Characterization and Modeling of the leading edge erosion of Wind Turbine Blades due to Sand Particles Impingement

Abdullah F. Alajmi

A dissertation in partial fulfilment of the

requirements for the degree of

Doctor of Philosophy

University of Washington

2021

Reading Committee:

Ramulu Mamidala, Chair

Mark Tuttle

Junlan Wang

Program Authorized to Offer Degree:

Mechanical Engineering

©Copyright 2021
Abdullah F. Alajmi

University of Washington

Abstract

Characterization and Modeling of the leading edge erosion of Wind Turbine Blades due to Sand Particles Impingement

Abdullah F. Alajmi

Chair of the Supervisory Committee:

Ramulu Mamidala

Department of Mechanical Engineering

Harsh environments such as desert and arid environments are showing a promising potential for energy production from wind turbine blades. However, when wind turbines are erected in such environments, unavoidable damage due to sand particle impingement during sandstorms, especially on the blade's leading edge, is expected. The leading edge erosion of wind turbine blades has a detrimental effect on the aerodynamic performance of the turbine. This investigation aims to experimentally study the erosion behavior of wind turbine blades when subjected to abrasive silica particles. The effect of multiple testing parameters on the intensity of erosion was investigated, such as the angle of impingement, erosion duration, and air pressure. The effect of protective coatings on reducing the intensity of erosion was also studied. Three types of coatings were used either as a single layer or in a multilayer coating system: graphene H-146, graphene IA-700, and polyurethane. It has been found that graphene has a great potential as a protective coating against erosion

since a single layer of H-146 provided up to 19% material removal reduction compared to an uncoated specimen. Moreover, combining a polyurethane layer on top of a graphene IA-700 layer showed a significant erosion reduction reaching up to 60% when protecting the leading edge of a wind turbine blade. The effect of these coatings on the aerodynamic performance of wind turbine blades was also studied. It has been found that the leading erosion causes an increase in drag coefficient, a decrease in lift coefficient, and a decrease in the amount of power generated. Protective coatings were able to reduce aerodynamic loss. In general, a combination of protective coatings made of graphene and polyurethane showed an excellent erosion resistance in terms of reduction in the amount of material removed, reduction in the depth of erosion scars, and reduction in the aerodynamic loss. In light of results presented in this investigation, polyurethane/graphene IA-700 coating can be used as a protective measure for wind turbine blades in erosion-prone environments and should be further investigated in terms of actual field applications.

Acknowledgement

I would like to express my deep thanks and gratitude to my mentor and guide **Ramulu Mamidala**, Professor of Mechanical Engineering, Adjunct Professor of Materials Science & Engineering, Adjunct Professor of Industrial & Systems Engineering, and Boeing - Pennell Professor of Engineering for his dedication, support, and keen interest in his students' growth, development, and success. The completion of this dissertation is thanks in large part to Professor Ramulu for his guidance that brought a great depth of knowledge to this work. I feel blessed and lucky to experience working with such a great teacher and human being. I would like also to express my gratitude to the Committee Members Mark Tuttle, Junlan Wang, and Dwayne Arola for their time, insight, and feedback that was essential and influential during the writing process.

Funding and sponsorship of this project greatly helped this dissertation to come to light. I would like to start with thanking the Government of Kuwait and the Mechanical Engineering department at Kuwait University for their support and sponsorship that was essential for the completion of this project. I would also like to thank the Department of Mechanical Engineering at University of Washington, Seattle, and Boeing - Pennell Professorship funds for their sponsorship of the project. A special thanks goes to AI Coatings for supplying this project with all the coatings needed, as well as using their facilities and personnel to apply these coatings.

Finally, I would like to thank my parents and siblings for believing in me and encouraging me to follow my dreams and for their emotional, psychological, and financial support. I would also like to thank my friends and my current and former colleagues at the Solheim Manufacturing Science and Technology Laboratory (MSTL).

Last but not least, I would like to thank the one person that without this project would not have been completed, my wife Rawan Alhayyan. Thank you so much for the daily doses of encouragement, support, and love. Thank you so much for the many sacrifices and for carrying the burdens which have fallen into your lap while I spent my time and energy pursuing my educational goals. Thank you for blessing us with Salman. Thank you for being you!

Table of Contents

ABSTRACT ..... **III**

ACKNOWLEDGEMENT ..... **V**

TABLE OF FIGURES ..... **X**

TABLE OF TABLES ..... **XIV**

NOMENCLATURE ..... **XVI**

CHAPTER 1: INTRODUCTION **1**

1.1 RENEWABLE ENERGY SOURCES 1

1.1.1 Hydroelectric energy *2*

1.1.2 Solar Photovoltaic *4*

1.2 WIND ENERGY 6

1.2.1 Horizontal-Axis vs. Vertical-Axis Wind Turbines *6*

1.2.2 Onshore vs. Offshore *7*

1.2.3 Size of Wind Turbines *9*

1.2.4 Number of blades *11*

1.2.5 Materials *11*

1.3 DRAWBACKS AND CHALLENGES 14

CHAPTER 2: LITERATURE REVIEW **17**

2.1 AERODYNAMIC PERFORMANCE 24

2.1.1 Wind Tunnel *24*

2.1.2 Xfoil *30*

2.2 LEADING EDGE EROSION 30

2.2.1 Addition of material *32*

2.2.2 Removal of material *37*

2.3 POSSIBLE SOLUTIONS 43

2.3.1 Design Solutions *43*

2.3.2 External Solutions *48*

2.4 SOLID PARTICLE EROSION 55

2.4.1 Erosion mechanisms *56*

2.4.2 Erosion parameters *66*

2.4.3 Erosion Models *73*

CHAPTER 3: MOTIVES AND OBJECTIVES **80**

3.1 Sandstorms *80*

3.2 Wind speed *82*

3.3 Characterization of sand particles *84*

3.4 Objectives and tasks *87*

CHAPTER 4: EXPERIMENTAL METHODOLOGY **89**

4.1 EXPERIMENTAL SETUP 89

4.1.1 Erosion Rig *89*

4.1.2 Test procedure *93*

4.1.3 Test parameters *93*

4.2 WIND TURBINE BLADES 95

4.3 SURFACE ROUGHNESS MEASUREMENTS 97

4.4 EROSION ANALYSIS 102

4.4.1 Optical Scanning (Profilometer) *102*

4.4.2 Scanning element Microscopy (SEM) *102*
4.4.3 Three-dimensional Scanning *103*
4.4.4 Statistical analysis and modeling *103*

CHAPTER 5: EROSION OF FLAT SURFACES 105
5.1 INTRODUCTION 105
5.1.1 Erosion of Ductile Material: *105*
5.1.2 Erosion of Brittle Material *113*
5.1.3 Erosion Experiments on GFRP *119*
5.2 EROSION OF COATED SURFACES 125
5.2.1 Erosion of single layer coated surfaces *131*
5.2.2 Erosion of Multi-layer coated surfaces *133*
5.3 DISCUSSION 136

CHAPTER 6: EROSION OF WIND TURBINE BLADES 151
6.1 TESTING PARAMETERS 155
6.1.1 Experimental procedure *156*
6.2 EROSION OF UNCOATED AIRFOILS 157
6.2.1 Material Removal Rate *158*
6.2.2 Depth of Erosion *160*
6.2.3 Erosion Mechanism *161*
6.2.4 Airfoil Shape After Erosion *162*
6.2.5 Total mass Loss *167*
6.3 EROSION OF COATED AIRFOILS 168
6.3.1 Inboard (Root) Section *169*
6.3.2 Midspan Section *170*
6.2.3 Outboard (Tip) Section *171*
6.4 DISCUSSION 173
6.4.1 Material Removal *173*
6.4.2 Depth of Erosion scars *174*
6.4.3 Erosion mechanism *175*
6.4.4 Surface Roughness *176*
6.3.4 Regression Analysis *178*

CHAPTER 7: ANALYSIS OF AERODYNAMIC PERFORMANCE 192
7.1 AERODYNAMIC PERFORMANCE 192
7.1.1 Uncoated blade *194*
7.1.2 coated blades *199*
7.1.3 Effects of coatings on Aerodynamic performance *209*
7.2 POWER GENERATION 214
7.2.1 Blade Element Momentum theory *214*
7.2.2 Power Estimation *225*
7.2.3 Discussion *226*

CHAPTER 8: CONCLUSION AND RECOMMENDATIONS 232

REFERENCES 236

APPENDIX I: MATERIAL REMOVAL DATA 247

APPENDIX II: PHOTOMICROGRAPHS OF EROSION SCARS OF FLAT SPECIMENS 254

APPENDIX III: MAXIMUM DEPTH OF EROSION SCARS 331

APPENDIX IV: ANALYSIS OF VARIANTS (ANOVA) 338

APPENDIX V: MATERIAL REMOVAL AND DEPTH OF EROSION SCARS OF THE LEADING EDGE 382

APPENDIX VI: PHOTOMICROGRAPHS OF THE EROSION SCARS OF THE LEADING EDGE 394

APPENDIX VII: XFOIL DOCUMENTATION 530

APPENDIX VIII: AERODYNAMIC PERFORMANCE BEFORE AND AFTER EROSION 565

Table of Figures

Fig. 1-1: Electric generating capacity for renewable sources for end of 2016 and 2017…….. 2
Fig. 1-2 Global renewable capacity growth by technology……. 3
Fig. 1-3: Levelized cost of electricity from utility-scale power generation technologies from 2010 to 2017. …….. 8
Fig. 1-4: Total installed costs of onshore wind projects and the global weighted average from 1983 to 2017 …… 10
Fig. 2-1: laminar to turbulent flow transition …… 18
Fig. 2-2: A schematic of an airfoil……. 19
Fig. 2-3: Flow visualization of the boundary layer of: (a) clean surface, and (b) rough surface …… 21
Fig. 2-4: Turbulence intensity due to roughness on a clean vs. rough surface…….. 22
Fig. 2-5: Clean and rough airfoils of the NACA 64-x18 family, a): Lift coefficient as a function of the angle of attack, and b) drag polar……... …… 23
Fig. 2-6: Wind Tunnel: (a) Open-circuit (b) Closed-Circuit……..... 25
Fig. 2-7: Resultant Force (F_R) components ..…… 29
Fig. 2-8: Ice adhesion and accretion on wind turbine blades…… 33
Fig. 2-9: Insect contamination on wind turbine blade…… 34
Fig. 2-10: Dust accumulation on wind turbine blades …….. 35
Fig. 2-11: Dust accumulation effects for nine months period on (a) Electrical power, (b) Mean power loss (MPL) percentage…… 36
Fig. 2-12: Annual Energy Production (AEP) as a function of velocity for the clean vs degraded profiles…….. 37
Fig. 2-13: leading edge erosion across years of service……... 38
Fig. 2-14: Erosion of the leading edge: pits, gouges, and delamination in: a) upper surface, and b) lower surface……. …….. 39
Fig. 2-15: Sand particles impact location and intensity of erosion rate at an angle of attack of (i) 0˚, (ii) 10˚, for: a) DU96 W180, b) NACA 63-415, and c) NREL S826.. 41
Fig. 2-16: Generator power comparison of SERI airfoils and AEROSTAR airfoils for clean and dirty blades……. ……. 45
Fig. 2-17: Design objective for optimum airfoil design …….…… 46
Fig. 2-18: Effect of surface geometry on the erosion rate: a) lower surface comparison, and b) upper surface comparison. Upper side erosion is shown in red. Lower side erosion is shown in cyan…… ……. 47
Fig. 2-19: Polyurethane-based coating compared to other types of coatings. Samples tested under the impact of rain droplet at 123-157 m/s at 30-35 mm/h. Top-to-bottom: Polyester gelcoat eroded for 1 hour, polyurethane tape- no UV-A exposure, polyurethane tape- 1000 hrs of UV-A exposure, ProBlade ™- 4000 hrs of UV-A exposure…… 52
Fig. 2-20: 3M W4600 compared to tape and competitive coatings……. 52
Fig. 2-21: Wear rate in humid and dry environments. ……..... 54
Fig. 2-22: The coefficient of friction (μ) of steel vs. steel interface is compared to the μ of steel vs. solution-processed graphene (SPG) coated steel…… 55
Fig. 2-23: Erosion rate vs. impact angle for ductile and brittle material……. 57

Fig. 2-24: Erosion stages as a function of time……..... 58
Fig. 2-25: Material removal mechanism of ductile material……...……. 59
Fig. 2-26: Material removal mechanism of brittle material……. 60
Fig. 2-27: Erosion of a glass plate by three different sizes of SiC particles in terms of angle of impingement…… 62
Fig. 2-28: Erosion rate as a function of impact velocity……... 67
Fig. 2-29: Erosion wear as a function of angle of impingement for: (a) Brittle materials, (b) Ductile materials. …….. 68
Fig. 2-30: Removal rate vs. standoff distance……... 69
Fig. 2-31: Erosion rate as a function of particle size…….....…… 70
Fig. 2-32: Effects of temperature on the wear rate of four types of steel: 1- St3, 2- U8A, 3- R9, and 4- cast iron Ch34L……... 73
Fig. 3-33: Idealized picture of a single particle scratching a ductile surface…… 75
Fig. 3-1: March 2009 dust storm metrological variables: (a) Visibility (b) Wind speed. ……. 81
Fig. 3-2: Visibility vs. wind speed data for ten years …… 84
Fig. 3-3: Particles size range percentage of dust fallout in Kuwait…… 87
Fig. 4-1: Experimental setup of the erosion rig……..... 91
Fig. 4-2: Silica abrasive particles used……. 93
Fig. 4-3: Cross-sectional view of the blade with glass fiber…… 96
Fig. 4-4: Roughness, waviness, and Lay in a surface…….. 98
Fig. 5-1: Material removal of aluminum as a function of angle of impingement ….. 107
Fig. 5-2: Erosion pattern of aluminum's erosion scars at an angle of attack of: (a) 10°, (b) 20°, (c) 30°, (d) 45°, (e) 60°, and (f) 90°…… 110
Fig. 5-3: Maximum depth of aluminum's erosion scars as a function of angle of attack……. 111
Fig. 5-4: Surface profile and maximum depth at an angle of Impingement of: (a) 10°, (b) 20°, (c) 30°, (d) 45°, (e) 60°, and (f) 90°…… 113
Fig. 5-5: Material removal of borosilicate glass as a function of angle of impingement …… 115
Fig. 5-6: Erosion pattern of glass's erosion scars at an angle of attack of: (a) 30˚, (b) 45˚, (c) 60˚, (d) 75˚, and (e) 90˚…….. 117
Fig. 5-7: Maximum depth of glass's erosion scars as a function of angle of attack…… 117
Fig. 5-8: Surface profiles for the three experimental sets at an angle of attack of: (a) 30˚, (b) 45˚, (c) 60˚, (d) 75˚, and (e) 90˚……..... 118
Fig. 5-9: Material removal of uncoated GFRP as a function of angle of attack …… 120
Fig. 5-10: Erosion pattern of GFRP's erosion scars at an angle of attack of: (a) 30˚, (b) 45˚, (c) 60˚, (d) 75˚, and (e) 90˚……..... 121
Fig. 5-11: Maximum depth of GFRP's erosion scars as a function of angle of attack……..... 122
Fig. 5-12: Surface profiles for the three experimental sets at an angle of attack of: (a) 30˚, (b) 45˚, (c) 60˚, (d) 75˚, and (e) 90˚…… 123
Fig. 5-13: Horizontal location of deepest point to length of erosion scar (x_d) as a function of angle of impingement for: (a) glass, and (b) GFRP…… 125
Fig. 5-14: SEM images of the surface of: a) H-146, b) IA-700, and c) Polyurethane…….. 127
Fig. 5-15: Cross section of coating systems: a) H-146, b) IA-700, c) Polyurethane, d)

Coating 4, e) Coating 5, f) Coating 6, and g) Coating 7…… 130
Fig. 5-16: Polyurethane layer getting removed from the top of H-146 layer …….. 130
Fig. 5-17: Analysis of single layer of coatings as a function of angle of attack a) maximum depth at 180 sec, and b) maximum depth at 360 sec, c) material removal at 180 sec, and d) material removal at 360 sec…….. 132
Fig. 5-18: Analysis of multilayer of coatings as a function of angle of attack a) maximum depth at 180 sec, and b) maximum depth at 360 sec, c) material removal at 180 sec, and d) material removal at 360 sec…….. 135
Fig. 5-19: Three-dimensional representation of material removal in terms of the angle of attack and erosion duration…… 138
Fig. 5-20: Three-dimensional representation of depth of erosion scars in terms of the angle of attack and erosion duration……. 140
Fig. 5-21: Micrographs of the erosion scar on the surface of: H-146: a) 30˚, b) 90˚, IA-700: c) 30˚, d) 90˚, and polyurethane: e) 30˚, f) 90˚…… 145
Fig. 5-22: Erosion scras at 45˚ for: a) SEM of Coating 5, b) SEM of Coating 7, c) transverse section of Coating 5, and d) transverse section of Coating 7…….. 147
Fig. 5-23: Surface roughness profile of a) H-146, b) IA-700, c) polyurethane, d) Coating 4, e) Coating 5, f) Coating 6, and g) Coating 7…….. 148
Fig. 6-1: Aeosol H 1-kW wind turbine blade: (a) full blade showing blade's sections and local, r, and total, R, radius of the blade, (b) cross-sectional view of Root section showing the A-A section, (c) cross sectional view of Midspan section showing the B-B section, and (d) cross-sectional view of Tip section showing the C-C section…….. 153
Fig. 6-2: Sand erosion rate at (a) r/R=0.35 at AOA= 5.5˚, (b) r/R=0.65 at AOA=6˚, and (c) r/R=0.75 at AOA=6˚. The blue circles of the airfoil indicate the location of sand particle impact and the red circle indicates the location of maximum erosion….. 154
Fig. 6-3: leading-edge erosion of Vestas 47 blade after 12 years of operation: (a) r/R=85%, (b) r/R= 90%, and (c) r/R=95%..... 155
Fig. 6-4: Schematic of NACA 63-215 airfoil with angles of attack of -5˚, 0˚, 5˚, and 10˚. …… 157
Fig. 6-5: Optical pictures of the erosion scars caused by: (a) -5˚, (b) 0˚, (c) 5˚, and (d) 10˚…….. 158
Fig. 6-6: Material removal as a function of angles of attack for root, midspan, and tip sections for an erosion duration of: (a) 180 seconds, and (b) 360 seconds …….. 159
Fig. 6-7: Maximum erosion depth as a function of angles of attack for root, midspan, and tip sections for an erosion duration of: (a) 180 seconds, and (b) 360 seconds …. 160
Fig. 6-8: SEM micrographs of 0˚ erosion scar showing matrix removal and fiber breakage at (a) 250x magnification, and (b) 1000x magnification……..... 162
Fig. 6-9: Extracting 2D profiles from 3D scanned before erosion airfoil……..... 163
Fig. 6-10: Before erosion (dashed line) and after erosion (solid line) tip section airfoil profiles after 360 seconds of: (a) -5˚, (b) 0˚, (c) 5˚, and (d) 10˚..... 165
Fig. 6-11: Expected shape of airfoil after erosion after combining the effects of different angles of attack……. 166
Fig. 6-12: Leading edge erosion of wind turbine blade with coating removed and laminate being exposed……. 167
Fig. 6-13: Comparison of the erosion behavior of Root section airfoils: (a) material removal at 180 seconds, (b) maximum depth at 180 seconds, (c) material removal at

360 seconds, and (d) maximum depth at 360 seconds……. 170
Fig. 6-14: Comparison of the erosion behavior of Midspan section airfoils: (a) material removal at 180 seconds, (b) maximum depth at 180 seconds, (c) material removal at 360 seconds, and (d) maximum depth at 360 seconds……. 171
Fig. 6-15: Comparison of the erosion behavior of Midspan section airfoils: (a) material removal at 180 seconds, (b) maximum depth at 180 seconds, (c) material removal at 360 seconds, and (d) maximum depth at 360 seconds……. 172
Fig. 6-16: (a) Surface Roughness parameters comparison, Surface profile of: (b) uncoated, (c) H-146, and (d) polyurethane/IA-700……. 177
Fig. 6-17: Mass loss due varying pressure, erosion duration, and angle of attack … 184
Fig. 6-18: Depth of erosion scars as a function of varying pressure, erosion duration, and angle of attack…….. 189
Fig. 6-19: Relationship between erosion scar depth and the amount of material removed…… 190
Fig. 7-1: Lift coefficient for the uncoated blade as a function of angle of attack before and after erosion for Root section a) 0˚, and b) 10˚, for Midspan section c) 0˚, and d)10˚, and for Tip section e) 0˚ and f) 10˚…….. 196
Fig. 7-2: Drag coefficient for the uncoated blade as a function of angle of attack before and after erosion for Root section a) 0˚, and b) 10˚, for Midspan section c) 0˚, and d)10˚, and for Tip section e) 0˚ and f)10˚…….. 198
Fig. 7-3: Lift coefficient for the H-146 coated blade as a function of angle of attack before and after erosion for Root section a) 0˚, and b) 10˚, for Midspan section c) 0˚, and d)10˚, and for Tip section e) 0˚ and f)10˚…….. 201
Fig. 7-4: Drag coefficient for the H-146 coated blade as a function of angle of attack before and after erosion for Root section a) 0˚, and b) 10˚, for Midspan section c) 0˚, and d)10˚, and for Tip section e) 0˚ and f)10˚……. 203
Fig. 7-5: Lift coefficient for the Polyurethane/IA-700 coated blade as a function of angle of attack before and after erosion for Root section a) 0˚, and b) 10˚, for Midspan section c) 0˚, and d)10˚, and for Tip section e) 0˚ and f)10˚……. 206
Fig. 7-6: Drag coefficient for the Polyurethane/IA-700 coated blade as a function of angle of attack before and after erosion for Root section a) 0˚, and b) 10˚, for Midspan section c) 0˚, and d)10˚, and for Tip section e) 0˚ and f)10˚……. 208
Fig. 7-7: Drag polar for the uncoated, H-146, and polyurethane/IA-700 blades at 0˚ and 10˚ angles of impingement……. 212
Fig. 7-8: Drag polar comparing the (a) before and (b) after erosion aerodynamic performance for the uncoated, H-146 coated, and polyurethane/Ia-700 coated blades……. 213
Fig. 7-9: A simple wind turbine rotor modeled as a permeable disc in 1-D flow … 215
Fig. 7-10: Control volume enclosing the flow through the ideal wind turbine rotor … 216
Fig. 7-11: velocities and angles at a blade element …… 220
Fig. 7-12: Lift-to-drag (Cl/Cd) ratio as a function of angle of attack for: (a) uncoated, (b) H-146 coated, and (c) polyurethane/IA-700 coated blades…… 228
Fig. 7-13: Power generation at 5˚ and 8˚ angle of attack for: a) before, and b) after erosion…… 231

Table of Tables

Table 1-1: Guide to silicon crystal solar cell efficiencies…….. 5
Table 2-1: Change in lift and drag coefficients after 12-month period ……. 37
Table 2-2: Erosion stages and description ……. 42
Table 2-3: Erosion stages and the resulting coefficients of lift (C_L) and drag (C_D). 42
Table 2-4: Four types of steel tested to study the effects of temperature on erosion 73
Table 3-1: Sand, silt, and clay particle size ranges …… 85
Table 3-2: Chemical composition of sand particles from multiple sites in Kuwait... 86
Table 4-1: Aeolos 1-kW wind turbine blades…… 96
Table 4-2: Abrasive water jet cutting conditions……... 97
Table 4-3: Roughness parameters and their formulations ……. 101
Table 4-4: Recommended cut-off length by ISO 4288 …..... 102
Table 4-5: Technical specifications for Keyence VR-3100 optical scanning profilometer ……..……..... 102
Table 4-6: Technical specifications of Creaform handyscan 700…..... 103
Table 5-1: Chemical Composition of Al 6061 – T6…..... 105
Table 5-2: Properties of Al 6061 – T6…..... 105
Table 5-3: Summary of testing parameters for erosion experiments on aluminum specimen …… 107
Table 5-4: Chemical composition of Borosilicate glass…..... 114
Table 5-5: Mechanical properties of borosilicate glass …..... 114
Table 5-6: Summary of testing parameters for erosion experiments on glass specimen 115
Table 5-7: Mechanical properties of GFRP…..... 117
Table 5-8: Summary of testing parameters for erosion experiments on GFRP specimen……. 120
Table 5-9: Mechanical Properties of the polyurethane coating…..... 128
Table 5-10: Mechanical properties of H-146 coating…..... 128
Table 5-11: Single and multilayer coatings of graphene and polyurethane…..... 129
Table 5-12: Optical photographs of typical erosion scars shape for the uncoated specimen, specimens coated with H-146, IA-700, and polyurethane…..... 133
Table 5-13: Optical photographs of typical erosion scars shape of Coatings 4 – 7..... 136
Table 5-14: A comparison of material removal data of the coated specimens to the uncoated specimen for an erosion duration of 180 seconds…….. 141
Table 5-15: A comparison of material removal data of the coated specimens to the uncoated specimen 141
Table 5-16: A comparison of maximum depth data of the coated specimens to the uncoated specimen for an erosion duration of 180 seconds……..... 142
Table 5-17: A comparison of maximum depth data of the coated specimens to the uncoated specimen 142
Table 6-1: Material removal experienced by H-146 coated blade and polyurethane/IA-700 coated in comparison to the uncoated blade for 360 seconds erosion duration ….. 174
Table 6-2: Maximum erosion depth experienced by H-146 coated blade and polyure-

thane/IA-700 coated in comparison to the uncoated blade for 360 seconds erosion duration…..... 174
Table 6-3: Ratio of material removal (and depth of erosion scar) of the leading edge of wind turbine blades to the material removal (and depth of erosion scar) of the flat GFRP surface……... 176
Table 6-4: A summary of variables used in regression analysis…….. 178
Table 6-5: Analysis of variance table to predict the mass loss of the uncoated blade … 180
Table 6-6: Analysis of variance table to predict the mass loss of the H-146 coated blade …… 180
Table 6-7: Analysis of variance table to predict the mass loss of the Polyurethane/IA-700 coated blade…….. 180
Table 6-8: Summary of results of regression analysis for mass loss response…… 181
Table 6-9: Coded factors of the depth of erosion scar equation for uncoated, H-146, and Polyurethane/IA-700 coated blades ……. 182
Table 6-10: Empirical constants needed to estimate the depth of erosion scars for the three blades …….. 182
Table 6-11: Analysis of variance table to predict the depth of erosion scars of the uncoated blade ……. 185
Table 6-12: Analysis of variance table to predict the depth of erosion scars of the H-146 coated blade……... 185
Table 6-13: Analysis of variance table to predict the depth of erosion scars of the Polyurethane/IA-700 coated blade……... 186
Table 6-14: Summary of results of regression analysis for the depth of erosion scar response……..... 186
Table 6-15: Coded factors of the depth of erosion scar equation for uncoated, H-146, and Polyurethane/IA-700 coated blades ……... 187
Table 6-16: Empirical constants needed to estimate the depth of erosion scars for the three blades ……... 187
Table 6-17: Empirical constants and R^2 values for Eqn. 6-6 …… 190
Table 7-1: Local velocity at representative r/R location in each section 193
Table 7-2: Change in lift and drag coefficient in the uncoated blade at Root, Midspan, and Tip sections for angles of impingement of -5˚, 0˚, 5˚, and 10˚ 199
Table 7-3: Change in lift and drag coefficient in the H-146 coated blade at Root, Midspan, and Tip sections for angles of impingement of -5˚, 0˚, 5˚, and 10˚…..... 204
Table 7-4: Change in lift and drag coefficient in the Polyurethane/IA-700 coated blade at Root, Midspan, and Tip sections for angles of impingement of -5˚, 0˚, 5˚, and 10˚..... 209
Table 7-5: Comparison of lift and drag coefficients changes for the uncoated, H-146 coated, and polyurethane/IA-700 coated blades 210
Table 7-6: Change in Cl/Cd at 8˚ angle of attack four the three blades 214
Table 7-7: Before and After erosion power generation for the uncoated blade…..... 225
Table 7-8: Before and After erosion power generation for H-146 coated blade…..... 226
Table 7-9: Before and After erosion power generation for H-146 coated blade……. 226
Table 7-10: Annual Energy Production (AEP) before and after erosion for the uncoated, H-146 coated, and Polyurethane/IA-700 coated blades ..…….. 227
Table 7-11: Change in Cl/Cd for the three blades at 5˚ angle of attack…….. 229

Nomenclature

Latin alphabets

A	Area of the rotor
A_1	Area of the nozzle section in a wind tunnel
A_2	Area of the test section in a wind tunnel
A_3	Area of the diffuser section in a wind tunnel
A_{cv}	Area of a controlled volume
A_{noz}	cross sectional area of the nozzle
A_s	defined area for measurement of surface roughness
a	axial induction factor
a'	angular induction factor
a_i	empirical constants
a_∞	speed of sound in the fluid
B	number of blades
b_i	empirical constants
C_A	axial force coefficient
C_d	drag coefficient
C_l	lift coefficient
C_n	normal force coefficient
C_R	resultant aerodynamic force coefficient
C_s	flow stress temperature-dependence constant
C_i	empirical factors
C_P	power coefficient
c	chord length
c_0	constant
c_i	first order coefficient
c_{ii}	second order coefficient
c_{ij}	interaction coefficient
D_0	reference particle diameter equal to 1 mm
D_s	diameter of the sphere abrasive particles

D_p diameter of the particle

D_i empirical factors

d_i diameter of the indentation

d_{noz} inner diameter of the nozzle

d_s depth of erosion scar

E Young's modulus

ER erosion rate (weight loss of target material per particle mass impacted in g/g)

ER_f erosion rate of fibers

ER_m erosion rate of matrix

ER_c erosion rate of composite

F Prandtl's tip loss factor

F_A Axial Aerodynamic force

F_D Drag force

F_L Lift force

F_n Normal Force

F_R Resultant aerodynamic force

g acceleration due to gravity

I moment of inertia of single particle

H head (vertical component of the water path)

H_C composite/measured hardness

H_F film (coating) hardness

H_S substrate hardness

Hv hardness

H_t hardness of the target material.

K velocity component normal to surface below which no erosion takes place in certain hard materials

K_1 proportionality constant

K_{Ic} fracture toughness

k adiabatic index

l_r sample lengths of roughness profiles

l_n evaluation length of roughness profiles

m_{air}	mass of airflow out of the nozzle
$\dot{m}_{side}$	mass of air flow inside a controlled volume
m_p	mass of the abrasive particles
m_{loss}	Amount of material removed from the leading edge
M	Mach number
M_T	total mass of impinging particles
P_0	Power generation
P_1	air pressure in the nozzle section in wind tunnel
P_2	air pressure in the test section in wind tunnel
P_3	air pressure in the diffuser section in wind tunnel
P	pressure
p_o	pressure at the cloud-base
p^+	pressure upstream of the rotor
p^-	pressure just behind the rotor
P_∞	freestream pressure
P_{in}	pressure at the inlet of the nozzle
P_{out}	atmospheric pressure
q	volumetric flow
q_∞	dynamic pressure
Q	Torque
r_p	radius of particle
r	local radius of rotor
R	blade length
R_a	arithmetical mean deviation of the assessed profile
R_c	Gas constant (287.05 J/kg)
R_q	Root mean square of the assessed profile
R_{ku}	kurtosis of assessed profile
R_p	maximum profile peak height
R_{sk}	skewness of assessed profile
R_v	maximum profile valley depth
R_z	maximum peak to valley height of a profile

Re	Reynolds number
S	airfoil reference area
S_a	arithmetic mean of the absolute of the ordinate values within a defined area A_s.
S_q	root mean square value of the ordinate values within a defined area A_s
S_{ku}	the quotient of the mean quartic value and the fourth power S_q respectively, within a defined area A_s
S_p	the largest profile peak height within a defined area A_s
S_{sk}	the quotient of the mean quartic value and the fourth power S_q respectively, within a defined area A_s
S_v	the largest profile valley depth within a defined area A_s.
S_z	the sum of height of the largest profile peak height and the largest profile valley depth within a defined area A_s
t	time
t_c	coating thickness
t_d	depth of indentation
T_e	temperature
T	Thrust force
T`	parcel temperature
ΔT	change in temperature
U_{max}	Peak wind speed
U_{th}	threshold of minimum kinetic energy of particles at which cracking can occur
u	reduced velocity in the rotor plane
u_1	velocity in the wake
V_o	undisturbed wind speed
V_1	air velocity in the nozzle section in wind tunnel
V_2	air velocity in the test section in wind tunnel
V_3	air velocity in the diffuser section in wind tunnel
V_∞	Freestream velocity
V_{rel}	relative velocity
v_p	velocity of the abrasives
v_{out}	airflow velocity

w	wind speed
w_o	vertical wind speed
w_f	weight fraction of fibers
w_m	weight fraction of matrix
x_d	the x-coordinate of the deepest point on an erosion scar
x_i	independent variable
x_j	independent variable
$x_{LE,old}$	x-coordinate of the leading edge of the airfoil before normalization
x_{new}	x-coordinate of the normalized airfoil
x_{old}	x-coordinate of the airfoil before normalization
x_T	Total length of erosion scar
$\dot{x}_t'$	horizontal velocity of tip of particle when cutting stops
$y(x)$	dependent variable
$y_{LE,old}$	y-coordinate of the leading edge of the airfoil before normalization
y_{new}	y-coordinate of the normalized airfoil
y_{old}	y-coordinate of the airfoil before normalization
y_t	depth of cut
z	film influence coefficient
$Z(x)$	height of the assessed profile at any position x
$Z(x,y)$	height of assessed profile area at any position x and y

Greek alphabets

α	Angle of attack
α_{p0}	impact angle at which horizontal velocity component has just become zero when particle leaves body
β	twist angle
δ	deformation wear factor, the amount of energy needed to remove unit volume of material
ε_v	erosive wear rate in mm^3/kg
ε_{VP}	volume of material removed due to plastic deformation mechanism (mm^3/kg)

ε_{VC}	volume removal due to cutting mechanism
ε_{VT}	total volume removal
η	fraction of particles cutting in an idealized manner
θ_p	pitch angle
κ	ratio of vertical to horizontal force components on the particle
λ_c	cut-off length
μ_∞	Dynamic viscosity of the fluid (air)
v	Kinematic viscosity
ρ	density of the fluid
ρ_∞	Freestream density
ρ_{air}	density of air
ρ_p	density of particle
σ_r	solidity
ϕ	flow angle
ϕ_i	Krumbein phi scale
χ	cutting wear factor, the quantity of energy needed to scratch out unit volume from a surface
ψ	ratio of depth of contact between abrasive particle and target surface (l) to depth of cut (y_t)
ω	angular velocity imparted to the wake
Ω	angular velocity of the rotor

Chapter 1: Introduction

As the demand for energy increases around the world, growing usage of fossil fuels is noticed, as well as the emission of greenhouse gases (GHG), especially carbon dioxide (CO2). According to the US Department of Energy, the global emissions of CO2 are estimated to rise from 31 billion metric tons in 2010 to 36 million metric tons in 2020 and 45 million metric tons in 2040 [1]. This increase in the production of CO2 and other toxic gases contributes to global warming, which accelerates the rate at which the ice melts and the raising of water levels endangering the lives of millions of human beings. Therefore, the use of energy sources with no/small GHG emissions is not only encouraged but also necessary.

The shift toward renewable energy sources is a promising and effective solution to the dangerous GHG emissions due to their cleaner and more environmentally friendly operations. According to U.S. Energy Information Administration (EIA), in 2017, about 63% of electricity generation came from fossil fuels (coal, natural gas, petroleum, and other gases), around 20% from nuclear energy, and 17% from renewable energy sources [2]. A brief overview of these renewable energy technologies is presented in the following sections.

1.1 Renewable Energy sources

Wind, hydroelectric, and solar photovoltaic (PV) represent the most renewable energy electricity generation, as shown in Fig. 1-1[2]. The fast growth of wind and solar PV is expected to compromise 82% of renewable energy growth in the five years of 2017-2022, as shown in Fig. 1-2 [3].

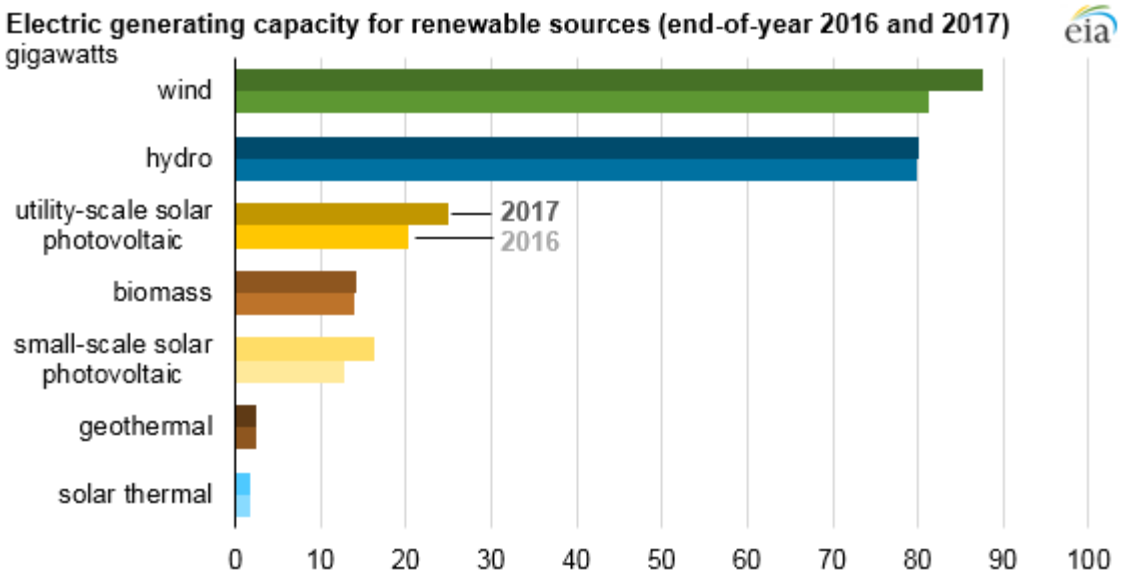


Fig. 1-1: Electric generating capacity for renewable sources for end of 2016 and 2017.

1.1.1 Hydroelectric energy

Compared to other renewable energy technologies, hydropower is the most mature, established, and widely used renewable energy resource. “Hydropower” as a term is restricted to the generation of shaft power from falling water for electricity generation or mechanical purposes. Electricity generation using hydro-turbines dates back to the 1880s and has been growing at a rate of about 5% since then [4]. In about one-third of the countries around the world, hydropower is responsible for more than 50% of the total electricity production. However, since the 1940s, most of the best sites in developed countries had already been exploited, and most of the new hydropower sites are in developing countries [4].

One of the advantages of hydropower plants is that it is long-lasting plants and with routine maintenance, the turbines can operate for about fifty years without major changes, and the dams can survive for around one hundred years. This long-lasting service is expected from hydropower systems because of their continuous operation without degrading factors such as high temperature or stress. Another major advantage of hydropower plants is the high

power generation efficiency, where efficiencies up to 90% have been achieved. On the other hand, the disadvantages include possible adverse environmental impacts such as affecting the fish, corrosion of water in some situations, and silting dams. It also has adverse social impacts such as displacement of people from reservoir sites and loss of potential productive lands.

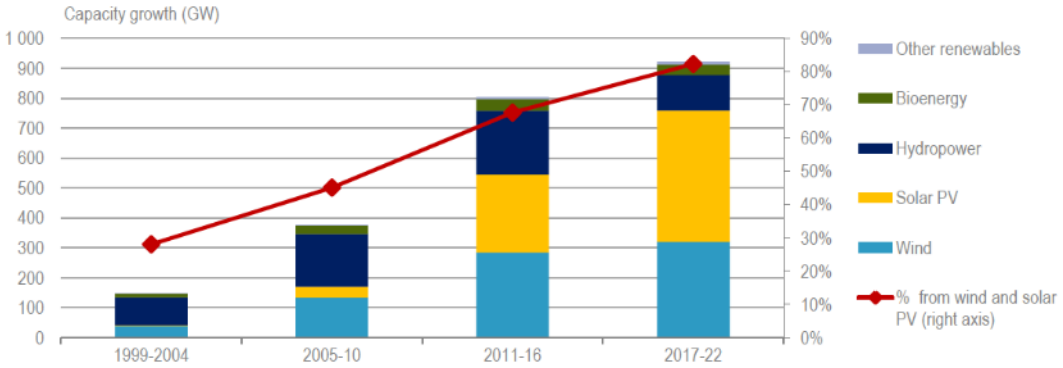


Fig. 1-2: Global renewable capacity growth by technology

To get a good estimate on whether a site should be considered for hydropower purposes the following equation is used:

$$P_0 = \rho q g H \tag{1-1}$$

where

P_0 is the power generation (in Watts).

ρ is the density of the fluid.

q is volumetric flow (volume per second)

g is acceleration due to gravity

H is head (vertical component of the water path)

Unlike the other energy sources, one of the advantages of hydropower systems is having no fundamental thermodynamic or dynamic reason for the power output to be lower than the power input P_0 apart of the frictional losses, which can be proportionally very small. In

any specific site, H is constant, q can be controlled and kept fairly constant, and therefore, it is not necessary to install a machine of capacity greater than usually required.

1.1.2 Solar Photovoltaic

Solar Energy is a form of renewable energy that can be used to produce electricity in two ways: thermally in concentrated solar power (CSP) plants, or photo-electrically via photovoltaic (PV) solar cells [4]. Solar thermal technology works by using sunbeam to raise the temperature concentrators to heat a fluid that can run turbines in CSP and produce electricity. There are two modes at which solar thermal power plants can be operated: either by directly heating the water/steam working fluid or by heating an intermediate fluid (e.g., molten salt), which is used to raise steam in a separate heat exchanger. The former system has the advantage of simplicity, while the latter, termed a thermal energy storage system, allows some flexibility for storing energy [5]. As shown in Fig. 1-1, solar thermal technology represents less than 5 GW of electricity production in 2017. This means it still has a long way to grow and needs more research and development to compete with other renewable energy and fossil fuels.

The second solar energy technology that has already proven its effectiveness and competitiveness is solar photovoltaic. The capacity of photovoltaic technology when combining both utility-scale with small-scale projects is around 40 GW, putting it in third place after wind energy and hydropower. Photovoltaic (PV) solar cells produce electricity by electromagnetic radiation, especially light that causes a separation of positive and negative charge carriers in the absorbing material. These charges produce a current to be used in an external circuit if an electric field is present. Such field exists inherently at junctions and inhomogeneities in PV cells as electrostatics fields and provides the electromotive force (EMF)

needed for useful power production. Semiconductors, especially silicon, are the most mature and well-established materials for PV power generation. In a clear sky with solar radiation of 1 kW/m^2, it is common for semiconductor/semiconductor or semiconductor/metal cells to produce potential differences of about 0.5 V and 400 A/m^2 current densities [4]. One of the most important disadvantages of PV cells is the generation efficiency, where commercial PV cells have 10-25% efficiency in ordinary sunshine. Table 1-1 below shows a guide to typical efficiency for silicon-based solar cells with silicon p-n (positive-negative) single crystal solar cells being the most common type of PV cells.

Table 1-1: Guide to silicon crystal solar cell efficiencies [4]

Type of silicon crystal solar cell	**Typical efficiency**
Laboratory, signal crystal	~ 25%
Laboratory, polycrystalline	~ 20%
Best commercial single crystal (e.g., for space)	~ 19%
General commercial, single crystal	~ 15%

The low efficiency of PV cells can be attributed to many factors; some are inherited in the science of electricity production from PV cells, and some are based on the way they are built. For example, power generation from PV cells is obtained by matching the radiation wavelengths of the incoming sunbeams, including inferred long wavelengths (~10 μm) to short ultraviolet wavelengths (~0.3 μm). Wavelengths longer than 1.1 μm cannot contribute to power generation, and the absorbance of the energy of these wavelengths causes the temperature of the cell to increase, leading to an approximate 23% efficiency loss. The same applies to very short wavelengths causing an approximate 33% efficiency loss. Top surface contact obstruction and reflection at top surface combined cause around 4% efficiency losses. With all that being said, PV cells have succeeded in becoming one of the most significant contributors to the power generation sector and reached a level of development where it is now competing with fossil fuels.

1.2 Wind Energy

In the last 40 years, wind energy succeeded in moving from a small activity used mainly to pump water in farms to an enormous power generation industry [6]. Furthermore, wind energy has seen an enormous growth where global wind production doubled every three and a half years [7]. Also, lifecycle energy estimates that the energy required for manufacturing, installing, and disposing of wind turbines can be recovered within six months of operation [8].

Wind energy is harvested through wind turbines, which could be divided into various categories based on different aspects. For example, a wind turbine could be categorized based on the direction of its axis of rotation, namely: Horizontal-Axis Wind Turbine (HAWT) and Vertical-Axis Wind Turbine (VAWT). Another common categorization is based on the location of their installation, either onshore or offshore. The sections below give a brief overview of these categories.

1.2.1 Horizontal-Axis vs. Vertical-Axis Wind Turbines

The first and most crucial categorization of wind turbines is based on the axis of rotation. Historically, wind turbines were made with a vertical axis of rotation from clothes as blades to pump water due to the ease of construction and the fact that VAWTs can accept wind from any direction without the need for a yaw system [9]. However, nowadays, HAWTs dominate the electricity production market because of their higher efficiency and energy output [10]. It has been found that the peak efficiency that a VAWT can achieve is 40%, while a HAWT can reach up to 50% [11]. Also, VAWTs need to be closer to the ground, which means it loses the opportunity of harvesting winds with higher speed at higher altitudes [10]. VAWTs are commonly used in small-scale projects, but in the case of utility-

scale projects, HAWTs dominate the market due to some inherent disadvantages in the VAWT system such as:

- They have suffered many fatigue failures due to the many natural resonances in the structure [4].
- They have a lower tip speed ratio and controlling rotor speeds is challenging. It has been found that efficiency increases with the increase of tip speed ratio [9]. A higher tip speed ratio means a higher rotational speed, and therefore a higher power can be generated with lower torque. A three-bladed wind turbine will typically run at a tip speed ratio of 7 to 8 for optimal performance [12].
- Complex tower support and because of the tower rotation with the blades, the bearings are susceptible to a considerable load [13].

1.2.2 Onshore vs. Offshore

Another essential categorization of wind turbine technology is based on the location of installation: onshore or offshore. Although the focus on onshore wind turbines is evident by the level of development and the number of units being installed globally, offshore wind turbines have attracted attention in the last decade [14]. Bloomberg New Energy Finance [15], in an analysis conducted in 2017, predicts a 16% compound annual growth rate making the offshore wind turbine industry reach a cumulative 115 GW capacity. Offshore wind turbine technology has the advantage of being away from the land where the winds blow harder, creating higher energy production. Also, the concerns about visual and noise pollution facing onshore wind technology are eliminated [7]. With the limited noise regulations on offshore wind turbines, the tip speed ratio can be increased. For example, Dykes et al. [16] studied the increase of tip speed from 80 m/s to 100 m/s results in

a 32% decrease in the gearbox size and, depending on the design approach, could decrease the Levelized cost of electricity (LCOE) by 1 to 9%. However, the trade-off when increasing the tip speeds is the increase of the energy at which airborne particles impact the blade, which leads to more severe damage.

Offshore wind technology is still facing some challenges that make onshore technology favorable, such as the LCOE of offshore wind technology is more than double that of onshore technology [14]. Fig. 1-3 shows an energy production cost comparison between different renewable energy technologies and fossil fuel during 2010-2017 [14]. The LCOE in 2016 of onshore wind turbine technology is at 6 cents/kWh while it is 14 cents/kWh for offshore wind turbine technology [14]. One of the main reasons for higher LCOE of offshore wind turbine technology is the difficult challenge of settling wind towers in waters that lay deeper and further from land, as well as the higher cost of maintenance due to the corrosive marine environment effects on the blades and their attachment [7].

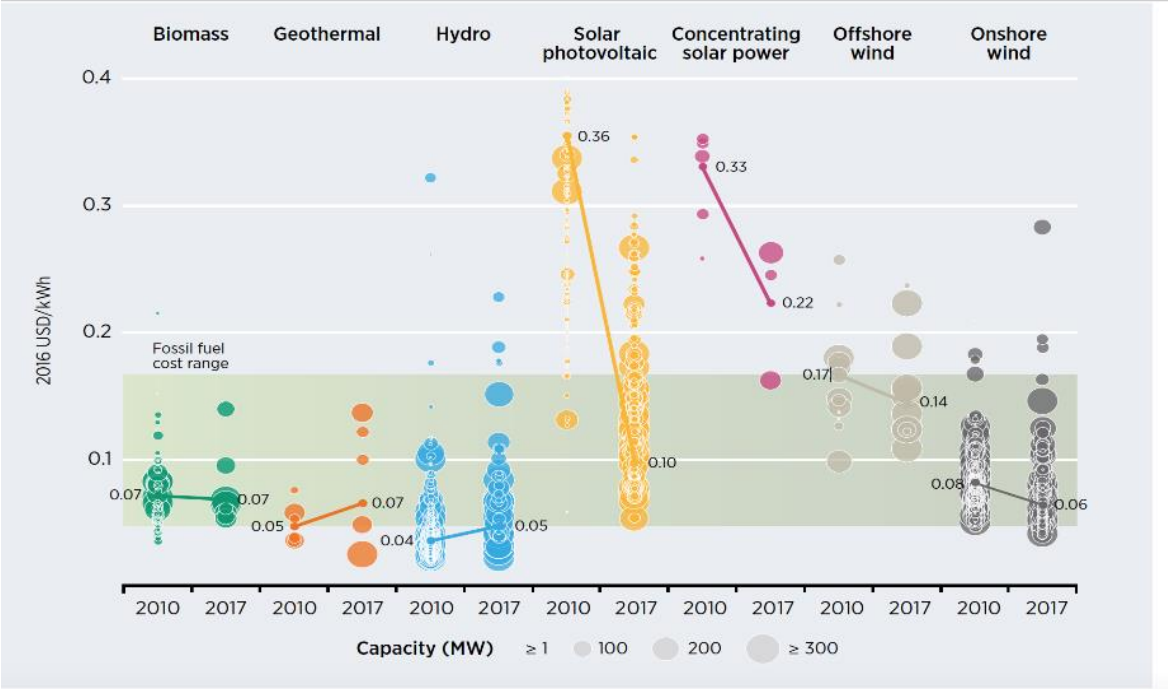


Fig. 1-3: Levelized cost of electricity from utility-scale power generation technologies from 2010 to 2017.

1.2.3 Size of Wind Turbines

According to Kaldellis and Zafirakis [17], the trend in the past few years is toward building bigger wind turbines with rotor lengths longer than 120 m. The reasons behind this trend are (1) to have better land exploitation, (2) the presence of economies of scale, and (3) the fact that bigger rotors at higher altitudes can catch winds with higher speed and at more stabilized flow due to lower turbulence. Also, it is estimated that a wind farm that is twice as tall will be subjected to roughly 10% higher wind speeds and 30% more power [18]. The hub height increased from around 20 meters in 1983 to around 100 meters in 2016 [14], with unit production increasing from around 100 kW to 2 MW, and it is expected to increase to 10-12 MW in the near future [6]. According to the World Energy Council [19], the blade length has been increasing at a rate of two meters per year for the last ten years, and if it continues its growth, a 15 MW will be commercialized in the 2030s. However, it should be noted that bigger wind turbines do not substantially increase the power output per unit of land because bigger wind turbines need to be spaced further apart [18].

The increase in the scale of wind turbines and the industry's maturity helped bring the cost of energy produced to competitive levels compared to other renewable energy industries and fossil fuel industries [9]. In Fig. 1-3, the cost of producing electricity for onshore wind turbines dropped from 0.08 $/kWh in 2010 to 0.06 $/kWh in 2016, which lies in the same range as fossil fuels (0.05 – 0.17 $/kWh). Fig. 1-4 shows the results of research and development on the historical total installed costs of onshore wind projects from 1983 to 2017 [14], where it can be seen that the global weighted average dropped from around 4,800 2016-USD per kW in 1983 to only around 1,500 2016-USD per kW.

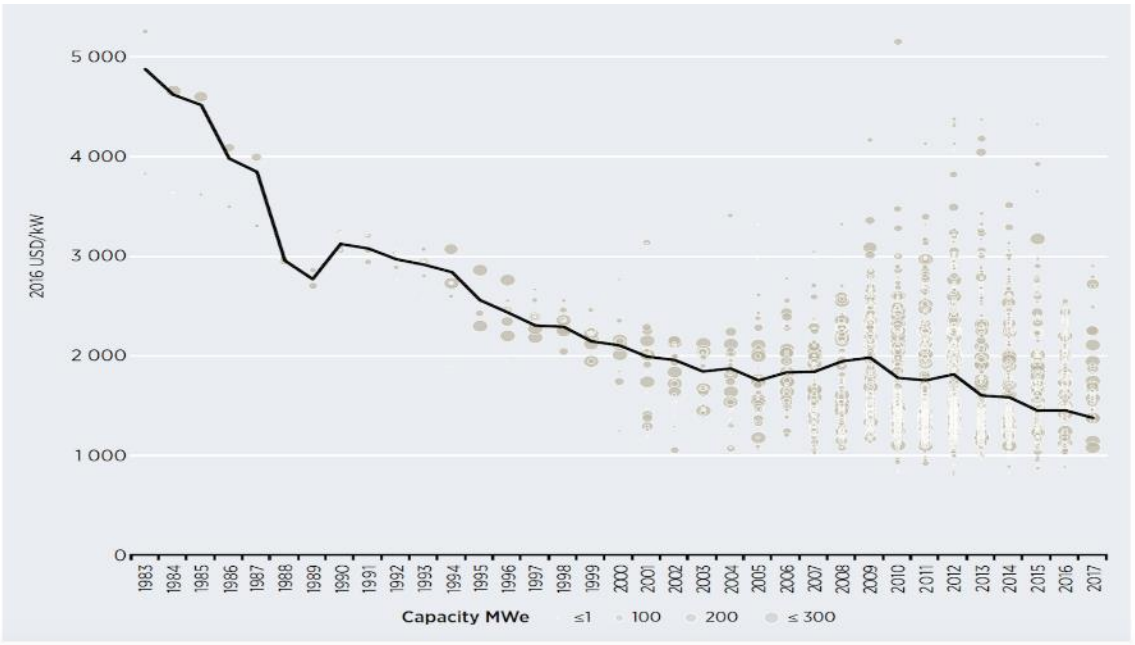


Fig. 1-4: Total installed costs of onshore wind projects and the global weighted average from 1983 to 2017 [8].

The increase in the size of wind turbines led to the rise of some challenges. For example, the weight of the rotor increases with the increase of the size of wind turbines, and as a result, the gravitational loads become the primary design driver. Also, with the increase of size, longer blades tend to have larger deflect; therefore, the stiffness-to-weight ratio is critical to ensure tip clearance (i.e., avoiding blades hitting the tower) [20]. Since larger blades represent a more massive amount of materials, it becomes crucial not to discard manufacturing defects since they are stress raisers and can become initiation points for further damage. Defects also can affect wind farm operators' ability to accurately predict the lifetime of the blades, which makes it challenging to schedule necessary repairs in advance and avoid blade damage and more downtime. Therefore, more damage tolerable materials without surface defects or impurities need to be developed [20].

1.2.4 Number of blades

One more critical aspect to examine is the number of blades on a wind turbine. Turbines with more than three blades need large initial torque to start but soon reach maximum power at a small rotational frequency; therefore, they are used more for water pumping and other low-frequency mechanical power [4]. On the other hand, turbines with a small number of blades may need starting but reach maximum power at a faster rotational frequency, which means it has fast shaft rotational frequency, and that is why it is used for electricity generation [4].

Two and three-bladed wind turbines are typical for electricity generation, but three-bladed is favorable due to its smoother and, generally, quieter operation compared to two-bladed rotors [4]. Increasing the number of blades from one to two yields a 4% increase in aerodynamic efficiency from 43% for one blade to 47% for two blades, while increasing from two to three blades yields a 3% efficiency increase [11]. Although four blades turbines have a marginal increase in efficiency over the three blades turbines, this small increase in efficiency does not justify the cost of manufacturing an extra blade [9].

1.2.5 Materials

Throughout history, different materials have been used to make wind turbines. Starting with cloths, wood, and stone in prehistoric Persia for usage in water pumping, to 1941, where steel blades were used to produce electricity, all the way to the 1970s where a shift toward composite materials was made [20]. Composite materials can be defined as a material system composed of two or more physically distinct phases whose combination pro-

duces better properties [21]. Composite materials are made of two main constituents: matrix (binder) and fibers (reinforcement), and every composite material must have at least one type of constituent.

Different parts of wind turbines play different roles and are subject to different loads; therefore, these parts must be made of different materials. For example, blades and nacelles are typically made of composite materials, while the tower and generator are made of metals [20]. Composite materials are used for making the blades because they have a high specific strength, good stiffness properties, and low weight, which is ideal for long slender load-bearing structures [22]. Also, composite materials are known for their excellent fatigue properties when compared to other high-performance alloys.

According to Mishnaevsky et al. [20], blades of wind turbines are typically made of E-glass fibers as the primary reinforcement in the composite, while recently, carbon fiber is represented as a promising alternative. Compared to fiberglass, carbon fibers show higher stiffness and lower density, thus allowing for thinner, lighter, and stiffer blades. However, carbon fibers show relatively low damage tolerance, compressive strength, and ultimate strain, and they are more expensive than E-glass fibers. Also, carbon fibers show sensitivity to waviness and fiber misalignment, where even slight misalignment could lead to a significant reduction in fatigue and compressive strength. Thus, when comparing the advantages and disadvantages of fiberglass and carbon fibers, it becomes clear why the dependence on fiberglass to build wind turbine blades.

Other types of glass fibers, such as S-glass, have been investigated. Compared to E-glass, S-glass has shown 40% higher tensile and flexural strengths, 10-20% higher compressive strength, and flexural modulus [20]. However, the price of S-glass fibers is around ten

times that of E-glass. Another attractive alternative to pure glass or carbon fibers is a hybrid E-glass/carbon reinforcement where it has been found that it would lead to an 80% decrease in weight while the cost will increase by 150% for an 8 m wind turbine [23]. Thus, it proves to be beneficial to use a mixture of carbon and glass fibers, with carbon being used mainly to increase the global blade stiffness.

For wind turbine blades, the composite material matrix is typically made of a thermoset material such as epoxy, polyester, and vinyl-Esther, and is rarely made of thermoplastic material [20]. Thermoset-based matrices constitute 80% of the market share of reinforced polymers, and they are preferable and dominating the market due to some advantages in their properties compared to thermoplastics [24]. For example, room/low cure temperature and low viscosity ease the infusion for manufacturing processes and increase production speed [20]. On the other hand, thermoplastics have higher processing temperatures leading to higher energy consumption during manufacturing and the possibility of influencing fiber properties [20]. Also, due to much higher viscosity in thermoplastics than thermosets, it is difficult to manufacture parts longer than 5 m and thicker than 5 mm [20]. When comparing fatigue behavior, thermosets generally demonstrate better behavior than thermoplastics when glass or carbon fibers are used [24].

Static and dynamic loads can cause various types of damages to the blades. Performing reliability analysis for wind turbines has shown that tip breakage and blade damage are two of the most common failure modes for wind turbines [25]. *Damage of the blades can cause harm in the wind turbines in two ways [26]: 1) mass imbalance, which will result in high loads on bearings, and even in the collapse of the tower; 2) turbulent airflow produced by the blades, which will negatively affect the neighboring wind turbines*.

The most common types of failures in the blades are: laminate delamination, failure of adhesive layers, and debonding and cracks in the coat/skin interface [20]. Also, when a fiber fails, load redistribution occurs, which induces a higher stress concentration [20]. Composite materials have some inherent drawbacks, such as performing poorly under the transverse impact (i.e., perpendicular to the direction of the fibers) and the sensitivity toward environmental factors such as moisture, UV light, and salinity [22]. These drawbacks must be taken into account when designing wind turbines.

Since the disassembling of wind turbine blades for factory inspection is costly, most inspections and servicing are done onsite. Damaged areas are visually inspected, and any surface alterations are smoothed using a primer and a protective polyurethane-based film [27, 28]. Barely visible damage may be missed during the inspection, which decreases the maximum structural load the blades are designed to sustain. Therefore, the use of non-destructive inspection tools such as ultrasonic scan and shearograpghy has gained some popularity. Nonetheless, some technical challenges are still present, such as wind turbine blades have a large surface area to be inspected visually and the fact that wind turbines are usually erected in poorly accessible locations [13, 25].

1.3 Drawbacks and Challenges

Although wind energy technology has made significant progress in the last 40 years, it still faces some inherent drawbacks and challenges. For example, similar to other renewable technologies, wind energy still faces the intermittency of the production problem. Since wind energy electricity production depends on winds blowing in a specific range of speeds,

meeting energy demand at a specific period of time might prove challenging, and the need for an energy storage system is necessary.

Another challenge facing wind energy technology is the aerodynamic noise and its critical effects on people's lives [29]. Many researchers have investigated the effects of the low frequency of aerodynamic noise on people's well-being, and its effects include: showing stress symptoms like headaches, sleep disturbance, hearing loss, and hurting the vestibular system [30, 31]. To minimize the harm caused by aerodynamic noise, researchers suggested installing wind turbines at least 2 km away from where people live or optimize house structures to block out the noise in areas close to wind farms [32].

Also, *when wind turbines are erected in harsh environments, unavoidable damage, especially on the blade's leading edge, is noticed*. Wind turbine blades account for 15 – 20% of the total cost of a wind turbine [33]. Harsh environments such as icy, dusty, and humid with a high concentration of insects can alter blades' airfoil design and increase their surface roughness. The effects of the increase of surface roughness on the aerodynamic performance are investigated in the next chapter.

Therefore, this investigation aims to study the leading edge erosion of wind turbine blades due to sand particles impingement during sandstorms. This goal is achieved by experimentally eroding wind turbine blades with silica sand particles. An imitation of an actual situation was taken into consideration to set up the parameters of this experiment. In order to mitigate the damage and the effects of using different types of protective coatings in order to reduce the erosion intensity were investigated. In addition, the effects of erosion on the aerodynamic performance of the blades with and without protective coatings were also studied.

This investigation is organized as follows: in Chapter 2, a literature survey is presented in order to understand the aerodynamic performance of wind turbine blades, leading edge erosion problem, possible solutions to the leading edge erosion problem, and an overview of the solid particle erosion process. Then in Chapter 3, the motivation, objectives, and the necessary tasks to achieve these objectives are discussed. In Chapter 4, the experimental setup, methodology, and procedures to study and analyze the erosion results are presented. In Chapter 5, the results of erosion experiments on flat surfaces are provided, as well as the study of different types of protective coatings. Then in Chapter 6, the leading edge of an uncoated wind turbine blade as well as a blade coated with H-146 graphene coating, and a blade coated with polyurethane/IA-700 coating are investigated. In Chapter 7, the aerodynamic performance of wind turbine blades before and after the leading edge erosion are presented. Finally, Chapter 8 provides the conclusion, recommendation, and future work suggested.

Chapter 2: Literature Review

The structural and aerodynamic properties of the blade are the fundamental factors for efficient wind power extraction [48]. One of the most critical challenges facing wind turbines is performance degradation due to the wind turbine blades' integrity being compromised. Efficient aerodynamic performance is achieved when airflow is attached to the blade. The increase of surface roughness at the leading edge increases the skin friction, which leads to early turbulence and premature flow separation. Consequently, the primary flow detaches earlier from the airfoil in the chord-wise direction than the optimal design, which is detrimental to aerodynamic efficiency [48].

Under two-phase conditions, the major interacting force between the gas and particles is the viscous drag. The degree of acceleration and deceleration achieved by the particles depends on the ratio of the viscous forces to the inertial forces experienced by the particles. As a result, a concentration gradient across the blade is formed, which leads to changes in the blade surface pressure distribution, and consequently, alters the performance of the turbine [49]. If the particles in the two-phase flow are erosive, the problem becomes more complicated. The impact of particles on the blade's surface can cause damage to the blades. This damage is manifested by cutting and pitting of the leading and trailing edge of the blade and a general increase of blade surface roughness. From an aerodynamic point of view, the effect of the impact of the erosive particle on the blade increases the total pressure loss across the blade.

From a fluid dynamics perspective, roughness can be defined as an extension of a body that penetrates the viscous layer causing an increase in the interaction between the fluid and the solid [50]. Therefore, more momentum and energy transfer occur between the two mediums, which affects the aerodynamic performance. According to the stability theory [51], there are small fluctuations in the flow parameters, such as pressure, velocity, density, and temperature. If these fluctuations are large enough to affect the flow parameters, a transitional period will occur where the flow transits from laminar to turbulent. Fig. 2-1 shows the stages of transition from laminar flow to turbulent flow. The flow at and up-stream of point 1 is laminar up to a critical point upstream of point 2. After that, various complex flow structures may form up to the point after which the flow is fully turbulent. At point 3 and 4, the origination and evolution of three-dimensional non-linear disturbance (∧ shape structure) occur, while at point 5, the interaction of turbulence spots can be seen. At point 6, the flow transition has been completed and the flow is fully turbulent. Depending on the flow parameters, some of these stages may be extended or bypassed.

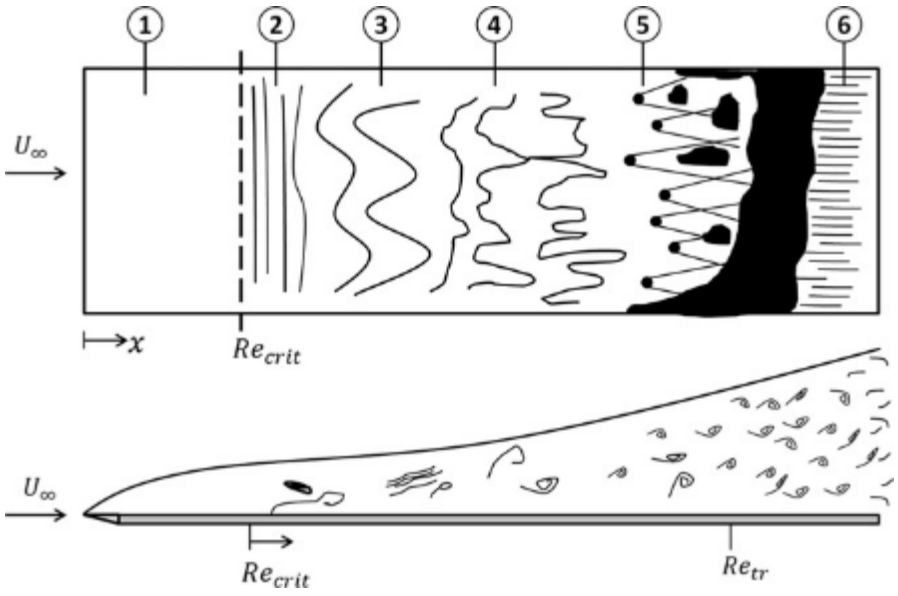


Fig. 2-1: laminar to turbulent flow transition [51].

There are some important geometrical parameters that differentiate one airfoil design from another, such as camber, thickness, and chord length. Fig. 2-2 shows a schematic diagram of an airfoil with the leading edge and trailing edge shown, as well as, chord line, mean camber line, maximum camber and maximum thickness. According to Anderson Jr [52], the *leading edge* is defined as the forward edge of the airfoil, while the *trailing edge* is the aft edge of the airfoil. A straight line connecting the leading edge and the trailing edge is called the *chord line*, which measures the length of the airfoil. The *mean camber line* is defined as a line drawn halfway between the upper surface and the lower surface. On the other hand, the *camber* is defined as the distance between the chord line and the mean camber line.

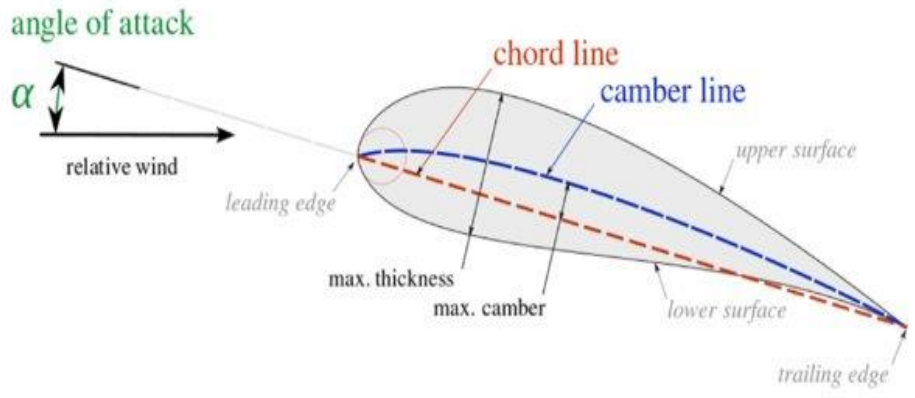


Fig. 2-2: A schematic of an airfoil [53]

The different types of airfoils are defined based on their geometrical and aerodynamical parameters. For example, the National Advisory Committee for Aeronautics (NACA) developed a systematic way to characterize the airfoils by dividing them into different series such as 4-digit series and 6-series. The 4-digit series is the simplest type of series, and it is defined as follows NACA xxxx [52]:

1. First digit describes the maximum camber as percentage of the chord.
2. Second digit describes the distance of maximum camber from the airfoil leading edge in tenths of the chord.
3. Last two digits describing maximum thickness of the airfoil as percent of the chord

For example, NACA 2412 means that the airfoil has a maximum camber of 2% of the chord located at 40% of the chord from the leading edge and the maximum thickness of the airfoil occurs at 12% of the chord.

On the other hand, for the 6-series NACA 6x-xxx:

1. The first digit simply identifies the series.
2. The second digit gives the location of minimum pressure in tenths of chord from the leading edge.
3. The third digit is design lift coefficient in tenths.
4. The last two digits give the maximum thickness in hundredths of chord.

For example, for NACA 63-215, the 6 is the series designation, while the minimum pressure occurs at 0.3 of chord. The design lift coefficient is 0.2, and the airfoil's maximum thickness is 15 percent of chord.

Several studies have investigated the effects of roughness on the aerodynamic performance of turbines. In a study conducted by Turner et al. [54] studying the boundary layers of clean and rough surfaces using flow visualization at a Reynolds number of 5×10^6, is shown in Fig. 2-3. As shown in the figure, the flow over the clean surface (a), the laminar flow can be seen, and the transition from laminar flow to turbulent flow. However, for the case of the rough surface (b), only turbulent flow is observed. In a numerical study on the effects

of roughness elements on the intensity of turbulence, Bragg et al. [55] studied both clean and rough NACA 0012 airfoil at a Reynolds number of 1.25 x 10^6. As can be seen in Fig. 2-4, roughness not only caused an early transition to turbulent flow, but it contributed toward higher turbulence intensity.

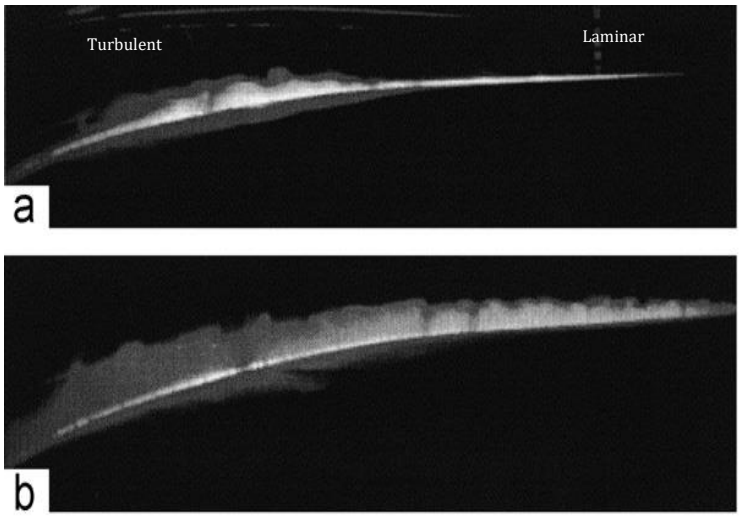


Fig. 2-3: Flow visualization of the boundary layer of: (a) clean surface, and (b) rough surface [54].

Several studies [55–57] investigated the effects of the location of roughness on the aerodynamic performance of the blade. *Aerodynamic lift* is defined as the force responsible for generating power by wind turbines, while *aerodynamic drag* is a resistant force that opposes the motion of the blades [9]. Therefore, for the best wind power extraction, lift must be maximized while drag must be minimized.

Roughness at the leading edge has a more detrimental effect on the aerodynamic performance of the blade than anywhere else on the blade. When studying the effects of roughness on the trailing edge up to 0.5 of the chord length, it has been found that the drag coefficient increased with a slight decrease in lift coefficient. Therefore, it can be concluded that the roughness of the trailing edge has minimal effect on the performance of the

blade. As the roughness reaches the leading edge, a 40% decrease in maximum lift coefficient and a 100% increase in drag coefficient have been observed.

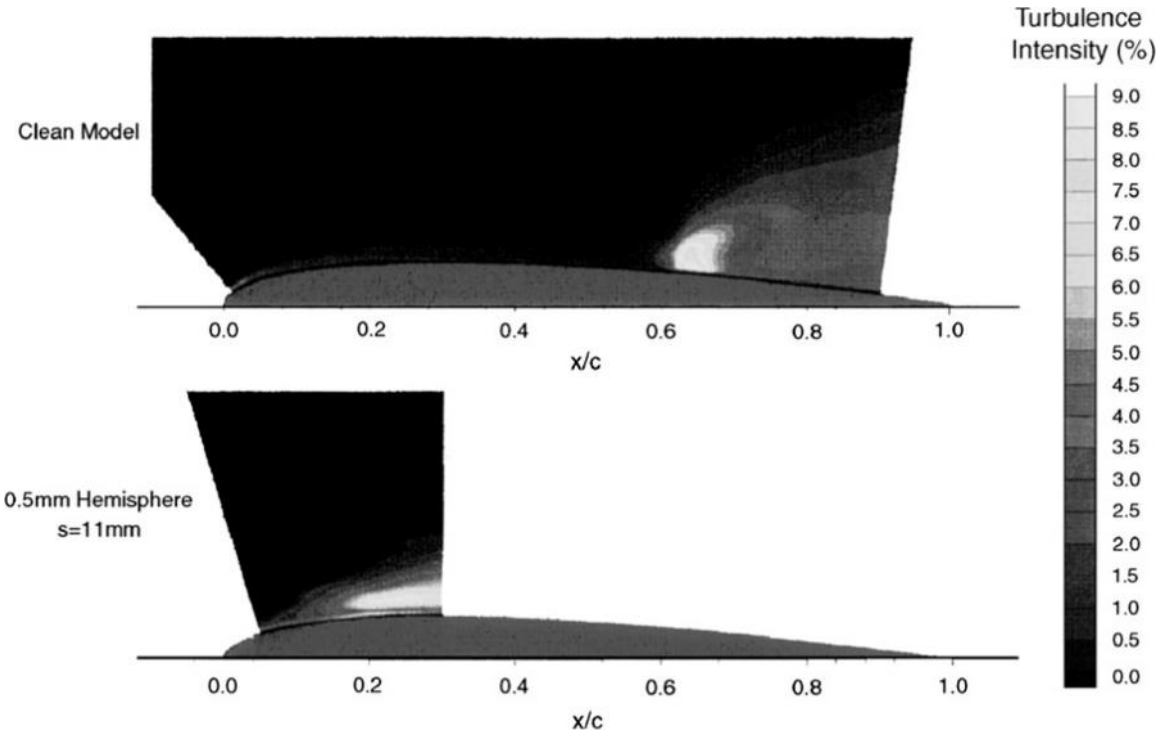


Fig. 2-4: Turbulence intensity due to roughness on a clean vs. rough surface [55].

In a study that investigated the effects of airfoil thickness and on roughness sensitivity, it has been concluded that airfoil thickness is proportional to roughness sensitivity [58], and for sections with thickness less than 18%, the effect of roughness on the lift-curve is small [12]. Timmer [59] studied the effects of roughness on 18% thick airfoils of a NACA 64-x18 family. Roughness was applied at the leading edge and up to 8% of the chord. Fig. 2-5 shows lift and drag coefficients for the clean and rough airfoils. It is clear that the lift coefficient decreased by approximately 20%, and the drag coefficient almost doubled.

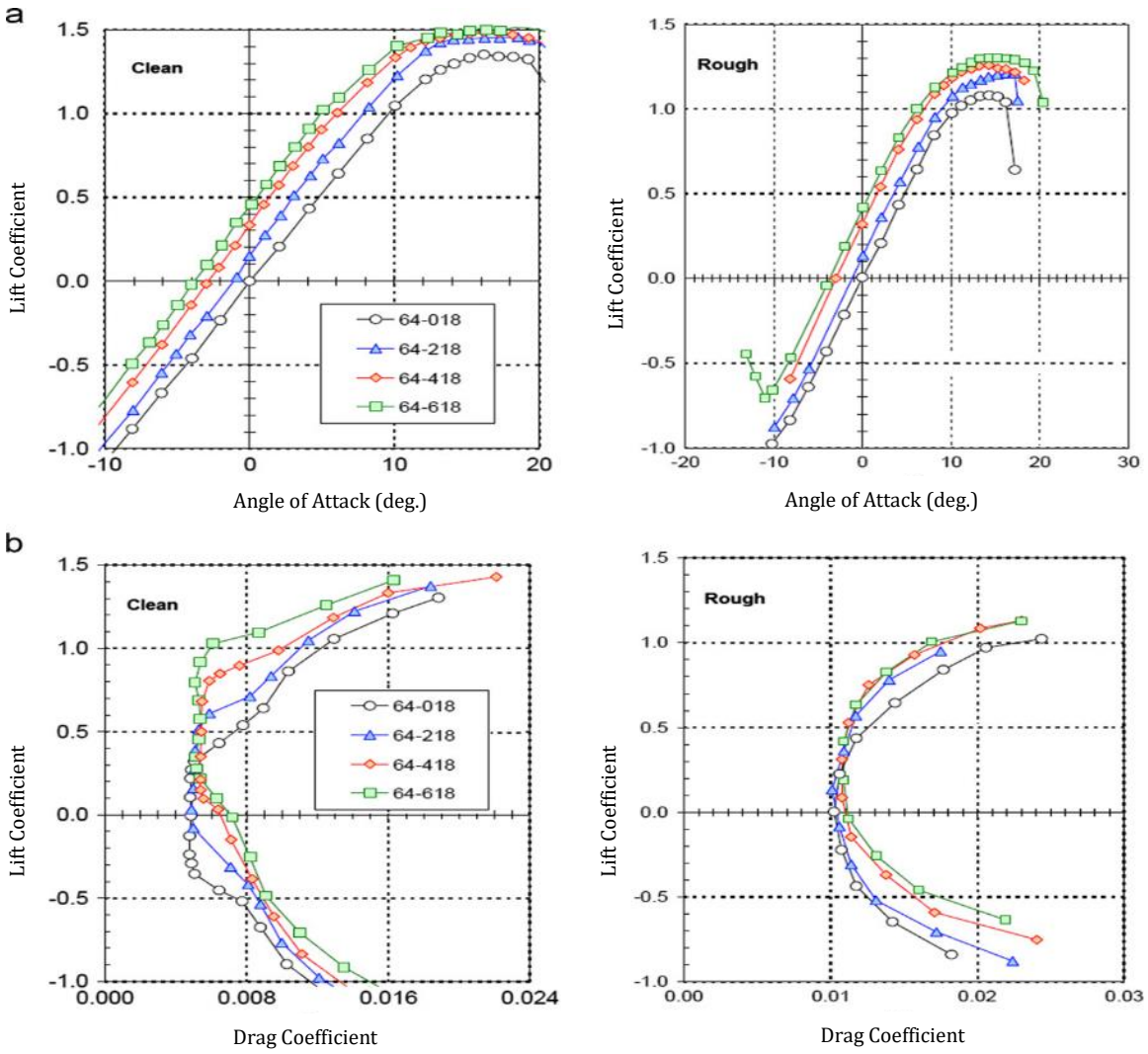


Fig. 2-5: Clean and rough airfoils of the NACA 64-x18 family, a): Lift coefficient as a function of the angle of attack, and b) drag polar [59].

In summary, roughness has three critical effects on the flow that affects the aerodynamic performance of wind turbine blades:

1. Roughness can contribute towards the increase of turbulence intensity, which is controlled by the size and location of roughness and Reynolds number of the flow.
2. The transition point from laminar to turbulent moves upstream, causing an early transition to turbulent flow.

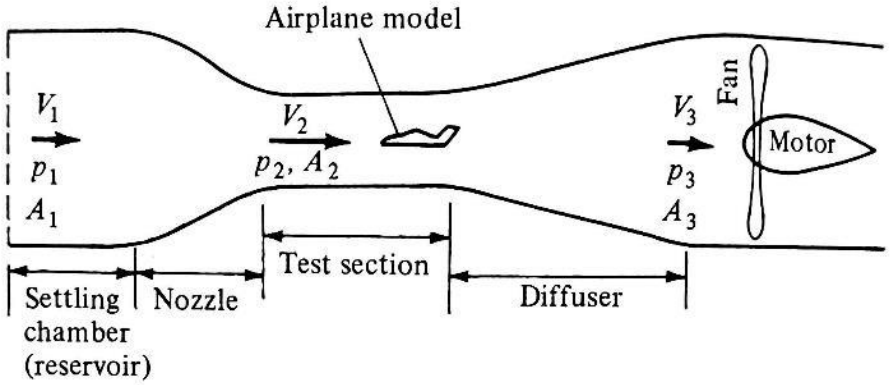
3. Roughness at the leading edge is highly detrimental to the aerodynamic performance, causing a decrease in lift coefficient and an increase in drag coefficient, consequentially decreasing aerodynamic efficiency.

2.1 Aerodynamic Performance

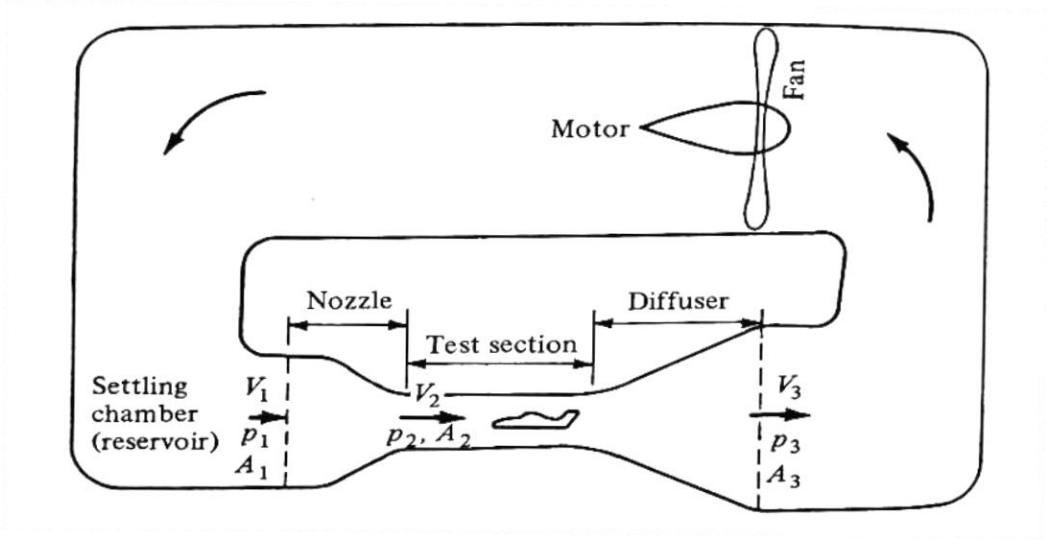
As discussed earlier, the erosion process caused the surface roughness of the blade to increase, leading to worse aerodynamic performance. The power output and the efficiency of wind turbine blades depend on the aerodynamic performance of the blades, and an efficient blade design will lead to higher energy capture. In this section, the aerodynamic performance of blades in terms of lift and drag coefficients will be investigated. Although a numerical simulation program will be used to estimate lift and drag coefficients, it is necessary to address the definition and how these coefficients are measured.

2.1.1 Wind Tunnel

A wind tunnel is commonly used to experimentally measure aerodynamic performance such as forces (lift and drag) and moments. In the wind tunnel, air is made to move across a test object with suitable sensors to measure aerodynamic forces, pressure distribution, and other wanted aerodynamic properties. A fan connected to a motor drives airflow in the wind tunnel. Wind tunnels could be classified into an open-circuit tunnel and a closed-circuit tunnel. In the open-circuit tunnel, air is drawn directly from the atmosphere and exhausted back to the atmosphere, as shown in Fig. 2-6 (a) [52]. On the other hand, air is circulated inside the tunnel in the closed-circuit tunnel without the need to draw new air from the atmosphere or to exhaust any out, as shown in Fig. 2-6 (b) [52].



(a)



(b)

Fig. 2-6: Wind Tunnel: (a) Open-circuit (b) Closed-Circuit [52].

Both types of wind tunnels consist of three main areas, namely: nozzle, test section, and diffuser. In the nozzle, air enters area A_1 with a low velocity V_1 and pressure P_1. Then it moves to the test section with smaller area A_2, a higher velocity V_2, and lower pressure P_2. After that, air leaves the test section to the diffuser with larger area A_3, lower velocity V_3, and higher pressure P_3. The relationship between area and velocity is governed by the continuity equation:

$$\rho_1 A_1 V_1 = \rho_2 A_2 V_2 \tag{3-1}$$

Considering that air is incompressible, where ρ is constant:

$$V_2 = \frac{A_1}{A_2} V_1 \tag{3-2}$$

The pressure in various locations in the wind tunnel is related to the velocity by Bernoulli's equation:

$$P_1 + \frac{1}{2}\rho V_1^2 = P_2 + \frac{1}{2}\rho V_2^2 \tag{3-3}$$

Combining the continuity equation with Bernoulli's equation and solving for V_2:

$$V_2 = \sqrt{\frac{2(P_1 - P_2)}{\rho[1-\left({}^{A_2}/_{A_1}\right)^2]}} \tag{3-4}$$

The contraction ratio A_2/A_1 is a fixed quantity for a given wind tunnel design.

2.1.1.1 Dimensionless analysis: The Buckingham PI Theorem

There are many physical quantities that can affect and determine the variations of the mentioned forces and moments. Some of these physical quantities are:

1- Freestream velocity V_∞.

2- Freestream density ρ_∞.

3- Viscosity of the fluid (air) μ_∞.

4- The size of the body represented by a chosen reference length (i.e. chord) c.

5- Speed of sound in the fluid a_∞.

6- Angle of attack α.

Therefore, a body with a given shape will have the resultant aerodynamic force R as a function of the mentioned physical quantities such as:

$$R = f(\rho_\infty, V_\infty, \mu_\infty, c, a_\infty, \alpha)$$

According to the Buckingham PI Theorem, this functional statement can be reduced to an equivalent dimensionless statement. In mechanics, all physical variables (N) can be expressed in terms of dimensions (K) of mass, length, and time. The number of dimensionless (PI) products is governed by N-K products, in this case, three PI products. If an equation describing a physical system has N dimensional variables and is expressed as:

$$y_1 = f(y_2, y_3, \dots\ y_N)$$

Then it can be rearranged and expressed in terms of (N-K) π-groups as

$$\pi_1 = F(\pi_2, \pi_3, \dots\ \pi_{N-K})$$

If these dimensionless products are the resultant force coefficient C_R, Reynolds number *Re*, and Mach number *M*:

$$\Pi_1 :\ C_R = \frac{F_R}{\frac{1}{2}\rho_\infty V_\infty^2 c^2} \tag{3-5}$$

$$\Pi_2 :\ Re = \frac{\rho_\infty V_\infty c}{\mu_\infty} \tag{3-6}$$

$$\Pi_3 :\ M = \frac{V_\infty}{a_\infty} \tag{3-7}$$

As a result, the resultant aerodynamic force (lift, drag) can be obtained for a given angle of attack α, by only varying Reynolds number and Mach number. Reynolds number and Mach number are called the similarity parameters, and they are the basis of wind tunnel testing. The aerodynamic performance of a model could predict the aerodynamic performance of a full-size object if the two flows are dynamically similar. Two flows are dynamically similar if [52]:

1- The streamline patterns are geometrically similar.

2- The distributions of V/V_∞, P/P_∞, etc., throughout the flow field are the same when plotted against dimensionless coordinates.

3- The similarity parameters are the same for both flows.

2.1.1.2 Lift and Drag Measurements

As seen in Π_1, the force coefficient is represented in terms of the resultant force F_R. The resultant force (F_R), as shown in Fig. 2-7, can be broken down into two components depending on either the direction of freestream (V_∞) or the chord line (c) of the airfoil. In terms of the freestream, lift (F_L) is the component of force acting upwards, perpendicular to the direction of the flight, or the freestream [60]. On the other hand, drag (F_D) is the component of the force parallel to the free stream that decreases the momentum [60]. In terms of the chord line (c), the resultant force can be broken down into normal and axial forces. The normal force is the force component perpendicular to c, while the axial force is the force component parallel to c.

Normal (F_N) and axial (F_A) forces data gathered from the wind tunnel tests will be used to calculate lift (F_L) and drag (F_D). Lift and drag can be calculated by the following two equations [52]:

$$F_L = F_N \cos\alpha - F_A \sin\alpha \tag{3-8}$$

$$F_D = F_N \sin\alpha + F_A \cos\alpha \tag{3-9}$$

The non-dimensional lift and drag coefficients are measured through the use of L and D [60]:

$$C_l = \frac{F_L}{q_\infty S} \tag{3-10}$$

$$C_d = \frac{F_D}{q_\infty S} \tag{3-11}$$

where

C_l is lift coefficient S is the reference area

C_d is drag coefficient While q_∞ is the dynamic pressure defined as

$$q_\infty = \frac{1}{2}\,\rho_\infty\,V_\infty \tag{3-12}$$

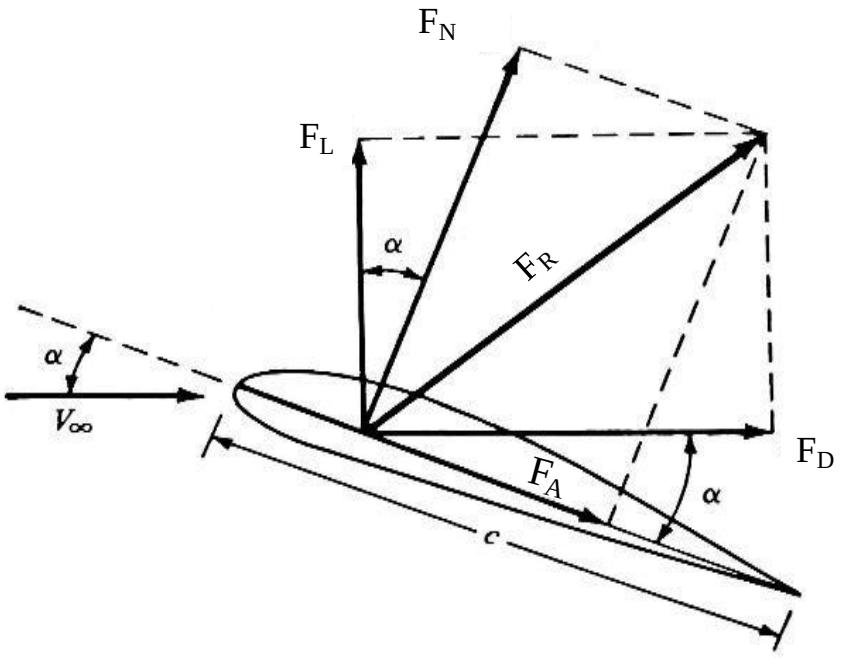


Fig. 2-7: Resultant Force (F_R) components

At low-to-moderate angle of attacks, the coefficient of lift increases linearly with the angle of attack. In this region, the flow moves smoothly over the airfoil and is attached to the surface for the most part. As the angle of attack increases, the flow tends to separate from the airfoil's upper surface, recirculate and flow in the opposite direction of the freestream. This separation of flow results in an increase in drag and decrease in lift, and under such conditions, the airfoil is said to be *stalled*. The maximum value of lift coefficient $C_{l,\,max}$ occurs just prior to the stall. On the other hand, the physical source of drag coefficient is both skin friction drag and pressure drag due to flow separation. The sum of these two drag sources leads to the drag coefficient C_d for the airfoil. Both sources of drag are generated due to viscous flow.

2.1.2 Xfoil

In this investigation, lift and drag coefficients will be obtained numerically using a publicly available software called Xfoil. Xfoil [61] was designed to rapidly predict airfoils' aerodynamic performance, especially at low Reynolds numbers. Xfoil calculates the viscous pressure distribution, and the convergence of analysis is reached through an iteration process between the outer and inner flow solutions on the boundary layer displacement thickness. When comparing experimental results and results predicted by Xfoil, Morgado et al. [62] found that Xfoil showed an excellent capability to predict airfoil performance. Also, they found that compared to other complex CFD softwares such as ANSYS Fluent® and OpenFoam, Xfoil showed similar prediction capability in a fraction of the time and effort.

After specifying the Reynolds number, the range of angles of attack needed for the analysis, lift and drag coefficients can be calculated. The angle at which the highest lift to drag ratio occurs is the angle at which the highest energy production is expected. Therefore, wind turbine blade manufacturers and operators want to run the turbines at or near this angle of attack. The lift and drag coefficients data obtained from Xfoil is crucial for calculating power output and loadings along the blade span.

2.2 Leading Edge Erosion

With the expansion of the wind turbine industry in the last few decades, interest in installing wind turbines in new harsh climatic zones with good wind speeds is rising. Some of these interesting new zones are the icy Nordic environments, humid regions with high insects population, and desert environments. In these harsh climatic zones, three major challenges are facing the wind turbine industry:

- ice adhesion and accretion on wind turbine blades in icy environments

- insect accumulation in humid regions
- dust accumulation and sand erosion of the blades in the desert environments.

These challenges lead to a common problem: the increase of surface roughness of the blades either positively (addition of material) in the case of ice adhesion, insect and dust accumulation, or negatively (removal of blade material) in the case of erosion.

Most of the previous studies focused on the effects of ice accretion, dust and insect debris on leading edge roughness, but little attention was given to blades erosion [63]. From the few papers that studied blade erosion, the majority of the studies focusing on erosion are on erosion caused by rain droplets, not by sand particles [63]. Trying to study the phenomena of erosion analytically using the classical approach can prove to be complex and highly specialized, and the introduction of composite materials can further complicate the problem [64]. Experimental and numerical approaches to evaluate the effects of sand erosion on wind turbine blades can be adopted. Experimental approach will act to inform and characterize the resulting damage modes and the erosive resistance of materials, while the numerical approach can reveal individual impact development [22].

Accurate numerical modeling of the erosion of composite materials is also not an easy task because of the need (in some cases) to go to microscopic, mesoscopic and macroscopic levels [64]. Moreover, one of the most challenging aspects of CFD simulation of wind turbine aerodynamics is turbulence modeling [38]. Nearly all the studies focusing on leading edge erosion used roughness strip or zigzag tape applied near the leading edge to simulate surface contamination, although this method is widely used, it does not accurately model the leading edge erosion [63]. Simulation of the real contamination accumulation

must be distributed throughout the blade with a higher concentration on the leading edge [65]. Also, for data to be an actual representation of the real situation, it must be taken from field measurements [65]. In the following sections, experimental and numerical studies on the effects of increasing surface roughness of the leading edge on the aerodynamic performance of wind turbine blades are presented and discussed.

2.2.1 Addition of material

As discussed earlier, a slight increase in surface roughness will, in turn, increase the drag coefficient, which could reach 20-50% at harsh sites leading to a reduction of the power output [66]. The uncertainty regarding wind turbine performance when there is ice accumulation on the blades resulted in several studies investigating accumulation shapes and sizes. Surface roughness has been found to degrade aerodynamic performance. In one study, glaze ice and rime ice effects were experimentally investigated with Reynolds numbers ranging between $2.65x10^5$ and $7.33x10^5$ on a NACA 63-415 airfoil design [67]. Glaze ice is horn-shaped and forms when a layer of water covers a thicker ice layer. The water layer does not freeze on impact with the ice layer, but it runs back toward the blade's trailing edge and freezes in its way in horn shape. On the other hand, rime ice contains ice layers that form at the intersection of solid surfaces and water droplet streamlines. The study showed that most of the accumulation was near the leading edge, where the masses of the glaze ice and rime ice was 11% and 6.7%, respectively, of the original mass of the blade (density of rime ice is lower due to air bubbles trapped in the ice). Lift coefficient at the leading edge decreased by 40%, while drag increased by 365% for glaze accretion and 250% for rime accretion.

Another study examined the effects of ice accretion on the performance of wind turbines numerically on a NACA 64-618 airfoil, and the results were verified using a wind tunnel test on an aircraft wing section and natural wind turbine icing [29]. It has been found that the lift coefficient dropped from 1.35 for a clean airfoil to 1.2, 1.1, 1.05 for ice droplet sizes of 12 μm, 17 μm, and 30 μm, respectively. Fig. 2-8 shows an example of ice adhesion and accretion on a wind turbine blade, and it is obvious how the shape of the leading edge of the original design has changed [68].

Similar to the ice accretion problem, the accumulation of insects on the leading edge of wind turbine blades can have detrimental effects depending on its concentration. For example, light insect accumulation was found to decrease power output by 8%, while high contamination can decrease power output by up to 55% [69]. Fig. 2-9 shows a blade contaminated by insect collusion [48].



Fig. 2-8: Ice adhesion and accretion on wind turbine blades [68].



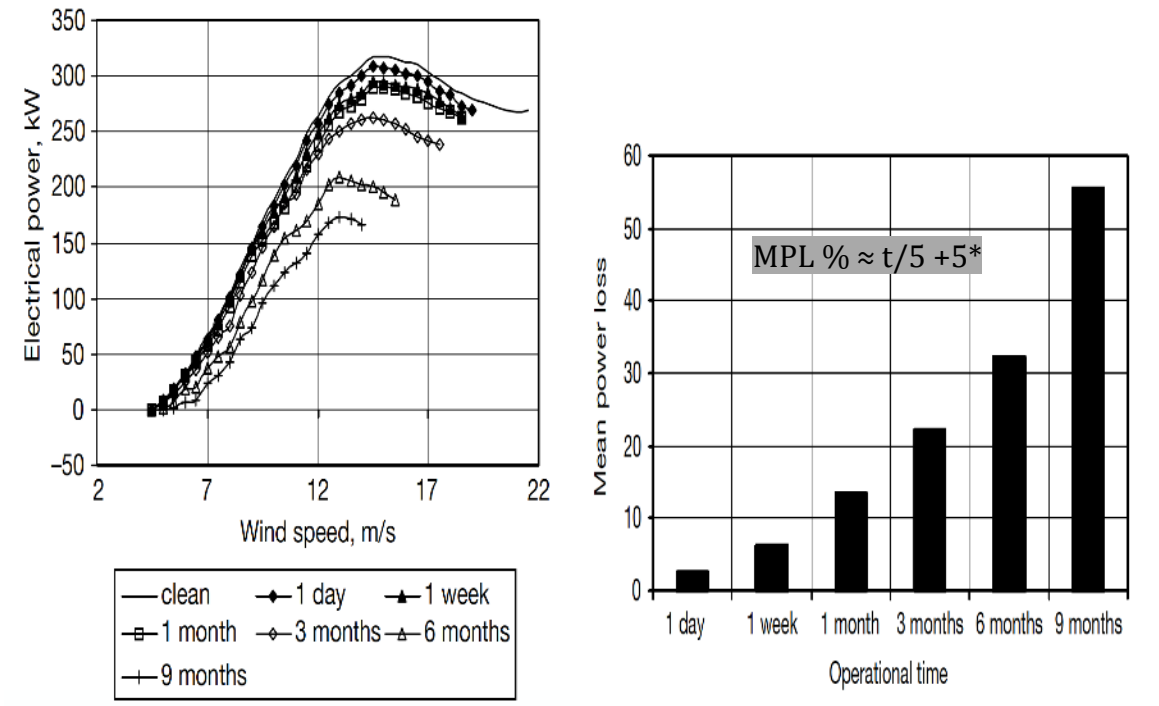
Fig. 2-9: Insect contamination on wind turbine blade [48].

Dust can accumulate on the blade in desert and arid environments, as shown in Fig. 2-10 [70]. Khalfallah and Koliub [71] conducted a study focusing on the effects of dust accumulation on power output, it has been found that subjecting a wind turbine to wind in a desert area for nine months without cleaning the blades (no rain was observed during this period) resulted in a decrease in electrical power production. Fig. 2-11(a) shows the production of wind turbines for the nine months as a function of wind speed. It can be seen that the power produced at speeds between 12 m/s and 17 m/s decreased from 320 kW for a clean wind turbine to around 160 kW after nine months of dust accumulation. Fig. 2-11(b) shows the mean power loss compared to clean blades for the nine months [71]. Accumulation of dust affects the surface roughness and increases the overall weight of the blades, which will expedite stall resulting in more stoppage time and more power loss.



Fig. 2-10: Dust accumulation on wind turbine blades [70].

In a numerical study, Ren and Ou [57] used a NACA 63-430 airfoil in a 2D simulation to explore the effects of dust accumulation and the increase of surface roughness on the aerodynamic performance. The simulation predictions were compared to experimental results, and they showed a good match. It was found that the lift coefficient decreases up to 50% in 20 months, while the drag coefficient increases because of the increase of surface roughness. Surface roughness height increased to 0.6 mm in 20 months of dust accumulation, and the critical roughness height was found to be 0.3 mm, where critical height is defined as the height at which the flow will transfer to a fully turbulent flow. At heights higher than 0.3 mm, flow separation is severe, and the effect of surface roughness on the aerodynamic performance becomes no longer evident.



(a) (b)

Fig. 2-11: Dust accumulation effects for nine months period on (a) Electrical power, (b) Mean power loss (MPL) percentage. * t is the time by day [71].

Moreover, due to the effects of relative speed, it is expected to have more dust deposition on the root section of the blade, while the tip section is more susceptible to erosion. This result has been reached in a numerical study by El-din et al. [72], where the change in the coefficient of drag and coefficient of lift for one year has been computed as shown in Table 2-1 below. The increase in drag coefficient due to erosion at the tip section reaches 67%, while at the root section of the blade, the increase in drag coefficient was at 40%. On the other hand, the increase in drag coefficient due to deposition at the root section reaches 200%, while at the tip section, the drag coefficient increase was at 4%. El-Din et al.[72] also compared the Annual Energy Production (AEP) between clean wind turbine blades and degraded blades subjected to sand deposition and erosion. As shown in Fig. 2-12, clean

blades always produced higher AEP than degraded blades. At the 12 m/s where the highest AEP is generated, the loss in AEP is around 10%.

Table 2-1: Change in lift and drag coefficients after 12-month period [72].

	$\%\Delta C_L$		$\%\Delta C_D$	
Blade section	Deposition	Erosion	Deposition	Erosion
Root	-15%	-1%	200%	40%
Mid-span	-12%	-2%	19%	50%
Tip	-0.1%	-10.5%	4%	67%

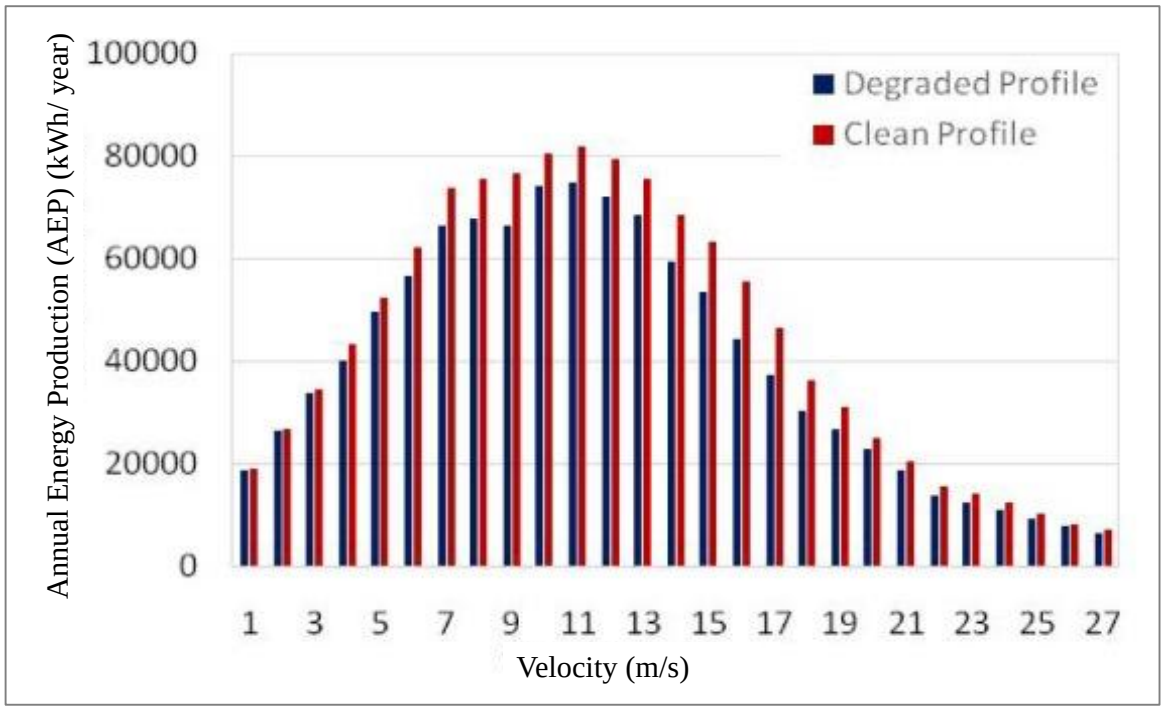


Fig. 2-12: Annual Energy Production (AEP) as a function of velocity for the clean vs degraded profiles [72]

2.2.2 Removal of material

The leading edge erosion is a serious challenge facing manufacturers and operators due to its role in aerodynamic load, power production, and the lifetime of the blades [22]. Wind carrying sand particles bombarding the leading edge of wind turbines leads to surface roughness changes, which in turn causes the aerodynamic performance to deteriorate. Combined with dust accumulation, erosion caused by sand particles is another problem

that faces wind turbine blades in arid environments leading to a change in the surface roughness of the blade. As shown in Fig. 2-13, the highest degree of erosion occurs at the leading edge and decreases in the chord direction [73]. Some operators noticed signs of wear and tear due to the leading-edge erosion as early as two years of operation, with the tips being most susceptible to wear. Therefore, this section will investigate the effects of the leading edge erosion on the aerodynamic performance of the blade.

Due to blade erosion, the blade profile and geometry change with time, causing a significant reduction in power output, efficiency, and availability [74]. The random pattern of material removal caused by the erosion process will also cause a mass imbalance in the wind turbine blades due to asymmetric masses causing a change in the original load distribution design, as well as increasing the possibility of the resonance due to the change of natural frequency, especially for smaller wind turbines [48].

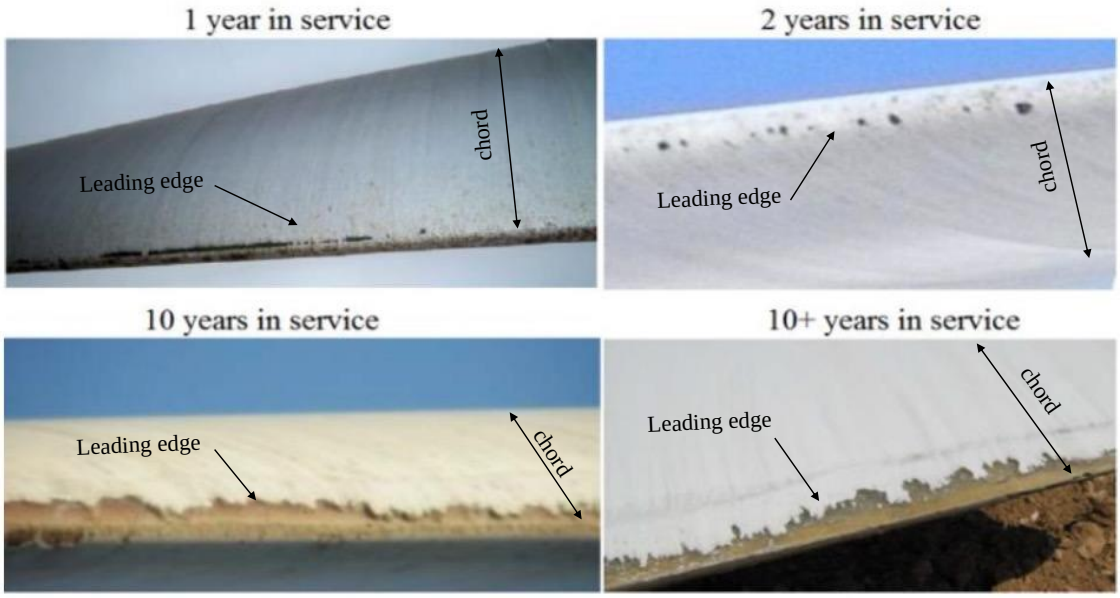
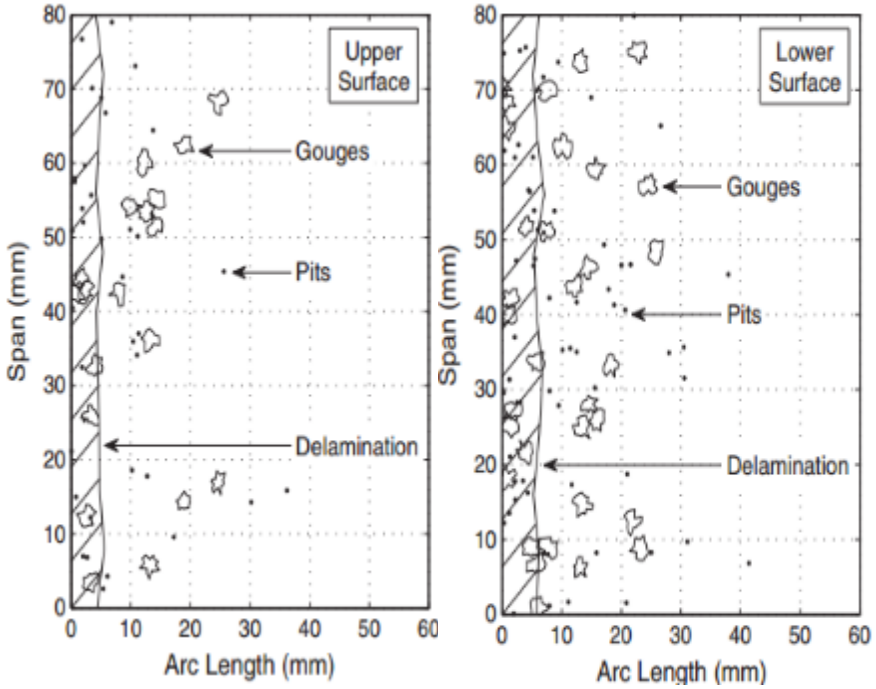


Fig. 2-13: leading edge erosion across years of service [73].

The erosion process typically starts with the formation of pits near the leading edge. As erosion continues, pits increase in number, depth, and density, forming gouges, which with

time elapsing combines forming delamination near the leading edge [63]. Bragg et al. [55] reports erosion on the lower and upper surface of wind turbine blades and divides it into pits, gouges and delamination, as shown in Fig. 2-14. Pits, gouges, and delamination not only can affect the aerodynamic performance of wind turbines but also can be the initiation sites for cracks, and if left unrepaired structural damage to the laminate material will soon develop, causing more complex problems.



a) b)

Fig. 2-14: Erosion of the leading edge: pits, gouges, and delamination in: a) upper surface, and b) lower surface [55].

The degradation of aerodynamic performance can be attributed to the early introduction of turbulence in the flow and the premature flow separation. The collision of airborne sand particles with wind turbine blades causes micro-cutting and ploughing in the coating material [75], which increases the surface roughness of the blade, especially at the leading edge. According to Fiore and Selig [76], the process of erosion of wind turbine blades over time can be summarized as:

1. Particles impact the wind turbine blade at the vicinity of the leading edge. Fig. 2-15 shows the trajectory of sand particles when impacting three different airfoils with similar thickness to chord ratio ~ 15% at two angles of attack: 0˚ and 10˚ [77].
2. Erosion due to sand particles impingement removes the coating layer and leaves a narrow strip of coating along the leading edge. Most current materials used for wind blade coating are polyurethane derivates [78] and show a maximum erosion at an angle of attack of 30˚ at upper and lower surfaces of wind turbine blade [76, 79].
3. The strip decays due to lack of coating integrity, and eventually, it gets removed due to continued sand particles erosion, and the composite substrate is exposed.
4. After the coating layer is removed, the composite substrate has the maximum erosion rate at a range of angles of attack of 45˚ – 55˚ [80], and the maximum erosion location move closer near the leading edge.

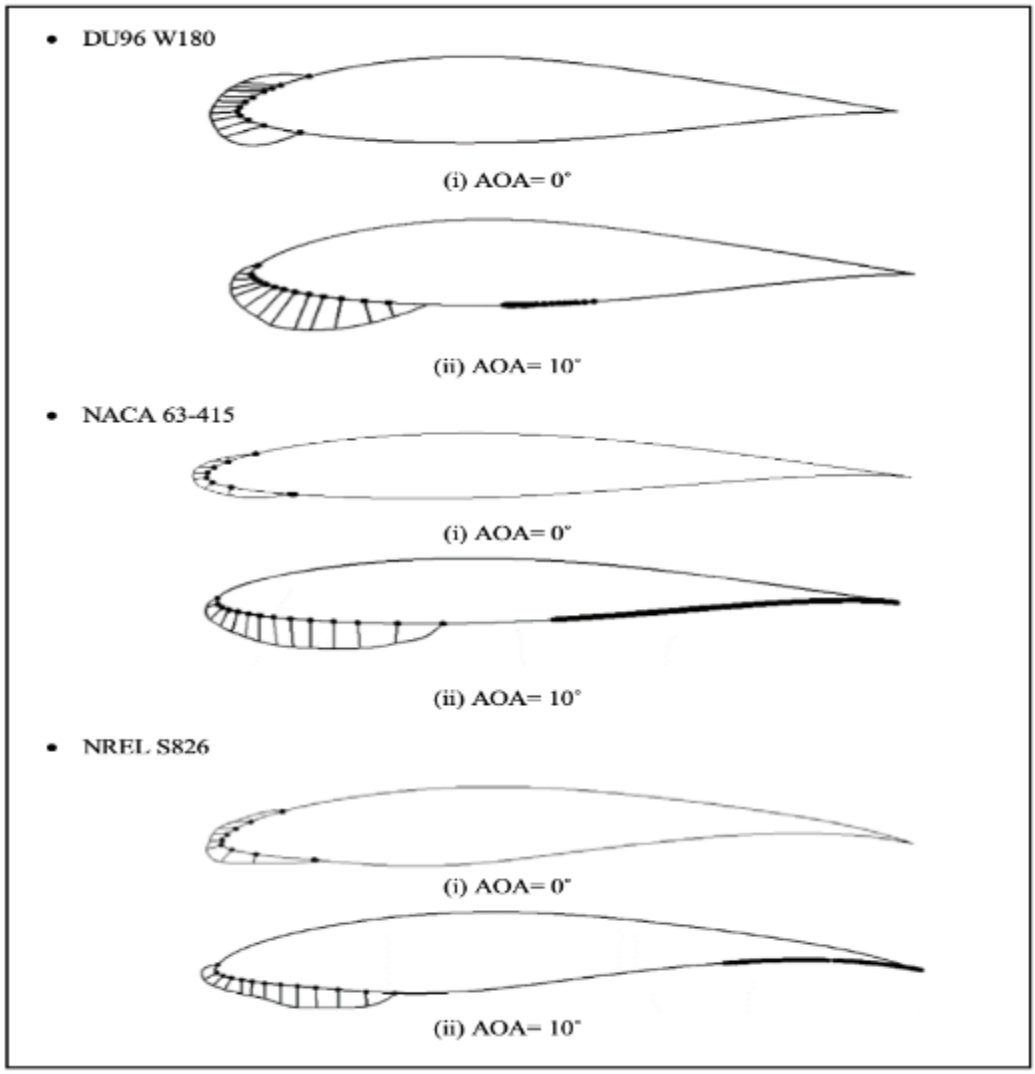


Fig. 2-15: Sand particles impact location and intensity of erosion rate at an angle of attack of (i) 0˚, (ii) 10˚, for: a) DU96 W180, b) NACA 63-415, and c) NREL S826 [77].

According to Sareen et al. [63], it has been found that light-to-heavy erosion could result in a 6-500% increase in drag [63]. An increase of 400-500% in drag coefficient coupled with a decrease in lift coefficient will result in a loss of annual energy production as high as 25%. In their studies of the leading-edge erosion of wind turbine blades, Sandia National Laboratories has shown that the annual power output can decrease between 5% and 25% [81].

In another study, Gaudern [82] studied and analyzed photographs and reports of Vestas wind turbines that had been operating for up to five years and divided the leading edge erosion into five stages based on their depth. Then erosion patterns from these stages were machined on the leading edge of the blades in patterns similar to those observed in the field. Then, the blades were experimentally tested for their aerodynamic performance to study the effects of surface roughness increase in a wind tunnel. Table 2-2 shows the description of these stages, while Table 2-3 shows the depth, diameter of the feature, the approximate percentage of chord coverage, average lift reduction, and drag increase at a 6˚ angle of attack. A clear trend can be seen where higher levels of erosion lead to higher drag coefficient and lower lift coefficient resulting in a severe loss in the airfoil performance.

Table 2-2: Erosion stages and description [82].

Stage	Description
1	Small pinholes of missing paint distributed across LE with some grouping
2	Pinholes have coalesced into larger eroded patches
3	The affected area has increased, with isolated larger patches with a greater depth
4	Patches have coalesced further, and depth has increased
5	Large areas of leading-edge laminate exposed

Table 2-3: Erosion stages and the resulting coefficients of lift (C_L) and drag (C_D) [82].

Stage	Erosion depth (mm)	Average feature diameter (mm)	Approx. % chord coverage	Average C_l decrease at 6°	Average C_d increase at 6°
1	0.1-0.2	2	3	4%	49%
2	0.1-0.2	15	3	4%	57%
3	0.3-0.5	20/40	5	5%	78%
4	0.5-0.8	40	5	6%	89%
5	0.8-1.2	>500	8	6%	86%

In another study, a CFD simulation has been used to study three erosion cases on S809 airfoil [83]. In these three cases, erosion thickness and length have been specified while simulating 2D airfoil design at three Reynolds numbers: 10^4, 10^5, and 10^6. It has been found

that with the increase of surface roughness lift coefficient decreased up to 76% for the most severe case. Previous experimental results validated the results from this model.

The wide disagreement in the results between the studies presented above could be attributed to many factors. For example, the rate at which wind turbine blades erode is dependent on tip speed, airfoil shape, and the environment in which it is situated [84]. Also, the authors tried to reproduce the damage caused by the abrasive particles on the leading edge, and the accuracy of that reproduction is debatable. Therefore, to better compare different wind turbine blades made of different airfoils and situated in different environments, using the Annual Energy Production (AEP) change as a measure will make the comparison possible and meaningful.

2.3 Possible Solutions

To minimize the significant effects of erosion of the leading edge on the aerodynamic performance, extend the life of the blades, and reduce the frequency of repairs, many possible solutions have been proposed. These solutions can be categorized as either design solutions or external solutions [50]. Design solutions are applied through the use of airfoils that are specifically designed to reduce the effects of surface roughness on its aerodynamic performance. In contrast, external solutions include various applications that can lessen the effects of roughness on aerodynamic performance.

2.3.1 Design Solutions

The National Renewable Energy Laboratory (NREL), formerly known as Solar Energy Research Institute (SERI), designed airfoils specifically for wind turbines instead of using airfoils used for aircraft for two reasons: first, airfoil used for aircraft generates excessive power at high wind speed, which leads to the burn-out of generators, and second, airfoils

designed for aircraft are very sensitive to surface roughness [85]. Therefore, many airfoil families have been designed specifically for wind turbine blades, and they have the following advantages [50]:

- Lower maximum lift coefficient for the tip section of the blade to control the power output and prevent the burn-out of the generator.
- Higher lift coefficient for the root section of the blade to be able to start up the turbine with lower wind velocities.
- Less sensitive to roughness by forcing laminar to turbulent transition on the lower and upper surfaces of the blade when maximum lift coefficient is reached.

In a study by Tangler et al.[85], comparing clean and dirty SERI airfoils, which are less sensitive to roughness, to AEROSTAR airfoils designed for aircraft. It has been found that the improvement in Annual Energy Production (AEP) that the clean SERI airfoils showed is 10% higher than that of the clean AEROSTAR blades, while for the dirty airfoils, the improvement was 30%. The SERI airfoils were designed not to exceed 65 kW in power production to prevent generator burn-out, as shown in Fig. 2-16.

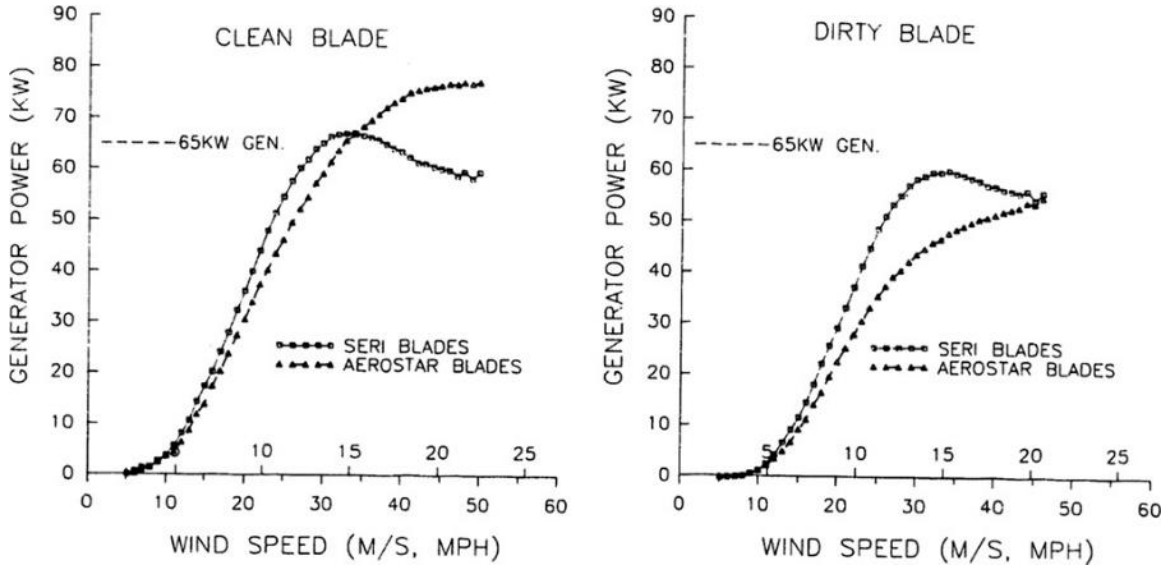


Fig. 2-16: Generator power comparison of SERI airfoils and AEROSTAR airfoils for clean and dirty blades [85].

Bak et al. [86] conducted a study to optimize the design of an airfoil family that is insensitive to roughness and turbulence intensity. The design variable for this optimization is the airfoil shape, and the design objective is to maximize the lift to drag ratio. A schematic of the design optimization strategy is shown in Fig. 2-17. As can be seen in the figure, the optimum zone to design the airfoil to have its maximum lift to drag ratio is the zone where angles of attack between 0˚ and the point of turbulent transition, that is, the low positive angle of attack zone. At this zone, when roughness is introduced to the blade surface, the angle of attack will slightly change, and this small change will not produce significant changes in the coefficient of lift. However, if designed to operate at the maximum lift, small changes in the angle of attack due to roughness will result in significant changes in the aerodynamic performance.

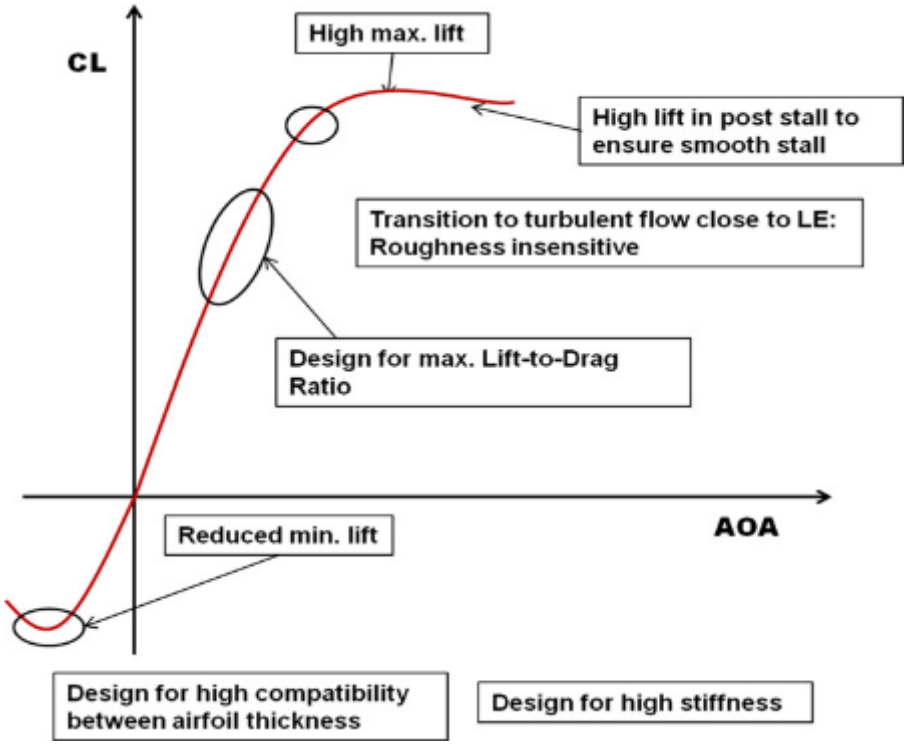
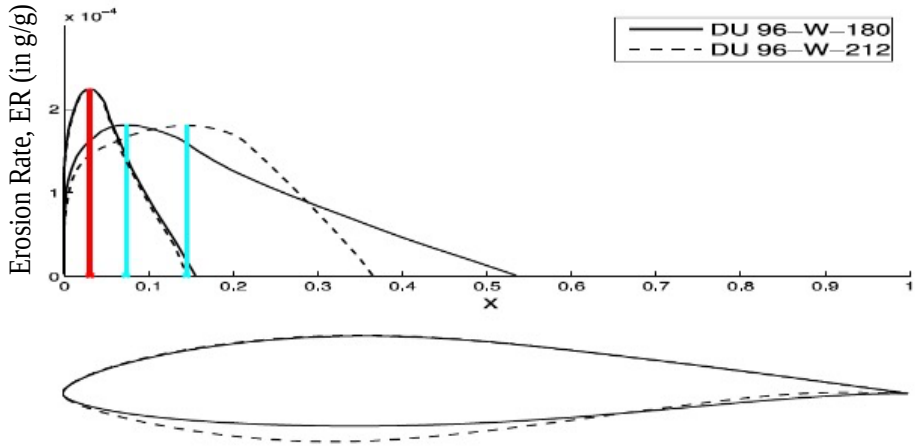


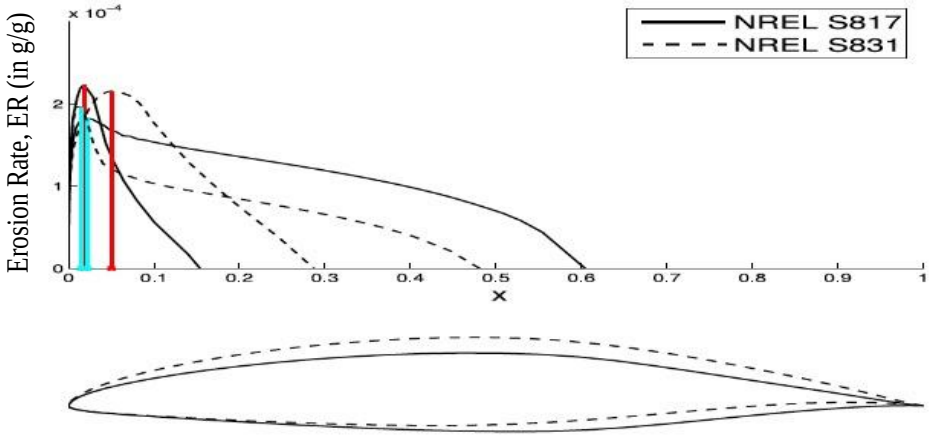
Fig. 2-17: Design objective for optimum airfoil design [86].

In a study conducted by Fiore and Selig [87], the effects of the airfoil's shape on the location at which the highest erosion rate occurred were studied. According to Wood [88], erosion rate (ER), can be defined as the mass or volume of material removed per unit mass of erodent impact. Therefore, Fiore and Selig [87] found that for the upper surface of the blade, a more bulbous shape appears to move the point at which the highest erosion rate occurs more downstream than thinner leading-edge geometries. For the lower surface, they found that a more slanted and flattened lower surface of the leading edge also caused the maximum erosion rate to occur more downstream. Fig. 2-18 shows a comparison of upper and lower surface geometries of commercially used airfoils. In Fig. 2-18 (a), a comparison of the lower surface of airfoils shows that thicker flattened shapes show a maximum erosion rate more downstream. The two airfoils have a general airfoil designation of DU yy-

W-xxx, with DU being Delft university followed by the last two digits of the year in which the airfoil was designed (1996 in this case) [89]. The W denotes wind energy application to distinguish it from airfoils designed for general aviation purposes. The last three digits give 10 times the maximum thickness in percent of the chord (18% and 21.2%, respectively). While in Fig. 2-18 (b), a thicker and bulbous upper surface shows a maximum erosion rate more downstream. The NREL S8xx designation represents the numerical order in which the airfoils were designed [90].



a) DU 96-W-180 vs. DU 96-W-212



b) NREL S817 vs. NREL S831

Fig. 2-18: Effect of surface geometry on the erosion rate: a) lower surface comparison, and b) upper surface comparison. Upper side erosion is shown in red. Lower side erosion is shown in cyan [87]

2.3.2 External Solutions

Two main external solutions have proven to be effective in reducing the leading-edge erosion of wind turbine blades. The first solution is the application of elastomeric material in the form of a tape to the leading edge of the blade [48], While the other solution is the addition of a layer (or more) of protective coating to the blades [22, 48].

2.3.2.1 Tape

The idea behind using tape is to use it as a sacrificial measure to protect the blades' surface integrity. Tape works by absorbing the incoming kinetic energy of the impacting abrasive particles bombarding the blade. After a while, the tape will start wearing off and, at that time, should be replaced. Although it is cheaper to sacrifice the tape and replace it than to get the blades damaged, it has been found that the application of tape causes a faster separation of the flow and an increase in drag [48]. The measured increase in drag ranges from 5-15%, depending on the tape placement and area size [91]. Also, the fact that the tape must be changed frequently means more stoppage time and a loss in production. Hence, using elastomeric tape as a solution might be a suitable solution for small wind turbines. However, the increase of drag makes it less suitable and more costly for big wind turbines [48].

2.3.2.2 Coatings

The other proposed solution to minimize the effects of erosion on wind turbine blades is the application of a layer of surface coating [22, 48]. It has been found that even a single layer of coating material could provide a multipurpose solution that might reduce the frequency of unscheduled shutdowns, according to Dalili et al. [48]. The coatings used for wind turbines mainly include water-based coatings and solvent-based coatings [33]. The

water-based coatings have some advantages such as low odor, environmentally friendliness, and convenience for construction. On the other hand, solvent-based coatings have a more stable performance when compared to water-based coatings and are therefore more commonly used in the wind turbine industry.

The primary purposes of protective layer coating are to assure consistent aerodynamic performance and adequate surface integrity throughout the life of the blade [92], as well as [33]:

- Erosion and wear resistance, the protection of composite substrate from impacts by foreign abrasives during manufacturing, installation, operation, and maintenance
- Weatherability, such as the protection from environmental factors such as UV lights and moister.
- High- and low-temperature flexibility
- Acid and alkali corrosion resistance
- Excellent adhesion between the blade and the coating since poor adhesion is cited as the most apparent reason for unsuccessful coating [93].
- Anti-icing
- Salt spray resistance and moist heat resistance
- Good construction performance
- Low environmental pollution

The surface roughness of the coating layer can affect the aerodynamics of the blades and can affect the erosion rate and behavior of the coated material. Since higher roughness means a higher number of contact points between the abrasive particles and the target, it

has been found that with an increase in surface roughness, the asperities on the surface can serve as damage initiation locations and a smoother surface led to a delay in erosion [94–96].

Nowadays, wind turbine blades are delivered with a factory-applied coating, which is usually polyurethane-based [97]. Current surface coatings utilized in the industry are proprietary matters, and the coating's information, such as chemical composition and method of preparation, are usually not fully disclosed [48]. In addition, the industry suffers from a certain level of ambiguity around the terminology of surface coatings, where they are generally called 'gel coat' without regard to the material used or the way of application [48]. Because of the ambiguity around the composition of the coatings used in the market, it is not easy to specify and compare the properties of coatings used in the industry.

2.3.2.2.1 Polyurethane

Polyurethane is mainly used for anti-erosion applications [98]. In many cases, polyurethane shows a segmented composite-like structure with hard segments determining the stiffness and soft/flexible segments determining the elastic deformation connected by chain-extenders, enabling the chemical cross-linking [99]. The solid particle erosion mechanism of segmented polyurethane at the nanoscale starts by first deforming the soft segments at the surface, and then brittle cracks are formed at the hard segments [99]. Cracks propagate and intersect in the hard segment leading to spalling, and fragments containing mainly soft segments are formed. During the cyclic loading by each abrasive particle bombarding the surface, elastic stretching occurs in the soft segments, while damage and yield occur in the hard segments leading to segments breakup and microfibrils [100].

However, polyurethane can show highly elastic and durable properties while providing superior resistance to solid particle erosion compared to metals [48]. In two studies on the application of polyurethane-based coatings on wind turbine blades to study the effects of erosion due to rain droplet impact, Haag [101] and Powell [73] showed the excellent performance of polyurethane on preventing leading edge erosion.

In Haag's experiment, a highly flexible 2-component solvent-free UV-resistant polyurethane-based coating has been developed and called ProBlade™. This coating has been subjected to 30-35 mm/h simulated rain at 123-157m/s, along with samples coated by typical Polyester gelcoat and polyurethane tape. All the samples were eroded for 6 hours except the Polyester gelcoat, which was eroded for only one hour. Fig. 2-19 below shows the degree of protection polyurethane-based coating supplied.

The experiment carried out by Powell [73] developed a polyurethane-based coating for 3M called W4600. This coating was compared to a tape and two competitive coatings under simulated rain at 134 m/s impact velocity. The tape and W4600 coating showed better resistance to erosion, as shown in Fig. 2-20. Although both experiments are not examples of erosion occurring in operational wind turbines, they show the potential of polyurethane-based coatings in preventing the leading edge erosion. The polyurethane-based coating has shown maximum wear due to erosion at an angle of impingement of 22˚ at the upper and lower surfaces of a wind turbine blade [76]. However, there is a lack of experimental data on the erosion of polyurethane-based coatings [92].

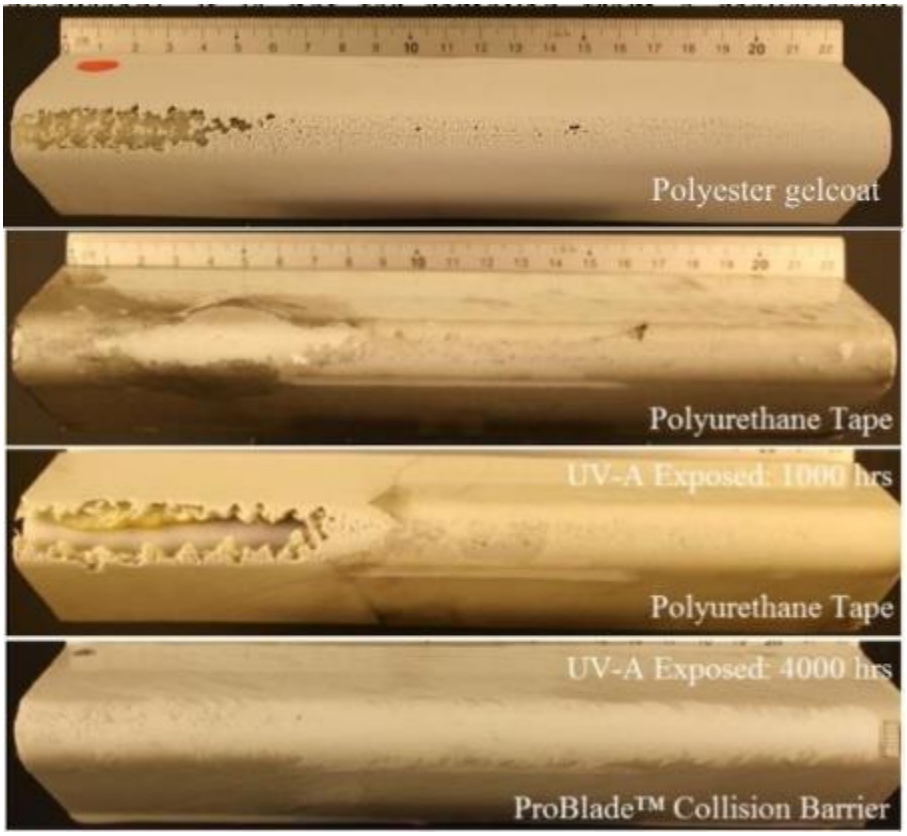


Fig. 2-19: Polyurethane-based coating compared to other types of coatings. Samples tested under the impact of rain droplet at 123-157 m/s at 30-35 mm/h. Top-to-bottom: Polyester gelcoat eroded for 1 hour, polyurethane tape- no UV-A exposure, polyurethane tape- 1000 hrs of UV-A exposure, ProBlade ™- 4000 hrs of UV-A exposure [101].

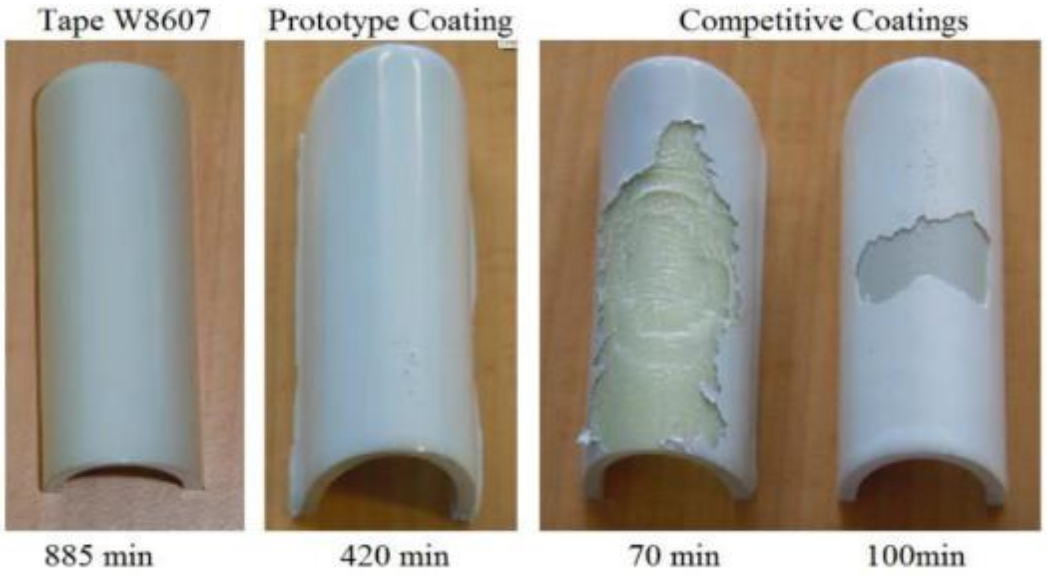


Fig. 2-20: 3M W4600 compared to tape and competitive coatings [73].

2.3.2.2.2 Graphene:

Graphene is a two-dimensional allotrope of carbon that attracted growing interest in research by demonstrating superior tribological properties, especially in reducing wear and friction [102]. Graphene can serve as a solid lubricant because of its extreme strength, high chemical inertness, and the capability of being easily sheared [103]. It is also confirmed as one of the thinnest, lightest, and strongest ever-measured nanomaterial, where Young's modulus of the defect-free graphene sheet is 1 TPa [104]. This extremely high strength could be attributed to the strong covalent bond between carbon atoms formed by sp2 hybridization atomic orbital in the hexagonal packed crystal structure with a bond length of 0.142 nm [104]. As a result, graphene has an easy shear capability on its densely packed atomically smooth surfaces. Moreover, graphene coatings are extremely chemically inert and impermeable to liquids and gases such as water and oxygen, thus reducing oxidation and corrosion processes, and as a result, reducing friction and wear [105].

In a study by Berman et al. [106], the wear protection of coatings was investigated, steel was coated with three different coatings, namely: solution-processed graphene (SPG), solution-processed graphene oxide (SPGO), and graphite. These three coatings were compared to bare steel as a baseline for the experiment. The comparison occurred in two environments, dry nitrogen to create dry and inert test conditions and humid air to create a humid environment. It has been found that graphene can provide up to four times higher wear protection, as shown in Fig. 2-21. The wear rate of graphene-coated steel is lower than steel covered by graphene oxide, graphite and significantly lower than bare steel. The coefficient of friction (μ) of steel/steel interface is compared to that of steel/solution-processed graphene (SPG) coated steel was also investigated, as shown in Fig. 2-22 [106].

Steel vs. SPG/steel always showed a lower coefficient of friction, where friction is reduced by 5-6 times, from 0.9- 1 for bare steel to 0.15- 0.16. A possible explanation for the reduction in friction coefficient and wear rate by graphene is because it is a two-dimensional nanomaterial working as a conformal protective coating on the friction interfaces, which makes it shears easier between sliding surfaces and protects against corrosion and oxidation, thus reducing wear drastically [106].

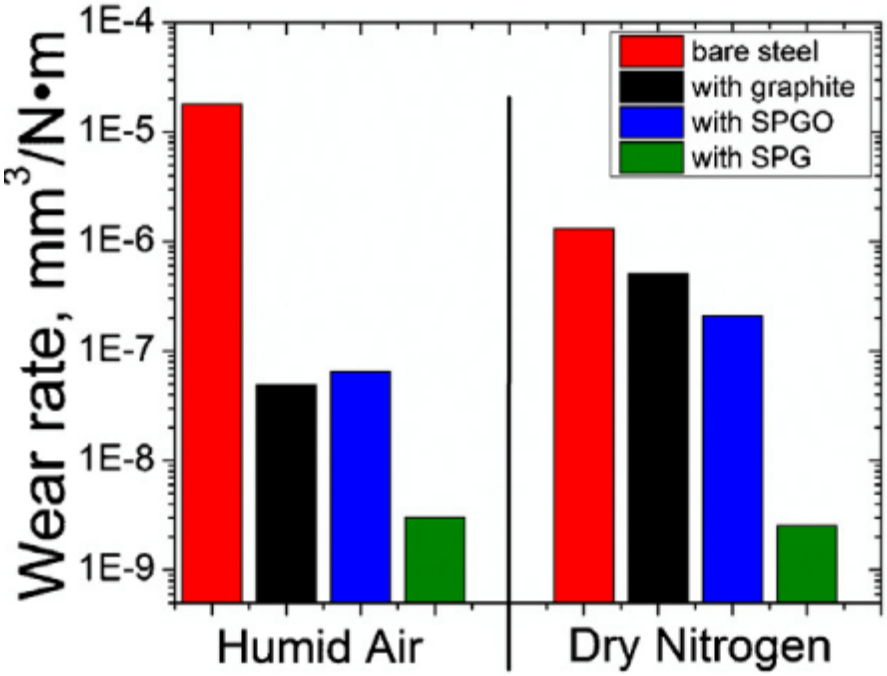


Fig. 2-21: Wear rate in humid and dry environments.

In summary, the increase of surface roughness due to the leading edge erosion of wind turbine blades has a detrimental effect on aerodynamic performance. Some solutions to this problem have been proposed, such as using tapes on the leading edge or using protective coatings. The degree of effectiveness of these solutions is still incomplete and needs more exploration [22, 67]. A deeper investigation of the solid particle erosion phenomenon will be discussed in the next section.

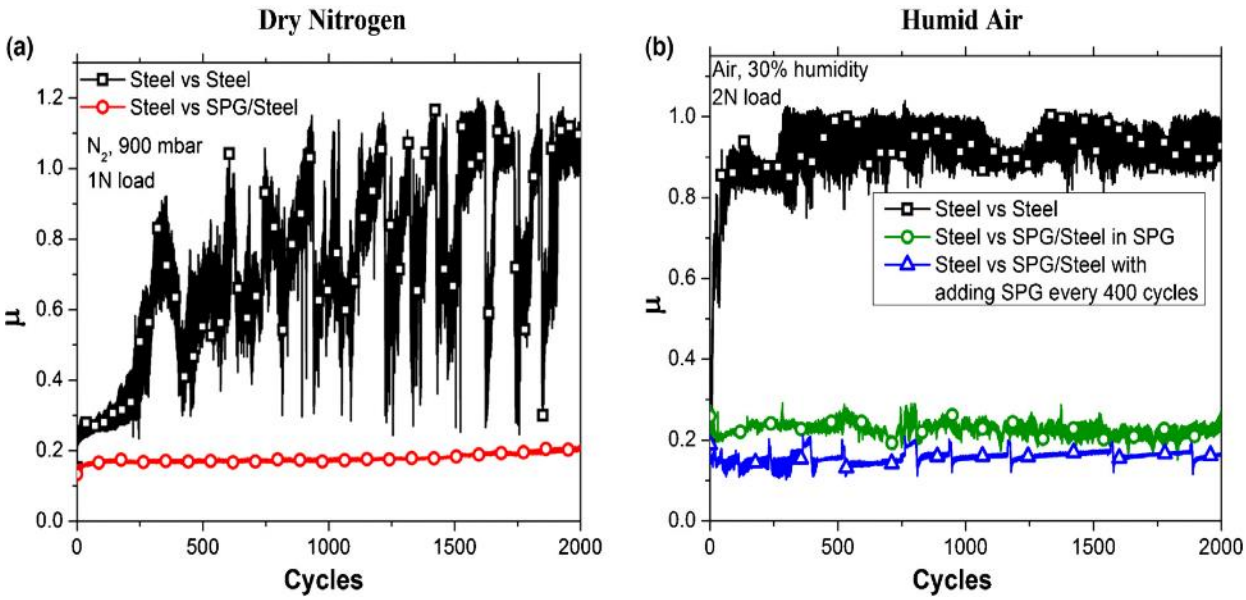


Fig. 2-22: The coefficient of friction (μ) of steel vs. steel interface is compared to the μ of steel vs. solution-processed graphene (SPG) coated steel.

2.4 Solid Particle Erosion

Solid particle erosion is the material wear due to the repeated impact of high-speed solid particles on a target surface. Solid particle erosion occurs in many industrial applications such as pipelines and valves wear in the oil industry [107], steam turbomachinery [49, 108, 109], fluidized bed combustion systems in power plants [110, 111], and wind turbines [63, 112]. Enormous effort has been put to investigate and predict the solid particle erosion process as early as the 1960s, such as in Finnie's [113, 114] and Bitter's work [115, 116], as well as recent contributions by Papini et al. [117–120] and Wang et al. [121]. However, due to the many physical properties involved in the erosion process as shown by Meng and Ludema [122], which will be discussed in this chapter, the solid particle erosion mechanism remains not fully understood, and the currently available models are too conservative [88, 107]. Currently, the models are not suitable for general application on materials or erosion

conditions other than those used to develop the models [123]. Therefore, further experimental studies are still needed to understand the erosion process better and develop more accurate erosion models. In this section, the different mechanisms of erosion and some of the proposed erosion models will be discussed, as well as the erosion parameters that have the most significant effects on the erosion process.

2.4.1 Erosion mechanisms

The erosion mechanism of ductile, brittle, and composite materials varies when bombarded by solid particles. The angle of impingement has been known to be the best indicator in which the erosion mechanisms can be best described. Ductile materials tend to lose the most weight when eroded at low angles (15˚ - 30˚), brittle materials, on the other hand, tend to lose the most weight when eroded at angles close to the normal incident (at or near 90˚). Polymer matrix composite materials tend to behave in a semi-ductile manner losing the most weight at angles ranging between 45˚-75˚ [124]. A comparison between erosion rates of ductile and brittle materials in terms of impingement angle is shown in Fig. 2-23 [125]. The sections below will describe in detail the different erosion mechanisms.

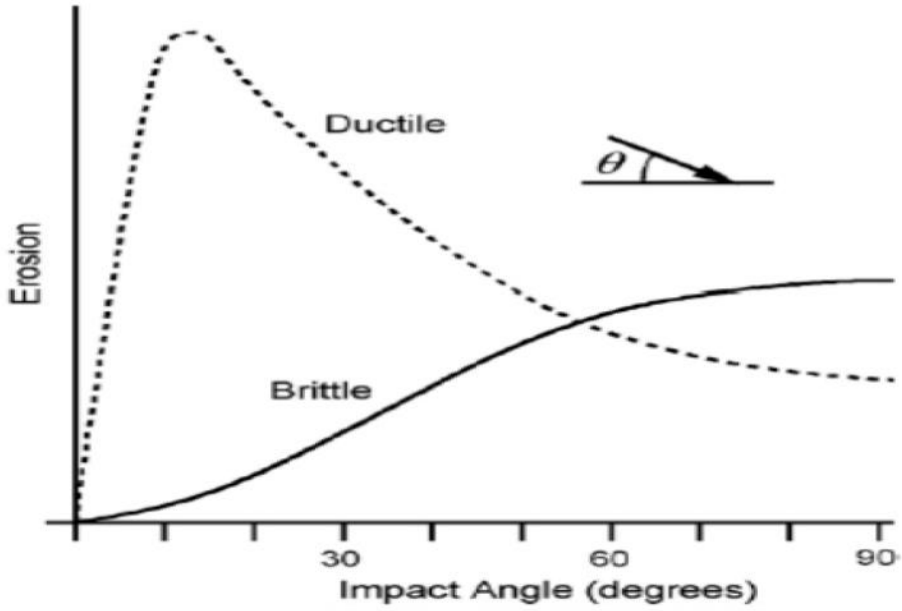


Fig. 2-23: Erosion rate vs. impact angle for ductile and brittle material [125].

The erosion progression can be broken down into three stages: Incubation period, Acceleration period, and Steady-state period [126]. In the incubation period, the surface seems unaffected, and no material removal is noticed, and sometimes, a weight gain will occur due to the impediment of abrasive particles into the target material. In the second stage, an increase in the material removal rate is observed until the rate starts reducing in the final steady-state stage. Fig. 2-24 below shows the weight or volume loss rate as a function of time [126].

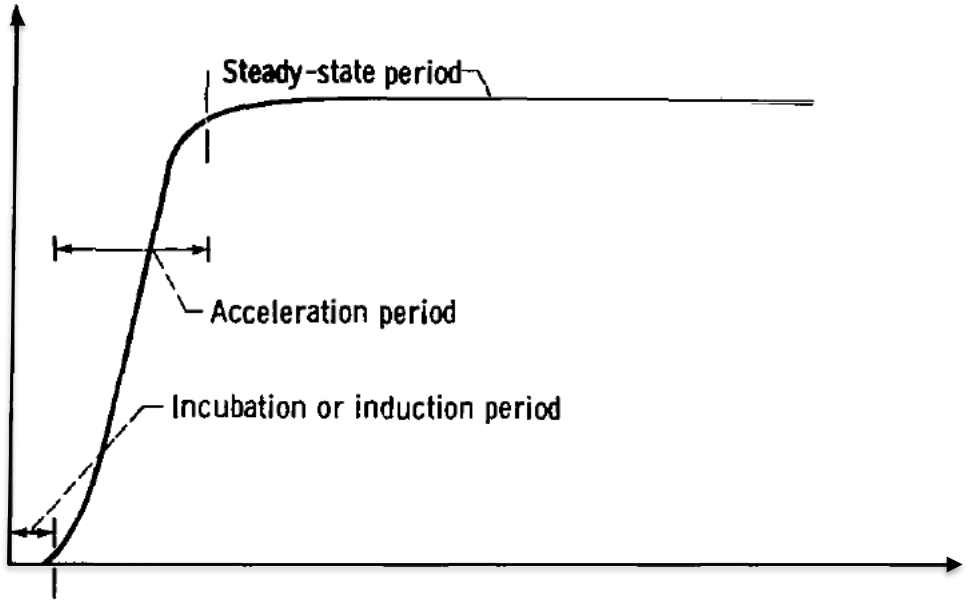


Fig. 2-24: Erosion stages as a function of time [126].

2.4.1.1 Erosion of Ductile Materials

When a particle hits the surface of a ductile material, it creates a crater-like scar. As more particles hit the surface, the crater gets larger, and material starts piling up around the crater. The piled-up material is eventually removed by the continued particle impact, as can be seen in Fig. 2-25 [127]. As a result of this process, Finnie in 1958 proposed that micro-cutting is the responsible mechanism of ductile materials erosion [128]. His model consisted of analyzing a single particle and the use of Newton's 2nd law and the horizontal and vertical components of the particle's force upon impact. The model underestimated the erosion because it neglected the effect of particle rotation and work hardening of the target material, which was added in a later model [113]. Bitter [115, 116] proposed a hypothesis that removal of material occurs as the sum of two processes. The first process is plastic deformation when the abrasives hit the target material with energy high enough to exceed

the target material's elastic limit resulting in the surface layer being destroyed, and fragments of it are removed. The second process is cutting due to abrasive particles scratching the surface and removing some of the target material in its way.

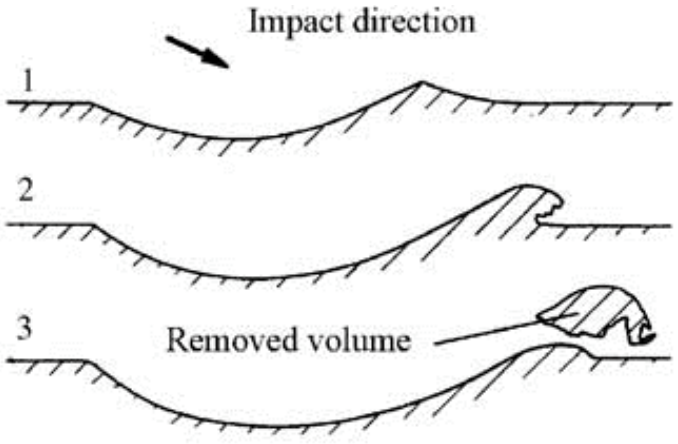


Fig. 2-25: Material removal mechanism of ductile material [127].

2.4.1.2 Erosion of Brittle Materials

When abrasives bombard a brittle target material, it initiates lateral and radial cracks. The continued particle impact causes the cracks to grow, intersect, and divide the surface into smaller pieces that can be easily removed by more abrasives impact, as shown in Fig. 2-26. Brittle material removal due to crack formation is a widely accepted mechanism by researchers such as Kleis and Kulu [129] and Sundararajan [130].

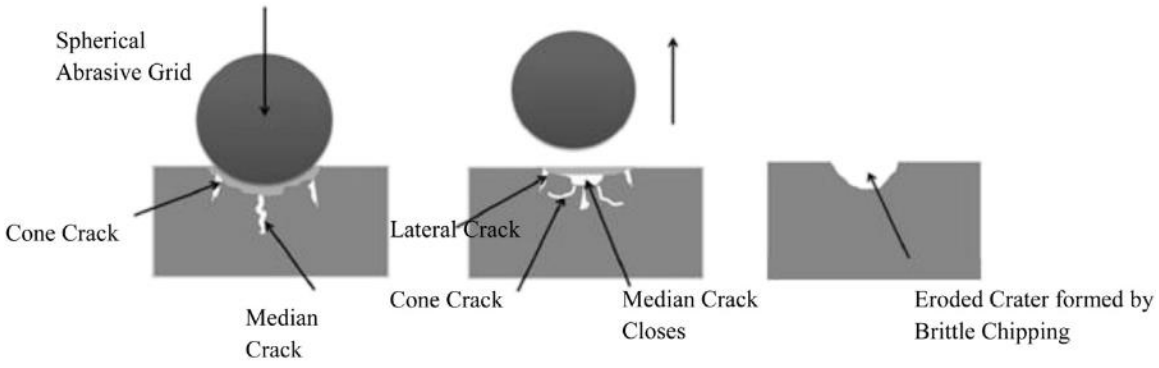


Fig. 2-26: Material removal mechanism of brittle material [131]

According to Finnie [132], two models were proposed to explain the behavior of brittle material under the impact of particles, namely: The Hertzian cracking model and the indenter model. The Hertzian crack model uses a spherical indenter with a large enough load to cause ring cracks around the contact area. Increasing the load increases the number of concentric ring cracks. The material removed by impacting particles is taken to be proportional to the volume of the outermost crack. In the indenter model, an elastic-plastic behavior is involved through loading and unloading. Load is applied to the surface, and at a threshold load, a median crack will propagate through the target material. This crack does not remove material, but it makes it weaker. When unloading, residual stresses lead to the propagation of lateral cracks, which results in material removal. The volume removed by a single particle is taken to be proportional to the cylindrical volume of the lateral crack and its depth. Both models show good agreement with experimental data.

2.4.1.3 Brittle-Ductile transition

As discussed earlier, the mechanisms of ductile and brittle erosion differ significantly. However, sometimes nominally brittle materials tend to have an erosion behavior similar to that of ductile materials. In such cases, the erosion mechanism shifts from brittle fracture (erosion behavior of brittle materials) to cutting (erosion behavior of ductile materials).

This behavior change is called the brittle-ductile transition. This transition occurs when the abrasives bombard a brittle material with small kinetic energy. In other words, when the abrasives have too small kinetic energy to initiate cracks that cause the brittle fracture in the target material, they will, eventually, only cause a plastic deformation [133]. Kinetic energy depends on particle size and velocity, and when one or both of these parameters is reduced below a critical limit, the brittle-ductile transition occurs.

Finnie and Sheldon [134] were the first to describe the brittle-ductile transition in their experiment on a plate of glass. They showed that small enough particles could produce behavior similar to ductile material in nominally brittle materials. Fig. 2-27 shows erosion as a function of the angle of impingement for three sizes of silicon carbide particles, 127 μm, 21 μm, and 9 μm, eroding a glass plate (nominally brittle). Their theory explained that the brittle-ductile transition is based on flaws. Cracking only occurs when there are flaws in the target material, and as the particle size decreases, the probability of encountering flaws and initiating cracks is decreased.

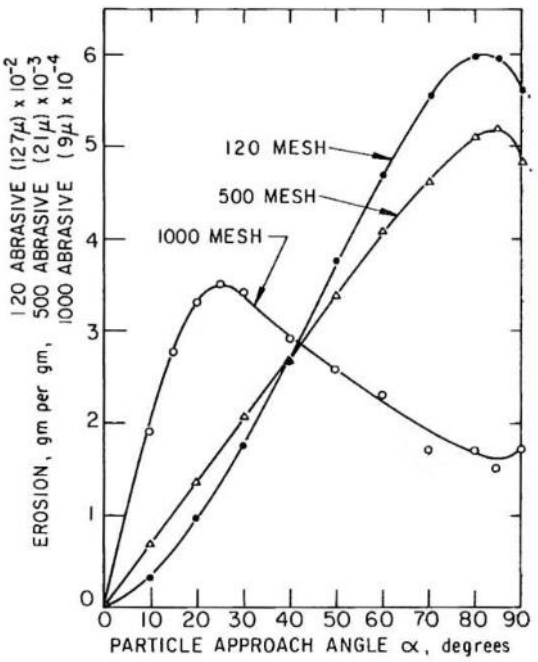


Fig. 2-27: Erosion of a glass plate by three different sizes of SiC particles in terms of angle of impingement.

2.4.1.4 Erosion of Composite Materials

Composite materials based on their matrix materials can be classified into three categories:

- Polymer matrix composite (PMC)

- Metal matrix composite (MMC)

- Ceramic matrix composite (CMC)

Since the airfoils that will be used in this experiment are made of PMC, it will be the focus of this investigation. The erosion of PMCs has been investigated thoroughly in the past. Based on SEM observations, Zahavi and Schmitt proposed that the erosion of composite materials follows the following process [135]:

1- Erosion and removal of the material of the resin locally

2- Erosion of the interference zones between fibers and the matrix

3- Erosion of fiber zones due to fiber breakage as a result of bending failure due to the removal of the resin

Pool et al. pointed out that the factors governing the erosion rate of PMCs could be summarized to three factors [136]: (a) brittleness of the fibers, (b) whether the matrix is thermosetting or thermoplastic, (c) Interfacial bond strength between the fibers and the matrix.

Many researchers have found that the maximum erosion rate as a function of the angle of impingement occurs at 45°-75°[135, 137–140]. This behavior is not similar to ductile erosion behavior where the maximum angle of impingement is 15°-30°, neither similar to brittle erosion where the maximum angle of impingement is close to 90°. Therefore, the erosion behavior seen in PMCs is called semi-ductile behavior. A possible reason behind this shift in the angle of impingement at which the maximum erosion rate occurs is the inclusion of brittle fibers into the otherwise ductile matrix.

Solid particles erosion experiments conducted by Ballout et al. [141] on S-glass glass-fiber (GF) and epoxy composites investigated the effects of changing the fiber and matrix weight ratios w_f / w_m from 65/35, 50/50, and 35/65. The angle of impingement at which the experiments were conducted varied from 10° to 90°. Using alumina particles (Al_2O_3) with 142-μm nominal diameter abrasives at particle velocity of 66 m/s resulted in semi-ductile erosion behavior for the 50/50 and 35/65 fibers to matrix ratio specimens, but a brittle behavior for the 65/35 specimens. This result is attributed to the high inclusion of GF. Composites showed higher erosion rates when compared to the neat resin (Epoxy), and the erosion rate increased with higher fiber content.

To predict the erosion rate of composite materials, Ballout et al. [141] used a linear rule of mixture (LROM) and an inverse rule of mixture (IROM) given as follows:

$$LROM: ER_c = w_f \times ER_f + w_m \times ER_m \quad (3\text{-}13)$$

$$IROM: \frac{1}{ER_c} = \frac{w_f}{ER_f} + \frac{w_m}{ER_m} \quad (3\text{-}14)$$

where ER represents the erosion rate (defined as weight loss of target material per particle mass impacted)

w is the weight fraction.

Subscripts c, f, and m represent composite, fiber, and matrix, respectively. Ballout et al. [141] concluded that when comparing these two methods of prediction, IROM showed better erosion rate predictions when compared to measured experimental results. The effect of fiber orientation in unidirectional composites on the erosion rate was also investigated [142]. Epoxy reinforced by unidirectional GF with a volume content of 68% was eroded by sharp angular alumina particles with 60 and 120 μm diameters. Erodent particle velocity was 70 m/s at impact angles of 30°, 60°, and 90°. It has been found that the erosion rate of composites with fibers parallel to the stream of erodent particles is lower than that of composites with fibers perpendicular to the stream of erodent particles. This result is accurate when the resin is a thermoset, as confirmed by other researchers [136, 143, 144]. Nevertheless, Barkoula and Karger-Kocsis [145] investigated this result when the resin is a thermoplastic instead of a thermoset using polypropylene as the resin and GF as the reinforcement. They found that the erosion of composites with parallel fibers to the erodent particles stream is higher than the perpendiculars.

Since the usage of carbon fibers (CF) and glass fibers (GF) as reinforcement in PMCs is widespread, many researchers tested and compared their erosion rates. It has been found

out that CF composites showed a higher weight erosion rate than GF composites if the fiber weights content is the same [139, 146, 147]. This result is due to the difference in densities between the two composites. CF composites have a lower density than GF composites under the same fiber weight conditions.

Erosion behavior of almost all PMCs has some common similarities that can be summarized as:

- The erosion rate of the composite material is larger than the corresponding neat resin.
- The angle at which maximum erosion rate occurs at a higher impact angle in comparison with the corresponding resin
- Strong adhesion between fillers and a matrix increases the erosion resistance and decreases the erosion rate. Better surface treatments of fillers will result in better erosion resistance.
- In a unidirectional fibers reinforced plastic, the erosion rate of composites with a fiber orientation perpendicular to the erodent flow direction is higher than that of parallel fiber orientation to the flow direction. This result is true when the resin is a thermoset, while the opposite is true when the resin is a thermoplastic.
- Glass-fiber and carbon-fiber are typical fillers in PMCs. The erosion rate of CF is higher than that of GF when both have the same content fiber to matrix ratio and the same resin matrix. The reason behind this result is that the density of CF composites being smaller than that of GF.

2.4.2 Erosion parameters

The erosion process is a complex phenomenon consisting of different variables interacting with each other. According to Aquaro and Fontani [148], these variables can be broken down into three types: impingement variables describing the particle flow, particle variables, and material variables. The impingement variables include particle velocity, angle of impingement, and standoff distance, while the particle variables include particle size and shape. Material variables include the properties of the target material, such as the hardness of the target material.

2.3.2.1 Particle velocity

With the increase of impact velocity, the rate of material removal increased [129]. Particles with higher velocity have higher kinetic energy, which gets transferred to the target material, causing higher erosion rates. As shown in Fig. 2-28, as the impact velocity increases, the erosion rate increases. In Fig. 2-28, particle size ranged from 300 to 600 μm divided into three sets of sizes, and the impact was at a 15° angle of impingement. Similar trends were obtained when the angle of impingement was changed [149].

Erosive wear rate is related to particle velocity through the following relation:

$$\varepsilon_v = b_1 . v_p^{b_2} \tag{3-15}$$

Where ε_v is the erosive wear rate in mm^3/kg, v_p is the particle velocity in m/s, while b_1 and b_2 are constants that depend on target material, angle of impingement, and properties of the eroding particles, and can be found experimentally.

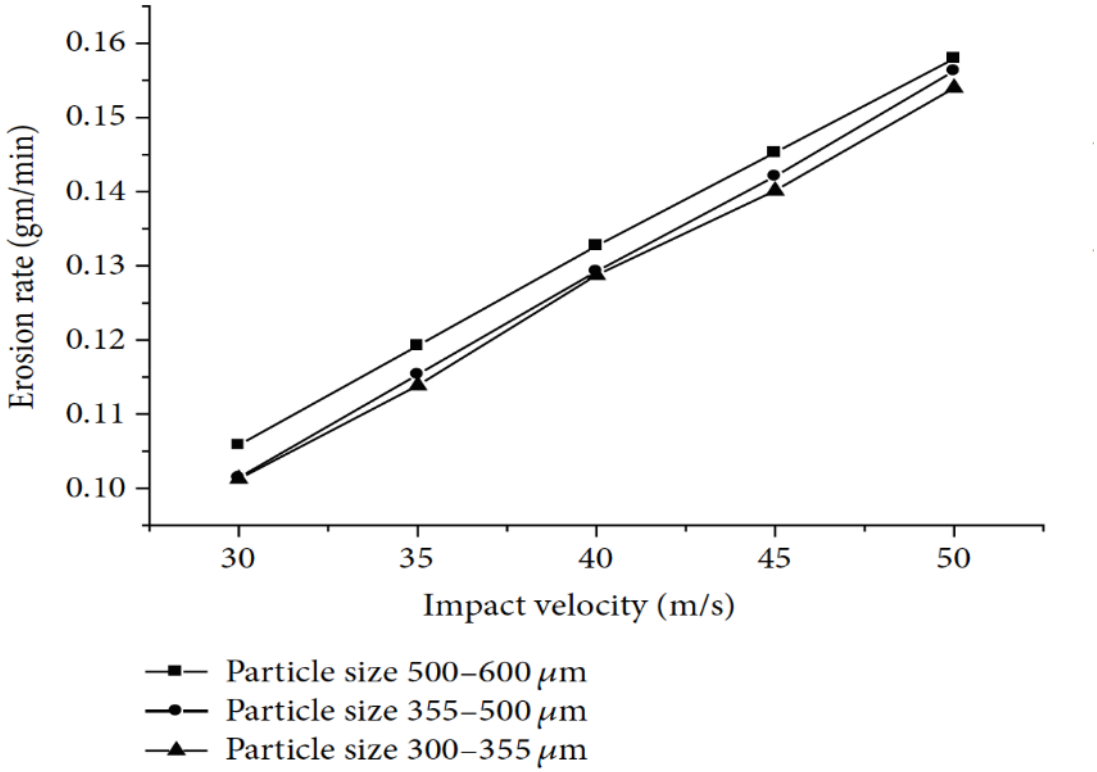


Fig. 2-28: Erosion rate as a function of impact velocity [149]

2.4.2.2 Angle of impingement

The second parameter that has a significant effect on the erosion process is the angle of impingement. It is noticed that ductile materials have a maximum erosion rate at 15°-30° due to micro-cutting, micro-ploughing, and other damage accumulation processes. In contrast, brittle materials have a maximum erosion rate at 60°- 90° due to mechanisms like plastic deformation and micro-cracking [149]. Fig. 2-29 shows the erosion rate of different brittle and ductile materials as a function of the angle of impingement, and it can be noticed that the maximum erosion rate occurs in the range of 15°-30° for ductile materials, and around 90˚ for brittle materials [150].

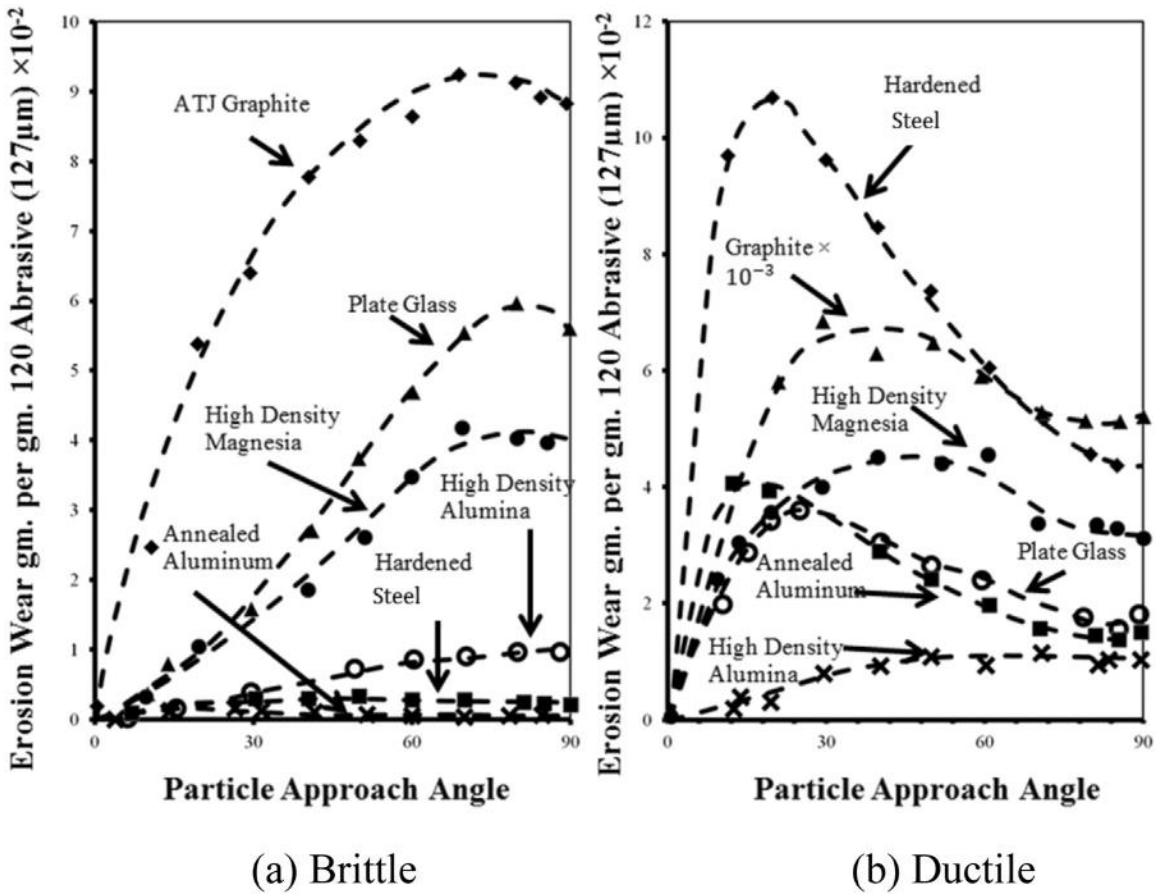


Fig. 2-29: Erosion wear as a function of angle of impingement for: (a) Brittle materials, (b) Ductile materials [150].

2.4.2.3 Standoff distance

The removal rate decreases with the increase in the standoff distance except when the nozzle is too close to the plate being eroded. When the nozzle is too close to the plate, particles rebound from the plate causing a backflow, which decreases removal rate. One study found that the optimal removal rate occurs at ≈ 5D (D is the diameter of the nozzle) because at this distance the stagnation pressure was found to be at its highest level with no backflow, while beyond at 26D no removal is expected to happen [129]. Fig. 2-30 shows the decrease in removal rate vs. the standoff distance (not showing when the nozzle is too close to the region being eroded) [149].

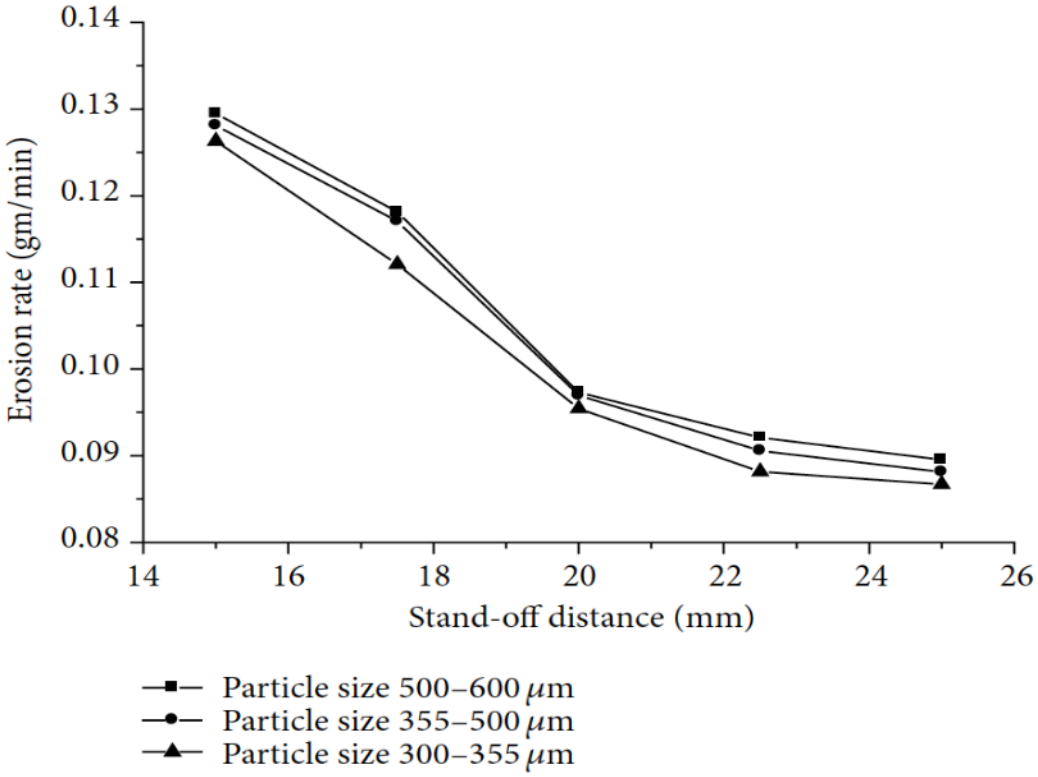


Fig. 2-30: Removal rate vs. standoff distance [149].

2.4.2.4 Particle size

According to Levy and Chik [151], the erosivity of impacting particles is dependent on their ability to concentrate force on a local area of the target material to create damage. When particles are weak and friable that they cannot maintain their integrity when hitting the target material, they will shatter into smaller pieces. When fragmentation occurs, 20 – 30% of the initial energy is transferred to the fragments instead of the target resulting in a reduction of the erosion rate [152]. Salman et al. [153] conducted an experiment on plexi-glass, glass, steel, and aluminum targets to study the effects of the target material on the number of fractured particles. They found that it is less likely for particles to fracture when impacting softer targets because a larger portion of the kinetic energy is transferred to the

soft target leaving less energy available to cause fragmentation. It was found that the likelihood of particle fracture depends on the ratio of fracture toughnesses, hardnesses, and elasticity moduli of particles and target material [154].

When particles reach a level of strength and integrity that they will not shatter upon impact, larger particles will have a more significant influence on the erosion magnitude than smaller particles, given that all other parameters are kept the same. Fig. 2-31 shows the relationship between erosion in terms of the mass of the target material (in mg)/ mass of impacting particles (in g). It can be seen that erosion increases with the increase of impacting particles size up to 100 μm, after that, it stabilizes.

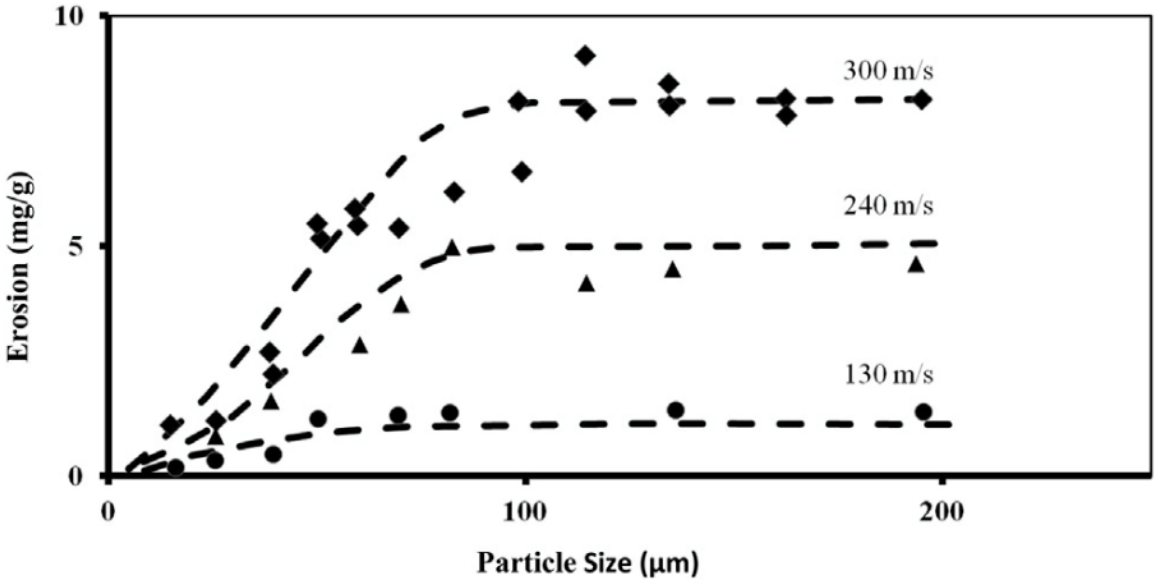


Fig. 2-31: Erosion rate as a function of particle size [155].

2.4.2.5 Particle shape

It has been observed that the shape of the impacting particles can have a significant influence on the magnitude of erosion [151]. Salik et al. [156] showed that this influence could be an order of magnitude when comparing sharp (angular) to rounded (blunt) particles.

When brittle materials are bombarded at low velocities by rounded and angular particles, rounded particles form cone cracks while angular particles form lateral cracks [157, 158]. Particle shape and angularity can also affect the impact angle at which the maximum erosion occurs [159].

2.4.2.6 Hardness

The hardness of target material and abrasive particles is one of the most critical factors in the erosion process. The relationship between the hardness of materials and erosion can be understood by the relationship between hardness and the indentation caused by abrasives [160]:

$$\frac{d_i}{D_s} = b_3\ (Hv)^{-b_4} \tag{3-16}$$

where d_i is the diameter of the indentation Hv is hardness value

D_s is the diameter of the sphere abrasive particles

b_3 and b_4 are constants.

Depending on the type of hardness test used, the values of the constants (b_3 and b_4) change. From this equation, it can be seen that the relationship between indentation and the reciprocal of hardness is linear. Finnie [113] stated that the erosion rate is inversely proportional to hardness. While Evans et al. [161] shown that the erosion rate is proportional to $H^{-1/4}$, as shown in the next section. Evans and Marshall [162] showed that the force at the fracture threshold is strongly influenced by the hardness, and the erosion rate is substantially reduced below this threshold. As a result, when the hardness of the target material increases, the ability to indent decreases, and consequently, the possibility of eroding the target material decreases.

2.4.2.7 Temperature

Many researchers have studied the effects of temperature on the erosion process and rate. Although a solid conclusion on the effects has not been agreed upon, many hypotheses have been proposed. Smeltzer et al. [163] tested different types of metal alloys (12-Cr stainless steel, 17-Cr and 7-Ni precipitation-hardening stainless steel, Ti-6Al-4V titanium alloy, and aluminum 2024) at 60˚ angle of impingement and a maximum temperature of 370˚C (700 F) and found that the erosion rate decreases as the temperature increases. According to Levy [164], this result is due to the increase in ductility in the target material, which helps absorb the kinetic energy of the incoming abrasives by plastically deforming instead of getting chipped away. Suur [165] in his study of elevated temperatures on four types of steel with composition shown in Table 2-4, found that up to 400-450 C, it is true that wear rate barely shows any change and in some cases, it decreases, but after that, a sharp increase occurs as shown in Fig. 2-32. Suur [165] explains this sharp increase by the formation of film oxides that are easier to erode. Similar to Suur's conclusion, Tabakoff et al. [166] performed a series of high-temperature erosion experiments on different target materials. In one experiment comparing 304 steel erosion behavior at 26˚C and 649 ˚C and 197 m/s, it was observed that the erosion volume increased by almost 2.5 times at the impingement angle where the maximum material removal occurred (25˚).

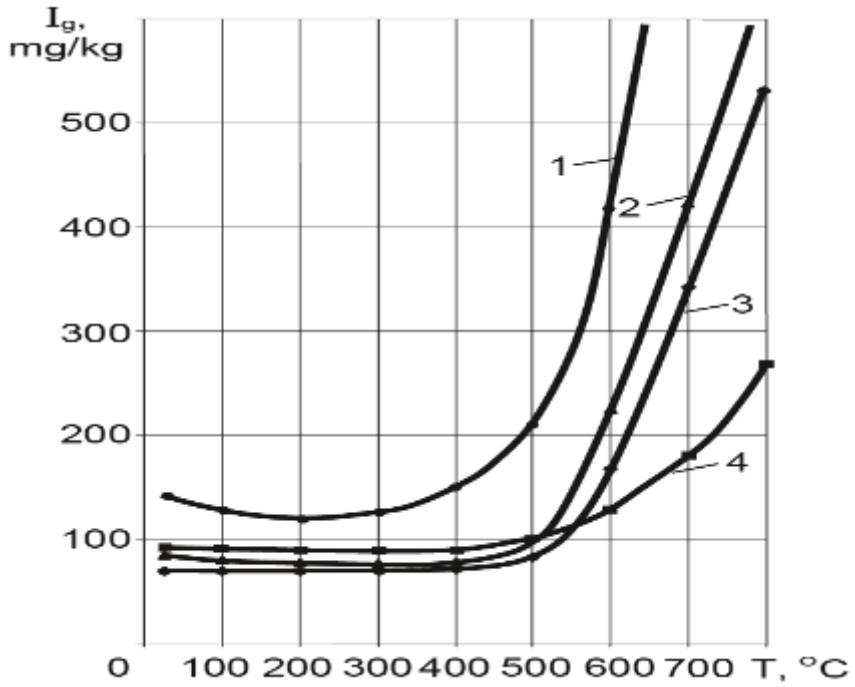


Fig. 2-32: Effects of temperature on the wear rate of four types of steel: 1- St3, 2- U8A, 3- R9, and 4- cast iron Ch34L [165].

Table 2-4: four types of steel tested to study the effects of temperature on erosion [165]

Steel (Russian standard)	Mean of constituent elements, wt%							
	C	Si	Mn	Cr	Ni	V	W	Mo
St3	0.2	~ 0.2	~ 0.5					
U8A	0.8	0.2	0.2	< 0.15				
R9	0.9			4		2.3	9	<0.3
Ch34L	2.0	1.5	0.7	34				

2.4.3 Erosion Models

Due to the importance of solid particle erosion, especially for oil and gas industries, researchers have tried to propose various scenarios and mechanisms to describe the characteristics of solid particle erosion. These various scenarios led to the introduction of a large number of physical parameters in the mathematical models proposed by researchers. Meng and Ludema [122] published a review paper that included 28 erosion equations with 33

physical parameters involved in the erosion process. Despite the numerous proposed erosion correlations, no model can be considered universal to precisely cover the wide variety of parameters involved. Nonetheless, some of these models and equations will be discussed below.

One of the earliest equations that fundamentally investigated solid particles erosion was proposed by Finnie [113], as discussed earlier. He considers the motion of a single particle striking the surface of a ductile material, causing a scratch or crater on the surface, as shown in Fig. 2-33. He provided two equations to predict the volume removed by a single particle for low and high angles of impingement as follows

$$\varepsilon_{VP} = \frac{m_p v_p^2}{P\psi\kappa} \left(\sin(2\alpha) - \frac{6}{\kappa}\sin^2(\alpha) \right) \qquad \text{for } \tan\alpha \leq \kappa/6 \qquad (3\text{-}17)$$

$$\varepsilon_{VP} = \frac{m_p v_p^2}{P\psi\kappa} \left(\frac{\kappa \cos^2\alpha}{6} \right) \qquad \text{for } \tan\alpha \geq \kappa/6 \qquad (3\text{-}18)$$

where, ε_{VP} is volume of material removed by single abrasive particle of mass

m_p is mass of abrasive particle

v_p is particle velocity

P is pressure

ψ is ratio of depth of contact to depth of cut (l/y_t)

κ is ratio of vertical to horizontal force components on the particle

α is angle of impingement

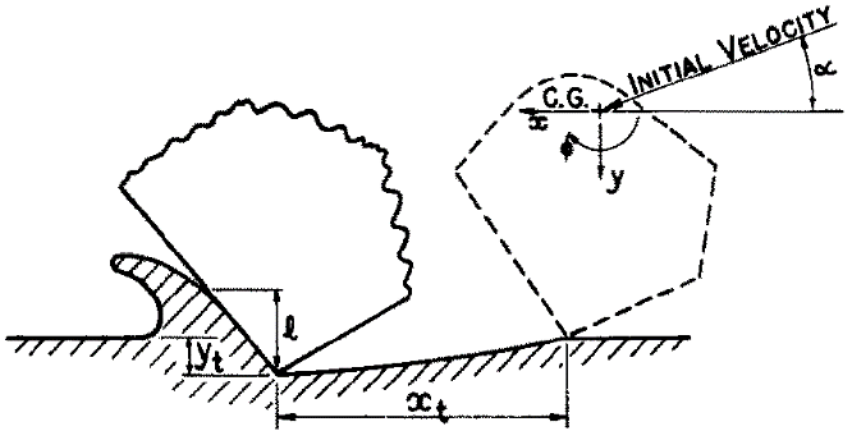


Fig. 2-33: Idealized picture of a single particle scratching a ductile surface.

Three assumptions were made to come up with these equations:

1. The ratio of the depth of contact to the depth of the cut (ψ) is constant.
2. The width of the particle cutting face is uniform and large compared to the depth of cut.
3. Plastic flow is constant upon particles' impact.

The main flaw of this model is that it predicts no erosion when the angle of impingement is 90˚. Although the model is based on single particle analysis, it showed good agreement with experimental data at small impingement angles when applied on multi-particle analysis.

Finnie later proposed a modification to his earlier model [114], where he solved the equation of motion of an abrasive particle and proposed the following equation:

$$\varepsilon_{VP} = \frac{\eta M_T v_P^2}{4P\left(1+\frac{m_p r_p^2}{I}\right)}\left(\cos^2\alpha - \frac{\dot{x_t'}}{v_p}\right) \tag{3-19}$$

$$\dot{x}_t' = v_p \cos\alpha - \frac{2v_p}{P}\sin\alpha \tag{3-20}$$

where, ε_{VP} is erosion rate (volume loss/impact mass)

η is fraction of particles cutting in an idealized manner

M_T is total mass of impinging particles

r_p is radius of particle

I is moment of inertia of single particle

$\dot{x}_t'$ is horizontal velocity of tip of particle when cutting stops

Finnie proposed two possibilities for the cutting mechanism to stop: cutting stops when the horizontal velocity component of the particle tip is zero or when the particle leaves the surface. Based on these two possibilities, the above equations are simplified, as follows:

$$\varepsilon_{VP} = \frac{\eta M v_P^2}{4P\left(1+\frac{m_p r^2}{I}\right)} \cos^2 \alpha \qquad \text{for } \dot{x}_t'=0 \qquad (3\text{-}21)$$

$$\varepsilon_{VP} = \frac{cMv_P^2}{4P\left(1+\frac{m_p r^2}{I}\right)} \left(sin(2\alpha) - \frac{2\sin^2 \alpha}{P}\right) \qquad \text{for } y_t = 0 \qquad (3\text{-}22)$$

where, y_t is depth of cut.

It is worth noting that this model has a low accuracy as the angle of impingement approaches 90˚.

Bitter [116], in his model, proposed two mechanisms for erosion: plastic deformation and cutting. He developed two models to predict the erosion rate caused by both mechanisms for ductile and brittle materials. In his first model [115], he developed an equation based on the balance of energy for an elastic-plastic collision to predict the erosion (ε_{VP}) caused by deformation:

$$\varepsilon_{VP} = \frac{1}{2}\frac{M(V_p \sin\alpha - K)^2}{\delta} \quad (3\text{-}23)$$

where, K is velocity component normal to surface below which no erosion takes place in certain hard materials

δ is deformation wear factor, the amount of energy needed to remove unit volume of material

Brittle materials showed a good agreement with this equation when compared to experimental data. In Bitter's second model, which focuses on the cutting mechanisms of erosion, he considered two scenarios on whether particles have a horizontal velocity component when leaving the target material after impact or not. He proposed two models for the cutting mechanism as follows:

$$\varepsilon_{VC1} = \frac{2MC_s(V_p \sin(\alpha) - K)^2}{(V_p \sin(\alpha))^{1/2}} \{V_p \cos(\alpha) - \frac{C_s(V_p \sin(\alpha) - K)^2}{(V_P \sin(\alpha))^{1/2}} \chi\} \quad \text{for } \alpha \geq \alpha_{p0} \quad (3\text{-}24)$$

$$\varepsilon_{VC2} = \frac{\frac{1}{2}M[V_P^2 \cos^2\alpha - K_1(V_p \sin\alpha - K)^{3/2}]}{\chi} \quad \text{for } \alpha \leq \alpha_{p0} \quad (3\text{-}25)$$

where, $\varepsilon_{VC1,2}$ is volumes of material removed by cutting mechanism 1, and 2

C_s is flow stress temperature dependence constant

χ is cutting wear factor, the quantity of energy needed to scratch out unit volume from a surface

K_1 proportionality constant

α_{P0} is impact angle at which horizontal velocity component has just become zero when particle leaves body

The total erosion rate is then the summation of the erosion due to each mechanism:

$$\varepsilon_{VT} = \varepsilon_{VP} + \varepsilon_{VC} \quad (3\text{-}26)$$

where, ε_{VT} is total volume removal

ε_{VP} is volume removal due to plastic deformation mechanism

ε_{VC} is volume removal due to cutting mechanism

Evans et al. [161] studied the damage in brittle materials in the elastic-plastic regime. Using impact dynamics features and fracture mechanics to analyze radial cracks (surface extension), lateral cracks (penetration), and fracture threshold to propose the following equation that relates radial crack formation and fracture toughness of target material:

$$\varepsilon_{VP} \propto \frac{V_p^{19/6} r^{11/3} \rho_p^{1/4}}{K_{Ic}^{4/3} H_t^{1/4}} \tag{3-27}$$

where, ρ_p is density of particle

K_{Ic} is fracture toughness

H_t is hardness of the target material.

According to Lawn [158], the critical load for crack initiations is found to be dependent on the flaw population of the surface. Static indenters use Hertzian models from indentation theories to predict the behavior of particle impact [133]. The use of blunt indenters provides good behavior predictions. However, it is not the case for sharp indenters since they can create their own flaws [158]. Marshall et al. [167] developed a model for lateral cracking due to sharp indenters by describing an apparent threshold for lateral cracking. Later Hutchings [168] related the apparent threshold to materials properties, and Slikkerveer et al. [169] quantified it as shown in the following equation:

$$U_{th} = 23225 \frac{E^{3/2} K_{Ic}^6}{H_t^{13/2}} \tag{3-28}$$

where, U_{th} is the threshold of minimum kinetic energy of particles at which cracking can occur

E is Young's modulus

In summary, the aerodynamic performance of wind turbine blades is affected by the roughness of the airfoil. It has been found by the presented studies that the increase of surface roughness at the leading edge can lead to an early transition of the flow from laminar to turbulent, which affects the pressure distribution on the blade and consequently decreases lift and increases drag. One way to reduce the effects of erosion on wind turbine blades is through the use of protective coatings, and it has been shown in this chapter that polyurethane and graphene coatings are good candidates for this job.

Moreover, the process of solid particle erosion depends on many physical parameters related to the flow, such as particle velocity and angle of impingement, particle parameters such as size and shape of the abrasive particles, and target parameters such as hardness and temperature of the target surface. Many researchers tried to model the erosion process, however, due to the complex nature of the erosion process and the high number of parameters involved, no model could be considered universal, and the available models work well only with the conditions used to derive them in the first place. Therefore, experimental solid particle erosion testing is still necessary to fully understand and characterize the erosion process.

Chapter 3: Motives and Objectives

In this chapter, the motives behind this research, objectives and goals, methodology, and the tasks required to accomplish these objectives will be discussed thoroughly. Wind turbine blades erected in desert and arid environments are subject to impingement by sand particles, especially during sandstorms. The erosion caused by sand particles impingement causes detrimental effects on the smoothness of the blade, the efficiency, and the annual energy production, as will be discussed in detail in the next chapter. To establish the needed test parameters, the situation during sandstorms in desert areas such as the Middle East and North Africa will be imitated.

3.1 Sandstorms

Strong winds cause sandstorms on loose, dry, and sparsely vegetated grounds, a common phenomenon in arid and semi-arid regions. The World Metrological Organization (WMO) defines sandstorms in terms of two factors, first the visibility, which must be reduced to below 1000 m, and second is wind speed, which must be at 22 knots (11.3 m/s) or more [34]. These two factors are not always present at the same time; for example, suspended dust can cause the visibility to be less than 1000 m when the dust is raised by light and calm winds [35]. According to Kuteil and Furman [36], he Arabian Peninsula is identified as the region with the highest occurrence of dust storms. The highest frequency of dust storms in the Arabian Peninsula occurs in the lower Mesopotamian Plains (southern Iraq and Kuwait), where the highest occurrence of 33 dust storms per annum is recorded in the city of Nasiriya in Iraq, followed by 27 dust storms per annum in Kuwait [34].

In one of the biggest recorded dust storms that hit the Arabian Peninsula in March 2009, Alharbi et al. [37], provided the impacts of this dust storm and five key meteorological variables (temperature, wind speed and direction, atmospheric pressure, and visibility). Fig. 3-1 shows the visibility and wind speed graphs for the three days, from noon of March 9th until noon of March 12th. Focusing on the 12 hours highlighted by circles on Fig. 3-1 between March 10th at noon (shown in the figure as 10/3/12) and March 11th at midnight (shown as 11/3/00), it can be seen that the visibility drops to levels below 1000 m, which means that this is the period at which the dust storm was occurring. At this period, the wind speed increased to the maximum of 28 m/s. A similar situation occurs in Egypt during the Khamasin sand storm with speeds up to 140 km/h (~39 m/s) carrying a tremendous amount of sand particles [38].

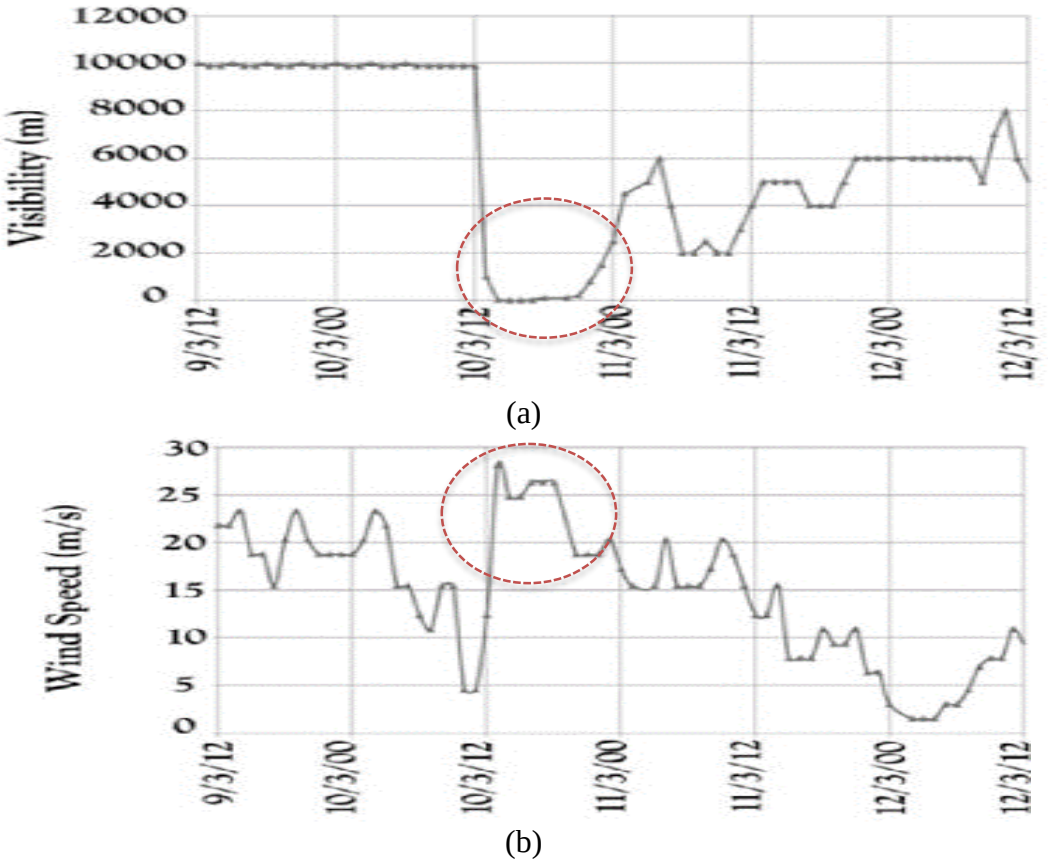


Fig. 3-1: March 2009 dust storm metrological variables: (a) Visibility (b) Wind speed.

3.2 Wind speed

Many theories and models have been used and proposed by researchers to predict the true peak wind speed during dust storms. For example, according to the buoyancy equation, parcel theory predicts and describes the descent of negatively buoyant air mass. As a result, wind speed could be calculated by:

$$\frac{1}{2}\,(w^2 - w_o^2) = -R_c \int_{p_o}^{p} (T' - T_e)\frac{dp}{p} \qquad (2\text{-}1)$$

where, w is wind speed w_o is the vertical wind speed

p is the environment pressure p_o is the pressure at cloud-base

T_e is the environment temperature T' is the parcel temperature

R_c is the gas constant

Proctor [39] proposed another way to estimate the peak wind speed by relating it to the peak temperatures difference between the environment and the cold pool, as follows:

$$U_{max} = -5\Delta T \qquad (2\text{-}2)$$

Haboob is an Arabic word meaning "strong wind" or "blow" that describes a metrological phenomenon of an immense wall of blowing sand and dust. The front of the storm is extremely dense and turbulent, and the wall of dust associated with these storms exceeds 1 km in height and an average maximum wind speed of 15 m/s [40]. Miller et al. [41], in their study of Haboob in the UAE using meteorological stations, satellite, radar, and lidar coverage, found out that eq. (2-1) and (2-2) underestimate the gathered wind speed data by approximately a factor of 2. Lawson [42] found out due to the redirection of the horizontal motion into the vertical along the forward edge, the speed of the dust front advance was approximately half the maximum wind speed measured behind the front. Miller et al. [41] gave two reasons for why their anemometer underestimated the speed data. The first reason

is that the occurrence of Haboob in remote, sparsely inhabited areas with considerable distance between the origination point and the nearest metrological station. Stations less than 20 km away underestimated the wind speed by less than 10%, and as the distance increased, exponential decay is noticed. Secondly, due to the nature of anemometers readings where they averaged the data every 15 min, underestimating the true peak value occurs. Anemometers' averaging tends to bias the low wind speed values, especially if the true peak value occurs over a duration significantly shorter than that of the averaging window.

In Kuwait, ten years of visibility and wind speed data from Kuwait International Airport is shown in Fig. 3-2. Data is measured and recorded every 30 min. The wind speed data has been multiplied by a factor of two following Lawson's estimation to acquire a better true peak value of wind speed. The cases where the visibility data is higher than 1000 m were removed, as well as the cases where wind speed data is below 11 m/s. Every circle in the graph represents a sandstorm incident with visibility less than 1000 m and wind speed higher than 11 m/s. It is noticeable that wind speed reached values near 35 m/s, consistent with what was measured in Egypt during the Khamasin sandstorm.

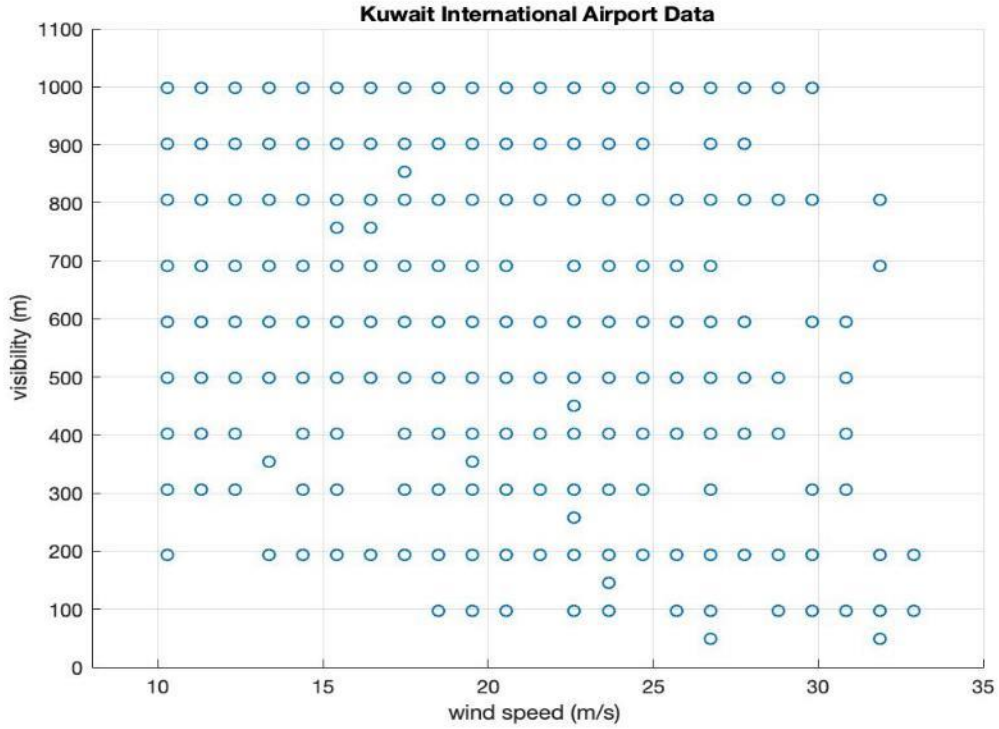


Fig. 3-2: Visibility vs. wind speed data for a ten years period (Larson modification is applied to wind speeds).

3.3 Characterization of sand particles

The size of sand particles can be classified into three categories according to ISO 14688 standard [43], coarse (0.63 mm – 2 mm), medium (0.2 mm – 0.63 mm), and fine (0.063 mm – 0.2 mm). On the other hand, silt is categorized into coarse (0.02 mm – 0.063 mm), medium (0.0063 mm – 0.02 mm), and fine (0.002 mm – 0.0063 mm). A smaller classification of particle size ranges for sand, silt, and clay is given in Table 3-1 [44]. In the United States, the Krumbein *phi* (ϕ_i) scale [45], a logarithmic scale, which is a modification of the Wentworth scale, has been commonly used. It is given by:

$$D_p = D_0 \times 2^{-\phi_i} \tag{2-3}$$

where,

D_p is the diameter of the particle in mm

D_0 is a reference diameter equal to 1 mm

ϕ_i is the Krumbein phi scale

Table 3-1: Sand, silt, and clay particle size ranges [44].

Particle size category (symbol)		Range of particle size	*Phi* Φ	ASTM mesh
Sand	Very Coarse (V.C.S)	1-2 mm	-1 – 0	10 – 18
	Coarse (C.S)	0.5-1 mm	0 – 1	18 – 25
	Medium (M.S)	0.25-0.5 mm	1 – 2	25 – 60
	Fine (F.S)	125-250 μm	2 – 3	60 – 120
	Very Fine (V.F.S)	62.5-125 μm	3 – 4	120 – 230
Silt	Coarse (C. Silt)	31.2-62.5 μm	4 – 5	--
	Medium (M. Silt)	15.6-31.2 μm	5 – 6	--
	Fine (F. Silt)	7.8-15.6 μm	6 – 7	--
	Very Fine (V.F. Silt)	3.9-7.8 μm	7 – 8	--
Clay	Clay	<3.9 μm	8 – 12	--

A study of the particle size distribution of the dust fall in multiple sites in Kuwait is shown in Fig. 3-3 [46]. It can be seen in the figure that the majority of the dust is from the Very Fine Silt (V.F.S.) category, followed by Fine Silt (F.S.). The chemical composition of sand collected from four desert sites in Kuwait is shown in Table 3-2 [47]. It can be seen that the composition consists mainly of silica, which on average is about 84% of the composition, followed by oxides such as aluminum oxide ~8%, calcium oxide ~3%, and magnesium oxide ~1%. Wind speed, sand particle size, and chemical composition data in Kuwait shown in this chapter will later be used to set up the testing parameters needed for the leading edge erosion experiments in order to imitate an actual situation.

Table 3-2: Chemical composition of Sand samples from multiple sites in Kuwait [47]

Site	Silica (SiO_2)	Ferric oxide (Fe_2O_3)	Aluminum oxide (Al_2O_3)	Calcium oxide (CaO)	Magnesium oxide (MgO)	Sulphate (SO_3^{-2})	Chloride (Cl^-)	Organic matter (O.M.)	Carbon Dioxide (CO_2)	Calcium sulphate ($CaSO_4$)	Calcium carbonate ($CaCO_3$)	Magnesium sulphate ($MgSO_4$)	Magnesium carbonate ($MgCO_3$)
Ashegaya	83.42	0.64	5.12	4.06	2.40	0.0083	0.016	1.03	3.26	Nil	7.25	Nil	0.134
Um-Alish	76.64	0.72	8.62	6.78	1.72	0.0083	0.023	0.48	3.68	0.114	8.36	Nil	Nil
Al-Wafra	89.28	0.48	4.42	2.12	0.81	0.0083	0.016	0.55	1.95	Nil	3.79	0.013	0.53
Kabd	84.32	0.60	8.24	3.14	1.07	0.0083	--	0.66	1.76	0.014	4	Nil	Nil

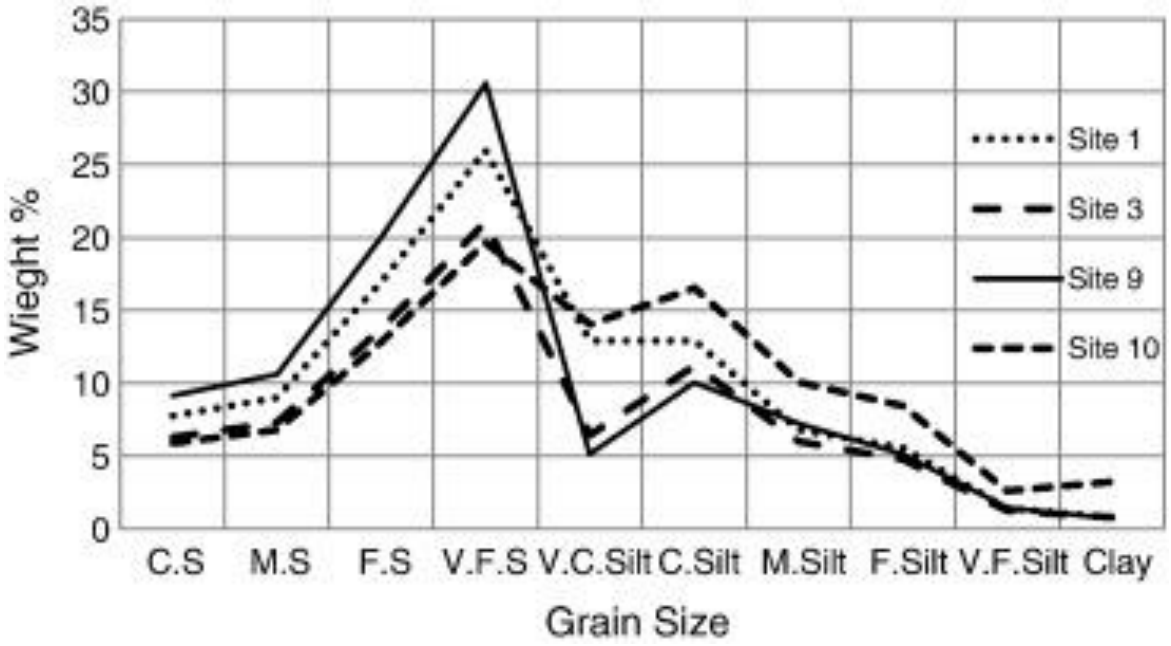


Fig. 3-3: Particles size range percentage of dust fallout in Kuwait

3.4 Objectives and tasks

The data presented in this chapter highlights the severe weather conditions in Kuwait and the high frequency of sandstorms occurrence, which is expected to cause erosive damage to wind turbine blades if they were constructed in that region. This erosive damage is expected to deteriorate the aerodynamic performance of wind turbines. Therefore, the motive behind this study is to give designers the ability to predict loads and energy losses due to the leading edge erosion problem in order to minimize the reduction in captured energy and, consequentially, profitability.

This investigation will focus on experimentally investigating, characterizing, and modeling the effects of the leading edge erosion on wind turbine blades. Also, the effects of protection that can be provided by single and multilayers of protective coatings, namely: polyurethane-based coating and graphene-based coating on minimizing the effects of erosion. Finally, the effects of erosion on the aerodynamic performance in terms of changes

in lift and drag coefficients and the change in power generation of coated and uncoated blades were studied and characterized. The tasks required to accomplish these research objectives are listed below:

- Task 1: Assembling erosion test rig where all erosion tests will be taking place
- Task 2: Eroding flat surfaces of ductile and brittle materials to verify the workability of the erosion rig set when compared to the available literature.
- Task 3: Erosion of multiple single and multilayer graphene and polyurethane-based coatings and specifying the ones providing the best erosion resistance.
- Task 4: Getting three small wind turbine blades and cutting them into smaller airfoils for testing.
- Task 5: Coating one set of airfoils with the best performing single layer coating and another set with the best performing multilayer coating.
- Task 6: Eroding the uncoated and coated airfoils and measure its erosion resistance in terms of material removal and depth of erosion scars in order to study the effects of coating on the erosion process.
- Task 7: Three-dimensional (3D) Scanning of all three sets of airfoils before and after erosion.
- Task 8: Extract 2D profiles at the location of the erosion scars and compare them to the before erosion profile to characterize the shape alterations due to erosion.
- Task 9: Numerically analyze the 2D profile in Xfoil to get their aerodynamic performance before and after erosion.
- Task 10: Use Blade Element Momentum Theory (BEMT) to calculate the change in power generation before and after erosion.

Chapter 4: Experimental methodology

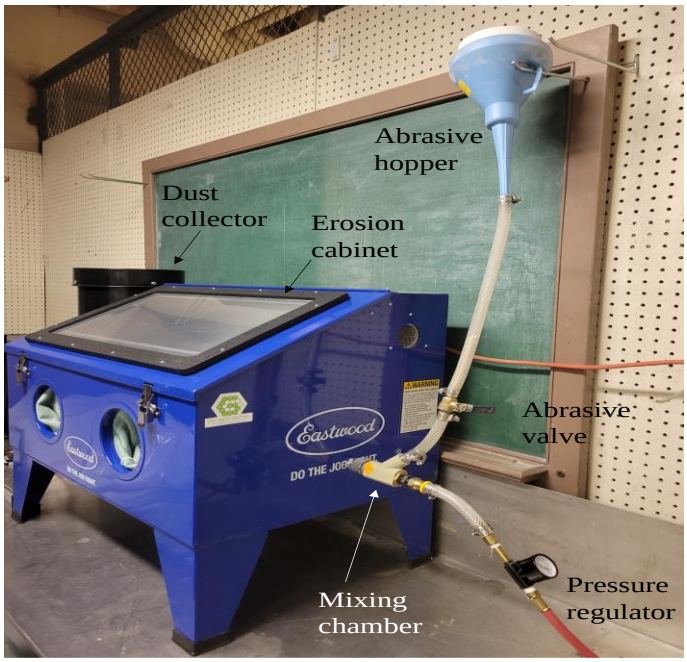
In this chapter, the experimental procedure followed to achieve the stated objectives and tasks presented in Chapter 3. The first and most crucial experimental task is building an erosion rig where all the erosion experiments can be conducted. Then the accuracy of the results generated by the erosion setup must be verified. After that, different types of coatings will be eroded to specify the coatings that should be used to coat wind turbine blades in preparation for erosion. The erosion results were analyzed using an electronic balance, contact profilometer, and optical scanner to obtain material removal, surface roughness, and depth and profile of erosion scars, respectively. After eroding wind turbine blades, a three-dimensional (3D) scanner was used to capture erosion shape and airfoil profiles and perform aerodynamic analysis using Xfoil. Details of the experimental procedure and methodology are discussed extensively in this chapter.

4.1 Experimental Setup

4.1.1 Erosion Rig

Following ASTM G76-13 standard for conducting erosion tests by solid particle impingement using gas jets [170], an erosion rig was assembled where all the erosion tests took place. The sole purpose of the erosion rig is to supply air at a specific pressure to drive abrasive particles to cause erosion/damage to a test specimen. A photograph of the setup is shown in a Fig. 4-1 (a) with the nozzle shown in Fig. 4-1 (b). A schematic of the components of the erosion rig used in this experiment is shown in Fig. 4-1 (c). The setup starts with pressurized air, which is controlled by the air valve. When the air valve is opened, the

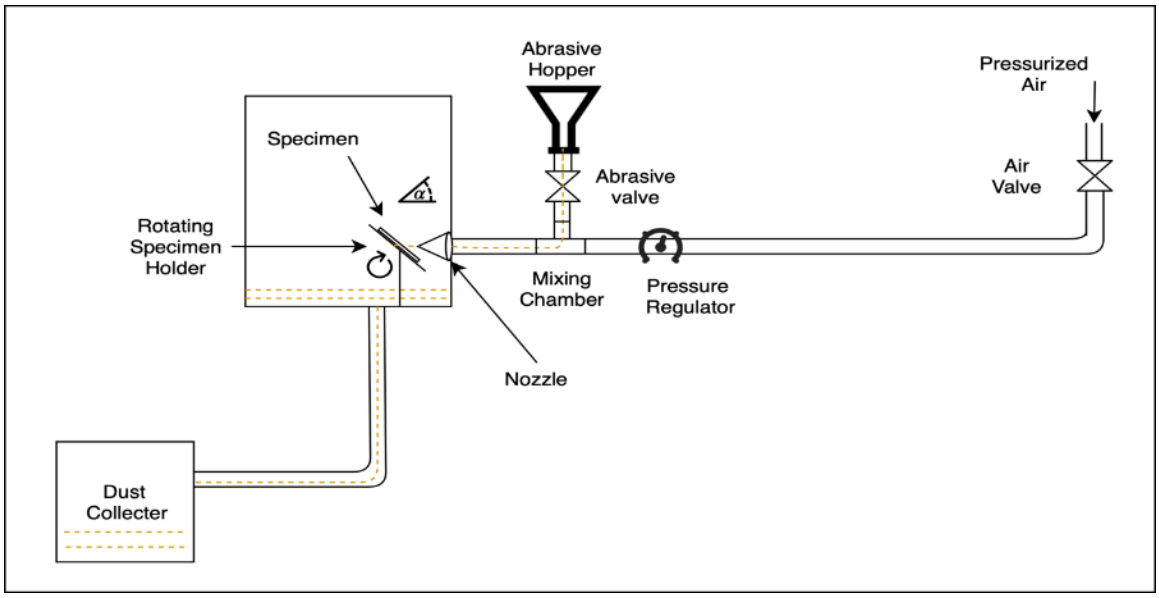
air has to go through a pressure regulator, which ensures that air entering the mixing chamber is at the exact pressure required at all times. An abrasive hopper is where the abrasive particles are stored, and it is connected to an abrasive particles valve. During erosion tests, the abrasives valve is opened. In the mixing chamber, the incoming pressurized air creates a Venturi effect that leads to the suction of abrasive particles and guides it toward the nozzle inside the erosion cabinet. The erosion cabinet, manufactured by Eastwood Inc., has internal dimensions of 71 cm by 30.5 cm by 46 cm, length x width x height, respectively. The abrasives gain momentum and bombard the target specimen, which is placed on a rotating specimen holder. Finally, a dust collector sucks abrasive particles and debris out of the erosion cabinet. The dust collector is manufactured by Eastwood Inc. with a 1.75-gallon capacity and 8 microns of filtration.



(a)



(b)



(c)

Fig. 4-1: Experimental setup of the erosion rig: (a) photograph of the testing setup, (b) Nozzle inside the erosion cabinet, and (c) schematic of the testing setup

4.1.1.1 Nozzle

One of the most crucial elements in the experimental erosion setups is the nozzle. Nozzles control the emerging fluid stream and its characteristics, such as flow rate, speed, shape,

and flow pressure. The material of the nozzle, orifice shape, dimensions, the distance between the nozzle tip and the target material, angle of impingement between the nozzle and the target material are some of the main parameters that give the nozzle its importance.

The nozzle used in this experiment has been chosen by following ASTM G76-13 standard [170], which requires that:

- The length to inner diameter ratio should be greater than 25:1 to achieve acceptable particle velocity distribution
- Made of an erosion-resistant material such as Tungsten carbide (WC) and Aluminum oxide (Al_2O_3).
- The increase in the inner diameter due to the erosion process must not exceed 10%.

The nozzle used in this experiment, manufactured by Kennametal Inc., is a straight-head nozzle made of tungsten carbide (WC) with the following dimensions 50.8 mm (2 in.) in length, and constant outer and inner diameters of 12.7 mm (0.5 in.) and 1.524 mm (0.06 in.), respectively. These dimensions give an approximate length to inner diameter ratio of 33:1.

4.1.1.2 Abrasive particles

The abrasive particles used in this experiment are round (blunt) silica sand abrasives with an average particle diameter of 206 μm. Silica sand with 99% purity is used since the majority of sand in Kuwait is made out of silica, as shown in Chapter 3. This particle size lies in the Fine Sand (F.S.) category, as shown in Chapter 3. The particle diameter size represents an average of 20% of the dust fallout in Kuwait, as shown in Fig. 3-3. Large particle size was chosen to expedite the erosion process and make it easier for analysis. Fig. 4-2 shows an optical picture of the silica abrasives.

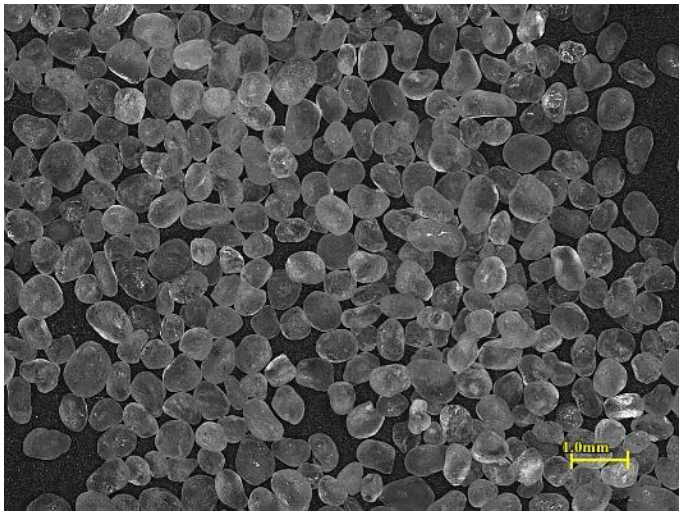


Fig. 4-2: Silica abrasive particles used

4.1.2 Test procedure

Before the erosion of any specimen, its mass must be measured. SA-310 electronic mass balance with the ability to measure with ±0.1 mg sensitivity is used to measure the specimen's mass. After that, the specimen is placed inside the erosion cabinet in preparation for erosion. Depending on the angle of impingement required, angle blocks are used to mount the specimen. The blocks can put the specimen at any angle of impingement required with an accuracy of ±1˚. After the erosion process is completed, the specimen is cleaned and remeasured to determine the amount of mass loss. Erosion rate is determined by dividing the mass of the material removed by the mass flow rate for abrasives, measured to be 0.067 g/s when operating at air pressure of 200 kPa.

4.1.3 Test parameters

Many test parameters can affect the erosion process, as discussed previously. Some of these parameters are studied in this investigation, such as the angle of impingement, erosion du-

ration, and air pressure. The variable and fixed parameters used for every erosion experiment will be discussed in the following chapters when discussing the different erosion tests. One important erosion parameter that will be estimated theoretically is the impact velocity of abrasive particles. Since varying air pressure will affect the impact velocity of abrasive particles, the following equations are used to estimate impact velocity.

Assuming a simple convergent nozzle situation, the relationship between Mach number and the pressure can be represented as [171]:

$$M = \left\{ \frac{2}{R_c - 1} \left[\left(\frac{P_{in}}{P_{out}} \right)^{(R_c - 1)/R_c} - 1 \right] \right\}^{1/2} \tag{4-1}$$

where M is Mach number

R_c is Gas constant (287.05 J/kg)

P_{in} is the pressure at the inlet of the nozzle

P_{out} is the atmospheric pressure

The Mach number can be obtained by

$$M = \frac{v_{out}}{a_\infty} \tag{4-2}$$

where v_{out} is the airflow velocity

a_∞ is the local speed of sound and is obtained by

$$a_\infty = \sqrt{k R_c T_e} \tag{4-3}$$

where k is the adiabatic index of air (k=1.4 for air at 293 K)

T_e is the temperature in K (293 K)

Therefore, the airflow velocity can be estimated by:

$$v_{out} = a_\infty M = \sqrt{k R_c T_e} \left\{ \frac{2}{R_c - 1} \left[\left(\frac{P_{in}}{P_{out}} \right)^{(R_c - 1)/R_c} - 1 \right] \right\}^{1/2} \tag{4-4}$$

To obtain the abrasives velocity, the law of conservation of linear momentum is used:

$$m_{air} v_{out} = \left(m_{air} + m_p\right) v_p \tag{4-5}$$

where m_{air} is the mass of airflow out of the nozzle

m_p is the mass of the abrasives

v_p is the velocity of the abrasives

The mass of the airflow out of the nozzle can be calculated by

$$m_{air} = \rho_{air} v_{out} A_{noz} = \frac{\pi}{4} \rho_{air} v_{out} d_{noz}^2 \tag{4-6}$$

where ρ_{air} is the density of air

A_{noz} cross sectional area of the nozzle

d_{noz} is the inner diameter of the nozzle

4.2 Wind turbine blades

The wind turbine blades used in these experiments are Aeosol H 1-kW. Table 4-1 shows some of its properties. Three 1.20 m blades made of a vinyl epoxy matrix, fiberglass, and polyurethane foam are used. A cross sectional view of the blade is shown in Fig. 4-3. The fiber to resin ratio is 45 to 55, and the fibers are woven in a radial orientation. Blades were cut to small airfoils of 20 cm lengths and a varying chord length resulting in 18 testing specimens. The blades were cut using an abrasive water jet, and the cutting conditions are shown in Table 4-2.

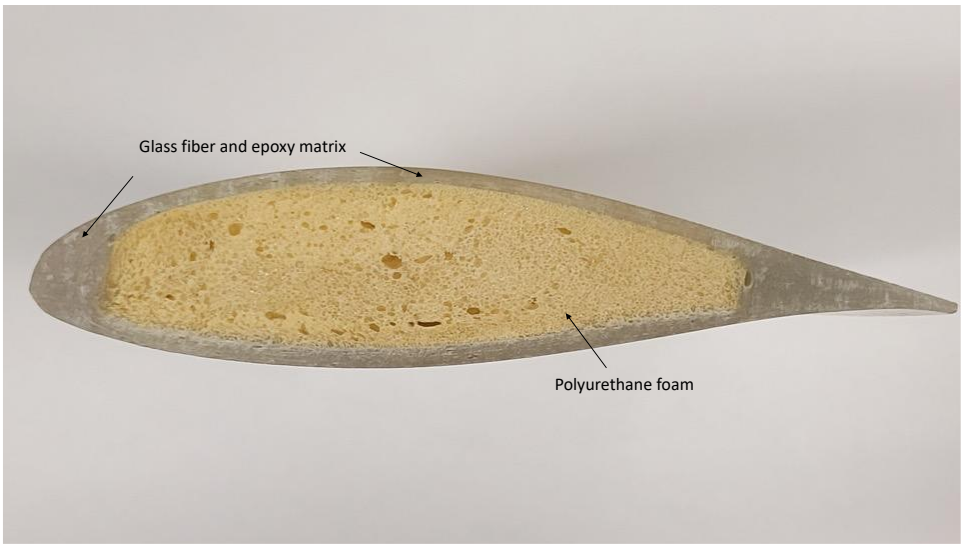


Fig. 4-3: Cross-sectional view of the blade with glass fiber

The airfoils are organized in three sets based on the type of coatings they will receive. The first will act as a baseline of comparison and will be uncoated. The second set will be coated with the best performing single layer coating, while the last set will be coated with the best performing multilayer coating, as will be discussed in Chapter 5.

Table 4-1: Aeolos 1-kW wind turbine blades [172]

Property	**Magnitude**
Rated Power	1 kW
Maximum Output Power	1.2 kW
Output Voltage	48 V
Blade Quantity	3 Glass Fiber Blades
Rotor Blade Diameter	3.2 m
Cut-in Wind Speed	2.5 m/s
Rated Wind Speed	12 m/s
Cut-out Wind Speed	25 m/s
Survival Wind Speed	45 m/s
Generator	Three Phase Permanent Magnetic Generator
Generator Efficiency	>0.96
Design Lifetime	20 Years

Table 4-2: Abrasive water jet cutting conditions

Property	Magnitude
Mixing tube diameter	1 mm (0.04 in.)
Mixing tube length	101.6 mm (4 in.)
Standoff distance	Minimum 2.8 mm (0.11 in) (variable due to curvature)
Orifice diameter	0.33 mm (0.013 in.)
Pressure	414 MPa (60,000 Psi)
Traverse Speed	127 mm/ min (5 in/min)
Material of the mixing tube	Tungsten carbide (WC)
Orifice material	Ruby
Abrasive flow rate	6.05 g/s

4.3 Surface Roughness measurements

As shown in Chapter 2, it is with no doubt that surface roughness plays a vital role in aerodynamic performance and energy production. The surface roughness will be measured before and after erosion. In the process of fabricating any new surface, prints and irregularities due to the machining process are always present. These irregularities are called roughness, which comes in the form of peaks and valleys deviating from a nominal surface's mean line. Every machine has its limits in terms of the degree of roughness it can create. Roughness can cause changes in the behavior of the materials in terms of wear, friction, corrosion, and lubrication.

In every surface, based on the wavelengths, the shape of the surface can be classified into three components: Roughness, Waviness, and Lay. Roughness represents the short wavelength, waviness represents the medium wavelength, and lay represents the long wavelength. Fig. 4-4 below demonstrates the difference between the three components. A surface is considered rough if the deviations from the nominal surface are large and smooth if the deviations are minor. However, the question is, what constitutes large and small? The

answer depends on the size and nature of the application. For example, rough surfaces for Nano-applications can be considered smooth for automotive parts.

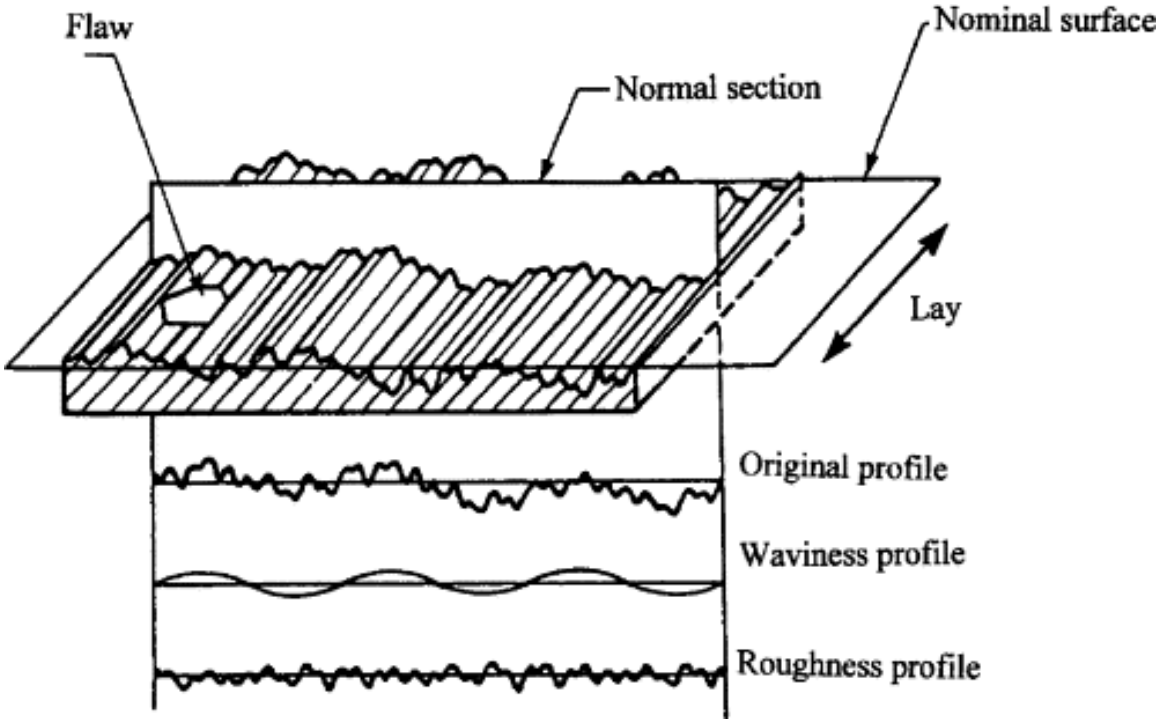


Fig. 4-4: Roughness, waviness, and Lay in a surface [173].

During the manufacturing of new surfaces, the shape, height, and the direction of roughness are created due to several factors such as [174]:

1. The machining variables, which include cutting speed, feed, and depth of cut.
2. The machining tool, which includes geometry and quality
3. The mechanical properties of the machined material and the tool

Measurement of surface roughness can be divided into three categories: subjective comparison with standard test surfaces, stylus electronic instruments, and optical techniques [21]. Compared with the standard test, surfaces work by scratching the surface of the specimen with fingernails and comparing the roughness with available surface finish blocks. In the electronic instruments, a cone-shaped diamond stylus is traversed across the test surface

at a constant low speed. The optical techniques work by subjecting the test surface to a light beam and, based on reflectance, scatter, or diffusion roughness, is measured.

4.3.1 Roughness Parameters:

The roughness of any surface can be defined by a single number, which is according to ISO 4287 [175], could be:

- Arithmetical mean deviation from the assessed profile (R_a): The arithmetical mean of the absolute values of the profile deviations from the mean line of the roughness profile.
- Root mean square deviation from the assessed profile (R_q): root square value within a sampling length
- Skewness of the assessed profile (R_{sk}): the quotient of the mean cube value and the cube of the R_q respectively within a sampling length.
- Kurtosis of the assessed profile (R_{ku}): the quotient of the mean quartic value and the fourth power R_q respectively, within a sampling length.
- Maximum profile peak height (R_p): the largest profile peak height within a sampling length
- Maximum profile valley depth (R_v): the largest profile valley depth within a sampling length.
- Maximum height of profile (R_z): the sum of height of the largest profile peak height and the largest profile valley depth within a sampling length

Another way to measure the surface roughness of a target material is through the measurement of the roughness of an area by using the following parameters according to ISO 25178:

- Arithmetical mean height (S_a): arithmetic mean of the absolute of the ordinate values within a defined area A_s.
- Root mean square height of a surface (S_q): root mean square value of the ordinate values within a defined area A_s.
- Skewness of the assessed profile (S_{sk}): the quotient of the mean cube value and the cube of the S_q respectively within a defined area A_s
- Kurtosis of the assessed profile (S_{ku}): the quotient of the mean quartic value and the fourth power S_q respectively, within a defined area A_s.
- Maximum profile peak height (S_p): the largest profile peak height within a defined area A_s.
- Maximum profile valley depth (S_v): the largest profile valley depth within a defined area A_s.
- Maximum height of profile (S_z): the sum of height of the largest profile peak height and the largest profile valley depth within a defined area A_s.

A summary of some of the roughness parameters and the formulations are shown in Table 4-3 below:

Table 4-3: Roughness parameters and their formulations [175]

Parameter	Formulation
R_a	$R_a = \frac{1}{l}\int_0^l \lvert Z(x)\rvert \, dx$
R_q	$R_q = \sqrt{\frac{1}{l}\int_0^l Z^2(x)\, dx}$
R_{sk}	$R_{sk} = \frac{1}{R_q^3}\left[\frac{1}{l_r}\int_0^{l_r} Z^3(x)\, dx\right]$
R_{ku}	$R_{ku} = \frac{1}{R_q^4}\left[\frac{1}{l_r}\int_0^{l_r} Z^4(x)\, dx\right]$
R_z	$R_z = R_p + R_v$
S_a	$S_a = \frac{1}{A_s}\iint \lvert z(x,y)\rvert dxdy$
S_q	$S_q = \sqrt{\frac{1}{A_s}\iint z^2(x,y)dxdy}$
S_{sk}	$S_{sk} = \frac{1}{S_q^3}\left[\frac{1}{A_s}\iint z^3(x,y)dxdy\right]$
S_{ku}	$S_{ku} = \frac{1}{S_q^4}\left[\frac{1}{A_s}\iint z^4(x,y)dxdy\right]$
S_z	$S_z = S_p + S_v$

To reduce or eliminate the effects of the unwanted long wavelength of waviness, a cut-off length is specified to measure the roughness wavelength. The cut-off length is also used to ensure that the measured surface is long enough to give a reliable roughness parameter value. After data has been recorded, it is broken into equal sample lengths (l_r), which is equal to the cut-off value (λ_c). According to ISO 4287 [175], an evaluation length (l_n) consists of five sampling lengths, and it is used for analysis. Table 4-4 below shows the recommended cut-off length and evaluation length based on the value of R_a.

Table 4-4: Recommended cut-off length by ISO 4288 [176]

R_a (µm)	$\lambda_c = l_r$ (µm)	l_n (µm)
0.006 – 0.02	0.08	0.4
>0.02 – 0.1	0.25	1.25
>0.1 – 2	0.8	4
>2 – 10	2.5	12.5
>10 – 80	8	40

4.4 Erosion Analysis

4.4.1 Optical Scanning (Profilometer)

After eroding specimens and measuring their removed mass, the dimensions of erosion scars are measure in terms of the length, width, and depth, as well as measuring the volume. These measurements are taken using a 3D measurement system through optical scanning using Keyence VR-3100. Table 4-5 shows the technical specifications of this instrument. Using the Keyence optical profilometer, the surface roughness profile of specimens is measured optically. Also, a Mahr GD-25 contact profilometer with a 2.5 µm stylus was used to verify the surface roughness data.

Table 4-5: Technical specifications for Keyence VR-3100 optical scanning profilometer

Parameter	**Value**
Magnification	12x – 160x
Measurable height	10 – 1 mm
Repeatability	0.5 µm
Accuracy	±3 µm
Image receiving element	4-megapixel monochrome CMOS
Transmitter lens	Two, double-telecentric lens
Receiver lens	Double-telecentric lens
Light source	White LED
Image size	1024 x 768, 2048 x 1536 pixels
Operating Temperature	15-30 ˚C

4.4.2 Scanning element Microscopy (SEM)

Scanning electron microscopy (SEM) was used to further understand the removal and erosion mechanism. Prior to SEM investigation, the specimens were cleaned using water at

55° C in an ultrasonic cleaner at a frequency of 40 kHz for 25 min**.** Then, SEM images were taken at different magnifications in the range of 25x to 5000x.

4.4.3 Three-dimensional Scanning

After eroding the leading edge of wind turbine blades, it is necessary to transform the new shape of the airfoil using a Creaform handyscan 700 scanner 3D scanner in order to be able to analyze it using Xfoil. The technical specifications of the 3D scanner are shown in Table 4-6 below. After the airfoils were scanned, Solidworks software was used to extract 2D profiles at the location of the erosion scar. These 2D profiles were used later in Xfoil to generate the aerodynamic performance data.

Table 4-6: Technical specifications of Creaform handyscan 700

Parameter	**Value**
Weight	0.85 kg
Dimensions	77 x 122 x 294 mm
Measurement Rate	480,000 measurements/s
Scanning Area	275 x 250 mm
Light source	7 laser crosses (+1 extra line)
Laser Class	2M (eye-safe)
Resolution	0.050 mm
Accuracy	Up to 0.030 mm
Operating Temperature Range	5-40 ˚C

4.4.4 Statistical analysis and modeling

A regression analysis attempt was made to characterize the erosion process using Response Surface methodology using the all the process parametric levels. This was achieved through the usage of Analysis of Variants (ANOVA) method to statistically study the impact and significance of the used variables. To do so, Design Expert® software (Version 9.0.3.1, Stat-Ease Inc.) has been utilized. The modeled responses (depth of erosion scars and mass loss) were modeled using the input variables of pressure, angle of impingement, and erosion duration.

In summary, an erosion rig was built following ASTM standard G76-13 to conduct erosion experiments on flat surfaces and the leading edge of airfoils. These experiments will investigate the effects of protective coating on reducing the erosion rate. Many instruments that have been presented on this chapter were used to analyze the erosion scars, such as electronic mass balance, optical and scanning microscope, and 3D scanners. The details on how and where these instruments were utilized will be covered in the following three chapters.

Chapter 5: Erosion of Flat Surfaces

5.1 Introduction

The workability of the erosion rig setup was investigated by testing its ability to reproduce erosion results of materials with known behavior. Erosion experiments were conducted on two types of flat surfaces: ductile and brittle materials. The materials used in this experiment are Aluminum 6061 – T6 representing ductile materials and borosilicate glass representing brittle materials. The amount of material removed of these materials was evaluated as a function of angle of attack. For all experimental tests on flat surfaces discussed in this chapter, a constant air pressure of 200 kPa was used, which resulted in a 20 m/s particle velocity, abrasive flow rate of 0.067 g/s, and the standoff distance was kept at 10 mm ± 1 mm. Subsequently, series of similar erosion experiment were conducted on glass fiber reinforced epoxy (GFRP) both coated and uncoated, and the results were presented and discussed in this chapter.

5.1.1 Erosion of Ductile Material:

The first type of material tested was aluminum 6061 – T6, chemical composition and properties of al 6061 – T6 are shown in Tables 5-1 and 5-2, respectively. The duration of the erosion experiments was 12 minutes for each angle. The dimensions of the specimens are 7.6 cm long by 1.27 cm width by 1.27 cm height (3 in x 0.5 in x 0.5 in). Aluminum specimens were eroded at six different angles of impingement: 10°, 20°, 30°, 45°, 60°, and 90°. Each experiment was duplicated three times to ensure repeatability of the erosion results, which resulted in a total of 18 erosion experiments. A summary of the used experimental test parameters is shown in Table 5-3.

Table 5-1: Chemical Composition of Al 6061 – T6 [177]

Component	**Wt. %**
Al	95.1 – 98.2
Cr	0.4 – 0.8
Cu	0.05 – 0.4
Mg	0.8 – 1.2
Si	0.4 – 0.8
Fe	Max 0.7
Mn	Max 0.15
Ti	Max 0.15
Ni	Max 0.05
Zn	Max 0.25
Zr	Max 0.25
Other elements	No more than 0.05% each, 0.15 total

Table 5-2: Properties of Al 6061 – T6 [177]

Property	**Magnitude**
Density	2.7 g/cm^3
Hardness, Brinell	95
Ultimate Tensile Strength	310 MPa
Yield Tensile Strength	276 MPa
Elongation at Break	12.5%
Modulus of Elasticity	68.9 GPa
Poisson's ratio	0.33
Fracture Toughness	29 MPa – $m^{1/2}$

The amount of material removed of aluminum as a function of the impingement angle is given in Fig.5-1. The erosion rate of each experiment is shown as well as the average erosion rate and one standard deviation from the mean. It can be seen that at smaller angles (10°, 20°, and 30°), the erosion was at its highest, while it decreased as the angle increased. The highest removal of material was noticed at 20°, while the lowest was at 90°. This behavior is expected from ductile materials due to the cutting mechanism for material removal. All material removal data is shown in Appendix I.

Table 5-3: Summary of testing parameters for erosion experiments on aluminum specimen

Parameter	**Magnitude**
Air pressure, P_{out}	200 kPa
Abrasive material	Silica sand
Abrasive size	200 μm
Abrasive flow rate	0.067 g/s
Standoff distance	10 mm
Nozzle diameter	1.5 mm
Erosion duration	720 seconds
Angle of attack	10˚, 20˚, 30˚, 45˚, 60˚, and 90˚

Due to impingement angle and plastic deformation effects, aluminum is displaced differently, and different erosion patterns are generated. In Fig. 5-2, optical and digital of the top views of the eroded areas are shown. All photomicrographs of erosion scars resulting from erosion experiments are shown in Appendix II. The incoming silica particles create a crater-like shape at the normal incident where the aluminum is displaced circularly around the erosion target. The 45° and 60° angles tend to displace material only in the way of the incoming abrasives, while smaller angles create ripples in the direction of the incoming abrasives.

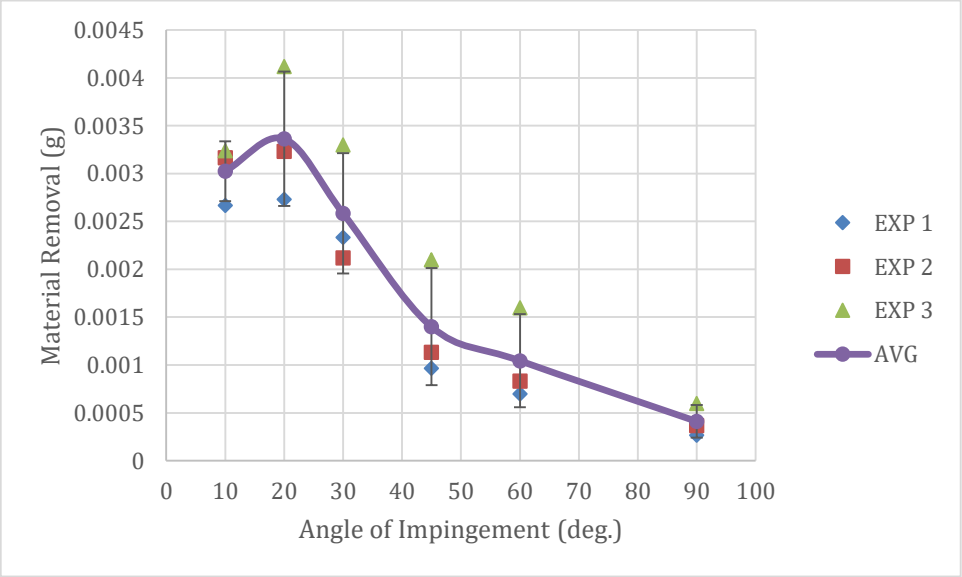
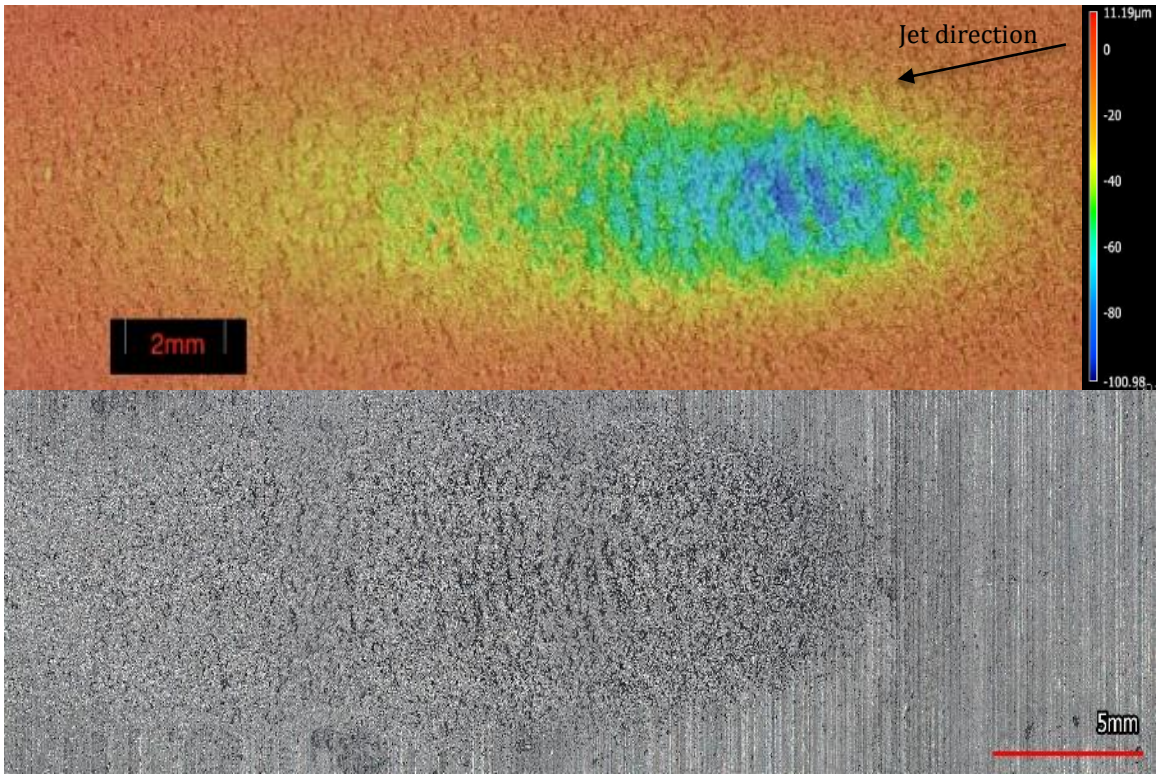
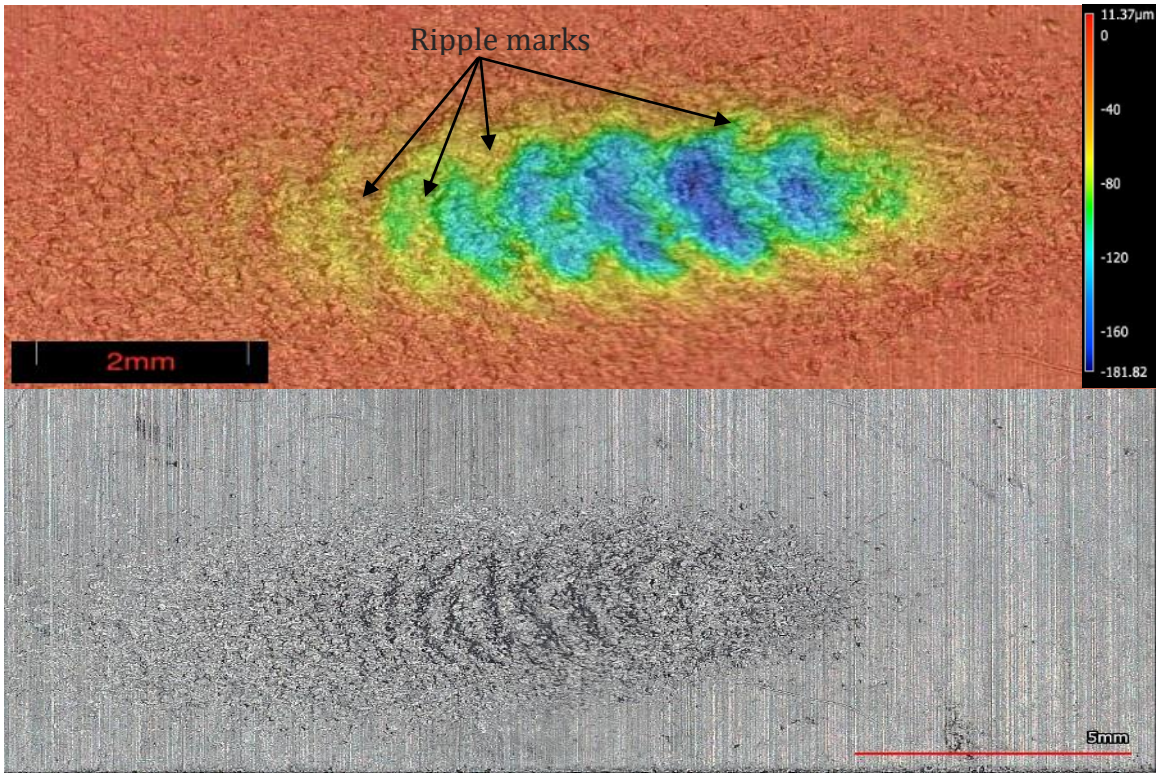


Fig. 5-1: Material removal of aluminum as a function of angle of impingement.

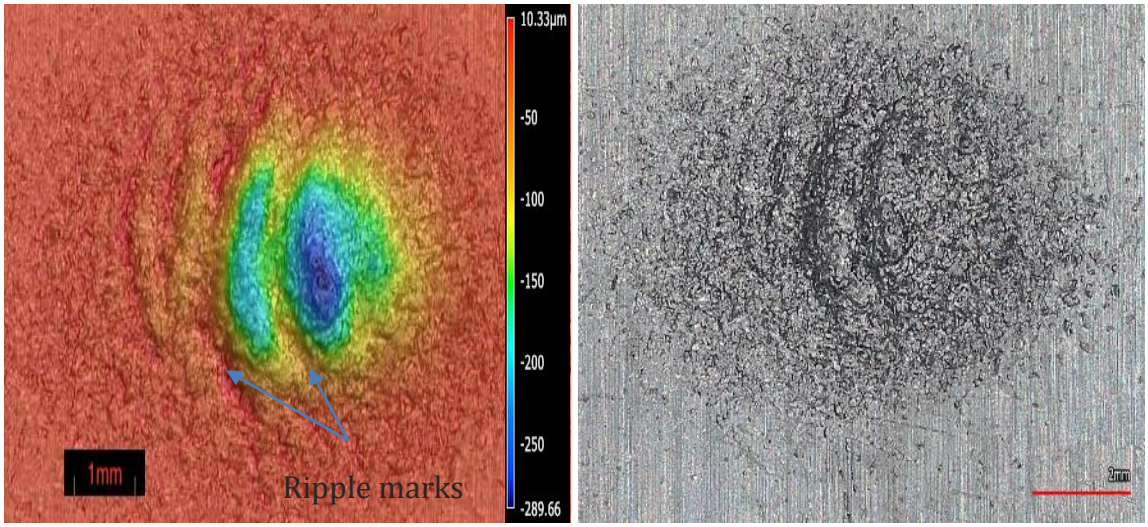
The maximum depth created by erosion is shown in Fig. 5-3. The maximum depth data for all erosion experiments can be found in Appendix III. The maximum depth was found to be at the 45° angle of impingement; this could be attributed to the fact that for ductile materials, the maximum shear occurs at 45°, making it easier for the planes to slip and move freely. The erosion scar profiles crossing at the deepest point of each experiment are shown in Fig. 5-4. It can be seen from the figures that the number of ripples decreases as the angle increases. These ripples can be noticed to be higher in number and shallower in depth for smaller angles, and as the angle increase toward 30˚, the number of ripples decrease and the depth of removal increases.



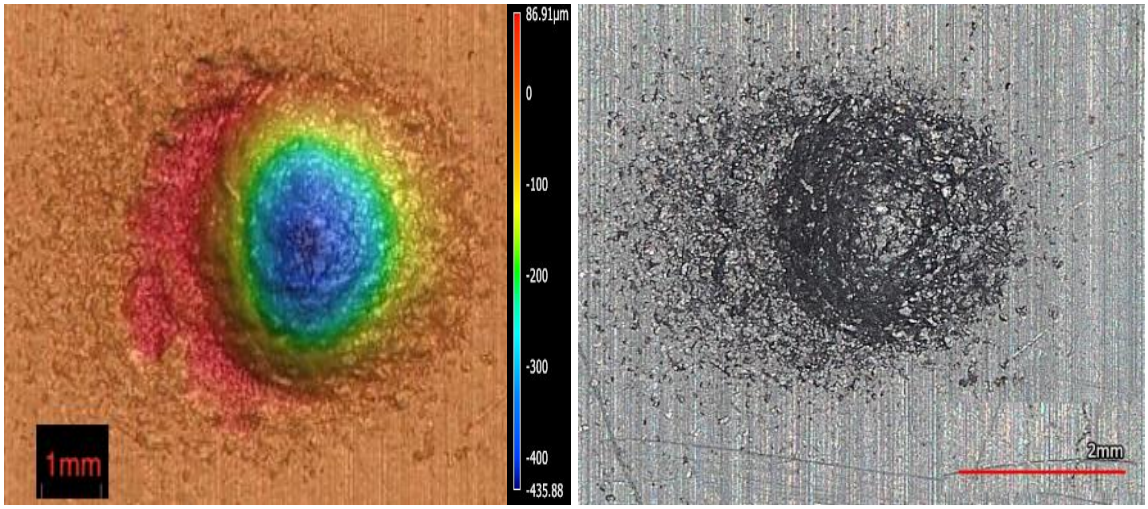
(a)


Ripple marks
11.37µm
0
-40
-80
-120
-160
-181.82
2mm
5mm

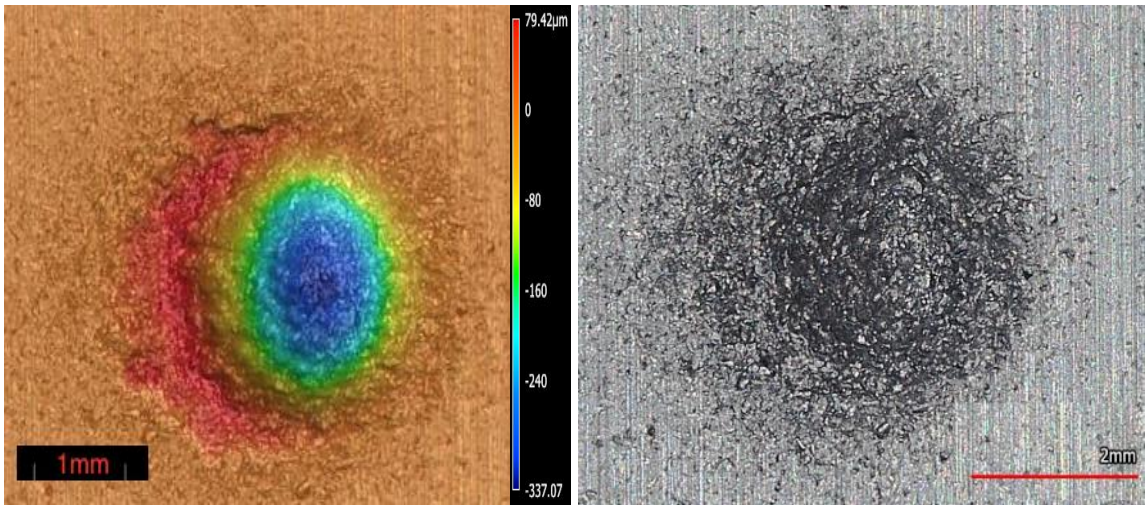
(b)


10.33µm
-50
-100
-150
-200
-250
-289.66
1mm
Ripple marks
2mm

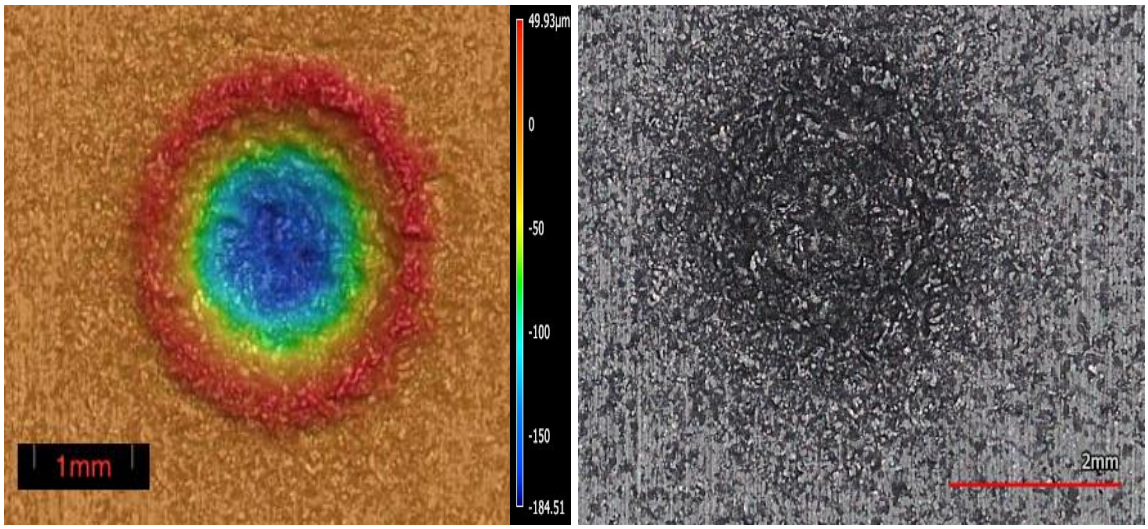
(c)



(d)



(e)



(f)

Fig. 5-2: Erosion pattern of aluminum's erosion scars at an angle of attack of: (a) 10°, (b) 20°, (c) 30°, (d) 45°, (e) 60°, and (f) 90°.

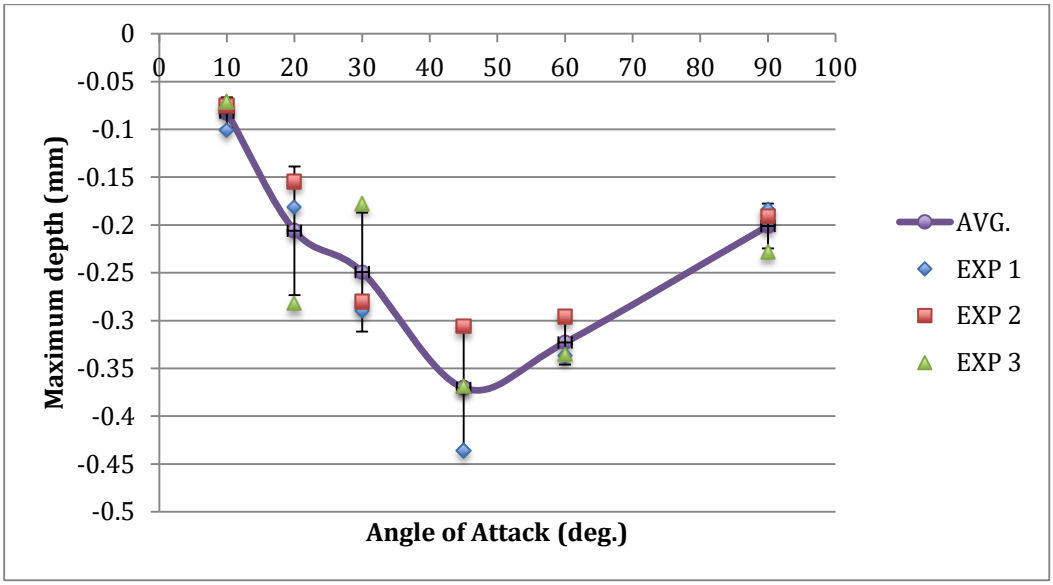
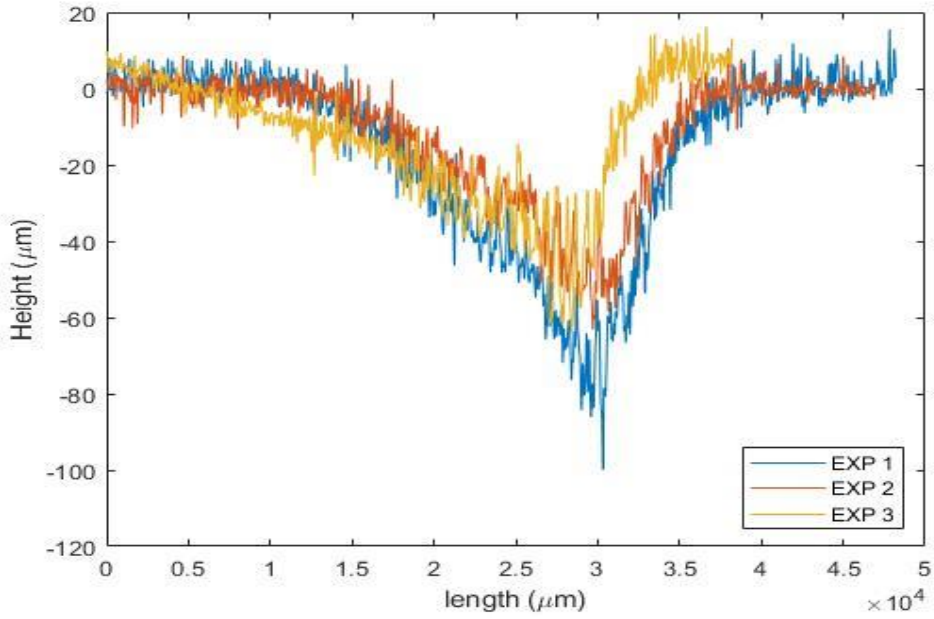
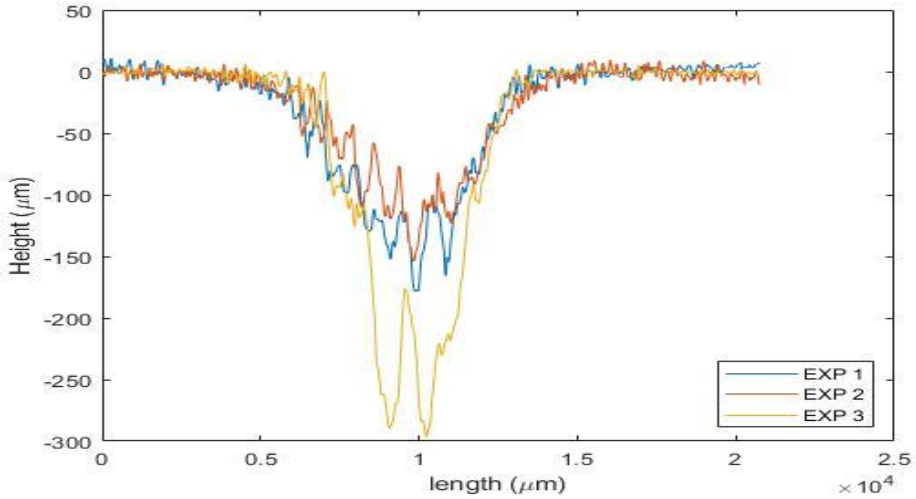


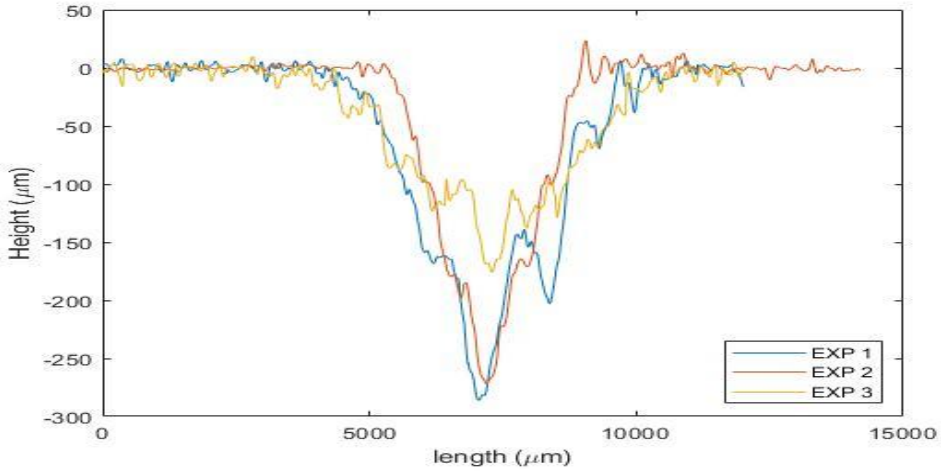
Fig. 5-3: Maximum depth of aluminum's erosion scars as a function of angle of attack



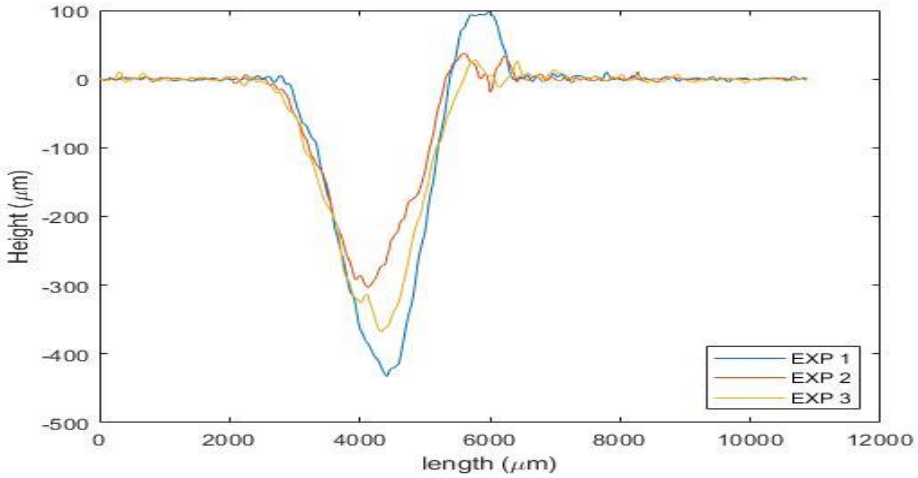
(a)


Height (μm)
length (μm)
$\times 10^4$
EXP 1
EXP 2
EXP 3

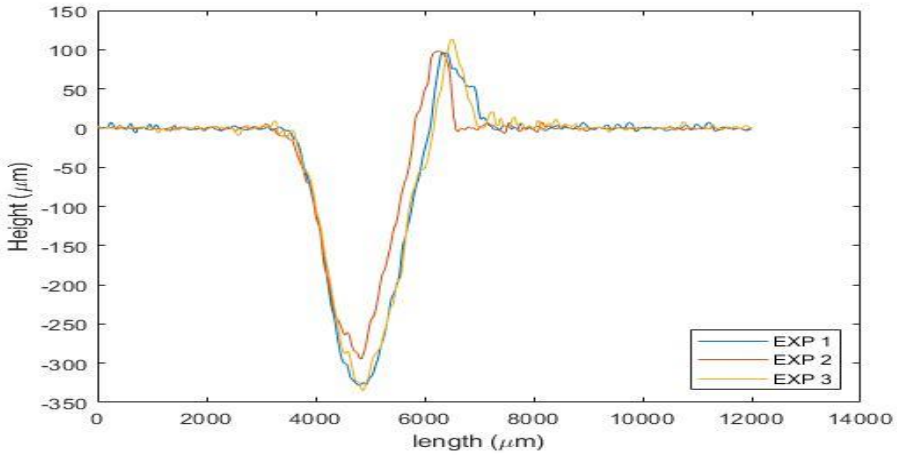
(b)


Height (μm)
length (μm)
EXP 1
EXP 2
EXP 3

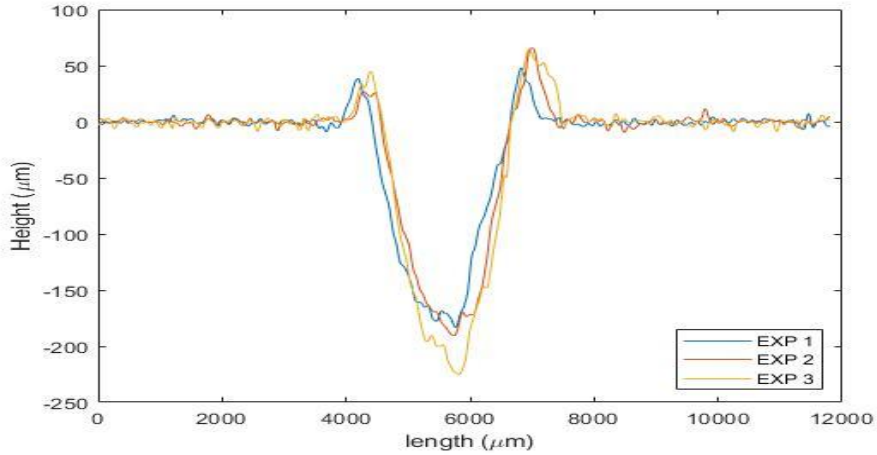
(c)


Height (μm)
length (μm)
EXP 1
EXP 2
EXP 3

(d)



(e)



(f)

Fig. 5-4: Surface profile and maximum depth at an angle of Impingement of: (a) 10°, (b) 20°, (c) 30°, (d) 45°, (e) 60°, and (f) 90°.

5.1.2 Erosion of Brittle Material

Brittle materials, as discussed earlier, have a different erosion mechanism that depends mainly on fracture. The brittle material chosen for this experiment is Borosilicate glass (also known as Pyrex). The dimensions of the eroded glass specimens are: 5.1cm by 5.1 cm by 0.635 cm (2in x 2in x 0.25in). Table 5-4 and Table 5-5 show the chemical composition and mechanical properties of borosilicate glass, respectively. Five angles of impingement were used, namely: 30°, 45°, 60°, 75°, and 90°. Five glass specimens were used for each angle of impingement. For each angle, the erosion duration of each experiment was

one minute, and each erosion experiment was repeated three times with a total number of 15 erosion experiments. A summary of the used experimental parameters is shown in Table 5-6. The material removal data for all erosion experiments is shown in Appendix I.

Table 5-4: Chemical composition of Borosilicate glass

Component	**Wt. %**
Aluminum Oxide	1-8%
Boron Trioxide	1-20%
Potassium Oxide	0-8%
Silicon Dioxide	70-87%
Sodium Oxide	0-15%

Table 5-5: Mechanical properties of borosilicate glass

Property	**Magnitude**
Density	2.21 g/cm^3
Modulus of Elasticity	63 GPa
Hardness	Knoop 418, KHN 100
Poisson's ratio	0.2
Compressive strength	2000 MPa
Ultimate Tensile Strength	280 MPa
Thermal conductivity	0.173 W/m-K @100°C
Maximum Temperature	230°C

As discussed earlier, brittle materials typically show the highest material removal at large impingement angles (60°-90°). The material removal of borosilicate glass as a function of angle of attack is shown in Fig. 5-5, where it can be seen that the typical brittle behavior occurred. All photomicrographs of erosion scars resulting from erosion experiments are shown in Appendix II. The optical and digital top views of eroded areas are shown in Fig. 5-6. It can be noticed that chipping of glass occurred at the edge of the erosion scar at 60˚ and 75˚ impingement angles. The chipping occurs when the abrasive particles leave the erosion scar, more material gets removed with the particles remaining momentum.

Table 5-6: Summary of testing parameters for erosion experiments on glass specimen

Parameter	**Magnitude**
Air pressure, P_{out}	200 kPa
Abrasive material	Silica sand
Abrasive size	200 µm
Abrasive flow rate	0.067 g/s
Standoff distance	10 mm
Nozzle diameter	1.5 mm
Erosion duration	60 seconds
Angle of attack	30˚, 45˚, 60˚, 75˚ and 90˚

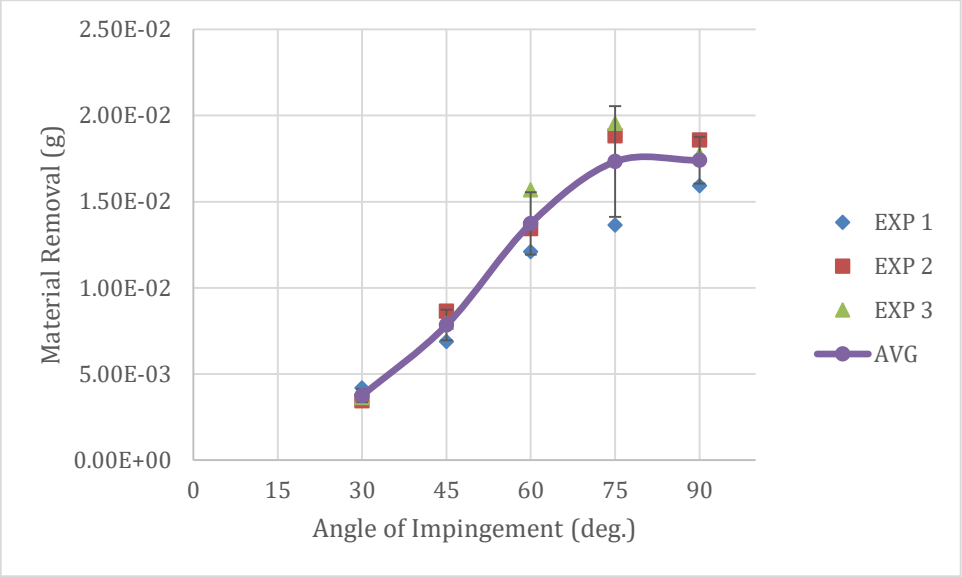
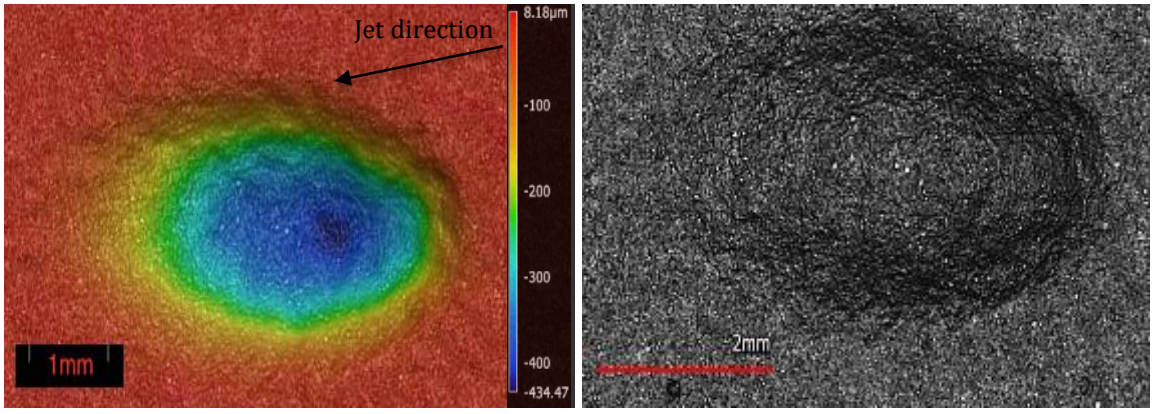
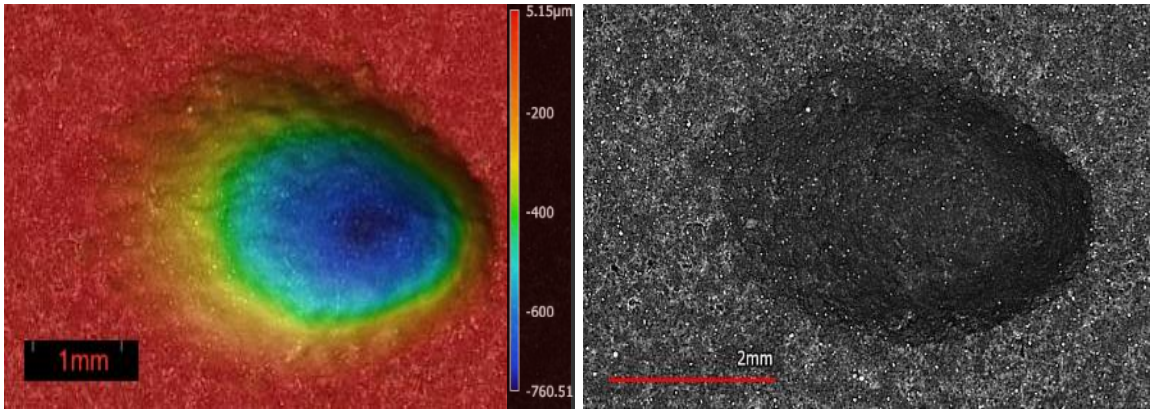


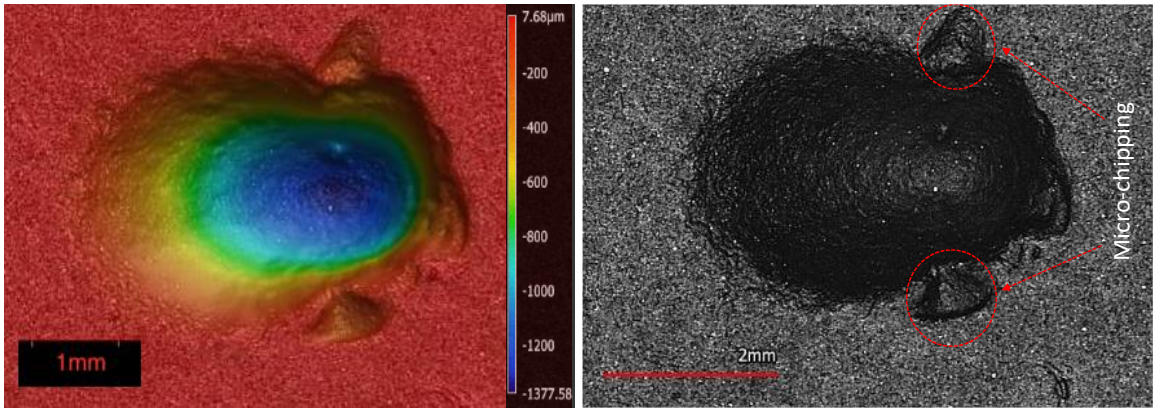
Fig. 5-5: Material removal of borosilicate glass as a function of angle of impingement.



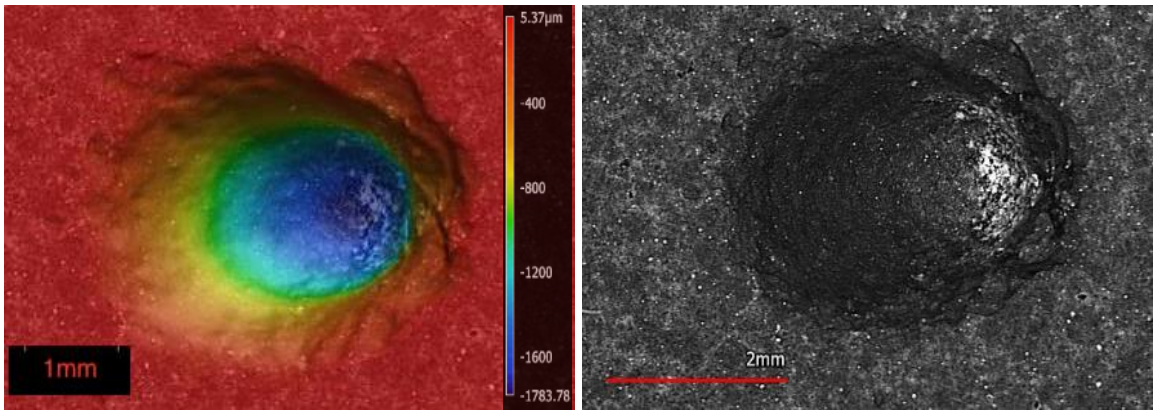
(a)


5.15µm
-200
-400
-600
-760.51
1mm
2mm

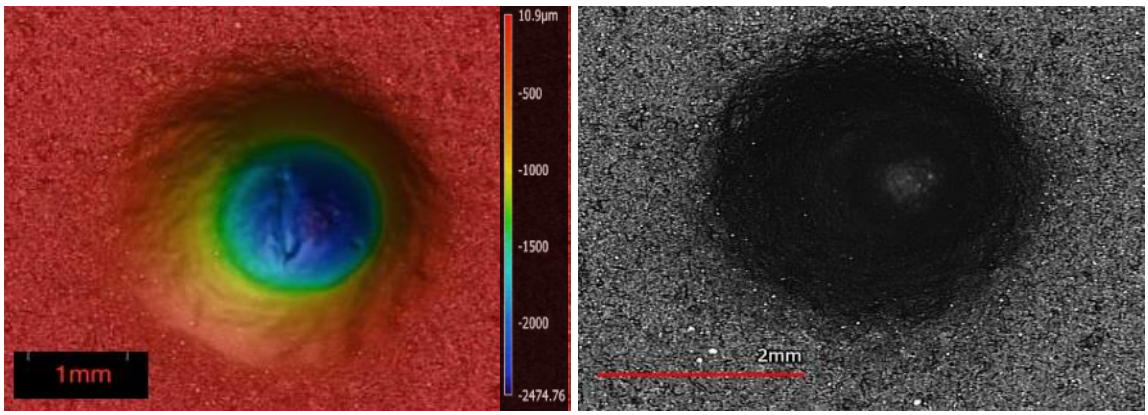
(b)


7.68µm
-200
-400
-600
-800
-1000
-1200
-1377.58
1mm
Micro-chipping
2mm

(c)


5.37µm
-400
-800
-1200
-1600
-1783.78
1mm
2mm

(d)



(e)

Fig. 5-6: Erosion pattern of glass's erosion scars at an angle of attack of: (a) 10°, (b) 20°, (c) 30°, (d) 45°, (e) 60°, and (f) 90°.

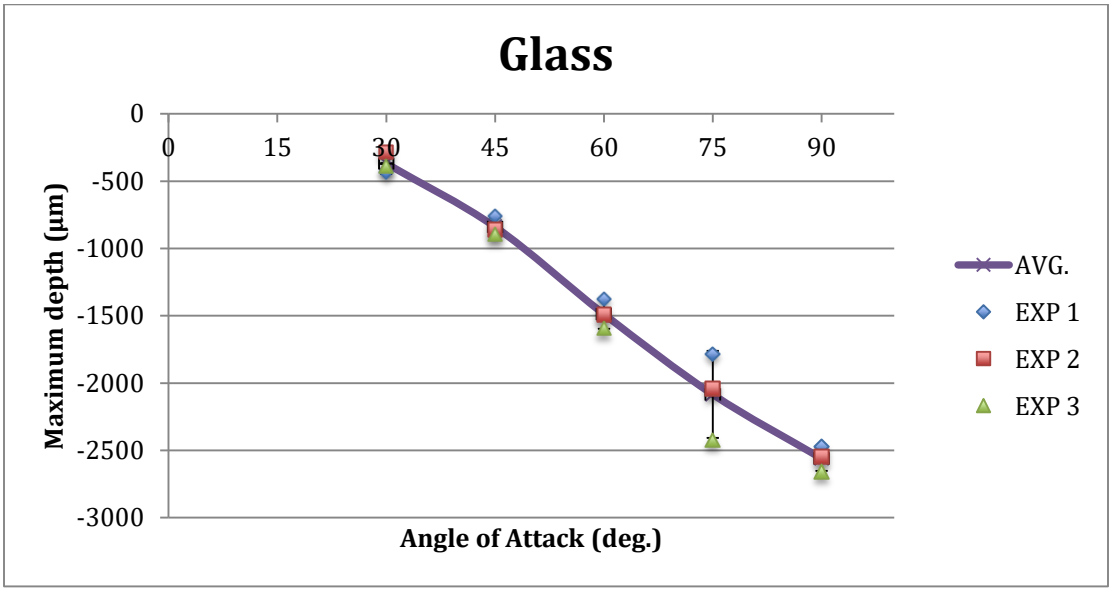


Fig. 5-7: Maximum depth of glass's erosion scars as a function of angle of attack

Contrary to the aluminum erosion result, the depth of erosion scars and the intensity of material removal are in agreement in terms of the impingement angle. The maximum erosion and maximum depth occur at 90˚, and they decrease as the angle becomes decreases. Fig. 5-7 shows the maximum depth as a function of the impingement angle for the three sets of experiments. The erosion scar profiles crossing through the maximum depth point for the eroded surfaces are shown in Fig. 5-8. The maximum depth data for all erosion scars is shown in Appendix III.

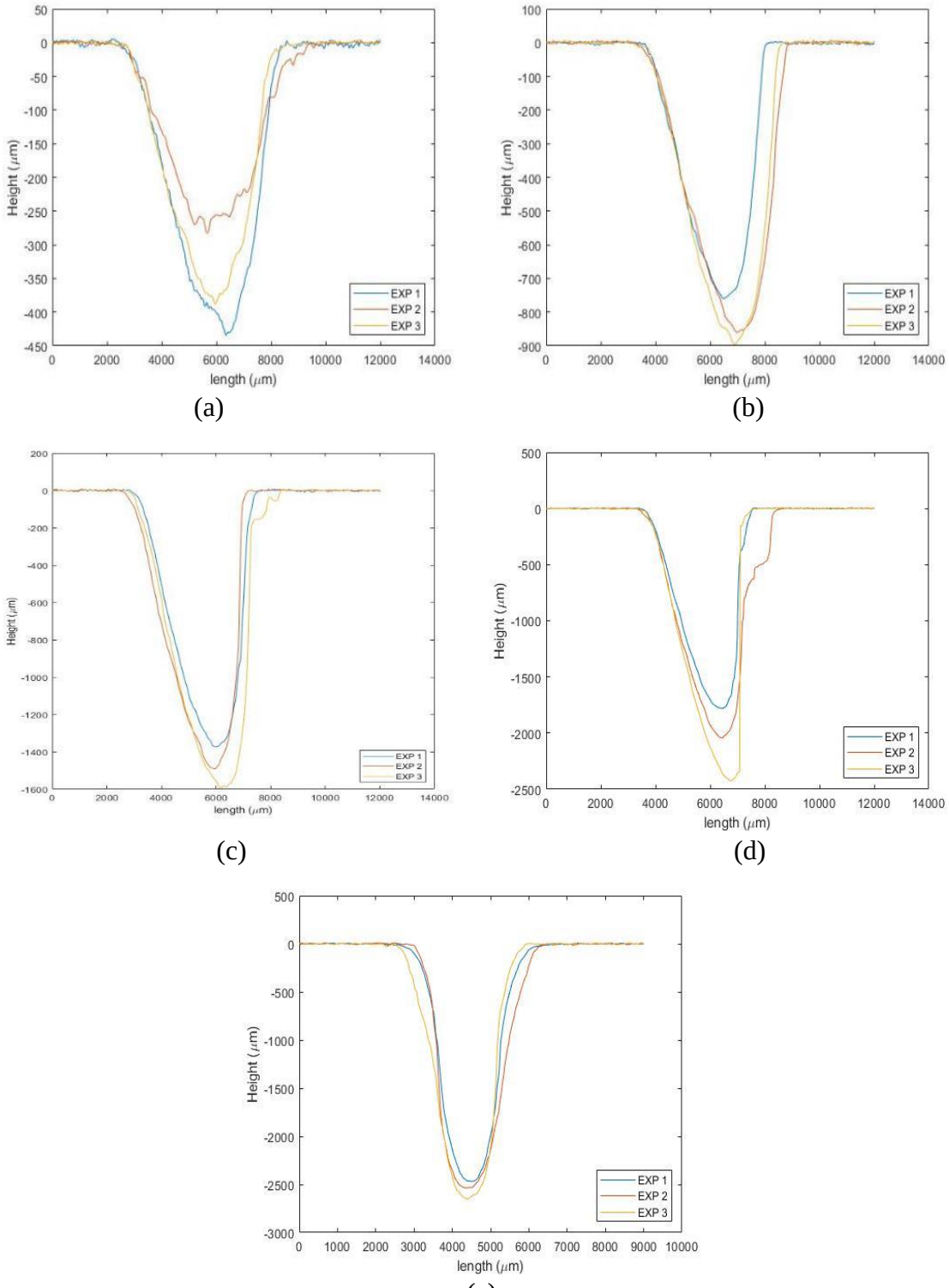


Fig. 5-8: Surface profiles for the three experimental sets at an angle of attack of: (a) 30˚, (b) 45˚, (c) 60˚, (d) 75˚, and (e) 90˚.

In summary, the erosion of ductile and brittle materials showed the typical and expected erosion behavior. Aluminum suffered the most loss of material at a 20˚ angle of impingement, while borosilicate glass showed the maximum loss at a 90˚ angle of impingement. Ductile and brittle materials tested prove the workability of the experimental setup of the erosion rig.

5.1.3 Erosion Experiments on GFRP

In this section, flat glass-fiber-reinforced Polymer (GFRP) will be investigated since wind turbine blades are typically made of GFRP. Both uncoated and coated GFRP with different coatings will be investigated to choose the best coating to use for wind turbine blades. To study the erosion behavior of composite materials, GFRP with 40% epoxy resin reinforced by woven 60% E-glass fibers is used. The mechanical properties of GFRP are shown in Table 5-7. One specimen has been used and it dimensions are 12.7 cm x 5.1 cm x 1.3 cm (5in x 2in x 0.5 in). Three sets of experiments have been conducted at five angles of impingement, namely: 30˚, 45˚, 60˚, 75˚, and 90˚. The effects of one more variable have been added to this investigation: erosion duration. Two erosion durations were investigated: 180 seconds and 360 seconds, which resulted in a total of 30 erosion experiment. A summary of the used experimental parameters is shown in Table 5-8. The material removal data for all erosion experiments is shown in Appendix I.

Table 5-7: Mechanical properties of GFRP

Property	**Magnitude**
Density	1.80 g/cm^3
Tensile Strength, MPa	262
Compressive strength, MPa	448
Flexural strength, MPa	448
Flexural modulus, GPa	16.5
Water absorption	0.1-0.15%
Hardness	115 Rockwell

The erosion of GFRP followed the expected trend and showed a semi-ductile erosion behavior. Fig. 5-9 shows the material removal of GFRP as a function of the angle of impingement. The removal rate increased as the impingement angle increased until it reached a maximum at 45˚, then decreased as the angle of impingement increased. Digital and optical top views of the eroded areas are shown in Fig. 5-10. It can be seen that compared to the digital and optical top views of ductile and brittle materials, GFRP followed a similar pattern of that of brittle material in terms of showing no plastic deformation or rippling, where no displacement of material can be seen but only material removal. All photomicrographs of erosion scars resulting from erosion experiments are shown in Appendix II.

Table 5-8: Summary of testing parameters for erosion experiments on GFRP specimen

Parameter	**Magnitude**
Air pressure, P_{out}	200 kPa
Abrasive material	Silica sand
Abrasive size	200 µm
Abrasive flow rate	0.067 g/s
Standoff distance	10 mm
Nozzle diameter	1.5 mm
Erosion duration	180 and 360 seconds
Angle of attack	30˚, 45˚, 60˚, 75˚ and 90˚

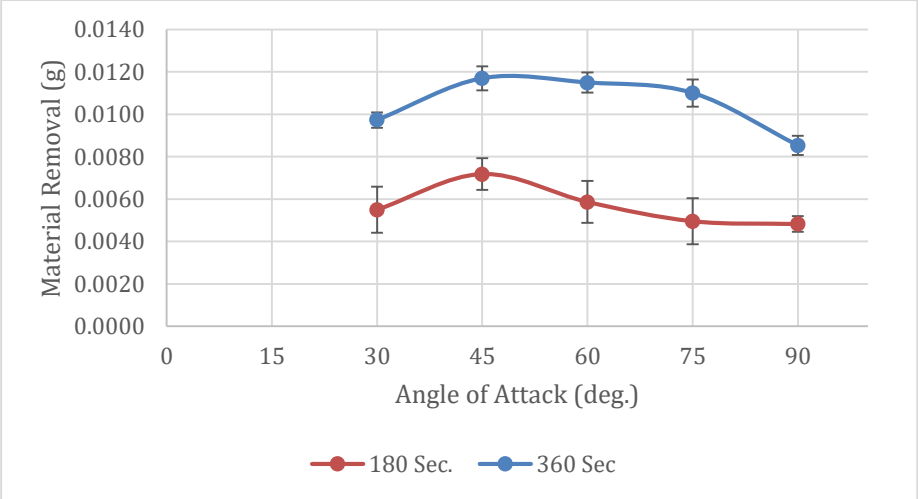
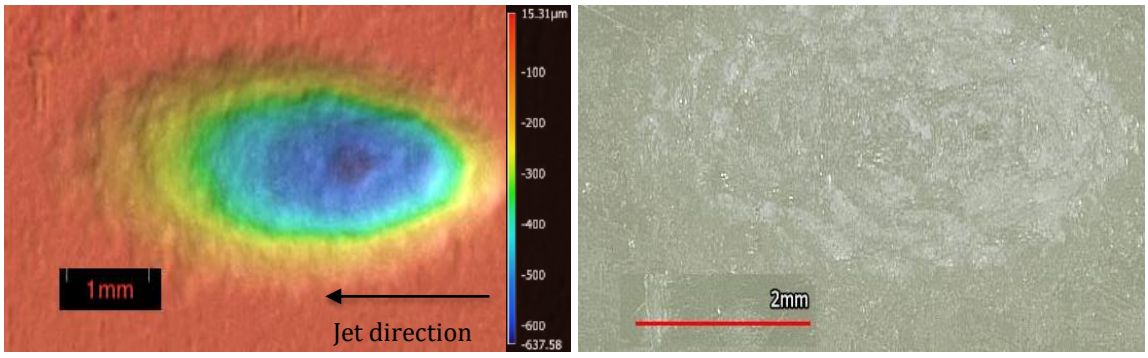
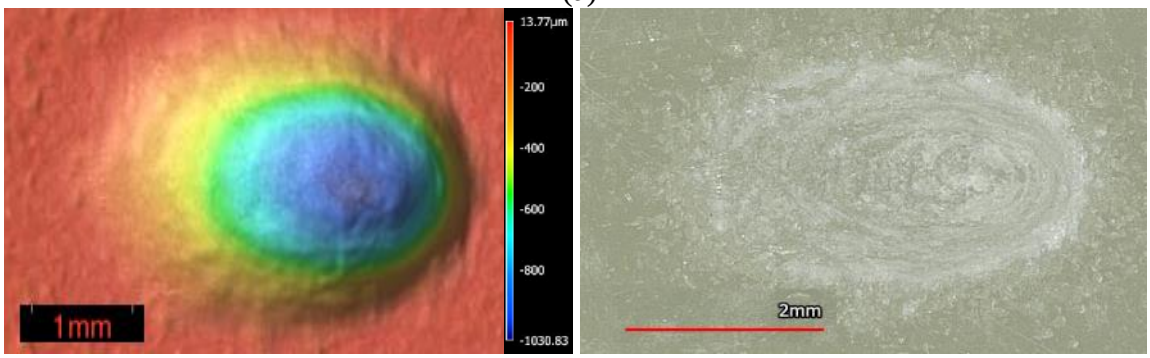


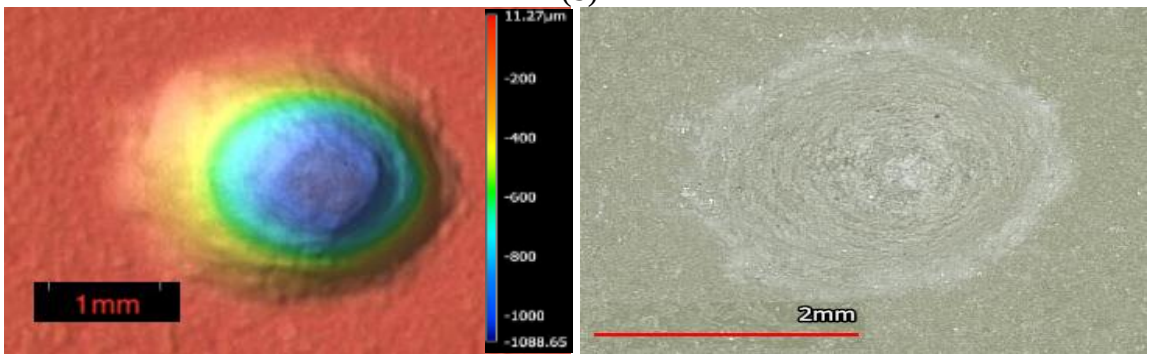
Fig. 5-9: Material removal of uncoated GFRP as a function of angle of attack.


15.31µm
-100
-200
-300
-400
-500
-600
-637.58
1mm
Jet direction
2mm

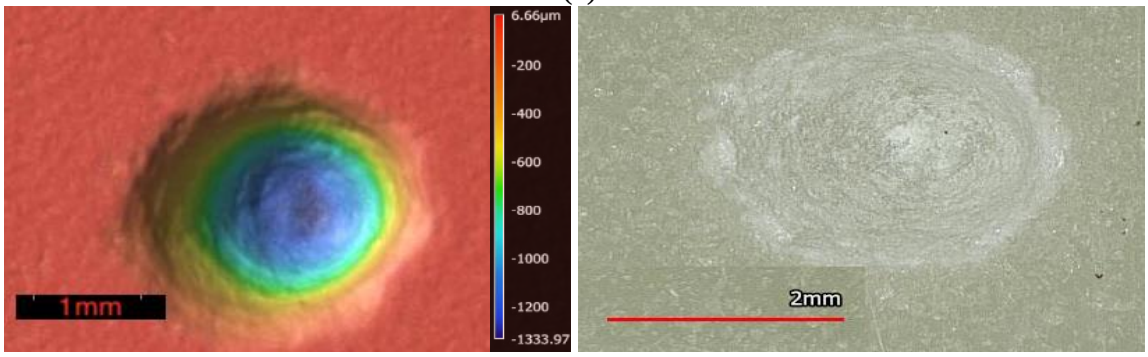
(a)


13.77µm
-200
-400
-600
-800
-1030.83
1mm
2mm

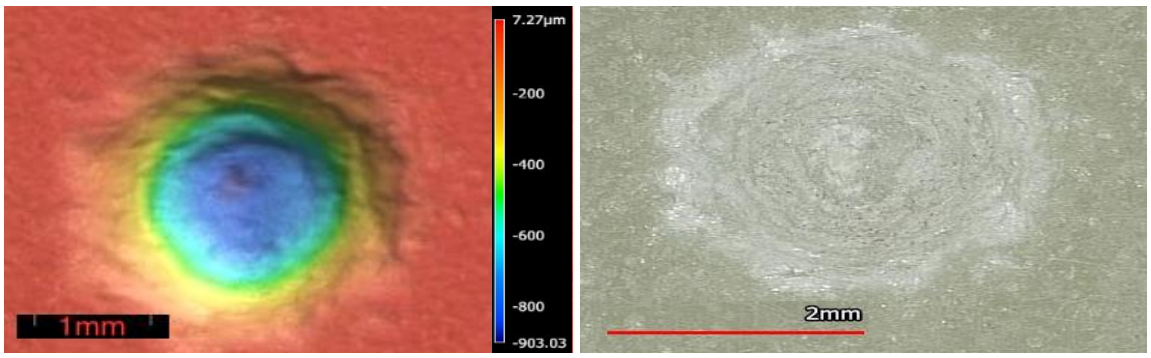
(b)


11.27µm
-200
-400
-600
-800
-1000
-1088.65
1mm
2mm

(c)


6.66µm
-200
-400
-600
-800
-1000
-1200
-1333.97
1mm
2mm

(d)



(e)

Fig. 5-10: Erosion pattern of GFRP's erosion scars at an angle of attack of: (a) 30˚, (b) 45˚, (c) 60˚, (d) 75˚, and (e) 90˚.

The depth of erosion scars resulting from the incoming abrasive particles as a function of angle of impingement is shown in Fig. 5-11. Compared to ductile and brittle behavior, the maximum depth occurred at an angle of 60˚, which is lower than that of brittle materials and higher than ductile materials. The erosion scar profiles passing through the maximum depth for each erosion experiment at every angle are shown in Fig. 5-12. The maximum depth data for all erosion scars is shown in Appendix III.

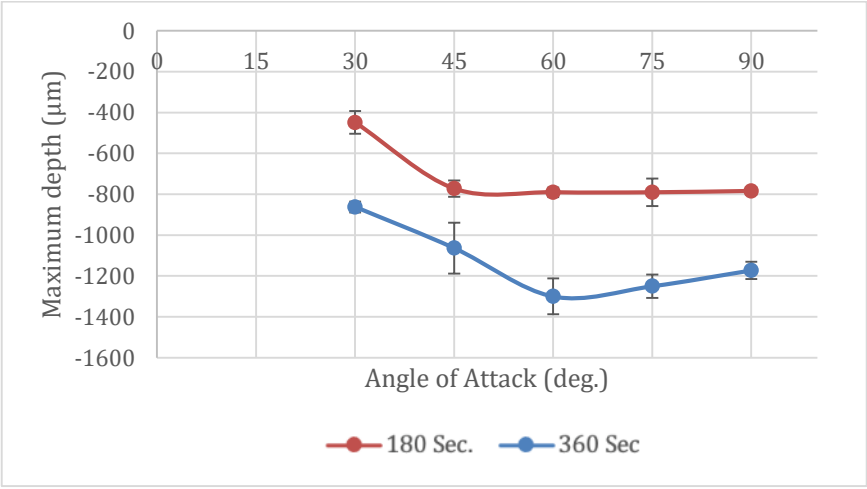


Fig. 5-11: Maximum depth of GFRP's erosion scars as a function of angle of attack

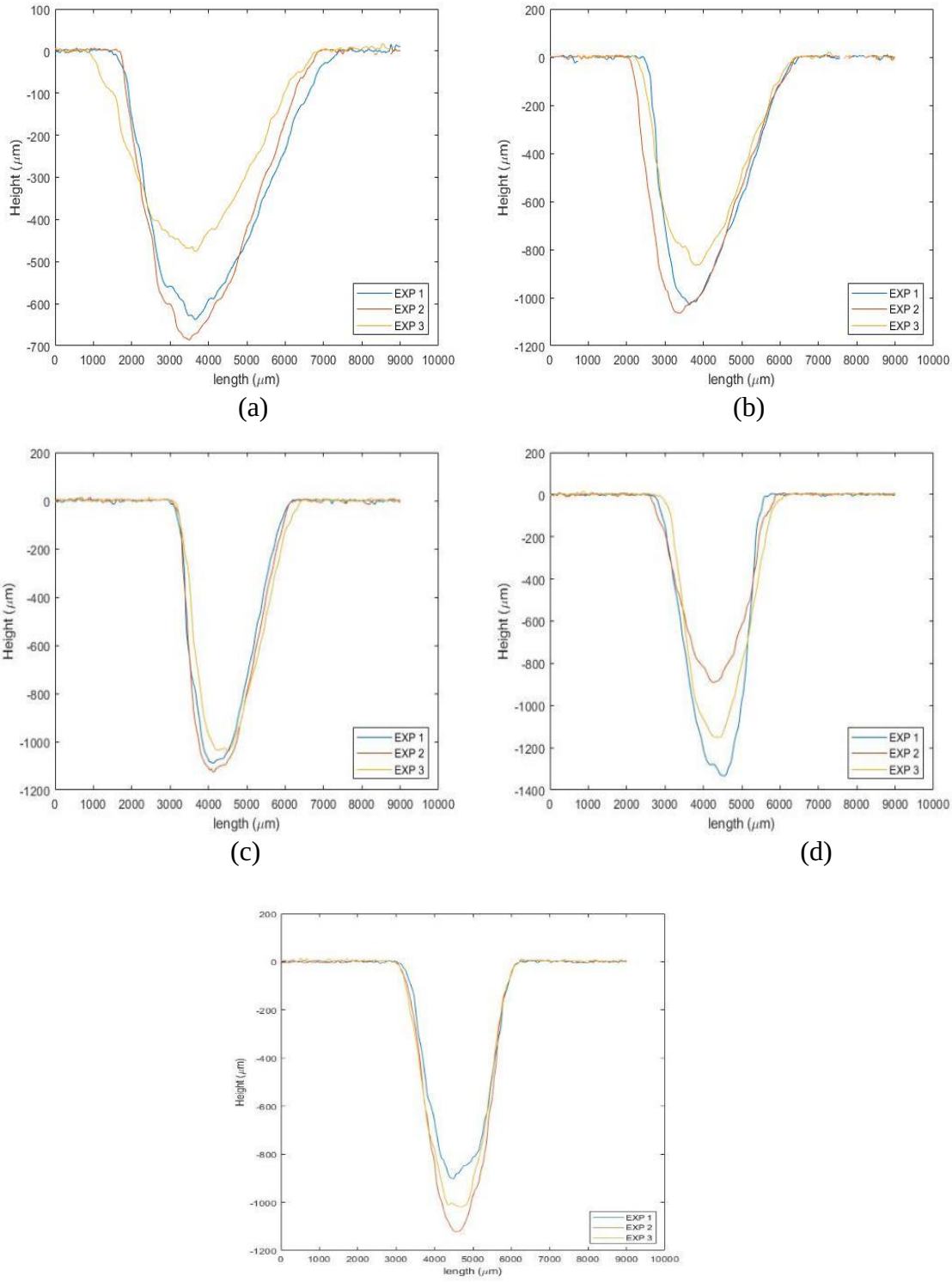
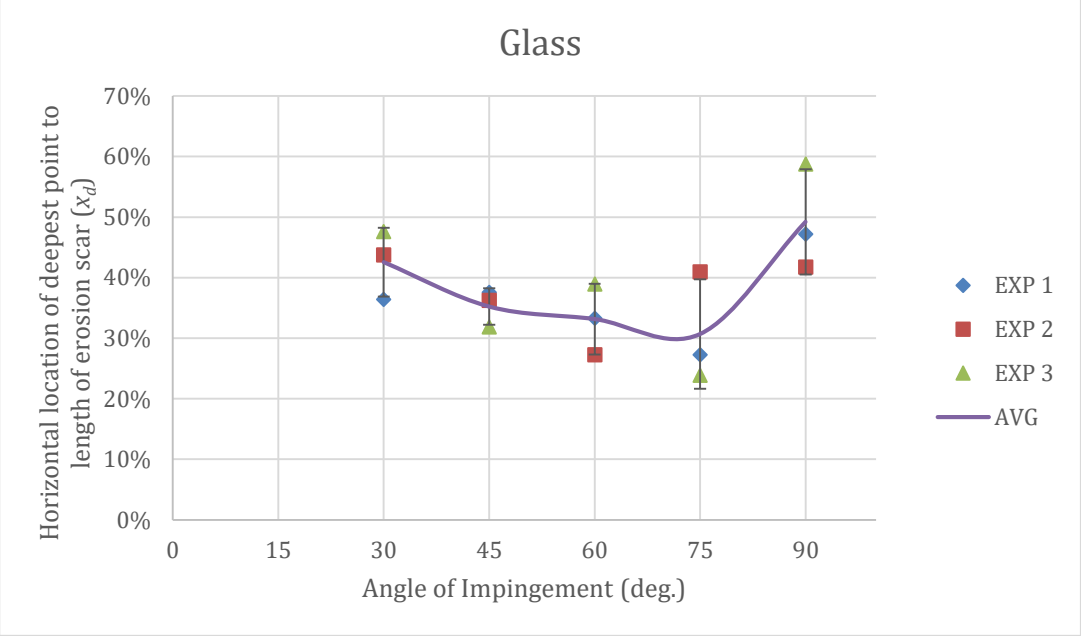
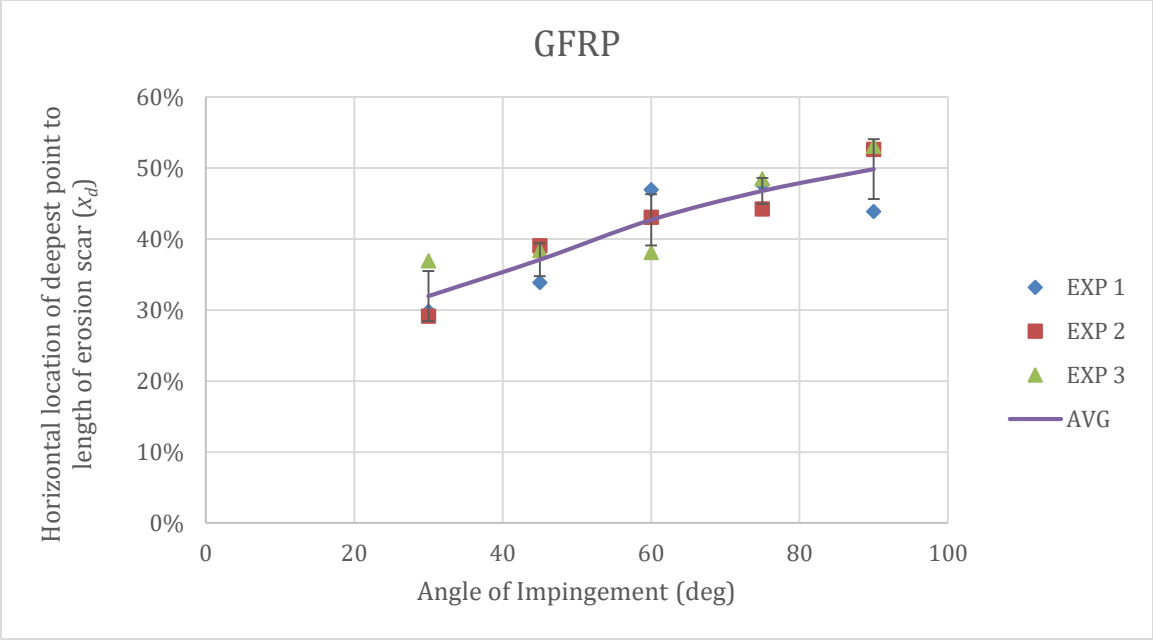


Fig. 5-12: Surface profiles for the three experimental sets at an angle of attack of: (a) 30˚, (b) 45˚, (c) 60˚, (d) 75˚, and (e) 90˚.

When studying the horizontal location of the deepest point in the erosion scar (x_d) as a percentage of the total length of erosion scar (x_T) it has been found that the angle of attack plays a major role. Also, it has been found that the type of material under study also has an effect on x_d, as can be seen in Fig. 5-13, which shows the behavior of the glass specimen and the uncoated GFRP. For the glass specimen, x_d started at around 45% for 30˚ angle of impingement and decreased to 30% for 75˚ and then increased up to 50% at 90˚. The decrease in x_d especially at 60˚ and 75˚ angles of impingement can be attributed to the micro-chipping phenomenon discussed in Fig. 5-6. On the other hand, x_d for GFRP specimen shows a linear increase from around 33% at 30˚ angle of impingement to 50% for 90˚ angle of impingement.



(a)



(b)

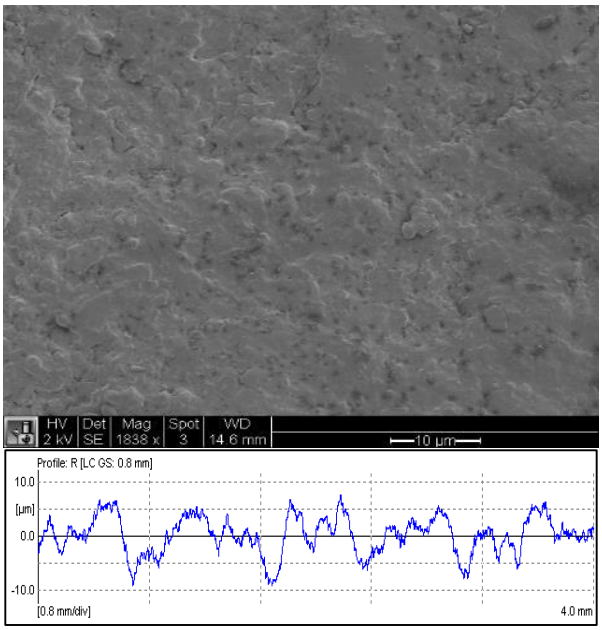
Fig. 5-13: Horizontal location of deepest point to length of erosion scar (x_d) as a function of angle of impingement for: (a) glass, and (b) GFRP

5.2 Erosion of coated surfaces

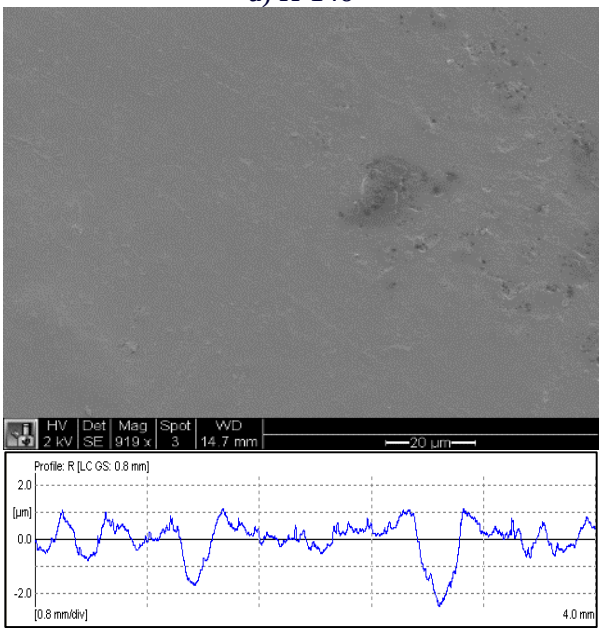
Three types of coatings have been used in this experiment: Polyurethane, H-146, and IA-700. The polyurethane used is an aliphatic acrylic polyurethane called Carbothane® 134 HG, conventionally sprayed with a coating thickness of 50 µm. The second coating used is H-146®, developed by NIC Industries, a ceramic-based coating with infused graphene that shows an excellent impact and abrasion resistance. The thickness of the H-146 coating layer is 25 µm. The last coating used in this experiment is IA-700, a graphene-infused coating developed by IA Coatings[1]. The thickness of the IA-700 coating layer is 75 µm. These three coatings are commercially available, and thus the chemical compositions cannot be disclosed here due to proprietary rights. Some of the mechanical properties of the

[1] IA Coatings, 16310 Hollister St, Houston, TX 77066. Phone: 832-666-3143,
Email: info@iacoatings.com

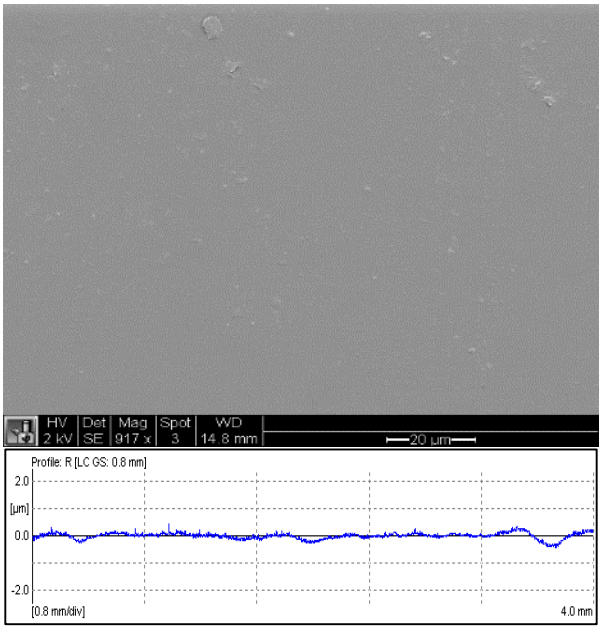
polyurethane coating and H-146 are shown in Table 5-9 and Table 5-10, respectively. The mechanical properties of IA-700 are not available yet since it is still under study. Fig. 5-14 shows scanning electron microscope (SEM) images of the surface of the three coatings.



a) H-146



b) IA-700



c) Polyurethane

Fig. 5-14: SEM images of the surface of: a) H-146, b) IA-700, and c) Polyurethane

The hardness of the coating layer has been measured using AMH43 Automatic Micro/Macro-indentation. The indentation microhardness test is a well-known and reliable measurement technique for coating hardness if the indentation depth does not exceed one-tenth of the coating thickness [178, 179]. If the indention does exceed this ratio, then the measured hardness is influenced by the substrate and no longer a characterization of the coating hardness. In order to determine the true hardness of the coating, the contribution of the substrate and the coating must be separated. Numerous mechanical and empirical models have been proposed based on a linear additive law called "series relation," which expresses the composite/measured hardness H_C as a function of the substrate hardness H_S and the film hardness H_F, as follows [180]:

$$H_C = H_S + z\,(H_F - H_S) \tag{5-1}$$

where z is the film influence coefficient

In a model proposed by Jönsson and Hogmark [181], z is defined as:

$$z = 2C\frac{t_c}{t_d} - C^2(\frac{t_c}{t_d})^2 \quad (5\text{-}2)$$

where t_c: coating thickness t_d: depth of indentation $C = \sin^2 22^\circ$

Using a Vickers indenter, the hardness of H-146, IA-700, and Polyurethane are (in MPa) 1160, 289, and 179, respectively. The indentation depth was calculated to ensure that the indenter did not penetrate through the coating layer using the following equation [182]:

$$t_d = \frac{t_c}{7} \quad (5\text{-}3)$$

The depth of indentation has been found to be (in μm) 19.1, 27.2, and 47.3 for H-146, IA-700, and Polyurethane, respectively.

Table 5-9: Mechanical Properties of the polyurethane coating [183].

Property	**Magnitude**
Adhesion Cross-Cut Tape (ASTM D3359)	5A
Adhesion (ASTM D4060)	70 mg. loss after 1000 cycles, CS17 wheel
Impact Resistance (ASTM D2794)	17.5 J
5% Salt Spray (ASTM B117)	No rusting, blistering, loss of bond or any measurable creepage from the scribe after 3000 hours.
Density	0.26 g/cm^3
Accelerated Weathering (ASTM G53, ASTM D4587)	No rusting, blistering or loss of adhesion; less than 5% gloss loss after 3000 hours

Table 5-10: Mechanical properties of H-146 coating [184].

Property	**Magnitude**
Adhesion Cross-Cut Tape (ASTM D3359)	5B
Impact (ASTM D2794)	18 J
5% Salt Spray (ASTM B117)	2,280 hours
Density (g/cm^3)	1.41
Abrasion (ASTM D4060)	6,666 cycles per mil
Viscosity (Brookfield Viscometer)	105.85 cP
Pencil Hardness (ASTM D3363)	9h
Scratch Hardness (ASTM D3363)	7h
Mandrel Bend (ASTM D522)	No coating loss with 180 rotations
Coefficient of friction (ASTM D1984)	0.233

Each of these three coatings was either used as a single layer coating or as part of a multi-layered coating system combined with one of the other coatings. Single- and multilayered coated targets have been eroded and compared to an uncoated specimen. A combination of the three mentioned coatings has been used for the multilayer coatings and presented in Table 5-11. As shown in Table 5-11, the combination of H-146 and Polyurethane is present in Coating 4, while the combination of IA-700 and Polyurethane is present in Coatings 5 and 7. The purpose of combining the graphene and polyurethane coatings in different order is to study the effects of having a softer or harder coating layer at the top on the solid particle erosion behavior. The cross-section of each of these coating combinations is shown in Fig. 5-15. Another coating combination was considered for this study, with Polyurethane as a top layer and H-146 as a base layer. However, as soon as the erosion experiments took place, the top coating layer got peeled off the base layer as shown in Fig. 5-16, which indicated a poor adhesion between the top and base layers. As a result, this coating combination was removed from the study. Similar to the uncoated GFRP specimen, all of the coated specimens were eroded at five angles of impingement: 30˚, 45˚, 60˚, 75˚, and 90˚ for two erosion durations: 180 seconds and 360 seconds.

Table 5-11: Single and multilayer coatings of graphene and polyurethane

Coating #	**Base layer**	**Top Layer**	**Total thickness (µm)**
1	H-146	---	25
2	IA-700	---	75
3	Polyurethane	---	50
4	Polyurethane	H-146	75
5	Polyurethane	IA-700	125
6	Polyurethane	Polyurethane	100
7	IA-700	Polyurethane	125

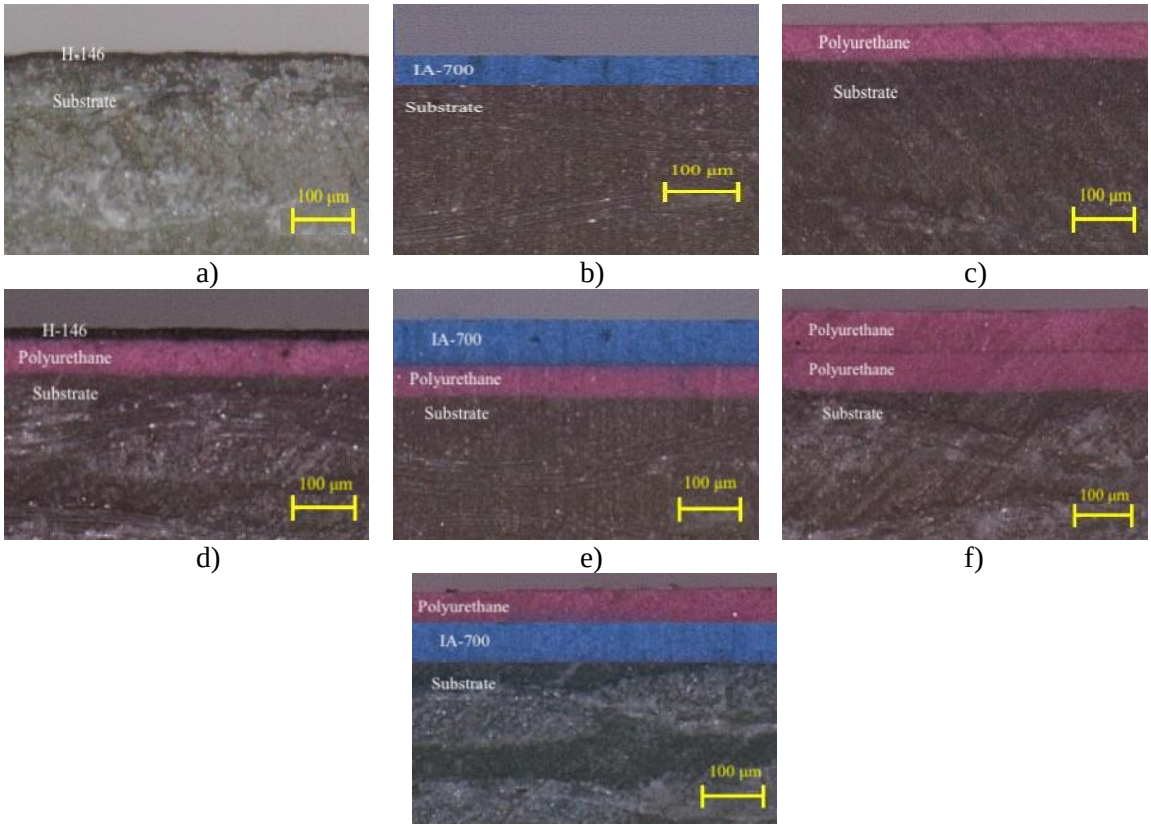


Fig. 5-15: Cross section of coating systems: a) H-146, b) IA-700, c) Polyurethane, d) Coating 4, e) Coating 5, f) Coating 6, and g) Coating 7.

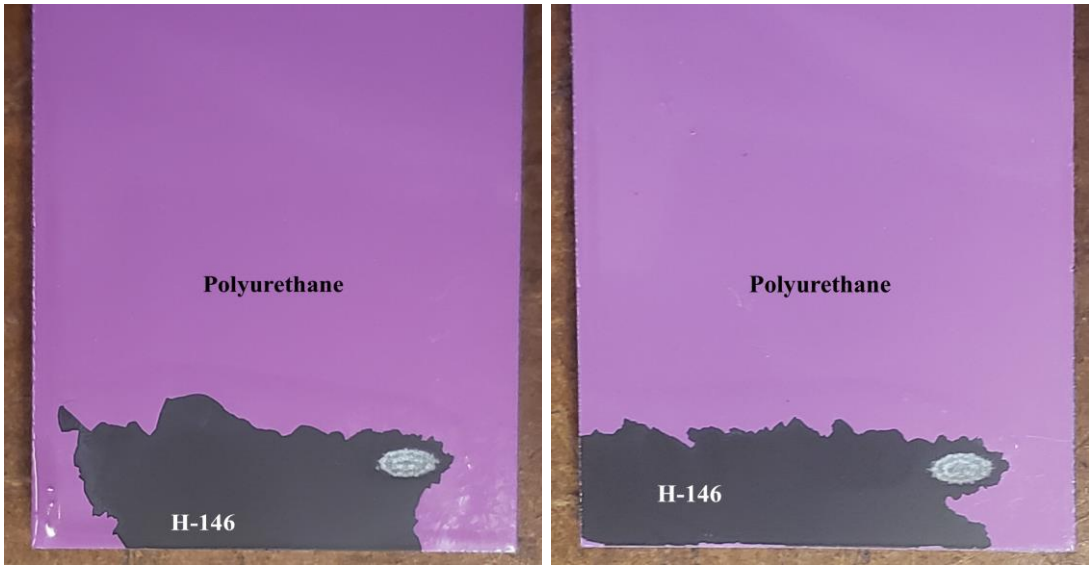
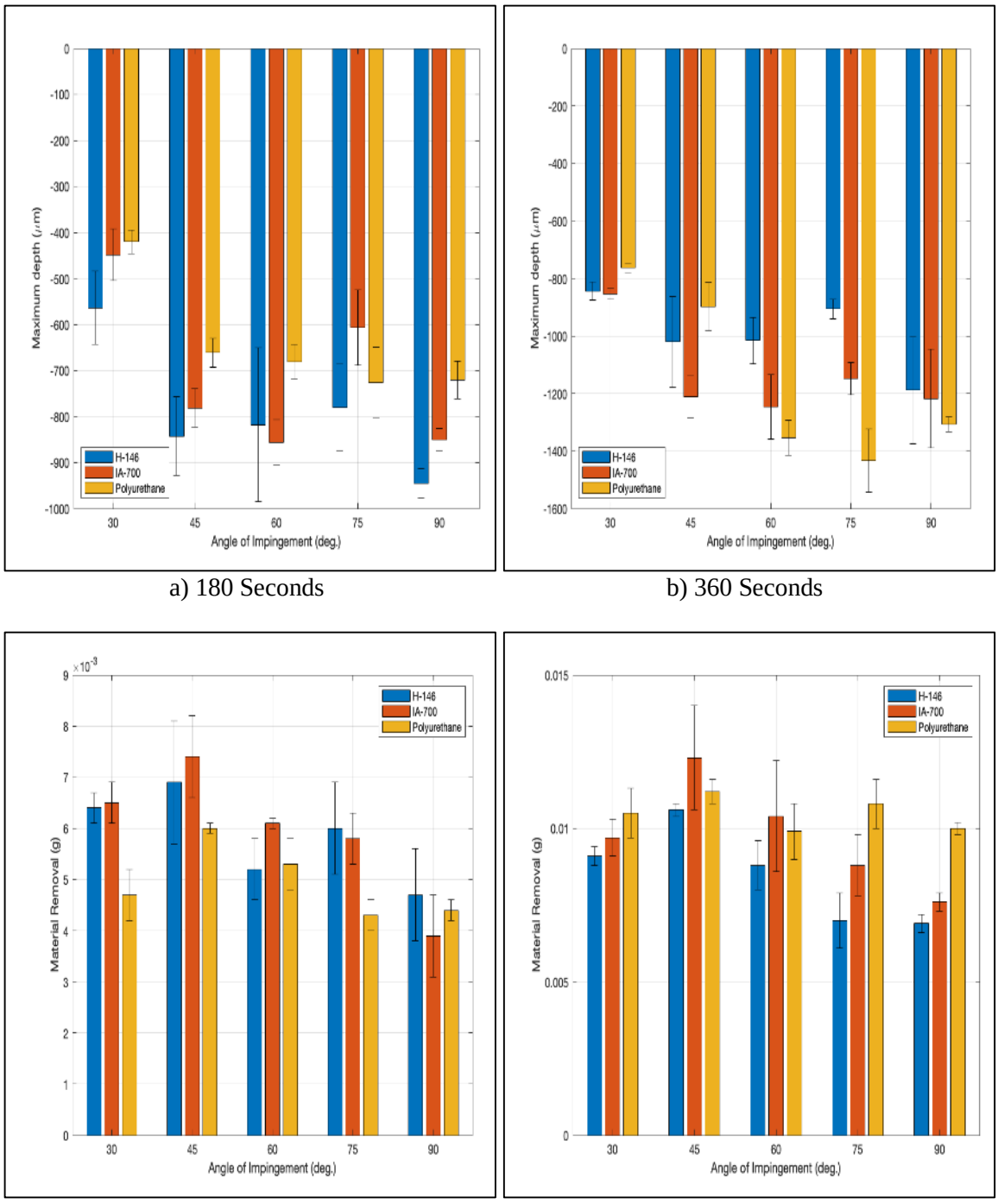


Fig. 5-16: Polyurethane layer getting removed from the top of H-146 layer

5.2.1 Erosion of single layer coated surfaces

Three GFRP specimens have been coated with a single layer of H-146, IA-700, and Polyurethane. The maximum depth of the three coatings as a function of the angle of impingement for the 180- and 360- seconds erosion durations is shown in Fig. 5-17 (a) and (b), while Fig. 5-17 (c) and (d) show the material removal behavior for the 180- and 360-seconds erosion duration, respectively. Material removal data for all erosion experiments is shown in Appendix I, while maximum depth data is shown in Appendix III. In terms of material removal, the maximum material removal occurred at 45˚, similar to the uncoated specimen for all three coatings. After 360 seconds of erosion, H-146 has shown the best erosion resistance behavior, and both graphene coatings showed better erosion resistance behavior than Polyurethane at high angles of impingement. Also, it can be noticed that the maximum depth for the polyurethane coating occurred at 75˚for both erosion durations, while for the graphene coatings, it remained similar to the uncoated specimen at 60˚. Table 5-12 shows optical photographs of typical erosion scars of the uncoated specimen and the three single-layer coated specimens. It is clear how the shape of the erosion scars shifts from shallow and elliptical at 30˚ and 45˚ toward more deep and circular shape for 60˚ - 90˚ angles of impingement.



a) 180 Seconds

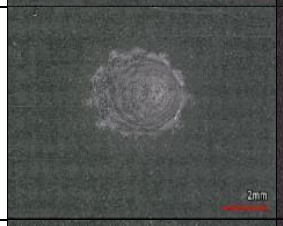
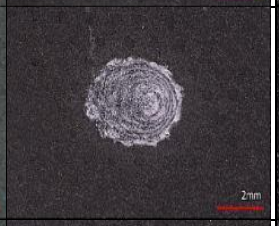
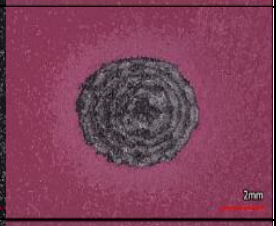
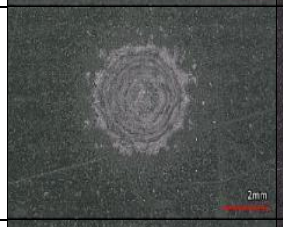
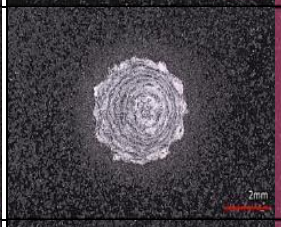
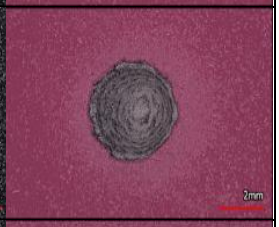
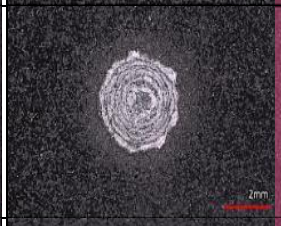
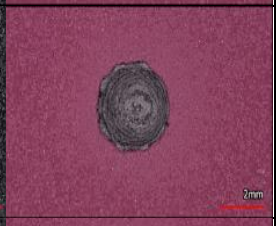
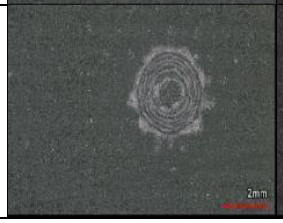
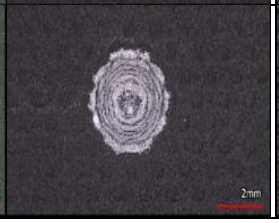
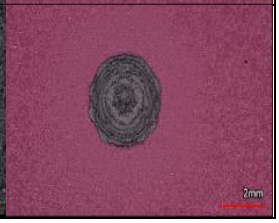
b) 360 Seconds

c) 180 Seconds

d) 360 Seconds

Fig. 5-17: Analysis of single layer of coatings as a function of angle of attack a) maximum depth at 180 sec, and b) maximum depth at 360 sec, c) material removal at 180 sec, and d) material removal at 360 sec

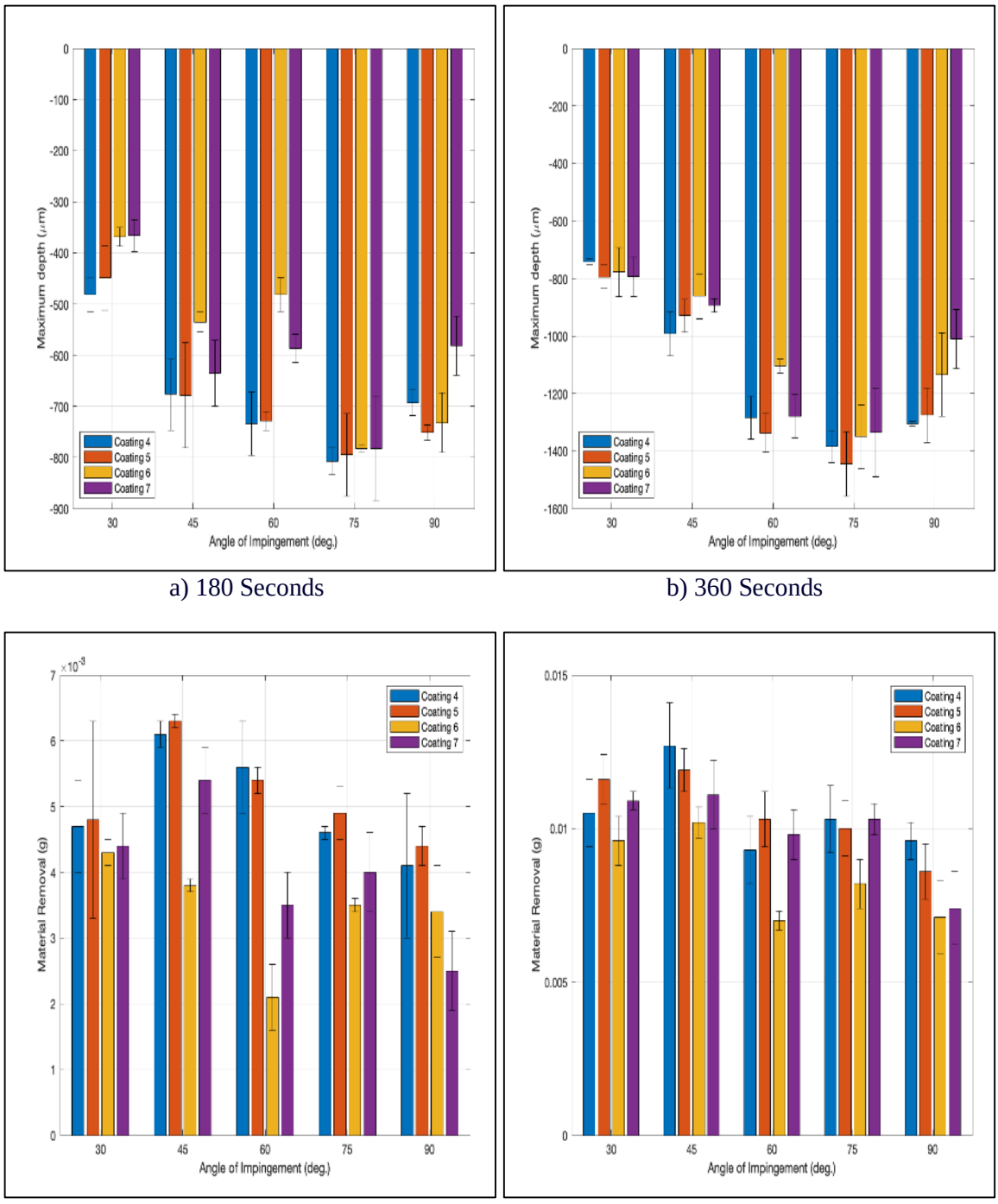
Table 5-12: Optical photographs of typical erosion scars shape for the uncoated specimen, specimens coated with H-146, IA-700, and polyurethane.

AOA	Uncoated	H-146	IA-700	Polyurethane
30˚				
45˚				
60˚				
75˚				
90˚				

5.2.2 Erosion of Multi-layer coated surfaces

The following analysis was on specimens coated with coatings 4 – 7 shown in Table 5-11. Fig. 5-18 (a-d) shows the maximum depth of the three coatings as a function of the angle of impingement for the 180 seconds (Fig. 5-18a) and 360 seconds (Fig. 5-18b) erosion durations, while Fig. 5-18c and 5-18d show the material removal behavior for the 180- and 360-seconds erosion duration, respectively. Material removal data for all erosion experiments is shown in Appendix I, while maximum depth data is shown in Appendix III. While

the erosion behavior stayed the same for the two erosion durations with the maximum material removal occurring at 45˚ angle of impingement, the maximum depth behavior has shifted for all the coatings at both erosion durations toward 75˚. After 360 seconds of erosion, Coating 6, which consists of two layers of Polyurethane, showed the best erosion resistance behavior, especially at low angles of attack. However, Coating 7 showed a shallower erosion scar at both erosion durations at 90˚ angle of impingement. Coating 4 and Coating 5 showed, in general, worse erosion resistance behavior than the other two coatings. Table 5-13 shows optical photographs of typical erosion scars of Coatings 4 – 7.



a) 180 Seconds

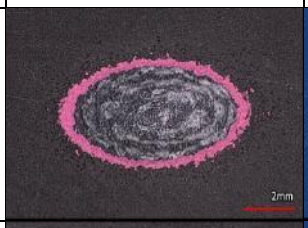
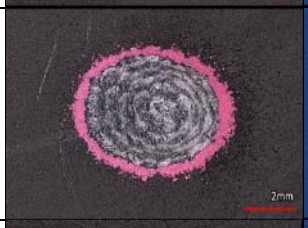
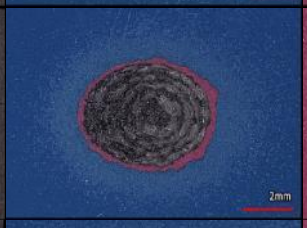
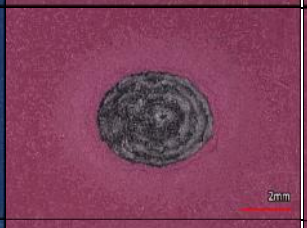
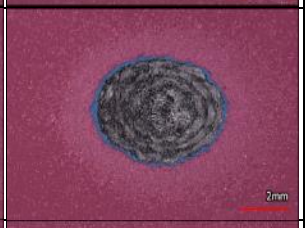
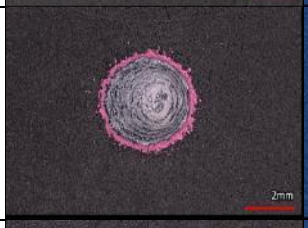
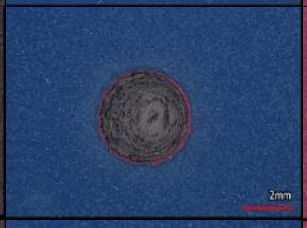
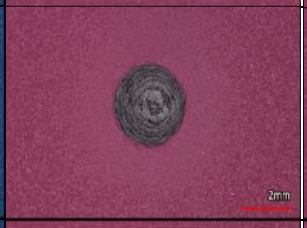
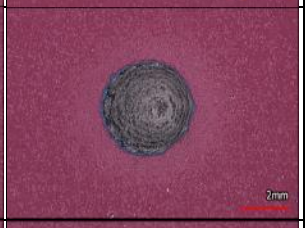
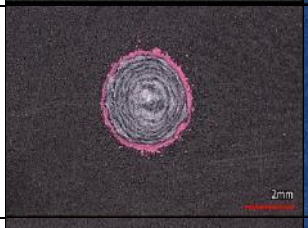
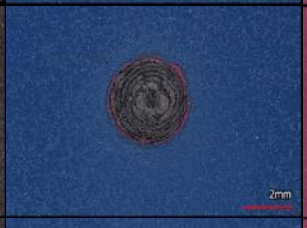
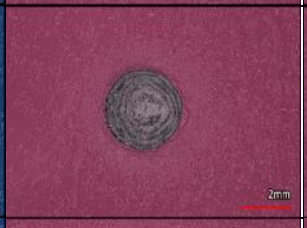
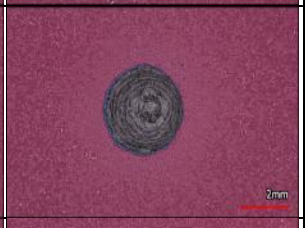
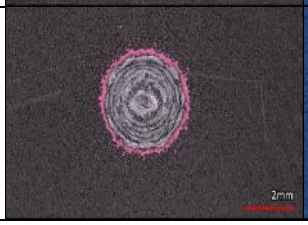
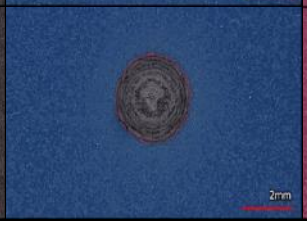
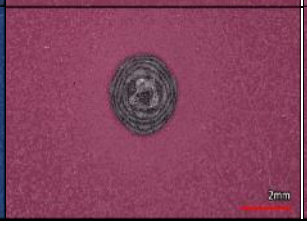
b) 360 Seconds

c) 180 Seconds

d) 360 Seconds

Fig. 5-18: Analysis of multilayer of coatings as a function of angle of attack a) maximum depth at 180 sec, and b) maximum depth at 360 sec, c) material removal at 180 sec, and d) material removal at 360 sec.

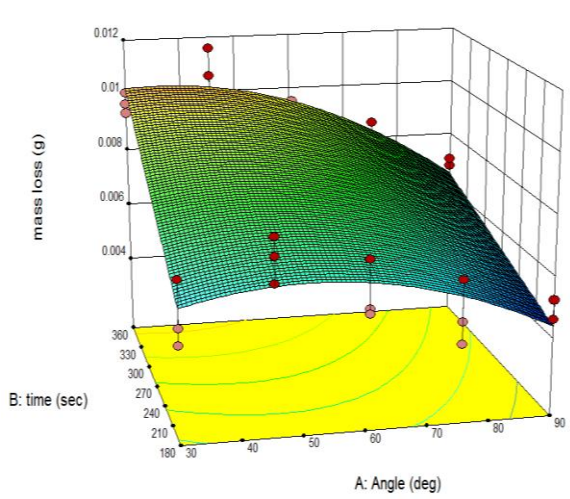
Table 5-13: Optical photographs of typical erosion scars shape of Coatings 4 – 7.

AOA	Coating 4	Coating 5	Coating 6	Coating 7
30˚				
45˚				
60˚				
75˚				
90˚				

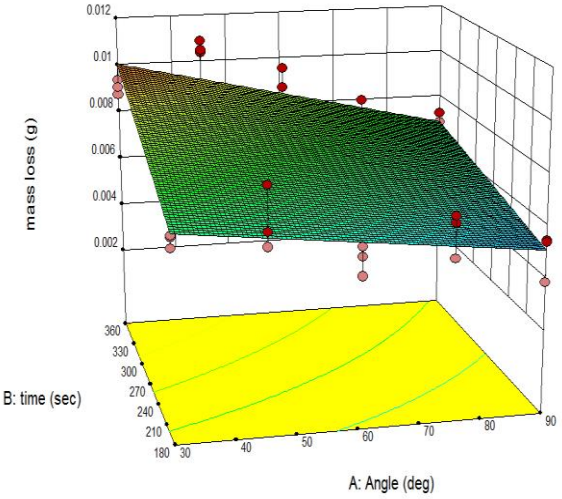
5.3 Discussion

Statistical Analysis of Variance (ANOVA) was used to study the behavior of uncoated, single-layer, and multilayer coated specimens. Angle of impingement and erosion duration were used as variables, while material removal and depth of erosion scars were used as outputs. Based on Response Surface modelling, Fig. 5-19 shows the material removal behavior while Fig. 5-20 shows the depth of erosion scar. It can be seen from both figures

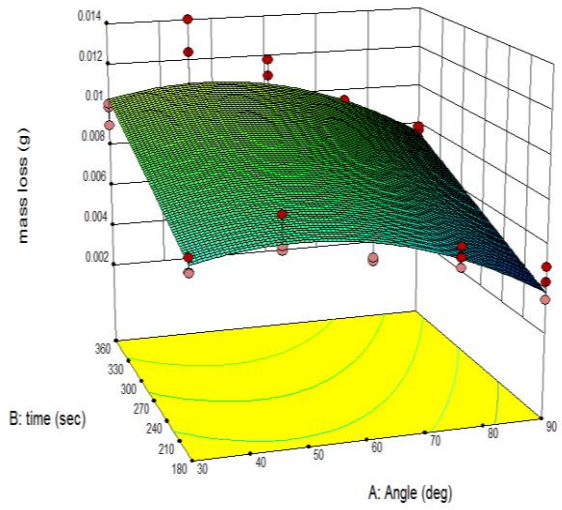
that the behavior changes with the change of the type of coatings used. The detailed ANOVA analysis is shown in Appendix IV.



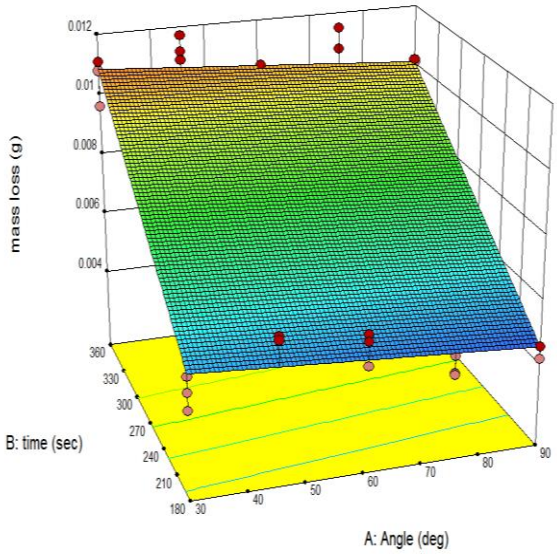
(a) Uncoated



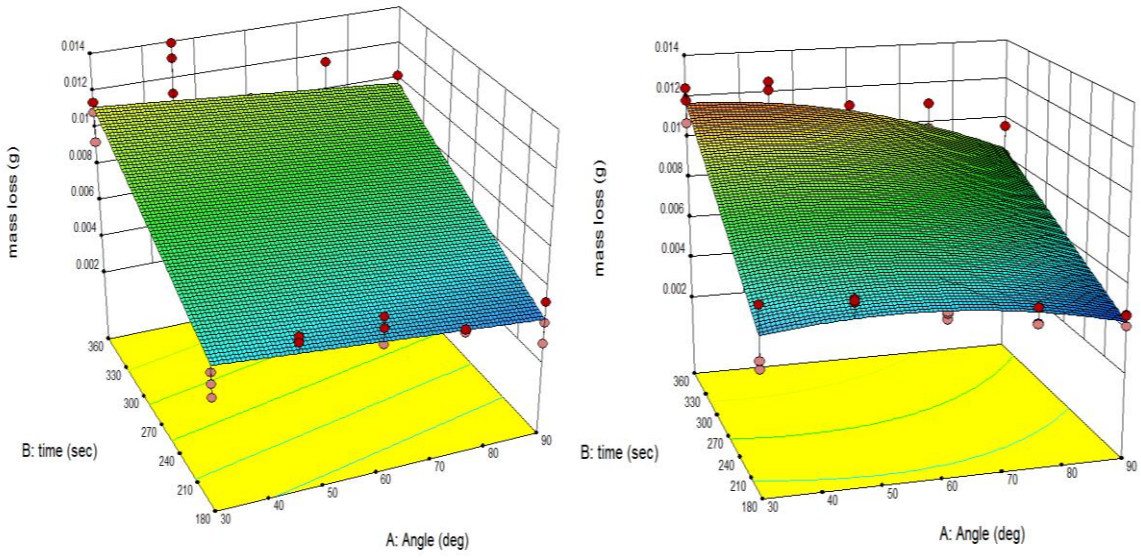
(b) H-146



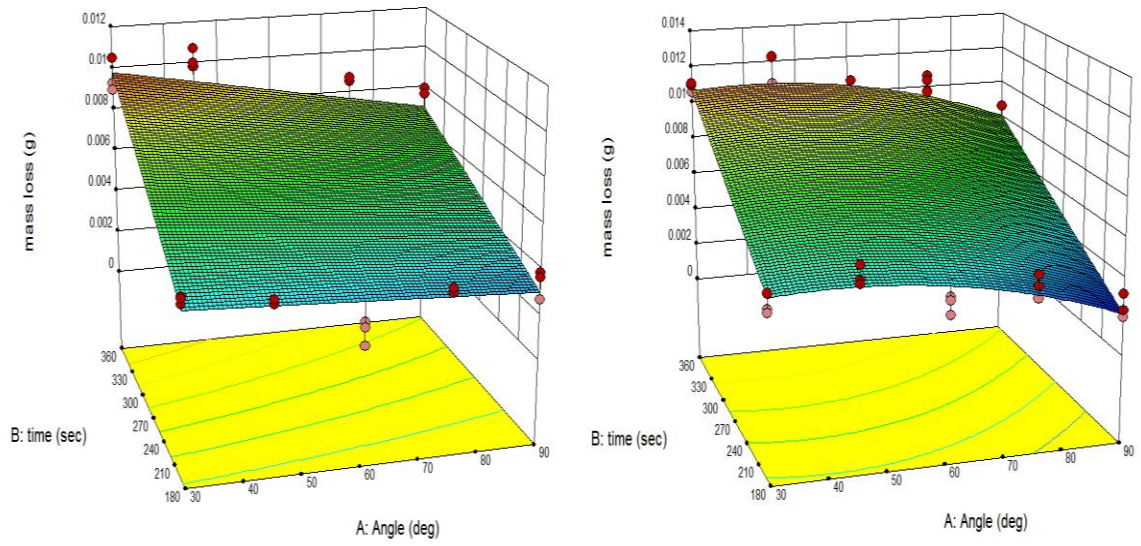
(c) IA-700



(d) Polyurethane

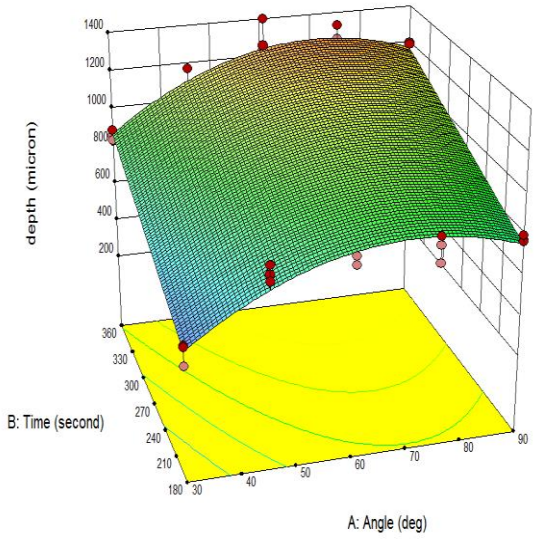


(e) Coating 4 (f) Coating 5

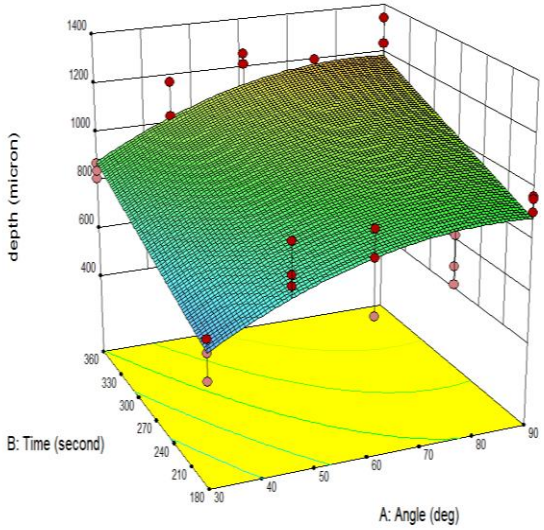


(g) Coating 6 (h) Coating 7

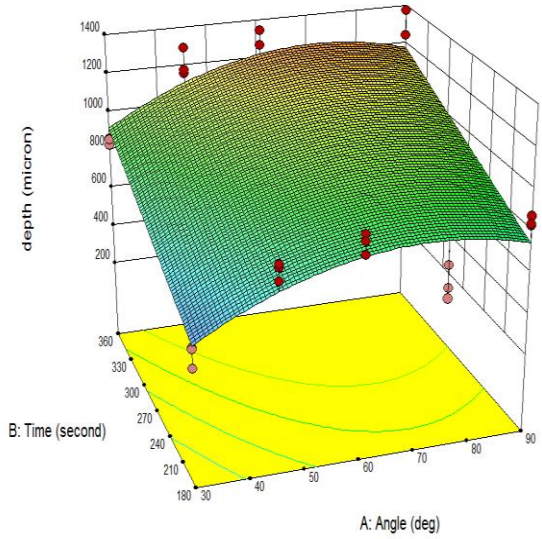
Fig. 5-19: Three-dimensional representation of material removal in terms of the angle of attack and erosion duration



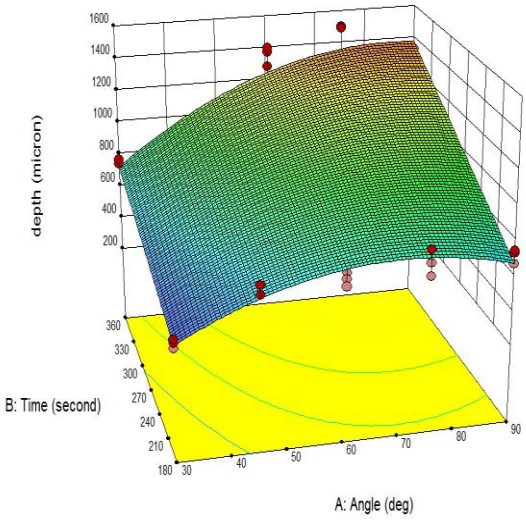
(a) Uncoated



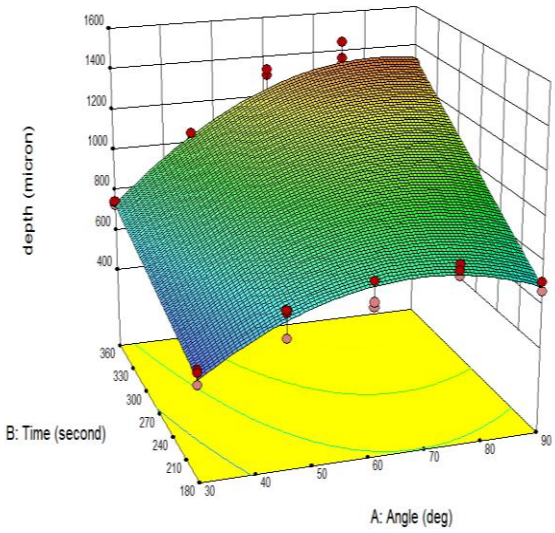
(b) H-146



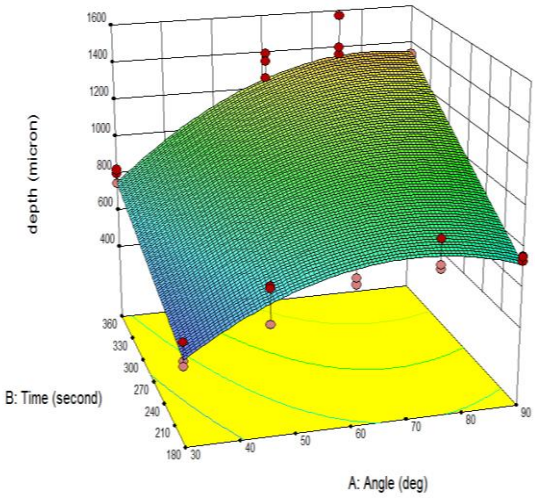
(c) IA-700



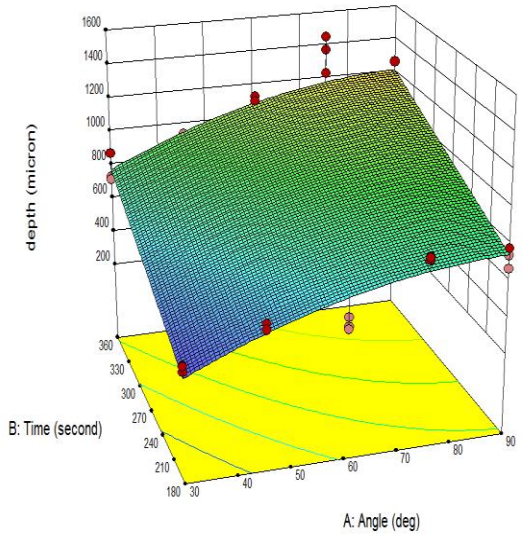
(d) Polyurethane



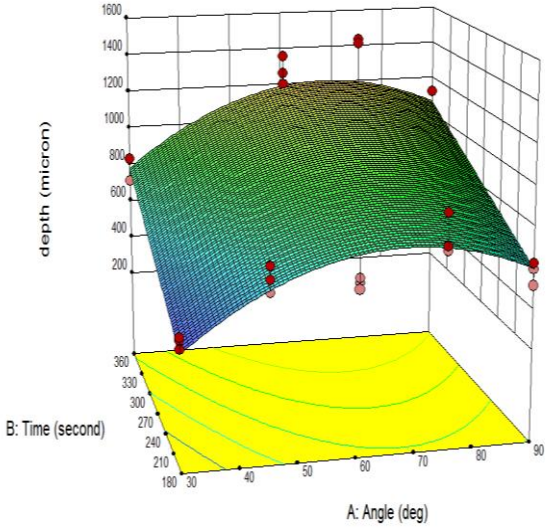
(e) Coating 4



(f) Coating 5



(g) Coating 6



(h) Coating 7

Fig. 5-20: Three-dimensional representation of depth of erosion scars in terms of the angle of attack and erosion duration

A comparison with the uncoated specimen performance is necessary to better analyze the effectiveness of the single layer and multilayer coating systems discussed above. Table 5-14 and 5-15 show the erosion resistance for the 180 seconds and 360 seconds, respectively, as the percentage change in material removal of the three single layer specimens and the four two-layers specimens compared to the uncoated specimen. While Table 5-16 and 5-

17 show the percentage change in the maximum depth for erosion durations of 180 and 360 seconds.

H-146 showed the best erosion resistance behavior for the single-layer specimens with a maximum material removal resistance of 19% at a 60˚ angle of impingement and 360 second erosion duration. On the other hand, the improvement in the maximum depth was less than 10% for most angles of impingement. It is worth noting that at 90˚, H-146 provided no erosion resistance improvement compared to the uncoated specimen and 2% deeper erosion scars. On the other hand, Polyurethane provided positive erosion resistance behavior between 45˚ - 75˚ with a maximum of 15% improvement at 60˚. However, when looking at the maximum depth, Polyurethane failed to provide better resistance than the uncoated specimen between 60˚ and 90˚ angles of attack.

Table 5-14: A comparison of material removal data of the coated specimens to the uncoated specimen for an erosion duration of 180 seconds

AOA	H-146	IA-700	Polyurethane	Coating 4	Coating 5	Coating 6	Coating 7
30˚	-17%	-17%	14%	14%	13%	22%	20%
45˚	4%	-3%	17%	16%	12%	47%	25%
60˚	11%	-5%	9%	4%	9%	65%	40%
75˚	-22%	-18%	14%	7%	2%	29%	20%
90˚	3%	18%	8%	14%	8%	29%	48%

Table 5-15: A comparison of material removal data of the coated specimens to the uncoated specimen for erosion duration of 360 seconds

AOA	H-146	IA-700	Polyurethane	Coating 4	Coating 5	Coating 6	Coating 7
30˚	7%	0%	-7%	-8%	-20%	2%	-12%
45˚	9%	-6%	3%	-10%	-2%	12%	5%
60˚	19%	0%	15%	18%	9%	38%	13%
75˚	14%	-4%	2%	6%	9%	25%	6%
90˚	0%	-20%	-15%	-12%	-1%	16%	13%

Table 5-16: A comparison of maximum depth data of the coated specimens to the uncoated specimen for an erosion duration of 180 seconds

AOA	H-146	IA-700	Polyurethane	Coating 4	Coating 5	Coating 6	Coating 7
30	-26%	0%	6%	-7%	0%	18%	18%
45	-9%	-1%	14%	12%	12%	31%	18%
60	-3%	-8%	14%	7%	8%	39%	26%
75	1%	23%	8%	-2%	0%	1%	1%
90	-20%	-8%	8%	12%	4%	7%	26%

Table 5-17: A comparison of maximum depth data of the coated specimens to the uncoated specimen for an erosion duration of 360 seconds

AOA	H-146	IA-700	Polyurethane	Coating 4	Coating 5	Coating 6	Coating 7
30	2%	1%	12%	14%	8%	10%	8%
45	4%	-14%	16%	7%	13%	19%	16%
60	8%	4%	-5%	1%	-3%	15%	1%
75	8%	9%	-13%	-9%	-14%	-7%	-5%
90	-2%	-3%	-10%	-10%	-8%	4%	15%

For specimens coated with two-layers, the two-layer Polyurethane (Coating 6) showed excellent erosion resistance behavior at 60˚ angle of impingement with improvements reaching up to 38%. Also, the improvement in terms of erosion scars depth is remarkable at angles of impingement ranging from 30˚ to 60˚, but not at high angles of impingement. While all coatings used in this experiment (except for Coating 6) showed a worse/no-change behavior at 90˚, Coating 7 showed the best improvement in the maximum depth category with 15% reduction and 13% reduction in material removal. Coating 4 and Coating 5 showed some improvement at low angles of attack when considering the maximum depth and some improvement at 60˚ and 75˚ when considering material removal.

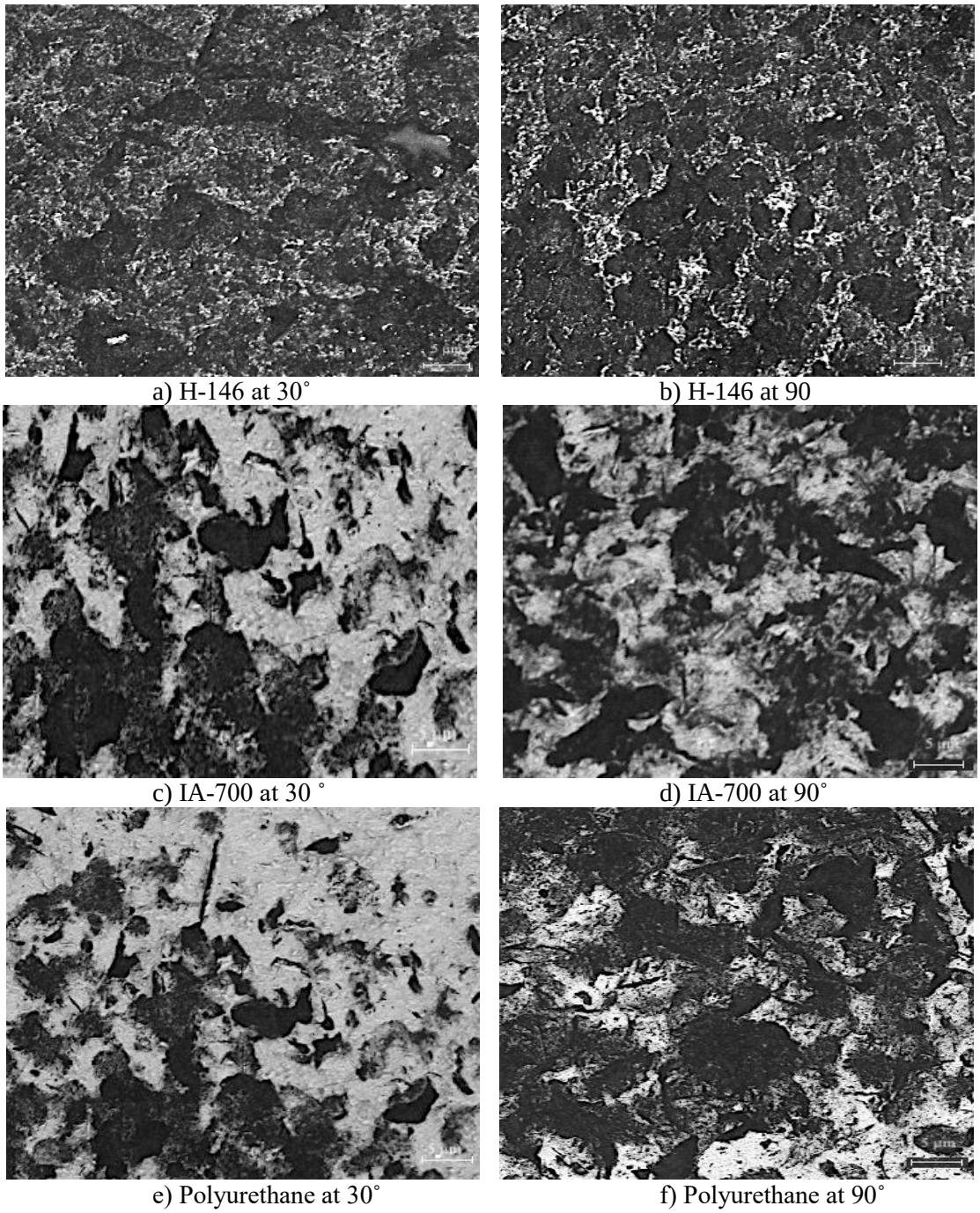
To understand the erosion mechanism of the coatings, Fig. 5-20 shows micrographs of the erosion scars for H-146, IA-700, and Polyurethane at 30˚ and 90˚. What can be noticed in the micrographs is that all erosion scars for all three coatings are in the form of ploughing, cutting, and pitting for both angles of attack. Looking at the 90˚ micrographs, it can be

noticed that the number and depth of the pitting scars are higher than those present in the 30˚ micrographs. Similarly, the depth and the number of the ploughing and cutting scars in the 30˚ micrographs are higher than those present in the 90˚ micrographs. Ploughing, cutting, and pitting are found to be common erosion scars in ductile materials, which is consistent with what other researchers found [185]. Therefore, H-146 and IA-700 coatings can be thought of as composite materials with ductile matrix and graphene acting as the reinforcement. When the coating is subjected to abrasive particles, the ductile matrix will be the first to fail with scars such as the one presented in the micrographs, then the interface between the matrix and graphene will be removed. Finally, graphene will be subjected to the incoming particles and start to fail. From Table 5-14 to Table 5-17, H-146 and IA-700 show similar trends with the worst performance at 90˚ followed by 30˚. At 30˚, the abrasive particles remove the ductile matrix easily, and then graphene provides some resistance until it fails. While at 90˚, the ductile matrix provides some erosion resistance, and the brittle graphene fails easier than it does at 30˚. It can be noticed that graphene provides more resistance at 30˚ than the resistance provided by the matrix at 90˚ and that is why the performance at 30˚ is better than 90˚.

To study the effect of alternating multilayer coating systems, two versions have been studied: a harder upper layer on top of a softer layer (Coating 5) and a soft upper layer on top of a harder layer (Coating 7). As mentioned earlier, the hardness of IA-700 is around 1.6 times that of Polyurethane. In this experiment, at 90˚ angle of impingement, it can be observed that Coating 7 (soft-upper/stiff-lower) showed a 13% reduction in terms of material removal while Coating 4 (stiff-upper/soft lower) shows a -1% performance compared to the uncoated specimen. Also, when considering the maximum depth, Coating

7 showed 15% shallower erosion scars while Coating 5 showed 8% deeper erosion scars than the uncoated specimen. The same conclusion has been noticed in almost all other angles of impingement, not only 90˚. As a result, a softer coating layer on top of a harder coating layer combination provides better erosion resistance than a harder layer on a softer layer. Similar observation was made in a numerical study with a similar purpose that was conducted by Mishnaevsky Jr et al. [186], to study the effect of water droplets on coatings in two versions: stiff-upper layer/soft-lower layer and soft upper layer/stiff lower layer. With droplets impacting the surface at 90˚, they found that the soft-upper/stiff-lower coating combination showed a lower stress magnitude than the stiff-upper/soft-lower coating combination.

This erosion resistance behavior can be explained by the ability of the soft layer to keep the stress upon impact relatively low by absorbing some of the incoming kinetic energy and working as a shock damper, which reduces the energy and the stress passing through the substrate. Fig. 5-22 shows SEMs of the erosion of coating 5 and coating 7 when eroded at 45˚, as well as the transverse sections of the coatings. It can be seen in Fig. 5-22 (a) and (b) that the amount of area of the base coating exposed in Coating 5 is larger than that of Coating 7, which shows how having a soft top layer would absorb energy and protect the hard lower layer.



a) H-146 at 30˚ b) H-146 at 90

c) IA-700 at 30 ˚ d) IA-700 at 90˚

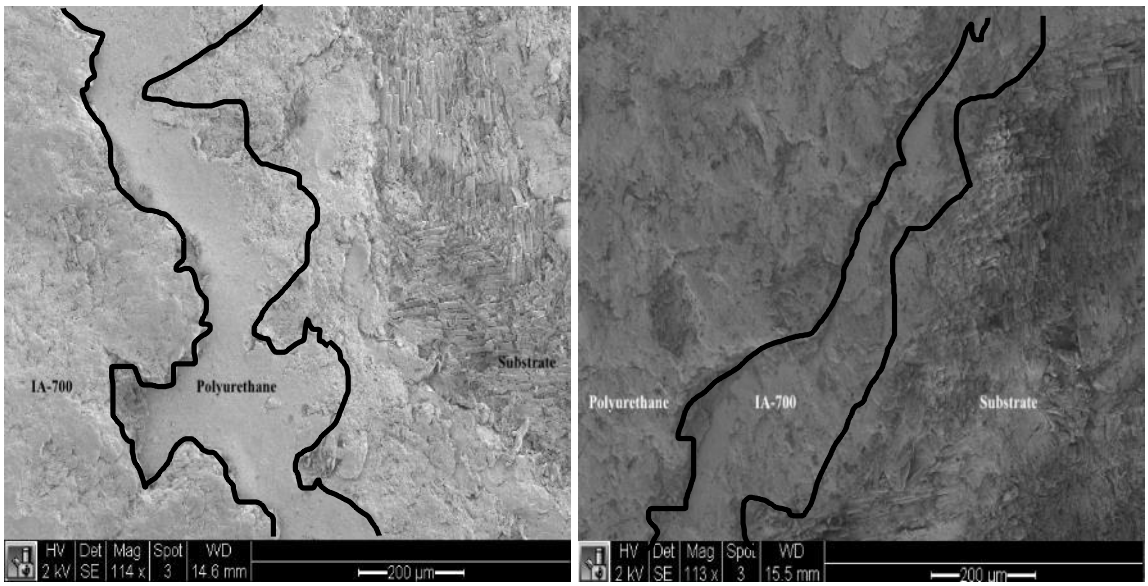
e) Polyurethane at 30˚ f) Polyurethane at 90˚

Fig. 5-21: Micrographs of the erosion scar on the surface of: H-146: a) 30˚, b) 90˚, IA-700: c) 30˚, d) 90˚, and polyurethane: e) 30˚, f) 90˚

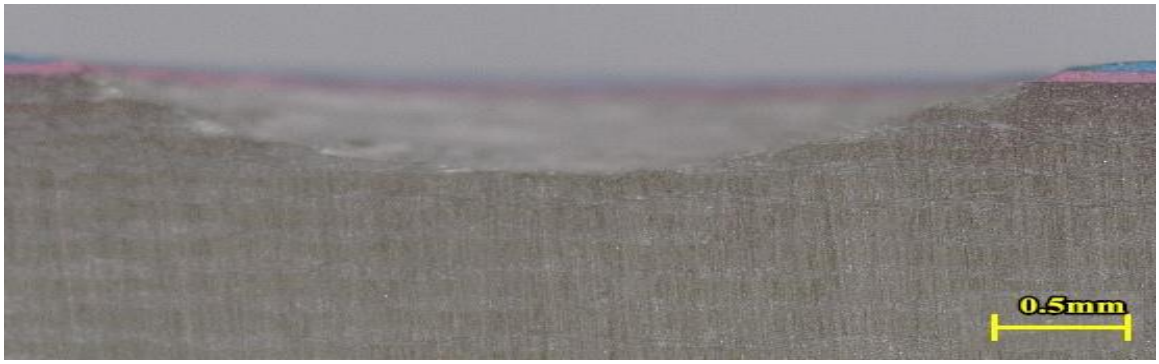
Comparing the erosion results of H-146 as a single layer and Coating 4, which is a layer of H-146 on top of a layer Polyurethane, it can be seen that the performance of H-146 deteriorated in the two-layer coating. This result is due to the inferior adhesion between these

two layers of the coating. As discussed earlier, one more coating combination was considered for this experiment that consisted of a layer of Polyurethane on top of a layer of H-146. However, the top layer got peeled off as soon as few abrasives impacted the surface as was shown in Fig. 5-16, proving that adhesion between these two layers contributed to the inferior behavior in the two-layer coating.

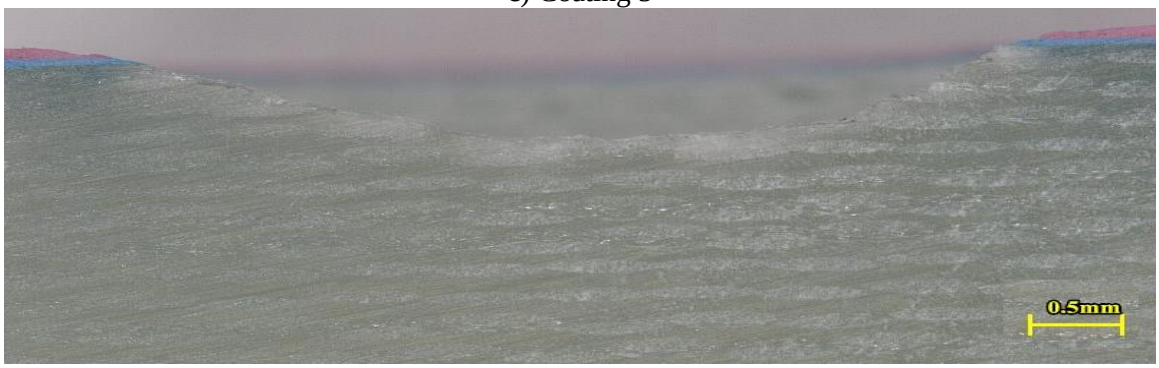
A comparison of the surface roughness profiles is shown in Fig. 5-23. It can be seen in the figure that coating with high surface roughness such as H-146, IA-700, Coating 4, and Coating 5 showed less erosion resistance than Coatings of smoother surfaces such as Coating 6 and Coating 7. Surface roughness can be one of the factors that affects the erosion behavior of materials. Higher surface roughness means that the number of contact points between the target material and the abrasive particles is increased, and since asperities on the surface serve as damage initiation sites, higher erosion rates are expected [95]. Reducing the initial surface roughness reduced the erosion rate and led to a delay in erosion [94].



a) Coating 5 b) Coating 7



c) Coating 5



d) Coating 7

Fig. 5-22: Erosion scras at 45˚ for: a) SEM of Coating 5, b) SEM of Coating 7, c) transverse section of Coating 5, and d) transverse section of Coating 7.

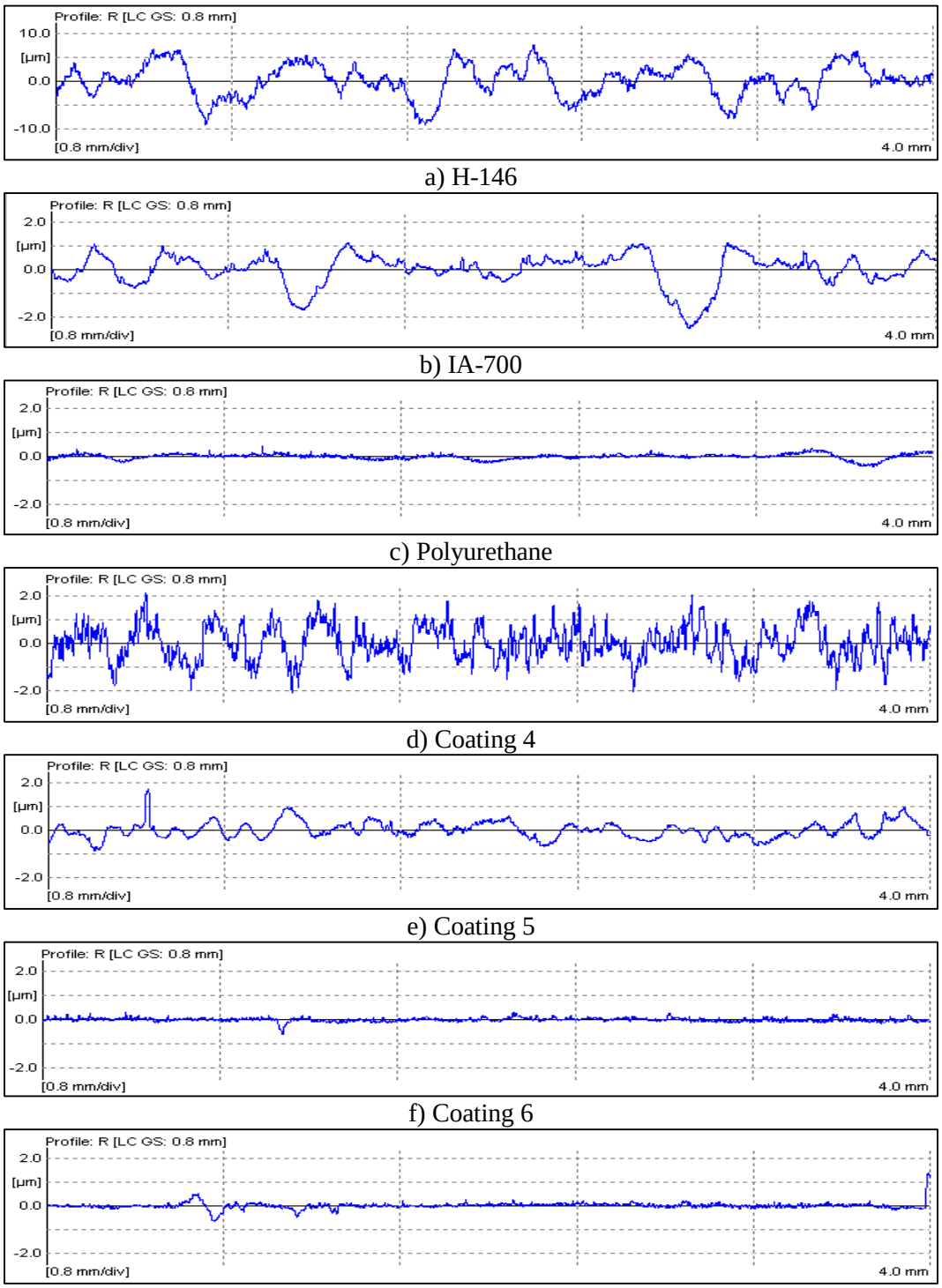


Fig. 5-23: Surface roughness profile of a) H-146, b) IA-700, c) polyurethane, d) Coating 4, e) Coating 5, f) Coating 6, and g) Coating 7.

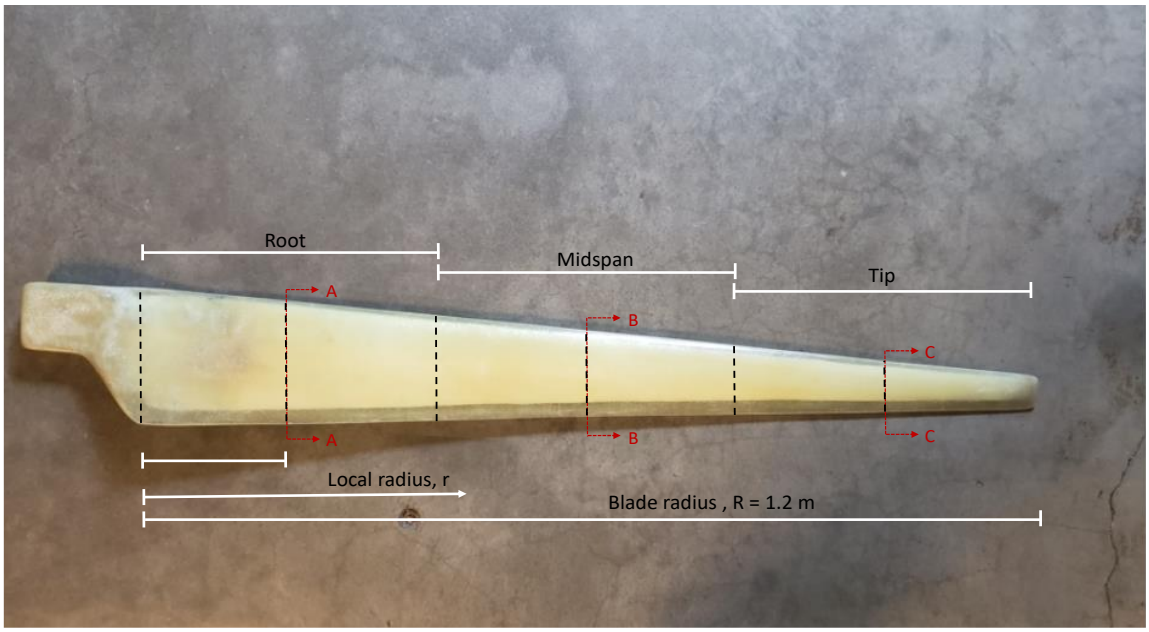
In summary, the erosion rig setup's workability has been confirmed by testing a ductile Al 6061-T6, which showed the highest erosion rate at 20˚ angle of impingement, and a brittle borosilicate glass, which showed the highest erosion rate at 90˚. Then erosion behavior of GFRP specimens has been investigated in terms of two variables, 1) the angle of attack, which was varied between 30˚ and 90˚ with 15˚ increments, and 2) erosion duration, which was 180 seconds and 360 seconds. The performance of the uncoated GFRP specimen in terms of material removal and maximum depth was compared to coated specimens. Two graphene-based coatings were used in this experiment: H-146 and IA-700, either as a single layer or in combination with Polyurethane as a multilayer coating system. It has been found that:

- A single layer of graphene-based coating H-146 showed the ability to increase erosion resistance behavior by decreasing the material removal up to 19% and decreasing the maximum depth by up to 8%.
- The use of multilayered coatings with graphene and polyurethane combination is an effective way to increase erosion resistance.
- A softer upper coating layer on top of a harder layer showed improvements in the erosion resistance compared to a hard-upper layer on top of a soft-lower layer. For example, Coating 7, a polyurethane layer on top of IA-700, showed better erosion resistance behavior than Coating 5 in terms of material removal and maximum depth.

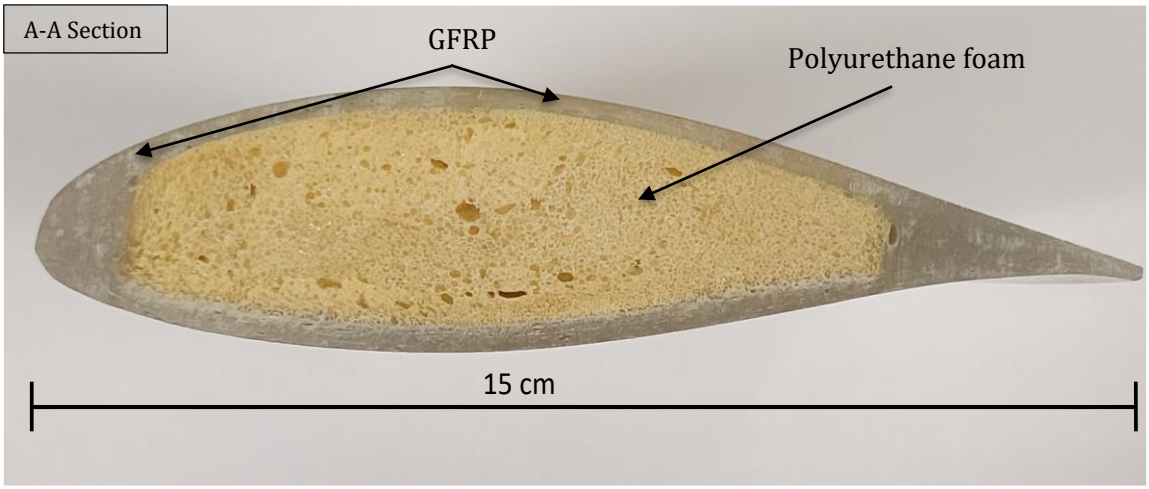
- The combination presented in Coating 7 demonstrated the best combination to resist erosion at a 90˚ angle of attack.
- Two layers of Polyurethane showed spectacular improvements reaching up to 38% improvement in material removal and 19% in maximum depth.

Chapter 6: Erosion of Wind turbine blades

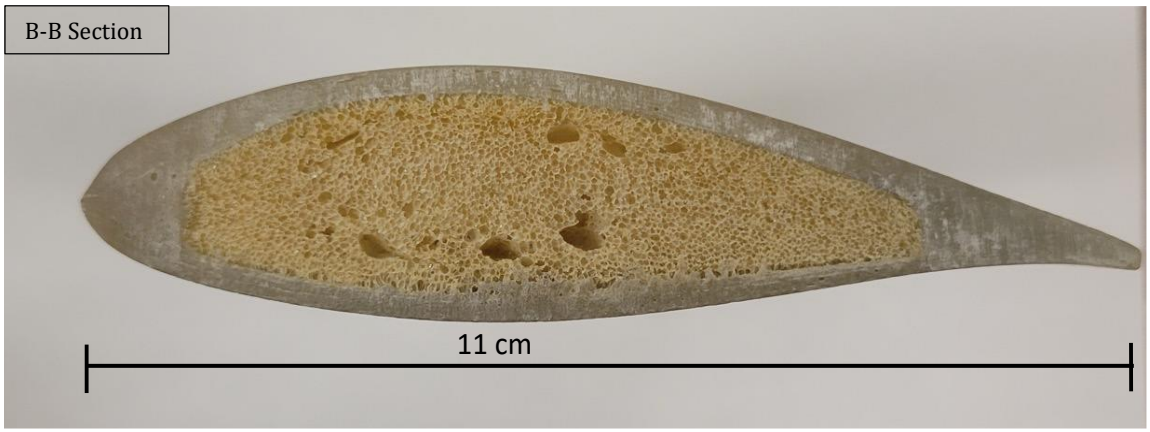
Since the increase of surface roughness of wind turbine blades has a detrimental effect on aerodynamic performance and, consequently, power generation, the erosion of the leading edge of 1.2 m long wind turbine blades, as shown in Fig. 6-1 (a), will be studied in this chapter. The blade can be divided into three sections: Root, Midspan, and Tip. Theses sections can be defined by the ratio of local blade radius, r, to the whole blade radius, R. Cross-sectional views from each section of the blade are shown in Fig. 6-1 (b) to (d). After eroding multiple types of coatings in the previous chapter on a flat surface, an investigation that considers the effects of coating on erosion behavior on wind turbine blades will be conducted in this chapter. To do so, three wind turbine blades have been studied: (i) a single layer of H-146 coated wind turbine blade since it was the coating that showed the highest erosion resistance in the single-layer category. The second blade (ii) was coated with a multilayer coating of polyurethane on top of IA-700 (Coating 7). Since the leading edge erosion is considered to occur at or near the normal incident (90˚ angle of impingement), Coating 7 was specifically chosen due to its superior performance compared to coatings in the same category. Finally, (iii) the third blade was left uncoated to serve as a baseline of comparison.



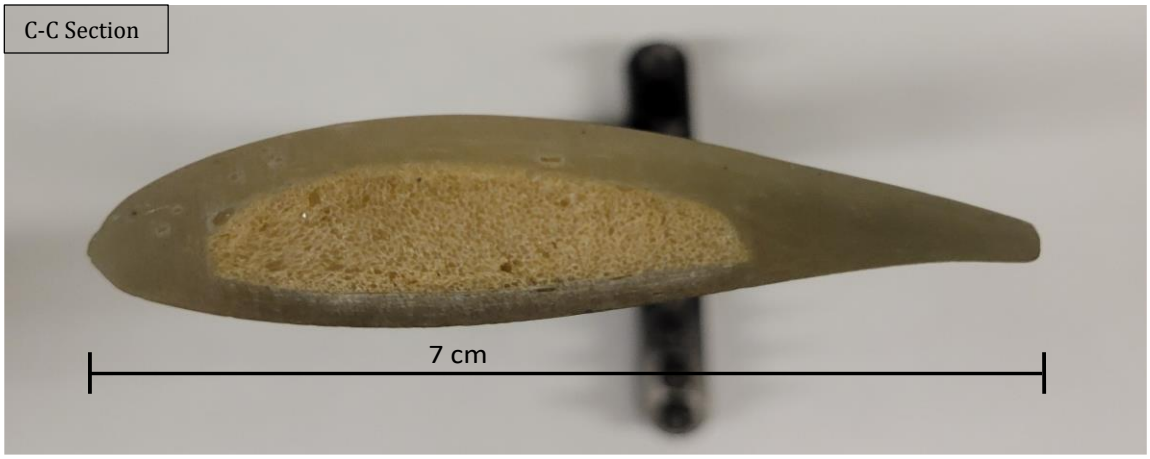
(a) 1.2 m long wind turbine blade



(b) Root section at r/R=17%



(c) Midspan section at r/R= 50%



(d) Tip section at r/R= 84%

Fig. 6-1: Aeosol H 1-kW wind turbine blade: (a) full blade showing blade's sections and local, r, and total, R, radius of the blade, (b) cross-sectional view of Root section showing the A-A section, (c) cross sectional view of Midspan section showing the B-B section, and (d) cross-sectional view of Tip section showing the C-C section

Although wind turbine blades are three-dimensional, the leading-edge damage along the spanwise direction after a long period of operation is the same and can be modeled as two-dimensional for simplicity [187]. The damage in the wind turbine blades is prominent at the outboard sections of the blade, where the local relative velocity is larger than the root section of the blade [188]. When wind turbines run at high wind speed, the tip speed could reach 100 m/s, and more than 60% of the energy extracted from the wind is from the out-bound section [189]. Being the thinnest part of the blade, the tip region in harsh environmental conditions is susceptible to wear, aging, and powdering until it breaks, affecting the power generation capacity and shortening the service life of the blade [188, 190]. In fact, Fiore and Selig [76] found that the erosion at the outboard (tip) section of the blade can be ten times higher than the inboard (root) section of the blade, while the freestream velocity was 50% at the inboard section of that of the outboard section. Fig. 6-2 shows the location and intensity of the sand erosion rate of the three sections of the blade, namely: root at r/R=35%, mid-span at r/R=65%, and tip at r/R=75% where r is the radial location on the

blade and R is the total length of the blade [76]. As shown in Fig. 6-2, the tip section is subjected to higher levels of erosion.

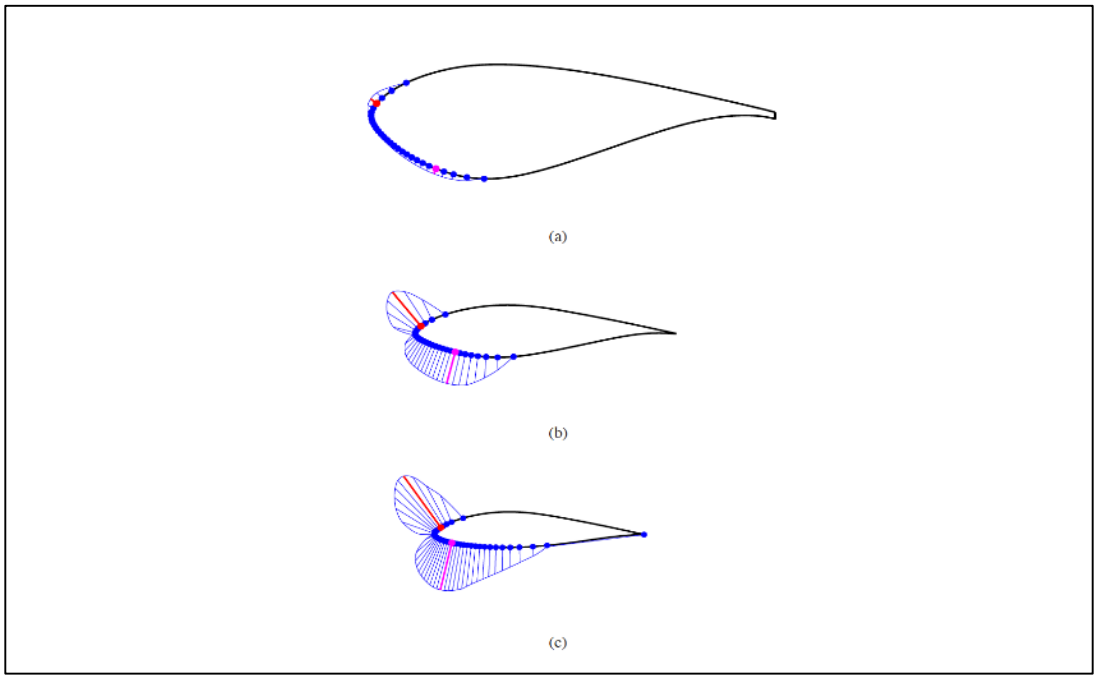
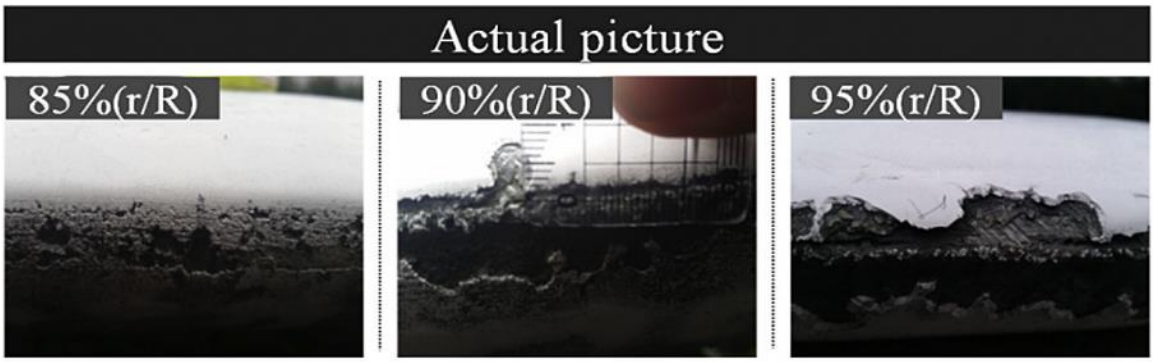


Fig. 6-2: Sand erosion rate at (a) r/R=35% at AOA= 5.5˚, (b) r/R=65% at AOA=6˚, and (c) r/R=75% at AOA=6˚. The blue circles of the airfoil indicate the location of sand particle impact and the red circle indicates the location of maximum erosion. The contour lines indicate the intensity of erosion [76].

An inspection of 201 blades of 67 wind turbines showed that 174 blades (87% of the blades) suffered from leading-edge erosion while 197 blades (98%) suffered from deposition of contaminations [191]. A study of the leading-edge of Vestas 47 blades that have been in operation for 12 years without any O&M activity showed that the tip section of the blade is the most damaged, and of that section, the most damaged area is the closest area to the tip as shown in Fig. 6-3 [190].



(a) r/R=85% (b) r/R= 90% (c) r/R=95%

Fig. 6-3: leading-edge erosion of Vestas 47 blade after 12 years of operation: (a) r/R=85%, (b) r/R= 90%, and (c) r/R=95% [190]**.**

6.1 Testing parameters

The blades used in this experiment are made of a vinyl epoxy matrix reinforced with glass fibers with polyurethane foam filler. The fiber to resin ratio is 45 to 55, and the fibers are woven. Each blade was cut into six small airfoils of 20 cm of lengths using abrasive water-jet techniques, as shown in Fig. 6-1. The largest two airfoils are treated as the Root section, the second two are treated as the Midspan section, and the smallest two are treated as the Tip section.

To incorporate the idea of increasing damage density toward the tip of the blade into our design, air pressure (and consequently particle impact velocity) has been increased from 100 kPa at the Root section to 125 kPa at the Midspan section to 200 kPa at the Tip section. To estimate the particle velocity at the different sections, equations (4-1) to (4-6) are used. Based on the air pressure, the mass flow rate has been experimentally measured to be 0.042 g/s, 0.048 g/s, and 0.067 g/s at 100 kPa, 125 kPa, and 200 kPa, respectively. The particle velocity upon departure from the nozzle is then estimated to be 12.1 m/s, 14.3 m/s, and 20.2 m/s for Root, Midspan, and Tip sections, respectively.

6.1.1 Experimental procedure

Since particles impact wind turbine blades at the vicinity of the leading edge, four angles of attack are used in this experiment. These angles of attack are -5˚, 0˚, 5˚, and 10˚ as shown in the schematic in Fig. 6-4. *The angle of attack was varied to imitate the randomness at which the sand particles bombard wind turbine blades during sandstorms and to understand the wear mechanism and severity of damage at each angle of attack.* On the other hand, two erosion durations, 180 seconds and 360 seconds, have been chosen to investigate the depth and shape alternation of the airfoil after different exposure lengths to sand particles and their effects on the aerodynamic performance of the blade. Therefore, each airfoil was be eroded at the four angles of attack at the two erosion durations. Each test was duplicated twice to verify the repeatability of the results. This leads to 16 erosion experiments for each airfoil and a total of 96 experiments for all airfoils. The mass of the specimens is measured before and after each erosion experiment. Then, optical photographs were taken to measure the depth and dimensions of erosion scars using the Keyence VR-3100 3D non-contact optical profilometer with a height measurement accuracy of ± 3 μm. In order to characterize the effects of the different erosion variables used in this experiment on the shape of the airfoil, Creaform handyscan 700 three-dimensional scanner has been used before and after erosion. To scan an airfoil, the 3D scanner with seven intersecting laser lines directed to the airfoil to triangulate and capture the shape of the airfoil accurately. Then the scan is transferred into a CAD model by using an accompanying software called VXmodel. In VXmodel, multiple operations can be done to optimize the scan such as filling any holes that were not captured by the scanner, creating a mesh, and specifying the point of origin

and axes on the scan. After the CAD model has been created, Solidworks was used for any further operations as will be discussed later.

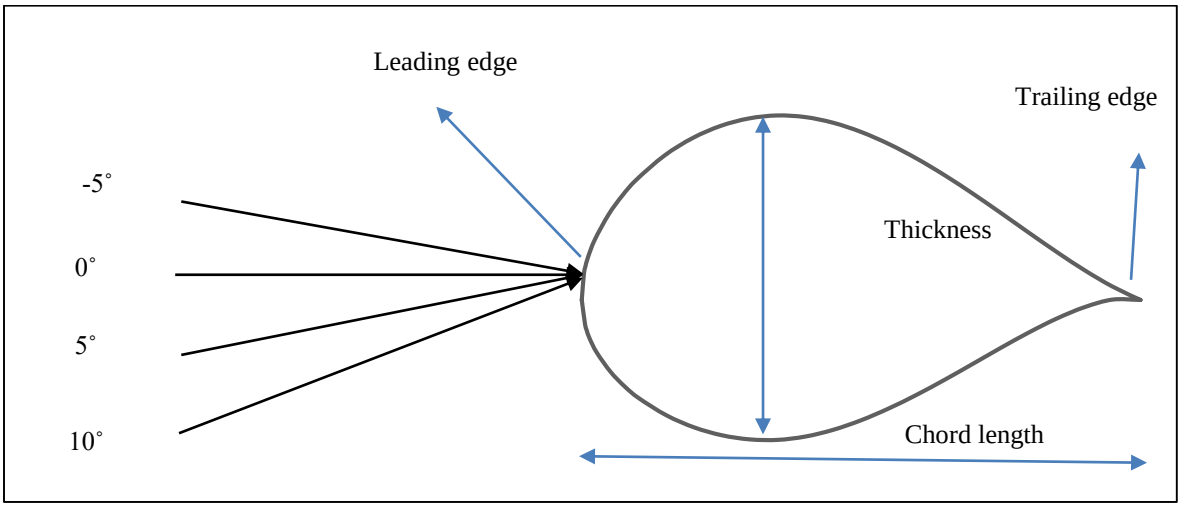


Fig. 6-4: Schematic of NACA 63-215 airfoil with angles of attack of -5˚, 0˚, 5˚, and 10˚.

6.2 Erosion of Uncoated Airfoils

The first blade that will be investigated is the uncoated blade to understand and characterize the erosion behavior without the effects of coatings. Eroding the leading edge of the wind turbine blade at the four angles of attack is shown in optical pictures in Fig. 6-5. All Photomicrographs of the erosion scars are shown in Appendix VI. It can be seen in the figure how the different impingement angles created erosion scars with different shapes. To understand the erosion behavior, material removal, depth of erosion, shape of the airfoil, and the total mass loss will be discussed thoroughly.

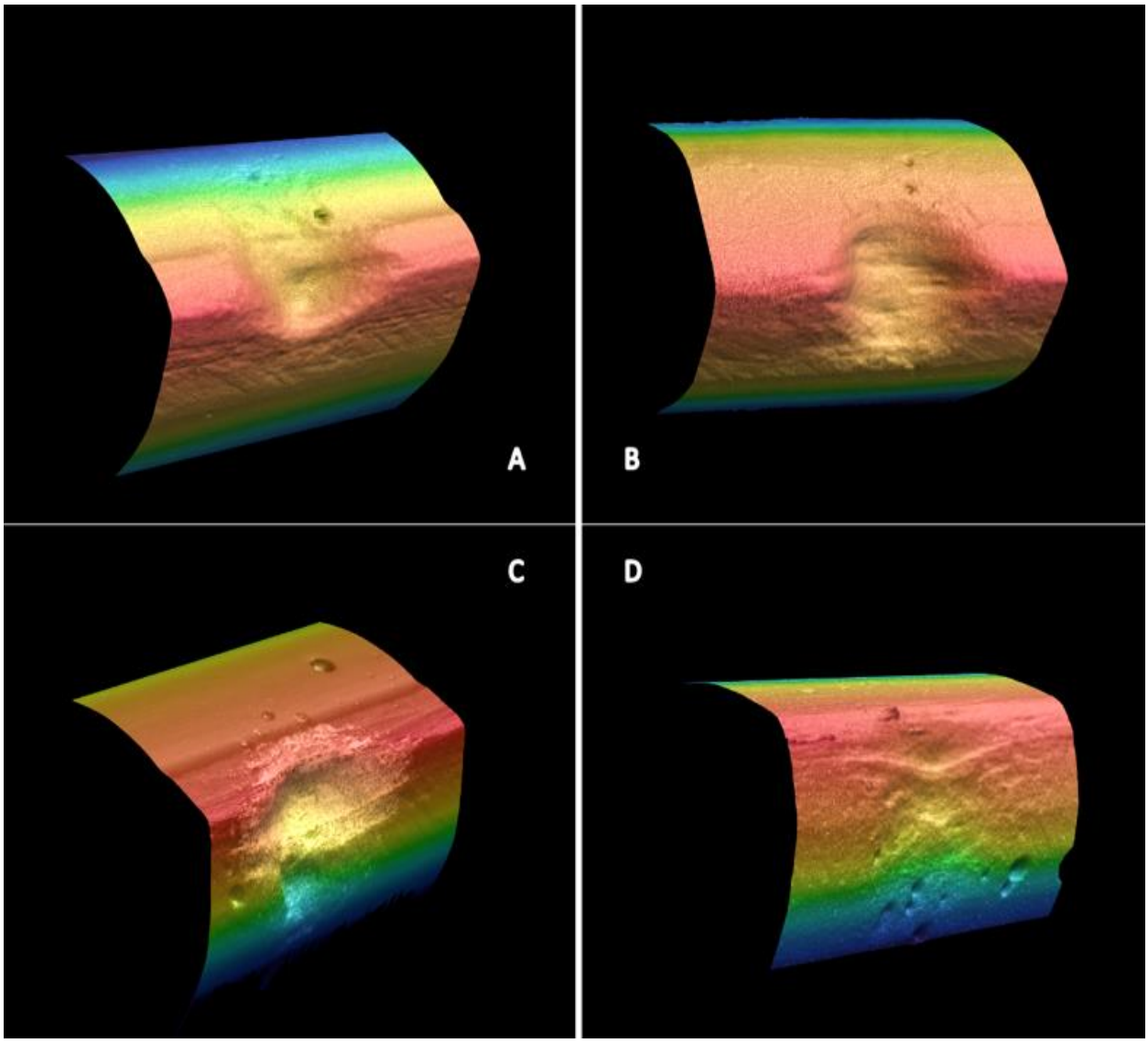
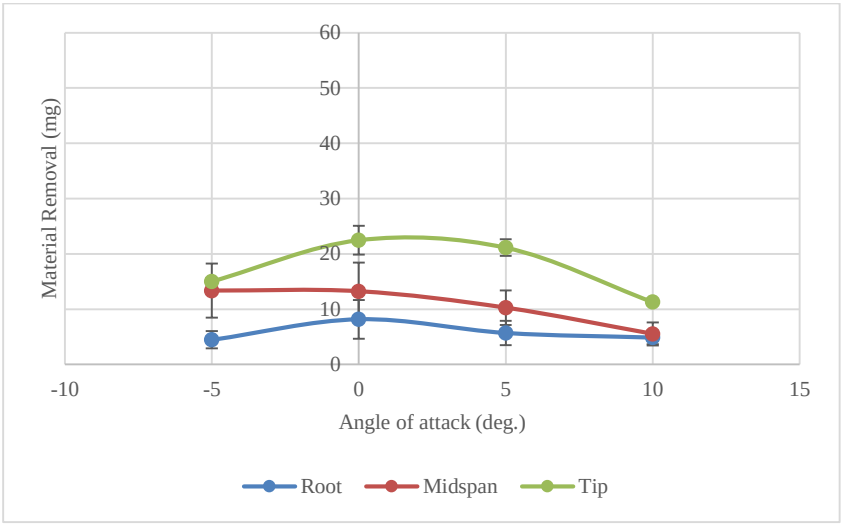


Fig. 6-5: Optical pictures of the erosion scars at 360 seconds erosion duration caused by: (a) -5˚, (b) 0˚, (c) 5˚, and (d) 10˚

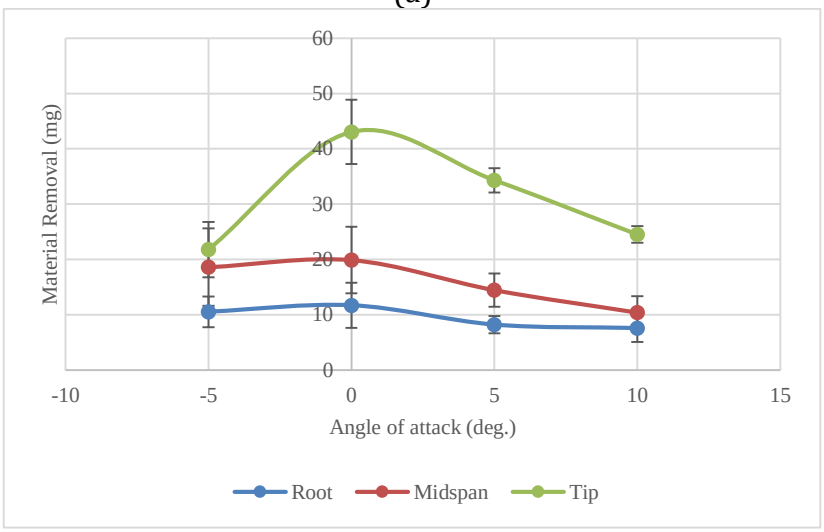
6.2.1 Material Removal Rate

The first parameter to analyze the erosion behavior is the amount of material removed. In Fig. 6-6, the amount of material removed in milligram (mg) is shown as a function of angle of attack at Root, Midspan, and Tip sections for an erosion duration of 180 seconds (Fig. 6-6 A) and for 360 seconds (Fig. 6-6 B). All experimental material removal data can be found in Appendix V. It can be seen that increasing air pressure and increasing erosion

duration increased the intensity of the damage. In all conditions, the maximum material removal occurred at 0˚ while the minimum occurred at 10˚. The higher erosion rate at 0˚ could be explained by the fact that the number of abrasive particles focused on the leading edge is higher than particles impacting at the other angles of attack.



(a)

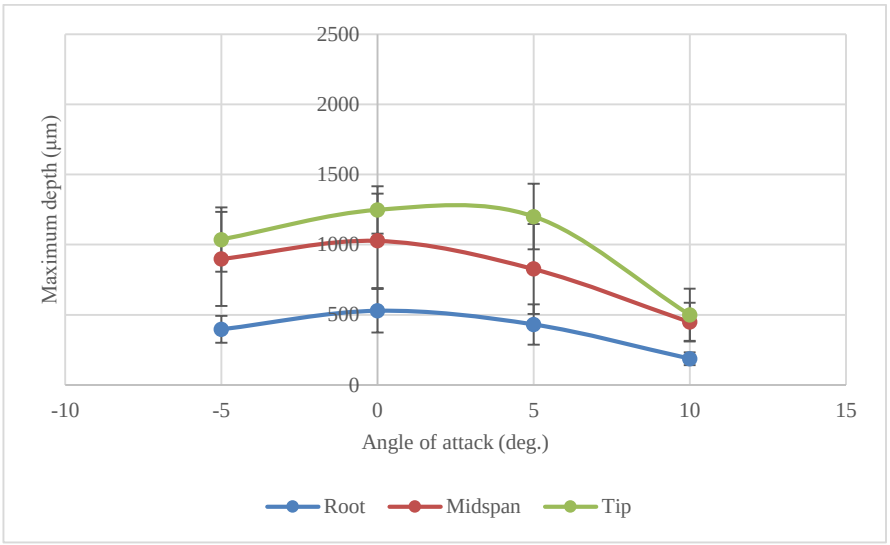


(b)

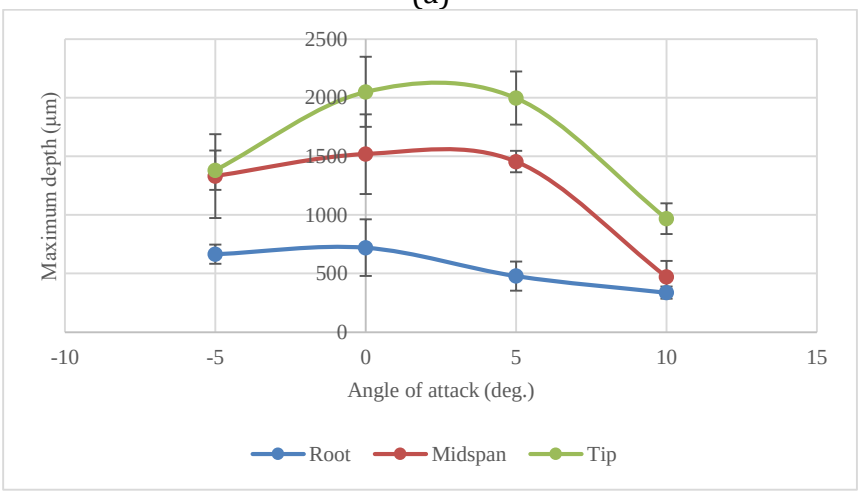
Fig. 6-6: Material removal as a function of angles of attack for root, midspan, and tip sections for an erosion duration of: (a) 180 seconds, and (b) 360 seconds

6.2.2 Depth of Erosion

The second parameter to analyze the erosion behavior is the depth of the erosion scar. In Fig. 6-7, the maximum depth of the erosion scars for the three sections of the blade at erosion duration of 180 seconds and 360 seconds is shown. All experimental depth of erosion data can be found in Appendix V. Similar to Fig. 6-6, the damage increased with increasing pressure and erosion duration. Also, the maximum depth now is still occurring at 0˚.



(a)



(b)

Fig. 6-7: Maximum erosion depth as a function of angles of attack for root, midspan, and tip sections for an erosion duration of: (a) 180 seconds, and (b) 360 seconds

6.2.3 Erosion Mechanism

It has been observed that the erosion process in composite materials can be divided into three steps: the first step is the erosion and removal of the resin, the second step is the erosion and removal of the adhesion between matrix and fibers, and finally, the erosion of fibers. This observation is consistent with observations noticed by other researchers [135]. Since the reinforcement used in the wind turbine blade in this experiment is brittle glass fibers, brittle materials are expected to show the highest erosion rate at the normal incident 90˚ angle of impingement (equals 0˚ angle of attack), the highest erosion rate was observed at 0˚ angle of attack. After removal of the matrix, scanning electron microscopy (SEM) micrographs in Fig. 6-8 (a) and (a) shows the broken glass fibers at 250X and 1000X magnification, respectively. The incoming particles bombard the glass fibers, causing them to bend and then break, making the dominant wear mechanism during erosion of wind turbine blades be fiber breakage with abrupt brittle fracture easily noticeable.

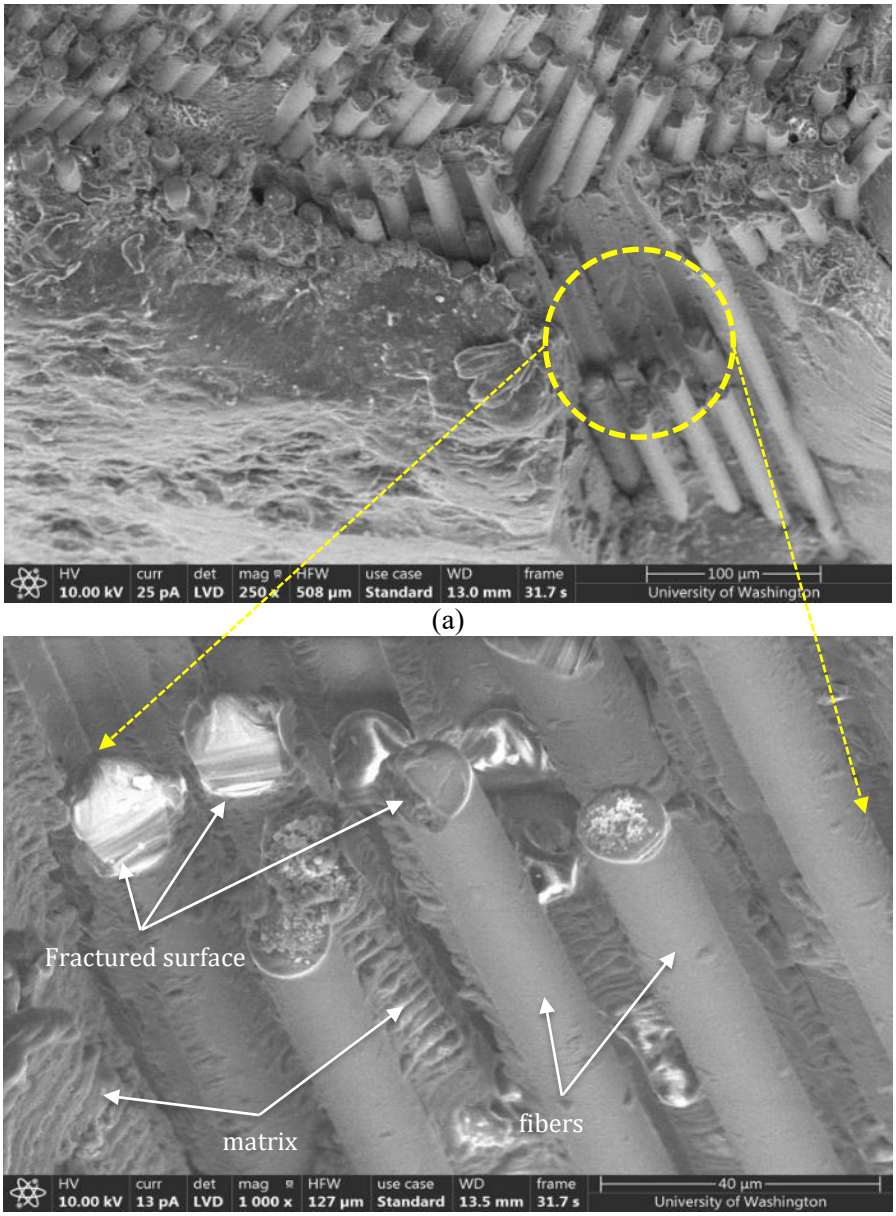


Fig. 6-8: SEM micrographs of 0˚ erosion scar showing matrix removal and fiber breakage at (a) 250x magnification, and (b) 1000x magnification

6.2.4 Airfoil Shape After Erosion

Since the shape of the airfoil after erosion can affect the aerodynamic behavior of the blade, the changes in the shape of the airfoils before and after erosion caused by the different angles of attack are discussed in this section. Three-dimensional scanning of the airfoils before and after erosion has been conducted, and then the scanned airfoils are imported to

Solidworks to extract a 2D profile, as shown in Fig. 6-9. The extracted 2D profile shown in Fig. 6-9 has an r/R ratio of 25%.

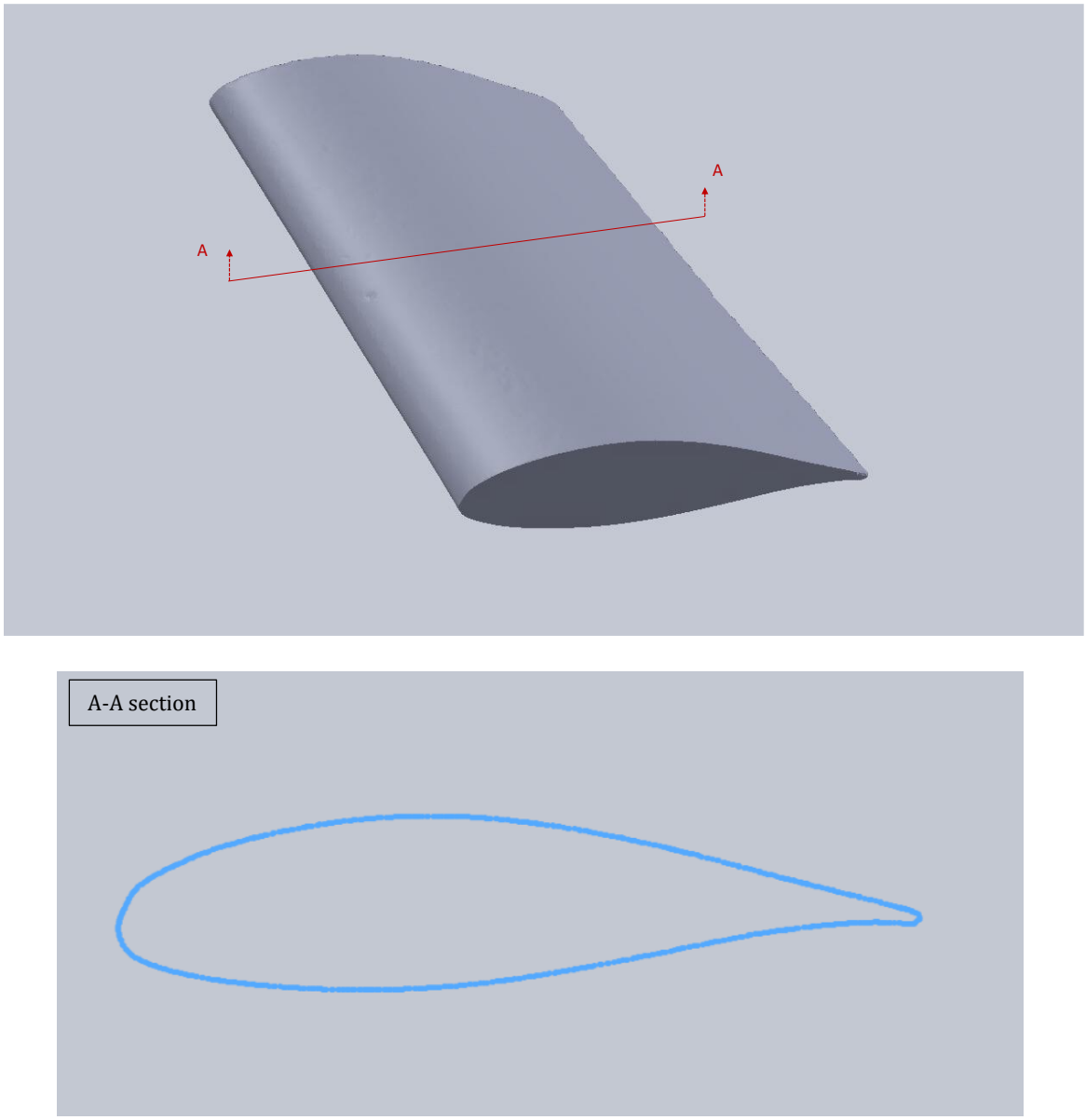


Fig. 6-9: Extracting 2D profiles from 3D scanned before erosion airfoil at r/R=25%.

The profiles shown in Fig. 6-10 come from the Tip section at 180- and 360-seconds erosion duration. The profiles shown in solid lines are the after-erosion profiles, while the dashed lines show the before-erosion profiles. Although the profiles are taken from the same blade section, the cord length decreases as we get closer to the tip of the blade. Therefore, the

chord length of the profiles depends on the exact location on the blade. The tip section is 40 cm long and the chord length changes from 9 to 3 cm. To avoid this problem, the chord length for each profile has been normalized (chord length of 1 unit) in both x and y coordinates. To normalize the chord length, the following equations have been used:

$$x_{new} = \frac{(x_{old} - x_{LE,old})}{c} \quad (6\text{-}1)$$

$$y_{new} = \frac{(y_{old} - y_{LE,old})}{c} \quad (6\text{-}2)$$

where x_{new} (y_{new}) the x-coordinate (y-coordinate) of the normalized airfoil

x_{old} (y_{old}) the x-coordinate (y-coordinate) of the airfoil before normalization

$x_{LE,old}$ ($y_{LE,old}$) the x-coordinate (y-coordinate) of the leading edge of the airfoil before normalization

c chord length

Similar to the results seen in Fig. 6-6 and 6-7, the most damage occurs at 0˚, and the lowest damage occurs at 10˚. It can be seen in Fig. 6-10 that the damage for -5˚ case affected the leading edge area with a focus on above the edge area. On the other hand, in the 5˚ and 10˚ cases, the damaged areas are at and below the leading edge, while the 0˚ case focused on the leading edge with some spread above and below. All airfoils' shapes of before and after erosion can be found in Appendix VII.

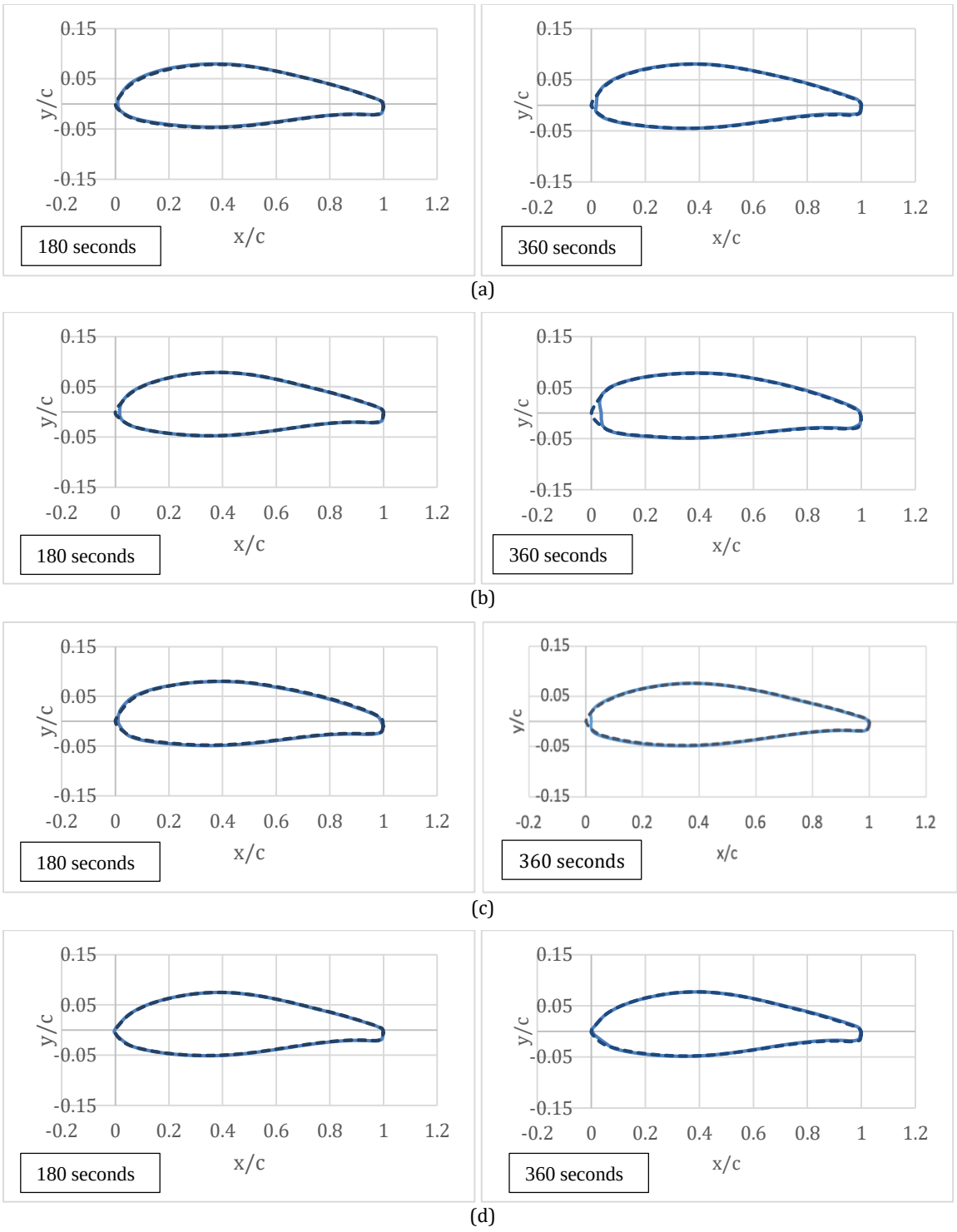


Fig. 6-10: Before erosion (dashed line) and after erosion (solid line) tip section airfoil profiles after 180- and 360-seconds of: (a) -5˚, (b) 0˚, (c) 5˚, and (d) 10˚

Since, during sandstorms, sand particles are expected to impact wind turbine blades in a random pattern, it is necessary to generate an airfoil shape that combines the damage

caused by the random impact. To do so, a superposition of the damage caused by each angle of attack is used to generate the expected after-erosion shape, as shown in Fig. 6-11. This final shape was reached by completing multiple steps: the starting point was the erosion scar of 0˚ angle of attack, then on that erosion scar the damage caused by 5˚ was added, which removed more material below the leading edge. Similarly, 10˚ increased the amount of material removed below the leading edge and finally -5˚ removed material from above the leading edge to reach the final shape shown in Fig. 6-11. Although more prolonged exposure to sandstorms is expected to increase the depth of the erosion scars on the leading edge, there is no reason to believe that the material loss pattern or the shape of the after-erosion profile will change. The reached shape is in agreement with pictures taken of wind turbine blades eroded in the field, as shown in Fig. 6-12.

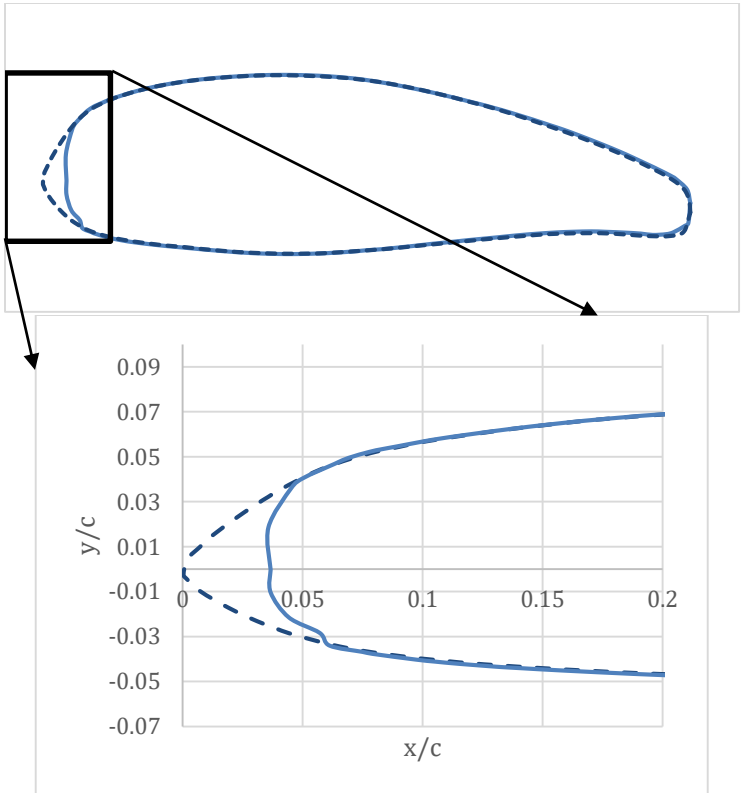


Fig. 6-11: Expected shape of airfoil after erosion after combining the effects of different angles of attack

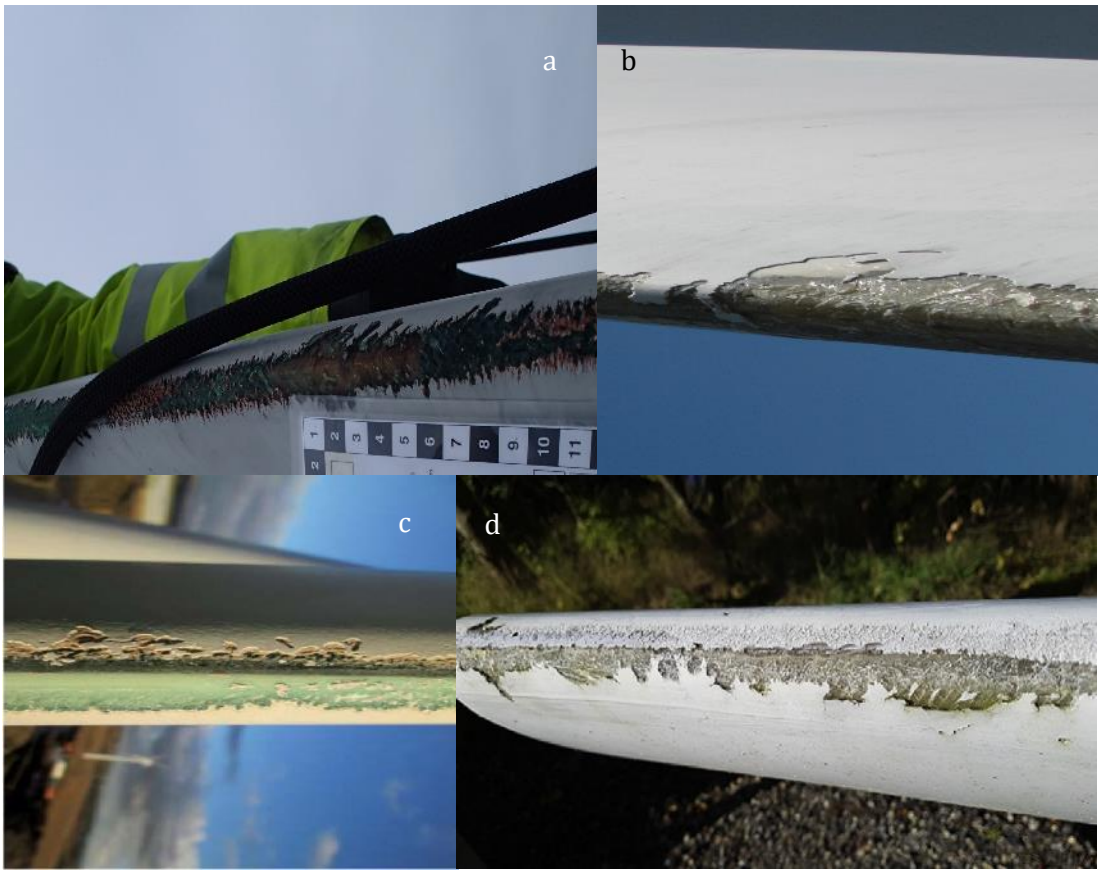


Fig. 6-12: Leading edge erosion of wind turbine blade with coating removed and laminate being exposed: (a) Ref [188], (b) Ref [27], (c) Ref [112], and (d) Ref [192]

6.2.5 Total mass Loss

In this experiment, discrete erosion scars on the leading edge have been formed to study the effects of different factors. However, in real life, the damage on the leading edge is continuous along the blade. Therefore, to calculate the total mass lost from the blade, the mass loss for erosion scars is extrapolated along each section of the blade then the result from the sections is added up. Although erosion scars have different mass loss and depth, the width of all erosion scars is the same since the width depends on the nozzle diameter and standoff distance which are constants for all testing conditions. Scar width has been measured to be 4.2 mm. Assuming the damage from the four angles of attack is combined in one scar (similar to Fig. 6-11), the resulting mass loss from that scar is 38 mg, 63.3 mg,

and 123.7 mg for Root, Midspan, and Tip sections, respectively. Extrapolating the damage to be continuous along the leading edge for each section (width of each section is 400 mm) yields a mass loss of 3,619 mg, 6,029 mg, and 11,781 mg for Root, Midspan, and Tip, respectively, with an overall mass loss for the whole blade of 21,429 mg. This amount of material loss represents 1.5% of the total mass of the blade.

In summary, the erosion behavior of the leading edge of an uncoated wind turbine blade using sand particles impact have been investigated by studying the effects of multiple variables such as the angle of attack, erosion duration, and impact velocity on the erosion behavior characterized by the amount of material removal, depth of erosion scars, and the changes in the shape of the airfoils after erosion. It has been found that:

- Increasing pressure and erosion duration resulted in more severe erosion damage, while different angles of attack resulted in different damage shapes on the leading edge.
- The maximum material removal and the maximum erosion depth occurred at an angle of attack of 0˚, while the least amount of damage occurred at 10˚.
- The expected airfoil shape after being subjected to erosion for extended periods has been generated through superposition of the shape changes due to all the angles of attack used in this experiment.

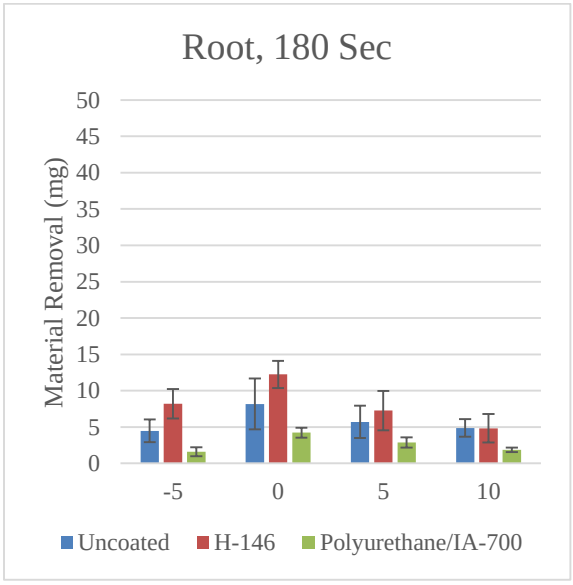
6.3 Erosion of Coated Airfoils

After characterizing the erosion behavior of the leading edge of an uncoated wind turbine blade, the effects of adding protective coatings will be studied in this section. Similar to the uncoated blade, both H-146 coated blade and Polyurethane/IA-700 coated blade were

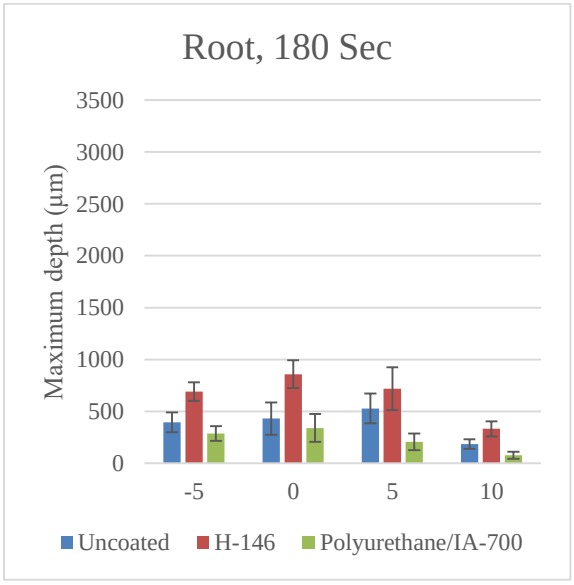
eroded with same air pressure (100 kPa at Root section, 125 kPa at Midspan section, and 200 kPa at Tip section), angles of attack (-5˚,0˚,5˚, and 10˚), and erosion duration (180 sec., and 360 sec.). All experimental material removal and depth of erosion data can be found in Appendix V, and all Photomicrographs of the erosion scars are shown in Appendix VI.

6.3.1 Inboard (Root) Section

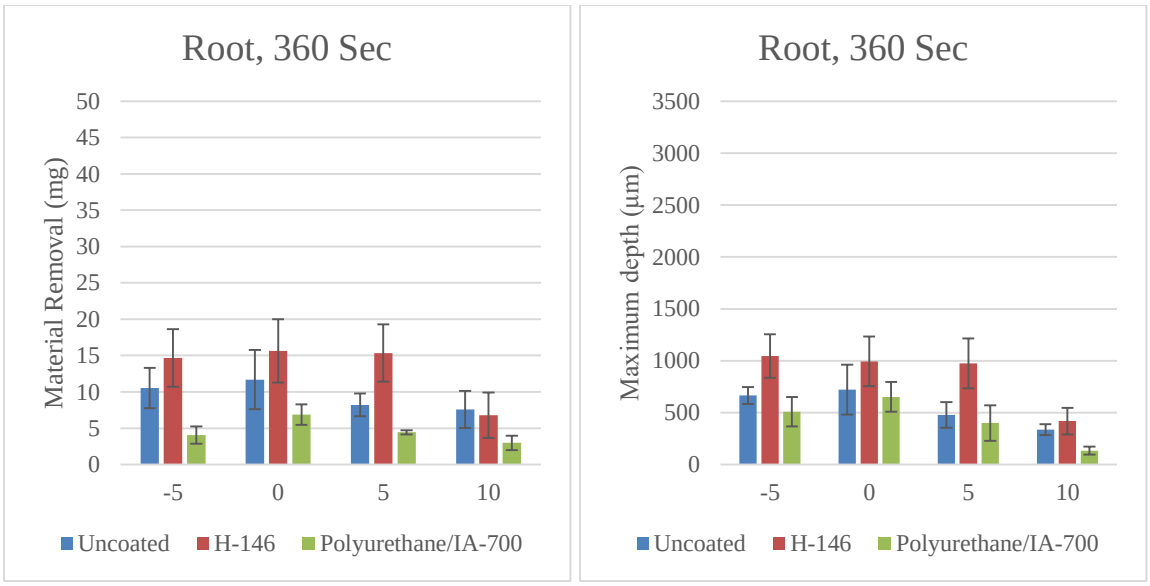
As discussed earlier, air pressure at the Root section was fixed at 100 kPa. Fig. 6-13 below compares the amount of material removed and the maximum erosion depth for all three blades at 180 seconds and 360 seconds erosion durations. It can be seen from Fig. 6-13 that the polyurethane and IA-700 graphene coating experienced less material removal and smaller erosion depth than both the uncoated and H-146 coated blades for all angles of attack. However, the H-146 coated airfoils showed worse erosion behavior than the un-coated airfoils.



(a)



(b)



(c) (d)

Fig. 6-13: Comparison of the erosion behavior of Root section airfoils: (a) material removal at 180 seconds, (b) maximum depth at 180 seconds, (c) material removal at 360 seconds, and (d) maximum depth at 360 seconds

6.3.2 Midspan Section

The air pressure for the midspan section was fixed at 125 kPa. Fig. 6-14 below compares the amount of material removed and the maximum erosion depth for all three blades at 180 seconds and 360 seconds erosion durations. It can be seen from Fig. 6-14 that the intensity of erosion has increased in terms of both material removal and erosion depth. Also, the behavior stayed the same with Polyurethane and IA-700 coating system showing the best results, while H-146 behaved worse than the uncoated blade in most cases.

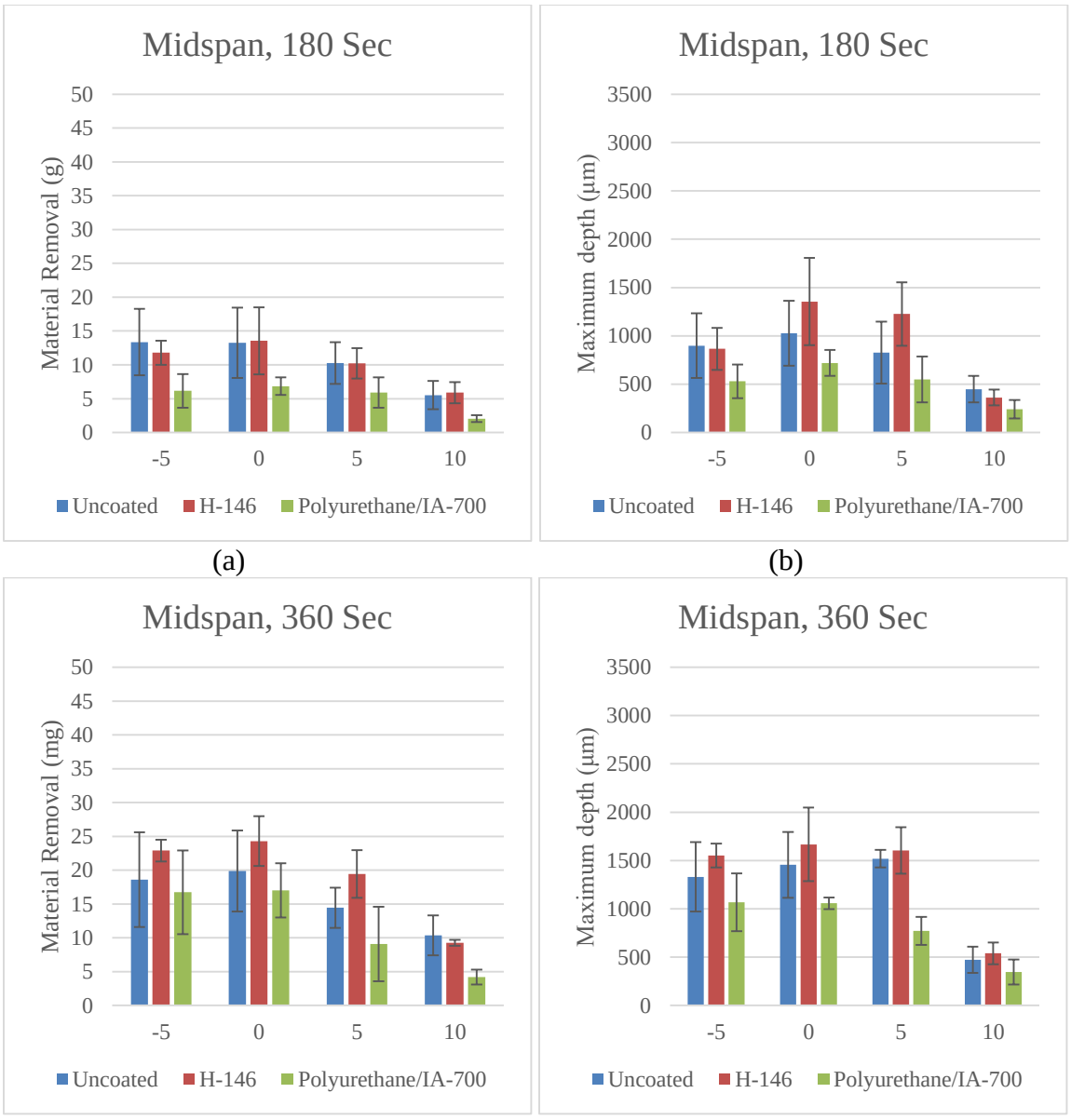


Fig. 6-14: Comparison of the erosion behavior of Midspan section airfoils: (a) material removal at 180 seconds, (b) maximum depth at 180 seconds, (c) material removal at 360 seconds, and (d) maximum depth at 360 seconds

6.2.3 Outboard (Tip) Section

For the smallest section of the blade, the air pressure was kept at 200 kPa. Fig. 6-15 shows material removal and erosion depth data of the three blades for the two erosion durations. Similar to Midspan section, the intensity of erosion has also increased in terms of material

removal and maximum depth. Polyurethane and IA-700 coating kept performing better than the other two blades. When comparing the performance of the uncoated and H-146 coated blades, no conclusion could be reached since their performance in all cases is within the margin of error.

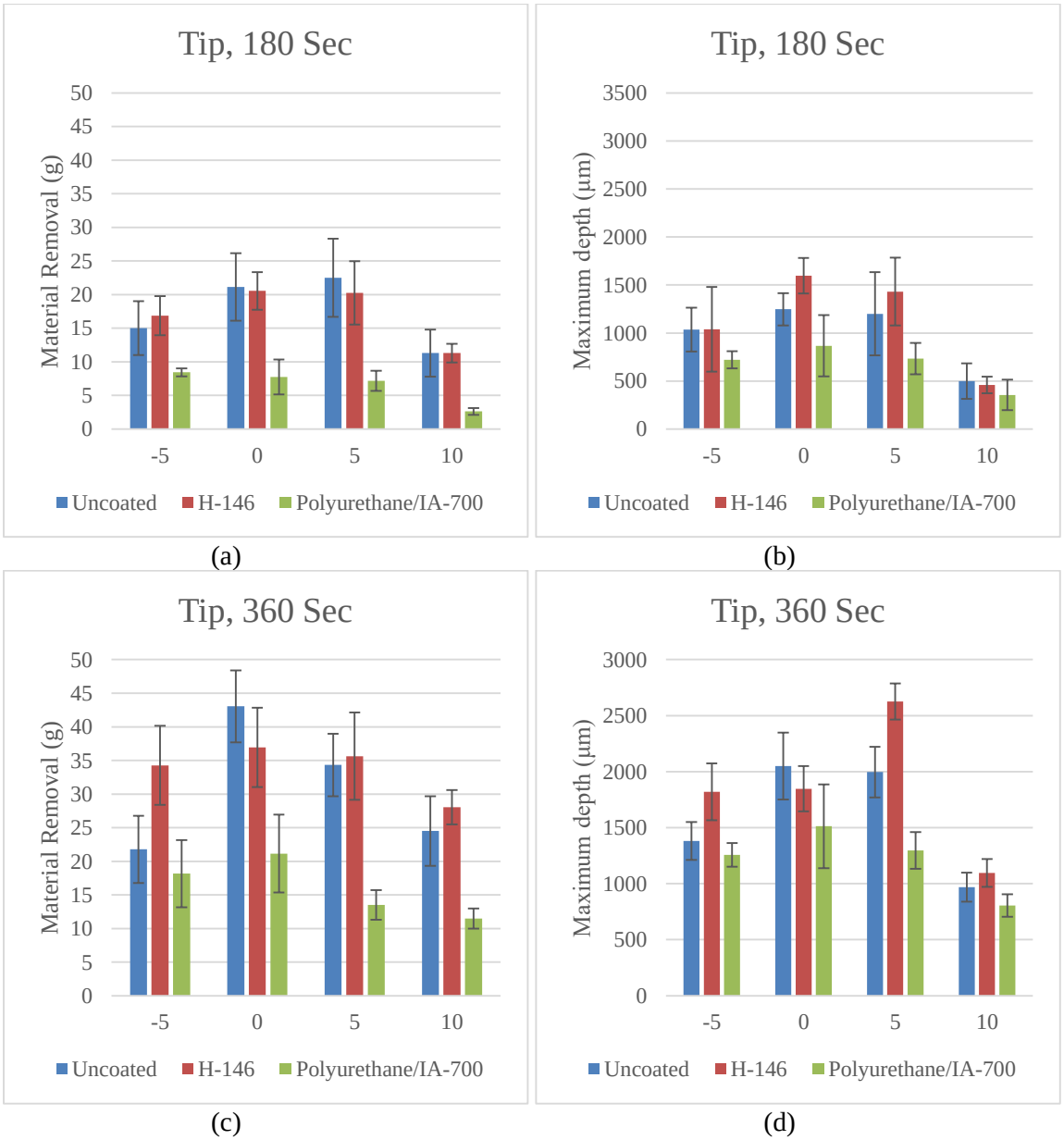


Fig. 6-15: Comparison of the erosion behavior of Midspan section airfoils: (a) material removal at 180 seconds, (b) maximum depth at 180 seconds, (c) material removal at 360 seconds, and (d) maximum depth at 360 seconds

6.4 Discussion

6.4.1 Material Removal

Looking at the material removal shown in Figs. 6-13 to 6-15 (a) and (c), it can be seen that the use of the Polyurethane/IA-700 coating improved the erosion resistance behavior of the blades across the three sections compared to the uncoated blade. On the other hand, H-146 coating showed a worse erosion resistance behavior in most of the cases when compared to the uncoated blade. It can be seen in all three blades that the highest amount of material removed occurred at 0˚ while the least amount removed at 10˚. Also, both material removal and depth of erosion scars increased with the increase of the pressure, and subsequentially the impact velocity, from 100 kPa (12.1 m/s) to 125 kPa (14.3 m/s) to 200 kPa (20.2 m/s). Moreover, both material removal and depth of erosion scars increased with the increase of erosion duration from 180 seconds to 360 seconds. Table 6-1 below shows a comparison of the material removal behavior of the two coated blades to the uncoated blade across all sections for the 360 seconds erosion case. Positive percentages mean that the amount of material removed from the coated blade is higher than the material removed from the uncoated blade and vice versa. From Table 6-1, it can be seen that polyurethane/IA-700 coating was able to show a considerable reduction in material removal, reaching up to 61% when compared to the uncoated material. Consistent high improvements were noticed at 10˚ with more than 50% in all sections of the blade.

Table 6-1: Material removal experienced by H-146 coated blade and polyurethane/IA-700 coated in comparison to the uncoated blade for 360 seconds erosion duration

Blade section	Root		Midspan		Tip	
Angle of Attack	H-146	Polyurethane/ IA-700	H-146	Polyurethane /IA-700	H-146	Polyurethane/ IA-700
-5˚	39%	-61%	23%	-10%	57%	-17%
0˚	34%	-41%	22%	-14%	-14%	-51%
5˚	87%	-46%	35%	-37%	4%	-61%
10˚	-11%	-61%	-11%	-59%	14%	-53%

6.4.2 Depth of Erosion scars

Similar to material removal rates, when measuring the maximum depth of erosion scars, it has been found that increasing pressure and time led to an increase in scars' depth, as can be seen in Figs. 6-13 to 6-15 (b) and (d). Also, the blade coated with polyurethane/IA-700 showed the shallowest scars' depth compared to the uncoated blade and the H-146 coated blade. The highest amount of material removed occurred at 0˚ while the least amount removed at 10˚. Table 6-2 shows a comparison of the depth of erosion scars of the two coated blades to the uncoated blade across all sections for the 360 seconds erosion case. Positive percentages mean that the amount of material removed from the coated blade is higher than the material removed from the uncoated blade and vice versa. It can be noticed in Table 6-2 that polyurethane/IA-700 coating showed a reduction in maximum depth up to 60% when compared to the uncoated blade.

Table 6-2: Maximum erosion depth experienced by H-146 coated blade and polyurethane/IA-700 coated in comparison to the uncoated blade for 360 seconds erosion duration

Blade section	Root		Midspan		Tip	
Angle of Attack	H-146	Polyurethane/ IA-700	H-146	Polyurethane/ IA-700	H-146	Polyurethane/ IA-700
-5˚	57%	-23%	45%	-20%	32%	-9%
0˚	38%	-10%	58%	-27%	-10%	-26%
5˚	104%	-17%	108%	-49%	32%	-35%
10˚	24%	-60%	14%	-27%	13%	-17%

6.4.3 Erosion mechanism

The significant improvement in erosion resistance showed by the Polyurethane/IA-700 coating is due to the combination of a soft layer of polyurethane on top of a harder layer of graphene IA-700. As discussed in the previous chapter, several layers of coatings with different properties can be used to reduce solid particle erosion by interrupting the stress distribution pattern upon impact and allowing for lower stresses [186]. The soft layer works as a damper absorbing the kinetic energy with the incoming abrasive particles, while the stiff layer provides support to the softer layer [193, 194]. On the other hand, although H-146 coating was the coating layer with the highest hardness, it showed worse resistance than the uncoated blade. Since the angles of attack used in this experiment to erode the leading edge are at or near the normal incident, a higher erosion rate is noticed for the stiff H-146 coating when compared to the uncoated blade.

To best compare the erosion behavior between the flat GFRP surface and the leading edge of the wind turbine blade, 90˚ angle of impingement for flat surface, which is equal to 0˚ angle of attack for the leading edge, is used. Also, since for the flat surface the pressure was always kept at 200 kPa, the pressure at the Tip section of the blade is going to be compared to the flat surface. This angle is specifically chosen since it is the only angle at which the erosion behavior for both types of surfaces is known. Table 6-3 below shows the ratio of material removed from the leading edge to the material removed from the flat GFRP at 90˚ angle of impingement from uncoated, H-146 coated, and Polyurethane/IA-700 coated flat and curved surfaces. Also, in Table 6-3, the ratio of the maximum depth of erosion scar of the leading edge to the maximum depth of erosion scar of the flat GFRP is

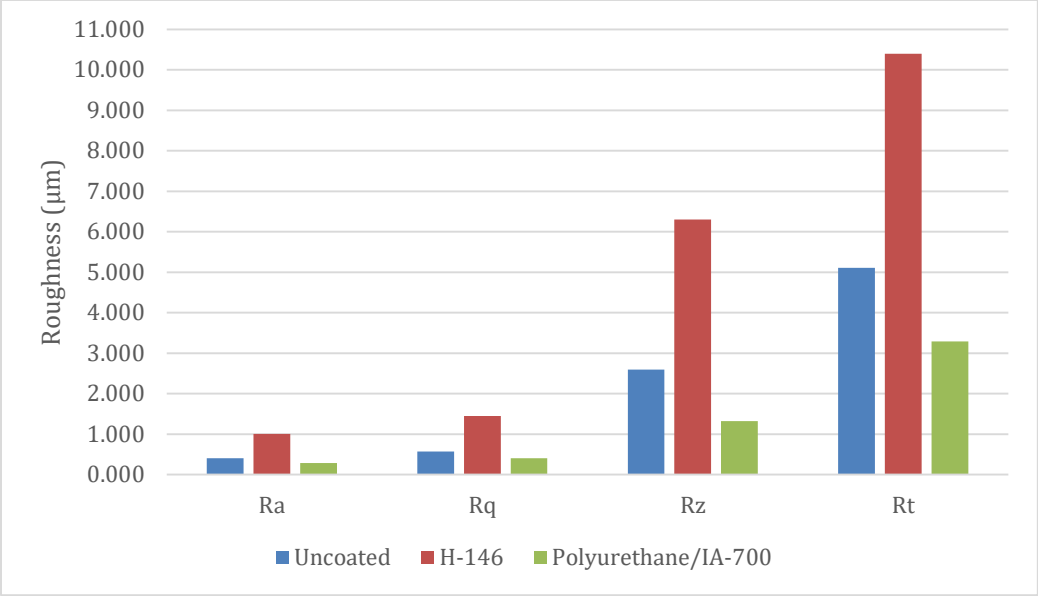
shown. It can be seen in the Table that the amount of material removed and the depth of erosion scars on the leading edge is higher than those of the flat GFRP for all three coating conditions. The ratio of material removed from the leading edge is between 2.8 and 6.4 times higher than that removed from the flat GFRP. Similarly, the depth of erosion scars of the leading edge is more consistent across all three coating conditions between 1.5 and 1.9 times higher than that of flat GFRP.

Table 6-3: Ratio of material removal (and depth of erosion scar) of the leading edge of wind turbine blades to the material removal (and depth of erosion scar) of the flat GFRP surface.

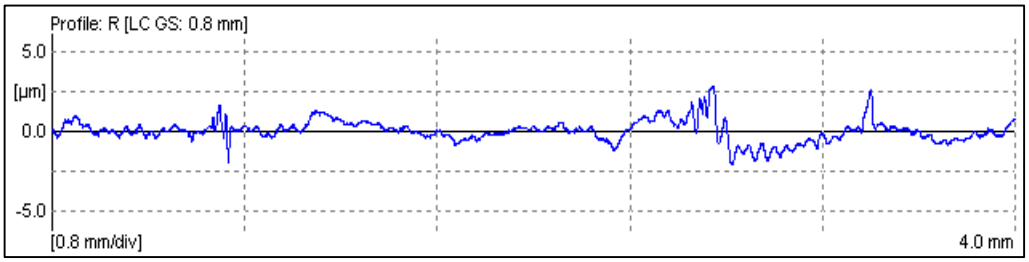
Output	Time (sec.)	Uncoated	H-146	Polyurethane/IA-700
Material re-moval	180	4.7	4.4	2.8
	360	6.4	5.3	3.6
Depth	180	1.6	1.7	1.5
	360	1.7	1.9	1.5

6.4.4 Surface Roughness

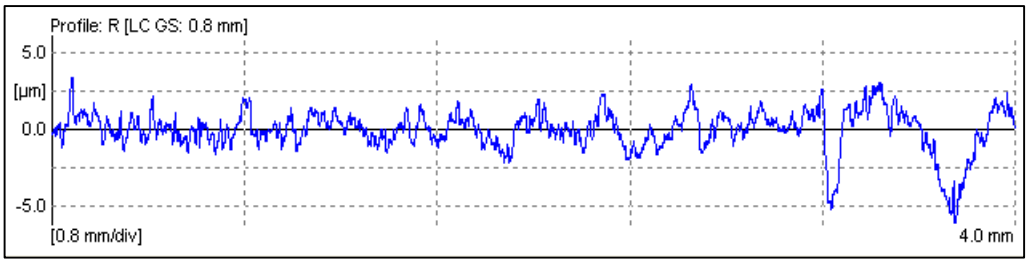
One other factor that could affect the erosion process is the surface roughness of the target material. Higher surface roughness means that the number of contact points between the target material and the abrasive particles is increased, and since asperities on the surface serve as damage initiation sites, higher erosion rates are expected [95]. Reducing the initial surface roughness reduced the erosion rate [94]. A comparison of some of the surface roughness parameters is shown in Fig. 6-16 (a), and surface profiles are shown in Fig. 6-16 (b), (c), and (d). It can be seen from the figure that H-146 showed the highest surface roughness, followed by the uncoated blade, then polyurethane/IA-700 surface, which has a similar trend to the erosion behavior seen in material removal and depth of erosion scars.



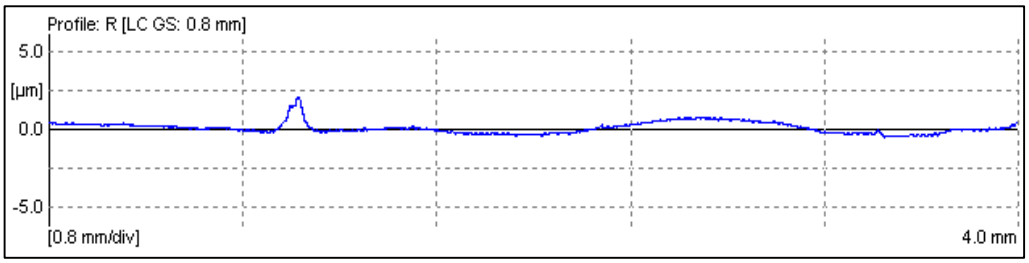
(a)



(b) Uncoated



(c) H-146



(d) Polyurethane/IA-700

Fig. 6-16: (a) Surface Roughness parameters comparison, Surface profile of: (b) uncoated, (c) H-146, and (d) polyurethane/IA-700

6.3.4 Regression Analysis

6.3.4.1 Effects of Erosion Parameters on Erosion behavior

A regression analysis has been adopted to understand the effects of the erosion parameters used in this experiment. Design Expert® software (Version 9.0.3.1, Stat-Ease Inc.) has been utilized to analyze the three variable factors used in this experiment. With pressure ranging from 100 kPa at the Root section to 125 kPa at the Midspan section to 200 kPa at the Tip section, pressure is the first factor to be studied. The second factor is erosion duration at 180 seconds and 360 seconds. The last factor is the angle of attack ranging from -5˚ to 10˚ at 5˚ increments. A summary of the variables used in this analysis is shown in Table 6-4. Equation 6-3 shows the standard second order polynomial generated using Design Expert® to predict the erosion behavior in terms of the mass loss and depth of erosion scars. Analysis of Variance (ANOVA) is used to statistically study the impact and significance of the used variables on the outcome of the erosion experiments.

Table 6-4: A summary of variables used in regression analysis

Variable	**Magnitude**
Pressure (kPa), x_1	100, 125, and 200
Erosion duration (seconds), x_2	180 and 360
Angle of Attack (deg.), x_3	-5, 0, 5, and 10

$$y(x) = c_0 + \sum_{i=1}^{3} c_i x_i + \sum_{i=1}^{3} c_{ii} x_i^2 + \sum_{i=1}^{2} \sum_{j=i+1}^{3} c_{ij} x_i x_j \qquad (6\text{-}3)$$

where $y(x)$ dependent variable

c_0 constant

c_i first order coefficient

c_{ii} second order coefficient

c_{ij} interaction coefficient

x_i independent variable

6.3.4.1.1 Mass loss

The mass loss data were analyzed for the three blades, and Tables 6-5 to 6-7 show the analysis of variance for the uncoated, H-146, and Polyurethane/IA-700, respectively. If a p-value is less than 0.05, the model or the factor under study is significant. The model p-value is less than 0.0001 for all three tables, which means the models proposed to estimate the mass loss are significant. For the uncoated blade, the factor that shows the highest significance, represented in the highest F-value and the lowest p-value, is pressure (A) followed by time (B), while the lowest was time*angle (BC). For the H-146 coated blade, the highest significance is shown by pressure (A) followed by time (B), while the lowest is shown by pressure^2 (A^2). Finally, the most significant factor for Polyurethane/IA-700 coated blade is shown by time (B) followed by pressure (A), while the least significant factor is pressure*angle (AC).

The regression analysis for the mass loss response for the uncoated, H-146, and Polyurethane/IA-700 blades is summarized in Table 6-8. R^2 values ranged from 0.8795 for the uncoated blade to 0.9039 for the Polyurethane/IA-700 coated blade, to 0.9806 for H-146 coated blade. The adequate precision measures the signal-to-noise ratio, with a ratio greater than 4 being desirable. The ratio for the uncoated, H-146, and Polyurethane/IA-700 models are 13.226, 35.044, and 15.105, respectively. These adequate precision ratios indicate adequate signals, meaning these models can navigate the design space.

Table 6-5: Analysis of variance table to predict the mass loss of the uncoated blade

Source	Sum of Squares	df	Mean Square	F Value	p-value Prob > F
Model	1811.24	8	226.40	13.69	< 0.0001
A-Pressure	1095.61	1	1095.61	66.25	< 0.0001
B-Time	396.67	1	396.67	23.99	0.0002
C-Angle	51.12	1	51.12	3.09	0.0991
AB	108.43	1	108.43	6.56	0.0217
AC	2.54	1	2.54	0.15	0.7007
BC	0.058	1	0.058	3.525E-3	0.9534
A^2	9.95	1	9.95	0.60	0.4499
C^2	174.34	1	174.34	10.54	0.0054
Residual	248.07	15	16.54		
Cor Total	2059.30	23			

Table 6-6: Analysis of variance table to predict the mass loss of the H-146 coated blade

Source	Sum of Squares	df	Mean Square	F Value	p-value Prob > F
Model	2001.54	8	250.19	94.73	< 0.0001
A-Pressure	884.39	1	884.39	334.84	< 0.0001
B-Time	694.05	1	694.05	262.78	< 0.0001
C-Angle	157.52	1	157.52	59.64	< 0.0001
AB	137.43	1	137.43	52.03	< 0.0001
AC	1.56	1	1.56	0.59	0.4543
BC	11.14	1	11.14	4.22	0.0579
A^2	0.56	1	0.56	0.21	0.6530
C^2	133.57	1	133.57	50.57	< 0.0001
Residual	39.62	15	2.64		
Cor Total	2041.16	23			

Table 6-7: Analysis of variance table to predict the mass loss of the Polyurethane/IA-700 coated blade

Source	Sum of Squares	df	Mean Square	F Value	p-value Prob > F
Model	668.34	8	83.54	17.64	< 0.0001
A-Pressure	235.72	1	235.72	49.77	< 0.0001
B-Time	250.79	1	250.79	52.95	< 0.0001
C-Angle	110.43	1	110.43	23.32	0.0002
AB	50.09	1	50.09	10.58	0.0054
AC	9.42	1	9.42	1.99	0.1789
BC	18.38	1	18.38	3.88	0.0676
A^2	43.60	1	43.60	9.21	0.0084
C^2	29.05	1	29.05	6.13	0.0256
Residual	71.04	15	4.74		
Cor Total	739.38	23			

Table 6-8: Summary of results of regression analysis for mass loss response

Blade	**Uncoated**	**H-146**	**Polyurethane/IA-700**
R^2	0.8795	0.9806	0.9039
Adjusted R^2	0.8153	0.9702	0.8527
Predicted R^2	0.5966	0.9478	0.7313
Standard deviation	4.07	1.63	2.18
C.V. %	27.08	9.60	27.92
Adequate Precision	13.326	35.044	15.105

The equation in terms of coded factors can be used to make predictions about the response for given levels of each factor. Table 6-9 shows the coded factors, while Table 6-10 shows the actual factors. By default, the high levels of the factors are coded as +1 and the low levels of the factors are coded as -1. The coded equation is useful for identifying the relative impact of the factors by comparing the factor coefficients. Fig. 6-17 shows mass loss graphs relating pressure with time at a constant angle of attack of 0˚, and relating pressure with the angle of attack at a constant erosion duration of 360 seconds for the three blades. It can be noticed that mass loss increases with the increase of pressure and time, and it increases with the angle of attack up to 0˚ and then start decreasing. The effects of these factors on mass loss are estimated in the following equation:

$$\begin{aligned}\text{Mass loss (in mg)} = {} & C_1 \\ & + C_2 * \text{Pressure} \\ & + C_3 * \text{Time} \\ & + C_4 * \text{Angle} \\ & + C_5 * \text{Pressure} * \text{Time} \\ & + C_6 * \text{Pressure} * \text{Angle} \\ & + C_7 * \text{Time} * \text{Angle} \\ & + C_8 * \text{Pressure}^2 \\ & + C_9 * \text{Angle}^2\end{aligned} \tag{6-4}$$

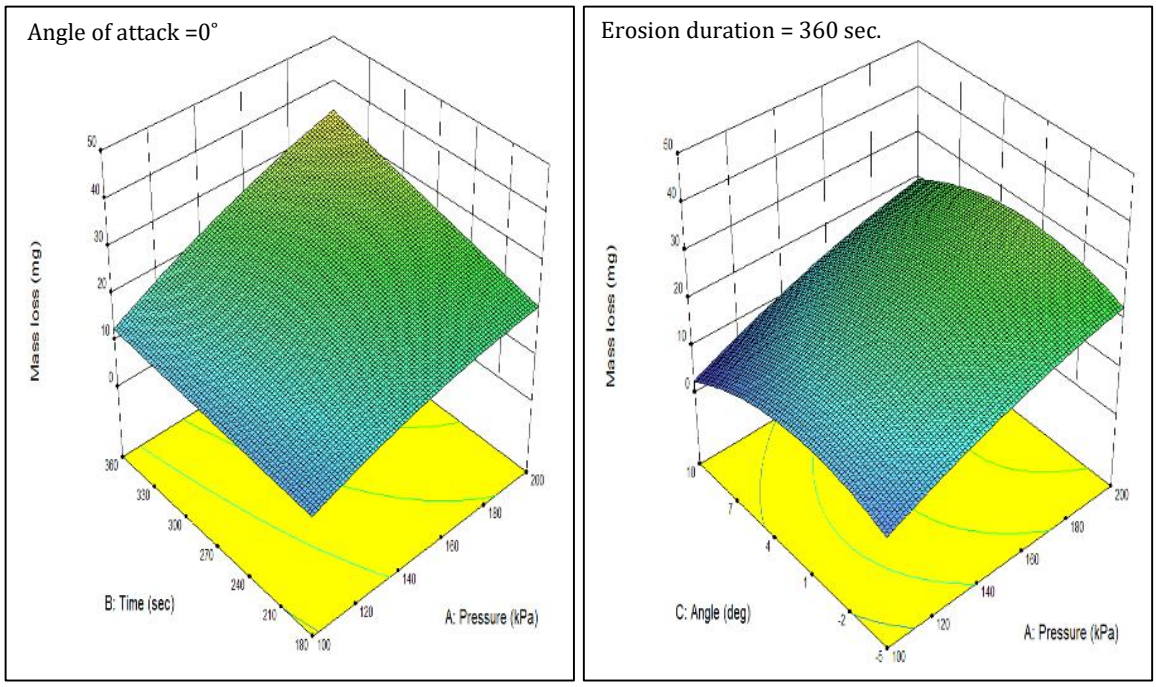
where C_1 to C_9 are empirical factors.

Table 6-9: Coded factors of the mass loss equation for the uncoated, H-146, and Polyurethane/IA-700 coated blades.

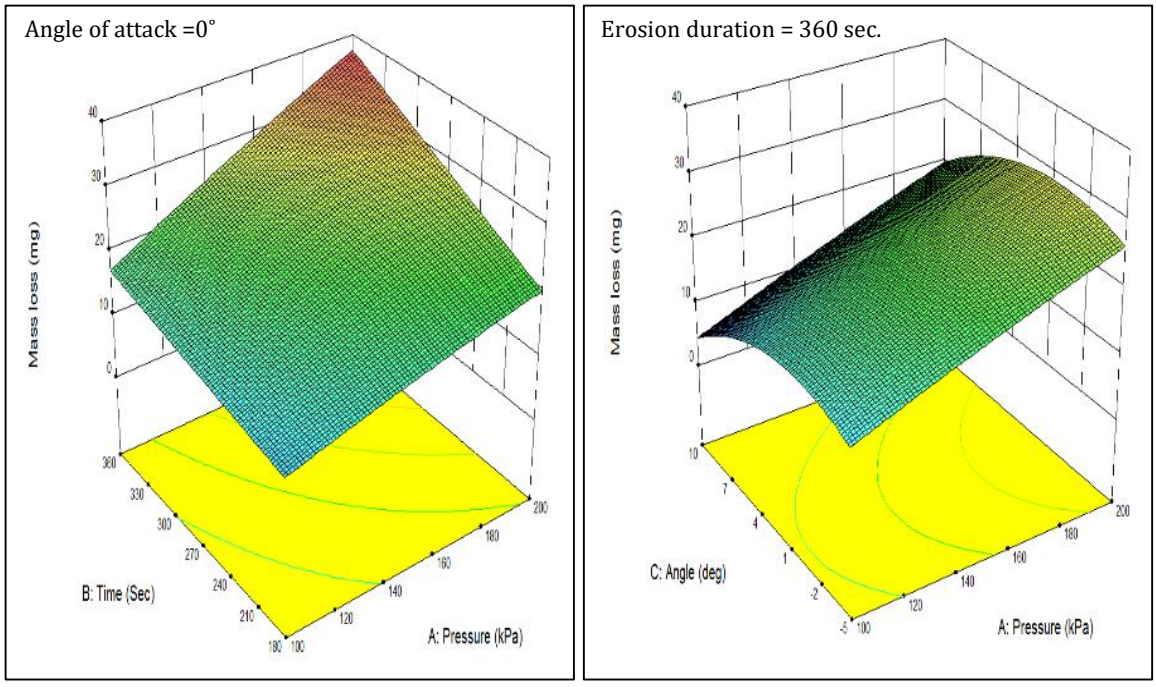
Factor	**Uncoated**	**H-146**	**Polyurethane/IA-700**
C_1 [mg]	+21.19	+21.45	+12.79
C_2 [mg/kPa]	+8.28	+7.43	+3.84
C_3 [mg/s]	+4.14	+5.48	+3.29
C_4 [mg/deg.]	-2.00	-3.50	-2.93
C_5 [mg/kPa- s]	+2.50	+2.82	+1.70
C_6 [mg/kPa-deg.]	+0.51	+0.40	-0.99
C_7 [mg/s-deg.]	-0.066	-0.91	-1.17
C_8 [mg/kPa^2]	-1.90	-0.45	-3.97
C_9 [mg/deg.^{2}]	-6.06	-5.31	-2.48

Table 6-10: Empirical constants needed for the mass loss estimation for the uncoated, H-146, and Polyurethane/IA-700

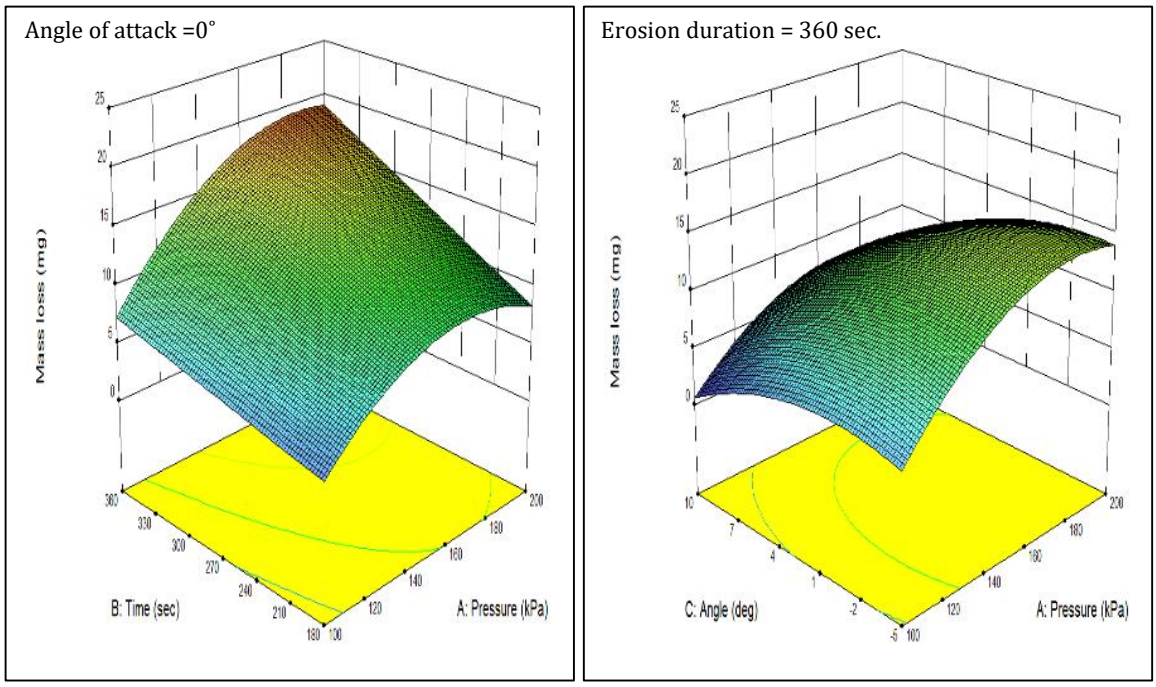
Factor	**Uncoated**	**H-146**	**Polyurethane/IA-700**
C_1 [mg]	-10.18	4.08	-30.49
C_2 [mg/kPa]	0.24	0.03	0.46
C_3 [mg/s]	-0.04	-0.03	-0.02
C_4 [mg/deg.]	0.09	0.21	0.69
C_5 [mg/kPa- s]	5.56E-04	6.26E-04	3.78E-04
C_6 [mg/kPa-deg.]	1.37E-03	1.07E-03	-2.64E-03
C_7 [mg/s-deg.]	-9.80E-05	-1.35E-03	-1.74E-03
C_8 [mg/kPa^2]	-7.58E-04	-1.79E-04	-1.59E-03
C_9 [mg/deg.^{2}]	-0.11	-0.09	-0.04



(a) Uncoated



(b) H-146



(c) Polyurethane/IA-700

Fig. 6-17: Mass loss due to varying pressure, erosion duration, and angle of attack.

6.3.4.1.2 Depth of Erosion scar

Similarly, ANOVA of depth of erosion scar in terms of the varying pressure, erosion duration, and angle of attack for the three blades is shown in Tables 6-11 to 6-13. The model p-value is less than 0.0001 for all three tables, which means the models proposed to estimate the depth of erosion scars are significant. The factor with highest significance for all three blades is pressure (A), while the factor of the least significance for all three blades is pressure*angle (AC).

Table 6-14 summarizes the regression analysis for the mass loss response for the uncoated, H-146, and Polyurethane/IA-700 blades. R^2 values ranged from 0.9113 for uncoated blade to 0.9532 for the H-146 coated blade, to 0.9598 for Polyurethane/IA-700 coated blade. The adequate precision ratio for the uncoated, H-146, and Polyurethane/IA-700 models are

16.574, 23.210, and 24.766, respectively. These adequate precision ratios are greater than the desirable ratio of 4, indicating adequate signals, meaning these models can be used to navigate the design space.

Table 6-11: Analysis of variance table to predict the depth of erosion scars of the un-coated blade

Source	Sum of Squares	df	Mean Square	F Value	p-value Prob > F
Model	5.587E+006	8	6.984E+005	19.27	< 0.0001
A-Pressure	2.754E+006	1	2.754E+006	76.00	< 0.0001
B-Time	1.023E+006	1	1.023E+006	28.25	< 0.0001
C-Angle	6.773E+005	1	6.773E+005	18.69	0.0006
AB	1.744E+005	1	1.744E+005	4.81	0.0444
AC	1944.16	1	1944.16	0.054	0.8199
BC	12636.50	1	12636.50	0.35	0.5636
A^2	5.106E+005	1	5.106E+005	14.09	0.0019
C^2	9.845E+005	1	9.845E+005	27.17	0.0001
Residual	5.435E+005	15	36232.11		
Cor Total	6.130E+006	23			

Table 6-12: Analysis of variance table to predict the depth of erosion scars of the H-146 coated blade

Source	Sum of Squares	df	Mean Square	F Value	p-value Prob > F
Model	6.047E+006	8	7.559E+005	38.22	< 0.0001
A-Pressure	1.879E+006	1	1.879E+006	95.01	< 0.0001
B-Time	1.098E+006	1	1.098E+006	55.54	< 0.0001
C-Angle	1.248E+006	1	1.248E+006	63.09	< 0.0001
AB	1.600E+005	1	1.600E+005	8.09	0.0123
AC	14169.62	1	14169.62	0.72	0.4106
BC	59942.70	1	59942.70	3.03	0.1022
A^2	2.402E+005	1	2.402E+005	12.15	0.0033
C^2	1.698E+006	1	1.698E+006	85.86	< 0.0001
Residual	2.967E+005	15	19776.98		
Cor Total	6.343E+006	23			

Table 6-13: Analysis of variance table to predict the depth of erosion scars of the Polyurethane/IA-700 coated blade

Source	***Sum of Squares***	***df***	***Mean Square***	***F Value***	***p-value Prob > F***
Model	*3.506E+006*	*8*	*4.383E+005*	*44.75*	*< 0.0001*
A-Pressure	*1.526E+006*	*1*	*1.526E+006*	*155.81*	*< 0.0001*
B-Time	*8.918E+005*	*1*	*8.918E+005*	*91.05*	*< 0.0001*
C-Angle	*6.042E+005*	*1*	*6.042E+005*	*61.69*	*< 0.0001*
AB	*1.187E+005*	*1*	*1.187E+005*	*12.12*	*0.0034*
AC	*773.56*	*1*	*773.56*	*0.079*	*0.7825*
BC	*54145.56*	*1*	*54145.56*	*5.53*	*0.0328*
A^2	*2.065E+005*	*1*	*2.065E+005*	*21.08*	*0.0004*
C^2	*3.738E+005*	*1*	*3.738E+005*	*38.16*	*< 0.0001*
Residual	*1.469E+005*	*15*	*9794.31*		
Cor Total	*3.653E+006*	*23*			

Table 6-14: Summary of results of regression analysis for the depth of erosion scar response

Blade	**Uncoated**	**H-146**	**Polyurethane/IA-700**
R^2	0.9113	0.9532	0.9598
Adjusted R^2	0.8641	0.9283	0.9383
Predicted R^2	0.7213	0.8670	0.8893
Standard deviation	190.35	140.63	98.97
C.V. %	20.67	12.63	15.19
Adequate precision	16.574	23.210	24.766

Fig. 6-18 shows the depth of erosion scars when relating pressure to erosion duration at a constant angle of attack of 0˚, and when relating pressure with angle of attack at a constant erosion duration of 360 seconds. From Fig. 6-18 it can be seen that the highest erosion rate occurs when pressure and erosion duration (time) are at their highest. On the other hand, for the pressure and angles of attack graphs, the highest erosion occurs at the highest pressure and 0˚ angle of attack. The following equation shows a quadratic model to predict the depth of erosion scars:

$$\begin{aligned} \text{Depth} = & \quad D_1 \\ & + D_2 * \text{Pressure} \\ & + D_3 * \text{Time} \\ & + D_4 * \text{Angle} \\ & + D_5 * \text{Pressure} * \text{Time} \\ & + D_6 * \text{Pressure} * \text{Angle} \\ & + D_7 * \text{Time} * \text{Angle} \\ & + D_8 * \text{Pressure}\text{\^{}}2 \\ & + D_9 * \text{Angle}\ \text{\^{}}2 \end{aligned} \tag{6-5}$$

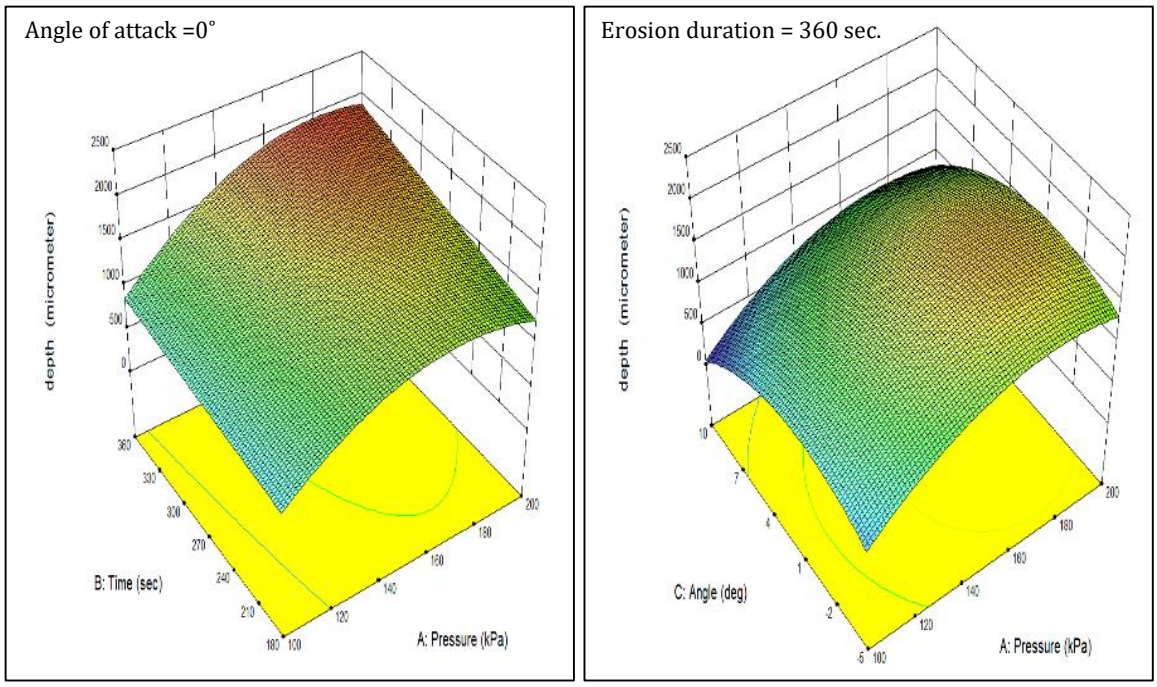
where D_1 to D_9 are empirical factors. The coded factors are shown in Table 6-15 while the actual factors are shown in Table 6-16.

Table 6-15: Coded factors of the depth of erosion scar equation for uncoated, H-146, and Polyurethane/IA-700 coated blades.

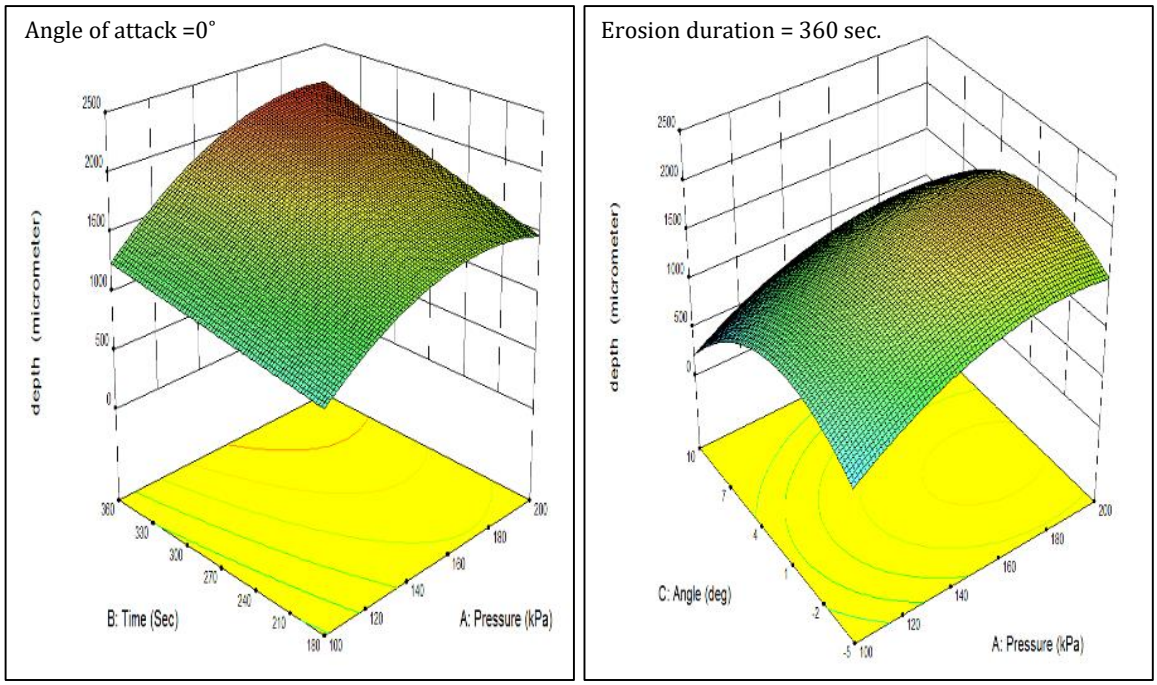
Factor	**Uncoated**	**H-146**	**Polyurethane/IA-700**
D_1 [μm]	+1565.05	+1723.85	+1063.70
D_2 [μm/kPa]	+414.85	+342.69	+308.83
D_3 [μm/s]	+210.44	+218.01	+196.44
D_4 [μm/deg.]	-229.67	-311.74	-216.92
D_5 [μm/kPa- s]	+100.32	+96.09	+82.74
D_6 [μm/kPa-deg.]	-14.21	-38.36	-8.96
D_7 [μm/s-deg.]	-30.79	-67.05	-63.73
D_8 [μm/kPa^2]	-429.38	-294.54	-273.06
D_9 [μm/deg.^{2}]	-455.71	-598.50	-280.79

Table 6-16: Empirical constants needed to estimate the depth of erosion scars for the three blades.

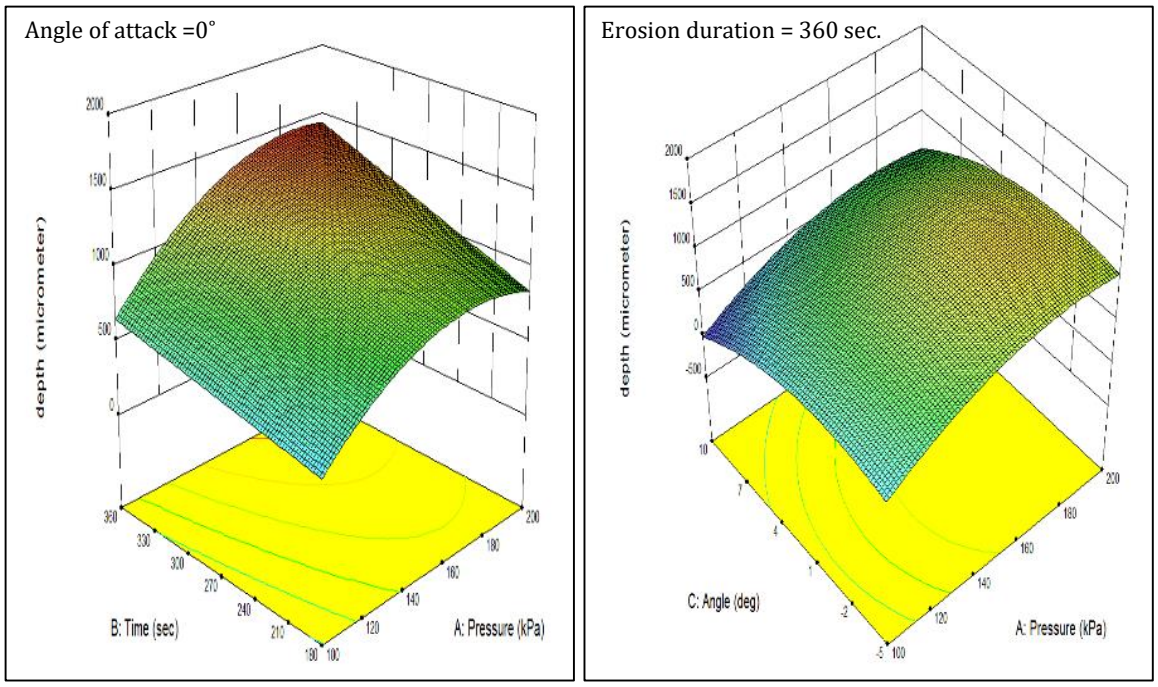
Factor	**Uncoated**	**H-146**	**Polyurethane/IA-700**
D_1 [μm]	-3291.50	-1812.34	-2196.50
D_2 [μm/kPa]	53.90	36.70	34.04
D_3 [μm/s]	-0.89	-0.53	-0.34
D_4 [μm/deg.]	27.88	53.80	25.11
D_5 [μm/kPa- s]	0.02	0.02	0.02
D_6 [μm/kPa-deg.]	-0.04	-0.10	-0.02
D_7 [μm/s-deg.]	-0.05	-0.10	-0.09
D_8 [μm/kPa^2]	-0.17	-0.12	-0.11
D_9 [μm/deg.^{2}]	-8.10	-10.64	-4.99



(a) uncoated



(b) H-146



(c) Polyurethane/IA-700

Fig. 6-18: Depth of erosion scars as a function of varying pressure, erosion duration, and angle of attack.

6.3.4.2 Mass loss and Erosion depth relationship

During maintenance, workers can easily measure the depth of erosion scar that they see on the leading edge of wind turbine blades. However, measuring the amount of material removed is extremely difficult. As discussed earlier, losing material from the blade is detrimental since it can make the turbine asymmetric due to mass imbalance and change the load distribution, affecting the turbine's structural stability. Therefore, an exponential relationship between the amount of material removed and the depth of erosion scar at the leading edge of wind turbine blades has been developed as:

$$m_{loss} = a_1 e^{a_2 d_s} \tag{6-6}$$

where a_1 and a_2 are constants.

Depth of erosion scars is measured in micrometers, while the mass loss in milligrams. Fig. 6-19 shows mass loss from the uncoated blade as a function of erosion depth. Table 6-17 shows the constants of Eqn. 6-6 for the uncoated, H-146, and polyurethane/IA-700 blades, as well as the R^2 for each blade. Therefore, from measuring the depth of erosion scars in the blade due to sand particle impingement, the amount of material removed can be estimated, and the structural stability of the blade can always be maintained.

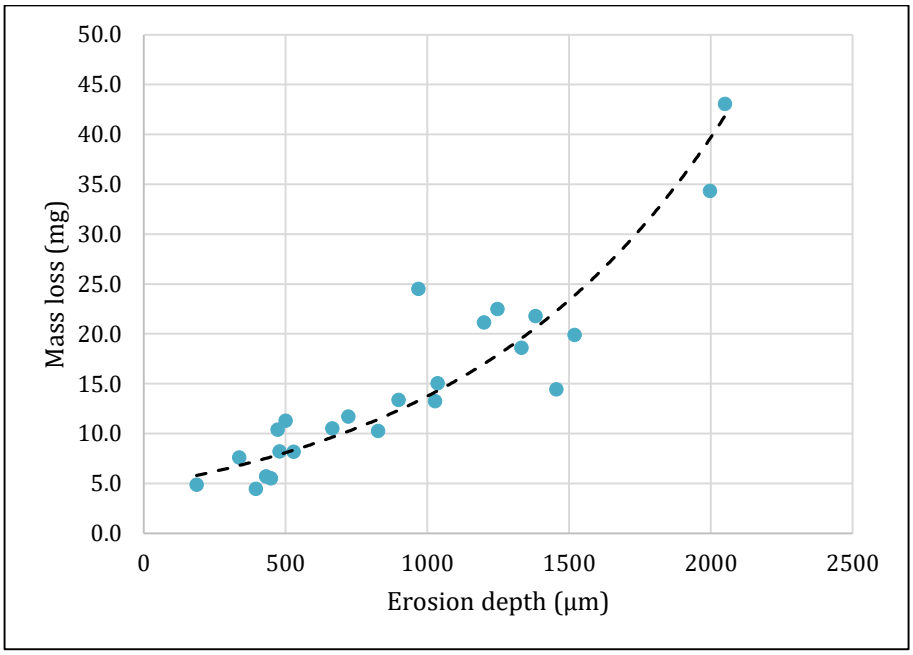


Fig. 6-19: Relationship between erosion scar depth and the amount of material removed

Table 6-17: Empirical constants and R^2 values for Eqn. 6-6

Parameters	Uncoated	H-146	Polyurethane/IA-700
a_1	4.7563	4.887	1.8692
a_2	0.0011	0.0010	0.0018
R^2	0.829	0.8065	0.879

In summary, the leading edge erosion of wind turbine blades has detrimental effects on structure stability as well as aerodynamic performance. In this chapter, the erosion behavior

due to varying angles of attack, varying erosion durations, and varying air pressures and impact velocities have been characterized. It has been found that the maximum erosion is characterized by the amount of material removed, and the maximum depth of erosion scar occurs at the leading edge when bombarded at 0˚. On the other hand, the least amount of damage has been noticed when the leading edge is attacked at 10˚. The use of protective coatings has been shown to reduce the intensity of erosion in the last chapter. A combination of graphene IA-700 as the base layer and polyurethane as the top layer shows improvements reaching 60% improvement in both material removal and depth of erosion. However, the use of a single layer of graphene H-146 did not show erosion resistance ability compared to the uncoated blade. Since the aerodynamic performance is of the wind turbine blades is expected to be affected by the leading edge erosion, the next chapter will investigate this relationship thoroughly.

Chapter 7: Analysis of Aerodynamic Performance

As shown in the previous chapter, the leading edge erosion of wind turbine blades affects the structural stability by material removal and alters the shape of airfoils. Changes in the shape of the airfoil will consequently change the aerodynamic performance of the whole blade, and it is expected to decrease the overall efficiency. Therefore, in this chapter, the aerodynamic performance of the uncoated blade, H-146 coated blade, and polyurethane/Ia-700 coated blade will be investigated.

7.1 Aerodynamic performance

To understand and characterize the aerodynamic performance of wind turbine blades with eroded leading edge, the uncoated blade will be studied first to exclude the effects of coatings on the performance. Three parameters will be used to analyze the aerodynamic performance: changes in lift coefficient, changes in drag coefficient, and changes in power generation.

In real life, after the wind turbines got eroded due to the harsh conditions during a sandstorm, the goal is to measure their aerodynamic performance throughout the year during normal and average conditions. The average wind speed in Kuwait at 10 m heigh is 3.7 – 5.5 m/s [195]. Since the chord length of the blade tapers from 16 cm to 5 cm, local relative velocity changes according to the following equation:

$$V_{\infty} = \frac{Re\, \nu}{c} \tag{7-1}$$

where Re is Reynolds number

ν is Kinematic viscosity (1.65×10^{-5} m^2/s at 35˚ C)

c is chord length

Taking Reynolds number to be 50 x10^3 results of local relative velocities are shown in Table 7-1 at representative location in each section.

Table 7-1: local velocity at representative r/R location in each section with R=120 cm.

r (cm)	r/R	c (cm)	V_∞ (m/s)
38.5	32%	14.1	5.85
78	65%	10.2	8.10
102	85%	8.5	10.77

As discussed in the previous chapter, the 2D profiles at the location of erosion scars were extracted before and after erosion. Then these 2D profiles were analyzed using Xfoil and lift and drag coefficients as a function of angle of attack were obtained. Full Xfoil documentations are shown in Appendix VII, and the full aerodynamic performance data are shown in Appendix VIII. To calculate the change in the lift coefficients before and after erosion, lift coefficient will be measured for a range of angles of attack and a specific angle of interest will be chosen, for example the angle at which the highest lift occurred, then lift coefficient before erosion will be compared to lift coefficient for after erosion at the same angle of attack. Change in drag coefficient will be measured in a similar manner. The performance of the airfoil was affected in terms of an increase in drag and a decrease in lift due to the erosion process. The change in aerodynamic coefficients was measure using the following equation:

$$\%\Delta C_l = \frac{C_{l,BE} - C_{l,AE}}{C_{l,BE}}\ x\ 100 \tag{7-2}$$

$$\%\Delta C_d = \frac{C_{d,BE} - C_{d,AE}}{C_{d,BE}}\ x\ 100 \tag{7-3}$$

where $\%\Delta C_l$ ($\%\Delta C_d$) is the change in lift (drag) coefficient before and after erosion

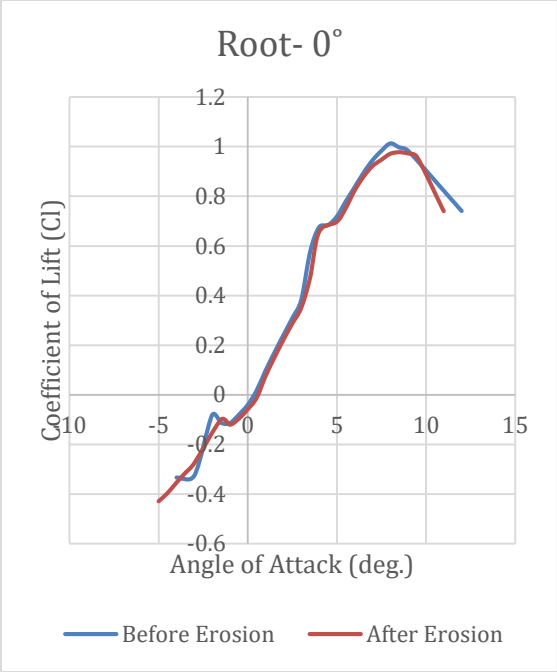
$C_{l,BE}$ ($C_{d,BE}$) is the lift (drag) coefficient before erosion

$C_{l,AE}$ ($C_{d,AE}$) is the lift (drag) coefficient after erosion

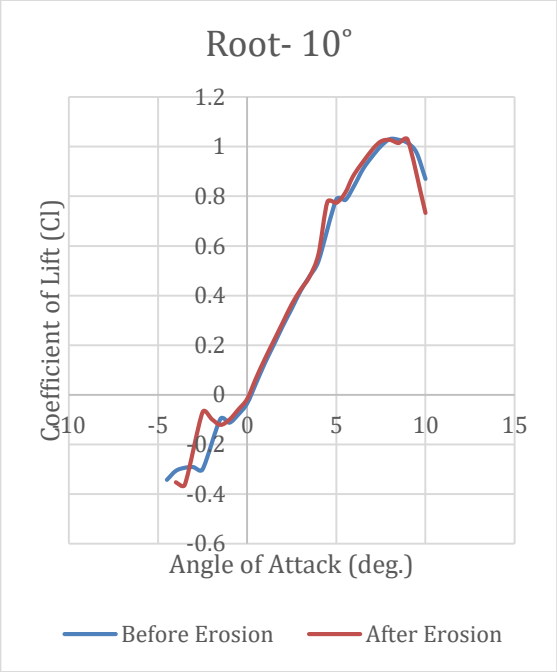
7.1.1 Uncoated blade

7.1.1.1 Lift coefficient

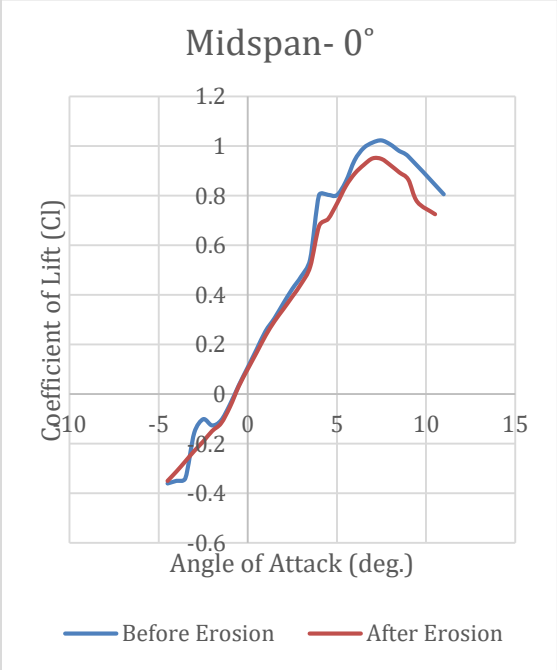
Starting with the lift coefficient, Fig.7-1 shows the changes in performance before and after erosion for the blade sections: Root, Midspan, and Tip. The graphs shown in Fig. 7-1 are for airfoils eroded at angles of impingement of 0˚ (highest erosion damage) and 10˚ (least erosion damage). It can be seen that with the increase in erosion intensity toward the tip, the change in lift increases, especially between 5˚ and 10˚ angles of attack. The change in lift coefficient is more noticeable in the 0˚ erosion case than 10˚. For example, for the 0˚ erosion case at the Root section at an 8˚ angle of attack, the highest lift coefficient before erosion was 1.01, while after erosion, the lift coefficient was 0.97, which means the coefficient of lift decreased by 4%. For the Tip section, a huge drop in lift can be noticed after 7˚ angle of attack, where the decrease in lift at 8˚ was 39%. On the other hand, the change in lift coefficient at 10˚ angle of impingement at 8˚ angle of attack is 1%, 4%, and 6% for Root, Midspan, and Tip sections, respectively.


Root- 0°
Coefficient of Lift (Cl)
Angle of Attack (deg.)
Before Erosion
After Erosion

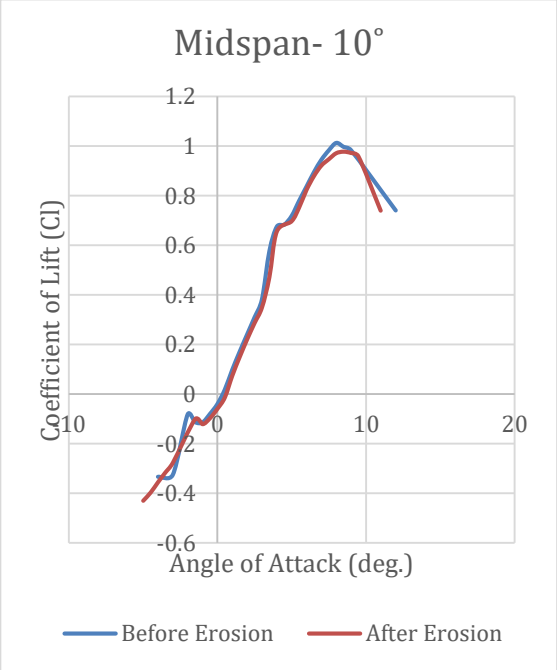
(a)


Root- 10°
Coefficient of Lift (Cl)
Angle of Attack (deg.)
Before Erosion
After Erosion

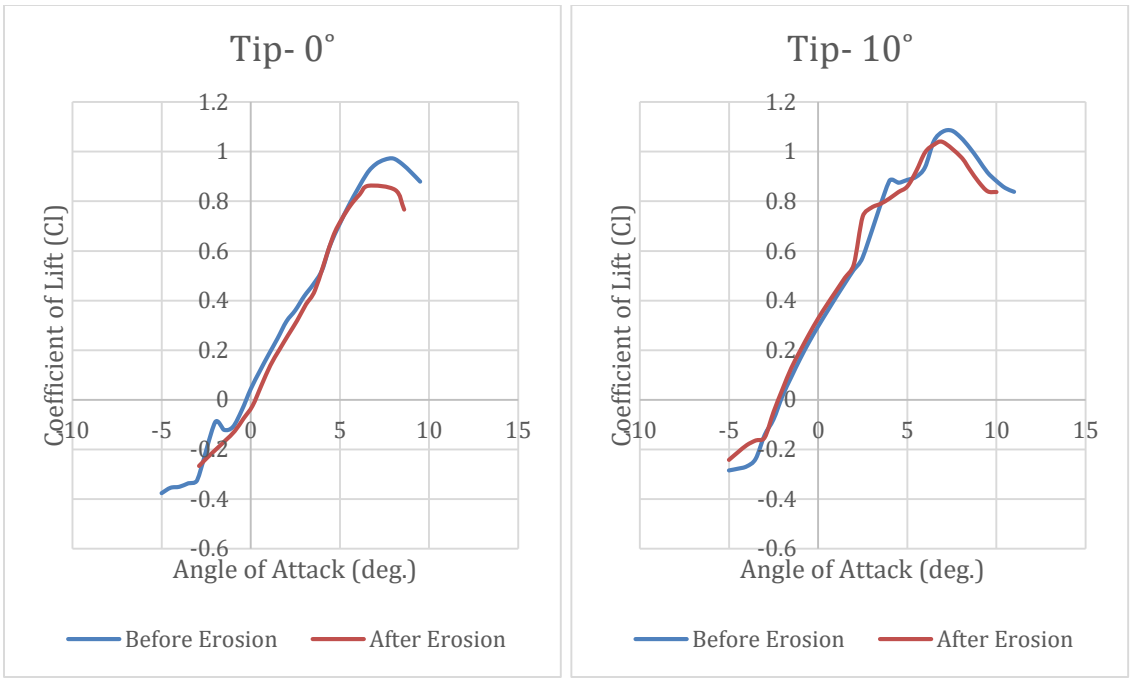
(b)


Midspan- 0°
Coefficient of Lift (Cl)
Angle of Attack (deg.)
Before Erosion
After Erosion

(c)


Midspan- 10°
Coefficient of Lift (Cl)
Angle of Attack (deg.)
Before Erosion
After Erosion

(d)

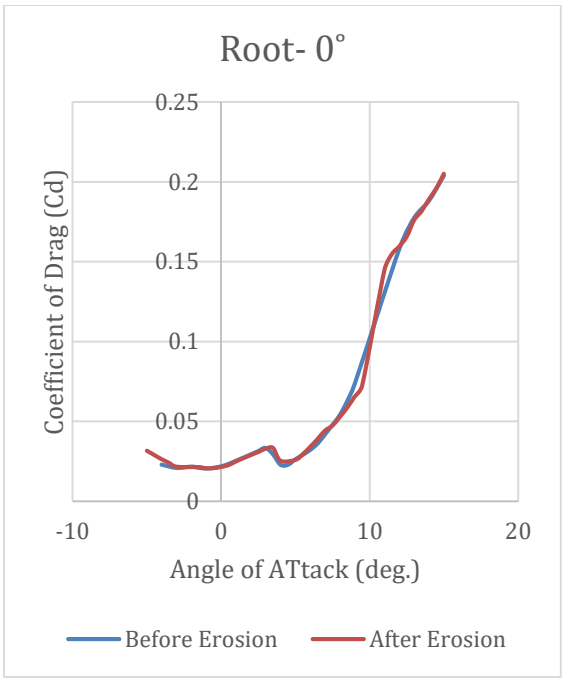


(e) (f)

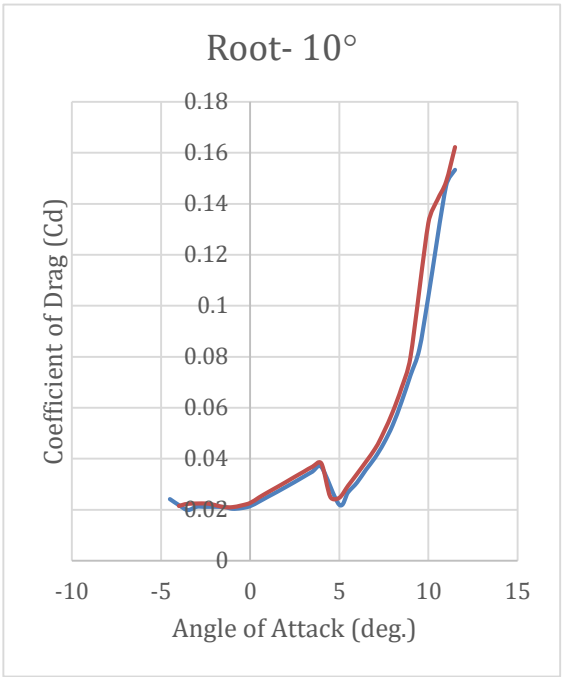
Fig. 7-1: Lift coefficient for the uncoated blade as a function of angle of attack before and after erosion for Root section a) 0˚, and b) 10˚, for Midspan section c) 0˚, and d)10˚, and for Tip section e) 0˚ and f)10˚

7.1.1.2 Drag Coefficient

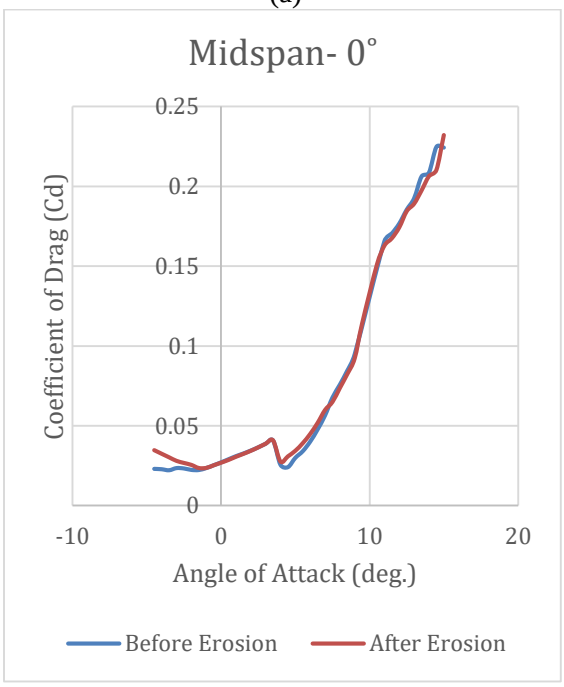
Drag Coefficient, also, is crucial to the aerodynamic performance of wind turbine blades. The change in drag coefficient before and after erosion for 0˚ and 10˚ angles of impingement is shown in Fig. 7-2 for Root, Midspan, and Tip. Similar to the performance of the lift coefficient, with the increase of the intensity of erosion toward the tip, the change in drag coefficient increased. Looking at the 0˚ angle of impingement graphs (a, c, and e), we see that at 8˚ angle of attack, the coefficient of drag increased by up to 230% at the tip section while at 10˚ angle of impingement (Fig. 7-2 b, d, and f), the highest increase was 13%.


Root- 0°
Coefficient of Drag (Cd)
0.25
0.2
0.15
0.1
0.05
0
-10
0
10
20
Angle of ATtack (deg.)
Before Erosion
After Erosion

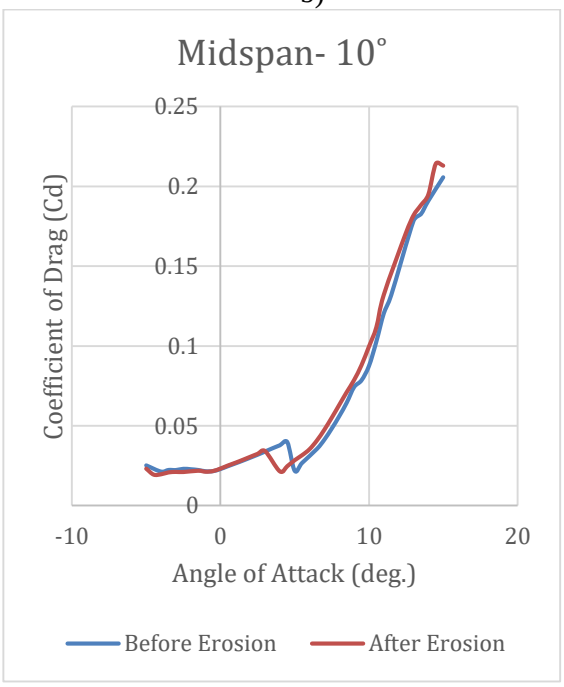
(a)


Root- 10°
Coefficient of Drag (Cd)
0.18
0.16
0.14
0.12
0.1
0.08
0.06
0.04
0.02
0
-10
-5
0
5
10
15
Angle of Attack (deg.)

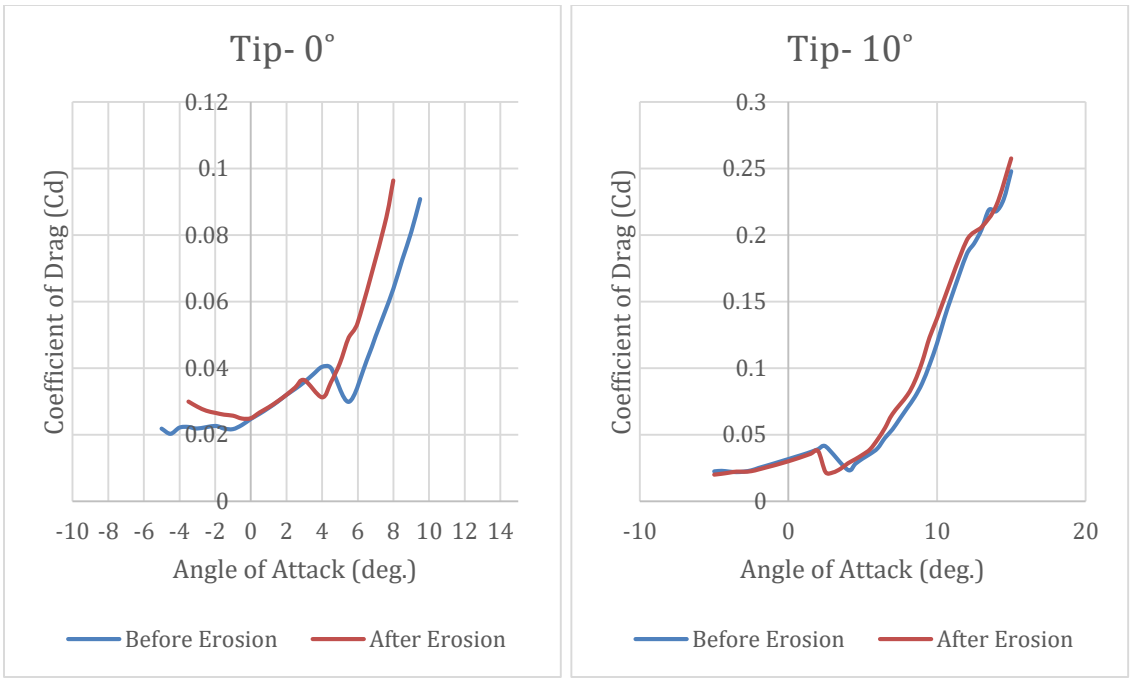
b)


Midspan- 0°
Coefficient of Drag (Cd)
0.25
0.2
0.15
0.1
0.05
0
-10
0
10
20
Angle of Attack (deg.)
Before Erosion
After Erosion

(c)


Midspan- 10°
Coefficient of Drag (Cd)
0.25
0.2
0.15
0.1
0.05
0
-10
0
10
20
Angle of Attack (deg.)
Before Erosion
After Erosion

(d)



(e) (f)

Fig. 7-2: Drag coefficient for the uncoated blade as a function of angle of attack before and after erosion for Root section a) 0˚, and b) 10˚, for Midspan section c) 0˚, and d)10˚, and for Tip section e) 0˚ and f)10˚

7.1.1.3 Lift and drag comparison

The best aerodynamic performance can be achieved when drag is at its lowest while lift is at its highest. Designers and operators use the point of highest lift-to-drag ratio as the point of optimal design. Table 7-2 shows the change in lift and drag coefficient before and after erosion for the four angles of impingement -5˚, 0˚, 5˚, and 10˚ at Root, Midspan, and Tip sections. The 8˚ angle of attack was chosen since it has shown the highest lift coefficient. It can be seen in the Table that, on average, the decrease in the lift coefficient ranged from 2% for the Root section, to 3% for the Midspan section, to 13% for the Tip section. On the other hand, the drag coefficient increased by 4%, 3%, and 49% for Root, Midspan, and Tip sections, respectively. Also, it can be noticed that drag is more sensitive to erosion with an increase up to 141% for 0˚ angle of impingement at the Tip section while the largest decrease in lift coefficient was 30% at the same location and conditions.

Table 7-2: Change in lift and drag coefficient in the uncoated blade at Root, Midspan, and Tip sections for angles of impingement of -5˚, 0˚, 5˚, and 10˚

Section	Root		Midspan		Tip	
Angle of Impingement	Lift	Drag	lift	Drag	Lift	Drag
-5	-5%	13%	-5%	6%	-8%	5%
0	-2%	2%	-4%	-2%	-30%	141%
5	-2%	-7%	0%	3%	-7%	37%
10	1%	9%	-4%	6%	-6%	12%
Average	**-2%**	**4%**	**-3%**	**3%**	**-13%**	**49%**

7.1.2 coated blades

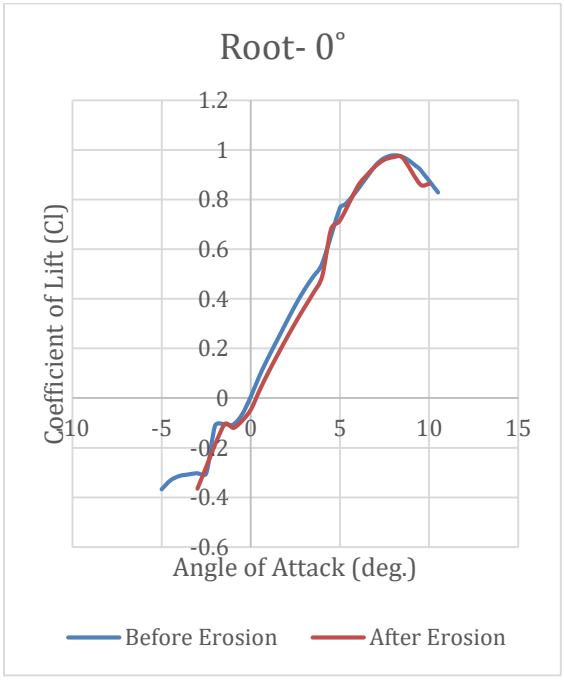
After characterizing the change in lift and drag coefficients for before and after erosion, studying and comparing the effects of coatings on the aerodynamic performance is necessary. The erosion behavior of the leading edge of the coated blade is different from that of the uncoated blade. Polyurethane/IA-700 coated blade showed higher erosion resistance by having a lower material removal rate and shallower depth of erosion scars. On the other hand, H-146 coated showed a worse erosion resistance behavior than the uncoated blade.

7.1.2.1 H-146 Coated

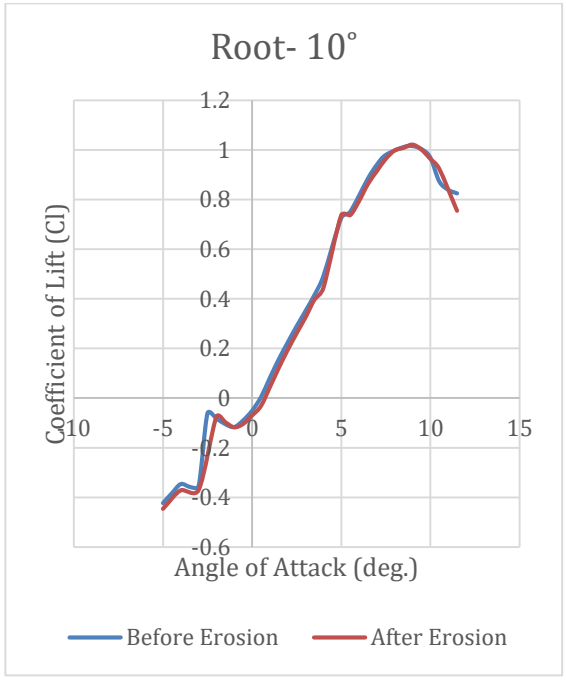
7.1.2.1.1 Lift coefficient

Staring with H-146 coated blade, the aerodynamic performance in terms of lift and drag coefficient was analyzed, as discussed in the following sections. When studying the performance of the H-146 coated blade before and after erosion, it has been noticed that the lift coefficient decreased more than the uncoated blade. Fig. 7-3 shows the lift coefficient as a function of angle of attack for 0˚ and 10˚ erosion conditions for Root, Midspan, and

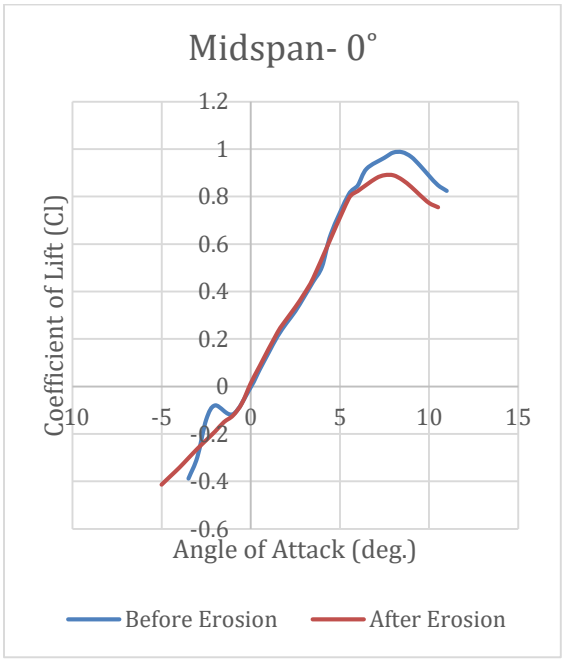
Tip sections. It can be noticed in the figure that the intensity of change was higher at 0˚, which showed the highest erosion rate as discussed in the previous chapter when compared to the change for 10˚. Like the uncoated, blade the change in lift coefficient becomes more visible at the tip section, which showed the highest erosion rate.



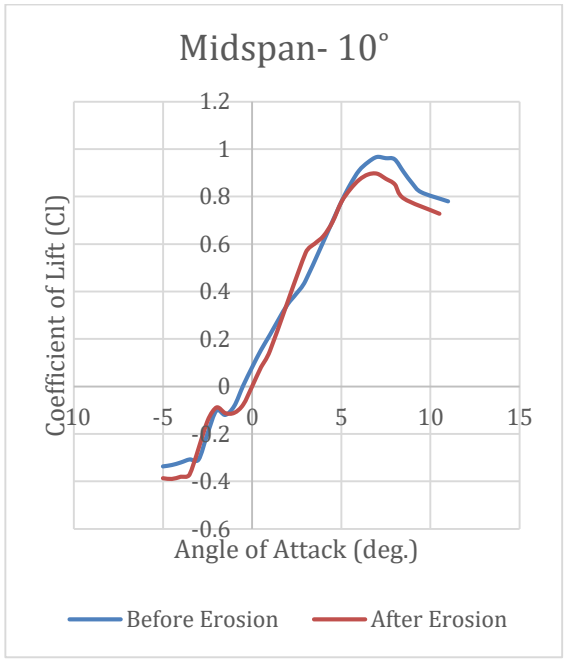
(a)



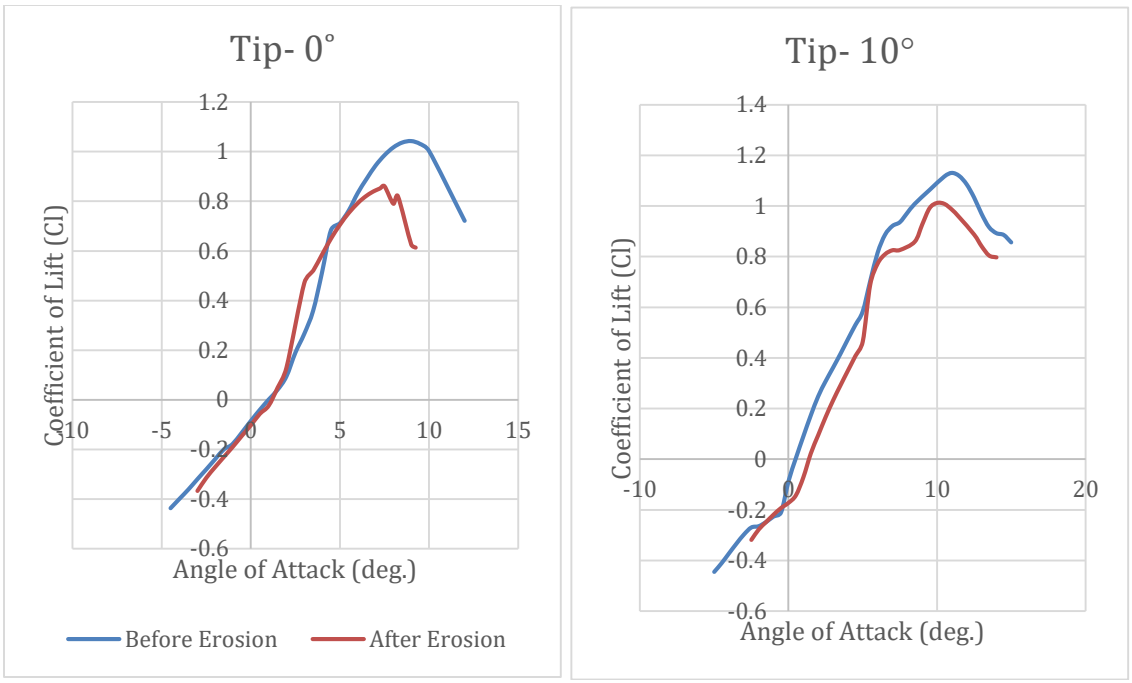
(b)



(c)



(d)

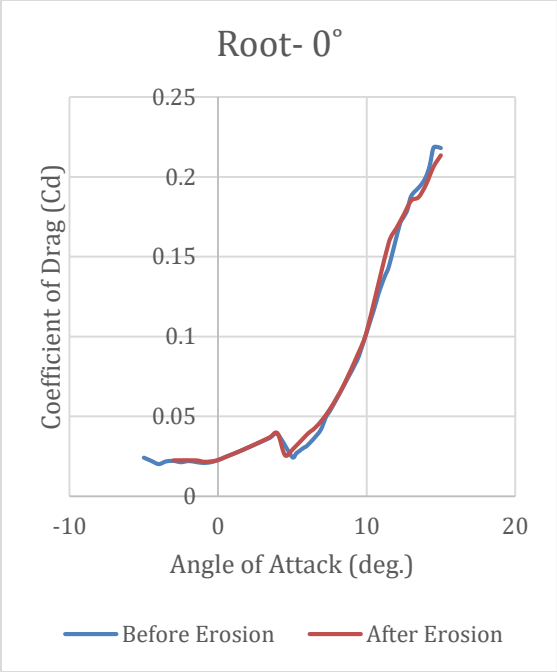


(e) (f)

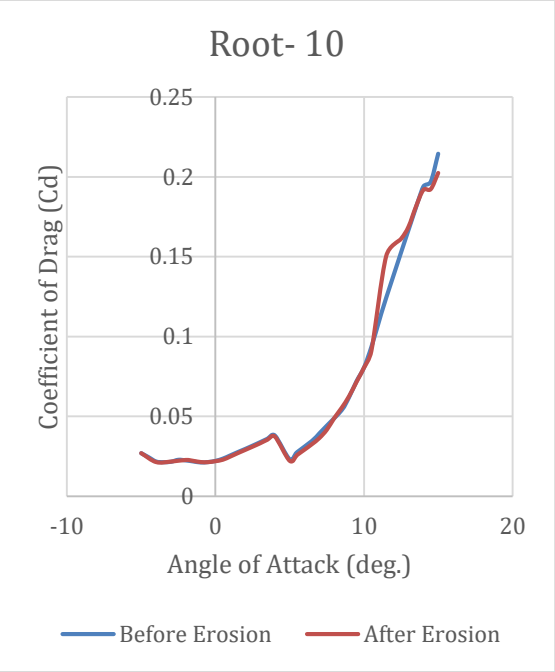
Fig. 7-3: Lift coefficient for the H-146 coated blade as a function of angle of attack before and after erosion for Root section a) 0˚, and b) 10˚, for Midspan section c) 0˚, and d)10˚, and for Tip section e) 0˚ and f)10˚

7.1.2.1.2 Drag coefficient

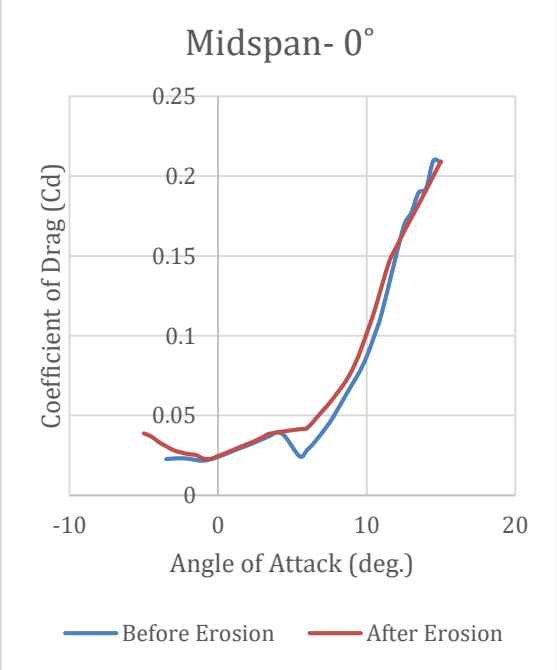
An increase in the coefficient of drag has also been noticed after erosion. Fig. 7-4 shows the drag coefficient as a function of angle of attack at 0˚ and 10˚ erosion conditions for the three sections of the blade. As expected, the change between the before and after erosion graphs is bigger for the 0˚ angle of impingement. Also, the change in the coefficient of drag increased with the increase of the intensity of erosion.


Root- 0°
Coefficient of Drag (Cd)
0.25
0.2
0.15
0.1
0.05
0
-10
0
10
20
Angle of Attack (deg.)
Before Erosion
After Erosion

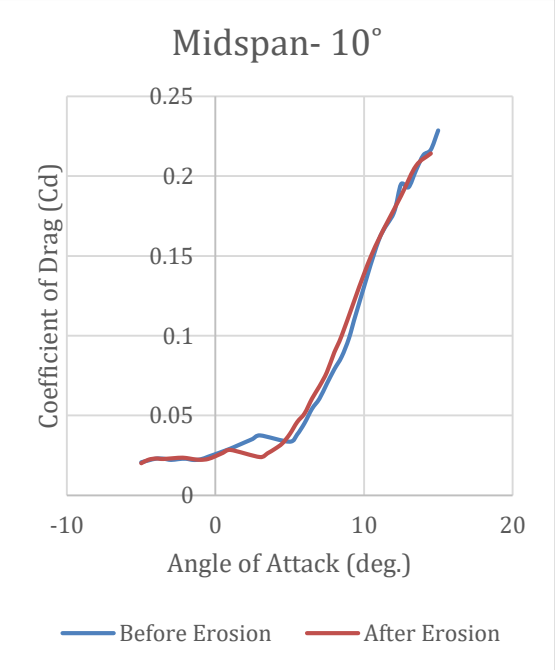
(a)


Root- 10
Coefficient of Drag (Cd)
0.25
0.2
0.15
0.1
0.05
0
-10
0
10
20
Angle of Attack (deg.)
Before Erosion
After Erosion

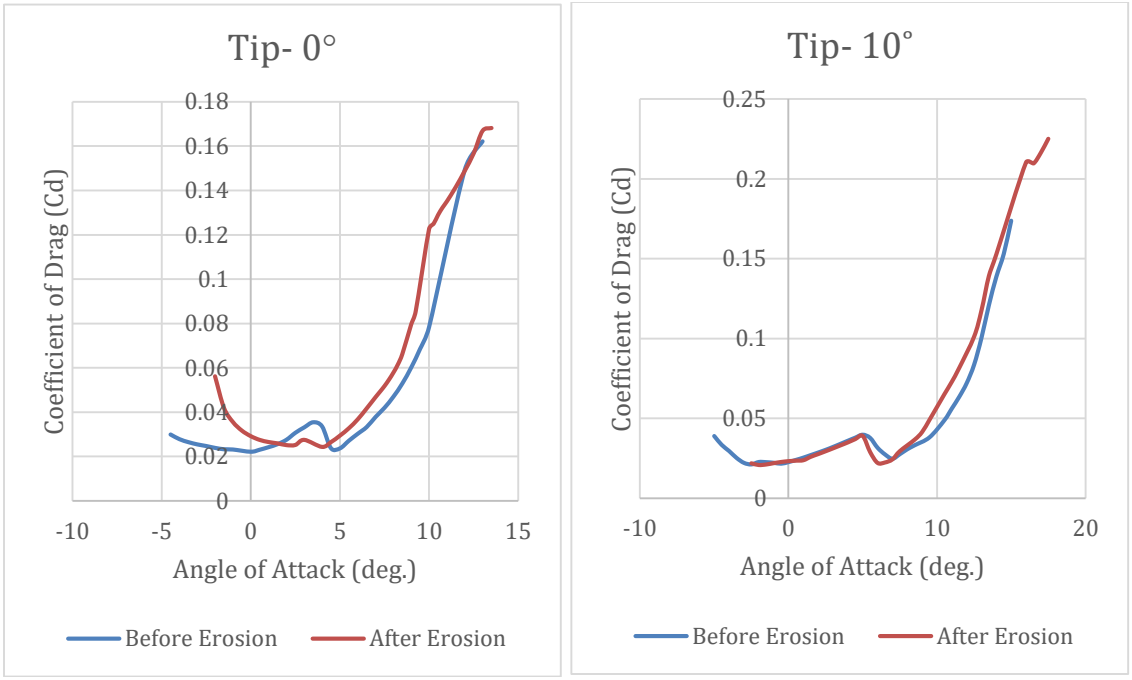
(b)


Midspan- 0°
Coefficient of Drag (Cd)
0.25
0.2
0.15
0.1
0.05
0
-10
0
10
20
Angle of Attack (deg.)
Before Erosion
After Erosion

(c)


Midspan- 10°
Coefficient of Drag (Cd)
0.25
0.2
0.15
0.1
0.05
0
-10
0
10
20
Angle of Attack (deg.)
Before Erosion
After Erosion

(d)



(e) (f)

Fig. 7-4: Drag coefficient for the H-146 coated blade as a function of angle of attack before and after erosion for Root section a) 0˚, and b) 10˚, for Midspan section c) 0˚, and d)10˚, and for Tip section e) 0˚ and f)10˚

7.1.2.1.3 Lift to drag comparison

To analyze the change in the aerodynamic performance that occurred due to erosion, the change in lift and drag coefficients at Root, Midspan, and Tip sections at 8˚ angle of attack is shown in Table 7-3. As discussed earlier, the drag coefficient is more sensitive to erosion than the lift coefficient, with the most significant change in drag reaching 38% at Tip section and 0˚ angle of impingement, while the biggest change in lift is 13%. It can be noticed in Table 7-3 that the average change in lift increased from 4% to 8% to 9 for Root, Midspan, and Tip sections, respectively, while the average change in drag increased from 14% to 18% to 33% for Root, Midspan, and Tip, respectively.

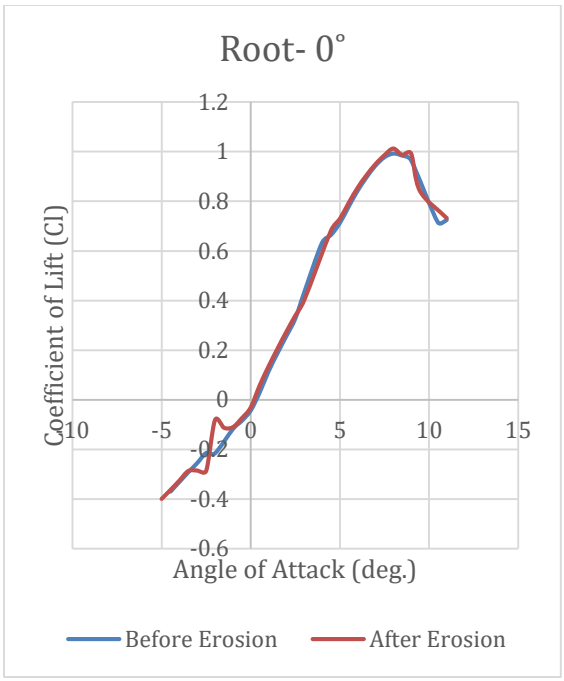
Table 7-3: Change in lift and drag coefficient in the H-146 coated blade at Root, Mid-span, and Tip sections for angles of impingement of -5˚, 0˚, 5˚, and 10˚

Section	Root		Midspan		Tip	
Angle of Impingement	Lift	Drag	lift	Drag	Lift	Drag
-5	-3%	11%	-4%	4%	-5%	29%
0	-11%	30%	-13%	27%	-11%	35%
5	-2%	4%	-11%	30%	-7%	38%
10	1%	10%	-6%	12%	-13%	32%
Average	**-4%**	**14%**	**-8%**	**18%**	**-9%**	**33%**

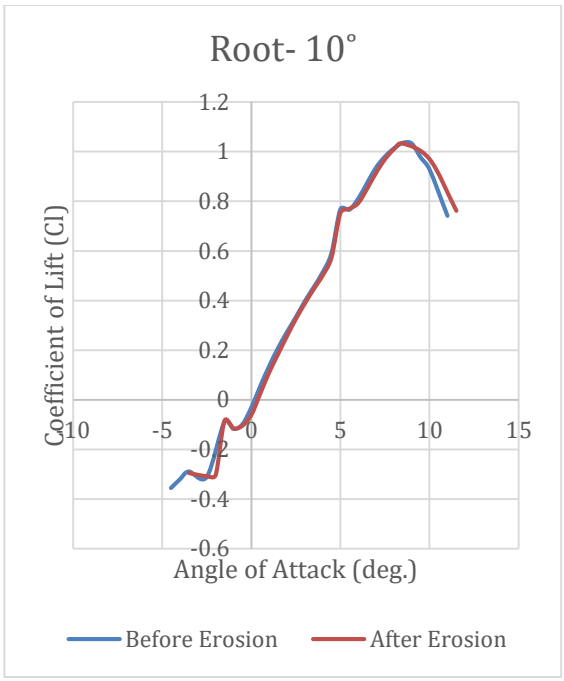
7.1.2.2 Polyurethane/IA-700 Coated blade

7.1.2.2.1 Lift coefficient

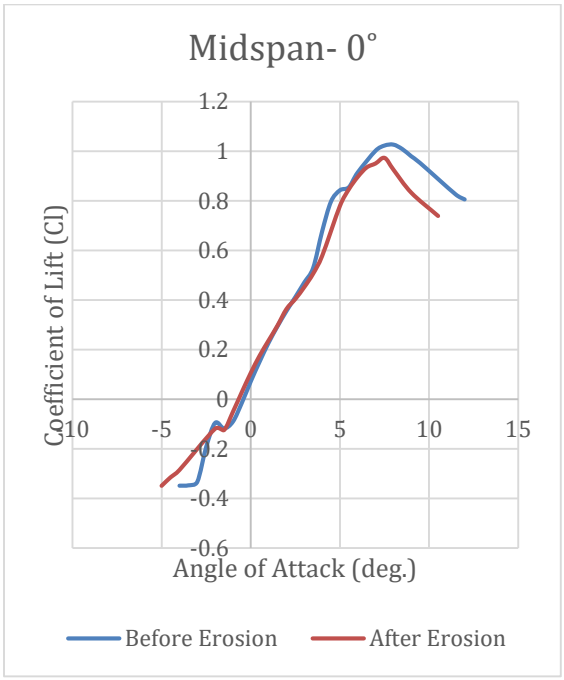
The last blade to be analyzed is the blade coated with a layer of Polyurethane on top of a layer of IA-700 graphene. Starting with the lift coefficient, Fig. 7-5 shows the lift coefficient as a function of the angle of attack for 0˚ and 10˚ erosion conditions for the Root, Midspan, and Tip. The same trend of increase in the gap between before and after erosion graphs with the increase of the intensity of damage noticed in the uncoated and H-146 coated blades can be noticed here. The change in lift coefficient increased toward the tip, and 0˚ angle impingement showed a bigger change than 10˚.


Root- 0°
Coefficient of Lift (Cl)
1.2
1
0.8
0.6
0.4
0.2
0
-0.2
-0.4
-0.6
-10
-5
0
5
10
15
Angle of Attack (deg.)
Before Erosion
After Erosion

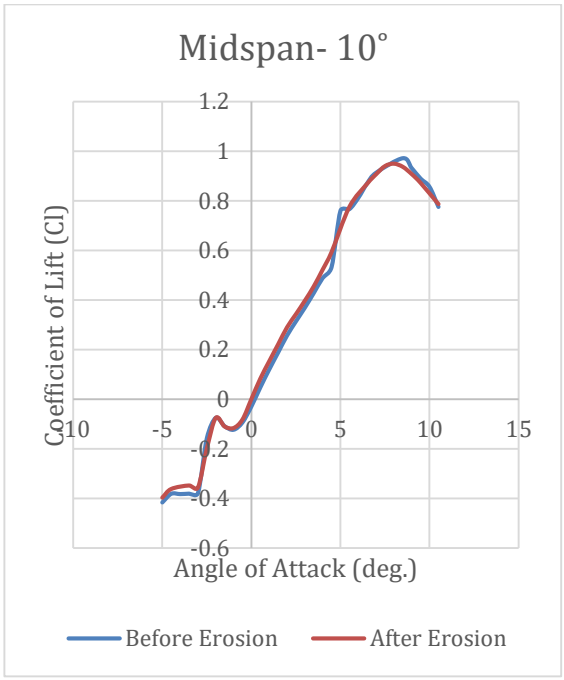
(a)


Root- 10°
Coefficient of Lift (Cl)
1.2
1
0.8
0.6
0.4
0.2
0
-0.2
-0.4
-0.6
-10
-5
0
5
10
15
Angle of Attack (deg.)
Before Erosion
After Erosion

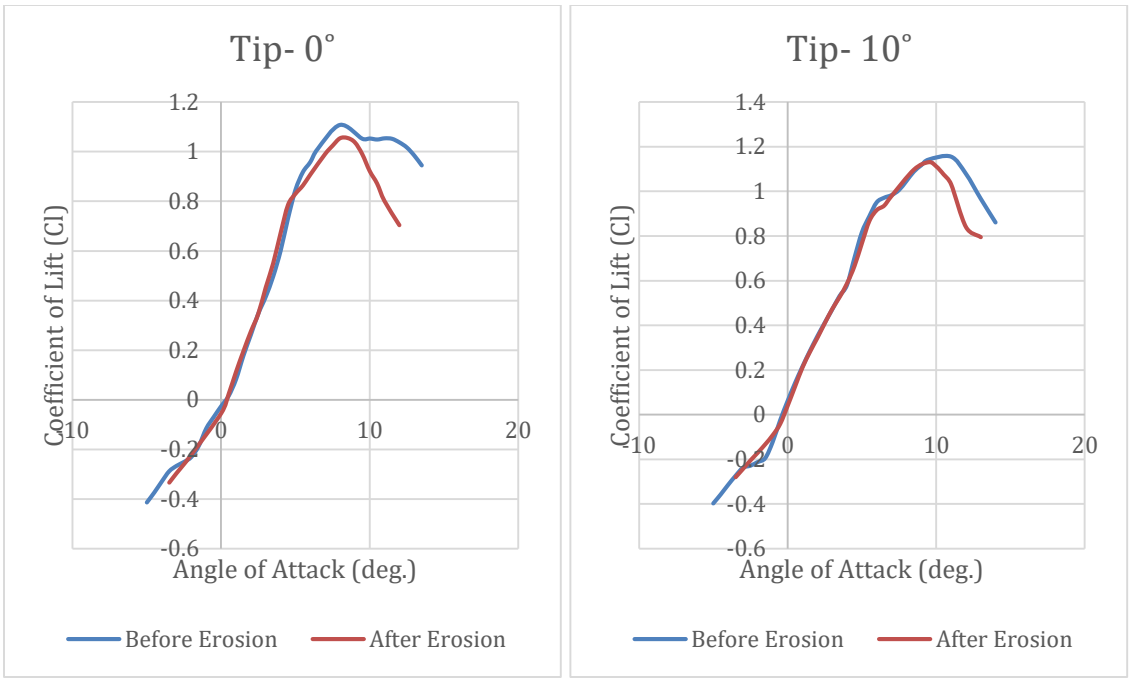
(b)


Midspan- 0°
Coefficient of Lift (Cl)
1.2
1
0.8
0.6
0.4
0.2
0
-0.2
-0.4
-0.6
-10
-5
0
5
10
15
Angle of Attack (deg.)
Before Erosion
After Erosion

(c)


Midspan- 10°
Coefficient of Lift (Cl)
1.2
1
0.8
0.6
0.4
0.2
0
-0.2
-0.4
-0.6
-10
-5
0
5
10
15
Angle of Attack (deg.)
Before Erosion
After Erosion

(d)



(e) (f)

Fig. 7-5: Lift coefficient for the Polyurethane/IA-700 coated blade as a function of angle of attack before and after erosion for Root section a) 0˚, and b) 10˚, for Midspan section c) 0˚, and d)10˚, and for Tip section e) 0˚ and f)10˚

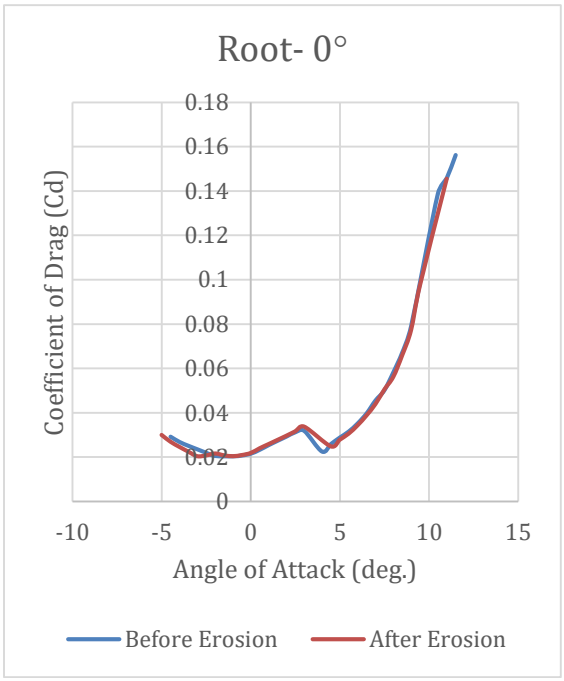
7.1.2.2.3 Lift to drag comparison

The change in both lift and drag coefficients for Root, Midspan, and Tip sections is shown in Table 7-4. It can be seen in the Table that on average the change in coefficient of lift before and after erosion increased from 1% for the Root section to 6% for the Midspan section to 5% for the Tip section. While the change in drag increased from 4% to 12% to 22% for Root, Midspan, and Tip, respectively. The highest change in drag coefficient was 43% at the Tip section for 0˚ angle of impingement while the highest change in lift was 10% at the same section and angle of impingement.

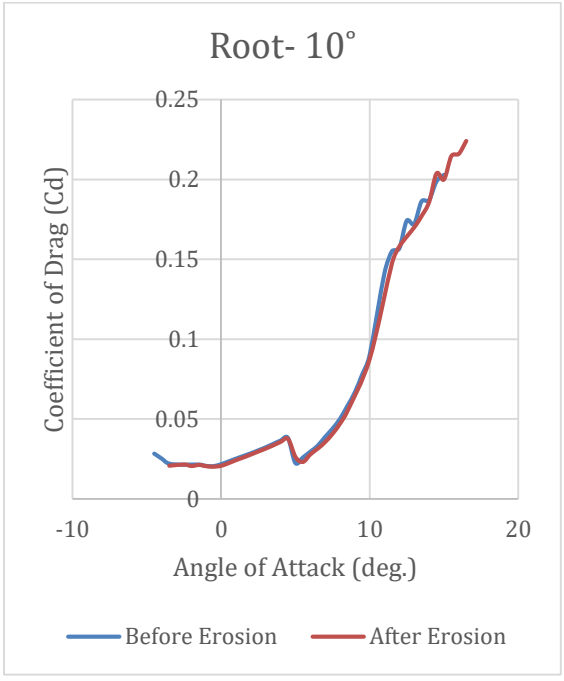
7.1.2.2.2 Drag coefficient

On the other hand, the change in the drag coefficient increased after erosion with the increase of intensity of erosion. Fig. 7-6 shows the before and after erosion drag coefficient

as a function of the angle of attack at 0˚ and 10˚ erosion conditions for the Root, Midspan, and Tip. A similar trend to what has been seen in the other two blades is noticed here. With the increase in erosion intensity toward the Tip, the change in drag coefficient increased for 0˚ and 10˚ erosion conditions. Also, the change in drag coefficient is more noticeable in the 0˚ erosion condition.



(a)



(b)

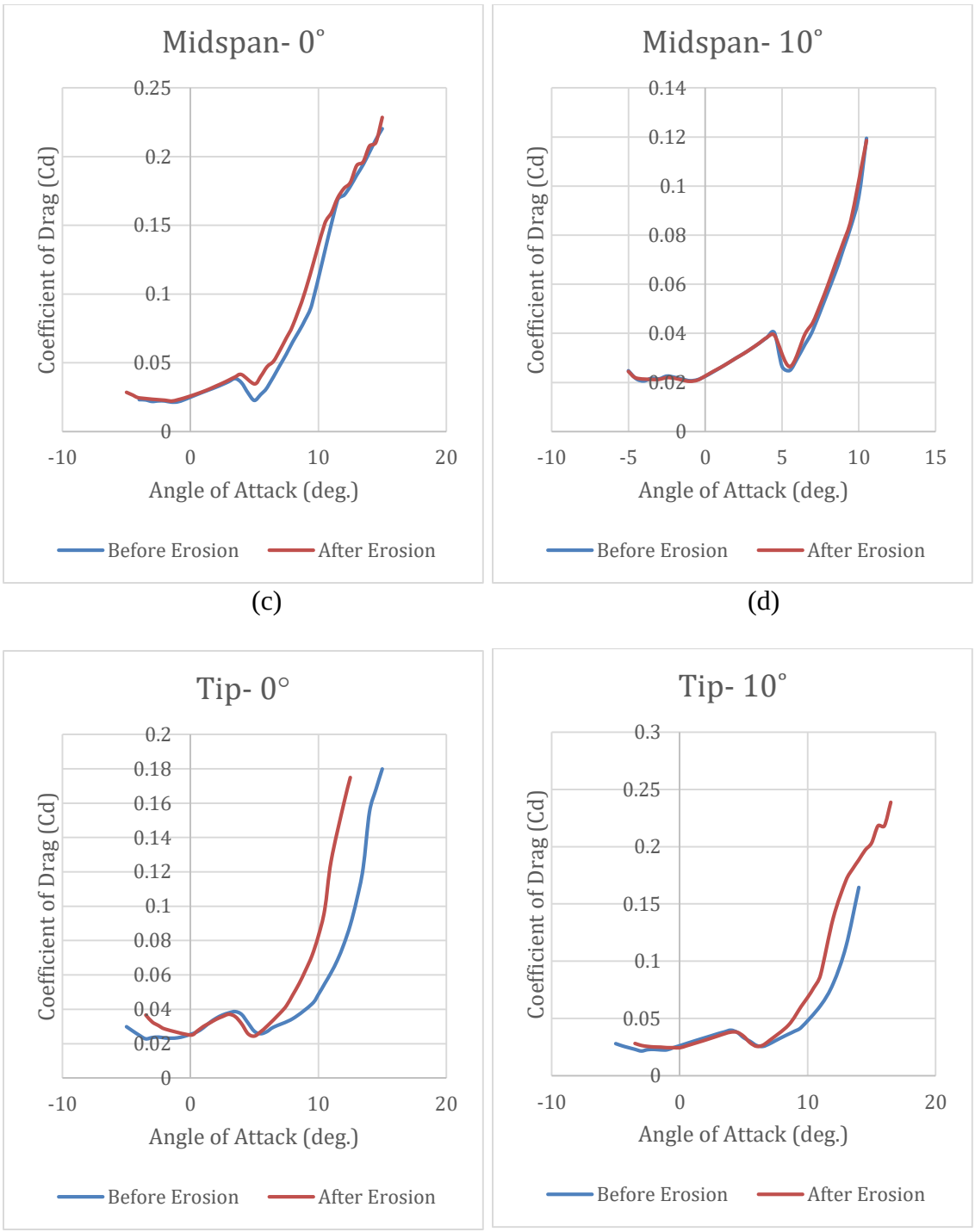


Fig. 7-6: Drag coefficient for the Polyurethane/IA-700 coated blade as a function of angle of attack before and after erosion for Root section a) 0˚, and b) 10˚, for Midspan section c) 0˚, and d)10˚, and for Tip section e) 0˚ and f)10˚

7.1.2.2.3 Lift to drag comparison

The changes in both lift and drag coefficients for Root, Midspan, and Tip sections are shown in Table 7-4. It can be seen in the Table that, on average, the change in the coefficient of lift before and after erosion increased from 1% for the Root section to 6% for the Midspan section to 5% for the Tip section. In comparison, the change in drag increased from 4% to 12% to 22% for Root, Midspan, and Tip, respectively. The biggest change in drag coefficient was 43% at the Tip section for 0˚ angle of impingement, while the biggest change in lift coefficient was 10% at the same section and angle of impingement.

Table 7-4: Change in lift and drag coefficient in the Polyurethane/IA-700 coated blade at Root, Midspan, and Tip sections for angles of impingement of -5˚, 0˚, 5˚, and 10˚

Section	Root		Midspan		Tip	
Angle of Impingement	Lift	Drag	lift	Drag	Lift	Drag
-5	-2%	12%	-4%	7%	-6%	2%
0	0%	0%	-8%	19%	-10%	43%
5	-1%	2%	-6%	12%	-3%	21%
10	1%	2%	-6%	9%	-7%	5%
Average	**-1%**	**4%**	**-6%**	**12%**	**-5%**	**22%**

7.1.3 Effects of coatings on Aerodynamic performance

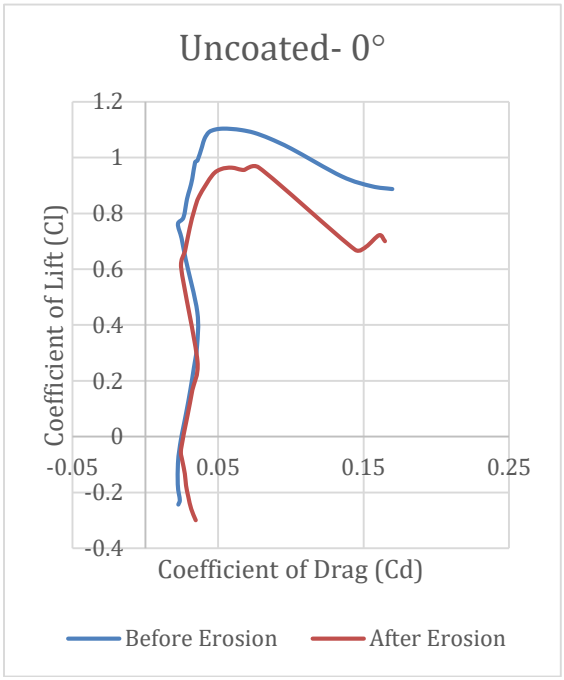
As discussed in the previous chapter, Polyurethane/IA-700 coating provided better erosion resistance compared to the uncoated blade, while H-146 coating showed worse erosion resistance. The effects of these coatings on aerodynamic performance will be investigated in this section. Table 7-5 combines the average change in Cl and Cd discussed in the previous sections and Tables 7-2 – 7-4. The aerodynamic performance of each blade shows a similar trend to that of erosion resistance. In terms of lift coefficient, the biggest change

was 7%, shown by H-146 coated blade followed by the uncoated blade with 6% change and finally, Polyurethane/IA-700 coated blade with 4% change. On the other hand, the biggest change in drag coefficient was shown again by H-146 with 22%, followed by the uncoated blade with 19% change and finally Polyurethane/IA-700 with 13%.

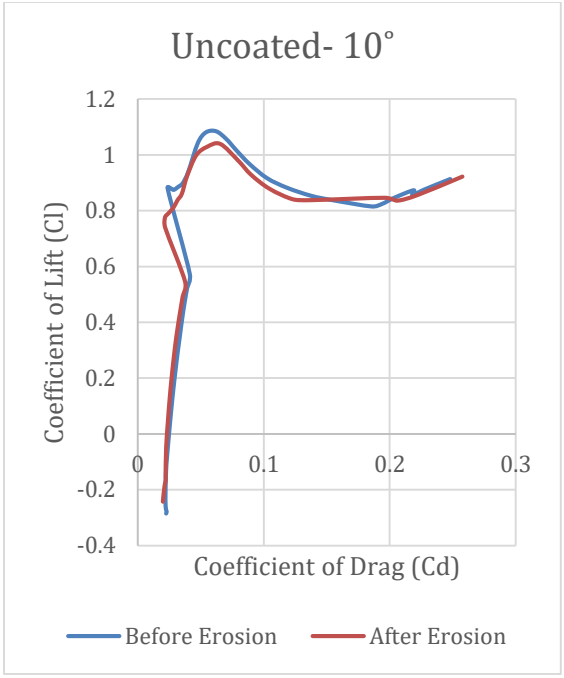
Table 7-5: Comparison of lift and drag coefficients changes for the uncoated, H-146 coated, and polyurethane/IA-700 coated blades

Section	Root		Midspan		Tip		Average	
Coefficient	Lift	Drag	lift	Drag	Lift	Drag	Lift	Drag
Uncoated	-2%	4%	-3%	3%	-13%	49%	**-6%**	**19%**
H-146	-4%	14%	-8%	18%	-9%	33%	**-7%**	**22%**
Polyurethane/ IA-700	-1%	4%	-6%	12%	-5%	22%	**-4%**	**13%**

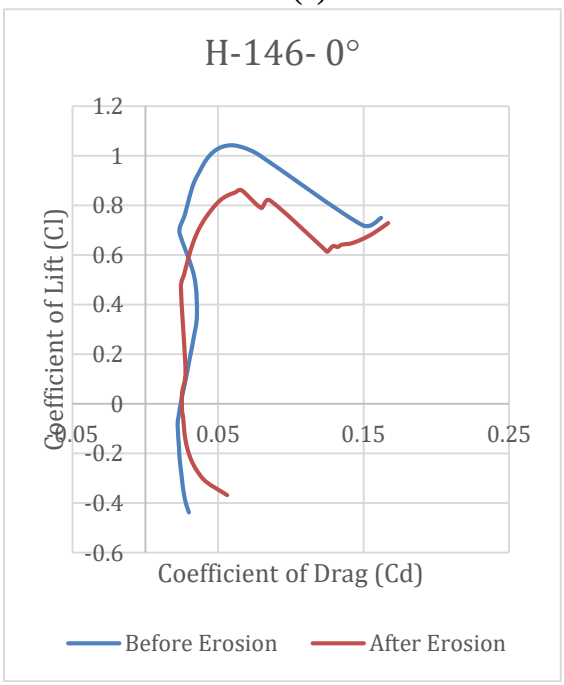
Since the best aerodynamic performance occurs when the lift is maximized, and drag is minimized, drag polar is used to compare the three blades. In drag polar, the drag coefficient is compared directly to the lift coefficient as shown in Fig. 7-7, which shows the drag polar of the before and after erosion performance at an angle of impingement of 0˚ and 10˚ at the tip section. The top left corner is the optimal place for the best aerodynamic performance since it has the highest lift coefficient at the lowest drag coefficient. Therefore, the graph that goes furthers to the top left corner has better aerodynamic performance.


Uncoated- 0°
Coefficient of Lift (Cl)
Coefficient of Drag (Cd)
Before Erosion
After Erosion

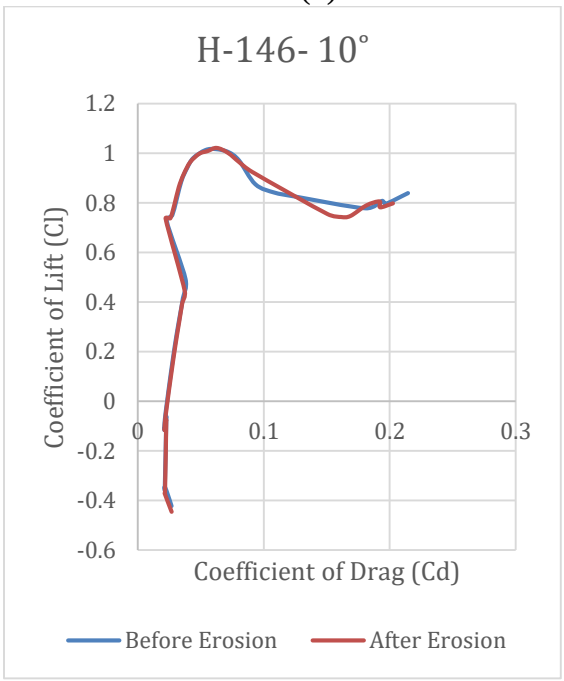
(a)


Uncoated- 10°
Coefficient of Lift (Cl)
Coefficient of Drag (Cd)
Before Erosion
After Erosion

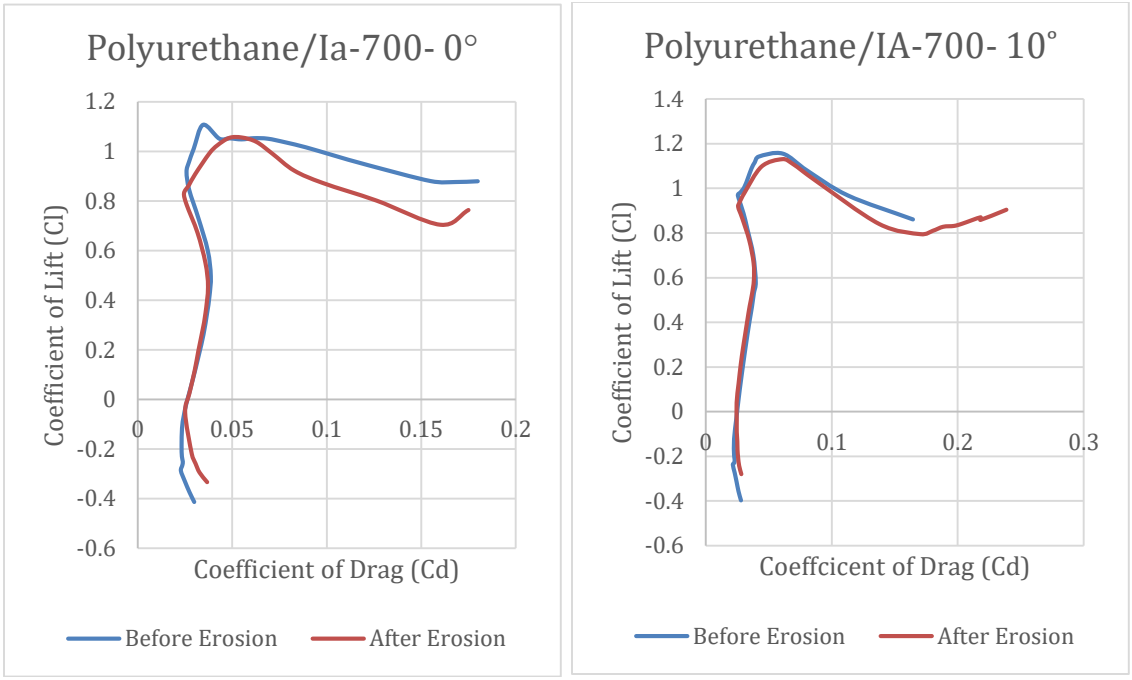
(b)


H-146- 0°
Coefficient of Lift (Cl)
Coefficient of Drag (Cd)
Before Erosion
After Erosion

(c)


H-146- 10°
Coefficient of Lift (Cl)
Coefficient of Drag (Cd)
Before Erosion
After Erosion

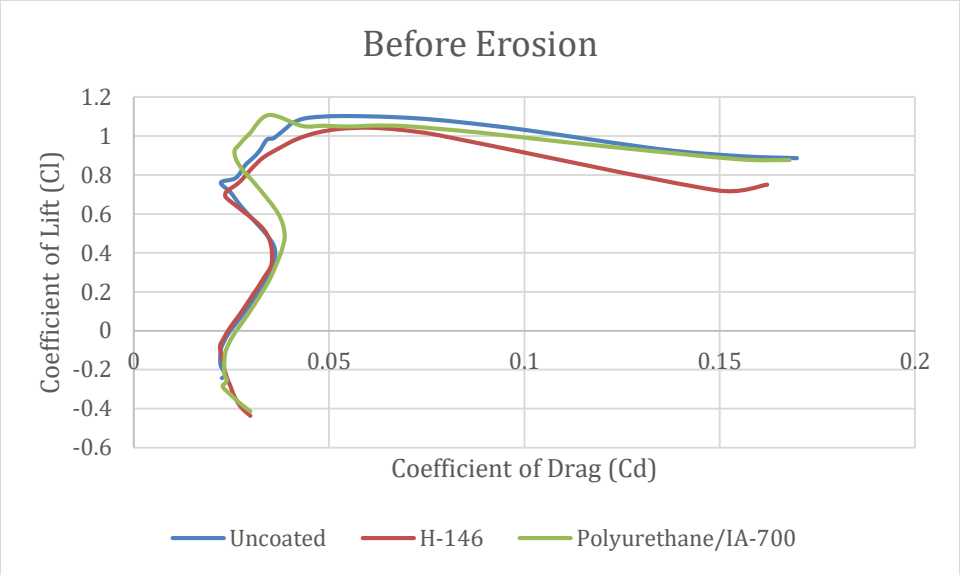
(d)



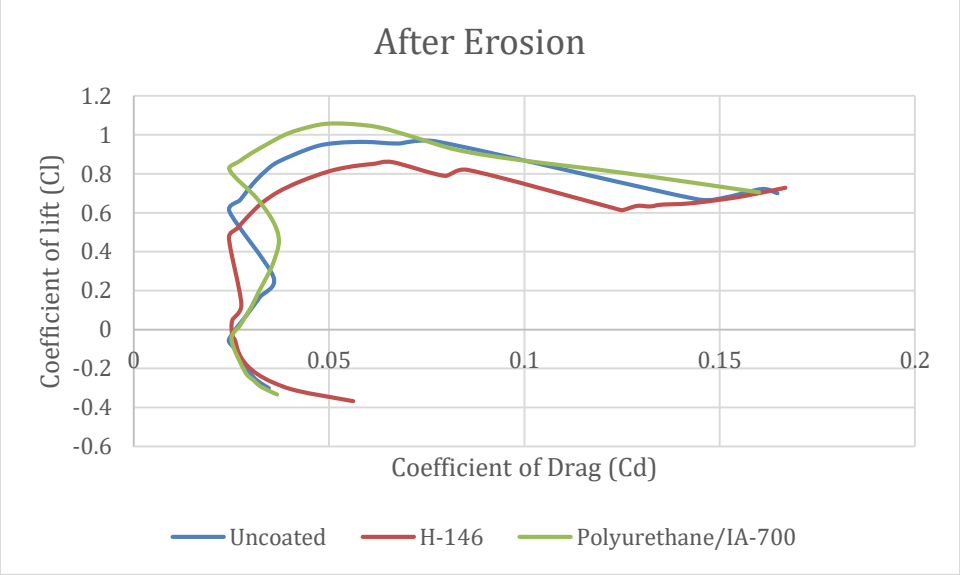
(e) (f)

Fig. 7-7: Drag polar for the uncoated, H-146, and polyurethane/IA-700 blades at 0˚ and 10˚ angles of impingement

It can be seen in all three graphs that the aerodynamic performance for the before erosion case is superior to that of the after erosion case. The closest after erosion drag polar to the before erosion can be seen in the polyurethane/IA-700 case. In contrast, the most significant difference between the before and after erosion can be seen in the H-146 case. Fig 7-8 shows the effects of coatings on the aerodynamic performance before and after erosion. The aerodynamic performance for the before-erosion case (Fig. 7-8a) shows that polyurethane/IA-700 has the best performance, followed by the uncoated blade, then the H-146 coated blade. Similarly, the after-erosion aerodynamic performance followed the same pattern. This aerodynamic performance is in agreement with the surface roughness measurements for the three blades as well as the erosion resistance behavior, with polyurethane/IA-700 being the smoothest and most resistant to erosion and H-146 being the roughest and the least resistant to erosion.



(a)



(b)

Fig. 7-8: Drag polar comparing the (a) before and (b) after erosion aerodynamic performance for the uncoated, H-146 coated, and polyurethane/Ia-700 coated blades

Another way to quantify the data shown in the drag polar graphs is by calculating the coefficient of lift to coefficient of drag ratio (Cl/Cd). Table 7-6 shows the average change of Cl/Cd at an 8˚ angle of attack for the four impingement angles for the three blades. It can

be seen that, on average, the biggest change in Cl/Cd occurred at H-146 with a 20% decrease followed by 14% for the uncoated blade and finally 11% for the polyurethane/IA-700 coated blade.

Table 7-6: change in Cl/Cd at 8˚ angle of attack four the three blades.

Coating	Uncoated	H-146	Polyurethane/ IA-700
-5	-13%	-13%	-4%
0	-23%	-28%	-20%
5	-10%	-21%	-13%
10	-11%	-19%	-8%
Average	**-14%**	**-20%**	**-11%**

In summary, due to the leading edge erosion of the wind turbine blades, an increase in drag coefficient and a decrease in the lift coefficient have been observed. The intensity of change in these coefficients depended on the intensity of erosion, with the Tip section showing more drastic changes than Root or Midspan sections. Also, it has been noticed that the type of coating applied to the wind turbine blade affects the change of these aerodynamic parameters. H-146 coated blade showed the biggest change while polyurethane/IA-700 coated blade showed the smallest change, consistent with both erosion rate and surface roughness results discussed in the previous chapter.

7.2 Power Generation

7.2.1 Blade Element Momentum theory

7.2.1.1 One-dimensional Momentum Theory

The one-dimensional momentum theory was originally developed by Froude and Rankine for marine propulsion applications more than 100 years ago, but can be applied to wind turbine rotor as will be shown below [196]. The rotor is modeled as a preamble disc where

a normal load is distributed over it giving rise to a constant velocity profile in the wake, as shown in Fig. 7-9. The main assumptions of the 1-D momentum theory are [196]:

- The flow is fluid, steady, and incompressible
- The flow is uniform through the disc and in the wake
- The disc extracts energy from the flow
- A pressure discontinuity is created across the disc
- The disc does not create any swirl to the flow

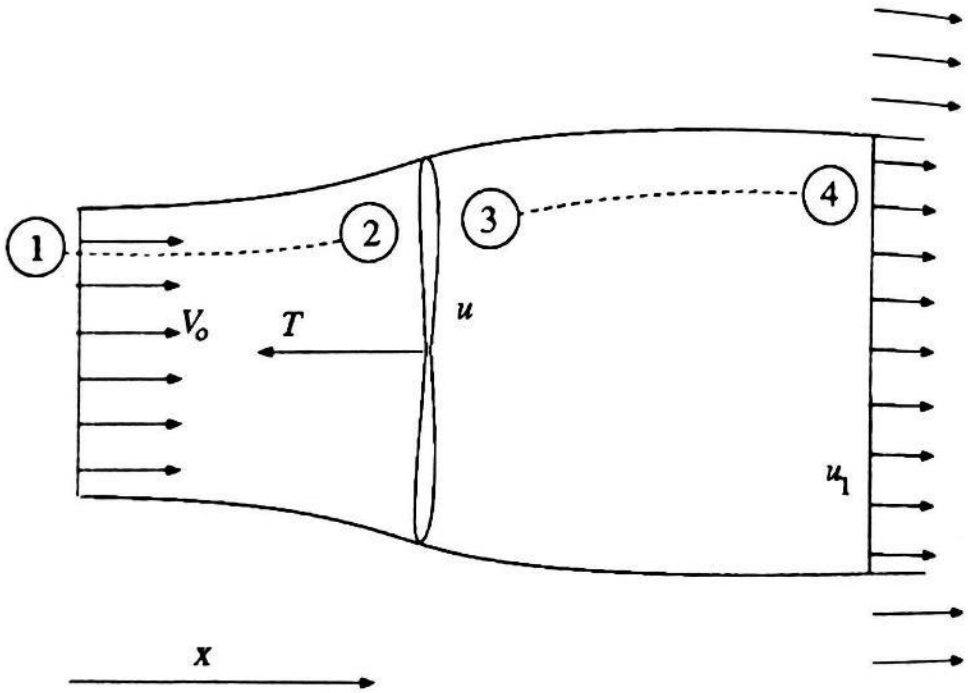


Fig. 7-9: A simple wind turbine rotor modeled as a permeable disc in 1-D flow [196]

Applying Bernoulli equation along the streamline from point 1 to point 2 in Fig. 7-9, and again from point 3 to point 4, gives the following equations:

$$p_o + \frac{1}{2}\rho V_o^2 = p^+ + \frac{1}{2}\rho u^2 \tag{7-4}$$

$$p^- + \frac{1}{2}\rho u^2 = p_o + \frac{1}{2}\rho u_1^2 \tag{7-5}$$

where p_o is the ambient pressure ρ is air density

p^+ is the pressure upstream of the rotor

p^- is the pressure just behind the rotor

V_o is the undisturbed wind speed

u is the reduced velocity in the rotor plane

u_1 is the velocity in the wake

These equations can be combined to calculate the pressure drop Δp:

$$\Delta p = p^+ - p^- = \frac{1}{2}\rho(V_o^2 - u_1^2) = \frac{1}{2}\rho(V_o + u_1)(V_o - u_1) \qquad (7\text{-}6)$$

Applying a cylindrical control volume totally enclosing the flow through the rotor as shown by the dashed line in Fig. 7-10. Since the lateral boundary of the control volume is horizontal, the pressure around the control volume can only contribute to an axial force in the inlet and outlet, and since at the inlet and the outlet of the control volume the pressure is ambient, the net pressure force is zero, and the only force left is the thrust force, T.

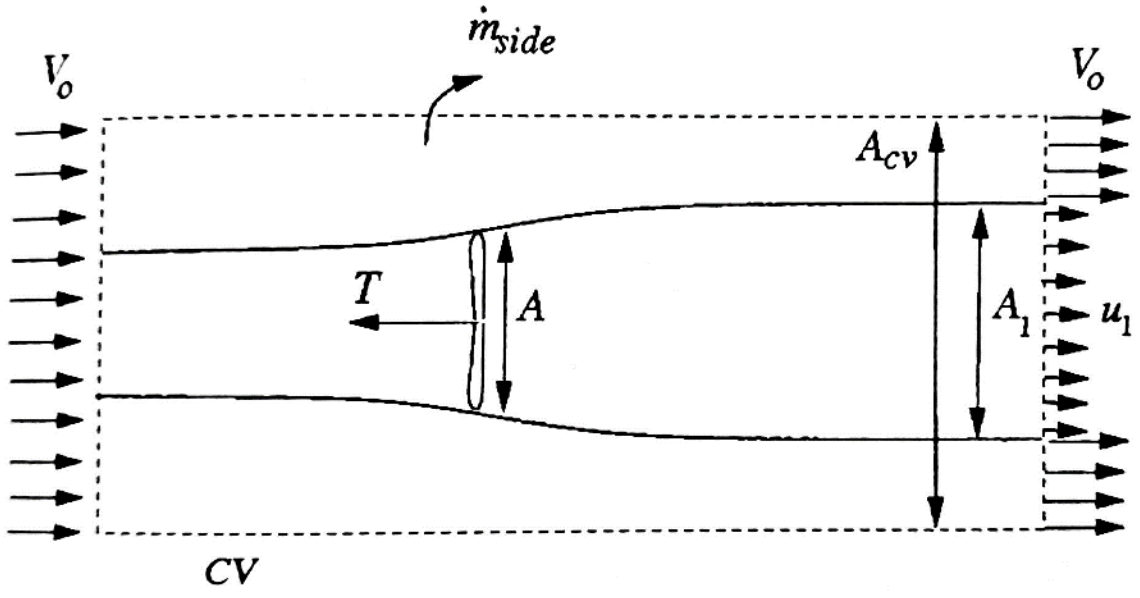


Fig. 7-10: Control volume enclosing the flow through the ideal wind turbine rotor

Summing the forces along the direction of the flow, ΣF_x

$$-T = \rho A_1 u_1^2 + \rho(A_{cv} - A_1)V_o^2 + \dot{m}_{side}V_o - \rho A_{cv}V_o^2 \tag{7-7}$$

And combining this with the conservation of mass

$$\dot{m}_{side} = \rho A_{cv}V_o - \rho A_1 u_1 - \rho(A_{cv} - A_1)V_o = \rho A_1(V_o - u_1) \tag{7-8}$$

Therefore

$$T = \rho A u(V_o - u_1) \tag{7-9}$$

Thrust can also be expressed in terms of pressure drop across the rotor times the area of the rotor

$$T = \Delta p A = \frac{1}{2}\rho A(V_o^2 - u_1^2) = \frac{1}{2}\rho A(V_o + u_1)(V_o - u_1) \tag{7-10}$$

Equating the two thrust equations leads to

$$u = \frac{1}{2}(V_o + u_1) \tag{7-11}$$

A new parameter that measures how much the wind velocity, V_o, has been affected by the rotor called axial induction factor, a, can be introduced

$$a = \frac{V_o - u}{V_o} \tag{7-12}$$

The power extracted from the wind by the rotor is equal to the thrust times the wind velocity at the rotor

$$P = Tu = 2\rho a(1 - a)^2 V_o^3 A \tag{7-13}$$

The power is often non-dimensionlized with the available power in the wind into the power coefficient

$$C_p = \frac{P}{\frac{1}{2}\rho V_o^3 A} \tag{7-14}$$

The power coefficient can also be expressed in terms of the axial induction factor using the power equation from the 1-D momentum theory, which assumes no losses as

$$C_p = \frac{2\rho a(1-a)^2 V_o^3 A}{\frac{1}{2}\rho V_o^3 A} = 4a\,(1-a)^2 \tag{7-15}$$

The maximum theoretical value C_p can reach is called the Betz limit, which equals 16/27≈ 0.593 when a is equal to 1/3.

7.2.1.2 Momentum theory with wake rotation

To include the effects of rotation in the wake of the flow downstream of the disc, two assumptions are made:

- The flow upstream of the rotor is not affected by the rotor rotation
- Immediately behind the rotor, a tangential flow is induced on the downstream wake.

Therefore, an angular induction factor a' is introduced to represent the tangential flow

$$a' = \frac{\omega}{2\Omega} \tag{7-16}$$

where ω is the angular velocity imparted to the wake

Ω is the angular velocity of the rotor

To calculate the power while including the effects of wake rotation in the equations, the torque must be known. The torque can be determined by applying conservation of angular momentum. This yields an equation for the differential torque acting on an angular ring at radius r of the rotor

$$dQ = d\dot{m}\omega r^2 \tag{7-17}$$

For the rotating annular element

$$d\dot{m} = \rho A u = \rho 2\pi r dr u \tag{7-18}$$

$$dQ = \rho 2\pi r dr u\omega r^2 = \rho u\omega r^2 2\pi r dr \tag{7-19}$$

Applying the angular induction factor and axial induction factor

$$dQ = 4a'(1-a)\rho V_o \Omega r^2 (2\pi r dr) \tag{7-20}$$

The differential power is

$$dP = \Omega dQ = 2a'(1-a)\rho V_o \Omega^2 r^2 (2\pi r dr) \quad (7\text{-}21)$$

7.2.1.3 Blade Element Momentum (BEM) Theory

The momentum theories discussed above provides simple formulas to calculate the power extracted by the rotor and the thrust force acting on the wind turbine rotor. Although there exists a large variety of methods to predict the performance of wind turbines, BEM theory is the only method used today by wind turbine manufacturers [197]. BEM theory provides a prediction of the performance of wind turbine blades as a function of the rotor blade design parameters such as blade chord, number of blades, rotor radius, blade twist, and airfoil shape. The advantage of BEM method is that it contains most of the physics representing rotary aerodynamics, it has proven to be accurate for most common low conditions and rotor configurations, and it is easy to implement and use on a computer. On the other hand, a drawback of the method is the dependence on empirical input that might not always be available. Additionally, the method in its simplest form neglects the effects of atmospheric turbulence, wind direction that change both in time and space, and the effects of wake of neighboring wind turbines.

In BEM, the blade is divided up into N elements and the flow is calculated at each element since each element will experience a slightly different flow. Numerical integration is used to sum the performance of each element and predict the overall performance characteristics along the blade span. In BEM two key assumptions are made: each element is independent where there are no aerodynamic interaction between the elements, and forces on each element can be determined only by lift and drag coefficients.

Looking at Fig. 7-11, relative velocity can be defined as the sum of wind speed and the rotational speed of the blade section

$$V_{rel} = \sqrt{[V_o(1-a)]^2 + [\omega r(1+a')]^2} \tag{7-22}$$

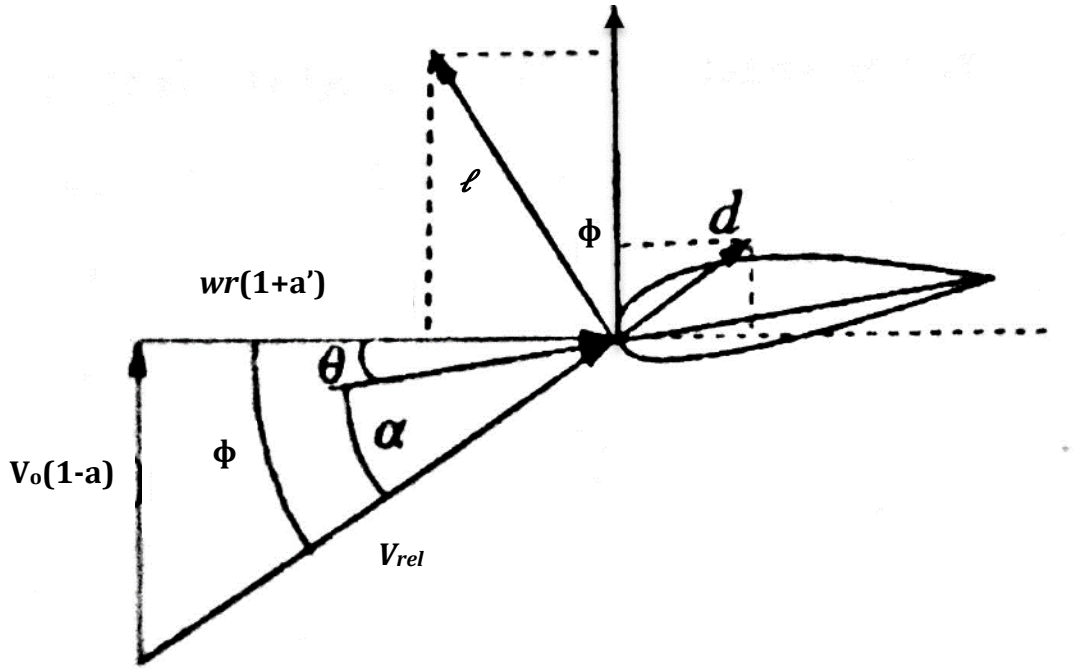


Fig. 7-11: velocities and angles at a blade element [196]

Provided the axial induction factor and the angular induction factor are known, the flow angle, ϕ, which is the angle between the incoming relative wind and the rotor plane is defined as

$$\tan\phi = \frac{(1-a)V_o}{(1+a')\omega r} \tag{7-23}$$

The local angle of attack, α, then can be calculated if the angle between the rotor plane and the airfoil chord, θ, is known

$$\alpha = \phi - \theta \tag{7-24}$$

where θ is the sum of the pitch angle, θ_p, which is the angle between the rotor plane and the tip airfoil.

β is the twist angle, which is the angle between a local airfoil along the blade and the tip airfoil.

Therefore, the local angle of attack is

$$\alpha(r) = \phi(r) - [\beta(r) + \theta_p] \tag{7-25}$$

where r is the local radius on the rotor

The normal and tangential forces acting on sections of the plane can be expressed in terms of differential lift and drag forces

$$dL = \frac{1}{2}\rho V_{rel}^2 c C_l(Re, \alpha) dr \tag{7-26}$$

$$dD = \frac{1}{2}\rho V_{rel}^2 c C_d(Re, \alpha) dr \tag{7-27}$$

where c is the cord length

Lift and drag coefficients are found by a table look up based on Reynolds number and the local angle of attack. The differential force normal to the rotation plane, and the force axial (tangential) to the rotation plane can be, respectively, calculated as

$$dF_n = dL\cos\phi + dD\sin\phi = \frac{1}{2}B\rho V_{rel}^2 c[C_l\cos\phi + C_d\sin\phi]dr \tag{7-28}$$

$$dF_A = dL\sin\phi - dD\cos\phi = \frac{1}{2}B\rho V_{rel}^2 c[C_l\sin\phi - C_d\cos\phi]dr \tag{7-29}$$

where B is the number of blades

defining C_n as

$$C_n = C_l\cos\phi + C_d\sin\phi \tag{7-30}$$

and C_t as

$$C_A = C_l\sin\phi - C_d\cos\phi \tag{7-31}$$

The normal and tangential forces then become

$$dF_n = \frac{1}{2}B\rho V_{rel}^2 c C_n dr \tag{7-32}$$

$$dF_A = \frac{1}{2} B \rho V_{rel}^2 c C_A dr \tag{7-33}$$

The differential torque then can be calculated as the differential of the tangential force multiplied by the radius

$$dQ = r dF_A = \frac{1}{2} B \rho V_{rel}^2 c C_A r dr \tag{7-34}$$

The differential power then equals to the differential torque multiplied by the angular velocity of the rotor

$$dP = \Omega dQ = \frac{1}{2} \Omega B \rho V_{rel}^2 c C_A r dr \tag{7-35}$$

Equating the differential thrust from the momentum theory with no wake with the differential normal force

$$2\rho V_o^2 a(1-a) 2\pi r dr = \frac{1}{2} B \rho V_{rel}^2 C_n c dr \tag{7-36}$$

Substituting

$$V_{rel} = \frac{V_o(1-a)}{\sin\phi} \tag{7-37}$$

Rearranging

$$\frac{a}{1-a} = \frac{B C_n c}{8\pi r \sin^2\phi} \tag{7-38}$$

Defining a new parameter called solidity as

$$\sigma_r = \frac{Bc}{2\pi r} \tag{7-39}$$

Leads to

$$a = \frac{1}{\frac{4\sin^2\phi}{\sigma_r C_n} + 1} \tag{7-40}$$

Similarly, equating the torque equation from momentum theory with wake rotation to and the torque equation from the BEM theory

$$2a'(1-a)\rho V_o \Omega r^2 2\pi r dr = \frac{1}{2} B \rho V_{rel}^2 c C_A r dr \quad (7\text{-}41)$$

Rearranging

$$a' = \frac{1}{\frac{4\sin\phi\cos\phi}{\sigma_r C_A} - 1} \quad (7\text{-}42)$$

7.2.1.3.1 Tip Correction

So far, the effects of vortices at the tip of the blades have not been included in the analysis. The BEM theory assumes each element is independent and should be analyzed as so. For the inboard portion of the blade, the assumption is valid, however, significant interference occurs at the tip of the blade element in the outer portion of the blade. This occurs due to the pressure from the high-pressure side of the rotor blade passes around the blade tip to the low-pressure side causing tip vortex. The vortices at the tip cause an increase in the overall drag, and to take care of the effect of tip vortices, Glauert [198] introduced Prandtl's tip loss factor, F,

$$F = \frac{2}{\pi}\cos^{-1}(e^{-f}) \quad (7\text{-}43)$$

where

$$f = \frac{B}{2}\frac{R-r}{r\sin\phi} \quad (7\text{-}44)$$

B is the number of blades R is the rotor radius

r is the local radius on the rotor

The tip loss factor is introduced into the differential equations discussed earlier as follows

Thrust: $$dT = 2F\rho V_o^2 a(1-a)2\pi r dr \quad (7\text{-}45)$$

Torque: $$dQ = 2Fa'(1-a)\rho V_o \Omega r^2 2\pi r dr \quad (7\text{-}46)$$

Power: $$dP = \frac{1}{2}\mathrm{F}\Omega B \rho V_{rel}^2 c C_A r dr \quad (7\text{-}47)$$

Axial induction factor: $$a = \frac{1}{\frac{4F\sin^2\phi}{\sigma_r C_n} + 1} \quad (7\text{-}48)$$

Angular induction factor: $$a' = \frac{1}{\frac{4F\sin\phi\cos\phi}{\sigma_r C_A} - 1} \quad (7\text{-}49)$$

7.2.1.3.2 BEM Theory method

There are some necessary inputs for BEM method before the start of the iterative process. First, the number of elements the blade will be divided into and their radial location, in this experiment is six which is the number of airfoils in each blade. The lift and drag coefficients as a function of angle of attack and Reynolds number. Lift and drag coefficients, which was acquired numerically using Xfoil. Chord length and the angle of twist for each element was measured, as well as some operational parameters such as wind speed V_o, pitch angle, and rotational speed ω.

For each blade element, the following steps must be followed:

1. Specify the angle of attack at which the blade will be operated, α
2. Compute the flow angle ϕ
3. Determine the lift and drag coefficients from the tabulated data acquired from Xfoil.
4. Calculate C_n and C_A
5. Calculate the new axial and angular induction factors
6. Calculate the differential thrust, dT, torque, dQ, and power, dP, for each of the blade elements
7. After reaching the last element, calculate the total thrust T, torque Q, and power P as a sum of the differential power from each of the elements.

7.2.2 Power Estimation

Lift and drag coefficients are crucial to the power generation expected from the wind turbine blade, and changes in these coefficients will directly affect the power generation. In this section, the power generation out of each blade before and after erosion will be explored. Using Blade Element Momentum Theory (BEMT), the power generation before and after erosion will be calculated for each of the six airfoils of the blade using the equations detailed in the previous section, and the total will be summed up.

7.2.2.1 Uncoated Blade

The change in lift and drag coefficient affected the power generation, as shown in Table 7-7, which shows the power generated before and after erosion and the change percentage for -5˚, 0˚, 5˚, and 10˚ angles of impingement. It can be noticed that the most significant change in power generation occurred where the biggest change in lift and drag coefficients occurred, that is 0˚. Also, it can be seen that the highest loss in power was 43% occurring at 0˚ angle of impingement.

Table 7-7: Before and After erosion power generation for the uncoated blade

Angle of Impingement	Before Erosion (W)	After Erosion (W)	Change Percent
-5˚	385.58	347.26	-10%
0˚	335.09	191.13	-43%
5˚	367.05	319.15	-13%
10˚	344.08	306.89	-11%
Average	**357.95**	**291.11**	**-19%**

7.2.2.2 Coated blades

7.2.2.2.1 H-146 coated blade

The change in lift and drag coefficients for the H-146 was the highest compared to the other two blades. Therefore, change in power generation before and after erosion is also

expected to be the highest. Table 7-8 shows before and after erosion power generation at the four impingement angles for the H-146 coated blade. Like the uncoated blade, the biggest change of 29% in power generation occurred at a 0˚ angle of impingement.

Table 7-8: Before and After erosion power generation for H-146 coated blade.

Angle of Impingement	Before Erosion (W)	After Erosion (W)	Change Percent
-5˚	336.56	305.97	-9%
0˚	313.99	223.11	-29%
5˚	347.64	270.46	-22%
10˚	336.26	250.62	-25%
Average	**333.61**	**262.54**	**-21%**

7.2.2.2.2 Polyurethane/IA-700 coated blade

Polyurethane/IA-700 coated blade showed the highest erosion resistance consequently the lowest change in lift and drag coefficients and therefore will show the lowest change in power generation. Table 7-9 shows the before and after erosion power generation for the polyurethane/IA-700 coated blade. The biggest change in power generation occurred at 0˚ angle of impingement, reaching 27%.

Table 7-9: Before and After erosion power generation for Polyurethane/IA-700 coated blade.

Angle of Impingement	Before Erosion (W)	After Erosion (W)	Change Percent
-5˚	395.62	363.12	-8%
0˚	358.89	260.35	-27%
5˚	350.90	296.43	-16%
10˚	347.69	294.27	-15%
Average	**363.28**	**303.54**	**-17%**

7.2.3 Discussion

Comparing the uncoated to the coated blade yields results similar to that of erosion, where the highest loss in power generation was observed for the H-146 coated blade with an average loss of 21%, followed by the uncoated blade at 19%, and finally, Polyurethane/IA-

700 coated blade at 17%. Since the rate at which wind turbine blades erode is dependent on tip speed, airfoil shape, and the environment in which it is situated [84], a better way to compare different wind turbine blades made of different airfoils and situated in different environments is through the use of the change of the Annual Energy Production (AEP). AEP is defined as the total electrical energy produced over a year, usually measured in kWh or MWh. To calculate AEP, the following equation is used:

$$AEP\ (kWh) = Power\ generated\ (kW) * capacity\ factor * 8760\ hr/year \tag{7-50}$$

Capacity factor is defined as the ratio of the amount of energy produced to the maximum possible energy output. According to Almutairi [199], the capacity factor in Shagaya Kuwait is measured to be 29.2%. Therefore, the average AEP for all three blades before and after erosion is shown in Table 7-10.

Table 7-10: Annual Energy Production (AEP) before and after erosion for the uncoated, H-146 coated, and Polyurethane/IA-700 coated blades

Coating	Before Erosion (kWh)	After Erosion (kWh)	Percent change
Uncoated	915.61	744.63	-19%
H-146	853.35	671.55	-21%
Polyurethane/IA-700	929.23	776.43	-17%

One suggestion to reduce the effects of erosion on the wind turbine production discussed in Chapter 2 was to operate the turbine at a low positive angle of attack that produces the highest lift to drag ratio instead of operating at the angle that generates the highest lift. Also, at low positive angles of attack, the change between before and after erosion is smaller than at 8˚, as shown in Fig. 7-1, 7-3, and 7-5. To test the validity of this suggestion, changes in lift and drag coefficients and power generation before and after erosion will be

investigated. It has been found that the highest lift to drag ratio for all three blades to be at or near a 5˚ angle of attack, as shown in Fig. 7-12, which shows Cl/Cd as a function of the angle of attack. Therefore, aerodynamic performance at 5˚ (highest lift to drag ratio) will be compared to the aerodynamic performance of 8˚ (highest lift).

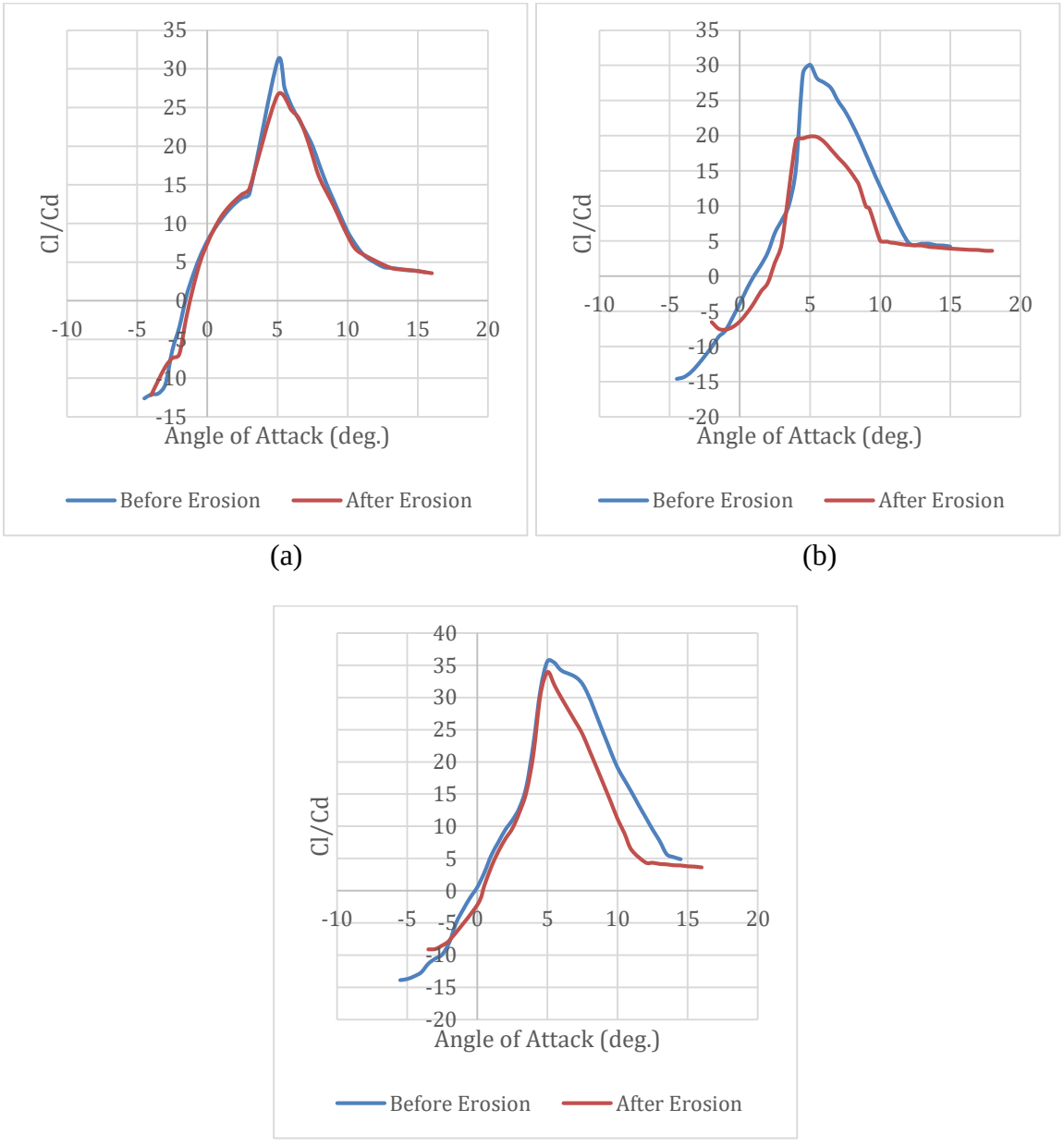


Fig. 7-12: Lift-to-drag (Cl/Cd) ratio as a function of angle of attack for: (a) uncoated, (b) H-146 coated, and (c) polyurethane/IA-700 coated blades.

7.2.3.1 performance at 5˚ vs. 8˚ angle of attack

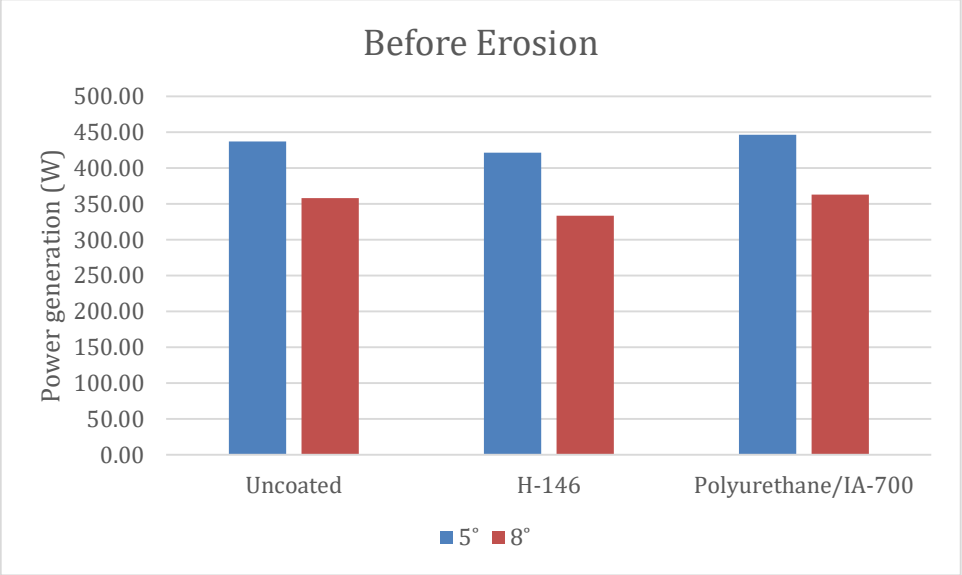
The change in lift and drag coefficients at a 5˚ angle of attack is shown in Table 7-11 for the -5˚, 0˚, 5˚, and 10˚ angles of impingement for the three blades. It can be seen that the change in lift coefficient on average is consistent across all three blades, with a 5% decrease for uncoated and H-146 coated blade and a 4% decrease for polyurethane/IA-700 coated blade. On the other hand, the change in drag coefficient is also consistent with an 11% increase for both uncoated and polyurethane/IA-700 coated blades and 15% for H-146 coated blade. It is noticeable that the changes in lift and drag coefficients had similar trends to the erosion rate for the three blades when looking at an 8˚ angle of attack. However, at a 5˚ angle of attack, the differences between the blades in terms of lift and drag changes are minor, although they had different erosion rates. The change in lift-to-drag ratio for 5˚ angle of attack has also been calculated to be 14%, 15%, and 13% for uncoated, H-146 coated, and polyurethane/IA-700 coated blades.

Table 7-11: Change in Cl/Cd for the three blades at 5˚ angle of attack

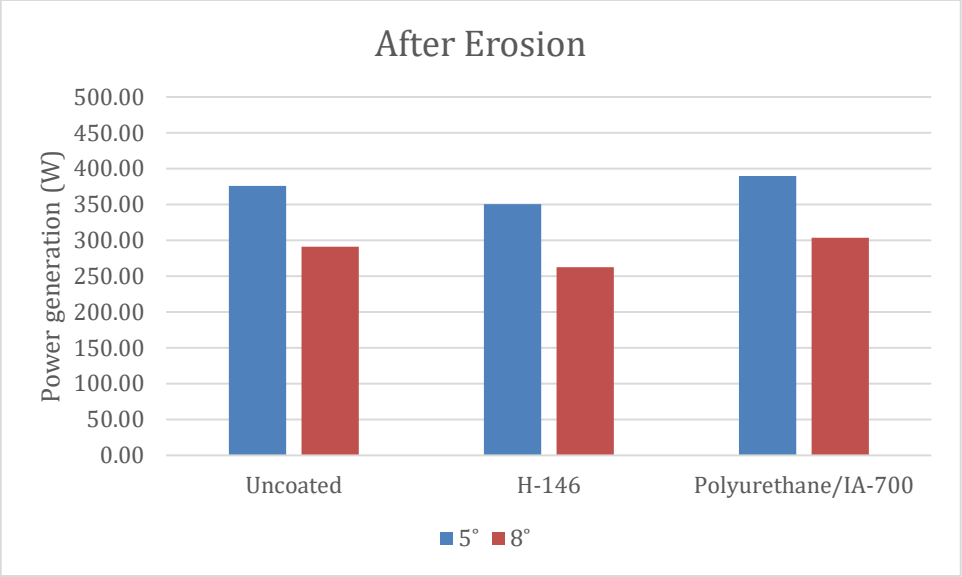
Coating	Uncoated		H-146		Polyurethane/IA-700	
Coefficient	Lift	Drag	lift	drag	lift	drag
-5	-2%	12%	-4%	15%	-3%	10%
0	-4%	13%	-3%	35%	-3%	13%
5	-9%	10%	-7%	4%	-5%	10%
10	-5%	9%	-6%	7%	-5%	11%
Average	**-5%**	**11%**	**-5%**	**15%**	**-4%**	**11%**

Power generation output for before and after erosion was calculated for the three blades at a 5˚ angle of attack. Fig. 7-13 (a) shows the before erosion comparison between 5˚ and 8˚ angles of attack while Fig. 7-13 (b) shows the after erosion performance. The figure shows higher power generation when operating the turbine at 5˚ angle of attack in all cases before and after erosion than 8˚ angle of attack. Decrease in after erosion power generation for 5˚

angle of attack was calculated to be 14%, 17%, and 13% for uncoated, H-146 coated, and Polyurethane/IA-700 coated blades. In comparison, the change in before and after erosion for the 8˚ case was 19%, 21%, and 17% for uncoated, H-146, and polyurethane/IA-700 coated blades. This confirms that operating at low positive angles of attack with the highest lift-to-drag ratio yields less change in aerodynamic performance and power generation due to erosion. Therefore, when operating a wind farm in a region with erosion-prone conditions, it is better to operate the wind turbines at low positive angles of attack since erosion will have smaller effects on the aerodynamic performance. As a result, power generation will be consistent for many years.



(a)



(b)

Fig. 7-13: Power generation at 5˚ and 8˚ angle of attack for: a) before, and b) after erosion

In summary, the effects of the leading edge erosion on the aerodynamic performance of wind turbine blades have been investigated in this chapter in terms of change in lift and drag coefficients and change in power generation. It has been observed that due to erosion, the lift coefficient decreased while the drag coefficient increased, which results in a decrease in the amount of power generated. It is noticeable that the drag coefficient is more sensitive to erosion, with the change in drag coefficient being around three times higher than the change in the lift coefficient. When operating the blade at the highest lift (8˚ angle of attack), it has been noticed that the intensity of erosion is consistent with the intensity of change in aerodynamic performance. However, to decrease the effects of erosion on the aerodynamic performance, it is recommended to operate the wind turbine at a low positive angle of attack (5˚), which showed better after erosion lift and drag coefficients as well as better power generation.

Chapter 8: Conclusion and Recommendations

Wind turbines operated in an environment subjected to sandstorms suffer from the leading edge erosion due to sand particles impingement. Erosion damage is a serious problem that causes a detrimental effect on the overall efficiency and power generation of the turbine. Therefore, the goal of this investigation was to experimentally study the leading edge erosion by eroding wind turbine blades with silica sand particles at varying testing parameters. Then, the effects of using different types of protective coatings in reducing the damage caused by erosion were investigated.

An erosion rig following ASTM G76 standard was built to conduct erosion experiments. Multiple materials were tested such as aluminum 6061 – T6, borosilicate glass, and Glass fiber reinforced epoxy (GFRP). The performance of the uncoated GFRP specimen in terms of material removal and maximum depth was compared to coated specimens. Two graphene-based coatings were used in this experiment, H-146, and IA-700, either as a single layer of coating or in combination with polyurethane as a multilayer coating system. It has been found that a single layer of graphene H-146 is capable of reducing material removal up to 19%. Also, it has been found that using a multilayer coating made of polyurethane as the top layer and graphene IA-700 as the base layer provided up to 15% reduction in erosion depth at 90˚ angle of impingement.

The erosion behavior of the leading edge of an uncoated wind turbine was investigated by studying the effects of multiple variables such as the angle of attack, erosion duration, and

impact velocity on the erosion behavior characterized by the amount of material removal, depth of erosion scars, and the changes in the shape of the airfoils after erosion. It has been found that increased pressure and erosion duration resulted in more severe erosion damage, while different angles of attack resulted in different damage shapes on the leading edge. Also, the maximum material removal and the maximum erosion depth occurred at an angle of attack of 0˚, while the least amount of damage occurred at 10˚. A combination of graphene IA-700 as the base layer and polyurethane as the top layer shows improvements reaching up to 60% improvement in material removal and depth of erosion scars.

Due to leading edge erosion of the wind turbine blades, an increase in drag coefficient, a decrease in the coefficient of lift, and a decrease in power generation have been observed. The level of change in the mentioned parameters depended on the intensity of erosion, with the Tip section showing more drastic changes than Root or Midspan sections. Also, it has been noticed that the type of coating applied to the wind turbine blade affects the change in these aerodynamic parameters. H-146 coated blade showed the largest change while the polyurethane/IA-700 coated blade showed the smallest change, which is consistent with both erosion rate and surface roughness results.

In light of this investigation, this work has been able to accomplish and contribute toward (i) experimentally characterizing the shape of erosion scars on the leading edge of wind turbine blades at different operating and testing conditions (ii) using graphene-based and polyurethane coatings, separately and combined, to protect the leading edge of wind turbine blades from erosion damage, and (iii) understanding the relationship between the shape of erosion and the resulting aerodynamic performance.

In conclusion, based on this investigation, the leading edge erosion of wind turbine blades is a problem that affects the efficiency of the blade, and it is recommended to:

1. Explore and develop graphene coatings with a focus on erosion resistance applications. In this exploratory investigation, graphene combined with polyurethane (Coating 7) has shown the potential to provide protections reaching up to 60% in material removal.
2. Use a protective multilayer coating system to reduce the damage intensity caused by erosion with alternating soft and stiff layers showing the best erosion resistance behavior.
3. Operate wind turbine blades at positive low angles of attack if the turbine is built in an erosion-prone area. Compared to before erosion aerodynamic performance, operating at low positive angles of attack after erosion has shown minimal levels of change in lift and drag coefficients, which means the turbine can generate power at a more consistent and predictable pattern.

Recommendation for future research:

1. Study the effects of temperature variations on the erosion behavior of the uncoated and coated wind turbine blades, since in this experiment only room temperature was considered.
2. Coating 7 (polyurethane on top of graphene IA-700) should be further investigated to examine its ability to provide excellent erosion resistance at different testing conditions.

3. In this investigation the erosion scars on the leading edge were discrete and separated, however, the actual erosion damage on the leading edge is continuous along the span of the blade. Therefore, instead of building a small erosion rig and cut the blades into small airfoils, it will be better to build a wind tunnel that can contain the whole blade and is capable of (i) blowing sand particles at a wind turbine blade, and (ii) measuring the change in aerodynamic performance instantaneously would yield more realistic results.
4. Investigate and develop roughness insensitive airfoils to be operated at erosion-prone areas.

References

[1] DOE and EIA, "The International Energy Outlook 2013," 2013.

[2] EIA, "Electric Power Monthly: Electricity generation from fossil fuels declined in 2017 as renewable generation rose," 2018.

[3] IEA, "Market Report Series: Renewables 2017 Analysis and Forecasts to 2022," 2017.

[4] J. Twidell and T. Weir, *Renewable energy resources*. Routledge, 2015.

[5] A. F. Alajmi, "Conceptual Design of a Circulating Fluidized Bed Reactor as a Thermochemical Thermal Energy Storage System for Applications in Concentrated Solar Thermal Power Plants," University of Wshington, 2016.

[6] M. R. Islam, S. Mekhilef, and R. Saidur, "Progress and recent trends of wind energy technology," *Renew. Sustain. Energy Rev.*, vol. 21, pp. 456–468, 2013.

[7] T. Ackermann and L. Söder, "Wind energy technology and current status: a review," *Renew. Sustain. energy Rev.*, vol. 4, no. 4, pp. 315–374, 2000.

[8] E. Martínez, F. Sanz, S. Pellegrini, E. Jiménez, and J. Blanco, "Life cycle assessment of a multi-megawatt wind turbine," *Renew. energy*, vol. 34, no. 3, pp. 667–673, 2009.

[9] P. J. Schubel and R. J. Crossley, "Wind turbine blade design," *Energies*, vol. 5, no. 9, pp. 3425–3449, 2012.

[10] Y. Kumar *et al.*, "Wind energy: Trends and enabling technologies," *Renew. Sustain. Energy Rev.*, vol. 53, pp. 209–224, 2016.

[11] E. Hau and H. von Renouard, *Wind turbines: fundamentals, technologies, application, economics*. Springer, 2003.

[12] M. R. Ahmed, "Blade sections for wind turbine and tidal current turbine applications – current status and future challenges," *Int. J. Energy Res.*, vol. 36, no. 7, pp. 829–844, 2012.

[13] B. Hayman, J. Wedel-Heinen, and P. Brøndsted, "Materials challenges in present and future wind energy," *MRS Bull.*, vol. 33, no. 4, pp. 343–353, 2008.

[14] IRENA, *Renewable Power Generation Costs in 2017.* 2018.

[15] "Bloomberg New Energy Finance. Offshore wind market outlook," New York, 2017.

[16] K. Dykes *et al.*, "Effect of Tip-Speed Constraints on the Optimized Design of a Wind Turbine," 2014.

[17] J. K. Kaldellis and D. Zafirakis, "The wind energy (r)evolution: A short review of a long history," *Renew. Energy*, vol. 36, no. 7, pp. 1887–1901, 2011.

[18] D. MacKay, *Sustainable Energy-without the hot air*. UIT Cambridge, 2008.

[19] "World Energy Concil," 2016.

[20] L. Mishnaevsky, K. Branner, H. N. Petersen, J. Beauson, M. McGugan, and B. F. Sørensen, "Materials for wind turbine blades: An overview," *Materials (Basel).*, vol. 10, no. 11, pp. 1–24, 2017.

[21] M. P. Groover, *Fundamentals of modern manufacturing: materials processes, and systems*. John Wiley & Sons, 2007.

[22] M. H. Keegan *et al.*, "On erosion issues associated with the leading edge of wind turbine blades," *J. Phys. D. Appl. Phys.*, vol. 383001, no. 38, p. 383001,

2013.
[23] C.-H. Ong and S. W. Tsai, “The use of carbon fibers in wind turbine blade design: a SERI-8 blade example,” 2000.
[24] R. P. L. Nijssen, “Fatigue life prediction and strength degradation of wind turbine rotor blade composites,” *Contract. Rep. SAND2006-7810P, Sandia Natl. Lab. Albuquerque, NM*, 2006.
[25] C. C. Ciang, J.-R. Lee, and H.-J. Bang, “Structural health monitoring for a wind turbine system: a review of damage detection methods,” *Meas. Sci. Technol.*, vol. 19, no. 12, p. 122001, 2008.
[26] D. Li, S. C. M. Ho, G. Song, L. Ren, and H. Li, “A review of damage detection methods for wind turbine blades,” *Smart Mater. Struct.*, vol. 24, no. 3, 2015.
[27] L. Rempel, “Rotor blade leading edge erosion - real life experiences,” *Wind Syst. Mag.*, pp. 22–24, 2012.
[28] A. Sareen, C. Sapre, and M. Selig, “Effects of leading-edge protection tape on wind turbine blade performance,” *Wind Eng.*, vol. 36, no. 5, pp. 525–534, 2012.
[29] D. Y. C. Leung and Y. Yang, “Wind energy development and its environmental impact: A review,” *Renew. Sustain. Energy Rev.*, vol. 16, no. 1, pp. 1031–1039, 2012.
[30] E. Torrance and K. Goff, “A quiet revolution,” *Eng. Technol.*, vol. 10, pp. 44–7, 2009.
[31] E. Pedersen, “Health aspects associated with wind turbine noise—Results from three field studies,” *Noise Control Eng. J.*, vol. 59, no. 1, pp. 47–53, 2011.
[32] J. Punch and D. Pabst, “Wind-turbine noise: what audiologists should know,” *Audiol. today*, vol. 22, no. 4, pp. 20–31, 2010.
[33] J. Chen, J. Wang, and A. Ni, “A review on rain erosion protection of wind turbine blades,” *J. Coatings Technol. Res.*, vol. 16, no. 1, pp. 15–24, 2019.
[34] N. J. Middleton, “Dust storms in the Middle East,” *J. Arid Environ.*, vol. 10, no. 2, pp. 83–96, 1986.
[35] A.-O. Abdulaziz, “A study of three types of wind-blown dust in Kuwait: Duststorms, Rising Dust and Suspen,” *J. Meteorol. THEN BRADFORD AVON-*, vol. 19, p. 19, 1994.
[36] H. Kutiel and H. Furman, “Dust storms in the Middle East: sources of origin and their temporal characteristics,” *Indoor Built Environ.*, vol. 12, no. 6, pp. 419–426, 2003.
[37] B. H. Alharbi, A. Maghrabi, and N. Tapper, “The March 2009 dust event in Saudi Arabia: Precursor and supportive environment,” *Bull. Am. Meteorol. Soc.*, vol. 94, no. 4, pp. 515–528, 2013.
[38] I. F. Zidane, K. M. Saqr, G. Swadener, X. Ma, and M. F. Shehadeh, “On the role of surface roughness in the aerodynamic performance and energy conversion of horizontal wind turbine blades: a review,” *Int. J. Energy Res.*, vol. 40, no. 15, pp. 2054–2077, 2016.
[39] F. H. Proctor, “Numerical simulations of an isolated microburst. Part I: Dynamics and structure,” *J. Atmos. Sci.*, vol. 45, no. 21, pp. 3137–3160, 1988.
[40] S. Dunlop, *A dictionary of weather*. OUP Oxford, 2008.
[41] S. D. Miller *et al.*, “Haboob dust storms of the southern Arabian Peninsula,” *J. Geophys. Res. Atmos.*, vol. 113, no. D1, 2008.

[42] T. J. Lawson, "Haboob structure at Khartoum," *Weather*, vol. 26, no. 3, pp. 105–112, 1971.
[43] "ISO 14688-1: 2002: Geotechnical investigation and testing. Identification and classification of soil. Identification and description." British Standards Institution London, 2002.
[44] C. K. Wentworth, "A scale of grade and class terms for clastic sediments," *J. Geol.*, vol. 30, no. 5, pp. 377–392, 1922.
[45] W. C. Krumbein, "Size frequency distributions of sediments," *J. Sediment. Res.*, vol. 4, no. 2, pp. 65–77, 1934.
[46] J. M. Al-Awadhi and A. A. Alshuaibi, "Dust fallout in Kuwait city: Deposition and characterization," *Sci. Total Environ.*, vol. 461–462, pp. 139–148, 2013.
[47] H. A. Al-Sanad, N. F. Ismael, and A. J. Nayfeh, "Geotechnical properties of dune sands in Kuwait," *Eng. Geol.*, vol. 34, no. 1–2, pp. 45–52, 1993.
[48] N. Dalili, A. Edrisy, and R. Carriveau, "A review of surface engineering issues critical to wind turbine performance," *Renew. Sustain. Energy Rev.*, vol. 13, no. 2, pp. 428–438, 2009.
[49] W. Tabakoff, "Review - Turbomachinery performance deterioration exposed to solid particulates environment," *J. Fluids Eng.*, vol. 106, pp. 125–134, 1984.
[50] E. Sagol, M. Reggio, and A. Ilinca, "Issues concerning roughness on wind turbine blades," *Renew. Sustain. Energy Rev.*, vol. 23, pp. 514–525, 2013.
[51] H. Schlichting and K. Gersten, *Boundary-layer theory*. Springer, 2016.
[52] J. D. Anderson Jr, *Fundamentals of aerodynamics*. Tata McGraw-Hill Education, 2010.
[53] M. Chakraborty, "A Computational Study on two horizontally close sequential airfoils to determine conjoined pressure distribution and aerodynamic influences on each other," Chittagong University of Engineering & Technology, 2015.
[54] A. B. Turner, S. E. Hubbe-Walker, and F. J. Bayley, "Fluid flow and heat transfer over straight and curved rough surfaces," *Int. J. Heat Mass Transf.*, vol. 43, no. 2, pp. 251–262, 2000.
[55] M. B. Bragg, A. P. Broeren, and L. A. Blumenthal, "Iced-airfoil aerodynamics," *Prog. Aerosp. Sci.*, vol. 41, no. 5, pp. 323–362, 2005.
[56] N. Gregory and C. L. O'reilly, "Low-speed aerodynamic characteristics of NACA 0012 aerofoil section, including the effects of upper-surface roughness simulating hoar frost," 1970.
[57] N. Ren and J. Ou, "Dust Effect on the Performance of Wind Turbine Airfoils," *J. Electromagn. Anal. Appl.*, vol. 01, no. 02, pp. 102–107, 2009.
[58] J. L. Tangler, "Effects of airfoil thickness and maximum lift on roughness sensitivity," in *Proceedings of the 3rd ASME/JSME Fluids Engineering Conference, CA, USA*, 1999.
[59] W. Timmer, "An overview of NACA 6-digit airfoil series characteristics with reference to airfoils for large wind turbine blades," in *47th AIAA aerospace sciences meeting including the new horizons forum and aerospace exposition*, 2009, p. 268.
[60] E. L. Houghton and P. W. Carpenter, *Aerodynamics for engineering students*. Elsevier, 2003.

[61] M. Drela, "XFOIL: An analysis and design system for low Reynolds number airfoils," in *Low Reynolds number aerodynamics*, Springer, 1989, pp. 1–12.
[62] J. Morgado, R. Vizinho, M. A. R. Silvestre, and J. C. Páscoa, "XFOIL vs CFD performance predictions for high lift low Reynolds number airfoils," *Aerosp. Sci. Technol.*, vol. 52, pp. 207–214, 2016.
[63] A. Sareen, C. A. Sapre, and M. S. Selig, "Effects of leading edge erosion on wind turbine blade performance," *Wind Energy*, vol. 17, no. 2014, pp. 1531–1542, 2014.
[64] O. Gohardani, "Impact of erosion testing aspects on current and future flight conditions," *Prog. Aerosp. Sci.*, vol. 47, no. 4, pp. 280–303, 2011.
[65] M. R. Soltani, A. H. Birjandi, and M. Seddighi Moorani, "Effect of surface contamination on the performance of a section of a wind turbine blade," *Sci. Iran.*, vol. 18, no. 3 B, pp. 349–357, 2011.
[66] W. J. Jasinski, S. C. Noe, M. S. Selig, and M. B. Bragg, "Wind turbine performance under icing conditions," *J. Sol. Energy Eng.*, vol. 120, no. 1, pp. 60–65, 1998.
[67] C. Hochart, G. Fortin, J. Perron, and A. Ilinca, "Wind turbine performance under icing conditions," *Wind Energy An Int. J. Prog. Appl. Wind Power Convers. Technol.*, vol. 11, no. 4, pp. 319–333, 2008.
[68] B. Tammelin, M. Cavaliere, H. Holttinen, C. Morgan, H. Seifert, and K. Säntti, "Wind energy production in cold climate (WECO). Finnish Meteorological Institute Rep," 2000.
[69] G. P. Corten and H. F. Veldkamp, "Aerodynamics: Insects can halve wind-turbine power," *Nature*, vol. 412, no. 6842, p. 41, 2001.
[70] A. Bellamy, "Why looking after blades will pay for itself," 2014.
[71] M. G. Khalfallah and A. M. Koliub, "Effect of dust on the performance of wind turbines," *Desalination*, vol. 209, no. 1-3 SPEC. ISS., pp. 209–220, 2007.
[72] A. M. H. El-Din, A. Diab, and Z. Ghoneim, "Assessment of losses in annual energy production of wind turbines subjected to sand erosion," in *Proceedings of International Conference on Fluid Dynamics*, 2016, pp. 1–12.
[73] "3M wind blade protection coating W4600," 2011.
[74] C. Arrighetti, G. M. De Pratti, and R. Ruscitti, "Performance decay analysis of new rotor blade profiles for wind turbines operating in offshore environments," *Wind Eng.*, vol. 27, no. 5, pp. 371–380, 2003.
[75] G. P. Tilly, "Erosion caused by airborne particles," *Wear*, vol. 14, no. 1, pp. 63–79, 1969.
[76] G. Fiore and M. S. Selig, "A simulation of operational damage for wind turbine blades," in *32nd AIAA Applied Aerodynamics Conference*, 2014, no. June, pp. 1–19.
[77] A. Hossam El-Din and A. Diab, "A preliminary study of the blade erosion for a wind turbine operating in a dusty environment," in *ASME Turbo Expo 2016: Turbomachinery Technical Conference and Exposition*, 2016.
[78] K. Wood, "Blade repair: Closing the maintenance gap," *Compos. World*, pp. 1–6, 2011.
[79] J. Zahavi and G. F. Schmitt, "Solid particle erosion of polymeric coatings," *Wear*, vol. 71, no. 2, pp. 191–210, 1981.
[80] S. Biswas, A. Satapathy, and A. Patnaik, "Erosion wear behavior of polymer

composites: A review," *J. Reinf. Plast. Compos.*, vol. 29, no. 19, pp. 2898–2924, 2010.
[81] R. S. Ehrmann, E. B. White, M. a Rumsey, R. Chow, C. M. Langel, and C. P. Van Dam, "Realistic Leading-Edge Roughness Effects on Airfoil Performance," *31st AIAA Appl. Aerodyn. Conf.*, pp. 1–19, 2013.
[82] N. Gaudern, "A practical study of the aerodynamic impact of wind turbine blade leading edge erosion," *J. Phys. Conf. Ser.*, vol. 524, no. 1, pp. 0–10, 2014.
[83] K. Gharali and D. A. Johnson, "Numerical modeling of an S809 airfoil under dynamic stall, erosion and high reduced frequencies," *Appl. Energy*, vol. 93, pp. 45–52, 2012.
[84] R. Herring, K. Dyer, F. Martin, and C. Ward, "The increasing importance of leading edge erosion and a review of existing protection solutions," *Renew. Sustain. Energy Rev.*, vol. 115, no. February, 2019.
[85] J. Tangler, B. Smith, and D. Jager, "SERI advanced wind turbine blades," 1992.
[86] C. Bak, P. Anderson, H. Madsen, M. Gaunaa, P. Fuglsang, and S. Bove, "Design and verification of airfoils resistant to surface contamination and turbulence intensity," in *26th AIAA applied aerodynamics conference*, 2008, pp. 1–11.
[87] G. Fiore and M. S. Selig, "Optimization of Wind Turbine Airfoils Subject to Particle Erosion," in *33rd AIAA Applied Aerodynamics Conference*, 2015, no. June, pp. 1–23.
[88] R. J. K. Wood, "Solid Particle Erosion," in *ASM handbook. Vol. 18, Friction, lubrication, and wear technology*, 2017, pp. 266–289.
[89] W. A. Timmer and R. Van Rooij, "Summary of the Delft University wind turbine dedicated airfoils," *J. Sol. Energy Eng.*, vol. 125, no. 4, pp. 488–496, 2003.
[90] J. L. Tangler and D. M. Somers, "NREL airfoil families for HAWTs," 1995.
[91] C. A. Sapre, "Turbine Blade Erosion and The Use Of Wind Protection Tape," University of Illinois at Urbana-Champaign, 2012.
[92] S. Arjula and A. P. Harsha, "Study of erosion efficiency of polymers and polymer composites," *Polym. Test.*, vol. 25, no. 2, pp. 188–196, 2006.
[93] D. W. Wheeler, "Chemical vapour deposition methods for protection against wear," *Surf. coatings Prot. against wear*, 2006.
[94] H. S. Kirols, D. Kevorkov, A. Uihlein, and M. Medraj, "The effect of initial surface roughness on water droplet erosion behaviour," *Wear*, vol. 342, pp. 198–209, 2015.
[95] A. S. Ellis, F. T. Smith, and A. H. White, "Droplet impact on to a rough surface," *Q. J. Mech. Appl. Math.*, vol. 64, no. 2, pp. 107–139, 2011.
[96] A. L. Yarin, "Drop impact dynamics: splashing, spreading, receding, bouncing…," *Annu. Rev. Fluid Mech.*, vol. 38, pp. 159–192, 2006.
[97] C. Challener, "Coatings critical for wind energy efficiency," *JCT CoatingsTech*, vol. 7, no. 1, p. 46, 2010.
[98] L. Mishnaevsky, "Toolbox for optimizing anti-erosion protective coatings of wind turbine blades: Overview of mechanisms and technical solutions," *Wind Energy*, no. May, pp. 1636–1653, 2019.
[99] N. S. Sigamani, "Characterization of polyurethane at multiple scales for erosion mechanisms under sand particle impact," Texas A & M University, 2010.

[100] E. M. Christenson, J. M. Anderson, A. Hiltner, and E. Baer, "Relationship between nanoscale deformation processes and elastic behavior of polyurethane elastomers," *Polymer (Guildf).*, vol. 46, no. 25, pp. 11744–11754, 2005.
[101] M. Haag, "Advances in leading edge protection of wind turbine blades," *EWEA (Vienna, Austria, 4-7, Febr. 2013)*, 2013.
[102] V. Singh, D. Joung, L. Zhai, S. Das, S. I. Khondaker, and S. Seal, "Graphene based materials: past, present and future," *Prog. Mater. Sci.*, vol. 56, no. 8, pp. 1178–1271, 2011.
[103] D. Berman, A. Erdemir, and A. V. Sumant, "Graphene: A new emerging lubricant," *Mater. Today*, vol. 17, no. 1, pp. 31–42, 2014.
[104] M. J. Nine, M. A. Cole, D. N. H. Tran, and D. Losic, "Graphene: a multipurpose material for protective coatings," *J. Mater. Chem. A*, vol. 3, no. 24, pp. 12580–12602, 2015.
[105] J. S. Bunch *et al.*, "Impermeable atomic membranes from graphene sheets," *Nano Lett.*, vol. 8, no. 8, pp. 2458–2462, 2008.
[106] D. Berman, A. Erdemir, and A. V Sumant, "Few layer graphene to reduce wear and friction on sliding steel surfaces," *Carbon N. Y.*, vol. 54, pp. 454–459, 2013.
[107] M. Parsi, K. Najmi, F. Najafifard, S. Hassani, B. S. McLaury, and S. A. Shirazi, "A comprehensive review of solid particle erosion modeling for oil and gas wells and pipelines applications," *J. Nat. Gas Sci. Eng.*, vol. 21, pp. 850–873, 2014.
[108] G. Grant and W. Tabakoff, "Erosion prediction in turbomachinery resulting from environmental solid particles," *J. Aircr.*, vol. 12, no. 5, pp. 471–478, 1975.
[109] A. A. Hamed, W. Tabakoff, R. B. Rivir, K. Das, and P. Arora, "Turbine Blade Surface Deterioration by Erosion," *J. Turbomach.*, vol. 127, no. 3, p. 445, 2005.
[110] J. M. Reichert and L. D. Norton, "Fluidized Bed Combustion Bottom-Ash Effects on Infiltration and Erosion of Variable-Charge Soils," *Soil Sci. Soc. Am. J.*, vol. 60, no. 1, pp. 275–282, 1996.
[111] B. Q. Wang, G. Q. Geng, and A. V Levy, "Surface behavior of heat exchanger tubes in fluidized-bed combustors," *Surf. Coatings Technol.*, vol. 42, no. 3, pp. 253–274, 1990.
[112] H. Law and V. Koutsos, "Leading edge erosion of wind turbines: Effect of solid airborne particles and rain on operational wind farms," *Wind Energy*, vol. 23, no. 10, pp. 1955–1965, 2020.
[113] I. Finnie, "Erosion of surfaces by Solid Particles," *Wear*, vol. 3, pp. 87–103, 1960.
[114] E. S. S. A and I. Finnie, "Some observations on the erosion of ductile metals," *Wear*, vol. 19, pp. 81–90, 1972.
[115] J. G. A. Bitter, "A Study of Erosion Phenomena Part I," *Wear*, vol. 6, pp. 5–21, 1963.
[116] J. G. A. Bitter, "A Study of Erosion Phenomena Part II," *Wear*, vol. 6, pp. 169–190, 1963.
[117] S. Ally, J. K. Spelt, and M. Papini, "Prediction of machined surface evolution in the abrasive jet micro-machining of metals," *Wear*, vol. 292–293, pp. 89–99, 2012.
[118] V. Hadavi, C. E. Moreno, and M. Papini, "Numerical and experimental analysis

of particle fracture during solid particle erosion, part I: modeling and experimental verification," *Wear*, vol. 356, pp. 135–145, 2016.
[119] V. Hadavi, C. E. Moreno, and M. Papini, "Numerical and experimental analysis of particle fracture during solid particle erosion, Part II: Effect of incident angle, velocity and abrasive size," *Wear*, vol. 356, pp. 146–157, 2016.
[120] R. H. M. Jafar, J. K. Spelt, and M. Papini, "Surface roughness and erosion rate of abrasive jet micro-machined channels: Experiments and analytical model," *Wear*, vol. 303, no. 1–2, pp. 138–145, 2013.
[121] Z. Wang, H. N. Li, T. B. Yu, H. Chen, and J. Zhao, "On the predictive modelling of machined surface topography in abrasive air jet polishing of quartz glass," *Int. J. Mech. Sci.*, vol. 152, no. August 2018, pp. 1–18, 2019.
[122] H. C. Meng and K. C. Ludema, "Wear models and predictive equations: their form and content," *Wear*, vol. 181, pp. 443–457, 1995.
[123] S. Hassani, M. Bielawski, W. Beres, L. Martinu, M. Balazinski, and J. E. Klemberg-Sapieha, "Predictive tools for the design of erosion resistant coatings," *Surf. Coatings Technol.*, vol. 203, no. 3–4, pp. 204–210, 2008.
[124] N. Miyazaki, *Solid particle erosion of composite materials: A critical review*, vol. 50, no. 23. 2016.
[125] I. Hutchings and P. Shipway, *Tribology: friction and wear of engineering materials*. Butterworth-Heinemann, 2017.
[126] P. V. Rao and D. H. Buckley, "Time dependence of solid-particle impingement erosion of an aluminum alloy," 1983.
[127] R. E. Winter and I. M. Hutchings, "Solid particle erosion studies using single angular particles," *Wear*, vol. 29, no. 2, pp. 181–194, 1974.
[128] I. Finnie, "The mechanism of erosion of ductile metals," in *3rd US national congress of applied mechanics*, 1958.
[129] I. Kleis and P. Kulu, *Solid Particle Erosion: Occurence, Prediction ans Control*. 2008.
[130] G. Sundararajan, "The depth of plastic deformation beneath eroded surfaces: The influence of impact angle and velocity, particle shape and material properties," *Wear*, vol. 149, no. 1–2, pp. 129–153, 1991.
[131] V. S. Sooraj and V. Radhakrishnan, "Elastic impact of abrasives for controlled erosion in fine finishing of surfaces," *J. Manuf. Sci. Eng. Trans. ASME*, vol. 135, no. 5, pp. 1–12, 2013.
[132] I. Finnie, "Some reflections on the past and future of erosion," *Wear*, vol. 186–187, P, no. 0, pp. 1–10, 1995.
[133] H. Wensink and M. C. Elwenspoek, "A closer look at the ductile-brittle transition in solid particle erosion," *Wear*, vol. 253, no. 9–10, pp. 1035–1043, 2002.
[134] G. L. Sheldon and I. Finnie, "On the Ductile Behavior of Nominally Brittle Materials During Erosive Cutting," *J. Eng. Ind.*, vol. 88, no. 4, p. 387, 1966.
[135] J. Zahavi and G. F. Schmitt Jr, "Solid particle erosion of reinforced composite materials," *Wear*, vol. 71, no. 2, pp. 179–190, 1981.
[136] K. V. Pool, C. K. H. Dharan, and I. Finnie, "Erosive wear of composite materials," *Wear*, vol. 107, no. 1, pp. 1–12, 1986.
[137] J. H. Williams Jr and E. K. Lau, "Solid particle erosion of graphite-epoxy

composites," *Wear*, vol. 29, no. 2, pp. 219–230, 1974.
[138] U. S. Tewari, A. P. Harsha, A. M. Häger, and K. Friedrich, "Solid particle erosion of unidirectional carbon fibre reinforced polyetheretherketone composites," *Wear*, vol. 252, no. 11–12, pp. 992–1000, 2002.
[139] N. Y. Sari, T. Sinmazcelik, and T. Yilmaz, "Erosive wear studies of glass fiber- and carbon fiber-reinforced polyetheretherketone composites at low particle speed," *J. Thermoplast. Compos. Mater.*, vol. 24, no. 3, pp. 333–350, 2011.
[140] T. Sinmazçelik and I. Taskiran, "Erosive wear behaviour of polyphenylenesulphide (PPS) composites," *Mater. Des.*, vol. 28, no. 9, pp. 2471–2477, 2007.
[141] Y. A. Ballout, S. K. Hovis, and J. E. Talia, "Erosion in glass-fiber reinforced epoxy composite," *Scr. Metall. Mater.*, vol. 24, no. 1, pp. 195–200, 1990.
[142] N.-M. Barkoula and J. Karger-Kocsis, "Solid particle erosion of unidirectional GF reinforced EP composites with different fiber/matrix adhesion," *J. Reinf. Plast. Compos.*, vol. 21, no. 15, pp. 1377–1388, 2002.
[143] N. Miyazaki and N. Takeda, "Solid particle erosion of fiber reinforced plastics," *J. Compos. Mater.*, vol. 27, no. 1, pp. 21–31, 1993.
[144] P. J. Mathias, W. Wu, K. C. Goretta, J. L. Routbort, D. P. Groppi, and K. R. Karasek, "Solid particle erosion of a graphite-fiber-reinforced bismaleimide polymer composite," *Wear*, vol. 135, no. 1, pp. 161–169, 1989.
[145] N.-M. Barkoula and J. Karger-Kocsis, "Effects of fibre content and relative fibre-orientation on the solid particle erosion of GF/PP composites," *Wear*, vol. 252, no. 1–2, pp. 80–87, 2002.
[146] A. P. Harsha, U. S. Tewari, and B. Venkatraman, "Solid particle erosion behaviour of various polyaryletherketone composites," *Wear*, vol. 254, no. 7–8, pp. 693–712, 2003.
[147] N. Miyazaki and T. Hamao, "Solid particle erosion of thermoplastic resins reinforced by short fibers," *J. Compos. Mater.*, vol. 28, no. 9, pp. 871–883, 1994.
[148] D. Aquaro and E. Fontani, "Erosion of ductile and brittle materials," *Meccanica*, vol. 36, no. 6, pp. 651–661, 2001.
[149] M. A. Chowdhury, U. K. Debnath, D. M. Nuruzzaman, and M. M. Islam, "Experimental evaluation of erosion of gunmetal under asymmetrical shaped sand particle," *Adv. Tribol.*, vol. 2015, 2015.
[150] G. L. Sheldon, "Similarities and differences in the erosion behavior of materials," *J. Basic Eng.*, vol. 92, no. 3, pp. 619–626, 1970.
[151] A. V. Levy and P. Chik, "The effects of erodent composition and shape on the erosion of steel," *Wear*, vol. 89, no. 2, pp. 151–162, 1983.
[152] G. P. Tilly and W. Sage, "The interaction of particle and material behaviour in erosion processes," *Wear*, vol. 16, no. 6, pp. 447–465, 1970.
[153] A. D. Salman, C. A. Biggs, J. Fu, I. Angyal, M. Szabo, and M. J. Hounslow, "An experimental investigation of particle fragmentation using single particle impact studies," *Powder Technol.*, vol. 128, no. 1, pp. 36–46, 2002.
[154] L. Murugesh and R. O. Scattergood, "Effect of erodent properties on the erosion of alumina," *J. Mater. Sci.*, vol. 26, no. 20, pp. 5456–5466, 1991.
[155] G. P. Tilly, "A two stage mechanism of ductile erosion," *Wear*, vol. 23, no. 1, pp. 87–96, 1973.

[156] J. Salik, D. Buckley, and W. A. Brainard, "The effect of mechanical surface and heat treatments on the erosion resistance of 6061 aluminum alloy," *Wear*, vol. 65, no. 3, pp. 351–358, 1981.
[157] S. M. Wiederhorn and B. J. Hockey, "Effect of material parameters on the erosion resistance of brittle materials," *J. Mater. Sci.*, vol. 18, pp. 766–780, 1983.
[158] B. Lawn and T. R. Wilshaw, *Fracture of brittle solids*. Cambridge university press, 1993.
[159] I. M. Hutchings, R. E. Winter, and J. E. Field, "Solid particle erosion of metals: the removal of surface material by spherical projectiles," *Proc. R. Soc. London. A. Math. Phys. Sci.*, vol. 348, no. 1654, pp. 379–392, 1976.
[160] Y. I. Oka, M. Matsumura, and T. Kawabata, "Relationship between surface hardness and erosion damage caused by solid particle impact," *Wear*, vol. 162–164, no. PART B, pp. 688–695, 1993.
[161] A. G. Evans, M. E. Gulden, and M. Rosenblatt, "Impact damage in brittle materials in the elastic-plastic response regime," *Proc. R. Soc. London. A. Math. Phys. Sci.*, vol. 361, no. 1706, pp. 343–365, 1978.
[162] A. G. Evans and D. B. Marshall, "Wear mechanism in ceramics, fundamentals of friction and wear of materials," *Wear*, p. 439, 1981.
[163] C. E. Smeltzer, M. E. Gulden, and W. A. Compton, "Mechanisms of metal removal by impacting dust particles," *J. Fluids Eng. Trans. ASME*, vol. 92, no. 3, pp. 639–652, 1970.
[164] A. V Levy, "The role of plasticity in erosion," in *International Conference on Erosion by Liquid and Solid Impact, 5 th, Cambridge, England*, 1979, pp. 31–39.
[165] U. Suur, "Device for erosion study at elevated temperatures," *Proc Techn Univ Talling*, vol. 192, pp. 51–67, 1962.
[166] W. Tabakoff, J. Ramachandran, and A. Hamed, "Temperature effects on the erosion of metals used in turbomachinery," in *International Conference on Erosion by Liquid and Solid Impact, 5 th, Cambridge, England, Proceedings*, 1979, vol. 3, no. 6.
[167] D. B. Marshall, B. R. Lawn, and A. G. Evans, "Elastic/plastic indentation damage in ceramics: the lateral crack system," *J. Am. Ceram. Soc.*, vol. 65, no. 11, pp. 561–566, 1982.
[168] K. Kendall, T. P. Weihs, and I. M. Hutchings, "Ductile-brittle transitions and wear maps for the erosion and abrasion of brittle materials Adhesion of nanoparticles within spray dried agglomerates Ductile-brittle transitions and wear maps for the erosion and abrasion of brittle materials," *J. Phys. D Appl. Phys. 25 A212 J. Phys. D Appl. Phys*, vol. 25, pp. 212–221, 1992.
[169] P. J. Slikkerveer, P. C. P. Bouten, F. H. In't Veld, and H. Scholten, "Erosion and damage by sharp particles," *Wear*, vol. 217, no. 2, pp. 237–250, 1998.
[170] ASTM, "G76 – 13 Standard Test Method forConducting Erosion Tests by Solid Particle Impingement Using Gas Jets."
[171] M. J. Zucrow and J. D. Hoffman, "Gas Dynamics, Vol. 1, 2," *John Wiley Sons, New York*, vol. 68, p. 69, 1976.
[172] "Aeolos - H 1KW Technical report."
[173] A. ANSI, "B46. 1: Surface Texture (Surface Roughness, Waviness, and Lay),"

ASME New York, NY, USA, 2009.
[174] J. de Villanueva Baygual, "Design and implementation of a calculation program in Matlab platform for evaluation of roughness," 2015.
[175] *ISO 4287. Geometrical Product Specifications (GPS). Surface Texture: Profile Method. Terms, Definitions and Surface Texture Parameters*. International Organization for Standardization, 1997.
[176] "ISO 4288. Geometric Product Specification (GPS). Surface texture: profile method—rules and procedures for the assessment of surface texture." British Standards Institution London, 1996.
[177] *ASM Handbook volume 2, Properties and Selection: Nonferrous alloys and special purpose materials*. 2001.
[178] Y. Sun, T. Bell, and S. Zheng, "Finite element analysis of the critical ratio of coating thickness to indentation depth for coating property measurements by nanoindentation," *Thin Solid Films*, vol. 258, no. 1–2, pp. 198–204, 1995.
[179] X. Cai and H. Bangert, "Hardness measurements of thin films-determining the critical ratio of depth to thickness using FEM," *Thin Solid Films*, vol. 264, no. 1, pp. 59–71, 1995.
[180] A. Tricoteaux, E. S. Puchi-Cabrera, and J. Lesage, "Method for fast determination of thin films hardness from standard microindentation tests," *Surf. Eng.*, vol. 23, no. 1, pp. 40–44, 2007.
[181] B. Jönsson and S. Hogmark, "Hardness measurements of thin films," *Thin Solid Films*, vol. 114, no. 3, pp. 257–269, 1984.
[182] E. Broitman, "Indentation Hardness Measurements at Macro-, Micro-, and Nanoscale: A Critical Overview," *Tribol. Lett.*, vol. 65, no. 1, p. 23, 2016.
[183] Carboline, "Carbothane HG 143 technical data sheet," 2011.
[184] NIC-Industries, "H-146 Graphite black technical data sheet."
[185] V. B. Nguyen, Q. B. Nguyen, Y. W. Zhang, C. Y. H. Lim, and B. C. Khoo, "Effect of particle size on erosion characteristics," *Wear*, vol. 348–349, pp. 126–137, 2016.
[186] L. Mishnaevsky, S. Fæster, L. P. Mikkelsen, Y. Kusano, and J. I. Bech, "Micromechanisms of leading edge erosion of wind turbine blades: X-ray tomography analysis and computational studies," *Wind Energy*, vol. 23, no. 3, pp. 547–562, 2020.
[187] Y. Wang, X. Zheng, R. Hu, and P. Wang, "Effects of Leading Edge Defect on the Aerodynamic and Flow Characteristics of an S809 Airfoil," *PLoS One*, vol. 11, no. 9, 2016.
[188] M. Schramm, H. Rahimi, B. Stoevesandt, and K. Tangager, "The Influence of Eroded Blades on Wind Turbine Performance Using Numerical Simulations," *Energies*, vol. 10, no. 9, pp. 1–15, 2017.
[189] S. Zhang, K. Dam-Johansen, P. L. Bernad Jr, and S. Kiil, "Rain erosion of wind turbine blade coatings using discrete water jets: Effects of water cushioning, substrate geometry, impact distance, and coating properties," *Wear*, vol. 328, pp. 140–148, 2015.
[190] W. Han, J. Kim, and B. Kim, "Effects of contamination and erosion at the leading edge of blade tip airfoils on the annual energy production of wind turbines," *Renew. Energy*, vol. 115, pp. 817–823, 2018.

[191] E. G. Perez, “Wind farm owner’s view on rotor blades from O&M to design requirements,” in *International Conference Wind Turbines Rotor Blade O&M*, 2014.
[192] L. Mishnaevsky, “Repair of wind turbine blades: Review of methods and related computational mechanics problems,” *Renew. Energy*, vol. 140, pp. 828–839, 2019.
[193] “Anti-erosion structure for aircrafts.,” United States Patent Application 20160046370.
[194] R. M. Gamache, C. B. Giller, G. Montella, D. Fragiadakis, and C. M. Roland, “Elastomer-metal laminate armor,” *Mater. \& Des.*, vol. 111, pp. 362–368, 2016.
[195] W. Al-Nassar, S. Alhajraf, A. Al-Enizi, and L. Al-Awadhi, “Potential wind power generation in the State of Kuwait,” *Renew. Energy*, vol. 30, no. 14, pp. 2149–2161, 2005.
[196] T. M. Letcher, *Wind energy engineering: a handbook for onshore and offshore wind turbines*. Academic Press, 2017.
[197] J. N. Sørensen, *General momentum theory for horizontal axis wind turbines*, vol. 4. Springer, 2016.
[198] H. Glauert, “Airplane propellers,” in *Aerodynamic theory*, Springer, 1935, pp. 169–360.
[199] B. L. Almutairi, “Investigating the feasibility and soil--structure integrity of onshore wind turbine systems in Kuwait,” Loughborough University, 2017.

Appendix I: Material removal data

In this appendix, the amount of material removed from flat surfaces is shown. Mass loss in the aluminum target is shown in Table AI-1, while mass loss of glass is shown in Table AI-2. On the other hand, material removal data for uncoated and coated GFRP for 180 seconds and 360 seconds are shown in Tables AI-3 to AI-18.

- Aluminum Material Removal:

Table AI-1: Amount of material removed from aluminum target as a function of angle of attack

Angle of impingement	EXP 1 (g)	EXP 2 (g)	EXP 3 (g)	Average (g)	Standard deviation
10˚	2.67E-03	3.17E-03	3.24E-03	3.02E-03	3.12E-04
20˚	2.73E-03	3.23E-03	4.12E-03	3.36E-03	7.02E-04
30˚	2.33E-03	2.12E-03	3.30E-03	2.58E-03	6.29E-04
45˚	9.67E-04	1.13E-03	2.10E-03	1.40E-03	6.12E-04
60˚	7.00E-04	8.33E-04	1.60E-03	1.04E-03	4.86E-04
90˚	2.67E-04	3.67E-04	6.00E-04	4.11E-04	1.71E-04

- Borosilicate Glass:

Table AI-2: Amount of material removed from glass target as a function of angle of attack

Angle of impingement	EXP 1 (g)	EXP 2 (g)	EXP 3 (g)	Average (g)	Standard deviation
30˚	5.84E-03	4.78E-03	3.98E-03	4.87E-03	9.33E-04
45˚	1.09E-02	1.04E-02	1.08E-02	1.07E-02	3.06E-04
60˚	1.79E-02	1.56E-02	1.72E-02	1.69E-02	1.16E-03
75˚	2.23E-02	1.95E-02	2.40E-02	2.19E-02	2.29E-03
90˚	2.44E-02	2.15E-02	2.20E-02	2.26E-02	1.53E-03

- Uncoated GFRP:
  - 180 seconds

Table AI-3: Amount of material removed from uncoated GFRP target as a function of angle of attack at an erosion duration of 180 seconds

Angle of impingement	EXP 1 (g)	EXP 2 (g)	EXP 3 (g)	Average (g)	Standard deviation
30˚	6.72E-03	4.62E-03	5.16E-03	5.50E-03	1.09E-03
45˚	6.40E-03	7.88E-03	7.26E-03	7.18E-03	7.43E-04
60˚	5.38E-03	7.00E-03	5.22E-03	5.87E-03	9.85E-04
75˚	4.74E-03	6.14E-03	4.00E-03	4.96E-03	1.09E-03
90˚	4.62E-03	5.26E-03	4.60E-03	4.83E-03	3.75E-04

  - 360 seconds

Table AI-4: Amount of material removed from uncoated GFRP target as a function of angle of attack at an erosion duration of 360 seconds

Angle of impingement	EXP 1 (g)	EXP 2 (g)	EXP 3 (g)	Average (g)	Standard deviation
30˚	9.38E-03	9.70E-03	1.01E-02	9.73E-03	3.61E-04
45˚	1.16E-02	1.16E-02	1.06E-02	1.13E-02	5.66E-04
60˚	8.68E-03	9.44E-03	9.56E-03	9.23E-03	4.77E-04
75˚	8.02E-03	8.64E-03	7.36E-03	8.01E-03	6.40E-04
90˚	6.84E-03	6.24E-03	7.12E-03	6.73E-03	4.50E-04

- H-146:
  - 180 seconds

Table AI-5: Amount of material removed from H-146 coated GFRP target as a function of angle of attack at an erosion duration of 180 seconds

Angle of impingement	EXP 1 (g)	EXP 2 (g)	EXP 3 (g)	Average (g)	Standard deviation
30˚	6.14E-03	6.54E-03	6.60E-03	6.43E-03	2.50E-04
45˚	5.94E-03	8.24E-03	6.50E-03	6.89E-03	1.20E-03
60˚	5.34E-03	4.60E-03	5.72E-03	5.22E-03	5.70E-04
75˚	5.04E-03	6.38E-03	6.66E-03	6.03E-03	8.66E-04
90˚	3.86E-03	5.50E-03	5.44E-03	4.68E-03	9.30E-04

- 360 seconds

Table AI-6: Amount of material removed from H-146 coated GFRP target as a function of angle of attack at an erosion duration of 360 seconds

Angle of impingement	EXP 1 (g)	EXP 2 (g)	EXP 3 (g)	Average (g)	Standard deviation
30˚	8.78E-03	9.38E-03	9.08E-03	9.08E-03	3.00E-04
45˚	1.04E-02	1.09E-02	1.05E-02	1.06E-02	2.27E-04
60˚	8.06E-03	9.58E-03	8.76E-03	8.80E-03	7.61E-04
75˚	6.86E-03	6.20E-03	8.04E-03	7.03E-03	9.32E-04
90˚	6.62E-03	7.28E-03	6.90E-03	6.93E-03	3.31E-04

- IA-700:
  - 180 seconds

Table AI-7: Amount of material removed from IA-700 coated GFRP target as a function of angle of attack at an erosion duration of 180 seconds

Angle of impingement	EXP 1 (g)	EXP 2 (g)	EXP 3 (g)	Average (g)	Standard deviation
30˚	6.26E-03	6.90E-03	6.22E-03	6.46E-03	3.82E-04
45˚	6.84E-03	7.04E-03	8.40E-03	7.43E-03	8.49E-04
60˚	6.04E-03	6.18E-03	6.20E-03	6.14E-03	8.72E-05
75˚	6.33E-03	5.84E-03	5.38E-03	5.85E-03	4.74E-04
90˚	3.54E-03	4.34E-03	5.04E-03	3.94E-03	7.51E-04

  - 360 seconds

Table AI-8: Amount of material removed from IA-700 coated GFRP target as a function of angle of attack at an erosion duration of 360 seconds

Angle of impingement	EXP 1 (g)	EXP 2 (g)	EXP 3 (g)	Average (g)	Standard deviation
30˚	9.90E-03	1.01E-02	9.02E-03	9.68E-03	5.82E-04
45˚	1.24E-02	1.40E-02	1.06E-02	1.23E-02	1.72E-03
60˚	8.34E-03	1.10E-02	1.18E-02	1.04E-02	1.80E-03
75˚	9.34E-03	7.66E-03	9.52E-03	8.84E-03	1.03E-03
90˚	7.68E-03	7.30E-03	7.90E-03	7.63E-03	3.04E-04

- Polyurethane:
  - 180 seconds

Table AI-9: Amount of material removed from Polyurethane coated GFRP target as a function of angle of attack at an erosion duration of 180 seconds

Angle of impingement	EXP 1 (g)	EXP 2 (g)	EXP 3 (g)	Average (g)	Standard deviation
30˚	5.22E-03	4.18E-03	4.72E-03	4.71E-03	5.20E-04
45˚	6.08E-03	5.92E-03	5.94E-03	5.98E-03	8.72E-05
60˚	5.74E-03	5.50E-03	4.74E-03	5.33E-03	5.22E-04
75˚	4.66E-03	4.12E-03	4.06E-03	4.28E-03	3.30E-04
90˚	4.58E-03	4.18E-03	4.56E-03	4.44E-03	2.25E-04

  - 360 seconds

Table AI-10: Amount of material removed from Polyurethane coated GFRP target as a function of angle of attack at an erosion duration of 360 seconds

Angle of impingement	EXP 1 (g)	EXP 2 (g)	EXP 3 (g)	Average (g)	Standard deviation
30˚	9.62E-03	1.08E-02	1.11E-02	1.05E-02	7.86E-04
45˚	1.17E-02	1.12E-02	1.09E-02	1.12E-02	4.01E-04
60˚	8.84E-03	1.03E-02	1.05E-02	9.86E-03	8.88E-04
75˚	9.94E-03	1.08E-02	1.15E-02	1.08E-02	8.01E-04
90˚	1.01E-02	9.76E-03	1.02E-02	1.00E-02	2.42E-04

- Coating 4 (H-146/Polyurethane):
  - 180 seconds

Table AI-11: Amount of material removed from H-146/Polyurethane (Coating 4) coated GFRP target as a function of angle of attack at an erosion duration of 180 seconds

Angle of impingement	EXP 1 (g)	EXP 2 (g)	EXP 3 (g)	Average (g)	Standard deviation
30˚	5.36E-03	4.06E-03	4.76E-03	4.73E-03	6.51E-04
45˚	6.06E-03	6.22E-03	5.90E-03	6.06E-03	1.60E-04
60˚	6.30E-03	4.86E-03	5.72E-03	5.63E-03	7.25E-04
75˚	4.70E-03	4.64E-03	4.54E-03	4.63E-03	8.08E-05
90˚	5.24E-03	4.14E-03	3.02E-03	4.13E-03	1.11E-03

- 360 seconds

Table AI-12: Amount of material removed from H-146/Polyurethane (Coating 4) coated GFRP target as a function of angle of attack at an erosion duration of 360 seconds

Angle of impingement	EXP 1 (g)	EXP 2 (g)	EXP 3 (g)	Average (g)	Standard deviation
30˚	9.30E-03	1.14E-02	1.09E-02	1.05E-02	1.11E-03
45˚	1.31E-02	1.12E-02	1.39E-02	1.27E-02	1.40E-03
60˚	8.10E-03	9.52E-03	1.03E-02	9.32E-03	1.13E-03
75˚	9.50E-03	9.84E-03	1.16E-02	1.03E-02	1.10E-03
90˚	9.10E-03	9.44E-03	1.02E-02	9.57E-03	5.52E-04

- Coating 5 (IA-700/Polyurethane):
  - 180 seconds

Table AI-13: Amount of material removed from IA-700/Polyurethane (Coating 5) coated GFRP target as a function of angle of attack at an erosion duration of 180 seconds

Angle of impingement	EXP 1 (g)	EXP 2 (g)	EXP 3 (g)	Average (g)	Standard deviation
30˚	6.52E-03	3.72E-03	4.10E-03	4.78E-03	1.52E-03
45˚	6.44E-03	6.28E-03	6.32E-03	6.35E-03	8.33E-05
60˚	5.18E-03	5.42E-03	5.50E-03	5.37E-03	1.67E-04
75˚	5.36E-03	4.64E-03	4.60E-03	4.87E-03	4.28E-04
90˚	4.12E-03	4.62E-03	4.60E-03	4.45E-03	2.83E-04

  - 360 seconds

Table AI-14: Amount of material removed from IA-700/Polyurethane (Coating 5) coated GFRP target as a function of angle of attack at an erosion duration of 360 seconds

Angle of impingement	EXP 1 (g)	EXP 2 (g)	EXP 3 (g)	Average (g)	Standard deviation
30˚	1.07E-02	1.18E-02	1.24E-02	1.16E-02	8.48E-04
45˚	1.11E-02	1.25E-02	1.21E-02	1.19E-02	7.02E-04
60˚	9.40E-03	1.03E-02	1.11E-02	1.03E-02	8.52E-04
75˚	9.22E-03	1.10E-02	9.74E-03	9.99E-03	9.15E-04
90˚	7.98E-03	9.60E-03	8.12E-03	8.57E-03	8.98E-04

- Coating 6 (Polyurethane/Polyurethane):
  - 180 seconds

Table AI-15: Amount of material removed from Polyurethane/Polyurethane (Coating 6) coated GFRP target as a function of angle of attack at an erosion duration of 180 seconds

Angle of impingement	EXP 1 (g)	EXP 2 (g)	EXP 3 (g)	Average (g)	Standard deviation
30˚	4.42E-03	4.08E-03	4.34E-03	4.28E-03	1.78E-04
45˚	3.90E-03	3.70E-03	3.90E-03	3.83E-03	1.15E-04
60˚	1.46E-03	2.50E-03	2.26E-03	2.07E-03	5.45E-04
75˚	3.38E-03	3.60E-03	3.62E-03	3.53E-03	1.33E-04
90˚	3.92E-03	2.68E-03	3.70E-03	3.43E-03	6.62E-04

  - 360 seconds

Table AI-16: Amount of material removed from Polyurethane/Polyurethane (Coating 6) coated GFRP target as a function of angle of attack at an erosion duration of 360 seconds

Angle of impingement	EXP 1 (g)	EXP 2 (g)	EXP 3 (g)	Average (g)	Standard deviation
30˚	1.05E-02	9.30E-03	8.96E-03	9.58E-03	7.98E-04
45˚	1.07E-02	9.82E-03	1.00E-02	1.02E-02	4.50E-04
60˚	7.16E-03	6.70E-03	7.20E-03	7.02E-03	2.78E-04
75˚	8.58E-03	8.78E-03	7.36E-03	8.24E-03	7.69E-04
90˚	5.70E-03	7.98E-03	7.70E-03	7.13E-03	1.24E-03

- Coating 7 (Polyurethane/IA-700):
  - 180 seconds

Table AI-17: Amount of material removed from Polyurethane/IA-700 (Coating 7) coated GFRP target as a function of angle of attack at an erosion duration of 180 seconds

Angle of impingement	EXP 1 (g)	EXP 2 (g)	EXP 3 (g)	Average (g)	Standard deviation
30˚	4.18E-03	4.96E-03	4.00E-03	4.38E-03	5.10E-04
45˚	5.16E-03	4.98E-03	5.94E-03	5.36E-03	5.10E-04
60˚	3.00E-03	3.90E-03	3.72E-03	3.54E-03	4.76E-04
75˚	4.00E-03	3.36E-03	4.60E-03	3.99E-03	6.20E-04
90˚	2.32E-03	3.18E-03	1.96E-03	2.49E-03	6.27E-04

- 360 seconds

Table AI-18: Amount of material removed from Polyurethane/IA-700 (Coating 7) coated GFRP target as a function of angle of attack at an erosion duration of 180 seconds

Angle of impingement	EXP 1 (g)	EXP 2 (g)	EXP 3 (g)	Average (g)	Standard deviation
30˚	1.06E-02	1.10E-02	1.11E-02	1.09E-02	2.91E-04
45˚	1.08E-02	1.02E-02	1.23E-02	1.11E-02	1.08E-03
60˚	9.36E-03	1.07E-02	9.44E-03	9.85E-03	7.75E-04
75˚	1.07E-02	1.04E-02	9.78E-03	1.03E-02	4.91E-04
90˚	8.68E-03	6.22E-03	7.40E-03	7.43E-03	1.23E-03

Appendix II: Photomicrographs of Erosion Scars of Flat Specimens

In this appendix, photomicrographs of the shape of erosion scars on flat specimens such as aluminum, glass, and coated and uncoated GFRP specimens are shown. The erosion tests conditions are shown in Tables 5-3, 5-6, and 5-8 for aluminum erosion, glass erosion, and GFRP (coated and uncoated) erosion, respectively. Each erosion experiment was repeated three times to verify the repeatability therefore for each condition figures in this appendix are showing EXP1, EXP 2, and EXP 3 erosion scars.

- Aluminum microphotographs
    - 10 degrees

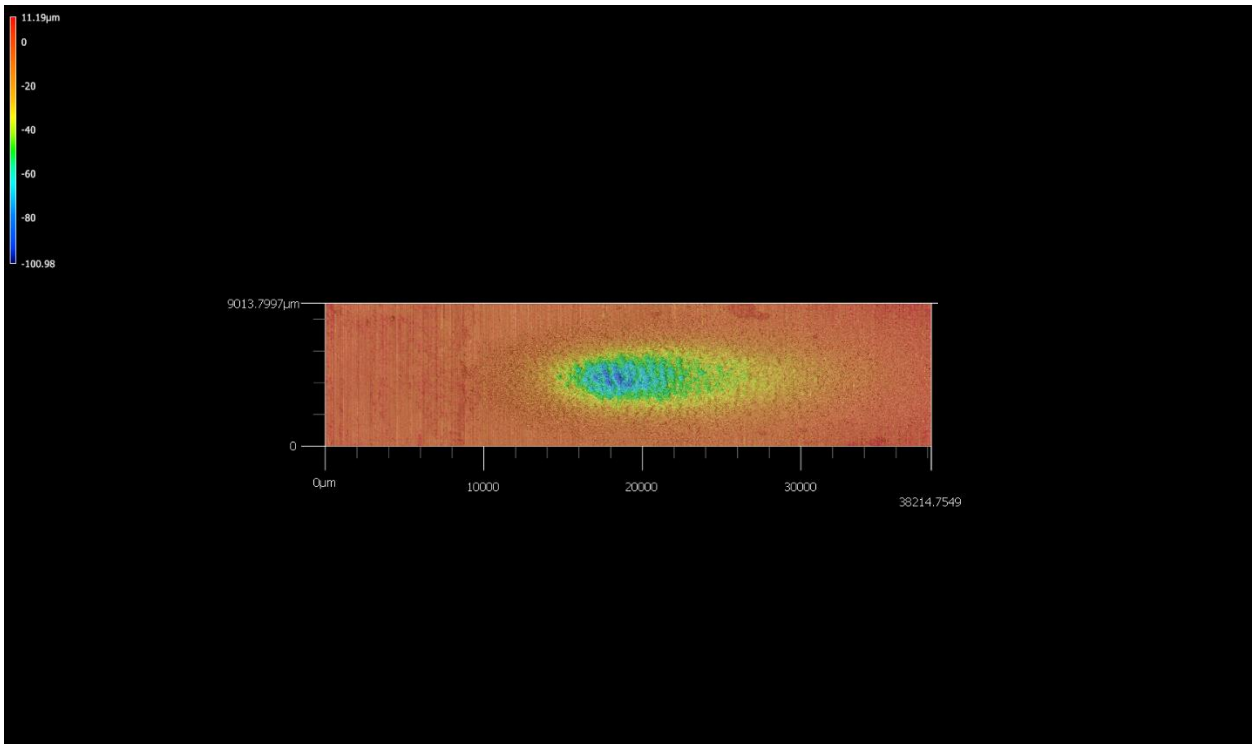


Fig. AII-1: Aluminum erosion scar EXP1 at 10° angle of attack

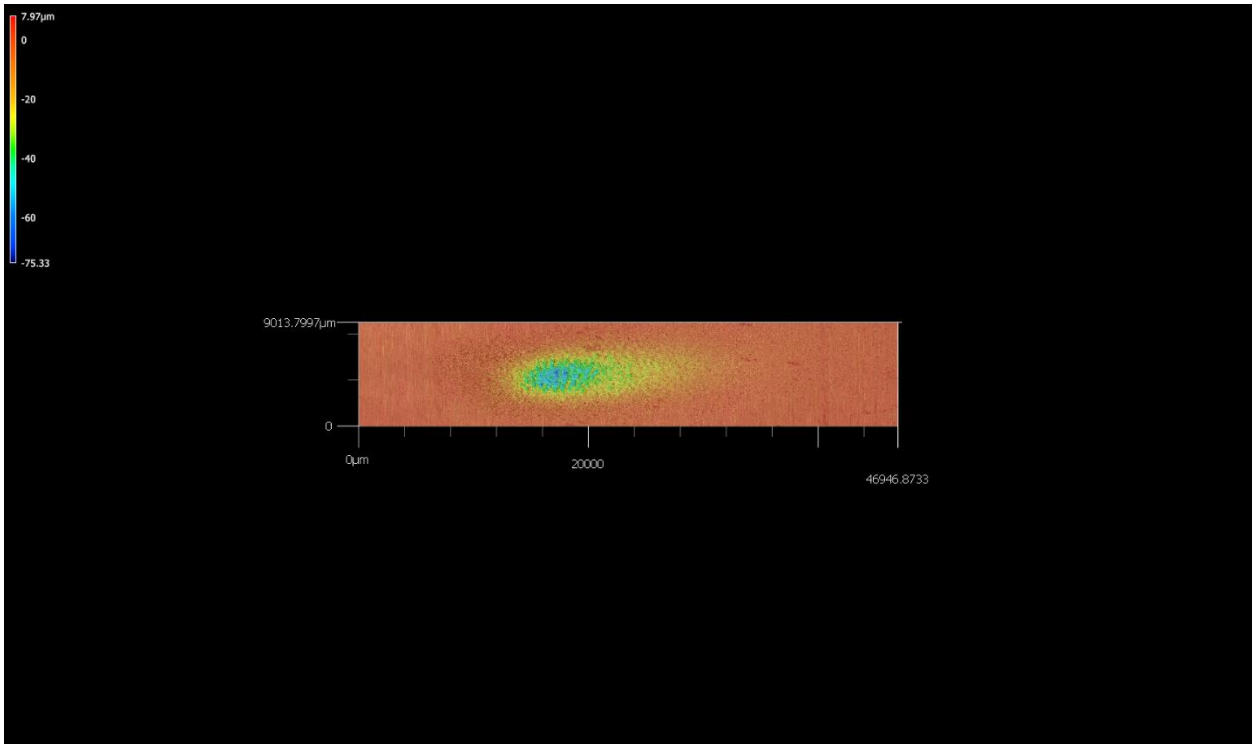


Fig. AII-2: Aluminum erosion scar EXP2 at 10° angle of attack

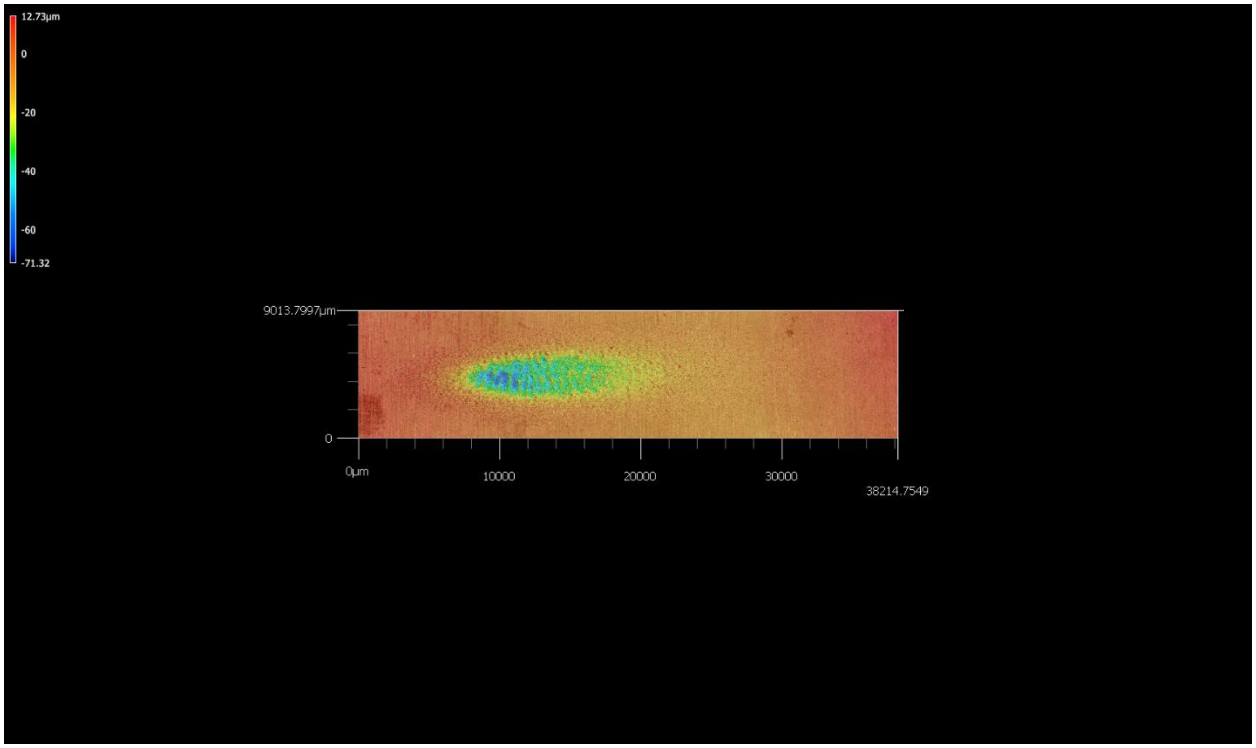


Fig. AII-3: Aluminum erosion scar EXP3 at 10° angle of attack

- 20 degrees

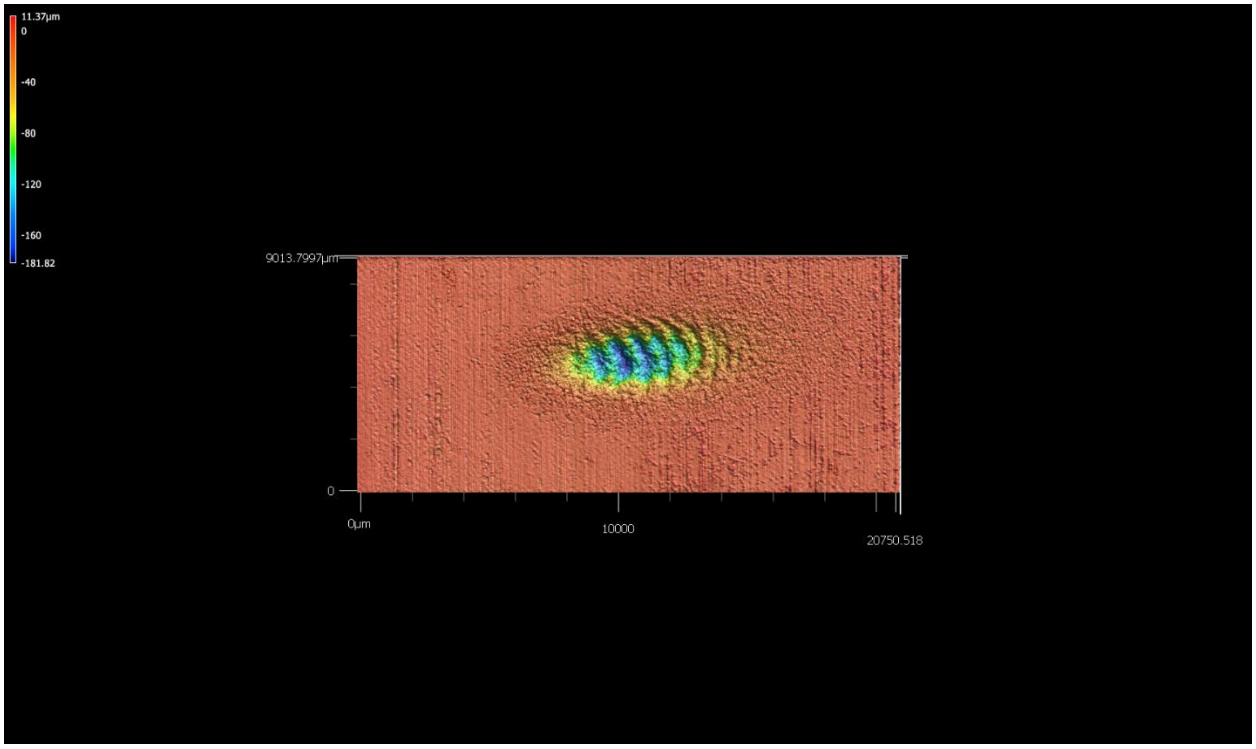


Fig. AII-4: Aluminum erosion scar EXP1 at 20° angle of attack

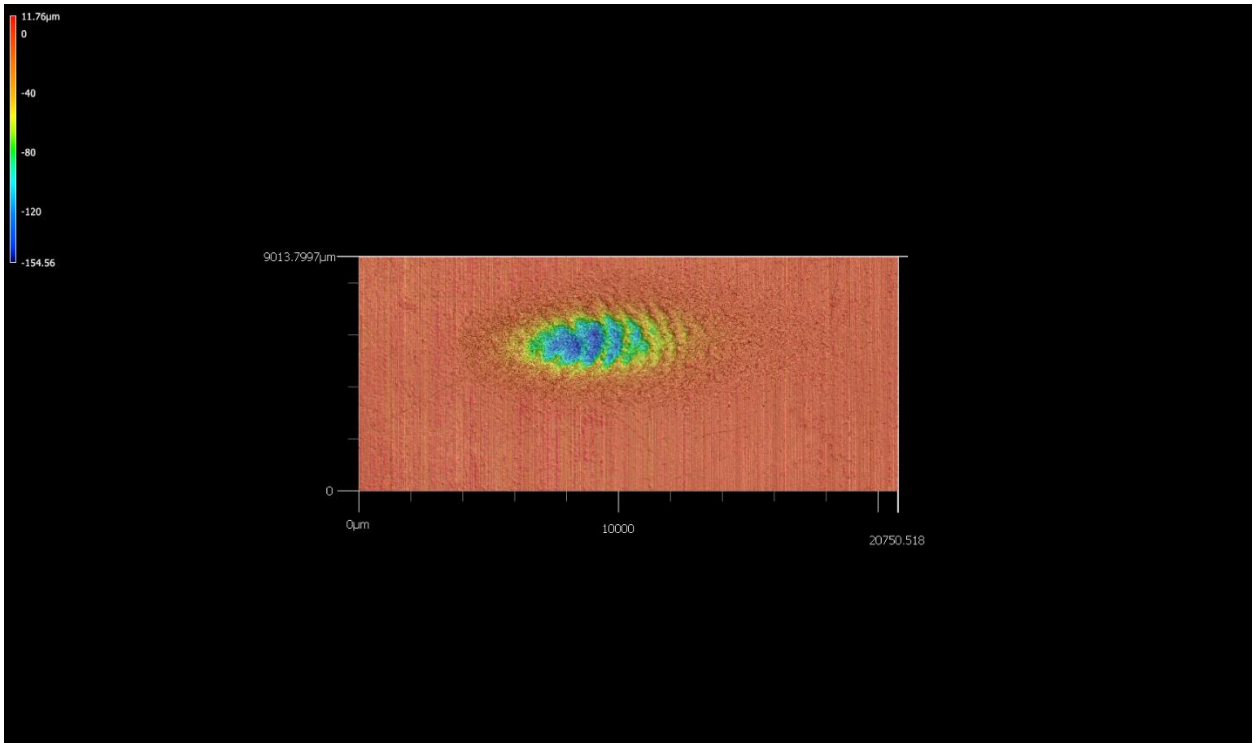


Fig. AII-5: Aluminum erosion scar EXP2 at 20° angle of attack

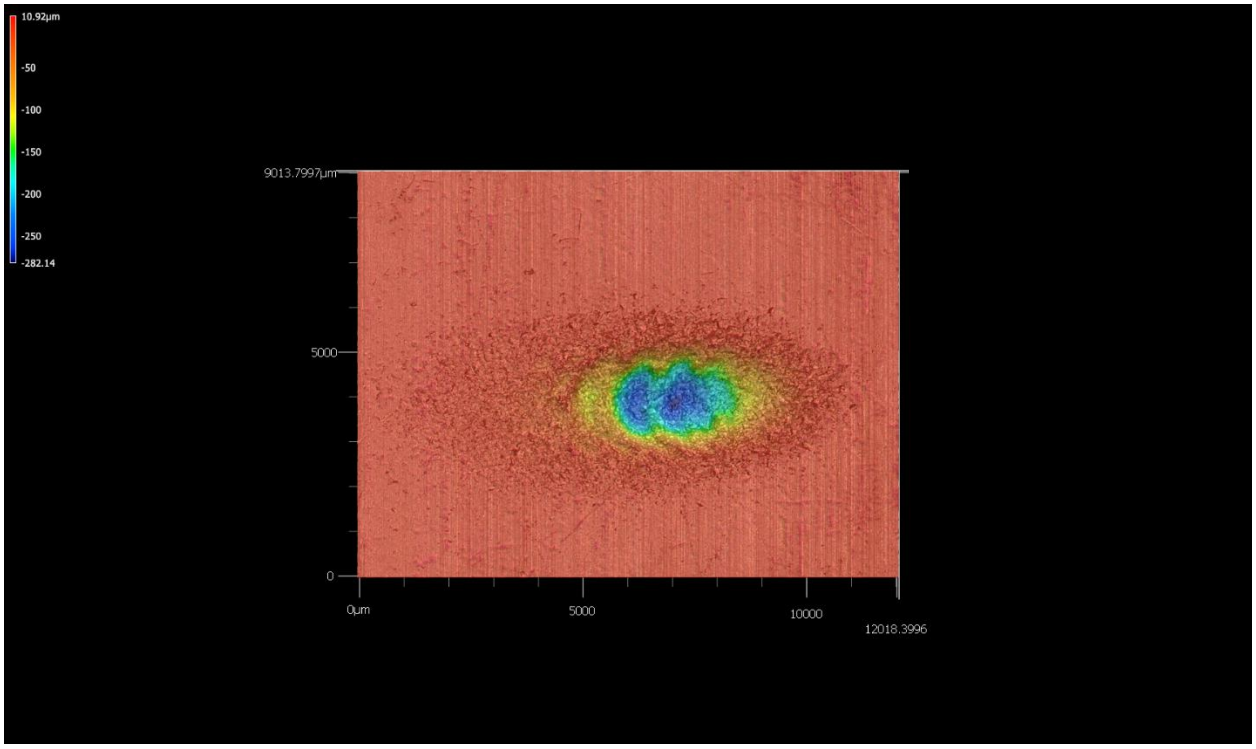


Fig. AII-6: Aluminum erosion scar EXP3 at 20° angle of attack

- 30 degrees

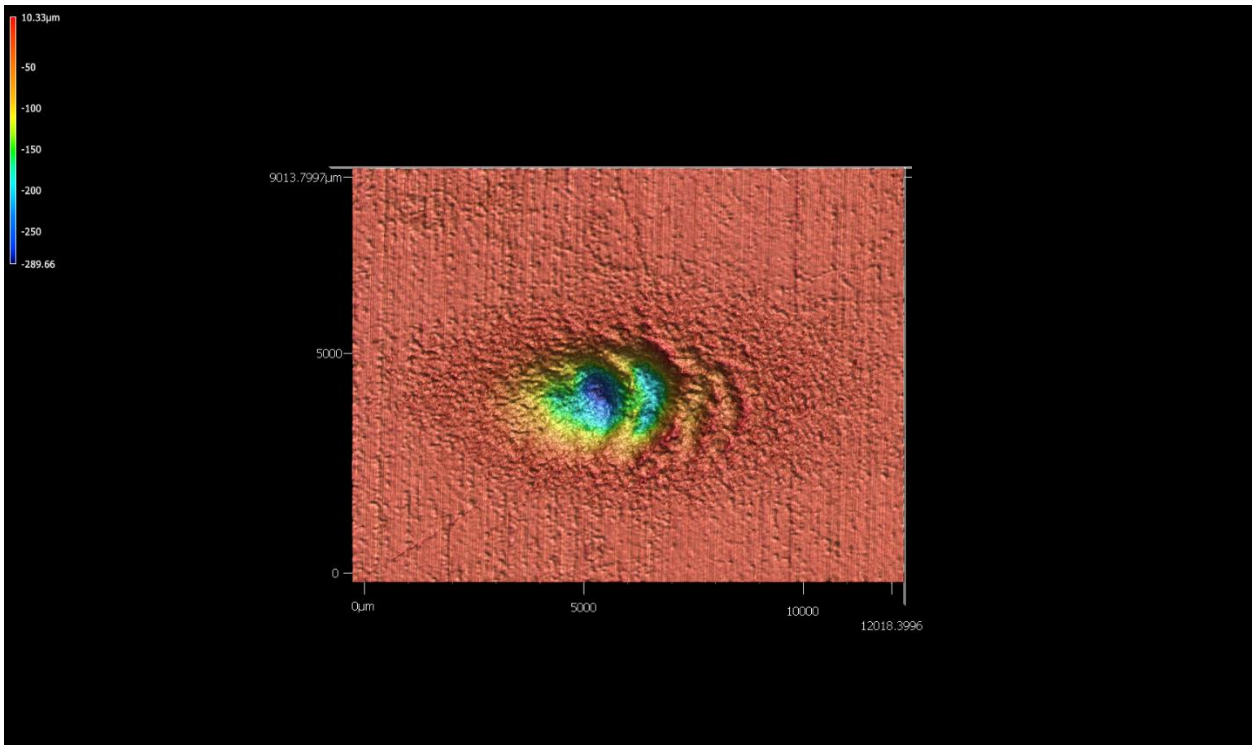


Fig. AII-7: Aluminum erosion scar EXP1 at 30° angle of attack

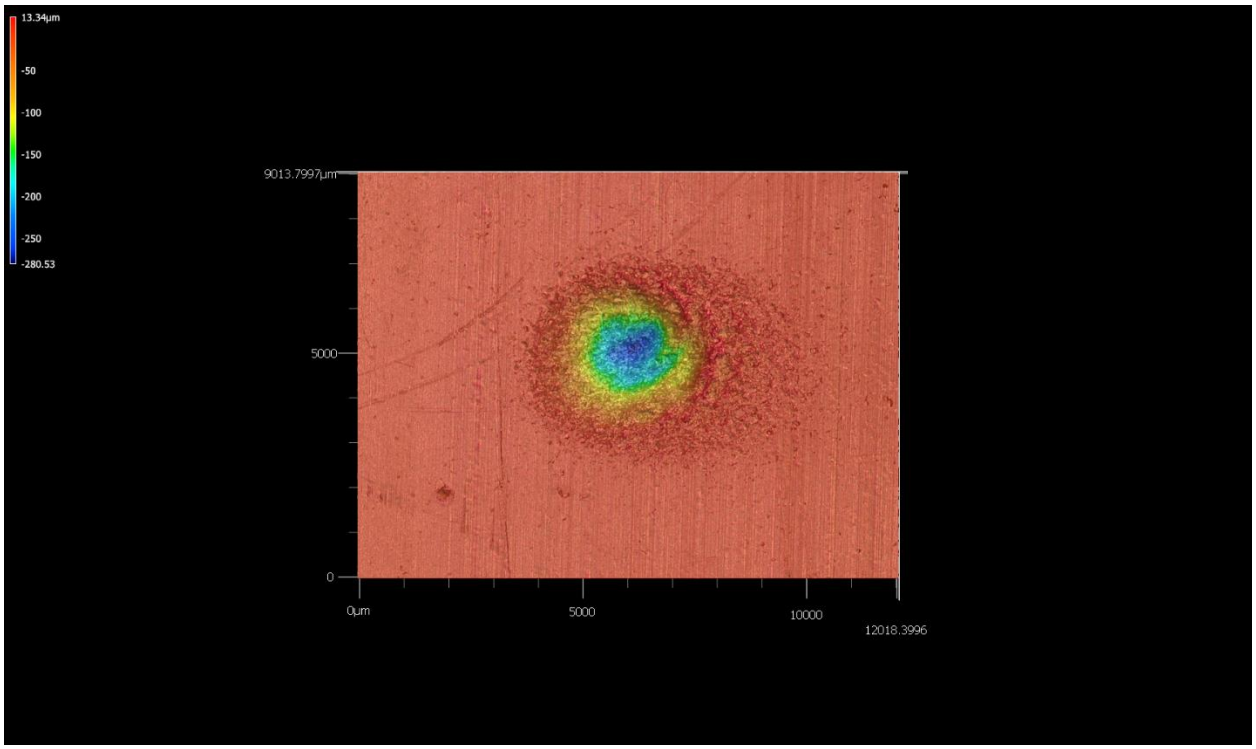


Fig. AII-8: Aluminum erosion scar EXP2 at 30° angle of attack

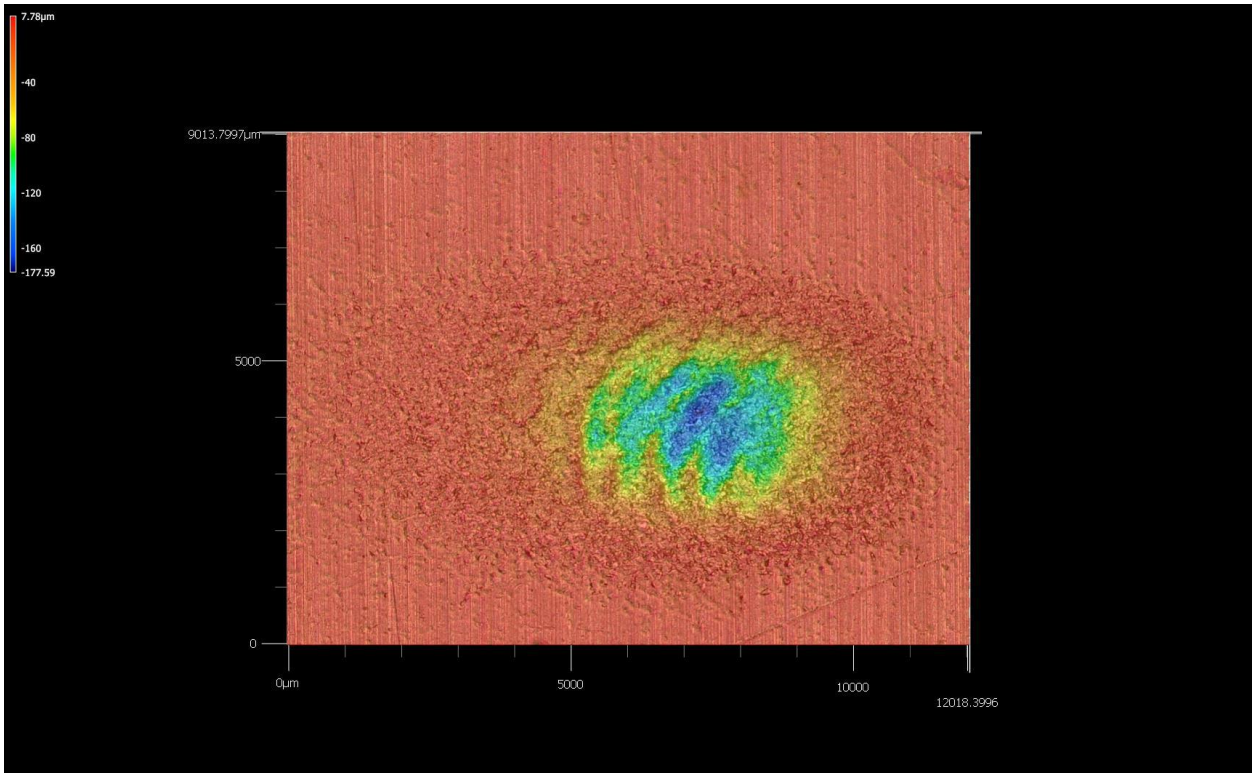


Fig. AII-9: Aluminum erosion scar EXP3 at 30° angle of attack

- 45 degrees

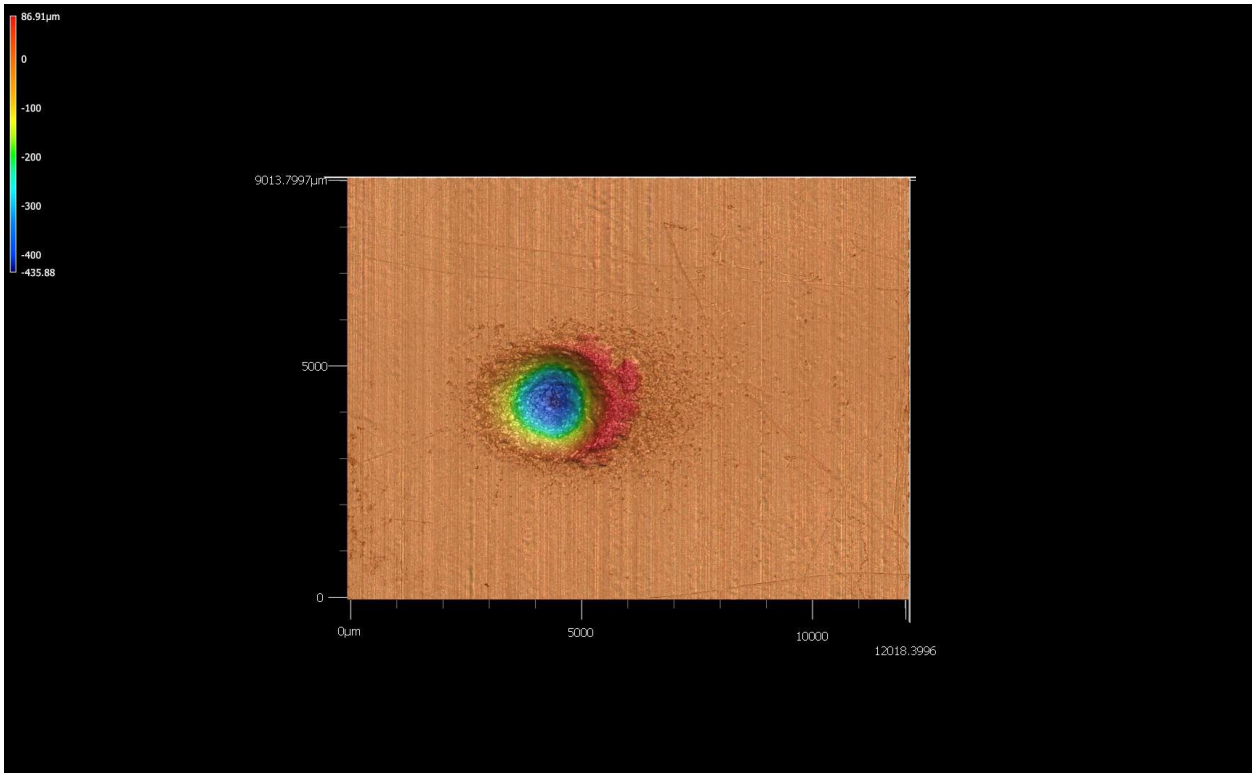


Fig. AII-10: Aluminum erosion scar EXP1 at 45° angle of attack

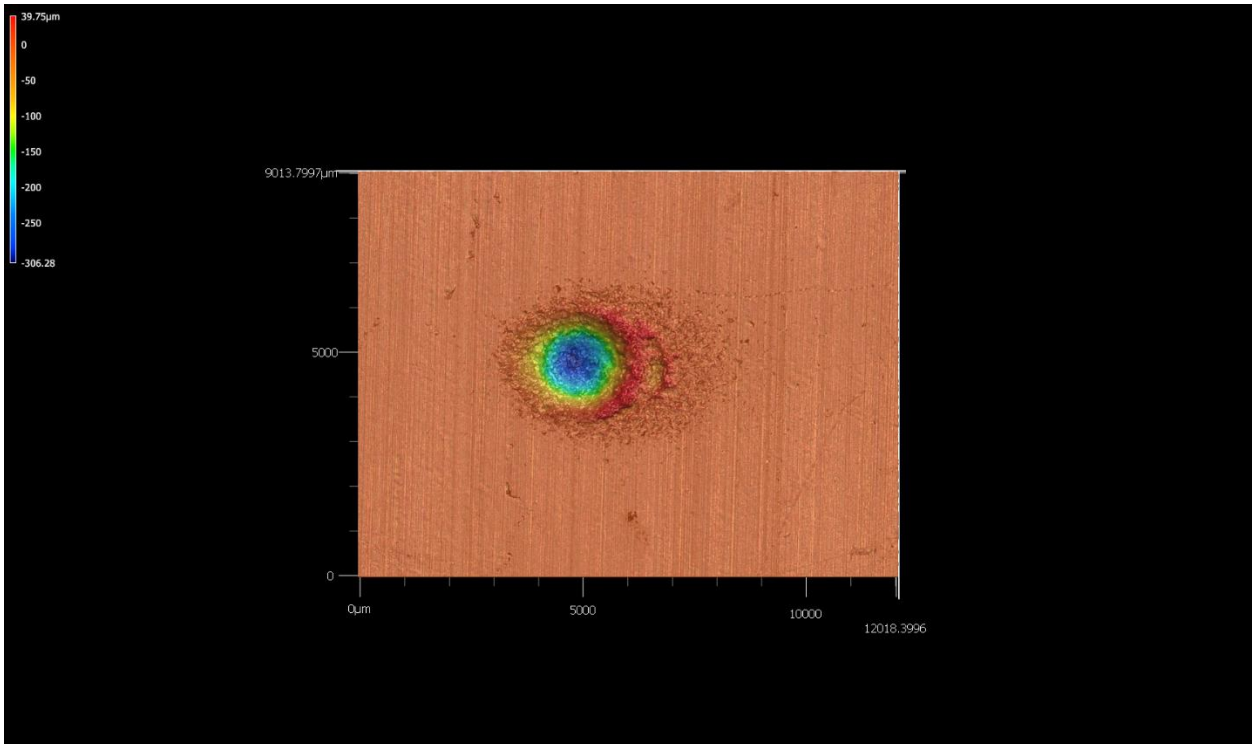


Fig. AII-11: Aluminum erosion scar EXP2 at 45° angle of attack

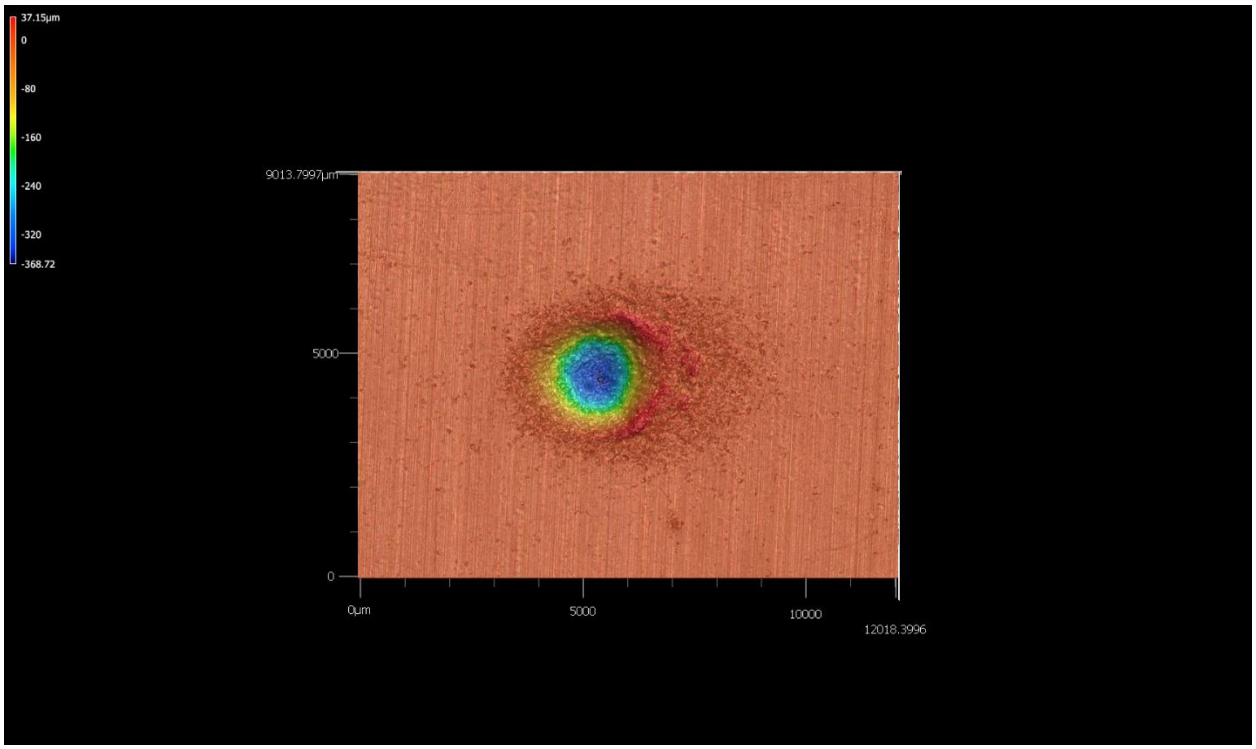


Fig. AII-12: Aluminum erosion scar EXP3 at 45° angle of attack

- 60 degrees

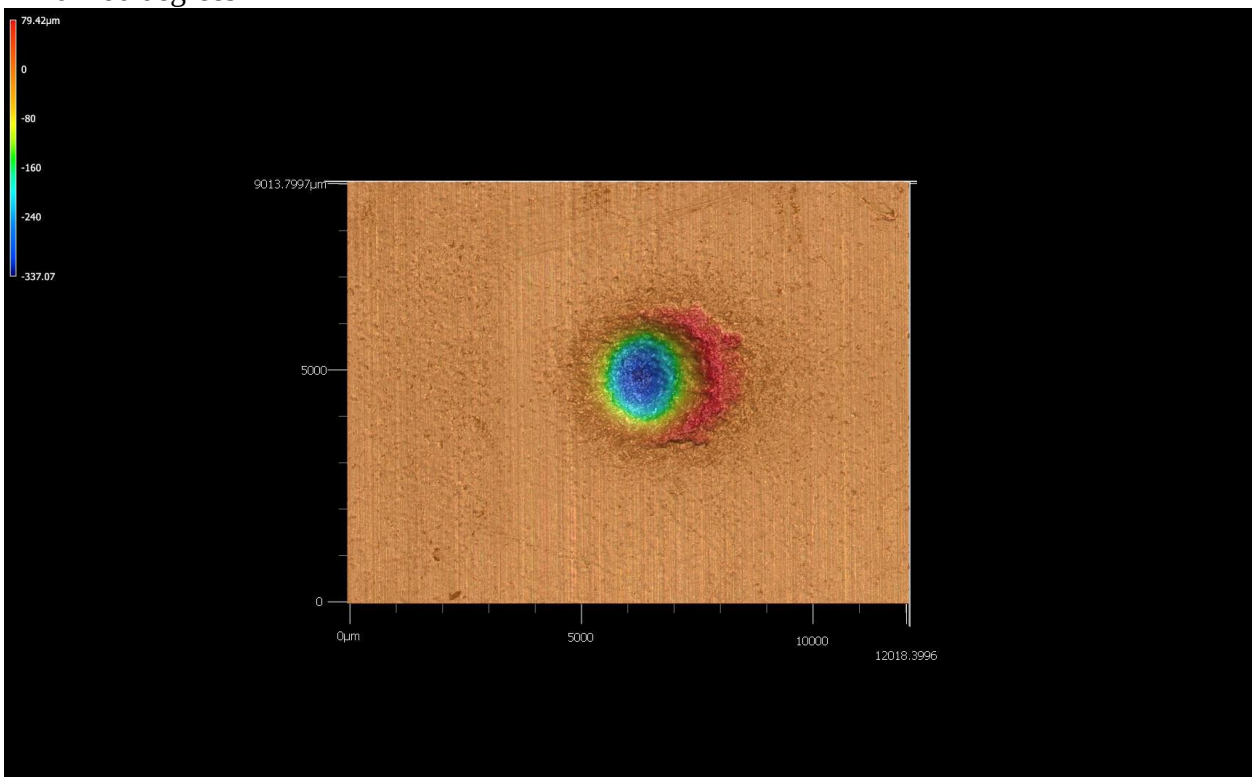


Fig. AII-13: Aluminum erosion scar EXP1 at 60° angle of attack

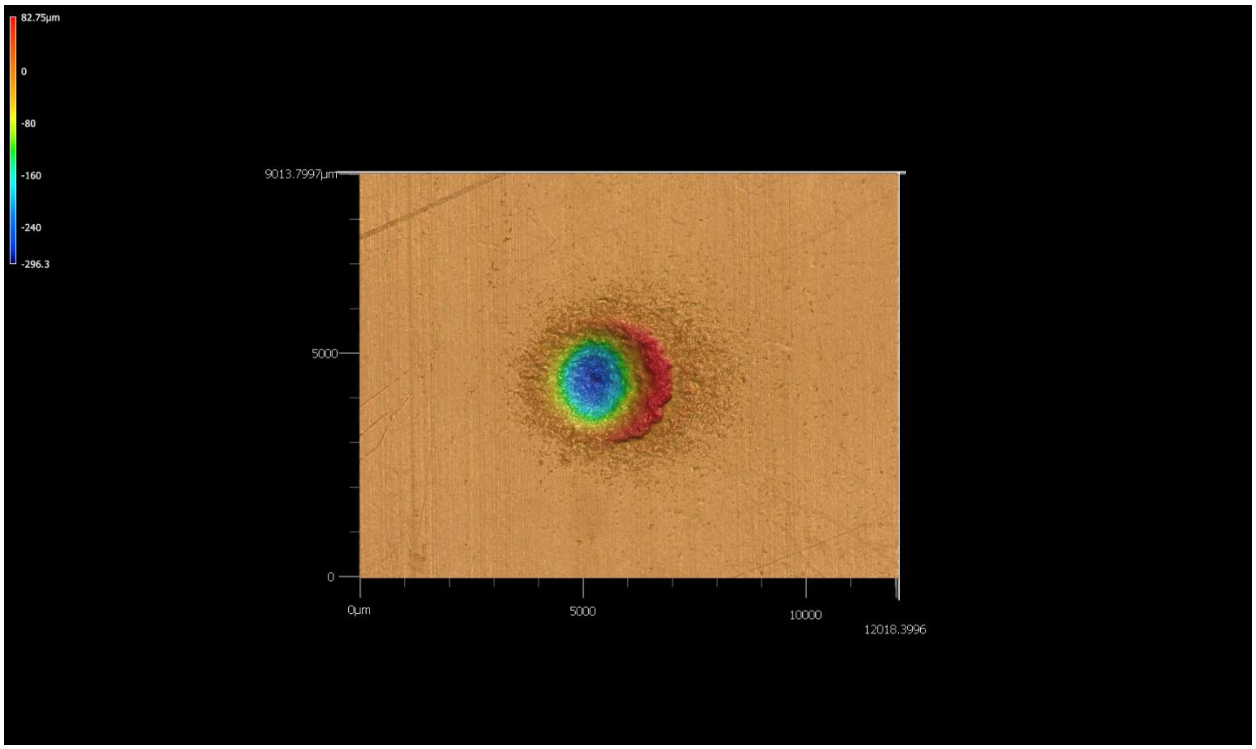


Fig. AII-14: Aluminum erosion scar EXP2 at 60° angle of attack

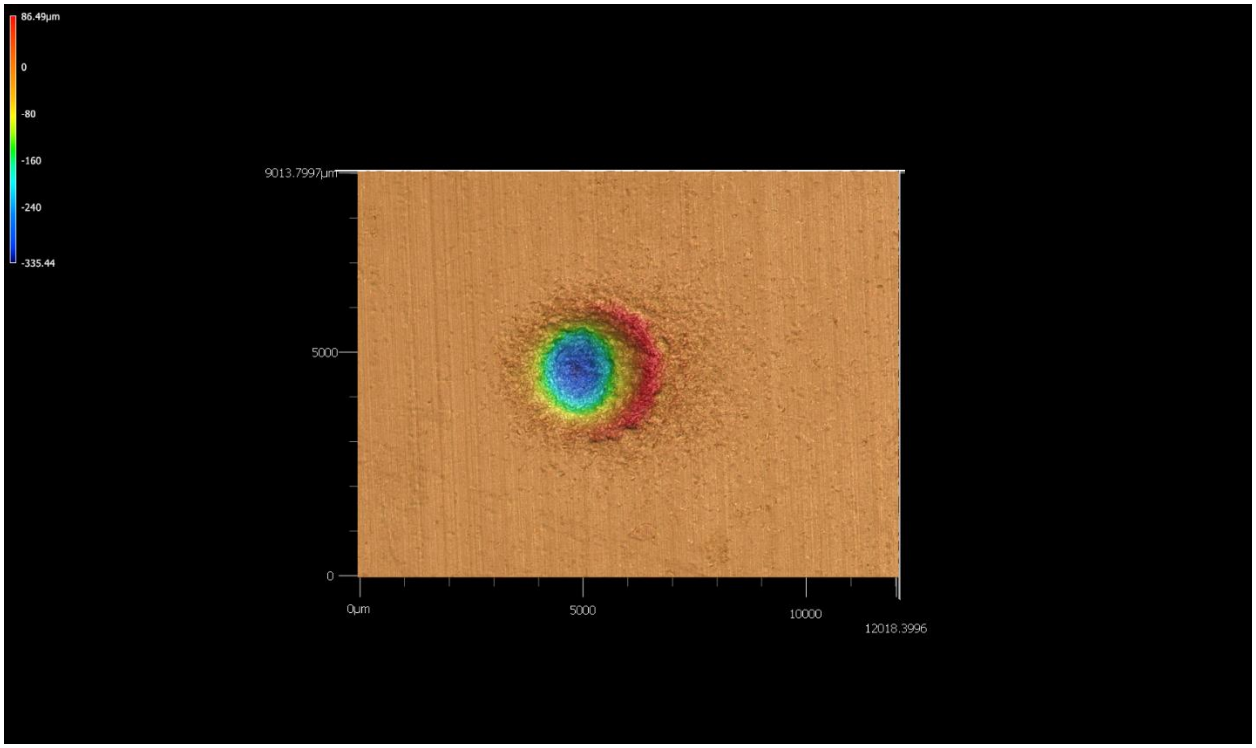


Fig. AII-15: Aluminum erosion scar EXP3 at 60° angle of attack

- 90 degrees

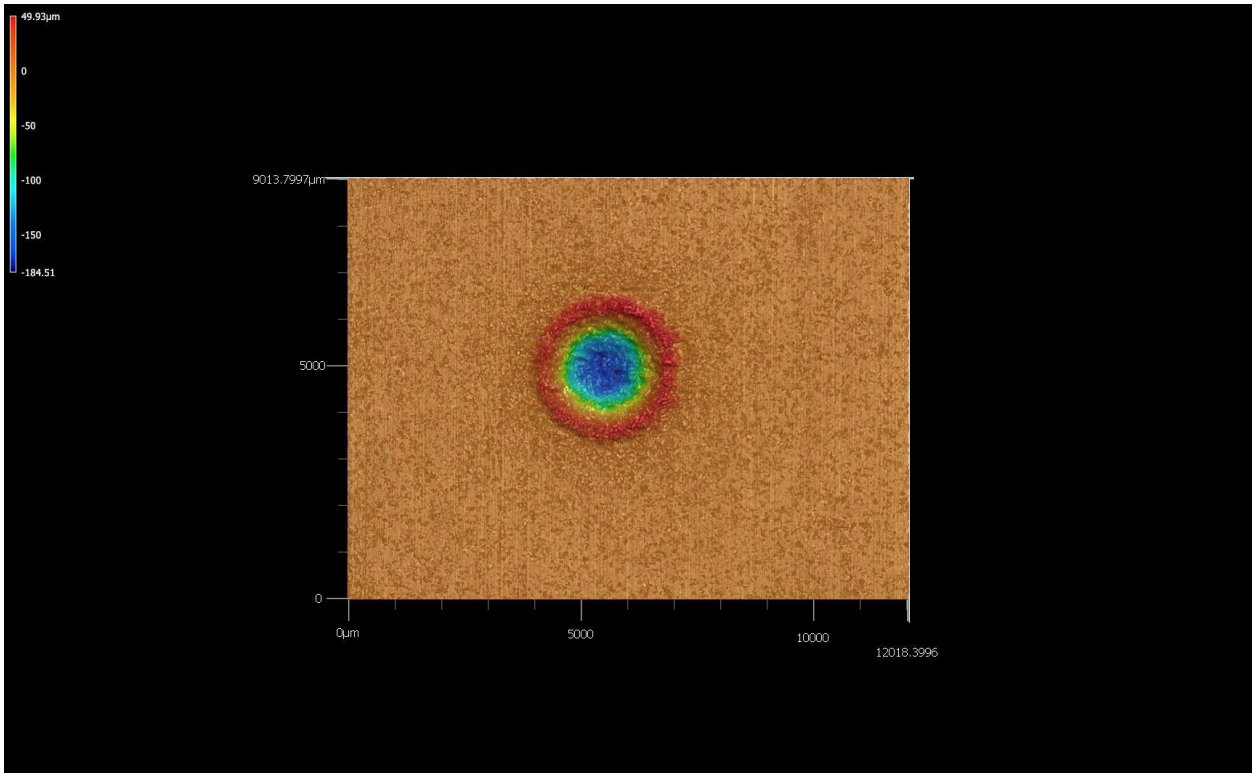


Fig. AII-16: Aluminum erosion scar EXP1 at 90° angle of attack

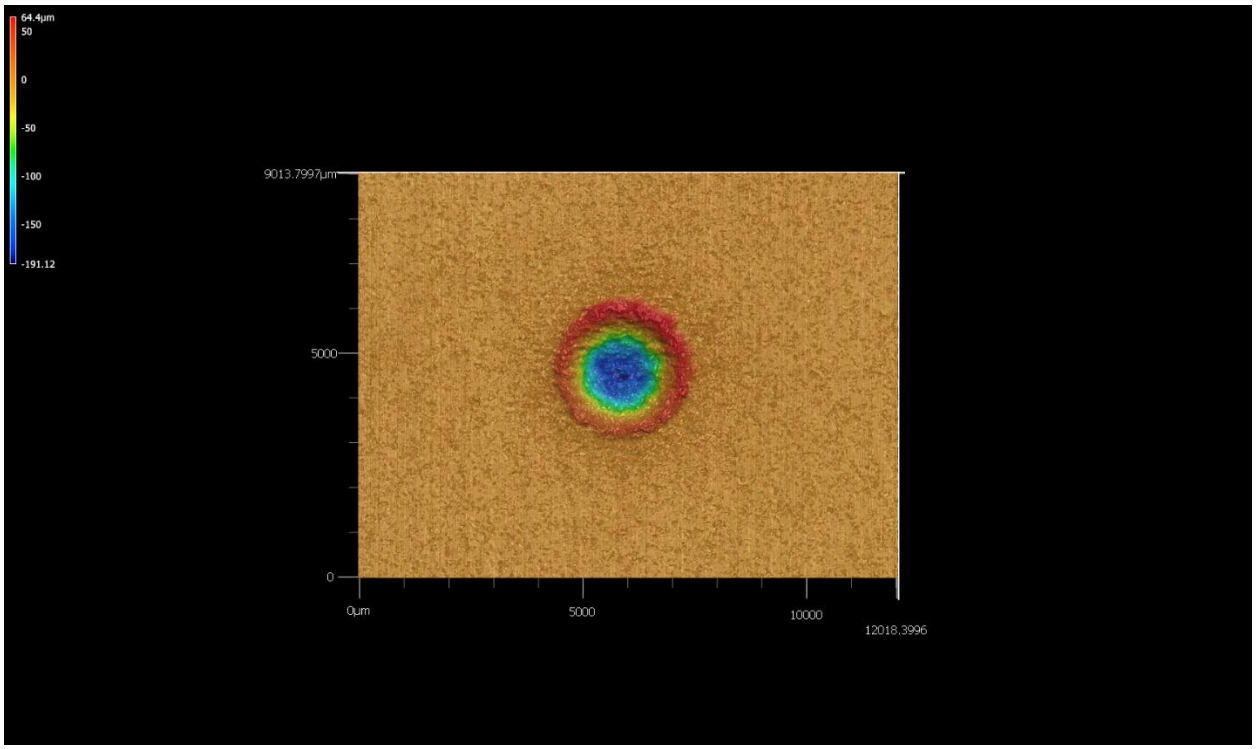


Fig. AII-17: Aluminum erosion scar EXP2 at 90° angle of attack

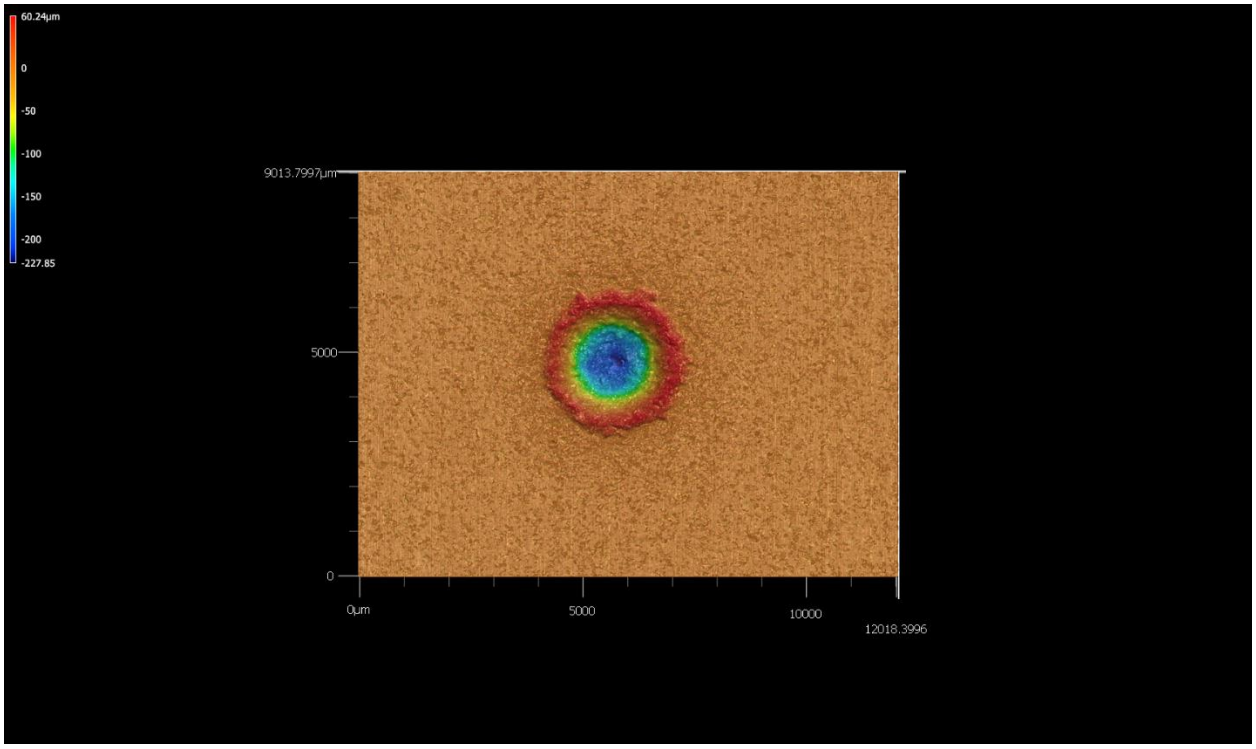


Fig. AII-18: Aluminum erosion scar EXP3 at 90° angle of attack

- Glass microphotographs
  - 30 degrees

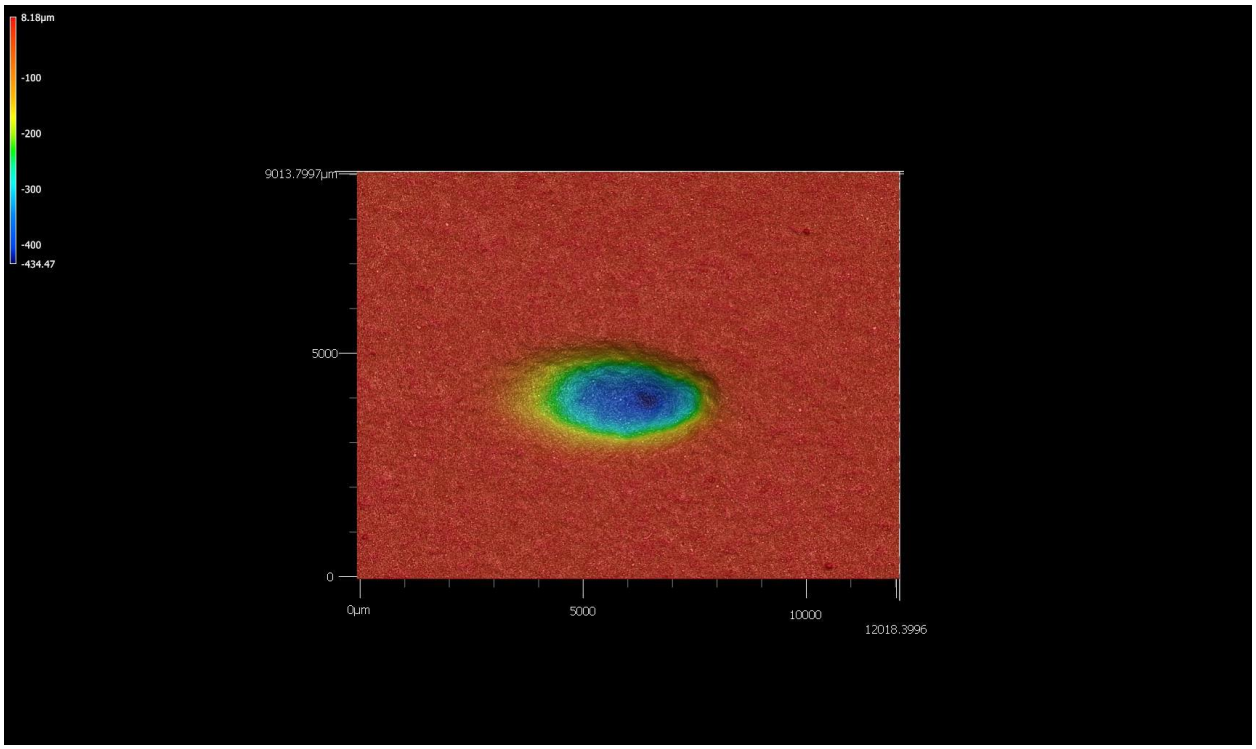


Fig. AII-19: Glass erosion scar EXP1 at 30° angle of attack

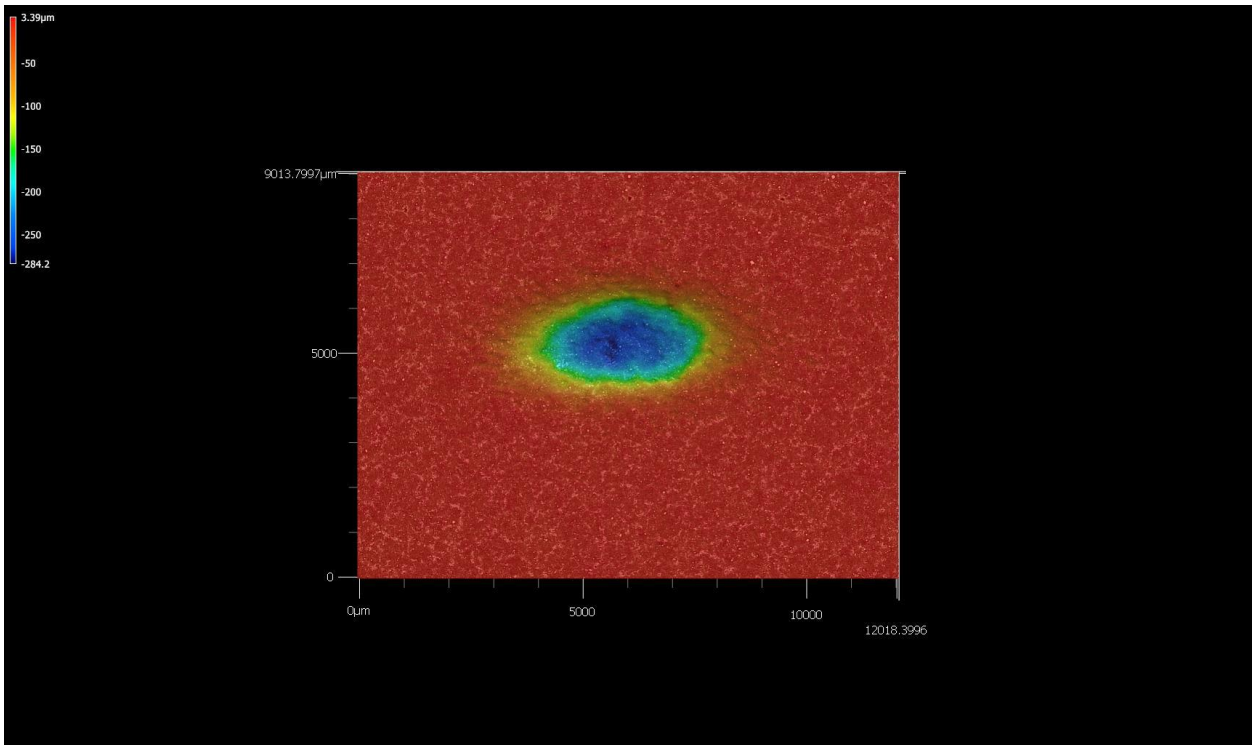


Fig. AII-20: Glass erosion scar EXP2 at 30° angle of attack

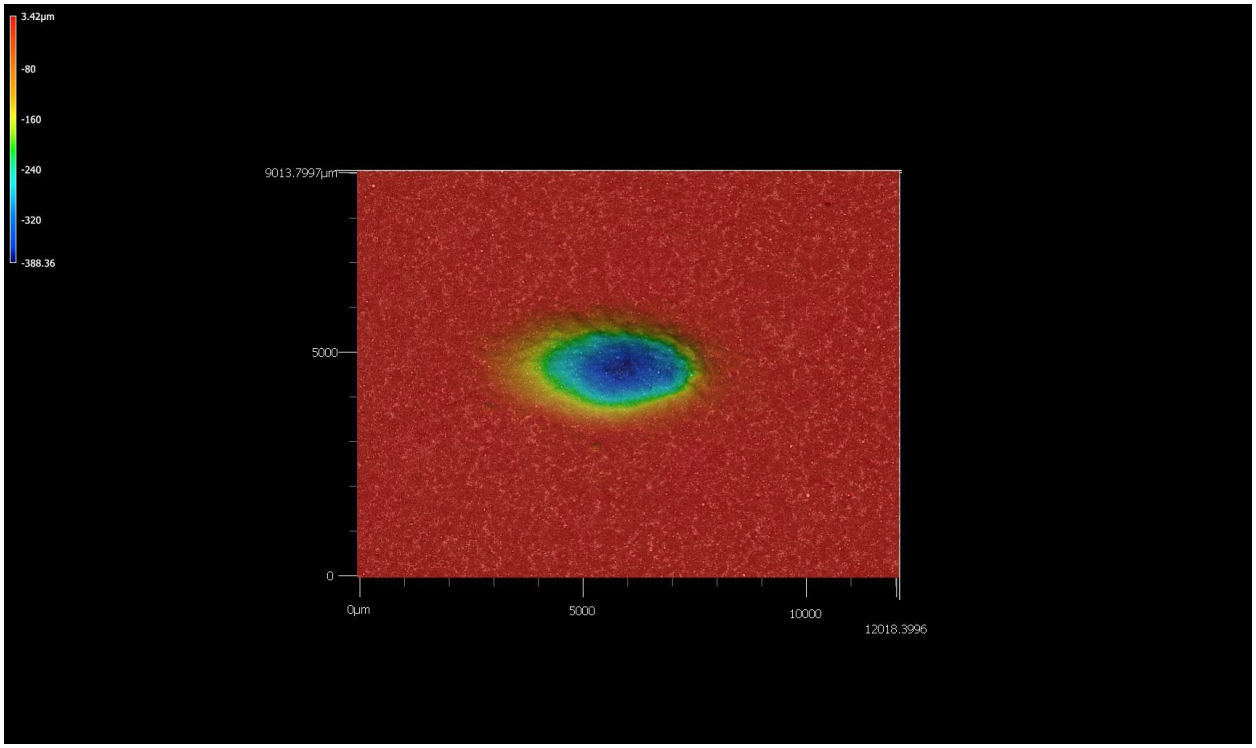


Fig. AII-21: Glass erosion scar EXP3 at 30° angle of attack

- 45 degrees

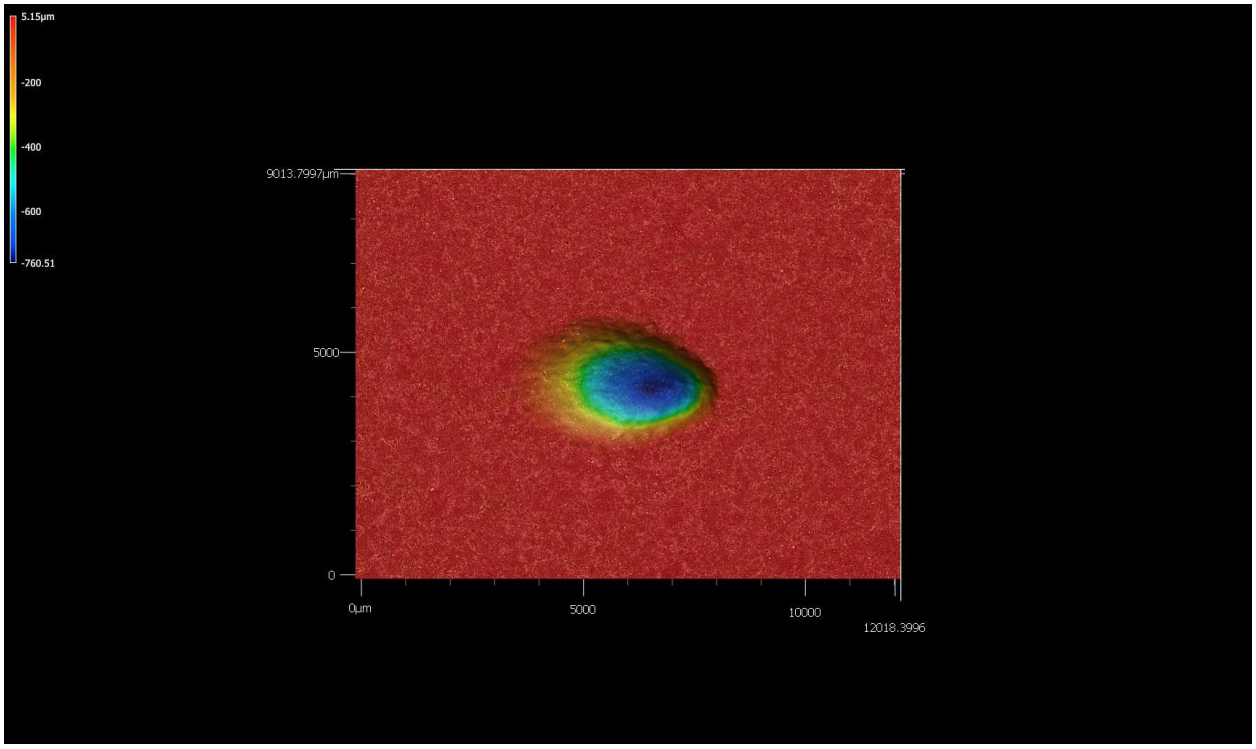


Fig. AII-22: Glass erosion scar EXP1 at 45° angle of attack

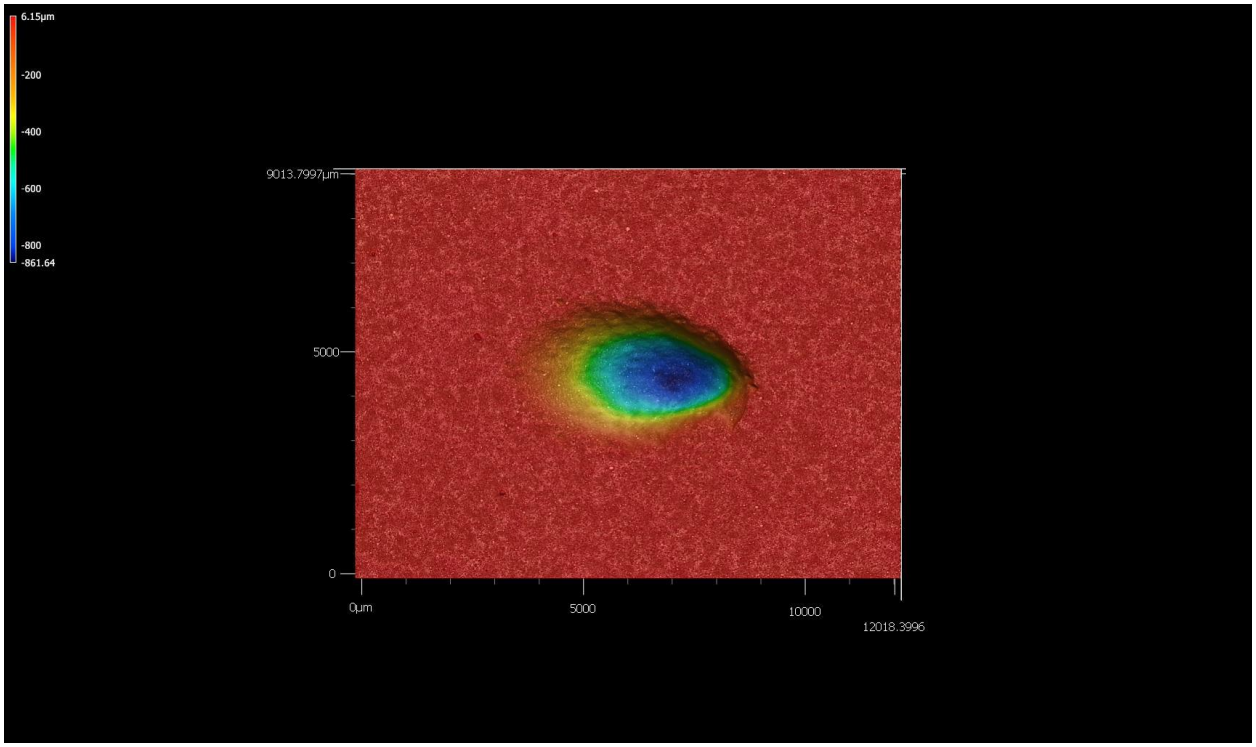


Fig. AII-23: Glass erosion scar EXP2 at 45° angle of attack

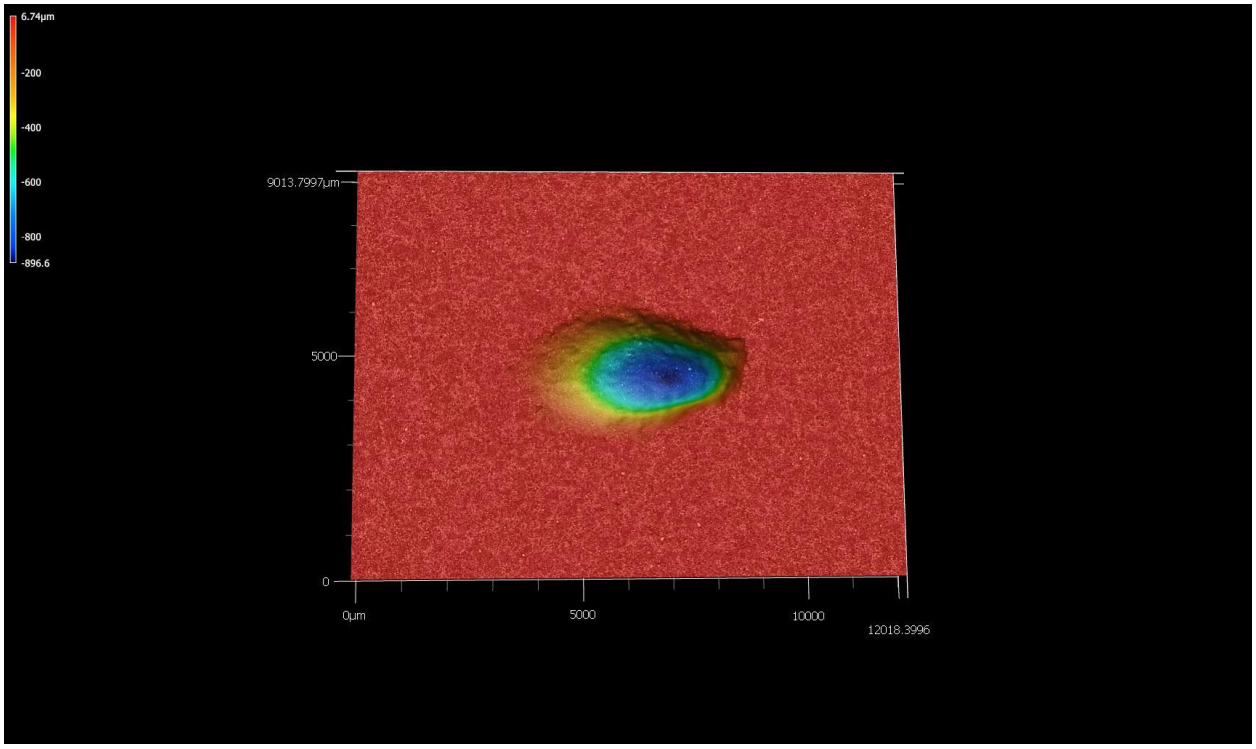


Fig. AII-24: Glass erosion scar EXP3 at 45° angle of attack

- 60 degrees

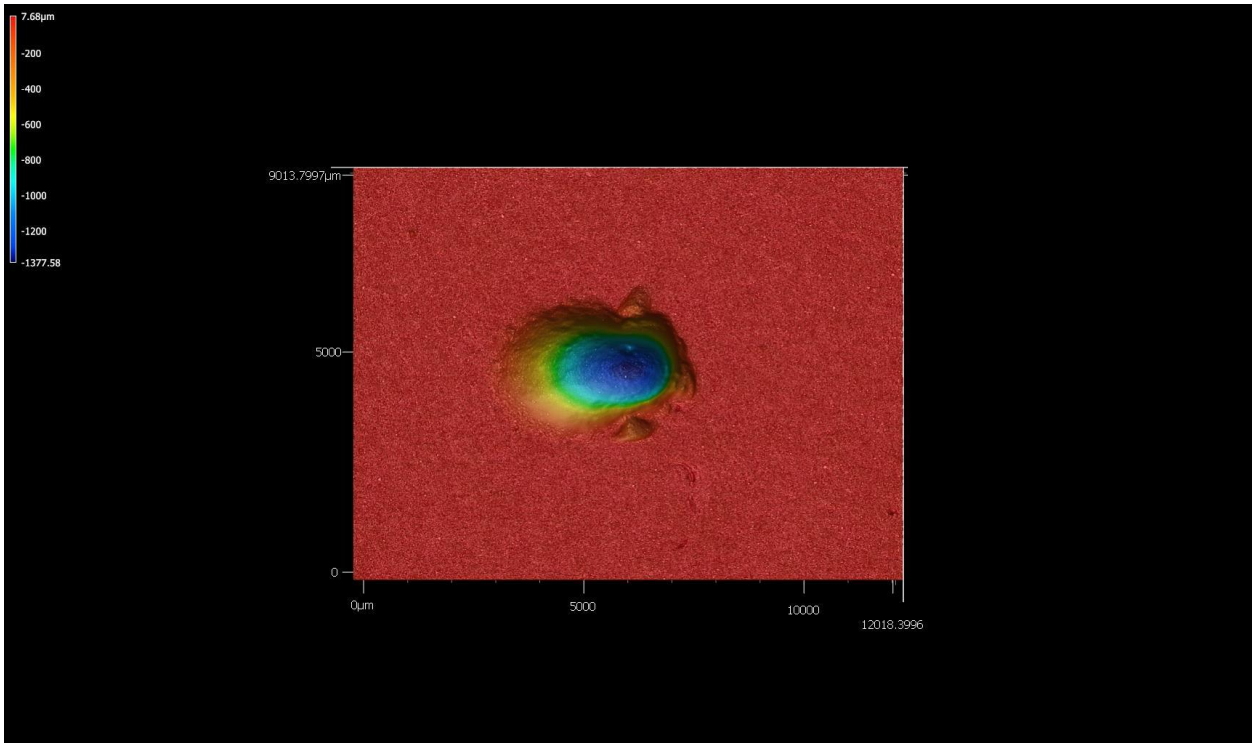


Fig. AII-25: Glass erosion scar EXP1 at 60° angle of attack

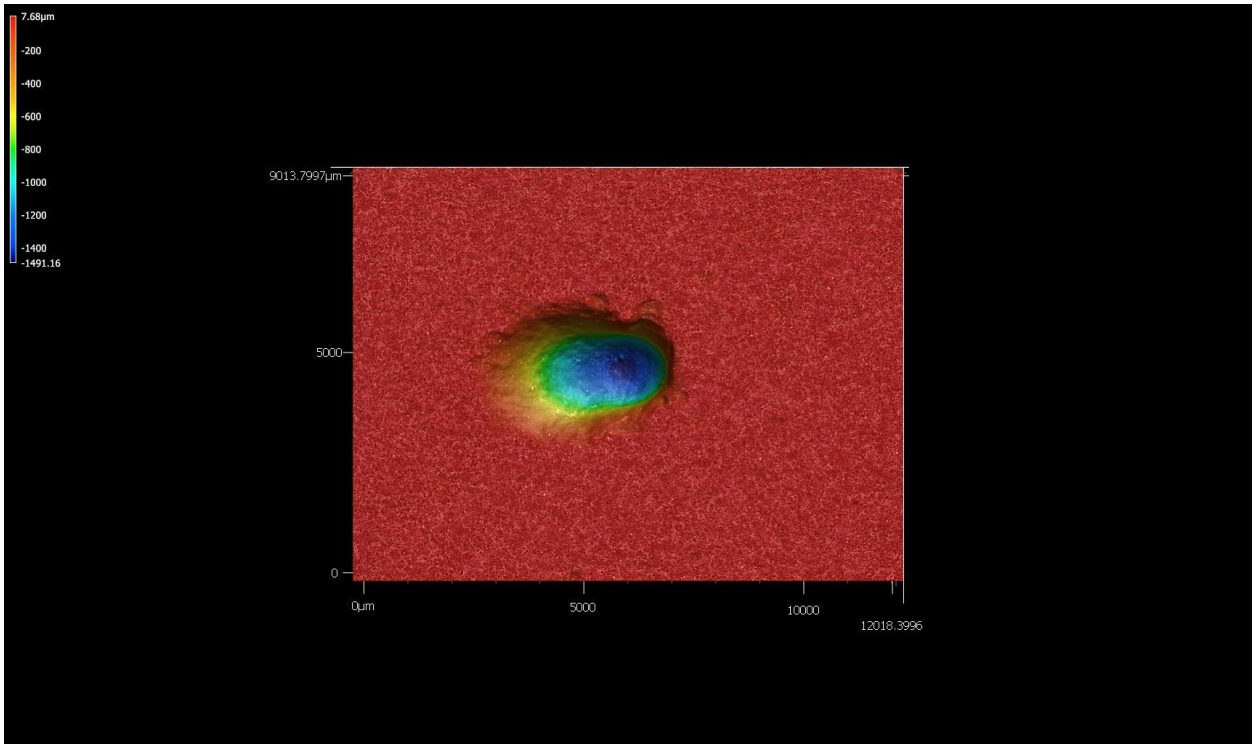


Fig. AII-26: Glass erosion scar EXP2 at 60° angle of attack

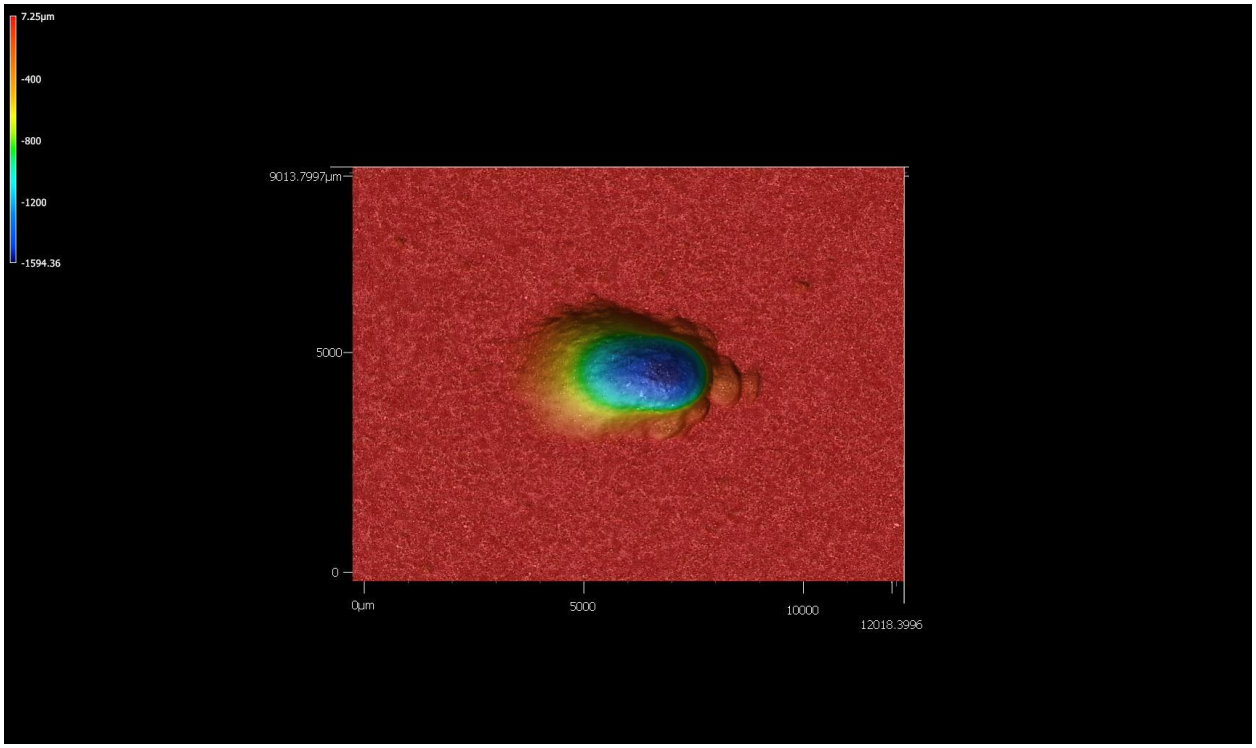


Fig. AII-27: Glass erosion scar EXP3 at 60° angle of attack

- 75 degrees

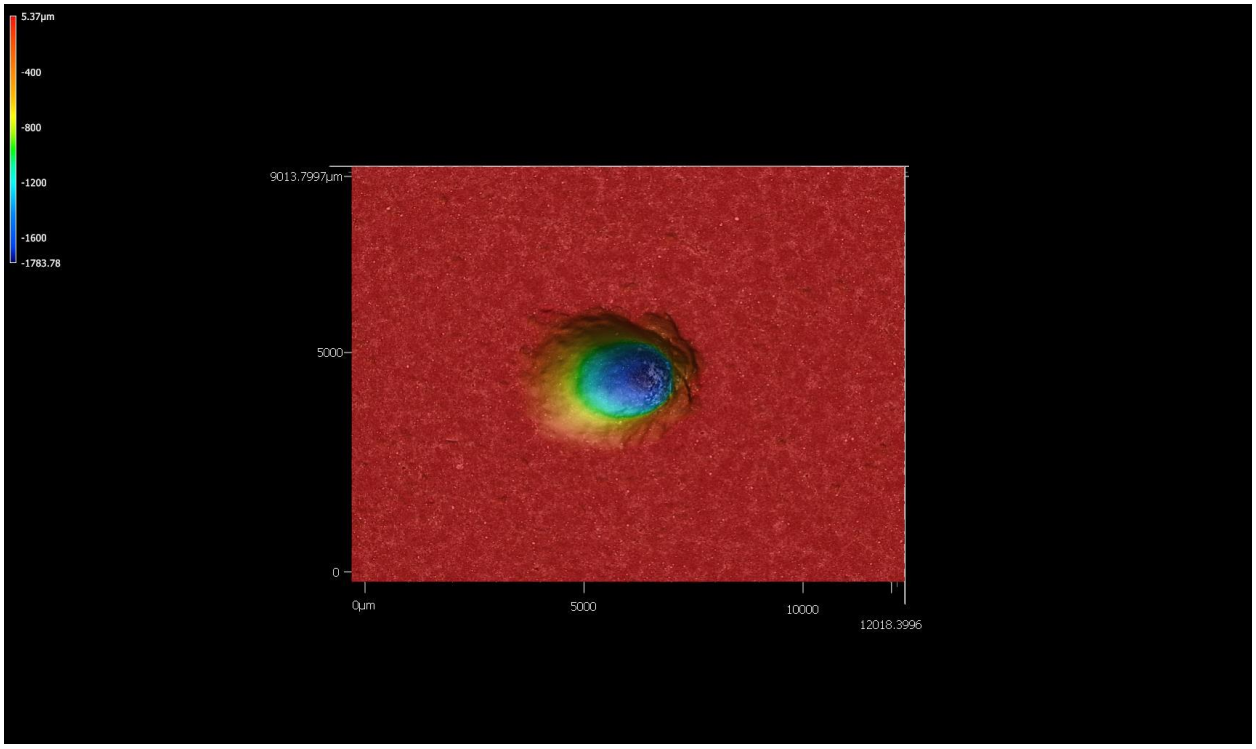


Fig. AII-28: Glass erosion scar EXP1 at 75° angle of attack

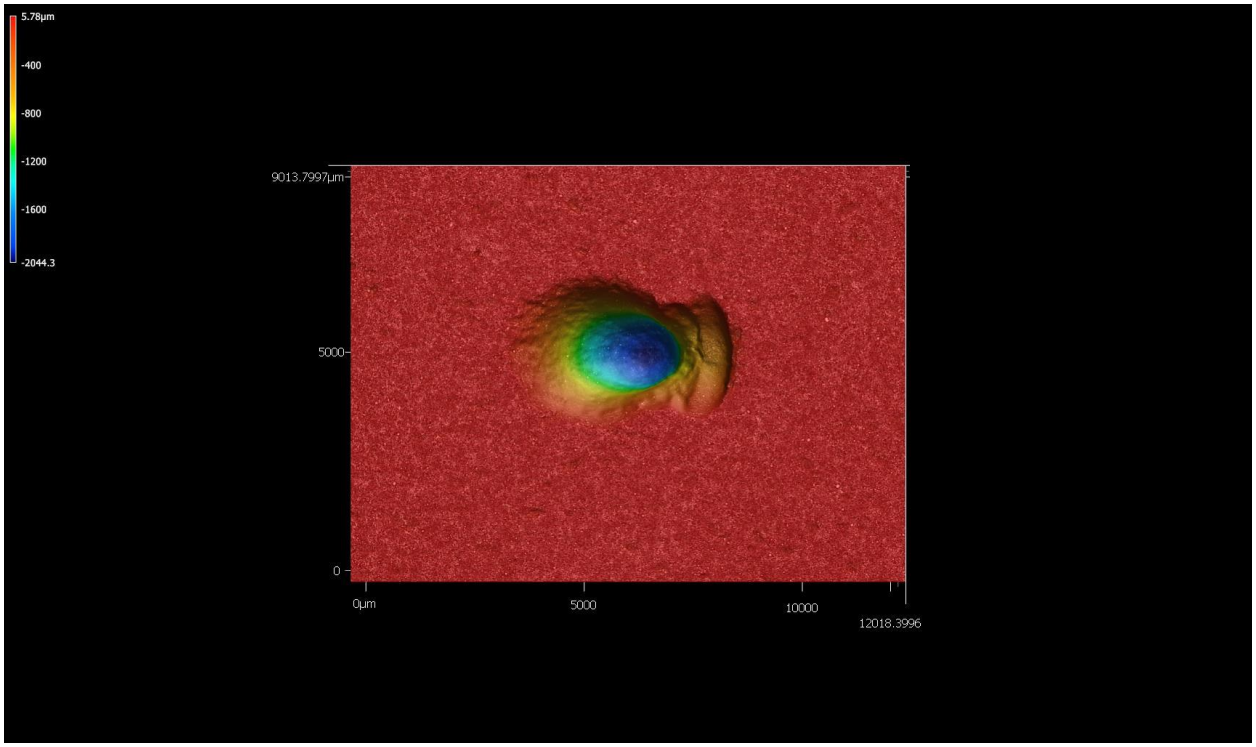


Fig. AII-29: Glass erosion scar EXP2 at 75° angle of attack

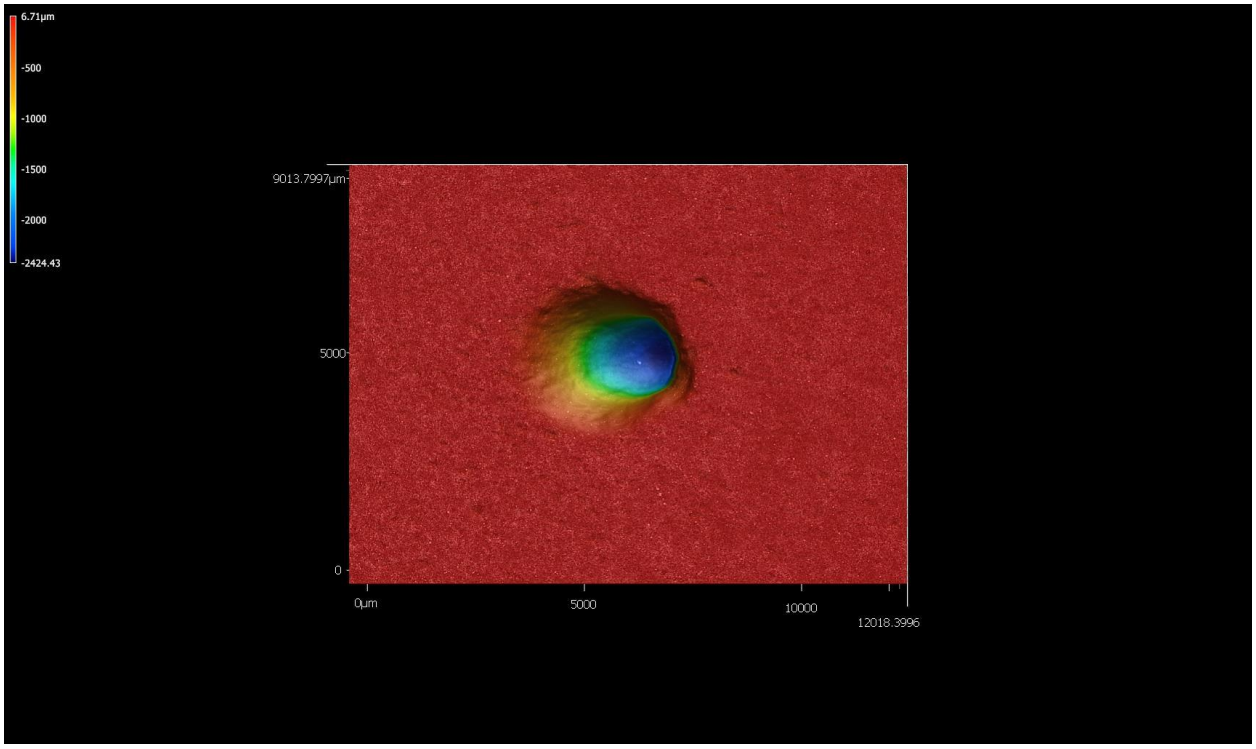


Fig. AII-30: Glass erosion scar EXP3 at 75° angle of attack

- 90 degrees

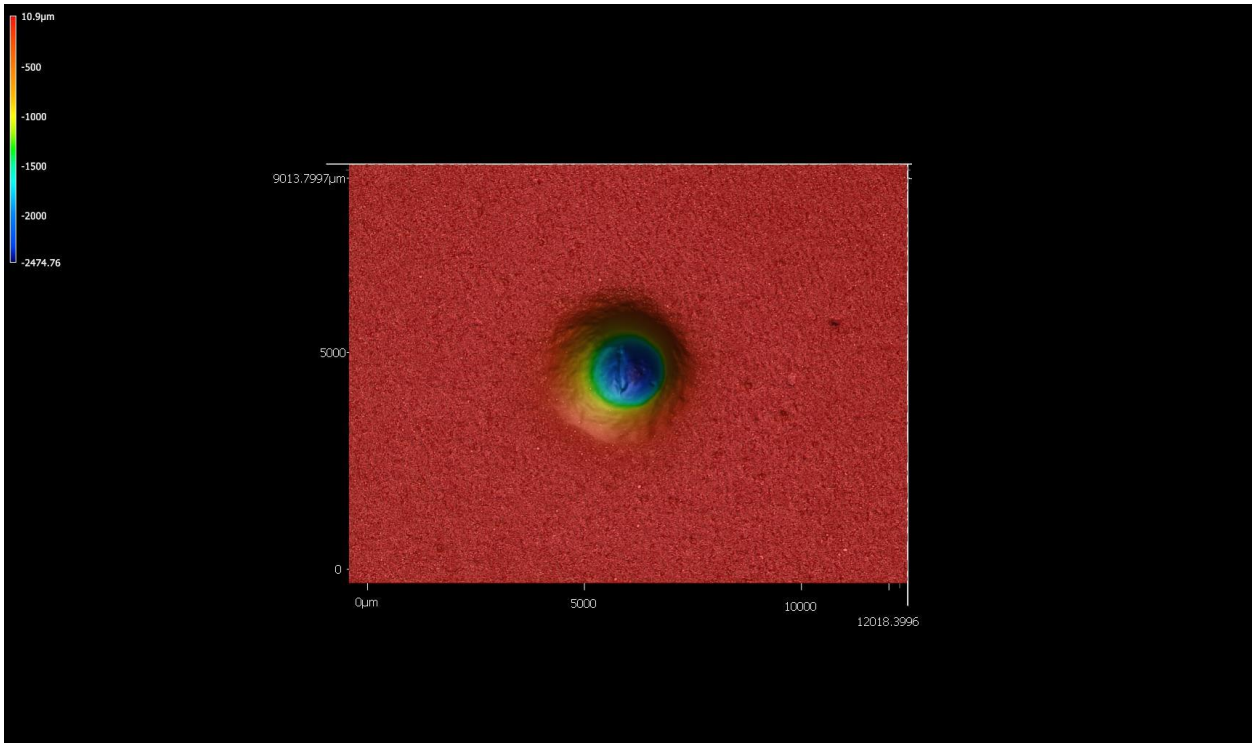


Fig. AII31: Glass erosion scar EXP1 at 90° angle of attack

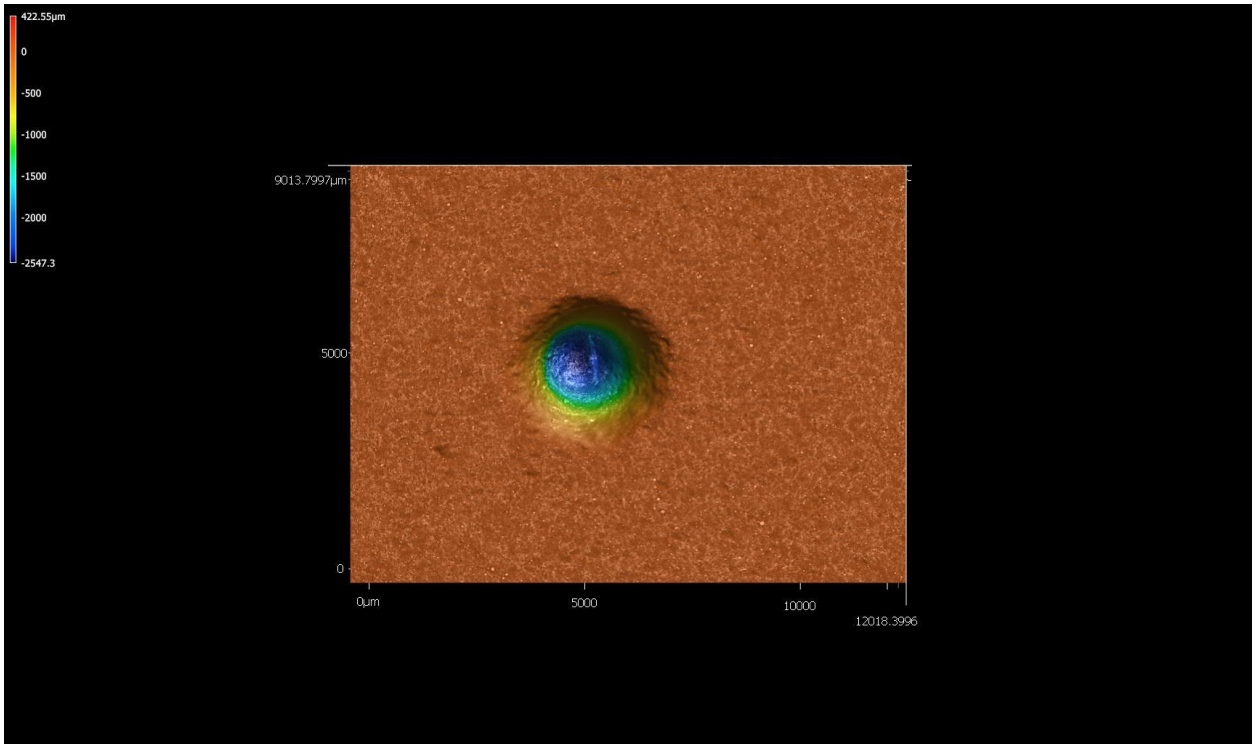


Fig. AII-32: Glass erosion scar EXP2 at 90° angle of attack

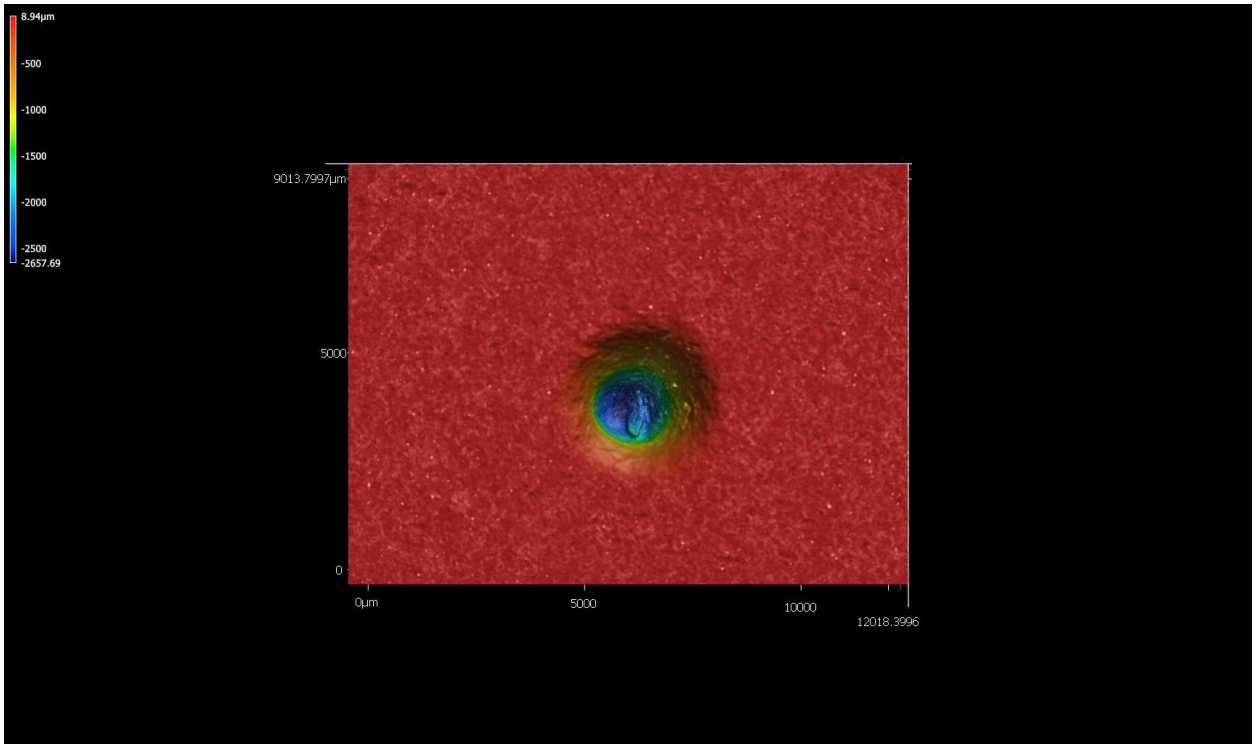


Fig. AII-33: Glass erosion scar EXP3 at 60° angle of attack

- GFRP microphotographs

Uncoated

- 30 degrees

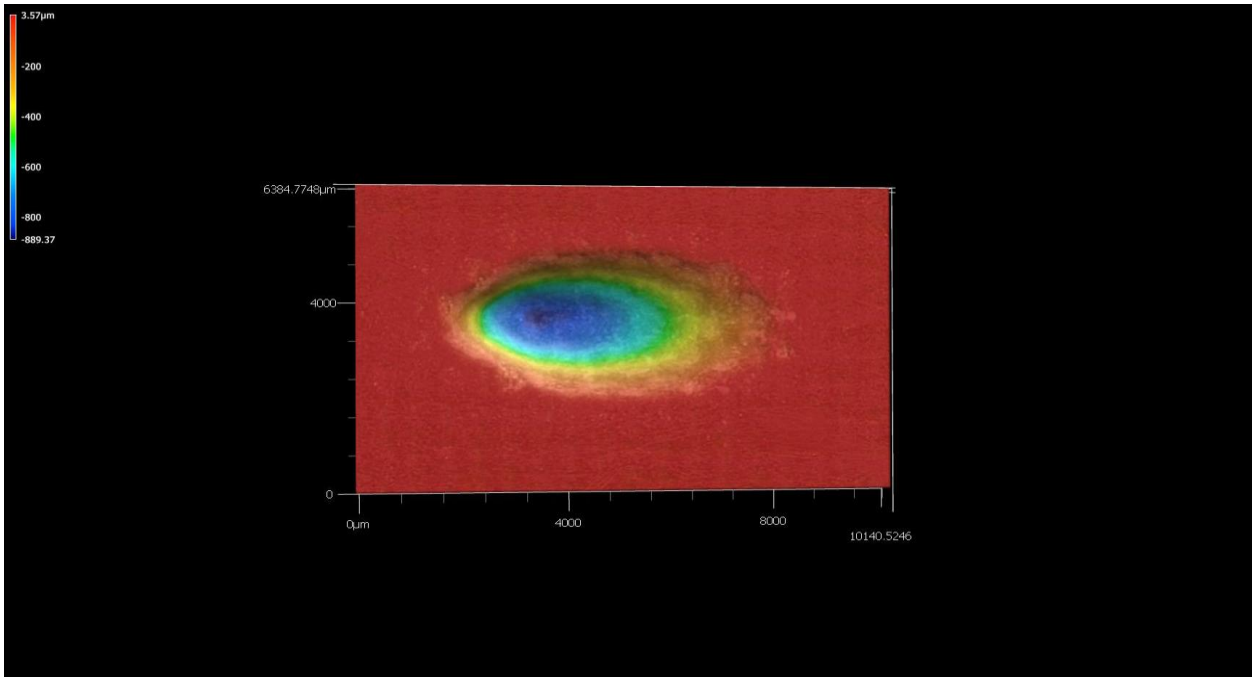


Fig. AII-34: Uncoated GFRP erosion scar EXP1 at 30° angle of attack

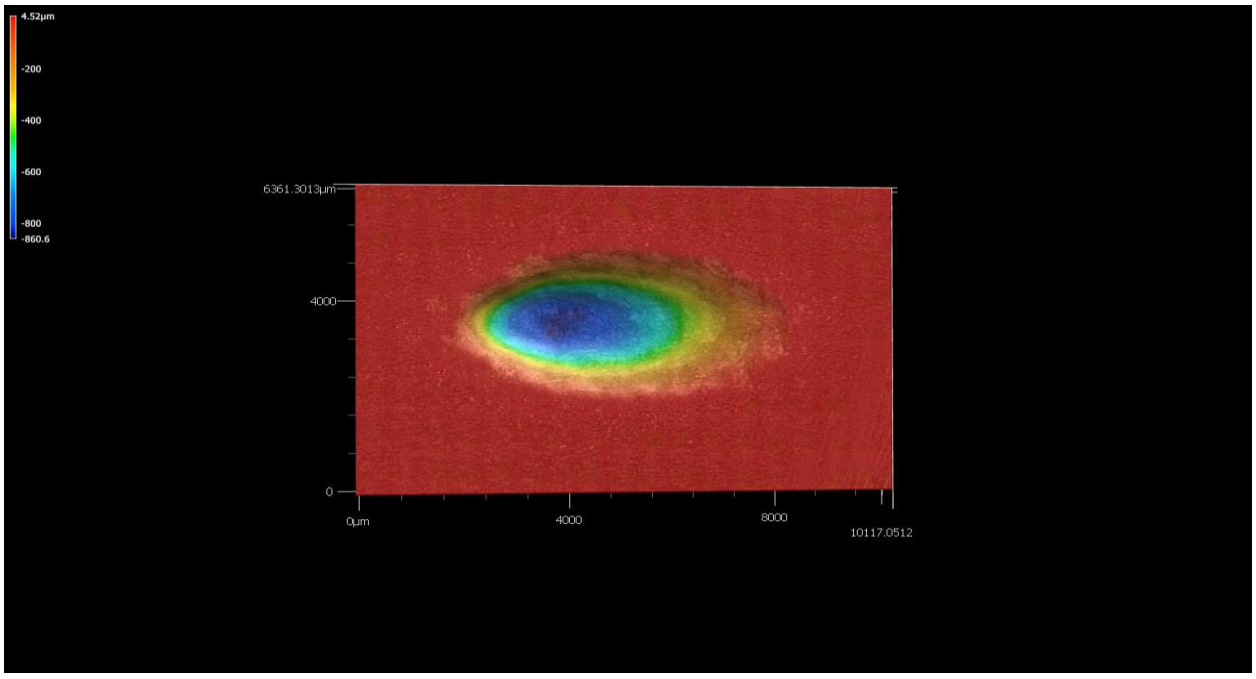


Fig. AII-35: Uncoated GFRP erosion scar EXP2 at 30° angle of attack

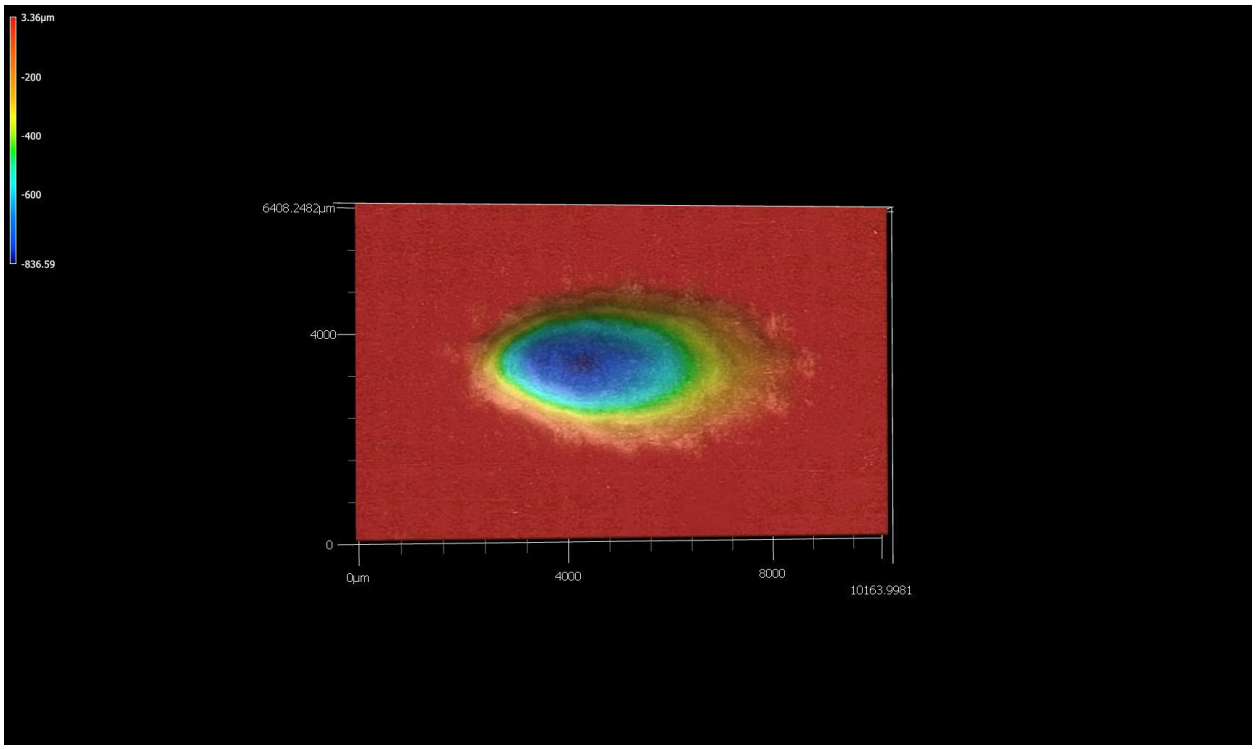


Fig. AII-36: Uncoated GFRP erosion scar EXP3 at 30° angle of attack

- 45 degrees

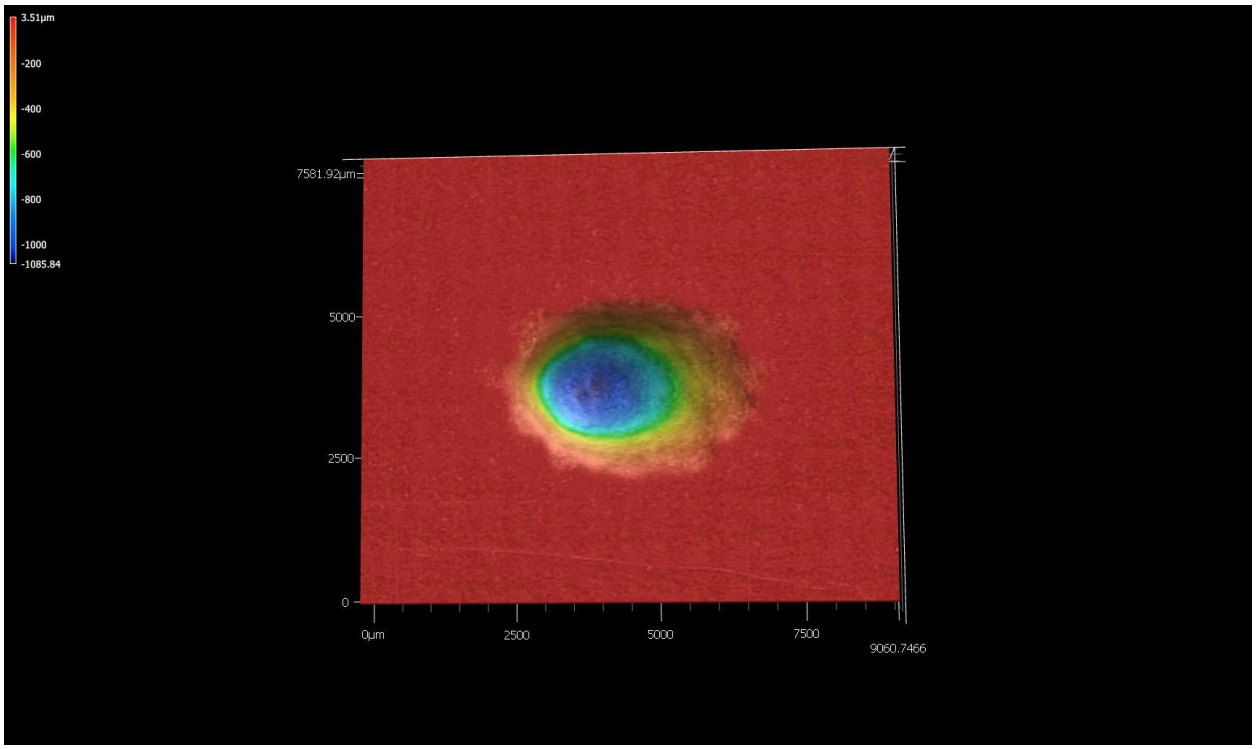


Fig. AII-37: Uncoated GFRP erosion scar EXP1 at 45° angle of attack

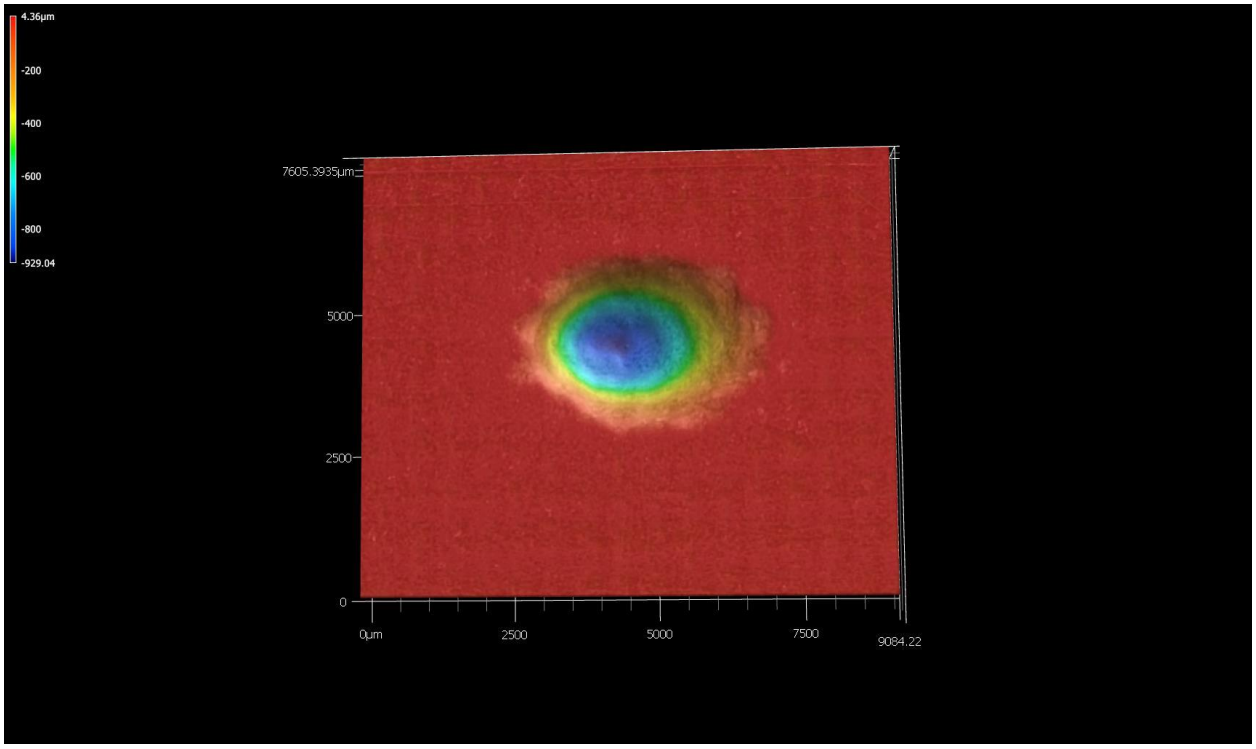


Fig. AII-38: Uncoated GFRP erosion scar EXP2 at 45° angle of attack

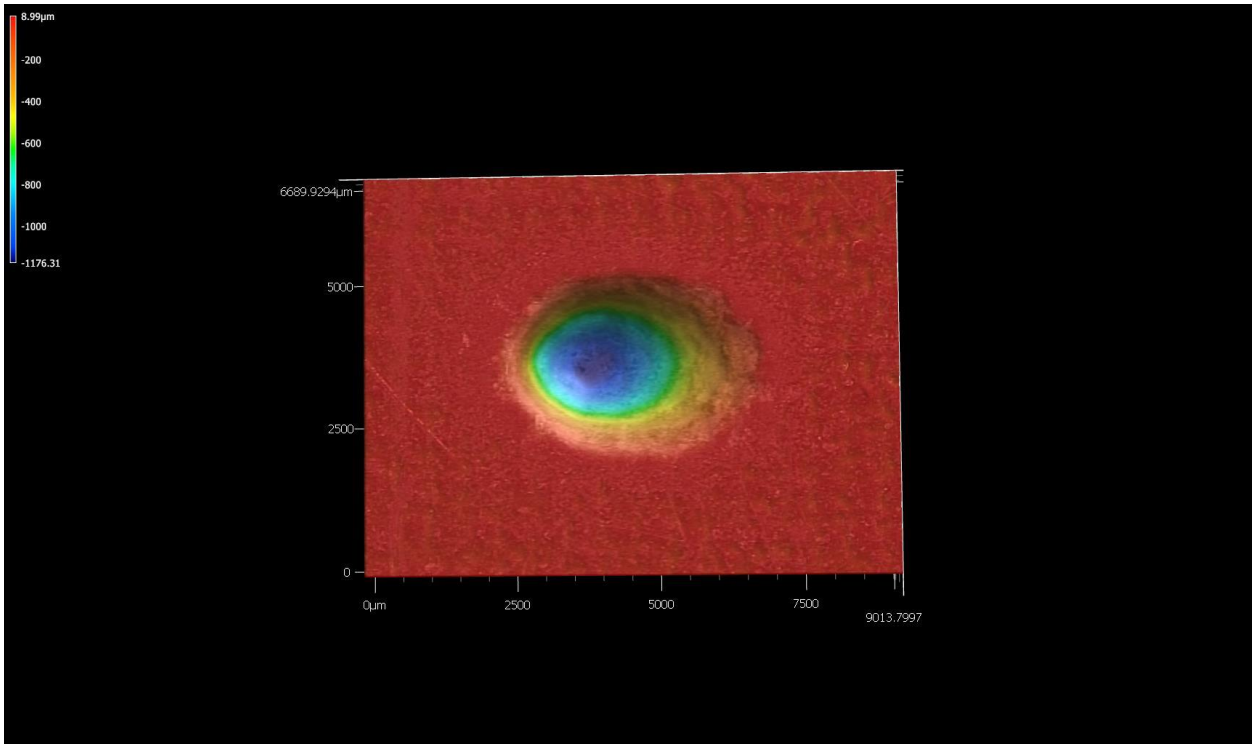


Fig. AII-39: Uncoated GFRP erosion scar EXP3 at 45° angle of attack

- 60 degrees

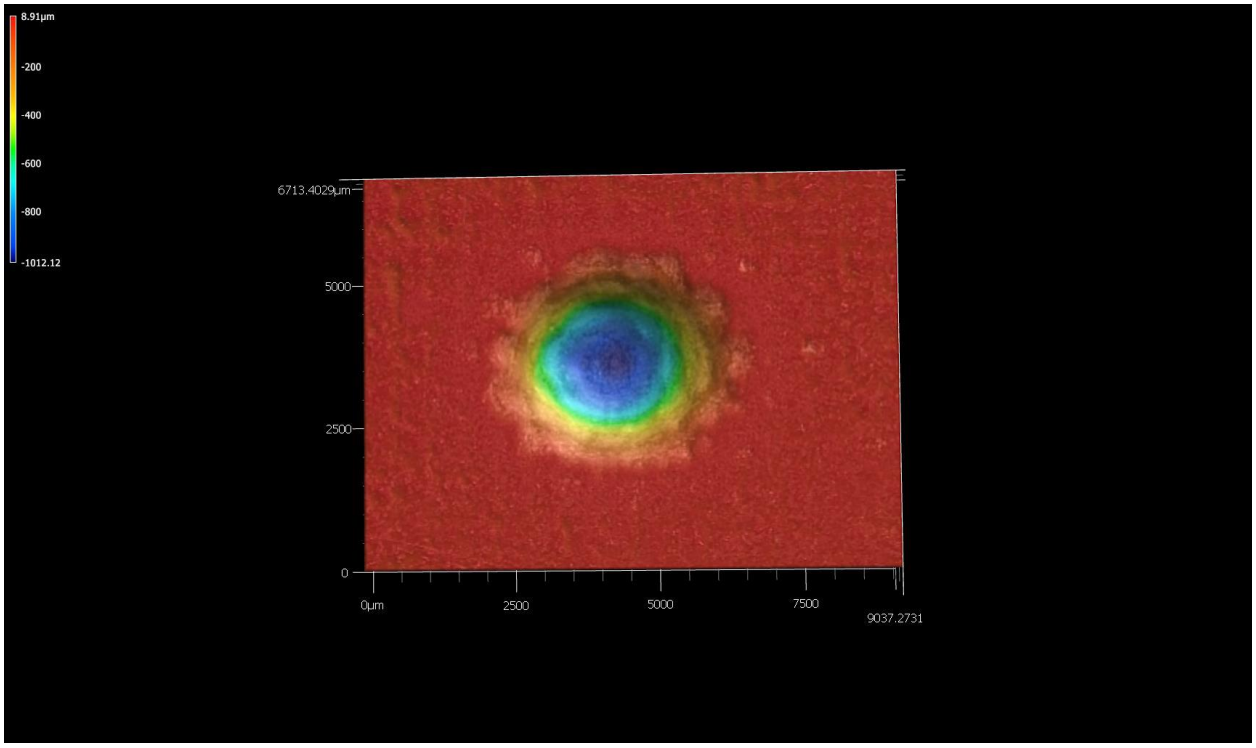


Fig. AII-40: Uncoated GFRP erosion scar EXP1 at 60° angle of attack

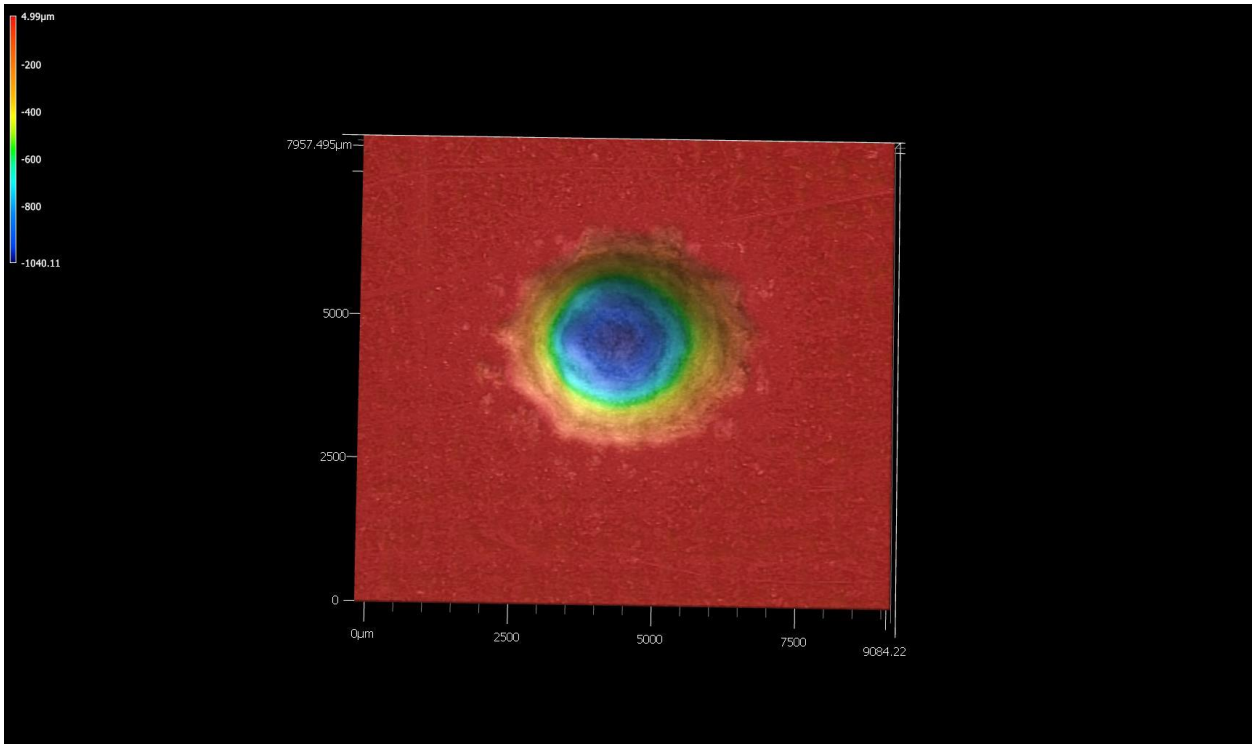


Fig. AII-41: Uncoated GFRP erosion scar EXP2 at 60° angle of attack

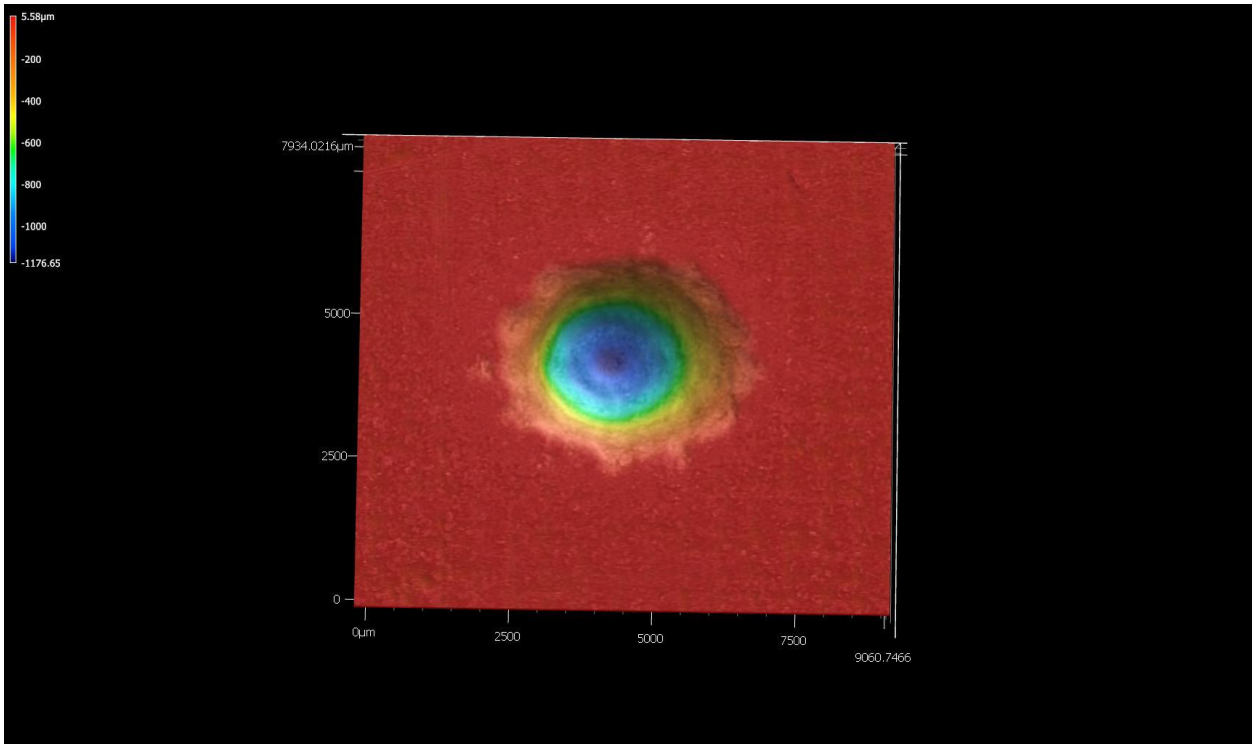


Fig. AII-42: Uncoated GFRP erosion scar EXP3 at 60° angle of attack

- 75 degrees

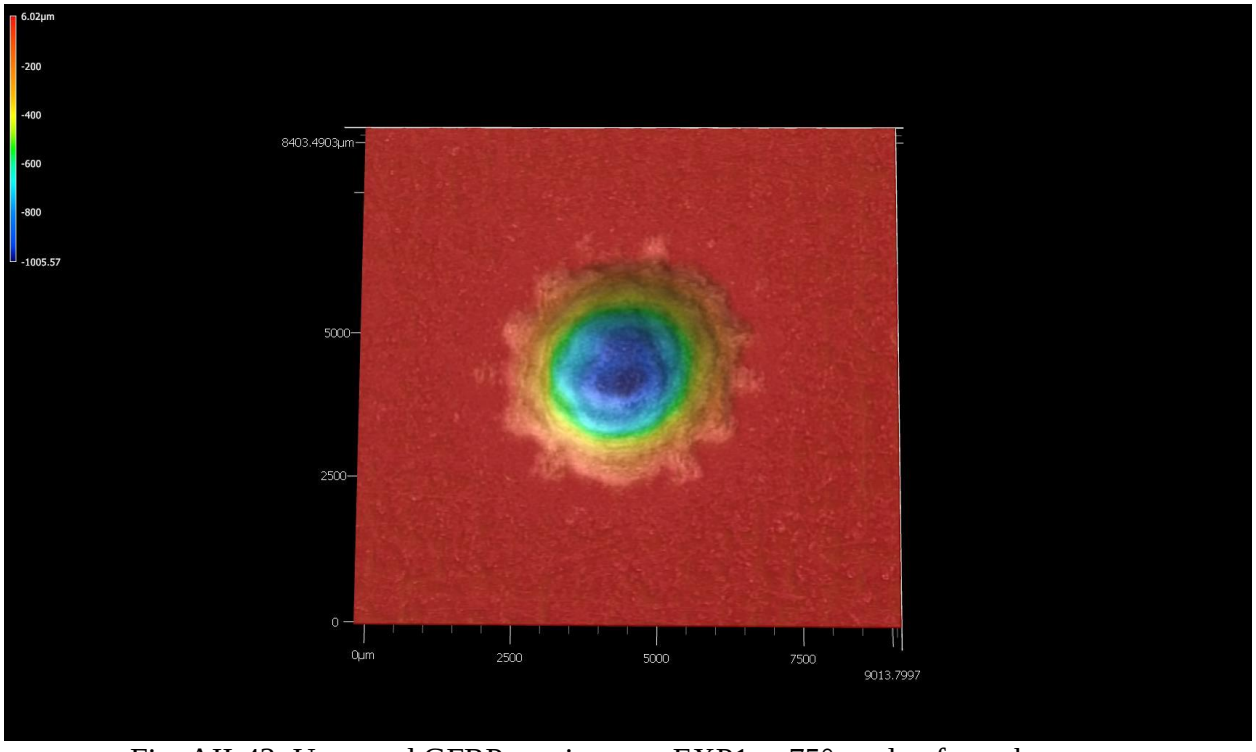


Fig. AII-43: Uncoated GFRP erosion scar EXP1 at 75° angle of attack

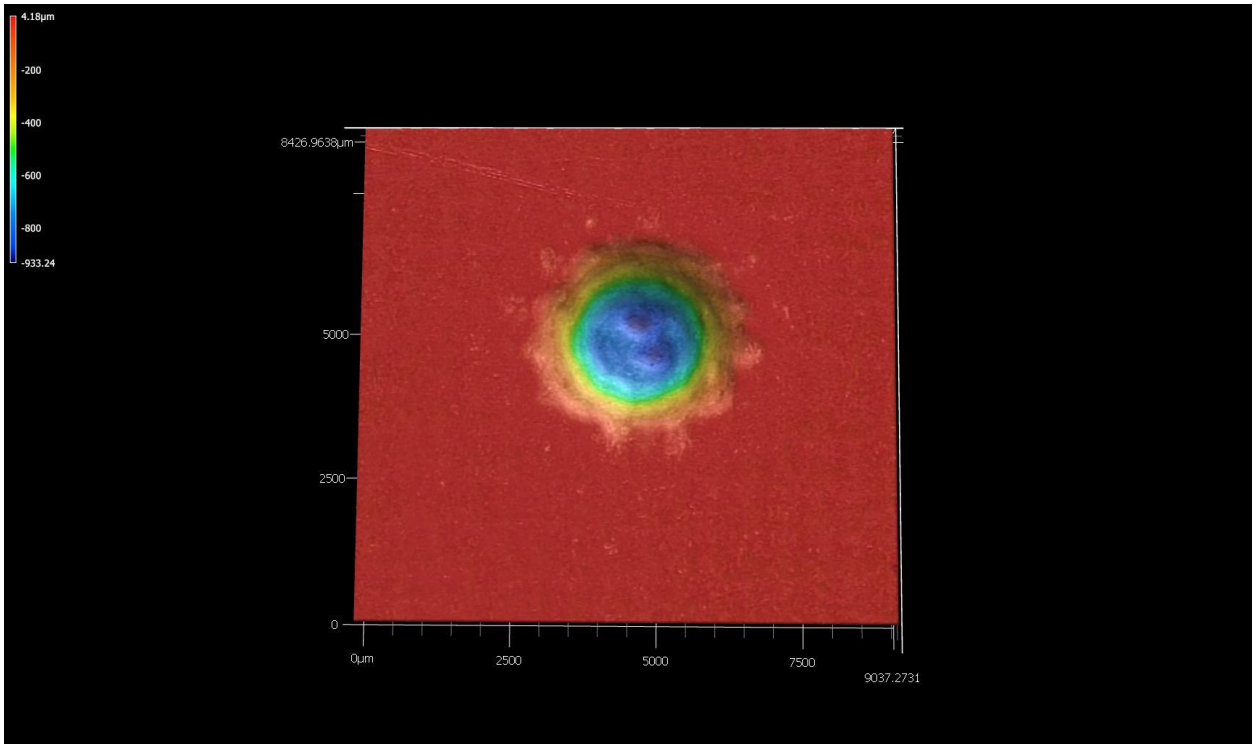


Fig. AII-44: Uncoated GFRP erosion scar EXP2 at 90° angle of attack

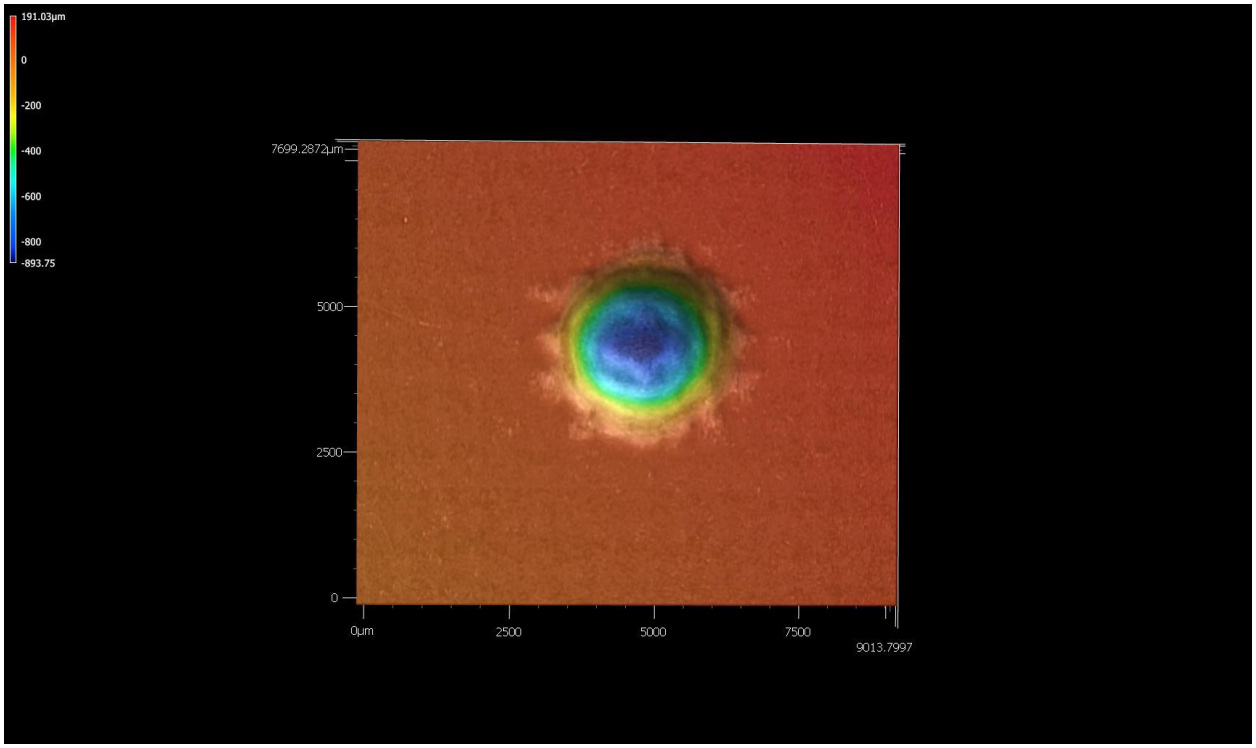


Fig. AII-45: Uncoated GFRP erosion scar EXP3 at 90° angle of attack

- 90 degrees

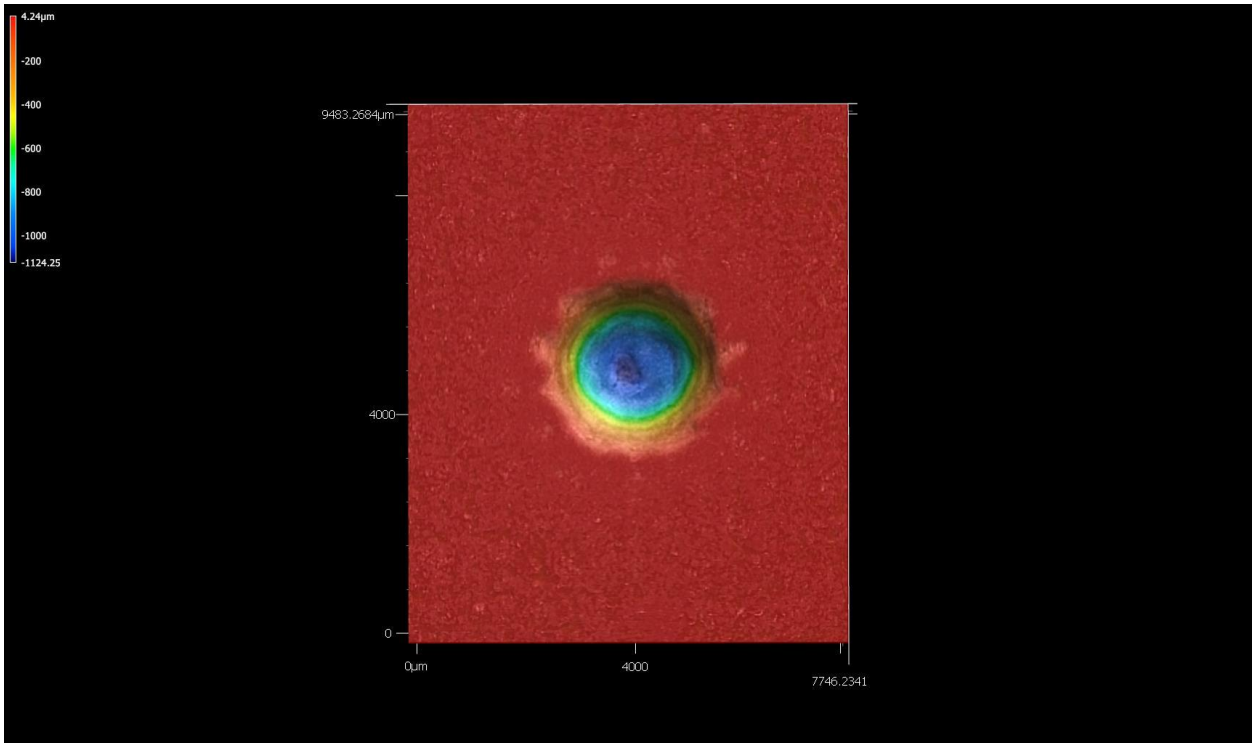


Fig. AII-46: Uncoated GFRP erosion scar EXP1 at 90° angle of attack

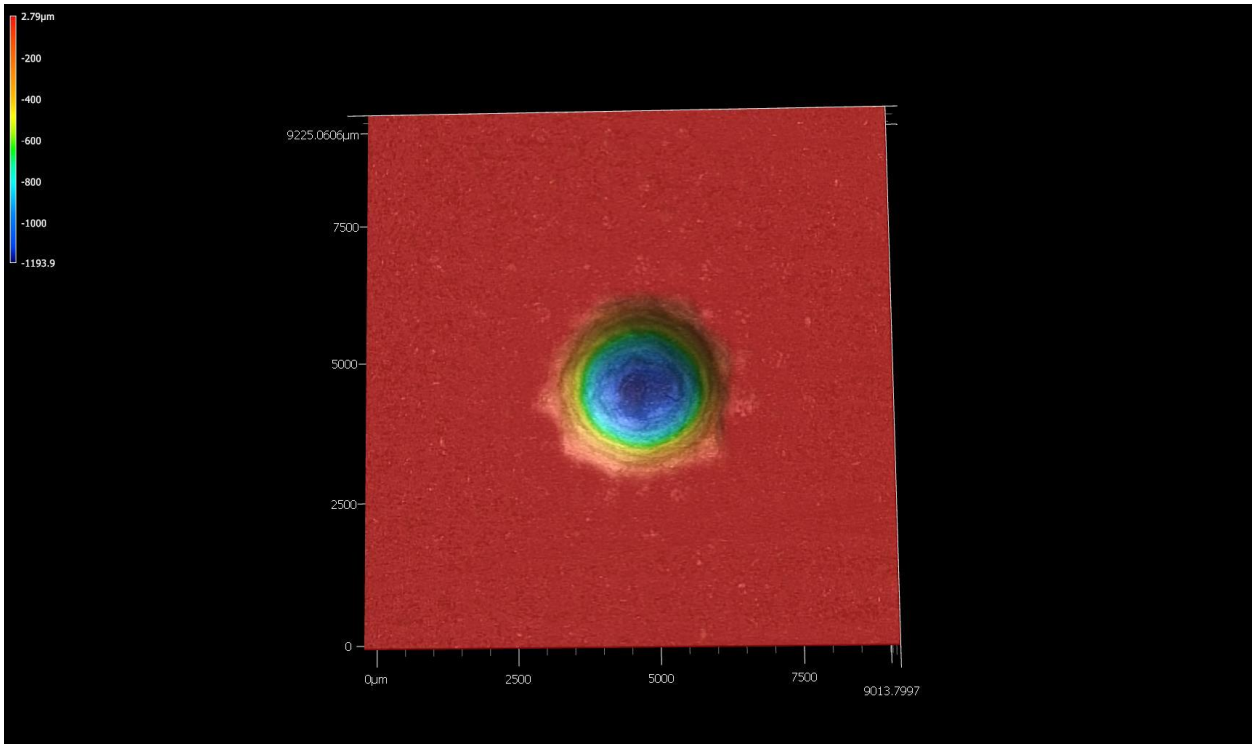


Fig. AII-47: Uncoated GFRP erosion scar EXP2 at 90° angle of attack

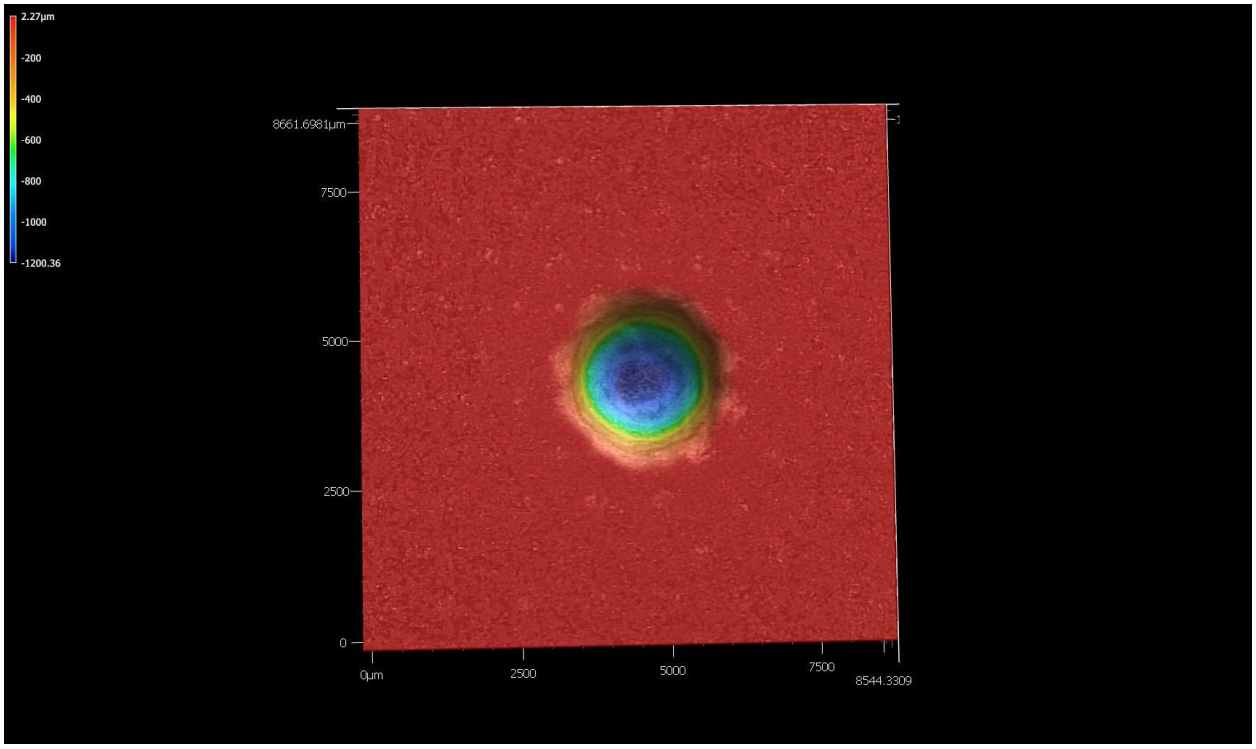


Fig. AII-48: Uncoated GFRP erosion scar EXP3 at 90° angle of attack

H-146

- 30 degrees

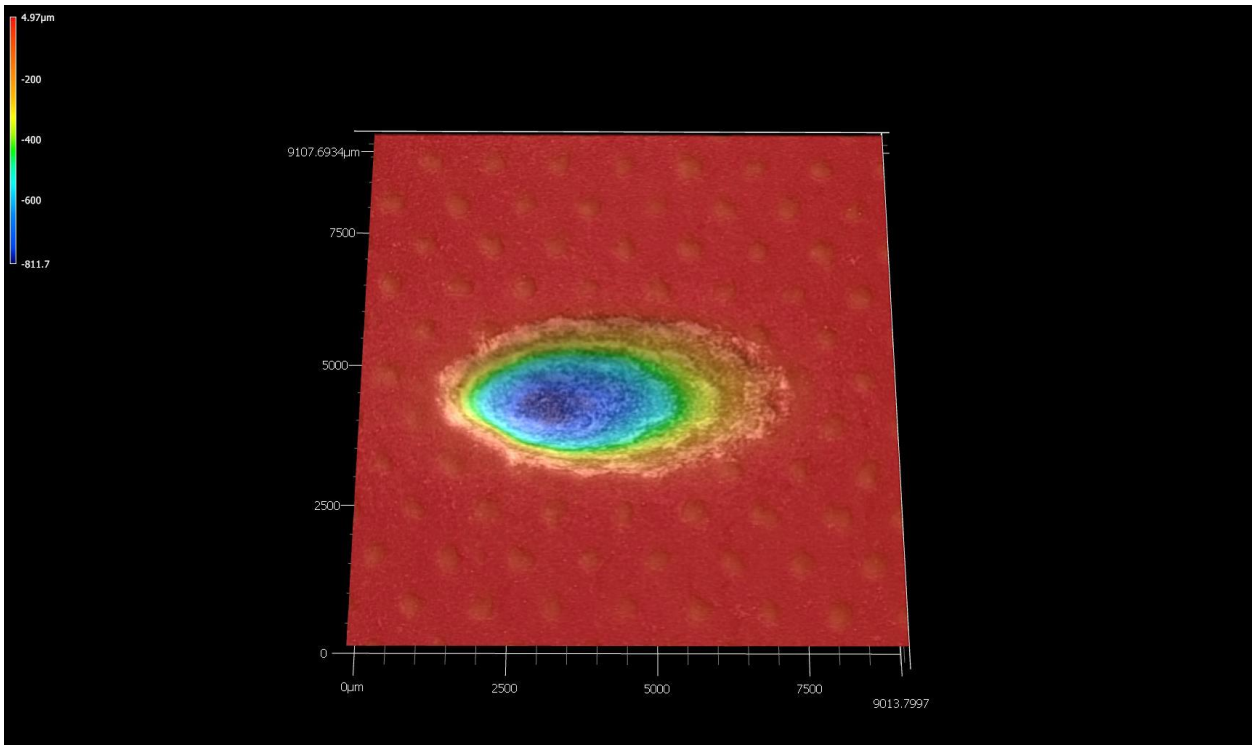


Fig. AII-49: H-146 coated GFRP erosion scar EXP1 at 30° angle of attack

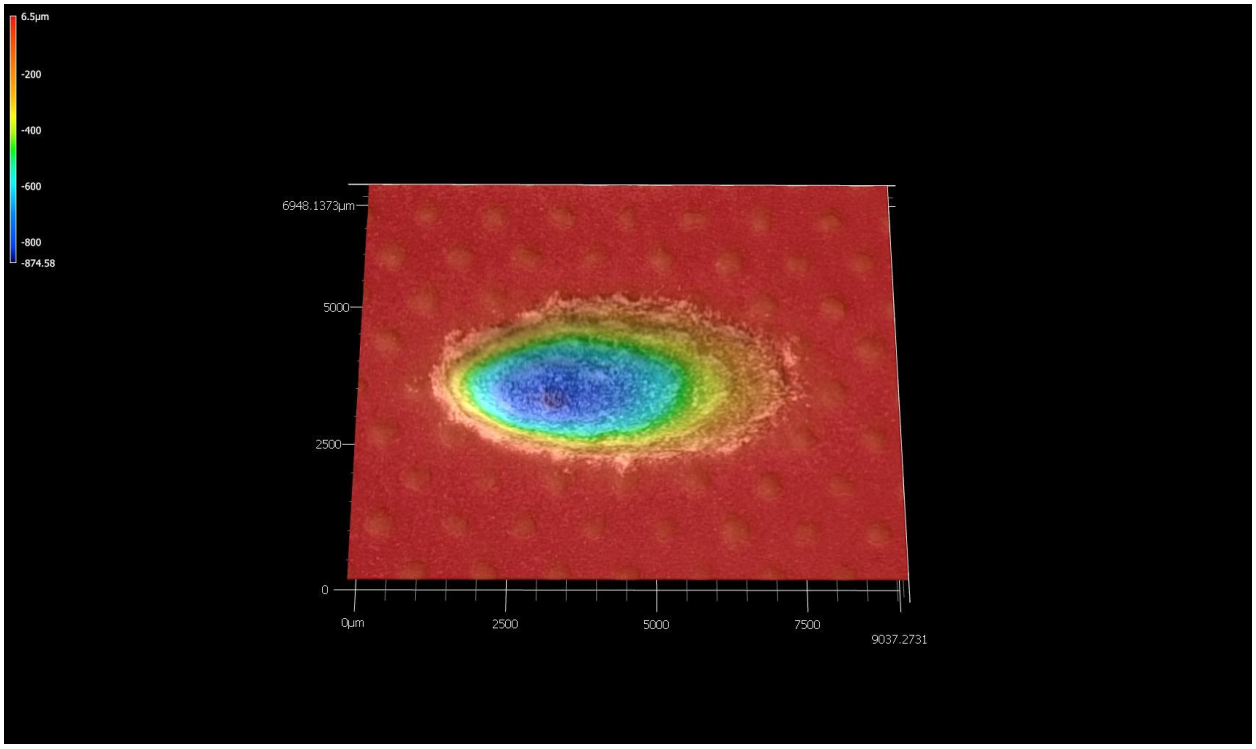


Fig. AII-50: H-146 coated GFRP erosion scar EXP2 at 30° angle of attack

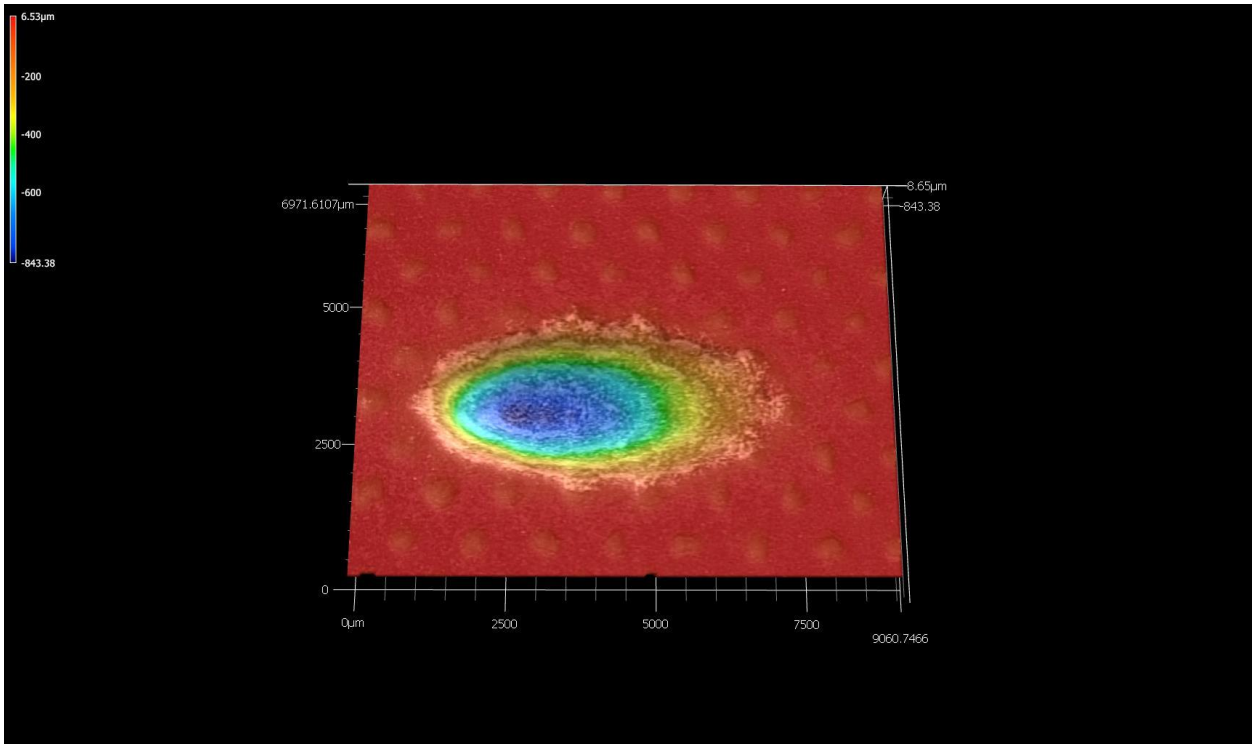


Fig. AII-51: H-146 coated GFRP erosion scar EXP2 at 30° angle of attack

- 45 degrees

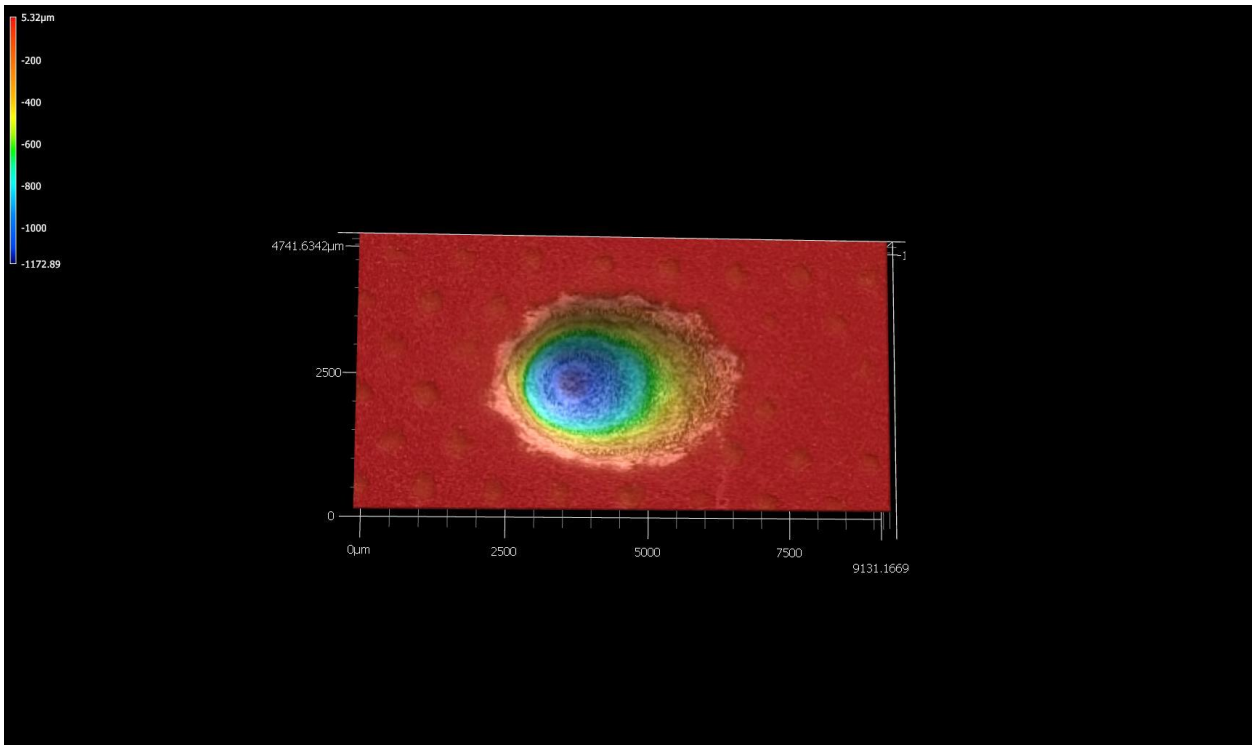


Fig. AII-52: H-146 coated GFRP erosion scar EXP1 at 45° angle of attack

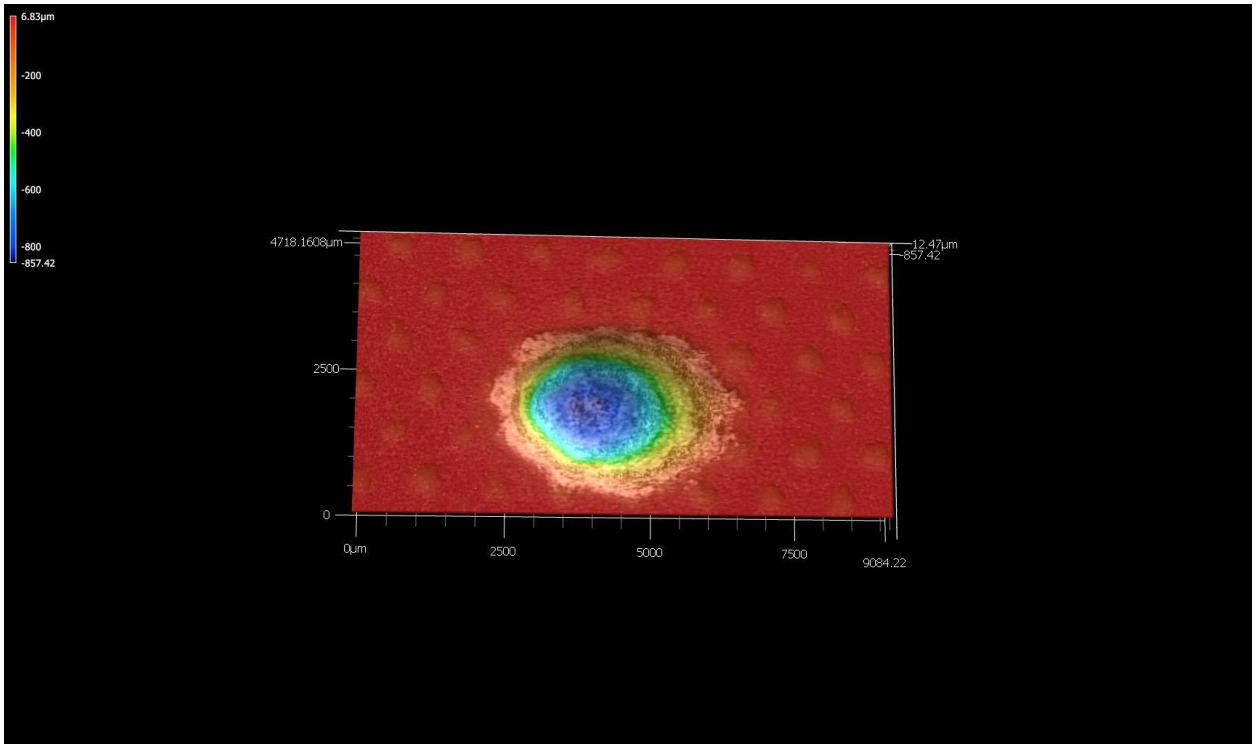


Fig. AII-53: H-146 coated GFRP erosion scar EXP2 at 45° angle of attack

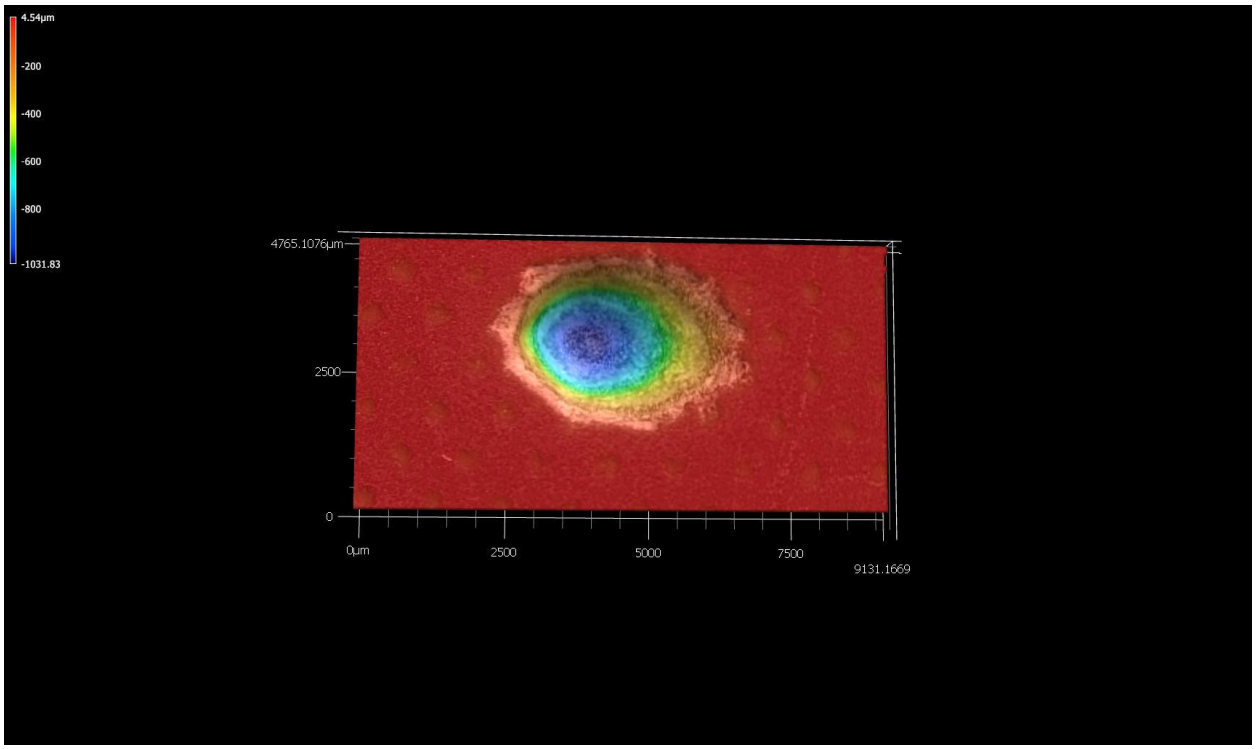


Fig. AII-54: H-146 coated GFRP erosion scar EXP3 at 45° angle of attack

- 60 degrees

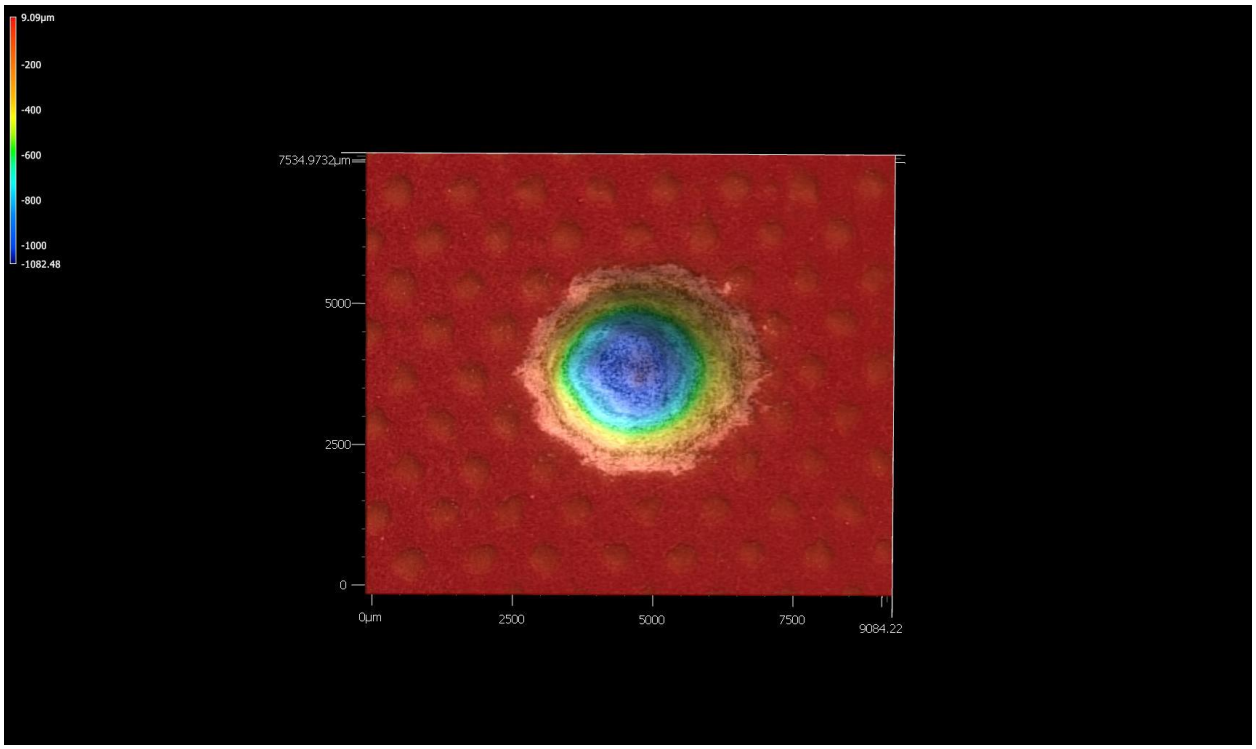


Fig. AII-55: H-146 coated GFRP erosion scar EXP1 at 60° angle of attack

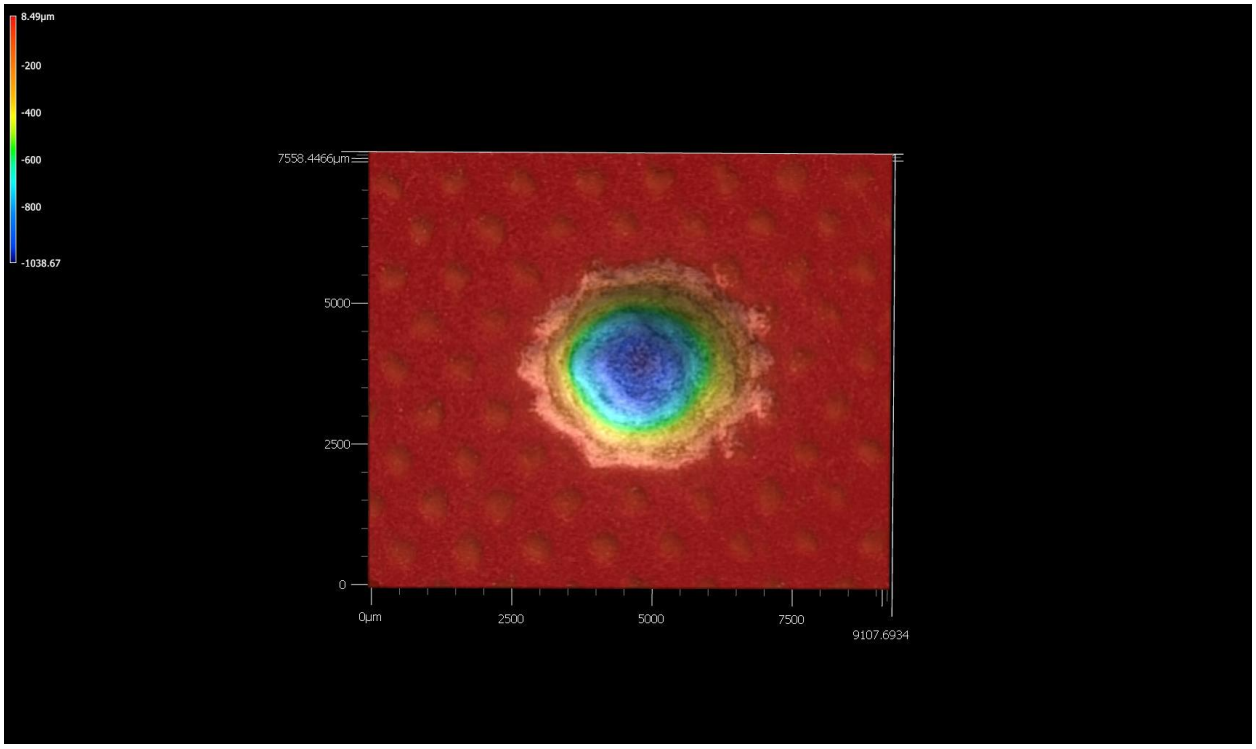


Fig. AII-56: H-146 coated GFRP erosion scar EXP2 at 60° angle of attack

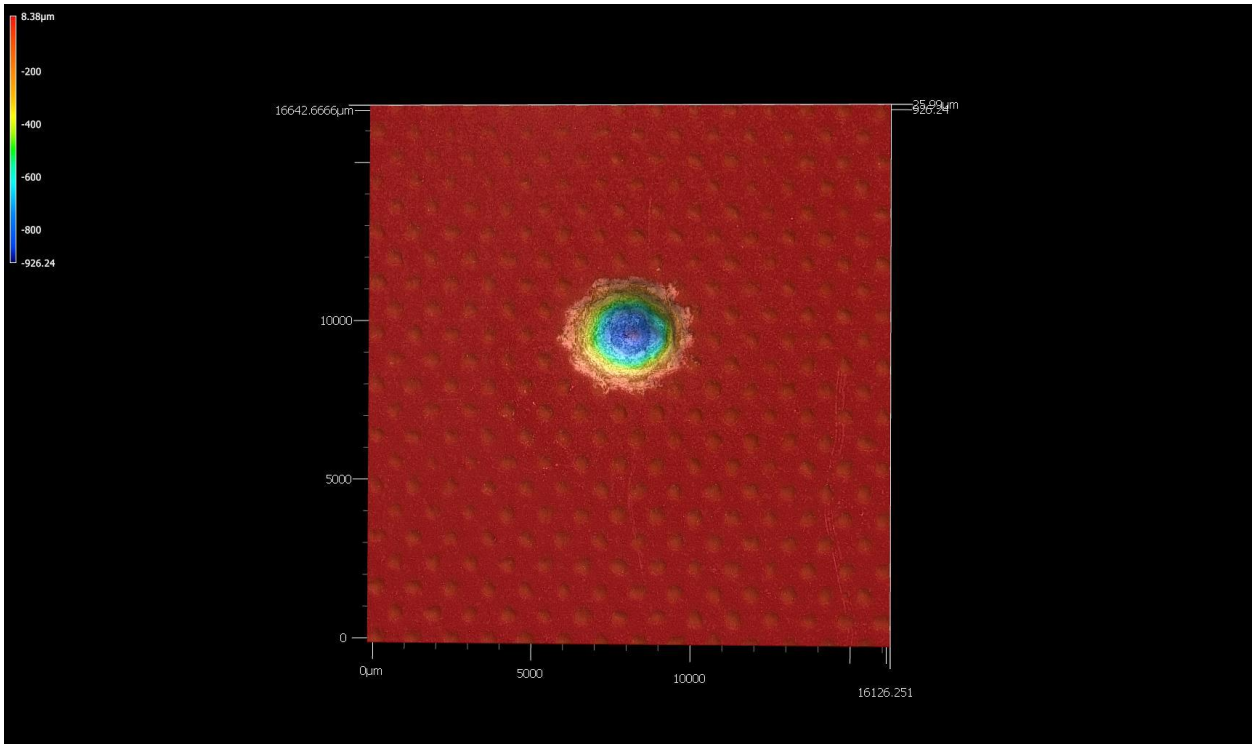


Fig. AII-57: H-146 coated GFRP erosion scar EXP3 at 60° angle of attack

- 75 degrees

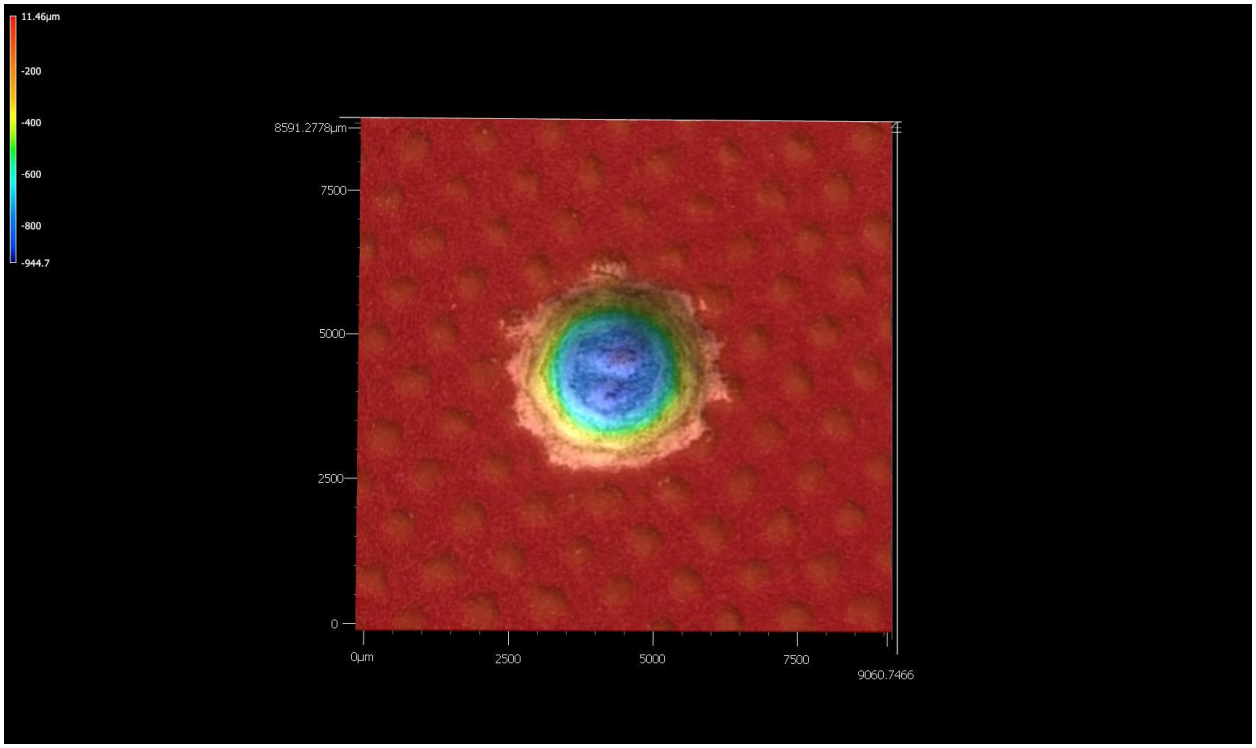


Fig. AII-58: H-146 coated GFRP erosion scar EXP1 at 75° angle of attack

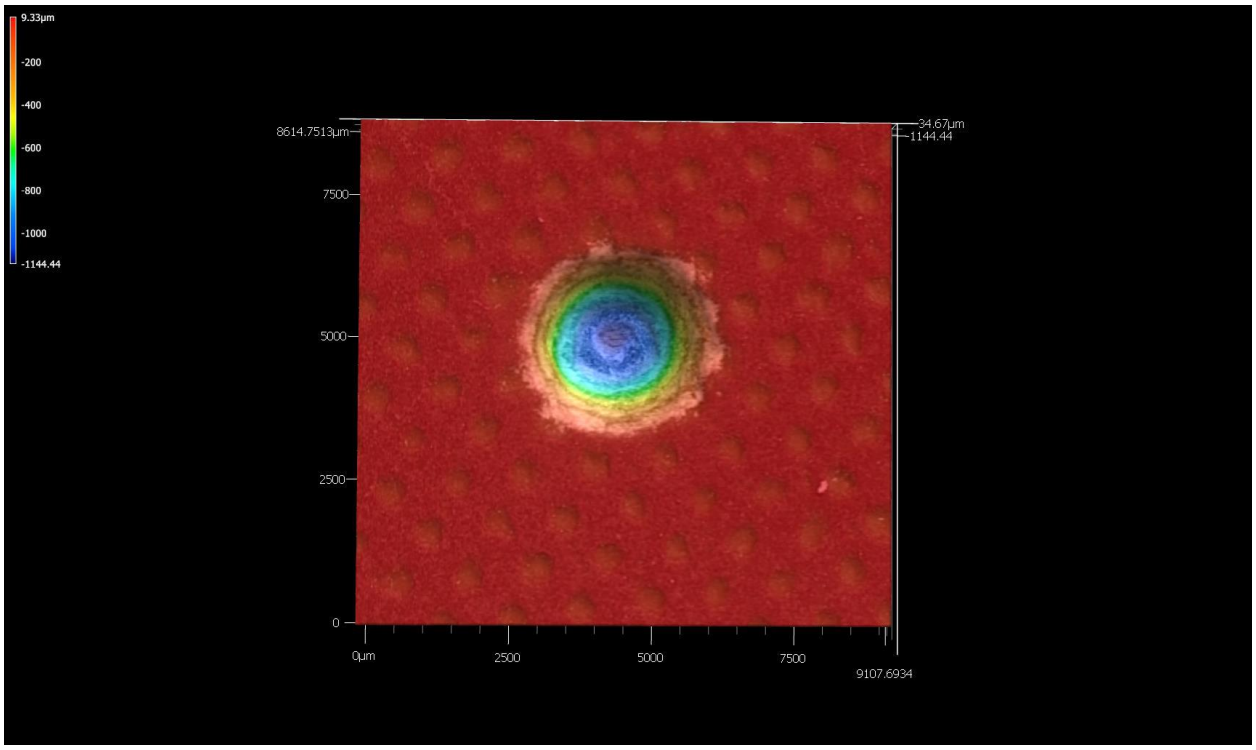


Fig. AII-59: H-146 coated GFRP erosion scar EXP2 at 75° angle of attack

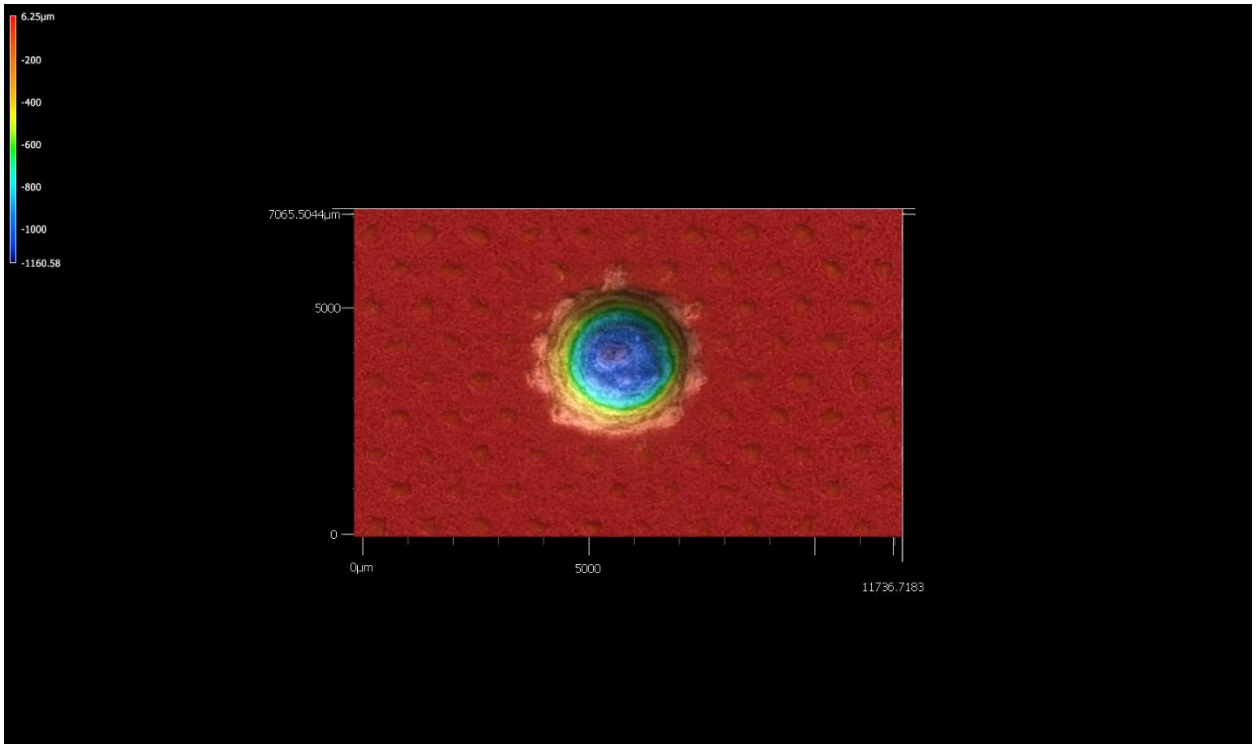


Fig. AII-60: H-146 coated GFRP erosion scar EXP3 at 75° angle of attack

- 90 degrees

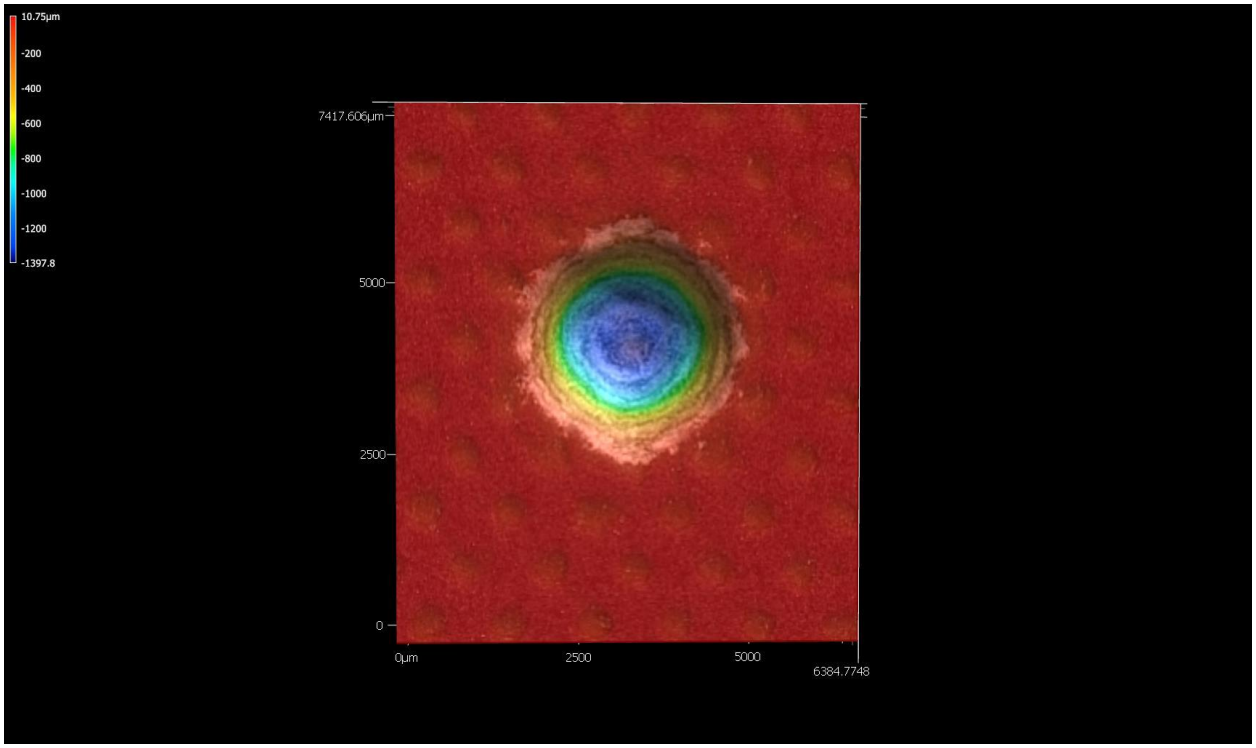


Fig. AII-61: H-146 coated GFRP erosion scar EXP1 at 90° angle of attack

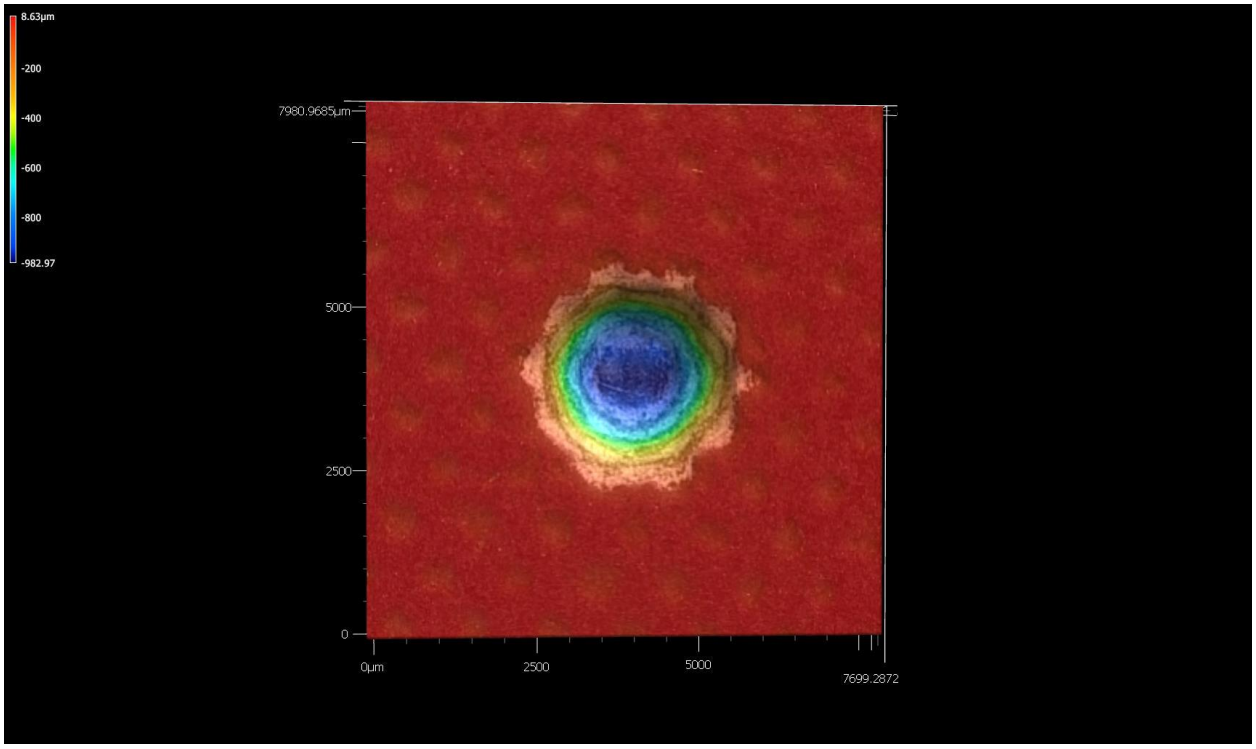


Fig. AII-62: H-146 coated GFRP erosion scar EXP2 at 90° angle of attack

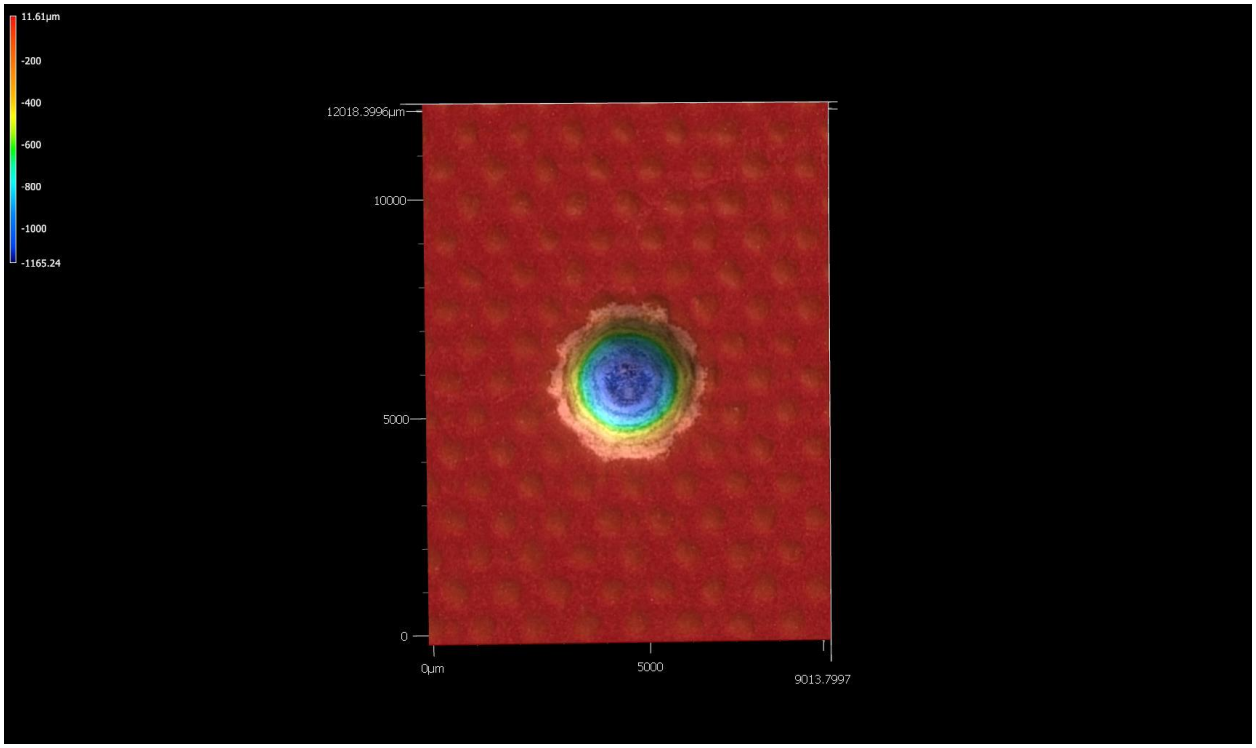


Fig. AII-63: H-146 coated GFRP erosion scar EXP3 at 90° angle of attack

IA-700:

- 30 degrees

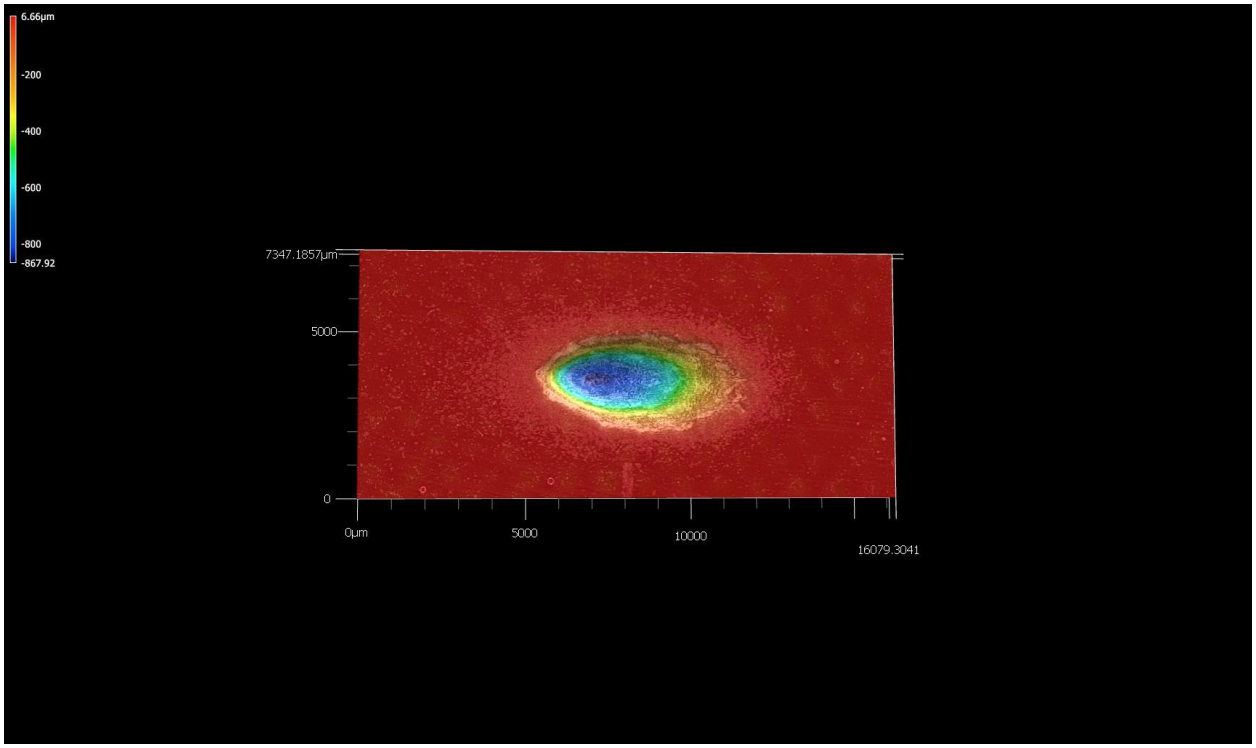


Fig. AII-64: IA-700 coated GFRP erosion scar EXP1 at 30° angle of attack

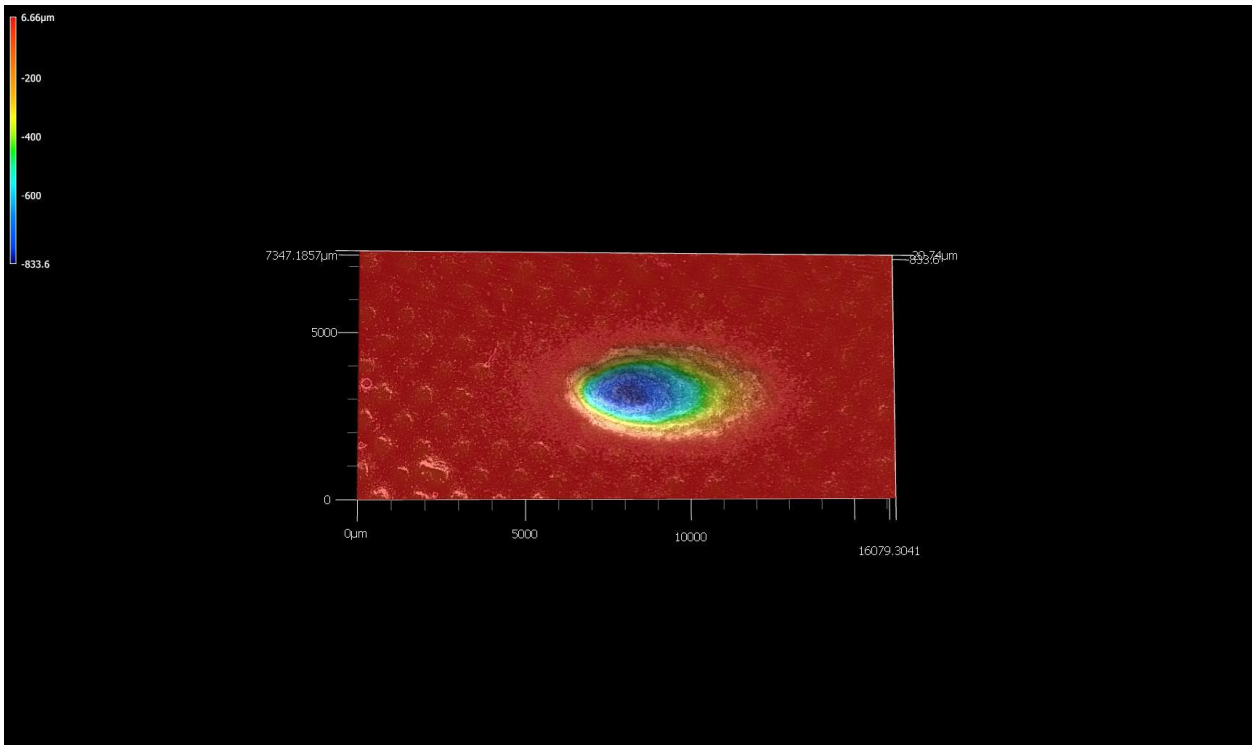


Fig. AII-65: IA-700 coated GFRP erosion scar EXP2 at 30° angle of attack

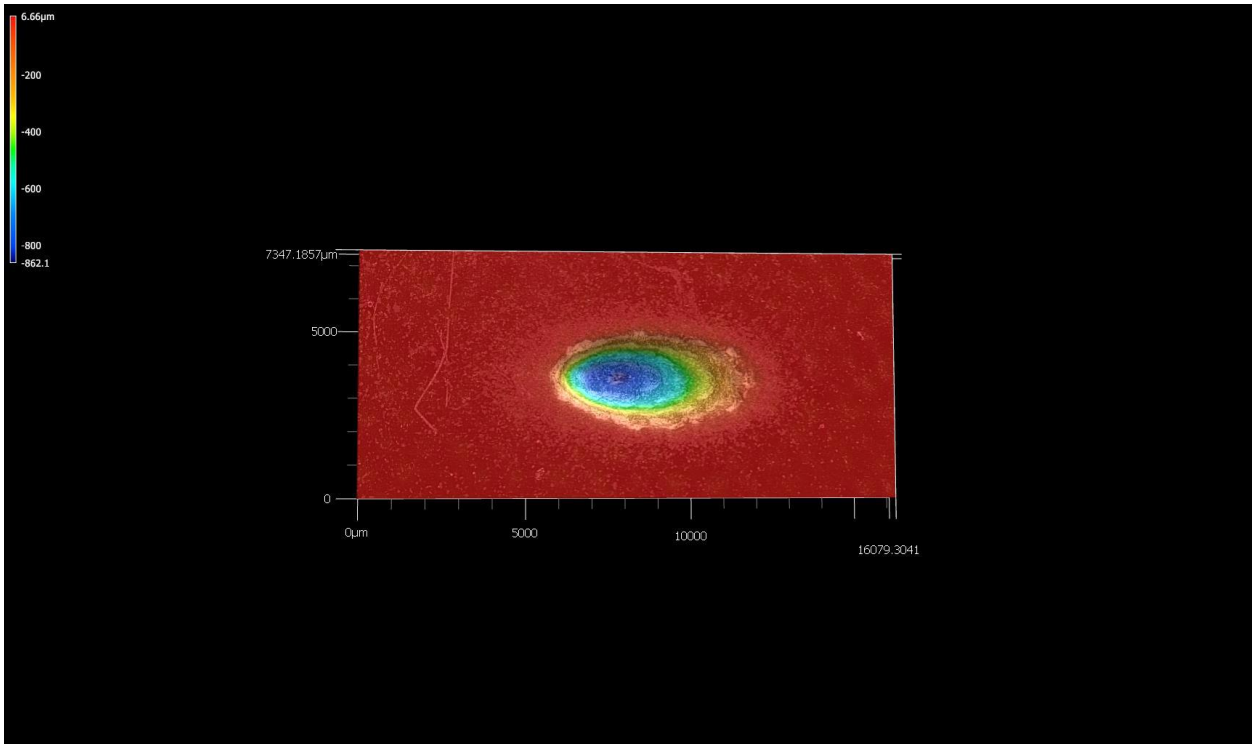


Fig. AII-66: IA-700 coated GFRP erosion scar EXP3 at 30° angle of attack

- 45 degrees

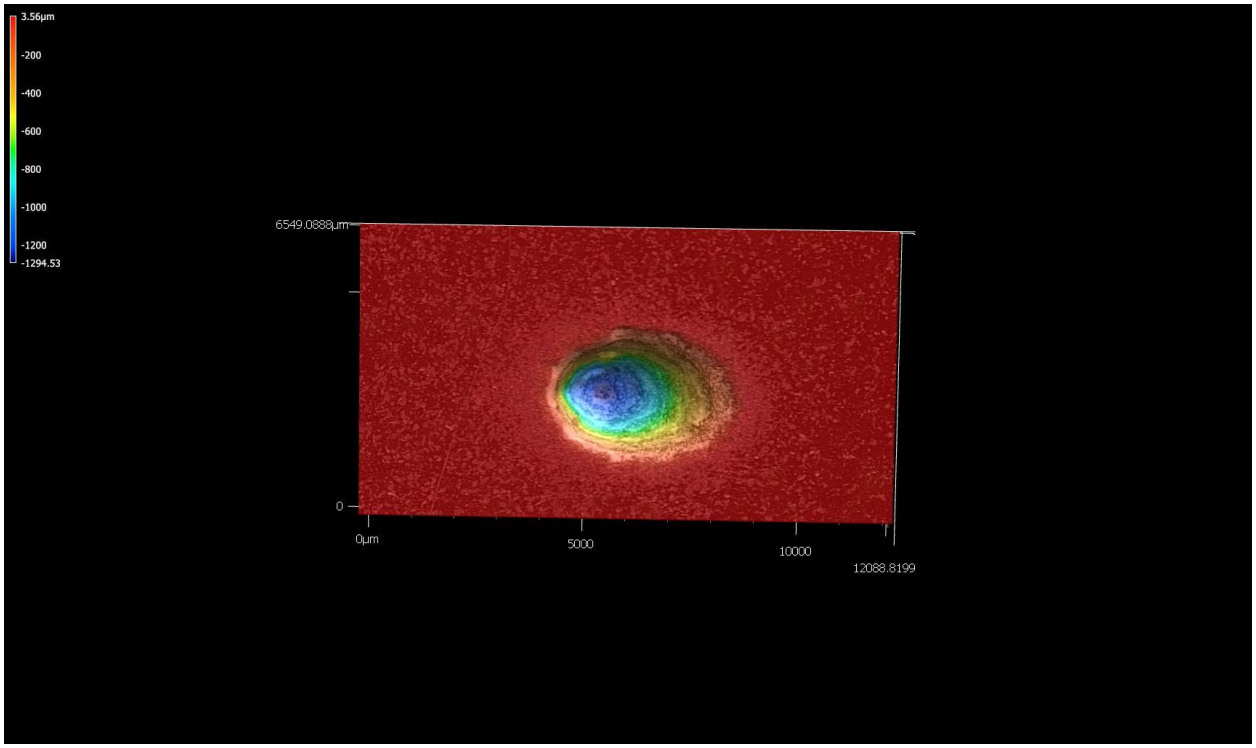


Fig. AII-67: IA-700 coated GFRP erosion scar EXP1 at 45° angle of attack

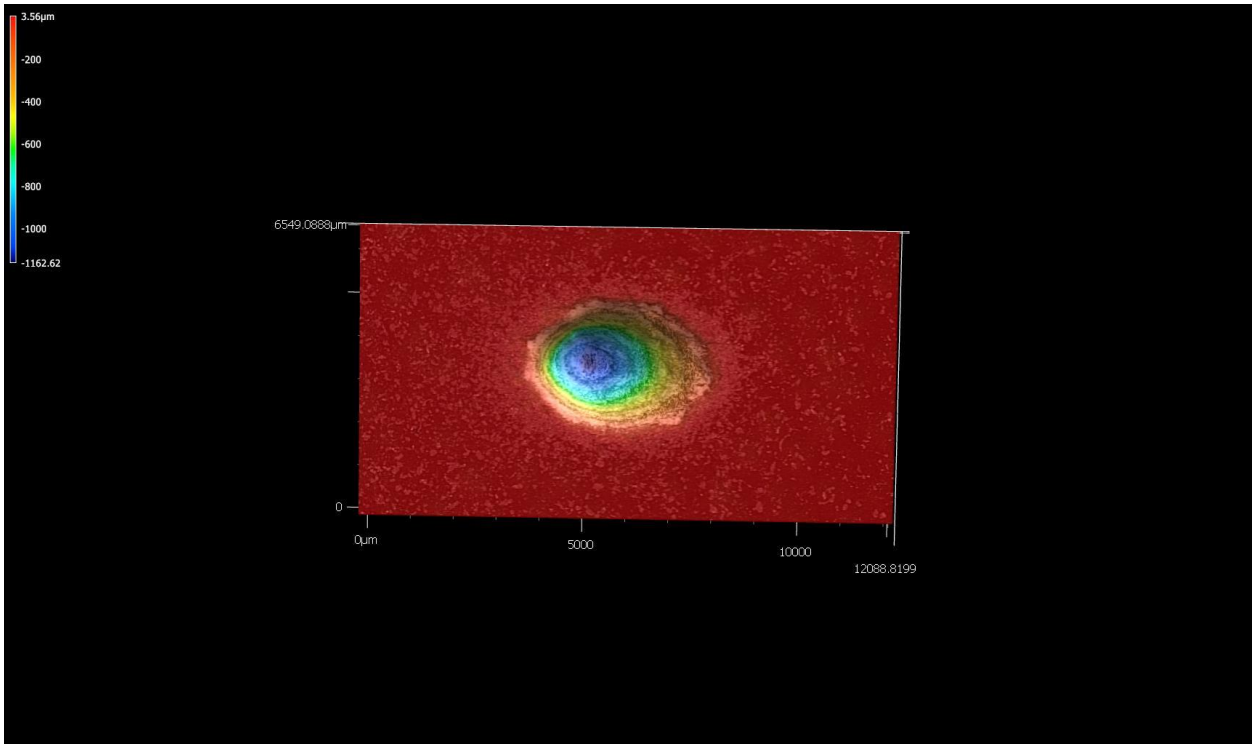


Fig. AII-68: IA-700 coated GFRP erosion scar EXP2 at 45° angle of attack

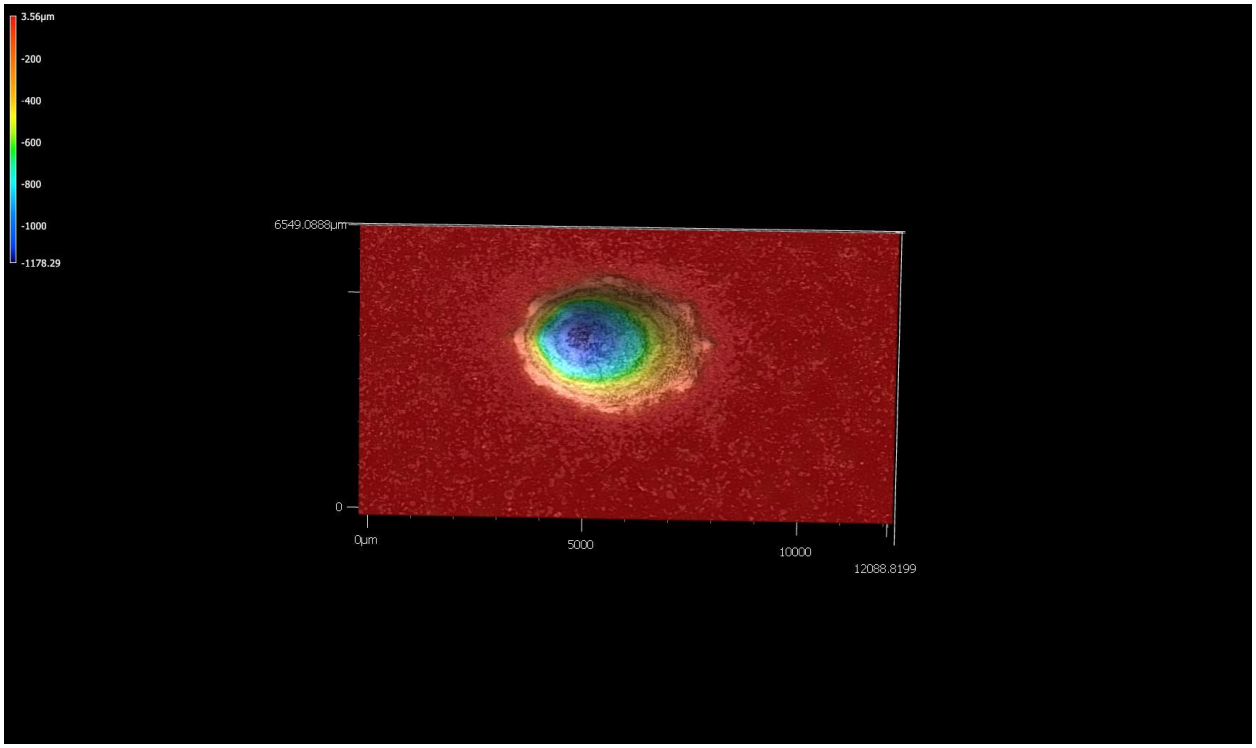


Fig. AII-69: IA-700 coated GFRP erosion scar EXP3 at 45° angle of attack

- 60 degrees

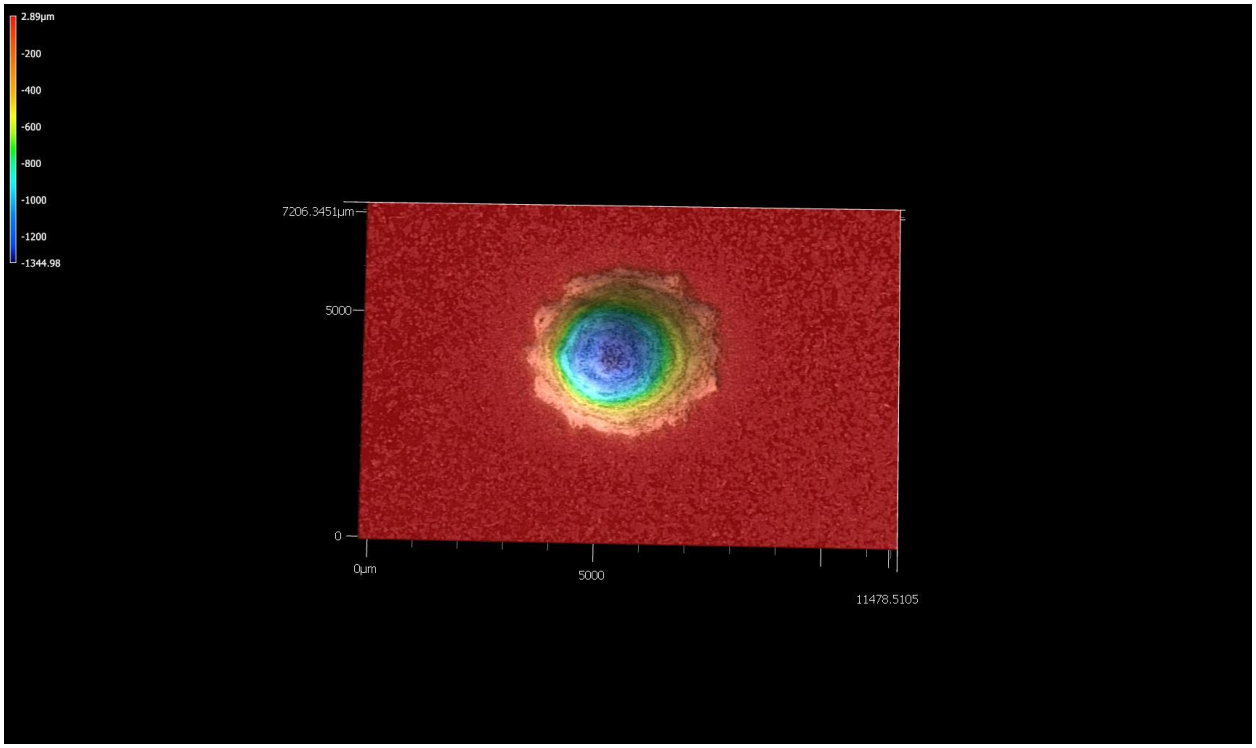


Fig. AII-70: IA-700 coated GFRP erosion scar EXP1 at 60° angle of attack

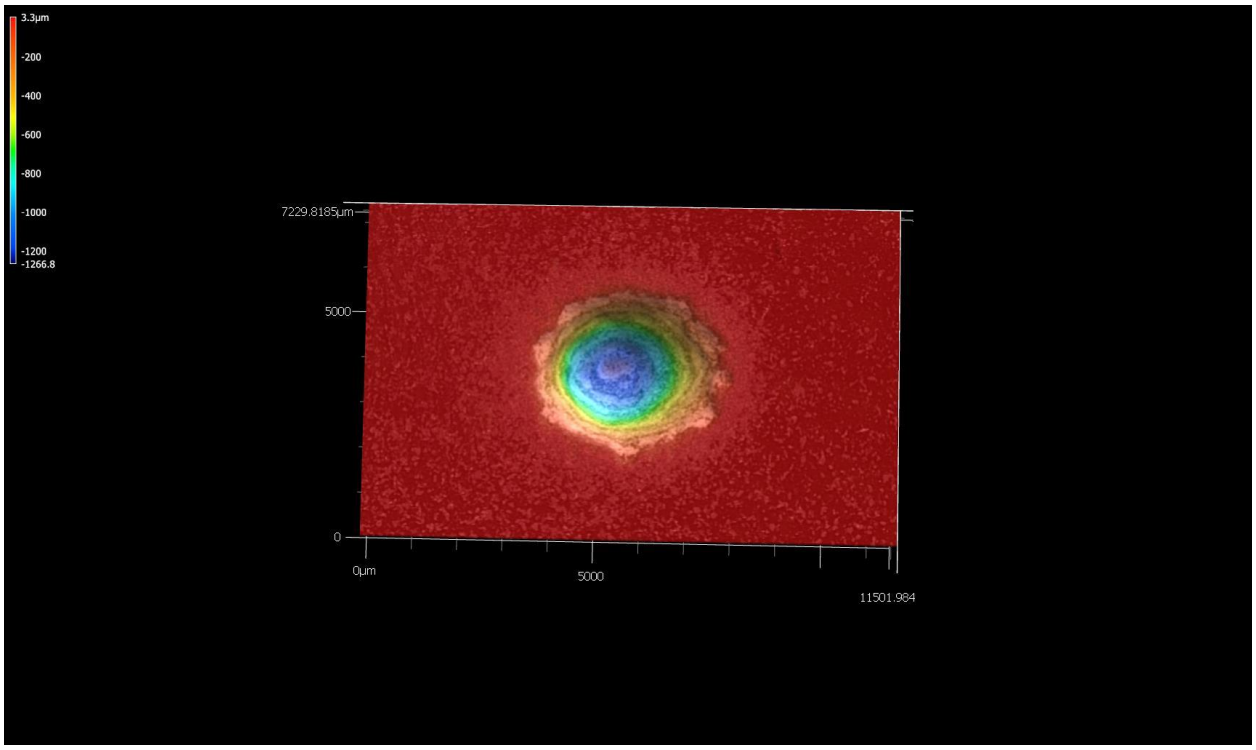


Fig. AII-71: IA-700 coated GFRP erosion scar EXP2 at 60° angle of attack

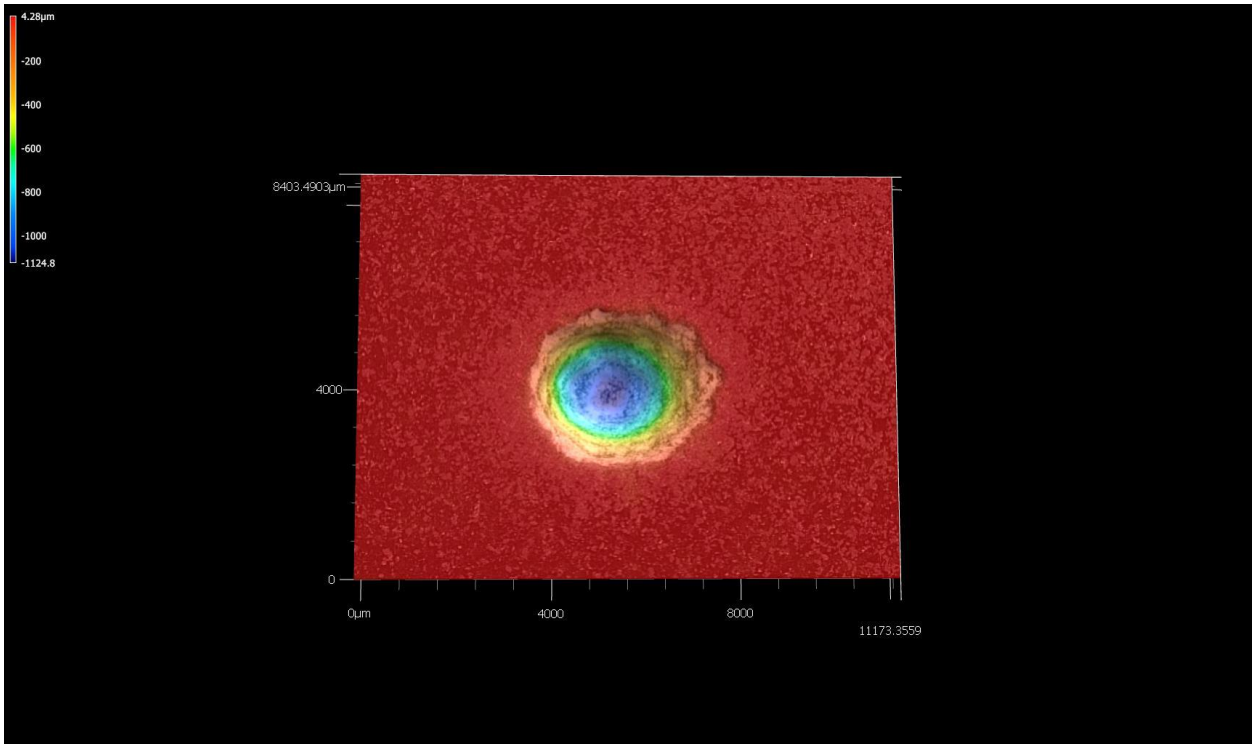


Fig. AII-72: IA-700 coated GFRP erosion scar EXP3 at 60° angle of attack

- 75 degrees

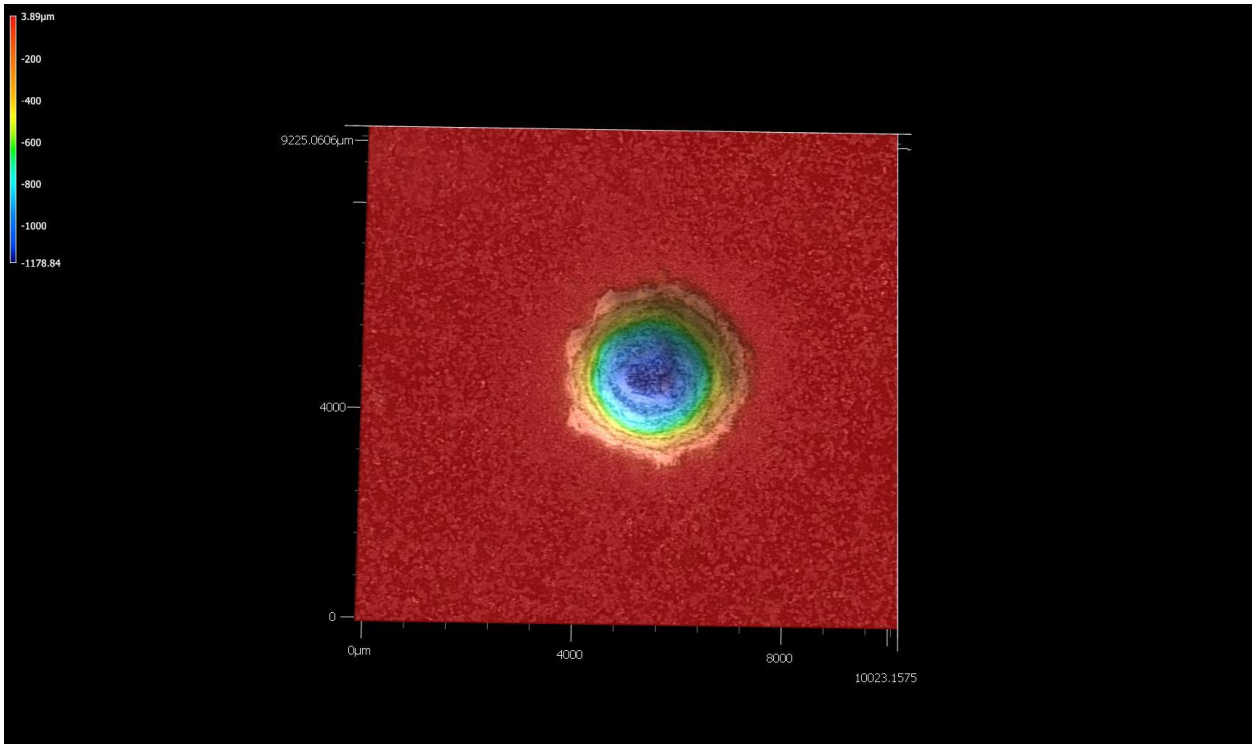


Fig. AII-73: IA-700 coated GFRP erosion scar EXP1 at 75° angle of attack

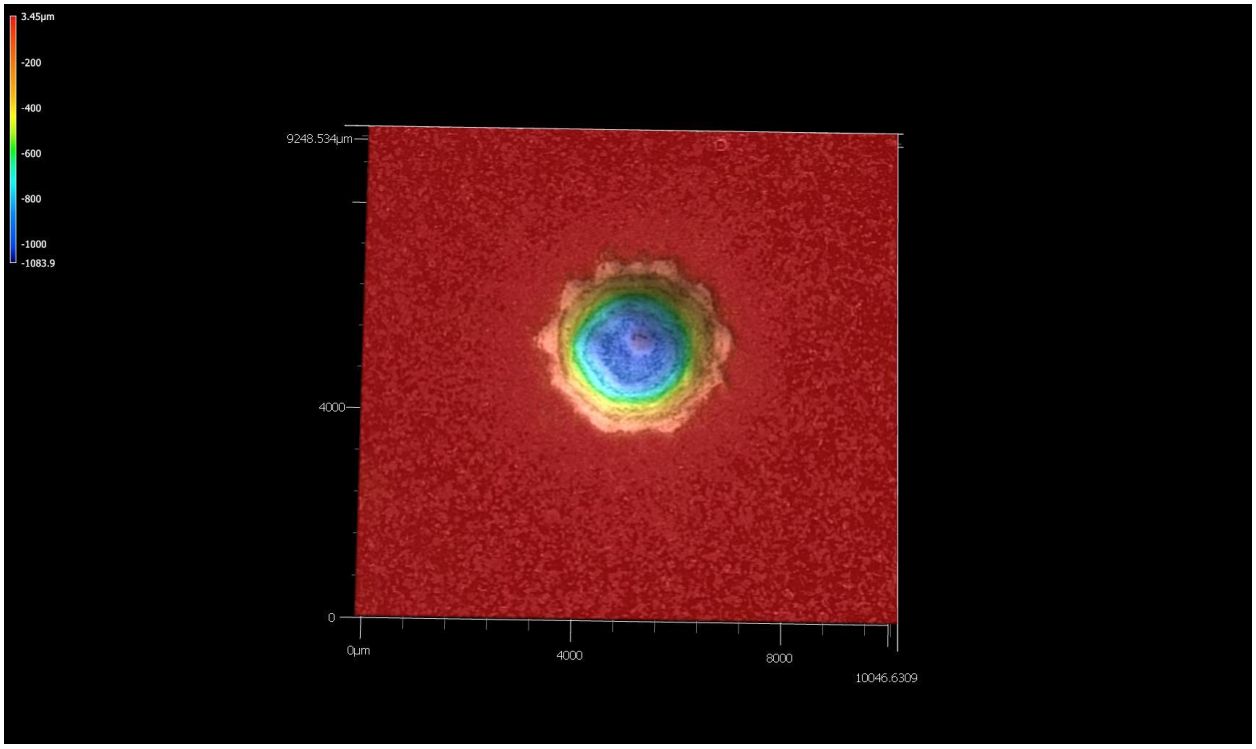


Fig. AII-74: IA-700 coated GFRP erosion scar EXP2 at 75° angle of attack

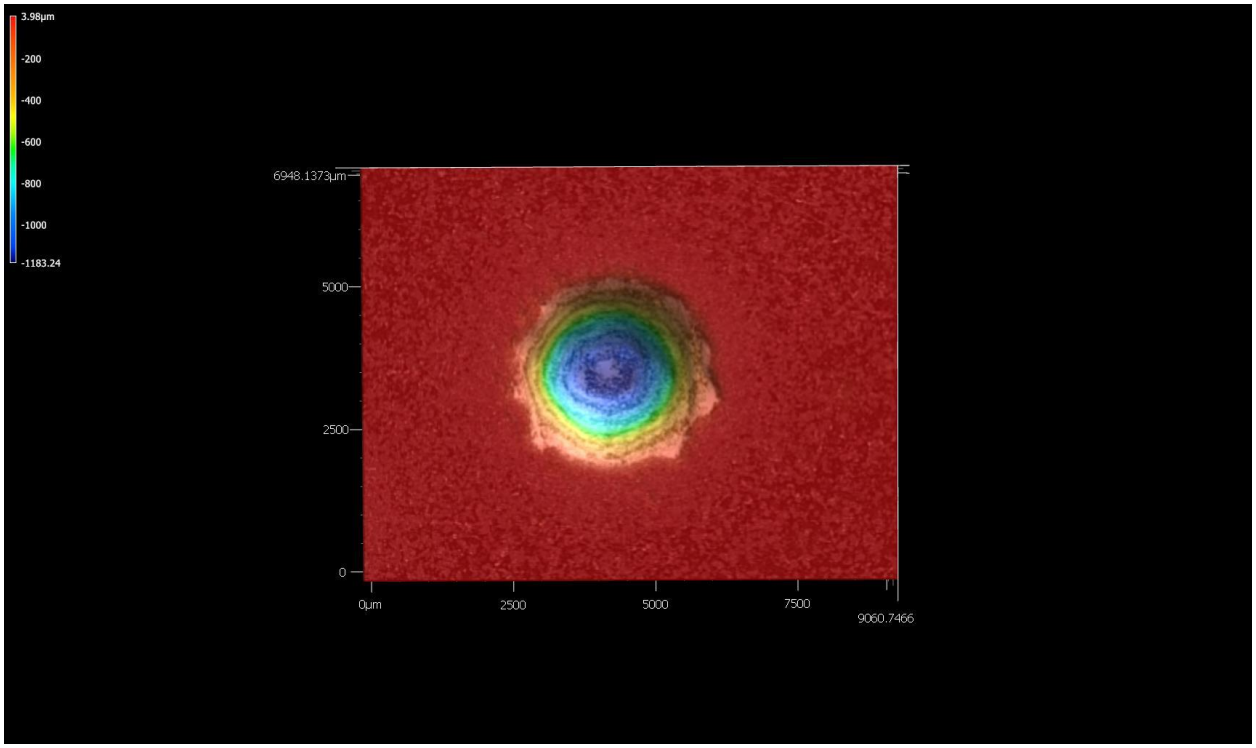


Fig. AII-75: IA-700 coated GFRP erosion scar EXP3 at 75° angle of attack

- 90 degrees

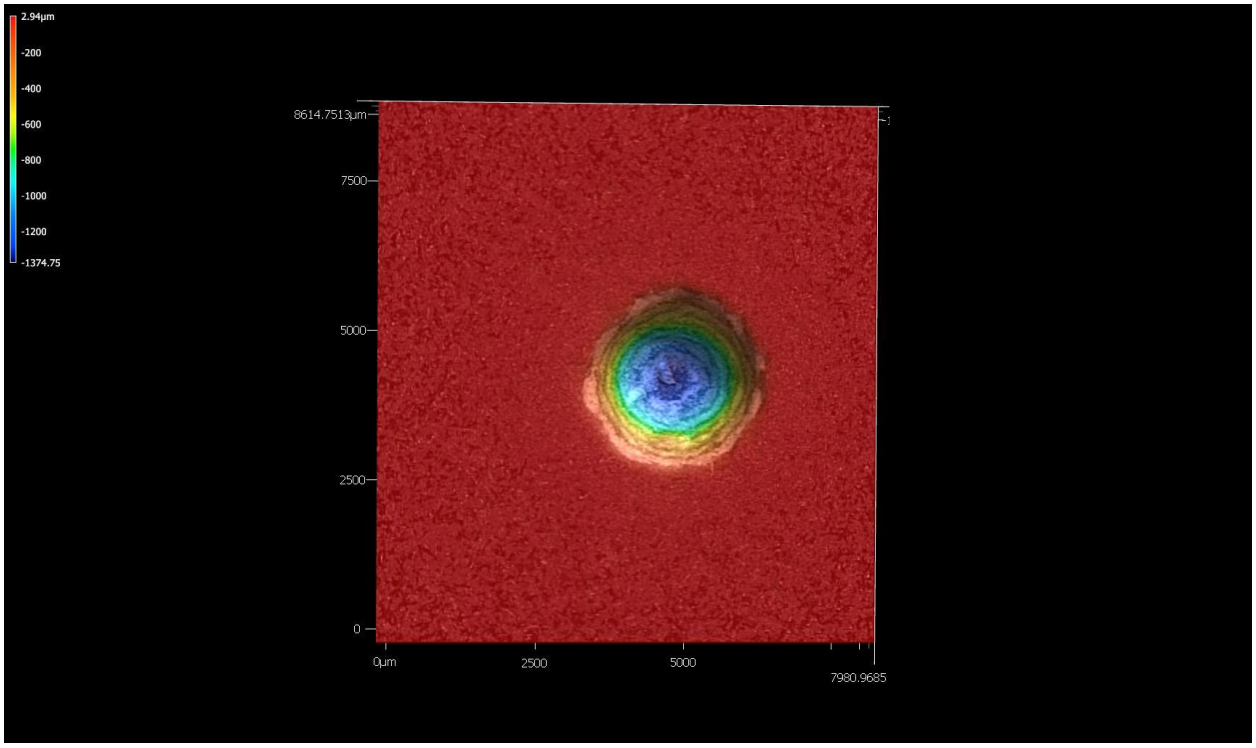


Fig. AII-76: IA-700 coated GFRP erosion scar EXP1 at 90° angle of attack

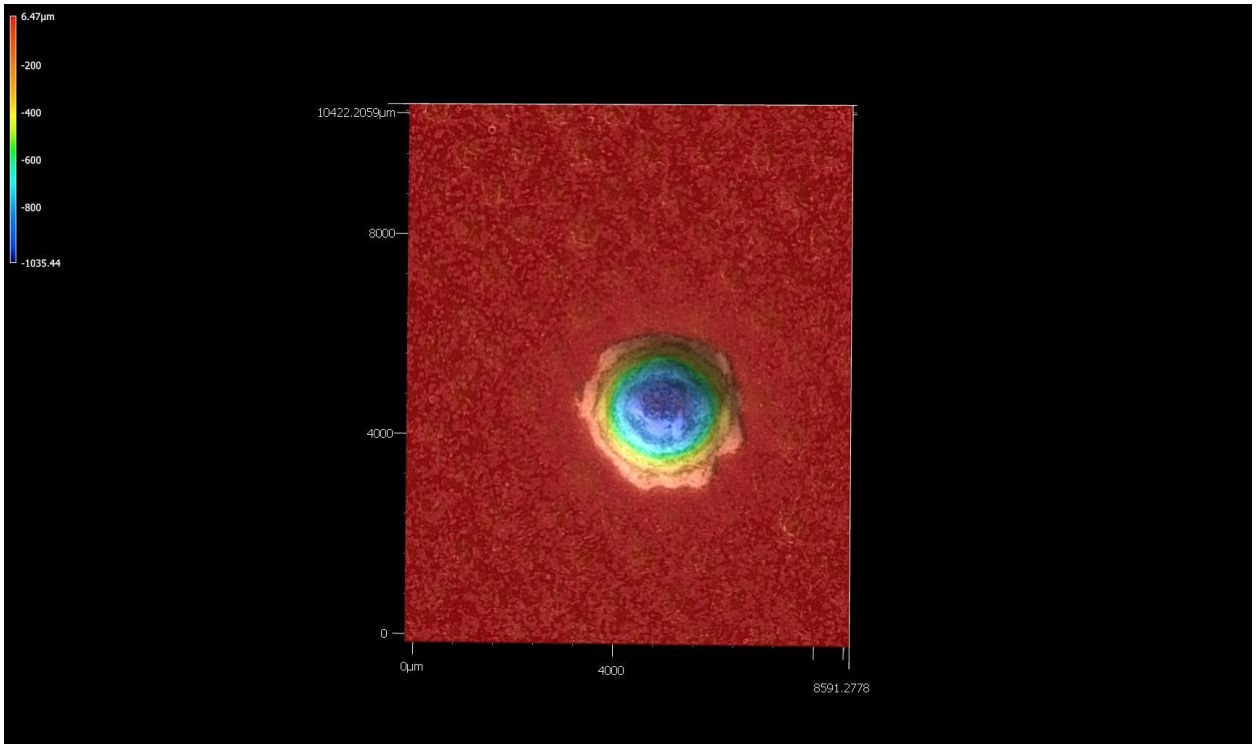


Fig. AII-77: IA-700 coated GFRP erosion scar EXP2 at 90° angle of attack

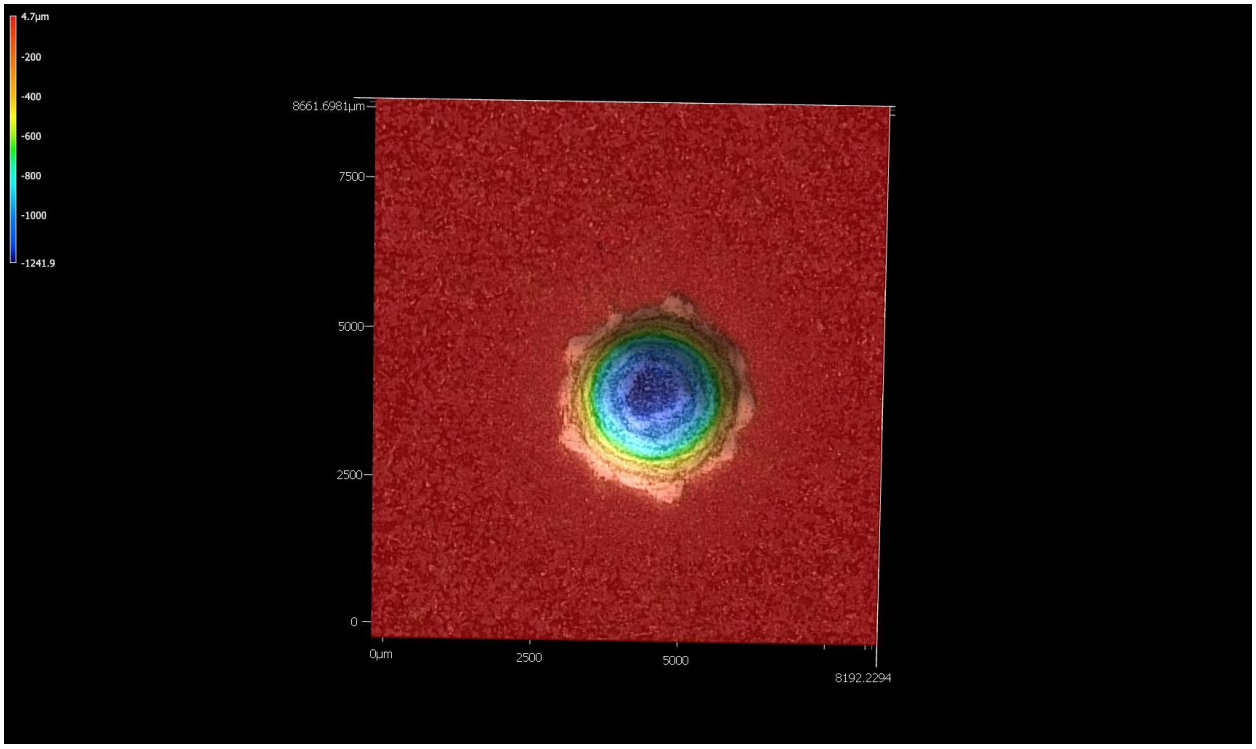


Fig. AII-78: IA-700 coated GFRP erosion scar EXP3 at 90° angle of attack

Polyurethane

- 30 degrees

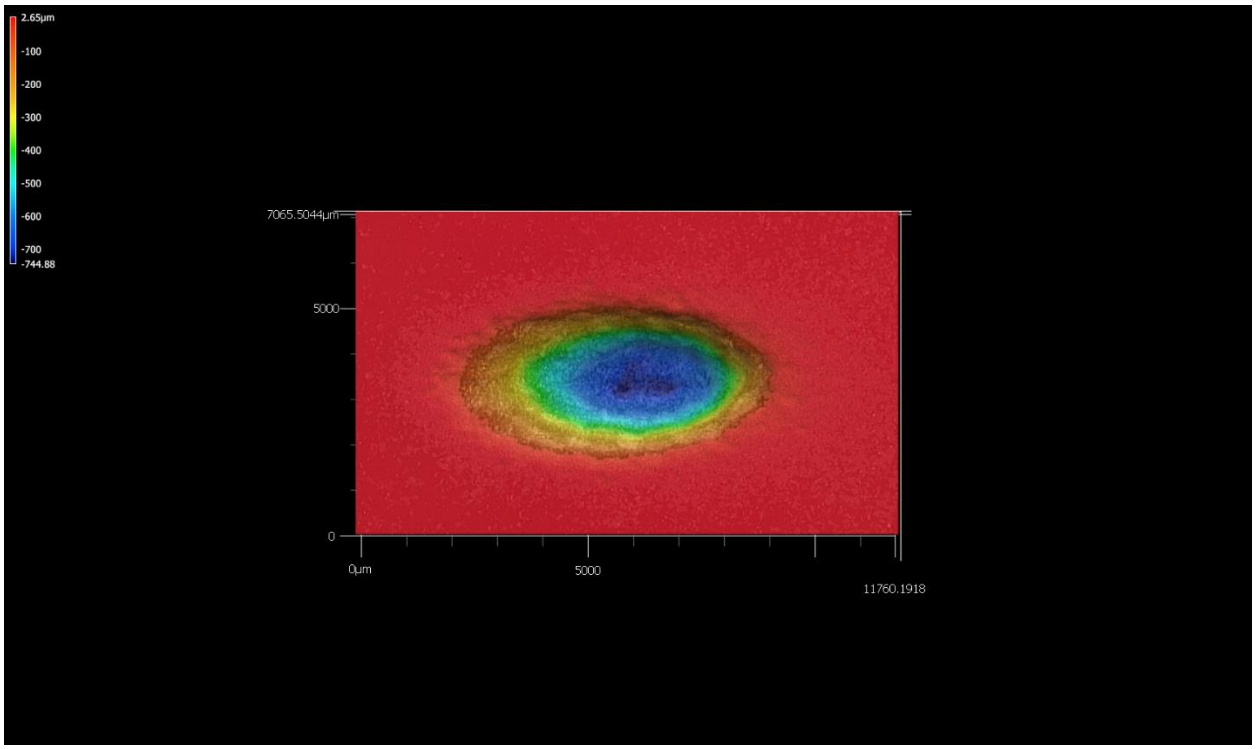


Fig. AII-79: Polyurethane coated GFRP erosion scar EXP1 at 30° angle of attack

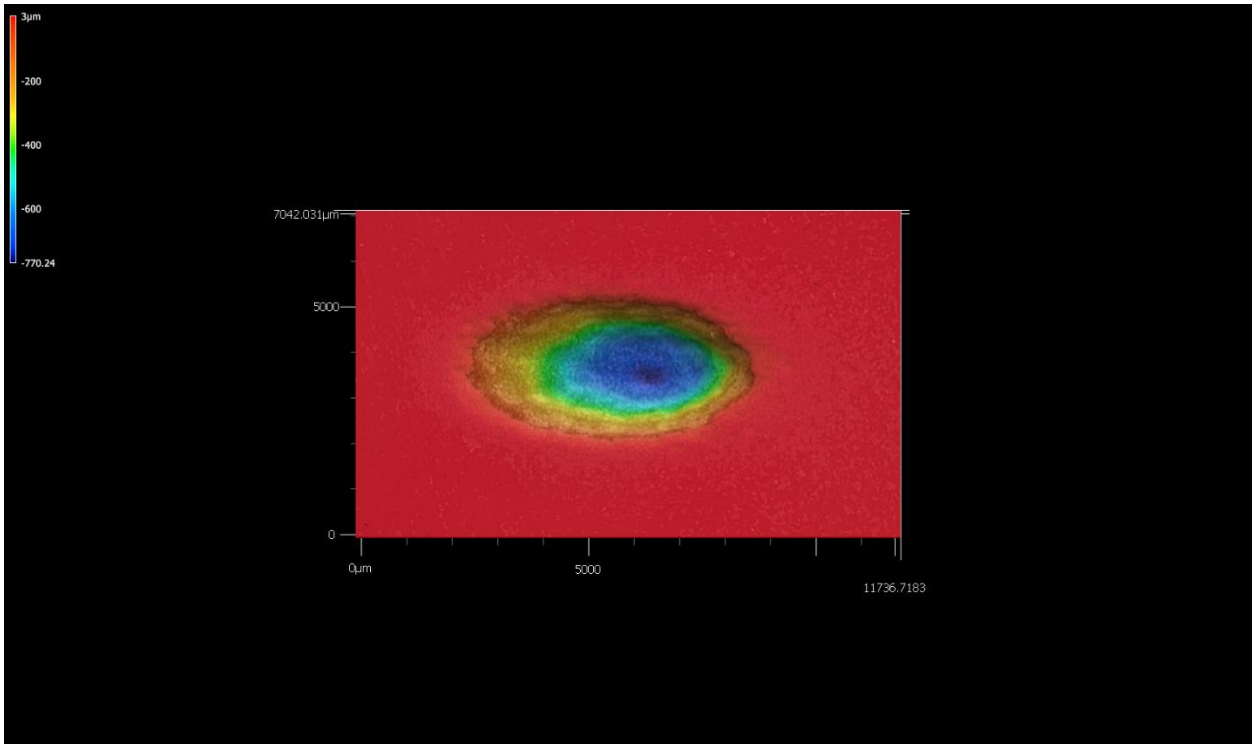


Fig. AII-80: Polyurethane coated GFRP erosion scar EXP2 at 30° angle of attack

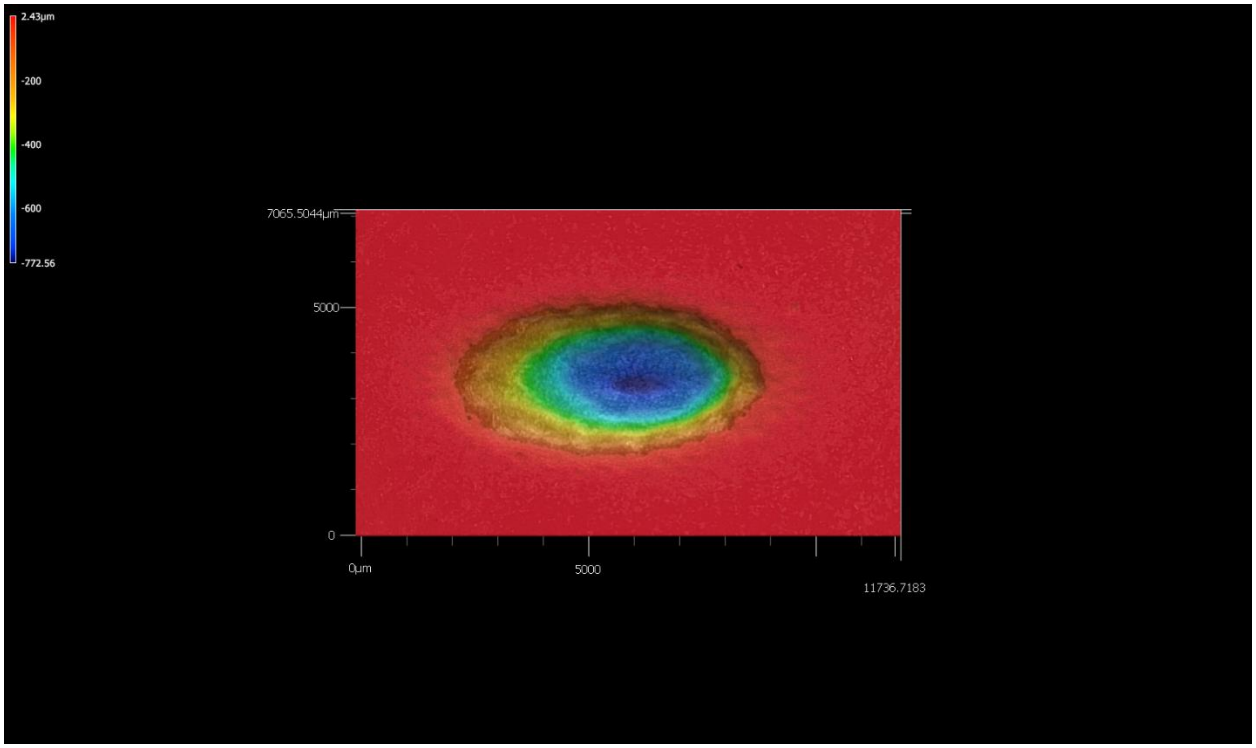


Fig. AII-81: Polyurethane coated GFRP erosion scar EXP3 at 30° angle of attack

- 45 degrees

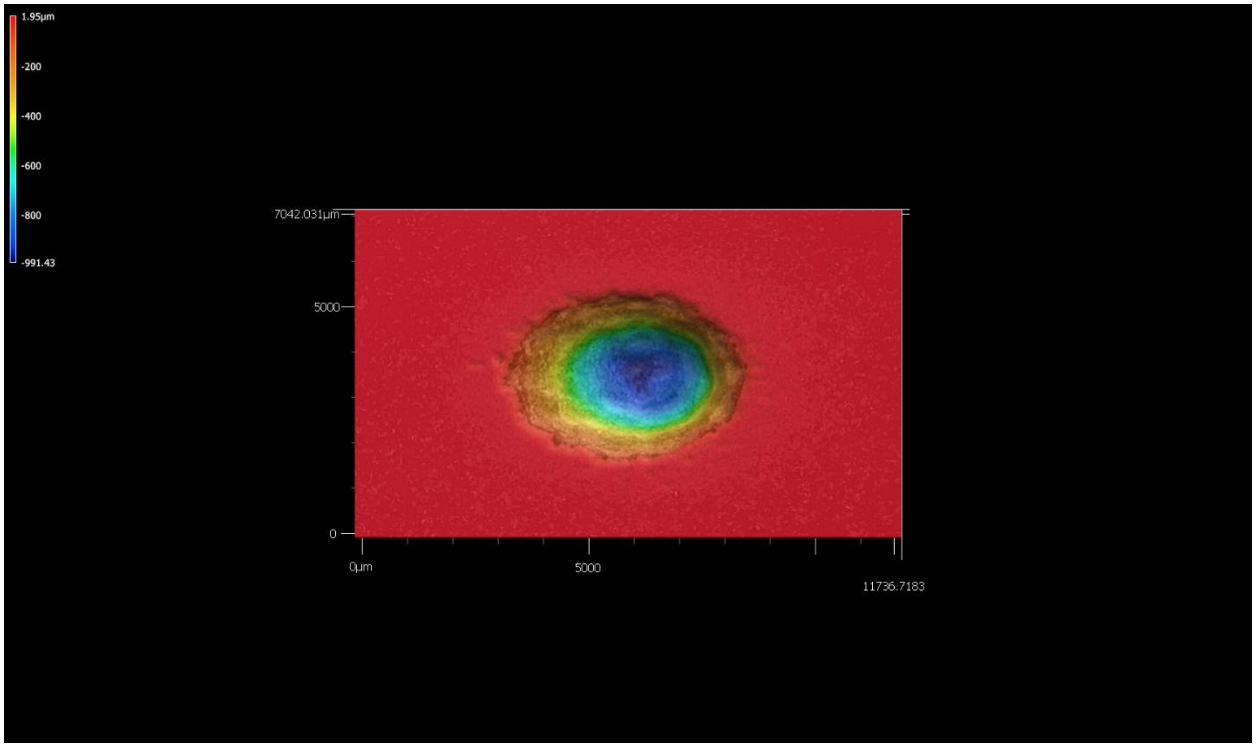


Fig. AII-82: Polyurethane coated GFRP erosion scar EXP1 at 45° angle of attack

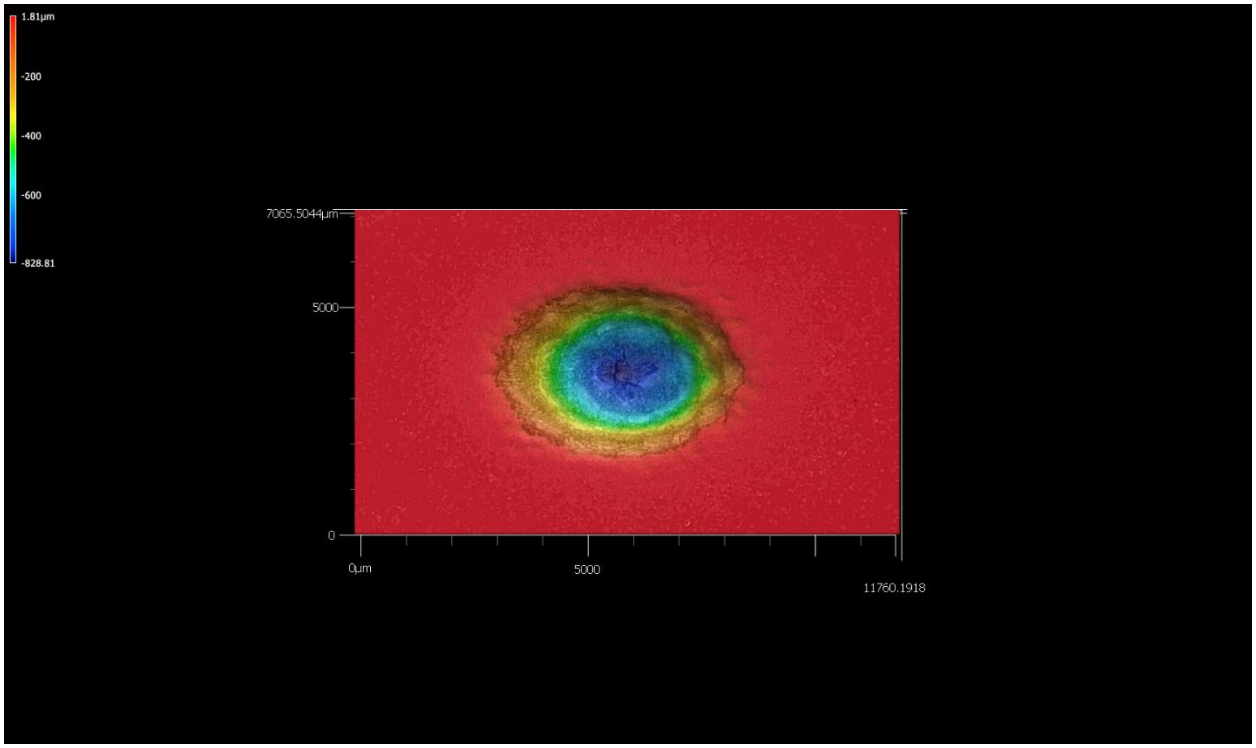


Fig. AII-83: Polyurethane coated GFRP erosion scar EXP2 at 45° angle of attack

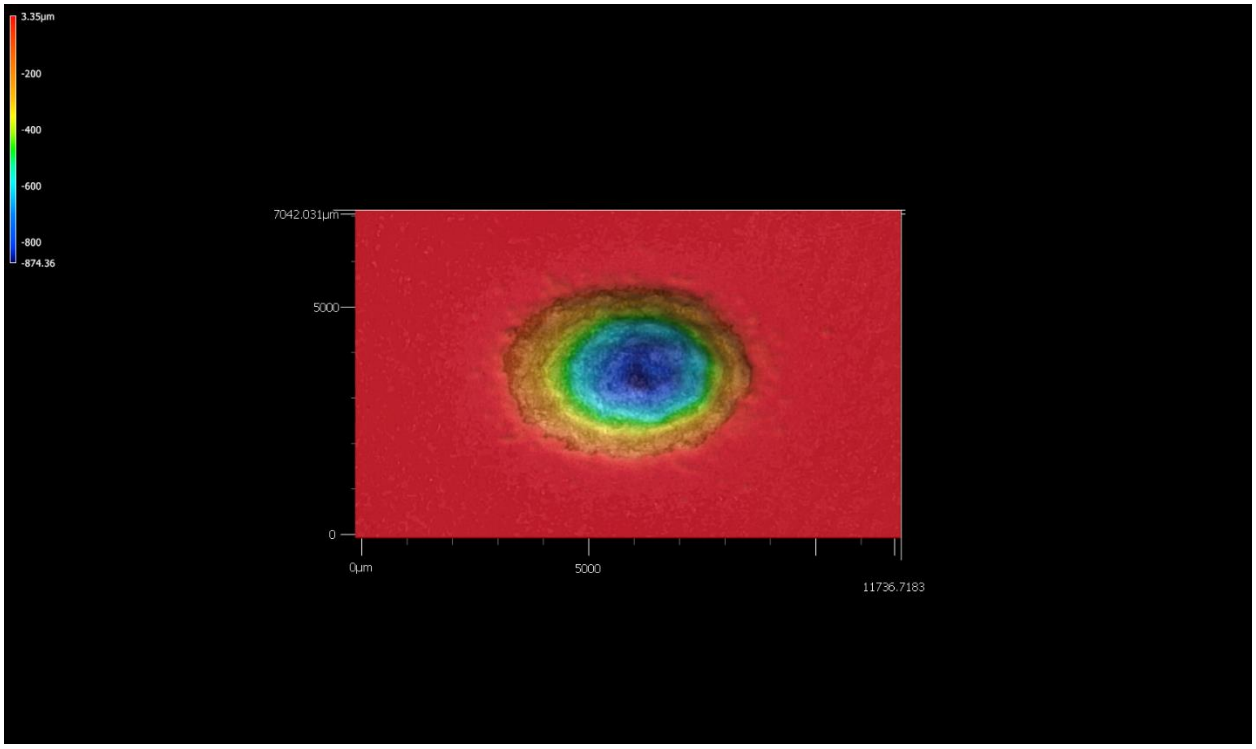


Fig. AII-84: Polyurethane coated GFRP erosion scar EXP3 at 45° angle of attack

- 60 degrees

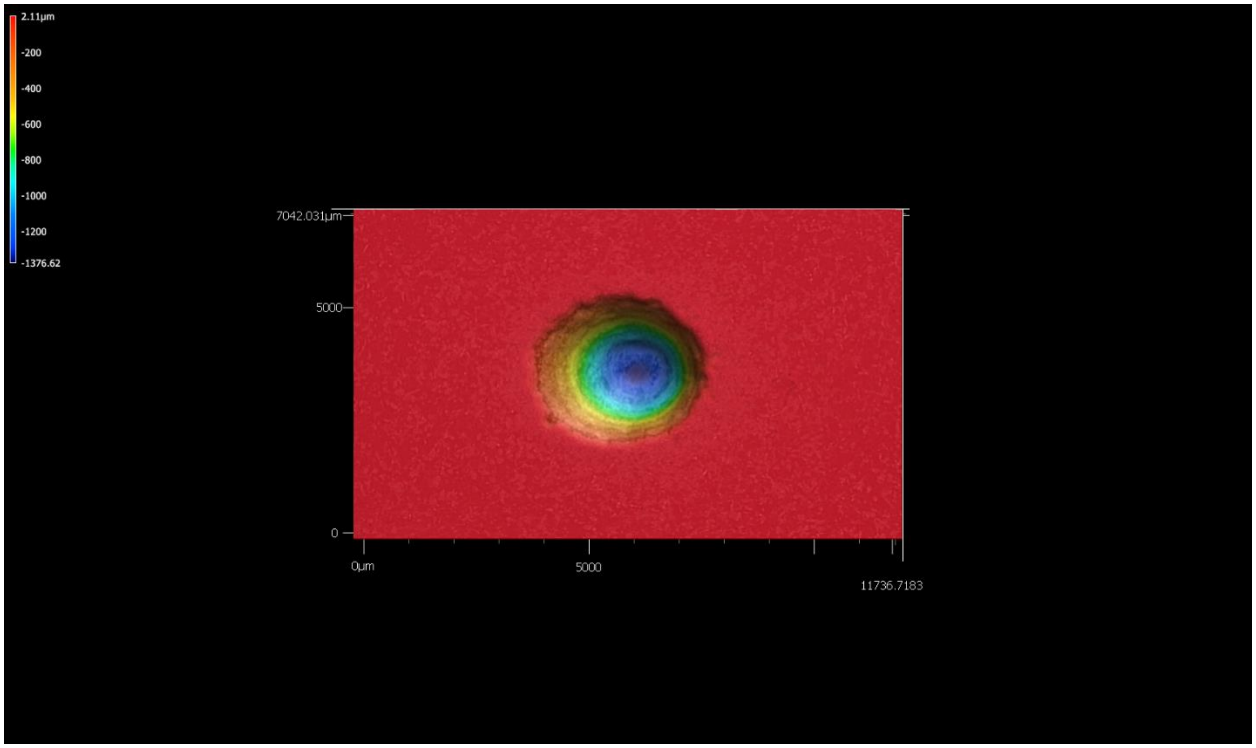


Fig. AII-85: Polyurethane coated GFRP erosion scar EXP1 at 60° angle of attack

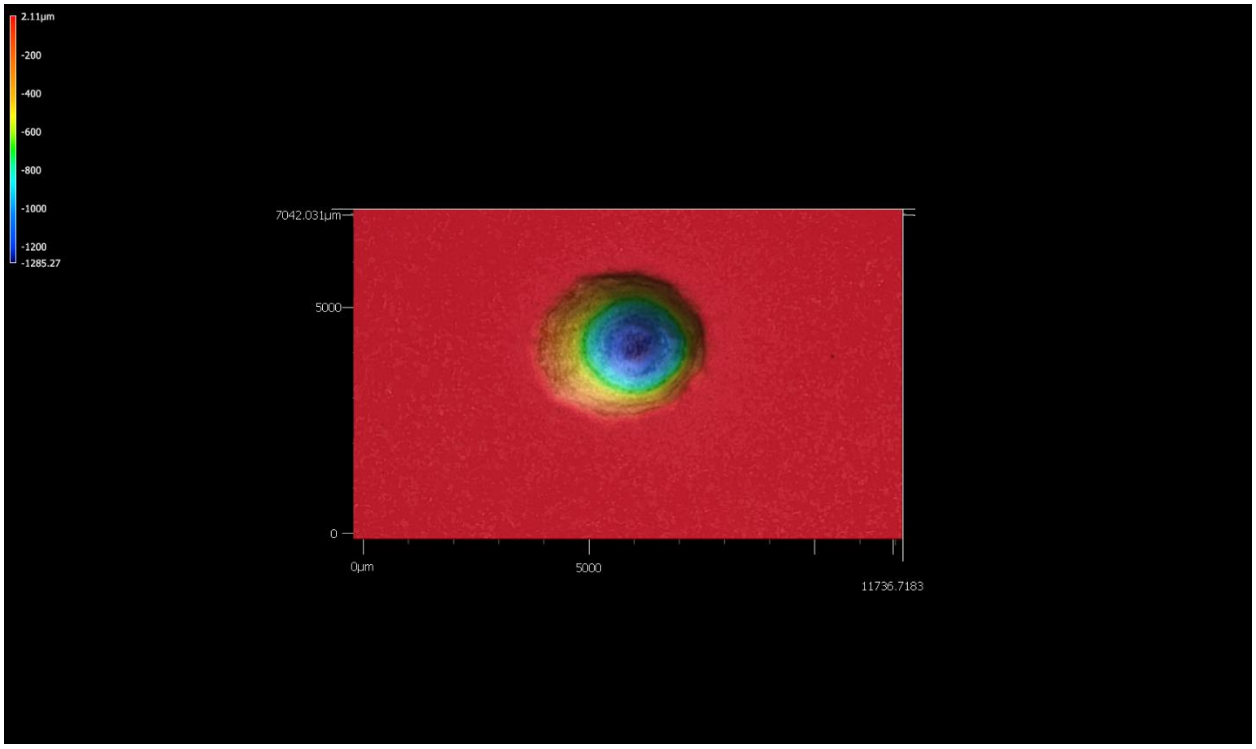


Fig. AII-86: Polyurethane coated GFRP erosion scar EXP2 at 60° angle of attack

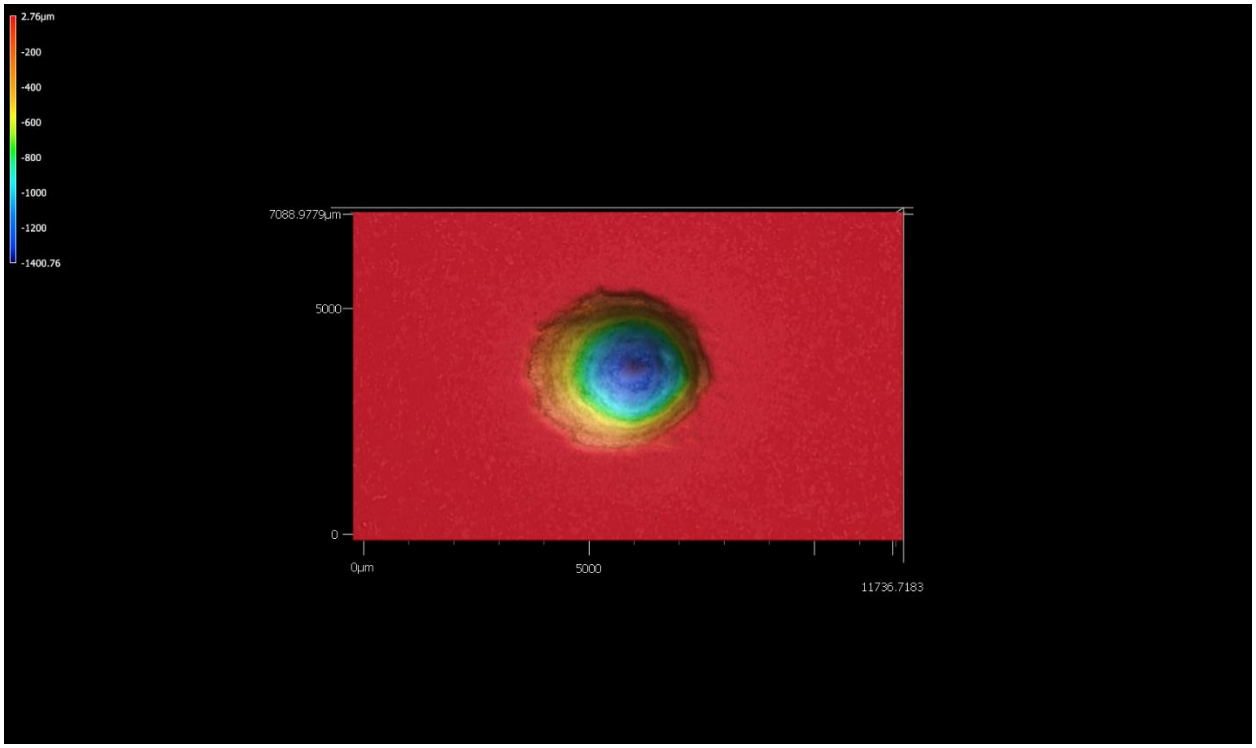


Fig. AII-87: Polyurethane coated GFRP erosion scar EXP3 at 60° angle of attack

- 75 degrees

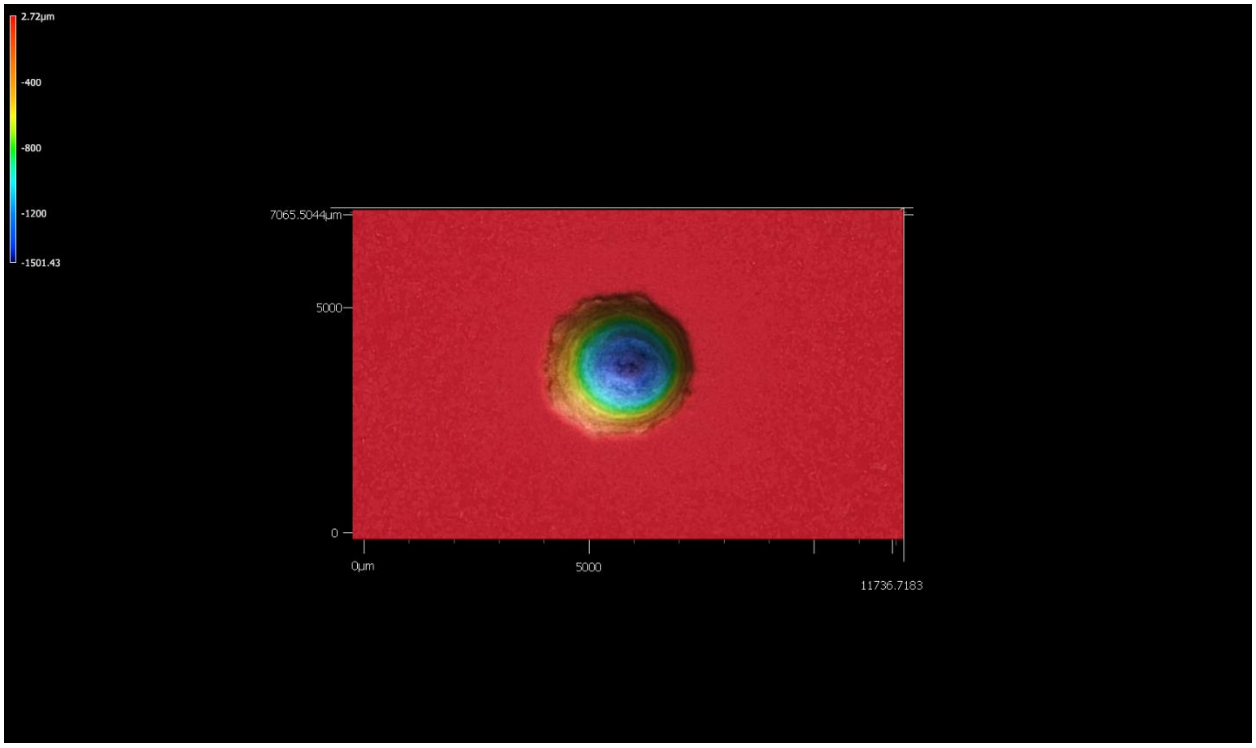


Fig. AII-88: Polyurethane coated GFRP erosion scar EXP1 at 75° angle of attack

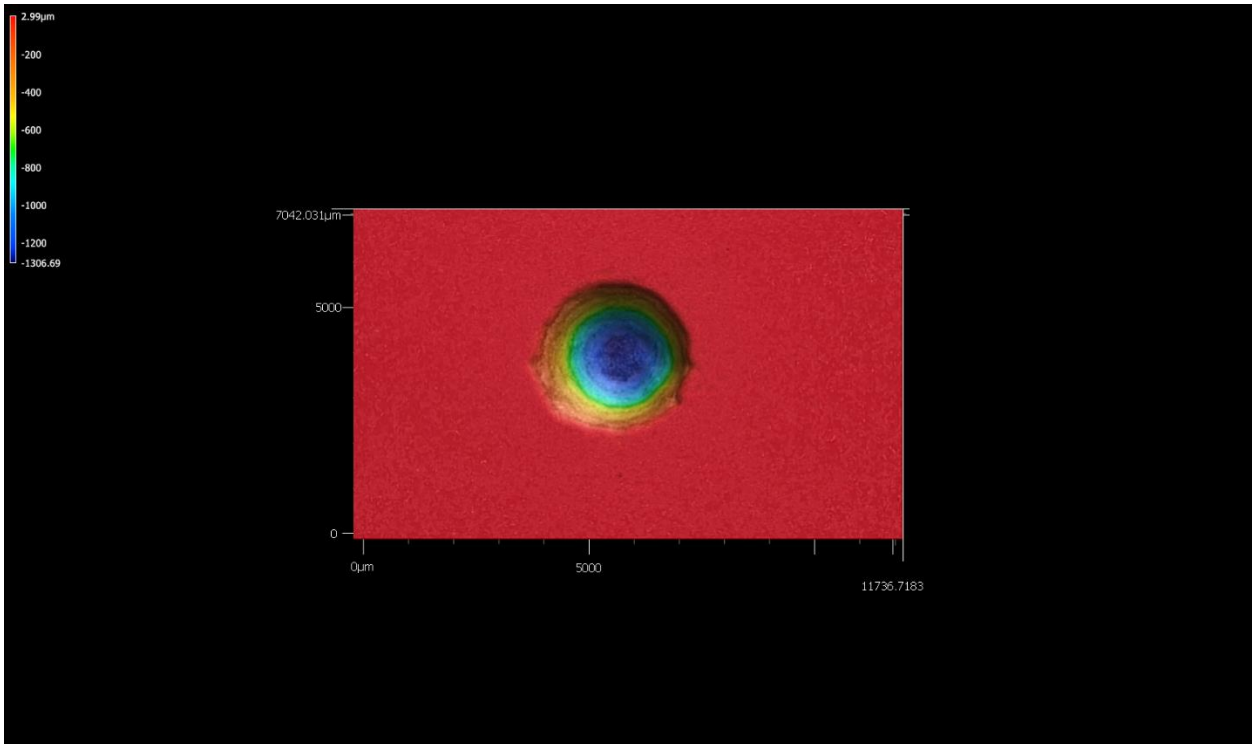


Fig. AII-89: Polyurethane coated GFRP erosion scar EXP2 at 75° angle of attack

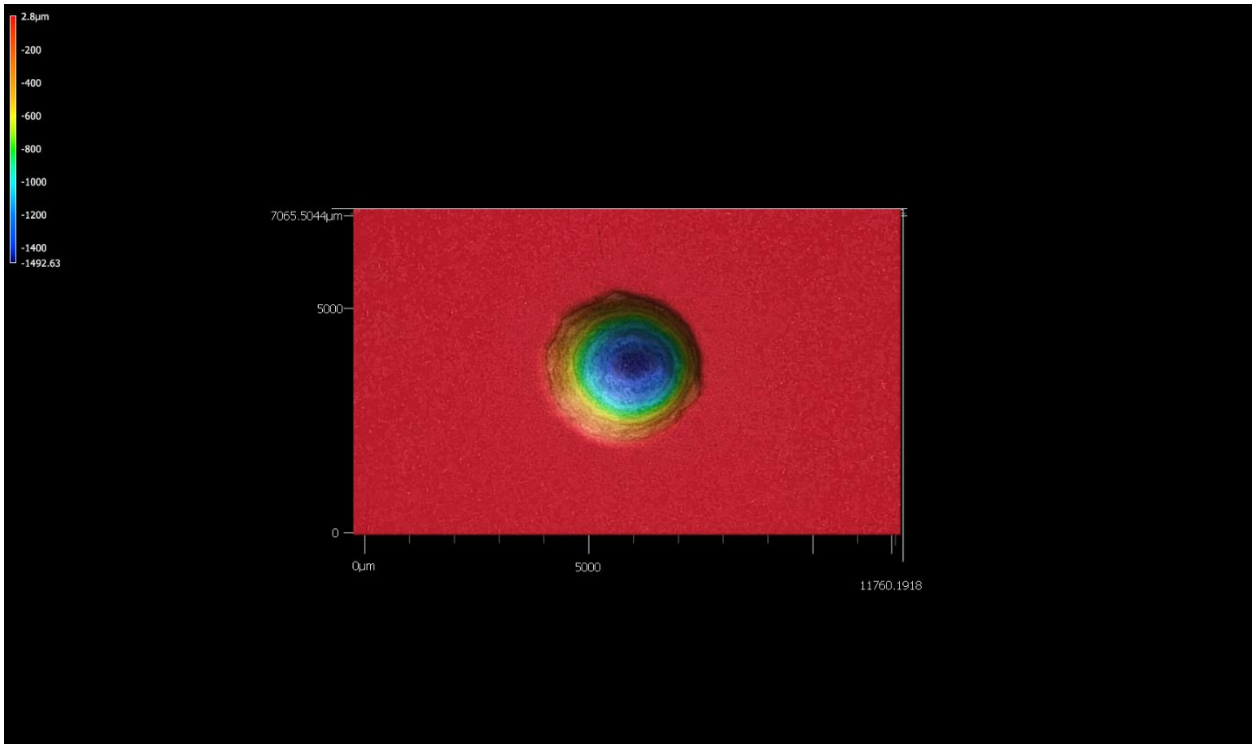


Fig. AII-90: Polyurethane coated GFRP erosion scar EXP3 at 75° angle of attack

- 90 degrees

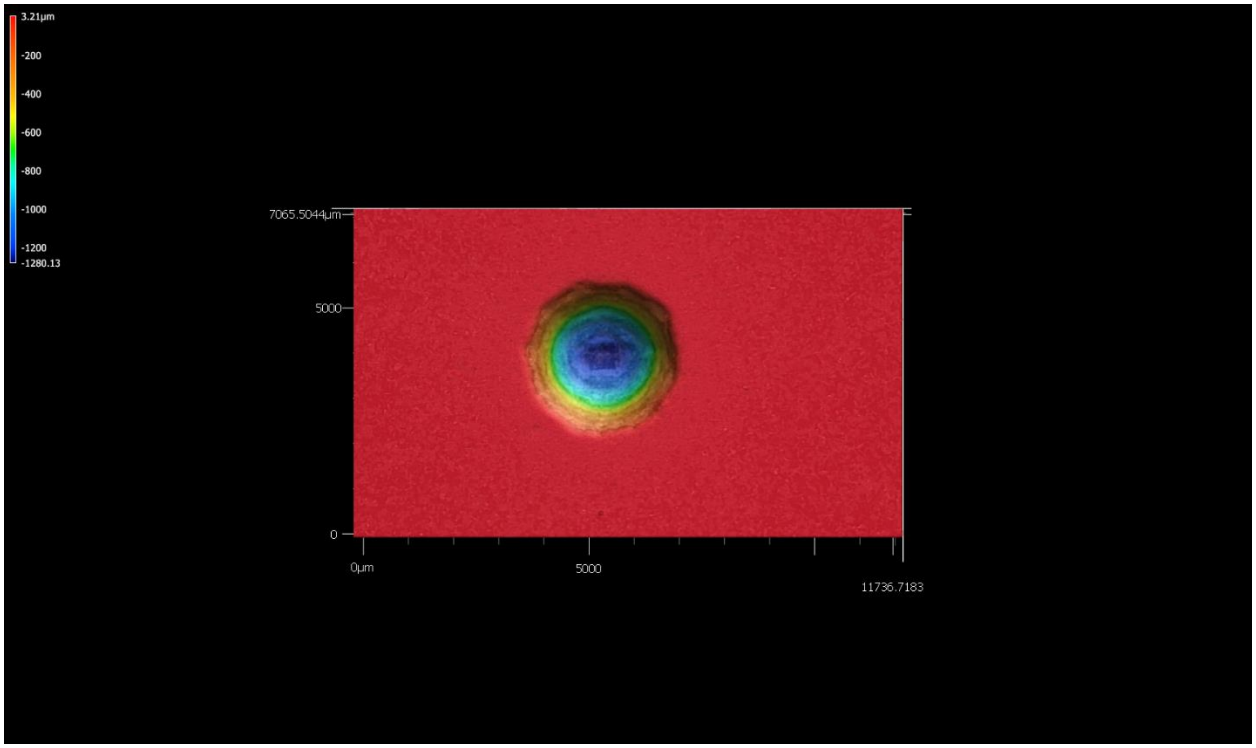


Fig. AII-91: Polyurethane coated GFRP erosion scar EXP1 at 90° angle of attack

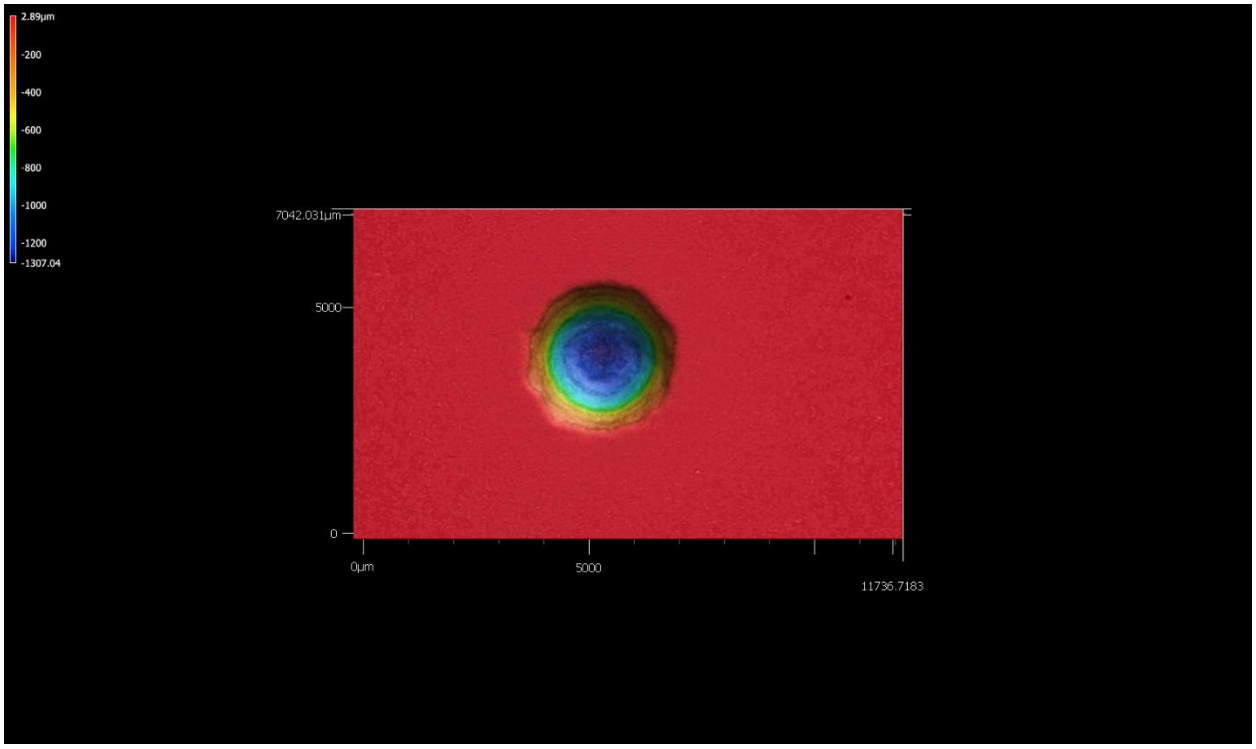


Fig. AII-92: Polyurethane coated GFRP erosion scar EXP2 at 90° angle of attack

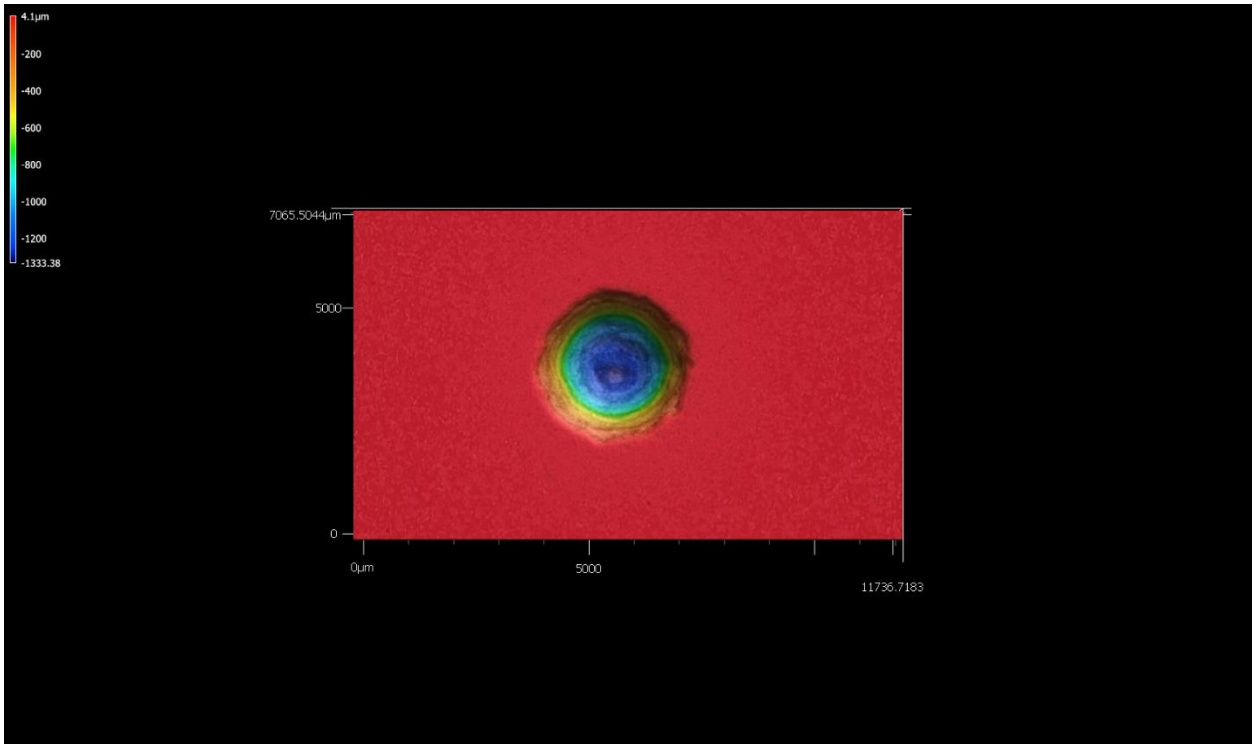


Fig. AII-93: Polyurethane coated GFRP erosion scar EXP3 at 90° angle of attack

Coating 4 (H-146/Polyurethane)

- 30 degrees

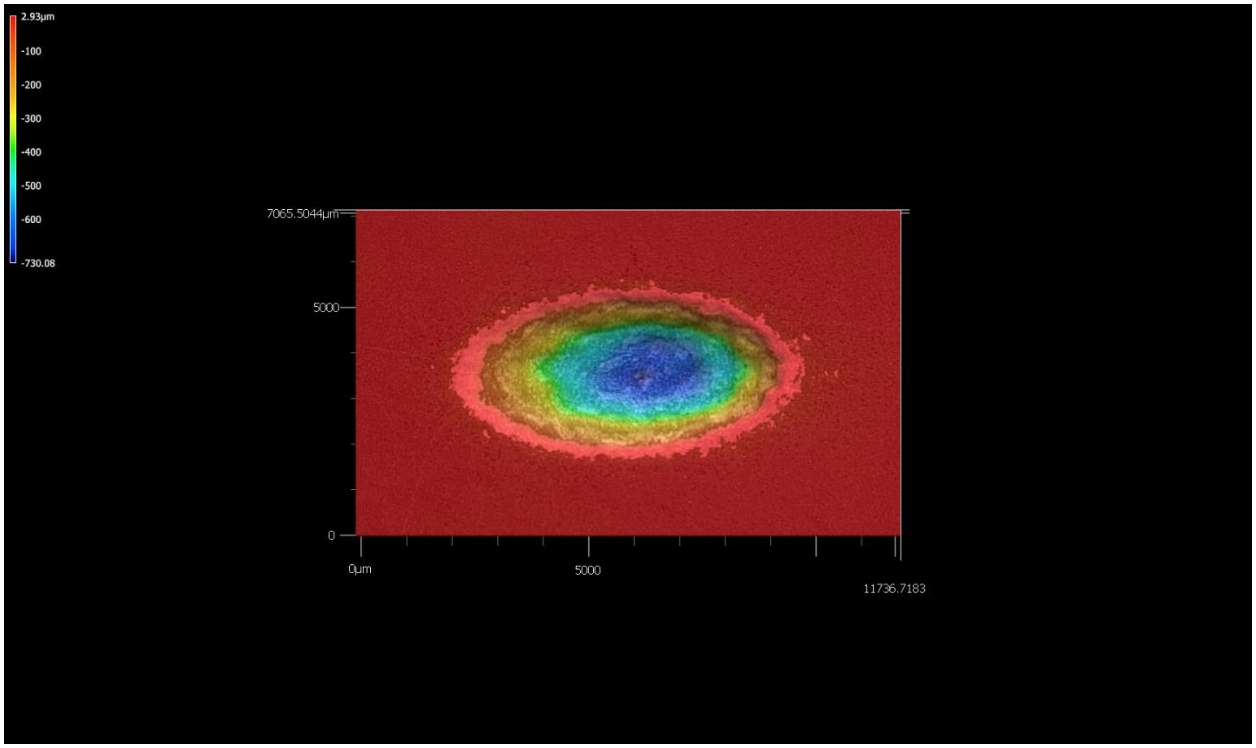


Fig. AII-94: H-146/Polyurethane coated GFRP erosion scar EXP1 at 30° angle of attack

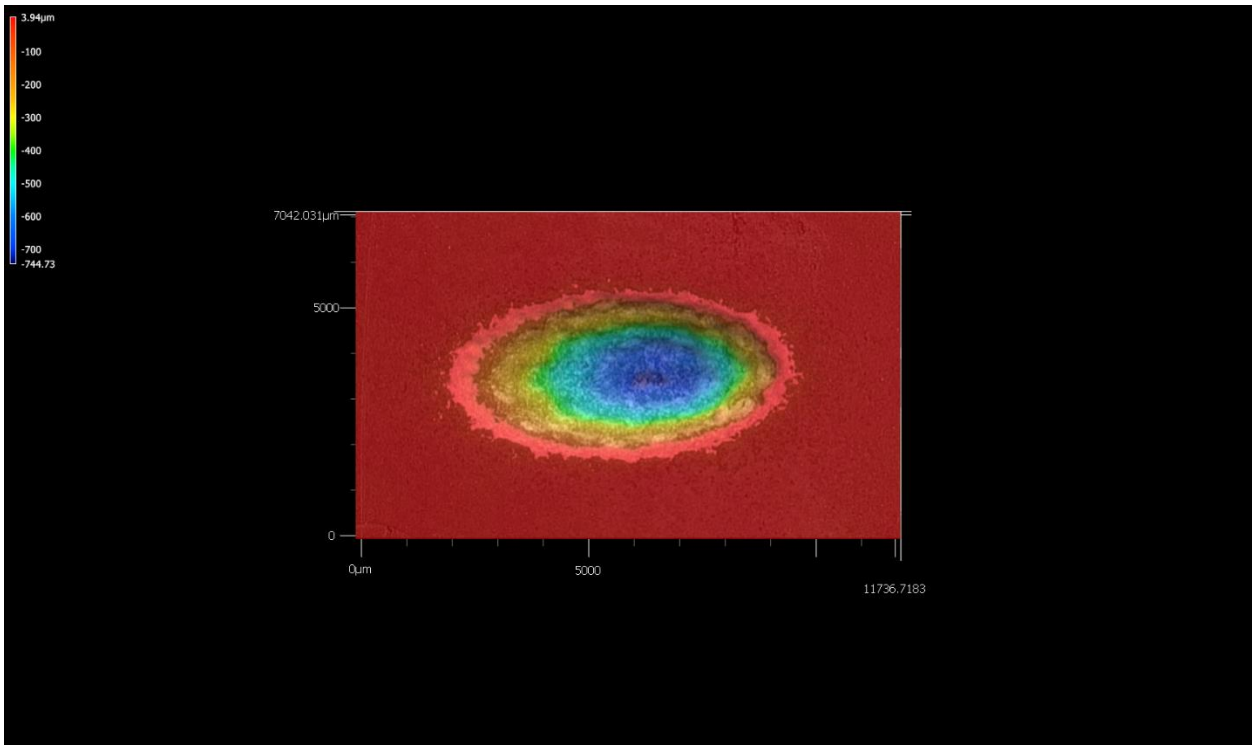


Fig. AII-95: H-146/Polyurethane coated GFRP erosion scar EXP2 at 30° angle of attack

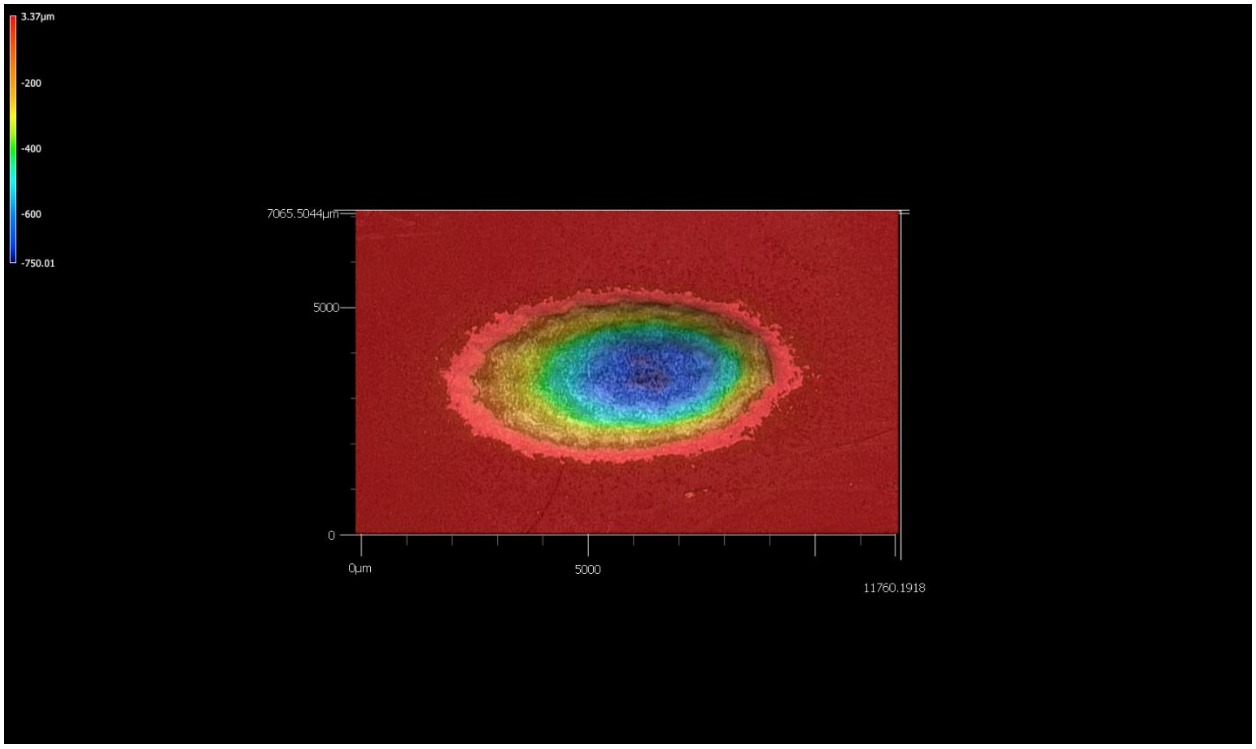


Fig. AII-96: H-146/Polyurethane coated GFRP erosion scar EXP3 at 30° angle of attack

- 45 degrees

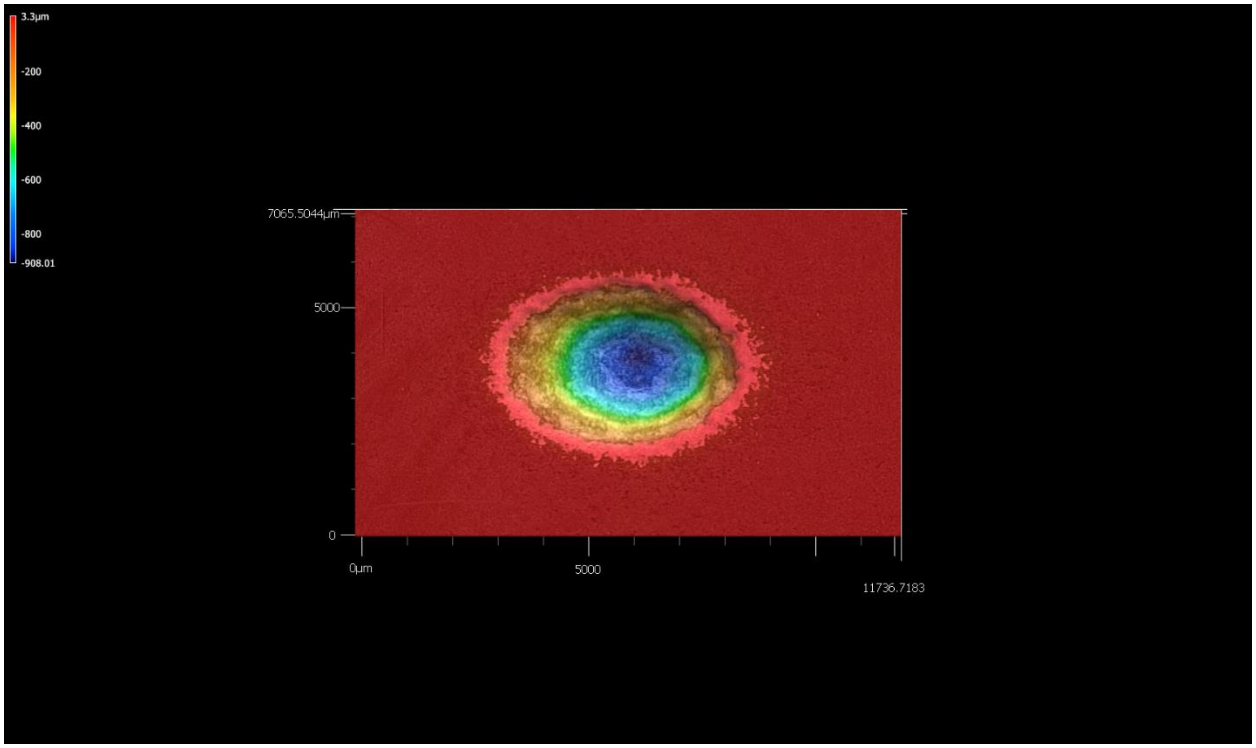


Fig. AII-97: H-146/Polyurethane coated GFRP erosion scar EXP1 at 45° angle of attack

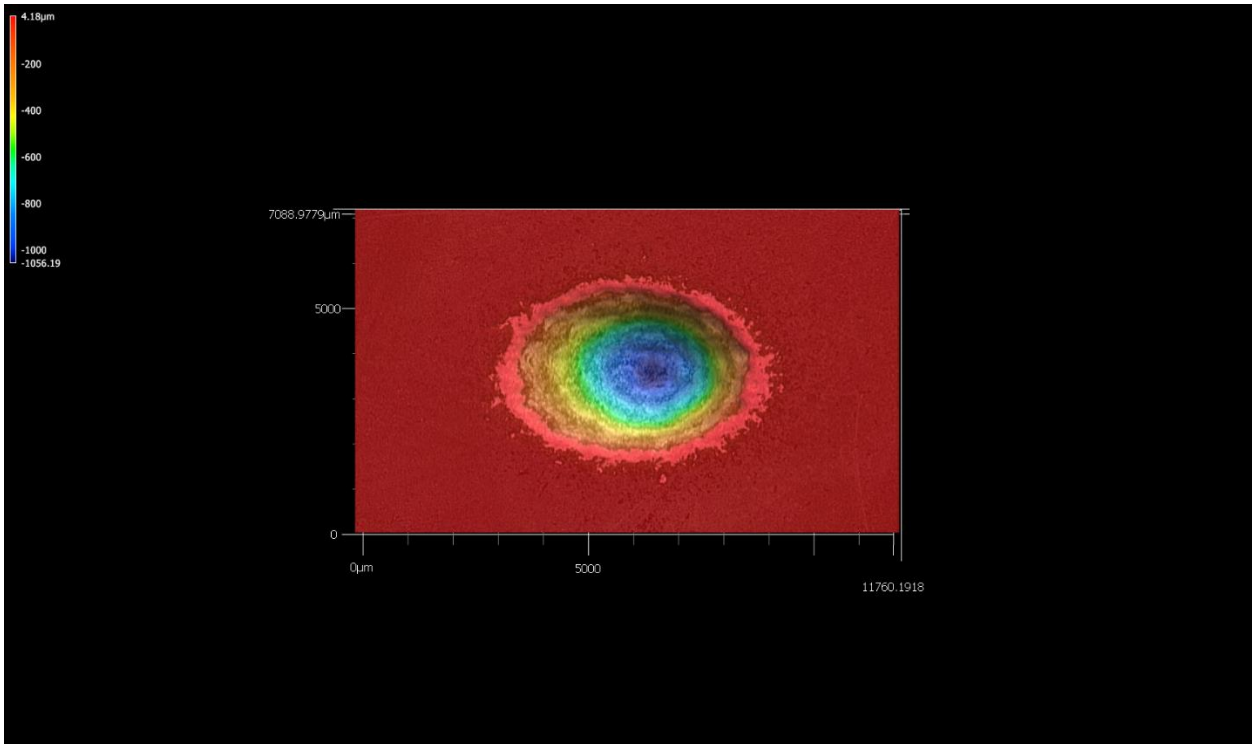


Fig. AII-98: H-146/Polyurethane coated GFRP erosion scar EXP2 at 45° angle of attack

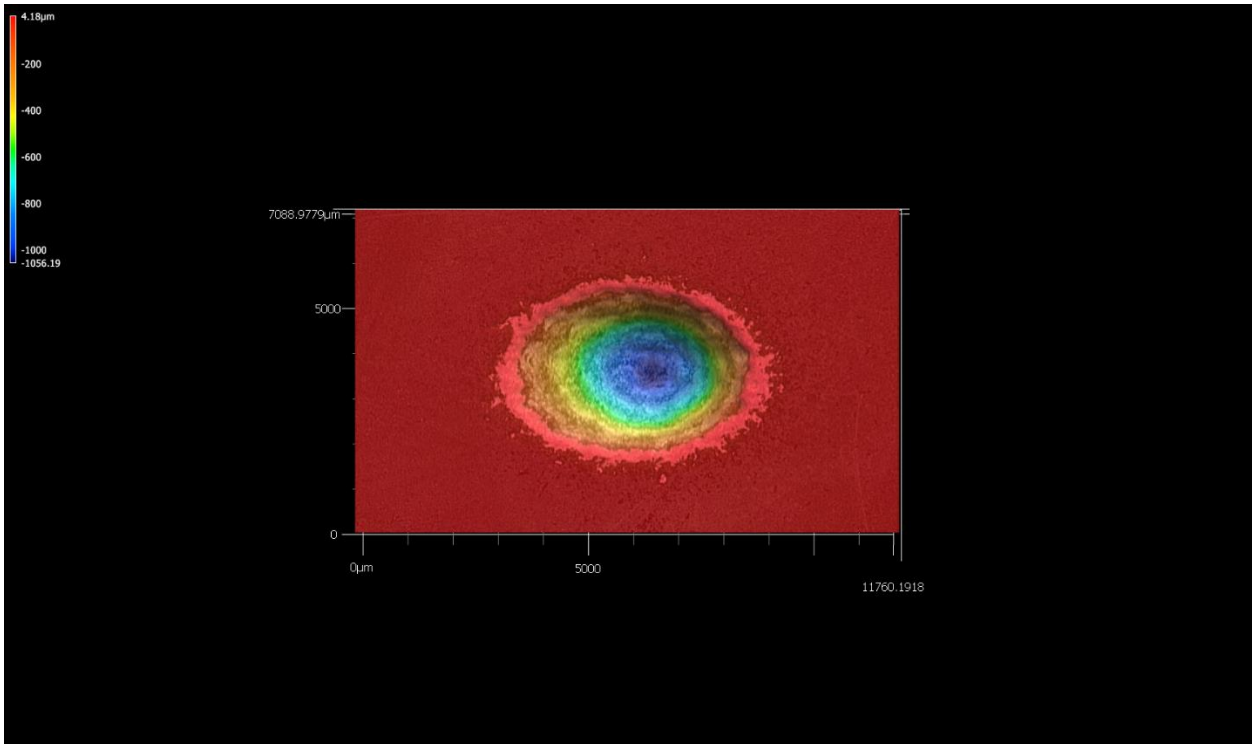


Fig. AII-99: H-146/Polyurethane coated GFRP erosion scar EXP3 at 45° angle of attack

- 60 degrees

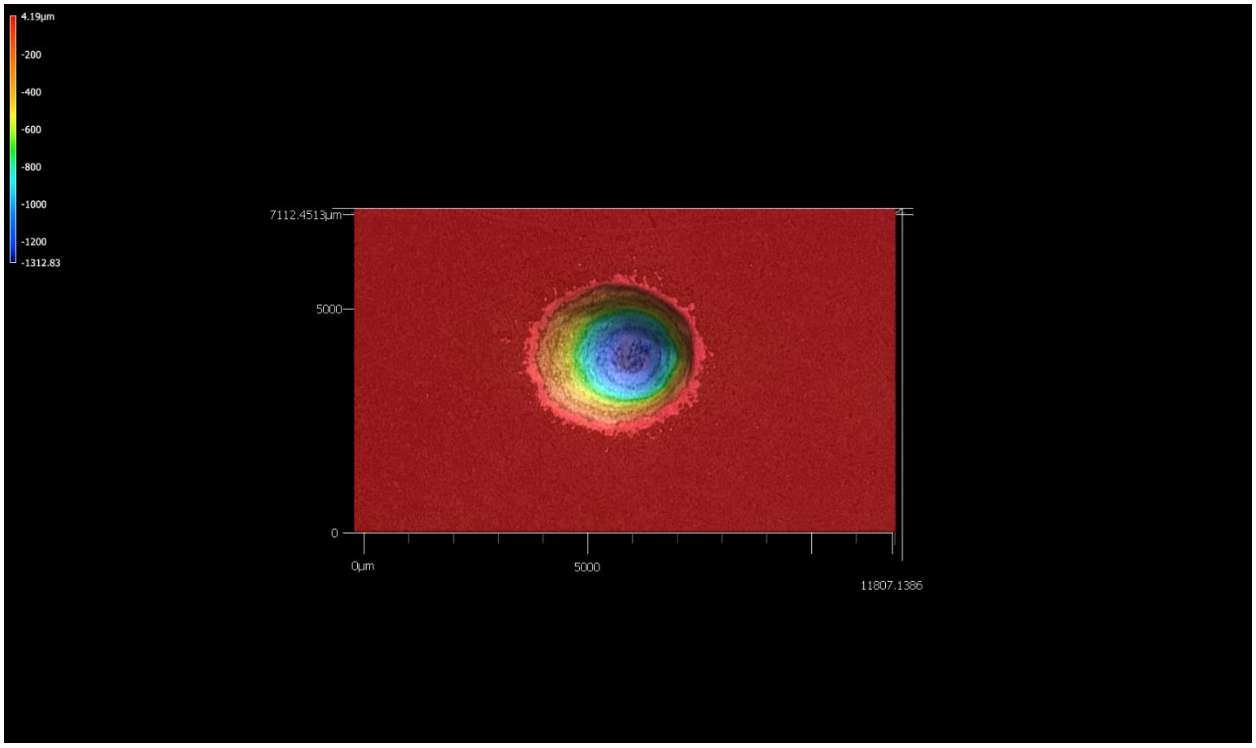


Fig. AII-100: H-146/Polyurethane coated GFRP erosion scar EXP1 at 60° angle of attack

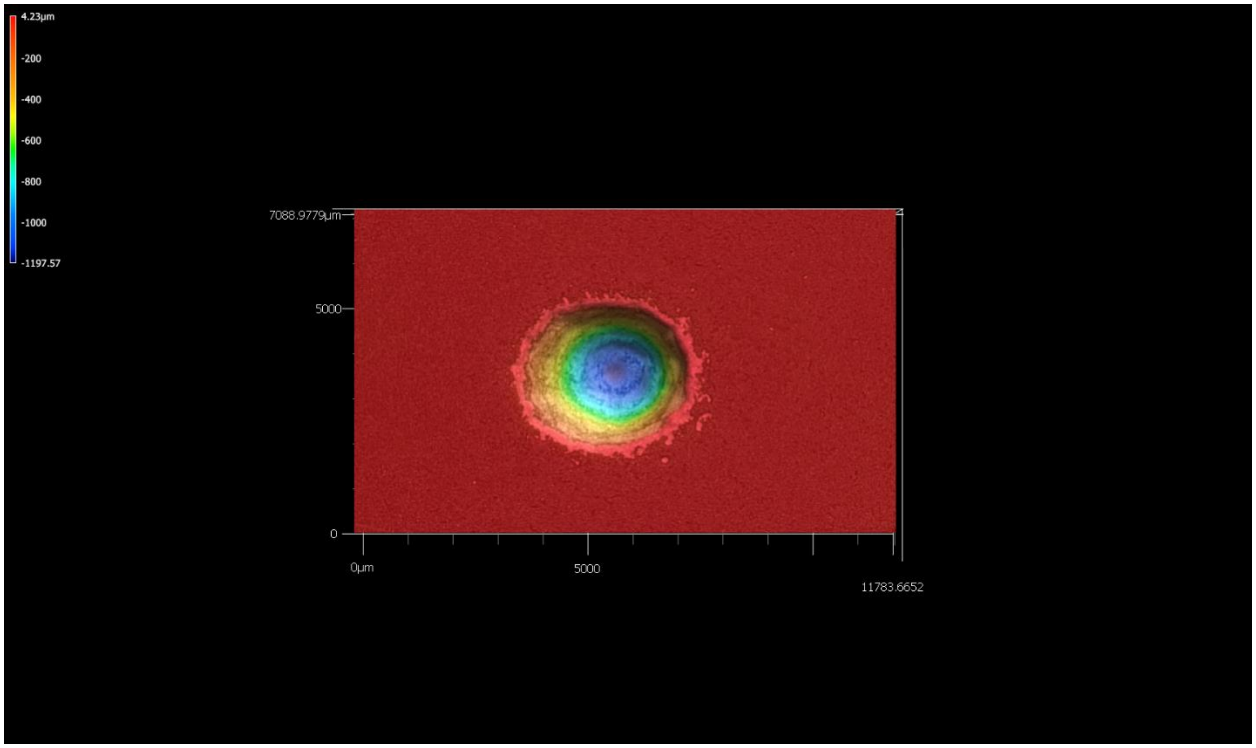


Fig. AII-101: H-146/Polyurethane coated GFRP erosion scar EXP2 at 60° angle of attack

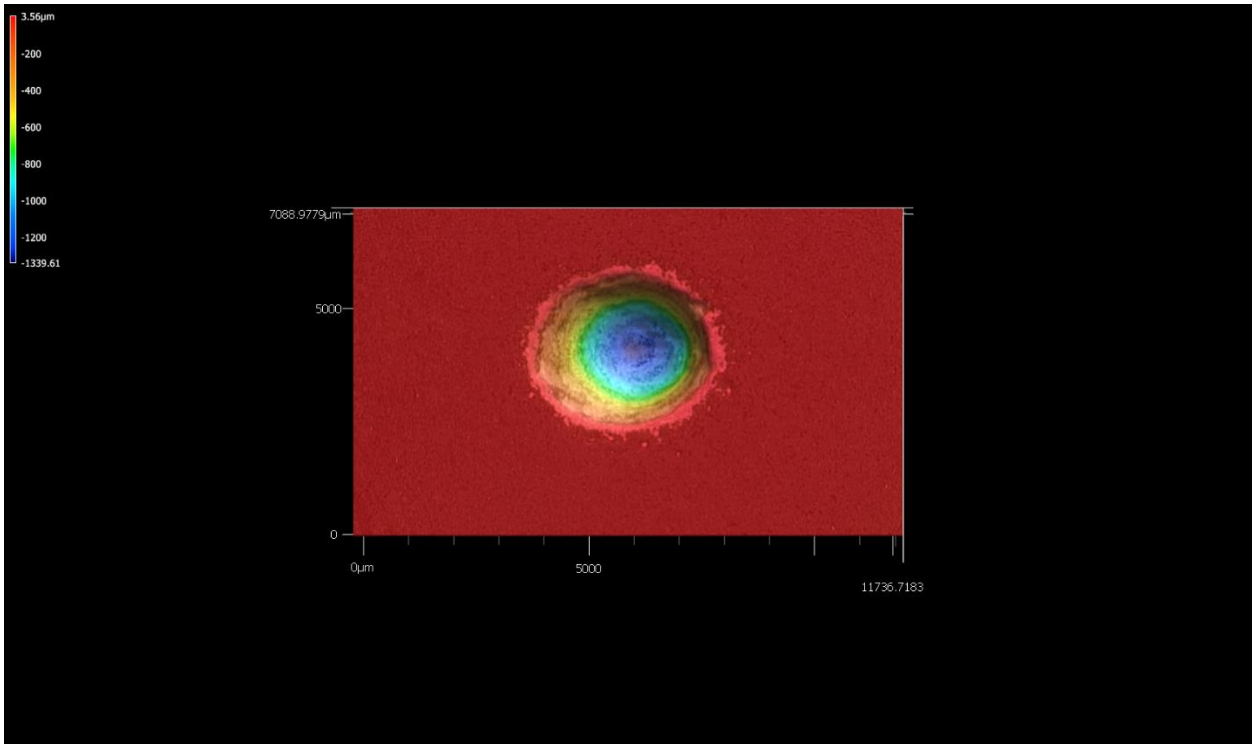


Fig. AII-103: H-146/Polyurethane coated GFRP erosion scar EXP3 at 60° angle of attack

- 75 degrees

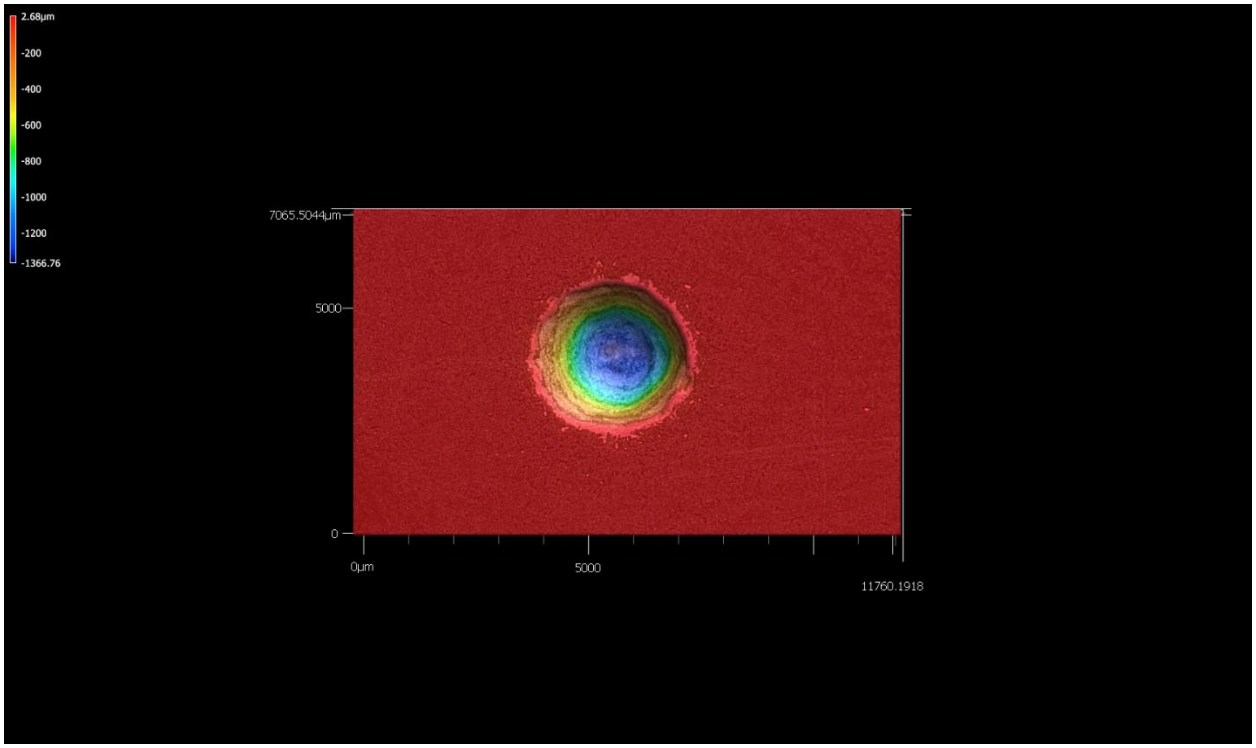


Fig. AII-104: H-146/Polyurethane coated GFRP erosion scar EXP1 at 75° angle of attack

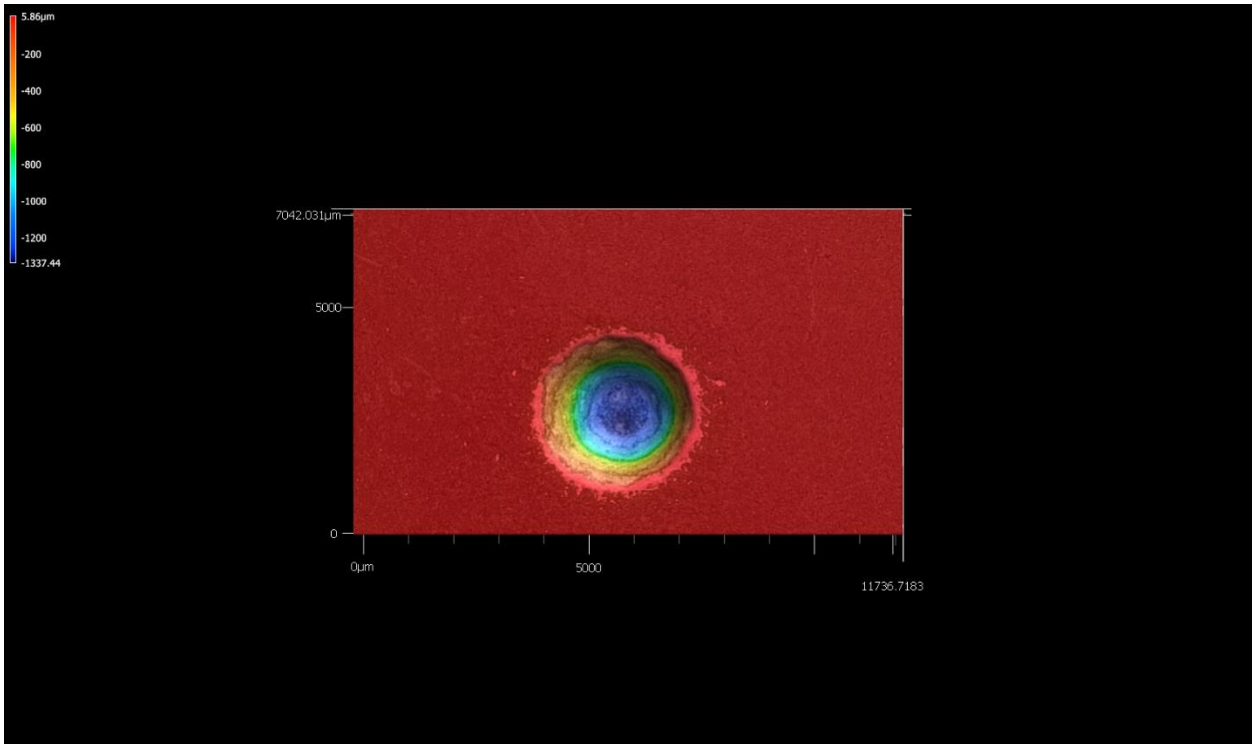


Fig. AII-105: H-146/Polyurethane coated GFRP erosion scar EXP2 at 75° angle of attack

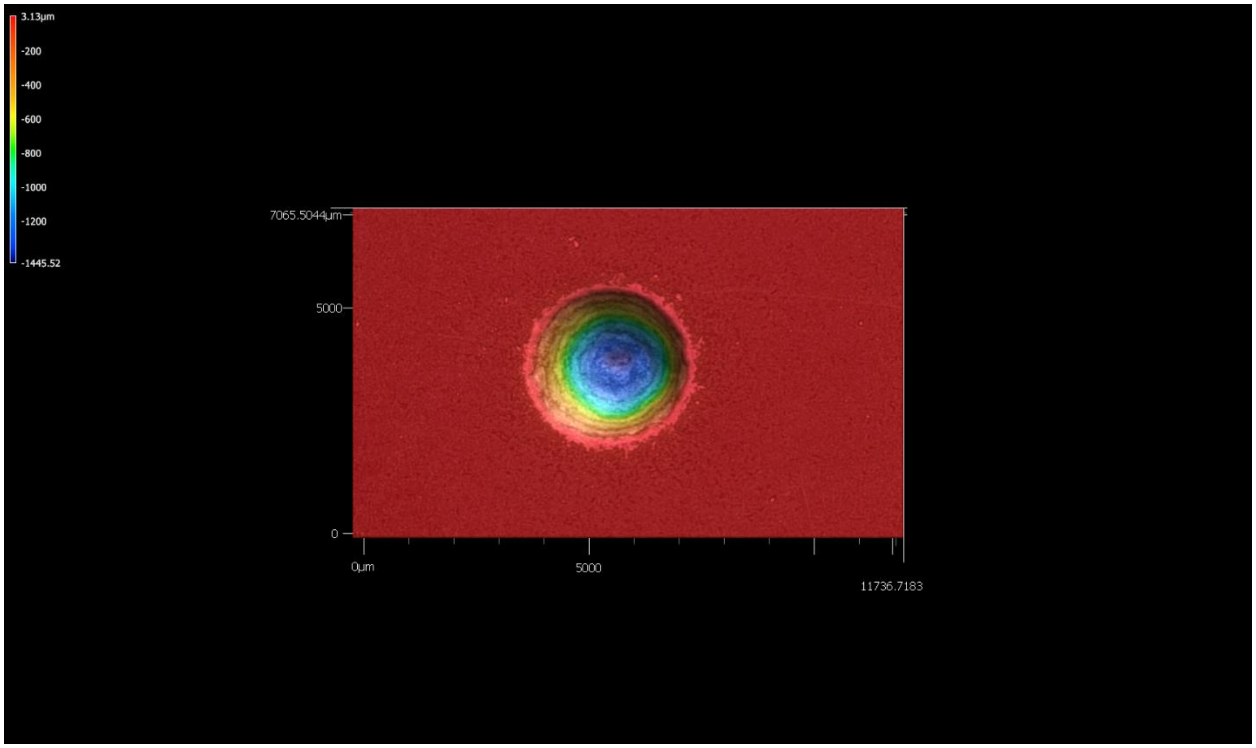


Fig. AII-106: H-146/Polyurethane coated GFRP erosion scar EXP3 at 75° angle of attack

- 90 degrees

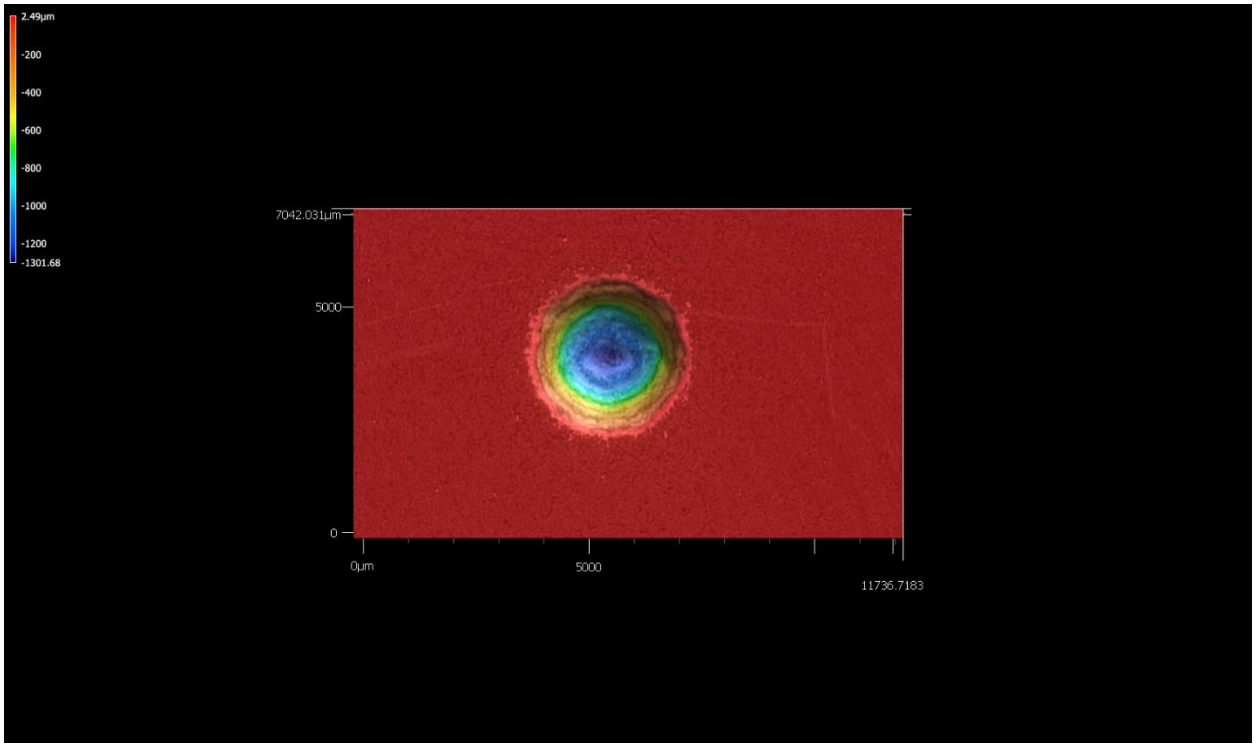


Fig. AII-107: H-146/Polyurethane coated GFRP erosion scar EXP1 at 90° angle of attack

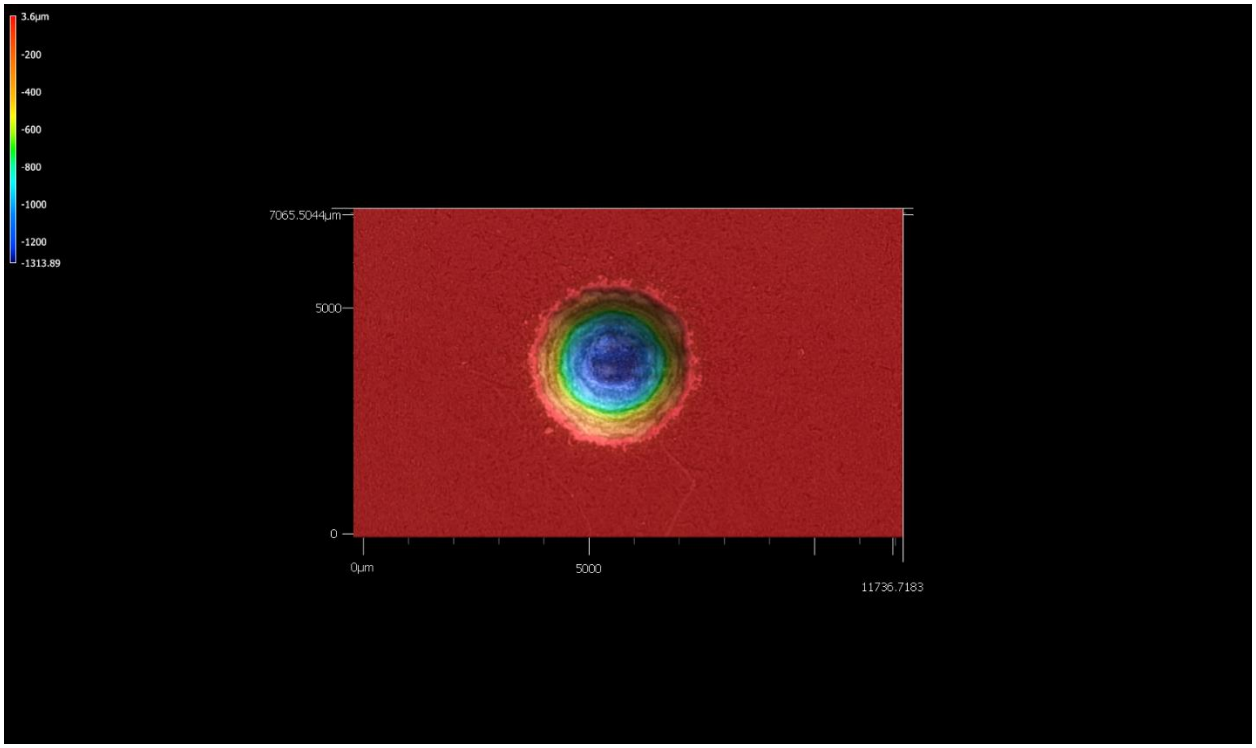


Fig. AII-108: H-146/Polyurethane coated GFRP erosion scar EXP2 at 90° angle of attack

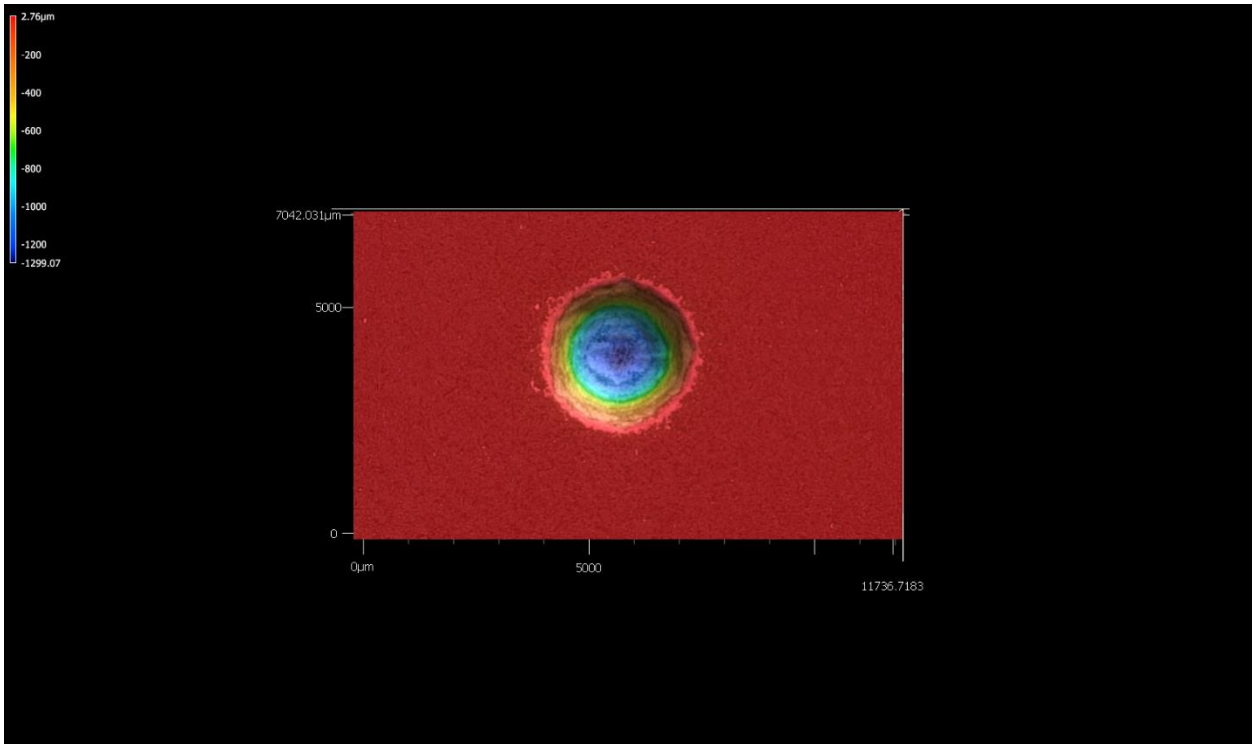


Fig. AII-109: H-146/Polyurethane coated GFRP erosion scar EXP2 at 90° angle of attack

Coating 5 (IA/Polyurethane)

- 30 degrees

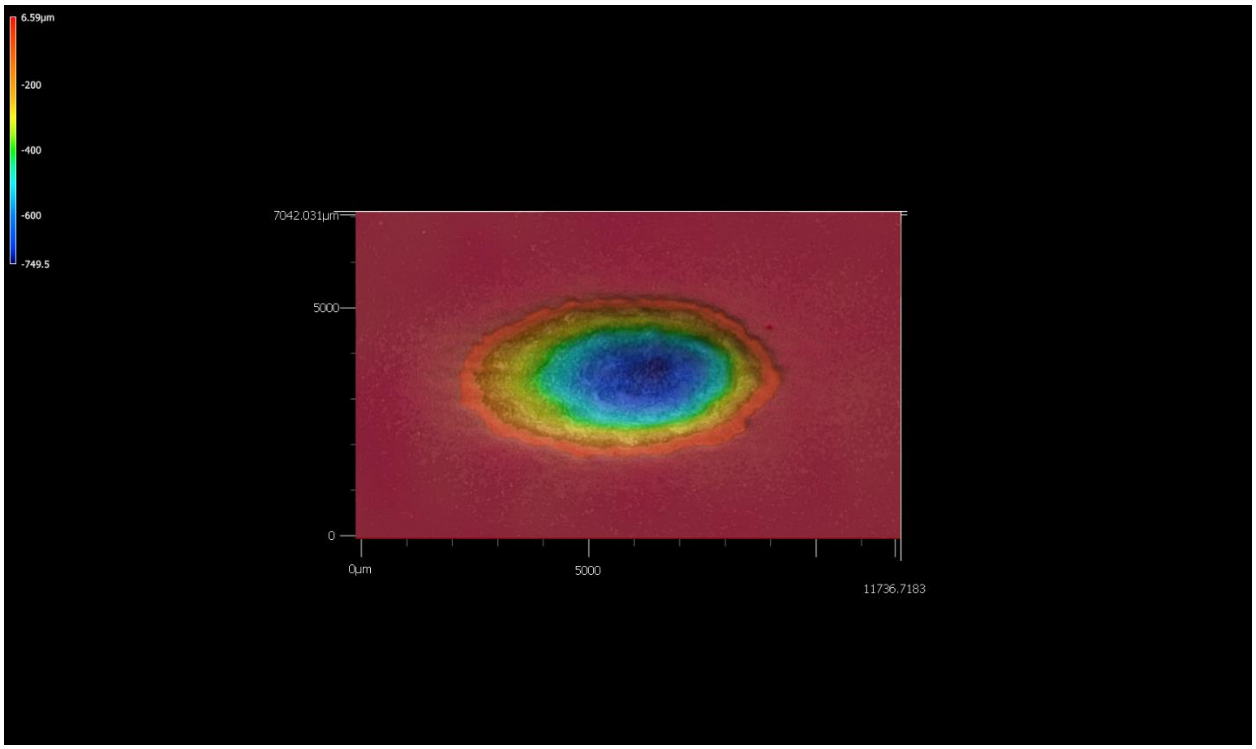


Fig. AII-110: IA-700/Polyurethane coated GFRP erosion scar EXP1 at 30° angle of attack

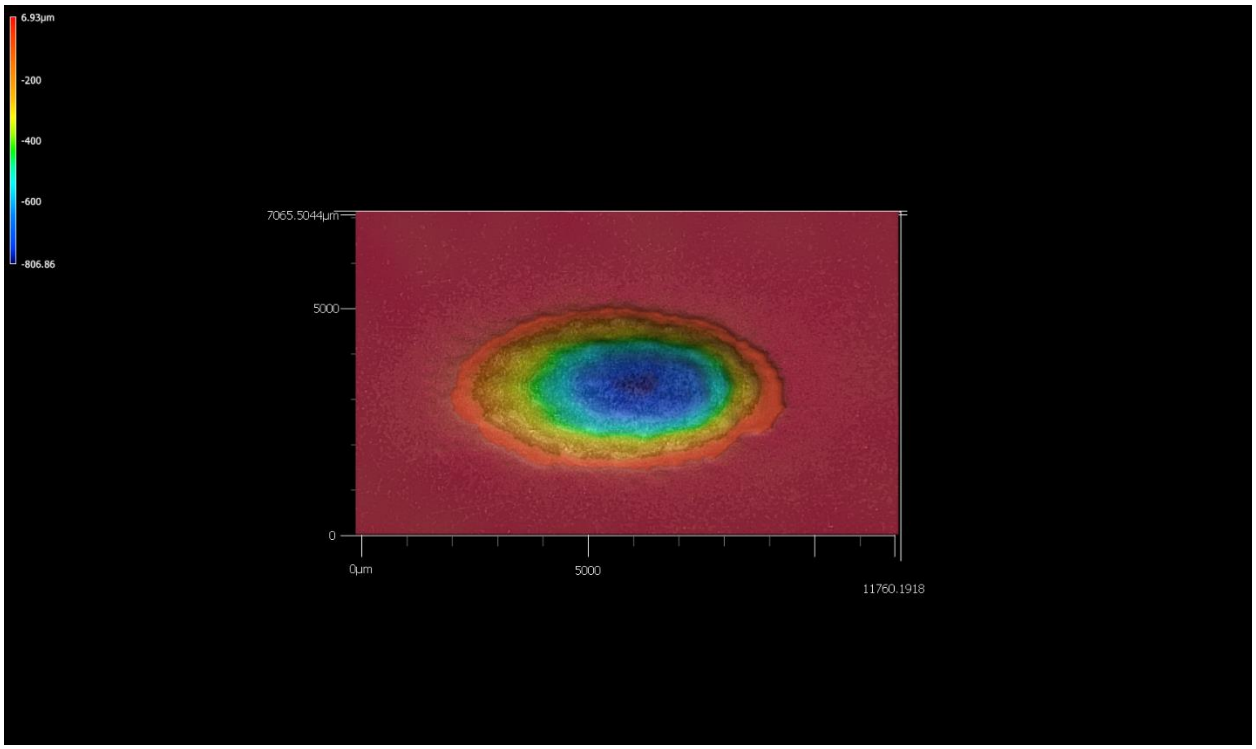


Fig. AII-111: IA-700/Polyurethane coated GFRP erosion scar EXP2 at 30° angle of attack

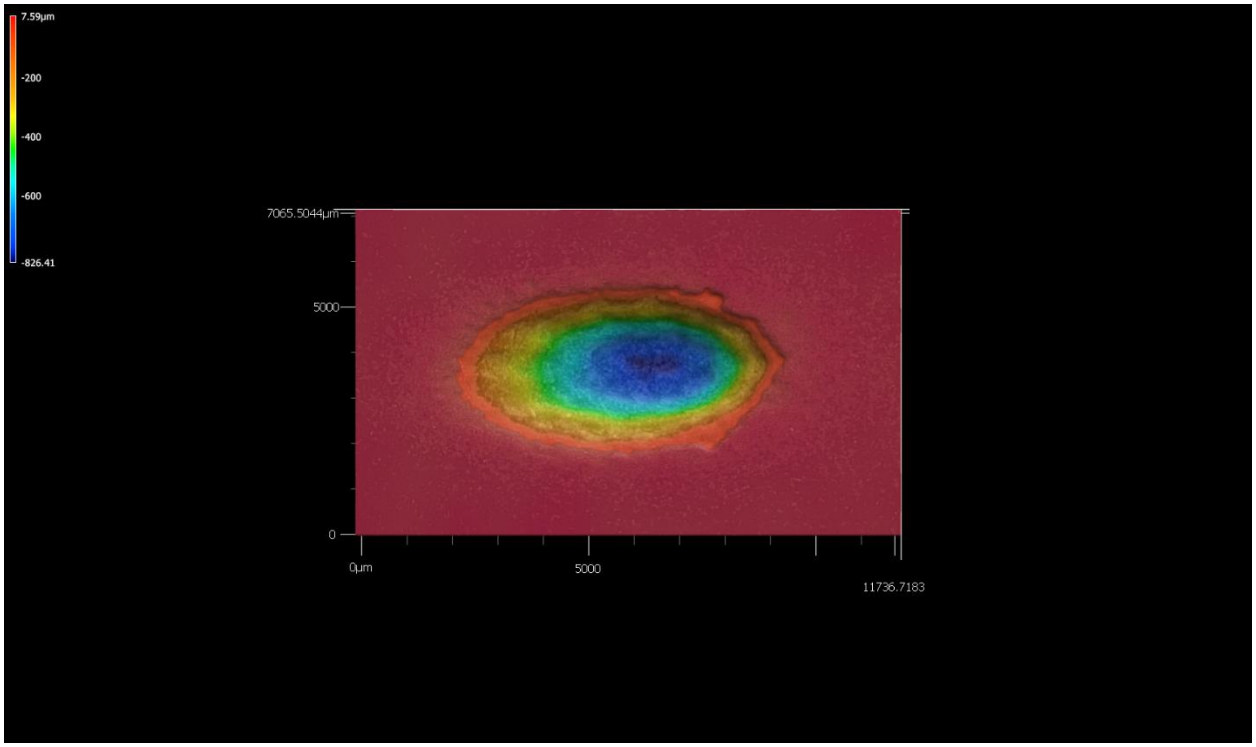


Fig. AII-112: IA-700/Polyurethane coated GFRP erosion scar EXP3 at 30° angle of attack

- 45 degrees

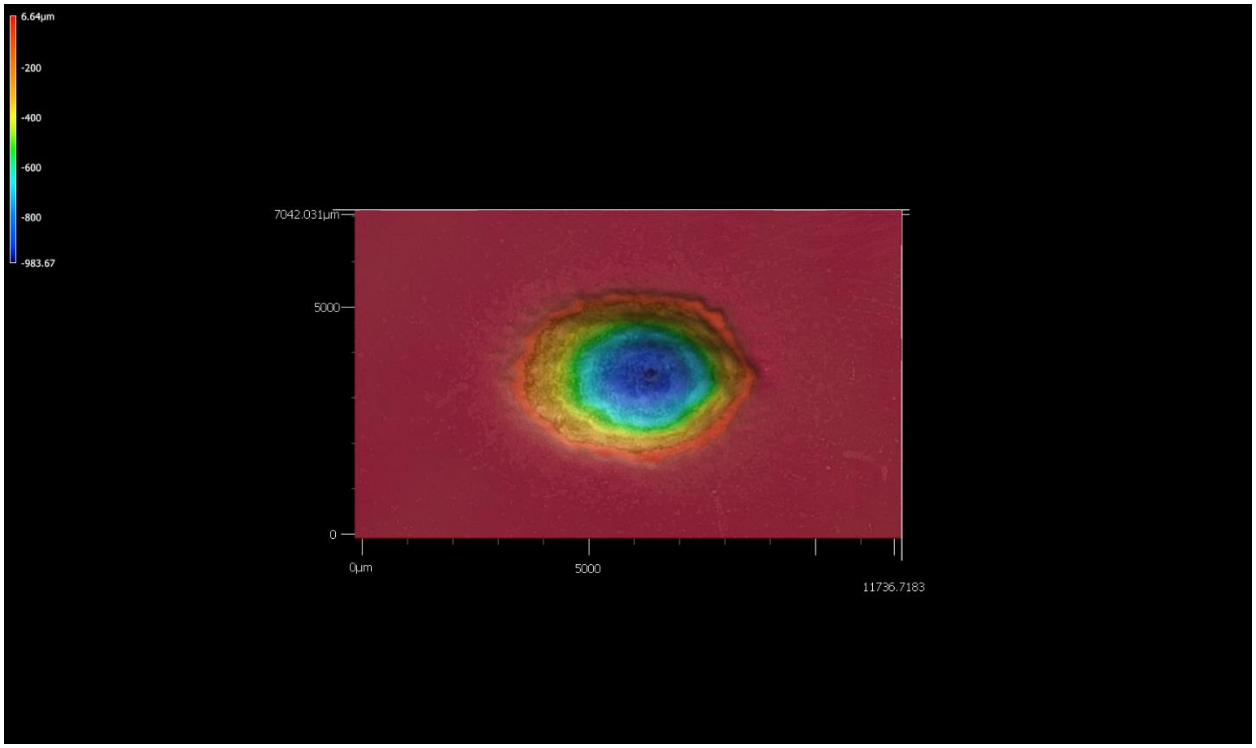


Fig. AII-113: IA-700/Polyurethane coated GFRP erosion scar EXP1 at 45° angle of attack

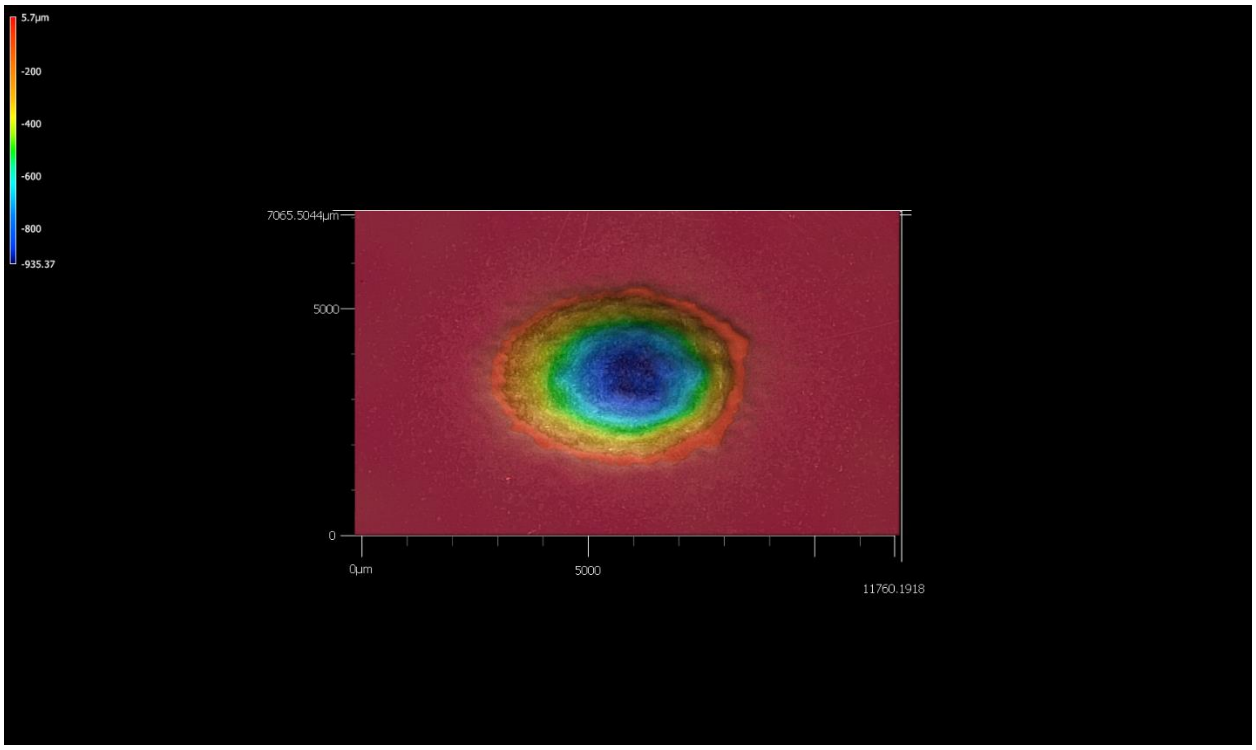


Fig. AII-114: IA-700/Polyurethane coated GFRP erosion scar EXP2 at 45° angle of attack

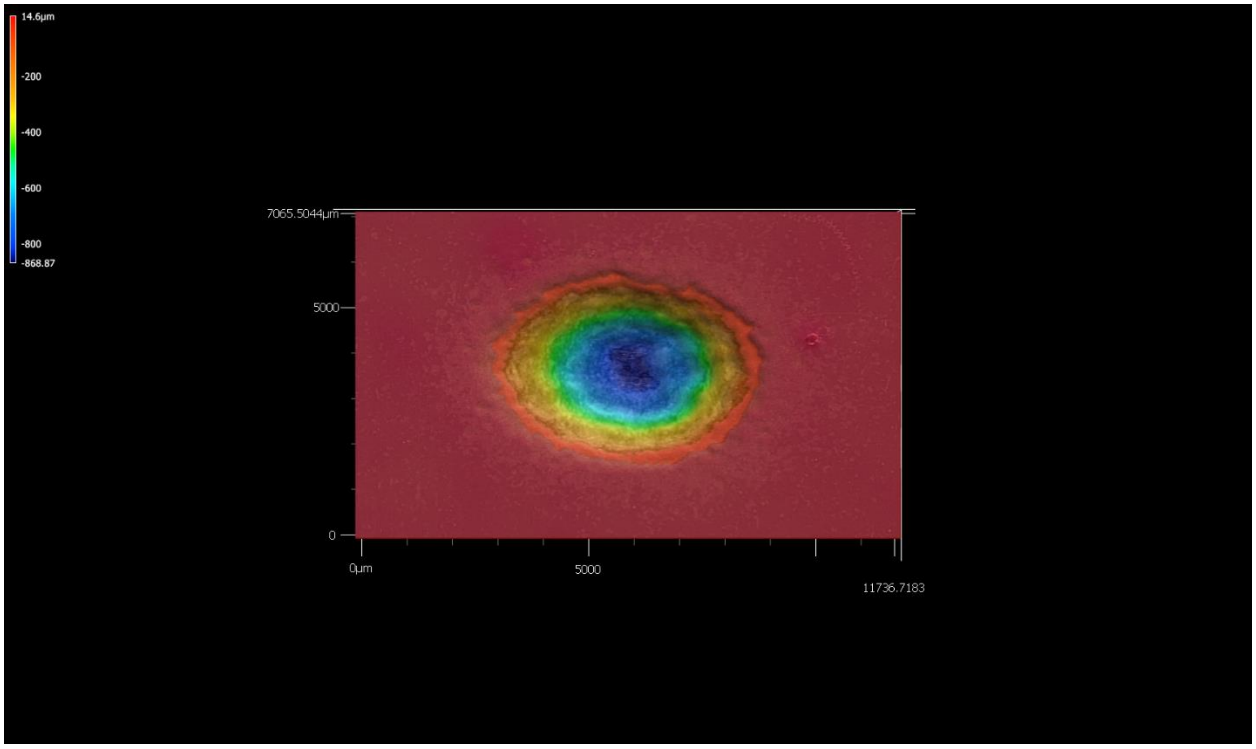


Fig. AII-116: IA-700/Polyurethane coated GFRP erosion scar EXP3 at 45° angle of attack

- 60 degrees

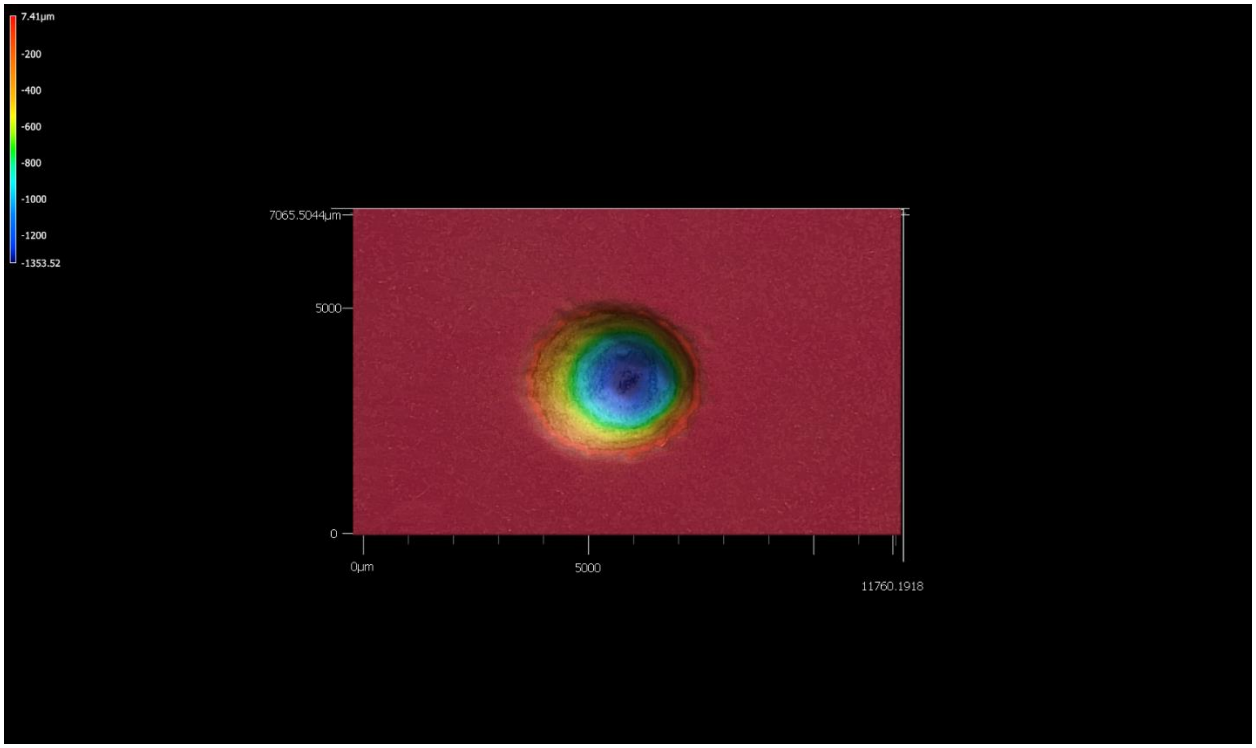


Fig. AII-117: IA-700/Polyurethane coated GFRP erosion scar EXP1 at 60° angle of attack

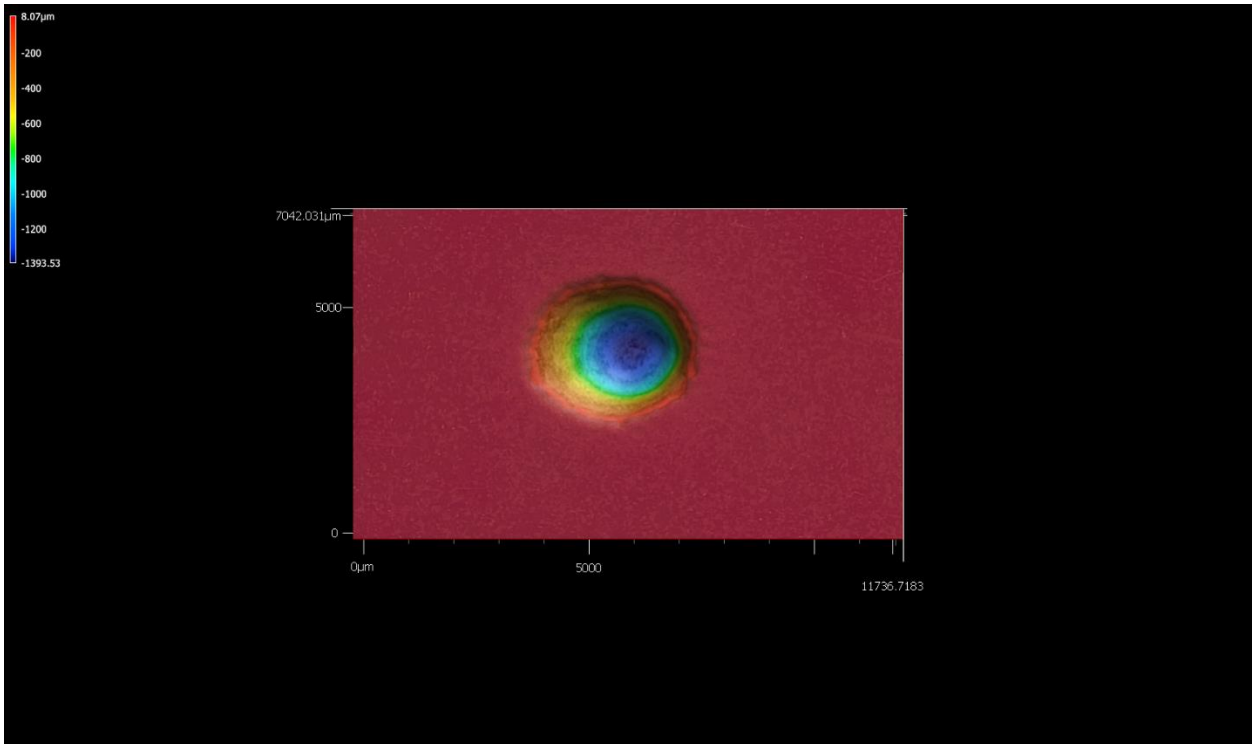


Fig. AII-118: IA-700/Polyurethane coated GFRP erosion scar EXP2 at 60° angle of attack

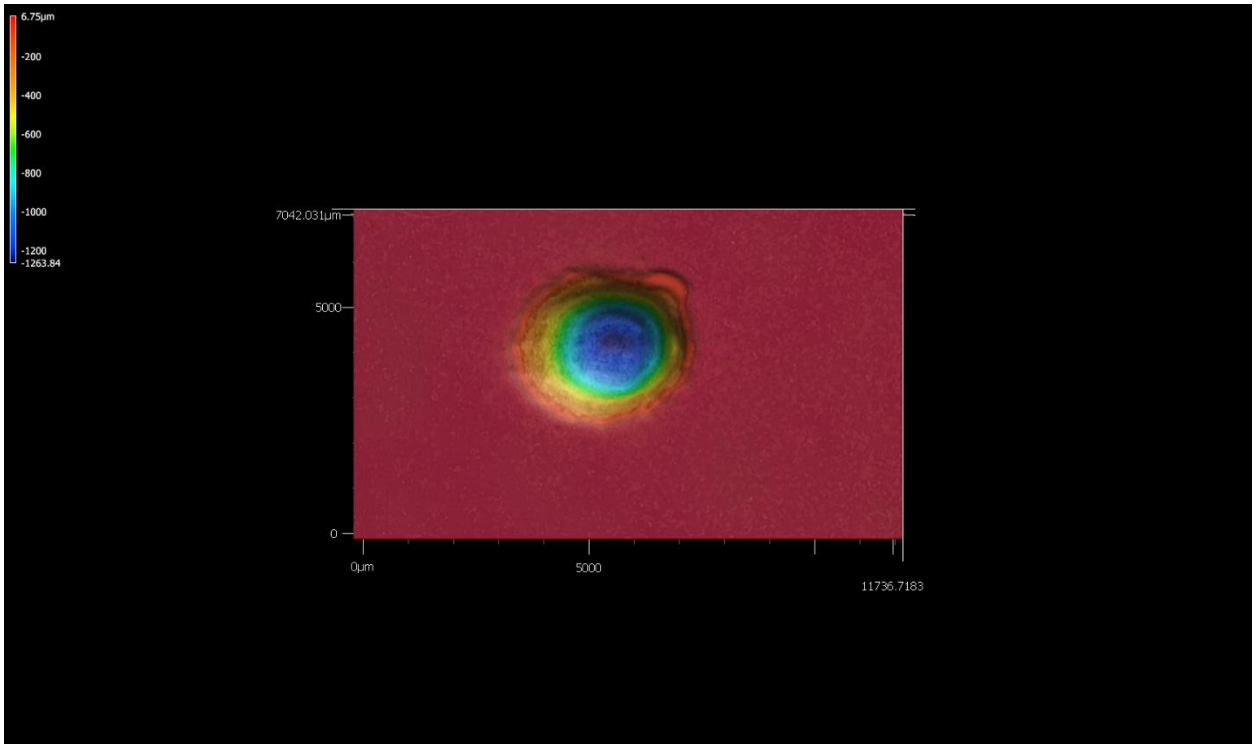


Fig. AII-119: IA-700/Polyurethane coated GFRP erosion scar EXP3 at 60° angle of attack

- 75 degrees

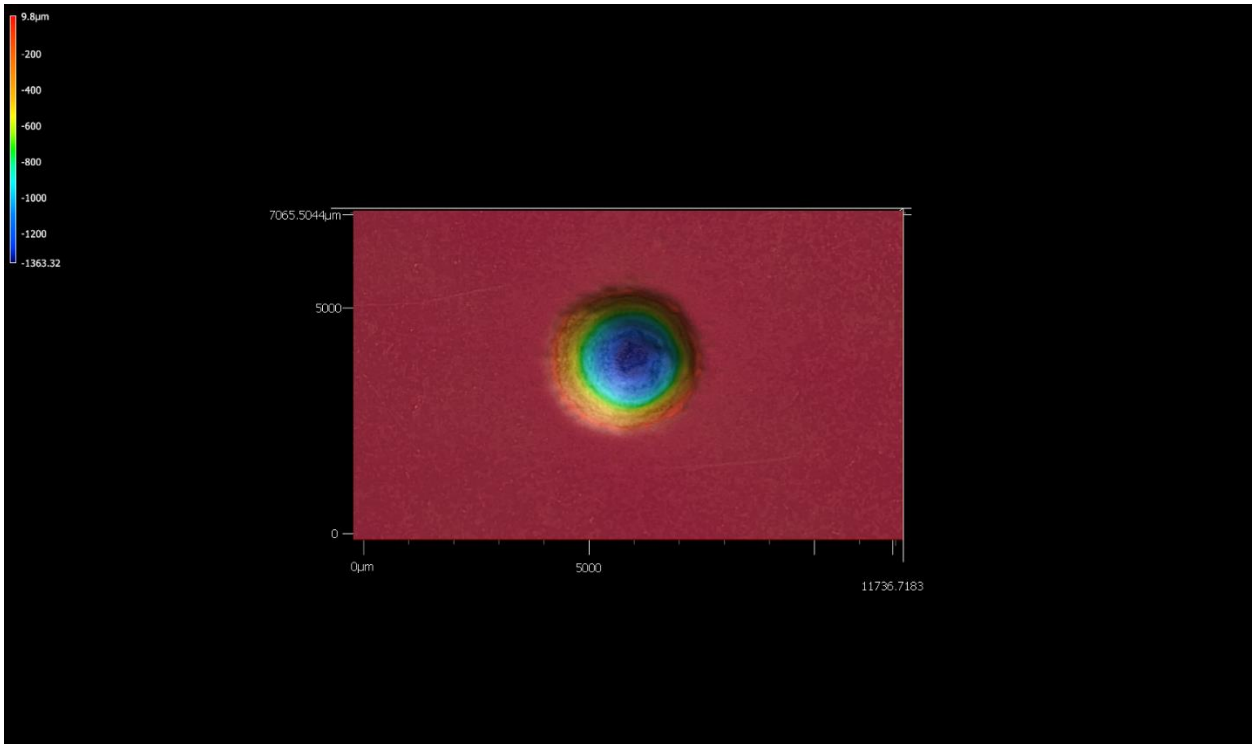


Fig. AII-120: IA-700/Polyurethane coated GFRP erosion scar EXP1 at 75° angle of attack

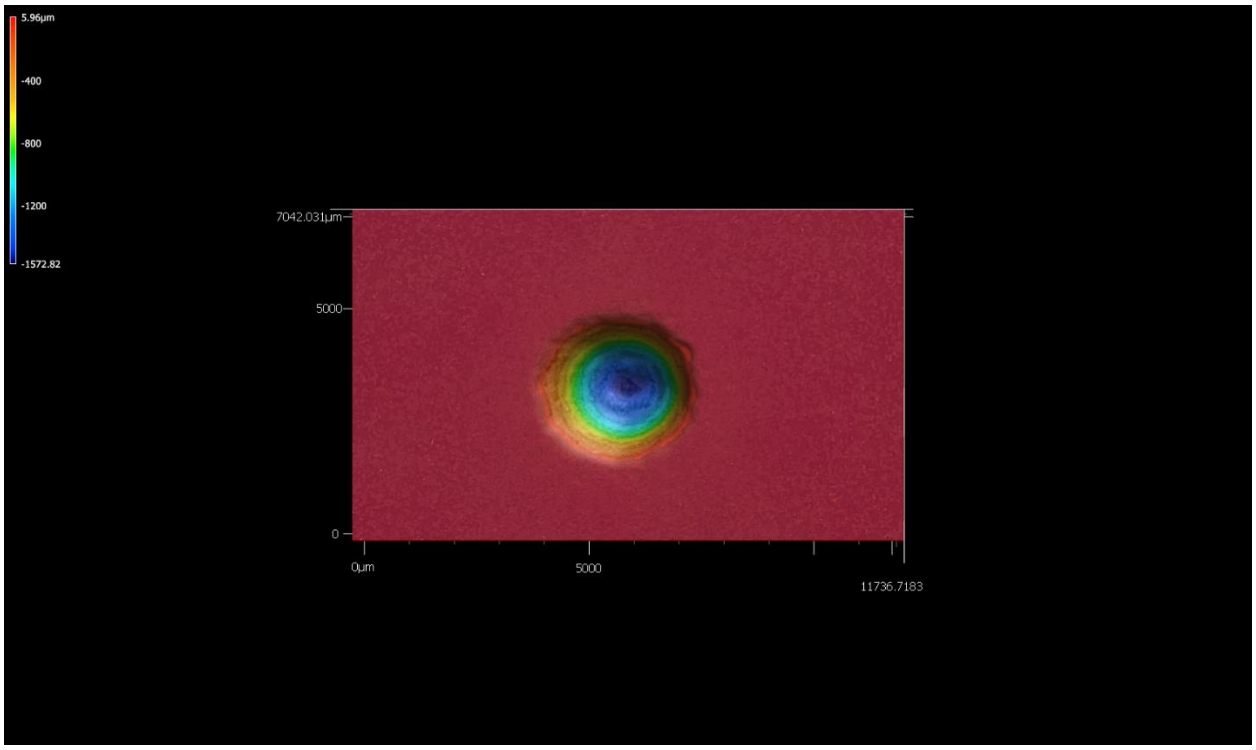


Fig. AII-121: IA-700/Polyurethane coated GFRP erosion scar EXP2 at 75° angle of attack

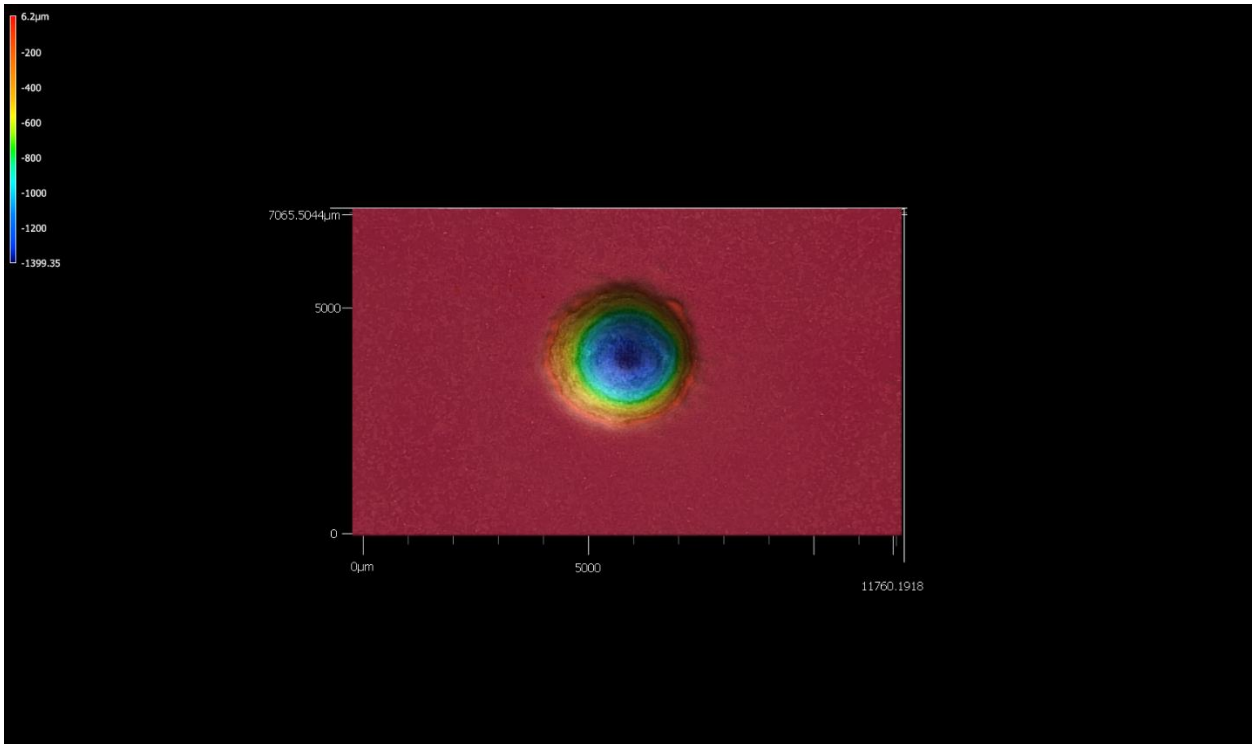


Fig. AII-122: IA-700/Polyurethane coated GFRP erosion scar EXP3 at 75° angle of attack

- 90 degrees

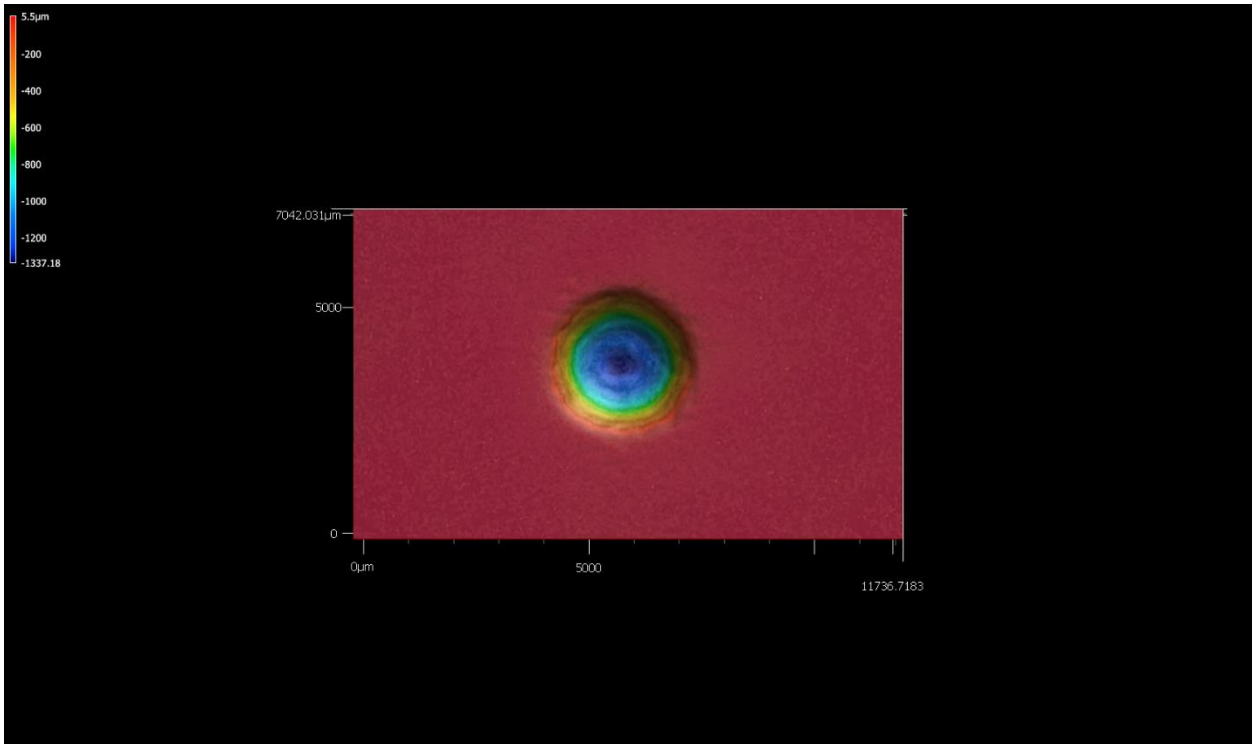


Fig. AII-123: IA-700/Polyurethane coated GFRP erosion scar EXP1 at 90° angle of attack

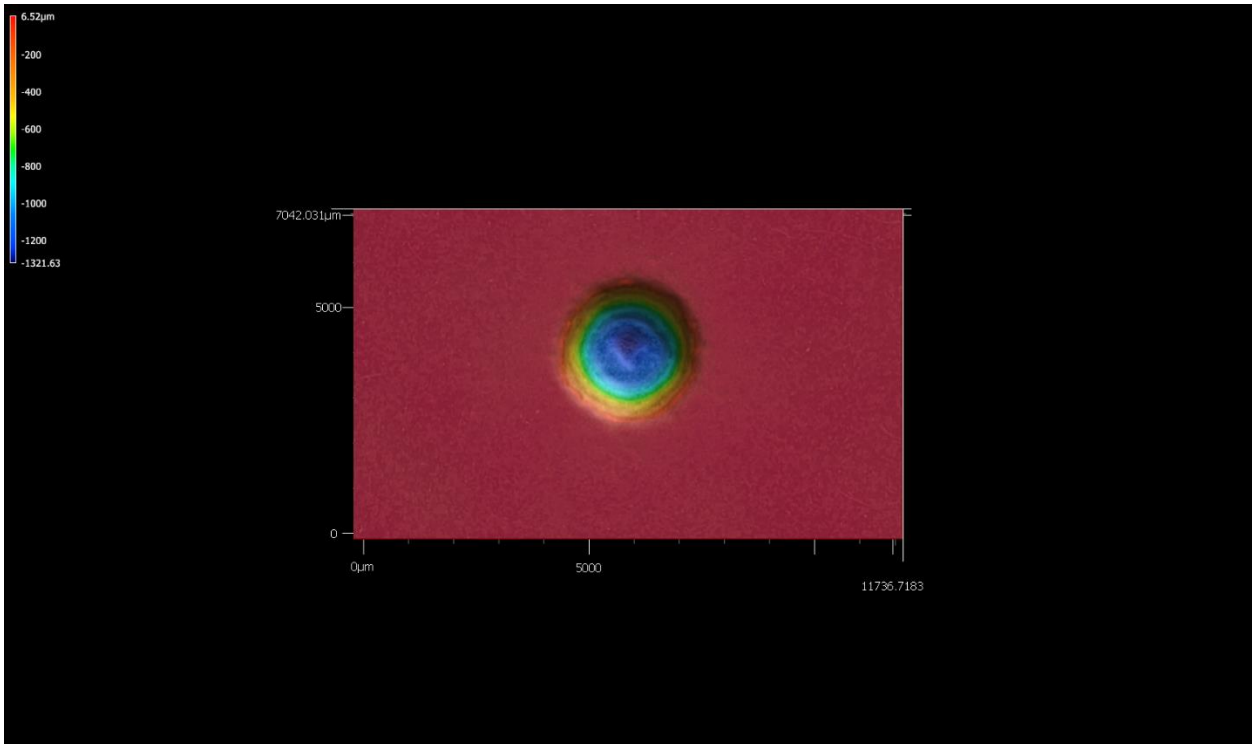


Fig. AII-124: IA-700/Polyurethane coated GFRP erosion scar EXP2 at 90° angle of attack

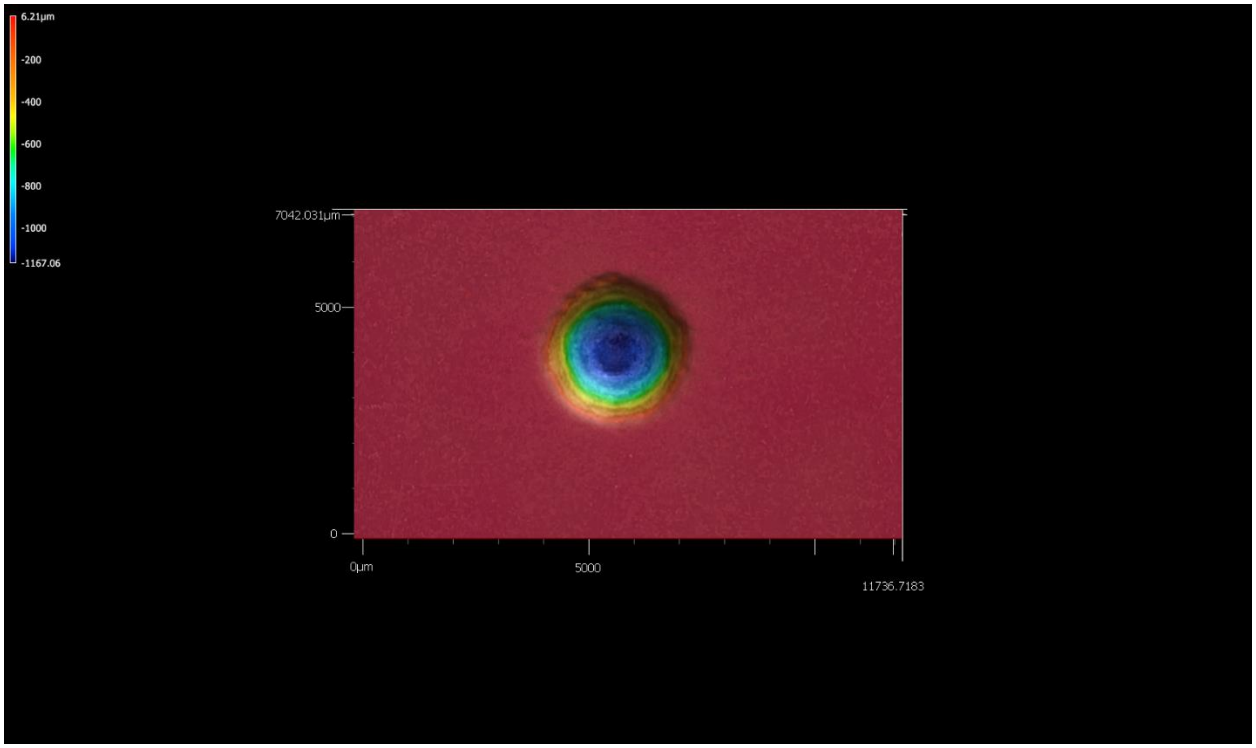


Fig. AII-125: IA-700/Polyurethane coated GFRP erosion scar EXP3 at 90° angle of attack

Coating 6 (polyurethane/Polyurethane)

- 30 degrees

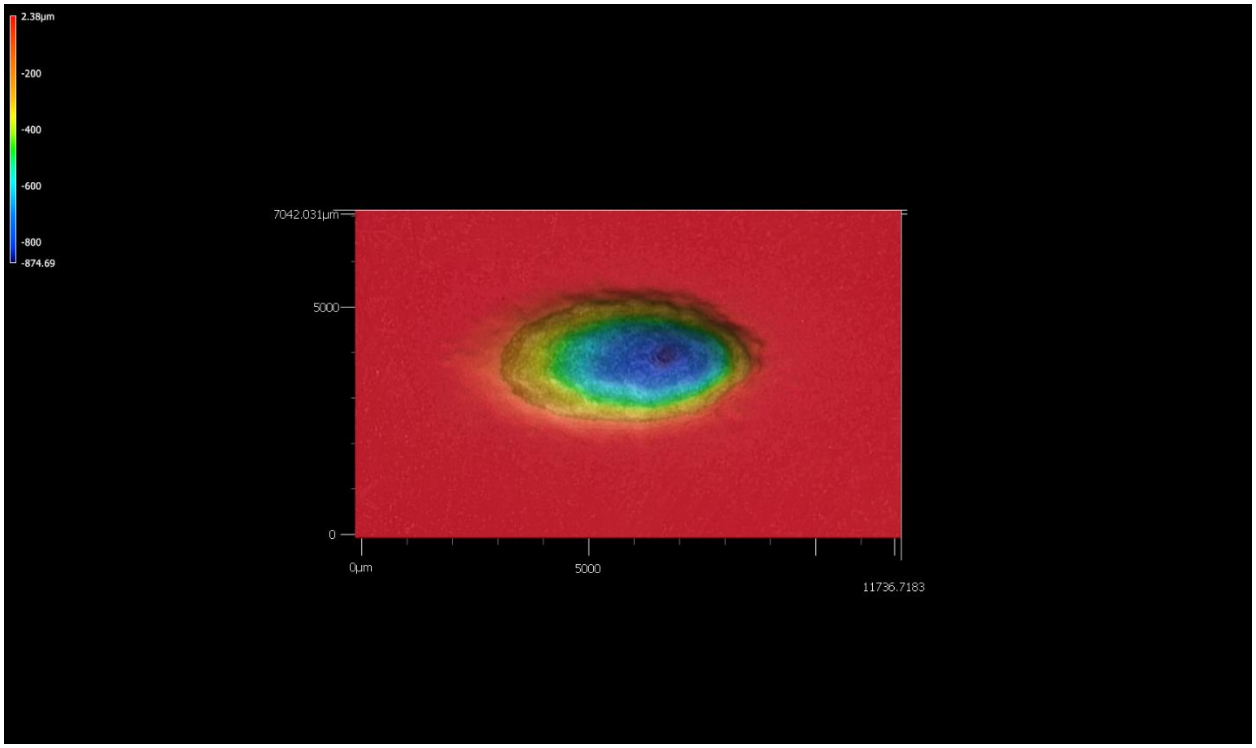


Fig. AII-126: Polyurethane/Polyurethane coated GFRP erosion scar EXP1 at 30° angle of attack

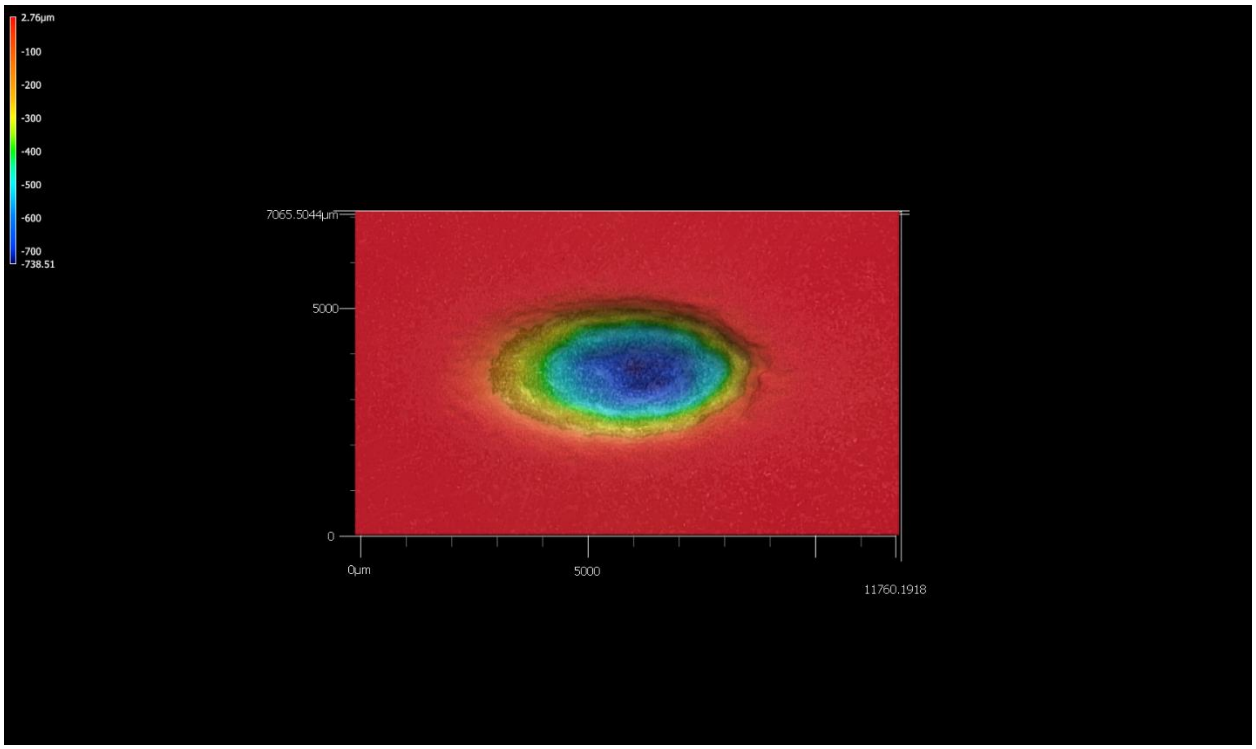


Fig. AII-127: Polyurethane/Polyurethane coated GFRP erosion scar EXP2 at 30° angle of attack

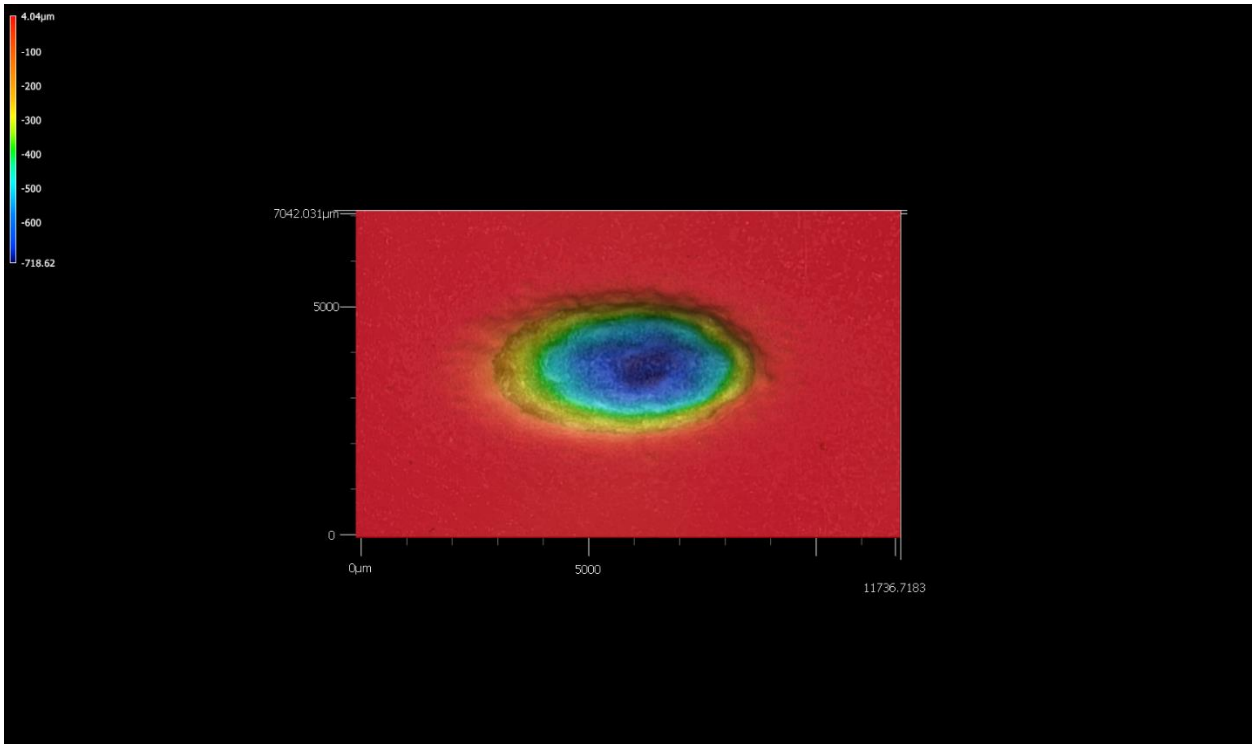


Fig. AII-128: Polyurethane/Polyurethane coated GFRP erosion scar EXP3 at 30° angle of attack

- 45 degrees

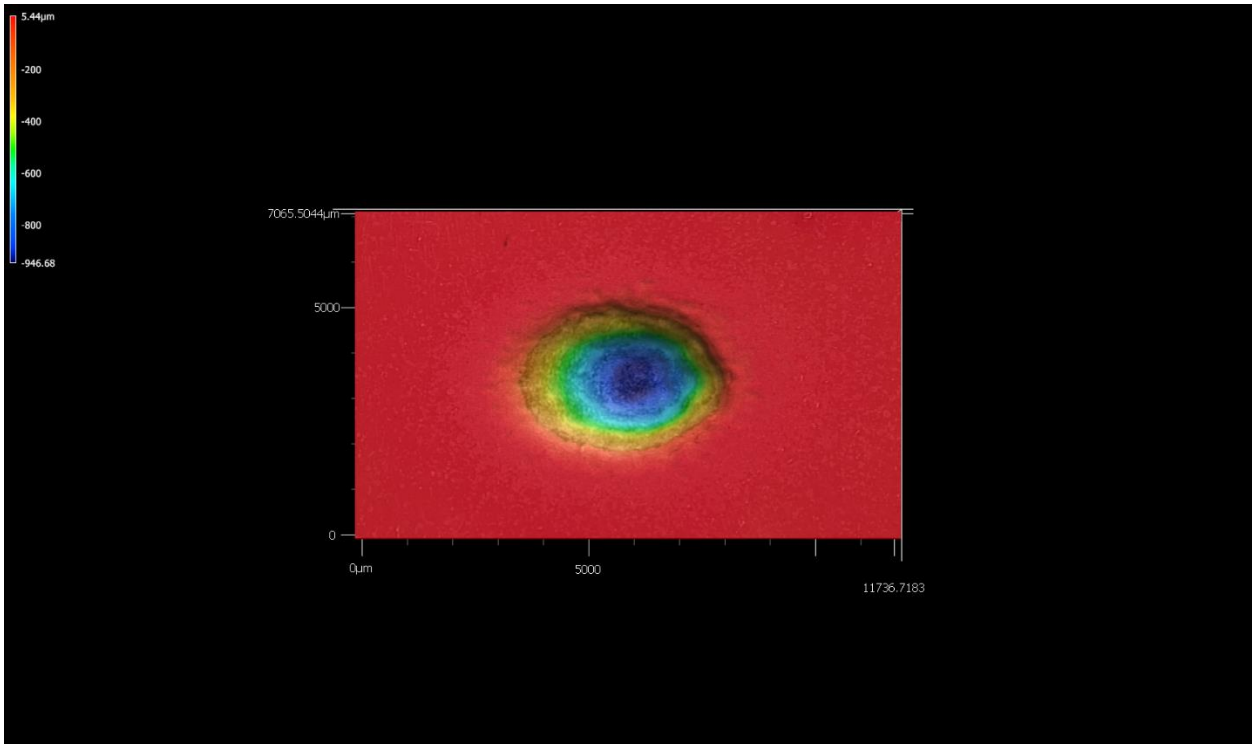


Fig. AII-129: Polyurethane/Polyurethane coated GFRP erosion scar EXP1 at 45° angle of attack

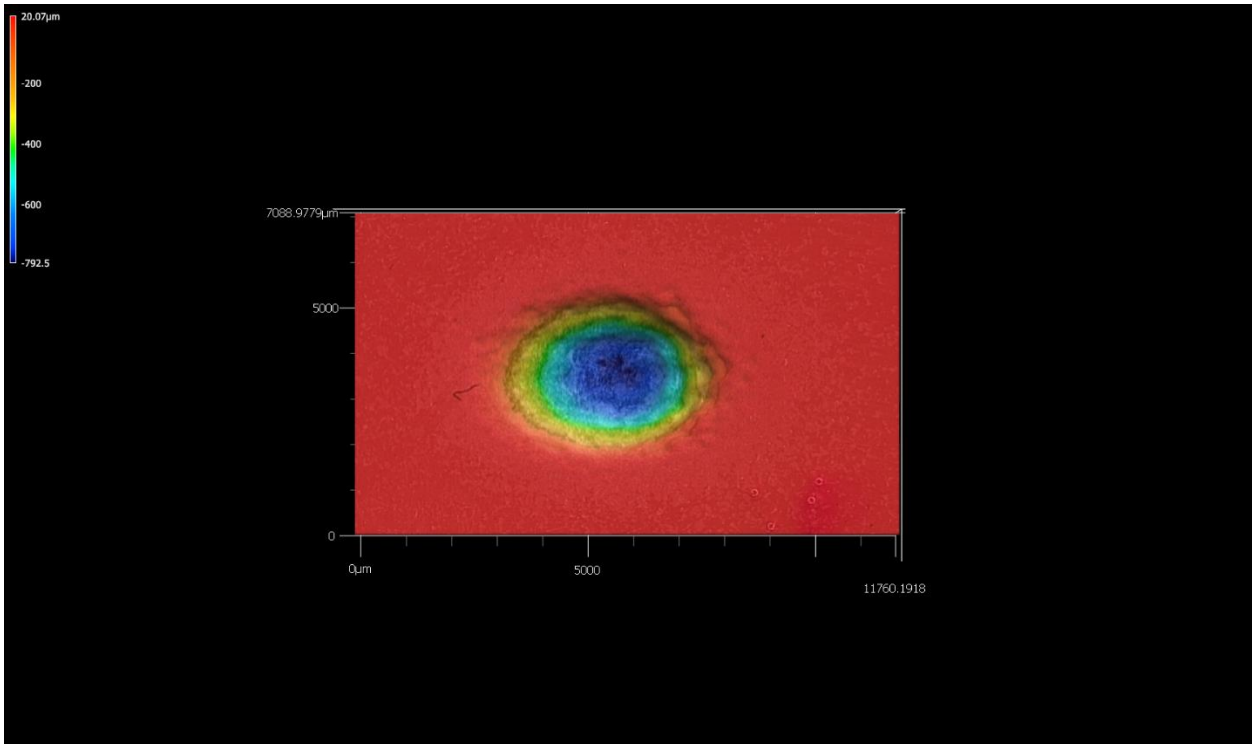


Fig. AII-130: Polyurethane/Polyurethane coated GFRP erosion scar EXP2 at 45° angle of attack

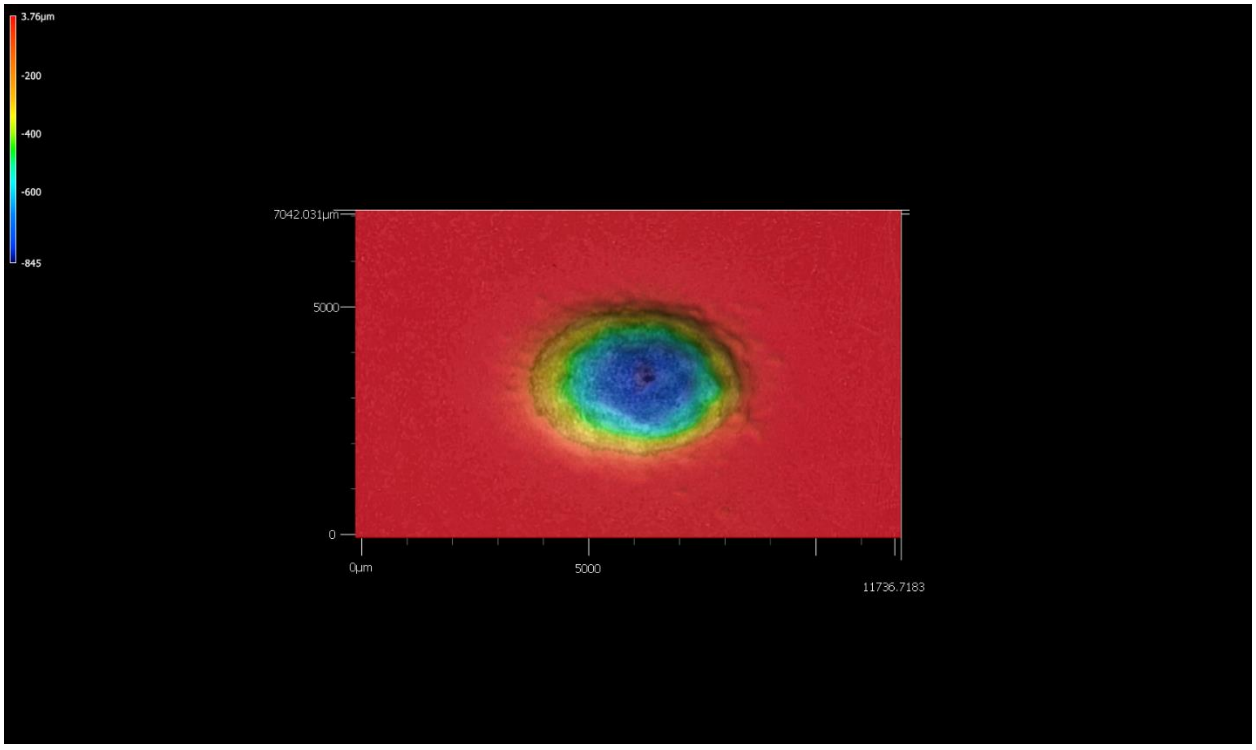


Fig. AII-131: Polyurethane/Polyurethane coated GFRP erosion scar EXP3 at 45° angle of attack

- 60 degrees

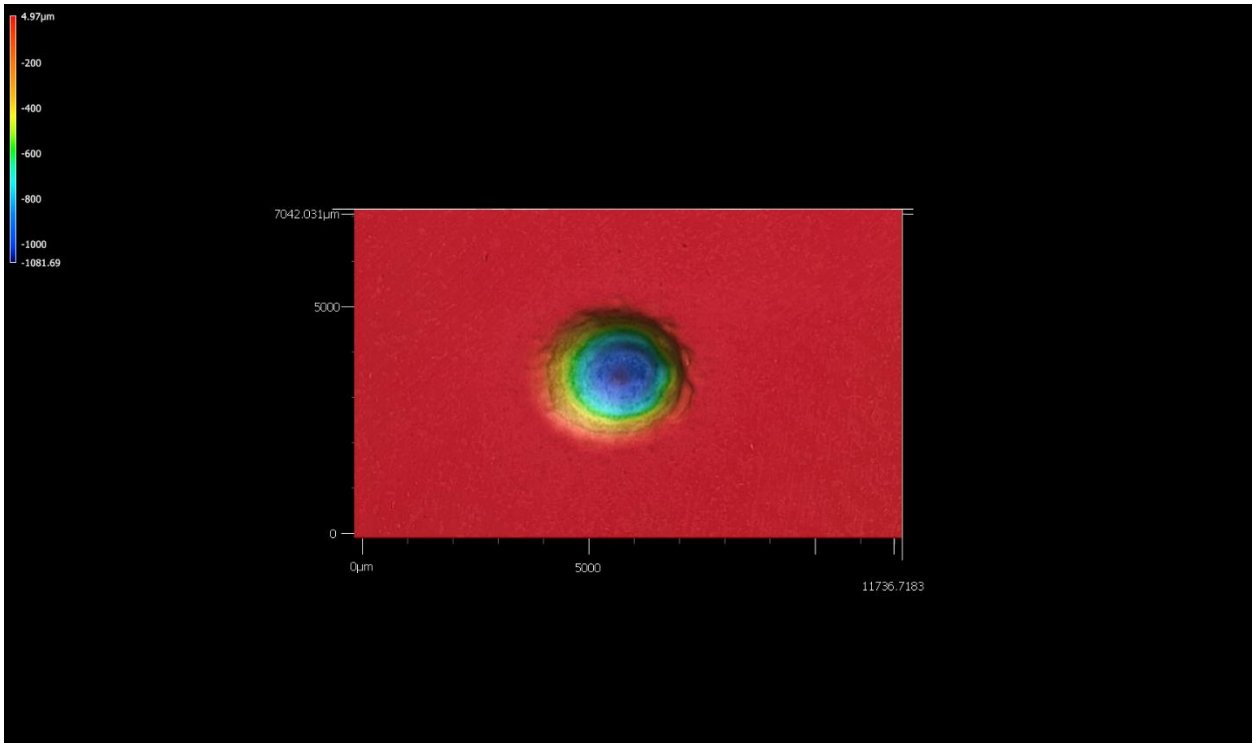


Fig. AII-132: Polyurethane/Polyurethane coated GFRP erosion scar EXP1 at 60° angle of attack

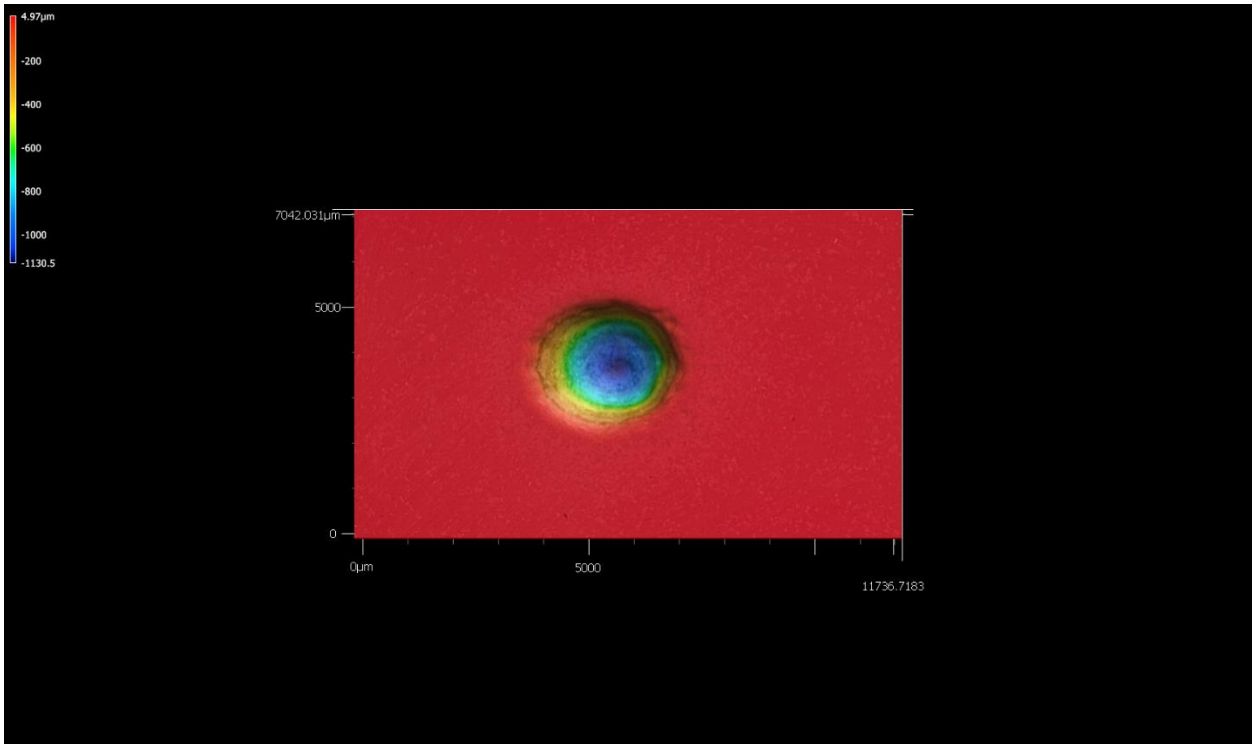


Fig. AII-133: Polyurethane/Polyurethane coated GFRP erosion scar EXP2 at 60° angle of attack

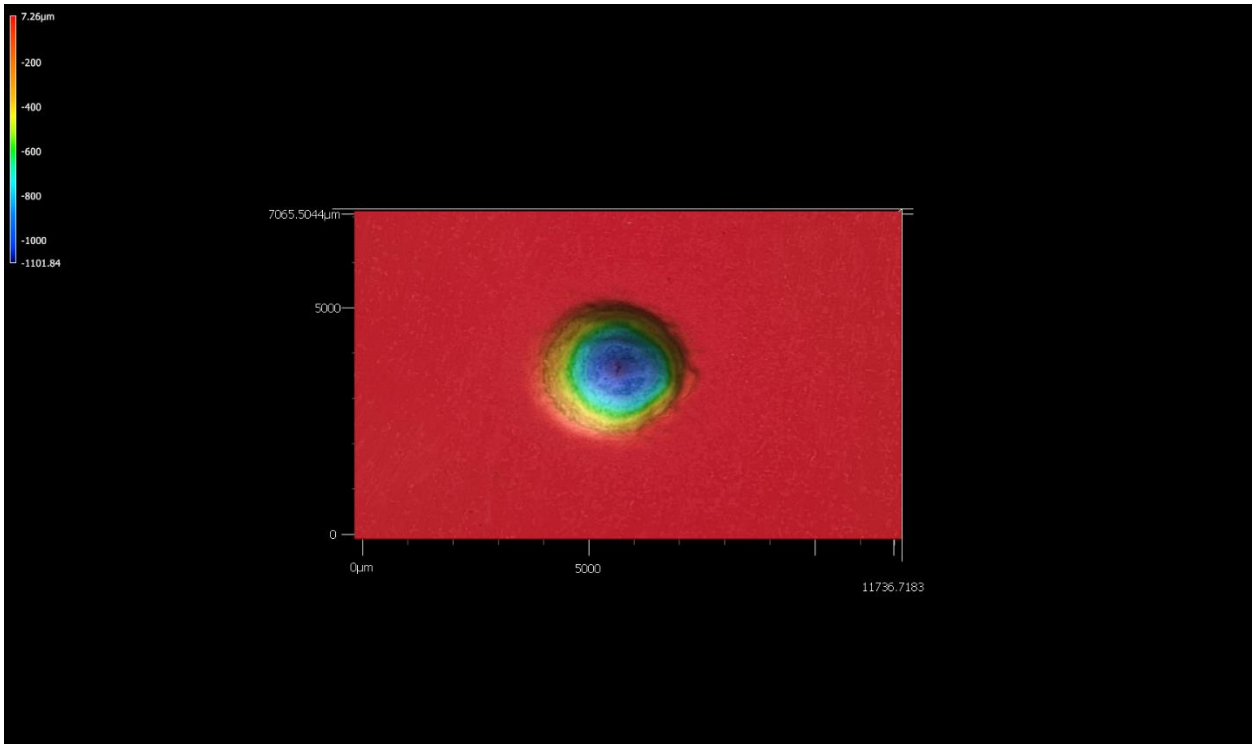


Fig. AII-134: Polyurethane/Polyurethane coated GFRP erosion scar EXP3 at 60° angle of attack

- 75 degrees

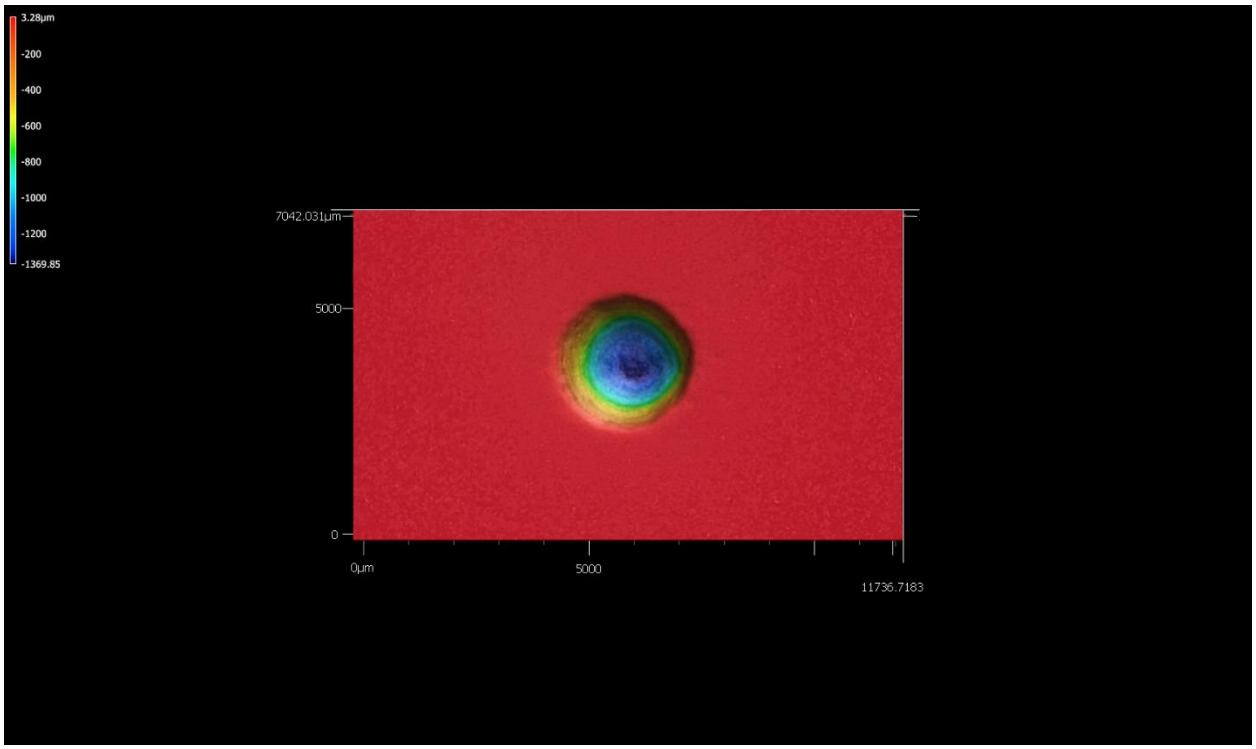


Fig. AII-135: Polyurethane/Polyurethane coated GFRP erosion scar EXP1 at 75° angle of attack

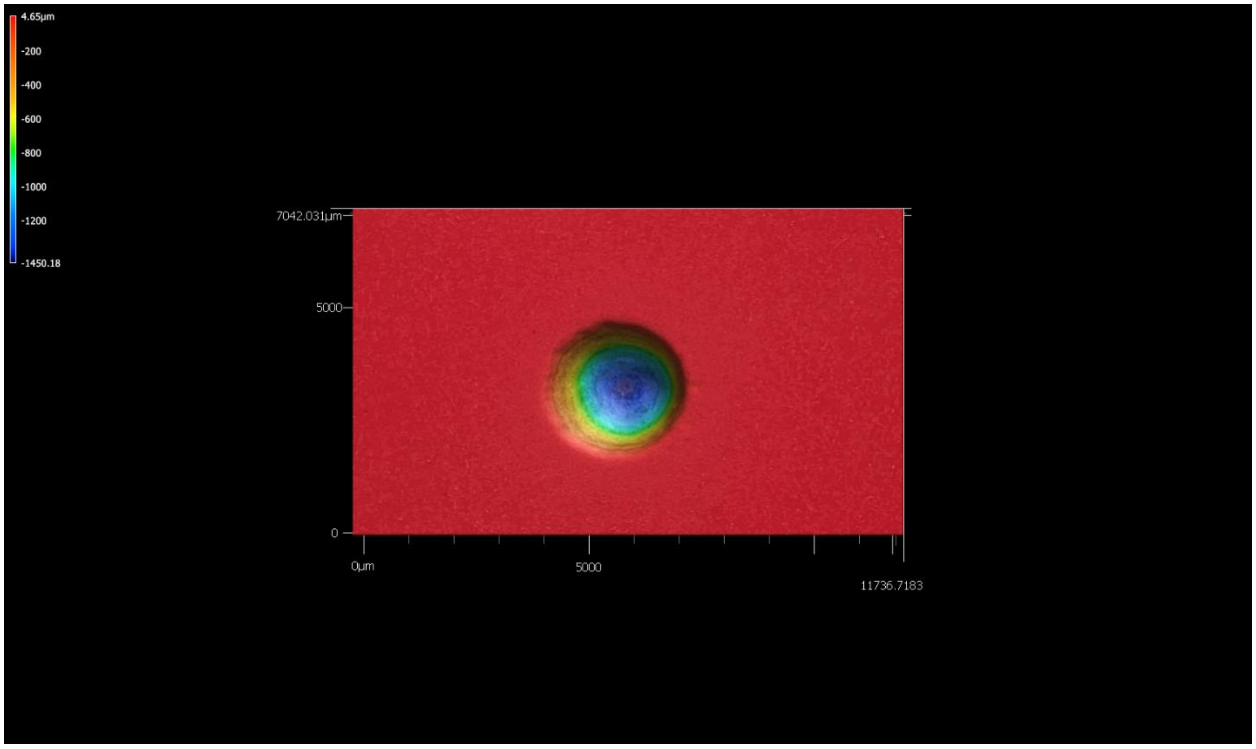


Fig. AII-136: Polyurethane/Polyurethane coated GFRP erosion scar EXP2 at 75° angle of attack

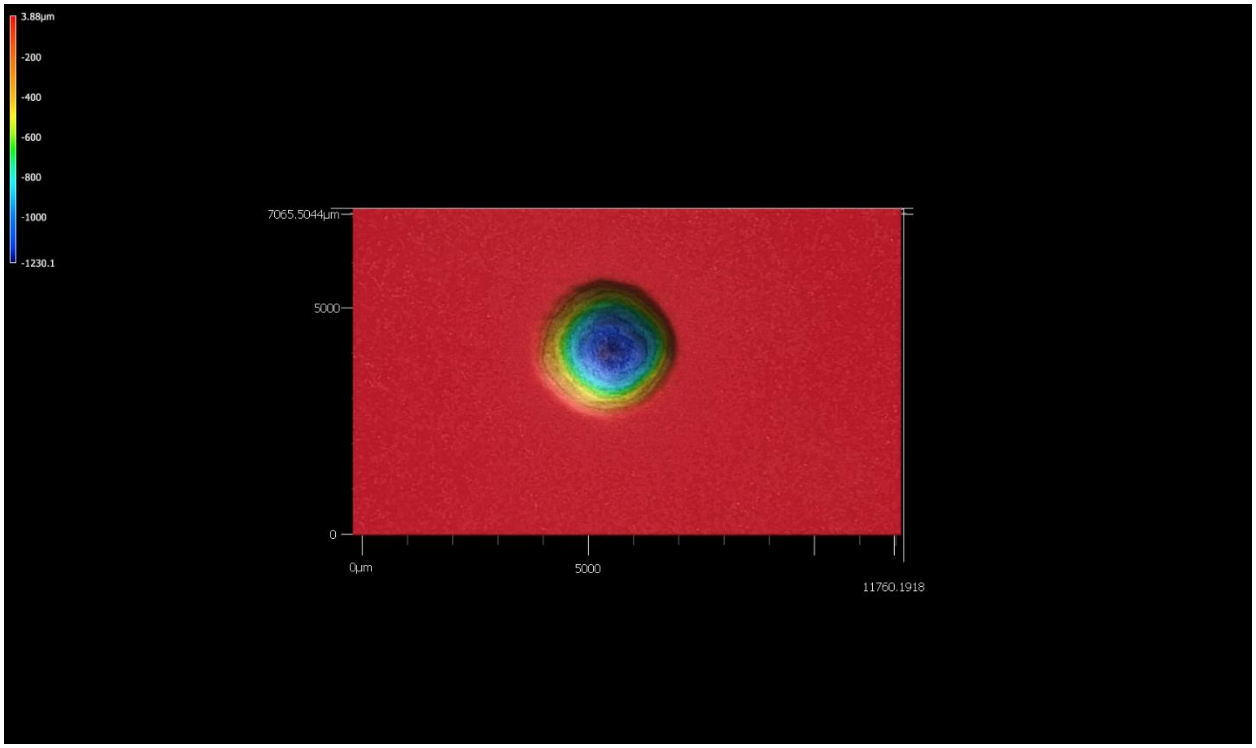


Fig. AII-137: Polyurethane/Polyurethane coated GFRP erosion scar EXP3 at 75° angle of attack

- 90 degrees

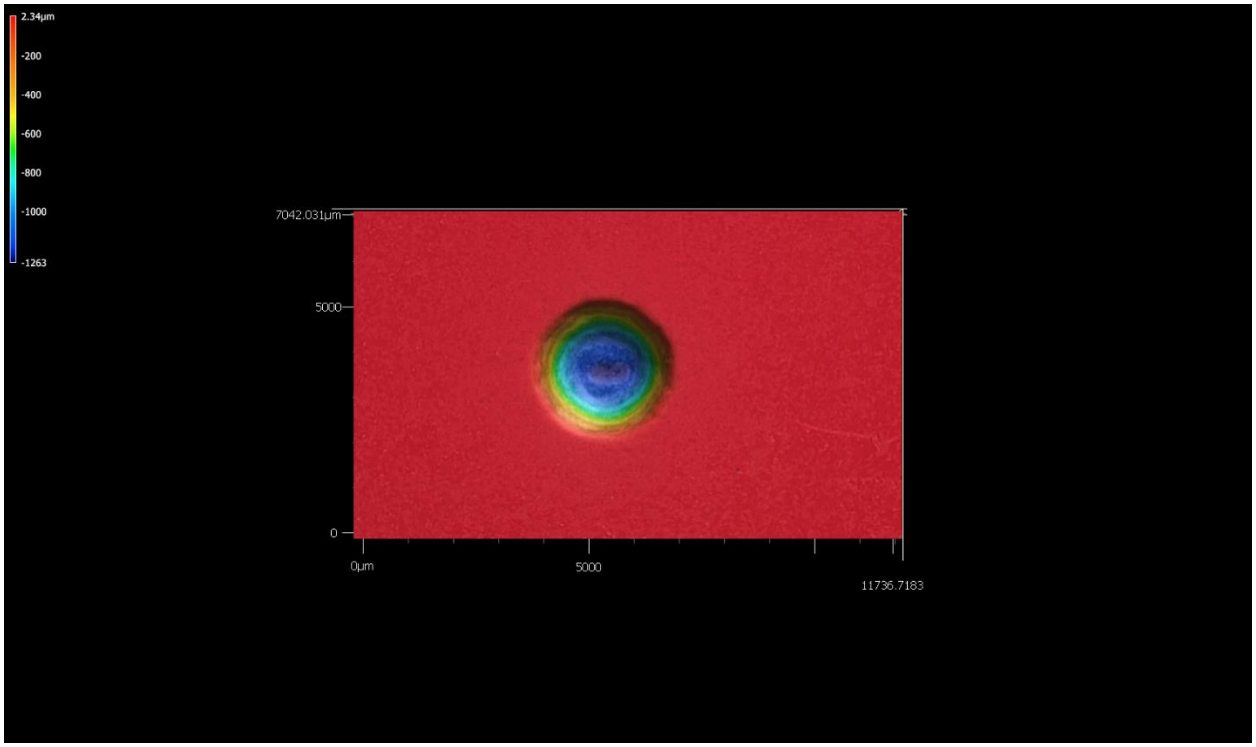


Fig. AII-138: Polyurethane/Polyurethane coated GFRP erosion scar EXP1 at 90° angle of attack

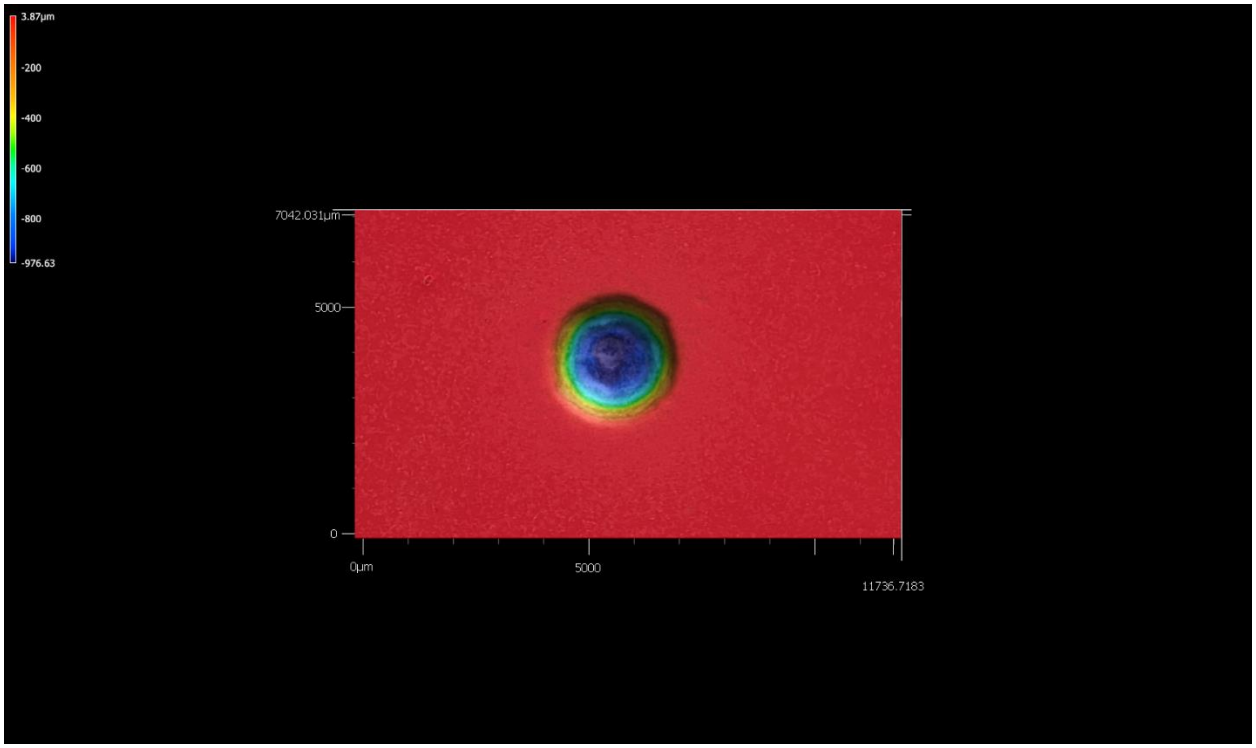


Fig. AII-139: Polyurethane/Polyurethane coated GFRP erosion scar EXP2 at 90° angle of attack

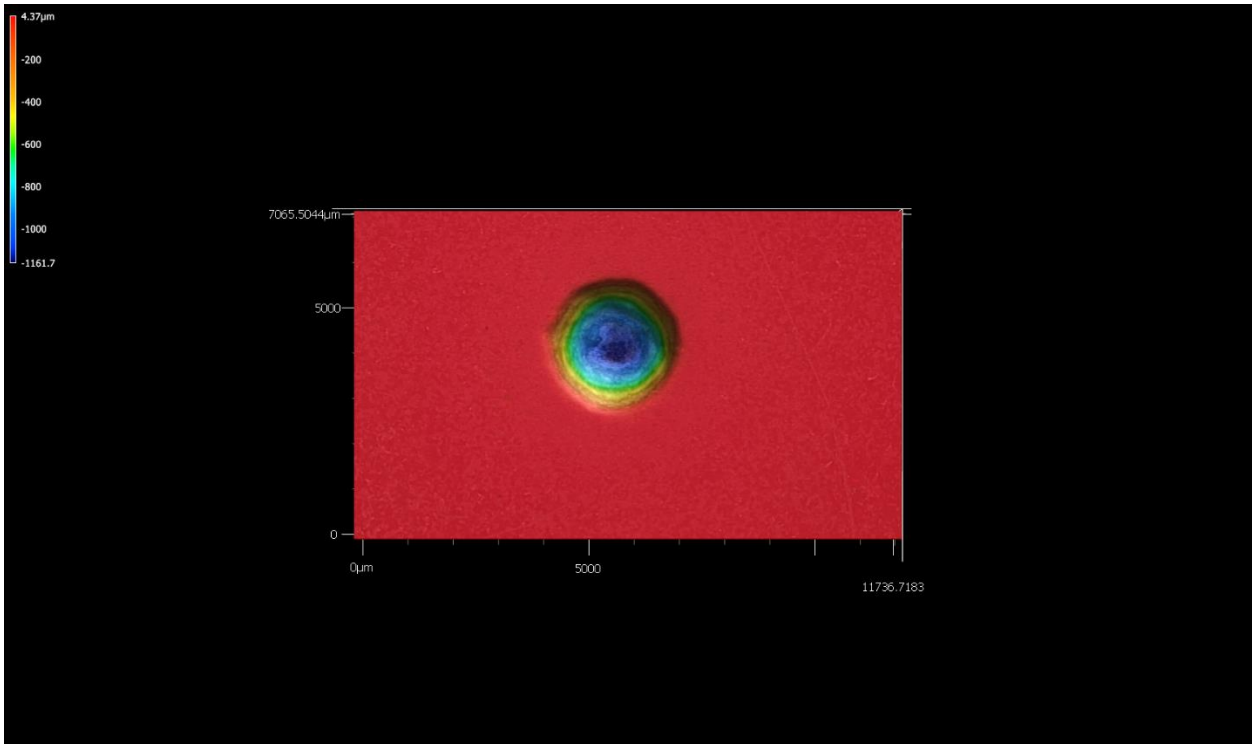


Fig. AII-140: Polyurethane/Polyurethane coated GFRP erosion scar EXP3 at 90° angle of attack

Coating 7 (Polyurethane/IA-700)

- 30 degrees

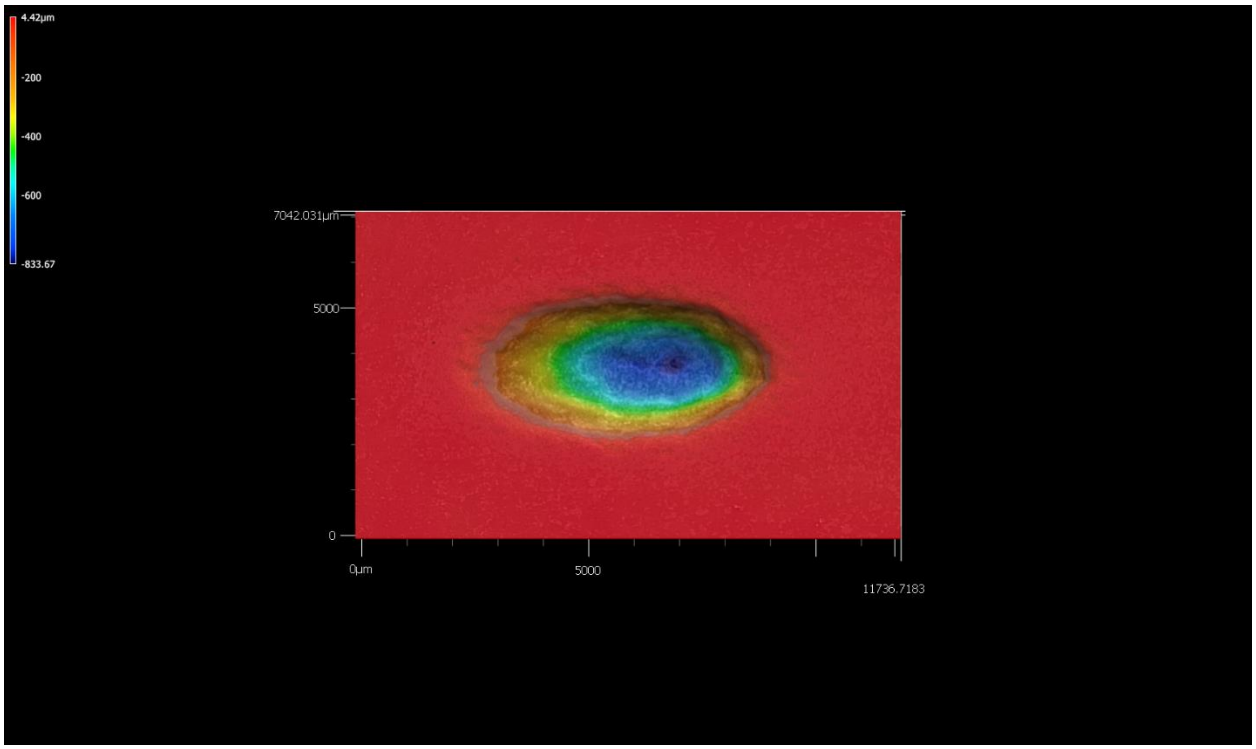


Fig. AII-141: Polyurethane/IA-700 coated GFRP erosion scar EXP1 at 30° angle of attack

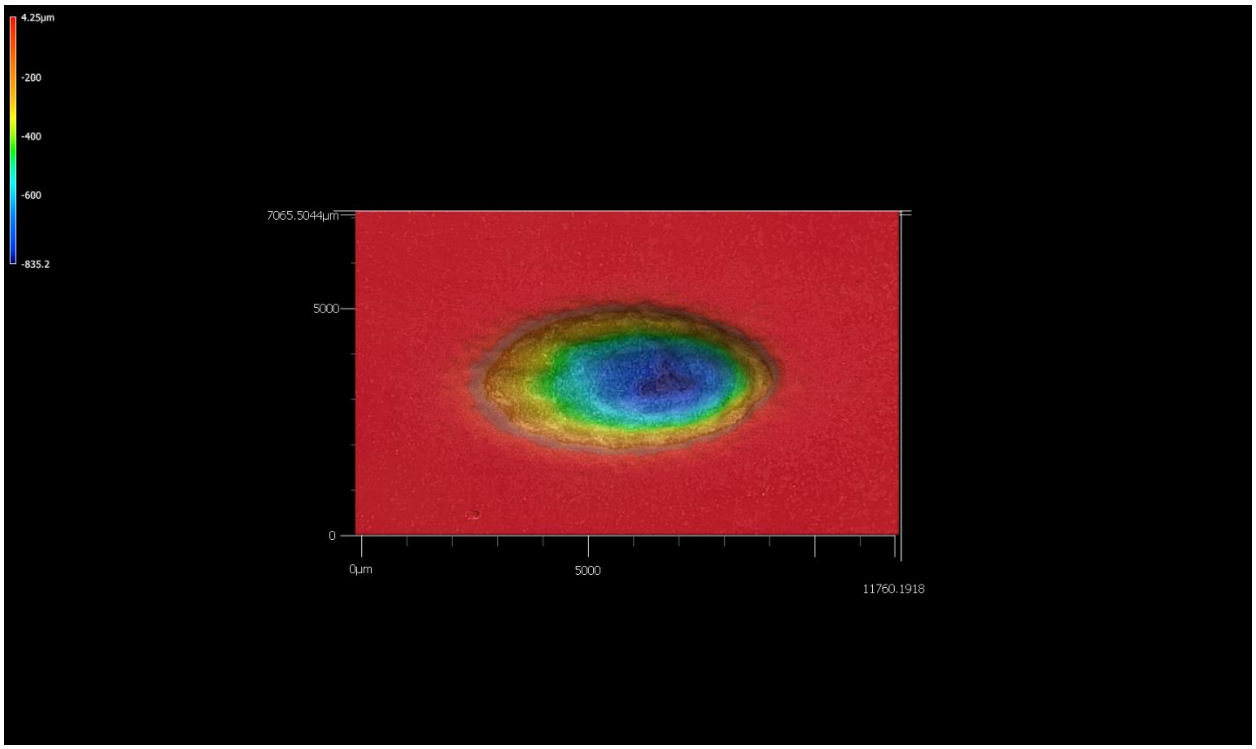


Fig. AII-142: Polyurethane/IA-700 coated GFRP erosion scar EXP2 at 30° angle of attack

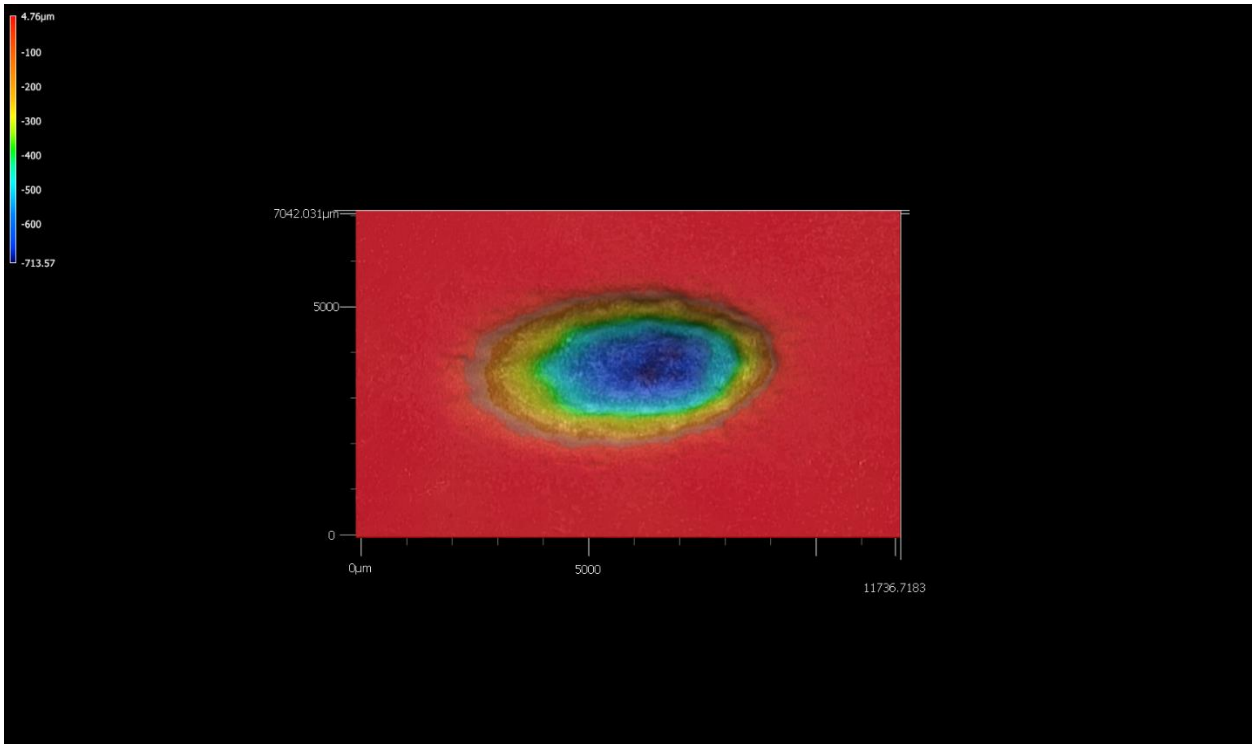


Fig. AII-143: Polyurethane/IA-700 coated GFRP erosion scar EXP3 at 30° angle of attack

- 45 degrees

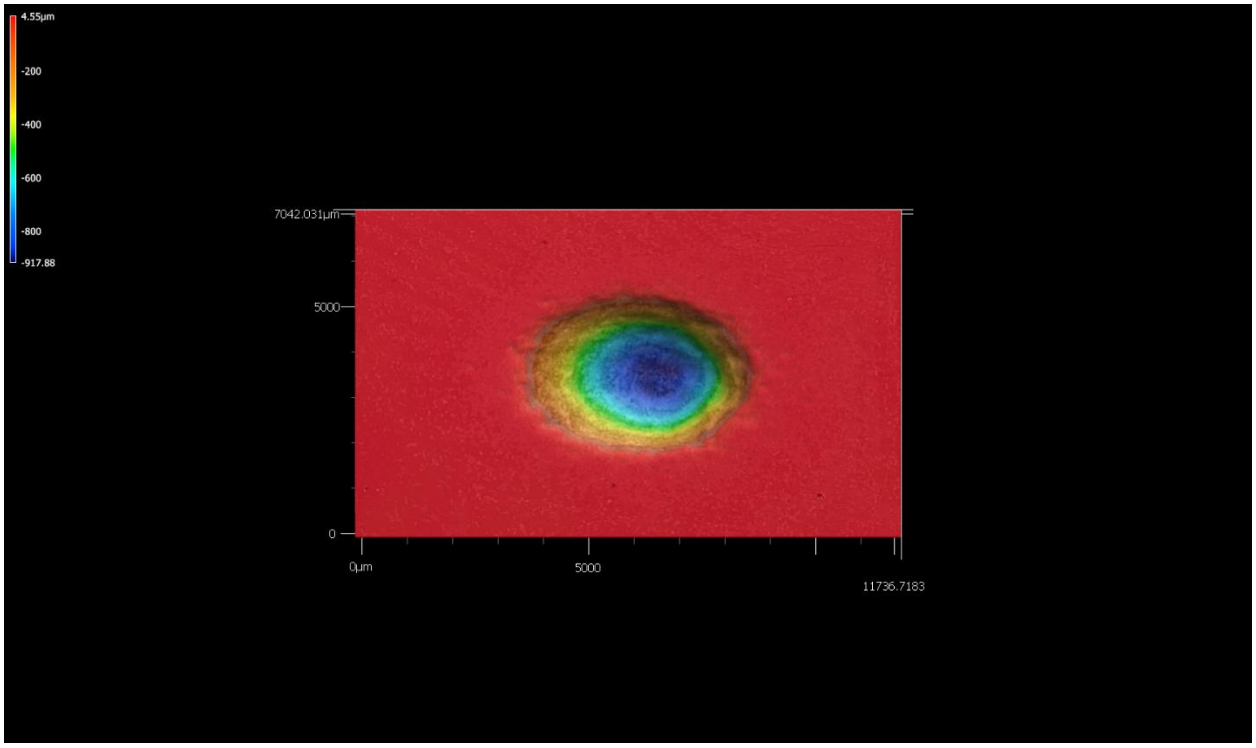


Fig. AII-144: Polyurethane/IA-700 coated GFRP erosion scar EXP1 at 45° angle of attack

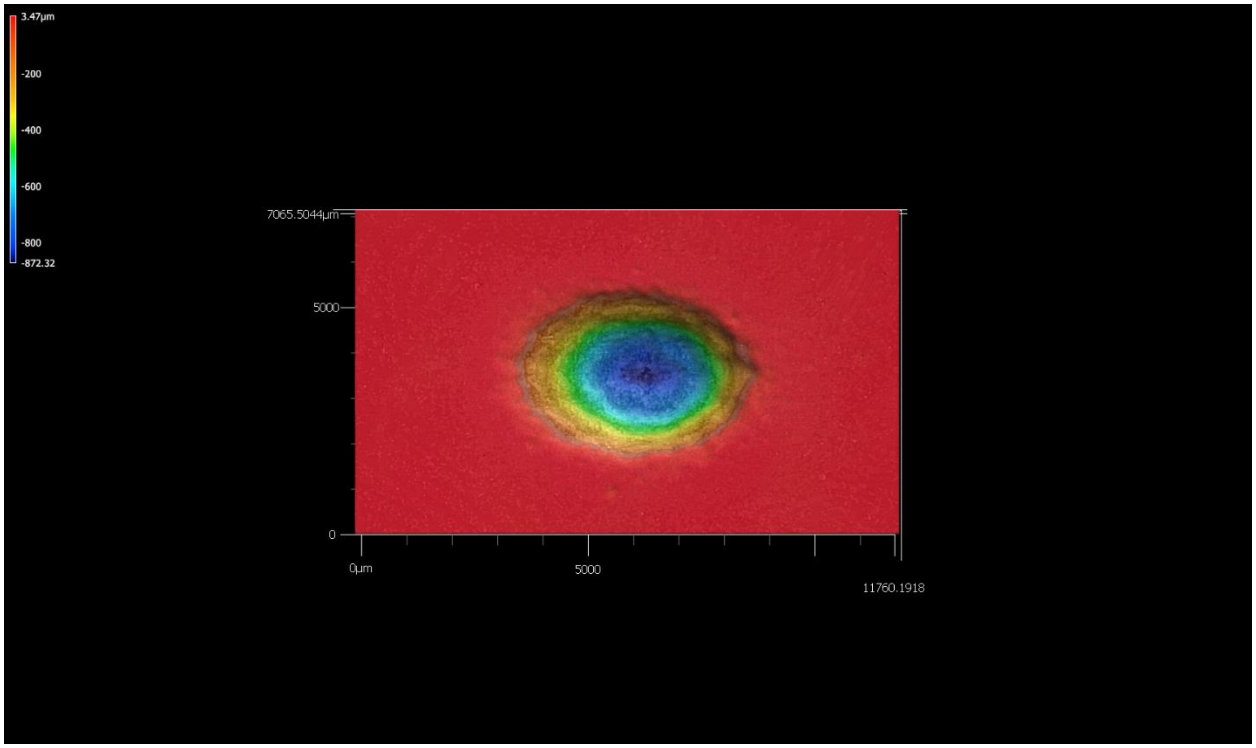


Fig. AII-145: Polyurethane/IA-700 coated GFRP erosion scar EXP2 at 45° angle of attack

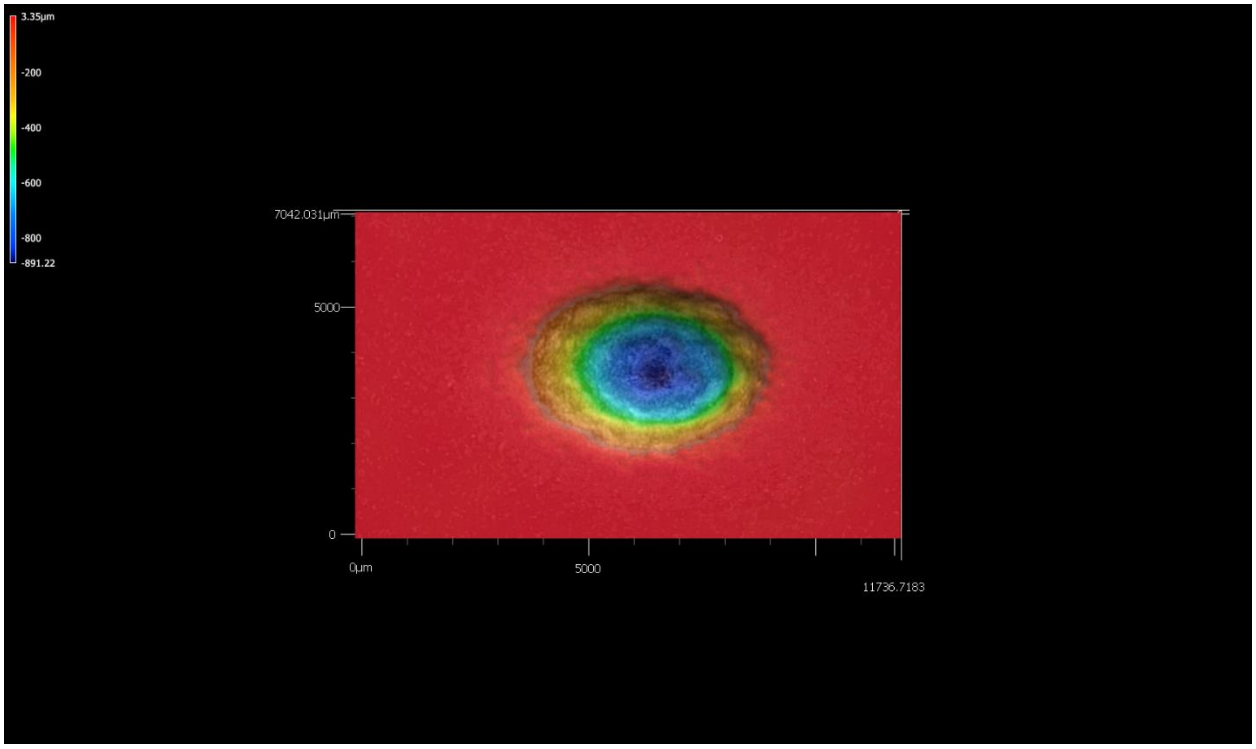


Fig. AII-146: Polyurethane/IA-700 coated GFRP erosion scar EXP3 at 45° angle of attack

- 60 degrees

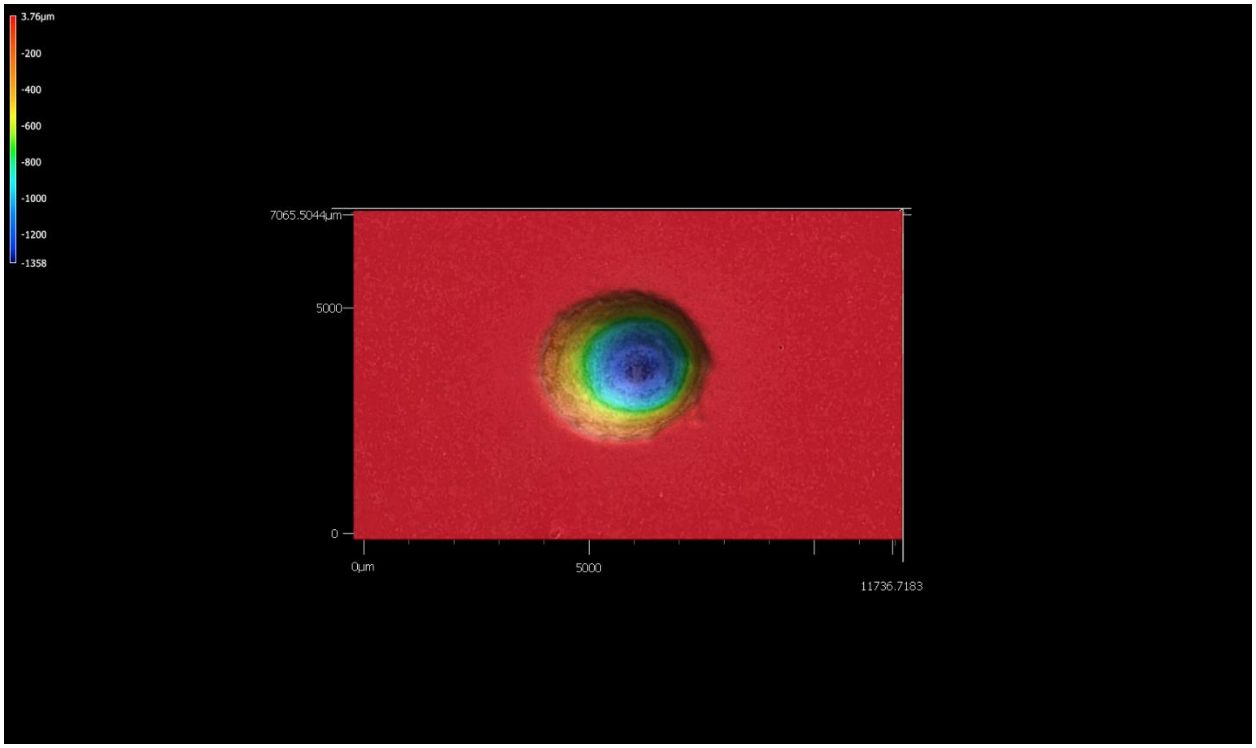


Fig. AII-147: Polyurethane/IA-700 coated GFRP erosion scar EXP1 at 60° angle of attack

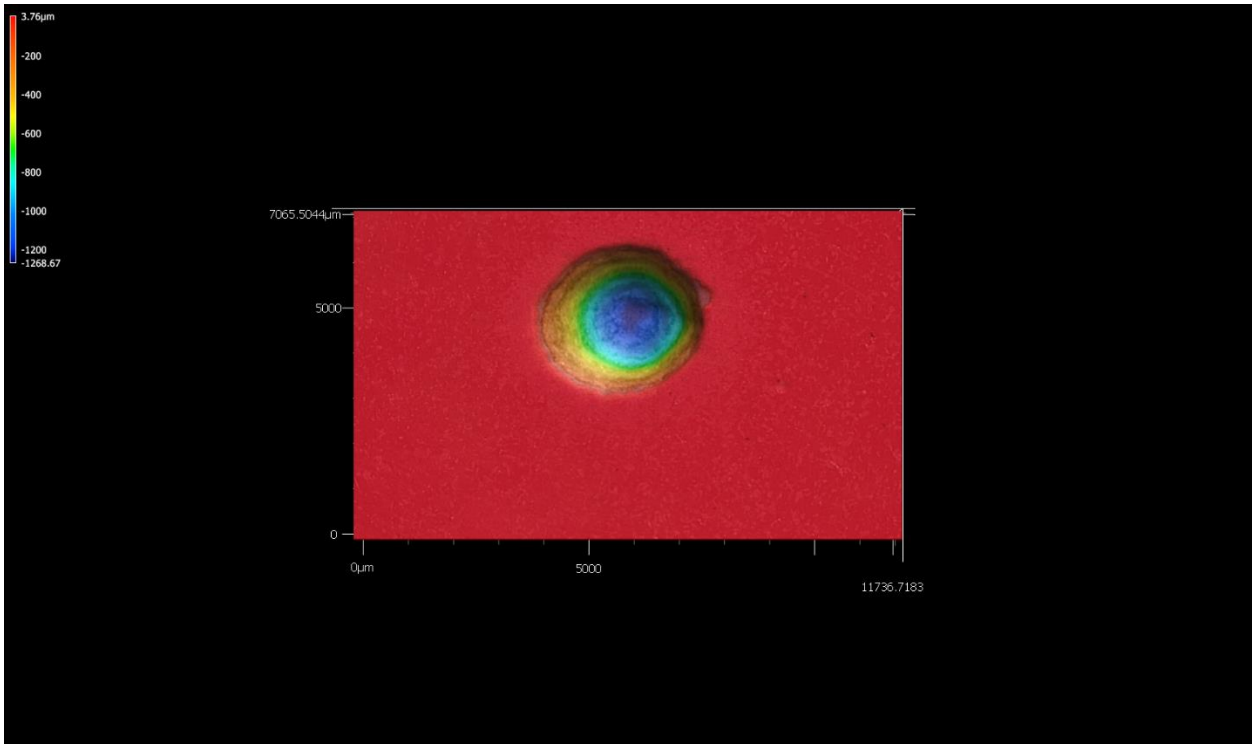


Fig. AII-148: Polyurethane/IA-700 coated GFRP erosion scar EXP2 at 60° angle of attack

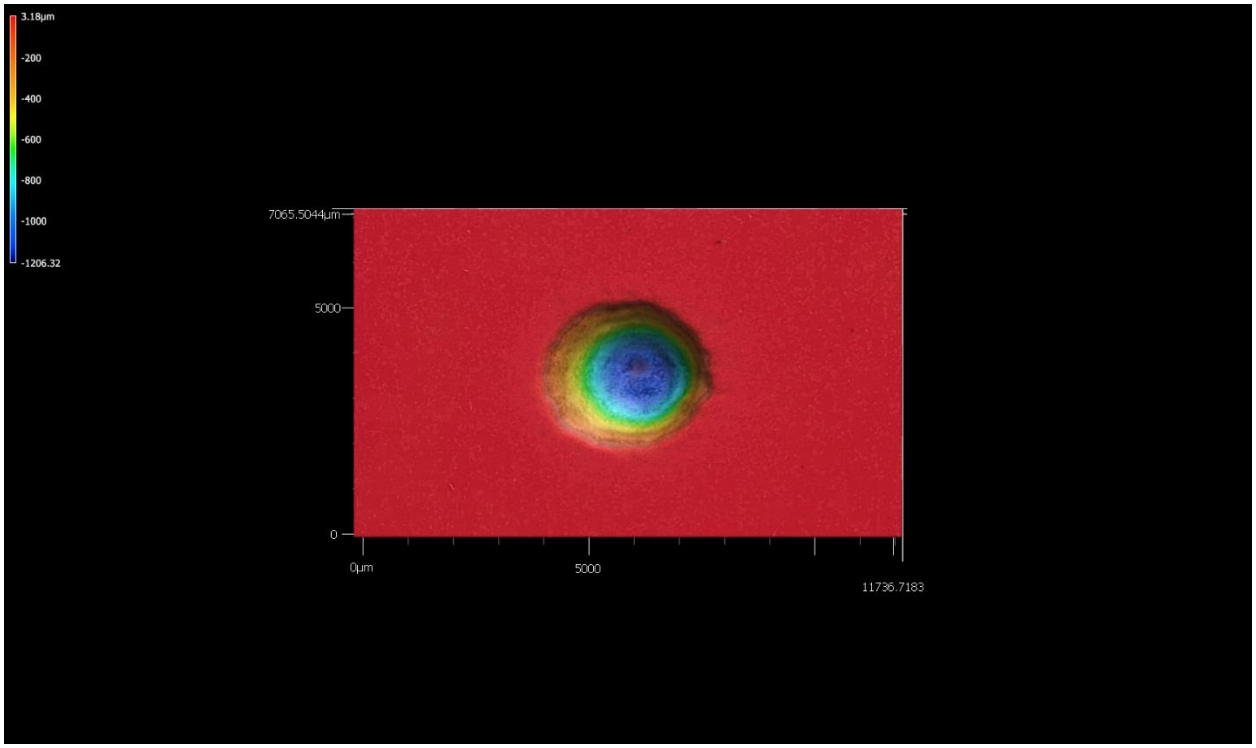


Fig. AII-149: Polyurethane/IA-700 coated GFRP erosion scar EXP3 at 60° angle of attack

- 75 degrees

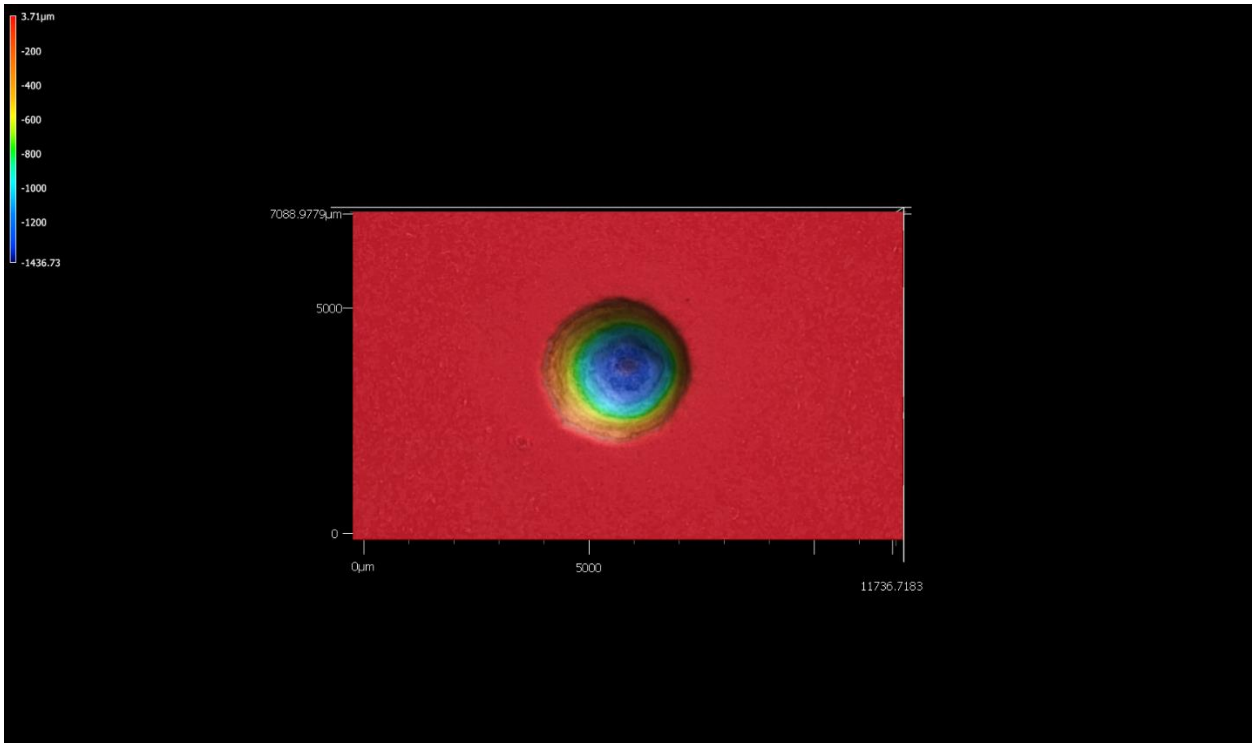


Fig. AII-150: Polyurethane/IA-700 coated GFRP erosion scar EXP1 at 75° angle of attack

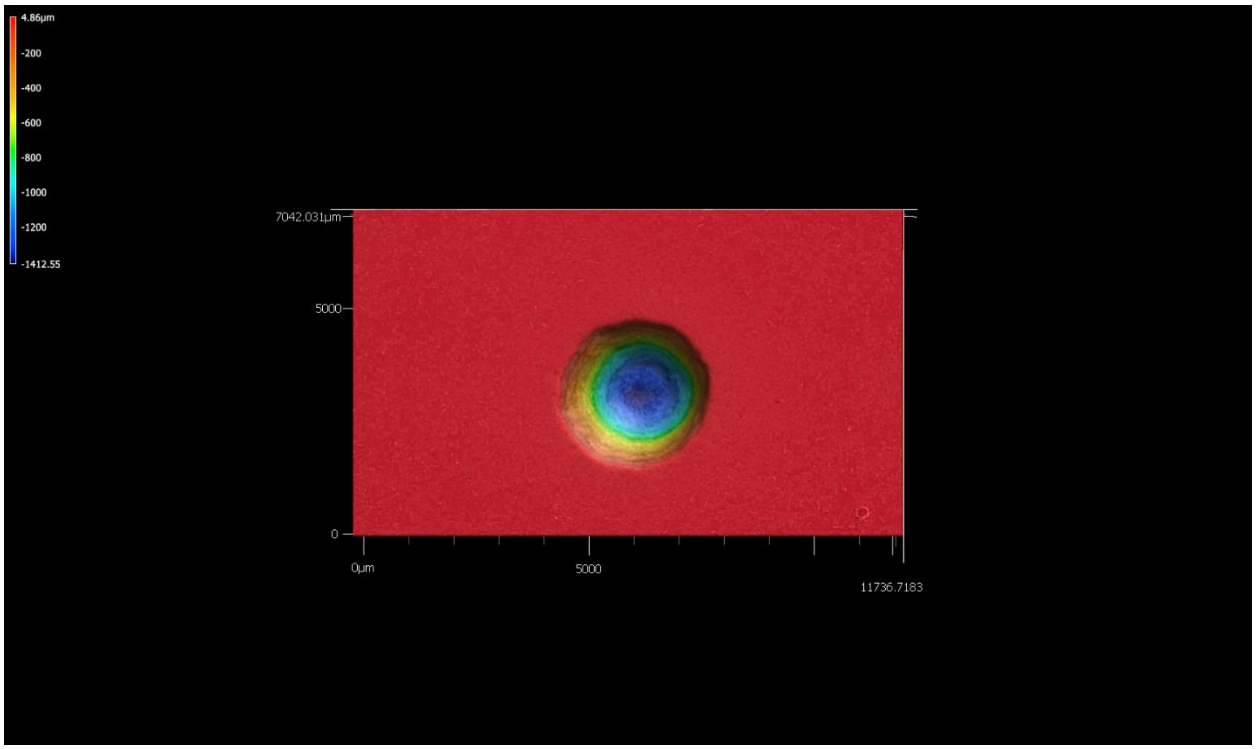


Fig. AII-151: Polyurethane/IA-700 coated GFRP erosion scar EXP2 at 75° angle of attack

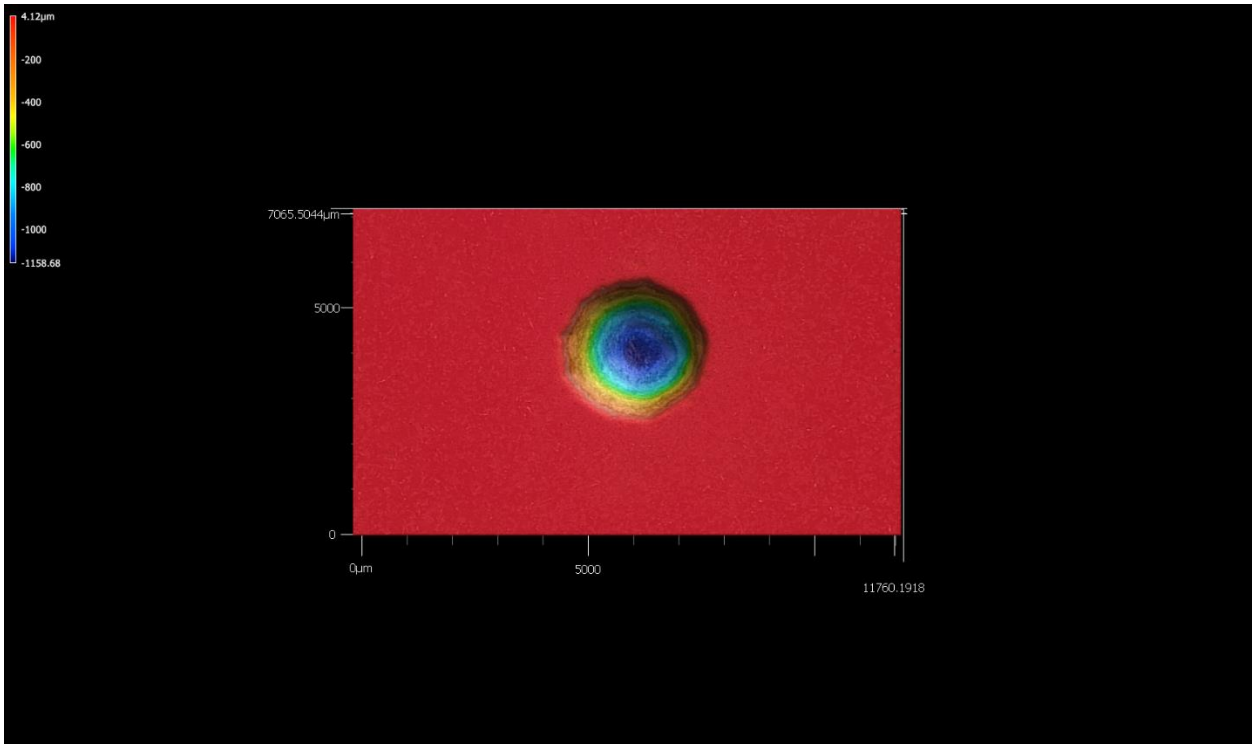


Fig. AII-152: Polyurethane/IA-700 coated GFRP erosion scar EXP3 at 75° angle of attack

- 90 degrees

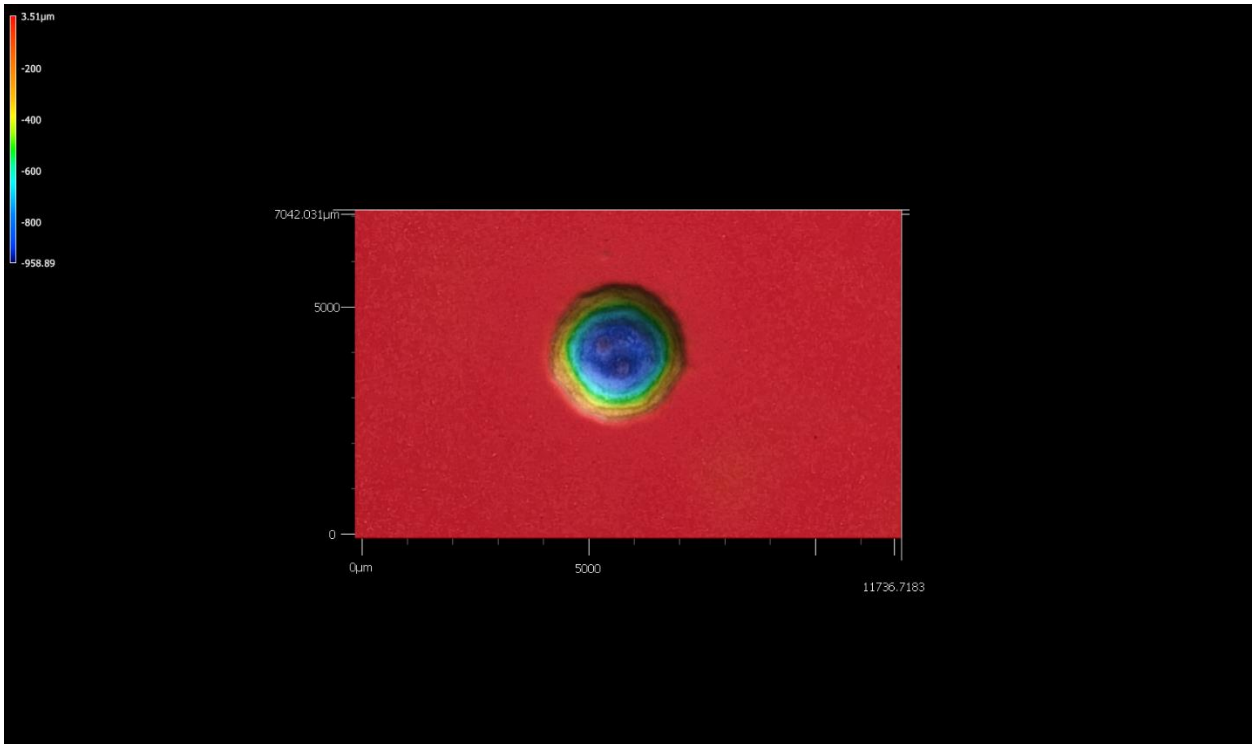


Fig. AII-153: Polyurethane/IA-700 coated GFRP erosion scar EXP1 at 90° angle of attack

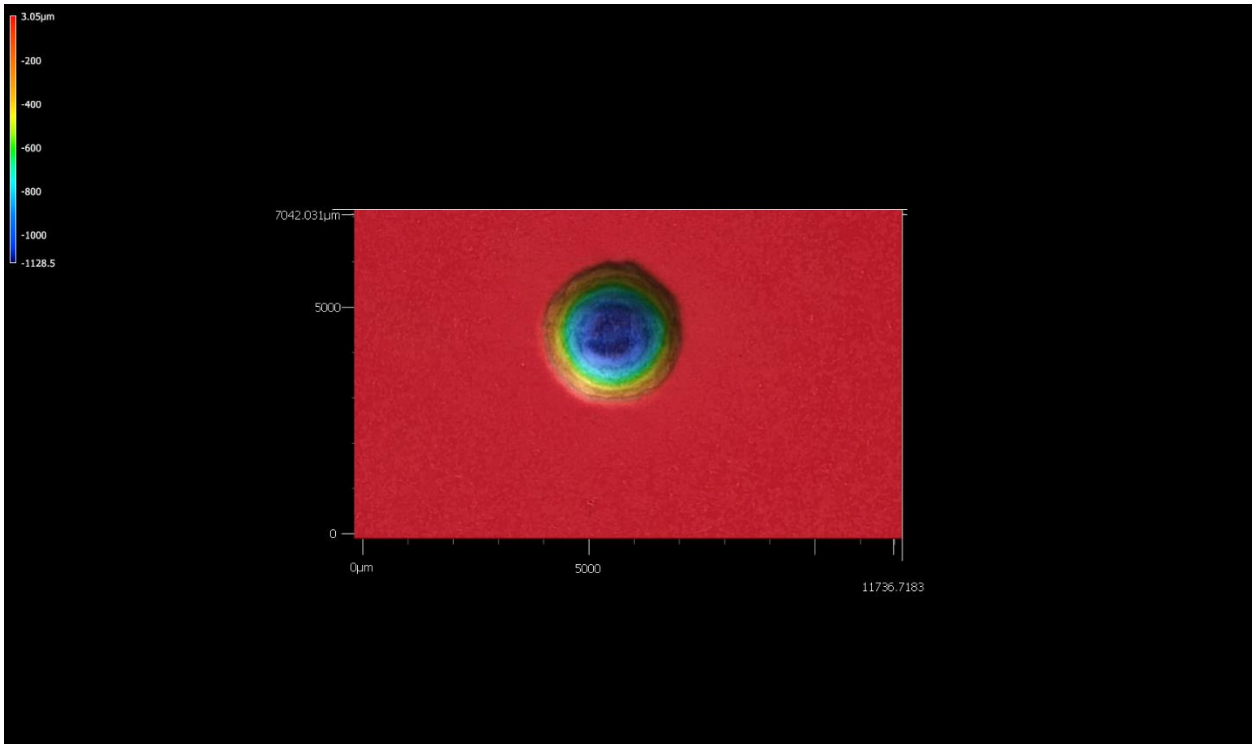


Fig. AII-154: Polyurethane/IA-700 coated GFRP erosion scar EXP2 at 90° angle of attack

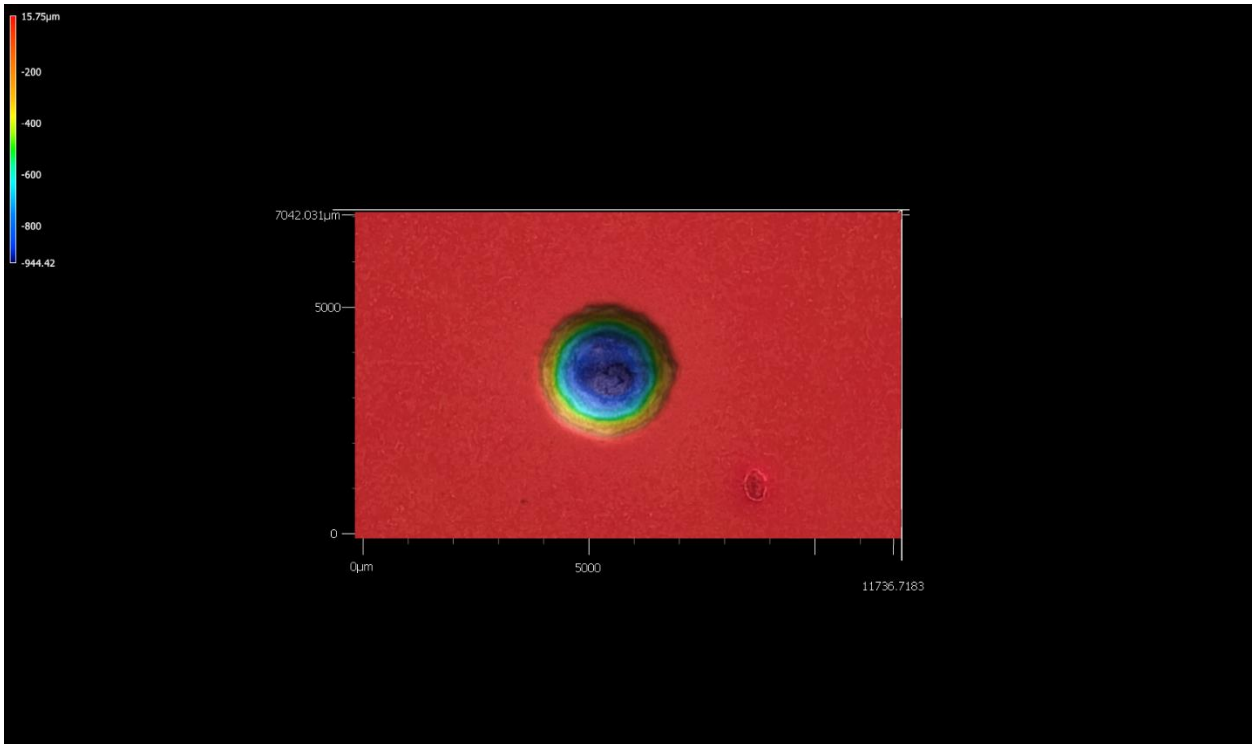


Fig. AII-155: Polyurethane/IA-700 coated GFRP erosion scar EXP3 at 90° angle of attack

Appendix III: Maximum depth of erosion scars

In this appendix, the amount of material removed from flat surfaces is shown. Mass loss in the aluminum target is shown in Table AIII-1, while mass loss of glass is shown in Table AIII-2. On the other hand, material removal data for uncoated and coated GFRP for 180 seconds and 360 seconds are shown in Tables AIII-3 to AIII-18.

- **Aluminum depth data:**

Table AIII-1: Maximum depth of erosion scars of aluminum target as a function of angle of attack

Angle of impingement	EXP 1 (μm)	EXP 2 (μm)	EXP 3 (μm)	Average (μm)	Standard deviation
10˚	-100.98	-75.33	-71.32	-82.54	16
20˚	-181.82	-154.56	-298.00	-211.46	76
30˚	-289.66	-280.53	-177.59	-249.26	62
45˚	-435.88	-306.28	-368.72	-370.29	65
60˚	-337.07	-296.30	-335.44	-322.94	23
90˚	-184.51	-191.12	-227.85	-201.16	23

- **Borosilicate Glass:**

Table AIII-2: Maximum depth of erosion scars of glass target as a function of angle of attack

Angle of impingement	EXP 1 (μm)	EXP 2 (μm)	EXP 3 (μm)	Average (μm)	Standard deviation
30˚	-434.47	-284.20	-388.36	-369.01	77
45˚	-760.51	-861.64	-896.60	-839.58	71
60˚	-1377.58	-1491.16	-1594.36	-1487.70	108
75˚	-1783.78	-2044.30	-2424.43	-2084.17	322
90˚	-2474.76	-2547.30	-2657.69	-2559.92	92

- **Uncoated GFRP:**
  - 180 seconds

Table AIII-3: Maximum depth of erosion scars of uncoated GFRP target as a function of angle of attack at an erosion duration of 180 seconds

Angle of impingement	EXP 1 (μm)	EXP 2 (μm)	EXP 3 (μm)	Average (μm)	Standard deviation
30˚	-484.79	-383.66	-476.76	-448.403	56
45˚	-769.31	-813.66	-734.38	-772.45	40
60˚	-762.83	-803.94	-804.78	-790.517	24
75˚	-716.88	-807.16	-848.67	-790.903	67
90˚	-779.52	-770.33	-802.99	-784.28	17

  - 360 seconds

Table AIII-4: Maximum depth of erosion scars of uncoated GFRP target as a function of angle of attack at an erosion duration of 360 seconds

Angle of impingement	EXP 1 (μm)	EXP 2 (μm)	EXP 3 (μm)	Average (μm)	Standard deviation
30˚	-860.6	-889.37	-836.59	-862.19	26
45˚	-1085.84	-929.04	-1176.31	-1063.73	125
60˚	-1232.12	-1396.65	-1258.71	-1295.83	88
75˚	-1328.57	-1256.24	-1216.75	-1267.19	57
90˚	-1124.25	-1200.36	-1193.9	-1172.84	42

- **H-146:**
  - 180 seconds

Table AIII-5: Maximum depth of erosion scars of H-146 coated GFRP target as a function of angle of attack at an erosion duration of 180 seconds

Angle of impingement	EXP 1 (μm)	EXP 2 (μm)	EXP 3 (μm)	Average (μm)	Standard deviation
30˚	-476.47	-633.48	-581.39	-563.78	80
45˚	-817.2	-773.26	-938.27	-842.91	85
60˚	-610.5	-938.12	-830.76	-818.018	167
75˚	-750.41	-868.69	-680.15	-779.772	95
90˚	-968.27	-959.02	-907.79	-945.027	33

- 360 seconds

Table AIII-6: Maximum depth of erosion scars of H-146 coated GFRP target as a function of angle of attack at an erosion duration of 360 seconds

Angle of impingement	EXP 1 (μm)	EXP 2 (μm)	EXP 3 (μm)	Average (μm)	Standard deviation
30˚	-811.7	-874.58	-843.38	-843.22	31
45˚	-857.42	-1172.89	-1031.83	-1020.71	158
60˚	-1256.48	-1212.67	-1100.24	-1189.8	81
75˚	-1198.7	-1140.76	-1140.76	-1160.07	33
90˚	-1345	-1237.2	-982.97	-1188.39	186

- **IA-700:**
  - 180 seconds

Table AIII-7: Maximum depth of erosion scars of IA-700 coated GFRP target as a function of angle of attack at an erosion duration of 180 seconds

Angle of impingement	EXP 1 (μm)	EXP 2 (μm)	EXP 3 (μm)	Average (μm)	Standard deviation
30˚	-484.79	-383.66	-476.74	-448.397	56
45˚	-796.31	-813.66	-734.38	-781.45	42
60˚	-899.19	-866.66	-801.35	-855.733	50
75˚	-696.27	-587.51	-535.91	-606.563	82
90˚	-877.34	-830.81	-841.3	-849.817	24

  - 360 seconds

Table AIII-8: Maximum depth of erosion scars of IA-700 coated GFRP target as a function of angle of attack at an erosion duration of 360 seconds

Angle of impingement	EXP 1 (μm)	EXP 2 (μm)	EXP 3 (μm)	Average (μm)	Standard deviation
30˚	-833.6	-867.92	-862.1	-854.54	18
45˚	-1294.53	-1162.62	-1178.29	-1211.81	72
60˚	-1344.98	-1266.8	-1124.8	-1245.53	112
75˚	-1178.84	-1083.9	-1183.24	-1148.66	56
90˚	-1374.75	-1035.44	-1241.9	-1217.36	171

- **Polyurethane:**
  - 180 seconds

Table AIII-9: Maximum depth of erosion scars of Polyurethane coated GFRP target as a function of angle of attack at an erosion duration of 180 seconds

Angle of impingement	EXP 1 (μm)	EXP 2 (μm)	EXP 3 (μm)	Average (μm)	Standard deviation
30˚	-423.32	-393.05	-444.63	-420.333	26
45˚	-643.12	-643.89	-696.8	-661.27	31
60˚	-717.96	-683.69	-641.69	-681.113	38
75˚	-804.2	-727.05	-649.43	-726.893	77
90˚	-737.88	-674.41	-749.48	-720.59	40

  - 360 seconds

Table AIII-10: Maximum depth of erosion scars of Polyurethane coated GFRP target as a function of angle of attack at an erosion duration of 360 seconds

Angle of impingement	EXP 1 (μm)	EXP 2 (μm)	EXP 3 (μm)	Average (μm)	Standard deviation
30˚	-770.24	-744.88	-772.56	-762.56	15
45˚	-991.43	-828.81	-874.36	-898.2	84
60˚	-1285.27	-1376.62	-1400.76	-1354.22	61
75˚	-1501.43	-1306.69	-1492.63	-1433.58	110
90˚	-1307.04	-1280.13	-1333.38	-1306.85	27

- **Coating 4 (H-146/Polyurethane):**
  - 180 seconds

Table AIII-11: Maximum depth of erosion scars of H-146/Polyurethane (Coating 4) coated GFRP target as a function of angle of attack at an erosion duration of 180 seconds

Angle of impingement	EXP 1 (μm)	EXP 2 (μm)	EXP 3 (μm)	Average (μm)	Standard deviation
30˚	-508.04	-442.65	-494.6	-481.763	35
45˚	-709.55	-723.87	-595.49	-676.303	70
60˚	-804.16	-688.37	-709.78	-734.103	62
75˚	-834.24	-781.27	-807.3	-807.603	26
90˚	-706.52	-707.81	-664.83	-693.053	24

- 360 seconds

Table AIII-12: Maximum depth of erosion scars of H-146/Polyurethane (Coating 4) coated GFRP target as a function of angle of attack at an erosion duration of 360 seconds

Angle of impingement	EXP 1 (μm)	EXP 2 (μm)	EXP 3 (μm)	Average (μm)	Standard deviation
30˚	-730.08	-744.73	-750.01	-741.607	10
45˚	-908.01	-1056.19	-1011.53	-991.91	76
60˚	-1312.83	-1197.57	-1339.61	-1283.34	75
75˚	-1337.44	-1366.76	-1445.52	-1383.24	56
90˚	-1301.68	-1313.89	-1299.07	-1304.88	8

- **Coating 5 (IA-700/Polyurethane):**
  - 180 seconds

Table AIII-13: Maximum depth of erosion scars of IA-700/Polyurethane (Coating 5) coated GFRP target as a function of angle of attack at an erosion duration of 180 seconds

Angle of impingement	EXP 1 (μm)	EXP 2 (μm)	EXP 3 (μm)	Average (μm)	Standard deviation
30˚	-519.87	-425.1	-400.74	-448.57	63
45˚	-743.5	-731.61	-558.96	-678.023	103
60˚	-739.99	-706.79	-738.64	-728.473	19
75˚	-886.78	-737.71	-759.14	-794.543	81
90˚	-762.3	-734.22	-756.95	-751.157	15

  - 360 seconds

Table AIII-14: Maximum depth of erosion scars of IA-700/Polyurethane (Coating 5) coated GFRP target as a function of angle of attack at an erosion duration of 360 seconds

Angle of impingement	EXP 1 (μm)	EXP 2 (μm)	EXP 3 (μm)	Average (μm)	Standard deviation
30˚	-749.5	-806.86	-826.41	-794.257	40
45˚	-983.67	-935.37	-868.87	-929.303	58
60˚	-1393.53	-1353.52	-1263.84	-1336.96	66
75˚	-1363.32	-1572.82	-1399.35	-1445.16	112
90˚	-1321.63	-1337.18	-1167.06	-1275.29	94

- **Coating 6 (Polyurethane/Polyurethane):**
  - 180 seconds

Table AIII-15: Maximum depth of erosion scars of Polyurethane/Polyurethane (Coating 6) coated GFRP target as a function of angle of attack at an erosion duration of 180 seconds

Angle of impingement	EXP 1 (μm)	EXP 2 (μm)	EXP 3 (μm)	Average (μm)	Standard deviation
30˚	-382.26	-347.37	-376.59	-368.74	19
45˚	-546.95	-544.57	-513.4	-534.973	19
60˚	-471.68	-518.46	-454.96	-481.7	33
75˚	-788.85	-773.83	-785.65	-782.777	8
90˚	-744.28	-668.47	-783.72	-732.157	59

  - 360 seconds

Table AIII-16: Maximum depth of erosion scars of Polyurethane/Polyurethane (Coating 6) coated GFRP target as a function of angle of attack at an erosion duration of 360 seconds

Angle of impingement	EXP 1 (μm)	EXP 2 (μm)	EXP 3 (μm)	Average (μm)	Standard deviation
30˚	-874.69	-738.51	-718.62	-777.273	85
45˚	-946.68	-792.5	-845	-861.393	78
60˚	-1130.5	-1081.69	-1101.84	-1104.68	25
75˚	-1369.85	-1450.18	-1230.1	-1350.04	111
90˚	-976.63	-1263	-1161.7	-1133.78	145

- **Coating 7 (Polyurethane/IA-700):**
  - 180 seconds

Table AIII-17: Maximum depth of erosion scars of Polyurethane/IA-700 (Coating 7) coated GFRP target as a function of angle of attack at an erosion duration of 180 seconds

Angle of impingement	EXP 1 (μm)	EXP 2 (μm)	EXP 3 (μm)	Average (μm)	Standard deviation
30˚	-376.06	-331.85	-390.63	-366.18	31
45˚	-700.64	-632.43	-572.18	-635.083	64
60˚	-589.59	-612.1	-557.72	-586.47	27
75˚	-736.84	-711.15	-900.42	-782.803	103
90˚	-516.81	-599.87	-627.43	-581.37	58

- 360 seconds

Table AIII-18: Maximum depth of erosion scars of Polyurethane/IA-700 (Coating 7) coated GFRP target as a function of angle of attack at an erosion duration of 360 seconds

Angle of impingement	EXP 1 (μm)	EXP 2 (μm)	EXP 3 (μm)	Average (μm)	Standard deviation
30˚	-833.67	-835.2	-713.57	-794.147	70
45˚	-917.88	-872.32	-891.22	-893.807	23
60˚	-1268.67	-1358	-1206.32	-1277.66	76
75˚	-1436.73	-1412.55	-1158.68	-1335.99	154
90˚	-1128.5	-958.89	-944.42	-1010.6	102

Appendix IV: Analysis of Variants (ANOVA)

Flat Surfaces

Uncoated

Response 1 depth

ANOVA for Response Surface Reduced Quadratic model
Analysis of variance table [Partial sum of squares - Type III]

Source	Sum of Squares	df	Mean Square	F Value	p-value Prob > F	
Model	1.888E+006	3	6.292E+005	128.26	< 0.0001	significant
A-Angle	*3.443E+005*	*1*	*3.443E+005*	*70.18*	*< 0.0001*	
B-Time	*1.292E+006*	*1*	*1.292E+006*	*263.36*	*< 0.0001*	
A^2	*2.513E+005*	*1*	*2.513E+005*	*51.23*	*< 0.0001*	
Residual	1.275E+005	26	4905.64			
Lack of Fit	*48975.07*	*6*	*8162.51*	*2.08*	*0.1019*	*not significant*
Pure Error	*78571.60*	*20*	*3928.58*			
Cor Total	2.015E+006	29				

The Model F-value of 128.26 implies the model is significant. There is only

a 0.01% chance that an F-value this large could occur due to noise.

Values of "Prob > F" less than 0.0500 indicate model terms are significant.

In this case A, B, A^2 are significant model terms.

Values greater than 0.1000 indicate the model terms are not significant.

The "Lack of Fit F-value" of 2.08 implies the Lack of Fit is not significant relative to the pure error. There is a 10.19% chance that a "Lack of Fit F-value" this large could occur due to noise. Non-significant lack of fit is good -- we want the model to fit.

Std. Dev.	70.04	R-Squared	0.9367
Mean	924.83	Adj R-Squared	0.9294
C.V. %	7.57	Pred R-Squared	0.9200
PRESS	1.612E+005	Adeq Precision	31.530

The "Pred R-Squared" of 0.9200 is in reasonable agreement with the "Adj R-Squared" of 0.9294; i.e. the difference is less than 0.2.

"Adeq Precision" measures the signal to noise ratio. A ratio greater than 4 is desirable. The ratio of 31.530 indicates an adequate signal. This model can be used to navigate the design space.

Factor	Coefficient Estimate	df	Standard Error	95% CI Low	95% CI High	VIF
Intercept	1034.23	1	19.93	993.27	1075.19	
A-Angle	151.50	1	18.08	114.32	188.67	1.00
B-Time	207.52	1	12.79	181.24	233.81	1.00
A^2	-218.79	1	30.57	-281.63	-155.96	1.00

Final Equation in Terms of Coded Factors:

depth =
+1034.23
+151.50 * A
+207.52 * B
-218.79 * A^2

The equation in terms of coded factors can be used to make predictions about the response for given levels of each factor. By default, the high levels of the factors are coded as +1 and the low levels of the factors are coded as -1. The coded equation is useful for identifying the relative impact of the factors by comparing the factor coefficients.

Final Equation in Terms of Actual Factors:

depth =
-766.49633
+34.22213 * Angle
+2.30579 * Time
-0.24310 * Angle^2

The equation in terms of actual factors can be used to make predictions about the response for given levels of each factor. Here, the levels should be specified in the original units for each factor. This equation should not be used to determine the relative impact of each factor because the coefficients are scaled to accommodate the units of each factor and the intercept is not at the center of the design space.

Response 2 mass loss

ANOVA for Response Surface Reduced Quadratic model
Analysis of variance table [Partial sum of squares - Type III]

Source	Sum of Squares	df	Mean Square	F Value	p-value Prob > F	
Model	1.193E-004	4	2.983E-005	36.34	< 0.0001	significant
A-Angle	*2.463E-005*	*1*	*2.463E-005*	*30.01*	*< 0.0001*	
B-time	*8.293E-005*	*1*	*8.293E-005*	*101.06*	*< 0.0001*	
AB	*4.839E-006*	*1*	*4.839E-006*	*5.90*	*0.0227*	
A^2	*6.903E-006*	*1*	*6.903E-006*	*8.41*	*0.0077*	
Residual	2.052E-005	25	8.207E-007			
Lack of Fit	*9.843E-006*	*5*	*1.969E-006*	*3.69*	*0.0158*	*significant*
Pure Error	*1.067E-005*	*20*	*5.337E-007*			
Cor Total	1.398E-004	29				

The Model F-value of 36.34 implies the model is significant. There is only

a 0.01% chance that an F-value this large could occur due to noise.

Values of "Prob > F" less than 0.0500 indicate model terms are significant.

In this case A, B, AB, A^2 are significant model terms.

Values greater than 0.1000 indicate the model terms are not significant.

The "Lack of Fit F-value" of 3.69 implies the Lack of Fit is significant. There is only a 1.58% chance that a "Lack of Fit F-value" this large could occur due to noise. Significant lack of fit is bad -- we want the model to fit.

Std. Dev.	9.059E-004	R-Squared	0.8533
Mean	7.329E-003	Adj R-Squared	0.8298
C.V. %	12.36	Pred R-Squared	0.7954
PRESS	2.861E-005	Adeq Precision	15.921

The "Pred R-Squared" of 0.7954 is in reasonable agreement with the "Adj R-Squared" of 0.8298; i.e. the difference is less than 0.2.

"Adeq Precision" measures the signal to noise ratio. A ratio greater than 4 is desirable. The ratio of 15.921 indicates an adequate signal. This model can be used to navigate the design space.

Factor	Coefficient Estimate	df	Standard Error	95% CI Low	95% CI High	VIF
Intercept	7.903E-003	1	2.577E-004	7.372E-003	8.434E-003	
A-Angle	-1.281E-003	1	2.339E-004	-1.763E-003	-7.996E-004	1.00
B-time	1.663E-003	1	1.654E-004	1.322E-003	2.003E-003	1.00
AB	-5.680E-004	1	2.339E-004	-1.050E-003	-8.627E-005	1.00
A^2	-1.147E-003	1	3.954E-004	-1.961E-003	-3.324E-004	1.00

Final Equation in Terms of Coded Factors:

mass loss =
+7.903E-003
-1.281E-003 * A
+1.663E-003 * B
-5.680E-004 * AB
-1.147E-003 * A^2

Final Equation in Terms of Actual Factors:

mass loss =
-2.51733E-003
+1.66978E-004 * Angle
+3.10963E-005 * time
-2.10370E-007 * Angle * time
-1.27407E-006 * Angle^2

H-146

Response 1 depth

ANOVA for Response Surface Reduced Quadratic model
Analysis of variance table [Partial sum of squares - Type III]

Source	Sum of Squares	df	Mean Square	F Value	p-value Prob > F	
Model	1.060E+006	3	3.534E+005	26.22	< 0.0001	significant
A-Angle	*3.446E+005*	*1*	*3.446E+005*	*25.56*	*< 0.0001*	
B-Time	*6.669E+005*	*1*	*6.669E+005*	*49.47*	*< 0.0001*	
A^2	*48835.29*	*1*	*48835.29*	*3.62*	*0.0681*	
Residual	3.505E+005	26	13480.55			
Lack of Fit	*1.108E+005*	*6*	*18461.21*	*1.54*	*0.2163*	*not significant*
Pure Error	*2.397E+005*	*20*	*11986.36*			
Cor Total	1.411E+006	29				

The Model F-value of 26.22 implies the model is significant. There is only

a 0.01% chance that an F-value this large could occur due to noise.

Values of "Prob > F" less than 0.0500 indicate model terms are significant.

In this case A, B are significant model terms.

Values greater than 0.1000 indicate the model terms are not significant.

The "Lack of Fit F-value" of 1.54 implies the Lack of Fit is not significant relative to the pure

error. There is a 21.63% chance that a "Lack of Fit F-value" this large could occur due

to noise. Non-significant lack of fit is good -- we want the model to fit.

Std. Dev.	116.11	R-Squared	0.7516
Mean	931.35	Adj R-Squared	0.7229
C.V. %	12.47	Pred R-Squared	0.6739
PRESS	4.601E+005	Adeq Precision	14.184

The "Pred R-Squared" of 0.6739 is in reasonable agreement with the "Adj R-Squared" of 0.7229; i.e. the difference is less than 0.2.

"Adeq Precision" measures the signal to noise ratio. A ratio greater than 4 is desirable. The ratio of 14.184 indicates an adequate signal. This model can be used to navigate the design space.

Factor	Coefficient Estimate	df	Standard Error	95% CI Low	95% CI High	VIF
Intercept	979.57	1	33.03	911.67	1047.47	
A-Angle	151.57	1	29.98	89.95	213.19	1.00
B-Time	149.09	1	21.20	105.52	192.67	1.00
A^2	-96.45	1	50.67	-200.61	7.71	1.00

Final Equation in Terms of Coded Factors:

depth =
+979.57
+151.57 * A
+149.09 * B
-96.45 * A^2

Final Equation in Terms of Actual Factors:

depth =
-156.63800
+17.91189 * Angle
+1.65659 * Time
-0.10716 * Angle^2

Response 2 mass loss

ANOVA for Response Surface 2FI model
Analysis of variance table [Partial sum of squares - Type III]

Source	Sum of Squares	df	Mean Square	F Value	p-value Prob > F	
Model	7.327E-005	3	2.442E-005	26.82	< 0.0001	significant
A-Angle	*2.058E-005*	*1*	*2.058E-005*	*22.59*	*< 0.0001*	
B-time	*5.028E-005*	*1*	*5.028E-005*	*55.21*	*< 0.0001*	
AB	*2.408E-006*	*1*	*2.408E-006*	*2.64*	*0.1160*	
Residual	2.368E-005	26	9.108E-007			
Lack of Fit	*1.337E-005*	*6*	*2.228E-006*	*4.32*	*0.0059*	*significant*
Pure Error	*1.032E-005*	*20*	*5.158E-007*			
Cor Total	9.696E-005	29				

The Model F-value of 26.82 implies the model is significant. There is only

a 0.01% chance that an F-value this large could occur due to noise.

Values of "Prob > F" less than 0.0500 indicate model terms are significant.

In this case A, B are significant model terms.

Values greater than 0.1000 indicate the model terms are not significant.

The "Lack of Fit F-value" of 4.32 implies the Lack of Fit is significant. There is only a

0.59% chance that a "Lack of Fit F-value" this large could occur due to noise.

Significant lack of fit is bad -- we want the model to fit.

Std. Dev.	9.544E-004	R-Squared	0.7557
Mean	7.195E-003	Adj R-Squared	0.7276
C.V. %	13.27	Pred R-Squared	0.6832
PRESS	3.072E-005	Adeq Precision	14.152

The "Pred R-Squared" of 0.6832 is in reasonable agreement with the "Adj R-Squared" of 0.7276; i.e. the difference is less than 0.2.

"Adeq Precision" measures the signal to noise ratio. A ratio greater than 4 is desirable. The ratio of 14.152 indicates an adequate signal. This model can be used to navigate the design space.

Factor	Coefficient Estimate	df	Standard Error	95% CI Low	95% CI High	VIF
Intercept	7.195E-003	1	1.742E-004	6.836E-003	7.553E-003	
A-Angle	-1.171E-003	1	2.464E-004	-1.678E-003	-6.648E-004	1.00
B-time	1.295E-003	1	1.742E-004	9.365E-004	1.653E-003	1.00
AB	-4.007E-004	1	2.464E-004	-9.072E-004	1.059E-004	1.00

Final Equation in Terms of Coded Factors:

mass loss =
+7.195E-003
-1.171E-003 * A
+1.295E-003 * B
-4.007E-004 * AB

Final Equation in Terms of Actual Factors:

mass loss =
+3.24933E-003
+1.02222E-006 * Angle
+2.32889E-005 * time
-1.48395E-007 * Angle * time

IA-700

Response 1 depth

ANOVA for Response Surface Reduced Quadratic model
Analysis of variance table [Partial sum of squares - Type III]

Source	Sum of Squares	df	Mean Square	F Value	p-value Prob > F	
Model	1.776E+006	3	5.918E+005	37.58	< 0.0001	significant
A-Angle	*2.498E+005*	*1*	*2.498E+005*	*15.86*	*0.0005*	
B-Time	*1.369E+006*	*1*	*1.369E+006*	*86.90*	*< 0.0001*	
A^2	*1.571E+005*	*1*	*1.571E+005*	*9.97*	*0.0040*	
Residual	4.095E+005	26	15750.60			
Lack of Fit	*2.794E+005*	*6*	*46569.31*	*7.16*	*0.0004*	*significant*
Pure Error	*1.301E+005*	*20*	*6504.98*			
Cor Total	2.185E+006	29				

The Model F-value of 37.58 implies the model is significant. There is only

a 0.01% chance that an F-value this large could occur due to noise.

Values of "Prob > F" less than 0.0500 indicate model terms are significant.

In this case A, B, A^2 are significant model terms.

Values greater than 0.1000 indicate the model terms are not significant.

The "Lack of Fit F-value" of 7.16 implies the Lack of Fit is significant. There is only a

0.04% chance that a "Lack of Fit F-value" this large could occur due to noise.

Significant lack of fit is bad -- we want the model to fit.

Std. Dev.	125.50	R-Squared	0.8126
Mean	921.99	Adj R-Squared	0.7910
C.V. %	13.61	Pred R-Squared	0.7553
PRESS	5.347E+005	Adeq Precision	16.377

The "Pred R-Squared" of 0.7553 is in reasonable agreement with the "Adj R-Squared" of 0.7910; i.e. the difference is less than 0.2.

"Adeq Precision" measures the signal to noise ratio. A ratio greater than 4 is desirable. The ratio of 16.377 indicates an adequate signal. This model can be used to navigate the design space.

Factor	Coefficient Estimate	df	Standard Error	95% CI Low	95% CI High	VIF
Intercept	1008.47	1	35.71	935.07	1081.87	
A-Angle	129.04	1	32.40	62.44	195.65	1.00
B-Time	213.59	1	22.91	166.50	260.69	1.00
A^2	-172.97	1	54.77	-285.56	-60.38	1.00

Final Equation in Terms of Coded Factors:

depth =
+1008.47
+129.04 * A
+213.59 * B
-172.97 * A^2

Final Equation in Terms of Actual Factors:

depth =
-582.27267
+27.36384 * Angle
+2.37327 * Time
-0.19219 * Angle^2

Response 2 mass loss

ANOVA for Response Surface Reduced Quadratic model
Analysis of variance table [Partial sum of squares - Type III]

Source	Sum of Squares	df	Mean Square	F Value	p-value Prob > F	
Model	1.456E-004	3	4.854E-005	41.69	< 0.0001	significant
A-Angle	*2.722E-005*	*1*	*2.722E-005*	*23.38*	*< 0.0001*	
B-time	*1.046E-004*	*1*	*1.046E-004*	*89.82*	*< 0.0001*	
A^2	*1.382E-005*	*1*	*1.382E-005*	*11.87*	*0.0019*	
Residual	3.027E-005	26	1.164E-006			
Lack of Fit	*1.165E-005*	*6*	*1.941E-006*	*2.08*	*0.1009*	*not significant*
Pure Error	*1.862E-005*	*20*	*9.312E-007*			
Cor Total	1.759E-004	29				

The Model F-value of 41.69 implies the model is significant. There is only

a 0.01% chance that an F-value this large could occur due to noise.

Values of "Prob > F" less than 0.0500 indicate model terms are significant.

In this case A, B, A^2 are significant model terms.

Values greater than 0.1000 indicate the model terms are not significant.

If there are many insignificant model terms (not counting those required to support hierarchy),

model reduction may improve your model.

The "Lack of Fit F-value" of 2.08 implies the Lack of Fit is not significant relative to the pure

error. There is a 10.09% chance that a "Lack of Fit F-value" this large could occur due

to noise. Non-significant lack of fit is good -- we want the model to fit.

Std. Dev.	1.079E-003	R-Squared	0.8279
Mean	7.904E-003	Adj R-Squared	0.8080
C.V. %	13.65	Pred R-Squared	0.7811
PRESS	3.851E-005	Adeq Precision	17.694

The "Pred R-Squared" of 0.7811 is in reasonable agreement with the "Adj R-Squared" of 0.8080; i.e. the difference is less than 0.2.

"Adeq Precision" measures the signal to noise ratio. A ratio greater than 4 is desirable. The ratio of 17.694 indicates an adequate signal. This model can be used to navigate the design space.

Factor	Coefficient Estimate	df	Standard Error	95% CI Low	95% CI High	VIF
Intercept	8.715E-003	1	3.070E-004	8.084E-003	9.346E-003	
A-Angle	-1.347E-003	1	2.786E-004	-1.920E-003	-7.743E-004	1.00
B-time	1.867E-003	1	1.970E-004	1.462E-003	2.272E-003	1.00
A^2	-1.622E-003	1	4.709E-004	-2.590E-003	-6.544E-004	1.00

Final Equation in Terms of Coded Factors:

mass loss =
+8.715E-003
-1.347E-003 * A
+1.867E-003 * B
-1.622E-003 * A^2

Final Equation in Terms of Actual Factors:

mass loss =
-6.81667E-004
+1.71417E-004 * Angle
+2.07444E-005 * time
-1.80265E-006 * Angle^2

Polyurethane

Response 1 depth

ANOVA for Response Surface Reduced Quadratic model
Analysis of variance table [Partial sum of squares - Type III]

Source	Sum of Squares	df	Mean Square	F Value	p-value Prob > F	
Model	3.069E+006	4	7.672E+005	88.16	< 0.0001	significant
A-Angle	*7.867E+005*	*1*	*7.867E+005*	*90.40*	*< 0.0001*	
B-Time	*1.943E+006*	*1*	*1.943E+006*	*223.32*	*< 0.0001*	
AB	*1.376E+005*	*1*	*1.376E+005*	*15.81*	*0.0005*	
A^2	*2.011E+005*	*1*	*2.011E+005*	*23.11*	*< 0.0001*	
Residual	2.176E+005	25	8702.42			
Lack of Fit	*1.486E+005*	*5*	*29716.68*	*8.62*	*0.0002*	*significant*
Pure Error	*68977.08*	*20*	*3448.85*			
Cor Total	3.286E+006	29				

The Model F-value of 88.16 implies the model is significant. There is only

a 0.01% chance that an F-value this large could occur due to noise.

Values of "Prob > F" less than 0.0500 indicate model terms are significant.

In this case A, B, AB, A^2 are significant model terms.

Values greater than 0.1000 indicate the model terms are not significant.

The "Lack of Fit F-value" of 8.62 implies the Lack of Fit is significant. There is only a

0.02% chance that a "Lack of Fit F-value" this large could occur due to noise.

Significant lack of fit is bad -- we want the model to fit.

Std. Dev.	93.29	R-Squared	0.9338
Mean	896.56	Adj R-Squared	0.9232
C.V. %	10.40	Pred R-Squared	0.9112
PRESS	2.917E+005	Adeq Precision	25.393

The "Pred R-Squared" of 0.9112 is in reasonable agreement with the "Adj R-Squared" of 0.9232; i.e. the difference is less than 0.2.

"Adeq Precision" measures the signal to noise ratio. A ratio greater than 4 is desirable. The ratio of 25.393 indicates an adequate signal. This model can be used to navigate the design space.

Factor	Coefficient Estimate	df	Standard Error	95% CI Low	95% CI High	VIF
Intercept	994.41	1	26.54	939.75	1049.08	
A-Angle	229.01	1	24.09	179.40	278.62	1.00
B-Time	254.52	1	17.03	219.44	289.60	1.00
AB	95.78	1	24.09	46.18	145.39	1.00
A^2	-195.71	1	40.71	-279.56	-111.85	1.00

Final Equation in Terms of Coded Factors:

depth =
+994.41
+229.01 * A
+254.52 * B
+95.78 * AB
-195.71 * A^2

Final Equation in Terms of Actual Factors:

depth =
-435.29600
+24.14950 * Angle
+0.69951 * Time
+0.035475 * Angle * Time
-0.21745 * Angle^2

Response 2 mass loss

ANOVA for Response Surface Linear model
Analysis of variance table [Partial sum of squares - Type III]

Source	Sum of Squares	df	Mean Square	F Value	p-value Prob > F	
Model	2.320E-004	2	1.160E-004	231.05	< 0.0001	significant
A-Angle	*2.083E-006*	*1*	*2.083E-006*	*4.15*	*0.0516*	
B-time	*2.300E-004*	*1*	*2.300E-004*	*457.95*	*< 0.0001*	
Residual	1.356E-005	27	5.022E-007			
Lack of Fit	*7.616E-006*	*7*	*1.088E-006*	*3.66*	*0.0105*	*significant*
Pure Error	*5.942E-006*	*20*	*2.971E-007*			
Cor Total	2.456E-004	29				

The Model F-value of 231.05 implies the model is significant. There is only

a 0.01% chance that an F-value this large could occur due to noise.

Values of "Prob > F" less than 0.0500 indicate model terms are significant.

In this case B is a significant model term.

Values greater than 0.1000 indicate the model terms are not significant.

The "Lack of Fit F-value" of 3.66 implies the Lack of Fit is significant. There is only a

1.05% chance that a "Lack of Fit F-value" this large could occur due to noise.

Significant lack of fit is bad -- we want the model to fit.

Std. Dev.	7.086E-004	R-Squared	0.9448
Mean	7.715E-003	Adj R-Squared	0.9407
C.V. %	9.18	Pred R-Squared	0.9329
PRESS	1.648E-005	Adeq Precision	28.036

The "Pred R-Squared" of 0.9329 is in reasonable agreement with the "Adj R-Squared" of 0.9407; i.e. the difference is less than 0.2.

"Adeq Precision" measures the signal to noise ratio. A ratio greater than 4 is desirable. The ratio of 28.036 indicates an adequate signal. This model can be used to navigate the design space.

Factor	Coefficient Estimate	df	Standard Error	95% CI Low	95% CI High	VIF
Intercept	7.715E-003	1	1.294E-004	7.450E-003	7.981E-003	
A-Angle	-3.727E-004	1	1.830E-004	-7.481E-004	2.752E-006	1.00
B-time	2.769E-003	1	1.294E-004	2.503E-003	3.034E-003	1.00

Final Equation in Terms of Coded Factors:

mass loss =
+7.715E-003
-3.727E-004 * A
+2.769E-003 * B

Final Equation in Terms of Actual Factors:

mass loss =
+1.54667E-004
-1.24222E-005 * Angle
+3.07630E-005 * time

Coating 4

Response 1 depth

ANOVA for Response Surface Reduced Quadratic model
Analysis of variance table [Partial sum of squares - Type III]

Source	Sum of Squares	df	Mean Square	F Value	p-value Prob > F	
Model	2.613E+006	4	6.532E+005	199.70	< 0.0001	significant
A-Angle	*6.438E+005*	*1*	*6.438E+005*	*196.84*	*< 0.0001*	
B-Time	*1.604E+006*	*1*	*1.604E+006*	*490.34*	*< 0.0001*	
AB	*1.394E+005*	*1*	*1.394E+005*	*42.62*	*< 0.0001*	
A^2	*2.257E+005*	*1*	*2.257E+005*	*69.00*	*< 0.0001*	
Residual	81769.87	25	3270.79			
Lack of Fit	*29761.26*	*5*	*5952.25*	*2.29*	*0.0847*	*not significant*
Pure Error	*52008.61*	*20*	*2600.43*			
Cor Total	2.694E+006	29				

The Model F-value of 199.70 implies the model is significant. There is only

a 0.01% chance that an F-value this large could occur due to noise.

Values of "Prob > F" less than 0.0500 indicate model terms are significant.

In this case A, B, AB, A^2 are significant model terms.

Values greater than 0.1000 indicate the model terms are not significant.

The "Lack of Fit F-value" of 2.29 implies there is a 8.47% chance that a "Lack of Fit F-

value" this large could occur due to noise. Lack of fit is bad -- we want the model to fit.

This relatively low probability (<10%) is troubling.

Std. Dev.	57.19	R-Squared	0.9697
Mean	909.78	Adj R-Squared	0.9648
C.V. %	6.29	Pred R-Squared	0.9598
PRESS	1.084E+005	Adeq Precision	37.712

The "Pred R-Squared" of 0.9598 is in reasonable agreement with the "Adj R-Squared" of 0.9648; i.e. the difference is less than 0.2.

"Adeq Precision" measures the signal to noise ratio. A ratio greater than 4 is desirable. The ratio of 37.712 indicates an adequate signal. This model can be used to navigate the design space.

Factor	Coefficient Estimate	df	Standard Error	95% CI Low	95% CI High	VIF
Intercept	1013.45	1	16.27	979.93	1046.96	
A-Angle	207.18	1	14.77	176.76	237.59	1.00
B-Time	231.21	1	10.44	209.71	252.72	1.00
AB	96.40	1	14.77	65.99	126.81	1.00
A^2	-207.33	1	24.96	-258.74	-155.93	1.00

Final Equation in Terms of Coded Factors:

depth =
+1013.45
+207.18 * A
+231.21 * B
+96.40 * AB
-207.33 * A^2

Final Equation in Terms of Actual Factors:

depth =
-345.48233
+24.91027 * Angle
+0.42684 * Time
+0.035704 * Angle * Time
-0.23037 * Angle^2

Response 2 mass loss

ANOVA for Response Surface Linear model
Analysis of variance table [Partial sum of squares - Type III]

Source	Sum of Squares	df	Mean Square	F Value	p-value Prob > F	
Model	2.307E-004	2	1.154E-004	81.09	< 0.0001	significant
A-Angle	*7.238E-006*	*1*	*7.238E-006*	*5.09*	*0.0324*	
B-time	*2.235E-004*	*1*	*2.235E-004*	*157.08*	*< 0.0001*	
Residual	3.841E-005	27	1.423E-006			
Lack of Fit	*2.207E-005*	*7*	*3.153E-006*	*3.86*	*0.0082*	*significant*
Pure Error	*1.634E-005*	*20*	*8.171E-007*			
Cor Total	2.691E-004	29				

The Model F-value of 81.09 implies the model is significant. There is only

a 0.01% chance that an F-value this large could occur due to noise.

Values of "Prob > F" less than 0.0500 indicate model terms are significant.

In this case A, B are significant model terms.

Values greater than 0.1000 indicate the model terms are not significant.

The "Lack of Fit F-value" of 3.86 implies the Lack of Fit is significant. There is only a

0.82% chance that a "Lack of Fit F-value" this large could occur due to noise.

Significant lack of fit is bad -- we want the model to fit.

Std. Dev.	1.193E-003	R-Squared	0.8573
Mean	7.764E-003	Adj R-Squared	0.8467
C.V. %	15.36	Pred R-Squared	0.8258
PRESS	4.689E-005	Adeq Precision	18.156

The "Pred R-Squared" of 0.8258 is in reasonable agreement with the "Adj R-Squared" of 0.8467; i.e. the difference is less than 0.2.

"Adeq Precision" measures the signal to noise ratio. A ratio greater than 4 is desirable. The ratio of 18.156 indicates an adequate signal. This model can be used to navigate the design space.

Factor	Coefficient Estimate	df	Standard Error	95% CI Low	95% CI High	VIF
Intercept	7.764E-003	1	2.178E-004	7.317E-003	8.211E-003	
A-Angle	-6.947E-004	1	3.080E-004	-1.327E-003	-6.277E-005	1.00
B-time	2.729E-003	1	2.178E-004	2.283E-003	3.176E-003	1.00

Final Equation in Terms of Coded Factors:

mass loss =
+7.764E-003
-6.947E-004 * A
+2.729E-003 * B

Final Equation in Terms of Actual Factors:

mass loss =
+9.65333E-004
-2.31556E-005 * Angle
+3.03259E-005 * time

Coating 5

Response 1 depth

ANOVA for Response Surface Reduced Quadratic model
Analysis of variance table [Partial sum of squares - Type III]

Source	Sum of Squares	df	Mean Square	F Value	p-value Prob > F	
Model	2.733E+006	4	6.833E+005	73.58	< 0.0001	significant
A-Angle	*7.257E+005*	*1*	*7.257E+005*	*78.15*	*< 0.0001*	
B-Time	*1.700E+006*	*1*	*1.700E+006*	*183.02*	*< 0.0001*	
AB	*85783.33*	*1*	*85783.33*	*9.24*	*0.0055*	
A^2	*2.220E+005*	*1*	*2.220E+005*	*23.90*	*< 0.0001*	
Residual	2.322E+005	25	9286.28			
Lack of Fit	*1.273E+005*	*5*	*25462.36*	*4.86*	*0.0045*	*significant*
Pure Error	*1.048E+005*	*20*	*5242.26*			
Cor Total	2.965E+006	29				

The Model F-value of 73.58 implies the model is significant. There is only

a 0.01% chance that an F-value this large could occur due to noise.

Values of "Prob > F" less than 0.0500 indicate model terms are significant.

In this case A, B, AB, A^2 are significant model terms.

Values greater than 0.1000 indicate the model terms are not significant.

The "Lack of Fit F-value" of 4.86 implies the Lack of Fit is significant. There is only a

0.45% chance that a "Lack of Fit F-value" this large could occur due to noise.

Significant lack of fit is bad -- we want the model to fit.

Std. Dev.	96.37	R-Squared	0.9217
Mean	918.17	Adj R-Squared	0.9092
C.V. %	10.50	Pred R-Squared	0.8918
PRESS	3.210E+005	Adeq Precision	23.446

The "Pred R-Squared" of 0.8918 is in reasonable agreement with the "Adj R-Squared" of 0.9092; i.e. the difference is less than 0.2.

"Adeq Precision" measures the signal to noise ratio. A ratio greater than 4 is desirable. The ratio of 23.446 indicates an adequate signal. This model can be used to navigate the design space.

Factor	Coefficient Estimate	df	Standard Error	95% CI Low	95% CI High	VIF
Intercept	1020.99	1	27.42	964.52	1077.45	
A-Angle	219.96	1	24.88	168.72	271.21	1.00
B-Time	238.02	1	17.59	201.79	274.26	1.00
AB	75.62	1	24.88	24.38	126.87	1.00
A^2	-205.62	1	42.06	-292.24	-119.00	1.00

Final Equation in Terms of Coded Factors:

depth =
+1020.99
+219.96 * A
+238.02 * B
+75.62 * AB
-205.62 * A^2

Final Equation in Terms of Actual Factors:

depth =
-501.75267
+27.18611 * Angle
+0.96416 * Time
+0.028009 * Angle * Time
-0.22847 * Angle^2

Response 2 mass loss

ANOVA for Response Surface Reduced Quadratic model
Analysis of variance table [Partial sum of squares - Type III]

Source	Sum of Squares	df	Mean Square	F Value	p-value Prob > F	
Model	2.355E-004	4	5.887E-005	87.27	< 0.0001	significant
A-Angle	*1.559E-005*	*1*	*1.559E-005*	*23.11*	*< 0.0001*	
B-time	*2.114E-004*	*1*	*2.114E-004*	*313.42*	*< 0.0001*	
AB	*5.222E-006*	*1*	*5.222E-006*	*7.74*	*0.0101*	
A^2	*3.257E-006*	*1*	*3.257E-006*	*4.83*	*0.0375*	
Residual	1.686E-005	25	6.745E-007			
Lack of Fit	*4.394E-006*	*5*	*8.788E-007*	*1.41*	*0.2634 not significant*	
Pure Error	*1.247E-005*	*20*	*6.235E-007*			
Cor Total	2.523E-004	29				

The Model F-value of 87.27 implies the model is significant. There is only

a 0.01% chance that an F-value this large could occur due to noise.

Values of "Prob > F" less than 0.0500 indicate model terms are significant.

In this case A, B, AB, A^2 are significant model terms.

Values greater than 0.1000 indicate the model terms are not significant.

The "Lack of Fit F-value" of 1.41 implies the Lack of Fit is not significant relative to the pure

error. There is a 26.34% chance that a "Lack of Fit F-value" this large could occur due

to noise. Non-significant lack of fit is good -- we want the model to fit.

Std. Dev.	8.213E-004	R-Squared	0.9332
Mean	7.816E-003	Adj R-Squared	0.9225
C.V. %	10.51	Pred R-Squared	0.8985
PRESS	2.562E-005	Adeq Precision	21.915

The "Pred R-Squared" of 0.8985 is in reasonable agreement with the "Adj R-Squared" of 0.9225; i.e. the difference is less than 0.2.

"Adeq Precision" measures the signal to noise ratio. A ratio greater than 4 is desirable. The ratio of 21.915 indicates an adequate signal. This model can be used to navigate the design space.

Factor	Coefficient Estimate	df	Standard Error	95% CI Low	95% CI High	VIF
Intercept	8.210E-003	1	2.337E-004	7.729E-003	8.691E-003	
A-Angle	-1.019E-003	1	2.121E-004	-1.456E-003	-5.826E-004	1.00
B-time	2.655E-003	1	1.499E-004	2.346E-003	2.963E-003	1.00
AB	-5.900E-004	1	2.121E-004	-1.027E-003	-1.533E-004	1.00
A^2	-7.876E-004	1	3.584E-004	-1.526E-003	-4.938E-005	1.00

Final Equation in Terms of Coded Factors:

mass loss =
+8.210E-003
-1.019E-003 * A
+2.655E-003 * B
-5.900E-004 * AB
-7.876E-004 * A^2

Final Equation in Terms of Actual Factors:

mass loss =
-4.40600E-003
+1.30038E-004 * Angle
+4.26074E-005 * time
-2.18519E-007 * Angle * time
-8.75132E-007 * Angle^2

Coating 6

Response 1 depth

ANOVA for Response Surface Reduced Quadratic model
Analysis of variance table [Partial sum of squares - Type III]

Source	Sum of Squares	df	Mean Square	F Value	p-value Prob > F	
Model	2.384E+006	3	7.946E+005	61.27	< 0.0001	significant
A-Angle	*7.104E+005*	*1*	*7.104E+005*	*54.78*	*< 0.0001*	
B-Time	*1.624E+006*	*1*	*1.624E+006*	*125.24*	*< 0.0001*	
A^2	*49258.64*	*1*	*49258.64*	*3.80*	*0.0622*	
Residual	3.372E+005	26	12968.58			
Lack of Fit	*2.317E+005*	*6*	*38620.49*	*7.32*	*0.0003*	*significant*
Pure Error	*1.055E+005*	*20*	*5273.01*			
Cor Total	2.721E+006	29				

The Model F-value of 61.27 implies the model is significant. There is only

a 0.01% chance that an F-value this large could occur due to noise.

Values of "Prob > F" less than 0.0500 indicate model terms are significant.

In this case A, B are significant model terms.

Values greater than 0.1000 indicate the model terms are not significant.

The "Lack of Fit F-value" of 7.32 implies the Lack of Fit is significant. There is only a

0.03% chance that a "Lack of Fit F-value" this large could occur due to noise.

Significant lack of fit is bad -- we want the model to fit.

Std. Dev.	113.88	R-Squared	0.8761
Mean	812.75	Adj R-Squared	0.8618
C.V. %	14.01	Pred R-Squared	0.8380
PRESS	4.407E+005	Adeq Precision	21.658

The "Pred R-Squared" of 0.8380 is in reasonable agreement with the "Adj R-Squared" of 0.8618; i.e. the difference is less than 0.2.

"Adeq Precision" measures the signal to noise ratio. A ratio greater than 4 is desirable. The ratio of 21.658 indicates an adequate signal. This model can be used to navigate the design space.

Factor	Coefficient Estimate	df	Standard Error	95% CI Low	95% CI High	VIF
Intercept	861.18	1	32.40	794.58	927.78	
A-Angle	217.63	1	29.40	157.19	278.07	1.00
B-Time	232.68	1	20.79	189.94	275.42	1.00
A^2	-96.86	1	49.70	-199.03	5.30	1.00

Final Equation in Terms of Coded Factors:

depth =
+861.18
+217.63 * A
+232.68 * B
-96.86 * A^2

Final Equation in Terms of Actual Factors:

depth =
-659.57600
+20.16949 * Angle
+2.58535 * Time
-0.10763 * Angle^2

Response 2 mass loss

ANOVA for Response Surface 2FI model
Analysis of variance table [Partial sum of squares - Type III]

Source	Sum of Squares	df	Mean Square	F Value	p-value Prob > F	
Model	2.027E-004	3	6.756E-005	70.29	< 0.0001	significant
A-Angle	*1.174E-005*	*1*	*1.174E-005*	*12.21*	*0.0017*	
B-time	*1.874E-004*	*1*	*1.874E-004*	*194.97*	*< 0.0001*	
AB	*3.543E-006*	*1*	*3.543E-006*	*3.69*	*0.0659*	
Residual	2.499E-005	26	9.612E-007			
Lack of Fit	*1.723E-005*	*6*	*2.871E-006*	*7.40*	*0.0003*	*significant*
Pure Error	*7.763E-006*	*20*	*3.882E-007*			
Cor Total	2.277E-004	29				

The Model F-value of 70.29 implies the model is significant. There is only

a 0.01% chance that an F-value this large could occur due to noise.

Values of "Prob > F" less than 0.0500 indicate model terms are significant.

In this case A, B are significant model terms.

Values greater than 0.1000 indicate the model terms are not significant.

The "Lack of Fit F-value" of 7.40 implies the Lack of Fit is significant. There is only a

0.03% chance that a "Lack of Fit F-value" this large could occur due to noise.

Significant lack of fit is bad -- we want the model to fit.

Std. Dev.	9.804E-004	R-Squared	0.8902
Mean	5.930E-003	Adj R-Squared	0.8776
C.V. %	16.53	Pred R-Squared	0.8597
PRESS	3.195E-005	Adeq Precision	18.906

The "Pred R-Squared" of 0.8597 is in reasonable agreement with the "Adj R-Squared" of 0.8776; i.e. the difference is less than 0.2.

"Adeq Precision" measures the signal to noise ratio. A ratio greater than 4 is desirable. The ratio of 18.906 indicates an adequate signal. This model can be used to navigate the design space.

Factor	Coefficient Estimate	df	Standard Error	95% CI Low	95% CI High	VIF
Intercept	5.930E-003	1	1.790E-004	5.562E-003	6.298E-003	
A-Angle	-8.847E-004	1	2.531E-004	-1.405E-003	-3.643E-004	1.00
B-time	2.499E-003	1	1.790E-004	2.131E-003	2.867E-003	1.00
AB	-4.860E-004	1	2.531E-004	-1.006E-003	3.433E-005	1.00

Final Equation in Terms of Coded Factors:

mass loss =
+5.930E-003
-8.847E-004 * A
+2.499E-003 * B
-4.860E-004 * AB

Final Equation in Terms of Actual Factors:

mass loss =
-2.71467E-003
+1.91111E-005 * Angle
+3.85704E-005 * time
-1.80000E-007 * Angle * time

Coating 7

Response 1 depth

ANOVA for Response Surface Reduced Quadratic model
Analysis of variance table [Partial sum of squares - Type III]

Source	Sum of Squares	df	Mean Square	F Value	p-value Prob > F	
Model	2.363E+006	3	7.878E+005	54.03	< 0.0001	significant
A-Angle	*3.168E+005*	*1*	*3.168E+005*	*21.72*	*< 0.0001*	
B-Time	*1.671E+006*	*1*	*1.671E+006*	*114.62*	*< 0.0001*	
A^2	*3.752E+005*	*1*	*3.752E+005*	*25.73*	*< 0.0001*	
Residual	3.791E+005	26	14581.09			
Lack of Fit	*2.490E+005*	*6*	*41491.94*	*6.38*	*0.0007*	*significant*
Pure Error	*1.302E+005*	*20*	*6507.83*			
Cor Total	2.742E+006	29				

The Model F-value of 54.03 implies the model is significant. There is only

a 0.01% chance that an F-value this large could occur due to noise.

Values of "Prob > F" less than 0.0500 indicate model terms are significant.

In this case A, B, A^2 are significant model terms.

Values greater than 0.1000 indicate the model terms are not significant.

The "Lack of Fit F-value" of 6.38 implies the Lack of Fit is significant. There is only a

0.07% chance that a "Lack of Fit F-value" this large could occur due to noise.

Significant lack of fit is bad -- we want the model to fit.

Std. Dev.	120.75	R-Squared	0.8618
Mean	826.41	Adj R-Squared	0.8458
C.V. %	14.61	Pred R-Squared	0.8233
PRESS	4.846E+005	Adeq Precision	20.197

The "Pred R-Squared" of 0.8233 is in reasonable agreement with the "Adj R-Squared" of 0.8458; i.e. the difference is less than 0.2.

"Adeq Precision" measures the signal to noise ratio. A ratio greater than 4 is desirable. The ratio of 20.197 indicates an adequate signal. This model can be used to navigate the design space.

Factor	Coefficient Estimate	df	Standard Error	95% CI Low	95% CI High	VIF
Intercept	960.08	1	34.36	889.46	1030.70	
A-Angle	145.32	1	31.18	81.23	209.41	1.00
B-Time	236.03	1	22.05	190.71	281.35	1.00
A^2	-267.34	1	52.70	-375.66	-159.01	1.00

Final Equation in Terms of Coded Factors:

depth =
+960.08
+145.32 * A
+236.03 * B
-267.34 * A^2

Final Equation in Terms of Actual Factors:

depth =
-1107.99067
+40.48868 * Angle
+2.62256 * Time
-0.29704 * Angle^2

Response 2 mass loss

ANOVA for Response Surface Reduced Quadratic model
Analysis of variance table [Partial sum of squares - Type III]

Source	Sum of Squares	df	Mean Square	F Value	p-value Prob > F	
Model	2.969E-004	3	9.896E-005	133.41	< 0.0001	significant
A-Angle	*2.496E-005*	*1*	*2.496E-005*	*33.65*	*< 0.0001*	
B-time	*2.665E-004*	*1*	*2.665E-004*	*359.33*	*< 0.0001*	
A^2	*5.381E-006*	*1*	*5.381E-006*	*7.25*	*0.0122*	
Residual	1.929E-005	26	7.417E-007			
Lack of Fit	*9.158E-006*	*6*	*1.526E-006*	*3.01*	*0.0290*	*significant*
Pure Error	*1.013E-005*	*20*	*5.064E-007*			
Cor Total	3.162E-004	29				

The Model F-value of 133.41 implies the model is significant. There is only

a 0.01% chance that an F-value this large could occur due to noise.

Values of "Prob > F" less than 0.0500 indicate model terms are significant.

In this case A, B, A^2 are significant model terms.

Values greater than 0.1000 indicate the model terms are not significant.

The "Lack of Fit F-value" of 3.01 implies the Lack of Fit is significant. There is only a

2.90% chance that a "Lack of Fit F-value" this large could occur due to noise.

Significant lack of fit is bad -- we want the model to fit.

Std. Dev.	8.612E-004	R-Squared	0.9390
Mean	6.931E-003	Adj R-Squared	0.9320
C.V. %	12.43	Pred R-Squared	0.9189
PRESS	2.564E-005	Adeq Precision	27.523

The "Pred R-Squared" of 0.9189 is in reasonable agreement with the "Adj R-Squared" of 0.9320; i.e. the difference is less than 0.2.

"Adeq Precision" measures the signal to noise ratio. A ratio greater than 4 is desirable. The ratio of 27.523 indicates an adequate signal. This model can be used to navigate the design space.

Factor	Coefficient Estimate	df	Standard Error	95% CI Low	95% CI High	VIF
Intercept	7.438E-003	1	2.450E-004	6.934E-003	7.941E-003	
A-Angle	-1.290E-003	1	2.224E-004	-1.747E-003	-8.329E-004	1.00
B-time	2.981E-003	1	1.572E-004	2.657E-003	3.304E-003	1.00
A^2	-1.012E-003	1	3.759E-004	-1.785E-003	-2.398E-004	1.00

Final Equation in Terms of Coded Factors:

mass loss =
+7.438E-003
-1.290E-003 * A
+2.981E-003 * B
-1.012E-003 * A^2

Final Equation in Terms of Actual Factors:

mass loss =
-2.97400E-003
+9.19841E-005 * Angle
+3.31185E-005 * time
-1.12487E-006 * Angle^2

Curved Surfaces

Uncoated

Response 1 depth

ANOVA for Response Surface Reduced Quadratic model
Analysis of variance table [Partial sum of squares - Type III]

Source	Sum of Squares	df	Mean Square	F Value	p-value Prob > F	
Model	5.587E+006	8	6.984E+005	19.27	< 0.0001	significant
A-Pressure	*2.754E+006*	*1*	*2.754E+006*	*76.00*	*< 0.0001*	
B-Time	*1.023E+006*	*1*	*1.023E+006*	*28.25*	*< 0.0001*	
C-Angle	*6.773E+005*	*1*	*6.773E+005*	*18.69*	*0.0006*	
AB	*1.744E+005*	*1*	*1.744E+005*	*4.81*	*0.0444*	
AC	*1944.16*	*1*	*1944.16*	*0.054*	*0.8199*	
BC	*12636.50*	*1*	*12636.50*	*0.35*	*0.5636*	
A^2	*5.106E+005*	*1*	*5.106E+005*	*14.09*	*0.0019*	
C^2	*9.845E+005*	*1*	*9.845E+005*	*27.17*	*0.0001*	
Residual	5.435E+005	15	36232.11			
Cor Total	6.130E+006	23				

The Model F-value of 19.27 implies the model is significant. There is only

a 0.01% chance that an F-value this large could occur due to noise.

Values of "Prob > F" less than 0.0500 indicate model terms are significant.

In this case A, B, C, AB, A^2, C^2 are significant model terms.

Values greater than 0.1000 indicate the model terms are not significant.

Std. Dev.	190.35	R-Squared	0.9113
Mean	920.69	Adj R-Squared	0.8641
C.V. %	20.67	Pred R-Squared	0.7213
PRESS	1.709E+006	Adeq Precision	16.574

The "Pred R-Squared" of 0.7213 is in reasonable agreement with the "Adj R-Squared" of 0.8641; i.e. the difference is less than 0.2.

"Adeq Precision" measures the signal to noise ratio. A ratio greater than 4 is desirable. The ratio of 16.574 indicates an adequate signal. This model can be used to navigate the design space.

Factor	Coefficient Estimate	df	Standard Error	95% CI Low	95% CI High	VIF
Intercept	1565.05	1	108.02	1334.80	1795.29	
A-Pressure	414.85	1	47.59	313.42	516.28	1.08
B-Time	210.44	1	39.59	126.05	294.84	1.04
C-Angle	-229.67	1	53.12	-342.90	-116.45	1.04
AB	100.32	1	45.72	2.87	197.77	1.04
AC	-14.21	1	61.34	-144.95	116.53	1.04
BC	-30.79	1	52.13	-141.90	80.32	1.00
A^2	-429.38	1	114.38	-673.19	-185.58	1.08
C^2	-455.71	1	87.42	-642.05	-269.37	1.00

Final Equation in Terms of Coded Factors:

depth =
+1565.05
+414.85 * A
+210.44 * B
-229.67 * C
+100.32 * AB
-14.21 * AC
-30.79 * BC
-429.38 * A^2
-455.71 * C^2

Final Equation in Terms of Actual Factors:

depth =
-3291.50429
+53.89871 * Pressure
-0.89162 * Time
+27.88233 * Angle
+0.022293 * Pressure * Time
-0.037890 * Pressure * Angle
-0.045608 * Time * Angle
-0.17175 * Pressure^2
-8.10151 * Angle^2

Response 2 mass loss

ANOVA for Response Surface Reduced Quadratic model
Analysis of variance table [Partial sum of squares - Type III]

Source	Sum of Squares	df	Mean Square	F Value	p-value Prob > F	
Model	1811.24	8	226.40	13.69	< 0.0001	significant
A-Pressure	*1095.61*	*1*	*1095.61*	*66.25*	*< 0.0001*	
B-Time	*396.67*	*1*	*396.67*	*23.99*	*0.0002*	
C-Angle	*51.12*	*1*	*51.12*	*3.09*	*0.0991*	
AB	*108.43*	*1*	*108.43*	*6.56*	*0.0217*	
AC	*2.54*	*1*	*2.54*	*0.15*	*0.7007*	
BC	*0.058*	*1*	*0.058*	*3.525E-003*	*0.9534*	
A^2	*9.95*	*1*	*9.95*	*0.60*	*0.4499*	
C^2	*174.34*	*1*	*174.34*	*10.54*	*0.0054*	
Residual	248.07	15	16.54			
Cor Total	2059.30	23				

The Model F-value of 13.69 implies the model is significant. There is only

a 0.01% chance that an F-value this large could occur due to noise.

Values of "Prob > F" less than 0.0500 indicate model terms are significant.

In this case A, B, AB, C^2 are significant model terms.

Values greater than 0.1000 indicate the model terms are not significant.

Std. Dev.	4.07	R-Squared	0.8795
Mean	15.02	Adj R-Squared	0.8153
C.V. %	27.08	Pred R-Squared	0.5966
PRESS	830.81	Adeq Precision	13.326

"Adeq Precision" measures the signal to noise ratio. A ratio greater than 4 is desirable. The ratio of 13.326 indicates an adequate signal. This model can be used to navigate the design space.

Factor	Coefficient Estimate	df	Standard Error	95% CI Low	95% CI High	VIF
Intercept	21.19	1	2.31	16.27	26.11	
A-Pressure	8.28	1	1.02	6.11	10.44	1.08
B-Time	4.14	1	0.85	2.34	5.95	1.04
C-Angle	-2.00	1	1.13	-4.41	0.42	1.04
AB	2.50	1	0.98	0.42	4.58	1.04
AC	0.51	1	1.31	-2.28	3.31	1.04
BC	-0.066	1	1.11	-2.44	2.31	1.00
A^2	-1.90	1	2.44	-7.10	3.31	1.08
C^2	-6.06	1	1.87	-10.05	-2.08	1.00

Final Equation in Terms of Coded Factors:

mass loss =
+21.19
+8.28 * A
+4.14 * B
-2.00 * C
+2.50 * AB
+0.51 * AC
-0.066 * BC
-1.90 * A^2
-6.06 * C^2

Final Equation in Terms of Actual Factors:

mass loss =
-10.17810
+0.23951 * Pressure
-0.037092 * Time
+0.094046 * Angle
+5.55791E-004 * Pressure * Time
+1.36938E-003 * Pressure * Angle
-9.79630E-005 * Time * Angle
-7.58333E-004 * Pressure^2
-0.10781 * Angle^2

H-146

Response 1 Depth

ANOVA for Response Surface Reduced Quadratic model
Analysis of variance table [Partial sum of squares - Type III]

Source	Sum of Squares	df	Mean Square	F Value	p-value Prob > F	
Model	6.047E+006	8	7.559E+005	38.22	< 0.0001	significant
A-Pressure	*1.879E+006*	*1*	*1.879E+006*	*95.01*	*< 0.0001*	
B-Time	*1.098E+006*	*1*	*1.098E+006*	*55.54*	*< 0.0001*	
C-Angle	*1.248E+006*	*1*	*1.248E+006*	*63.09*	*< 0.0001*	
AB	*1.600E+005*	*1*	*1.600E+005*	*8.09*	*0.0123*	
AC	*14169.62*	*1*	*14169.62*	*0.72*	*0.4106*	
BC	*59942.70*	*1*	*59942.70*	*3.03*	*0.1022*	
A^2	*2.402E+005*	*1*	*2.402E+005*	*12.15*	*0.0033*	
C^2	*1.698E+006*	*1*	*1.698E+006*	*85.86*	*< 0.0001*	
Residual	2.967E+005	15	19776.98			
Cor Total	6.343E+006	23				

The Model F-value of 38.22 implies the model is significant. There is only

a 0.01% chance that an F-value this large could occur due to noise.

Values of "Prob > F" less than 0.0500 indicate model terms are significant.

In this case A, B, C, AB, A^2, C^2 are significant model terms.

Values greater than 0.1000 indicate the model terms are not significant.

Std. Dev.	140.63	R-Squared	0.9532
Mean	1113.33	Adj R-Squared	0.9283
C.V. %	12.63	Pred R-Squared	0.8670
PRESS	8.437E+005	Adeq Precision	23.210

The "Pred R-Squared" of 0.8670 is in reasonable agreement with the "Adj R-Squared" of 0.9283; i.e. the difference is less than 0.2.

"Adeq Precision" measures the signal to noise ratio. A ratio greater than 4 is desirable. The ratio of 23.210 indicates an adequate signal. This model can be used to navigate the design space.

Factor	Coefficient Estimate	df	Standard Error	95% CI Low	95% CI High	VIF
Intercept	1723.85	1	79.81	1553.75	1893.96	
A-Pressure	342.69	1	35.16	267.75	417.62	1.08
B-Time	218.01	1	29.25	155.66	280.37	1.04
C-Angle	-311.74	1	39.25	-395.40	-228.09	1.04
AB	96.09	1	33.78	24.09	168.08	1.04
AC	-38.36	1	45.32	-134.95	58.23	1.04
BC	-67.05	1	38.51	-149.14	15.04	1.00
A^2	-294.54	1	84.51	-474.67	-114.42	1.08
C^2	-598.50	1	64.59	-736.17	-460.83	1.00

Final Equation in Terms of Coded Factors:

Depth =

+1723.85
+342.69 * A
+218.01 * B
-311.74 * C
+96.09 * AB
-38.36 * AC
-67.05 * BC
-294.54 * A^2
-598.50 * C^2

Final Equation in Terms of Actual Factors:

Depth =

-1812.34295
+36.68929 * Pressure
-0.53217 * Time
+53.79808 * Angle
+0.021353 * Pressure * Time
-0.10229 * Pressure * Angle
-0.099333 * Time * Angle
-0.11782 * Pressure^2
-10.64000 * Angle ^2

2 mass loss

Response

ANOVA for Response Surface Reduced Quadratic model
Analysis of variance table [Partial sum of squares - Type III]

Source	Sum of Squares	df	Mean Square	F Value	p-value Prob > F	
Model	2001.54	8	250.19	94.73	< 0.0001	significant
A-Pressure	*884.39*	*1*	*884.39*	*334.84*	*< 0.0001*	
B-Time	*694.05*	*1*	*694.05*	*262.78*	*< 0.0001*	
C-Angle	*157.52*	*1*	*157.52*	*59.64*	*< 0.0001*	
AB	*137.43*	*1*	*137.43*	*52.03*	*< 0.0001*	
AC	*1.56*	*1*	*1.56*	*0.59*	*0.4543*	
BC	*11.14*	*1*	*11.14*	*4.22*	*0.0579*	
A^2	*0.56*	*1*	*0.56*	*0.21*	*0.6530*	
C^2	*133.57*	*1*	*133.57*	*50.57*	*< 0.0001*	
Residual	39.62	15	2.64			
Cor Total	2041.16	23				

The Model F-value of 94.73 implies the model is significant. There is only

a 0.01% chance that an F-value this large could occur due to noise.

Values of "Prob > F" less than 0.0500 indicate model terms are significant.

In this case A, B, C, AB, C^2 are significant model terms.

Values greater than 0.1000 indicate the model terms are not significant.

Std. Dev.	1.63	R-Squared	0.9806
Mean	16.92	Adj R-Squared	0.9702
C.V. %	9.60	Pred R-Squared	0.9478
PRESS	106.52	Adeq Precision	35.044

The "Pred R-Squared" of 0.9478 is in reasonable agreement with the "Adj R-Squared" of 0.9702; i.e. the difference is less than 0.2.

"Adeq Precision" measures the signal to noise ratio. A ratio greater than 4 is desirable. The ratio of 35.044 indicates an adequate signal. This model can be used to navigate the design space.

Factor	Coefficient Estimate	df	Standard Error	95% CI Low	95% CI High	VIF
Intercept	21.45	1	0.92	19.48	23.41	
A-Pressure	7.43	1	0.41	6.57	8.30	1.08
B-Time	5.48	1	0.34	4.76	6.20	1.04
C-Angle	-3.50	1	0.45	-4.47	-2.54	1.04
AB	2.82	1	0.39	1.98	3.65	1.04
AC	0.40	1	0.52	-0.71	1.52	1.04
BC	-0.91	1	0.45	-1.86	0.035	1.00
A^2	-0.45	1	0.98	-2.53	1.63	1.08
C^2	-5.31	1	0.75	-6.90	-3.72	1.00

Final Equation in Terms of Coded Factors:

mass loss =
+21.45
+7.43 * A
+5.48 * B
-3.50 * C
+2.82 * AB
+0.40 * AC
-0.91 * BC
-0.45 * A^2
-5.31 * C^2

Final Equation in Terms of Actual Factors:

mass loss =
+4.07841
+0.030825 * Pressure
-0.029584 * Time
+0.20943 * Angle
+6.25723E-004 * Pressure * Time
+1.07285E-003 * Pressure * Angle
-1.35389E-003 * Time * Angle
-1.79194E-004 * Pressure^2
-0.094364 * Angle ^2

Polyurethane/IA-700

Response 1 Depth

ANOVA for Response Surface Reduced Quadratic model
Analysis of variance table [Partial sum of squares - Type III]

Source	Sum of Squares	df	Mean Square	F Value	p-value Prob > F	
Model	3.506E+006	8	4.383E+005	44.75	< 0.0001	significant
A-Pressure	*1.526E+006*	*1*	*1.526E+006*	*155.81*	*< 0.0001*	
B-Time	*8.918E+005*	*1*	*8.918E+005*	*91.05*	*< 0.0001*	
C-Angle	*6.042E+005*	*1*	*6.042E+005*	*61.69*	*< 0.0001*	
AB	*1.187E+005*	*1*	*1.187E+005*	*12.12*	*0.0034*	
AC	*773.56*	*1*	*773.56*	*0.079*	*0.7825*	
BC	*54145.56*	*1*	*54145.56*	*5.53*	*0.0328*	
A^2	*2.065E+005*	*1*	*2.065E+005*	*21.08*	*0.0004*	
C^2	*3.738E+005*	*1*	*3.738E+005*	*38.16*	*< 0.0001*	
Residual	1.469E+005	15	9794.31			
Cor Total	3.653E+006	23				

The Model F-value of 44.75 implies the model is significant. There is only

a 0.01% chance that an F-value this large could occur due to noise.

Values of "Prob > F" less than 0.0500 indicate model terms are significant.

In this case A, B, C, AB, BC, A^2, C^2 are significant model terms.

Values greater than 0.1000 indicate the model terms are not significant.

Std. Dev.	98.97	R-Squared	0.9598
Mean	651.44	Adj R-Squared	0.9383
C.V. %	15.19	Pred R-Squared	0.8893
PRESS	4.044E+005	Adeq Precision	24.766

The "Pred R-Squared" of 0.8893 is in reasonable agreement with the "Adj R-Squared" of 0.9383; i.e. the difference is less than 0.2.

"Adeq Precision" measures the signal to noise ratio. A ratio greater than 4 is desirable. The ratio of 24.766 indicates an adequate signal. This model can be used to navigate the design space.

Factor	Coefficient Estimate	df	Standard Error	95% CI Low	95% CI High	VIF
Intercept	1063.70	1	56.16	943.99	1183.40	
A-Pressure	308.83	1	24.74	256.09	361.56	1.08
B-Time	196.44	1	20.59	152.56	240.32	1.04
C-Angle	-216.92	1	27.62	-275.79	-158.06	1.04
AB	82.74	1	23.77	32.08	133.41	1.04
AC	-8.96	1	31.89	-76.94	59.01	1.04
BC	-63.73	1	27.10	-121.49	-5.96	1.00
A^2	-273.06	1	59.47	-399.82	-146.30	1.08
C^2	-280.79	1	45.45	-377.67	-183.91	1.00

Final Equation in Terms of Coded Factors:

Depth =
+1063.70
+308.83 * A
+196.44 * B
-216.92 * C
+82.74 * AB
-8.96 * AC
-63.73 * BC
-273.06 * A^2
-280.79 * C^2

Final Equation in Terms of Actual Factors:

Depth =
-2196.50419
+34.03853 * Pressure
-0.33945 * Time
+25.11121 * Angle
+0.018387 * Pressure * Time
-0.023901 * Pressure * Angle
-0.094408 * Time * Angle
-0.10922 * Pressure^2
-4.99185 * Angle^2

Response 2 Mass loss

ANOVA for Response Surface Reduced Quadratic model
Analysis of variance table [Partial sum of squares - Type III]

Source	Sum of Squares	df	Mean Square	F Value	p-value Prob > F	
Model	668.34	8	83.54	17.64	< 0.0001	significant
A-Pressure	*235.72*	*1*	*235.72*	*49.77*	*< 0.0001*	
B-Time	*250.79*	*1*	*250.79*	*52.95*	*< 0.0001*	
C-Angle	*110.43*	*1*	*110.43*	*23.32*	*0.0002*	
AB	*50.09*	*1*	*50.09*	*10.58*	*0.0054*	
AC	*9.42*	*1*	*9.42*	*1.99*	*0.1789*	
BC	*18.38*	*1*	*18.38*	*3.88*	*0.0676*	
A^2	*43.60*	*1*	*43.60*	*9.21*	*0.0084*	
C^2	*29.05*	*1*	*29.05*	*6.13*	*0.0256*	
Residual	71.04	15	4.74			
Cor Total	739.38	23				

The Model F-value of 17.64 implies the model is significant. There is only

a 0.01% chance that an F-value this large could occur due to noise.

Values of "Prob > F" less than 0.0500 indicate model terms are significant.

In this case A, B, C, AB, A^2, C^2 are significant model terms.

Values greater than 0.1000 indicate the model terms are not significant.

Std. Dev.	2.18	R-Squared	0.9039
Mean	7.79	Adj R-Squared	0.8527
C.V. %	27.92	Pred R-Squared	0.7313
PRESS	198.68	Adeq Precision	15.105

The "Pred R-Squared" of 0.7313 is in reasonable agreement with the "Adj R-Squared" of 0.8527; i.e. the difference is less than 0.2.

"Adeq Precision" measures the signal to noise ratio. A ratio greater than 4 is desirable. The ratio of 15.105 indicates an adequate signal. This model can be used to navigate the design space.

Factor	Coefficient Estimate	df	Standard Error	95% CI Low	95% CI High	VIF
Intercept	12.79	1	1.23	10.15	15.42	
A-Pressure	3.84	1	0.54	2.68	5.00	1.08
B-Time	3.29	1	0.45	2.33	4.26	1.04
C-Angle	-2.93	1	0.61	-4.23	-1.64	1.04
AB	1.70	1	0.52	0.59	2.81	1.04
AC	-0.99	1	0.70	-2.48	0.51	1.04
BC	-1.17	1	0.60	-2.44	0.096	1.00
A^2	-3.97	1	1.31	-6.76	-1.18	1.08
C^2	-2.48	1	1.00	-4.61	-0.35	1.00

Final Equation in Terms of Coded Factors:

Mass loss =
+12.79
+3.84 * A
+3.29 * B
-2.93 * C
+1.70 * AB
-0.99 * AC
-1.17 * BC
-3.97 * A^2
-2.48 * C^2

Final Equation in Terms of Actual Factors:

Mass loss =
-30.48611
+0.45753 * Pressure
-0.015713 * Time
+0.69426 * Angle
+3.77756E-004 * Pressure * Time
-2.63733E-003 * Pressure * Angle
-1.73938E-003 * Time * Angle
-1.58722E-003 * Pressure^2
-0.044011 * Angle^2

Appendix V: Material removal and depth of erosion scars of the leading edge

In this appendix, the erosion of the leading edge of coated and uncoated wind turbine blades is shown in terms of material removal and depth of erosion scars. In Table V-1, data for the uncoated blade is shown, while the data for the H-146 coated blade is shown in V-2 and finally the data for the polyurethane/IA-700 coated blade is shown in Table V-3.

- **Uncoated blade**

Table V-1: Results of erosion of leading edge of the uncoated blade in terms of mass loss and depth of erosion scars.

	Testing condition			Output	
Section	**Pressure (kPa)**	**Time (s)**	**Angle (deg.)**	**Mass loss (mg)**	**Depth (µm)**
Root	100	180	-5	6.68	541
	100	180	-5	3.26	338
	100	180	-5	4.4	361
	100	180	-5	3.5	342
	100	180	0	11.58	708
	100	180	0	10.34	596
	100	180	0	6.2	474
	100	180	0	4.54	335
	100	180	5	2.68	
	100	180	5	5.48	299
	100	180	5	6.96	405
	100	180	5	7.68	588
	100	180	10	4.02	
	100	180	10	5.12	154
	100	180	10	6.48	235
	100	180	10	3.86	170
	100	360	-5	11.18	660

	100	360	-5	14.2	781
	100	360	-5	8.48	620
	100	360	-5	8.24	598
	100	360	0	16.04	992
	100	360	0	14.08	853
	100	360	0	7.3	496
	100	360	0	9.34	542
	100	360	5	9.96	599
	100	360	5	7.08	312
	100	360	5	6.7	465
	100	360	5	9.08	538
	100	360	10	5.78	
	100	360	10	6.22	278
	100	360	10	11.32	352
	100	360	10	7.02	378
Midspan	125	180	-5	10.78	802
	125	180	-5	8.06	490
	125	180	-5	17.32	999
	125	180	-5	17.28	1301
	125	180	0	8.48	595
	125	180	0	9.90	926
	125	180	0	18.76	1299
	125	180	0	15.82	1289
	125	180	5	7.80	537
	125	180	5	7.78	683
	125	180	5	10.96	783
	125	180	5	14.52	1303
	125	180	10	3.84	255
	125	180	10	4.48	437
	125	180	10	5.02	549

	125	180	10	8.74	551
	125	360	-5	13.58	965
	125	360	-5	12.31	960
	125	360	-5	21.15	1566
	125	360	-5	27.30	1579
	125	360	0	13.30	1048
	125	360	0	15.88	1576
	125	360	0	24.72	1590
	125	360	0	25.62	1861
	125	360	5	11.71	1326
	125	360	5	15.20	1500
	125	360	5	18.34	1536
	125	360	5	12.54	1460
	125	360	10	9.02	587
	125	360	10	14.80	589
	125	360	10	8.70	334
	125	360	10	8.98	377
Tip	200	180	-5	13.22	799
	200	180	-5	14.40	
	200	180	-5	18.18	1252
	200	180	-5	14.32	1058
	200	180	0	17.02	1008
	200	180	0	25.36	1382
	200	180	0	23.46	1247
	200	180	0	24.12	1351
	200	180	5	19.02	977
	200	180	5	18.60	783
	200	180	5	24.46	1329
	200	180	5	22.44	1303
	200	180	10	7.92	255

	200	180	10	8.68	288
	200	180	10	14.74	549
	200	180	10	13.84	496
	200	360	-5	18.55	1220
	200	360	-5	16.50	960
	200	360	-5	25.68	
	200	360	-5	26.39	1579
	200	360	0	47.74	2463
	200	360	0	45.46	2053
	200	360	0	34.14	1851
	200	360	0	44.86	1830
	200	360	5	28.52	1755
	200	360	5	33.68	1848
	200	360	5	36.92	2120
	200	360	5	38.16	2265
	200	360	10	24.40	853
	200	360	10	22.34	859
	200	360	10	24.32	1061
	200	360	10	26.96	1101

- **H-146 coated blade**

Table V-2: Results of erosion of leading edge of the H-146 coated blade in terms of mass loss and depth of erosion scars.

	Testing condition			Output	
Section	**Pressure (kPa)**	**Time (s)**	**Angle (deg.)**	**Mass loss (mg)**	**Depth (µm)**
Root	100	180	-5	10.26	787
	100	180	-5	5.94	602
	100	180	-5	9.48	746
	100	180	-5	7.08	631
	100	180	0	11.54	765
	100	180	0	12.82	889
	100	180	0	14.48	1035
	100	180	0	10.08	747
	100	180	5	5.24	684
	100	180	5	4.74	548
	100	180	5	8.4	844
	100	180	5	10.6	999
	100	180	10	2.48	236
	100	180	10	7.24	401
	100	180	10	4.5	342
	100	180	10	5.06	352
	100	360	-5	17.08	1188
	100	360	-5	13.62	870
	100	360	-5	14.66	1153
	100	360	-5	13.28	761
	100	360	0	13.32	907
	100	360	0	22.06	1330
	100	360	0	15.48	1101
	100	360	0	11.68	842
	100	360	5	11.66	754

	100	360	5	15.9	1188
	100	360	5	15.44	766
	100	360	5	17.4	1191
	100	360	10	6.1	364
	100	360	10	5.1	312
	100	360	10	8.7	579
	100	360	10	7.14	
Midspan	125	180	-5	9.52	635
	125	180	-5	14.7	1070
	125	180	-5		
	125	180	-5	11.14	891
	125	180	0	16.34	2118
	125	180	0	13.8	1678
	125	180	0	9.8	1184
	125	180	0	14.3	1690
	125	180	5	12.34	1723
	125	180	5	7.6	982
	125	180	5	11.78	1147
	125	180	5	9.16	1052
	125	180	10	4.7	292
	125	180	10	6.1	396
	125	180	10	7.54	460
	125	180	10	5.24	298
	125	360	-5	21.48	1419
	125	360	-5	22.56	1578
	125	360	-5	24.66	1662
	125	360	-5		
	125	360	0	24.58	1690
	125	360	0	21.44	1184
	125	360	0	21.76	1678

	125	360	0	29.38	2118
	125	360	5	18.2	1588
	125	360	5	20.6	1734
	125	360	5	20.86	1820
	125	360	5	18.08	1272
	125	360	10	9.24	569
	125	360	10	8.86	414
	125	360	10		
	125	360	10	9.74	635
Tip	200	180	-5	17.58	1072
	200	180	-5	19.36	1623
	200	180	-5	15.24	569
	200	180	-5	15.3	892
	200	180	0	18.46	1549
	200	180	0	16.96	1377
	200	180	0	21.98	1645
	200	180	0	24.84	1818
	200	180	5	15.52	1031
	200	180	5	19.78	1238
	200	180	5	21.68	1716
	200	180	5	24.04	1742
	200	180	10	11.32	397
	200	180	10	9.78	390
	200	180	10	13.12	575
	200	180	10	10.98	472
	200	360	-5	39.1	2068
	200	360	-5	36.6	1893
	200	360	-5	36.12	1828
	200	360	-5	25.22	1493
	200	360	0	37.06	2203

	200	360	0	41.9	2432
	200	360	0	28.84	1934
	200	360	0	40	2334
	200	360	5	30.9	1745
	200	360	5	29.5	1729
	200	360	5	41.82	2101
	200	360	5	40.34	1817
	200	360	10	25.64	946
	200	360	10	26.62	1078
	200	360	10	31.1	1231
	200	360	10	28.8	1129

- **Polyurethane/IA-700 coated blade**

Table V-3: Results of erosion of leading edge of the Polyurethane/IA-700 coated blade in terms of mass loss and depth of erosion scars.

	Testing condition			Output	
Section	**Pressure (kPa)**	**Time (s)**	**Angle (deg.)**	**Mass loss (mg)**	**Depth (μm)**
Root	100	180	-5	0.82	213
	100	180	-5	1.30	245
	100	180	-5	1.88	306
	100	180	-5	2.36	384
	100	180	0	5.08	402
	100	180	0	4.48	324
	100	180	0	3.74	
	100	180	0	3.56	295
	100	180	5		
	100	180	5	2.76	142
	100	180	5	2.98	302
	100	180	5	2.82	175
	100	180	10	2.14	124
	100	180	10	2.04	77
	100	180	10	1.44	44
	100	180	10	1.76	64
	100	360	-5	2.26	
	100	360	-5	4.38	388
	100	360	-5	4.70	530
	100	360	-5	4.98	611
	100	360	0	7.10	632
	100	360	0	7.14	858
	100	360	0	6.60	577
	100	360	0	6.60	541
	100	360	5	4.04	199

	100	360	5	4.74	618
	100	360	5	4.62	403
	100	360	5	4.32	378
	100	360	10	3.20	82
	100	360	10	4.04	135
	100	360	10	2.14	146
	100	360	10	2.54	173
Midspan	125	180	-5	4.04	497
	125	180	-5	4.46	521
	125	180	-5	8.42	707
	125	180	-5	7.70	591
	125	180	0	6.02	1271
	125	180	0	5.48	1182
	125	180	0	7.74	1309
	125	180	0	8.08	1310
	125	180	5		
	125	180	5		626
	125	180	5	7.69	729
	125	180	5	4.11	291
	125	180	10	1.54	134
	125	180	10	1.56	184
	125	180	10	2.36	310
	125	180	10	2.72	332
	125	360	-5	10.12	756
	125	360	-5	12.96	916
	125	360	-5	24.30	1451
	125	360	-5	19.58	1111
	125	360	0	11.16	1182
	125	360	0	17.78	1271
	125	360	0	20.22	1309

	125	360	0	18.86	1310
	125	360	5	12.22	867
	125	360	5	6.44	
	125	360	5	14.42	1024
	125	360	5	15.70	1115
	125	360	10	4.74	
	125	360	10	2.36	208.76
	125	360	10	4.86	369
	125	360	10	4.90	462
Tip	200	180	-5	8.48	709
	200	180	-5	7.66	
	200	180	-5	8.52	690
	200	180	-5	9.12	766
	200	180	0	10.78	1135
	200	180	0	9.34	1147
	200	180	0	5.12	540
	200	180	0	5.70	645
	200	180	5	8.90	925
	200	180	5	7.84	805
	200	180	5	5.92	654
	200	180	5	5.98	553
	200	180	10	2.12	181
	200	180	10	2.56	395
	200	180	10	3.20	490
	200	180	10		
	200	360	-5	20.64	1320
	200	360	-5	19.30	1233
	200	360	-5	14.54	
	200	360	-5		1216
	200	360	0	18.06	1447

	200	360	0	24.50	1683
	200	360	0	14.68	1024
	200	360	0	27.34	1895
	200	360	5	15.26	1442
	200	360	5	14.98	1422
	200	360	5	10.58	1097
	200	360	5	13.16	1225
	200	360	10	11.26	824
	200	360	10	11.88	811
	200	360	10	13.22	913
	200	360	10	9.54	670

Appendix VI: Photomicrographs of the erosion scars of the leading edge

In this appendix, photomicrographs of the leading edge erosion of uncoated and coated wind turbine blades are presented. This appendix is divided into three sections: Root section, Midspan section, and Tip section. Each section is subdivided into four sections: -5°, 0°, 5°, and 10°. In each subsection, the erosion behavior for the three blades (uncoated blade, H-146 coated blade, and polyurethane/IA-700 coated blade) are shown.

- Root Section
  - **-5 degrees**
    - **Uncoated**

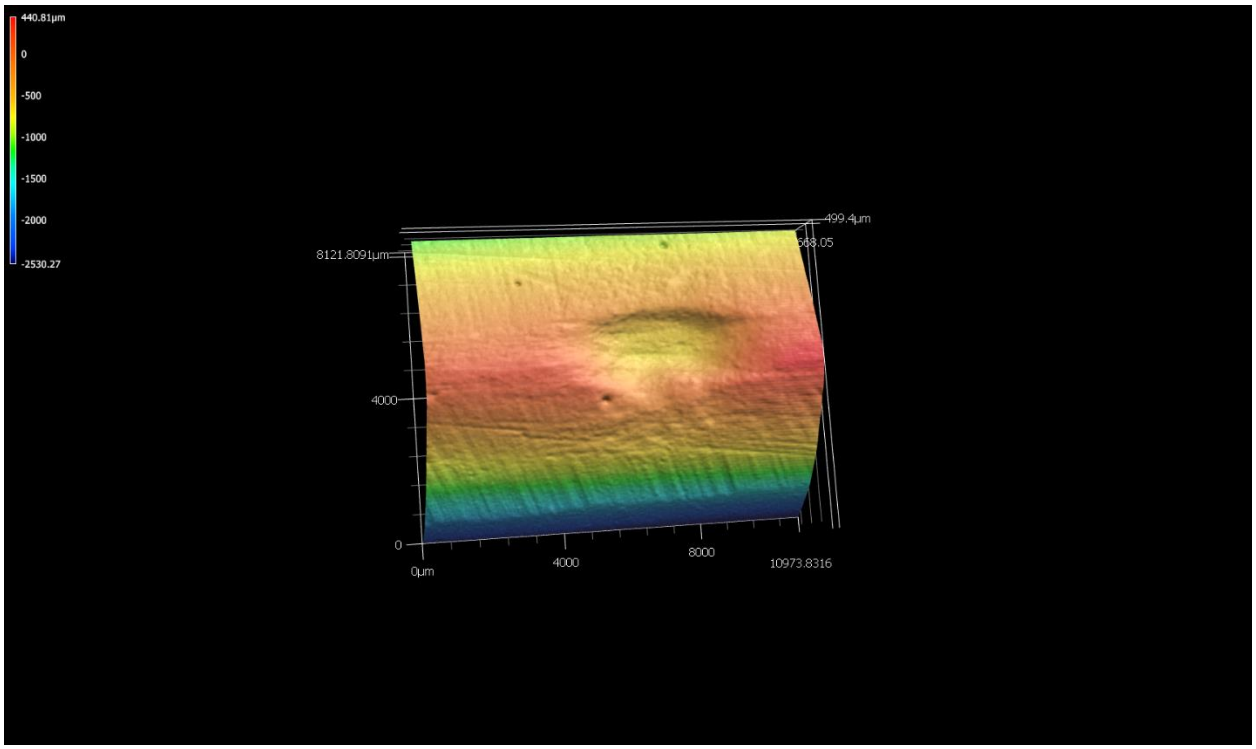


Fig. AVI-1: Erosion scar at -5° angle of impingement on the uncoated blade EXP1

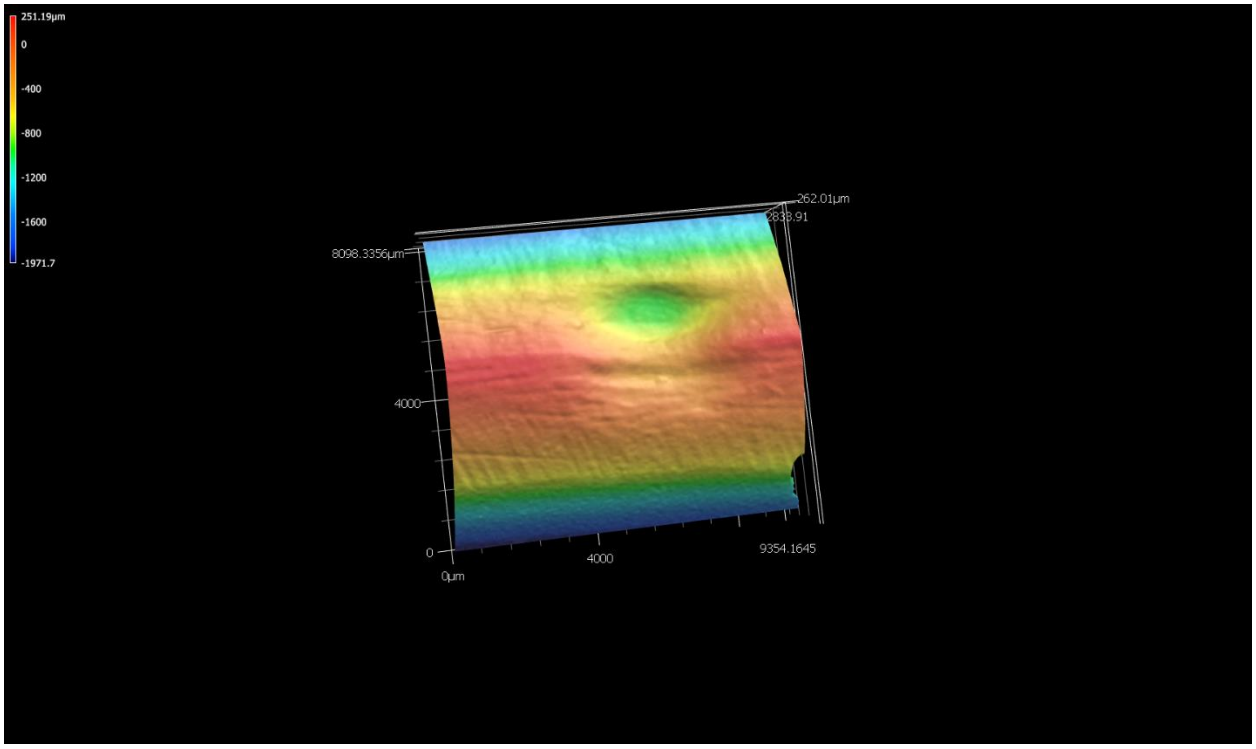


Fig. AVI-2: Erosion scar at -5° angle of impingement on the uncoated blade EXP2

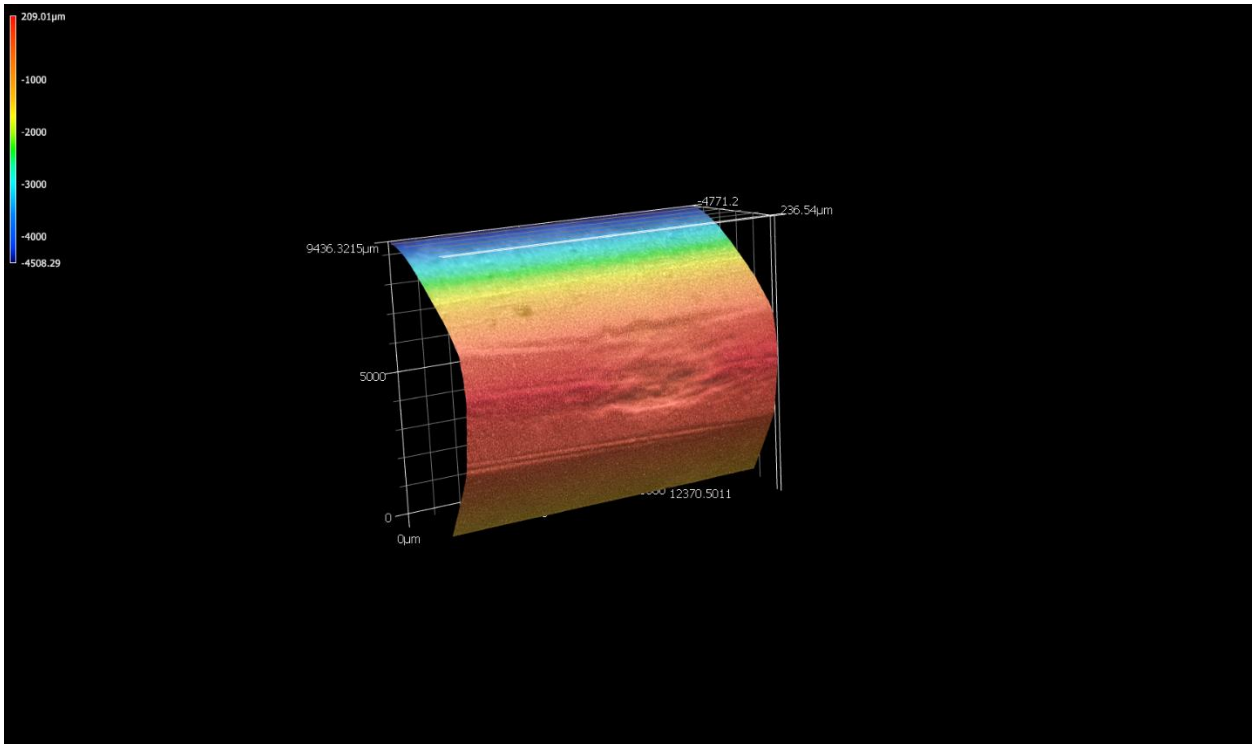


Fig. AVI-3: Erosion scar at -5° angle of impingement on the uncoated blade EXP3

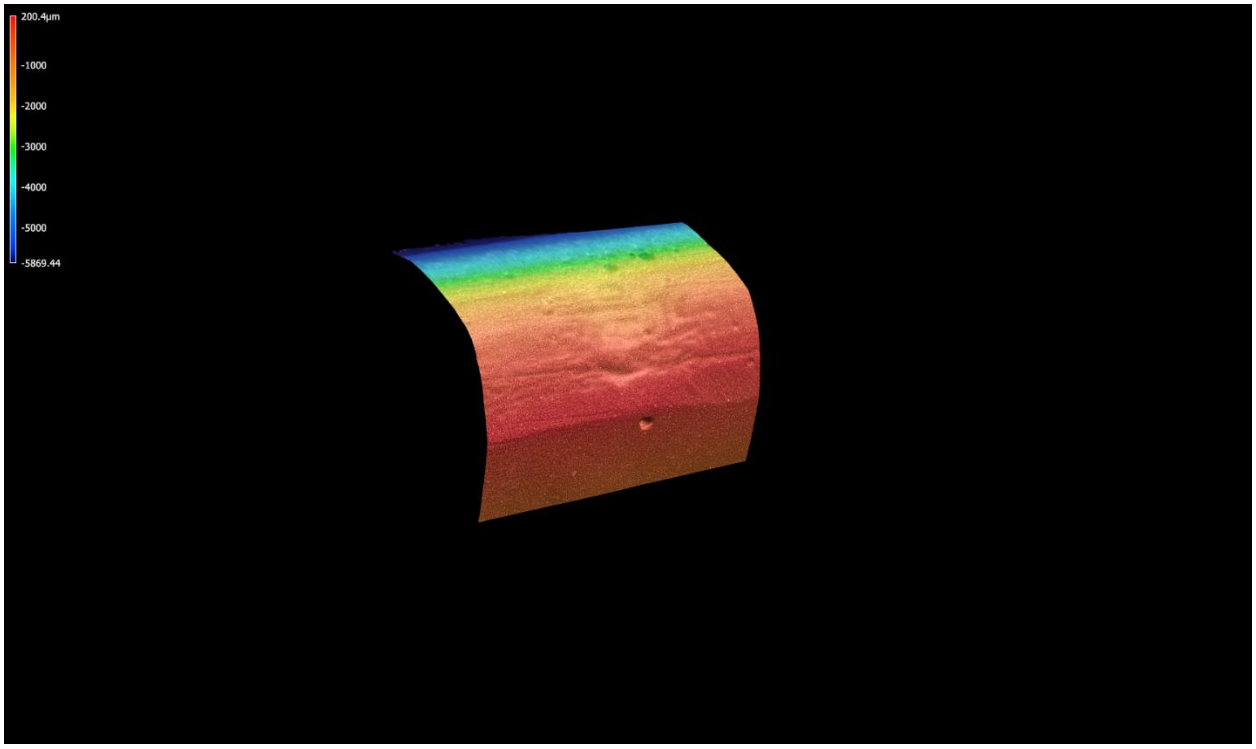


Fig. AVI-4: Erosion scar at -5° angle of impingement on the uncoated blade EXP4

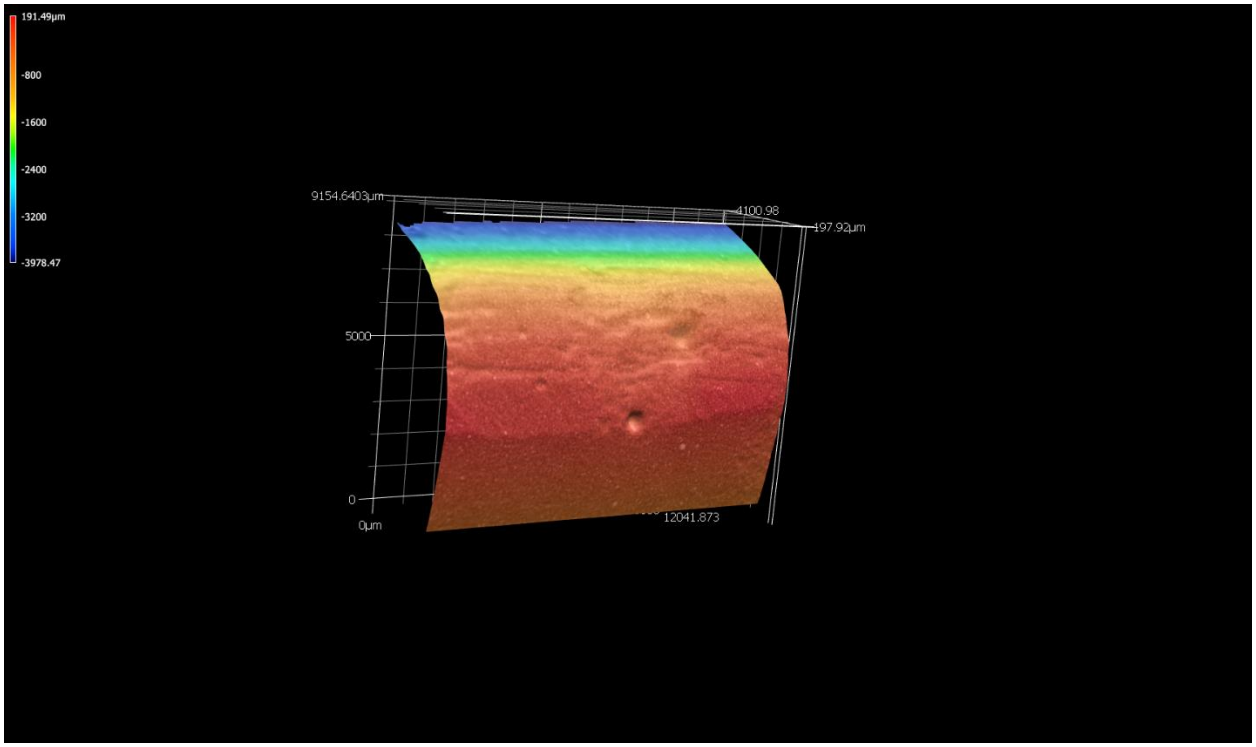


Fig. AVI-5: Erosion scar at -5° angle of impingement on the uncoated blade EXP5

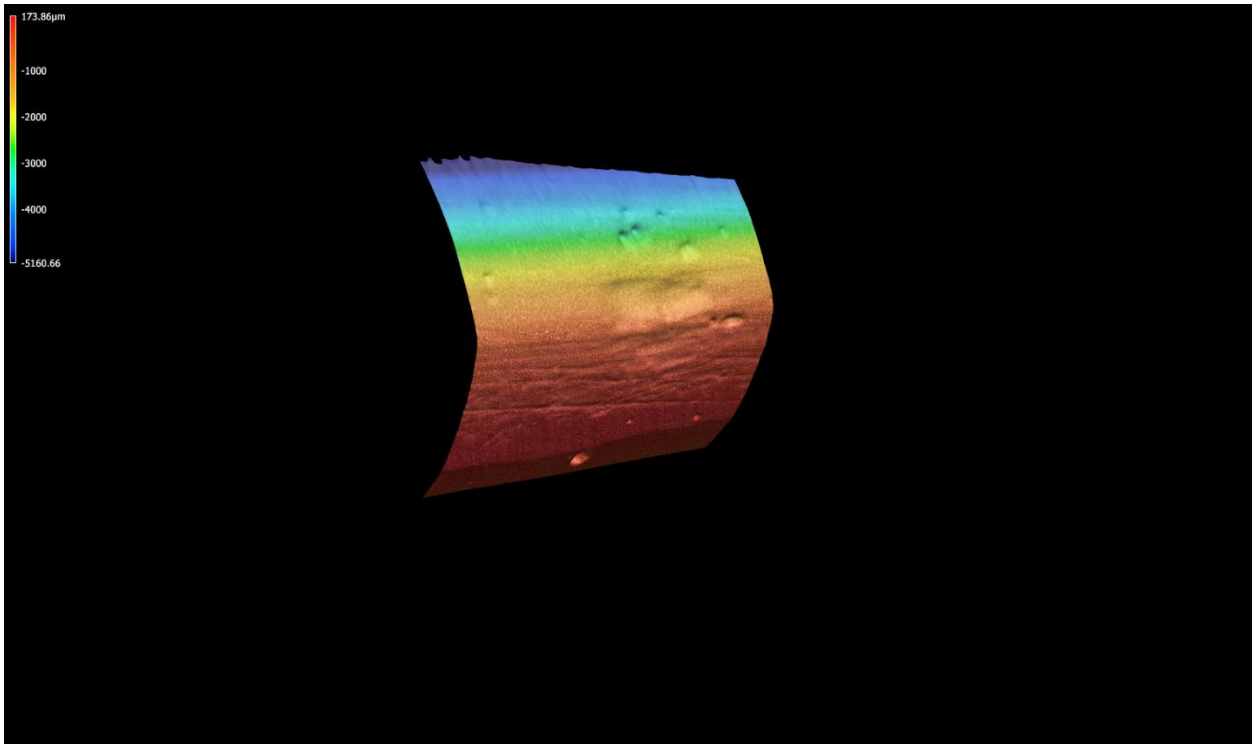


Fig. AVI-6: Erosion scar at -5° angle of impingement on the uncoated blade EXP6

- **H-146**

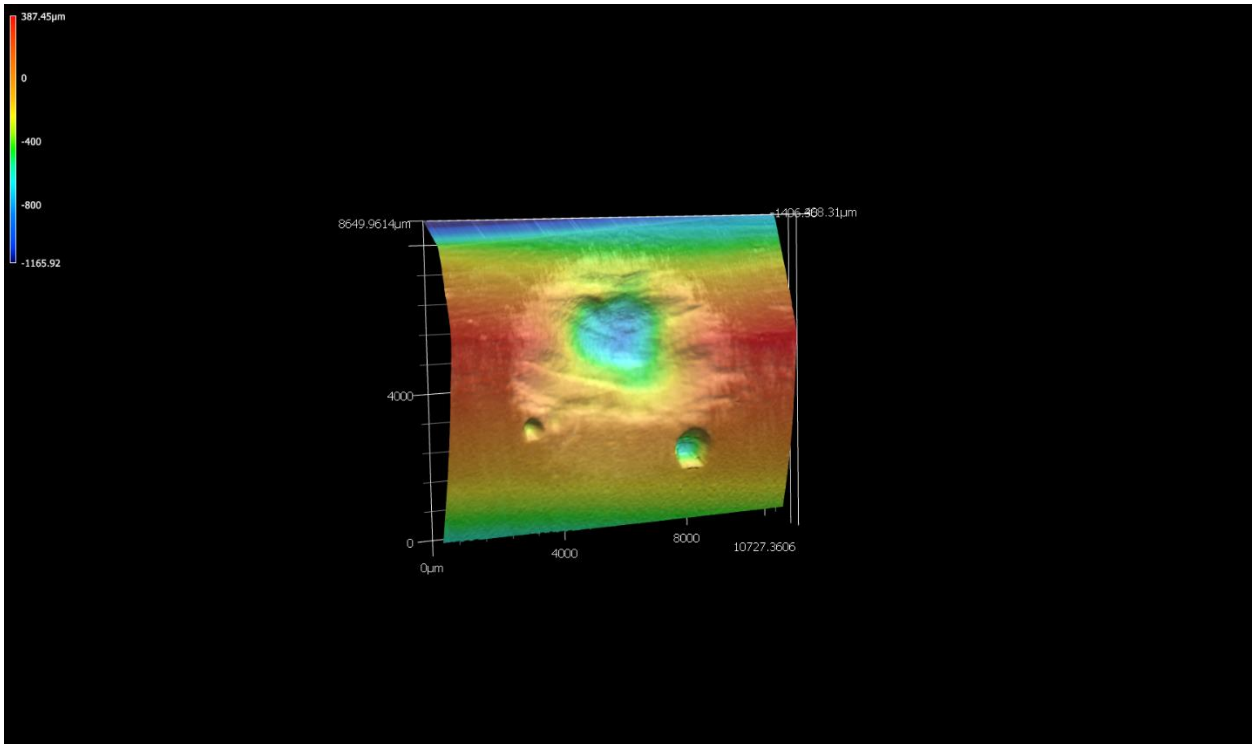


Fig. AVI-7: Erosion scar at -5° angle of impingement on the H-146 coated blade EXP1

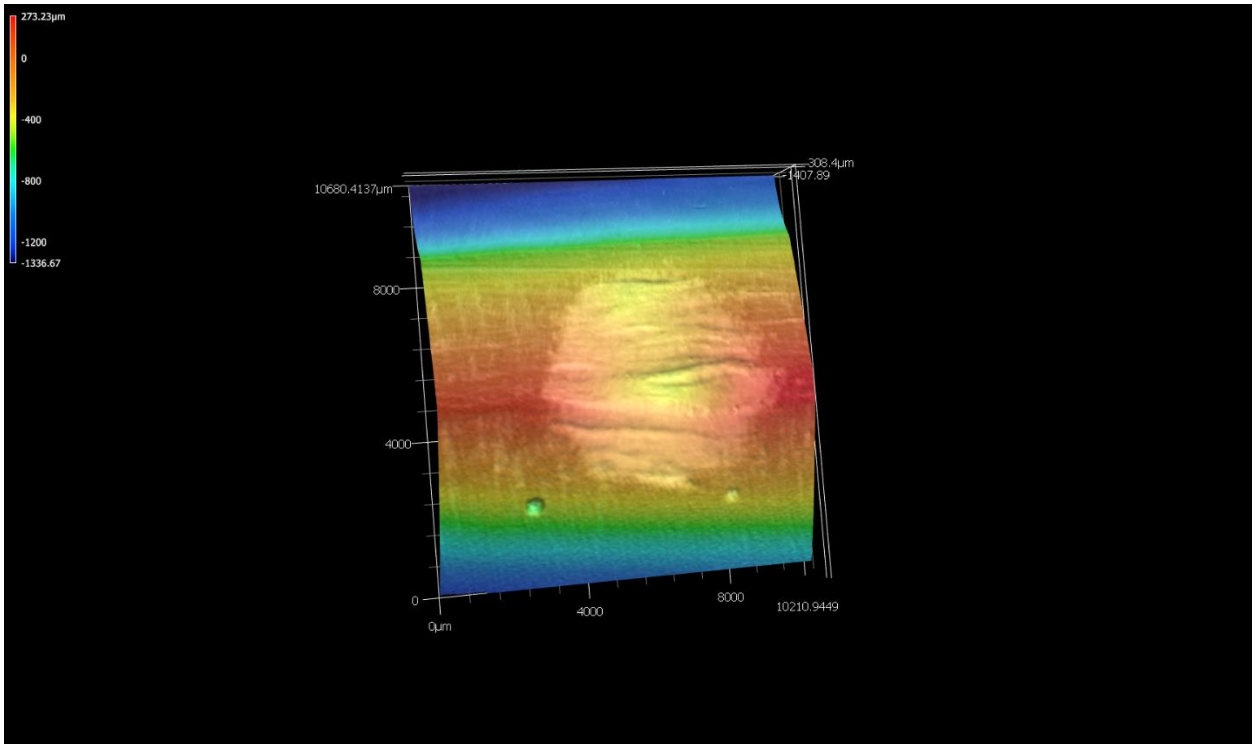


Fig. AVI-8: Erosion scar at -5° angle of impingement on the H-146 coated blade EXP2

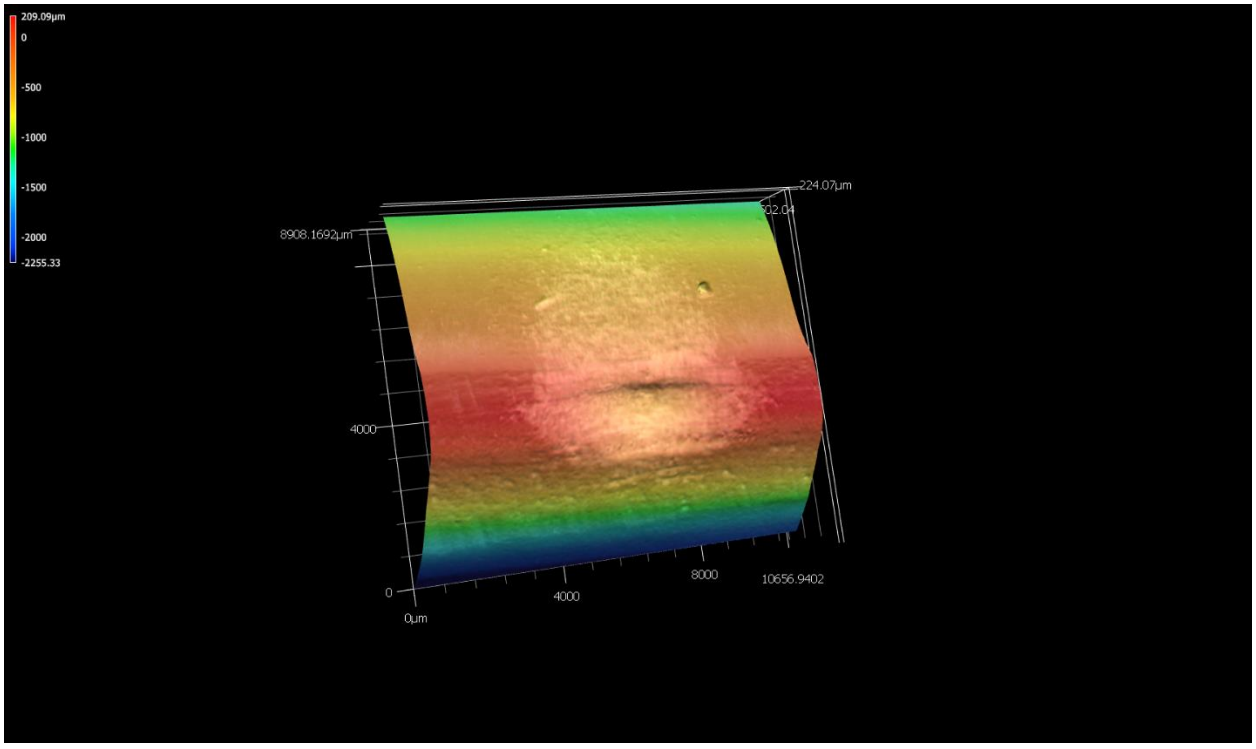


Fig. AVI-9: Erosion scar at -5° angle of impingement on the H-146 coated blade EXP3

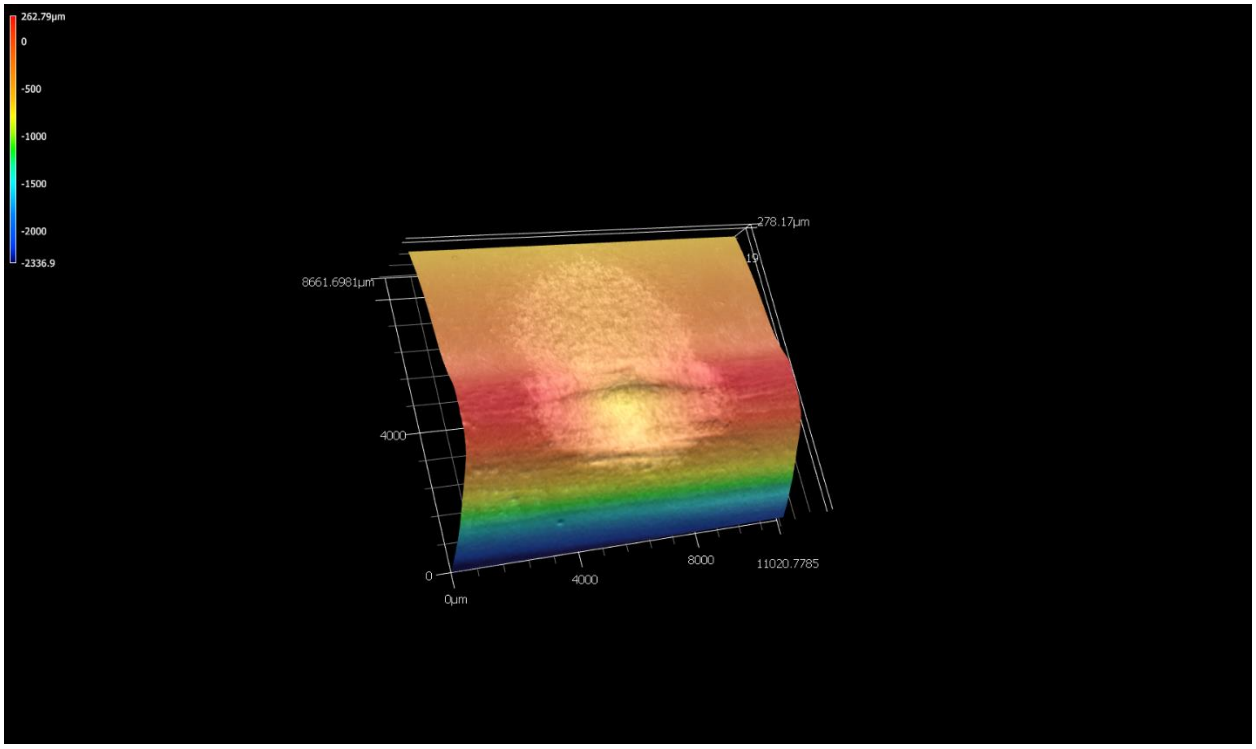


Fig. AVI-10: Erosion scar at -5° angle of impingement on the H-146 coated blade EXP4

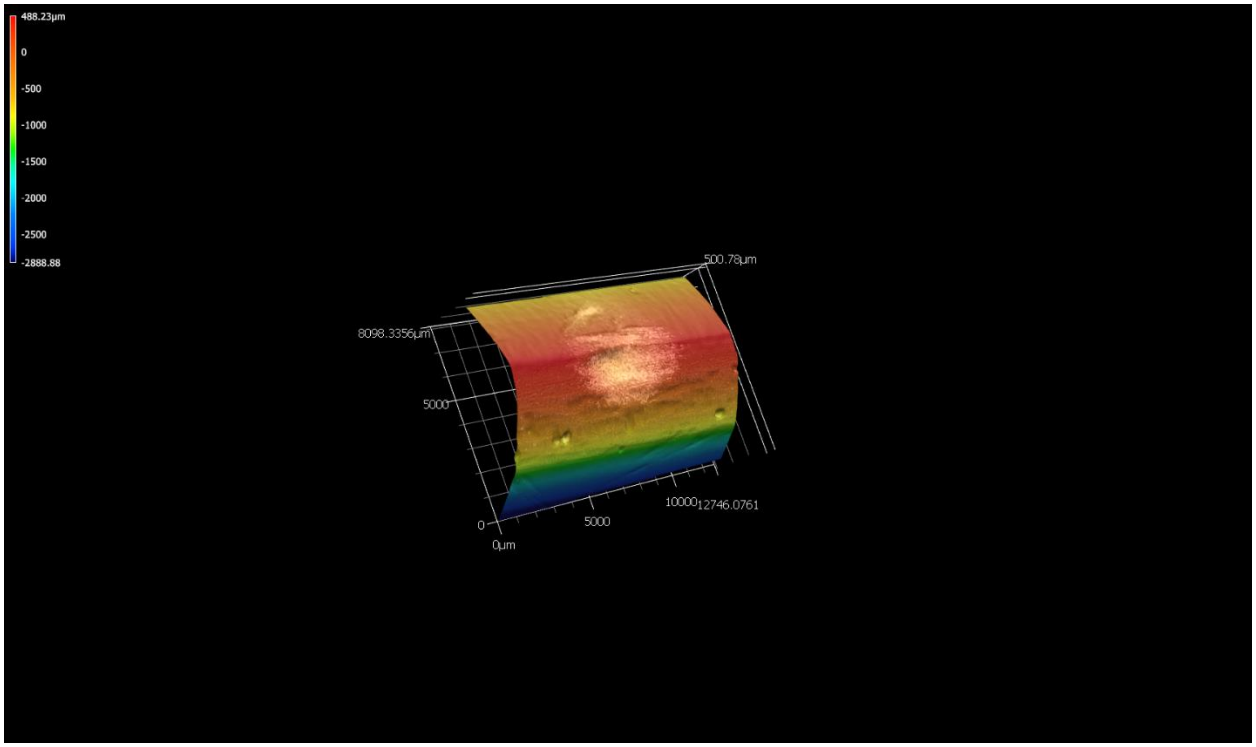


Fig. AVI-11: Erosion scar at -5° angle of impingement on the H-146 coated blade EXP5

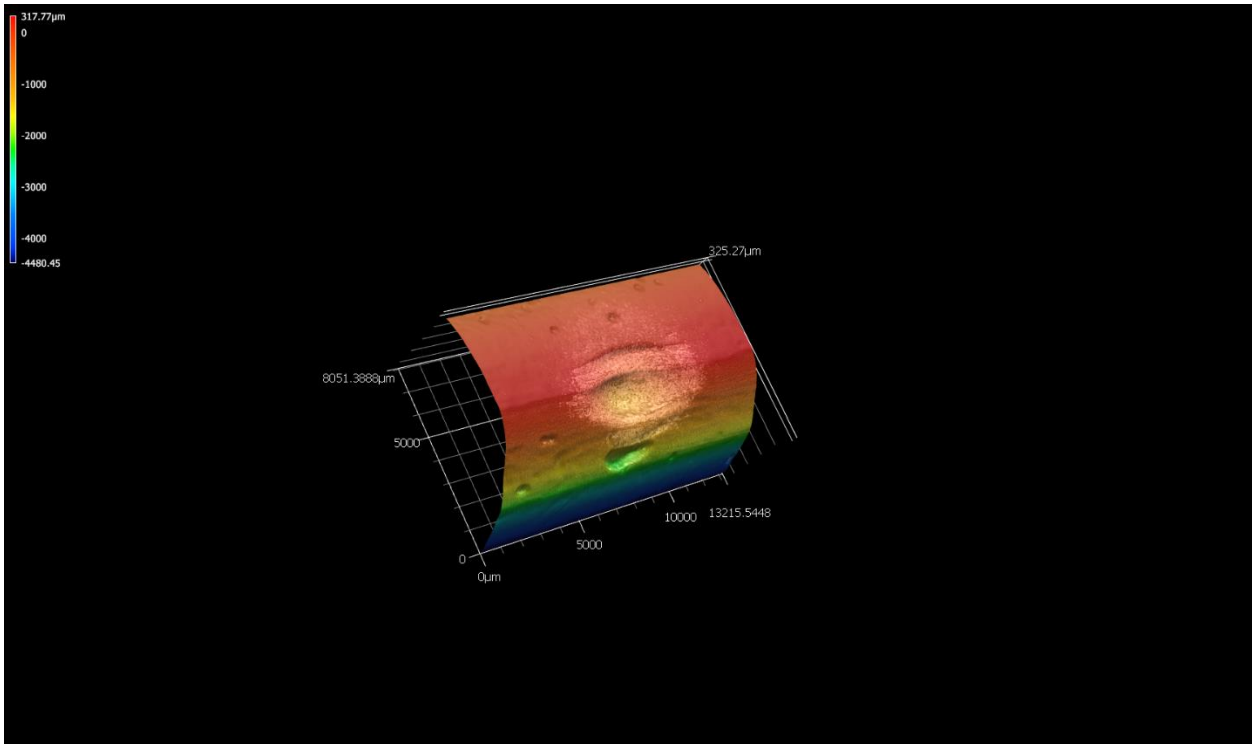


Fig. AVI-12: Erosion scar at -5° angle of impingement on the H-146 coated blade EXP6

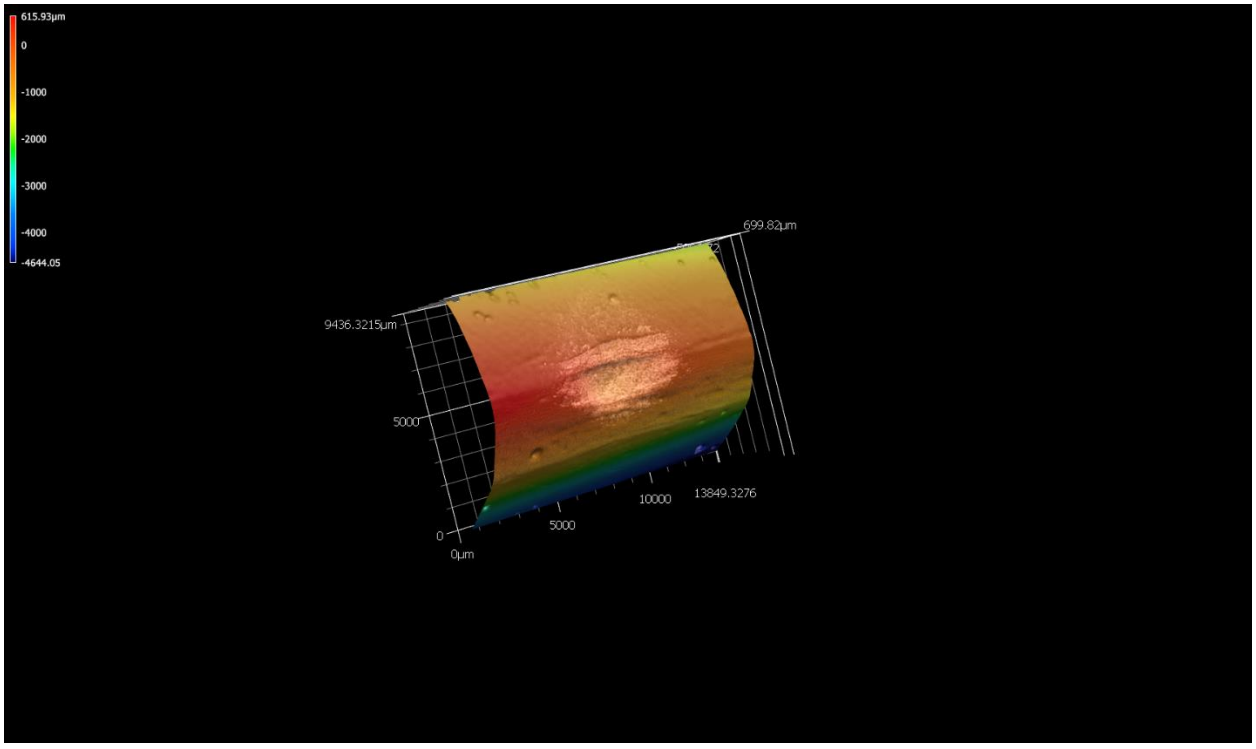


Fig. AVI-13: Erosion scar at -5° angle of impingement on the H-146 coated blade EXP7

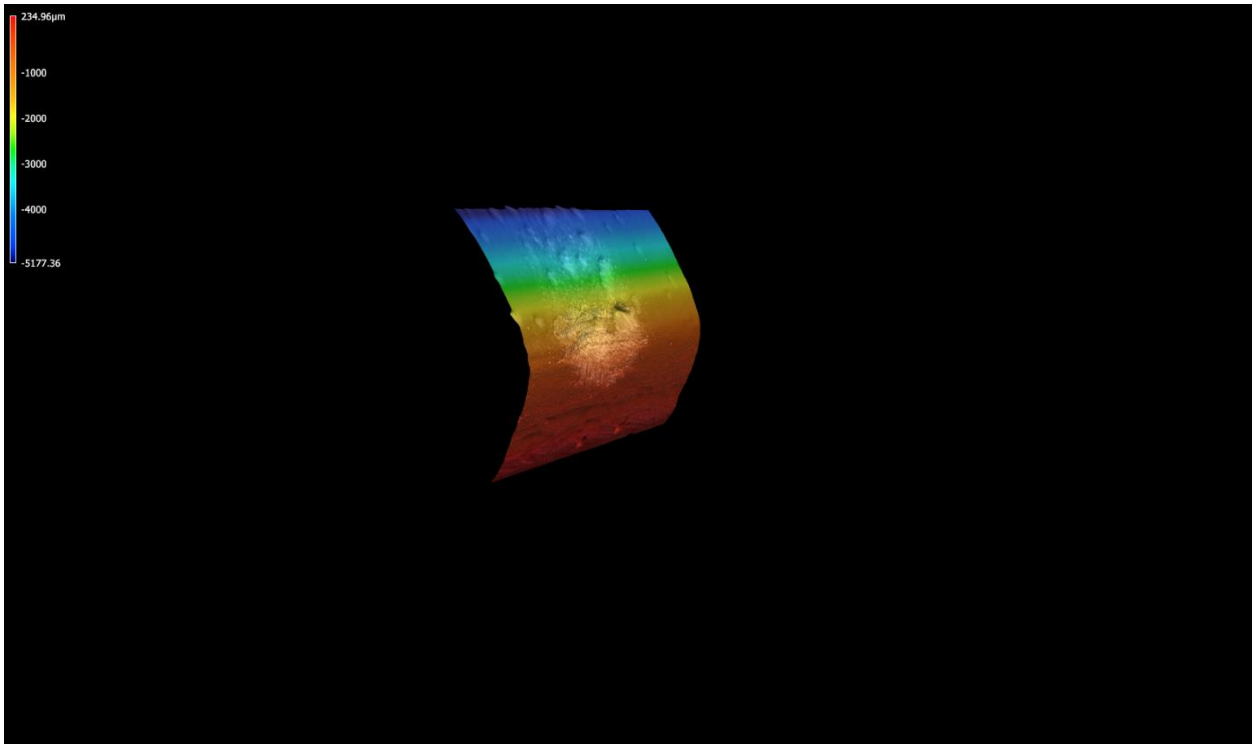


Fig. AVI-14: Erosion scar at -5° angle of impingement on the H-146 coated blade EXP8

- **Polyurethane/IA-700**

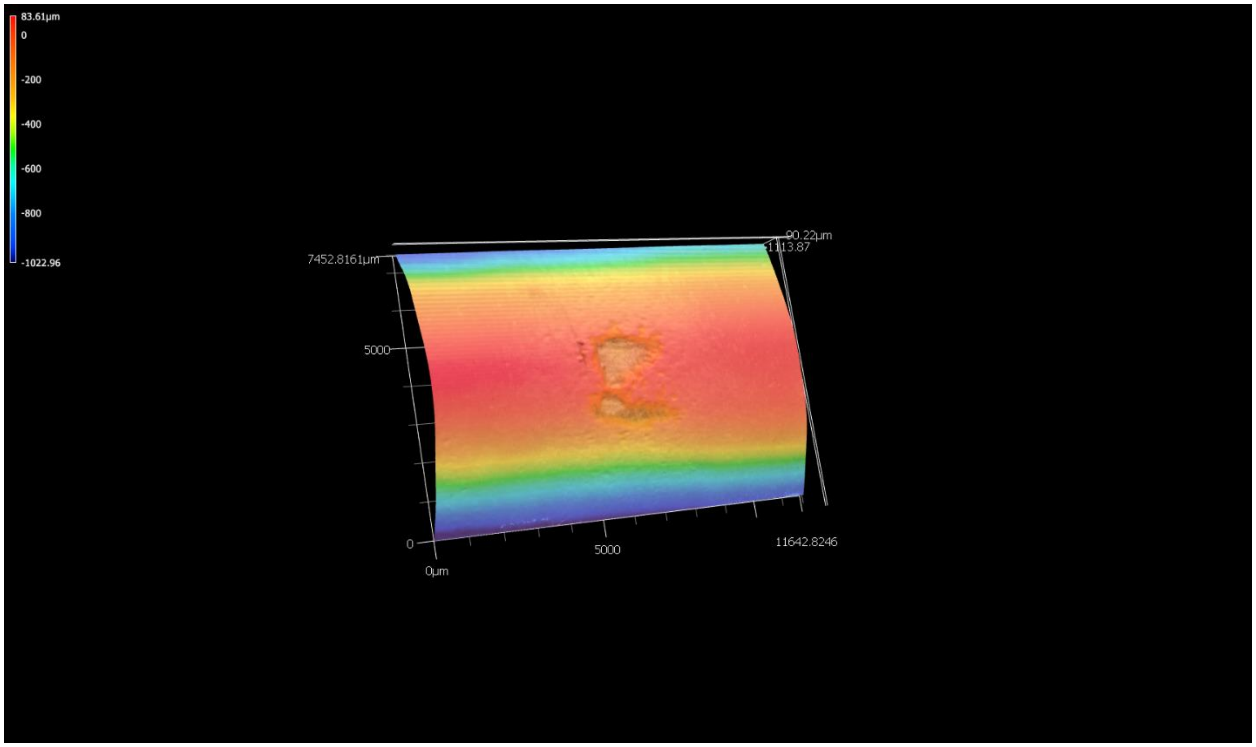


Fig. AVI-15: Erosion scar at -5° angle of impingement on the Polyurethane/IA-700 coated blade EXP1

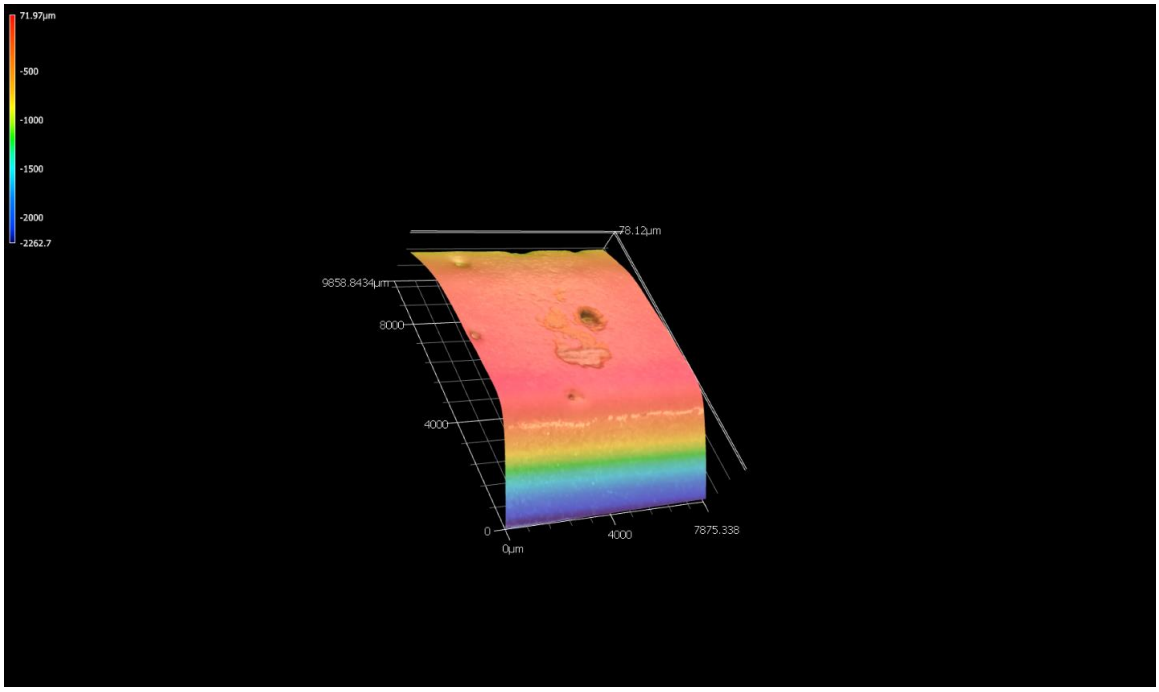


Fig. AVI-16: Erosion scar at -5° angle of impingement on the Polyurethane/IA-700 coated blade EXP2

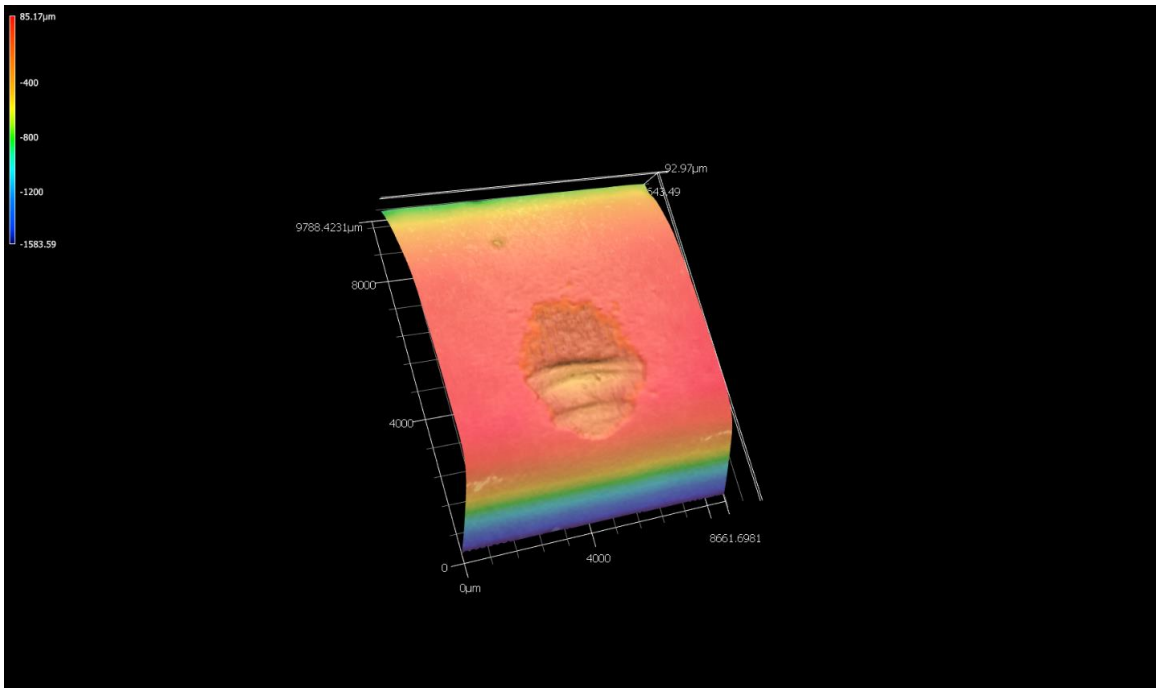


Fig. AVI-17: Erosion scar at -5° angle of impingement on the Polyurethane/IA-700 coated blade EXP3

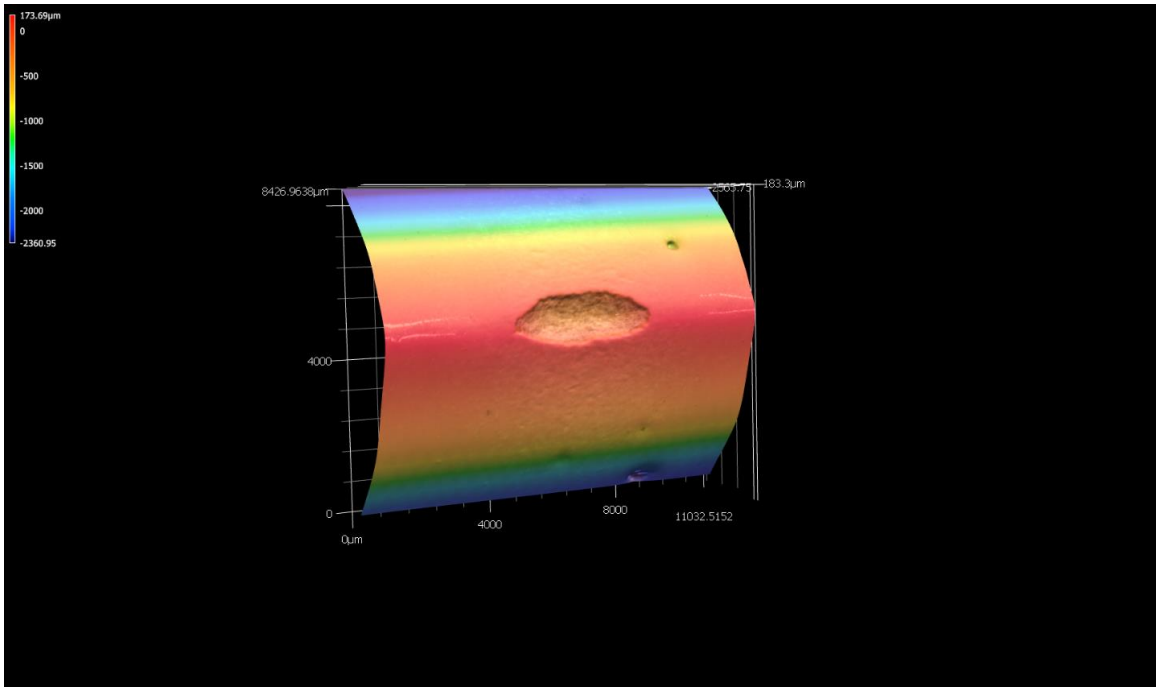


Fig. AVI-18: Erosion scar at -5° angle of impingement on the Polyurethane/IA-700 coated blade EXP4

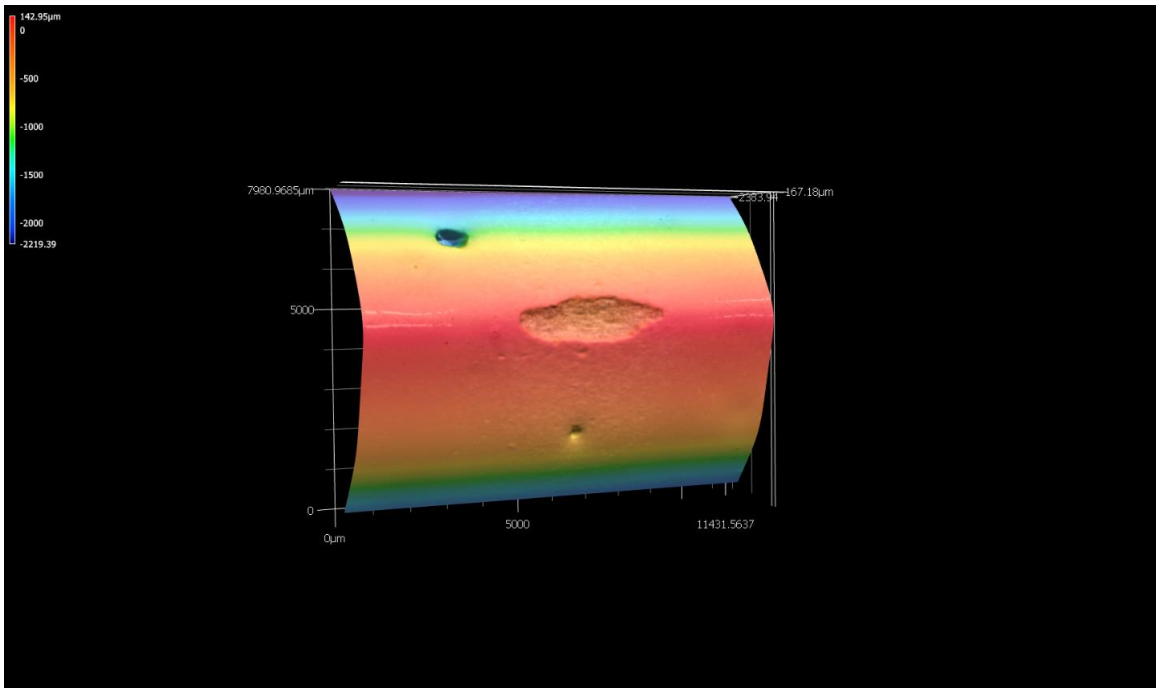


Fig. AVI-19: Erosion scar at -5° angle of impingement on the Polyurethane/IA-700 coated blade EXP5

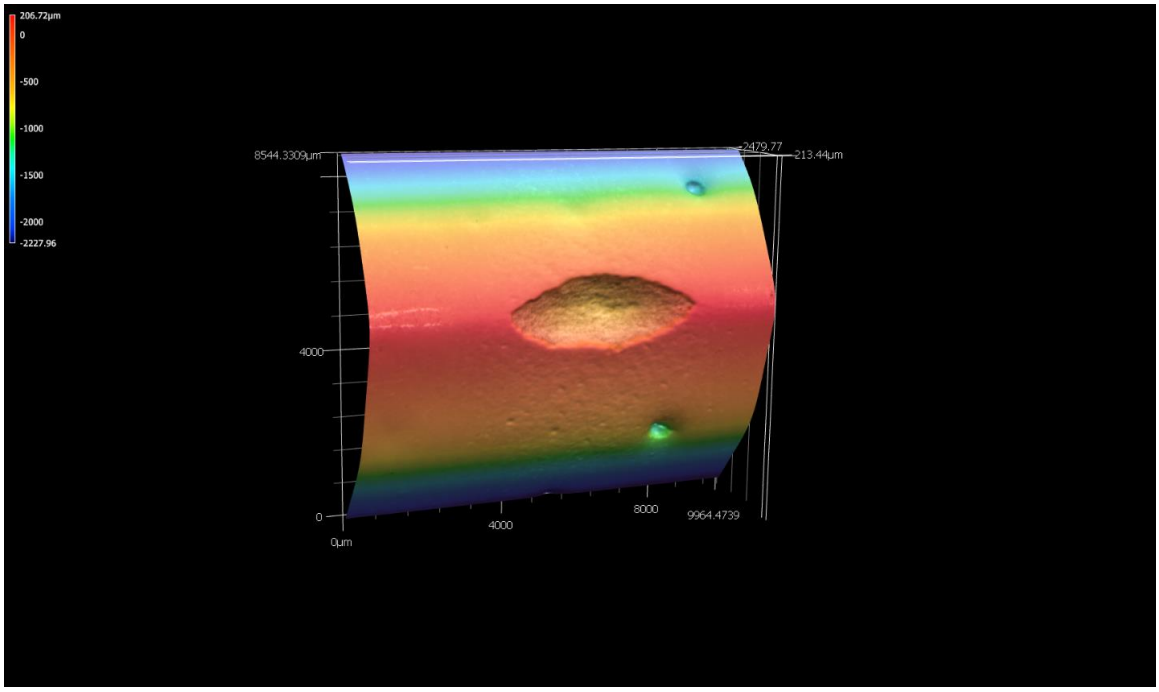


Fig. AVI-20: Erosion scar at -5° angle of impingement on the Polyurethane/IA-700 coated blade EXP6

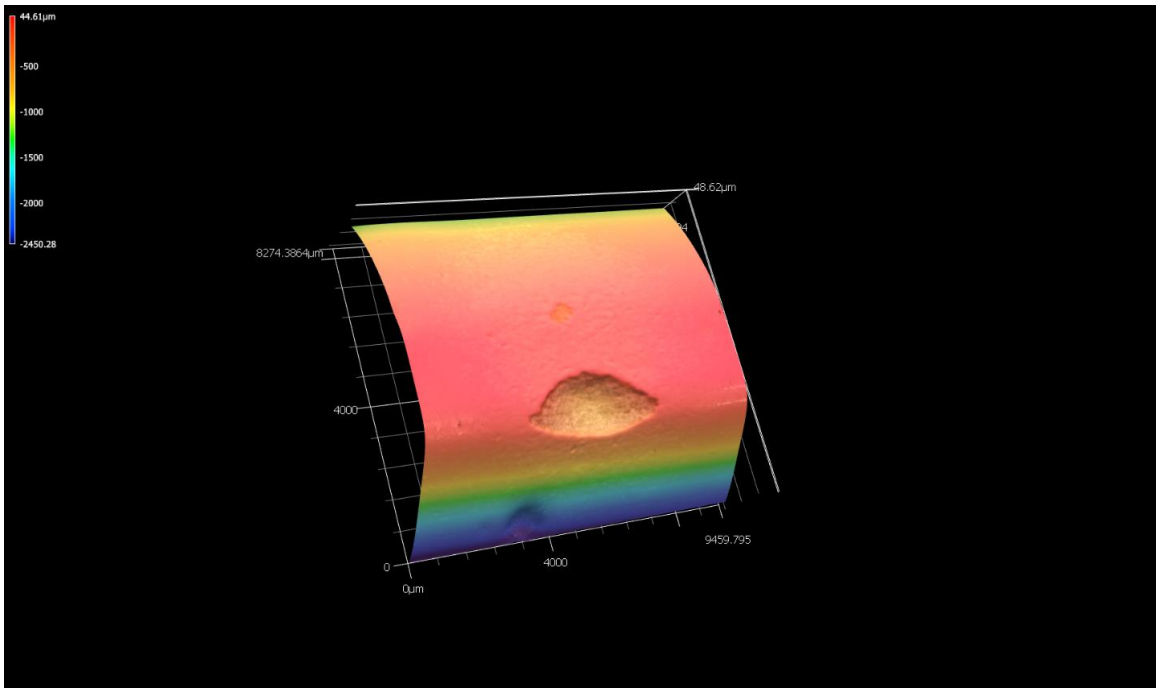


Fig. AVI-21: Erosion scar at -5° angle of impingement on the Polyurethane/IA-700 coated blade EXP7

- **0 degrees**
  - **Uncoated**

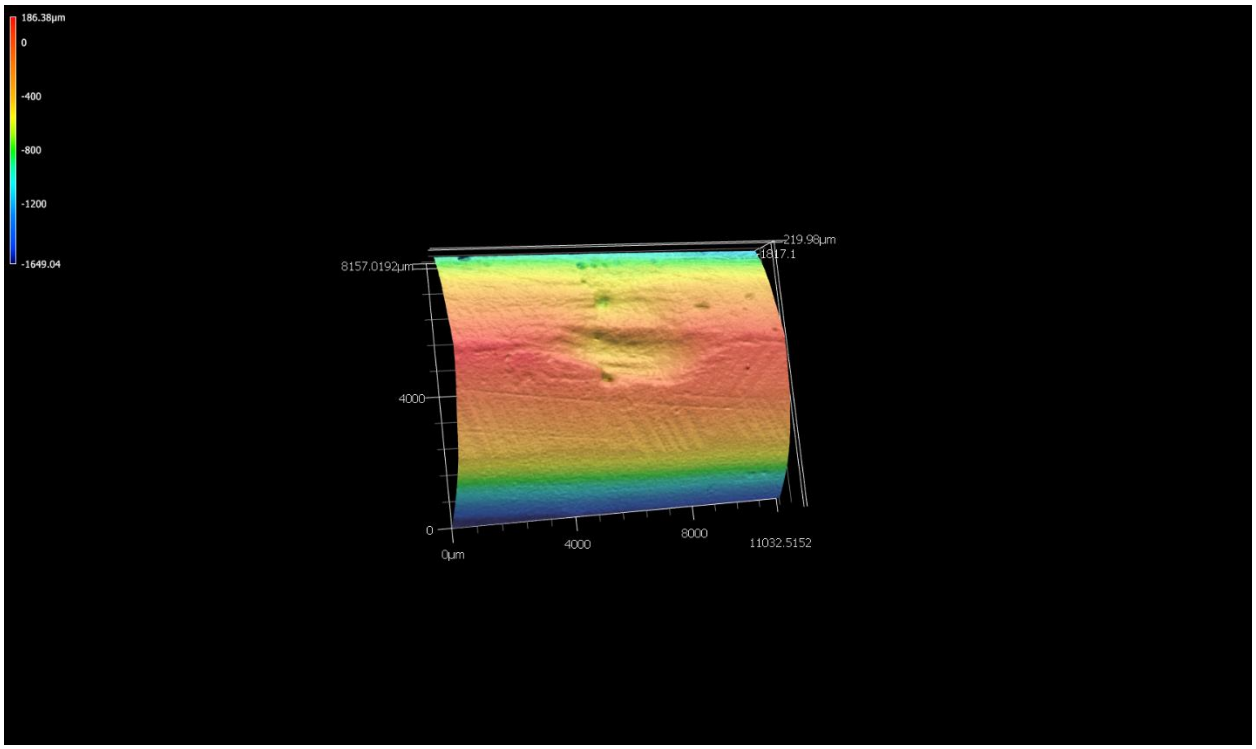


Fig. AVI-22: Erosion scar at 0° angle of impingement on the uncoated blade EXP1

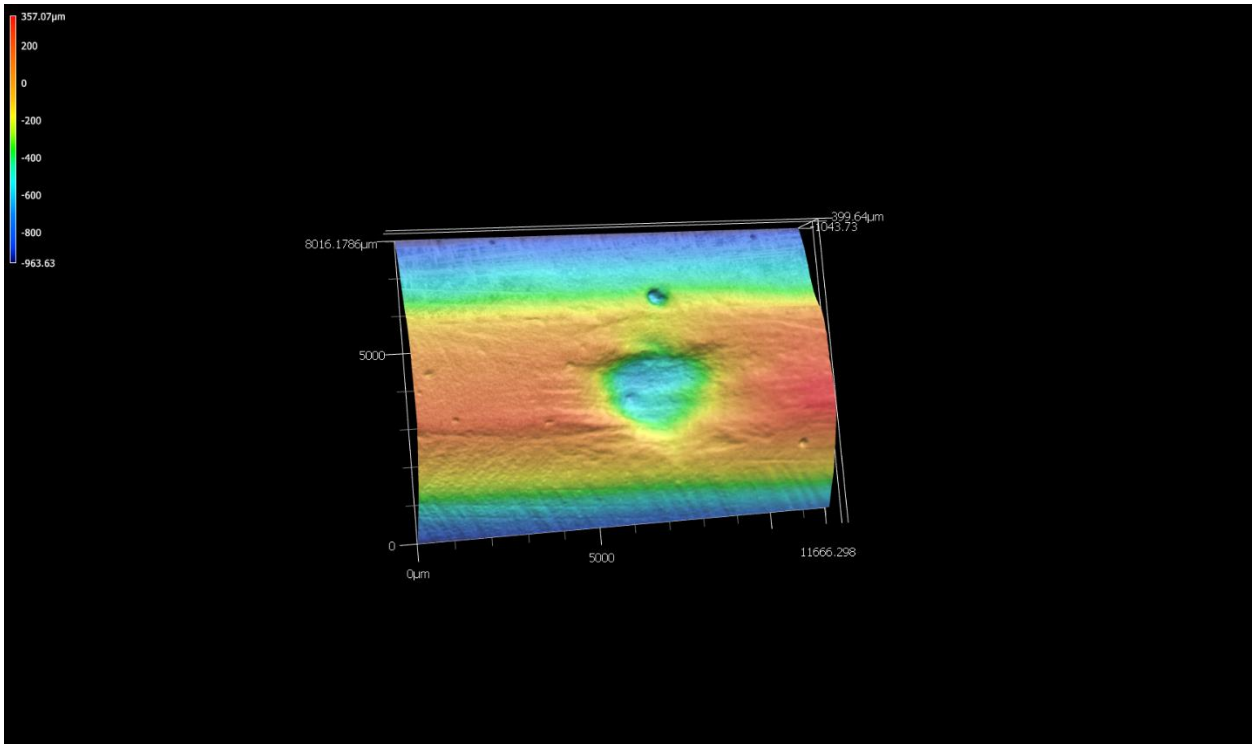


Fig. AVI-23: Erosion scar at 0° angle of impingement on the uncoated blade EXP2

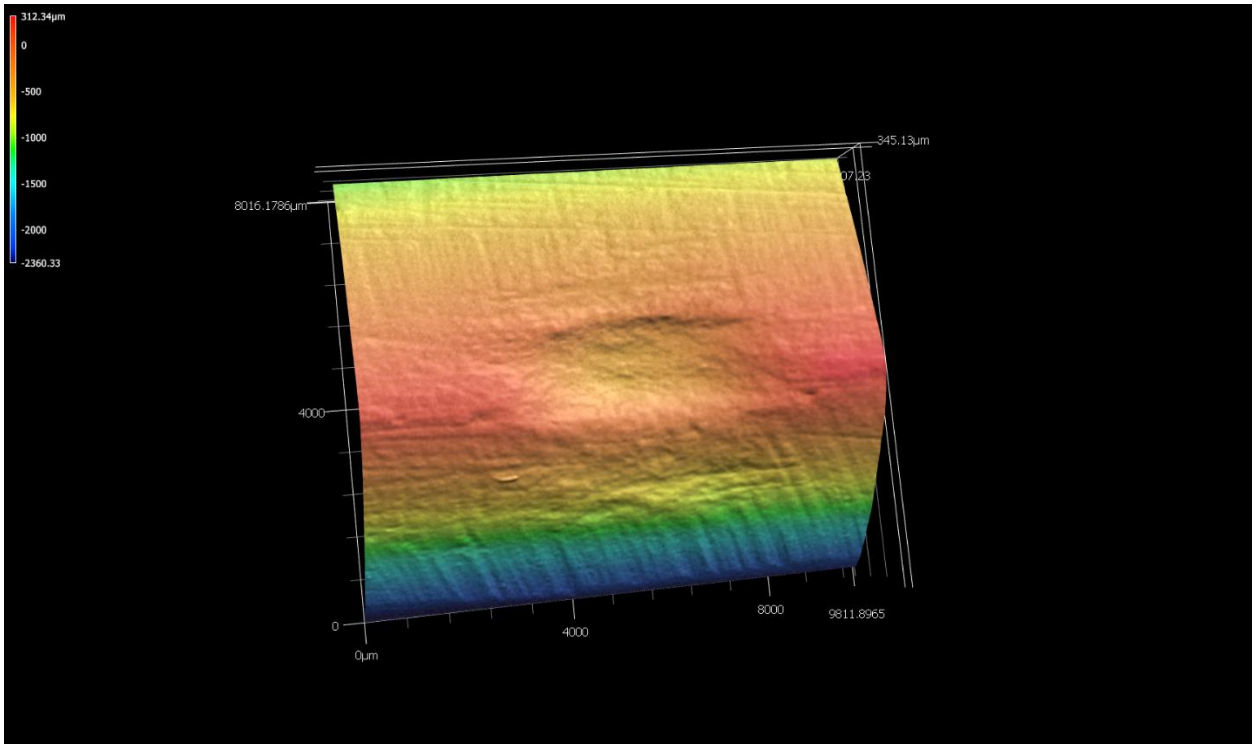


Fig. AVI-24: Erosion scar at 0° angle of impingement on the uncoated blade EXP3

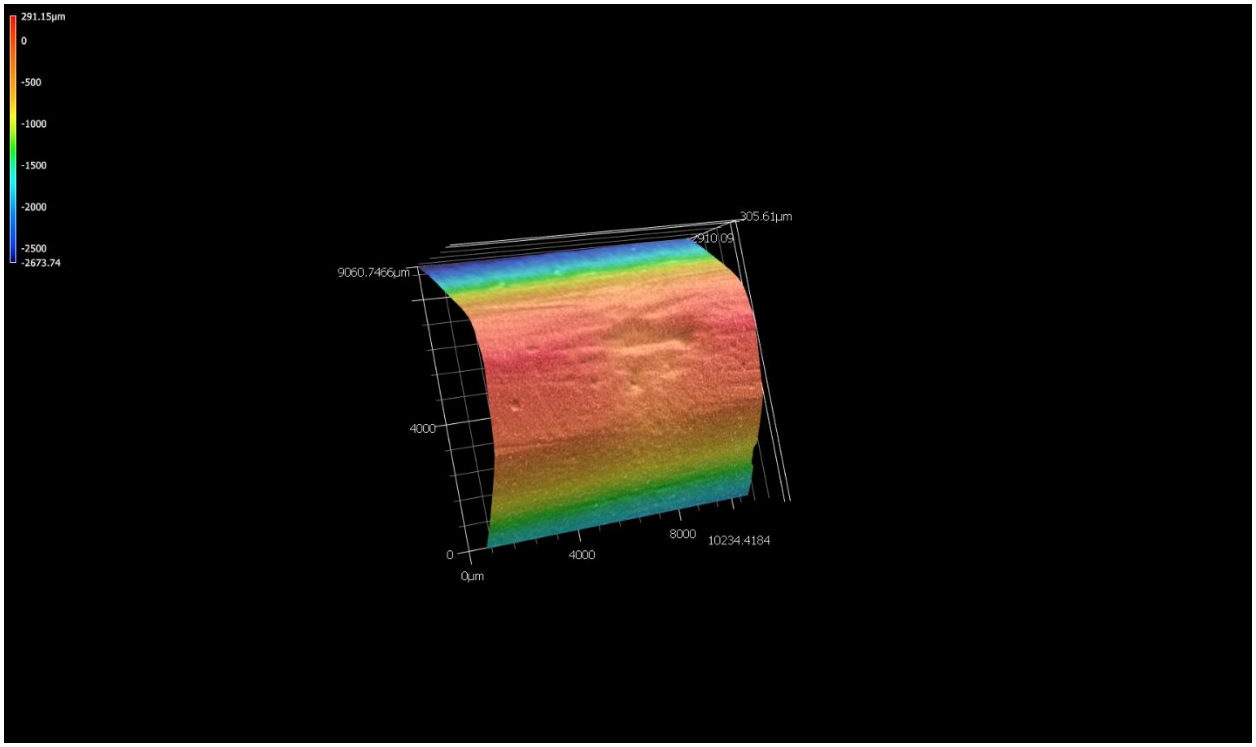


Fig. AVI-25: Erosion scar at 0° angle of impingement on the uncoated blade EXP4

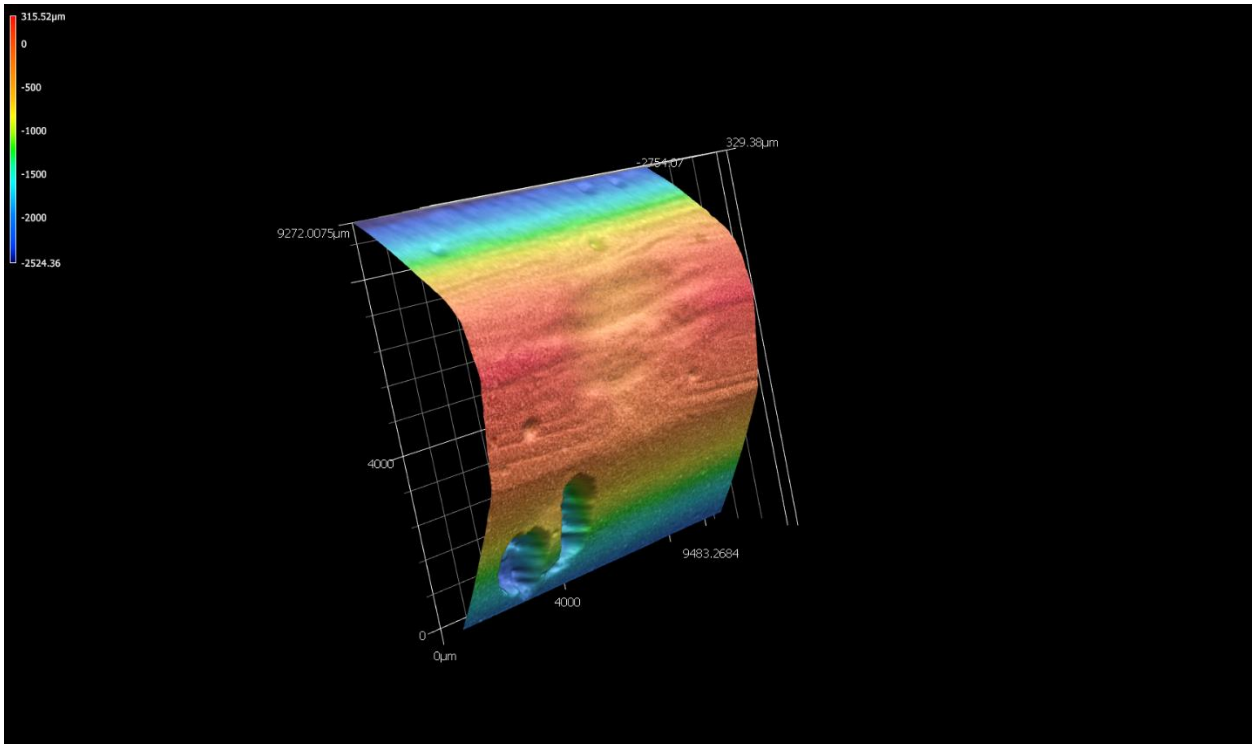


Fig. AVI-26: Erosion scar at 0° angle of impingement on the uncoated blade EXP5

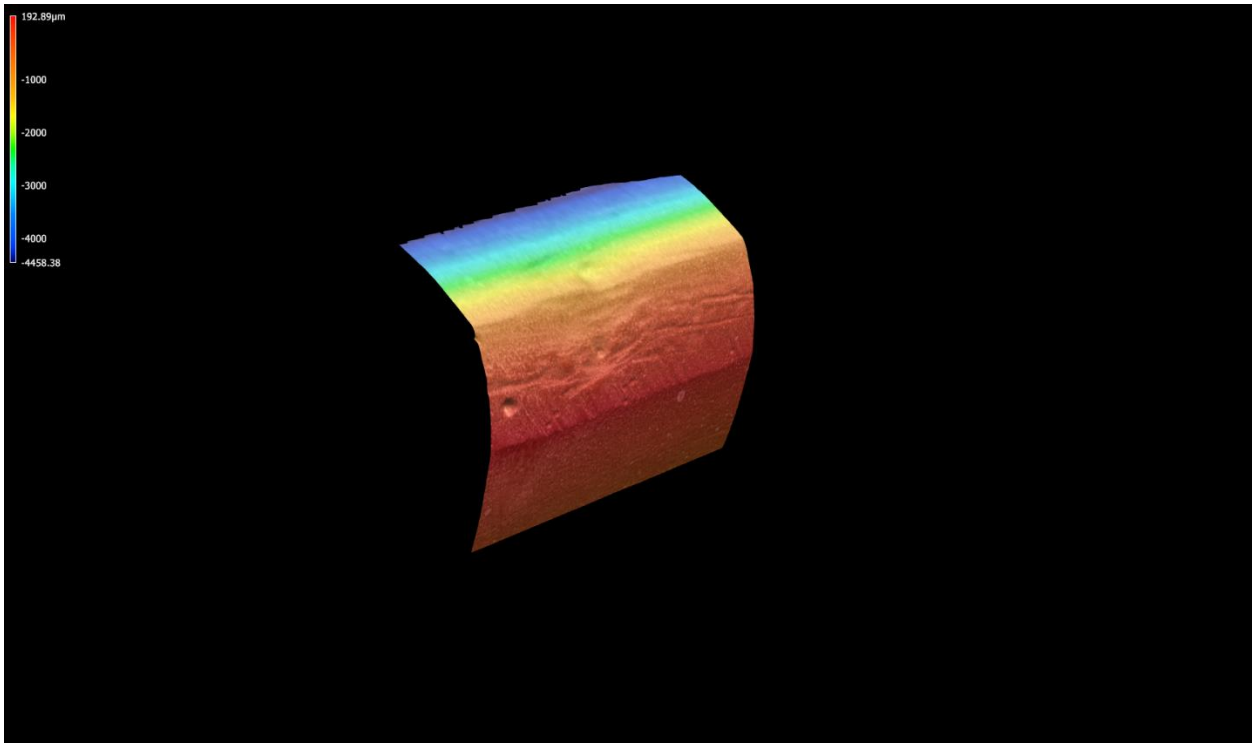


Fig. AVI-27: Erosion scar at 0° angle of impingement on the uncoated blade EXP7

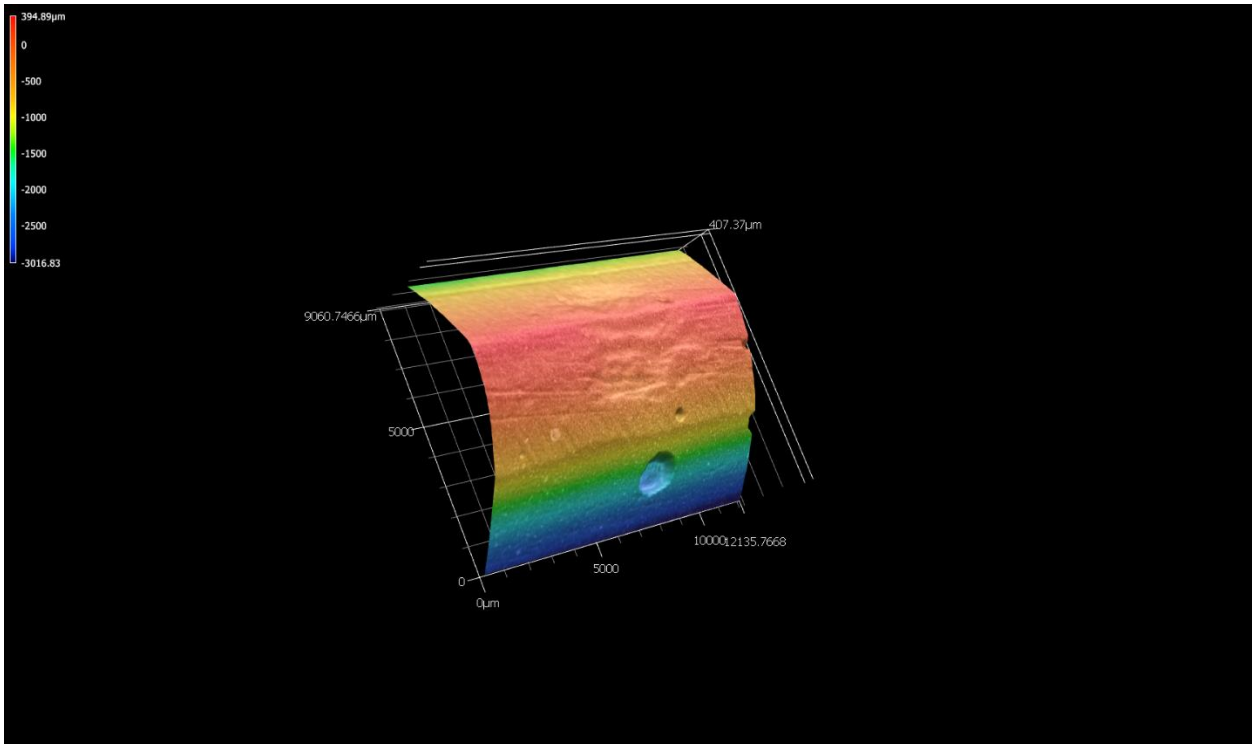


Fig. AVI-28: Erosion scar at 0° angle of impingement on the uncoated blade EXP8

- **<u>H-146</u>**

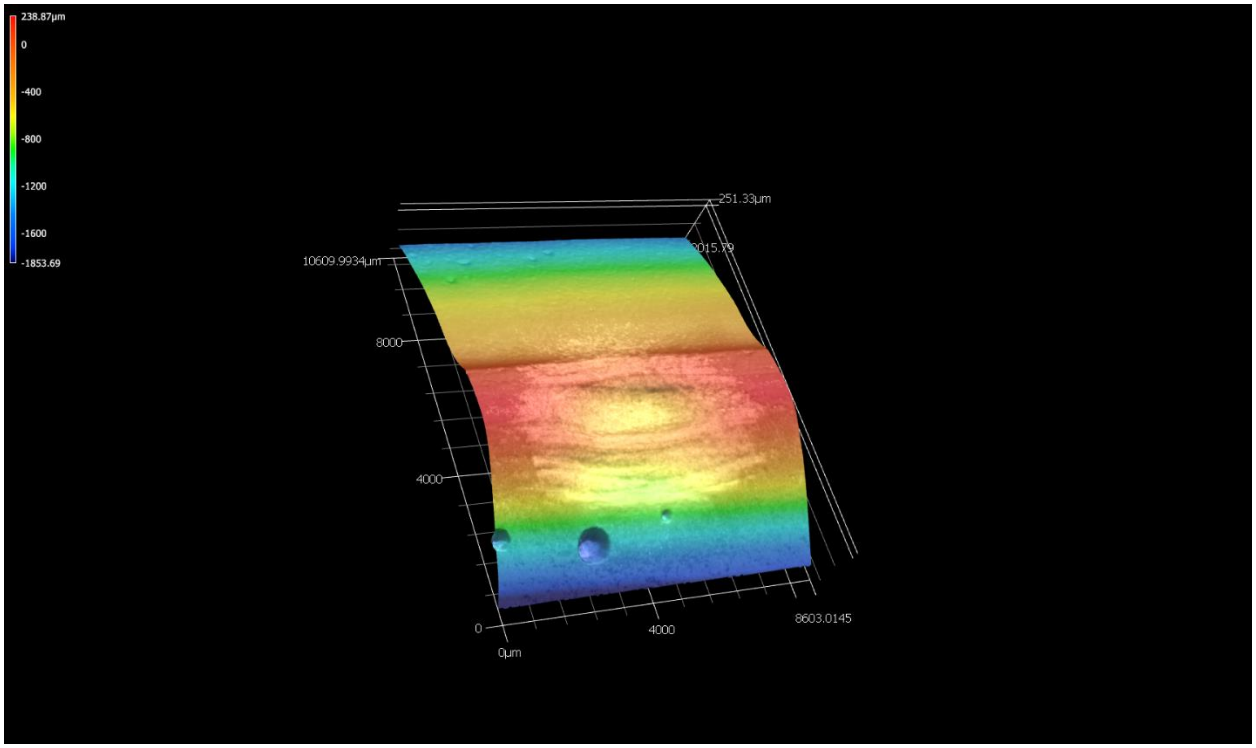


Fig. AVI-29: Erosion scar at 0° angle of impingement on the H-146 coated blade EXP1

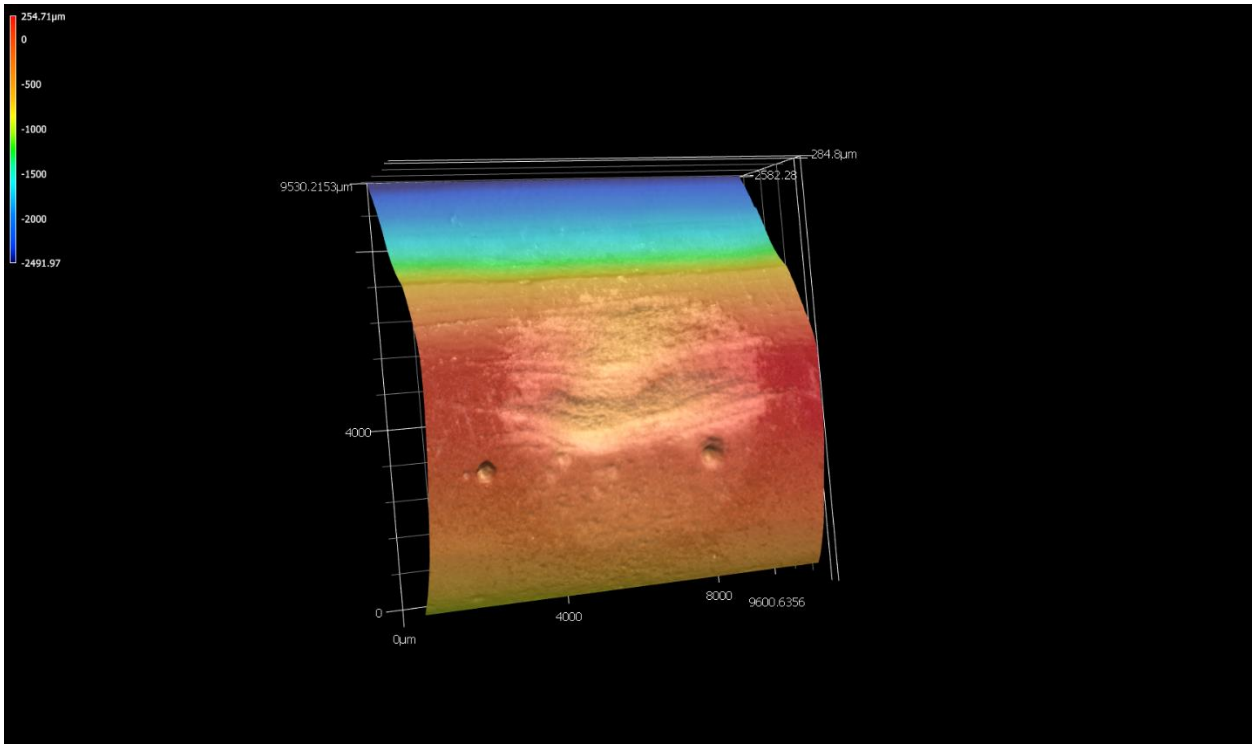


Fig. AVI-30: Erosion scar at 0° angle of impingement on the H-146 coated blade EXP2

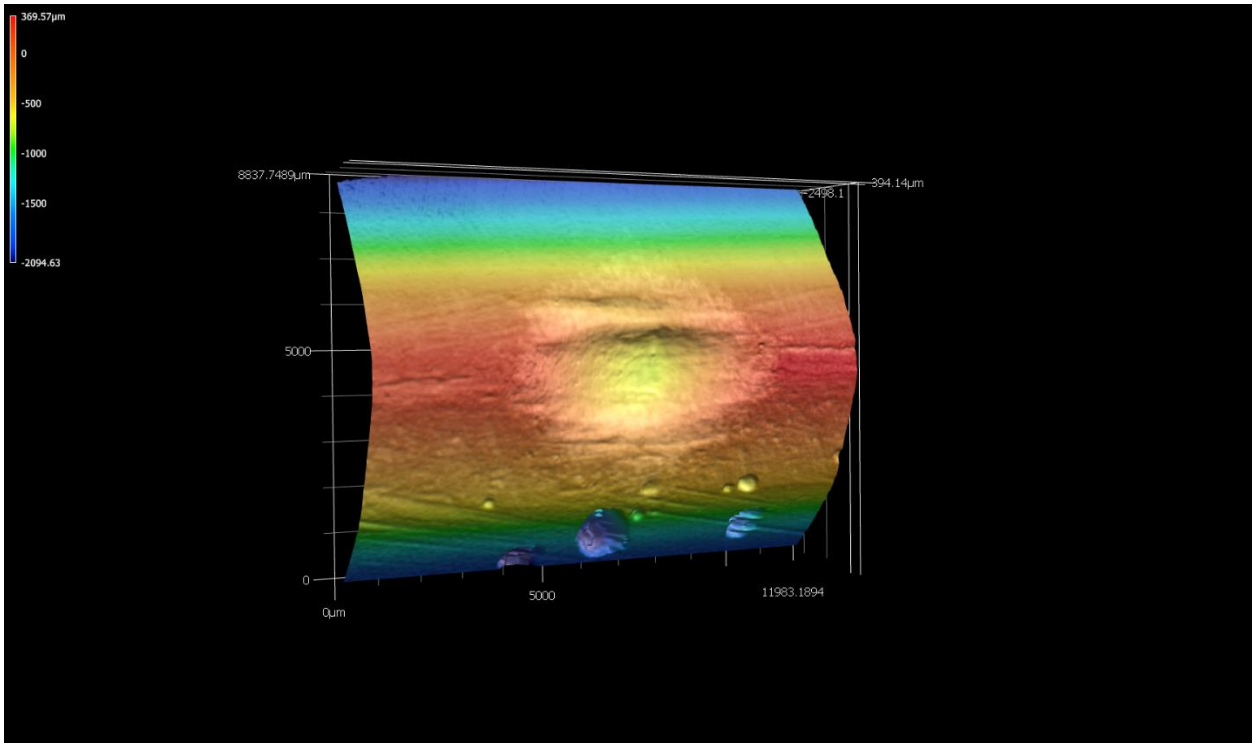


Fig. AVI-31: Erosion scar at 0° angle of impingement on the H-146 coated blade EXP3

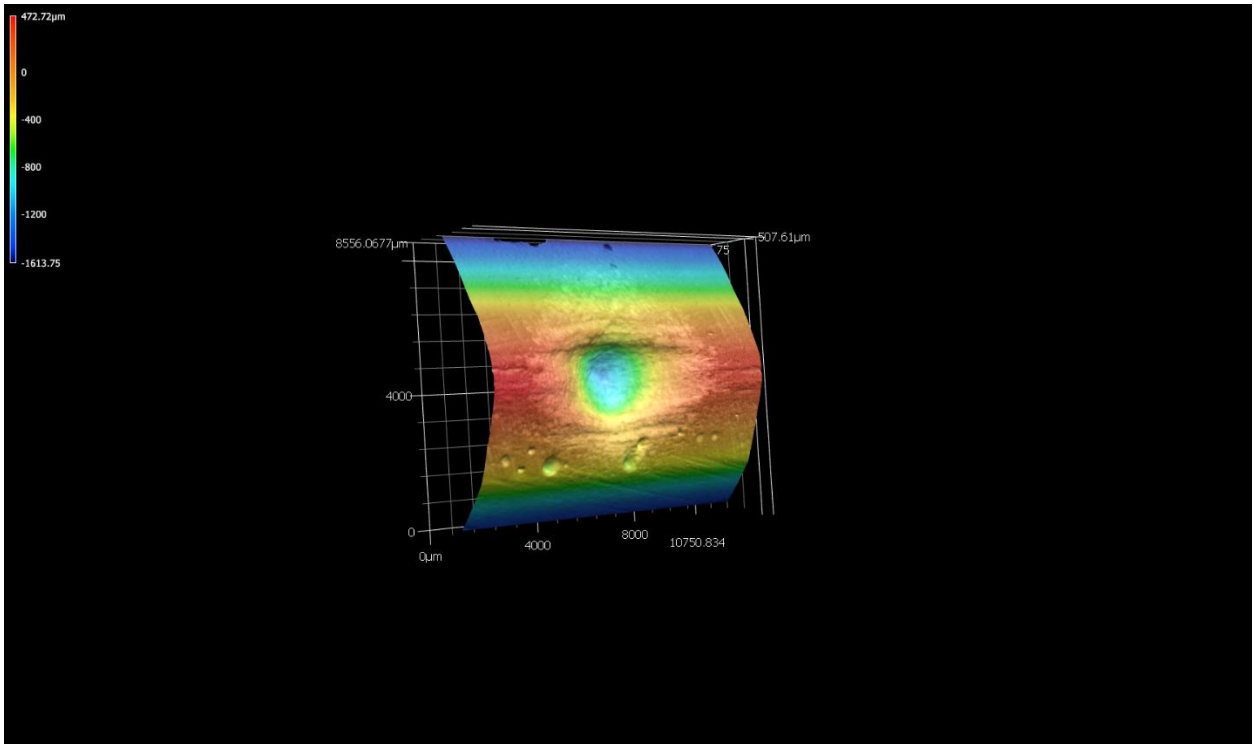


Fig. AVI-32: Erosion scar at 0° angle of impingement on the H-146 coated blade EXP4

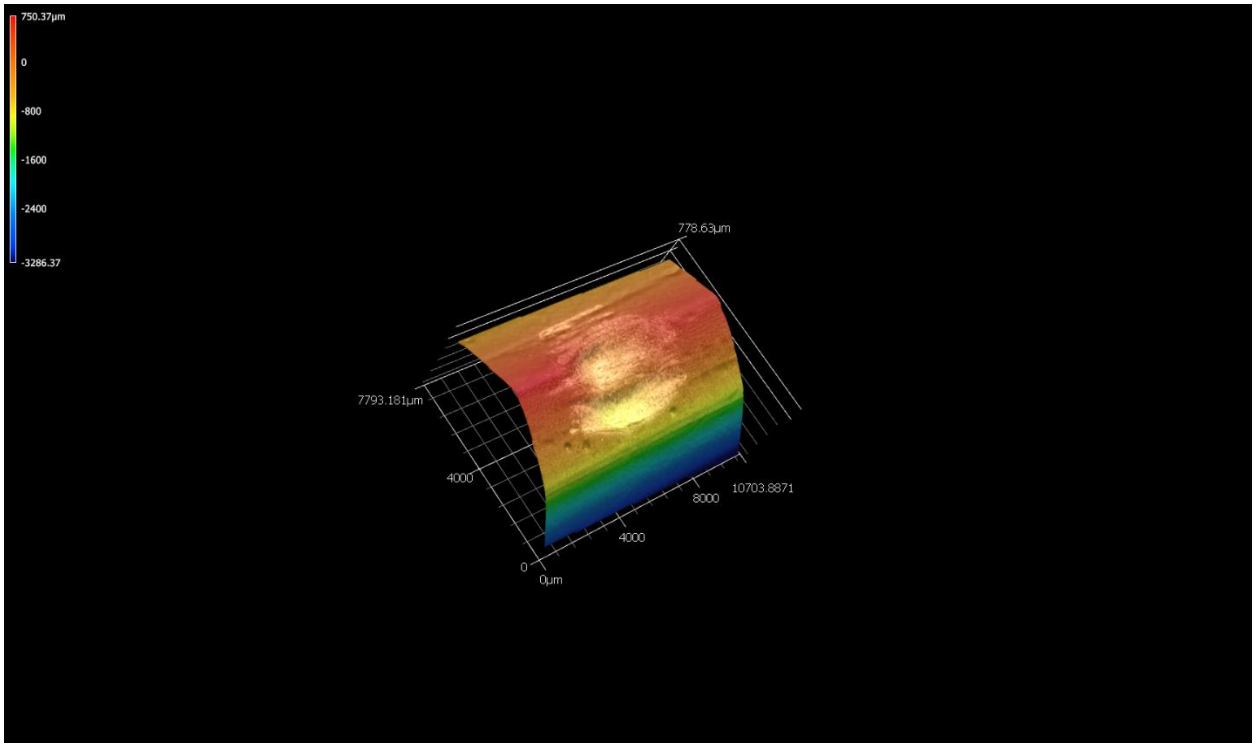


Fig. AVI-33: Erosion scar at 0° angle of impingement on the H-146 coated blade EXP5

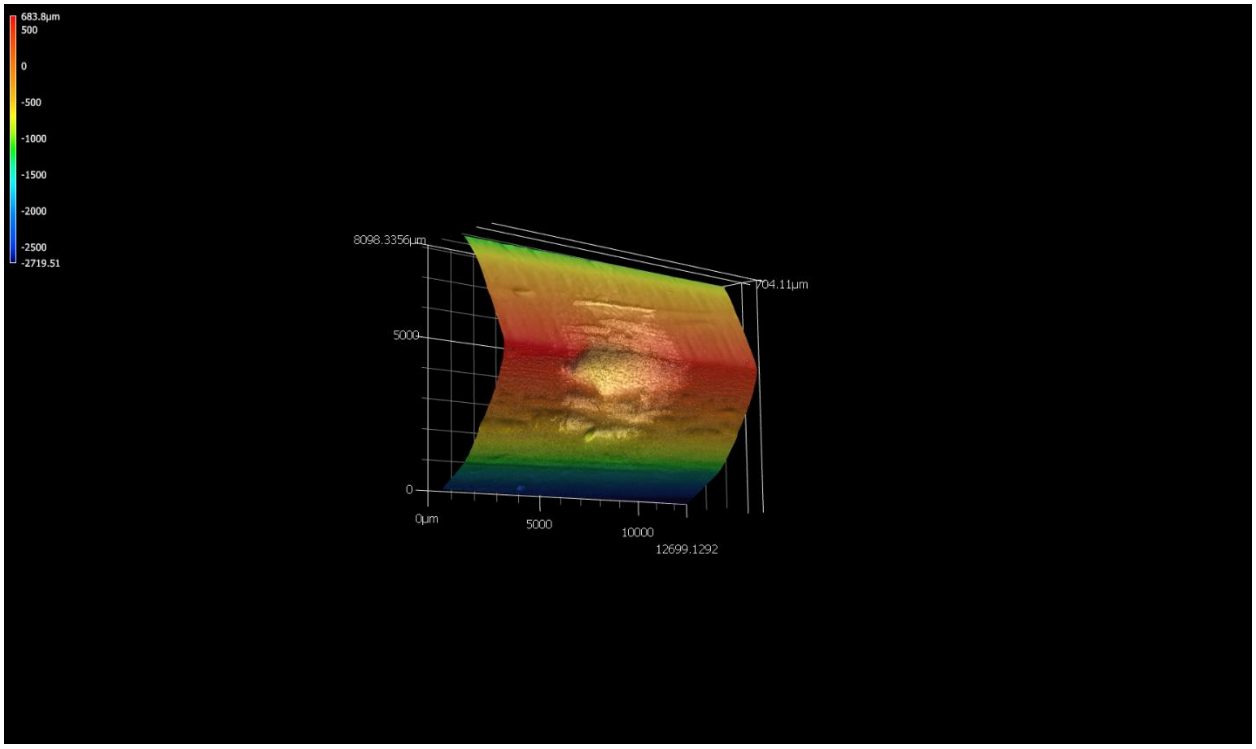


Fig. AVI-34: Erosion scar at 0° angle of impingement on the H-146 coated blade EXP6

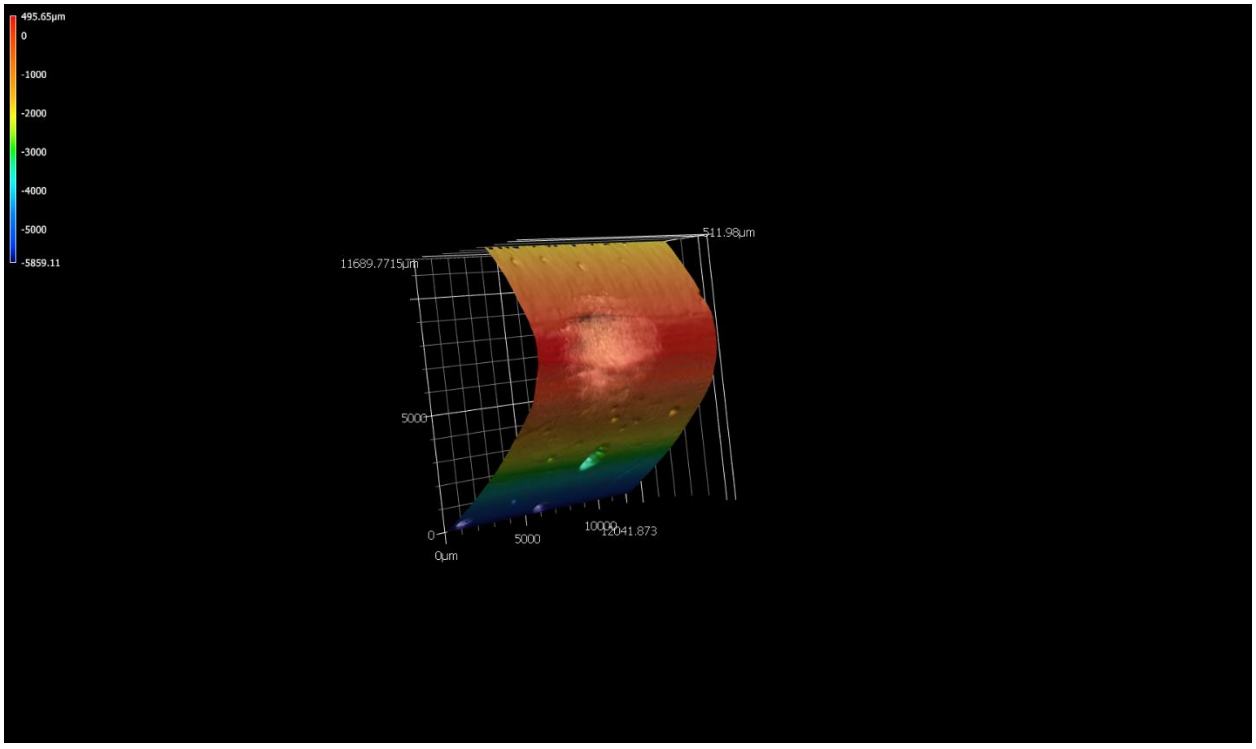


Fig. AVI-35: Erosion scar at 0° angle of impingement on the H-146 coated blade EXP7

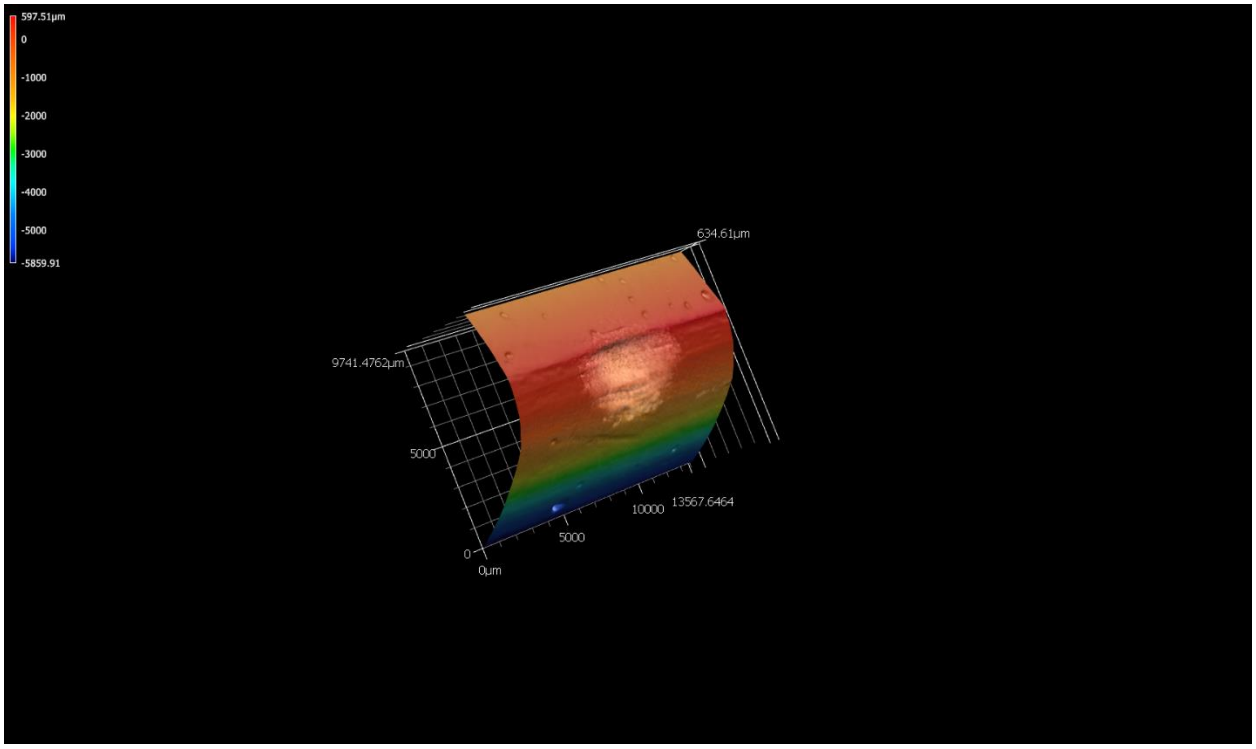


Fig. AVI-36: Erosion scar at 0° angle of impingement on the H-146 coated blade EXP8

- **<u>Polyurethane/IA-700</u>**

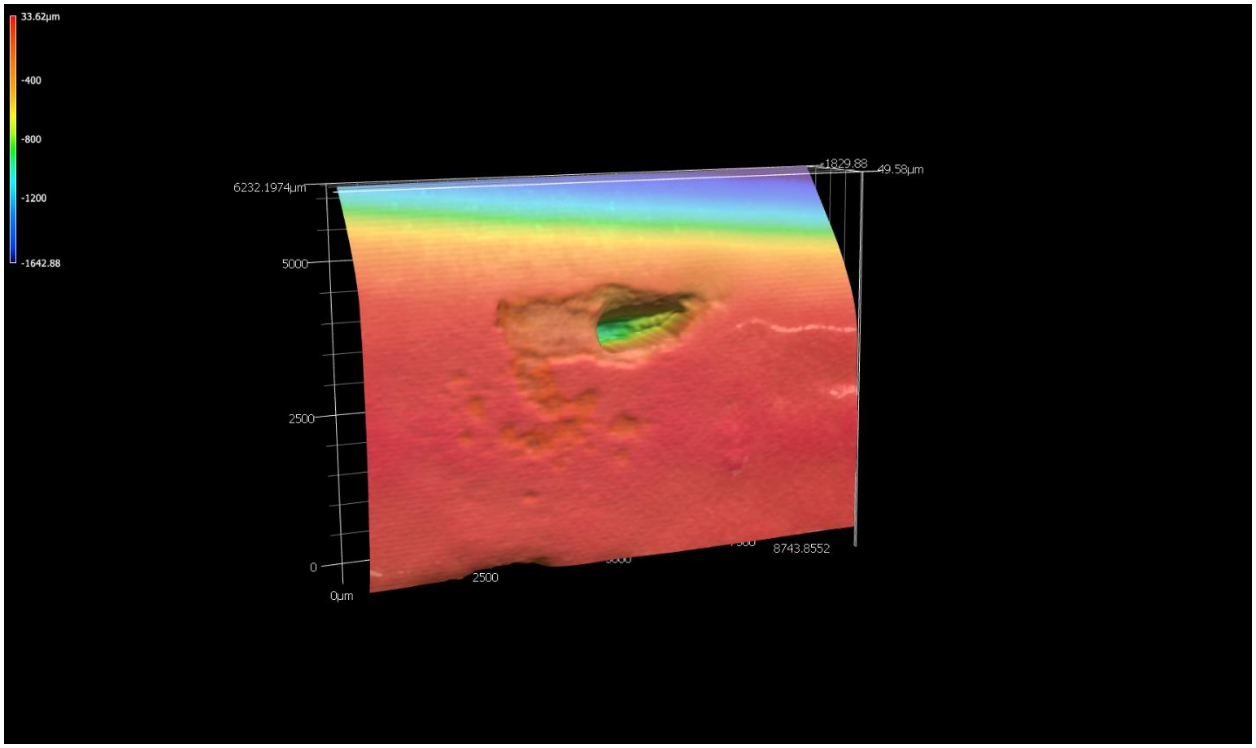


Fig. AVI-37: Erosion scar at 0° angle of impingement on the Polyurethane/IA-700 coated blade EXP1

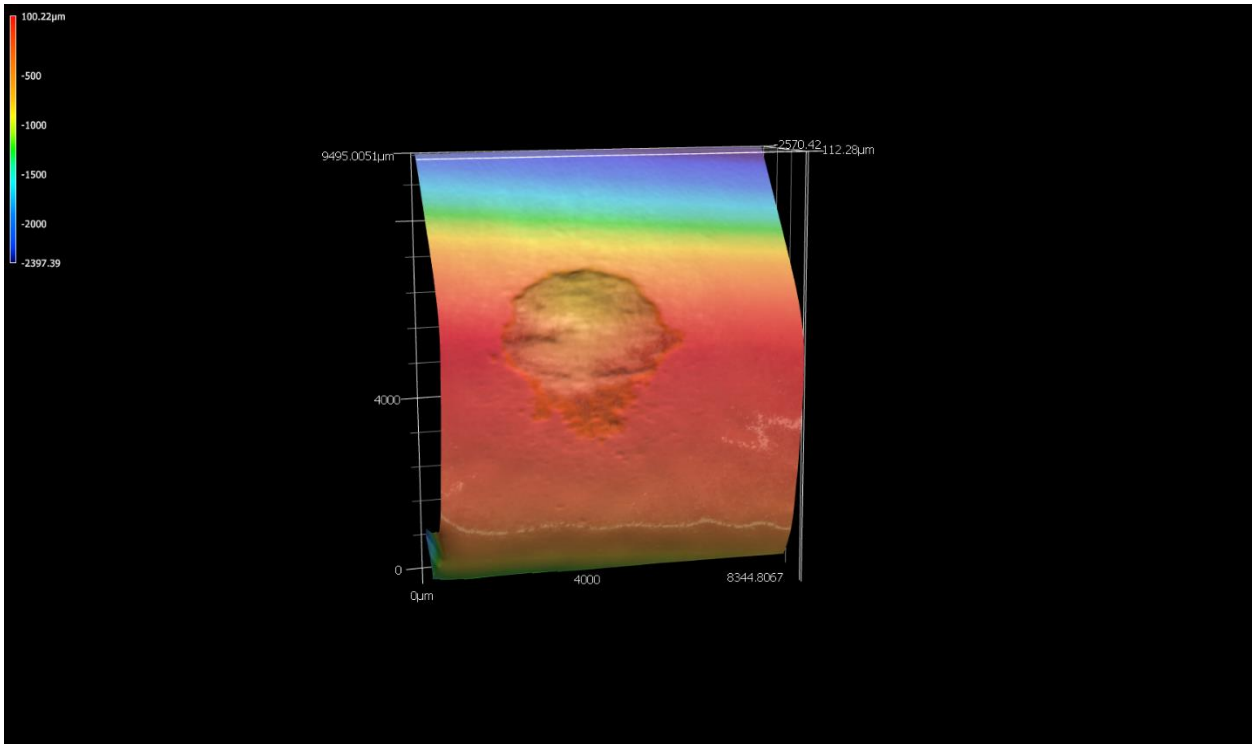


Fig. AVI-38: Erosion scar at 0° angle of impingement on the Polyurethane/IA-700 coated blade EXP2

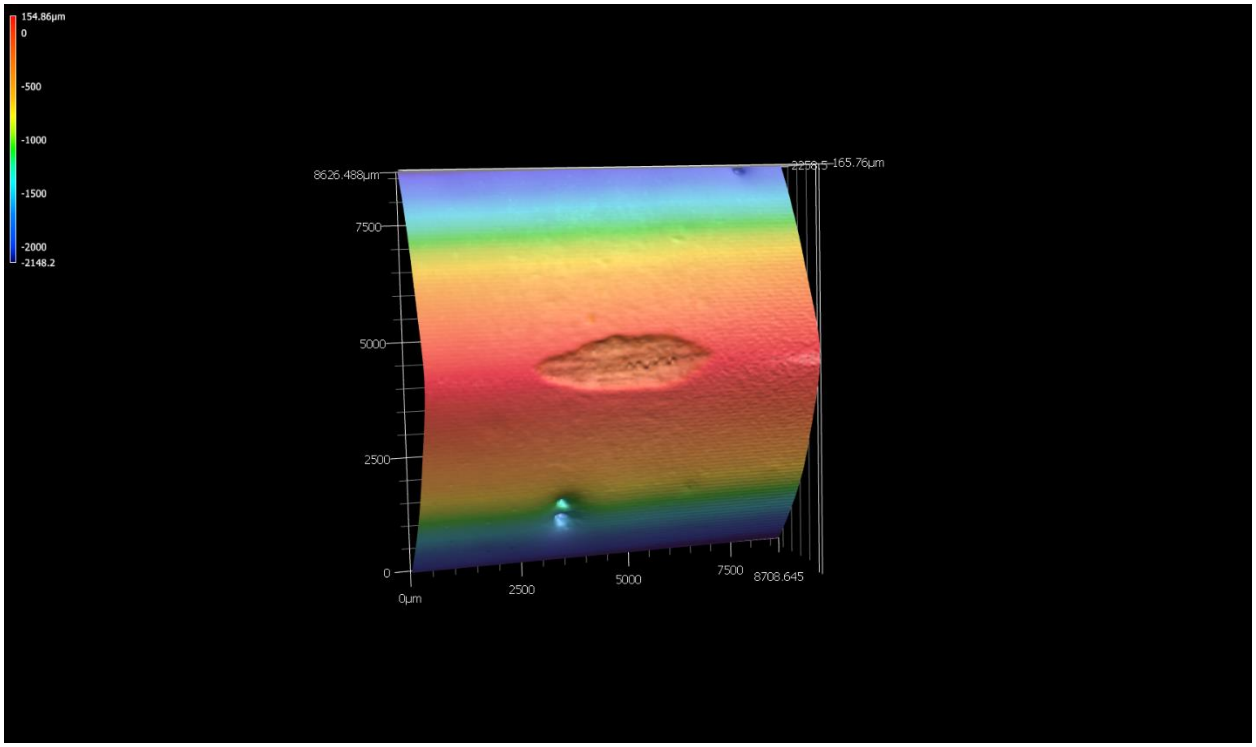


Fig. AVI-39: Erosion scar at 0° angle of impingement on the Polyurethane/IA-700 coated blade EXP3

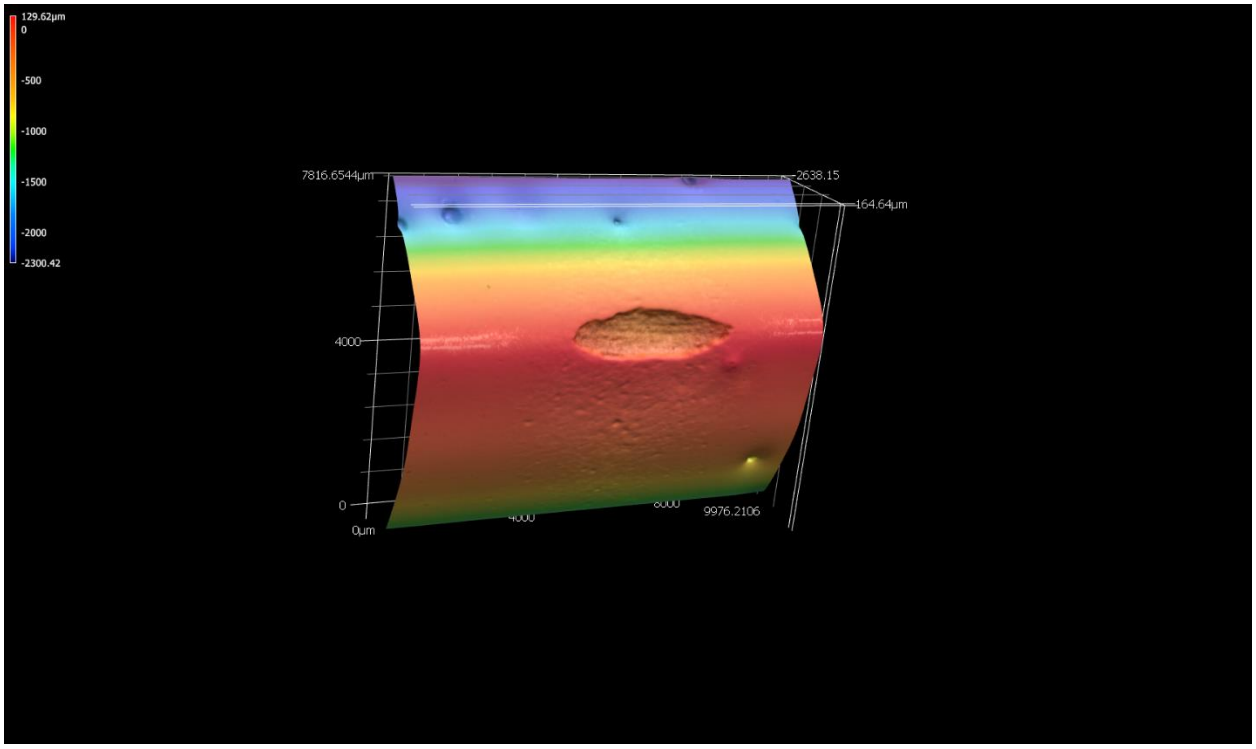


Fig. AVI-40: Erosion scar at 0° angle of impingement on the Polyurethane/IA-700 coated blade EXP4

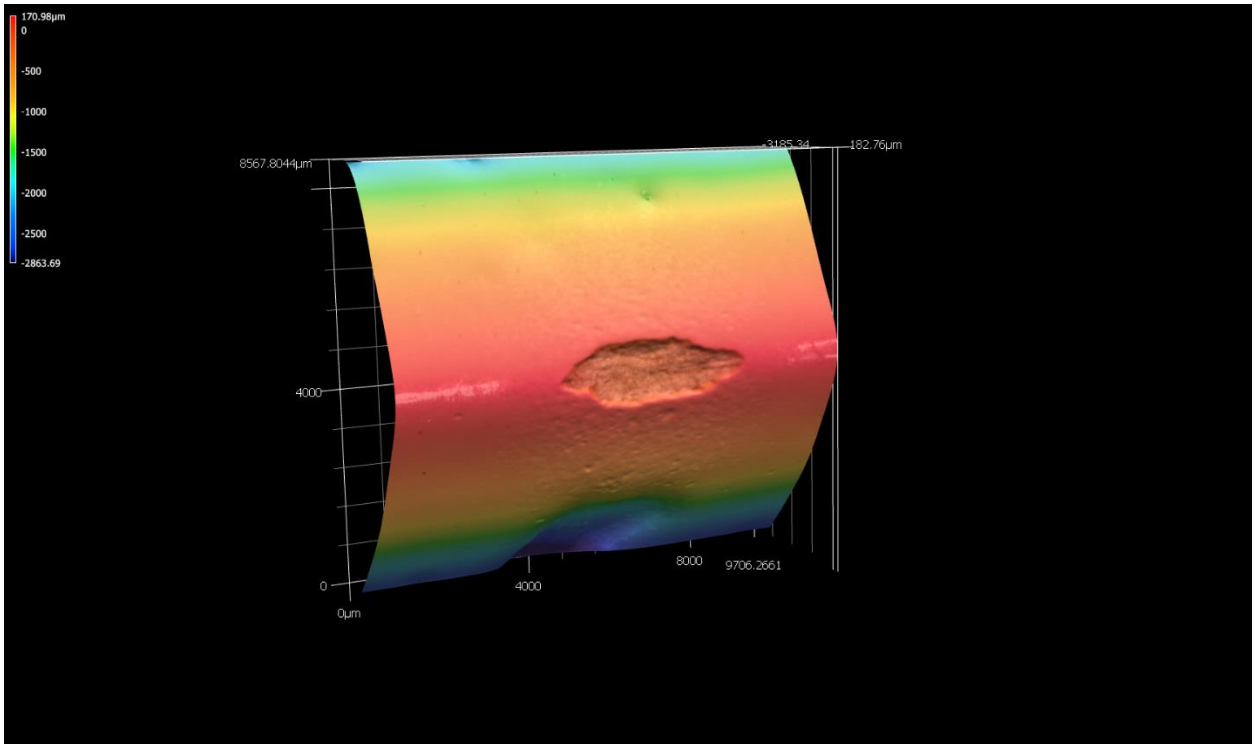


Fig. AVI-41: Erosion scar at 0° angle of impingement on the Polyurethane/IA-700 coated blade EXP5

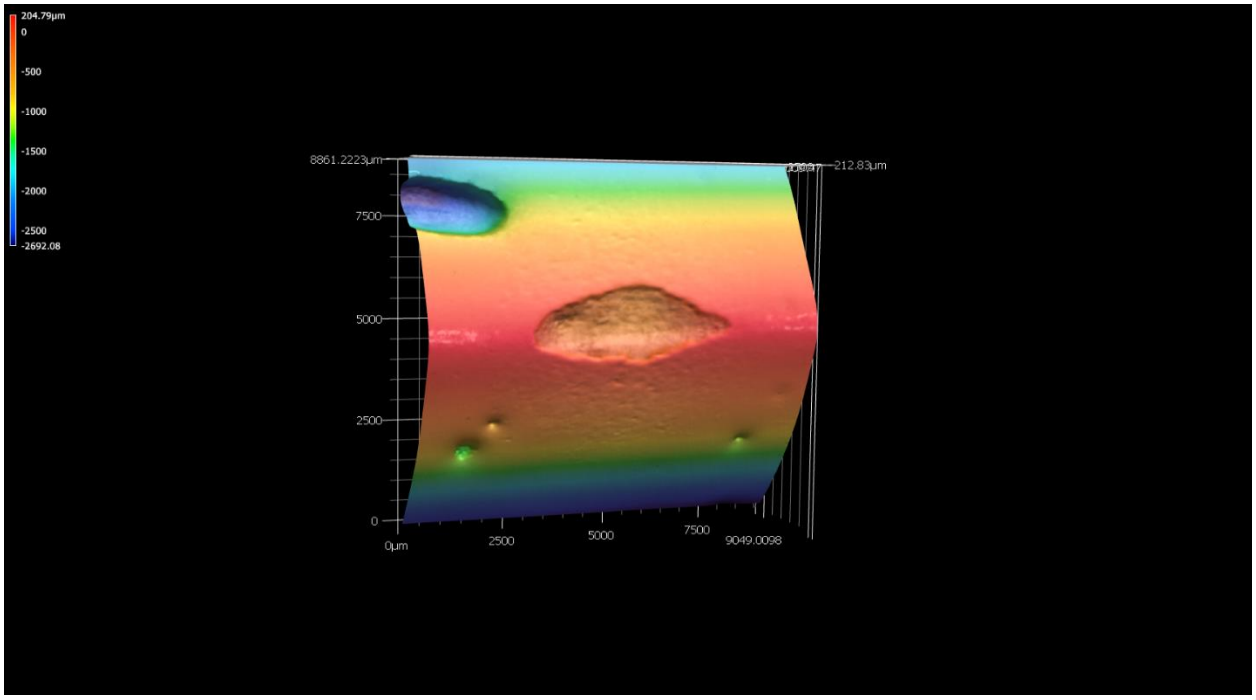


Fig. AVI-42: Erosion scar at 0° angle of impingement on the Polyurethane/IA-700 coated blade EXP6

- **5 degrees**
  - **Uncoated**

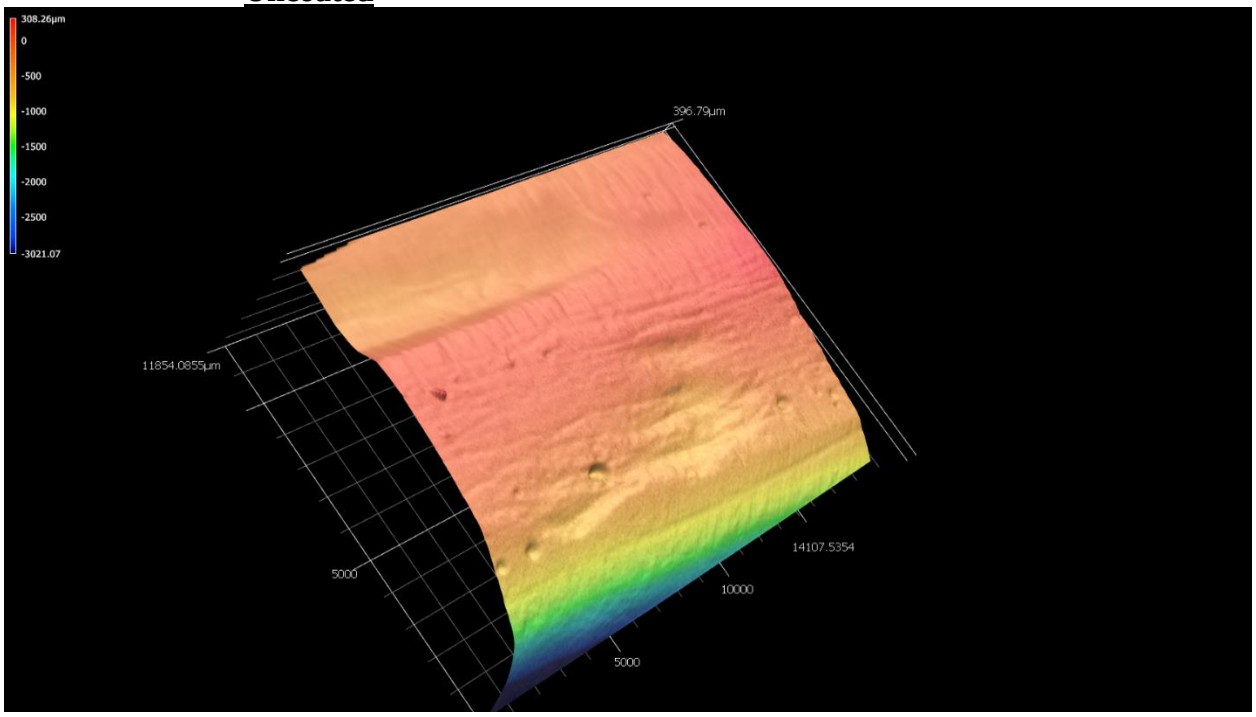


Fig. AVI-43: Erosion scar at 5° angle of impingement on the uncoated blade EXP1

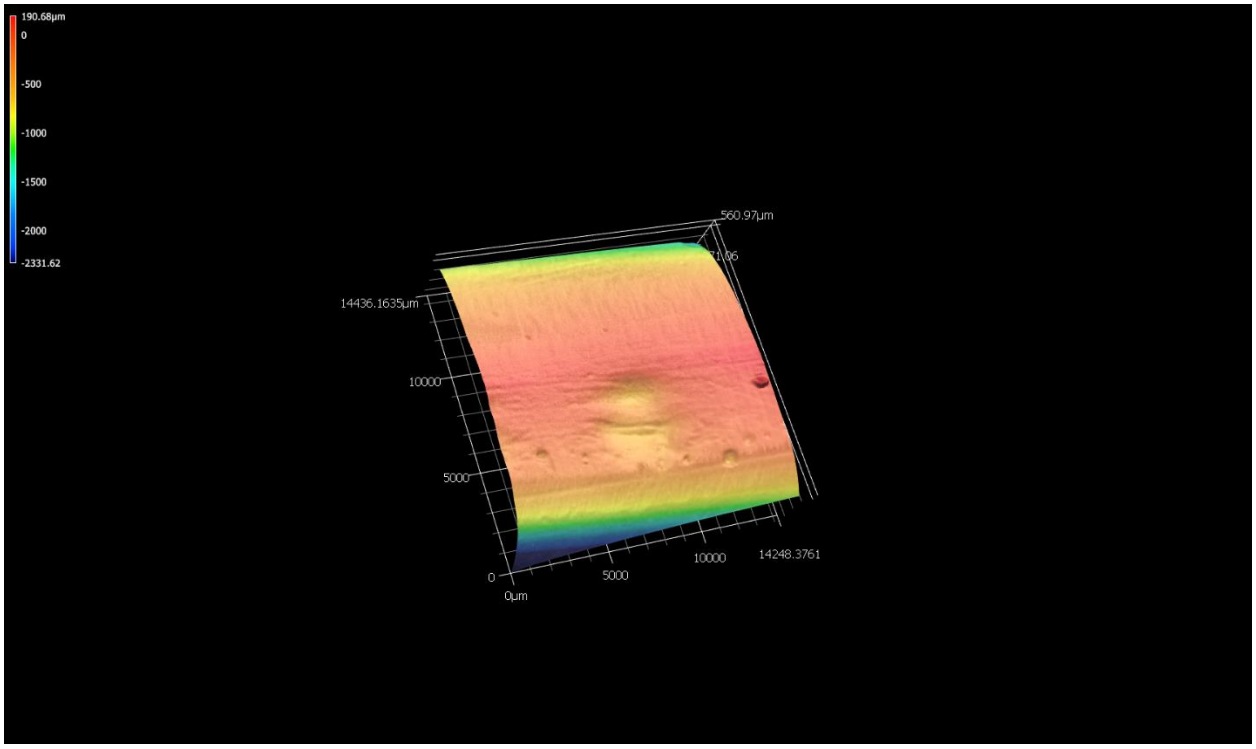


Fig. AVI-44: Erosion scar at 5° angle of impingement on the uncoated blade EXP2

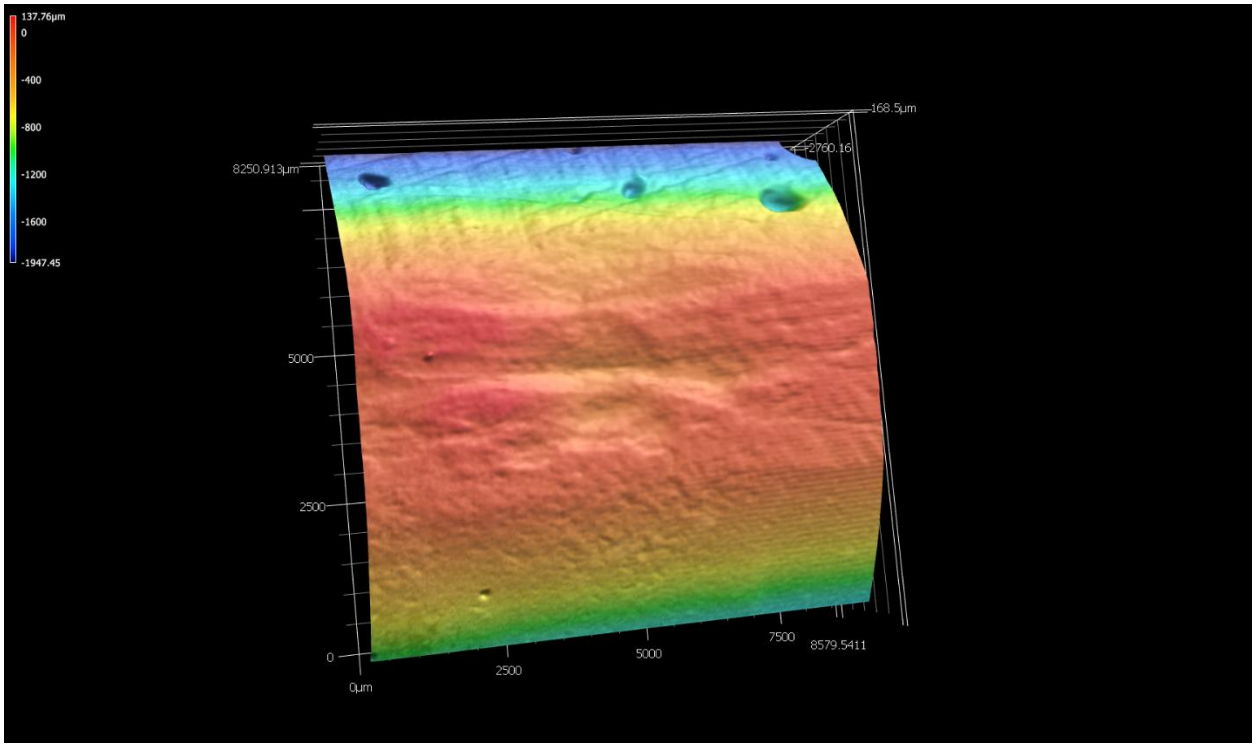


Fig. AVI-45: Erosion scar at 5° angle of impingement on the uncoated blade EXP3

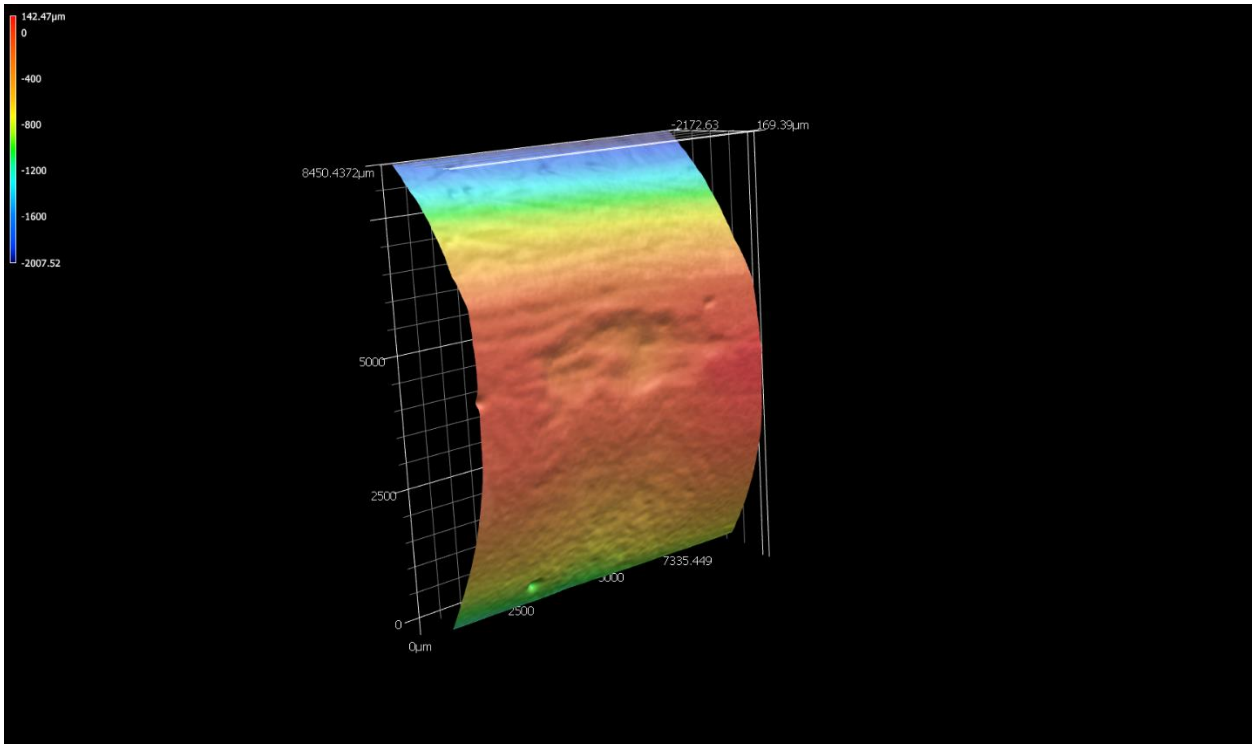


Fig. AVI-46: Erosion scar at 5° angle of impingement on the uncoated blade EXP4

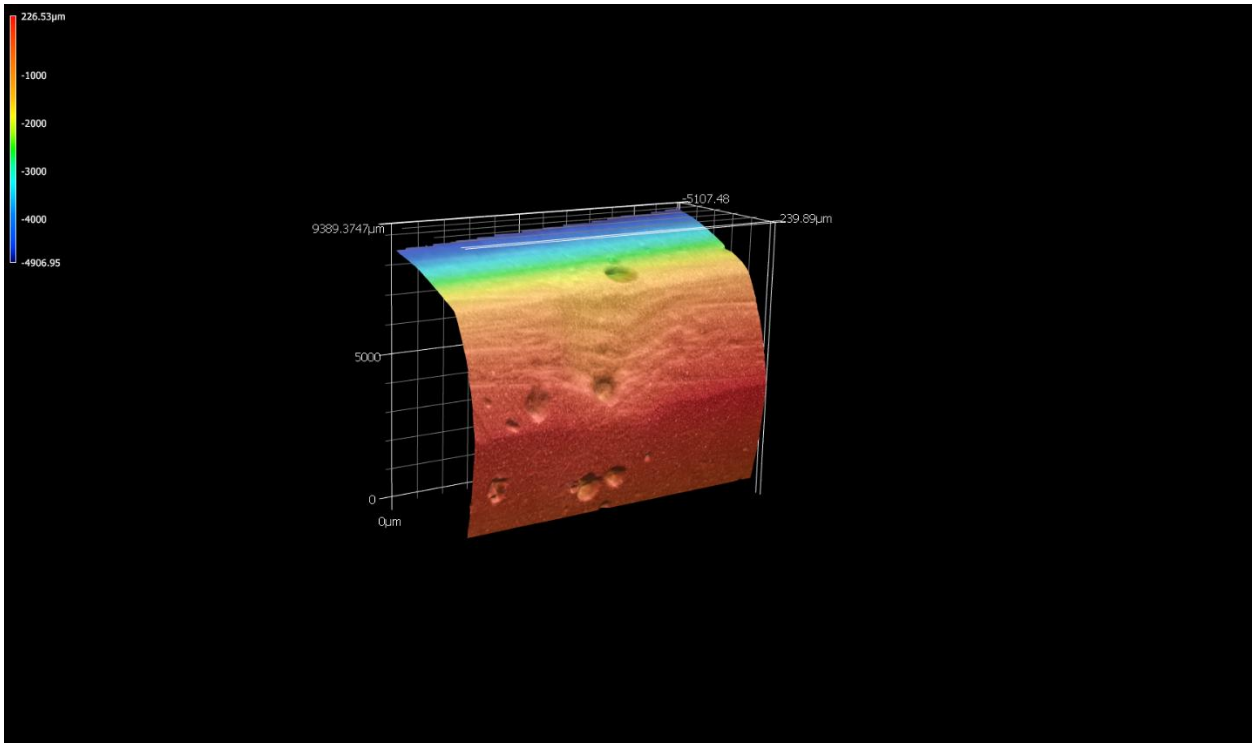


Fig. AVI-47: Erosion scar at 5° angle of impingement on the uncoated blade EXP5

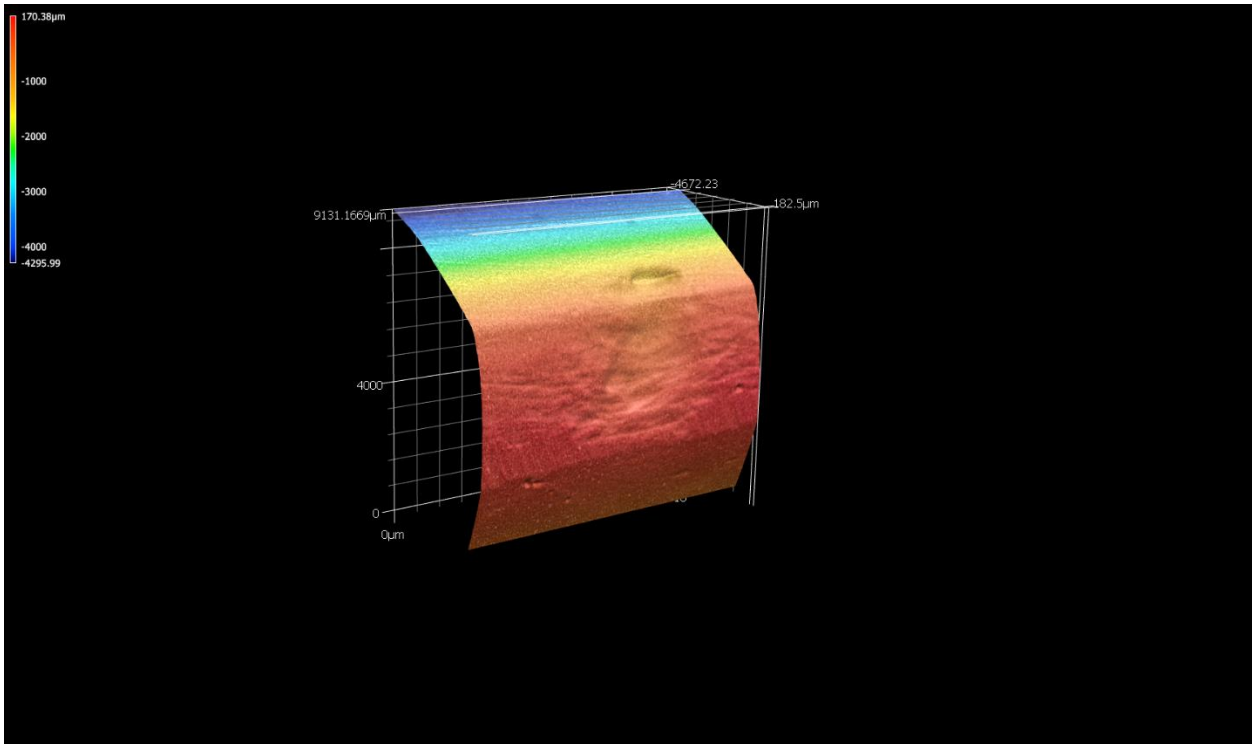


Fig. AVI-48: Erosion scar at 5° angle of impingement on the uncoated blade EXP6

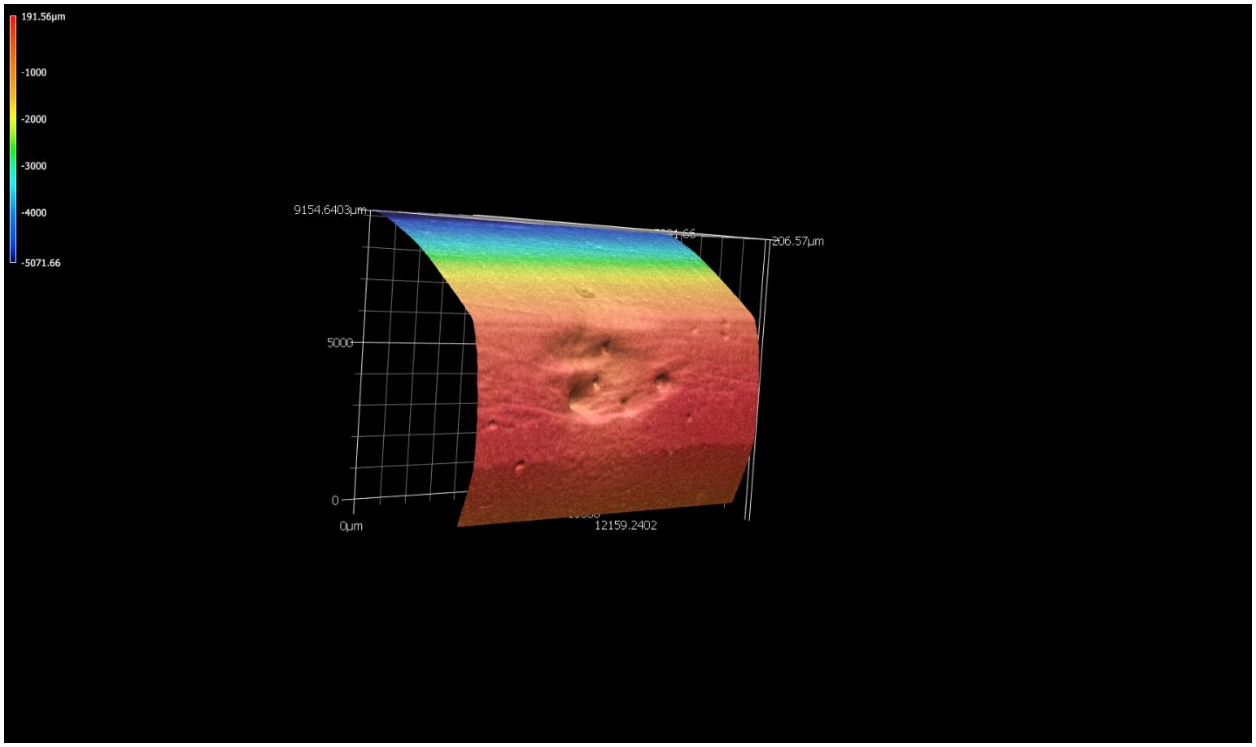


Fig. AVI-49: Erosion scar at 5° angle of impingement on the uncoated blade EXP7

- **H-146**

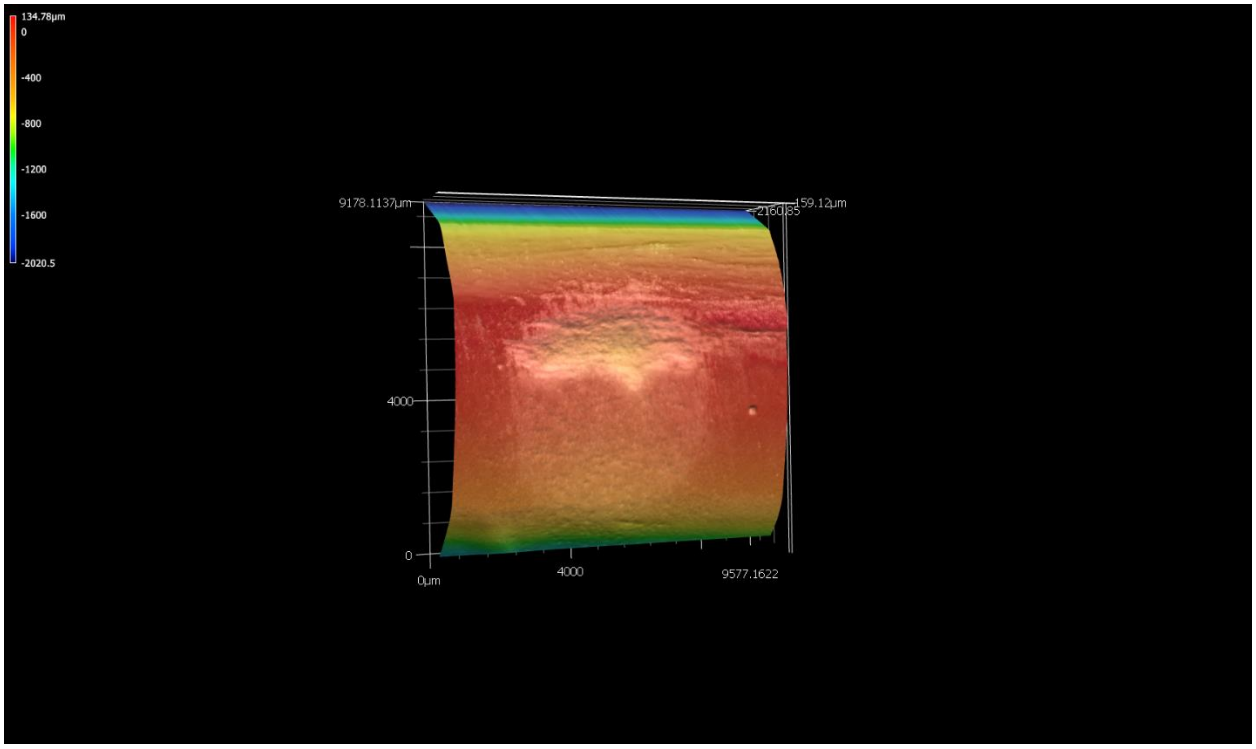


Fig. AVI-50: Erosion scar at 5° angle of impingement on the H-146 coated blade EXP1

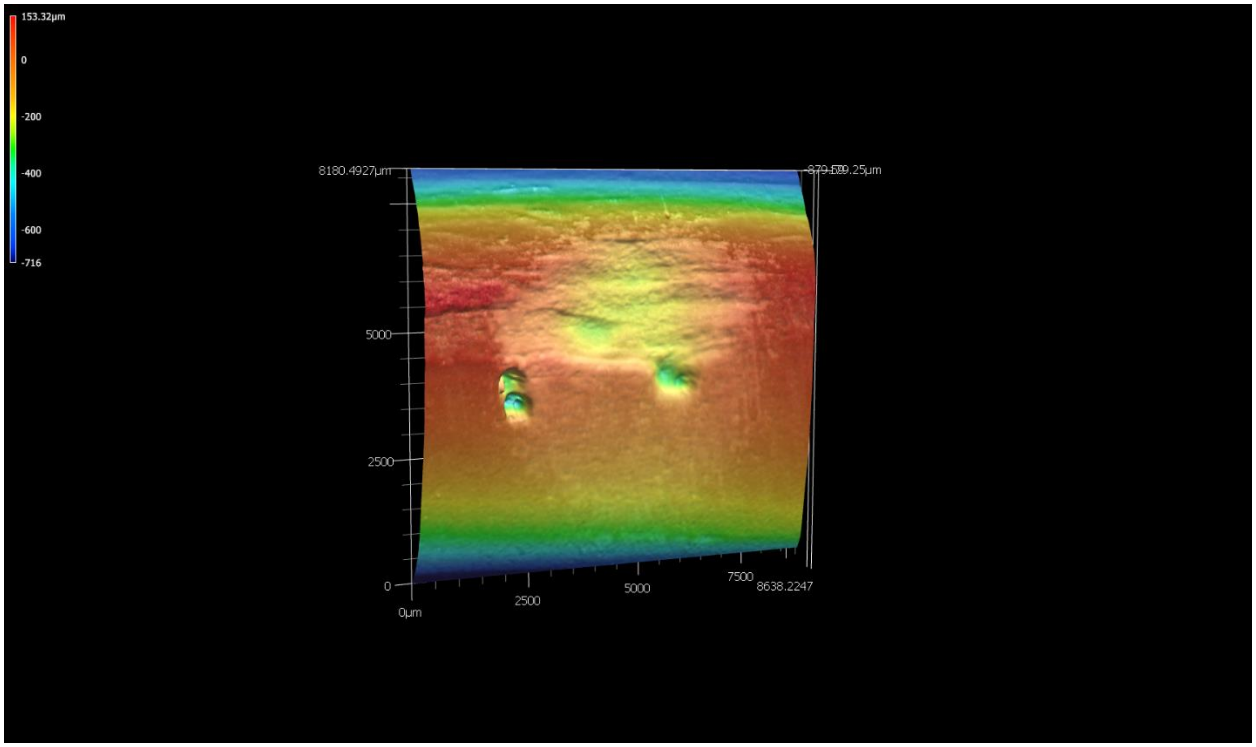


Fig. AVI-51: Erosion scar at 5° angle of impingement on the H-146 coated blade EXP2

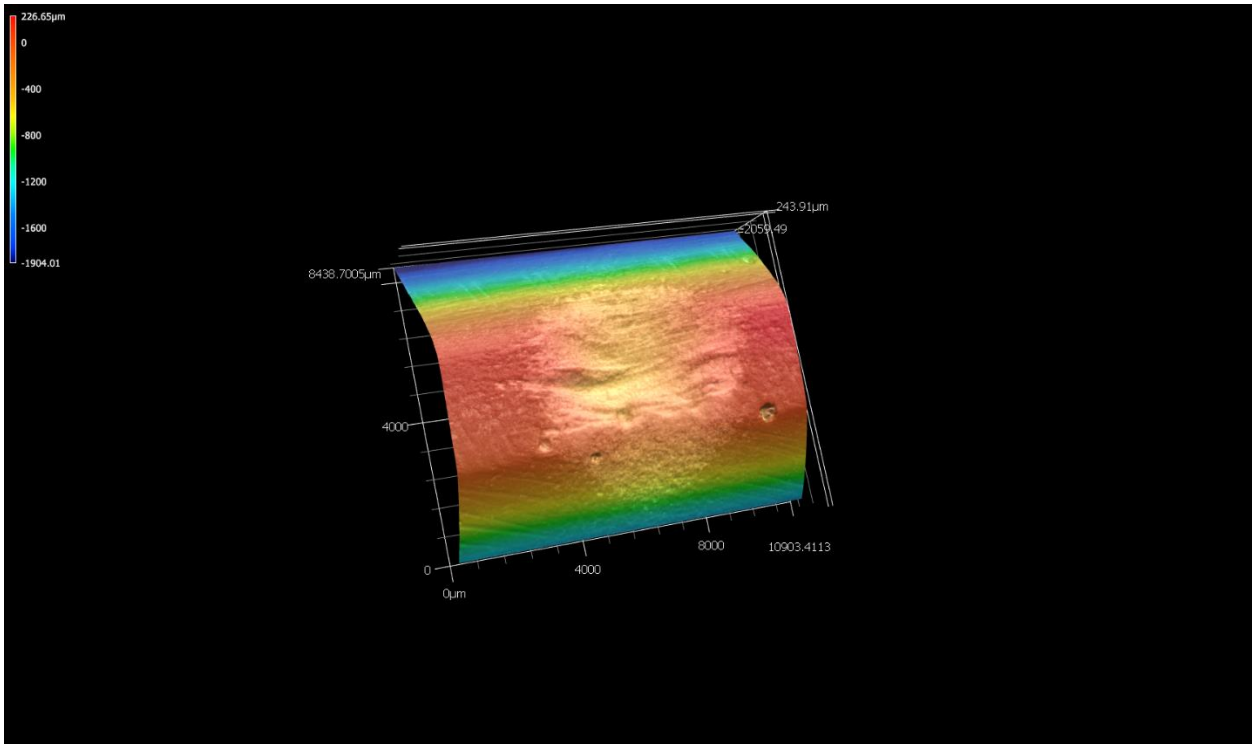


Fig. AVI-52: Erosion scar at 5° angle of impingement on the H-146 coated blade EXP3

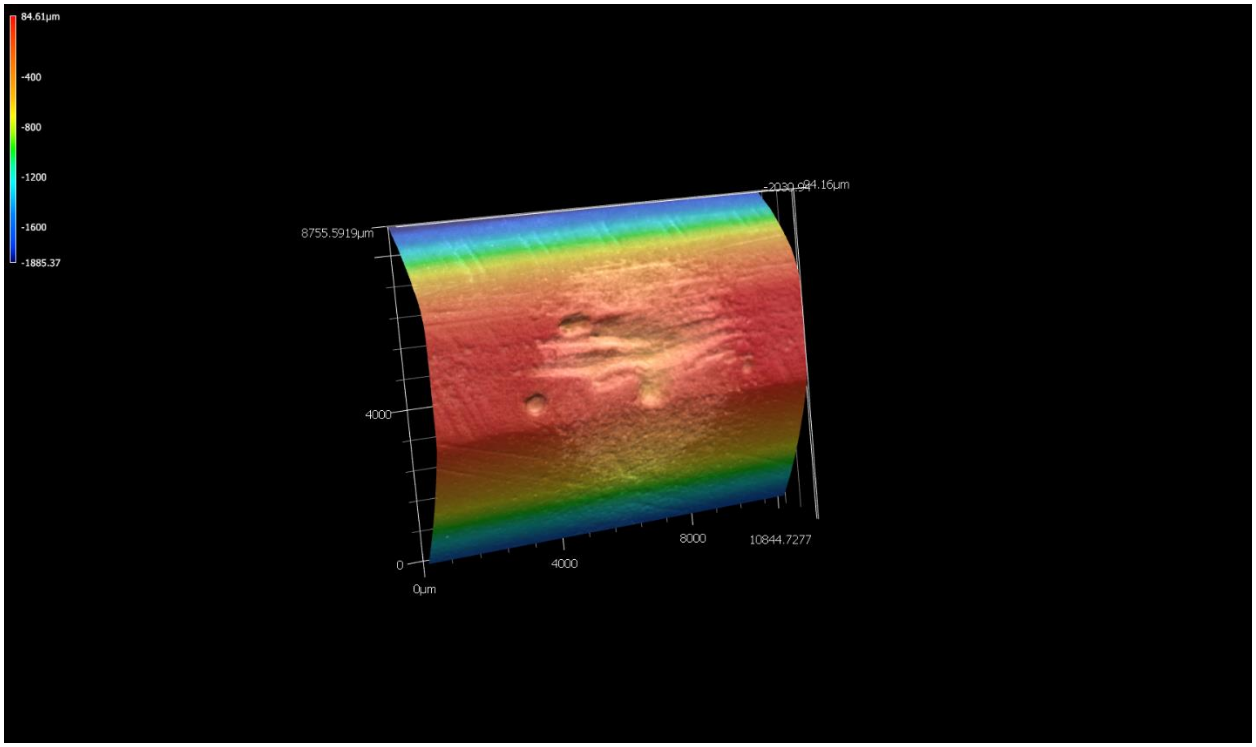


Fig. AVI-53: Erosion scar at 5° angle of impingement on the H-146 coated blade EXP4

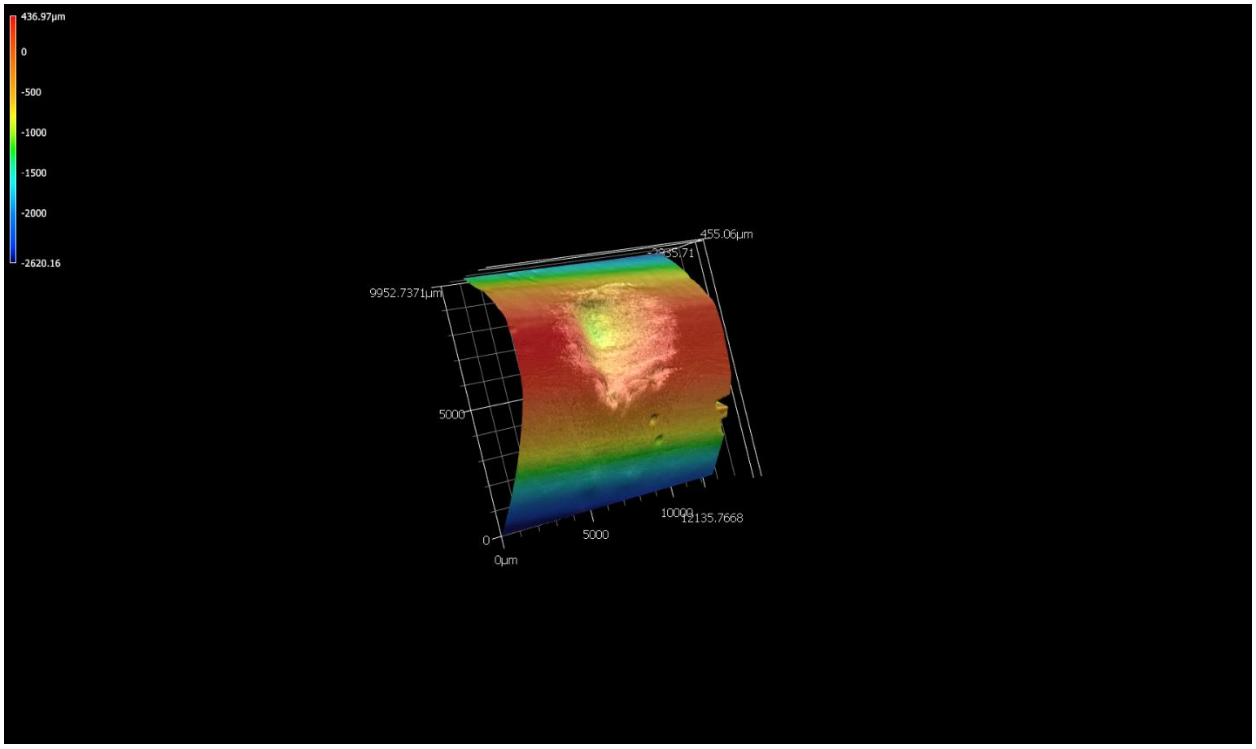


Fig. AVI-54: Erosion scar at 5° angle of impingement on the H-146 coated blade EXP5

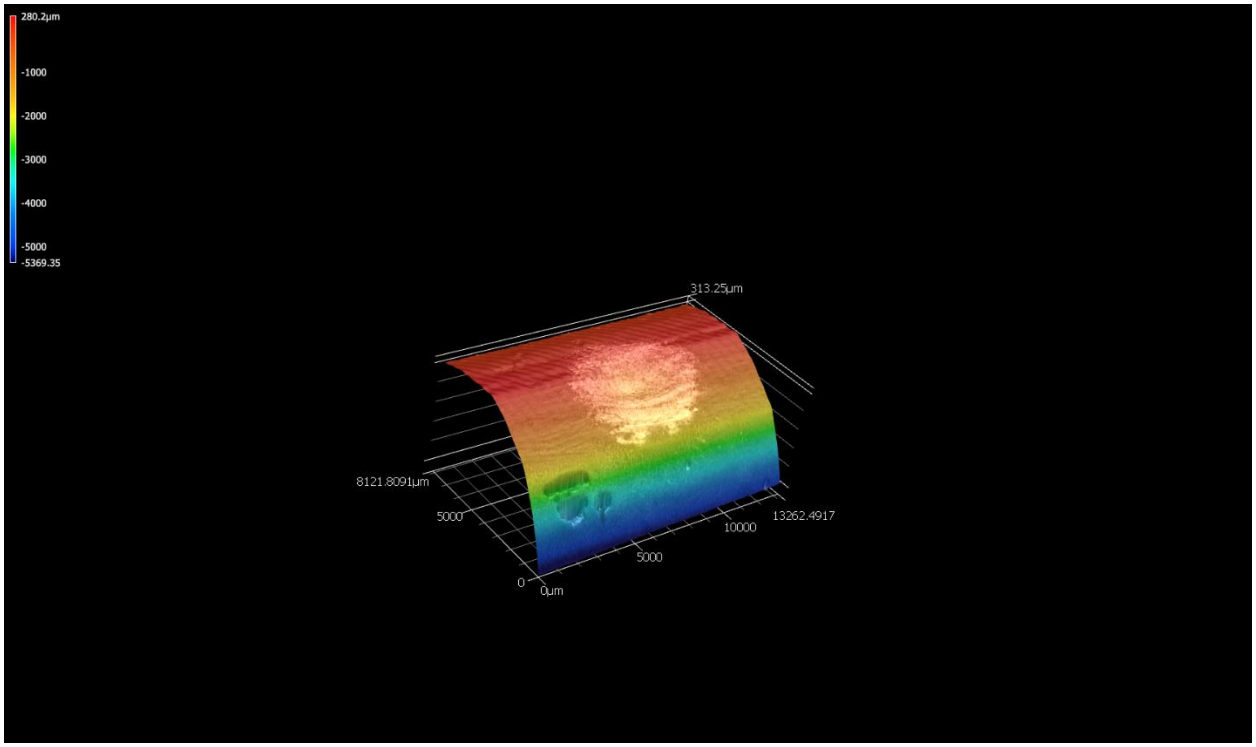


Fig. AVI-55: Erosion scar at 5° angle of impingement on the H-146 coated blade EXP6

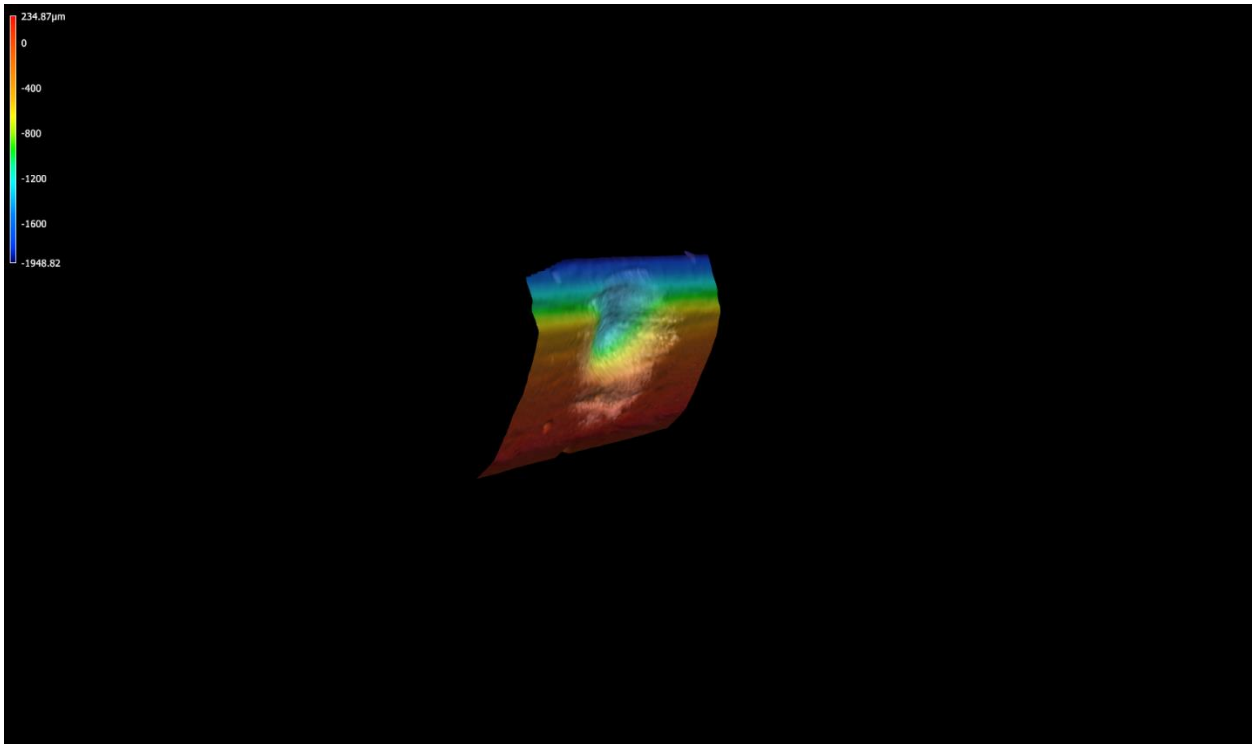


Fig. AVI-56: Erosion scar at 5° angle of impingement on the H-146 coated blade EXP7

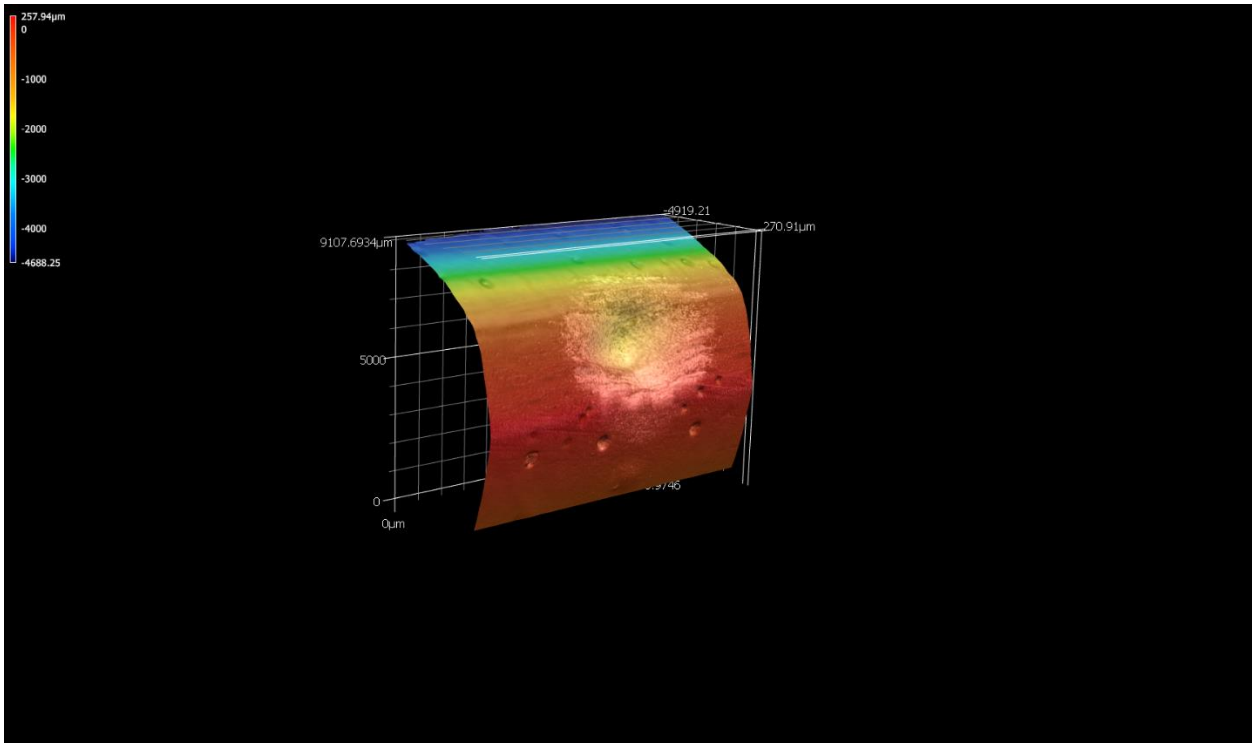


Fig. AVI-57: Erosion scar at 5° angle of impingement on the H-146 coated blade EXP8

- **Polyurethane/IA-700**

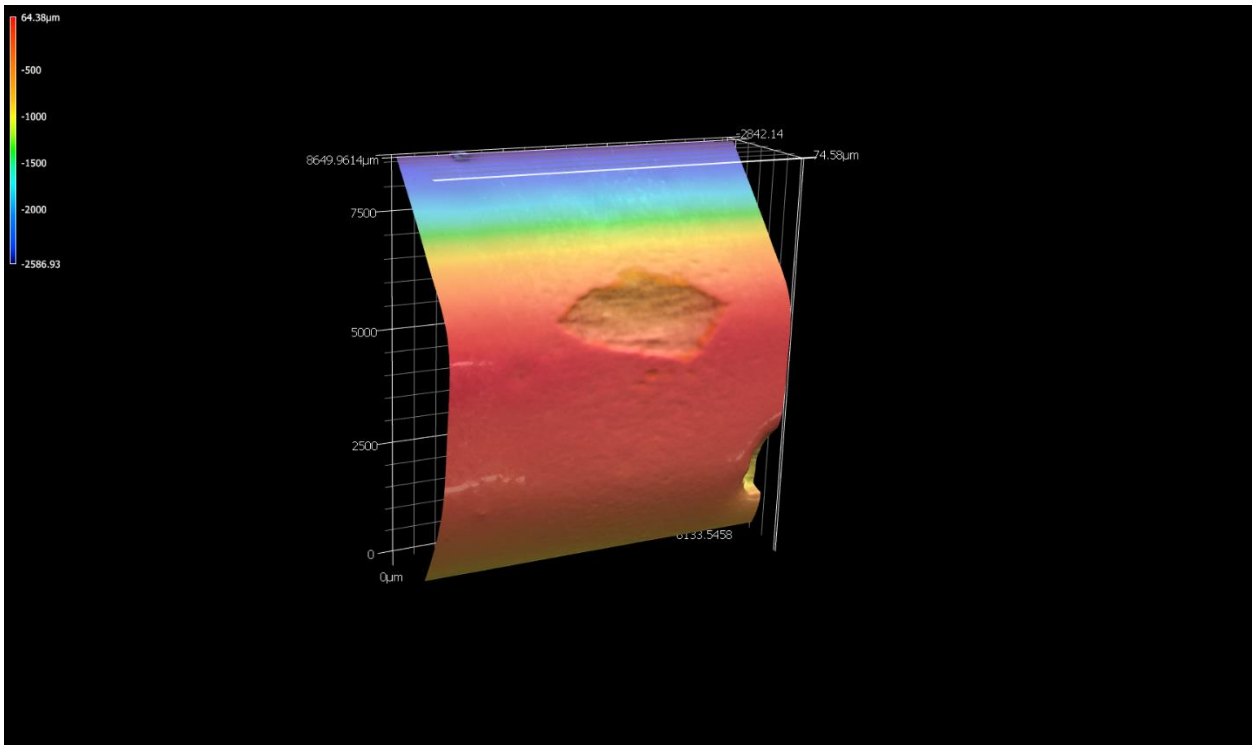


Fig. AVI-58: Erosion scar at 5° angle of impingement on the Polyurethane/IA-700 coated blade EXP1

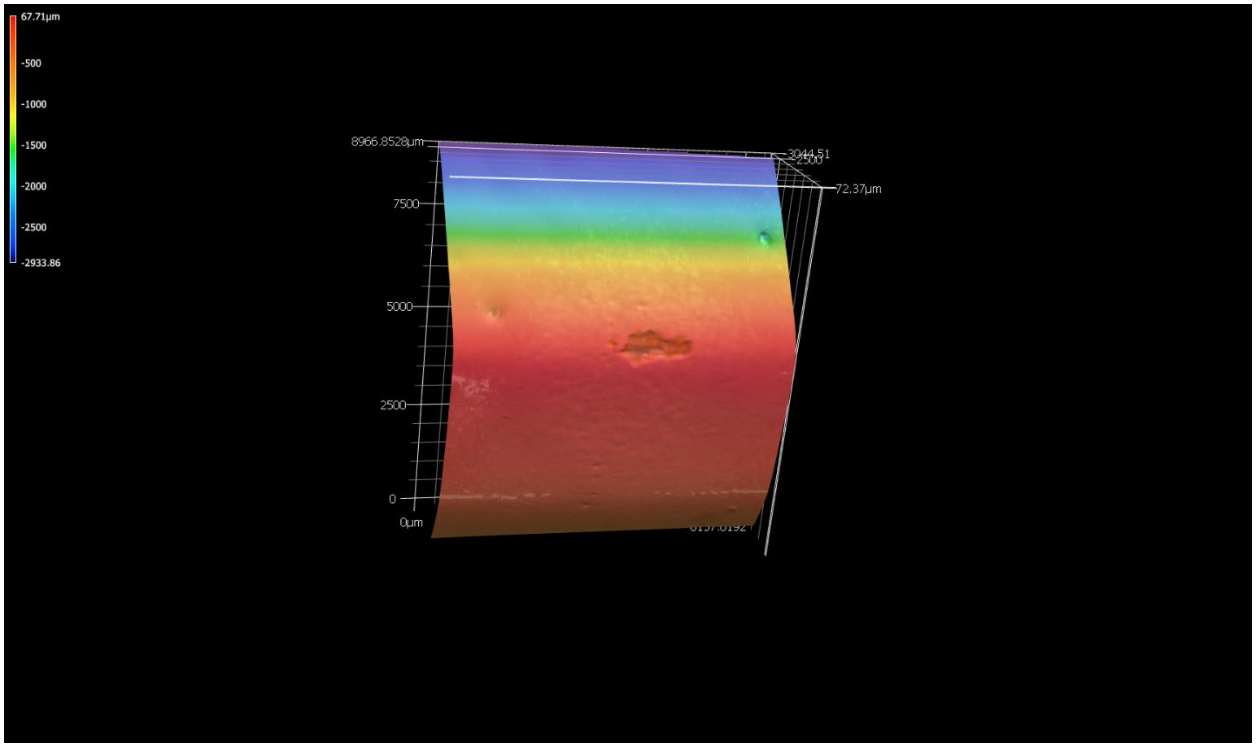


Fig. AVI-59: Erosion scar at 5° angle of impingement on the Polyurethane/IA-700 coated blade EXP2

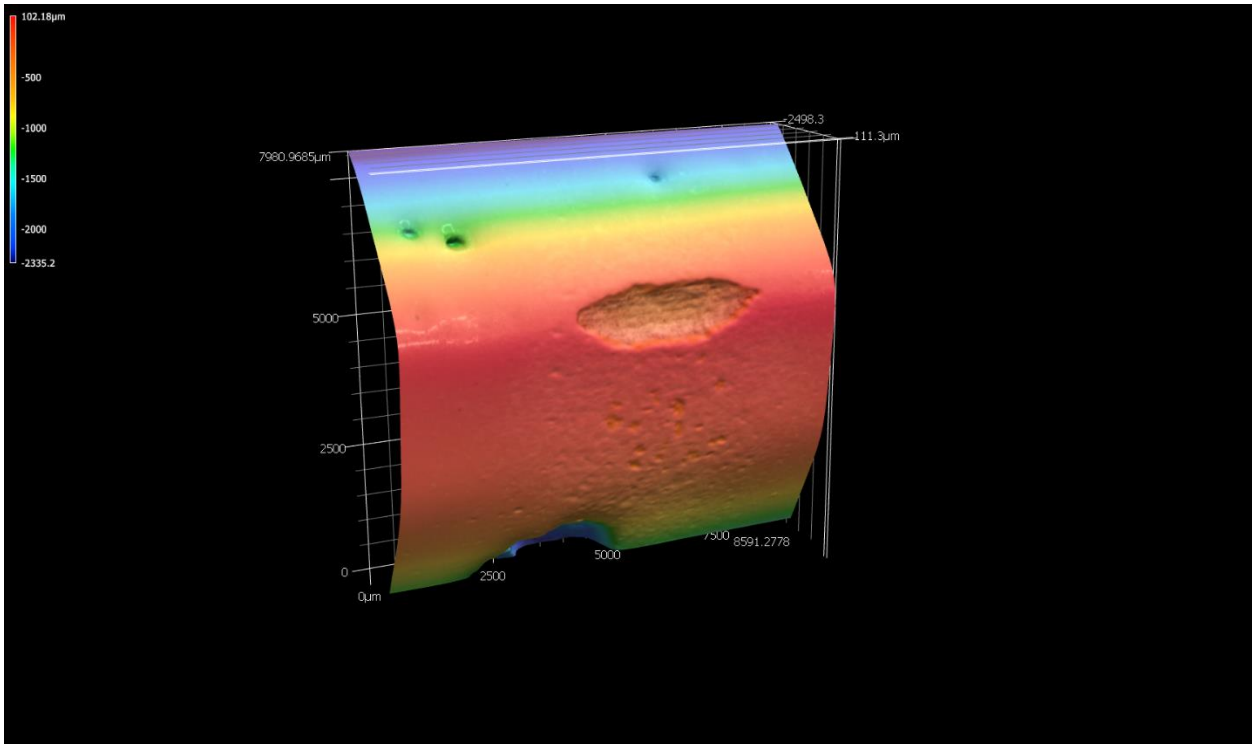


Fig. AVI-60: Erosion scar at 5° angle of impingement on the Polyurethane/IA-700 coated blade EXP3

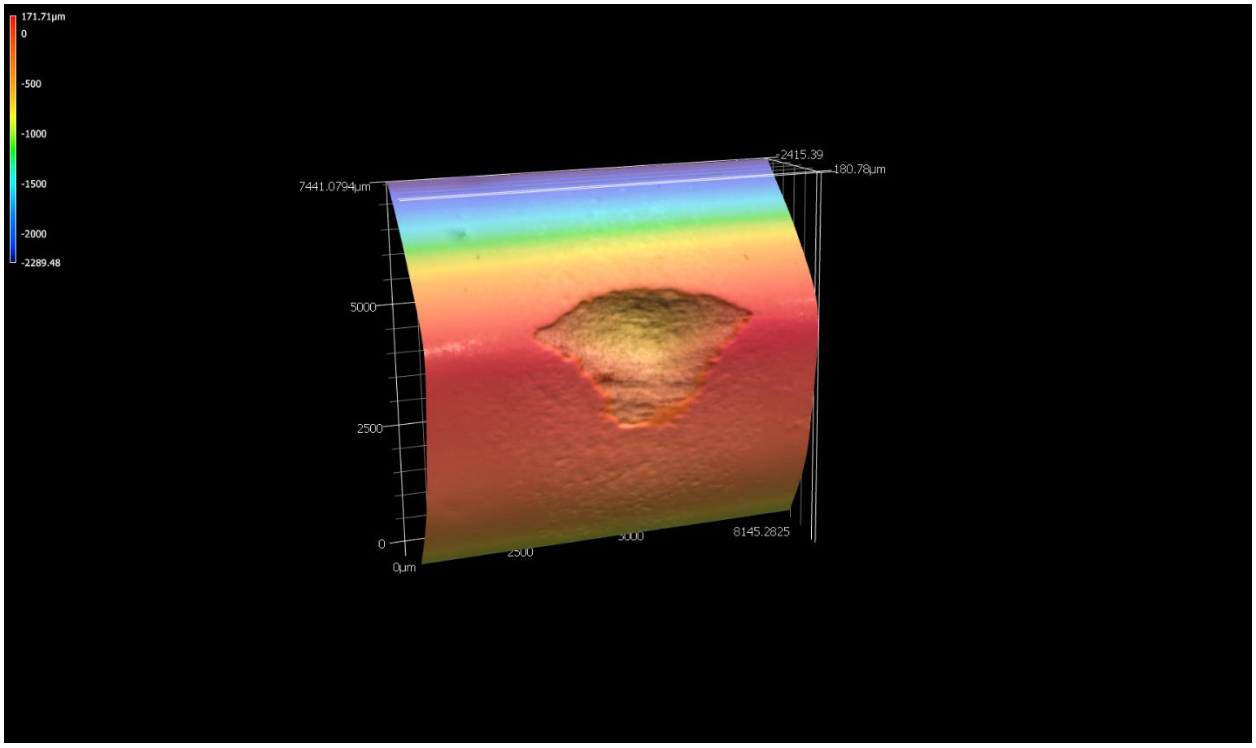


Fig. AVI-61: Erosion scar at 5° angle of impingement on the Polyurethane/IA-700 coated blade EXP4

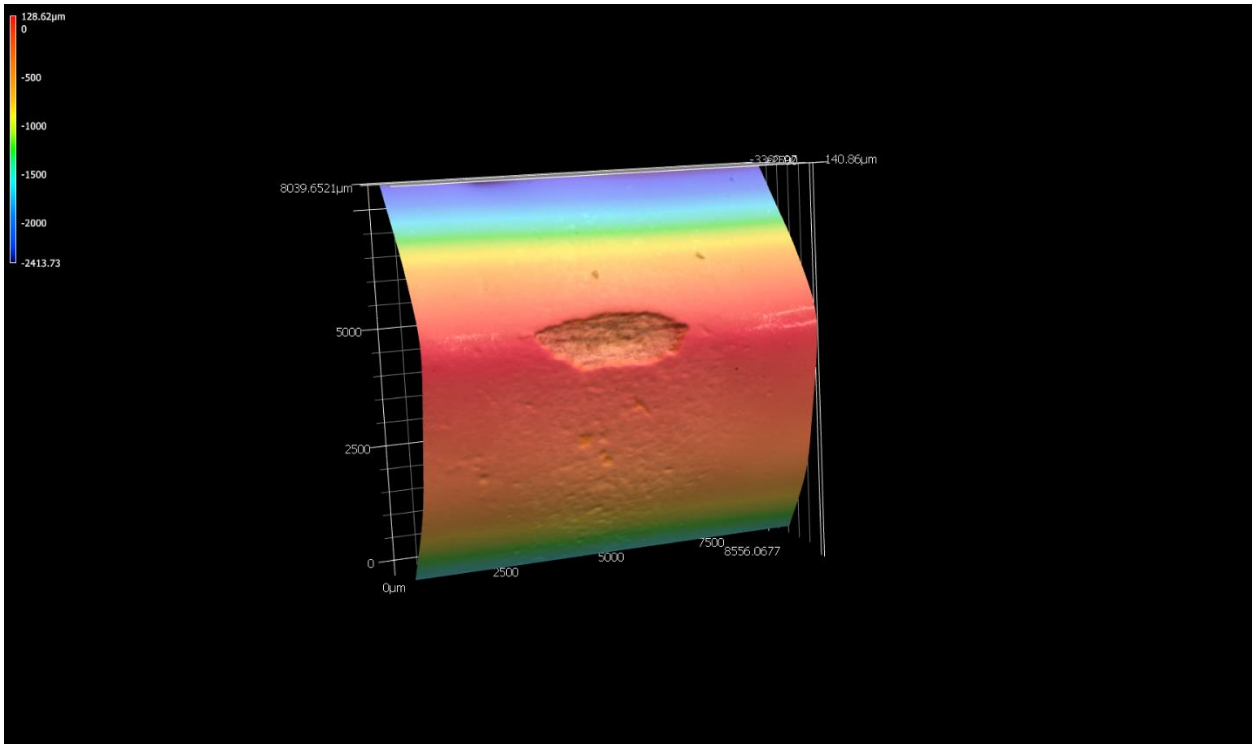


Fig. AVI-62: Erosion scar at 5° angle of impingement on the Polyurethane/IA-700 coated blade EXP5

- **10 degrees**
  - **Uncoated**

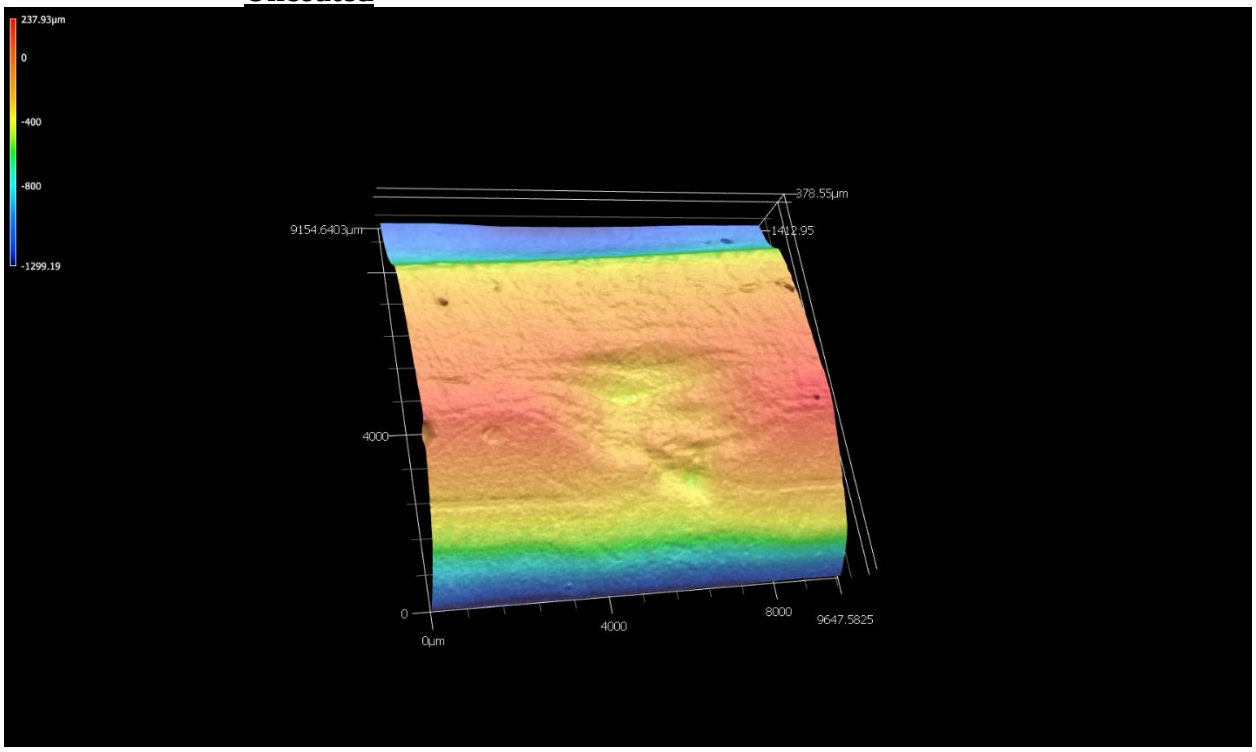


Fig. AVI-63: Erosion scar at 10° angle of impingement on the uncoated blade EXP1

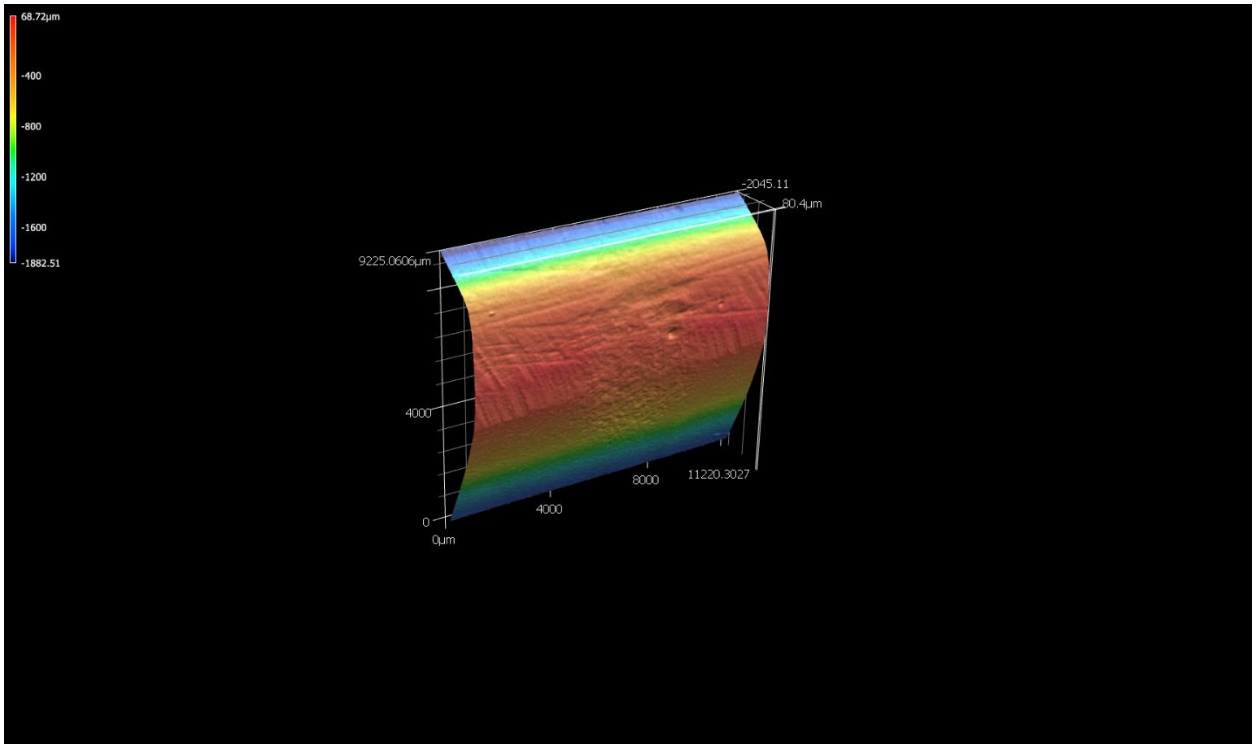


Fig. AVI-64: Erosion scar at 10° angle of impingement on the uncoated blade EXP2

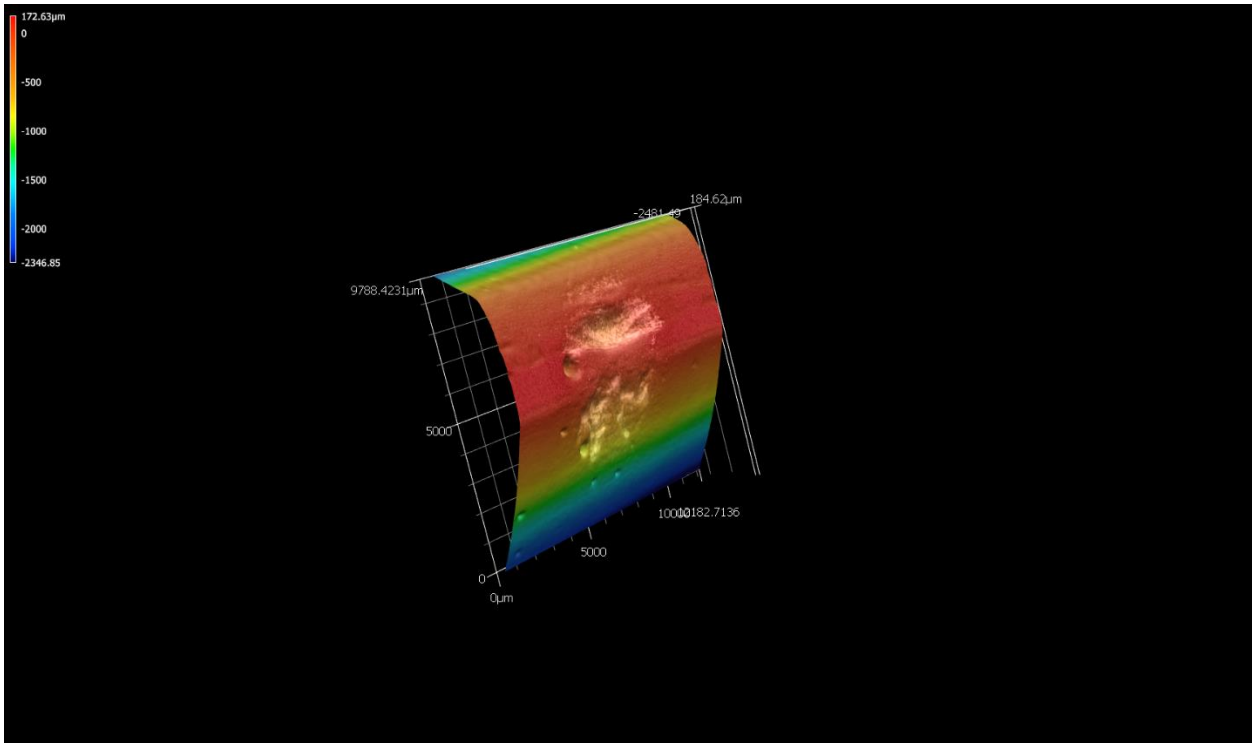


Fig. AVI-65: Erosion scar at 10° angle of impingement on the uncoated blade EXP3

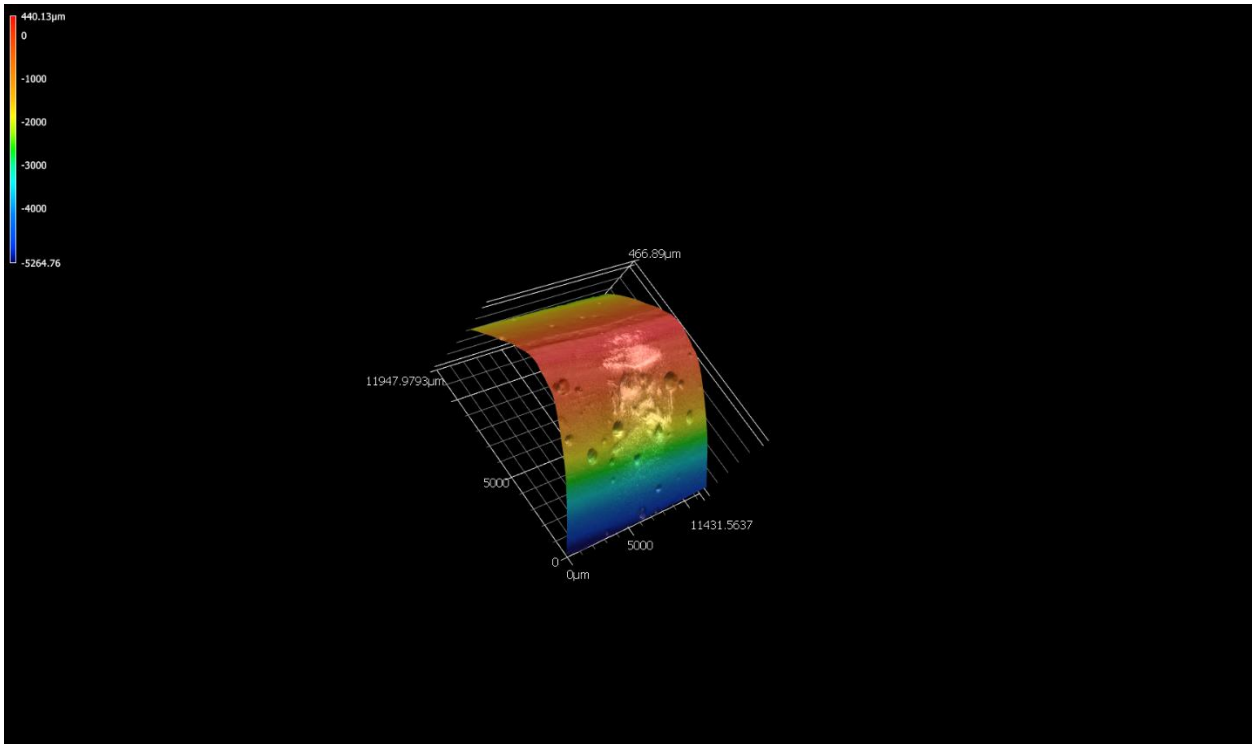


Fig. AVI-66: Erosion scar at 10° angle of impingement on the uncoated blade EXP4

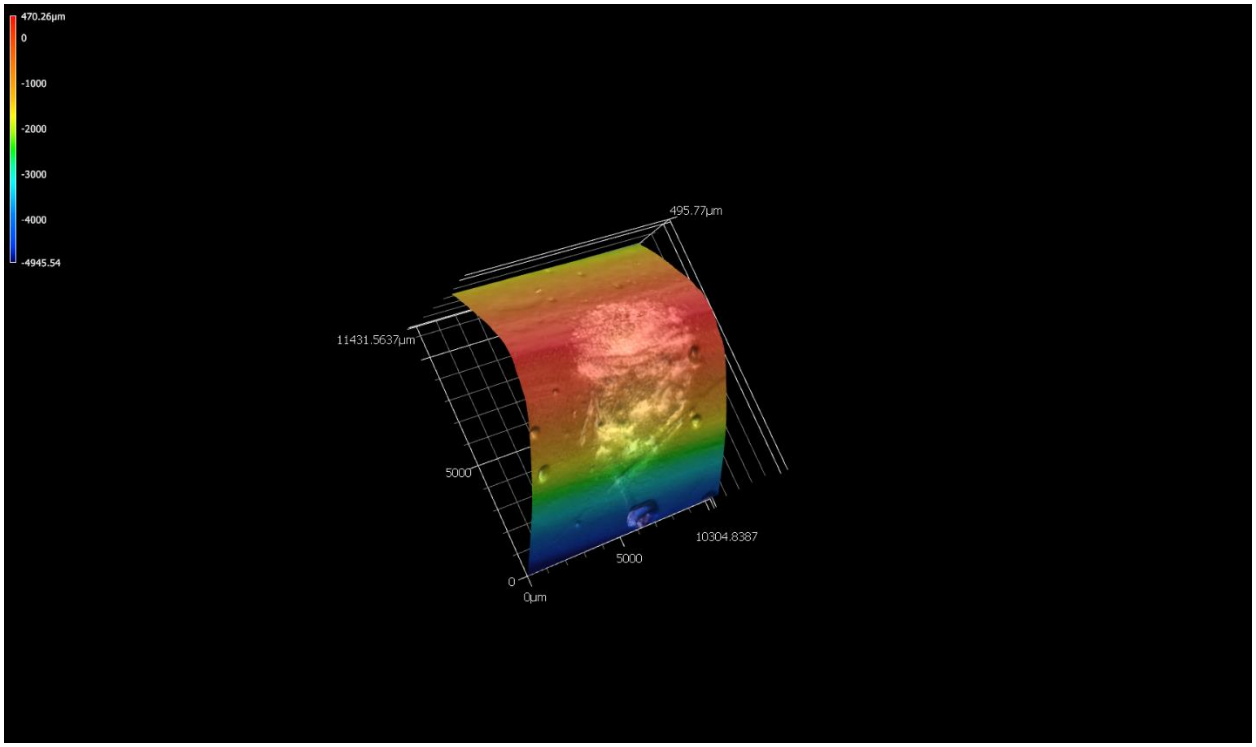


Fig. AVI-67: Erosion scar at 10° angle of impingement on the uncoated blade EXP5

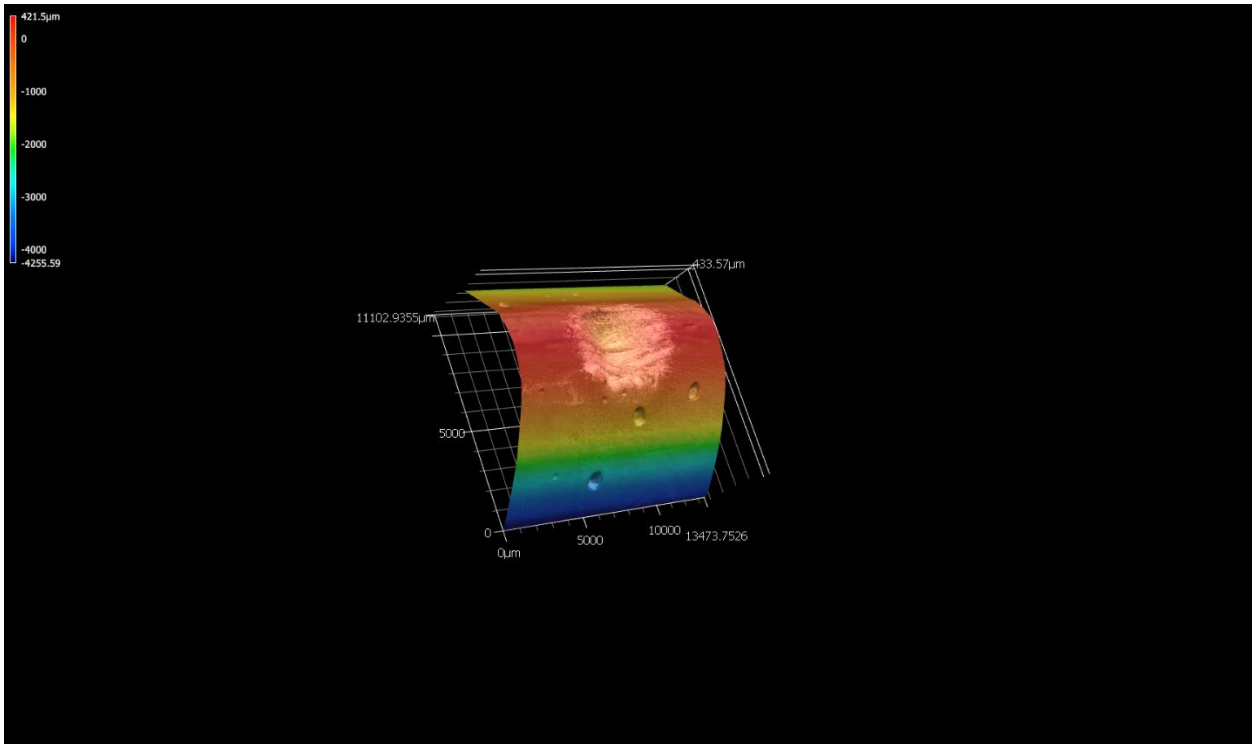


Fig. AVI-68: Erosion scar at 10° angle of impingement on the uncoated blade EXP6

- **<u>H-146</u>**

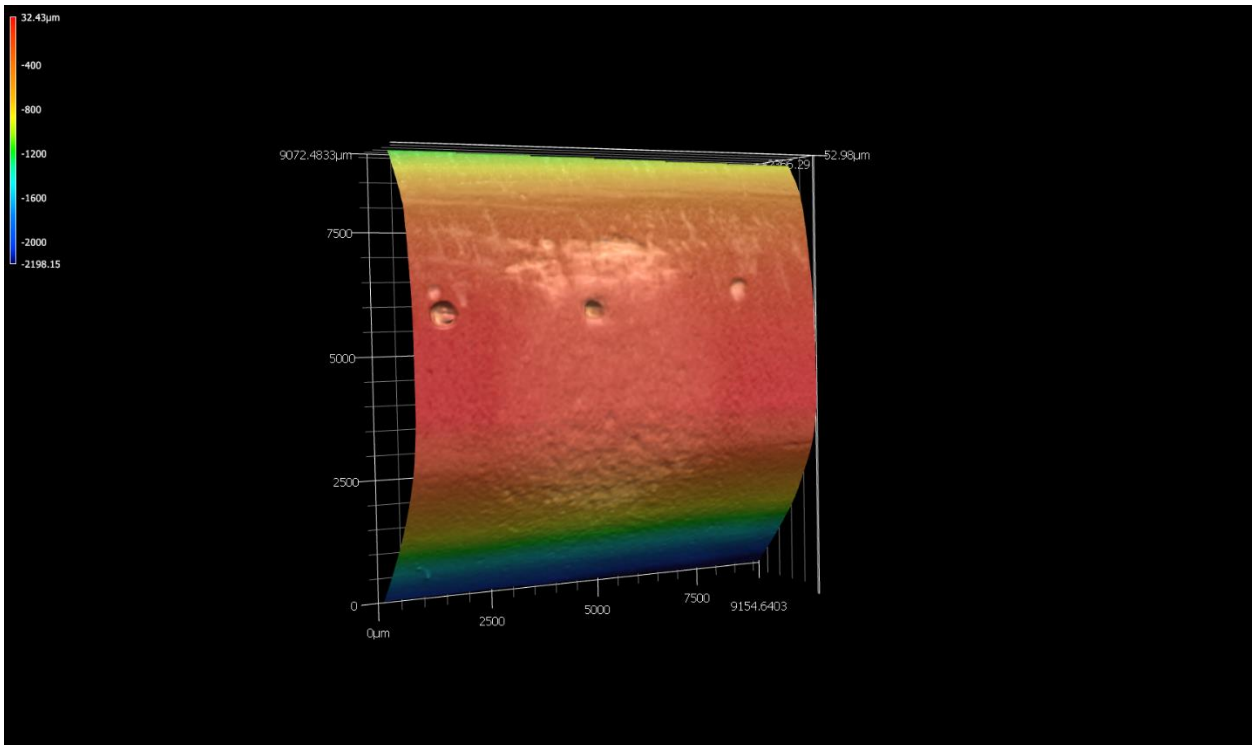


Fig. AVI-69: Erosion scar at 10° angle of impingement on the H-146 coated blade EXP1

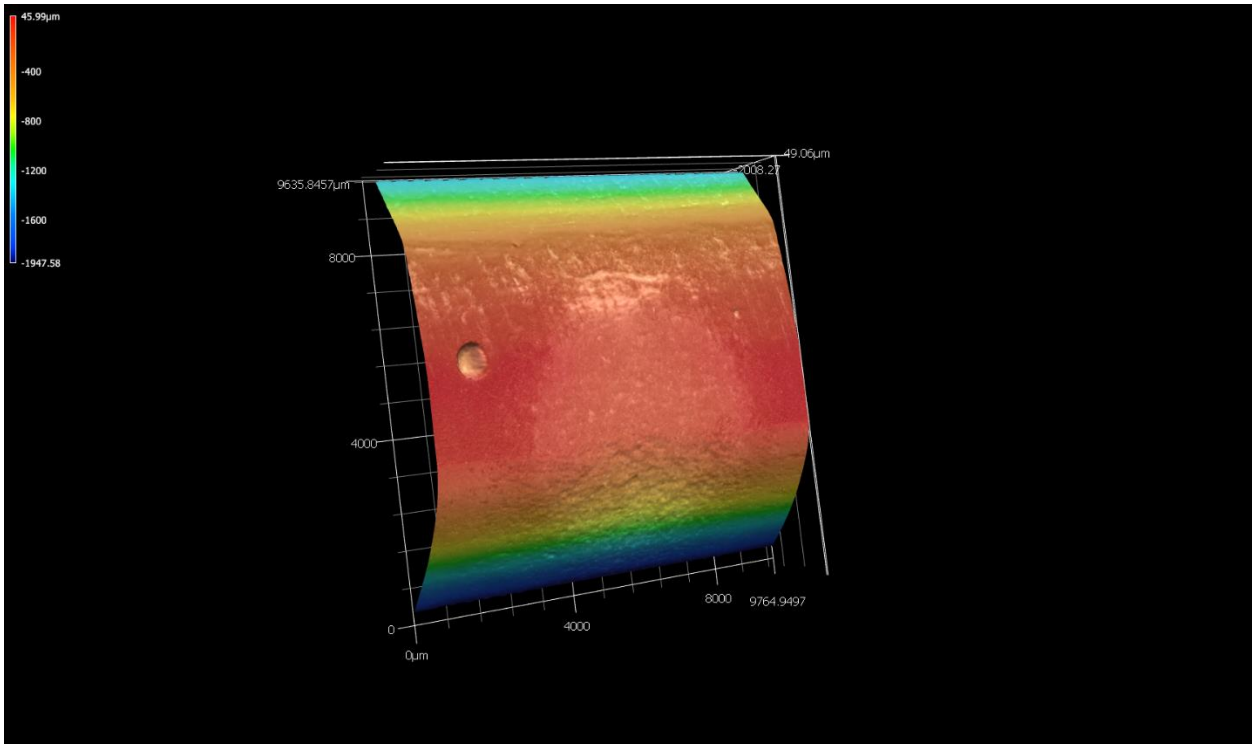


Fig. AVI-70: Erosion scar at 10° angle of impingement on the H-146 coated blade EXP2

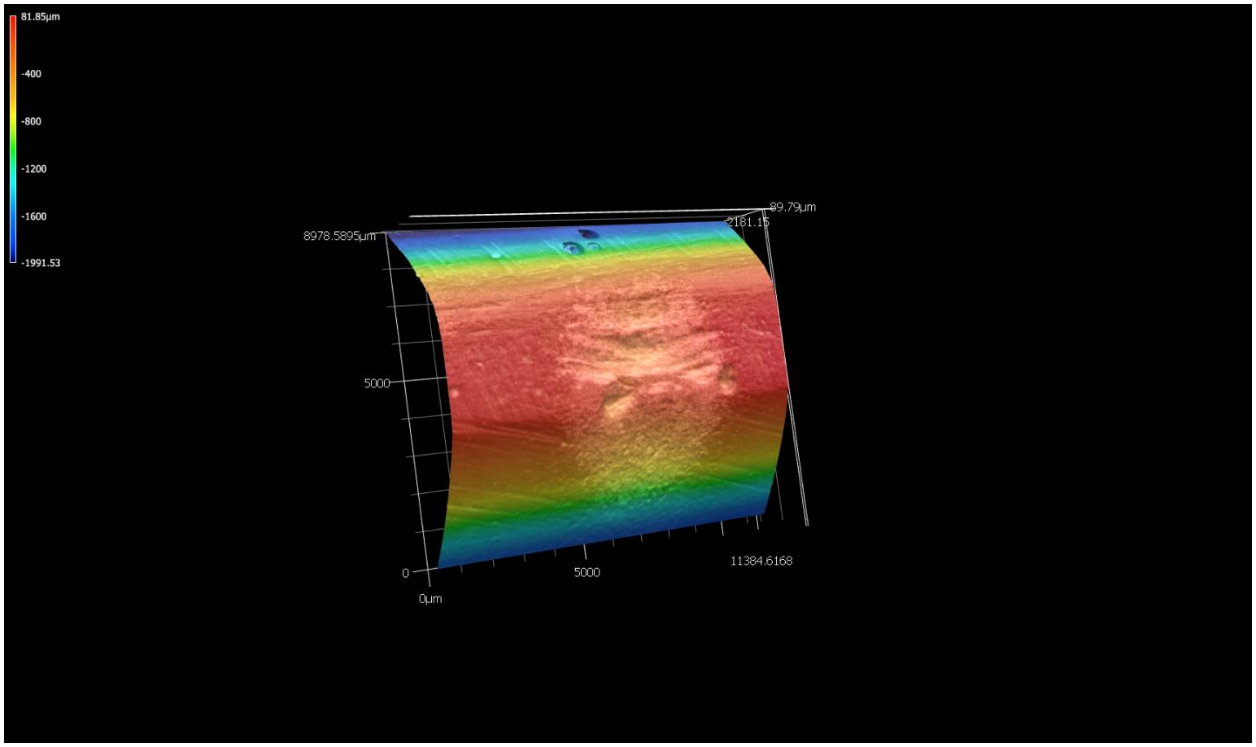


Fig. AVI-71: Erosion scar at 10° angle of impingement on the H-146 coated blade EXP3

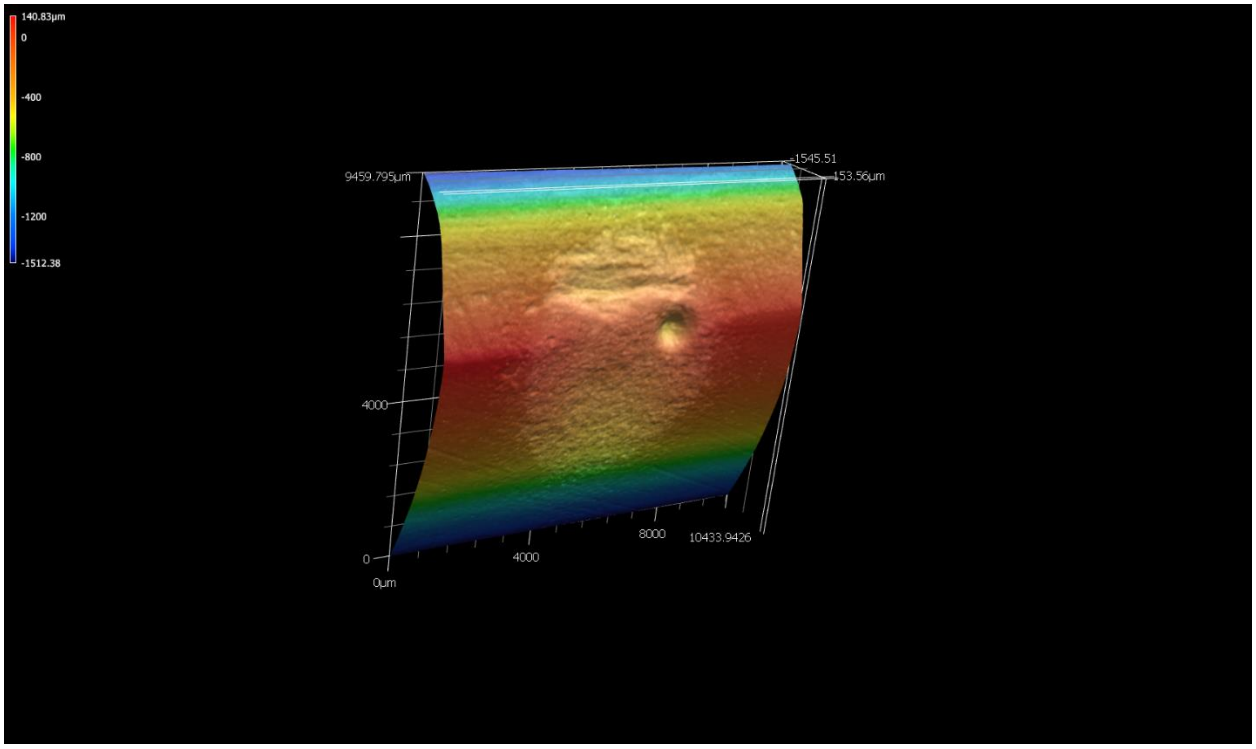


Fig. AVI-72: Erosion scar at 10° angle of impingement on the H-146 coated blade EXP4

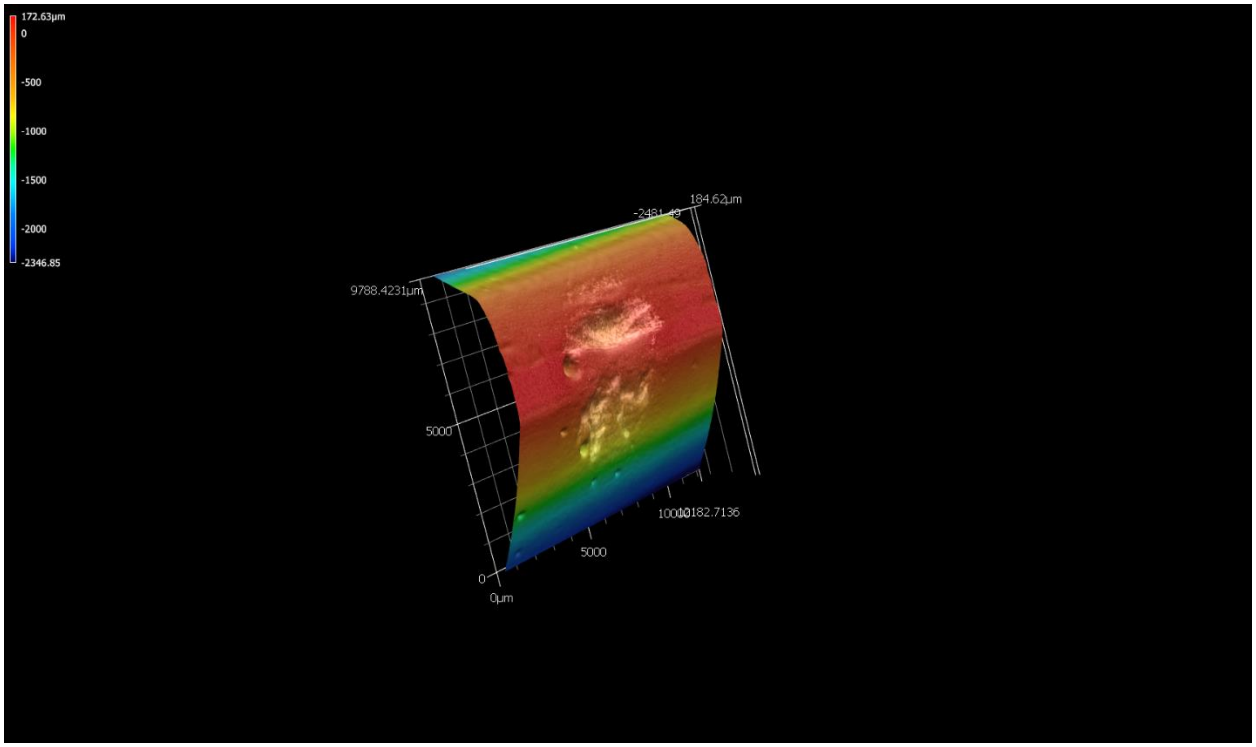


Fig. AVI-73: Erosion scar at 10° angle of impingement on the H-146 coated blade EXP5

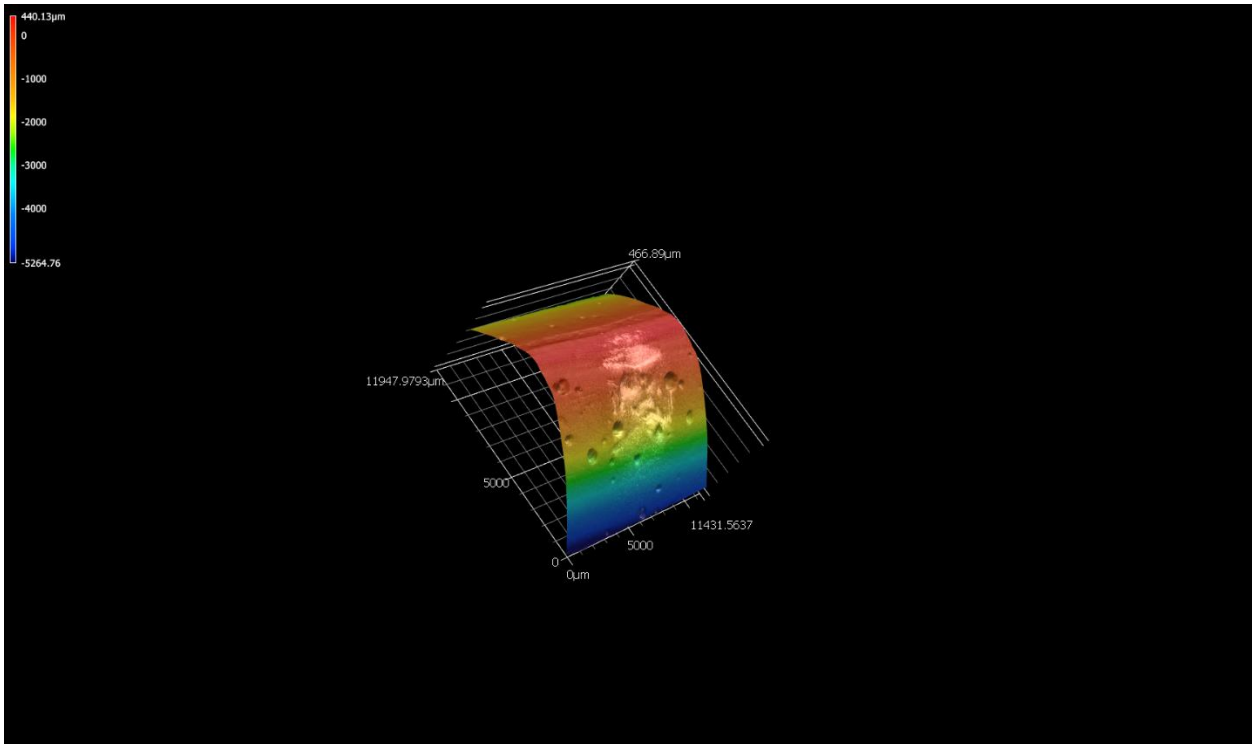


Fig. AVI-74: Erosion scar at 10° angle of impingement on the H-146 coated blade EXP6

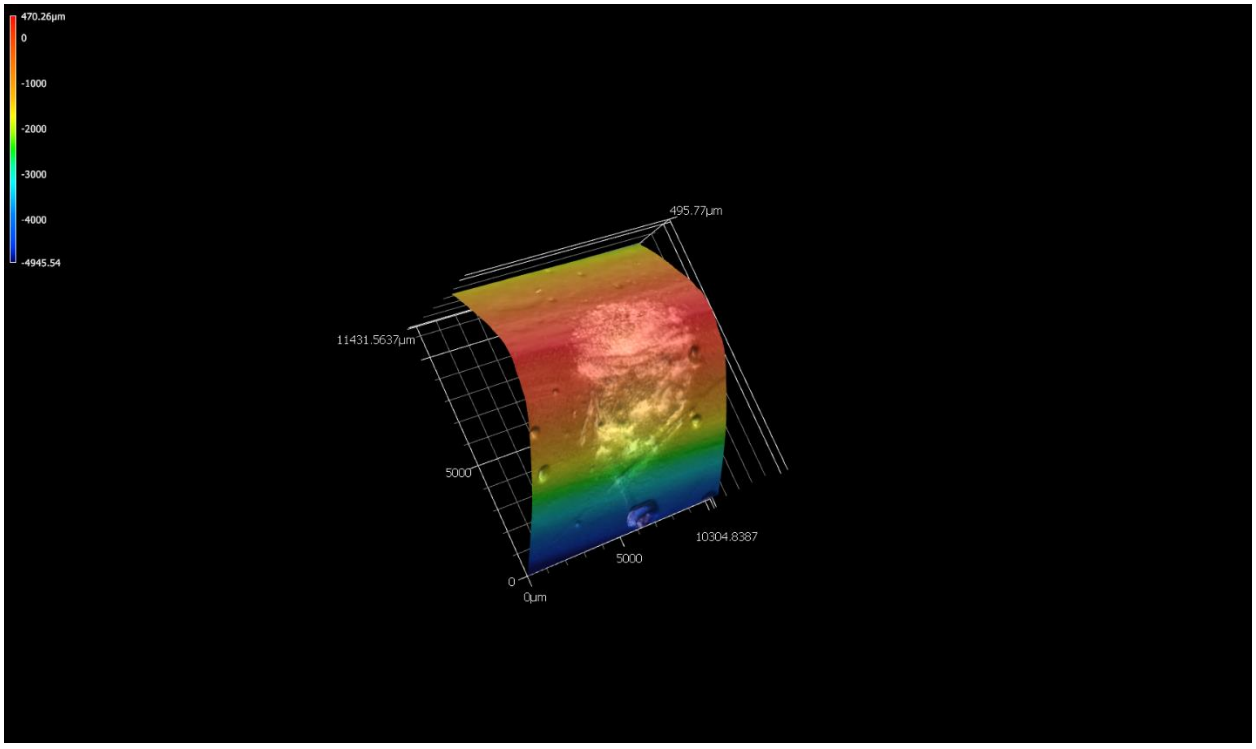


Fig. AVI-75: Erosion scar at 10° angle of impingement on the H-146 coated blade EXP7

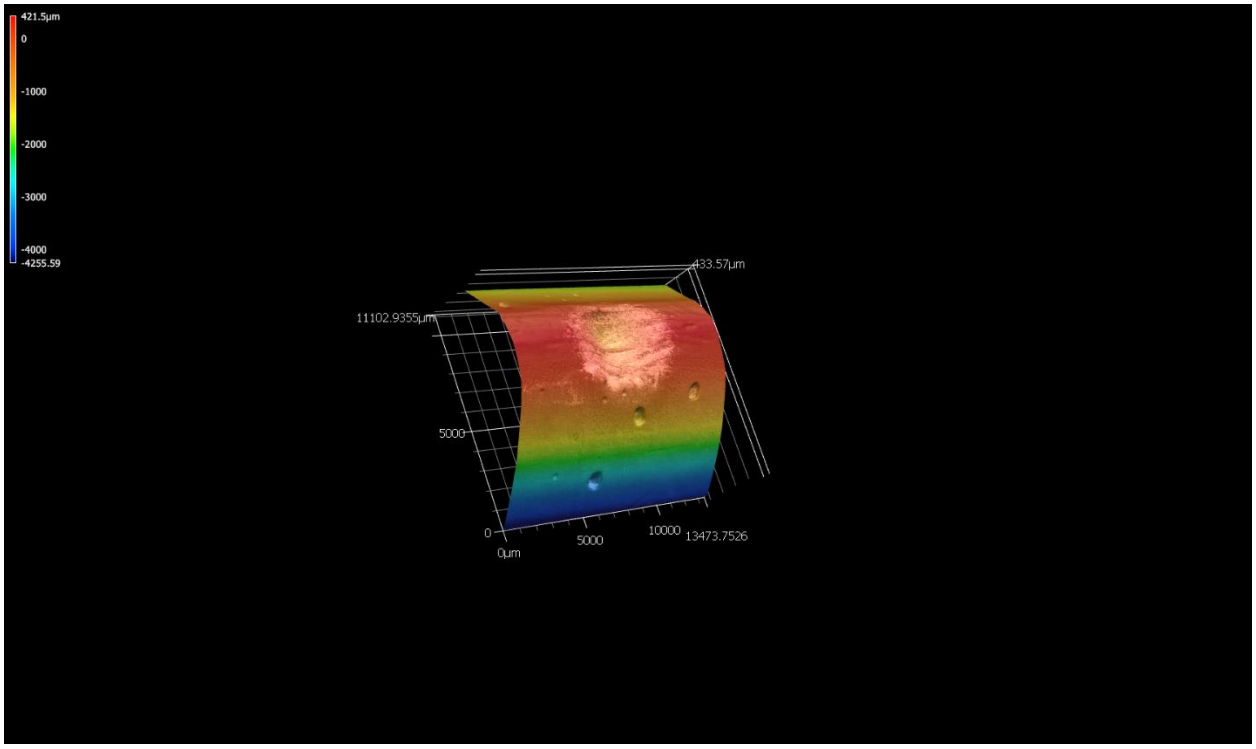


Fig. AVI-76: Erosion scar at 10° angle of impingement on the H-146 coated blade EXP8

- **<u>Polyurethane/IA-700</u>**

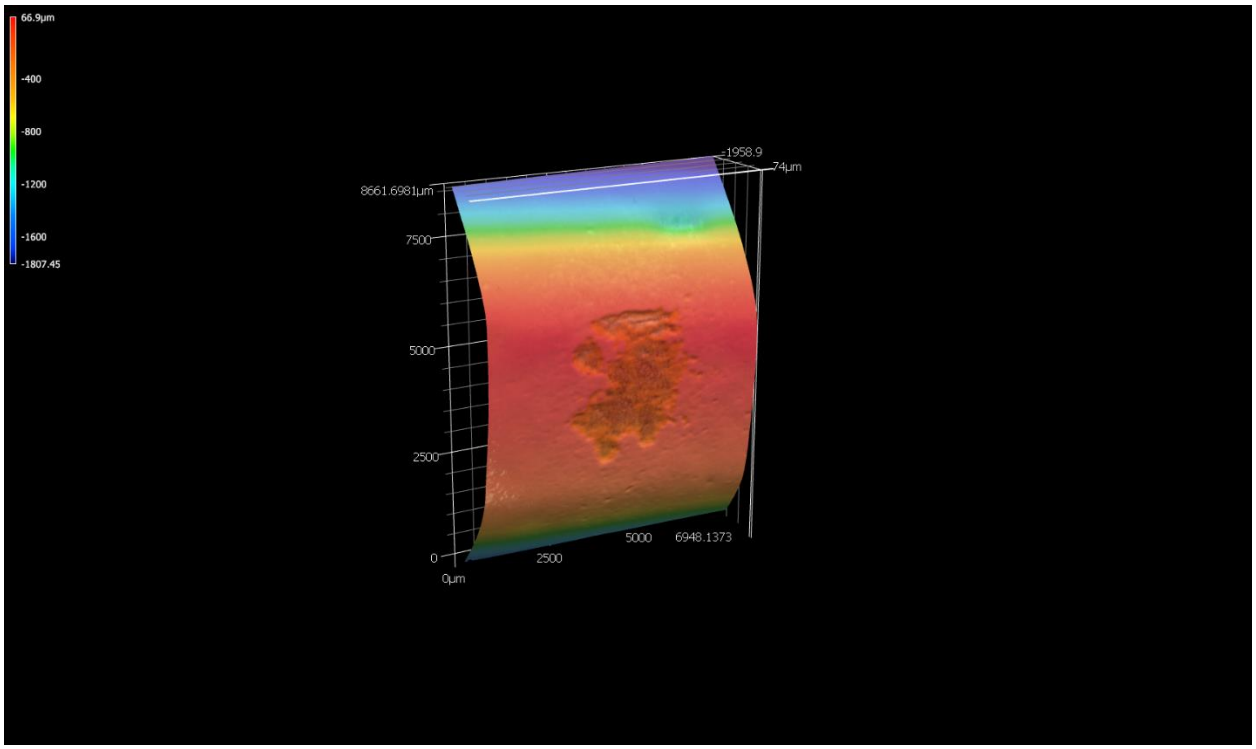


Fig. AVI-77: Erosion scar at 10° angle of impingement on the Polyurethane/IA-700 coated blade EXP1

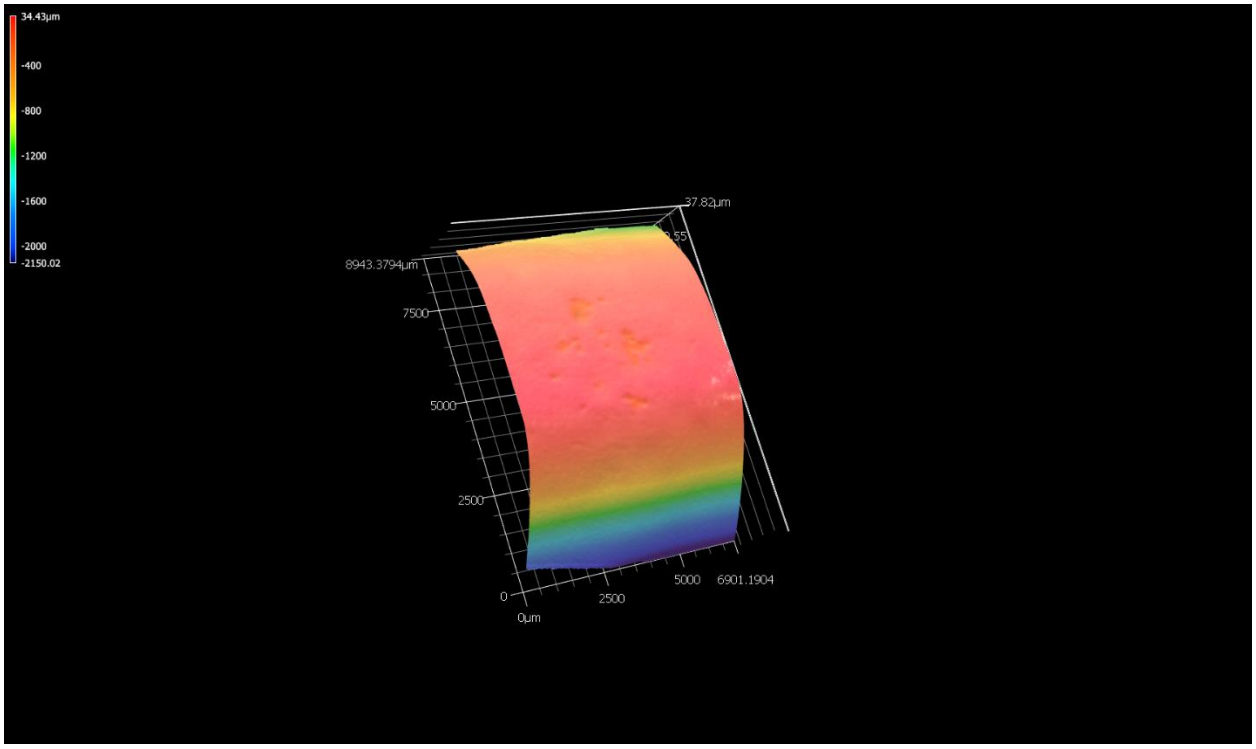


Fig. AVI-78: Erosion scar at 10° angle of impingement on the Polyurethane/IA-700 coated blade EXP2

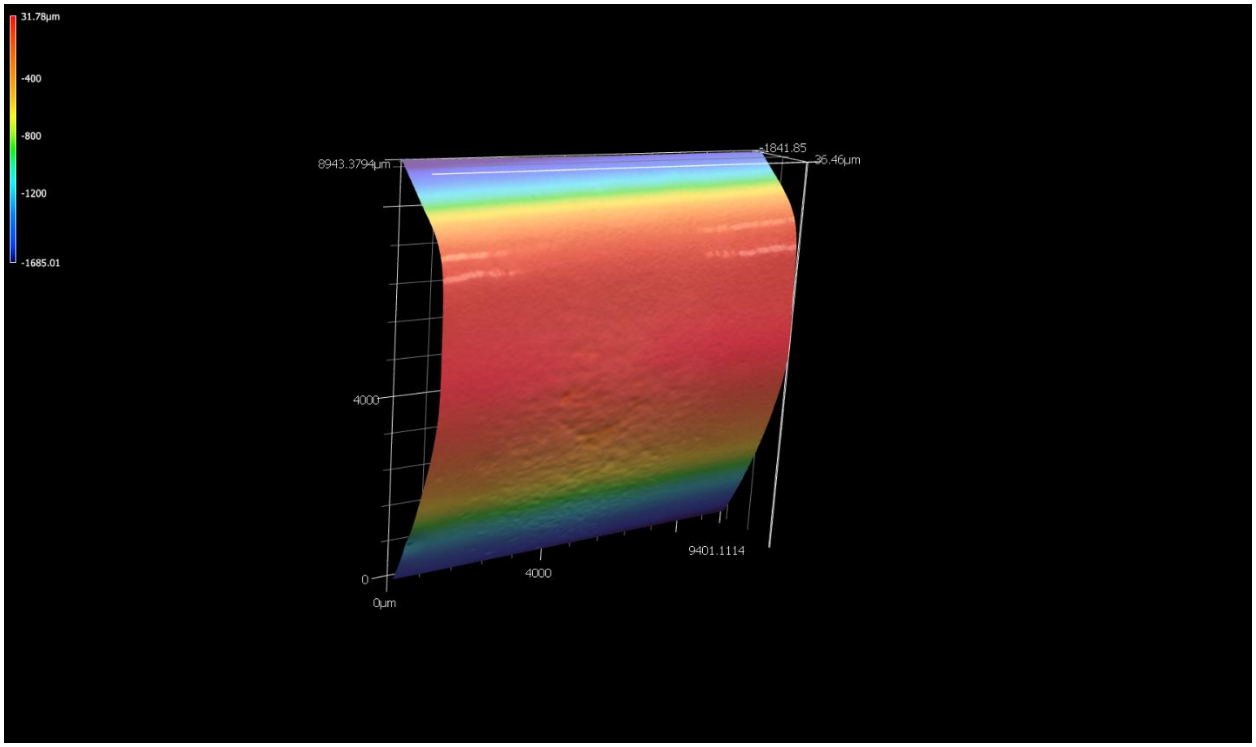


Fig. AVI-79: Erosion scar at 10° angle of impingement on the Polyurethane/IA-700 coated blade EXP3

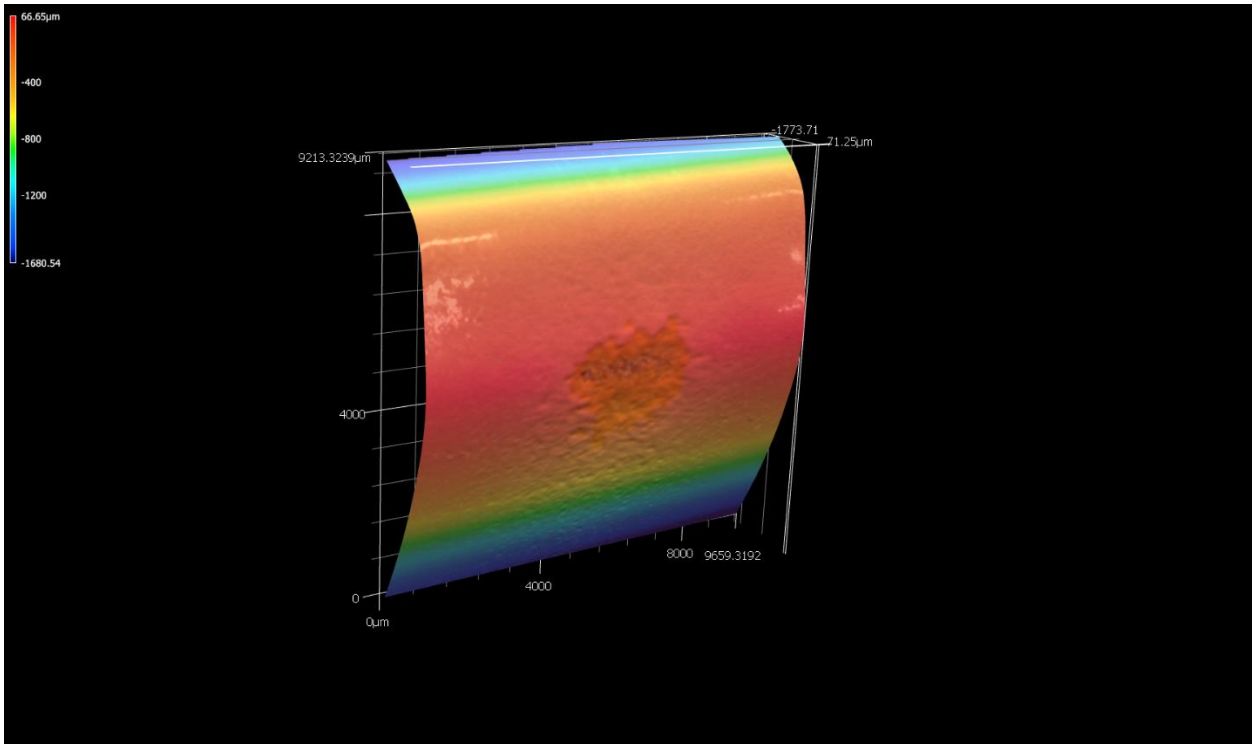


Fig. AVI-80: Erosion scar at 10° angle of impingement on the Polyurethane/IA-700 coated blade EXP4

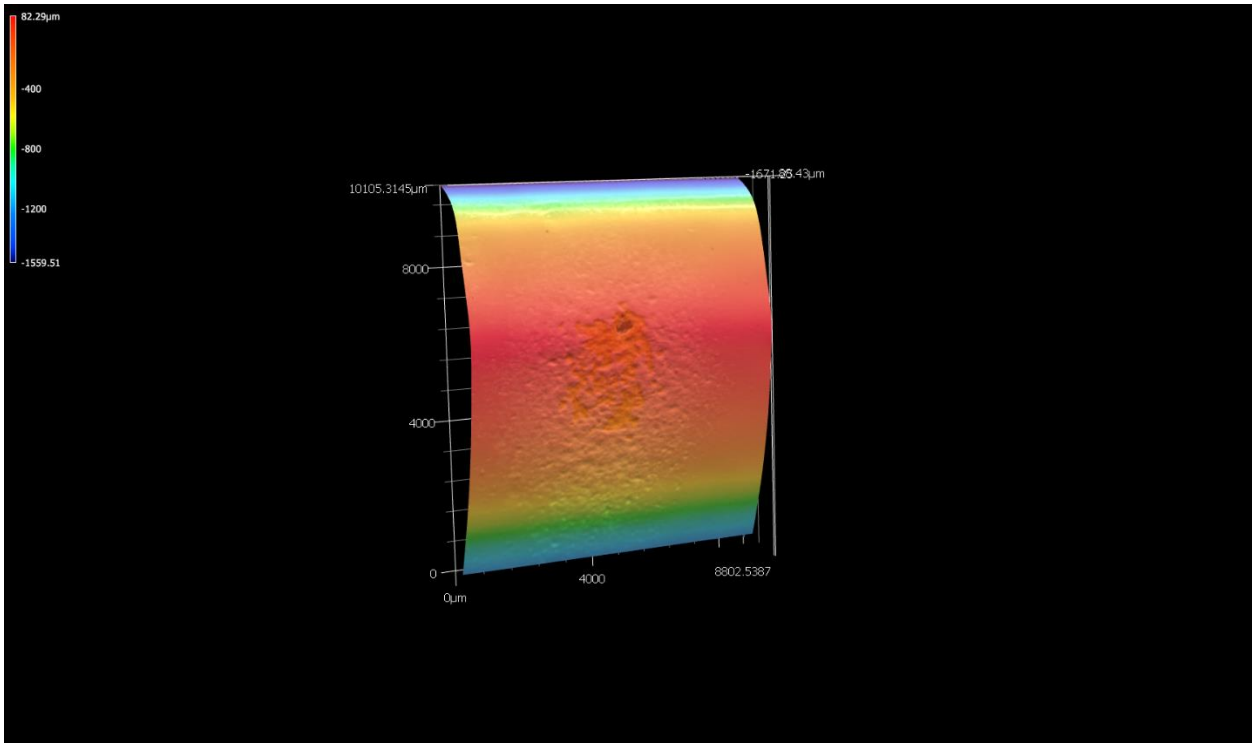


Fig. AVI-81: Erosion scar at 10° angle of impingement on the Polyurethane/IA-700 coated blade EXP5

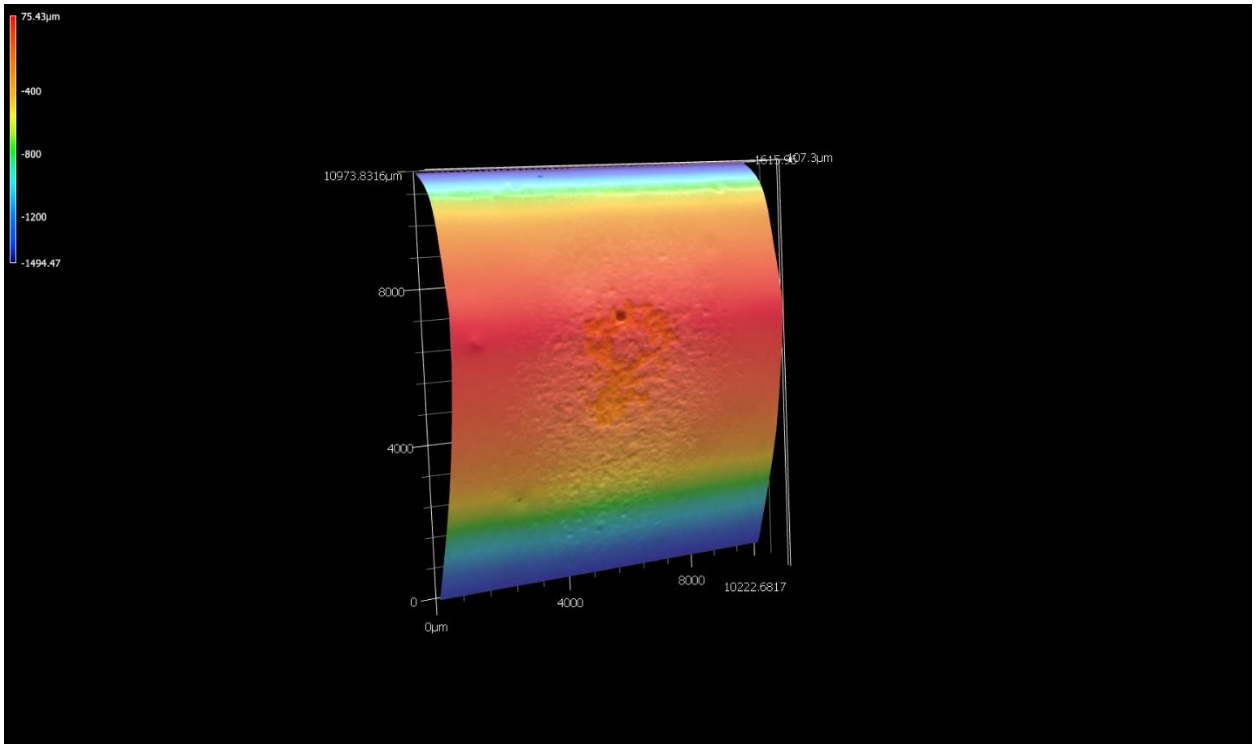


Fig. AVI-82: Erosion scar at 10° angle of impingement on the Polyurethane/IA-700 coated blade EXP6

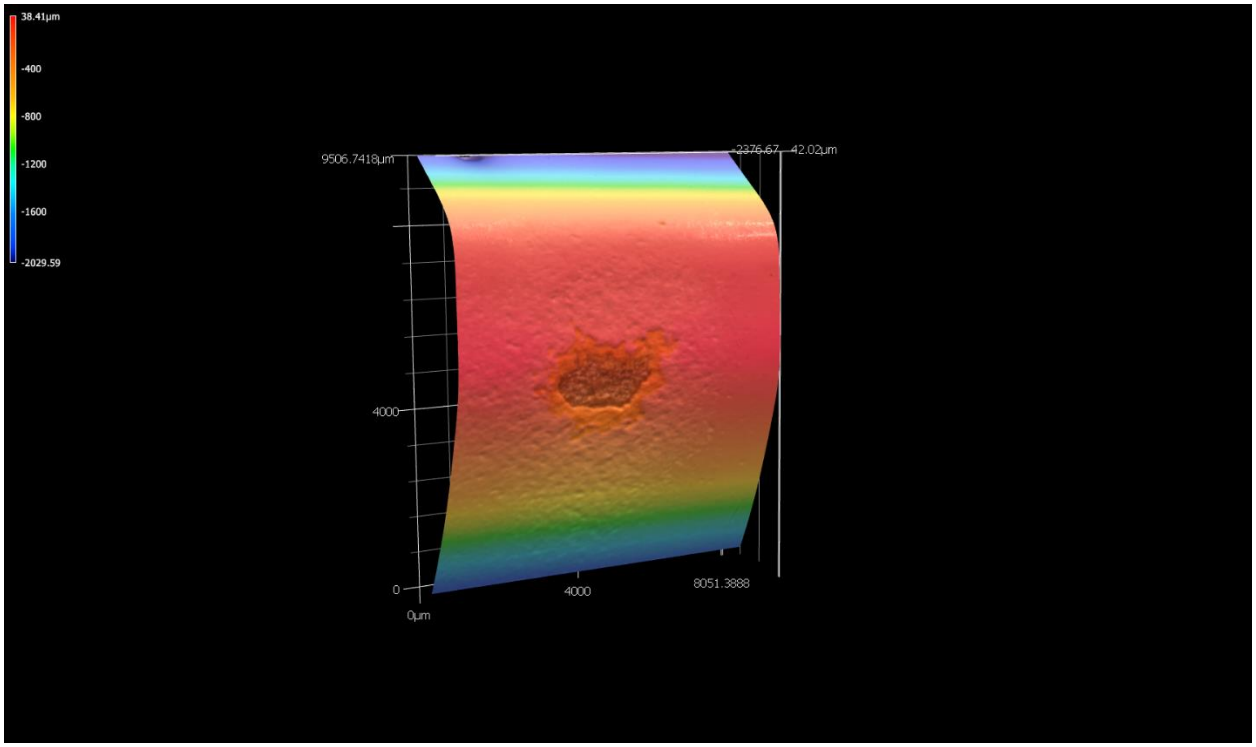


Fig. AVI-83: Erosion scar at 10° angle of impingement on the Polyurethane/IA-700 coated blade EXP7

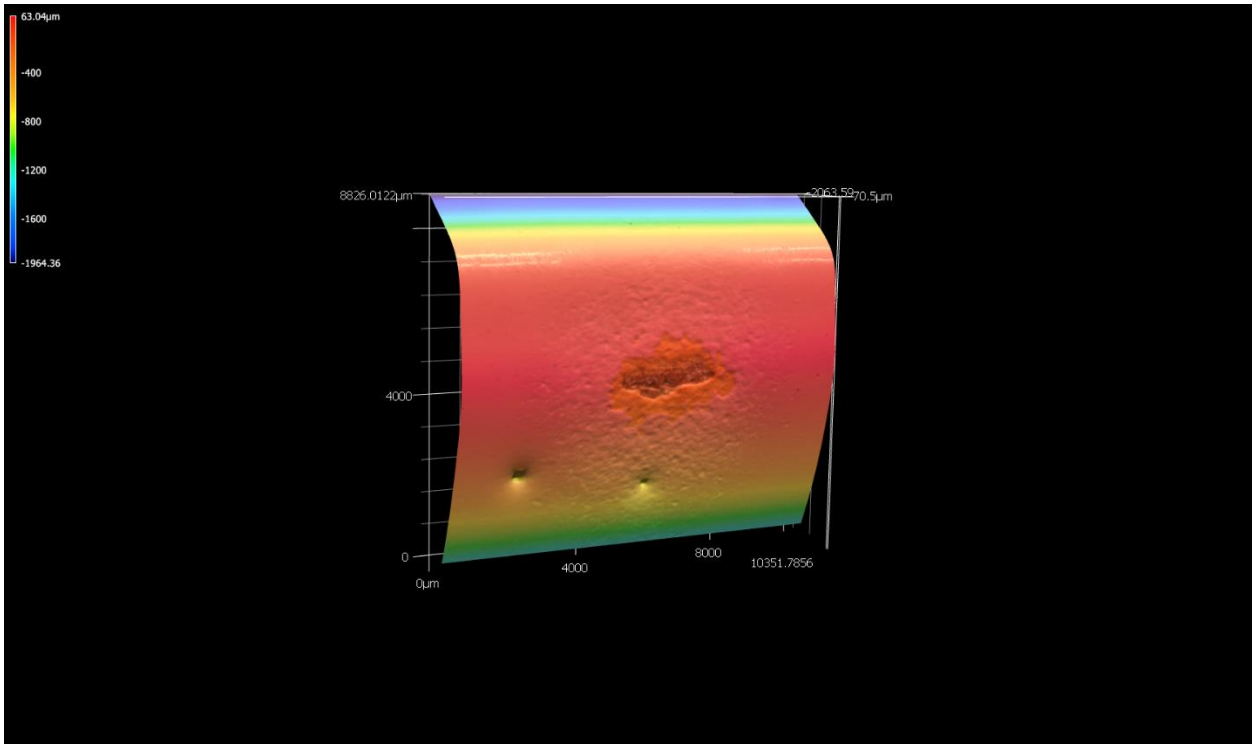


Fig. AVI-84: Erosion scar at 10° angle of impingement on the Polyurethane/IA-700 coated blade EXP8

- Midspan Section
  - **-5 degrees**
    - **Uncoated**

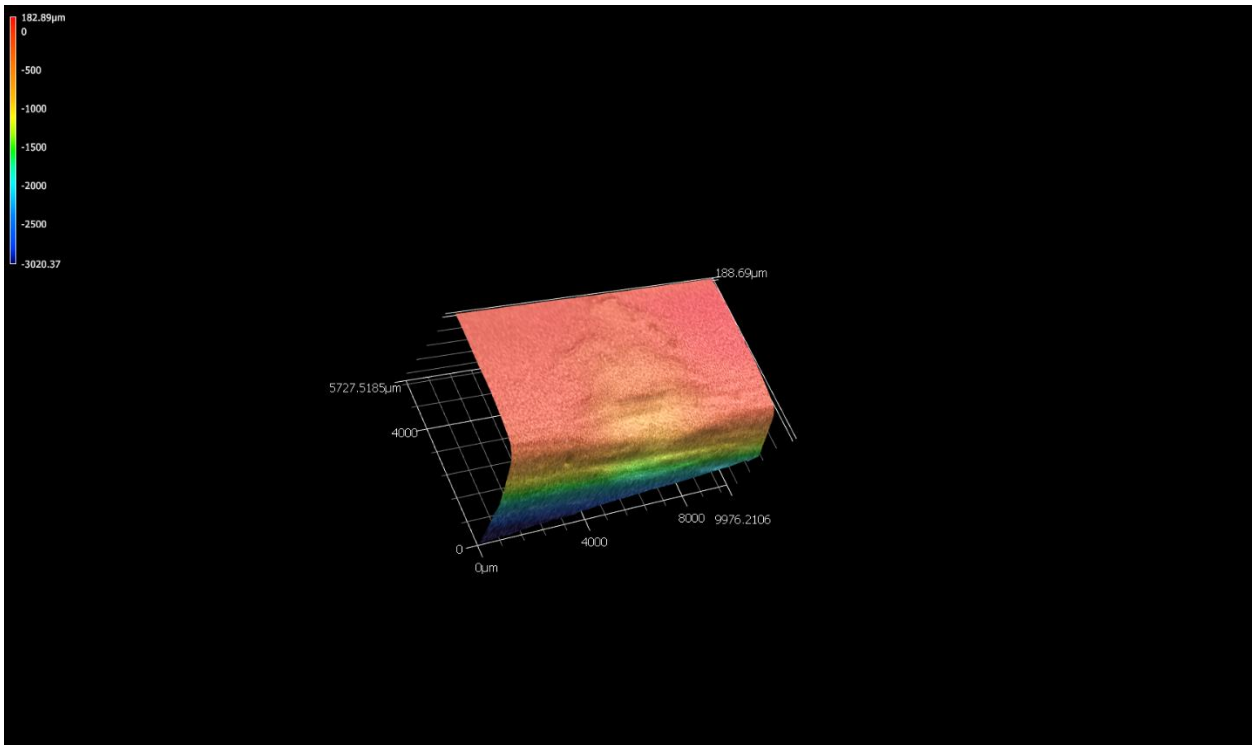


Fig. AVI-85: Erosion scar at -5° angle of impingement on the uncoated blade EXP1

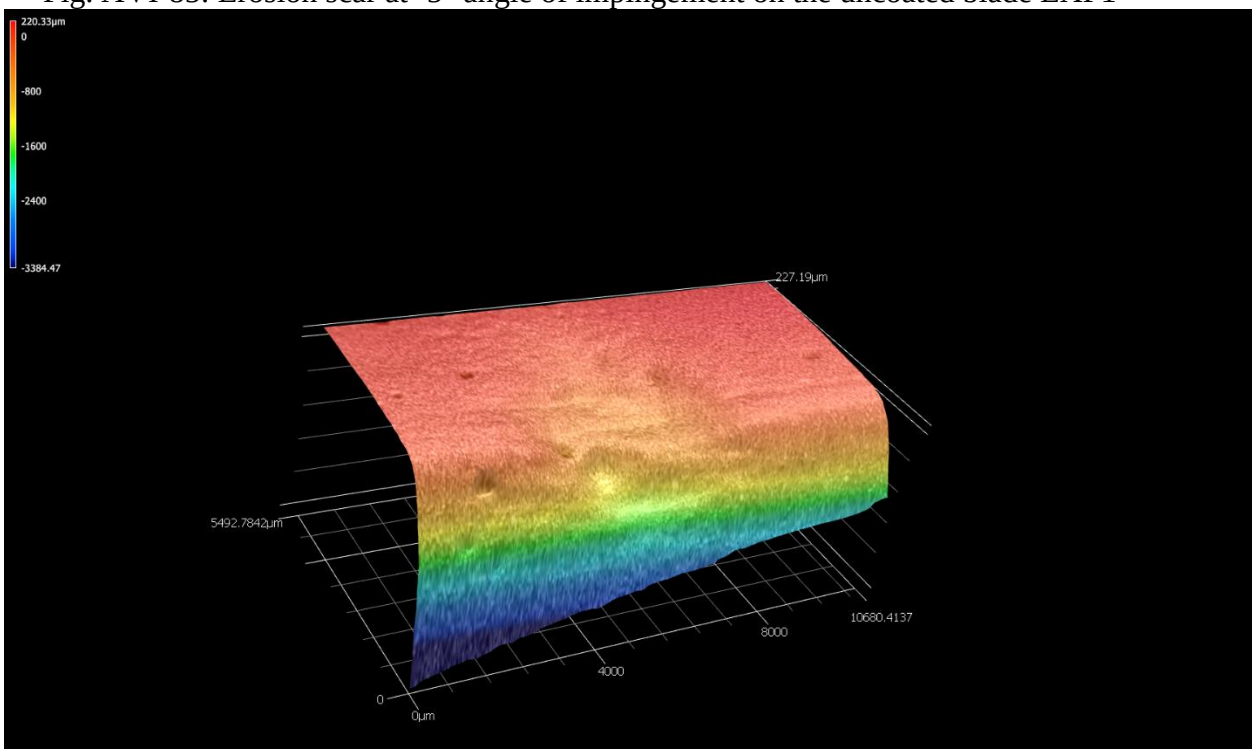


Fig. AVI-86: Erosion scar at -5° angle of impingement on the uncoated blade EXP2

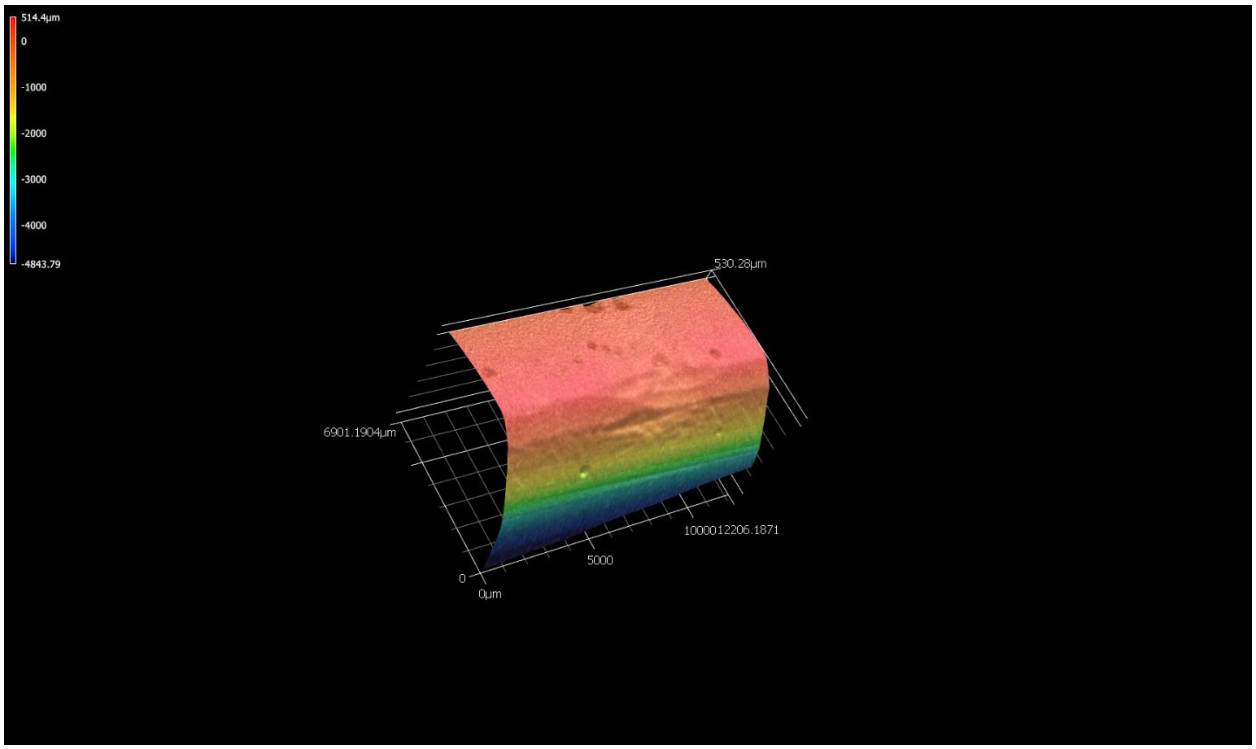


Fig. AVI-87: Erosion scar at -5° angle of impingement on the uncoated blade EXP3

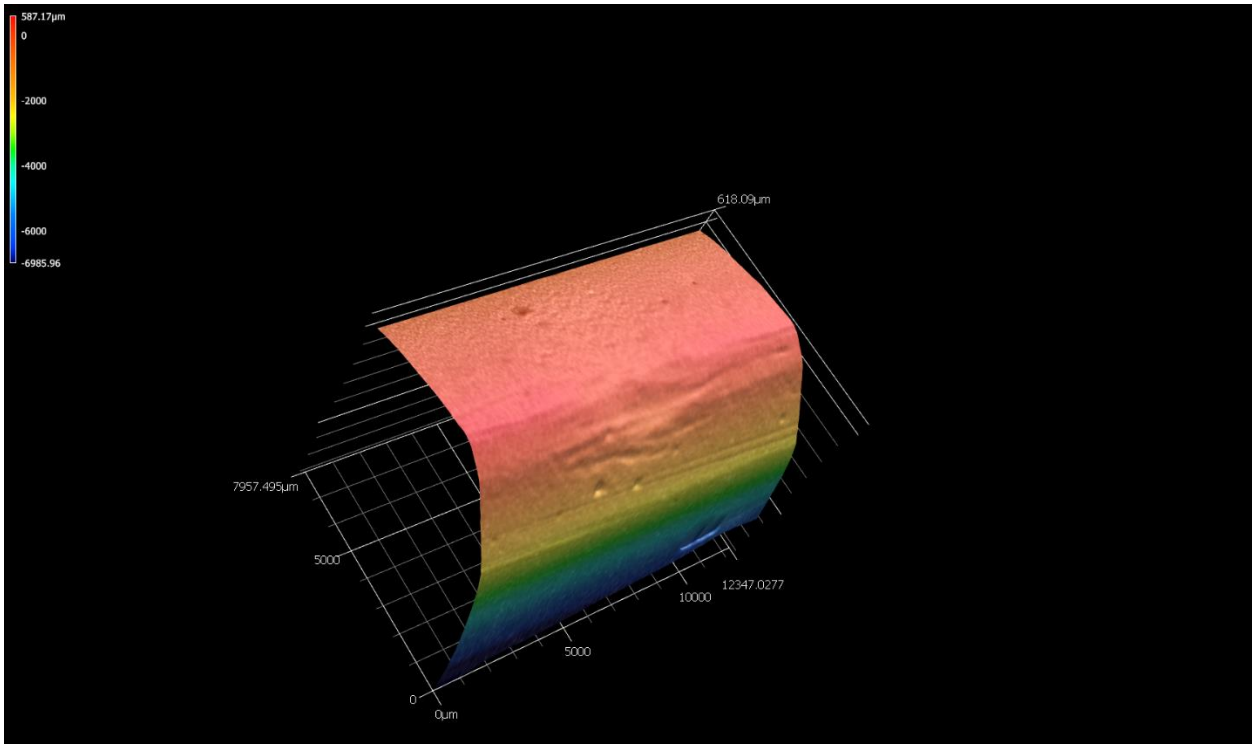


Fig. AVI-88: Erosion scar at -5° angle of impingement on the uncoated blade EXP4

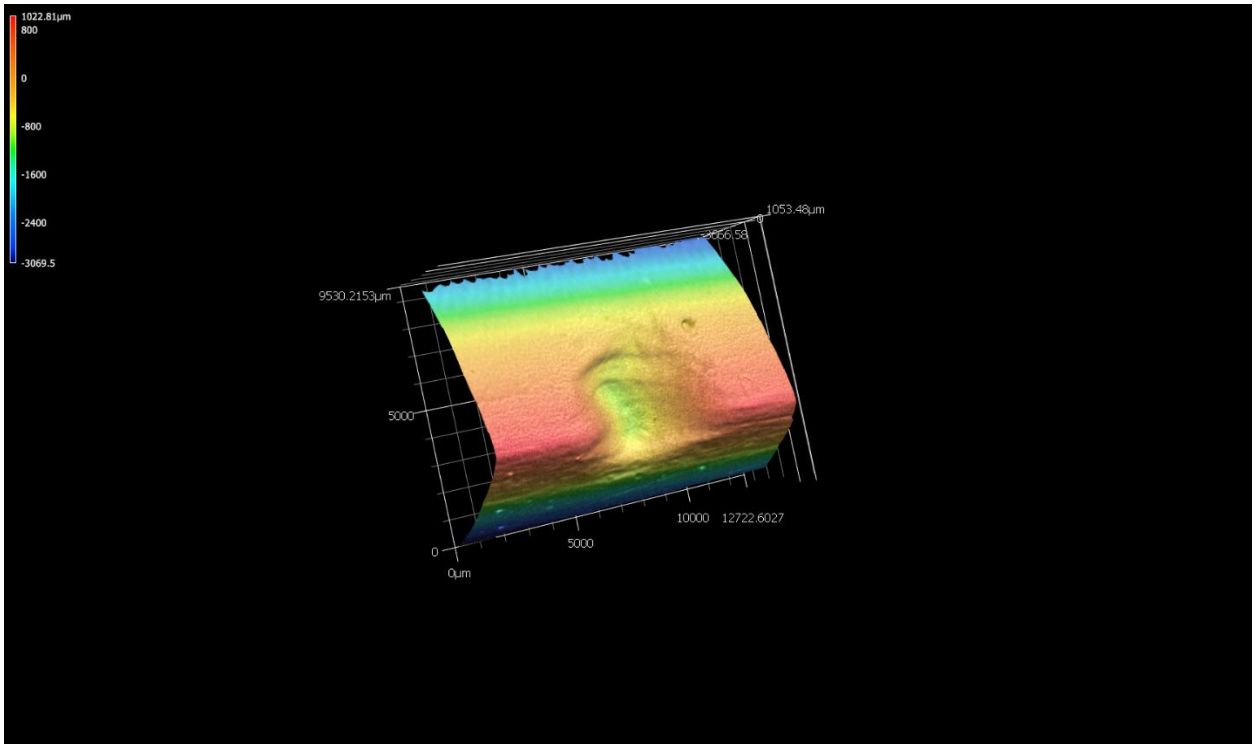


Fig. AVI-89: Erosion scar at -5° angle of impingement on the uncoated blade EXP5

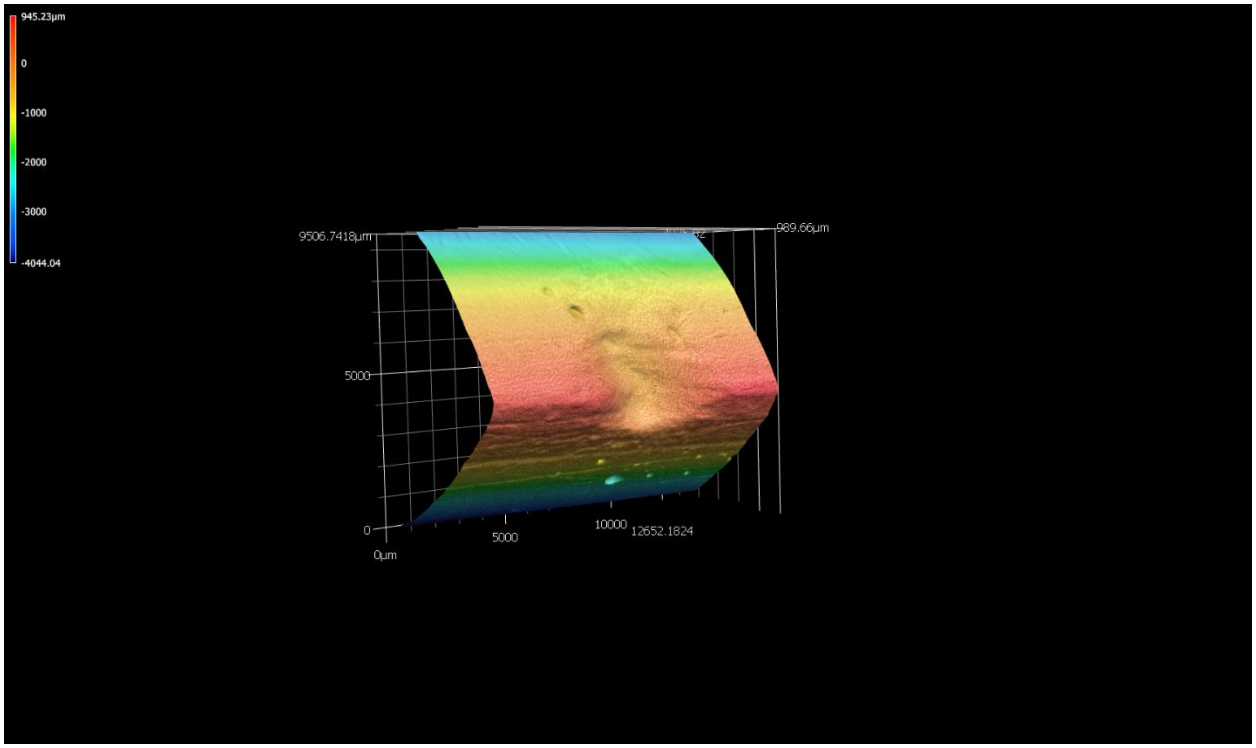


Fig. AVI-90: Erosion scar at -5° angle of impingement on the uncoated blade EXP6

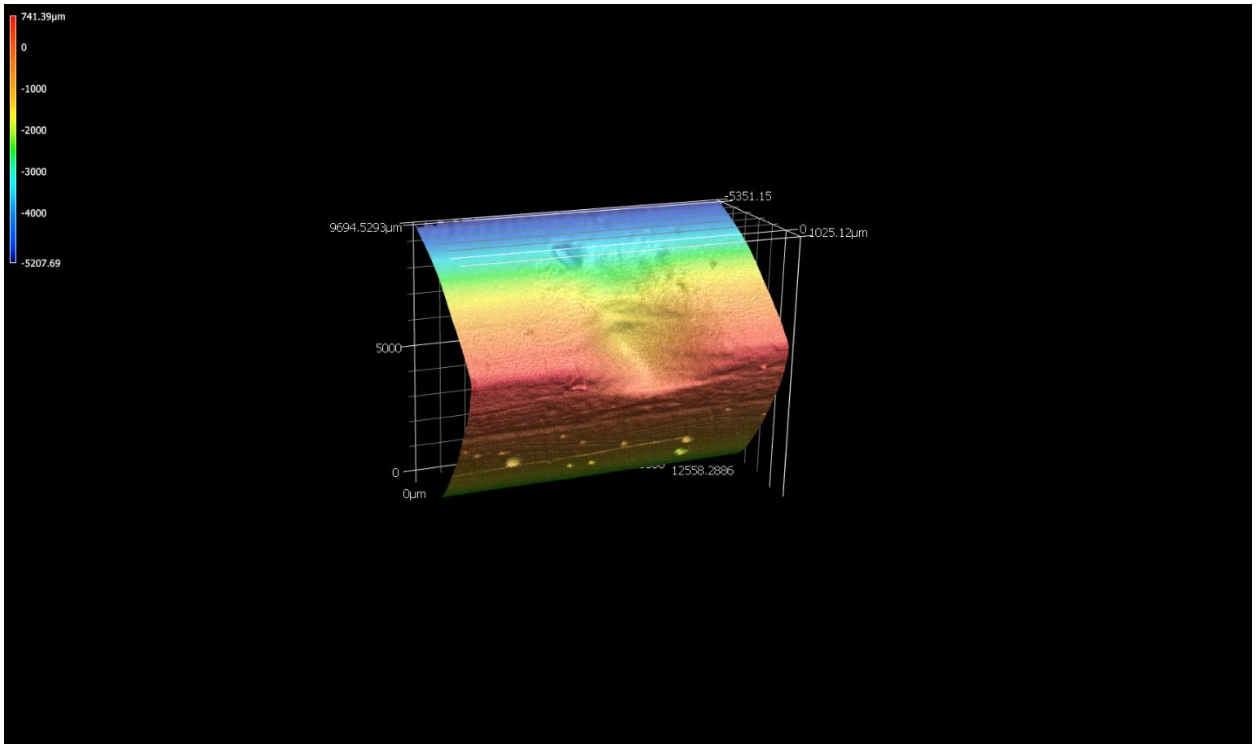


Fig. AVI-91: Erosion scar at -5° angle of impingement on the uncoated blade EXP7

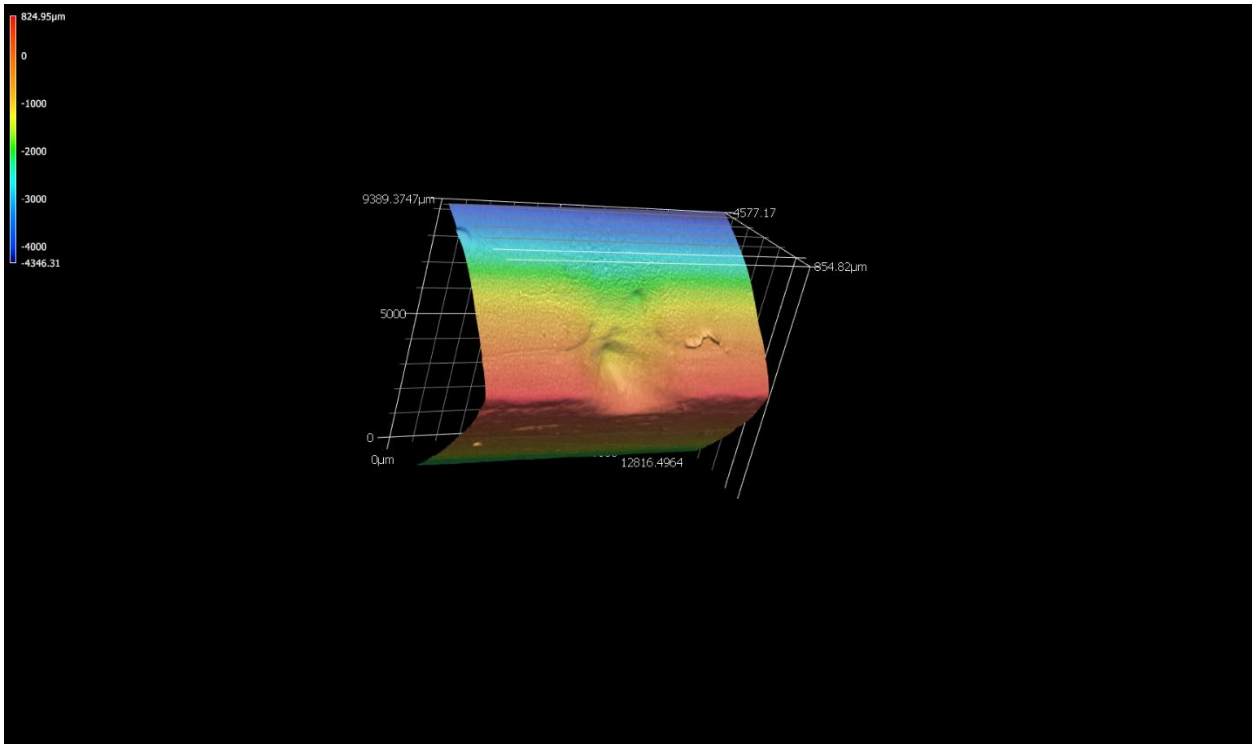


Fig. AVI-92: Erosion scar at -5° angle of impingement on the uncoated blade EXP8

- **H-146**

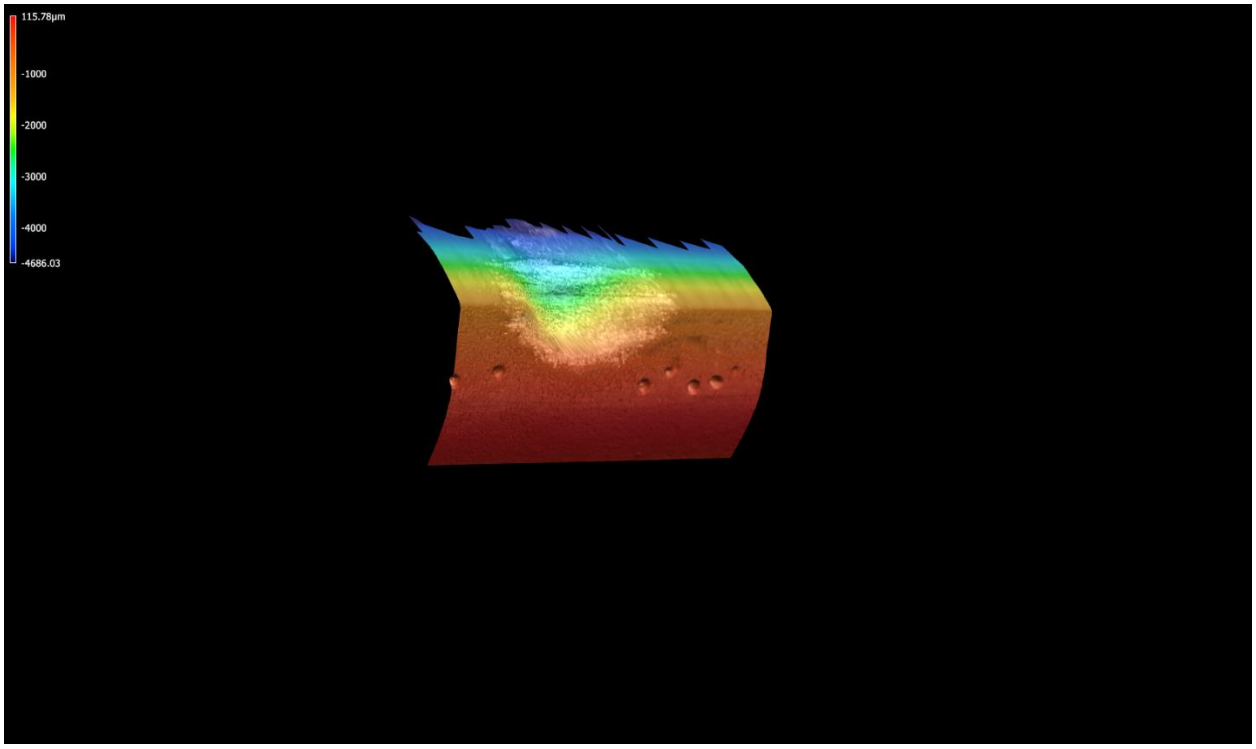


Fig. AVI-93: Erosion scar at -5° angle of impingement on the H-146 coated blade EXP1

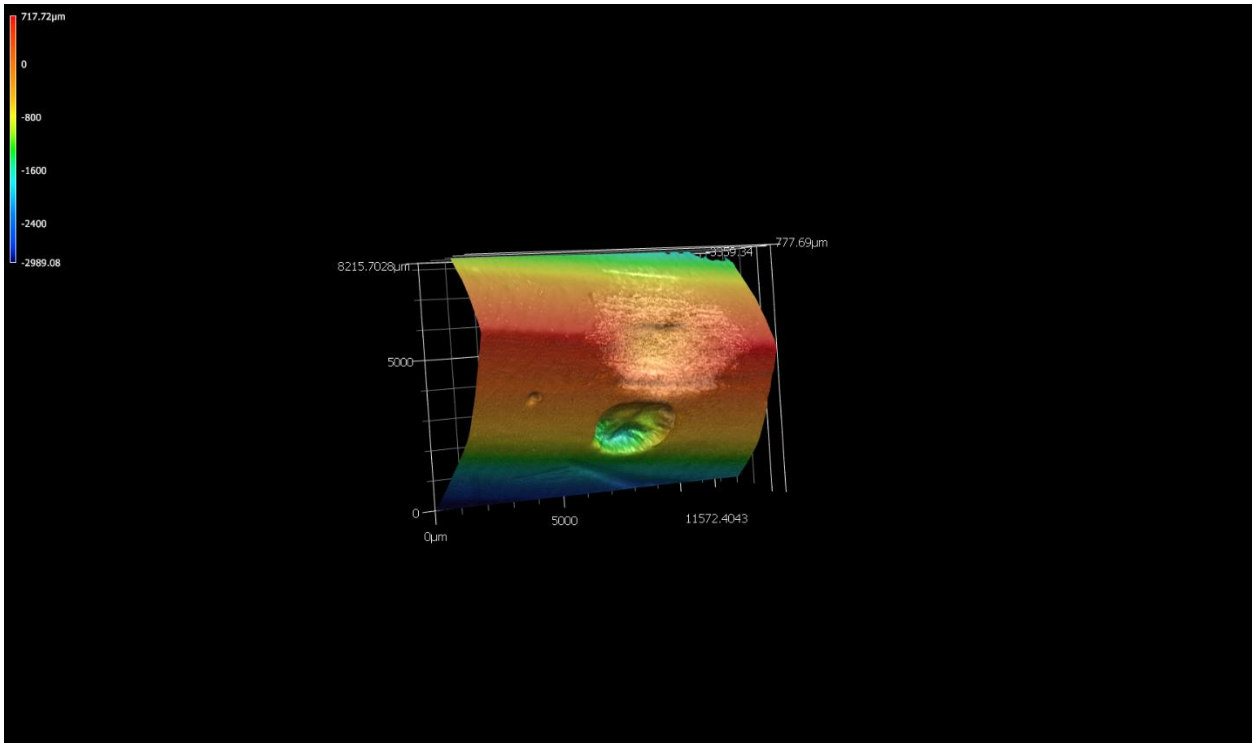


Fig. AVI-94: Erosion scar at -5° angle of impingement on the H-146 coated blade EXP2

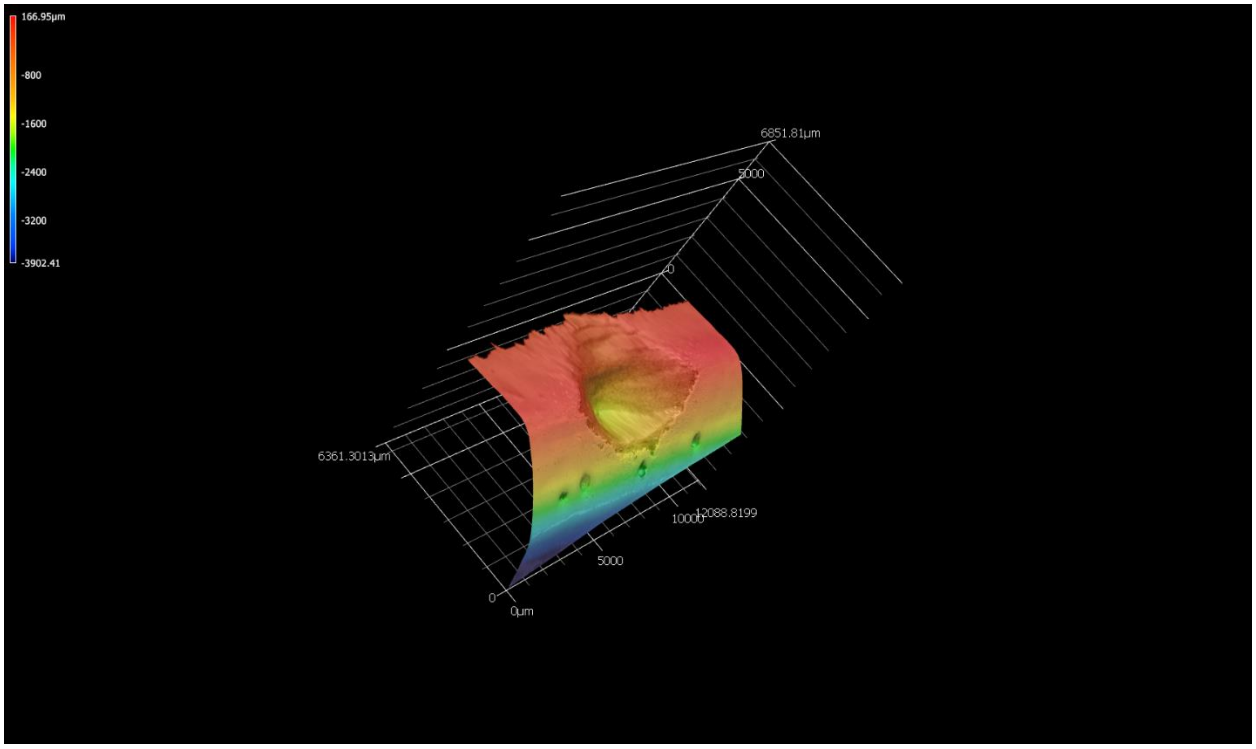


Fig. AVI-95: Erosion scar at -5° angle of impingement on the H-146 coated blade EXP3

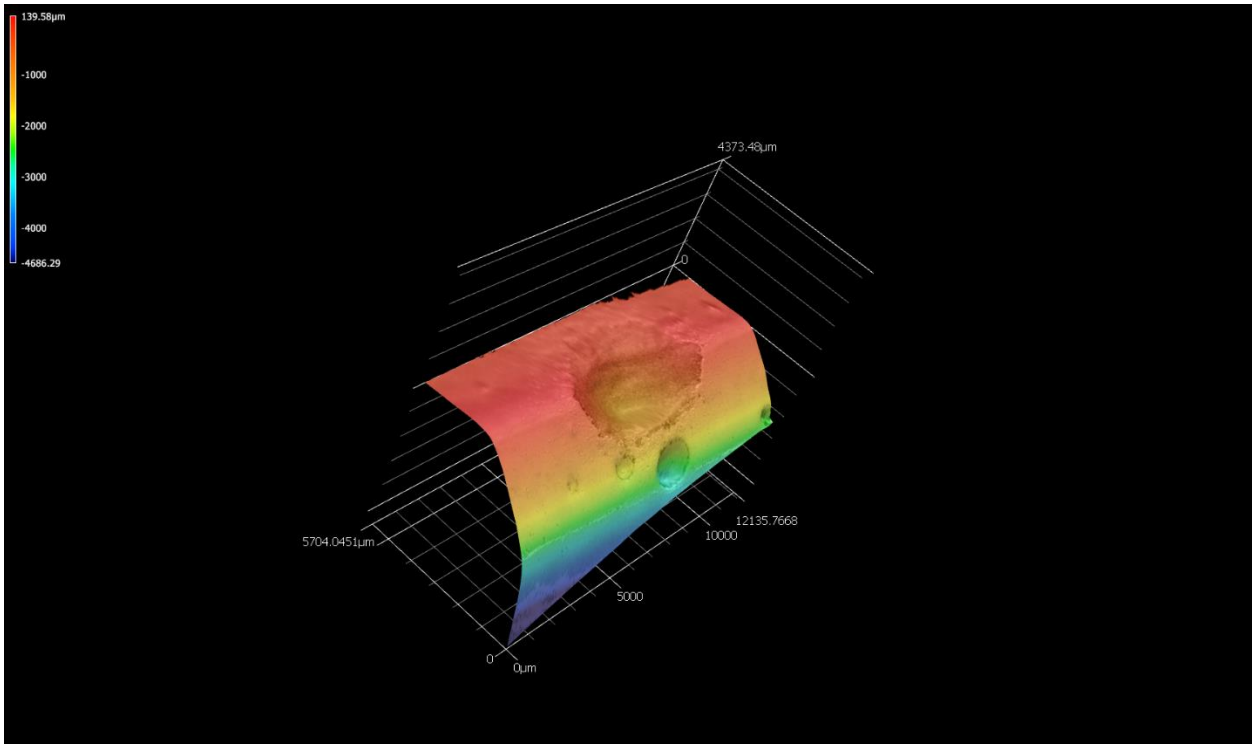


Fig. AVI-96: Erosion scar at -5° angle of impingement on the H-146 coated blade EXP4

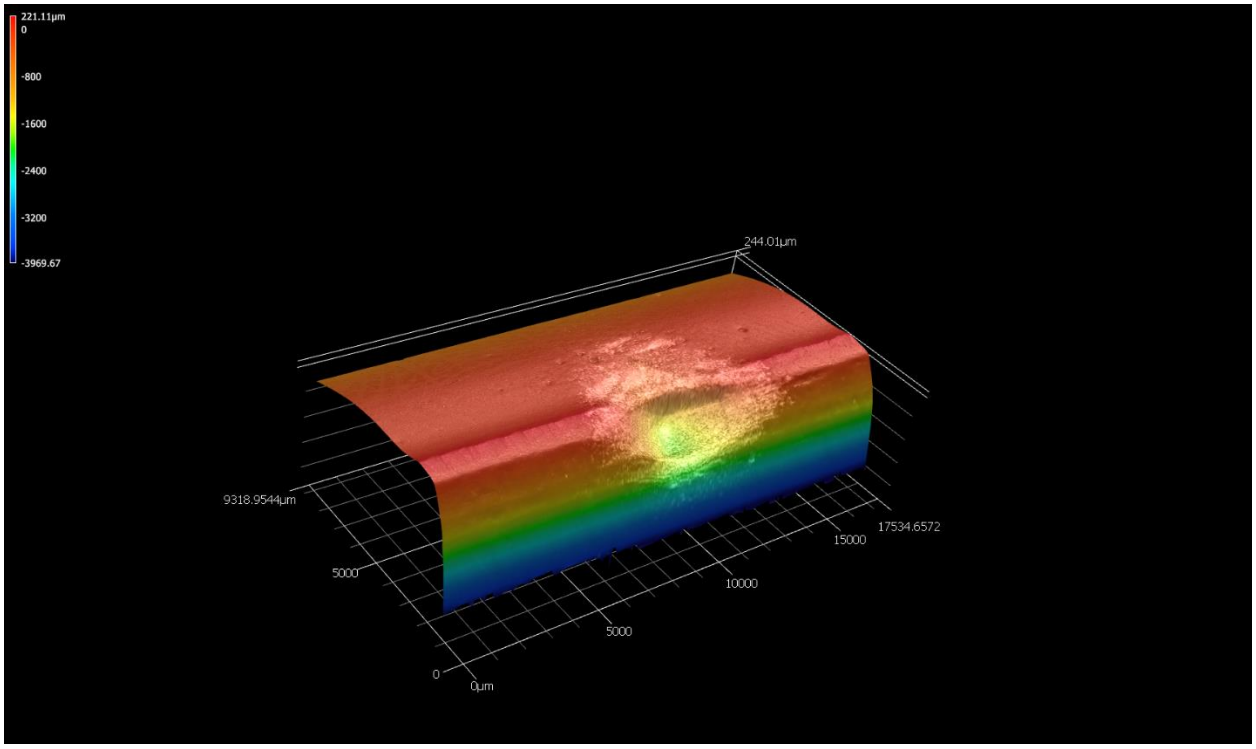


Fig. AVI-97: Erosion scar at -5° angle of impingement on the H-146 coated blade EXP5

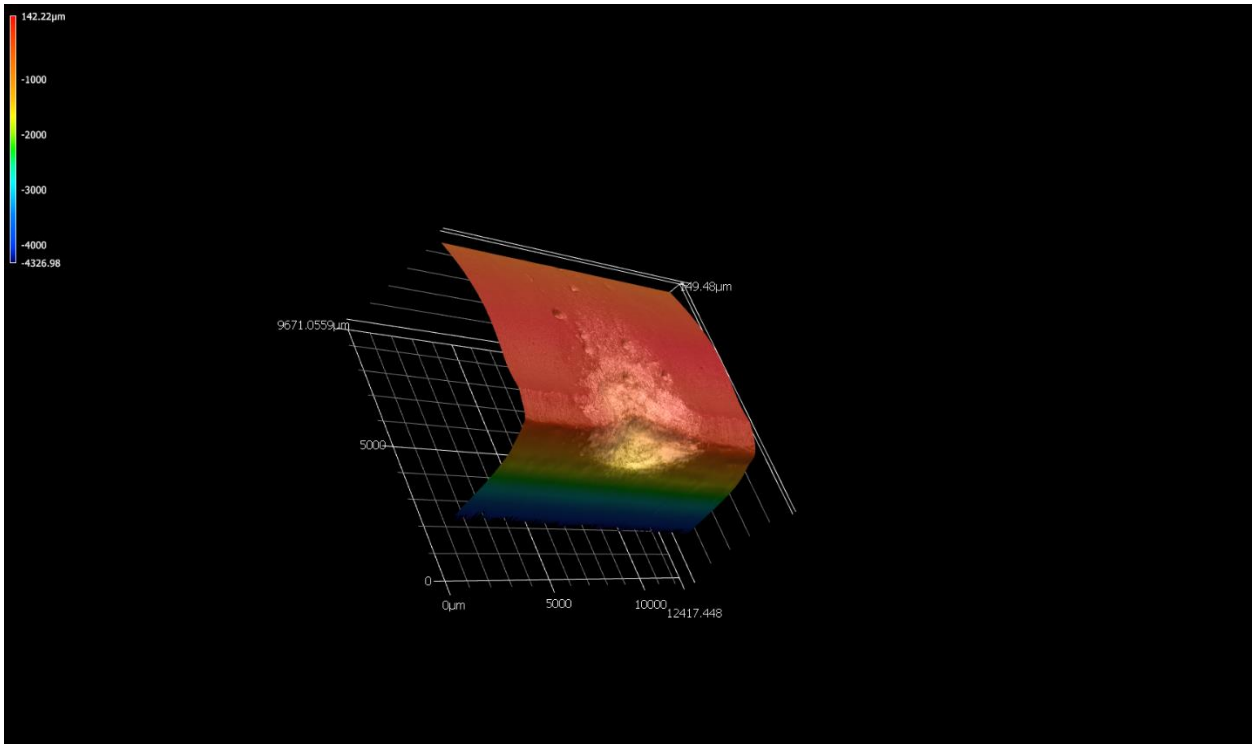


Fig. AVI-98: Erosion scar at -5° angle of impingement on the H-146 coated blade EXP6

- **Polyurethane/IA-700**

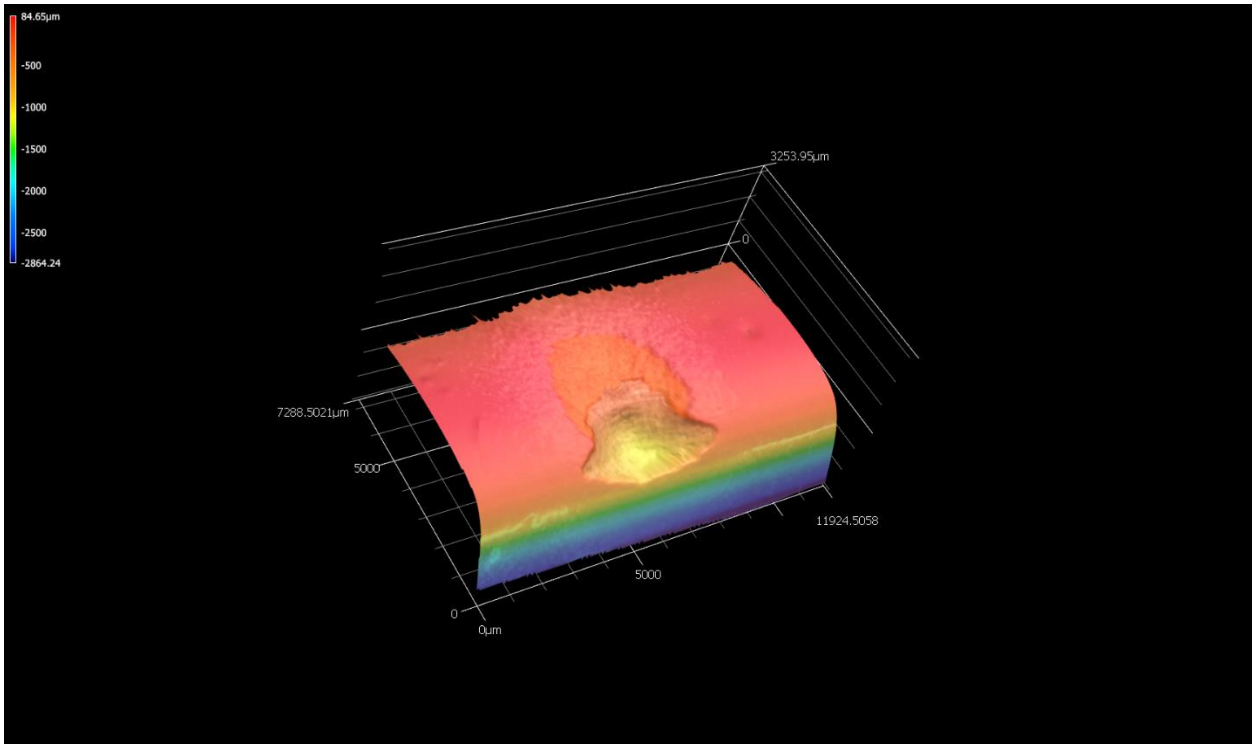


Fig. AVI-99: Erosion scar at -5° angle of impingement on the Polyurethane/IA-700 coated blade EXP1

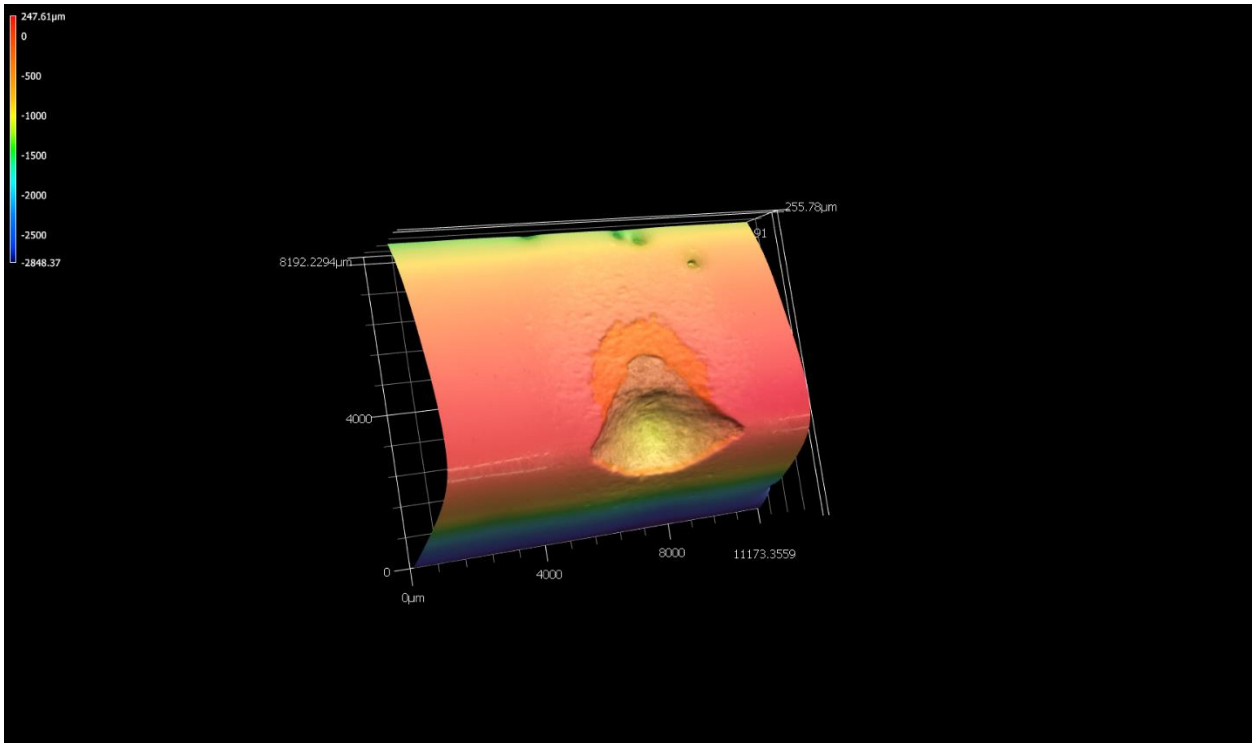


Fig. AVI-100: Erosion scar at -5° angle of impingement on the Polyurethane/IA-700 coated blade EXP2

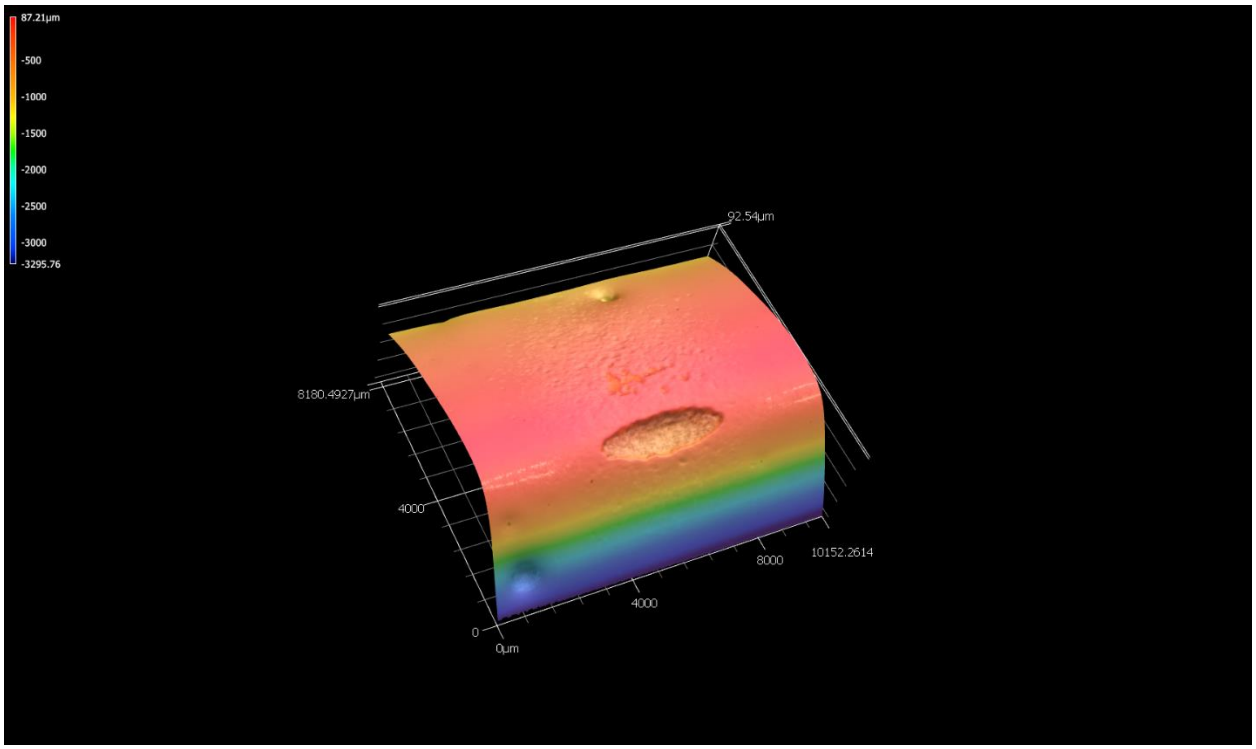


Fig. AVI-101: Erosion scar at -5° angle of impingement on the Polyurethane/IA-700 coated blade EXP3

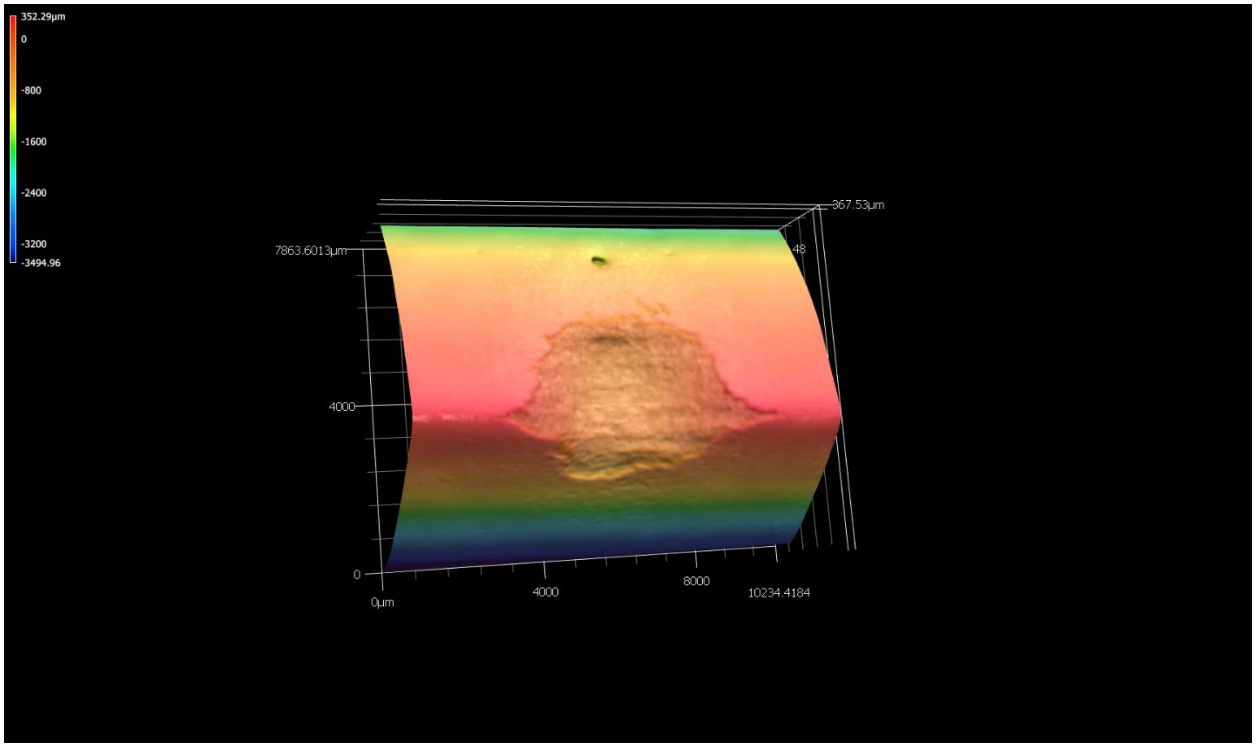


Fig. AVI-102: Erosion scar at -5° angle of impingement on the Polyurethane/IA-700 coated blade EXP4

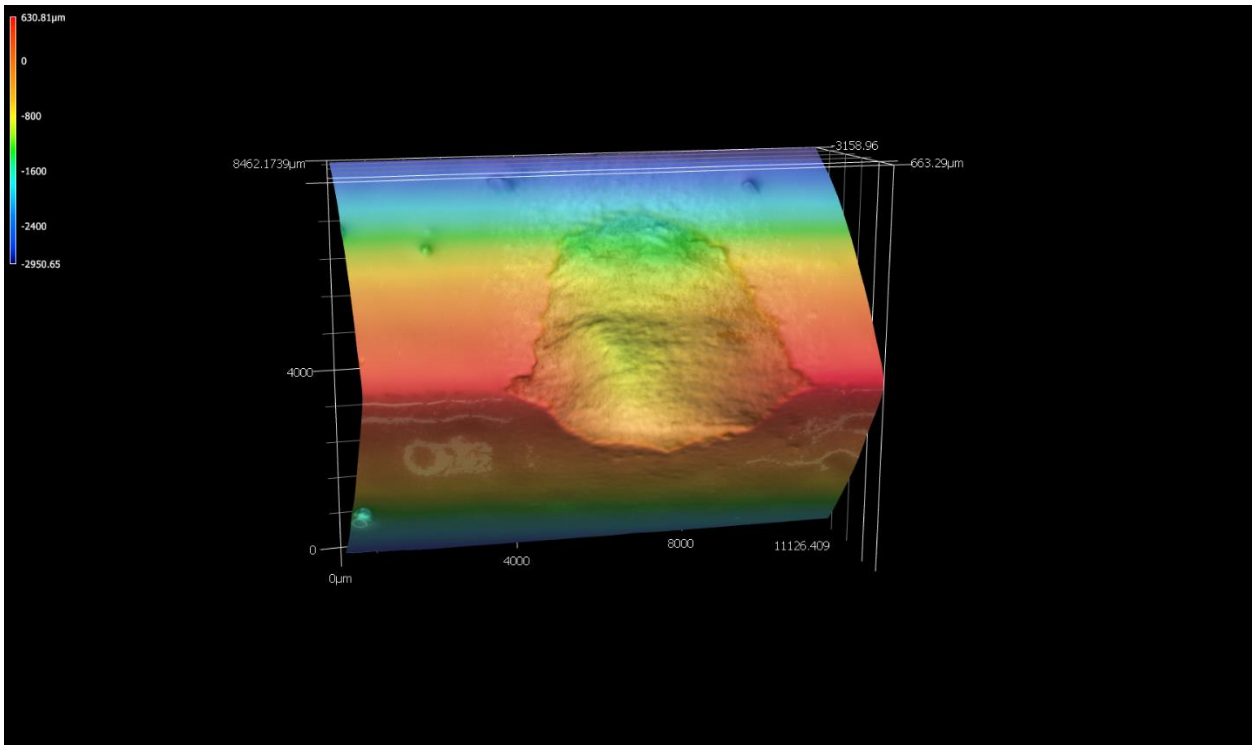


Fig. AVI-103: Erosion scar at -5° angle of impingement on the Polyurethane/IA-700 coated blade EXP5

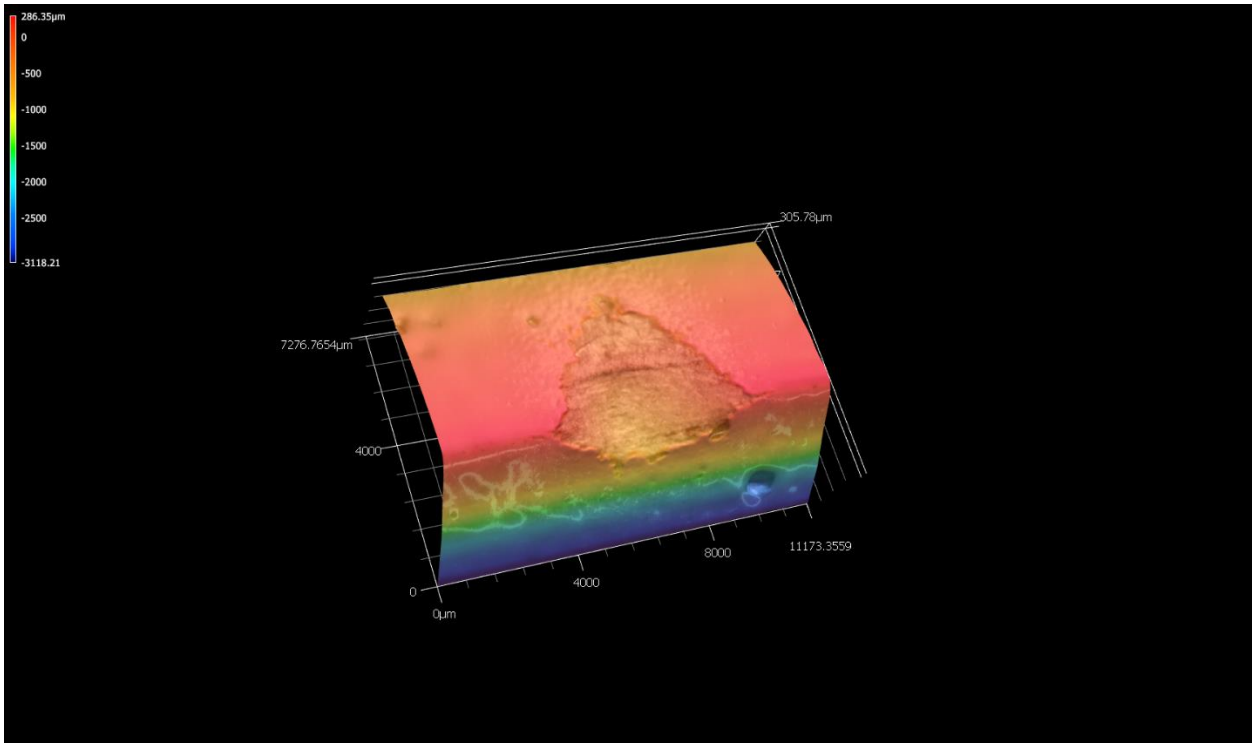


Fig. AVI-104: Erosion scar at -5° angle of impingement on the Polyurethane/IA-700 coated blade EXP6

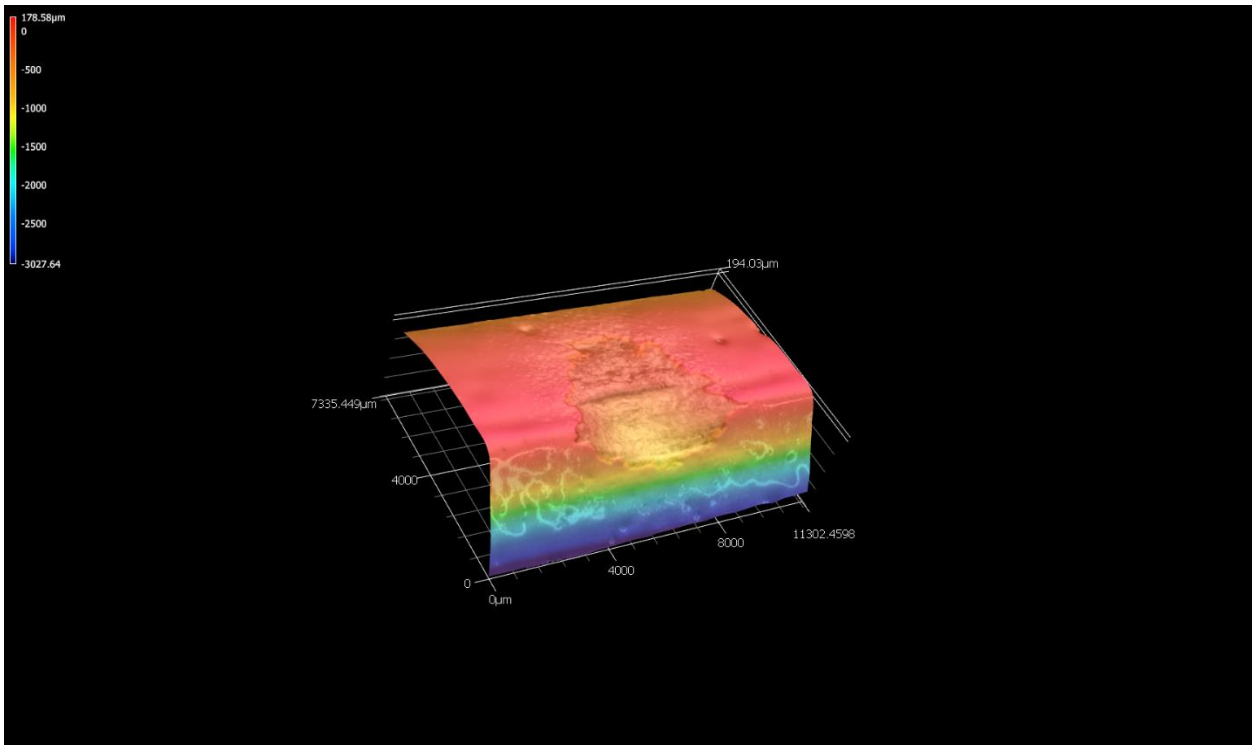


Fig. AVI-105: Erosion scar at -5° angle of impingement on the Polyurethane/IA-700 coated blade EXP7

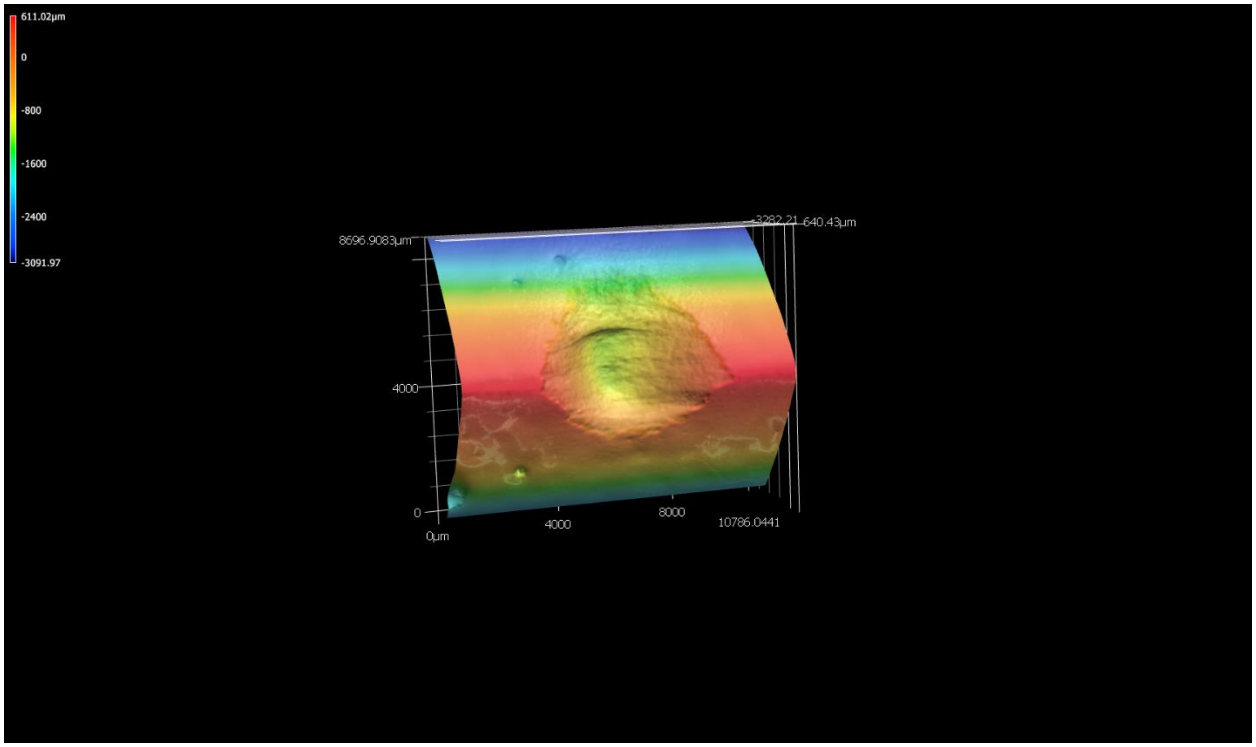


Fig. AVI-106: Erosion scar at -5° angle of impingement on the Polyurethane/IA-700 coated blade EXP8

- **0 degrees**
  - **Uncoated**

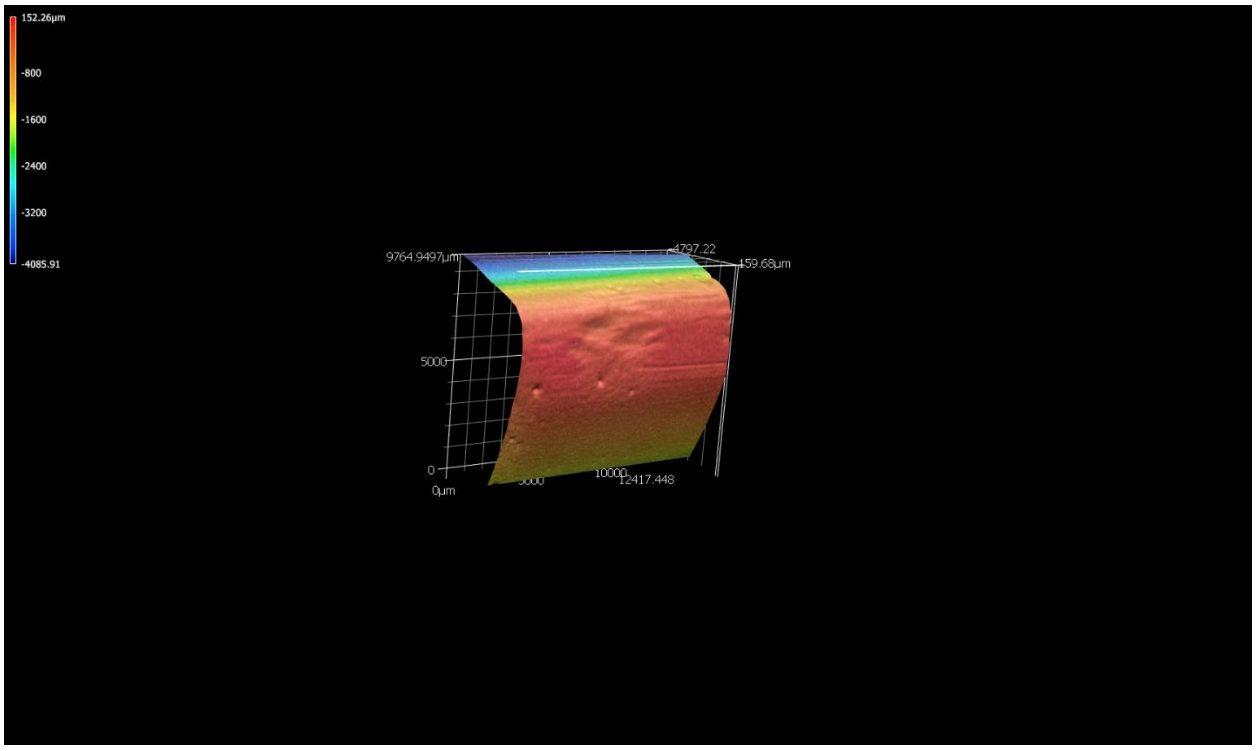


Fig. AVI-107: Erosion scar at 0° angle of impingement on the uncoated blade EXP1

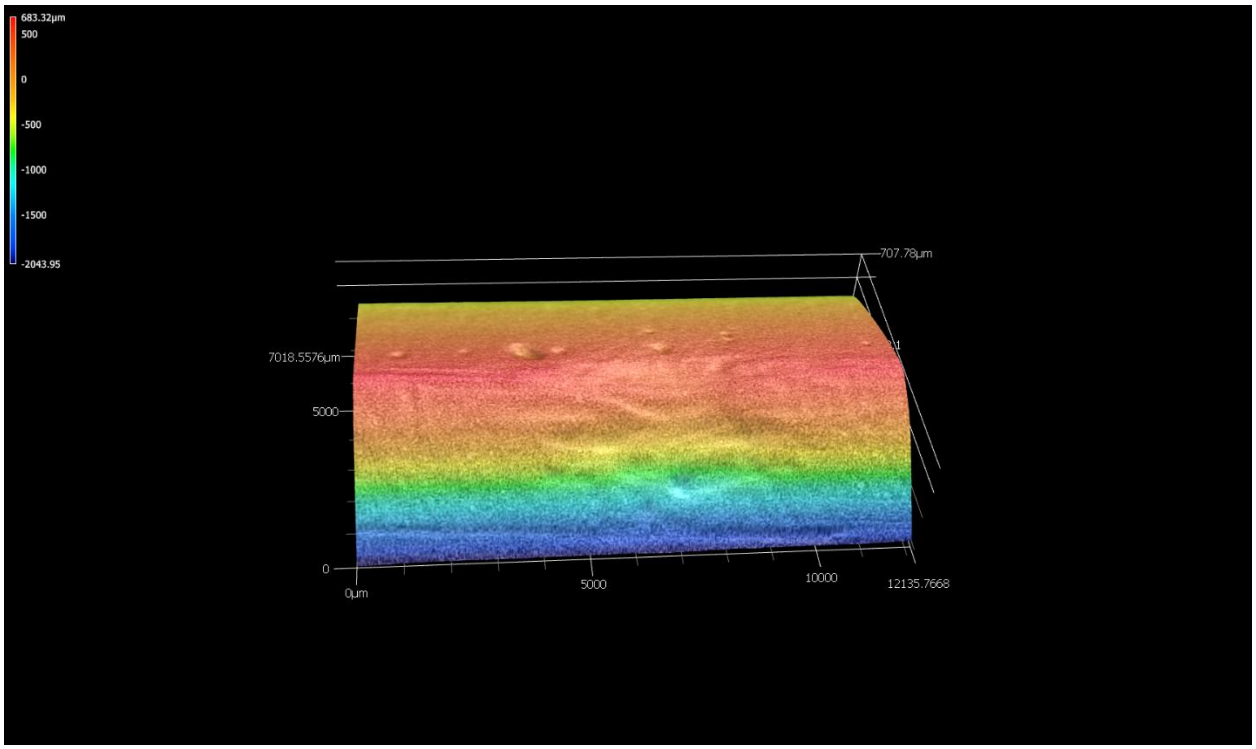


Fig. AVI-108: Erosion scar at 0° angle of impingement on the uncoated blade EXP2

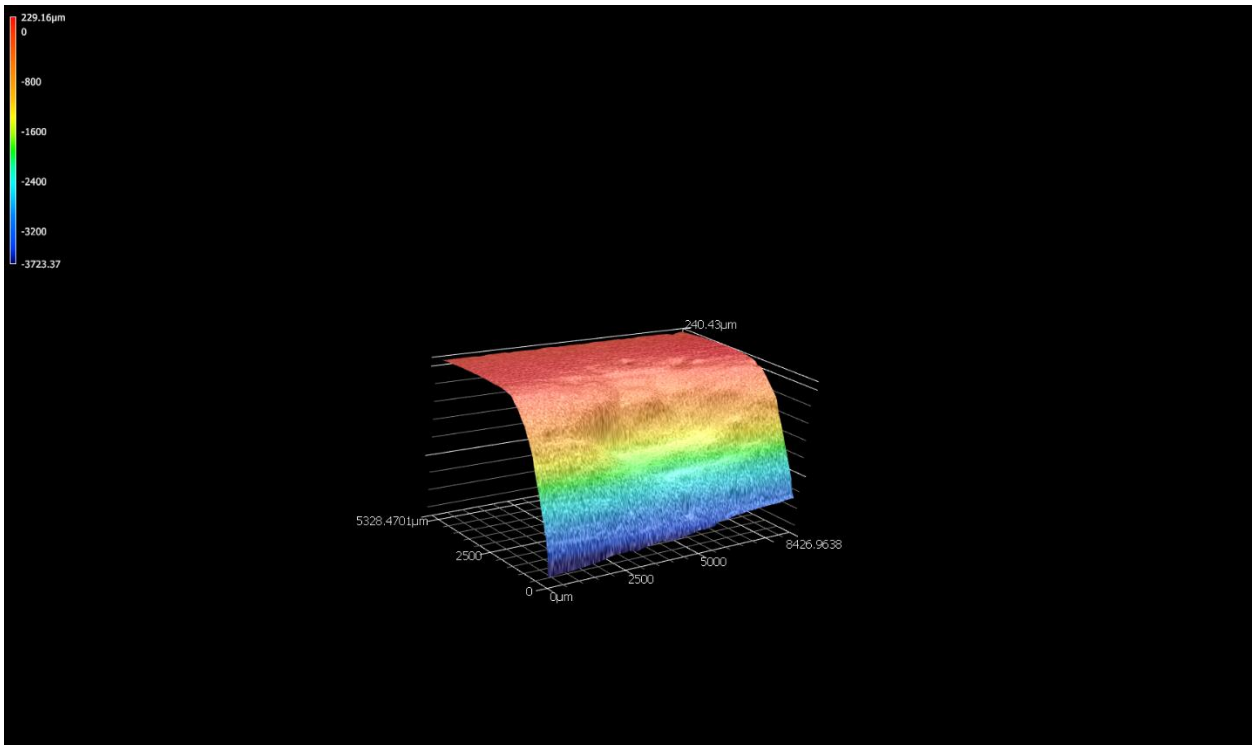


Fig. AVI-109: Erosion scar at 0° angle of impingement on the uncoated blade EXP3

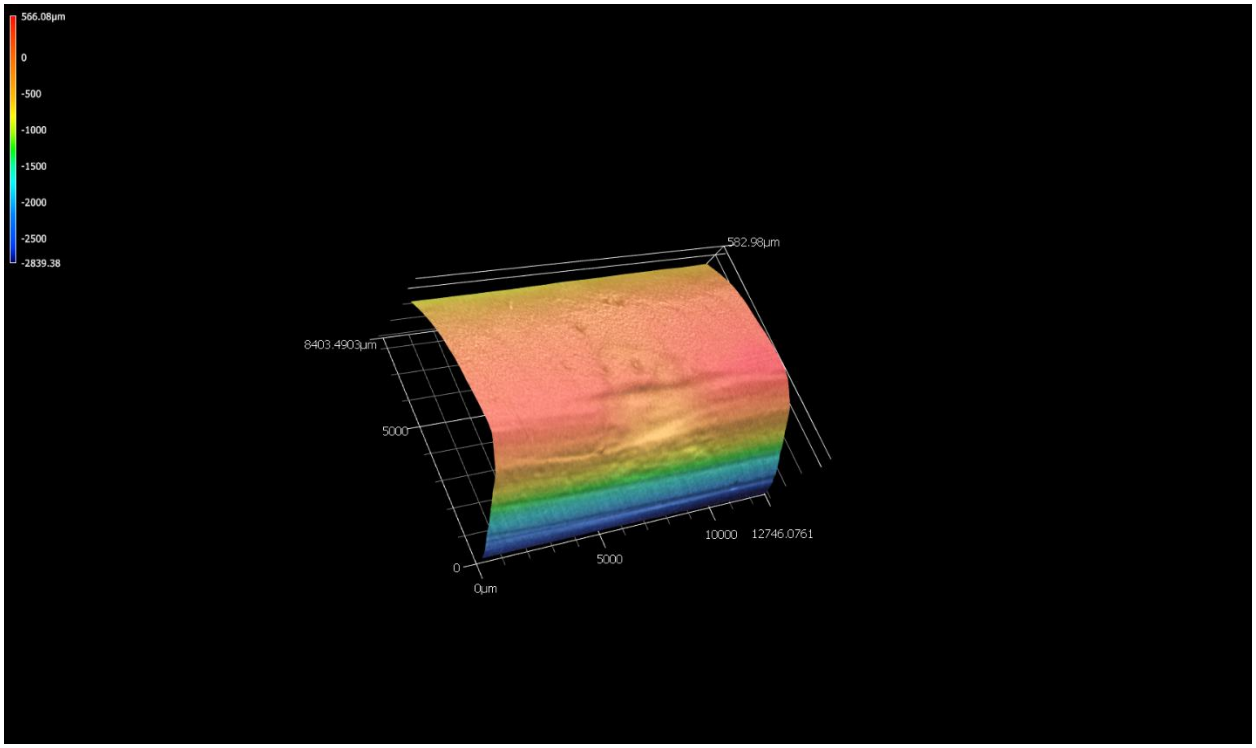


Fig. AVI-110: Erosion scar at 0° angle of impingement on the uncoated blade EXP4

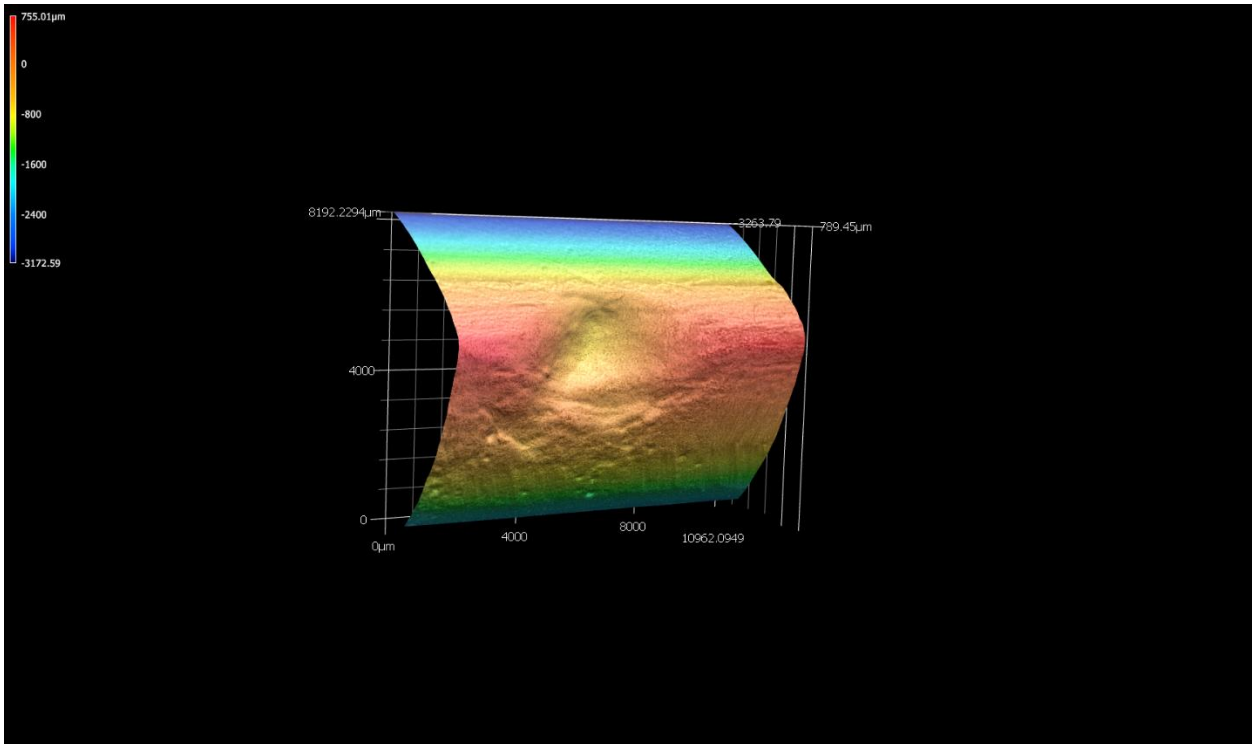


Fig. AVI-111: Erosion scar at 0° angle of impingement on the uncoated blade EXP5

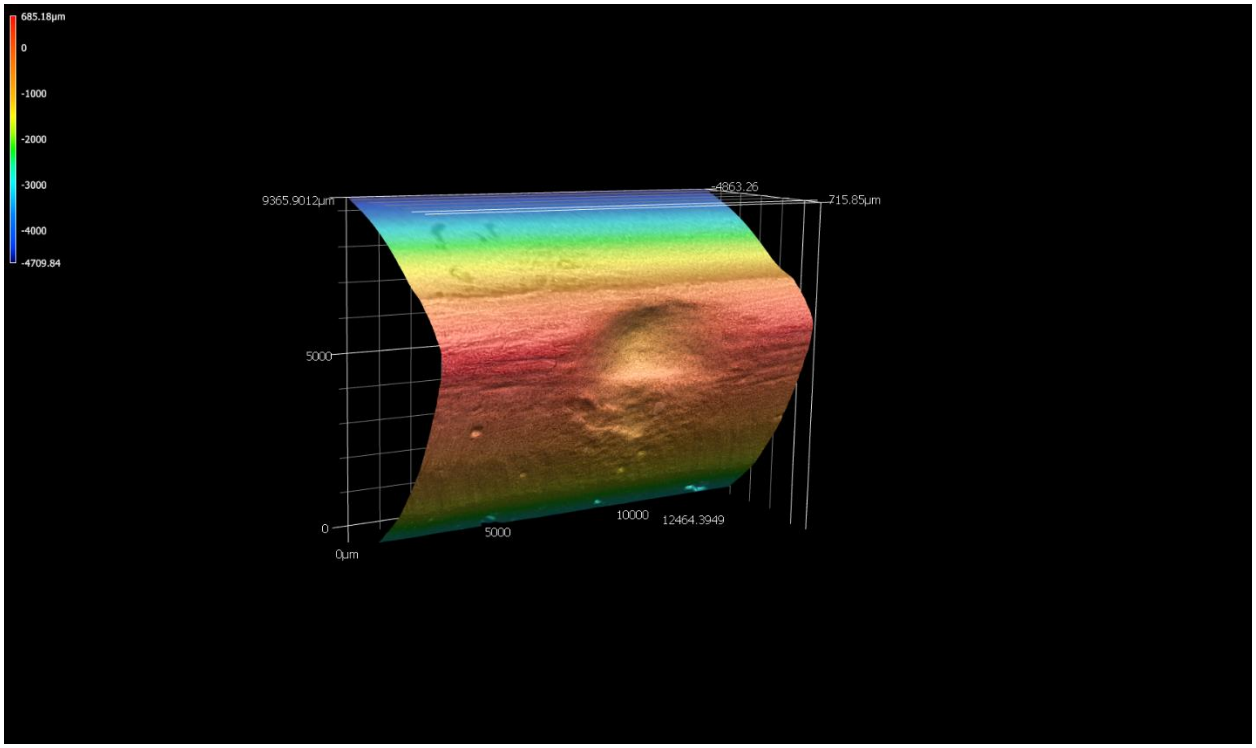


Fig. AVI-112: Erosion scar at 0° angle of impingement on the uncoated blade EXP6

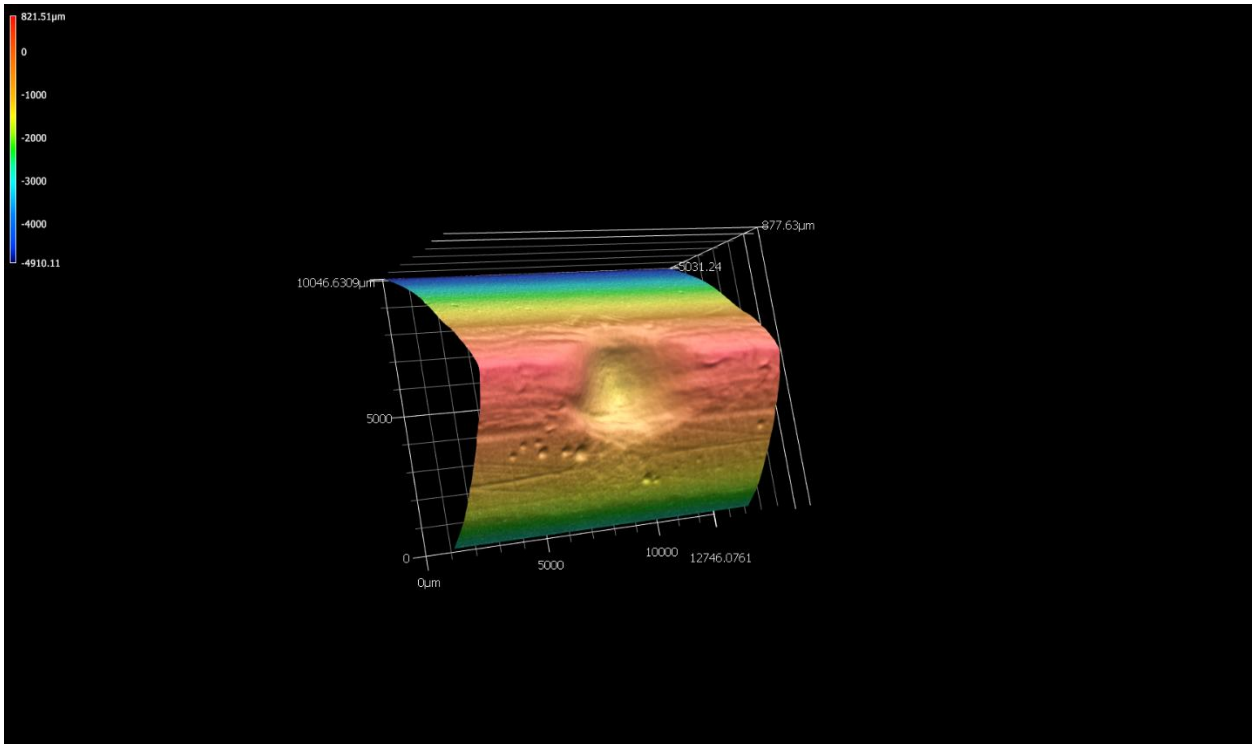


Fig. AVI-113: Erosion scar at 0° angle of impingement on the uncoated blade EXP7

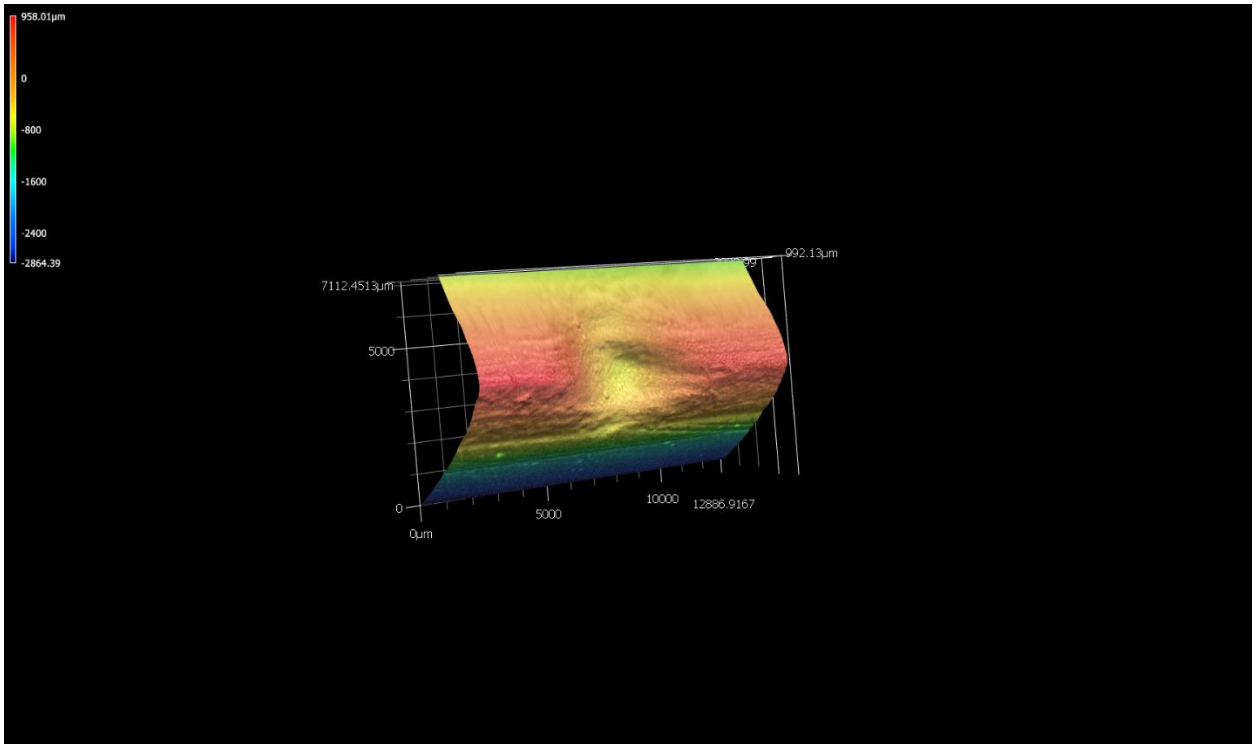


Fig. AVI-114: Erosion scar at 0° angle of impingement on the uncoated blade EXP8

- **H-146**

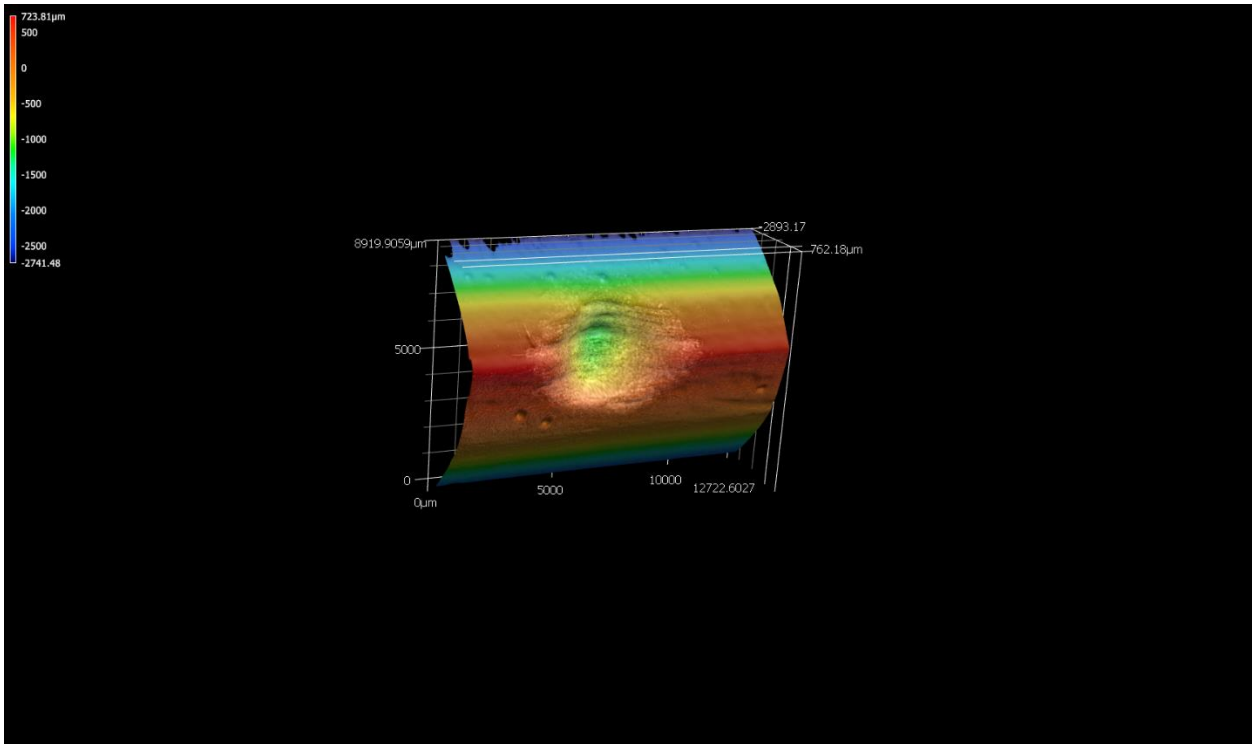


Fig. AVI-115: Erosion scar at 0° angle of impingement on the H-146 coated blade EXP1

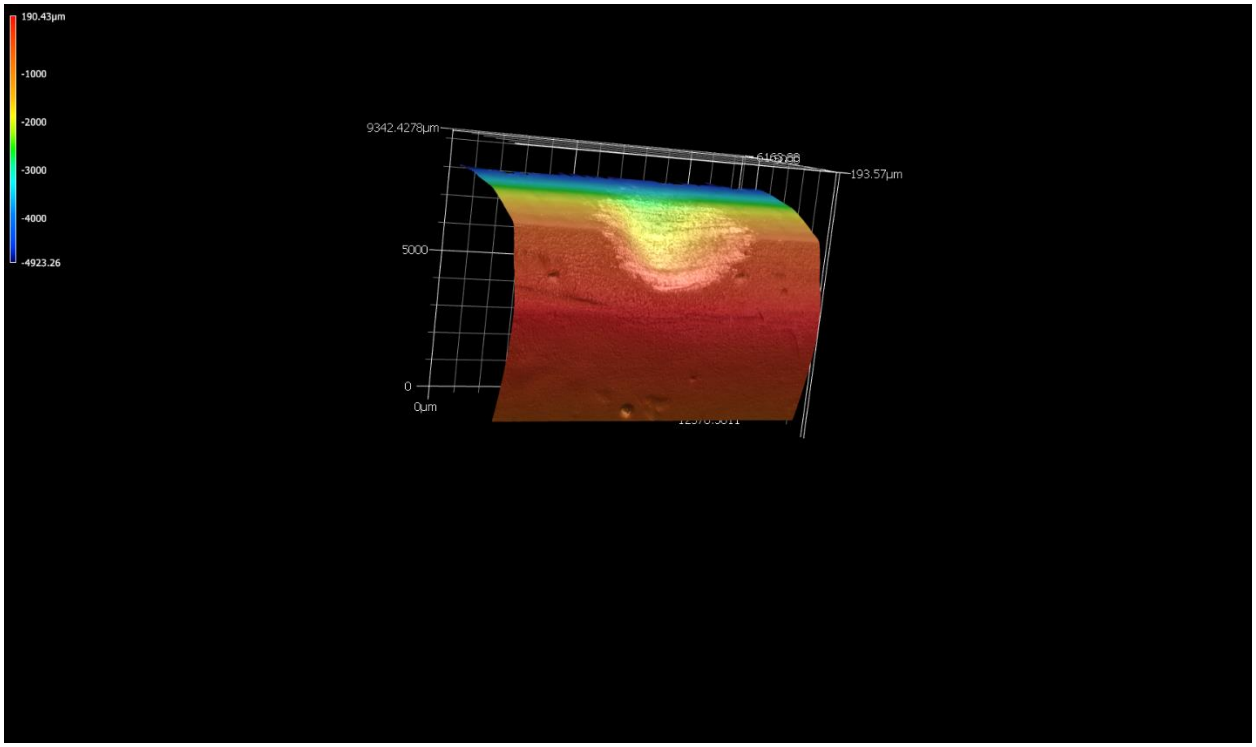


Fig. AVI-116: Erosion scar at 0° angle of impingement on the H-146 coated blade EXP2

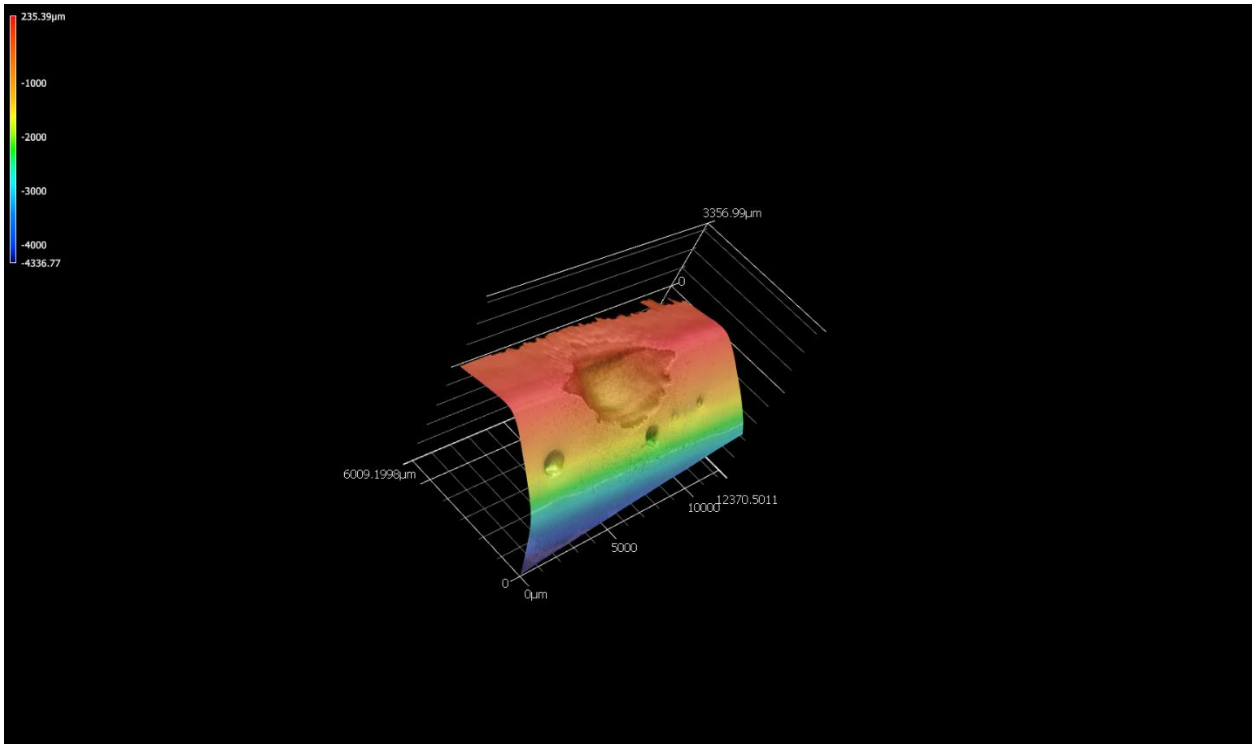


Fig. AVI-117: Erosion scar at 0° angle of impingement on the H-146 coated blade EXP3

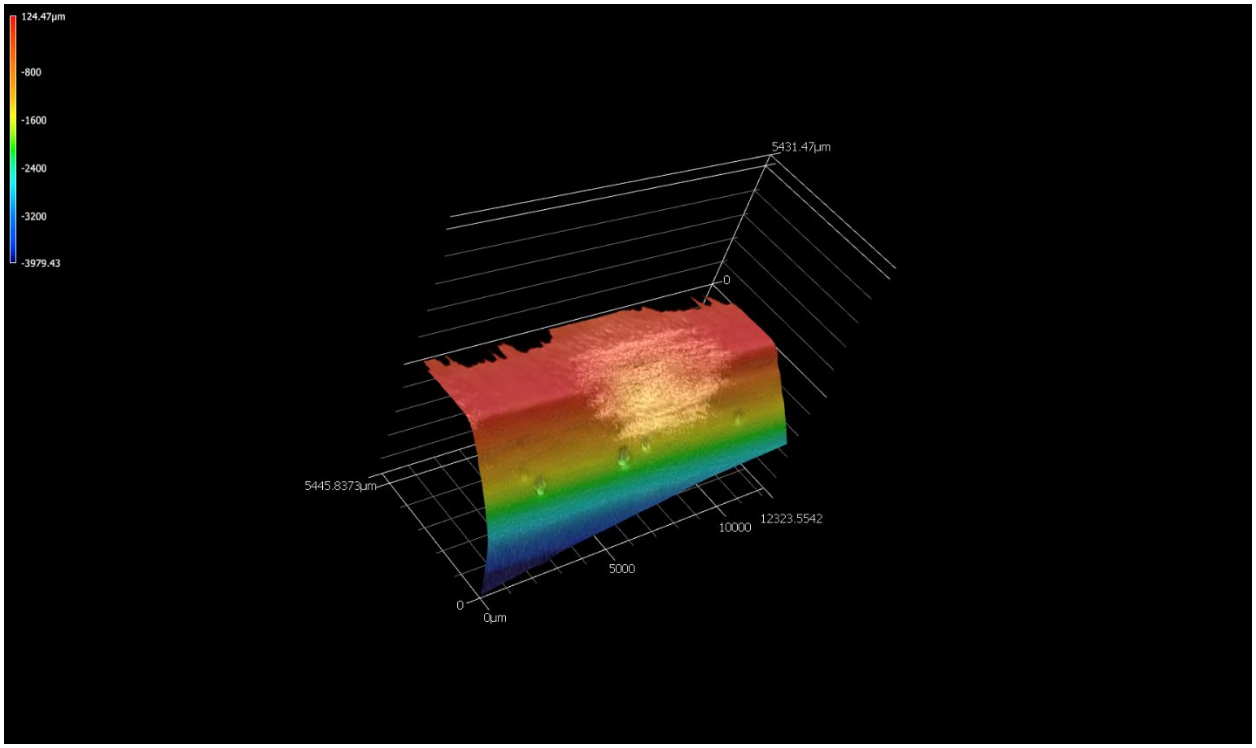


Fig. AVI-118: Erosion scar at 0° angle of impingement on the H-146 coated blade EXP4

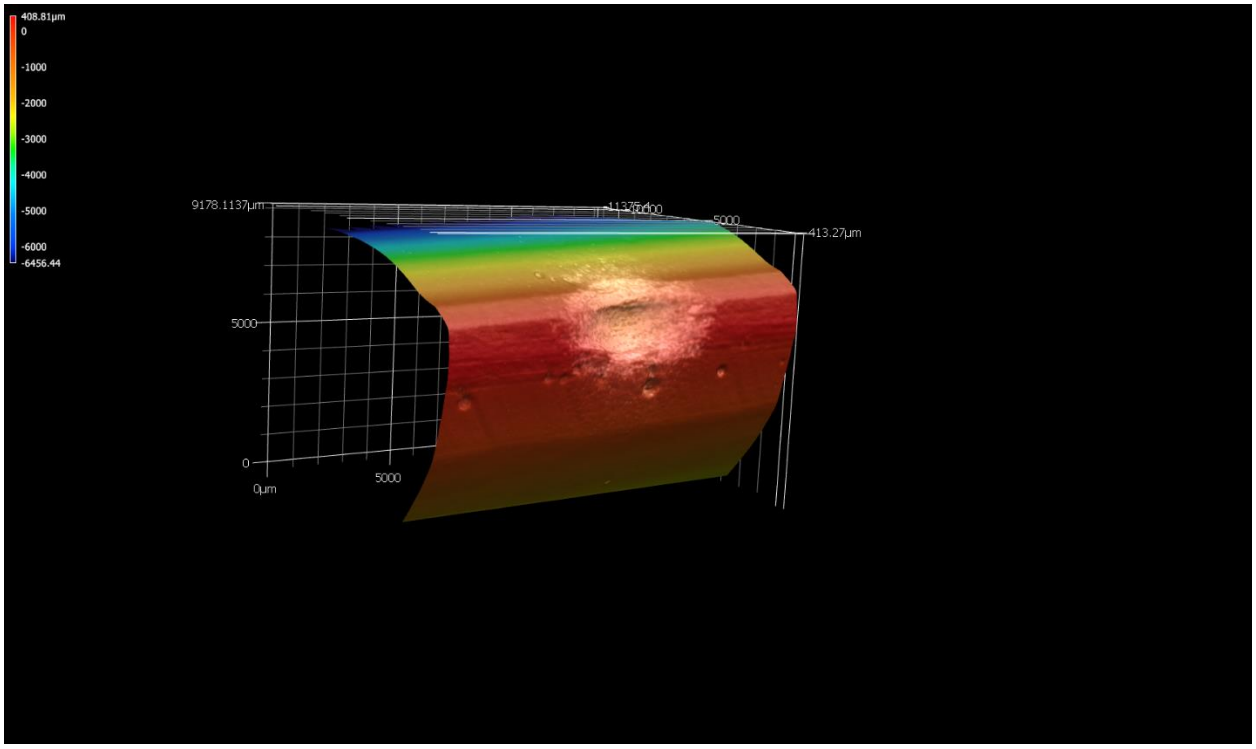


Fig. AVI-119: Erosion scar at 0° angle of impingement on the H-146 coated blade EXP5

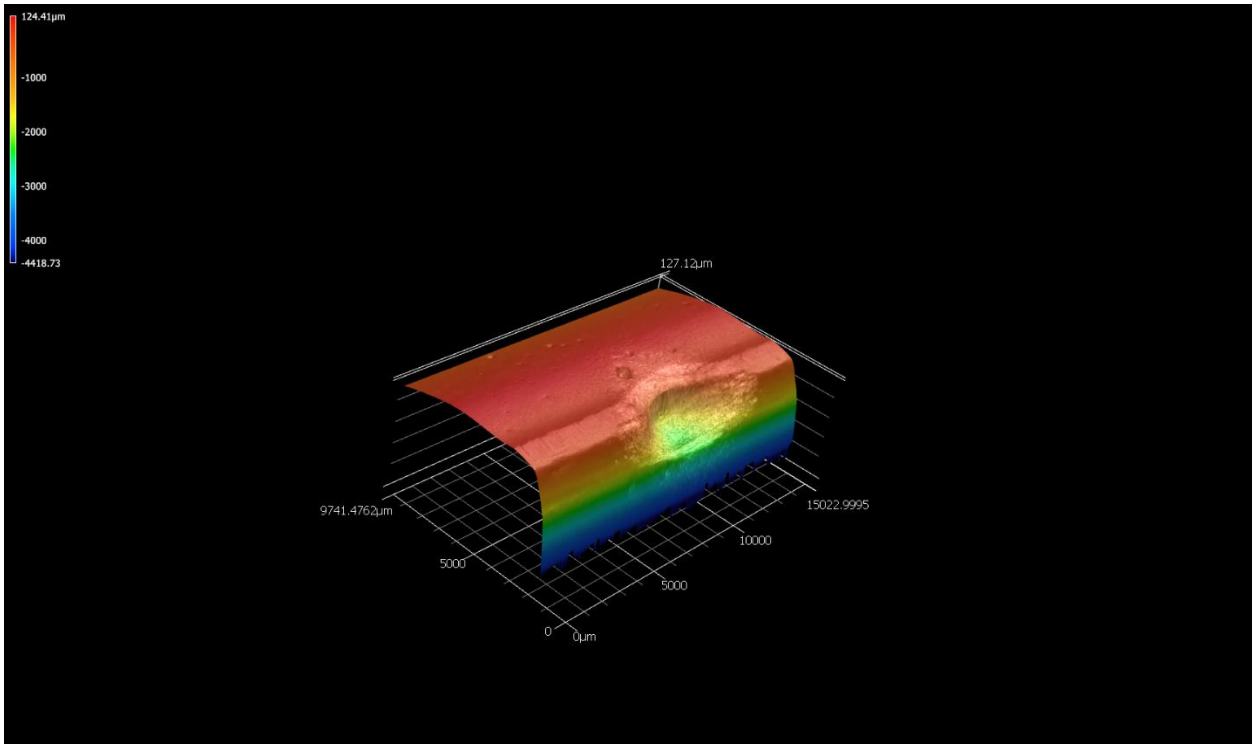


Fig. AVI-120: Erosion scar at 0° angle of impingement on the H-146 coated blade EXP6

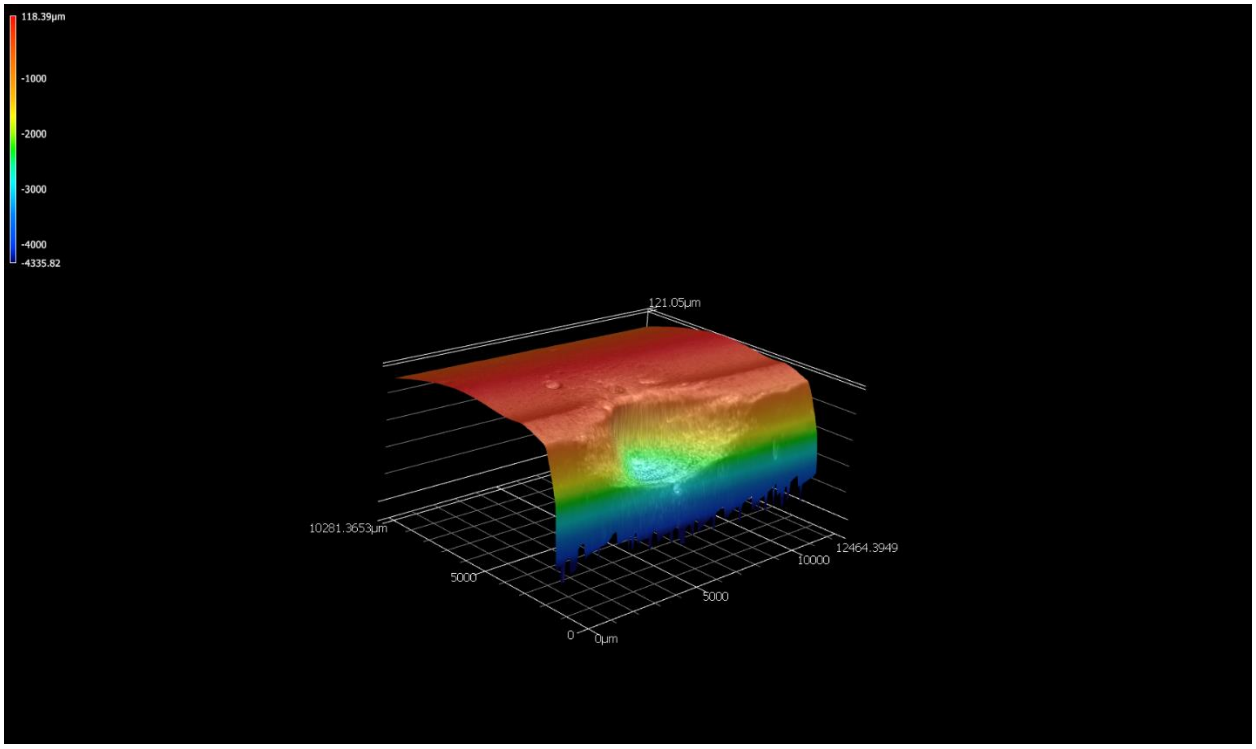


Fig. AVI-121: Erosion scar at 0° angle of impingement on the H-146 coated blade EXP7

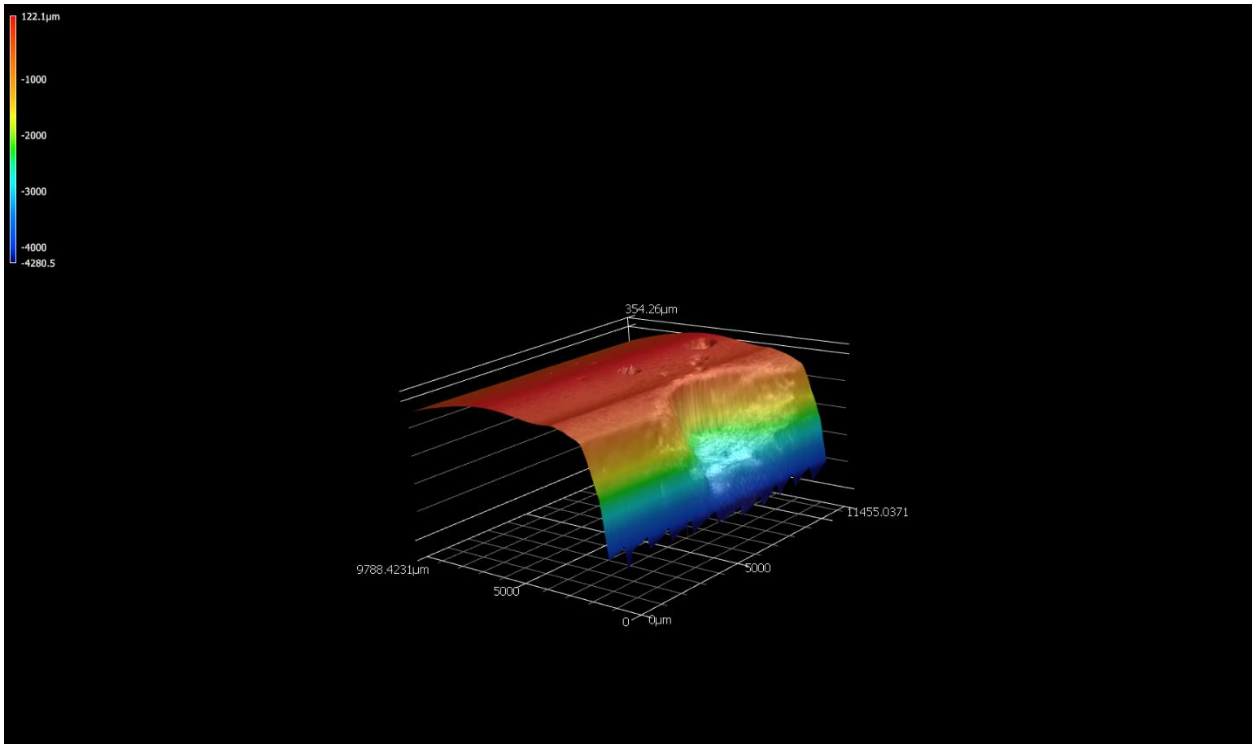


Fig. AVI-122: Erosion scar at 0° angle of impingement on the H-146 coated blade EXP8

- **Polyurethane/IA-700**

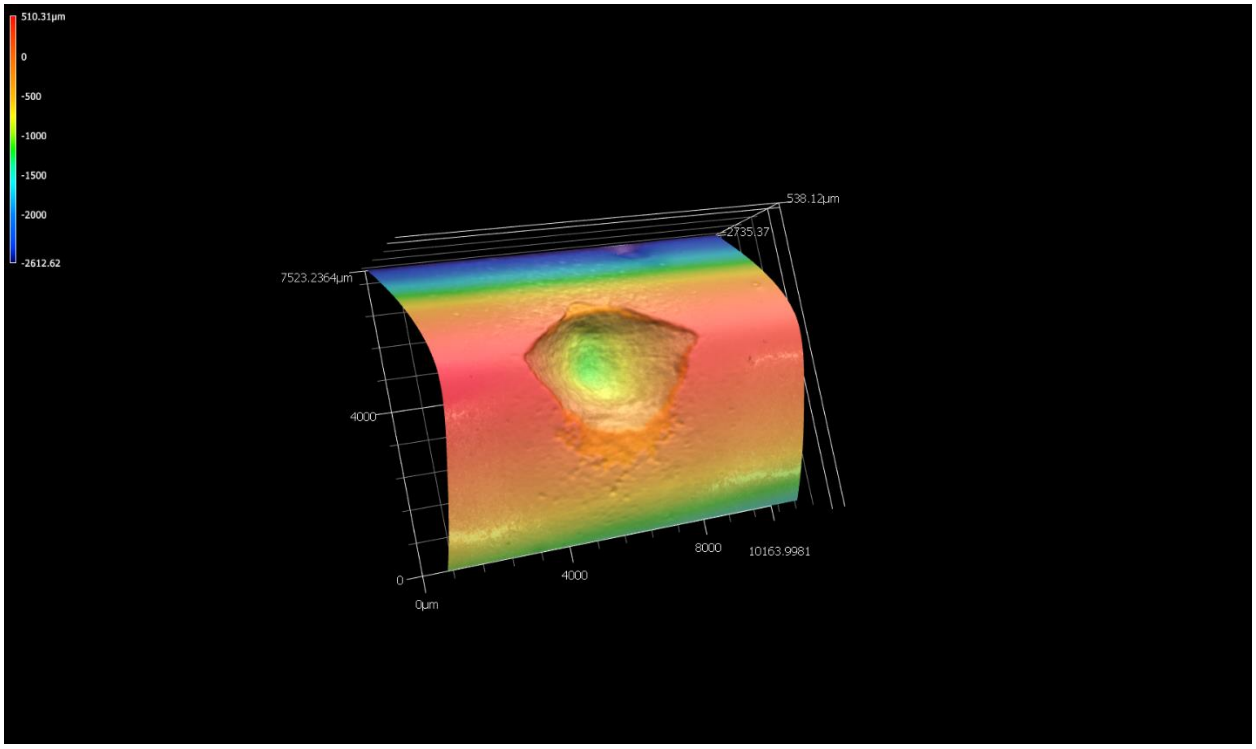


Fig. AVI-123: Erosion scar at 0° angle of impingement on the Polyurethane/IA-700 coated blade EXP1

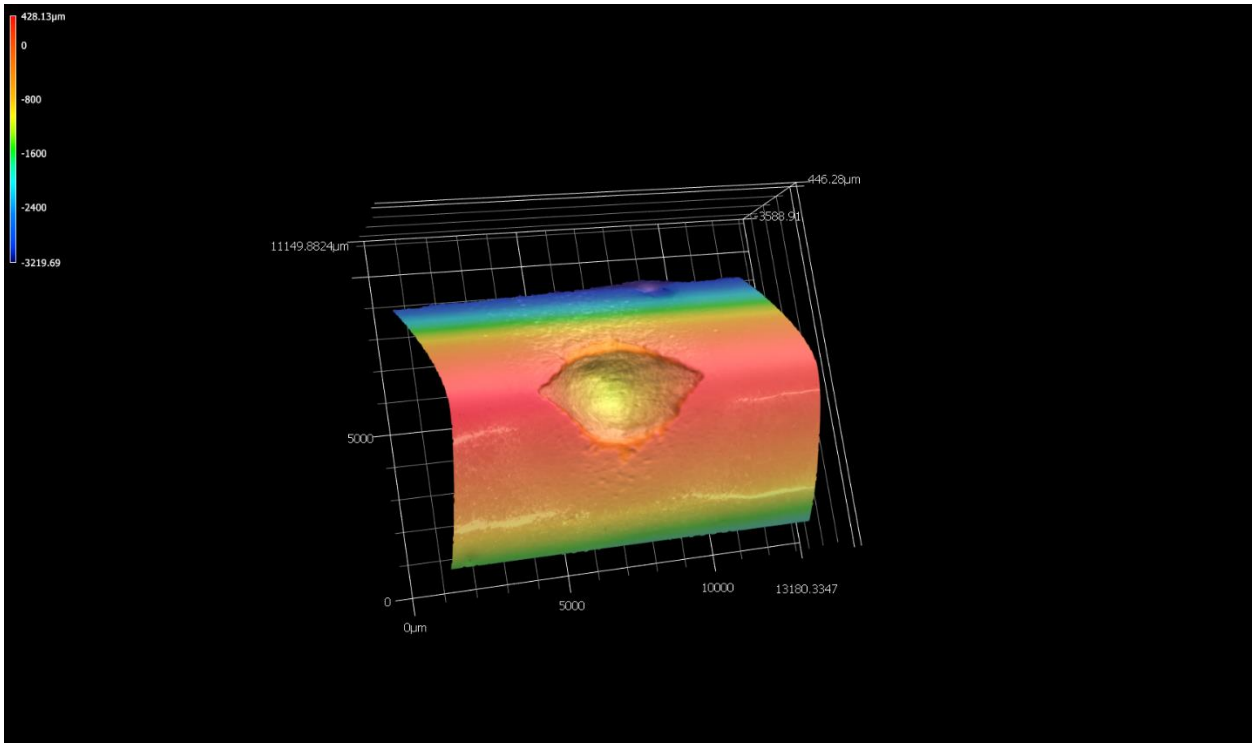


Fig. AVI-124: Erosion scar at 0° angle of impingement on the Polyurethane/IA-700 coated blade EXP2

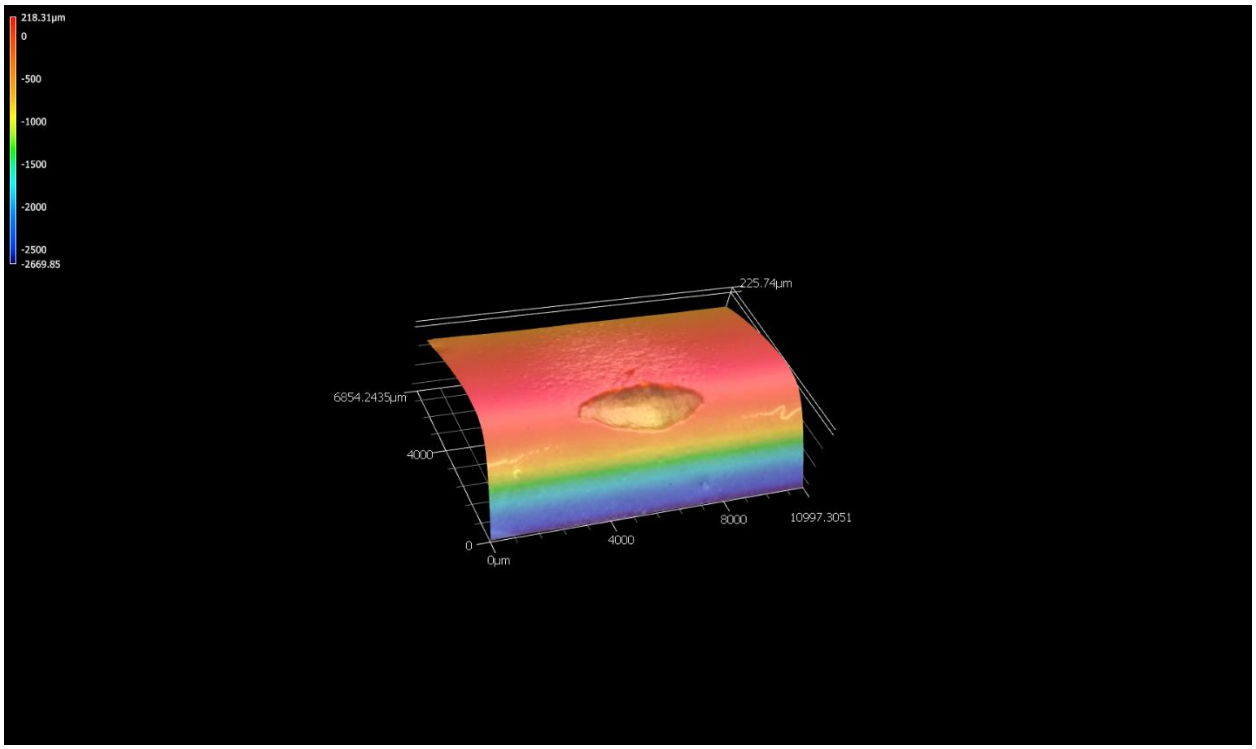


Fig. AVI-125: Erosion scar at 0° angle of impingement on the Polyurethane/IA-700 coated blade EXP3

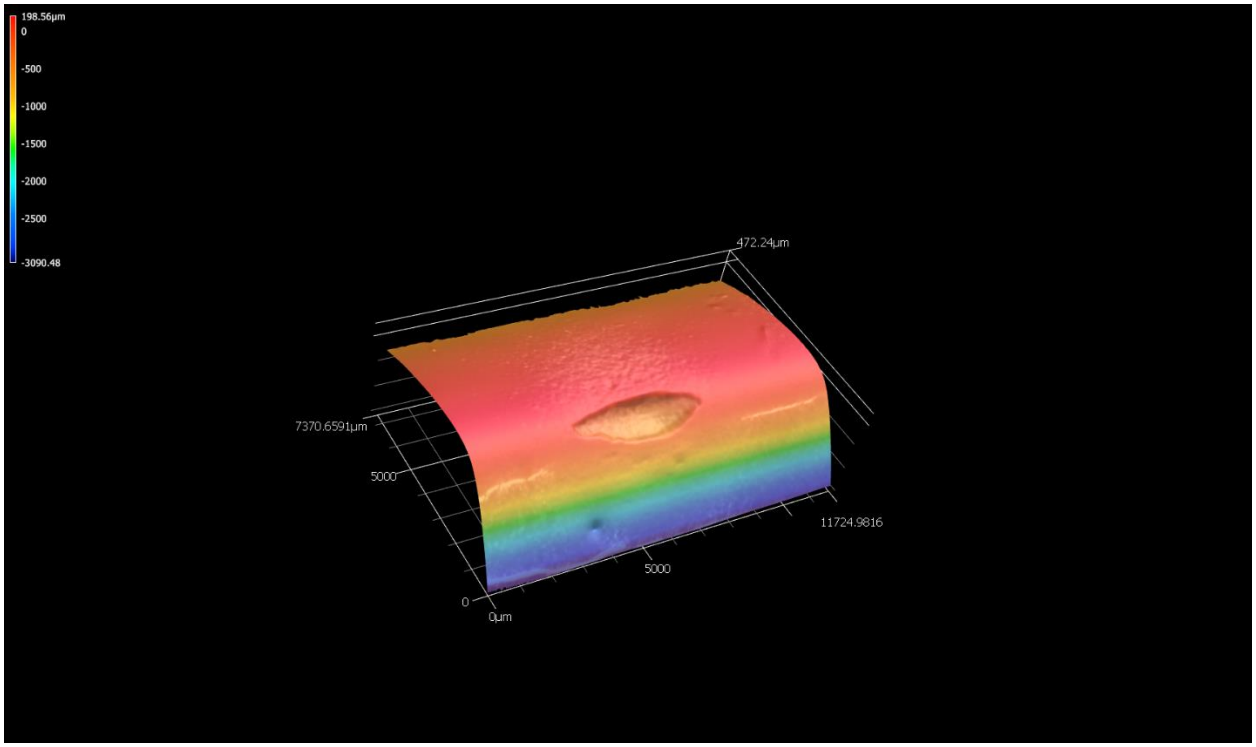


Fig. AVI-126: Erosion scar at 0° angle of impingement on the Polyurethane/IA-700 coated blade EXP4

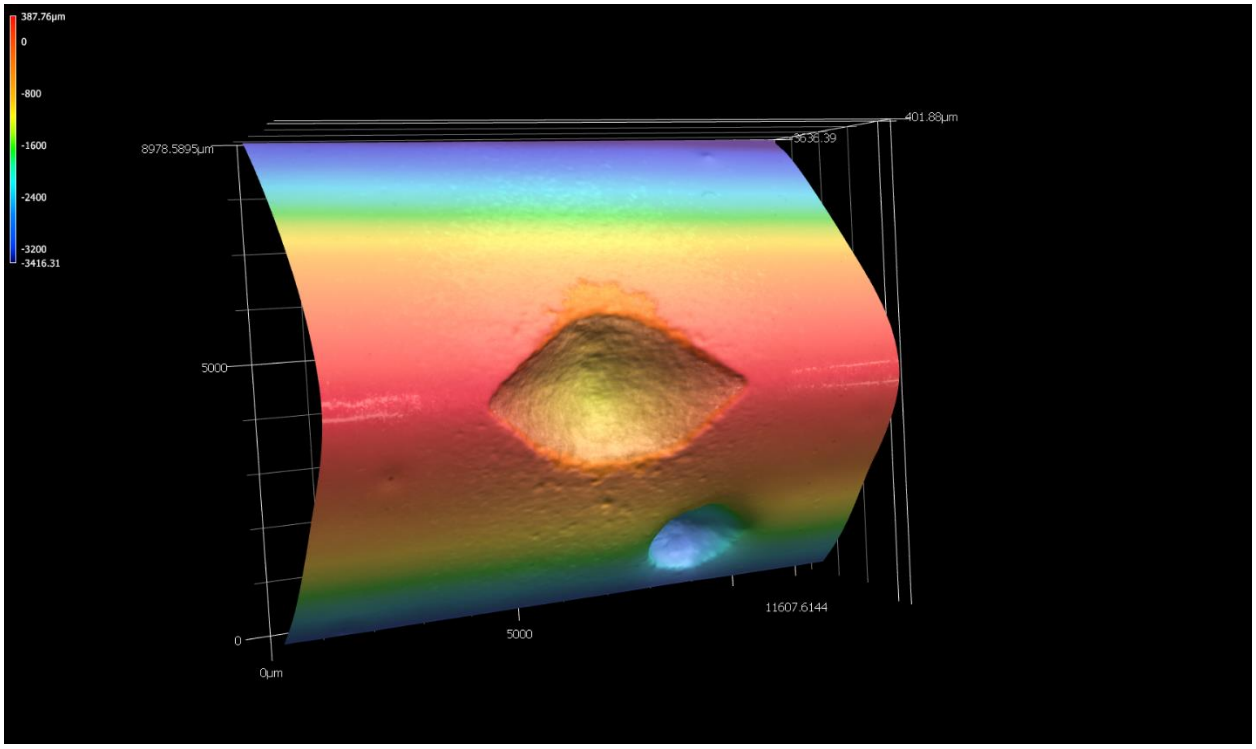


Fig. AVI-127: Erosion scar at 0° angle of impingement on the Polyurethane/IA-700 coated blade EXP5

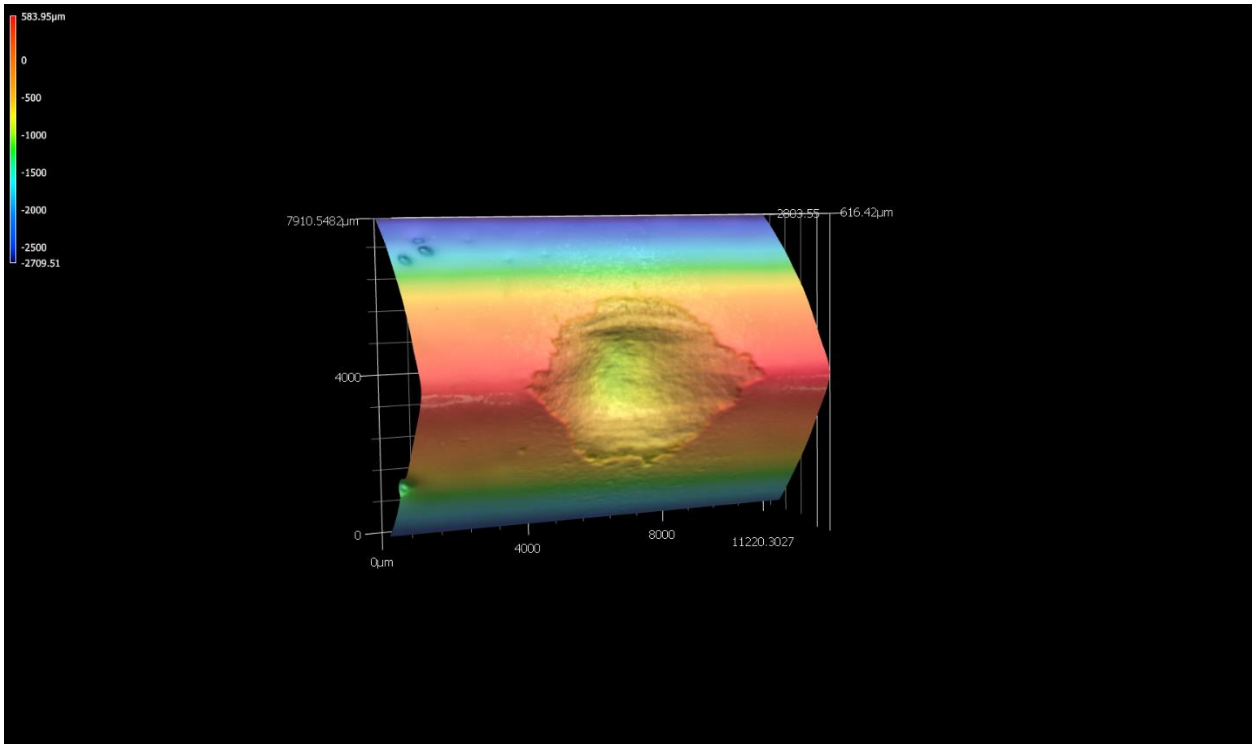


Fig. AVI-128: Erosion scar at 0° angle of impingement on the Polyurethane/IA-700 coated blade EXP6

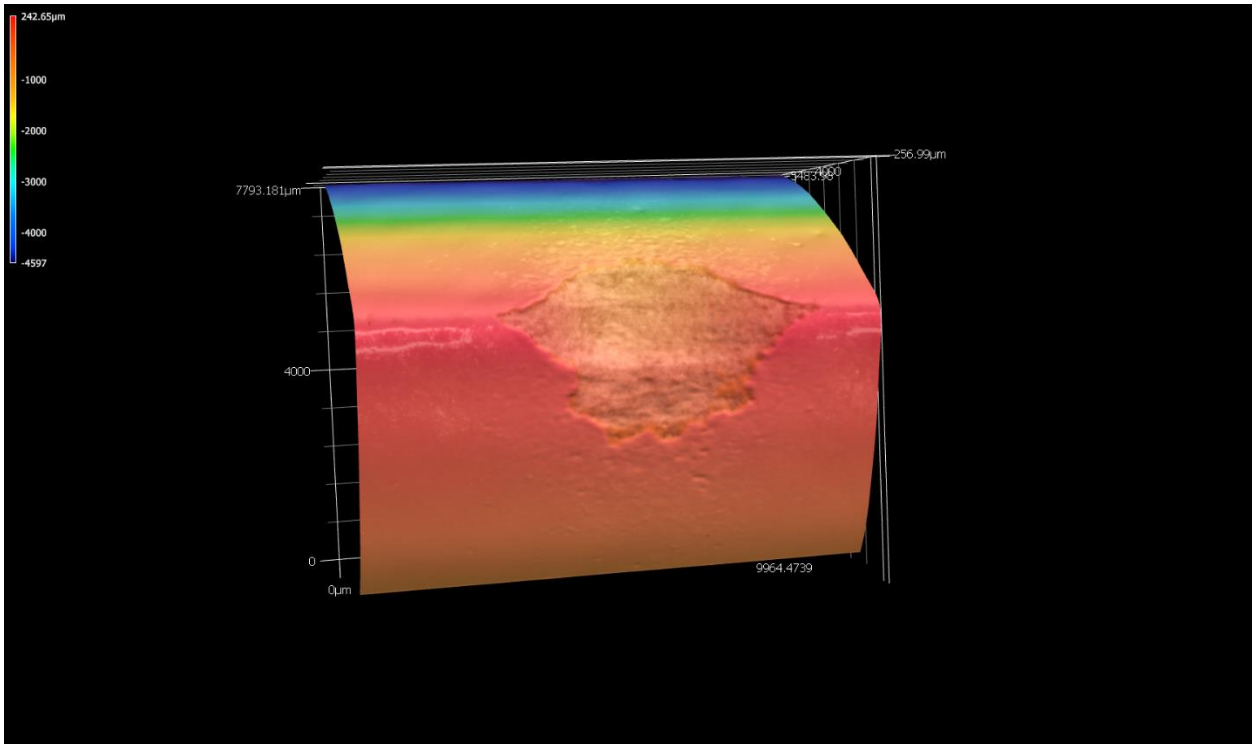


Fig. AVI-129: Erosion scar at 0° angle of impingement on the Polyurethane/IA-700 coated blade EXP7

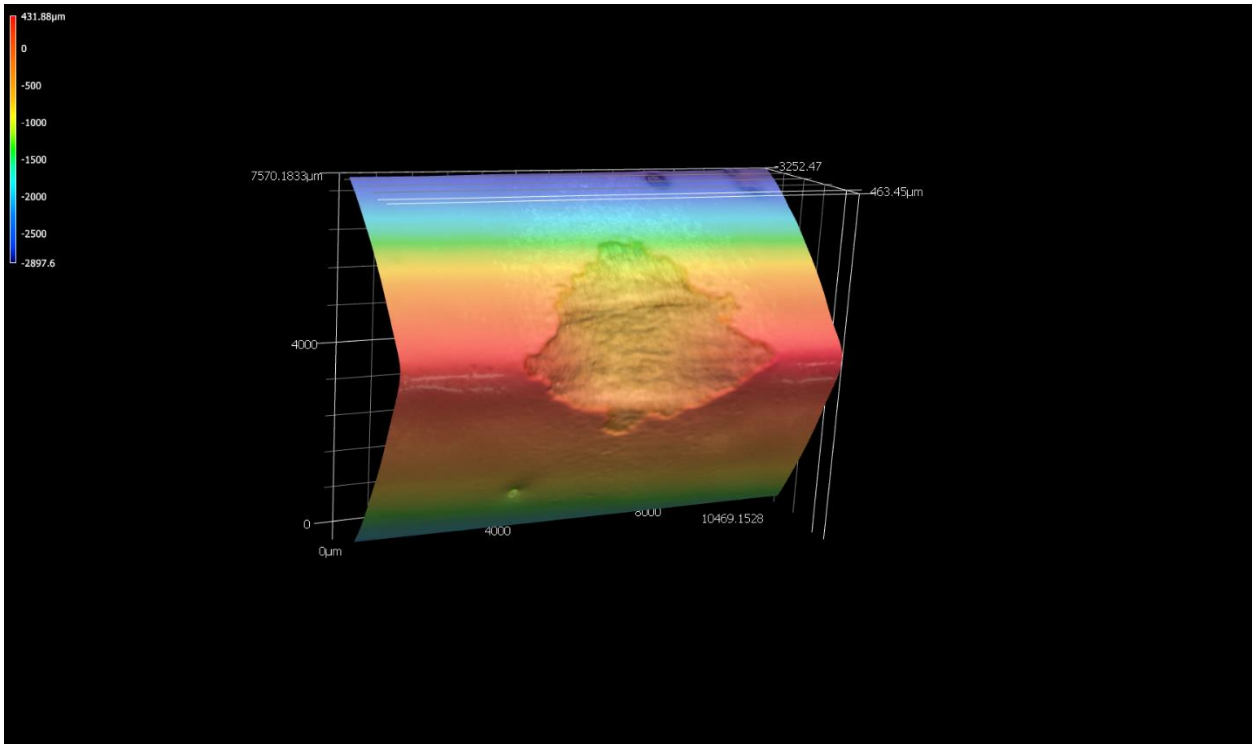


Fig. AVI-130: Erosion scar at 0° angle of impingement on the Polyurethane/IA-700 coated blade EXP8

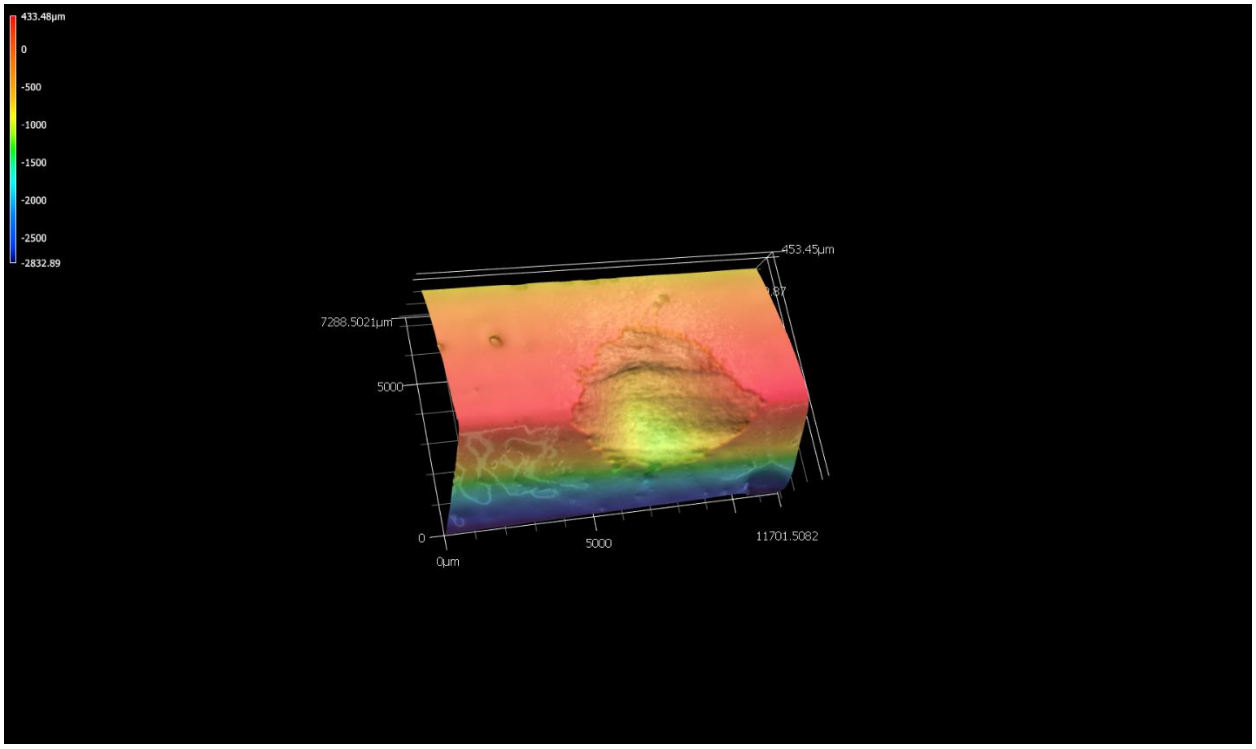


Fig. AVI-131: Erosion scar at 0° angle of impingement on the Polyurethane/IA-700 coated blade EXP9

- **5 degrees**
  - **Uncoated**

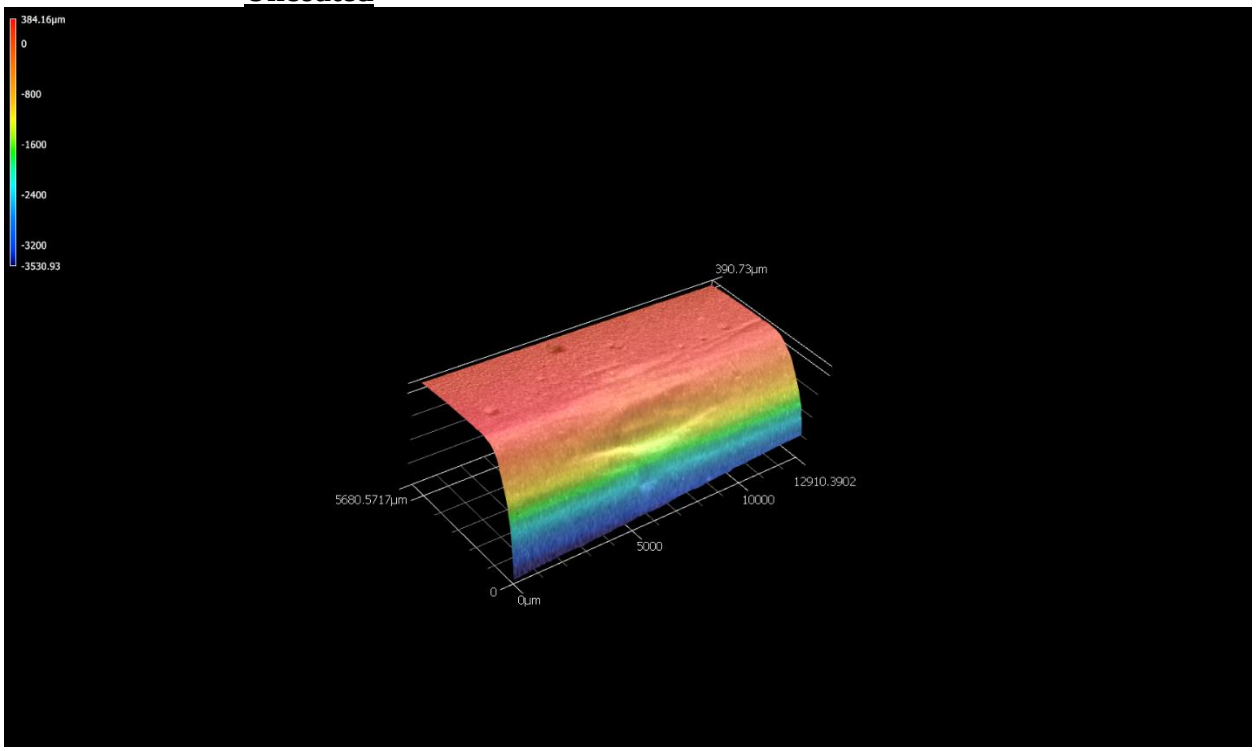


Fig. AVI-132: Erosion scar at 5° angle of impingement on the uncoated blade EXP1

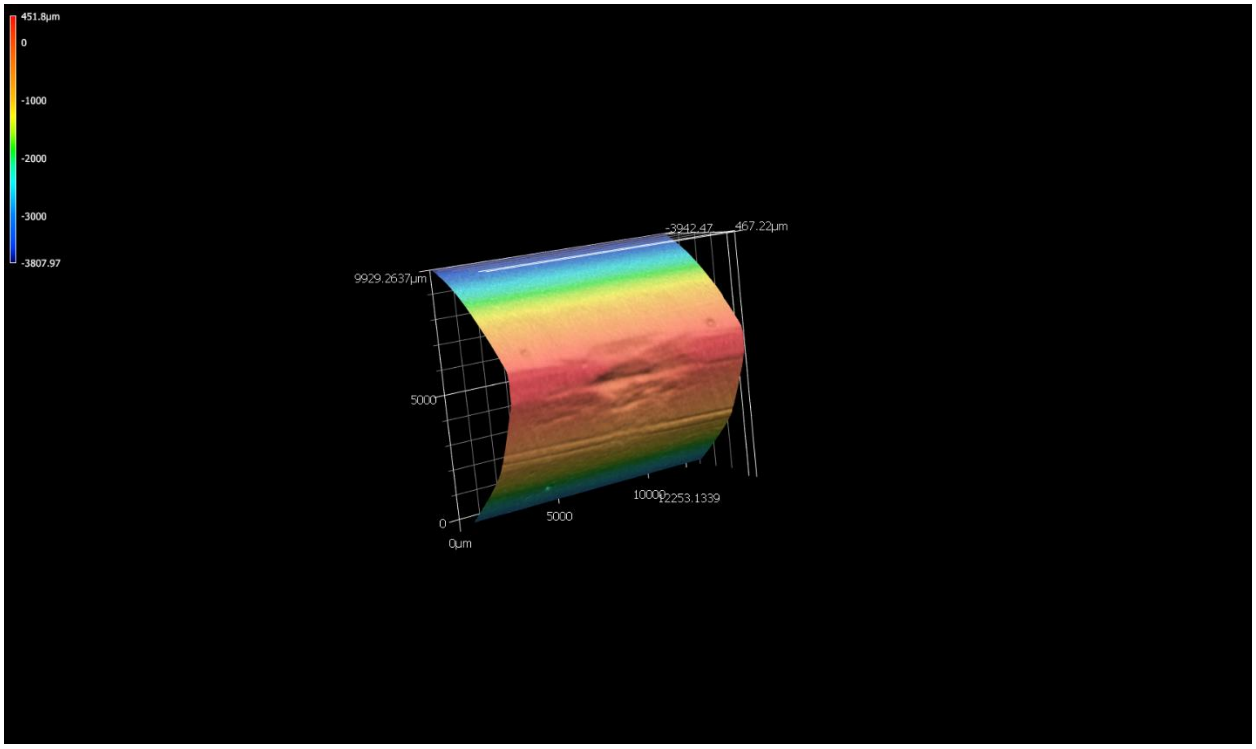


Fig. AVI-133: Erosion scar at 5° angle of impingement on the uncoated blade EXP2

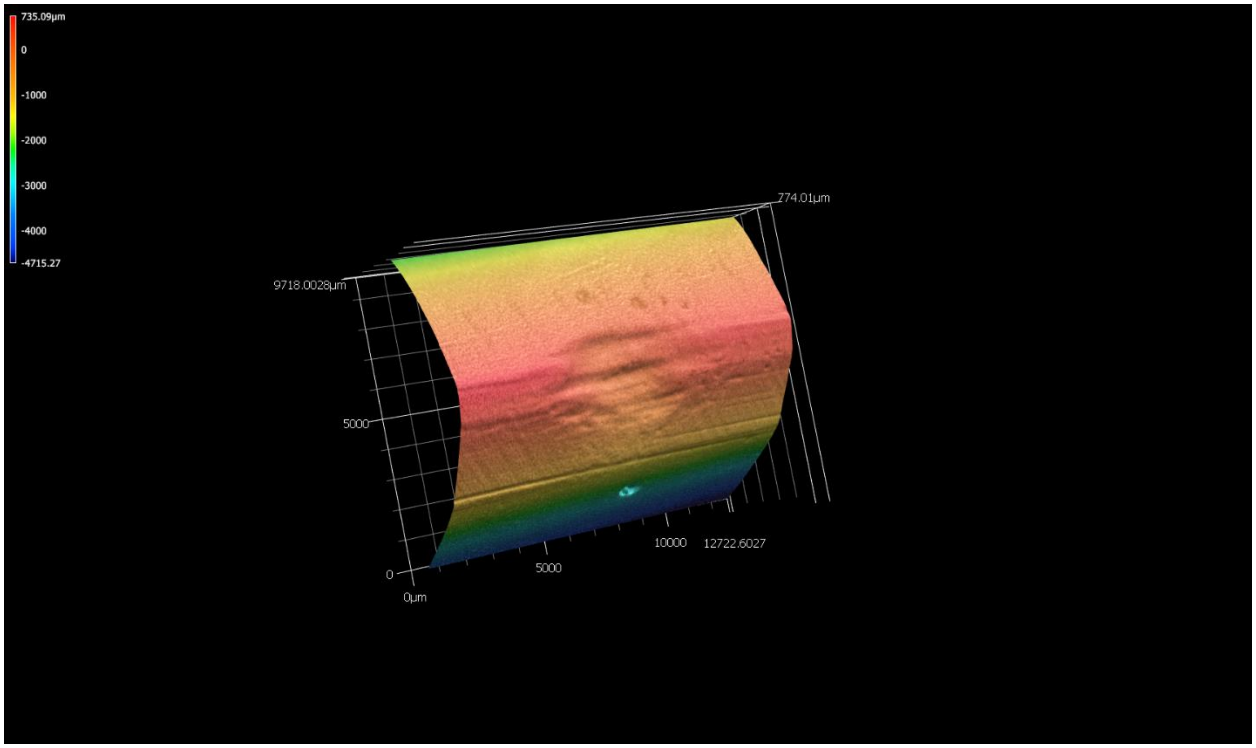


Fig. AVI-134: Erosion scar at 5° angle of impingement on the uncoated blade EXP3

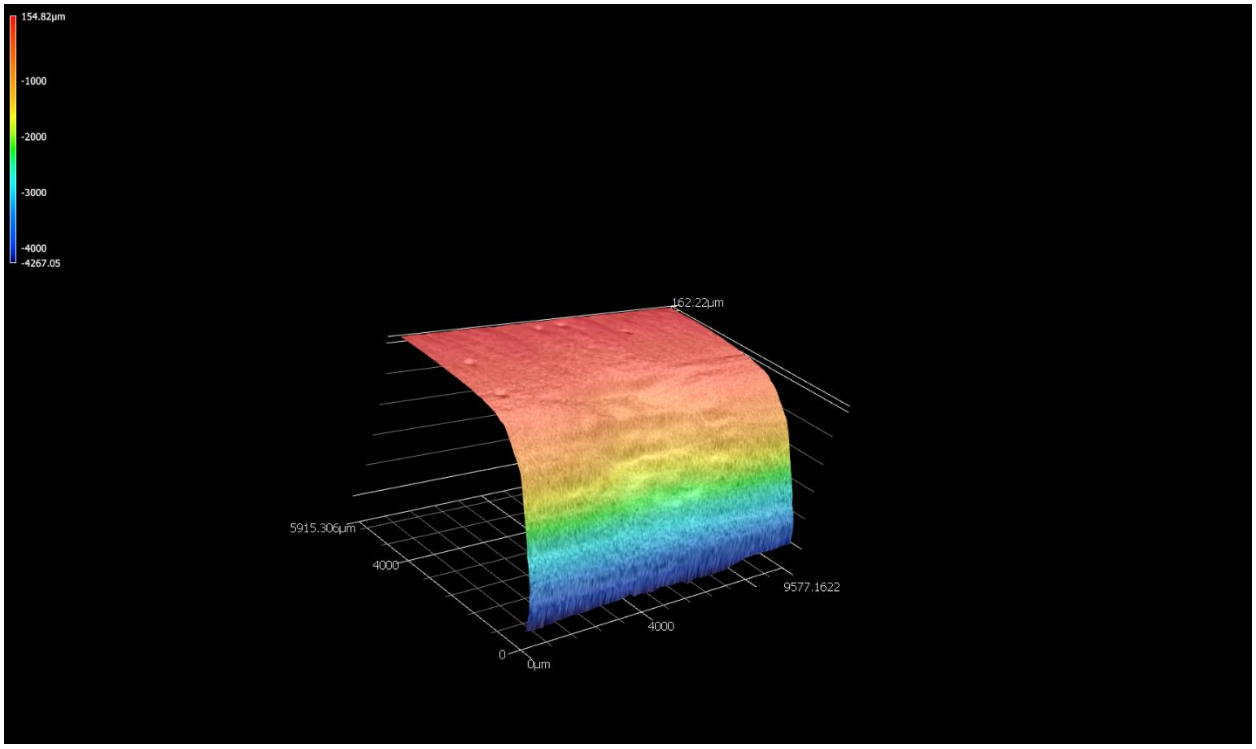


Fig. AVI-135: Erosion scar at 5° angle of impingement on the uncoated blade EXP4

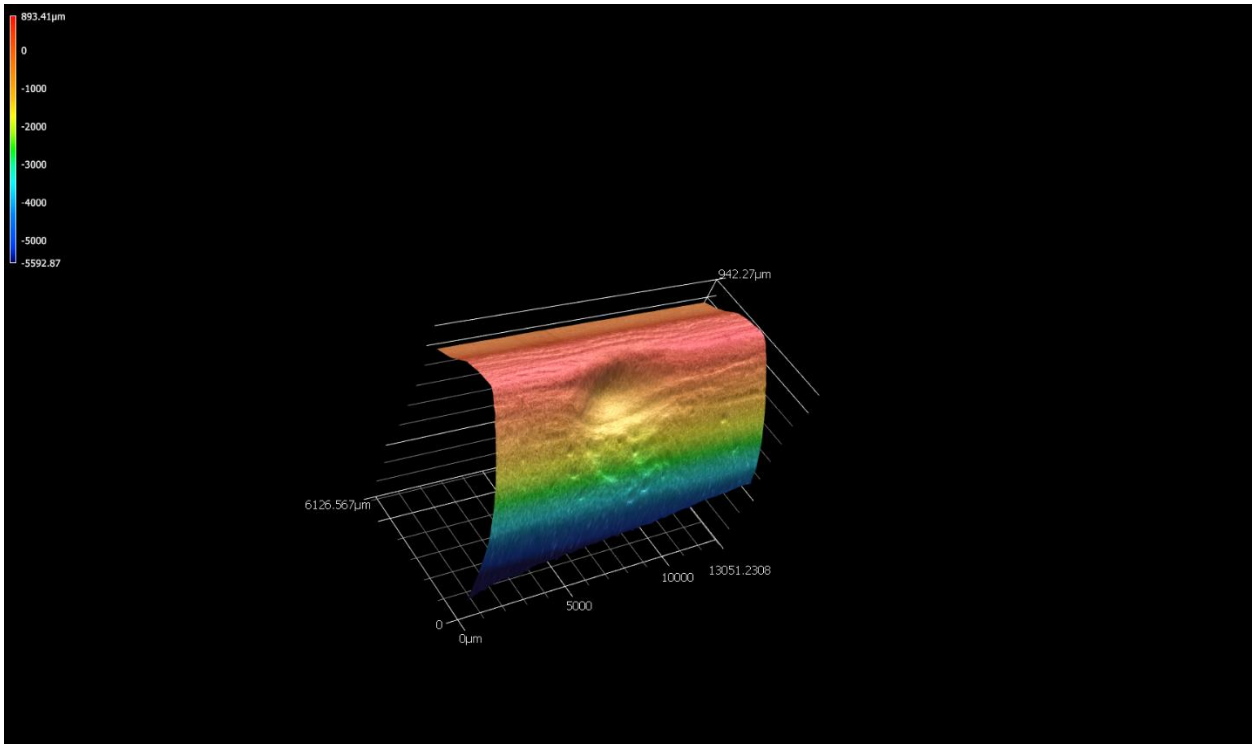


Fig. AVI-136: Erosion scar at 5° angle of impingement on the uncoated blade EXP5

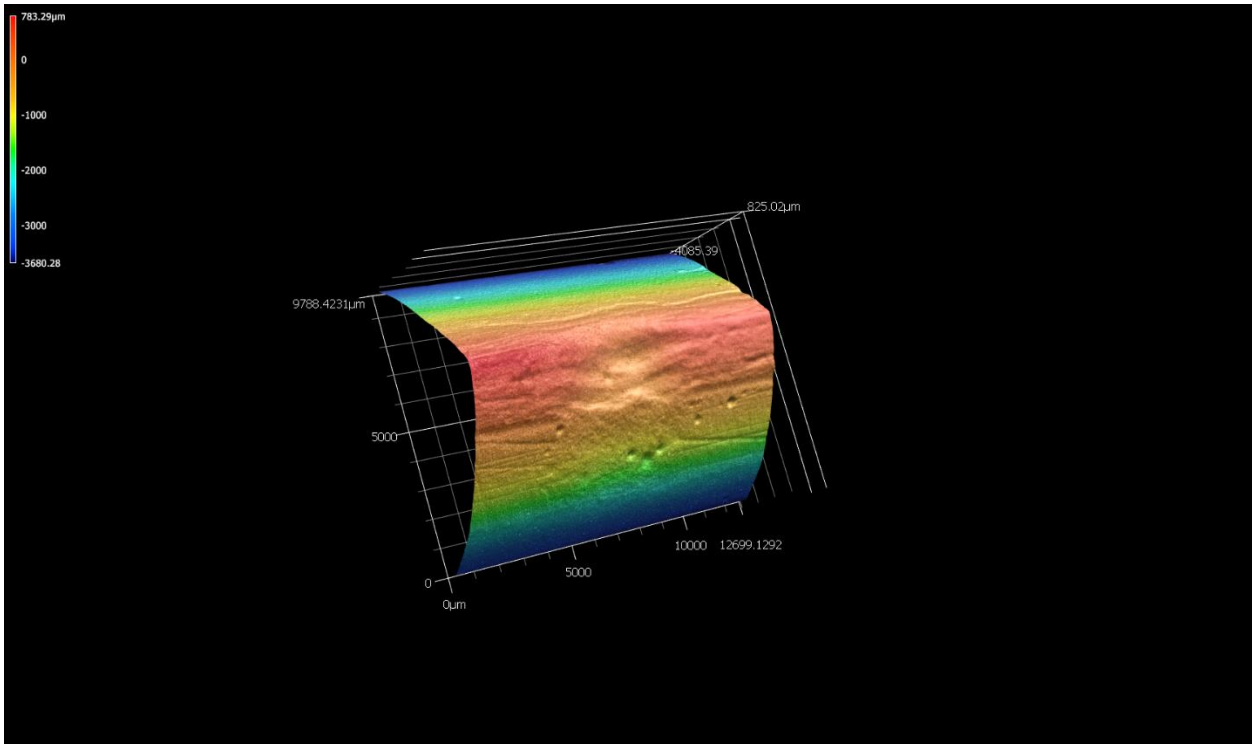


Fig. AVI-137: Erosion scar at 5° angle of impingement on the uncoated blade EXP6

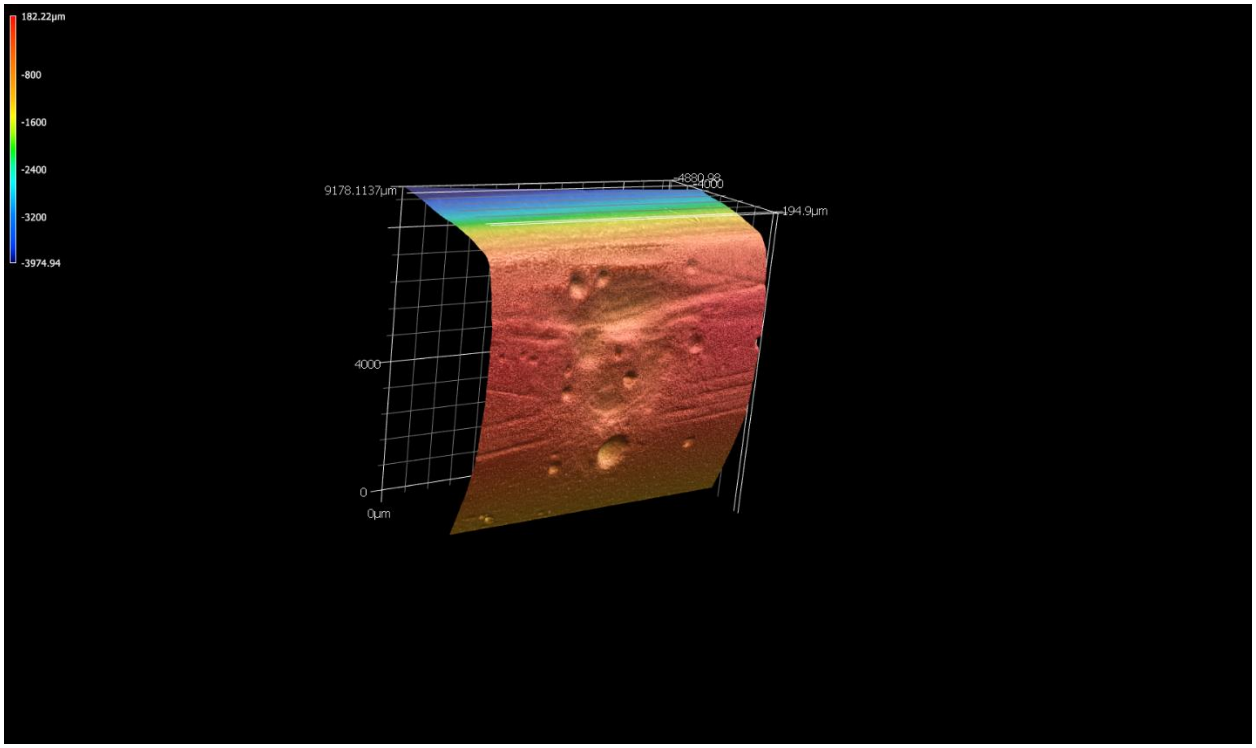


Fig. AVI-138: Erosion scar at 5° angle of impingement on the uncoated blade EXP7

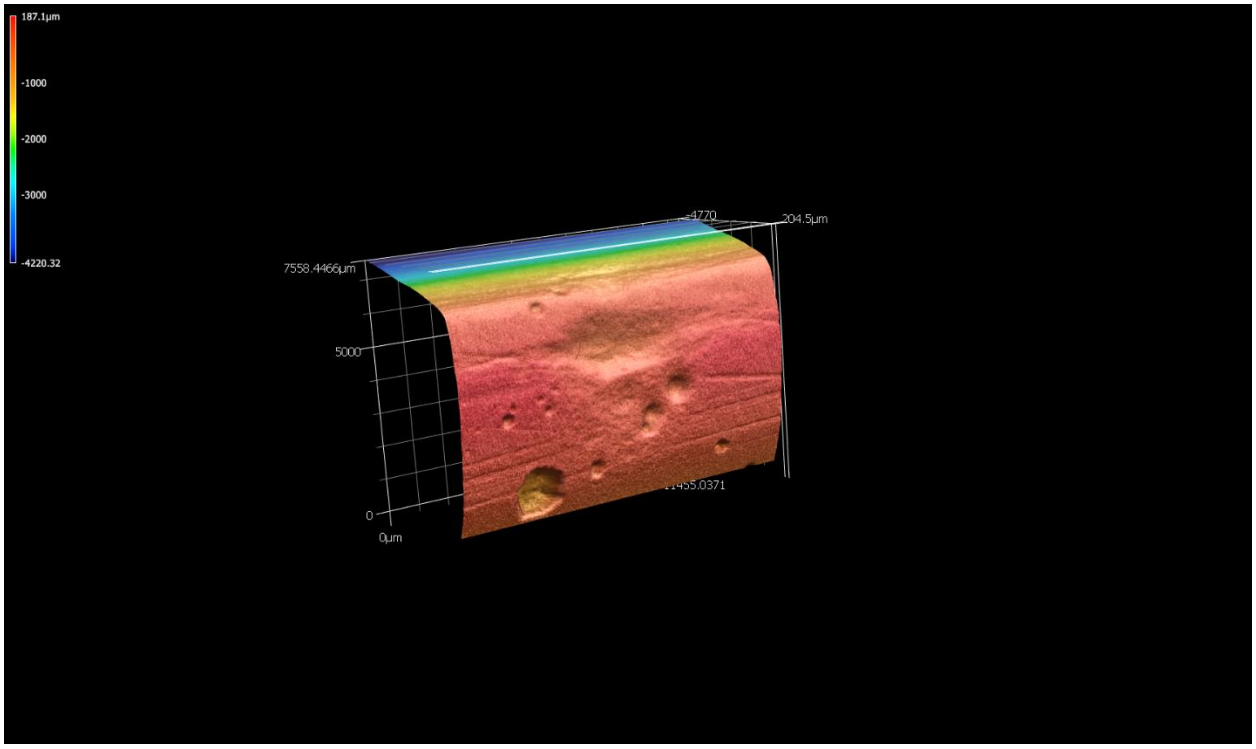


Fig. AVI-139: Erosion scar at 5° angle of impingement on the uncoated blade EXP8

- **H-146**

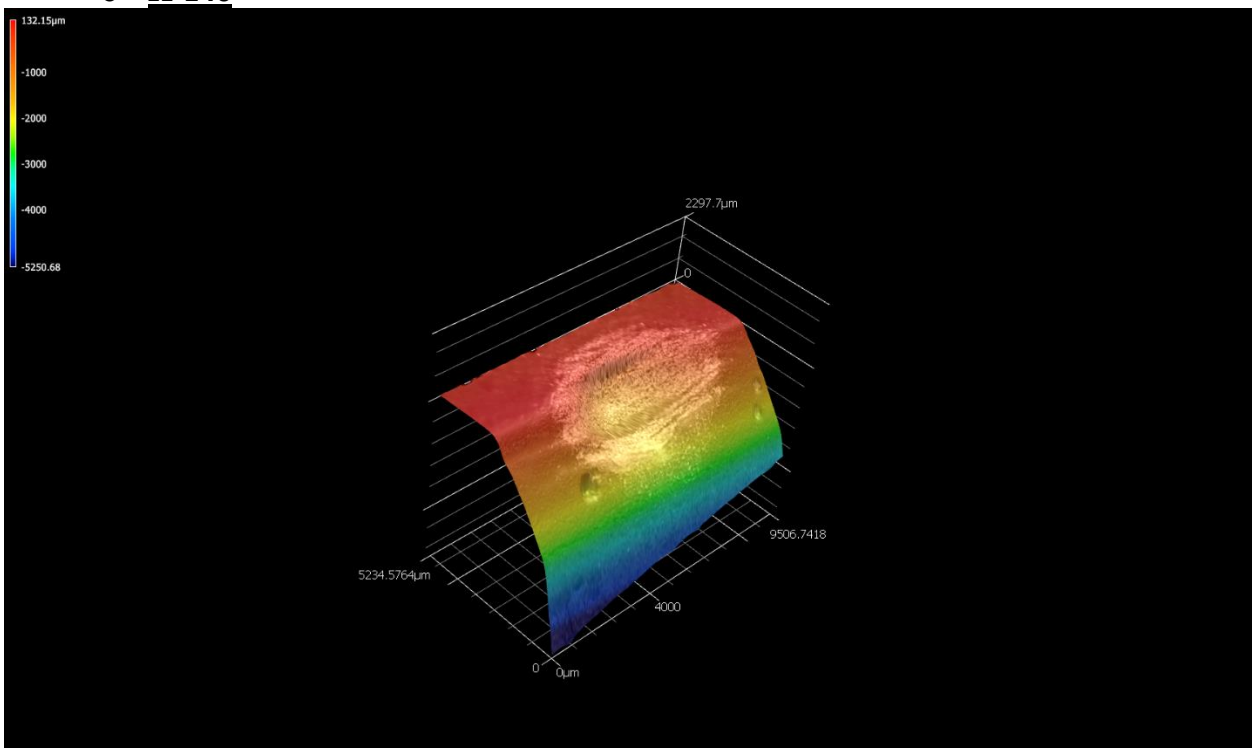


Fig. AVI-140: Erosion scar at 5° angle of impingement on the H-146 coated blade EXP1

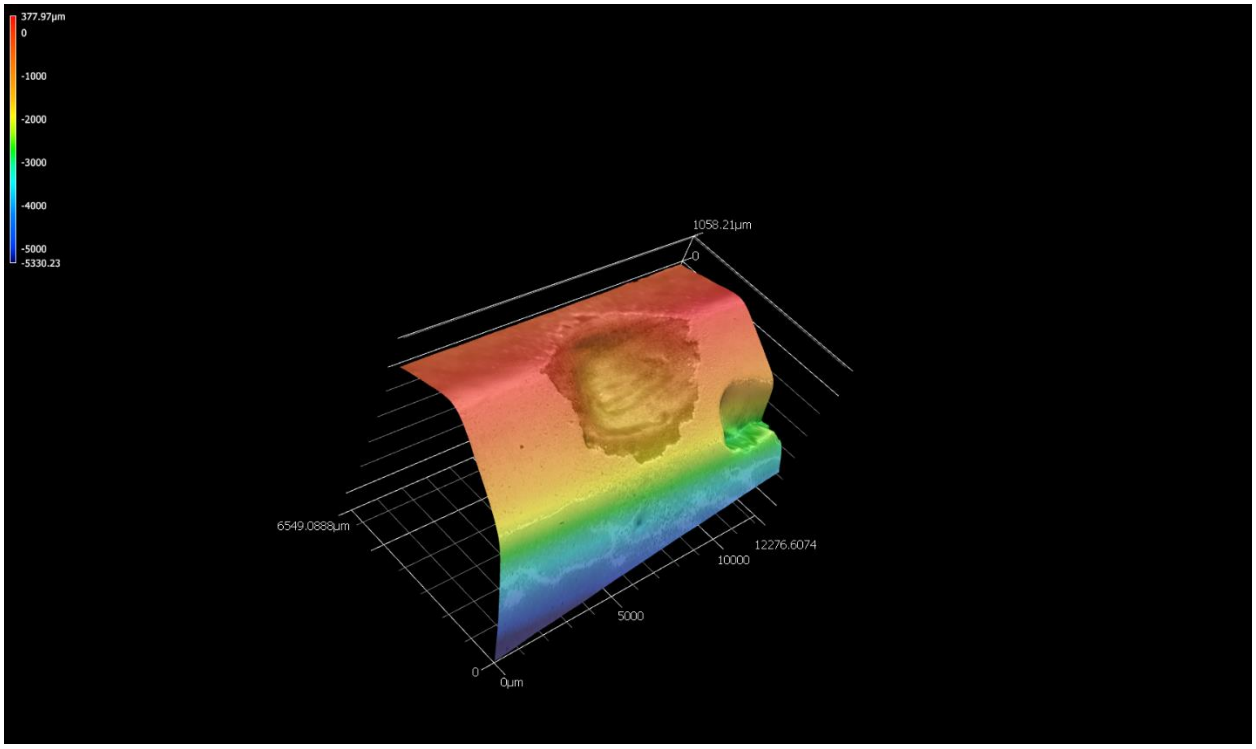


Fig. AVI-141: Erosion scar at 5° angle of impingement on the H-146 coated blade EXP2

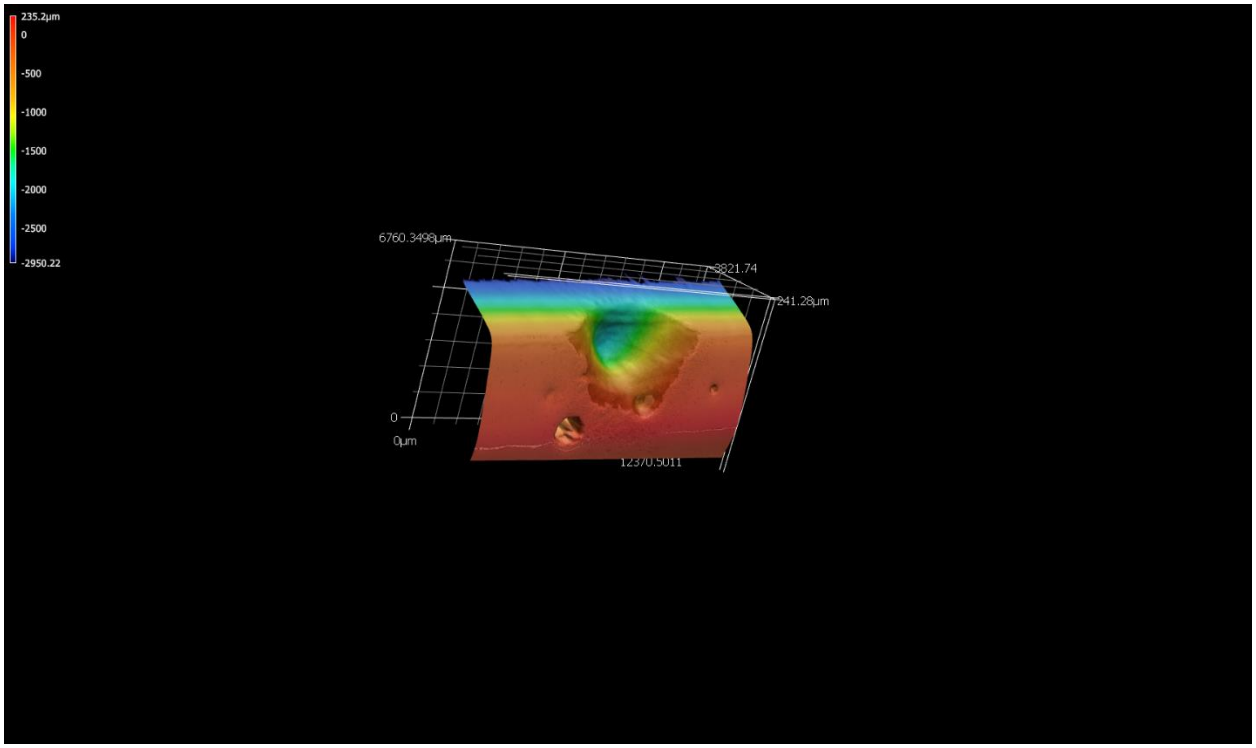


Fig. AVI-142: Erosion scar at 5° angle of impingement on the H-146 coated blade EXP3

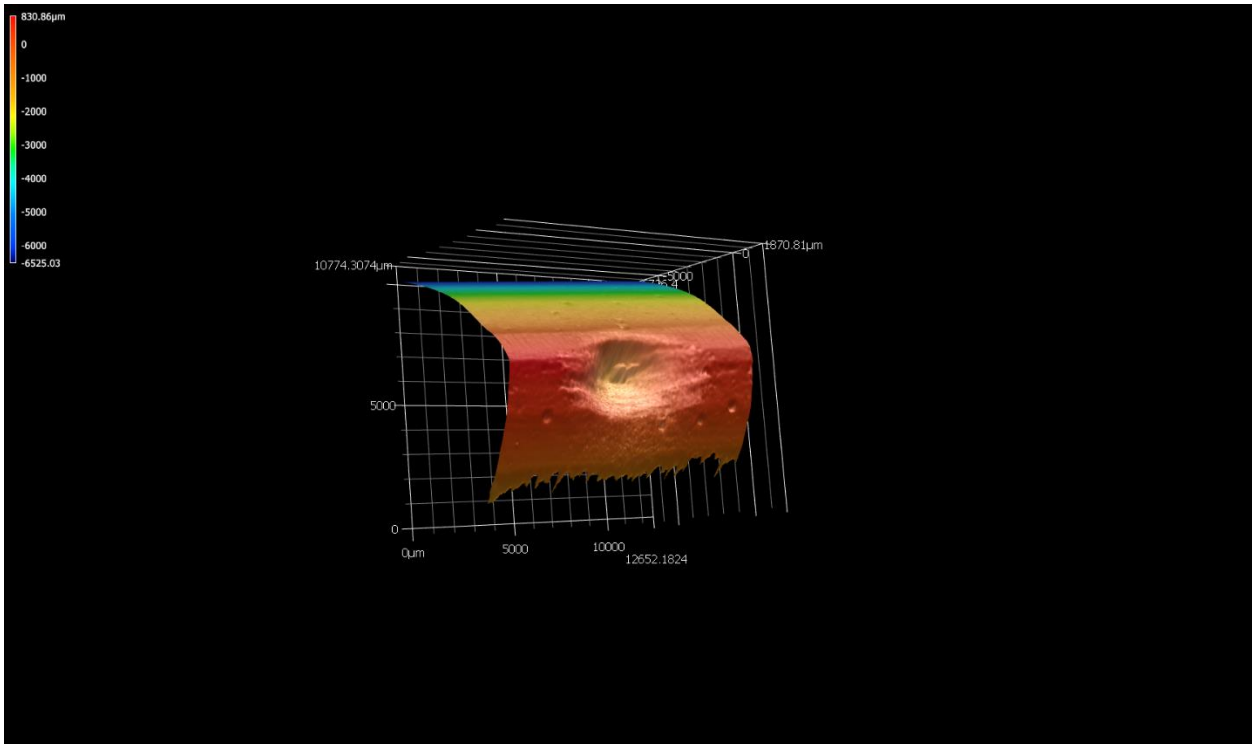


Fig. AVI-143: Erosion scar at 5° angle of impingement on the H-146 coated blade EXP4

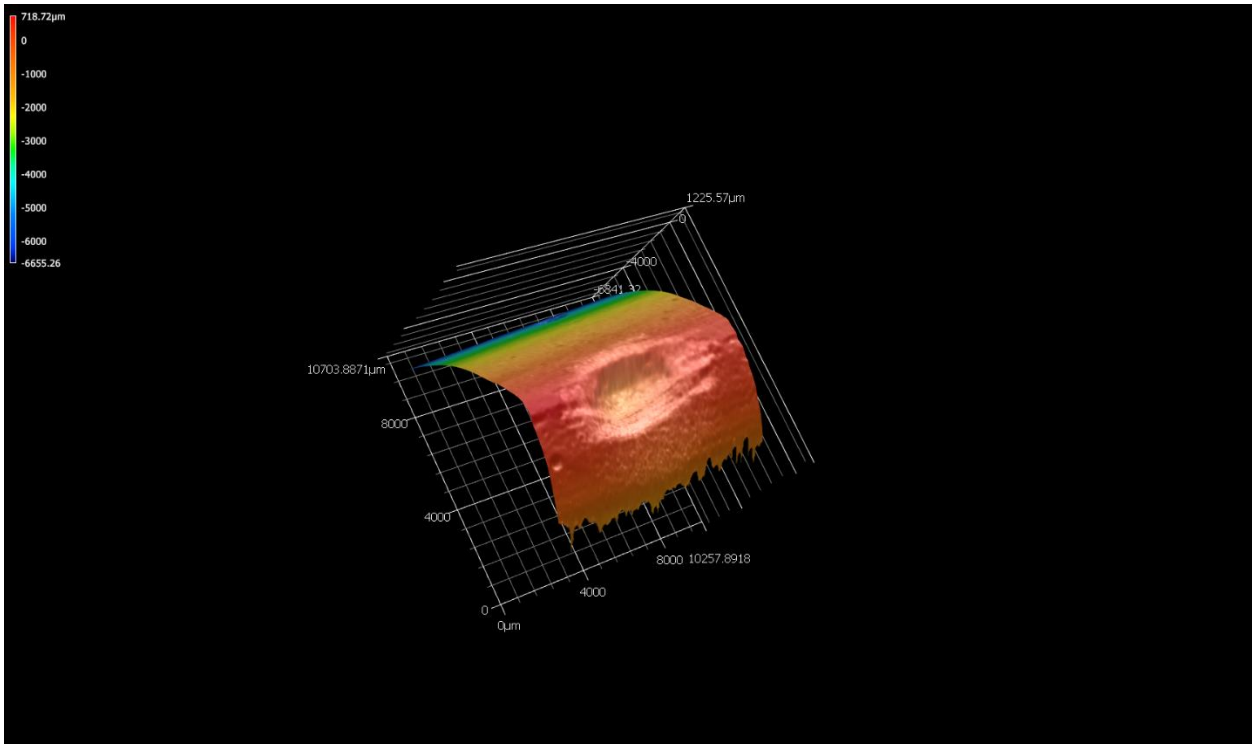


Fig. AVI-144: Erosion scar at 5° angle of impingement on the H-146 coated blade EXP5

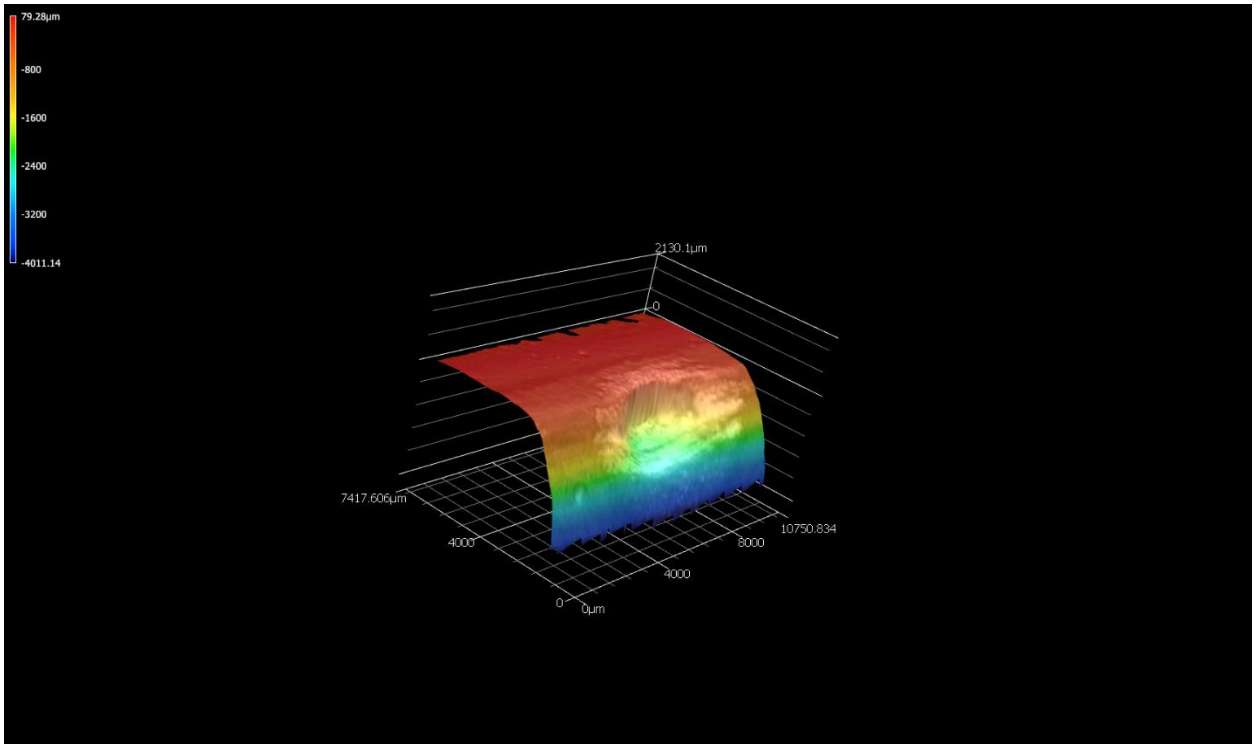


Fig. AVI-145: Erosion scar at 5° angle of impingement on the H-146 coated blade EXP6

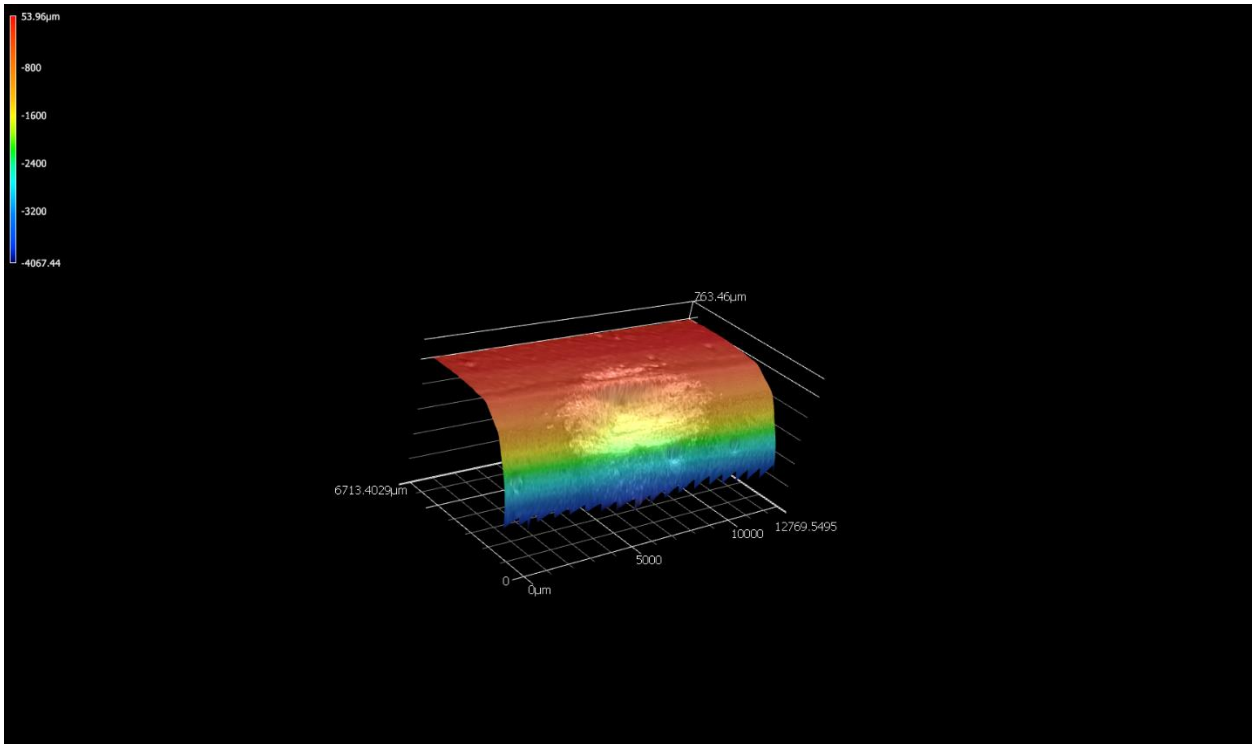


Fig. AVI-146: Erosion scar at 5° angle of impingement on the H-146 coated blade EXP7

- **Polyurethane/IA-700**

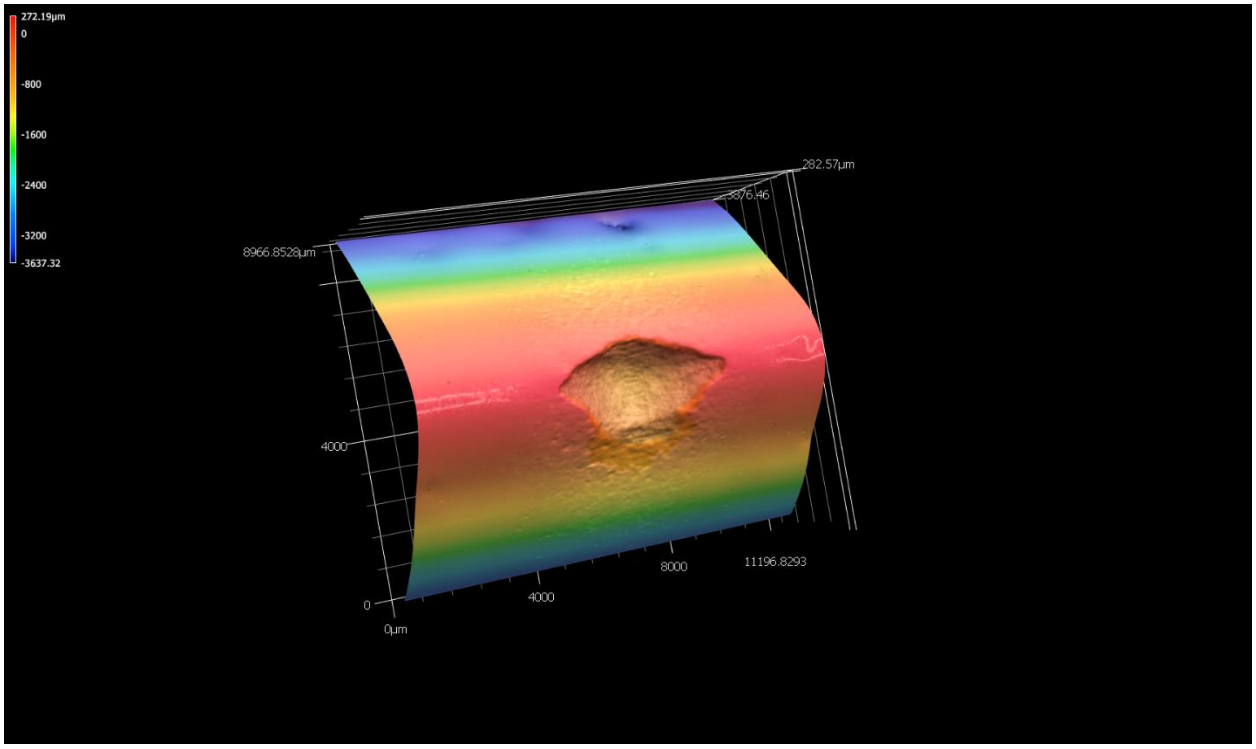


Fig. AVI-147: Erosion scar at 5° angle of impingement on the Polyurethane/IA-700 coated blade EXP1

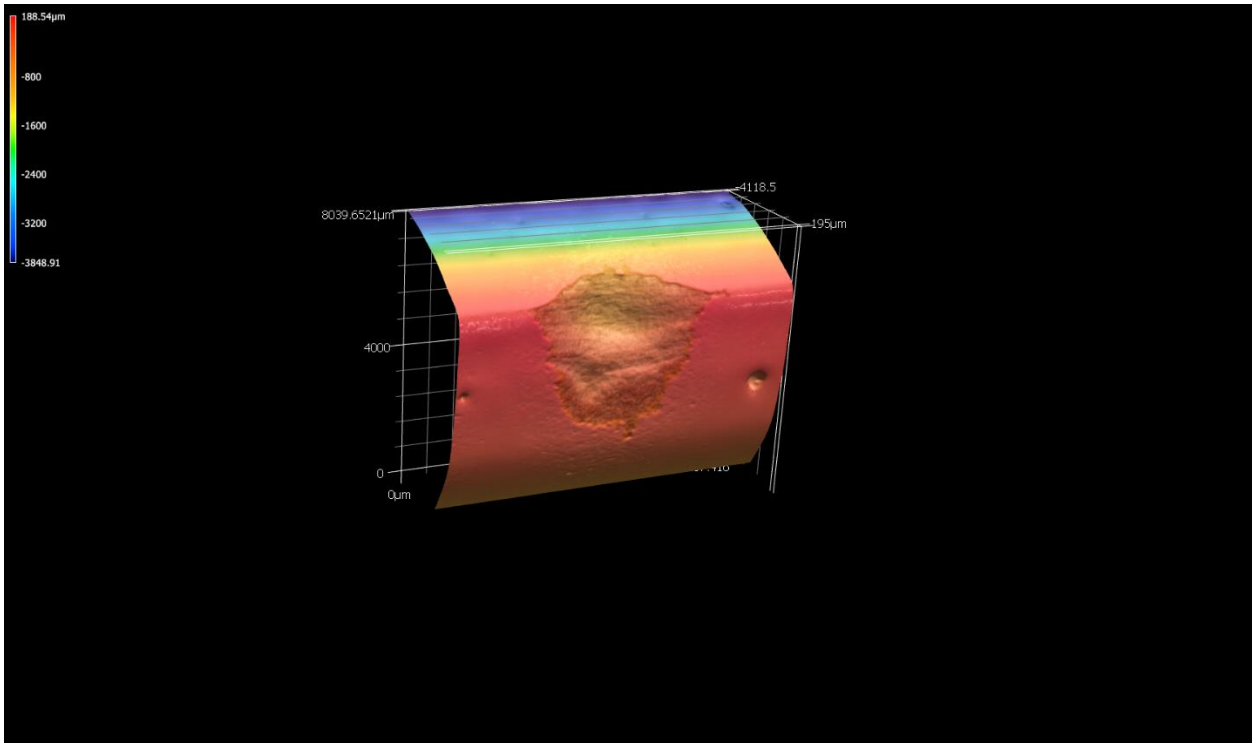


Fig. AVI-148: Erosion scar at 5° angle of impingement on the Polyurethane/IA-700 coated blade EXP2

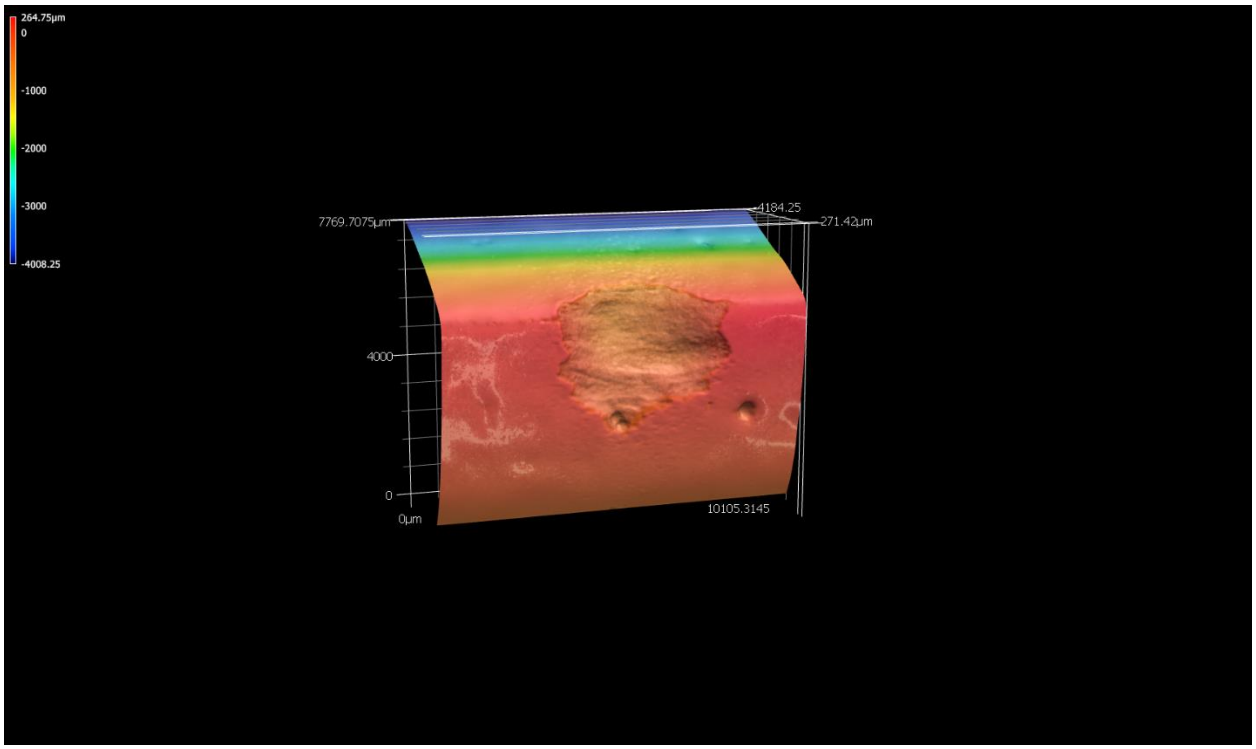


Fig. AVI-149: Erosion scar at 5° angle of impingement on the Polyurethane/IA-700 coated blade EXP3

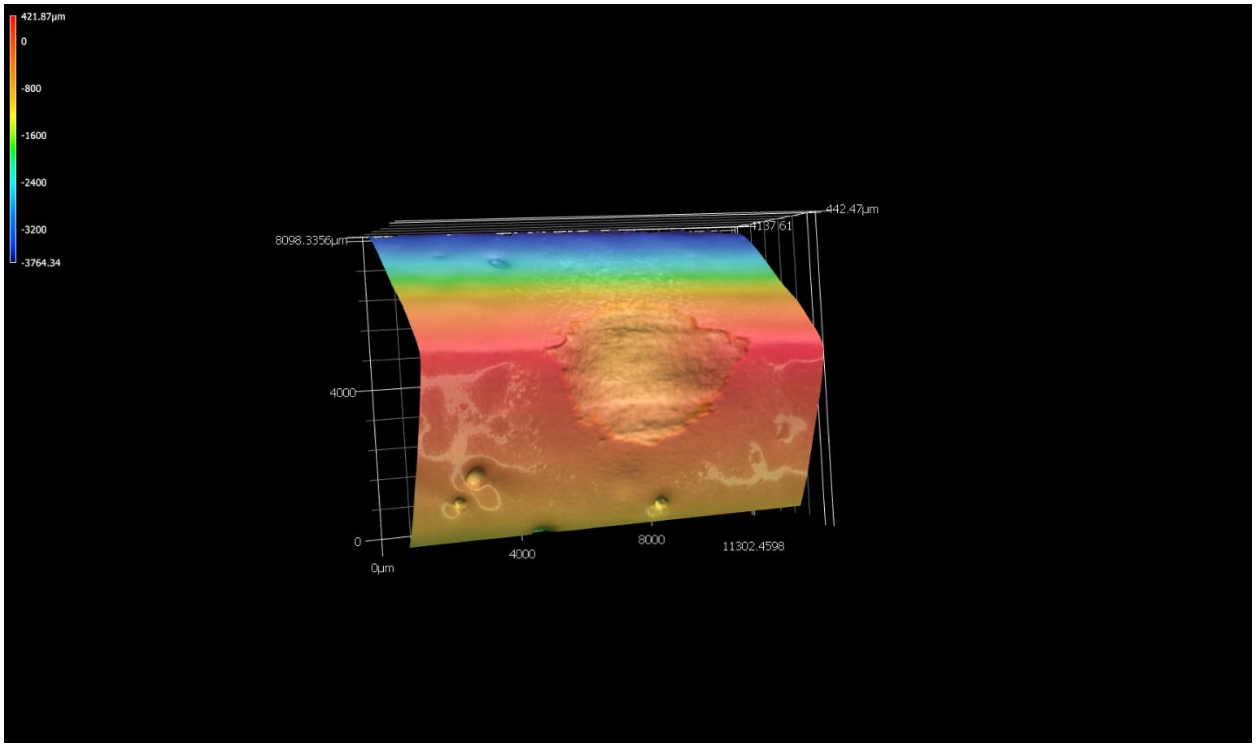


Fig. AVI-150: Erosion scar at 5° angle of impingement on the Polyurethane/IA-700 coated blade EXP4

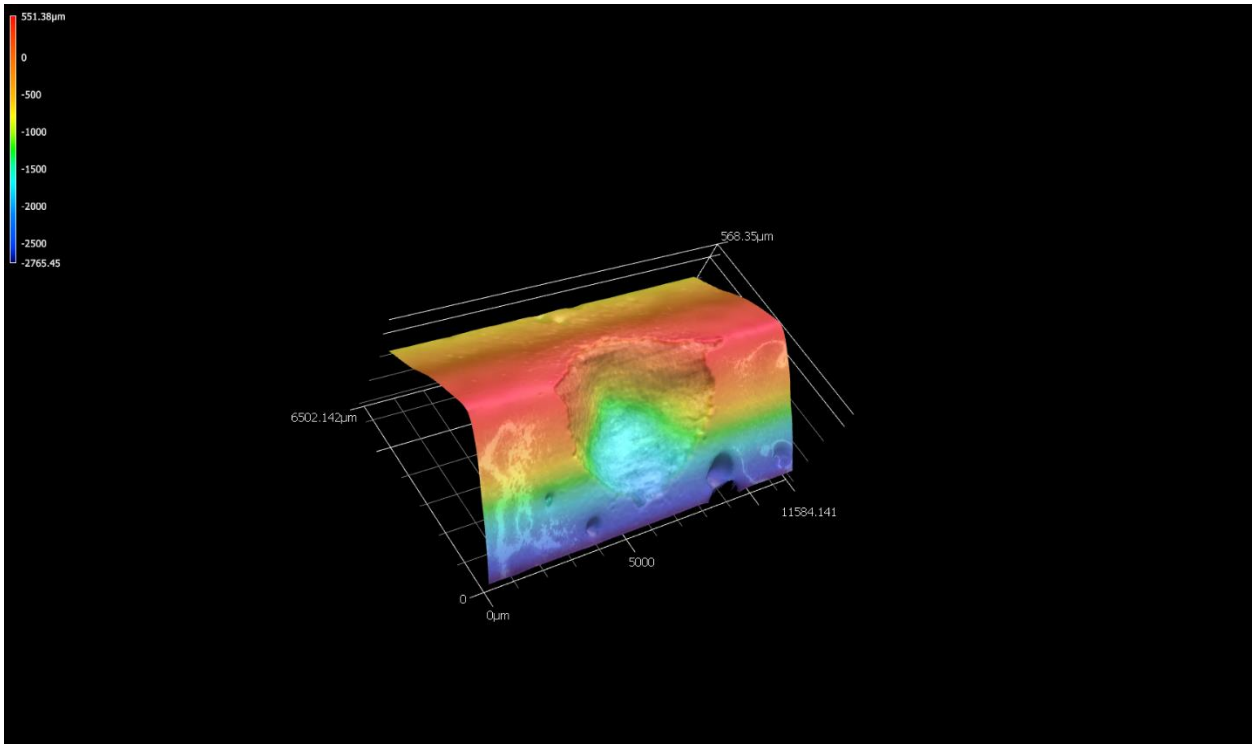


Fig. AVI-151: Erosion scar at 5° angle of impingement on the Polyurethane/IA-700 coated blade EXP5

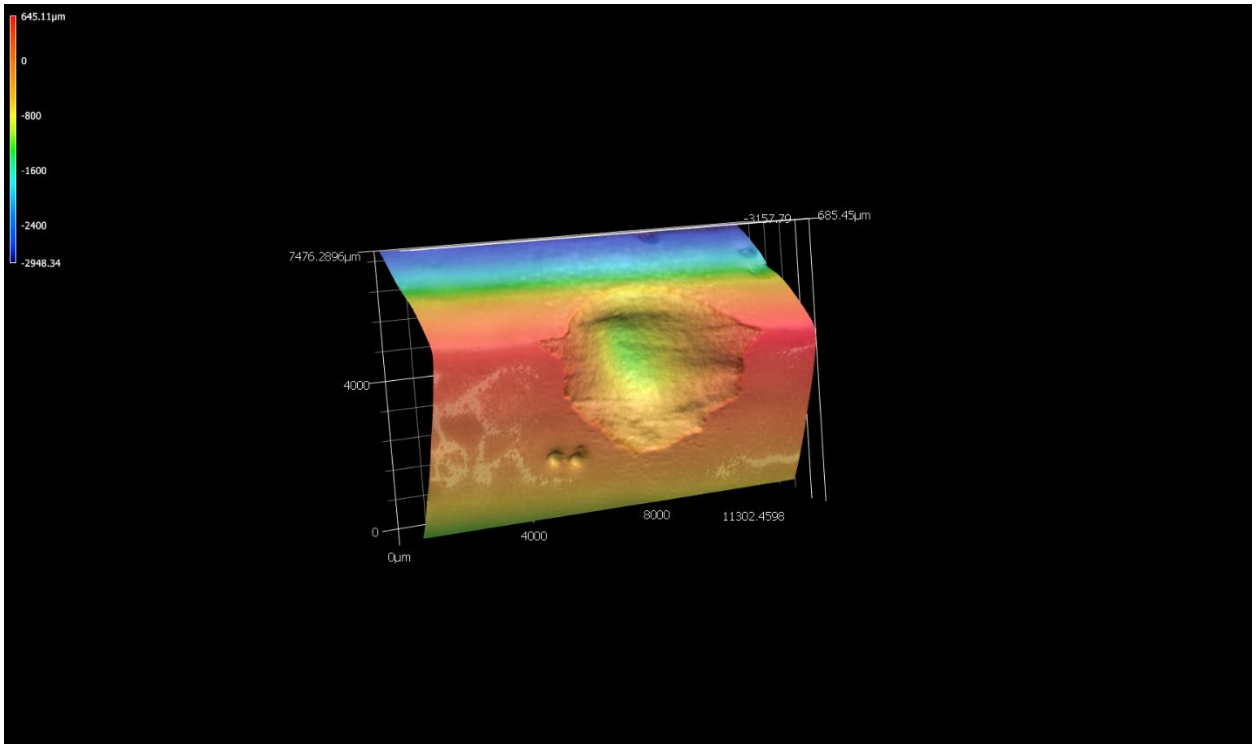


Fig. AVI-152: Erosion scar at 5° angle of impingement on the Polyurethane/IA-700 coated blade EXP6

- **10 degrees**
  - **Uncoated**

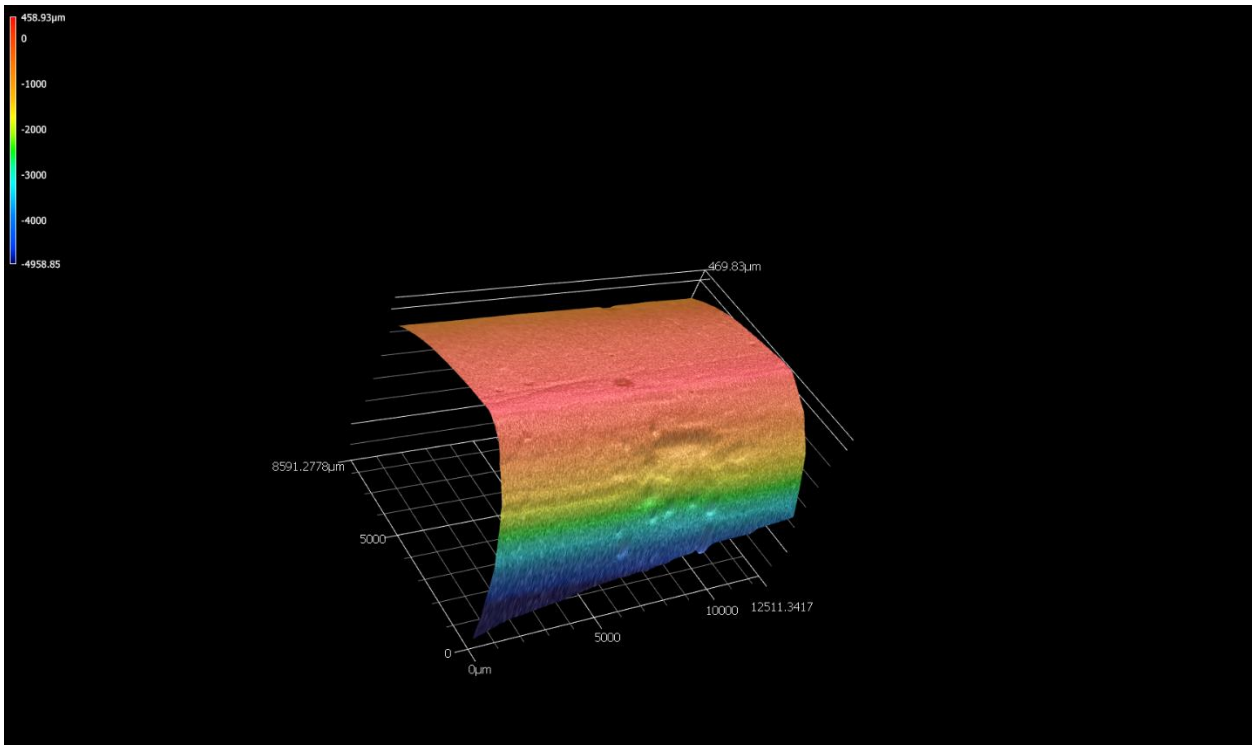


Fig. AVI-153: Erosion scar at 10° angle of impingement on the uncoated blade EXP1

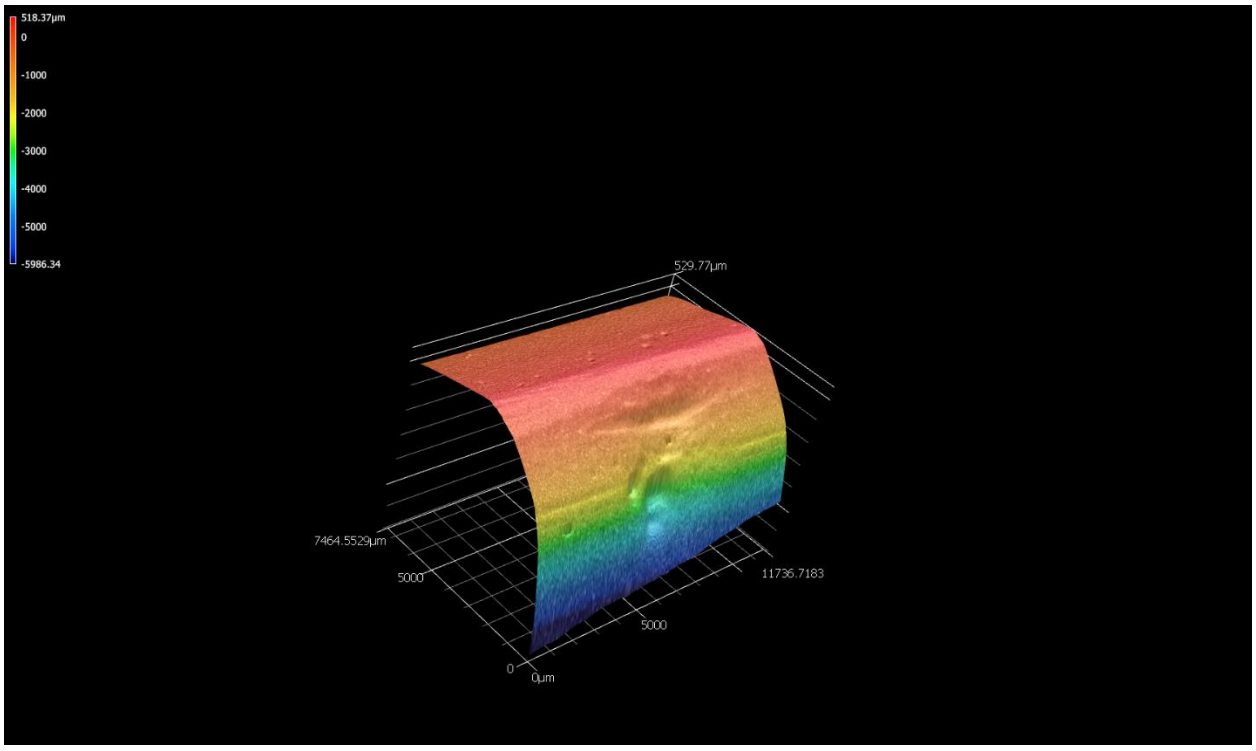


Fig. AVI-154: Erosion scar at 10° angle of impingement on the uncoated blade EXP2

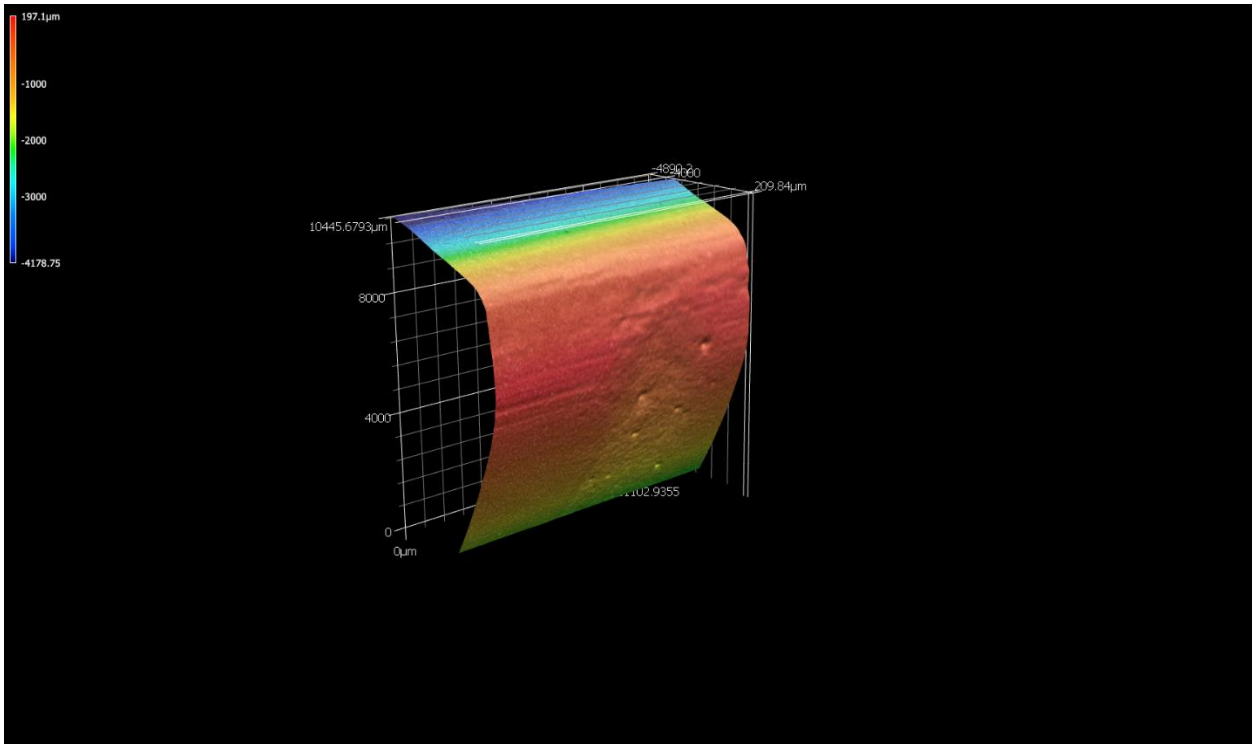


Fig. AVI-155: Erosion scar at 10° angle of impingement on the uncoated blade EXP3

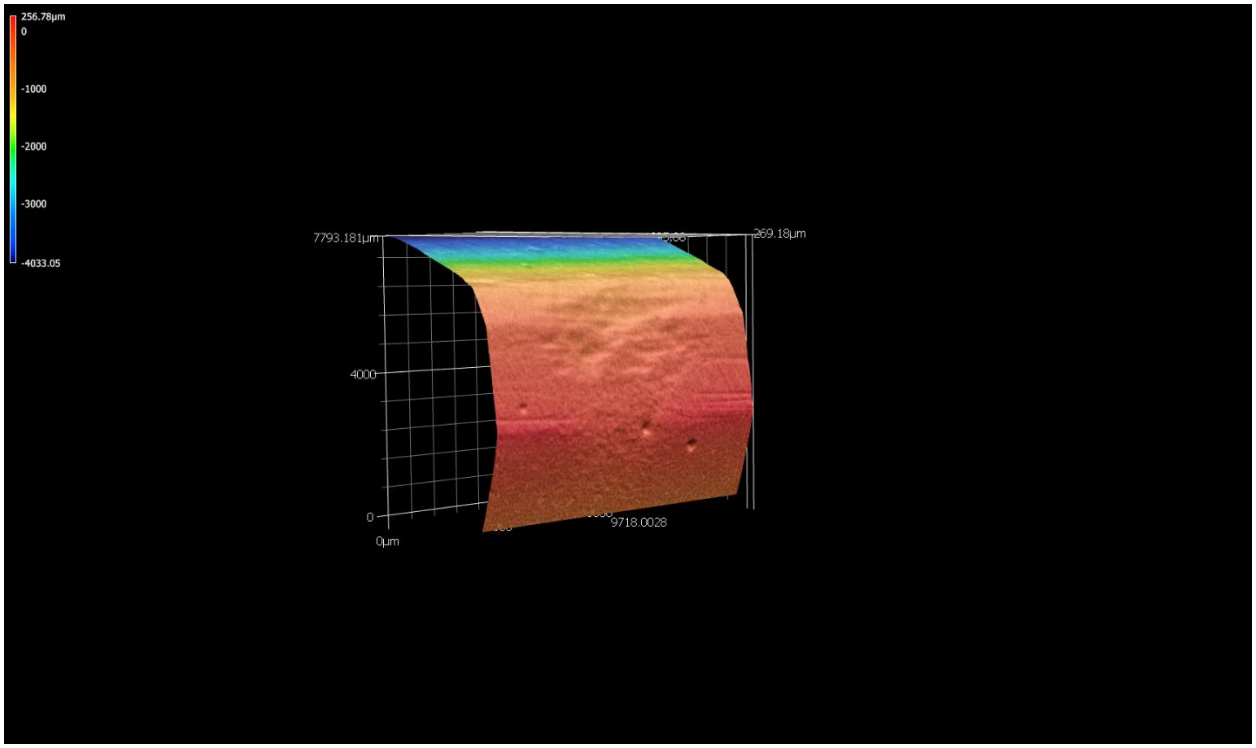


Fig. AVI-156: Erosion scar at 10° angle of impingement on the uncoated blade EXP4

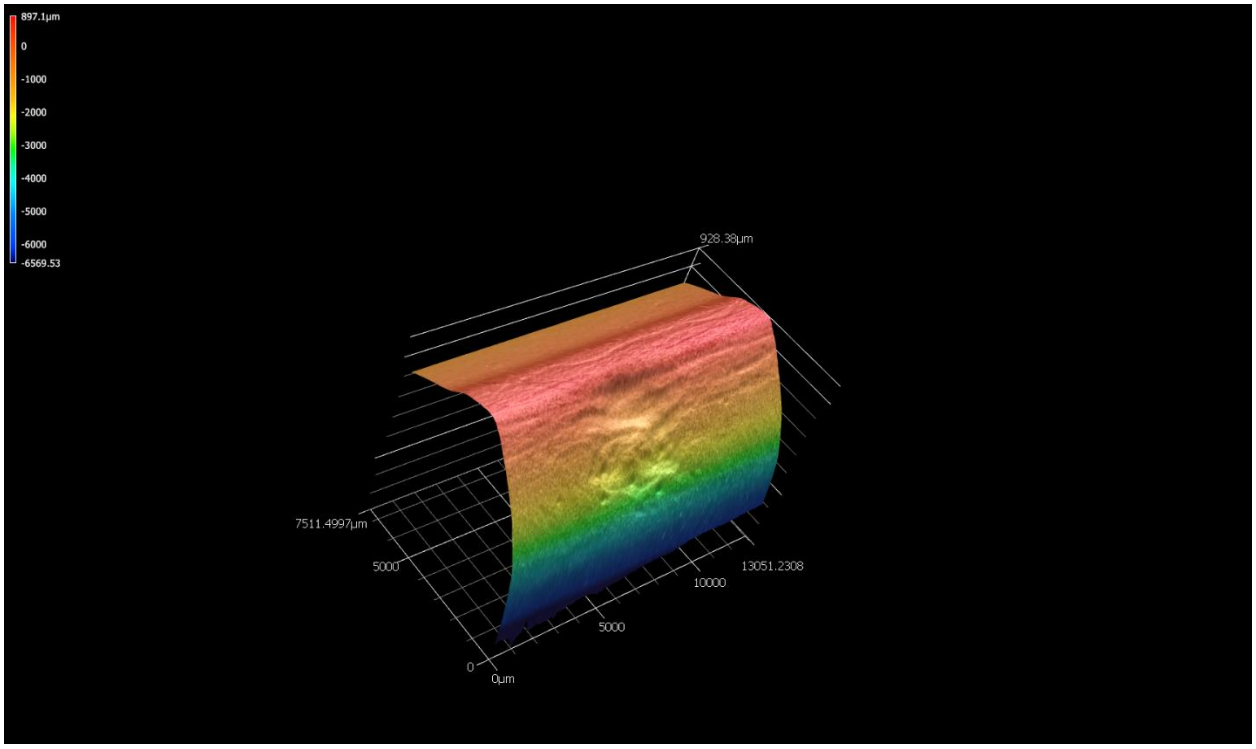


Fig. AVI-157: Erosion scar at 10° angle of impingement on the uncoated blade EXP5

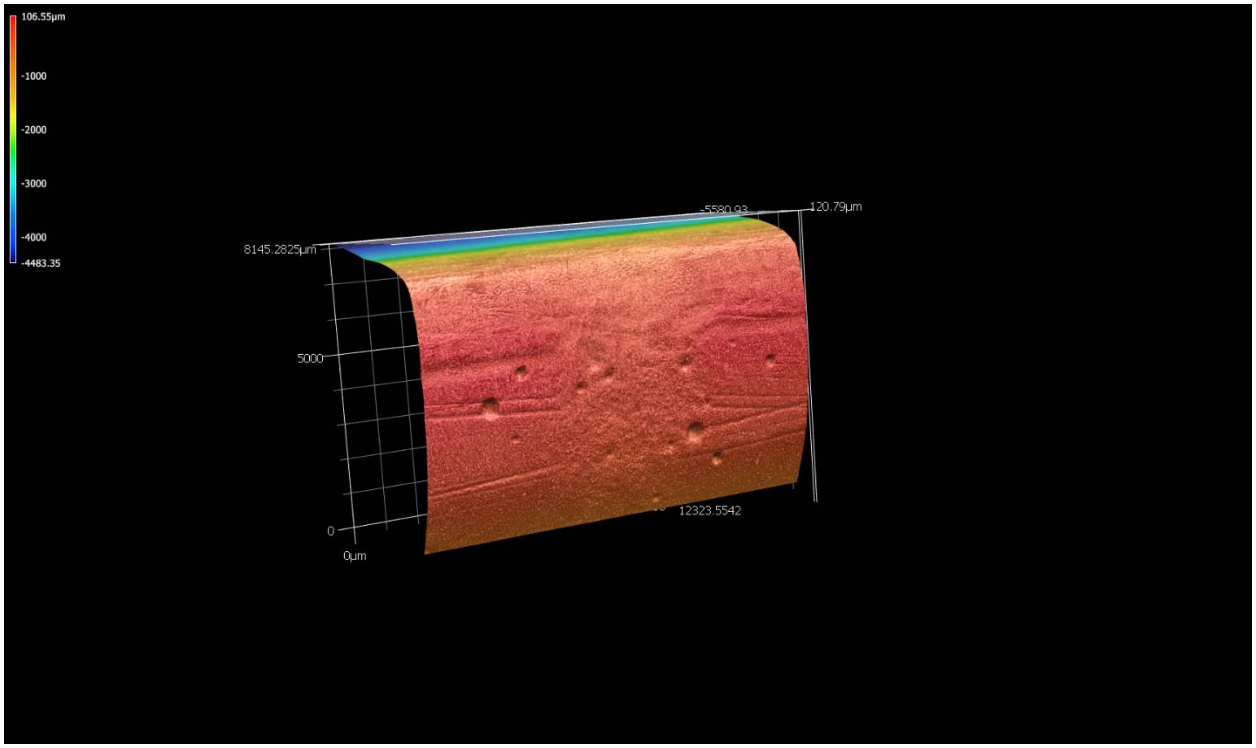


Fig. AVI-158: Erosion scar at 10° angle of impingement on the uncoated blade EXP6

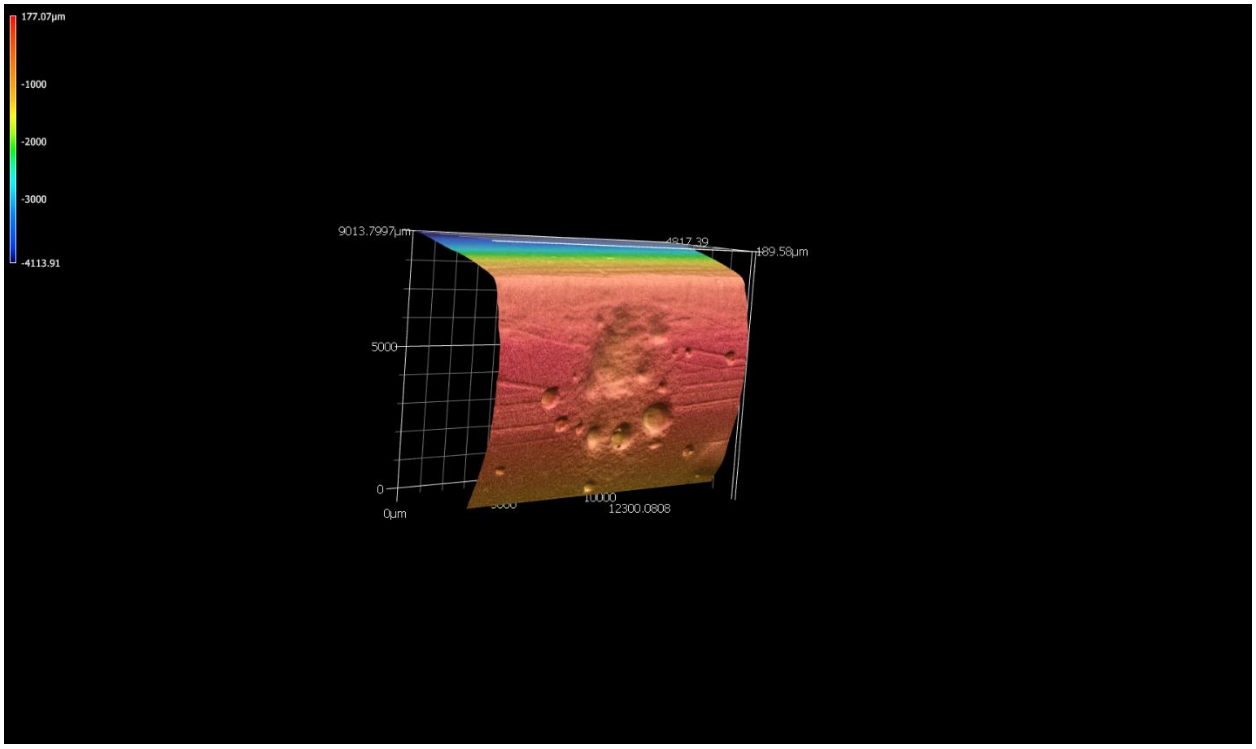


Fig. AVI-159: Erosion scar at 10° angle of impingement on the uncoated blade EXP7

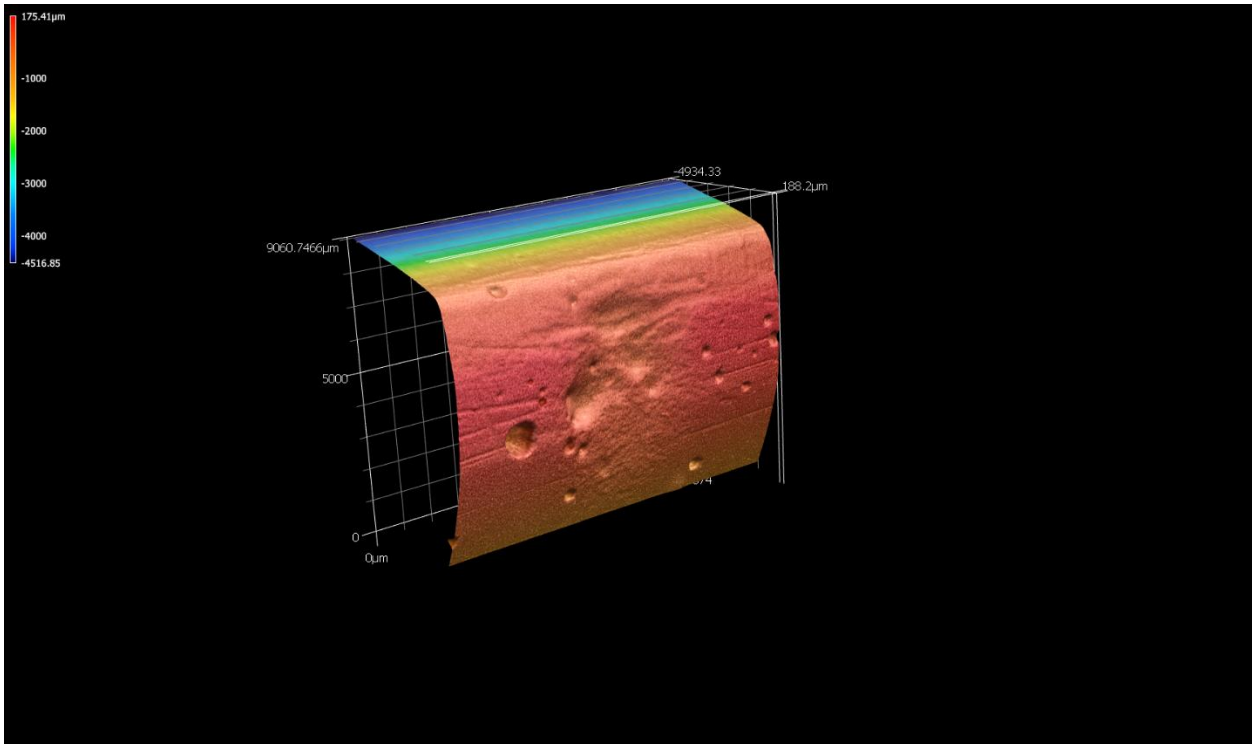


Fig. AVI-160: Erosion scar at 10° angle of impingement on the uncoated blade EXP8

- **H-146**

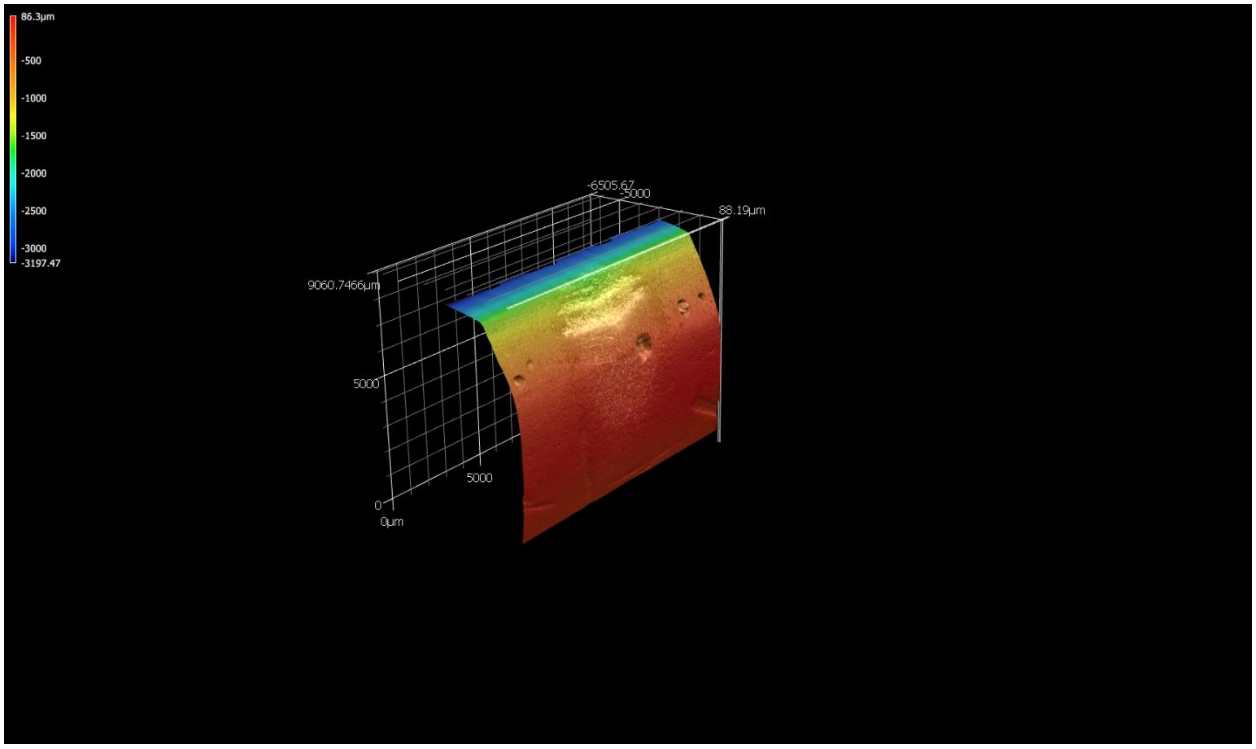


Fig. AVI-161: Erosion scar at 10° angle of impingement on the H-146 coated blade EXP1

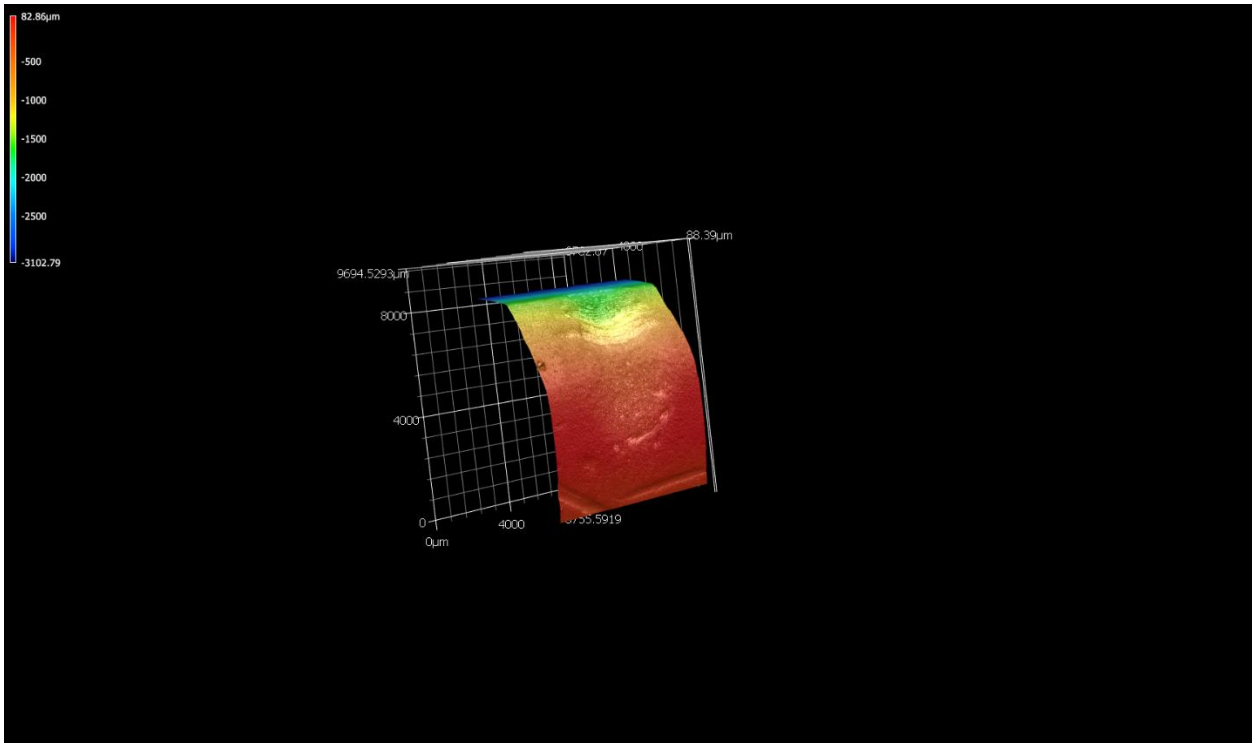


Fig. AVI-162: Erosion scar at 10° angle of impingement on the H-146 coated blade EXP2

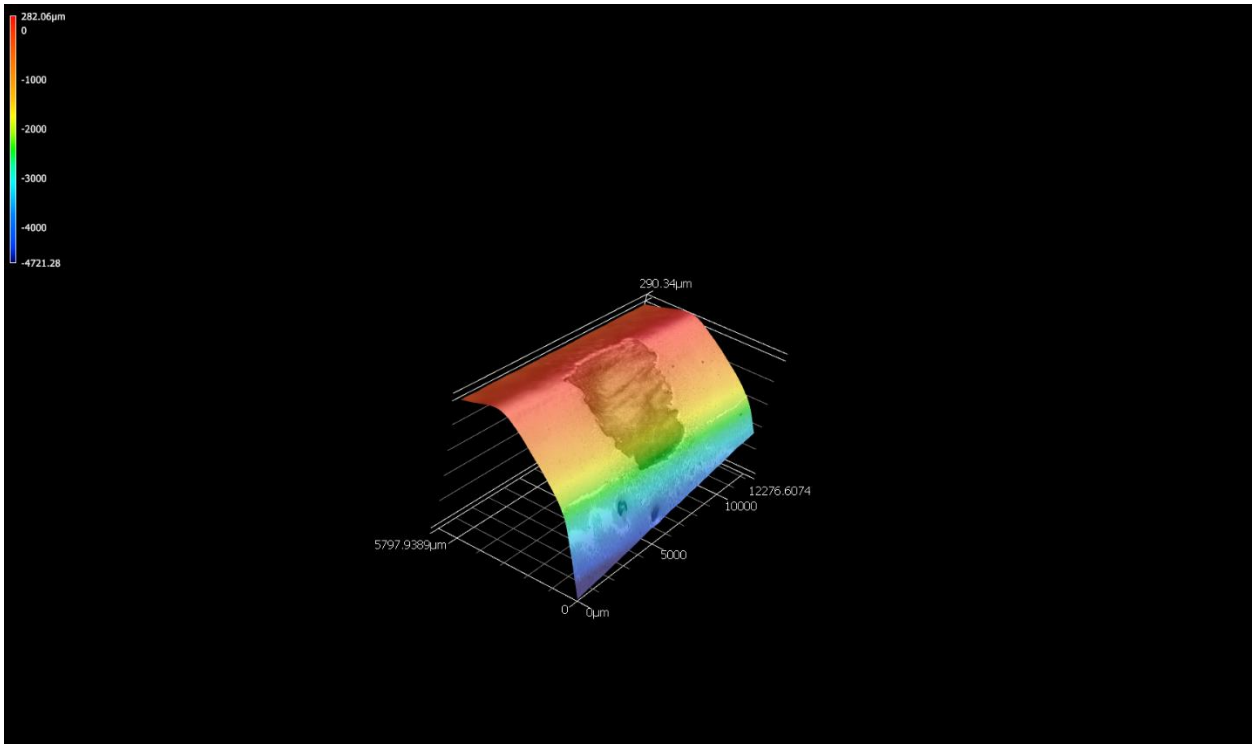


Fig. AVI-163: Erosion scar at 10° angle of impingement on the H-146 coated blade EXP3

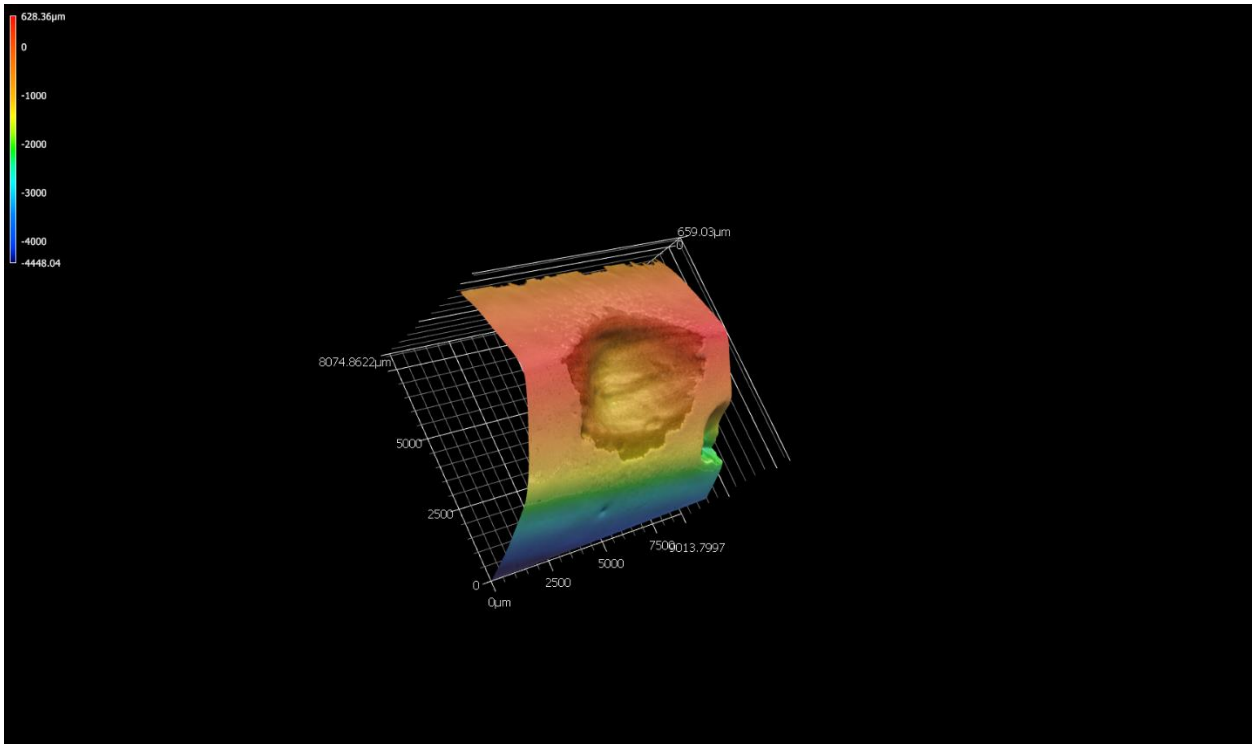


Fig. AVI-164: Erosion scar at 10° angle of impingement on the H-146 coated blade EXP4

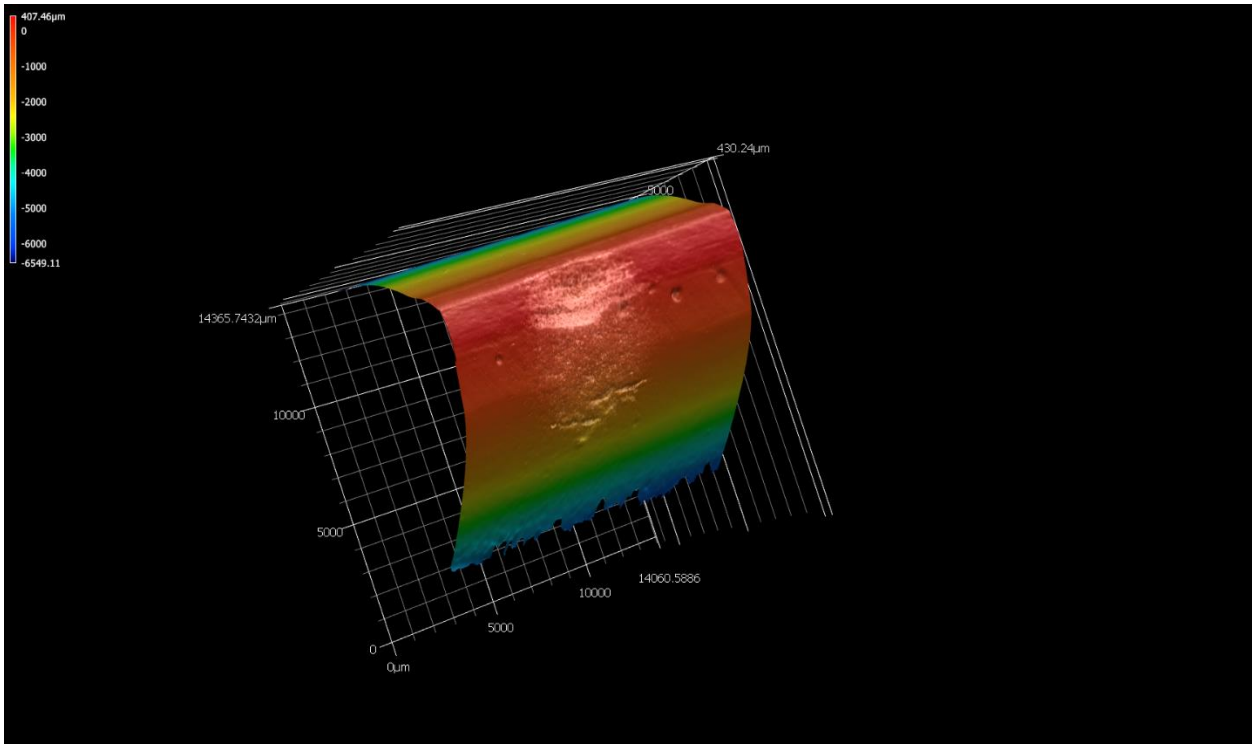


Fig. AVI-165: Erosion scar at 10° angle of impingement on the H-146 coated blade EXP5

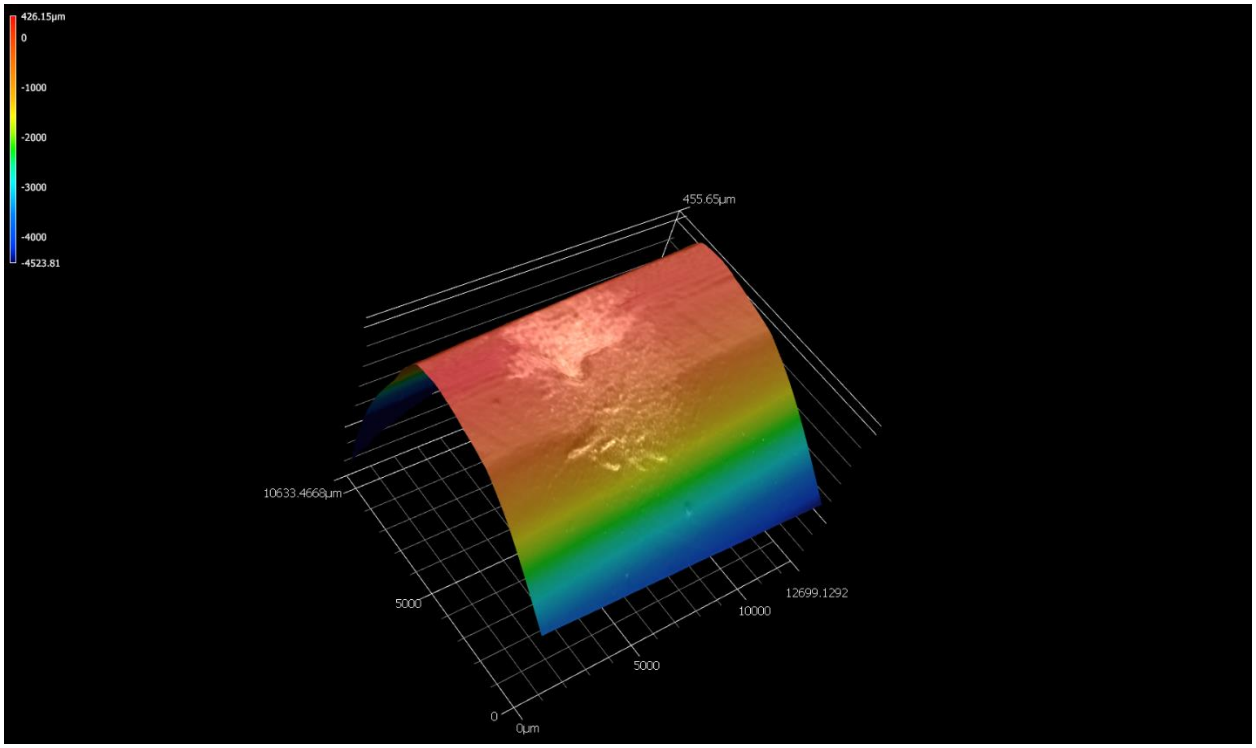


Fig. AVI-166: Erosion scar at 10° angle of impingement on the H-146 coated blade EXP6

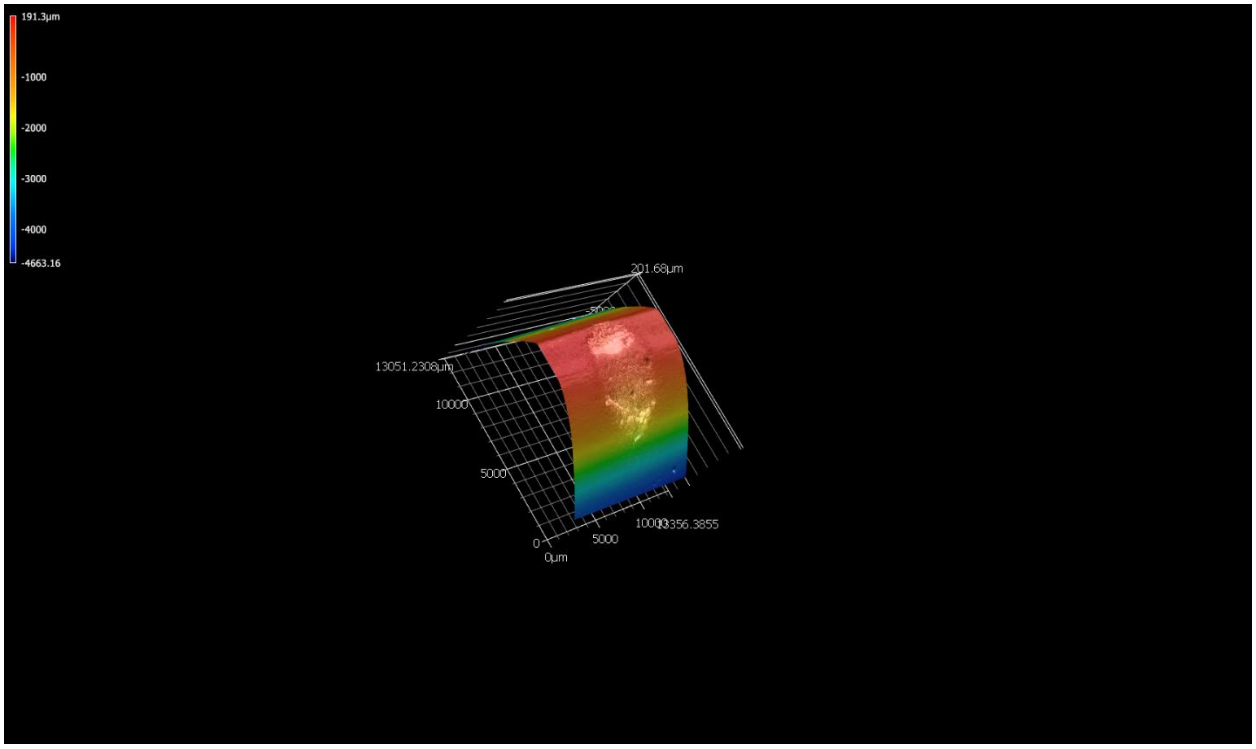


Fig. AVI-167: Erosion scar at 10° angle of impingement on the H-146 coated blade EXP7

- **Polyurethane/IA-700**

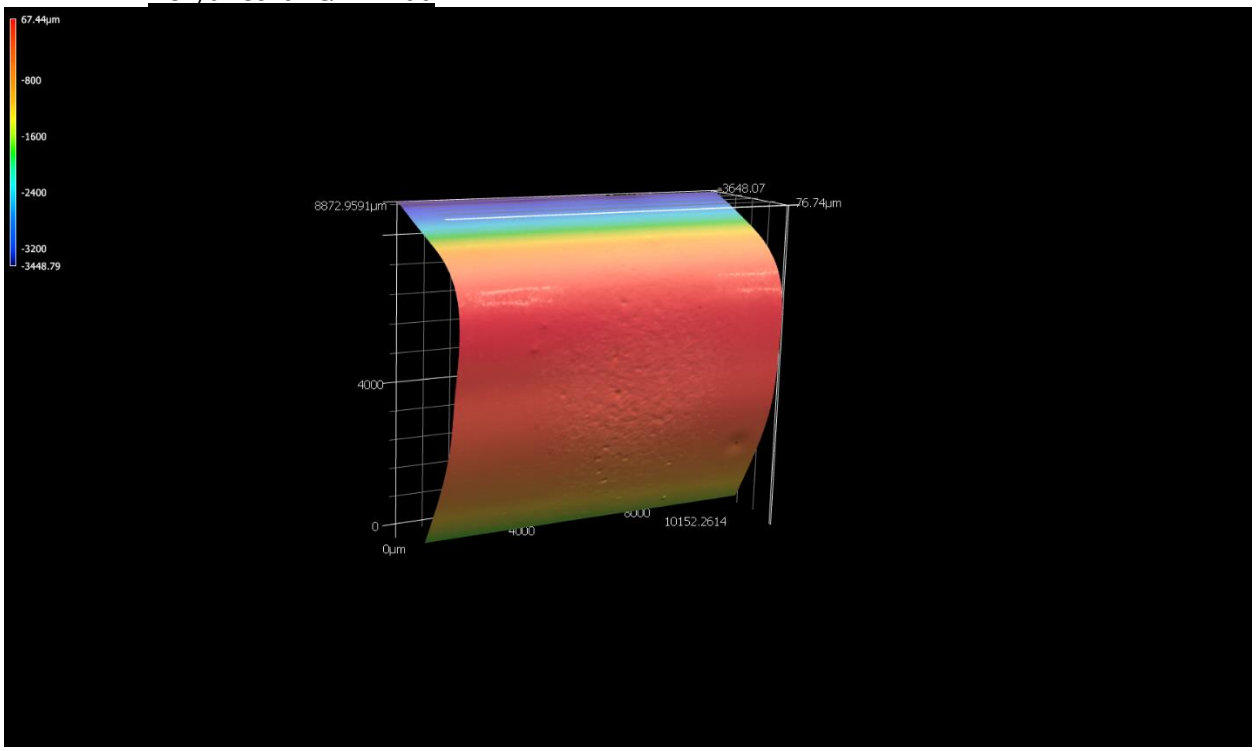


Fig. AVI-168: Erosion scar at 10° angle of impingement on the Polyurethane/IA-700 coated blade EXP1

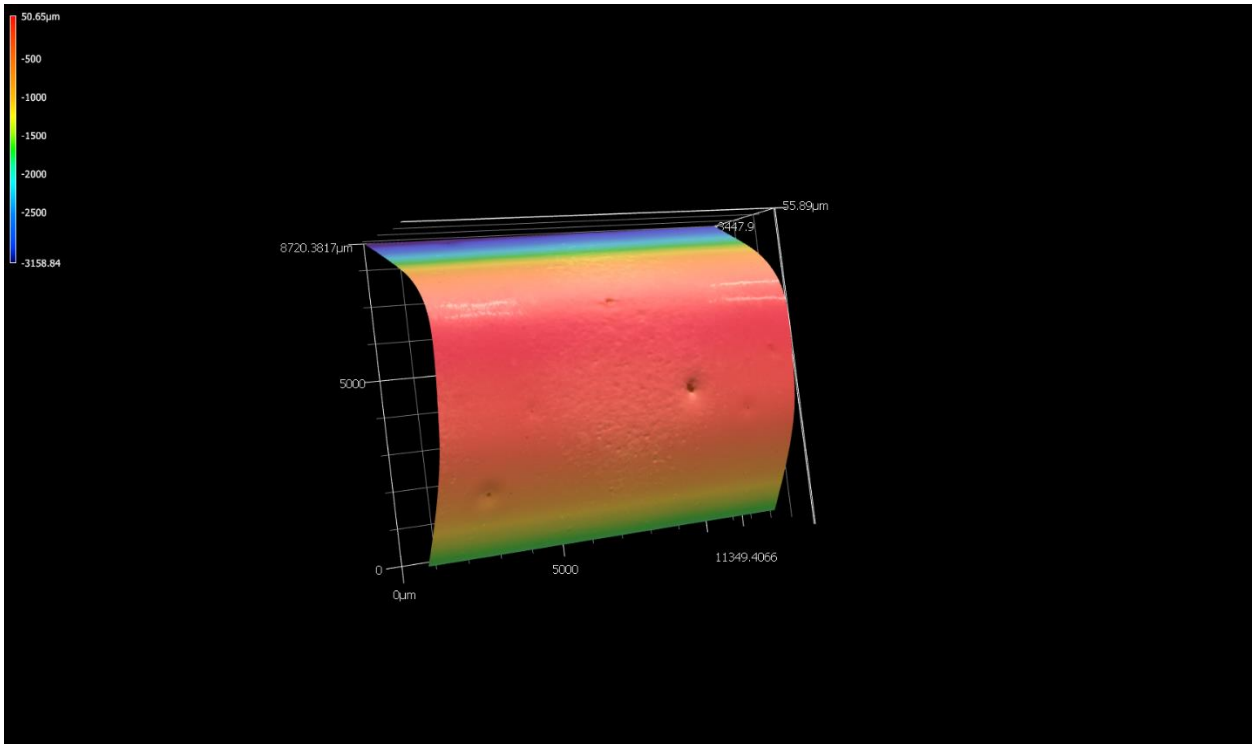


Fig. AVI-169: Erosion scar at 10° angle of impingement on the Polyurethane/IA-700 coated blade EXP2

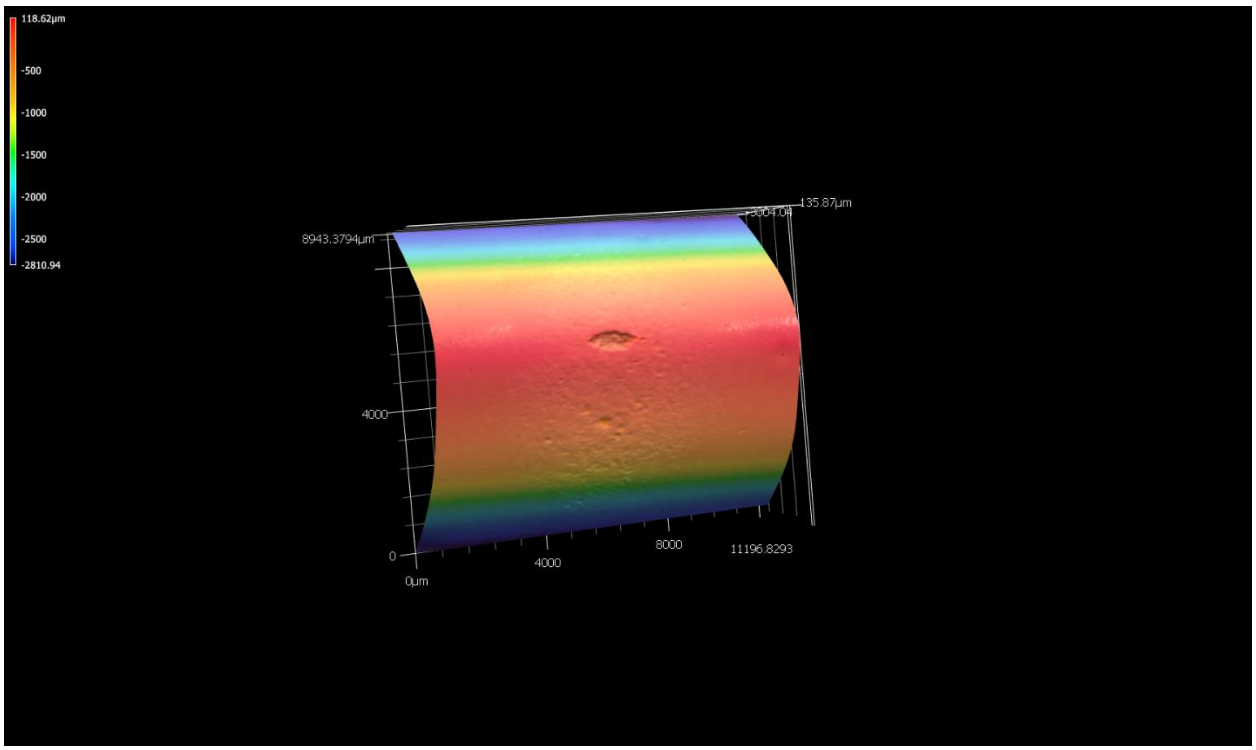


Fig. AVI-170: Erosion scar at 10° angle of impingement on the Polyurethane/IA-700 coated blade EXP3

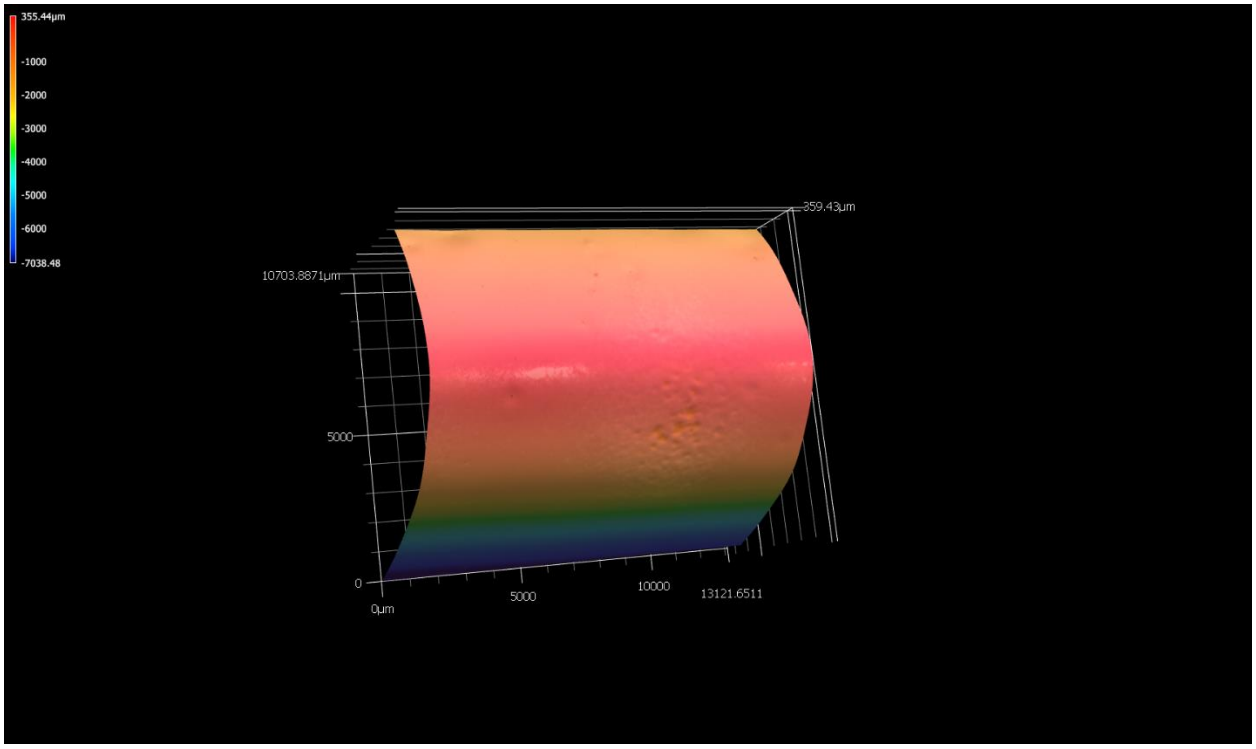


Fig. AVI-171: Erosion scar at 10° angle of impingement on the Polyurethane/IA-700 coated blade EXP4

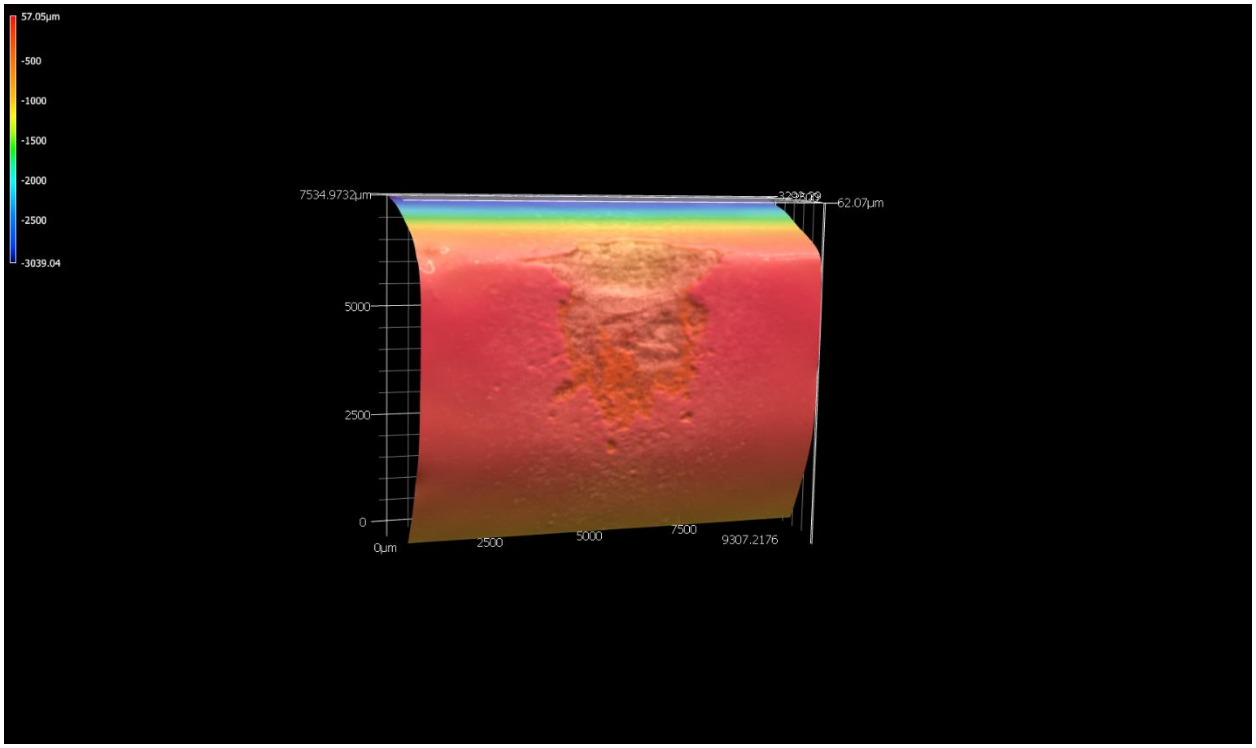


Fig. AVI-172: Erosion scar at 10° angle of impingement on the Polyurethane/IA-700 coated blade EXP5

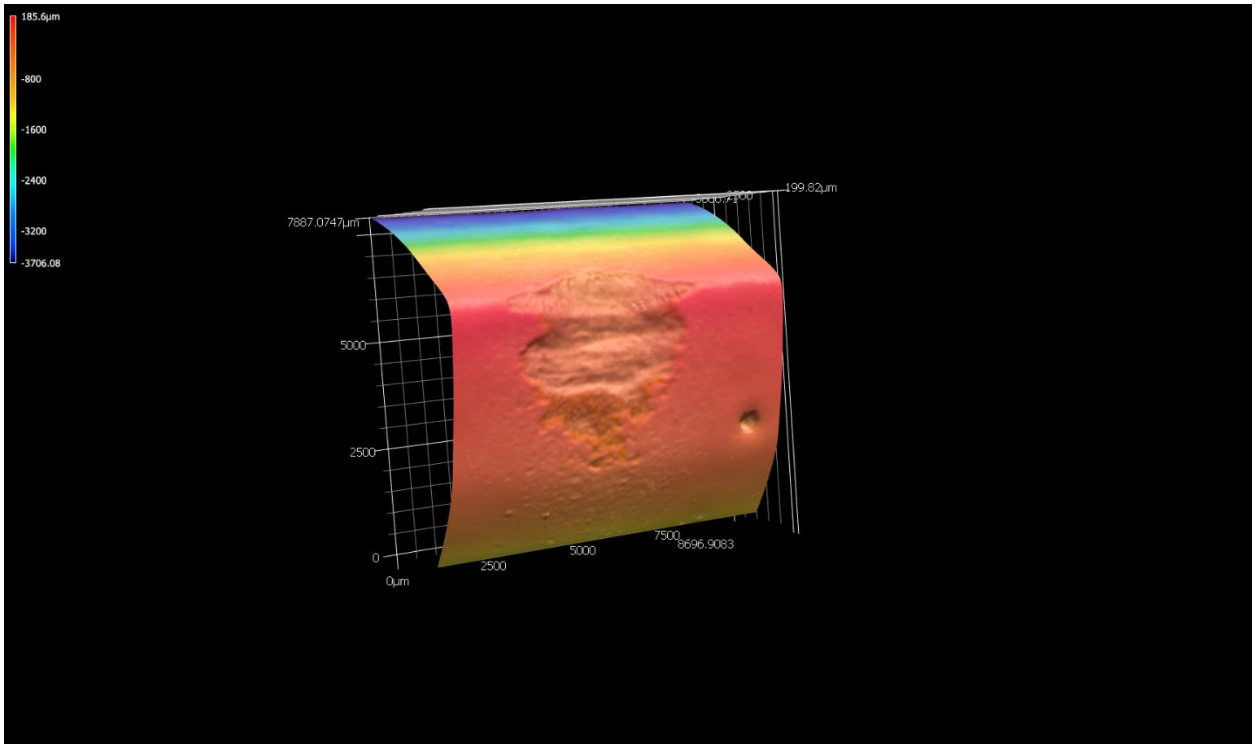


Fig. AVI-173: Erosion scar at 10° angle of impingement on the Polyurethane/IA-700 coated blade EXP6

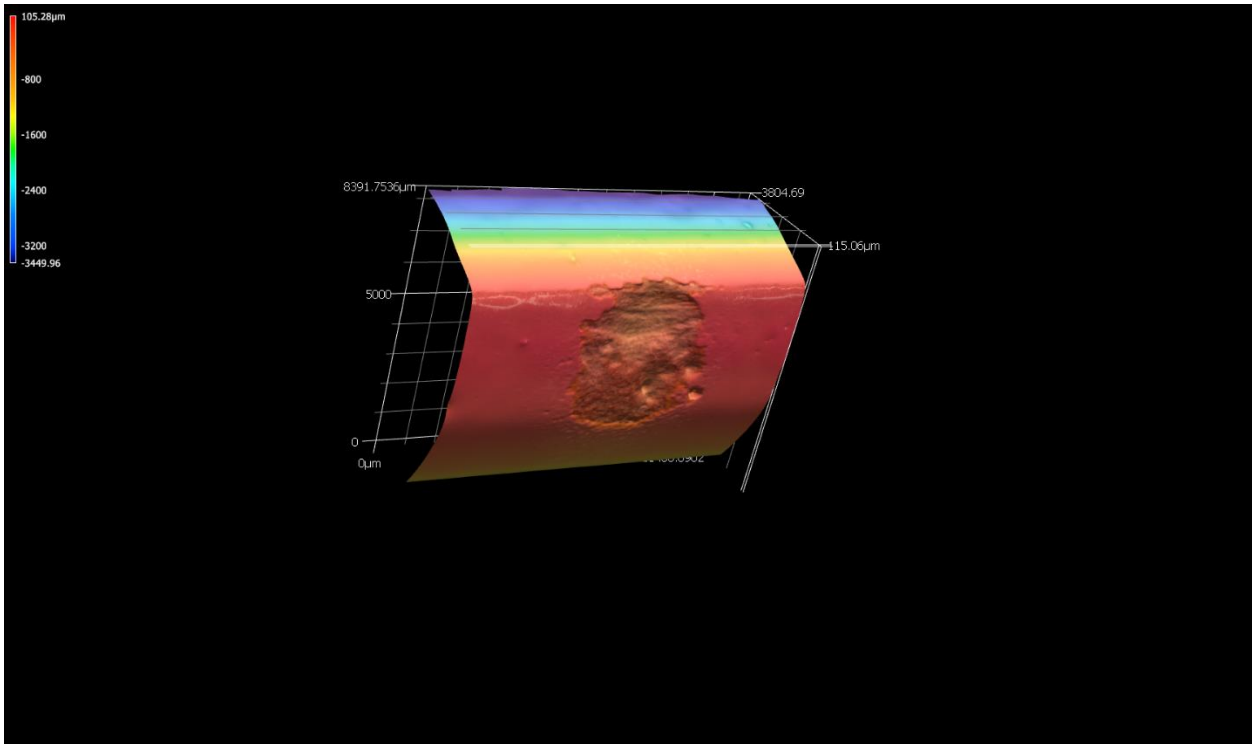


Fig. AVI-174: Erosion scar at 10° angle of impingement on the Polyurethane/IA-700 coated blade EXP7

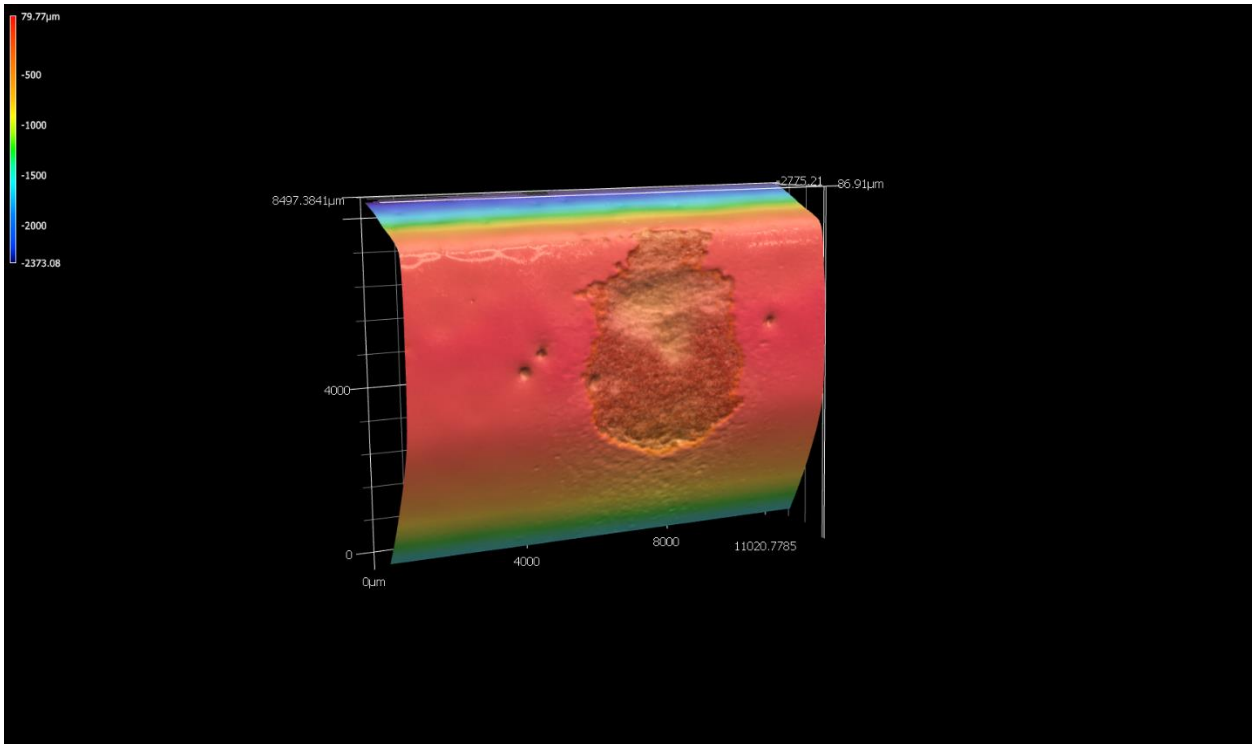


Fig. AVI-175: Erosion scar at 10° angle of impingement on the Polyurethane/IA-700 coated blade EXP8

- Tip Section
  - **-5 degrees**
    - **Uncoated**

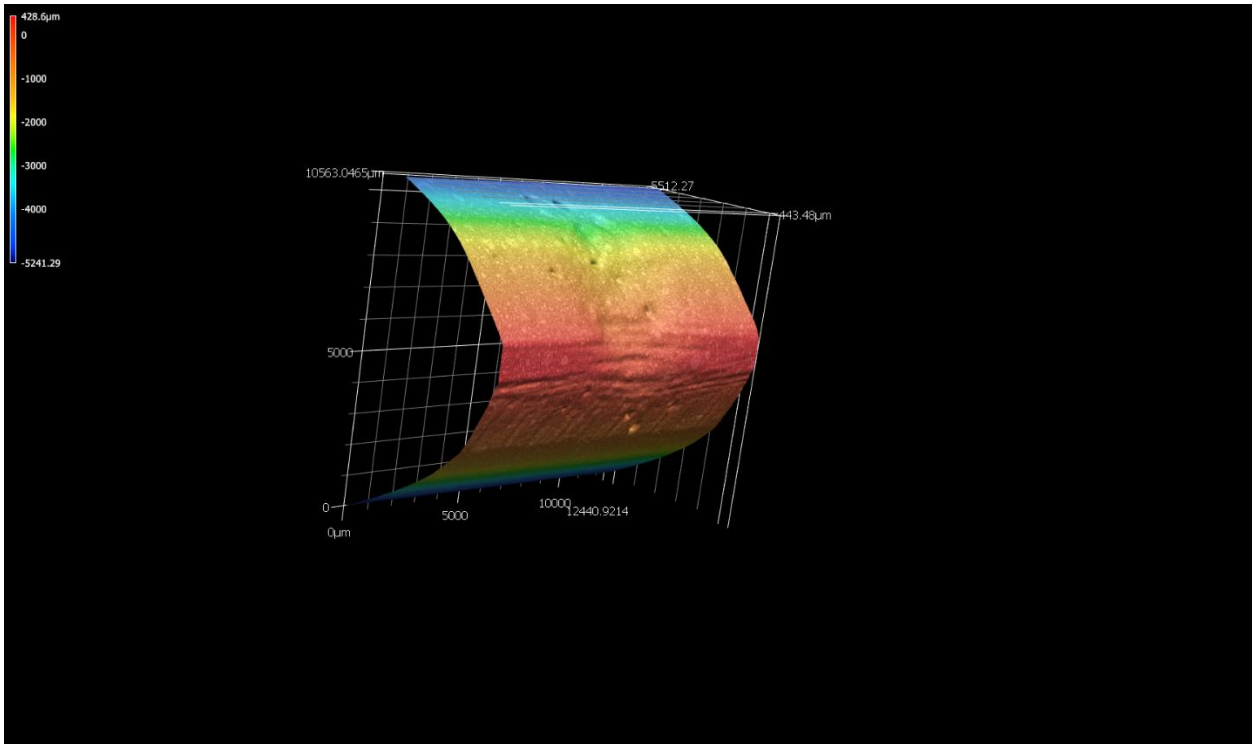


Fig. AVI-176: Erosion scar at -5° angle of impingement on the uncoated blade EXP1

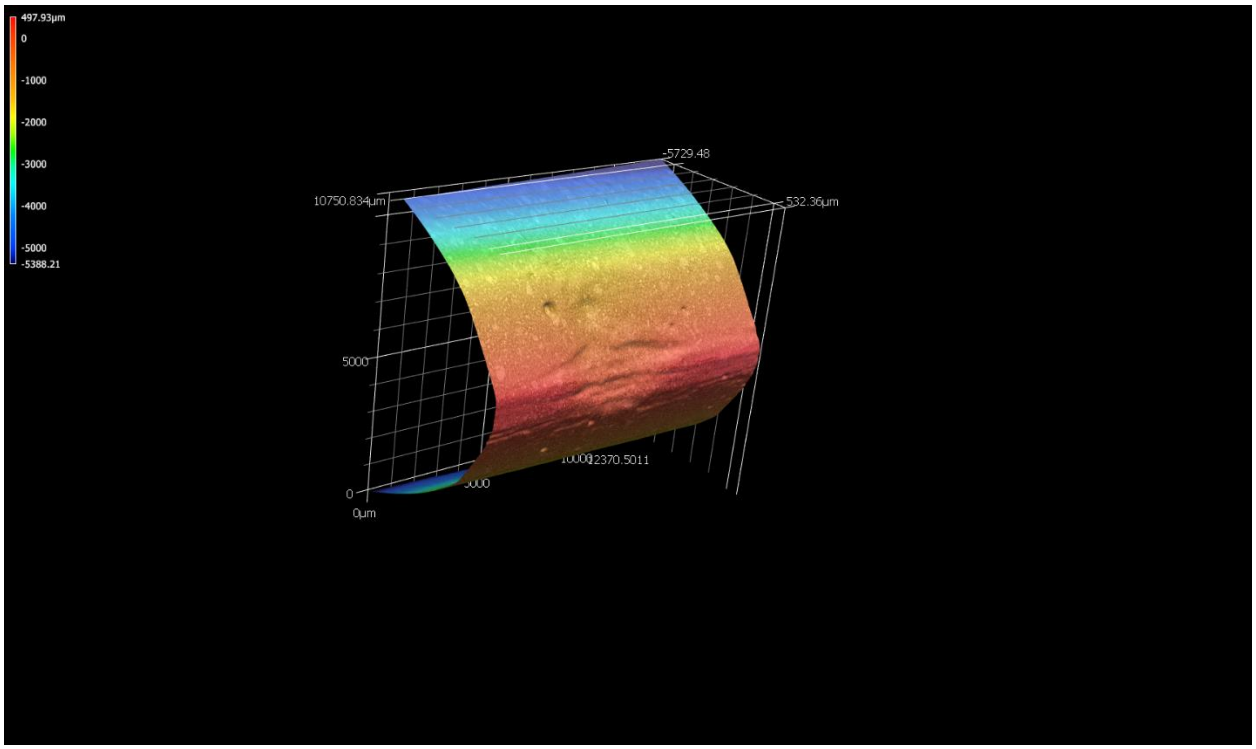


Fig. AVI-176: Erosion scar at -5° angle of impingement on the uncoated blade EXP2

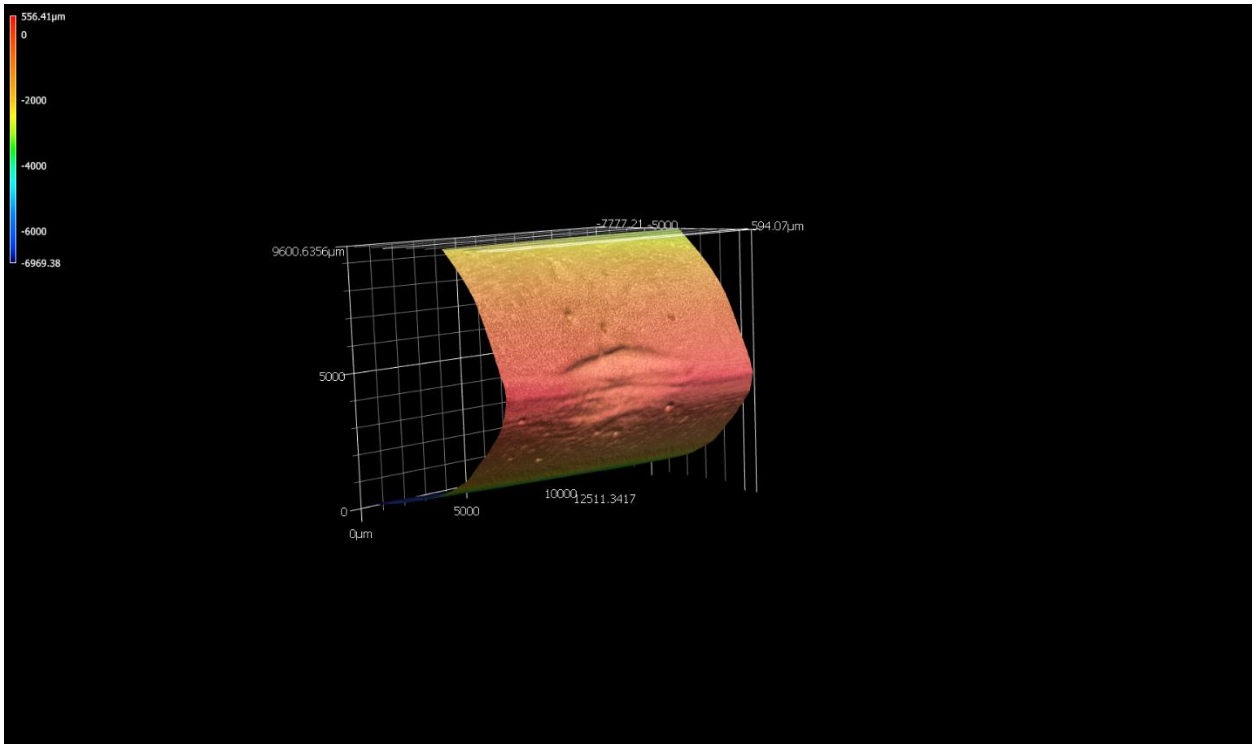


Fig. AVI-177: Erosion scar at -5° angle of impingement on the uncoated blade EXP3

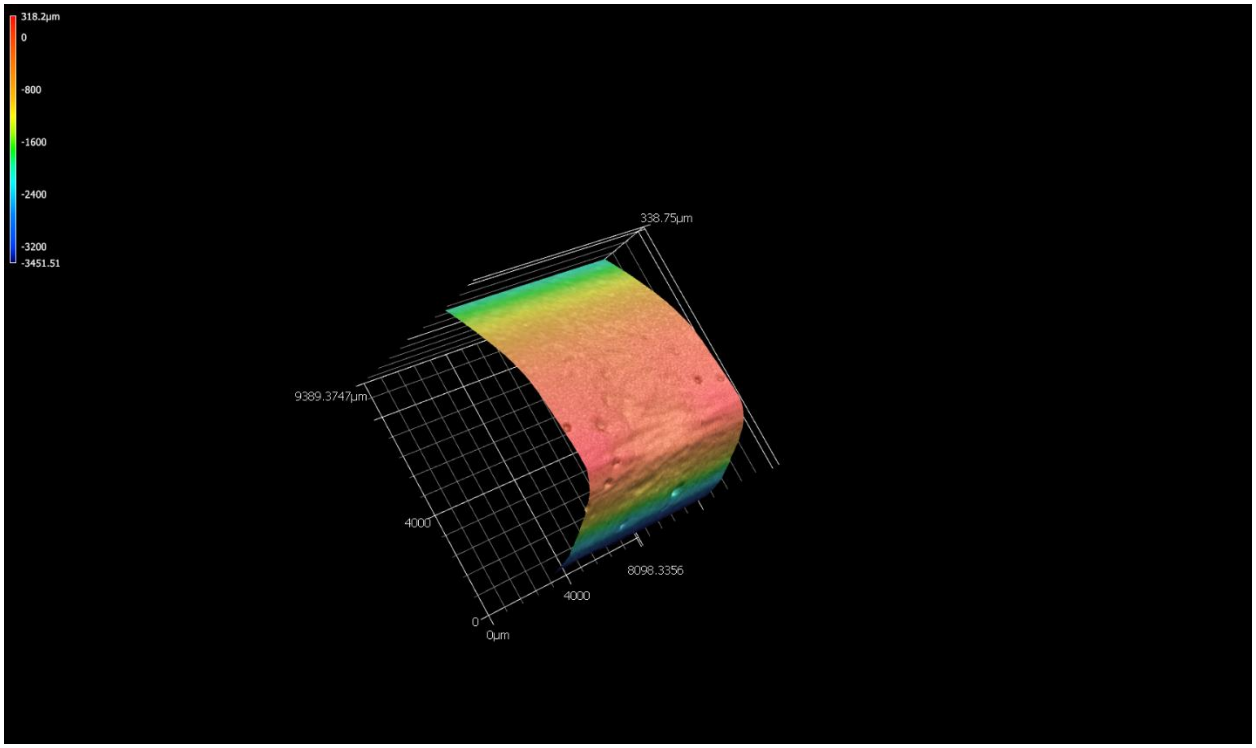


Fig. AVI-178: Erosion scar at -5° angle of impingement on the uncoated blade EXP4

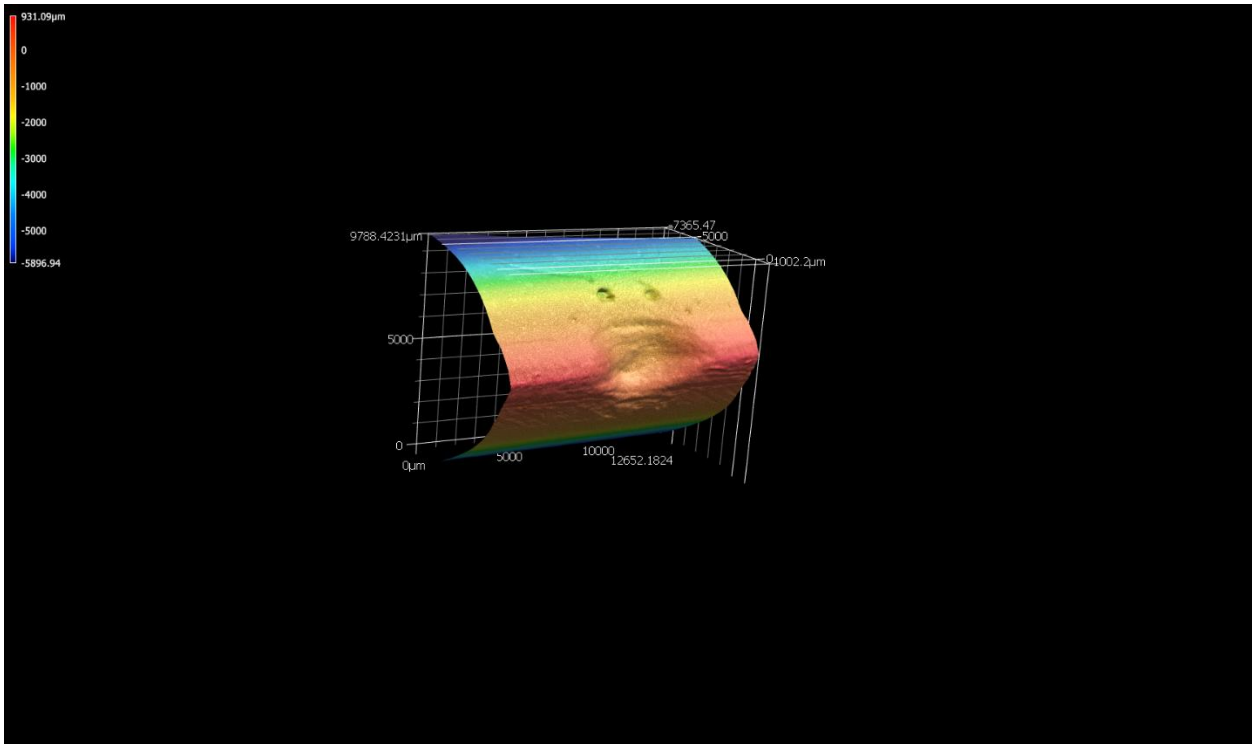


Fig. AVI-179: Erosion scar at -5° angle of impingement on the uncoated blade EXP5

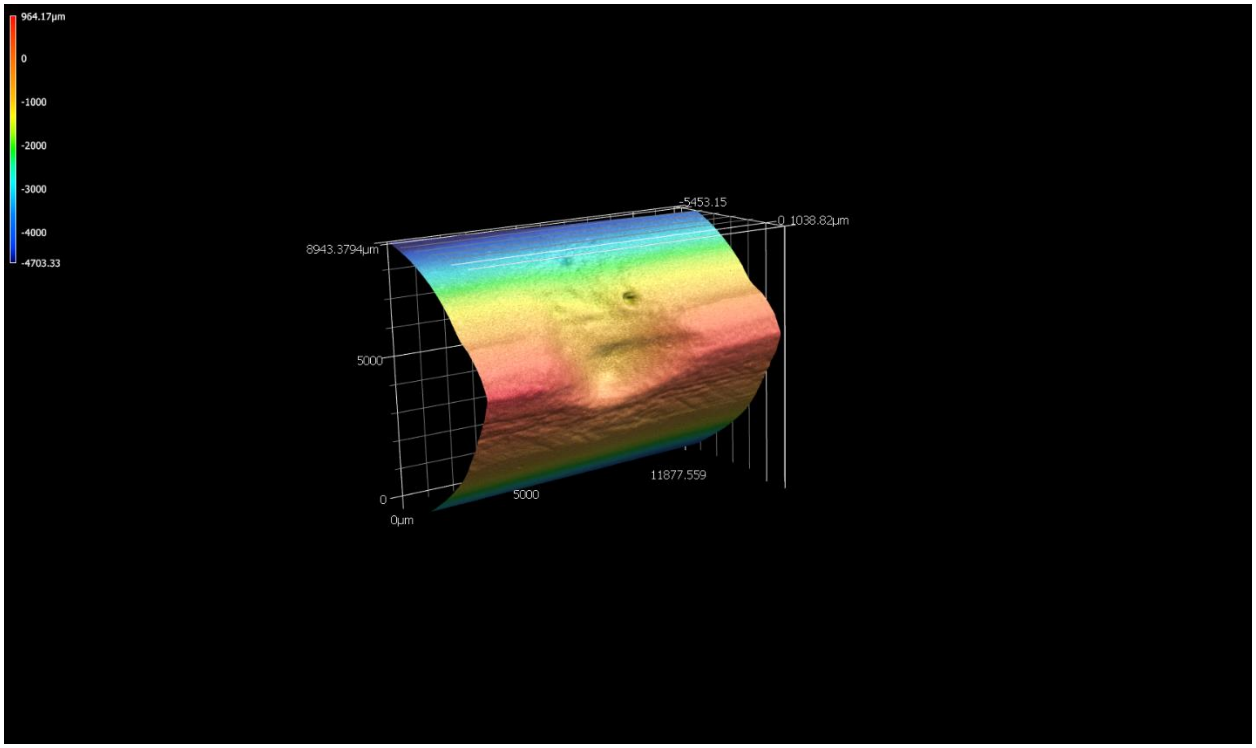


Fig. AVI-180: Erosion scar at -5° angle of impingement on the uncoated blade EXP6

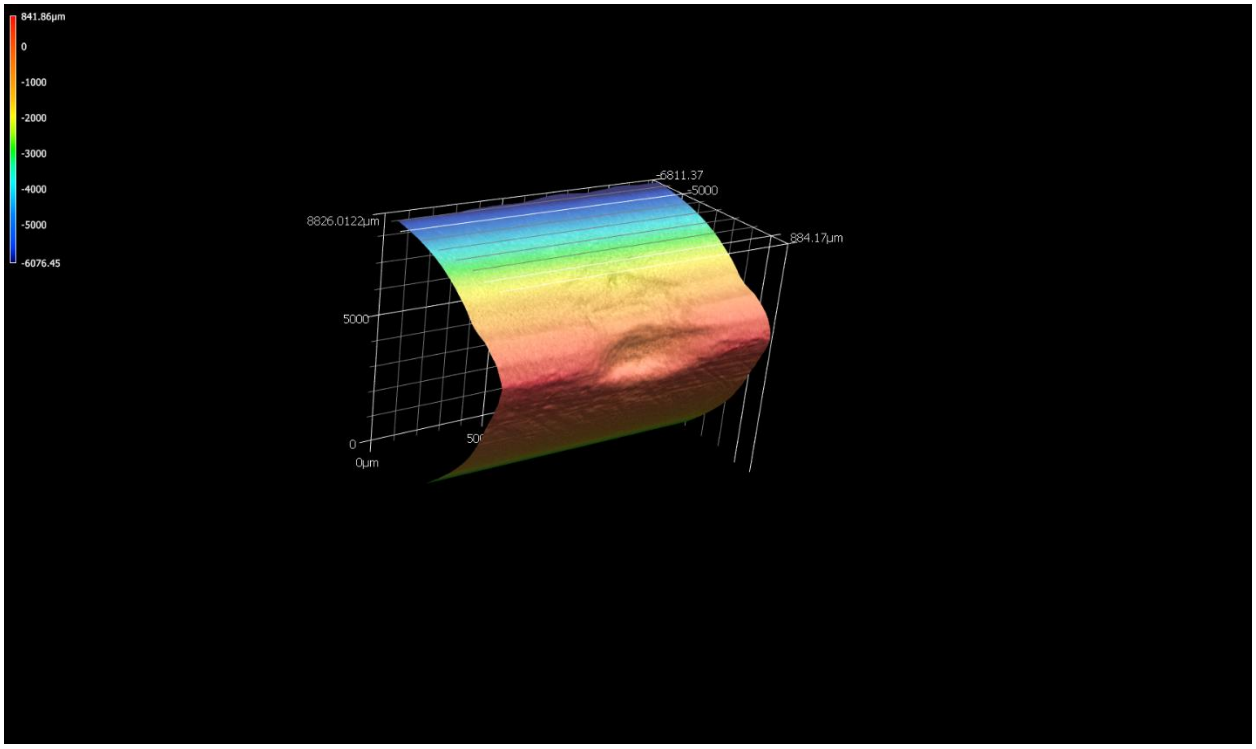


Fig. AVI-181: Erosion scar at -5° angle of impingement on the uncoated blade EXP7

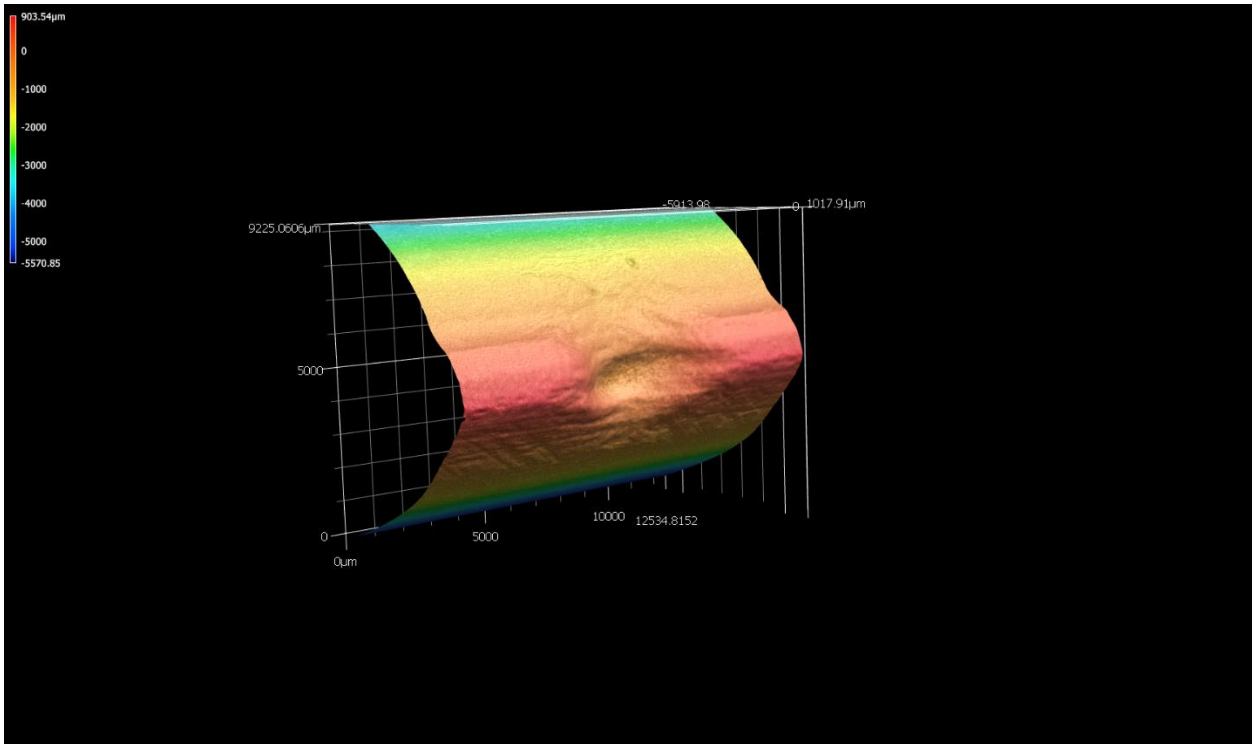


Fig. AVI-182: Erosion scar at -5° angle of impingement on the uncoated blade EXP8

- **H-146**

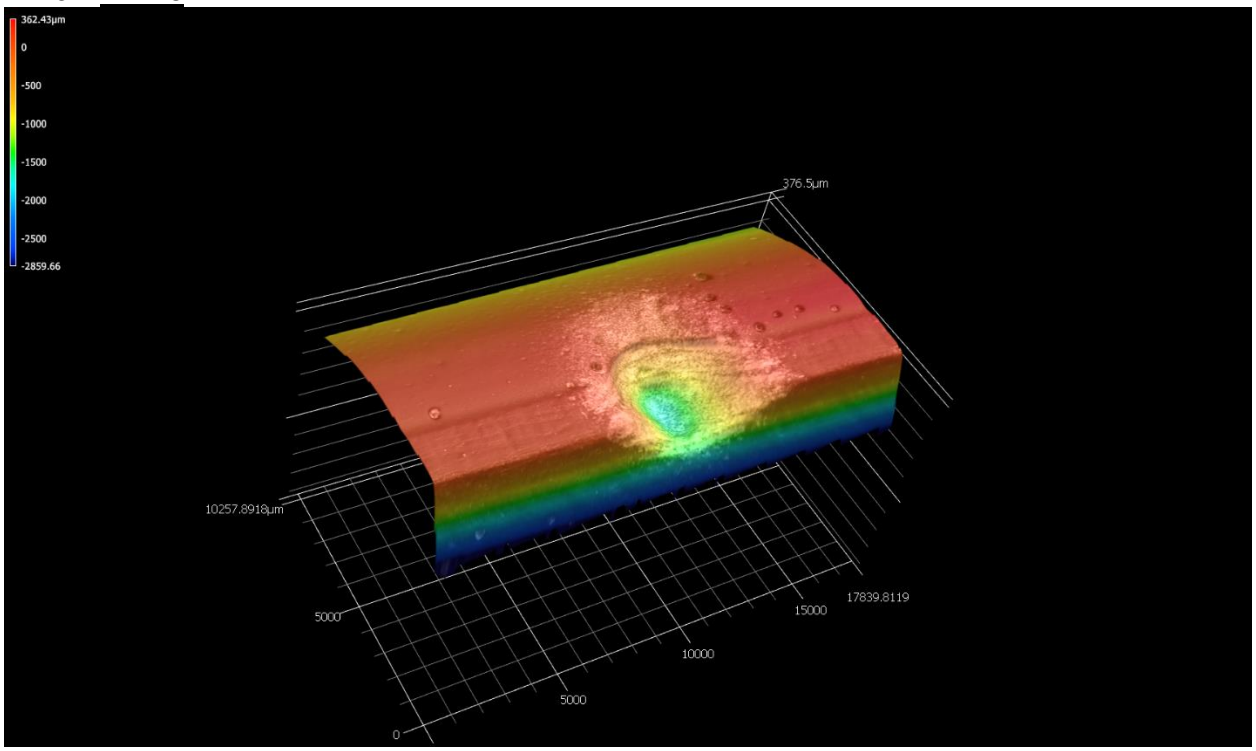


Fig. AVI-183: Erosion scar at -5° angle of impingement on the H-146 coated blade EXP1

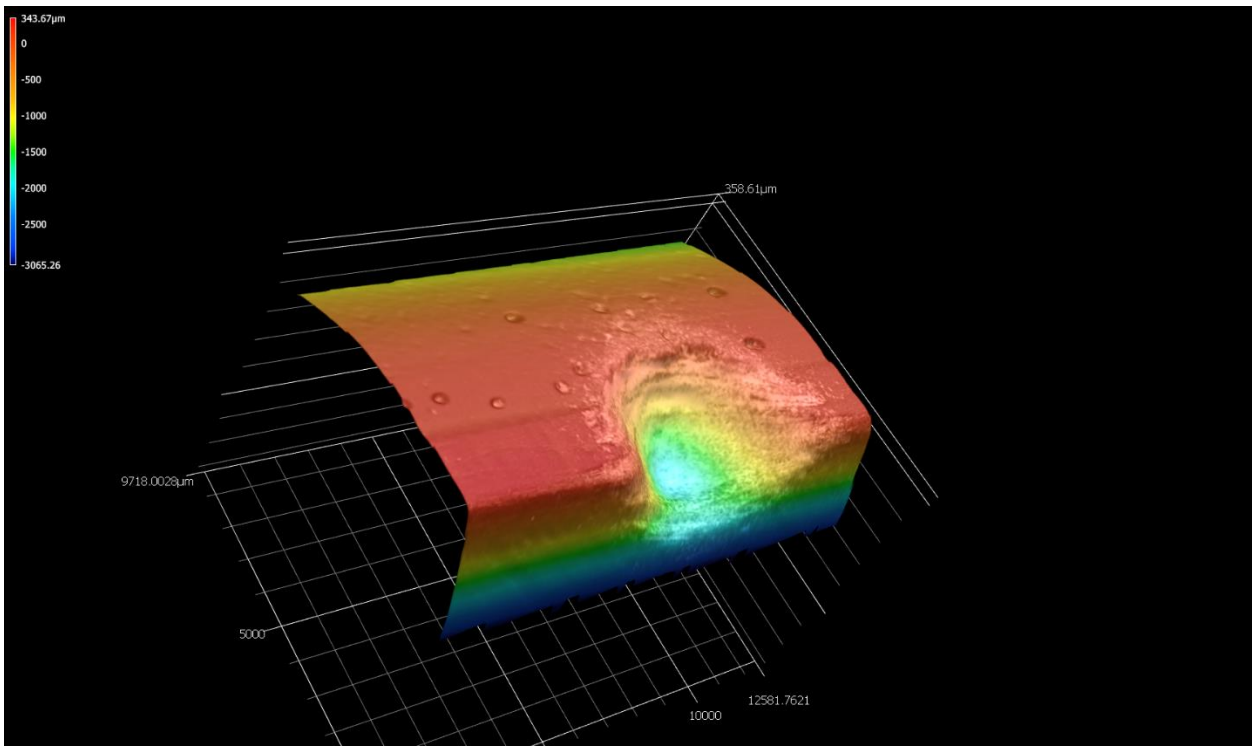


Fig. AVI-184: Erosion scar at -5° angle of impingement on the H-146 coated blade EXP2

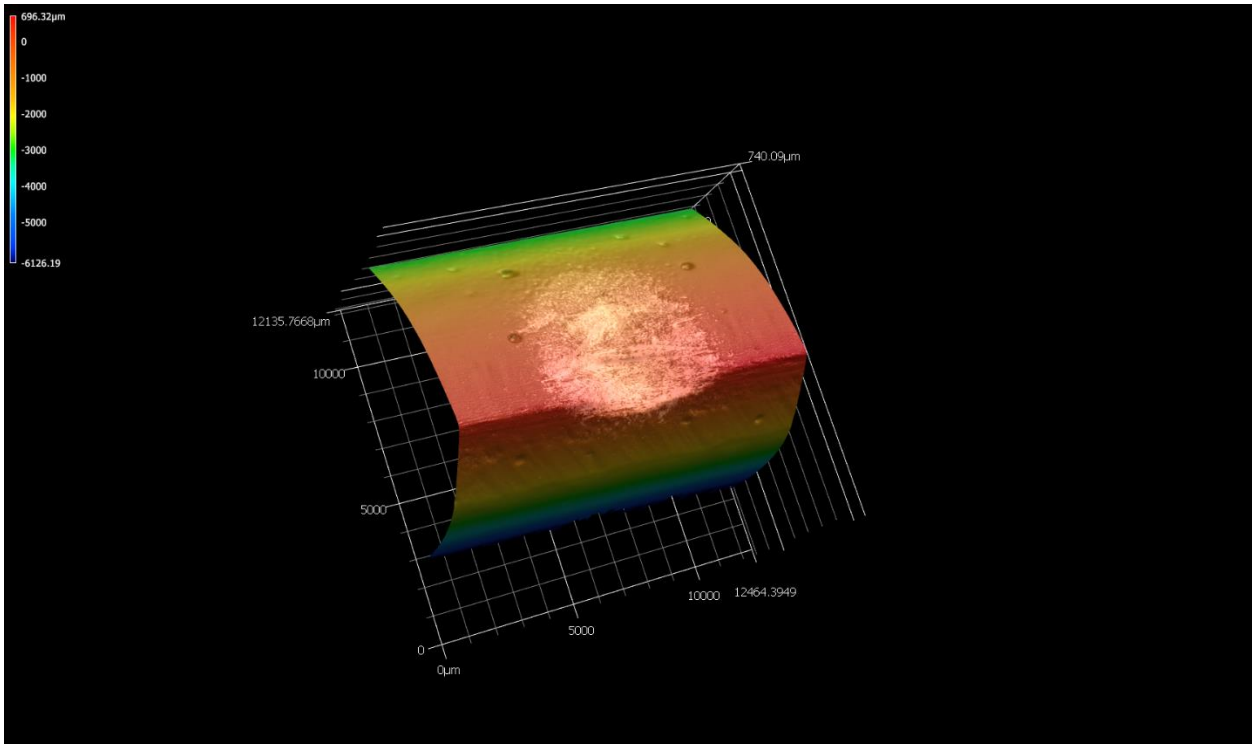


Fig. AVI-185: Erosion scar at -5° angle of impingement on the H-146 coated blade EXP3

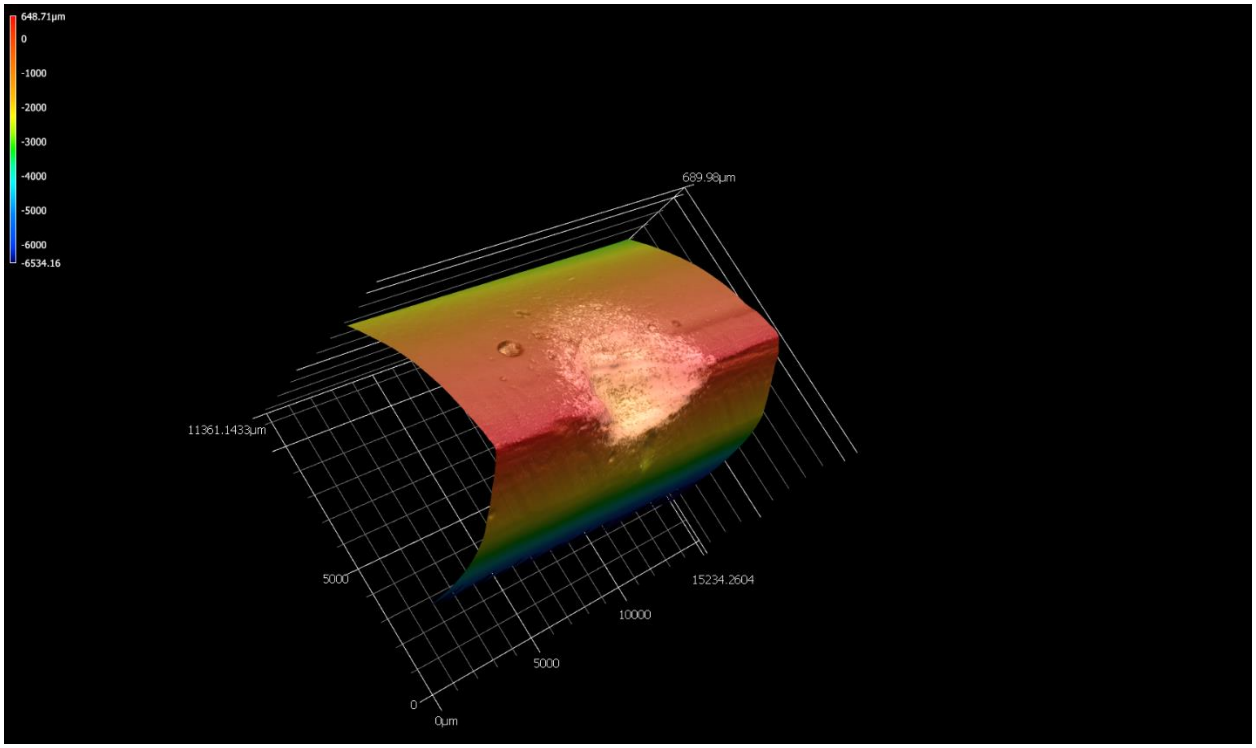


Fig. AVI-186: Erosion scar at -5° angle of impingement on the H-146 coated blade EXP4

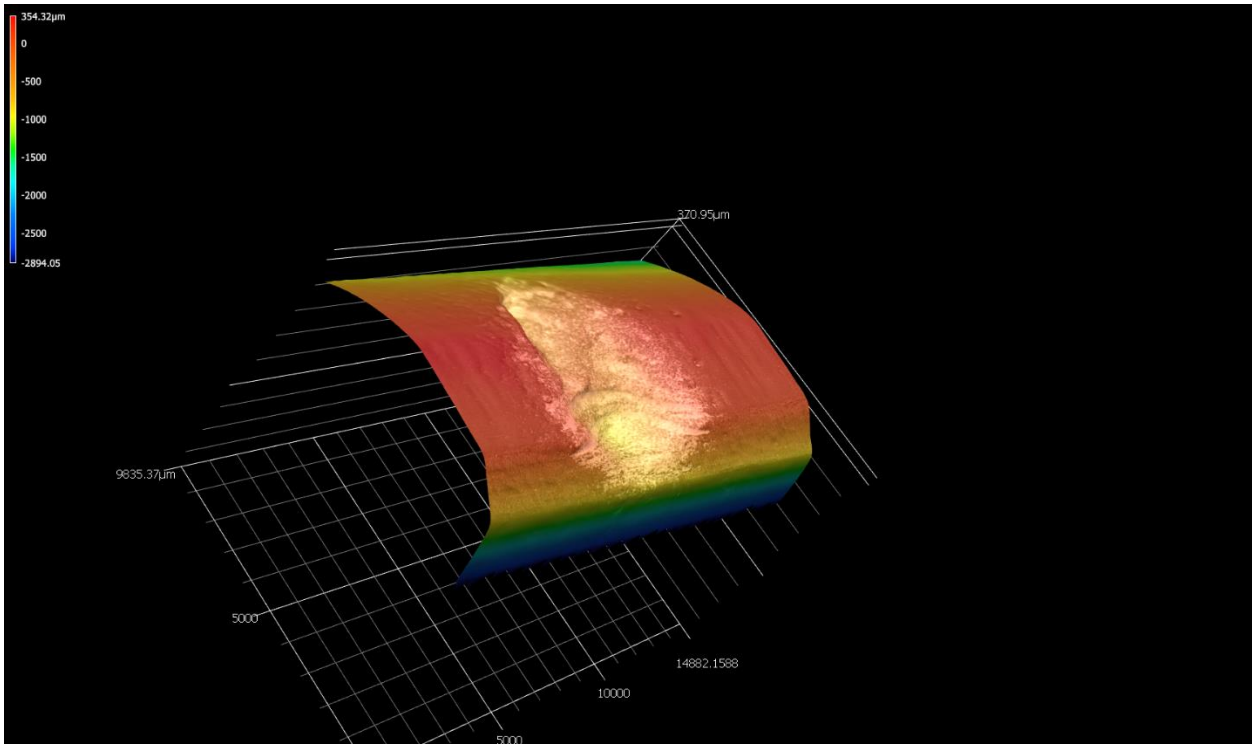


Fig. AVI-187: Erosion scar at -5° angle of impingement on the H-146 coated blade EXP5

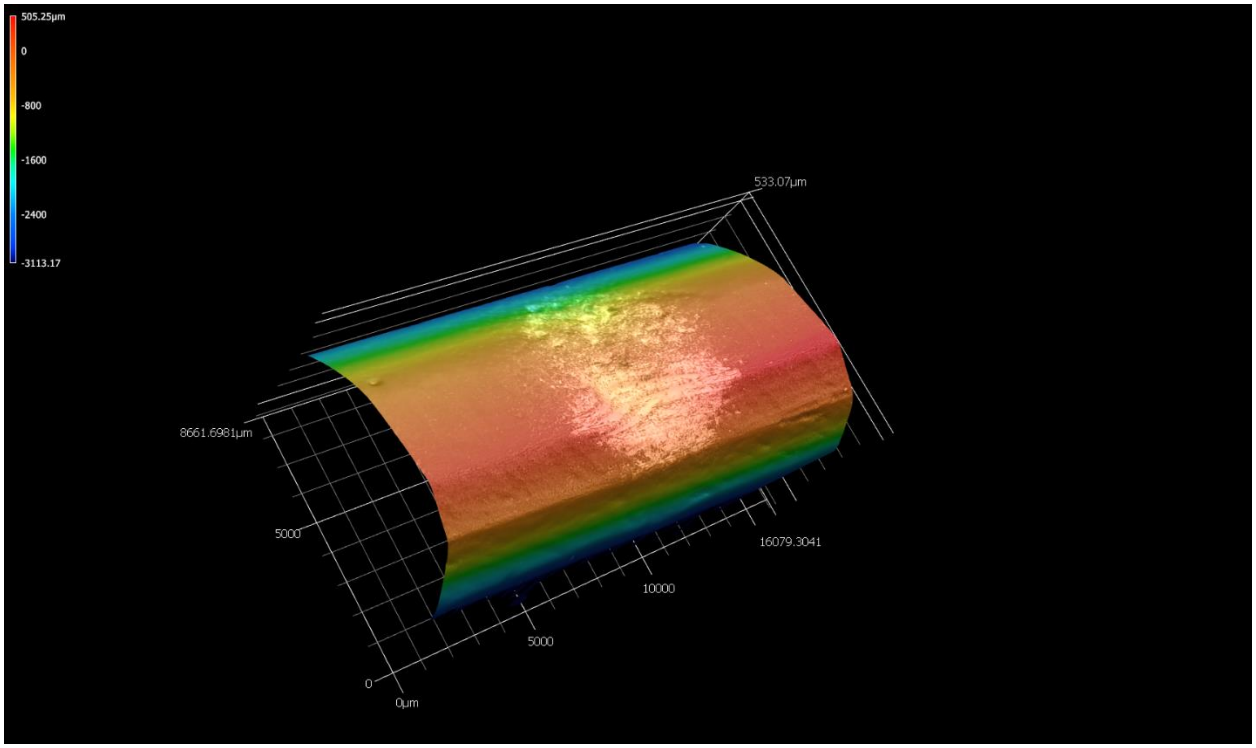


Fig. AVI-188: Erosion scar at -5° angle of impingement on the H-146 coated blade EXP6

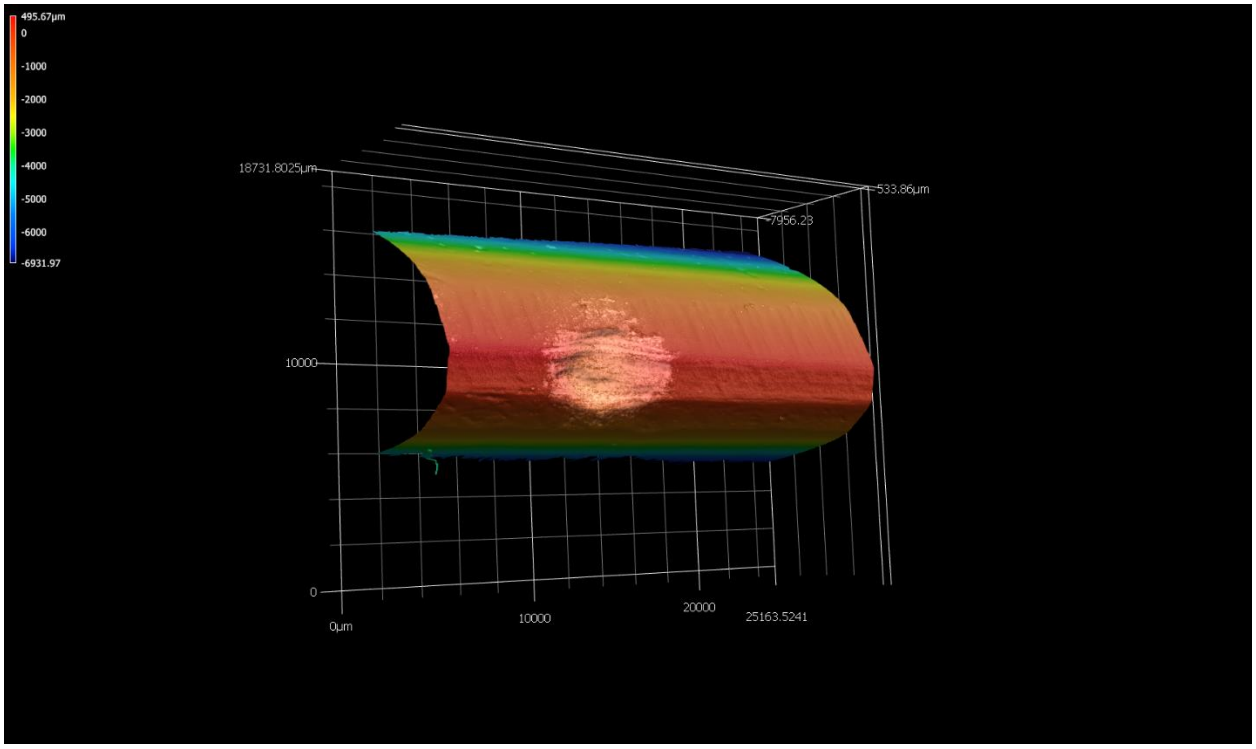


Fig. AVI-189: Erosion scar at -5° angle of impingement on the H-146 coated blade EXP7

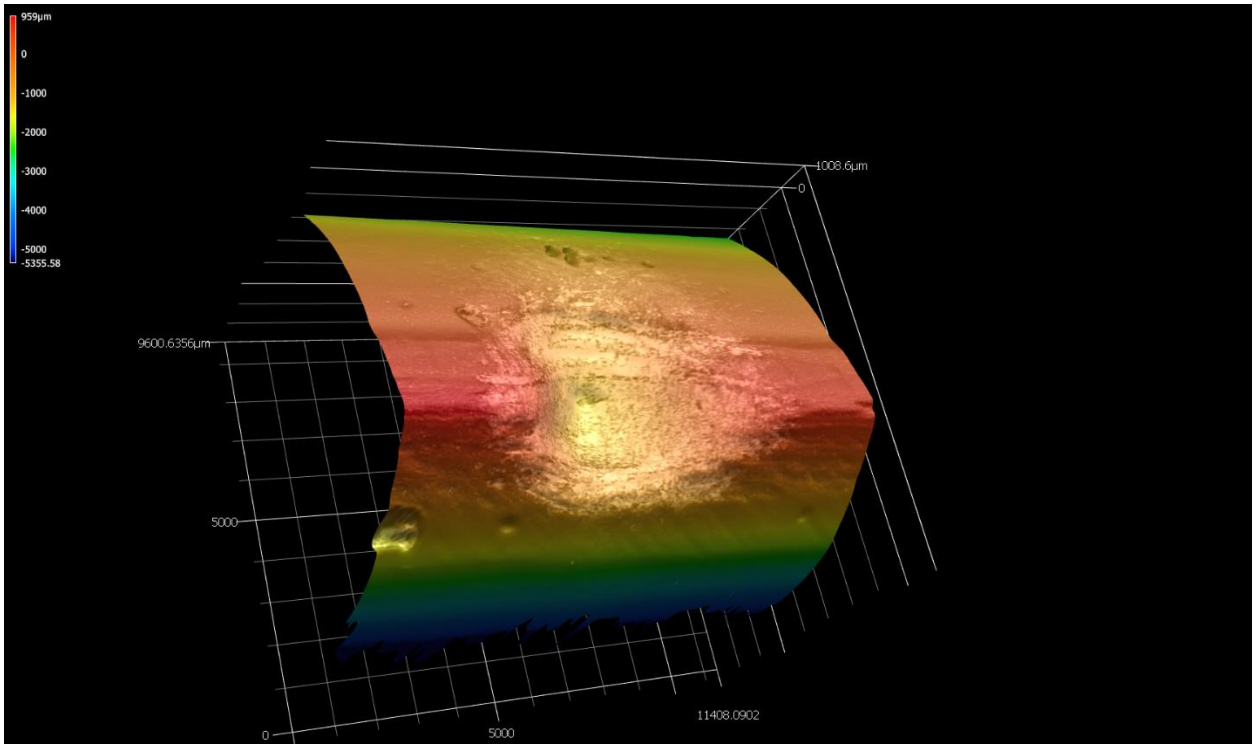


Fig. AVI-190: Erosion scar at -5° angle of impingement on the H-146 coated blade EXP8

- **Polyurethane/IA-700**

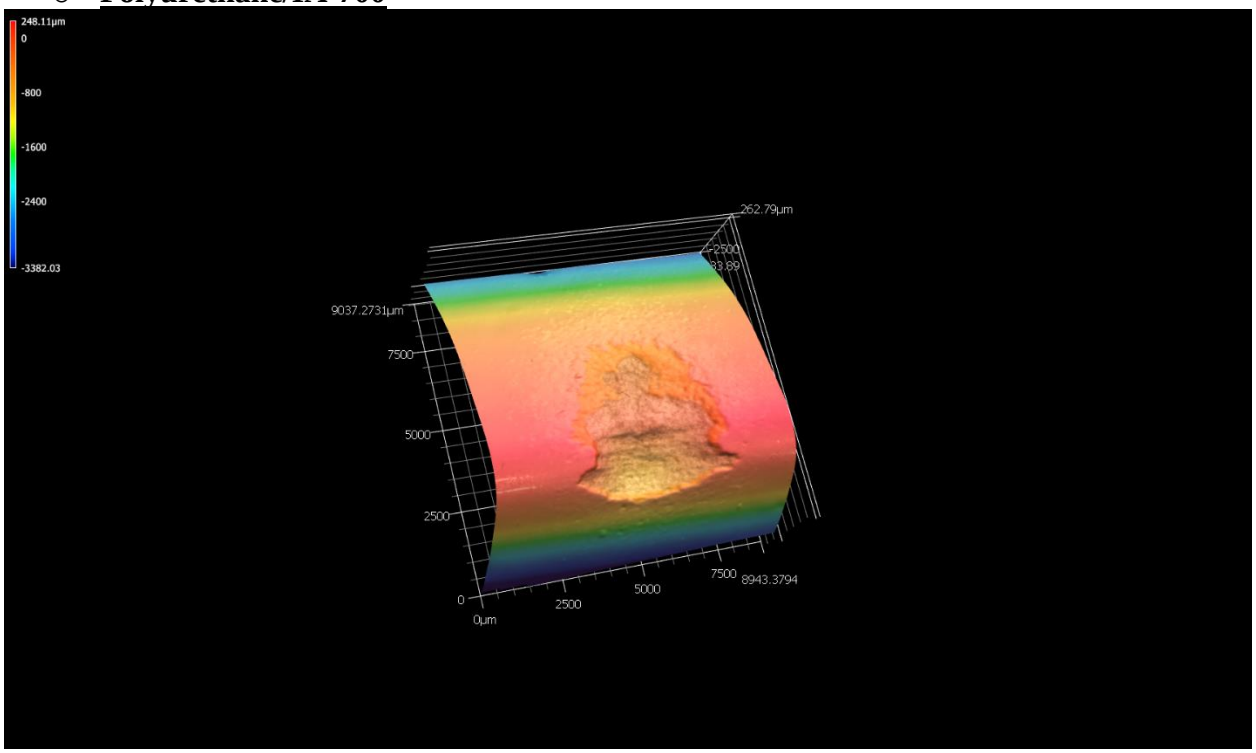


Fig. AVI-191: Erosion scar at -5° angle of impingement on the Polyurethane/IA-700 coated blade EXP1

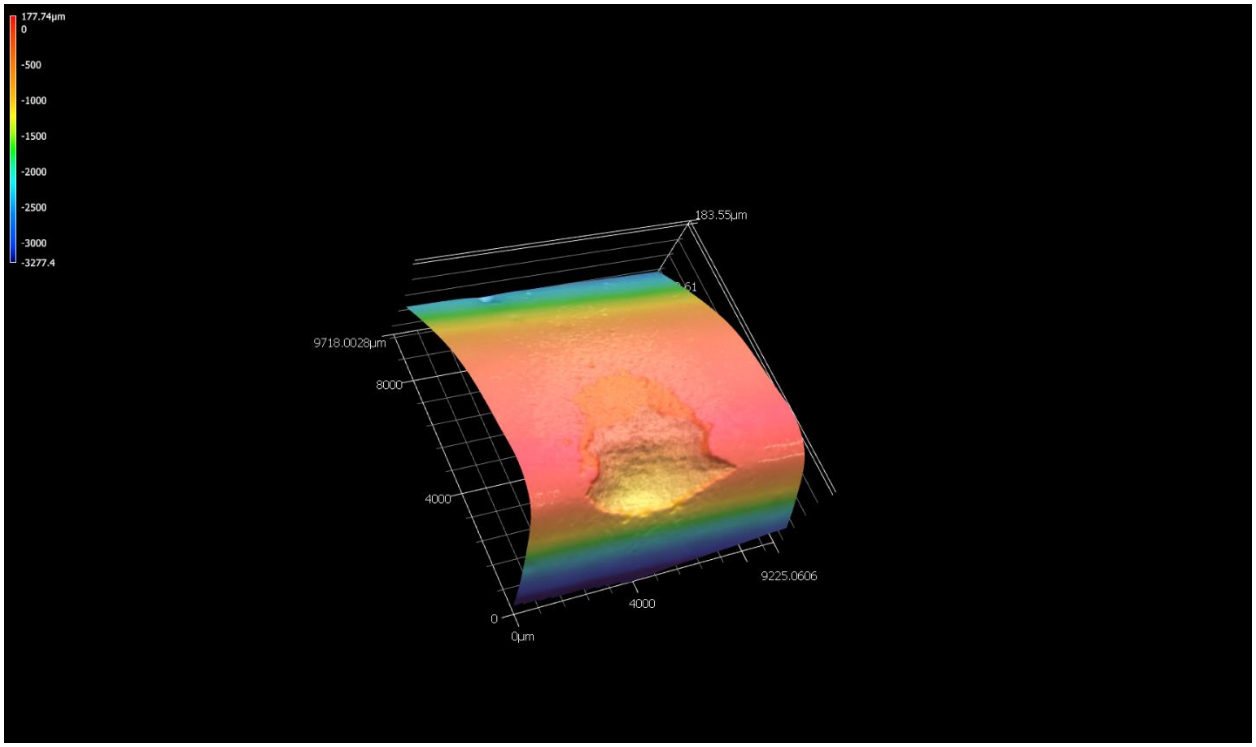


Fig. AVI-192: Erosion scar at -5° angle of impingement on the Polyurethane/IA-700 coated blade EXP2

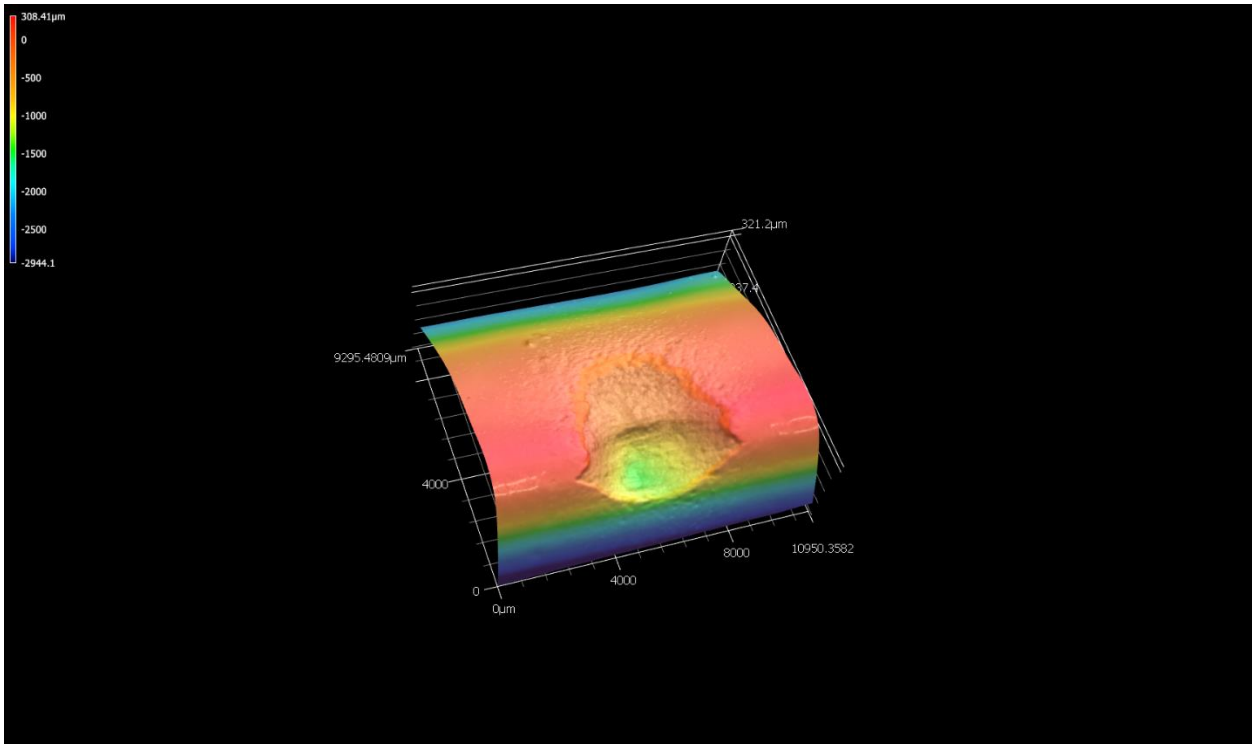


Fig. AVI-193: Erosion scar at -5° angle of impingement on the Polyurethane/IA-700 coated blade EXP3

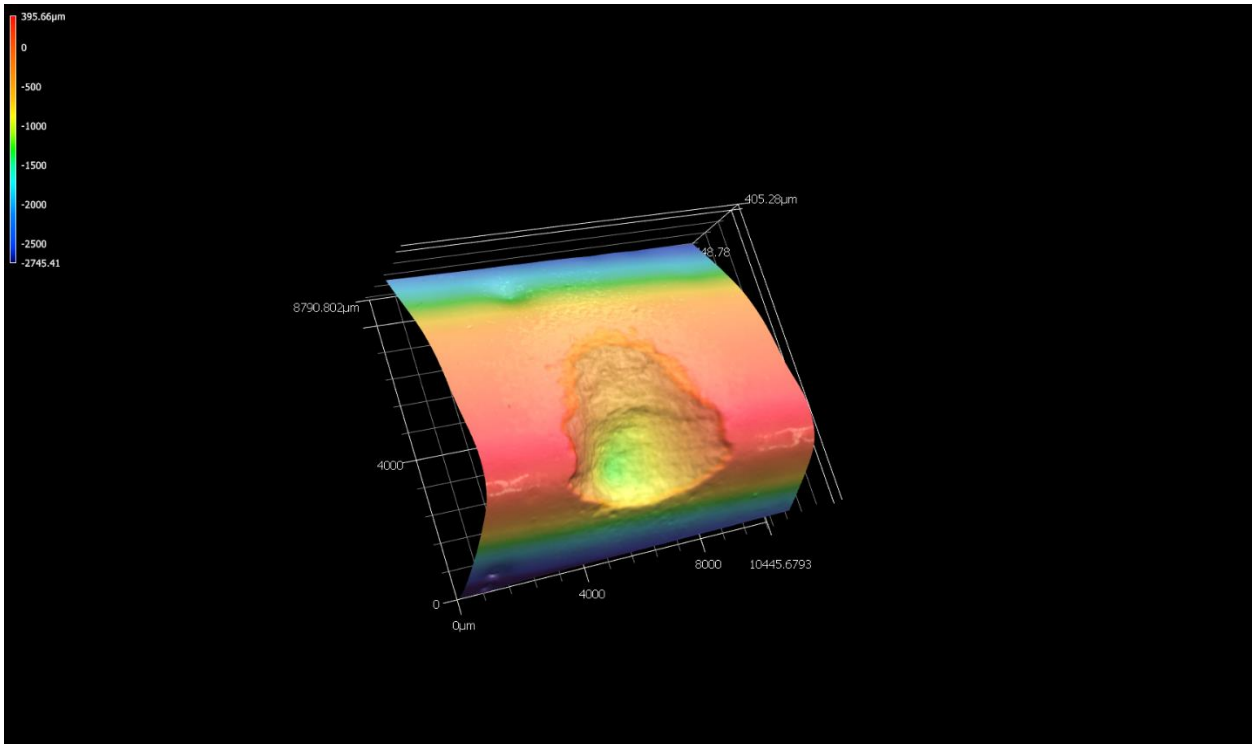


Fig. AVI-194: Erosion scar at -5° angle of impingement on the Polyurethane/IA-700 coated blade EXP4

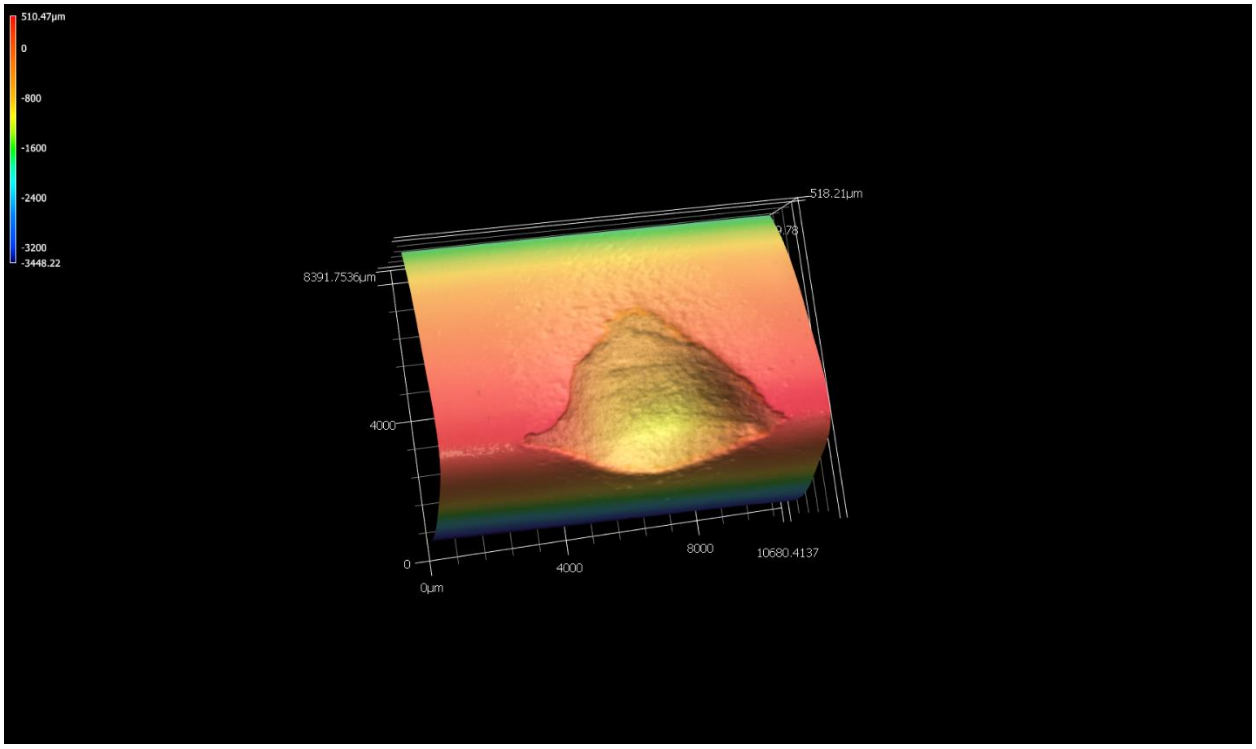


Fig. AVI-195: Erosion scar at -5° angle of impingement on the Polyurethane/IA-700 coated blade EXP5

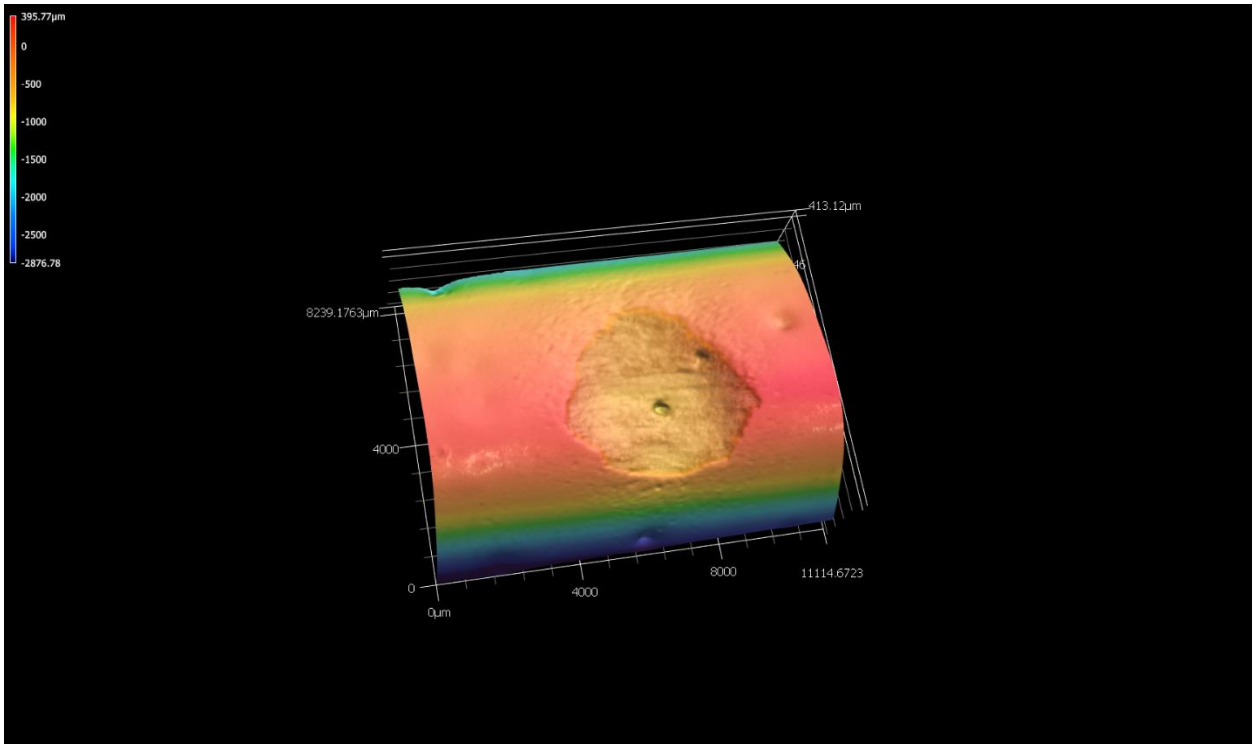


Fig. AVI-196: Erosion scar at -5° angle of impingement on the Polyurethane/IA-700 coated blade EXP6

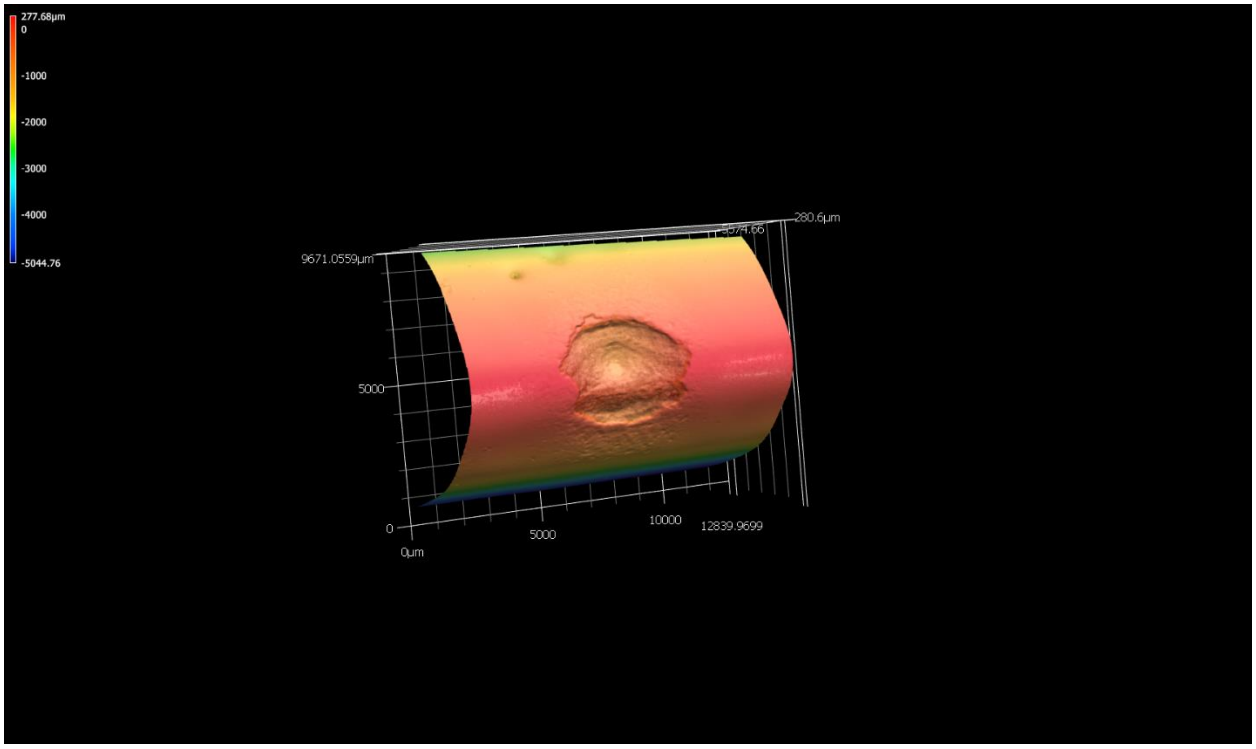


Fig. AVI-197: Erosion scar at -5° angle of impingement on the Polyurethane/IA-700 coated blade EXP7

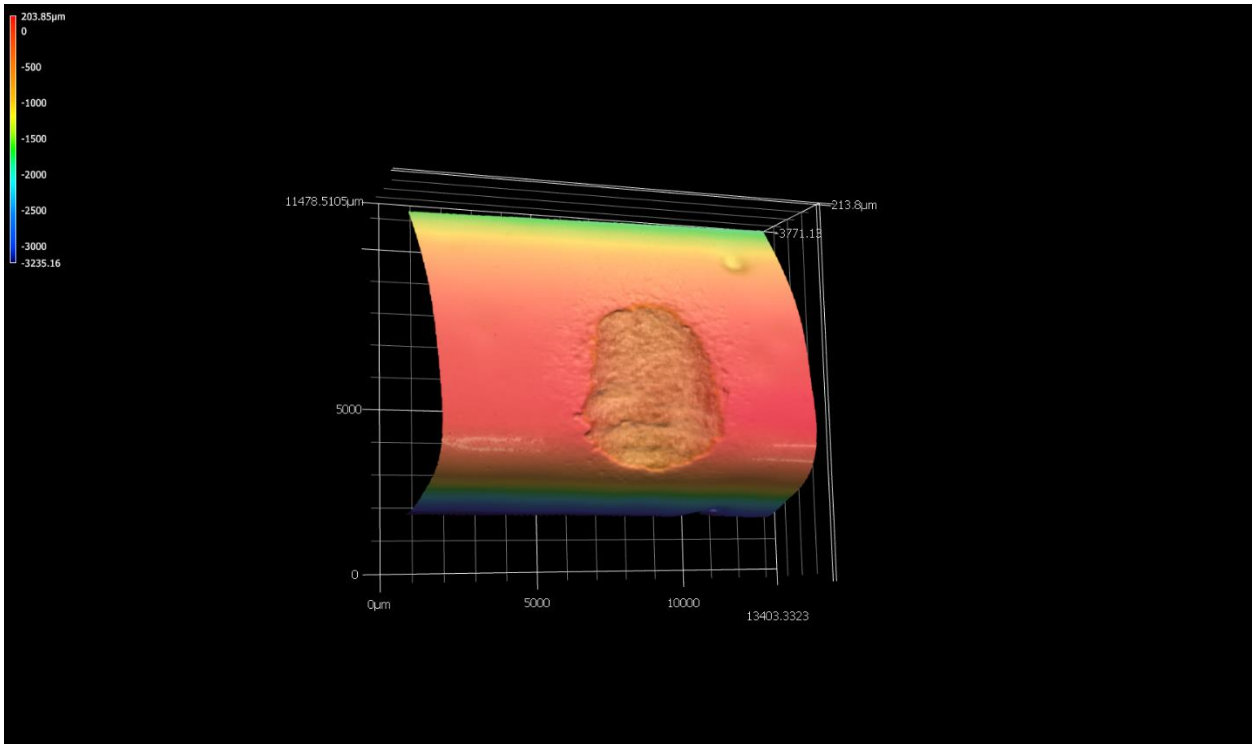


Fig. AVI-198: Erosion scar at -5° angle of impingement on the Polyurethane/IA-700 coated blade EXP8

- **0 degrees**
  - **Uncoated**

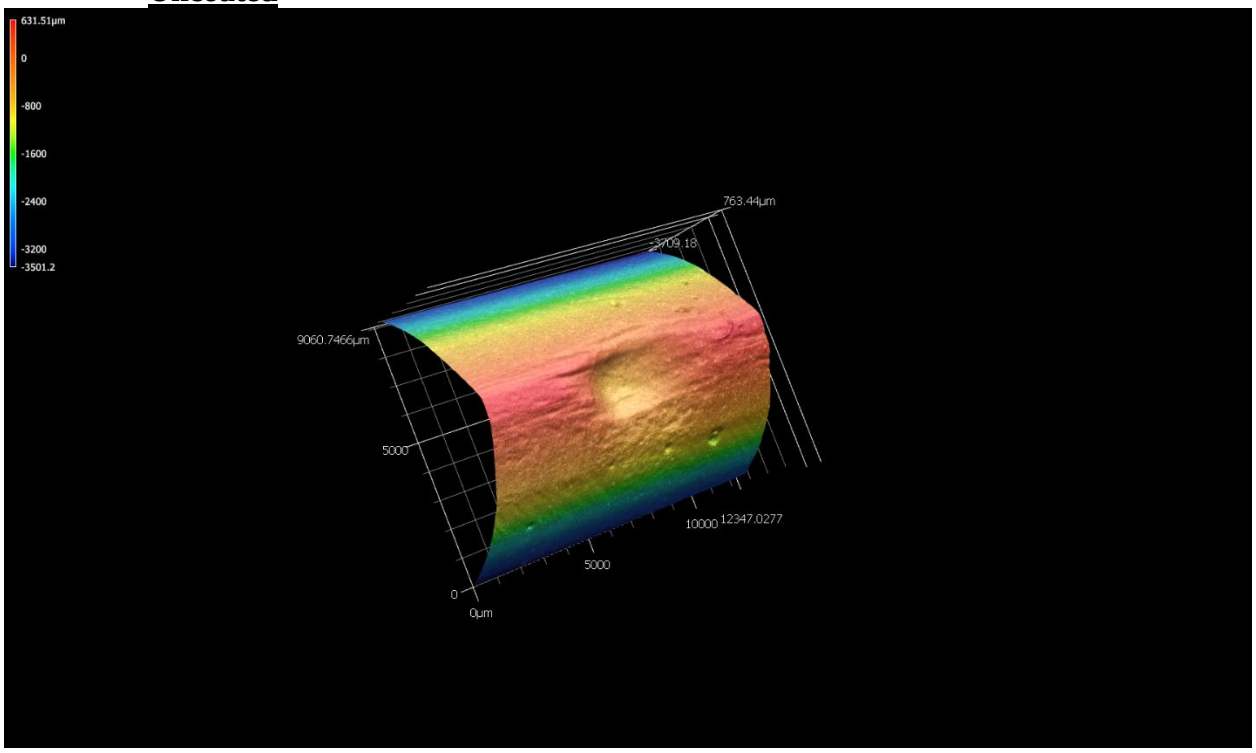


Fig. AVI-199: Erosion scar at 0° angle of impingement on the uncoated blade EXP1

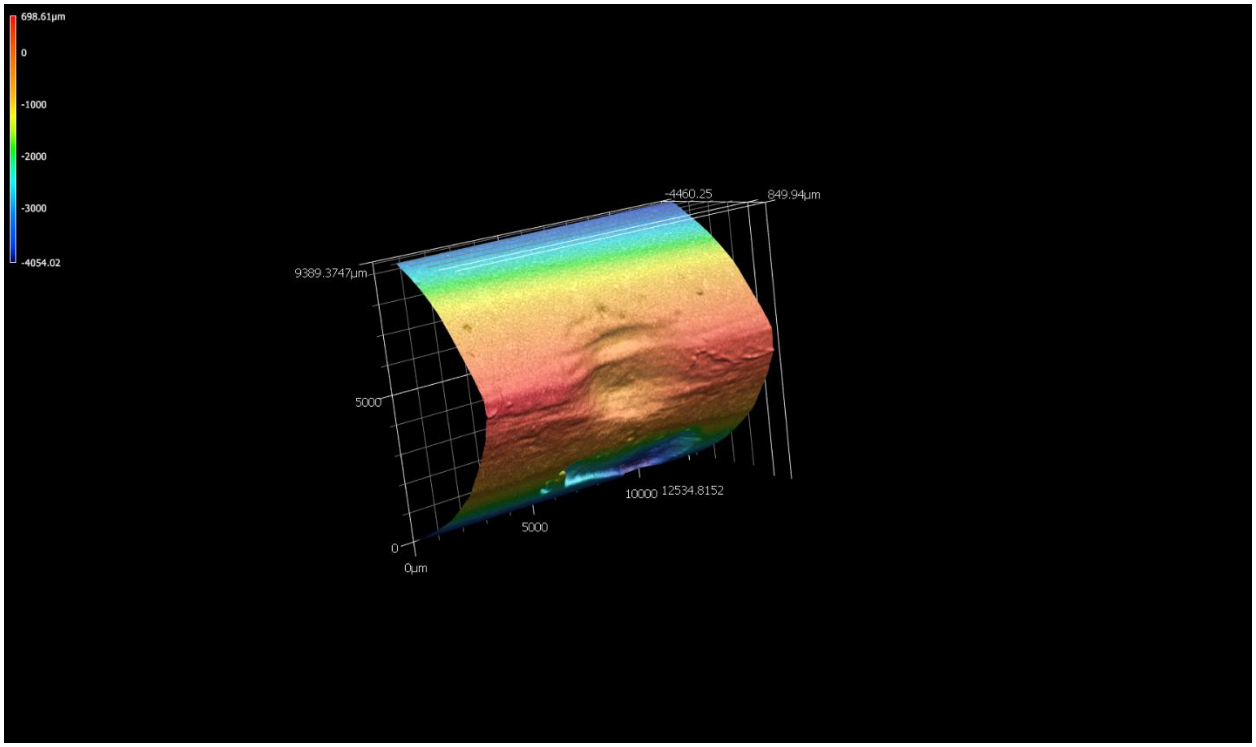


Fig. AVI-200: Erosion scar at 0° angle of impingement on the uncoated blade EXP2

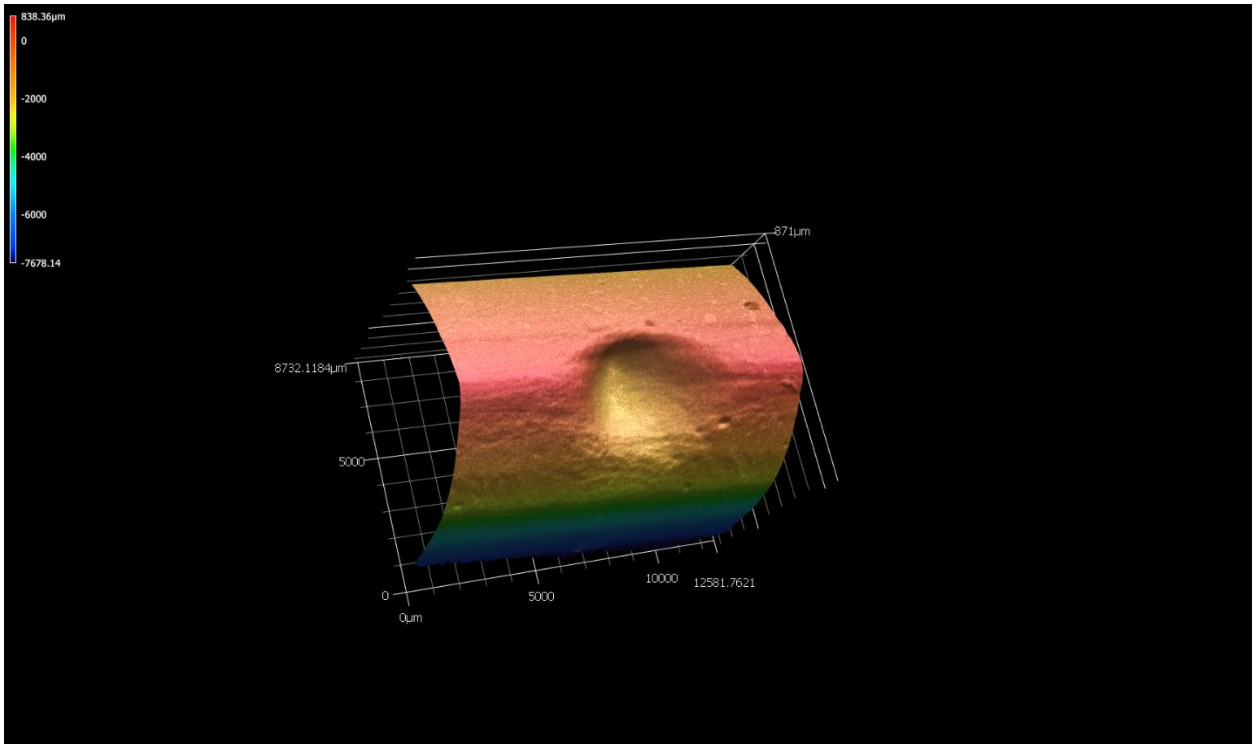


Fig. AVI-201: Erosion scar at 0° angle of impingement on the uncoated blade EXP3

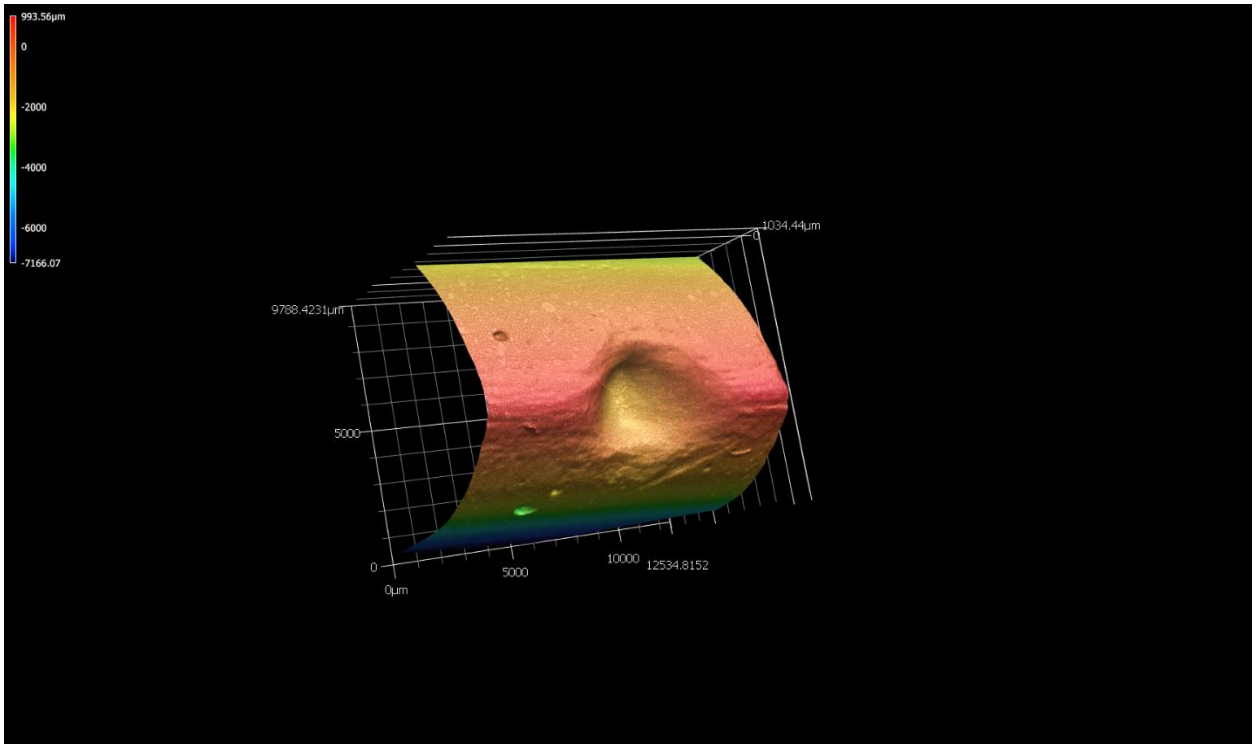


Fig. AVI-202: Erosion scar at 0° angle of impingement on the uncoated blade EXP4

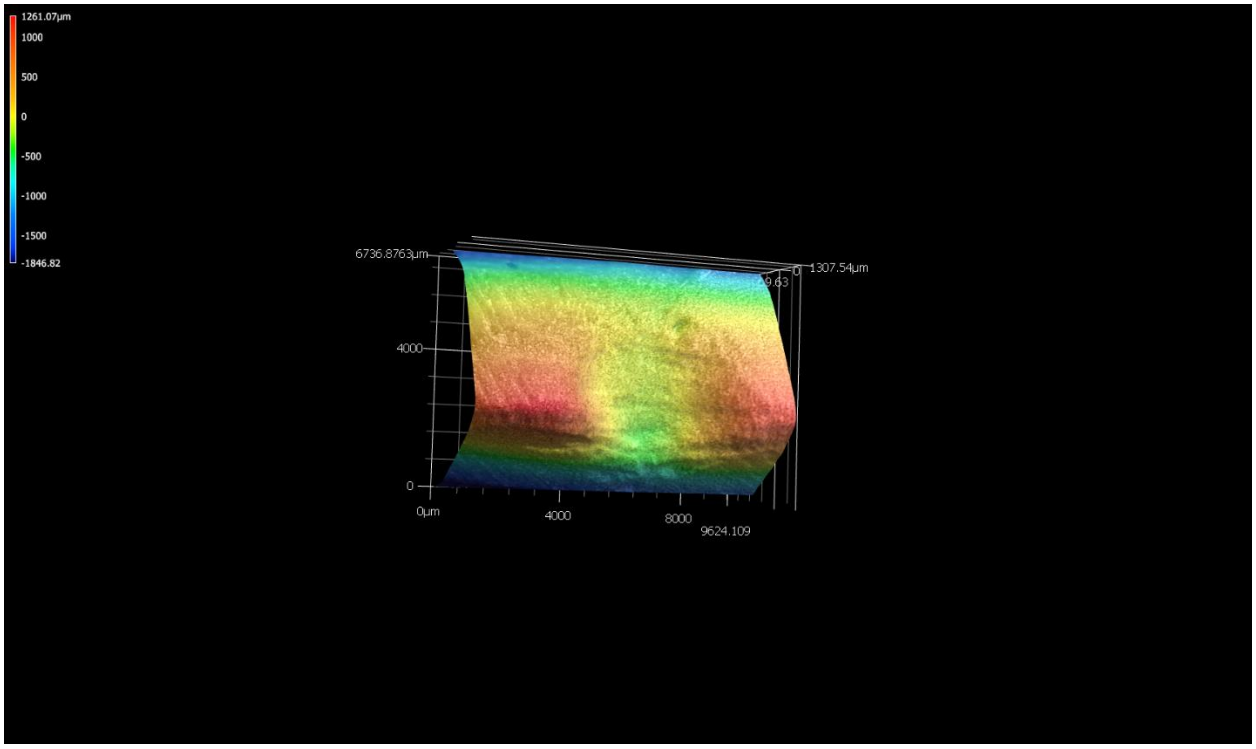


Fig. AVI-203: Erosion scar at 0° angle of impingement on the uncoated blade EXP5

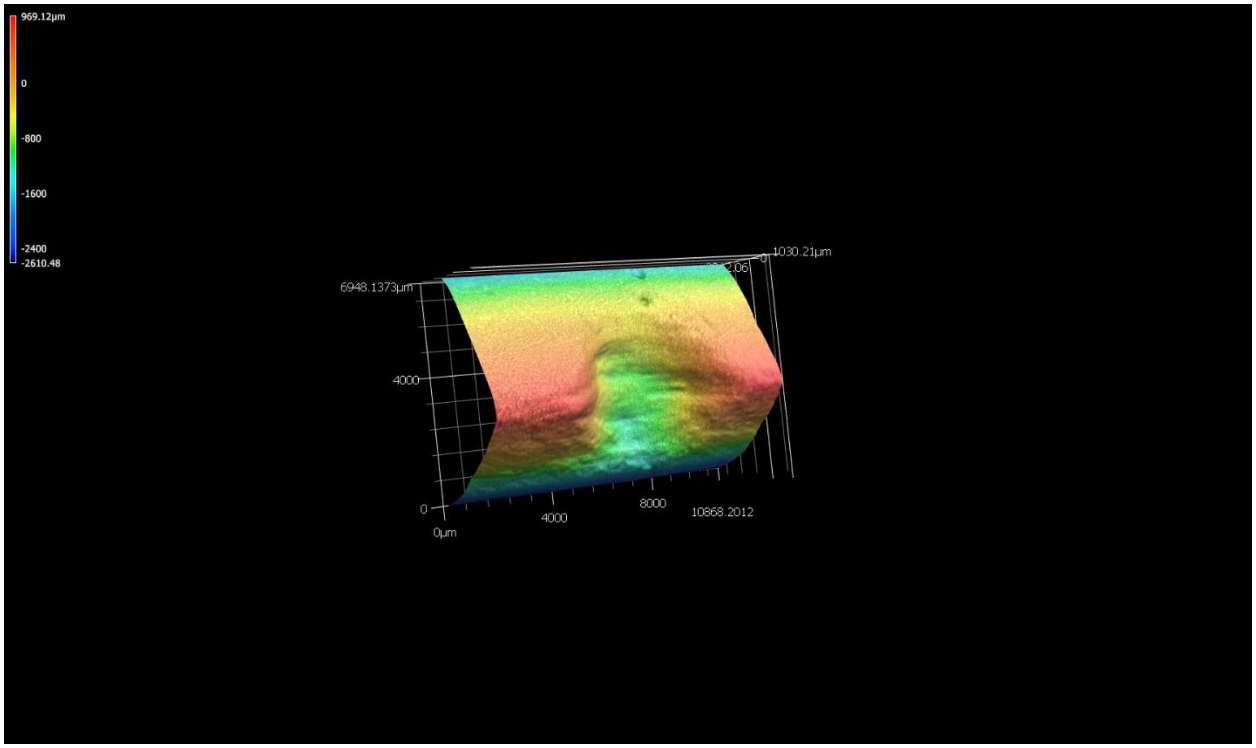


Fig. AVI-204: Erosion scar at 0° angle of impingement on the uncoated blade EXP6

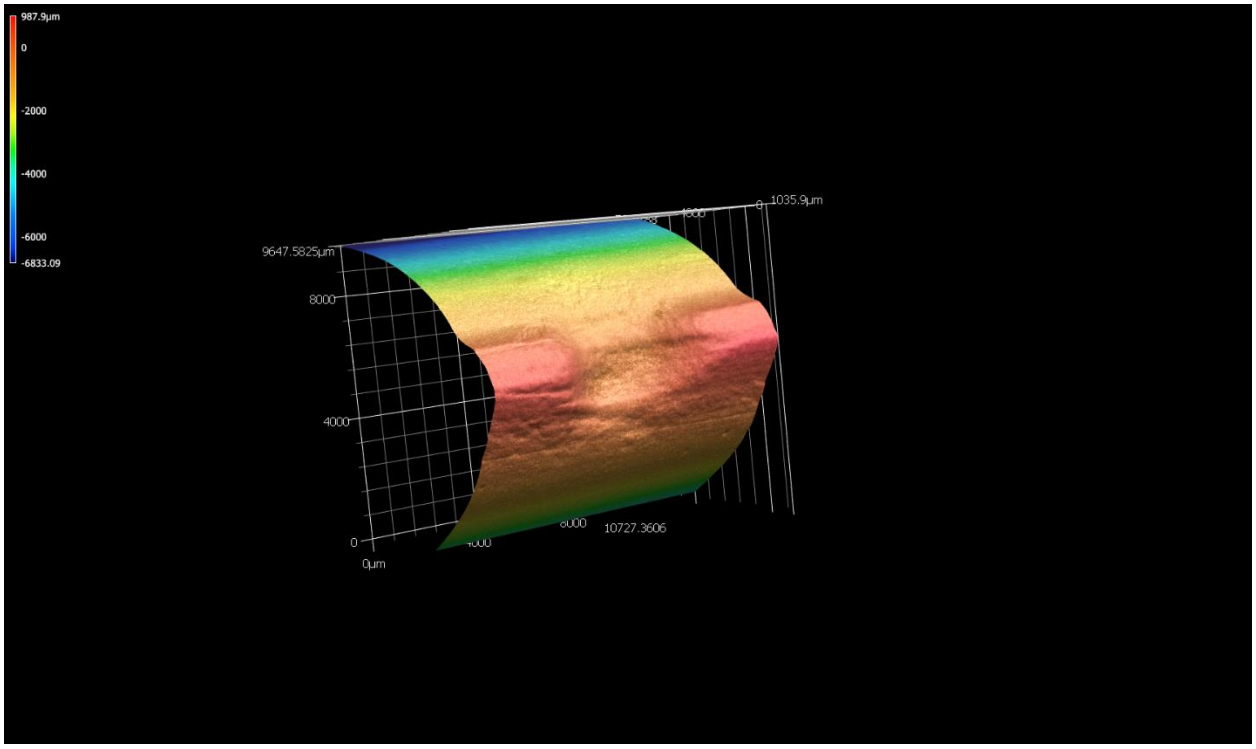


Fig. AVI-205: Erosion scar at 0° angle of impingement on the uncoated blade EXP7

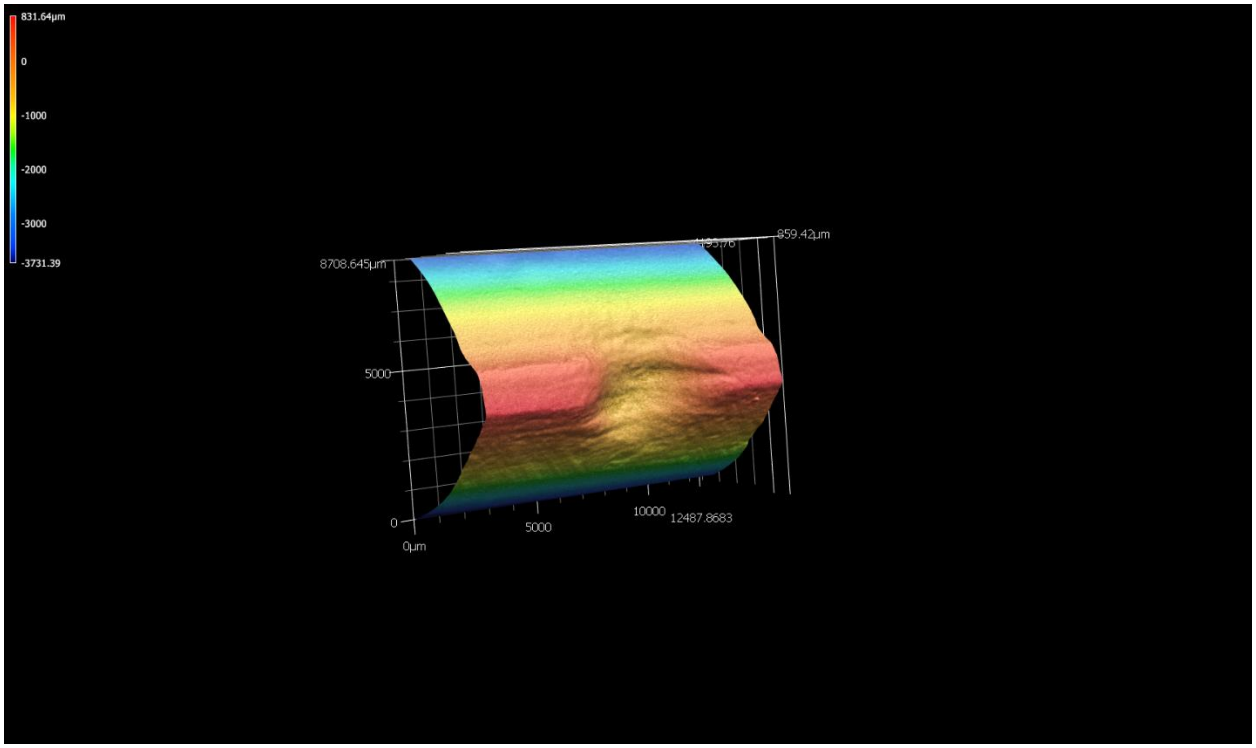


Fig. AVI-206: Erosion scar at 0° angle of impingement on the uncoated blade EXP8

- **H-146**

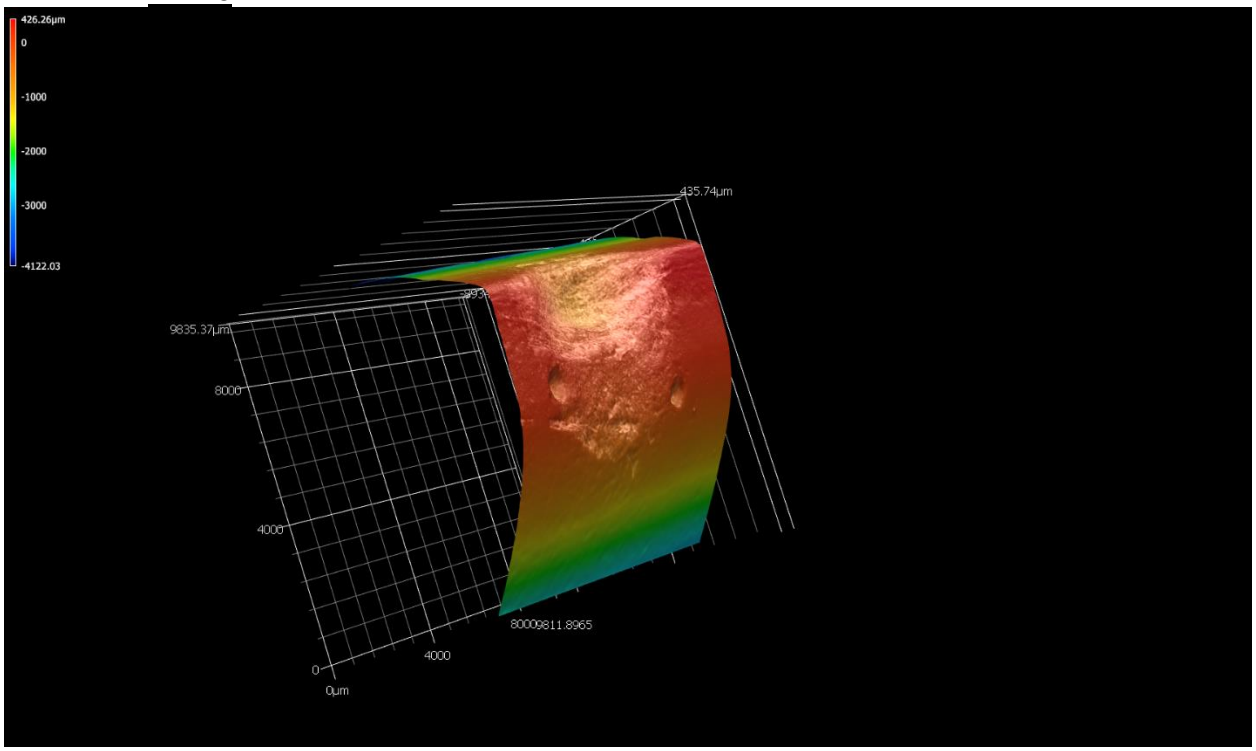


Fig. AVI-207: Erosion scar at 0° angle of impingement on the H-146 coated blade EXP1

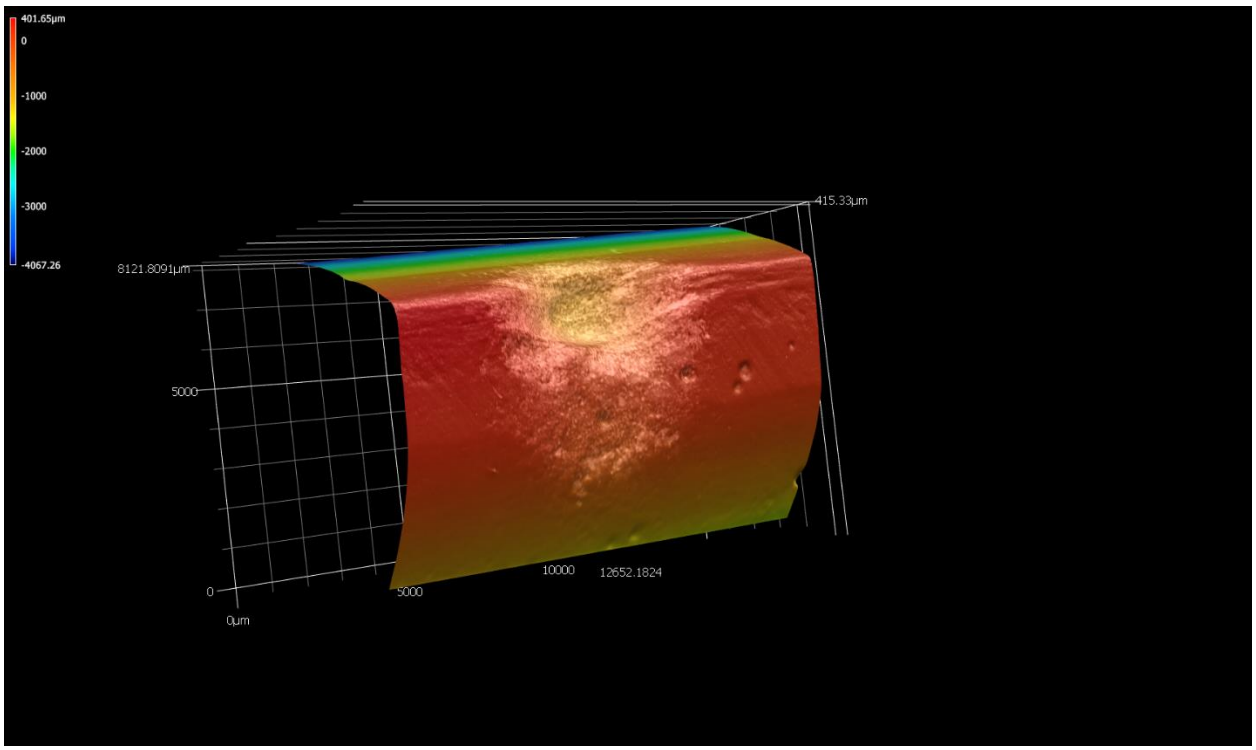


Fig. AVI-208: Erosion scar at 0° angle of impingement on the H-146 coated blade EXP2

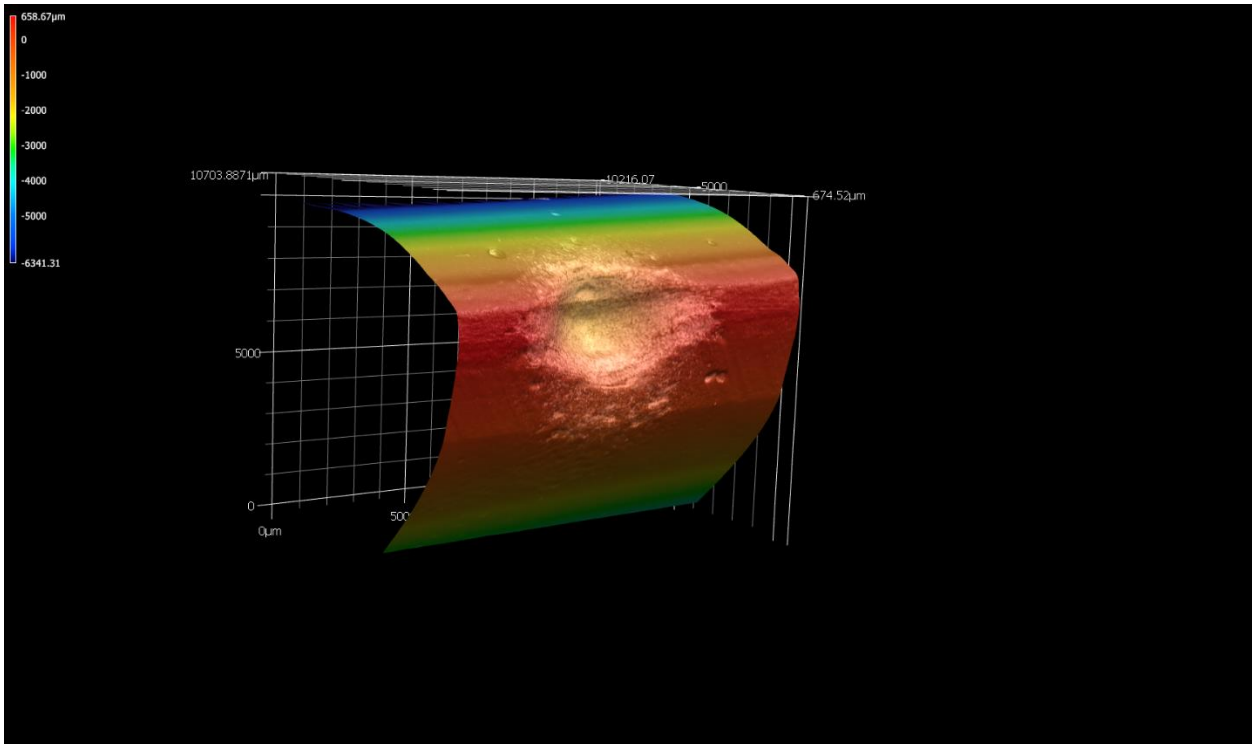


Fig. AVI-209: Erosion scar at 0° angle of impingement on the H-146 coated blade EXP3

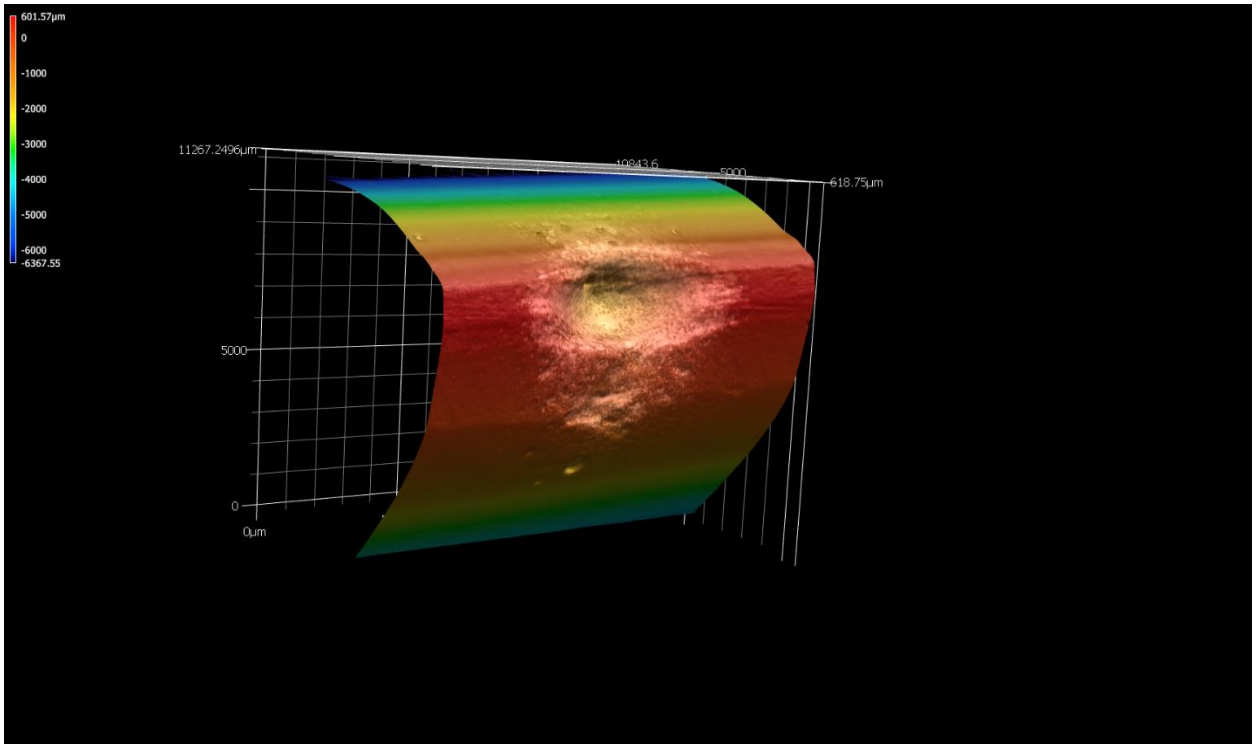


Fig. AVI-210: Erosion scar at 0° angle of impingement on the H-146 coated blade EXP4

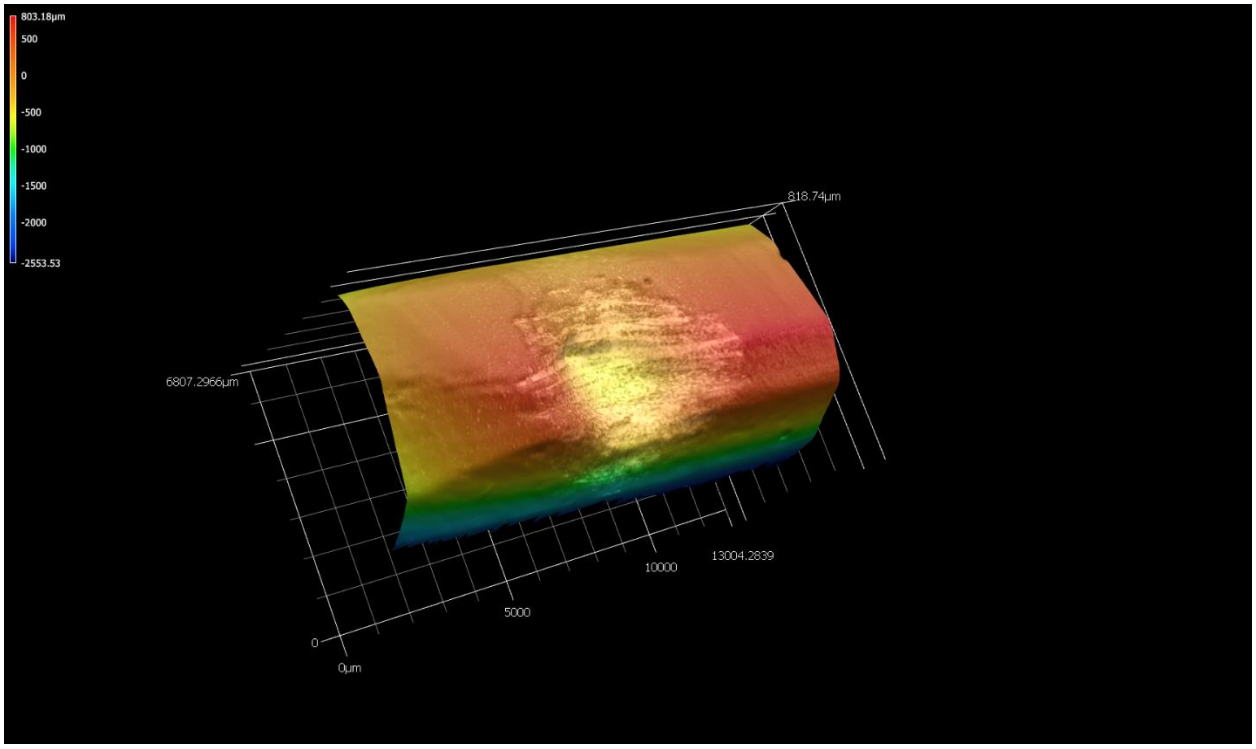


Fig. AVI-211: Erosion scar at 0° angle of impingement on the H-146 coated blade EXP5

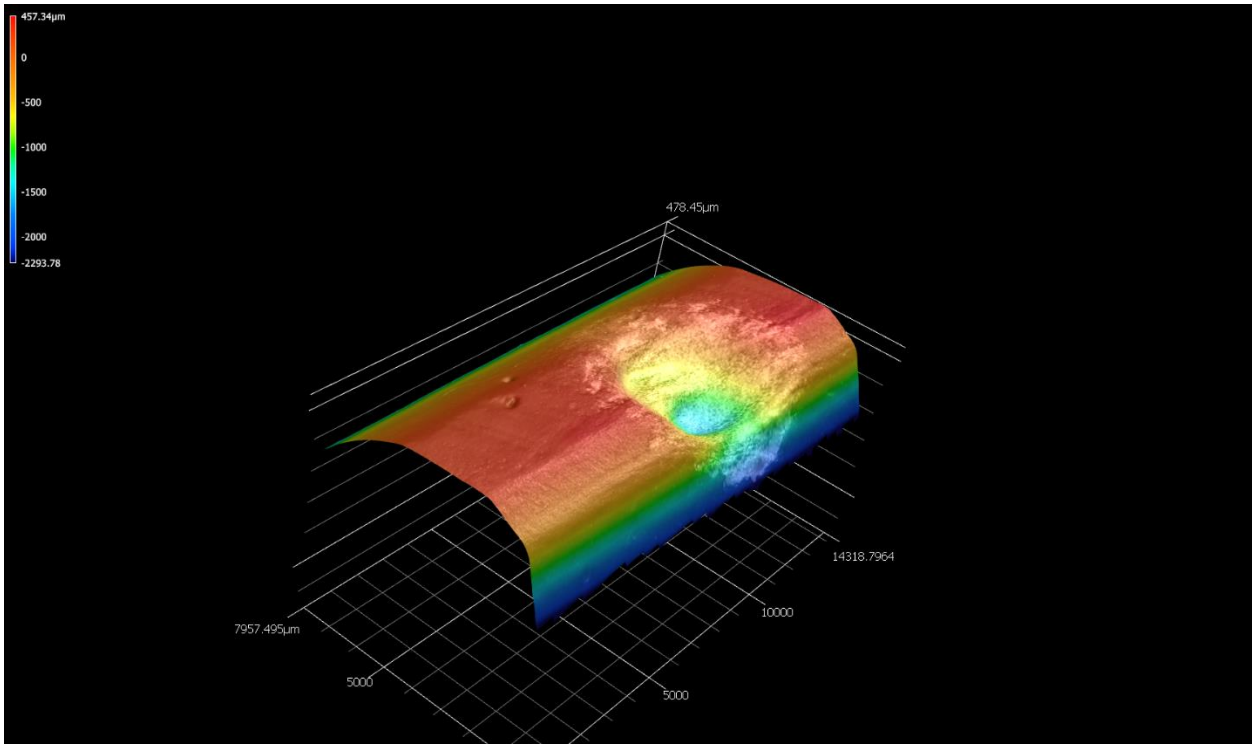


Fig. AVI-212: Erosion scar at 0° angle of impingement on the H-146 coated blade EXP6

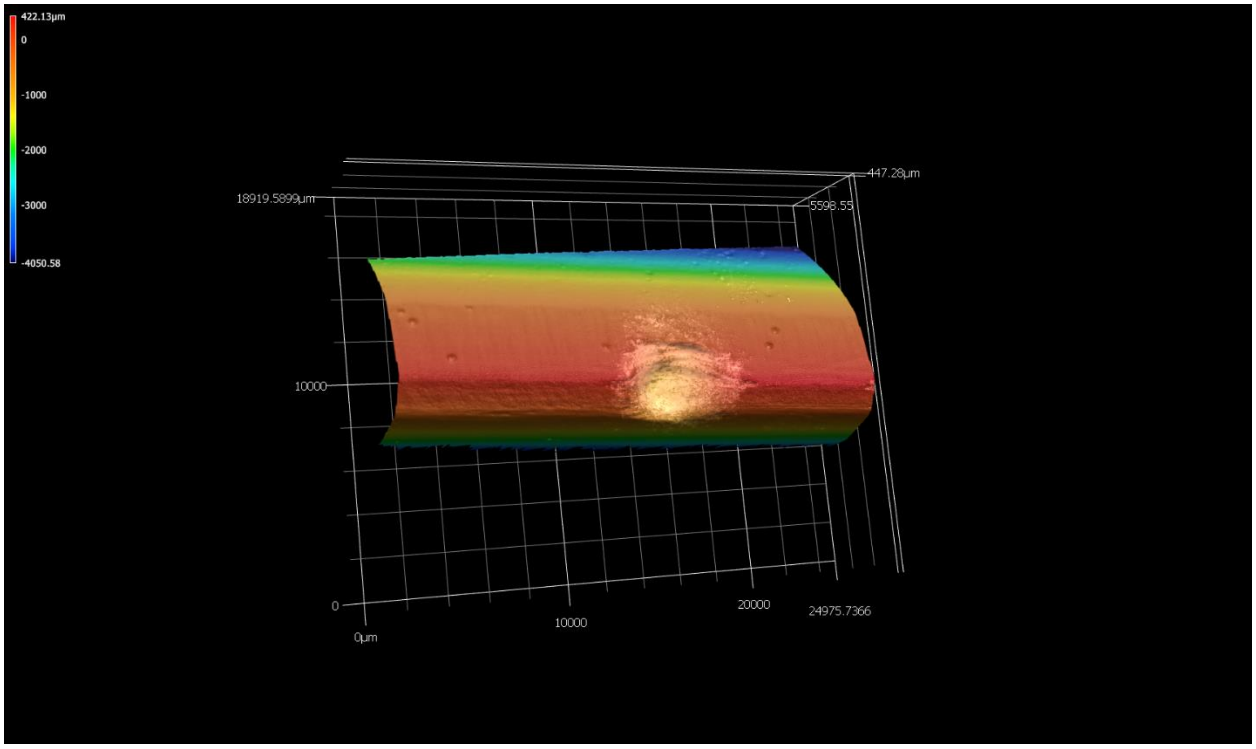


Fig. AVI-213: Erosion scar at 0° angle of impingement on the H-146 coated blade EXP7

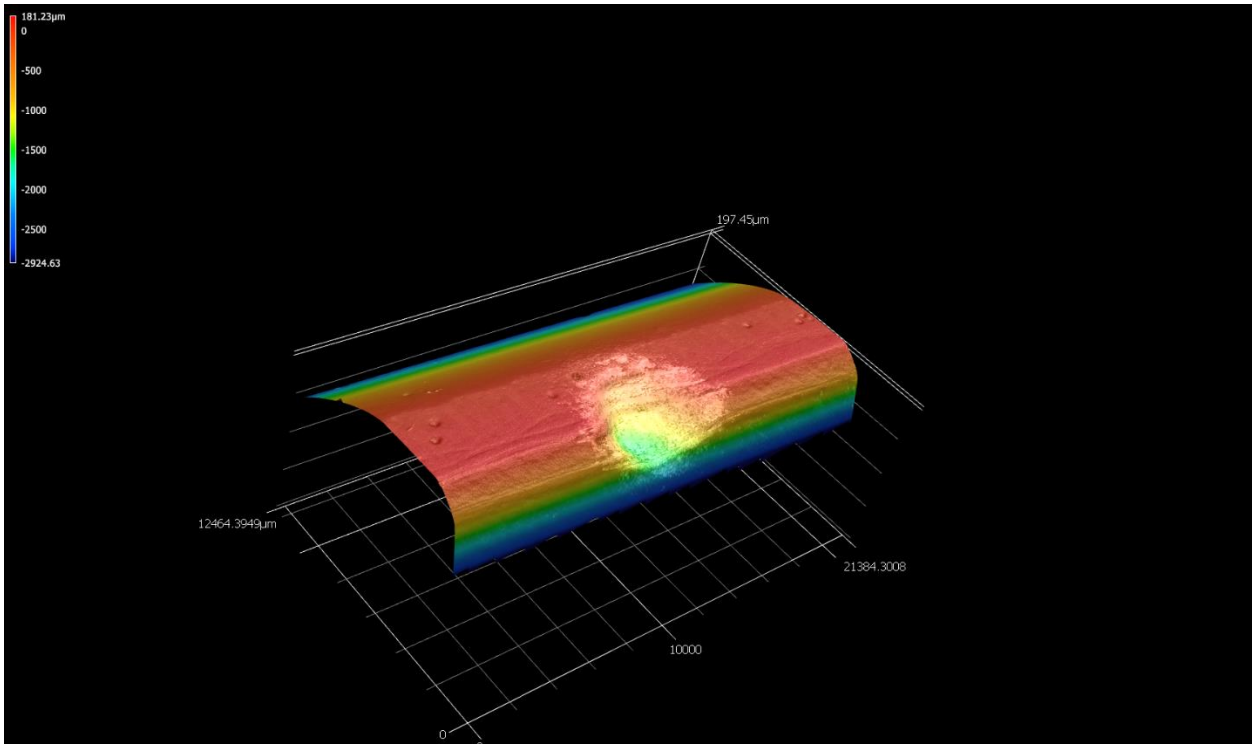


Fig. AVI-214: Erosion scar at 0° angle of impingement on the H-146 coated blade EXP8

- **Polyurethane/IA-700**

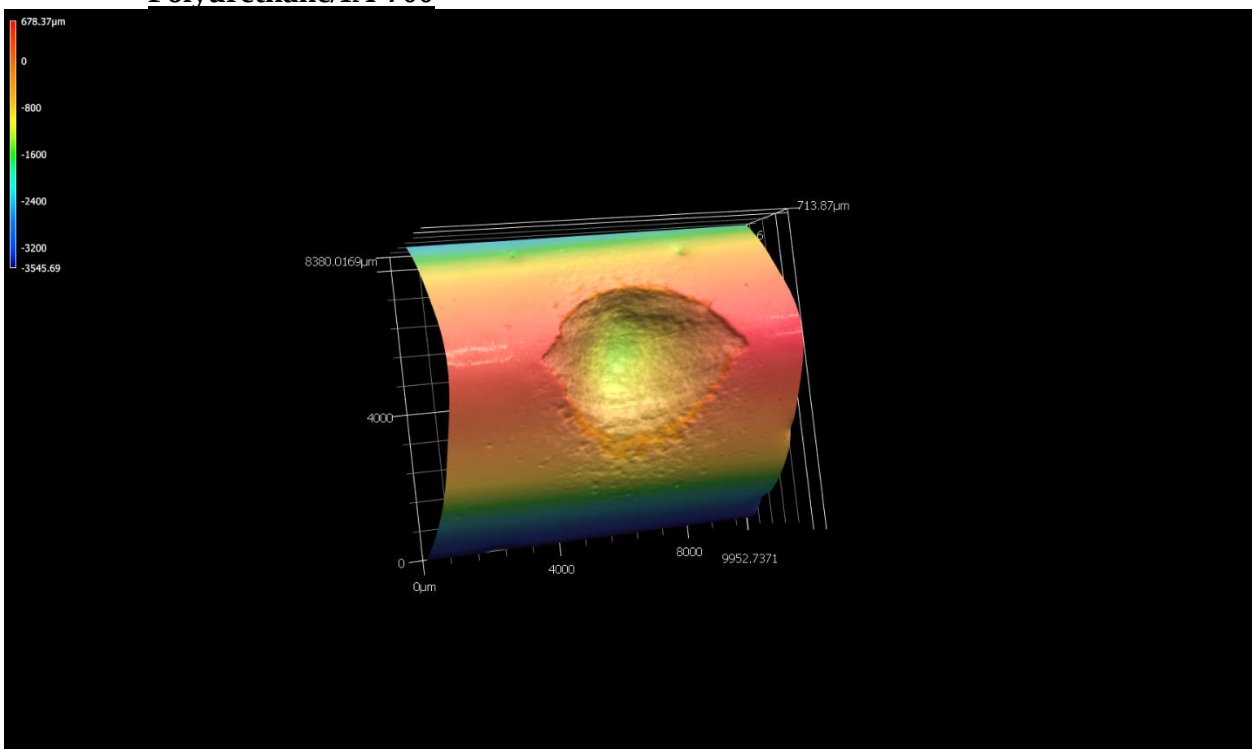


Fig. AVI-215: Erosion scar at 0° angle of impingement on the Polyurethane/IA-700 coated blade EXP1

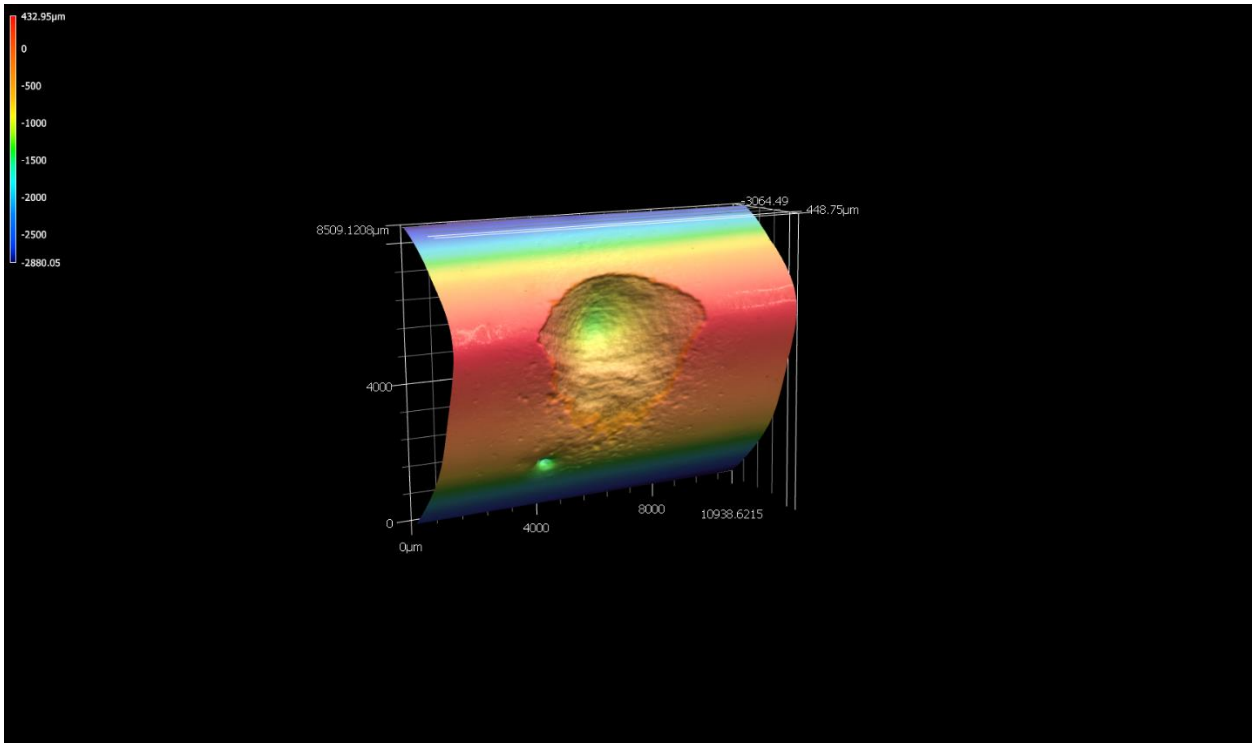


Fig. AVI-216: Erosion scar at 0° angle of impingement on the Polyurethane/IA-700 coated blade EXP2

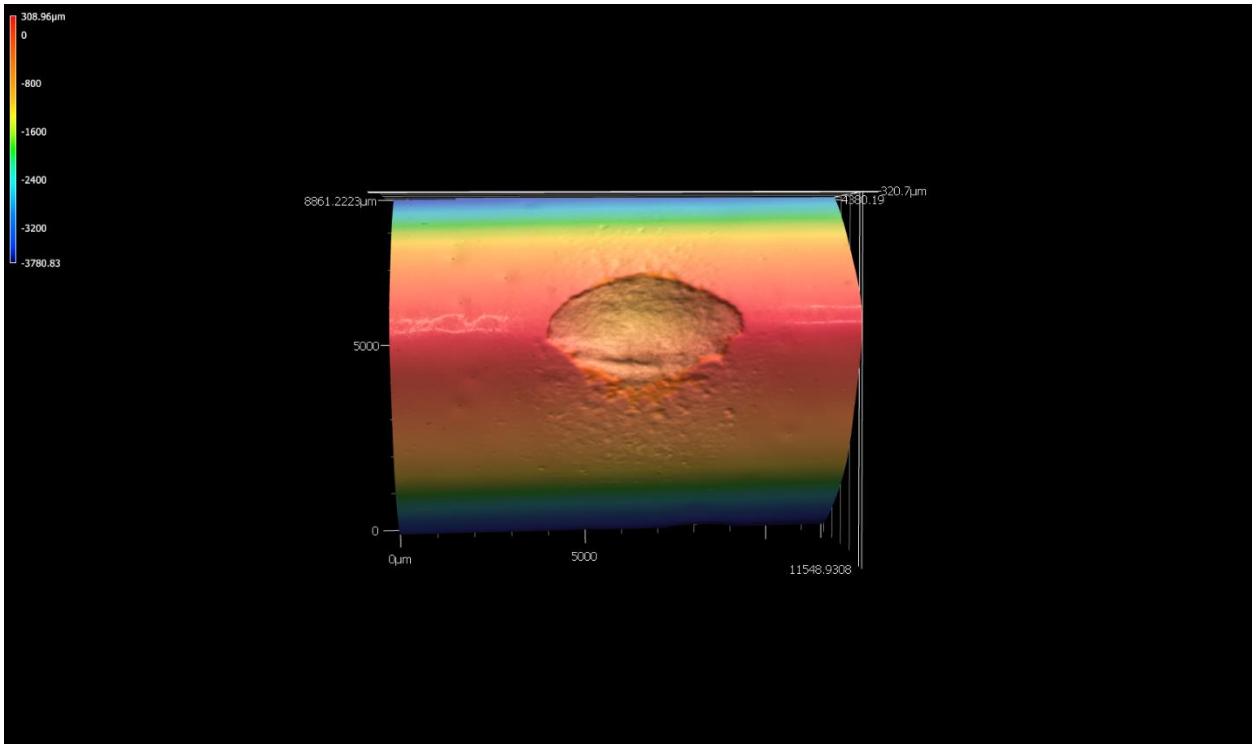


Fig. AVI-217: Erosion scar at 0° angle of impingement on the Polyurethane/IA-700 coated blade EXP3

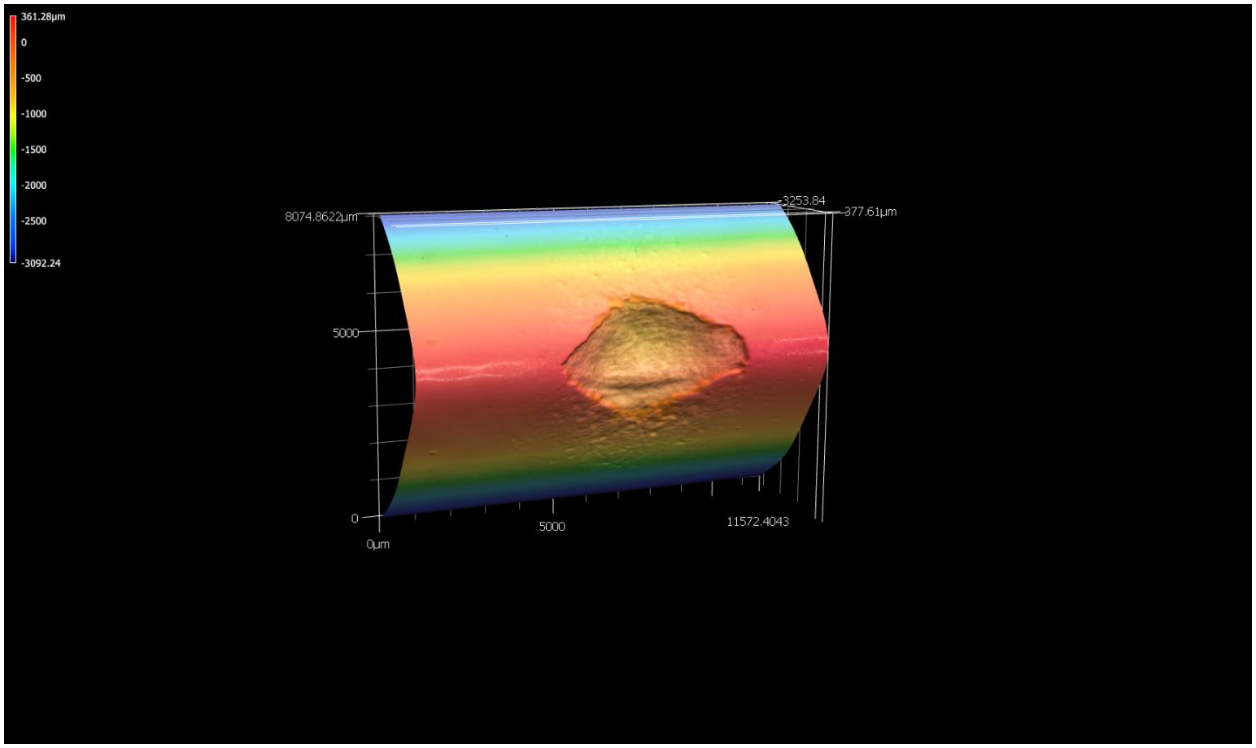


Fig. AVI-218: Erosion scar at 0° angle of impingement on the Polyurethane/IA-700 coated blade EXP4

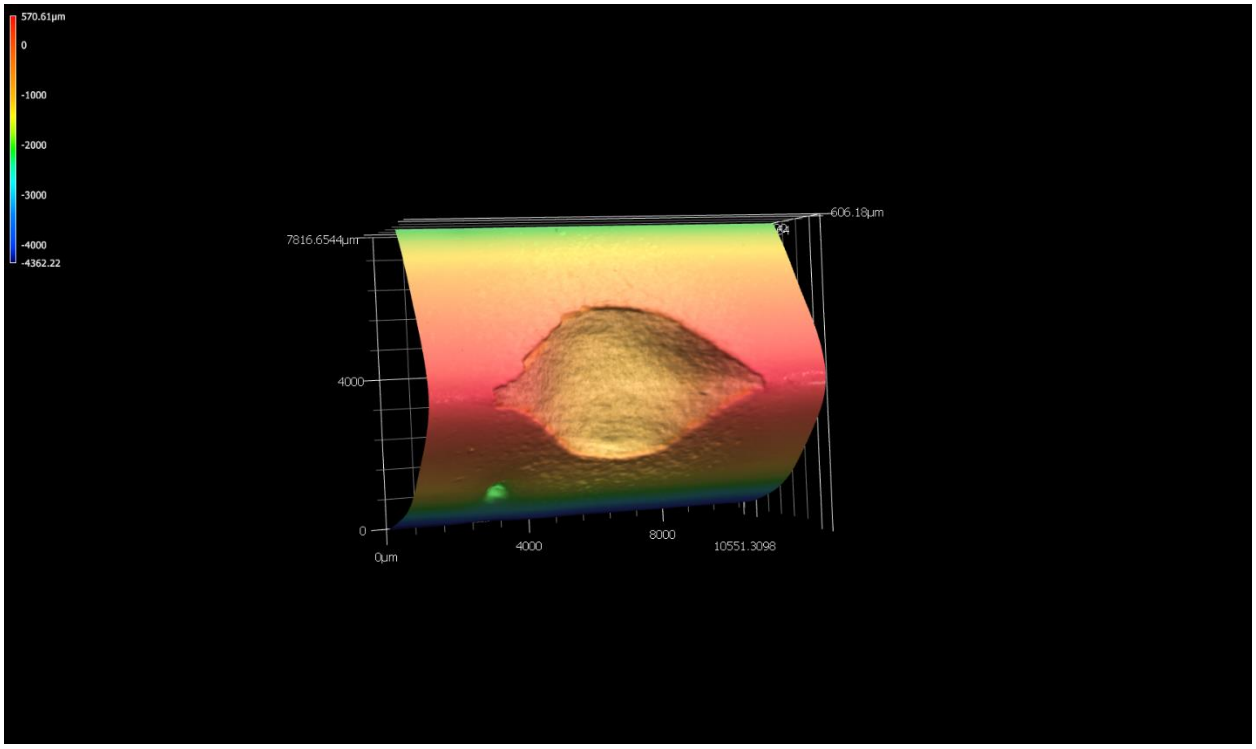


Fig. AVI-219: Erosion scar at 0° angle of impingement on the Polyurethane/IA-700 coated blade EXP5

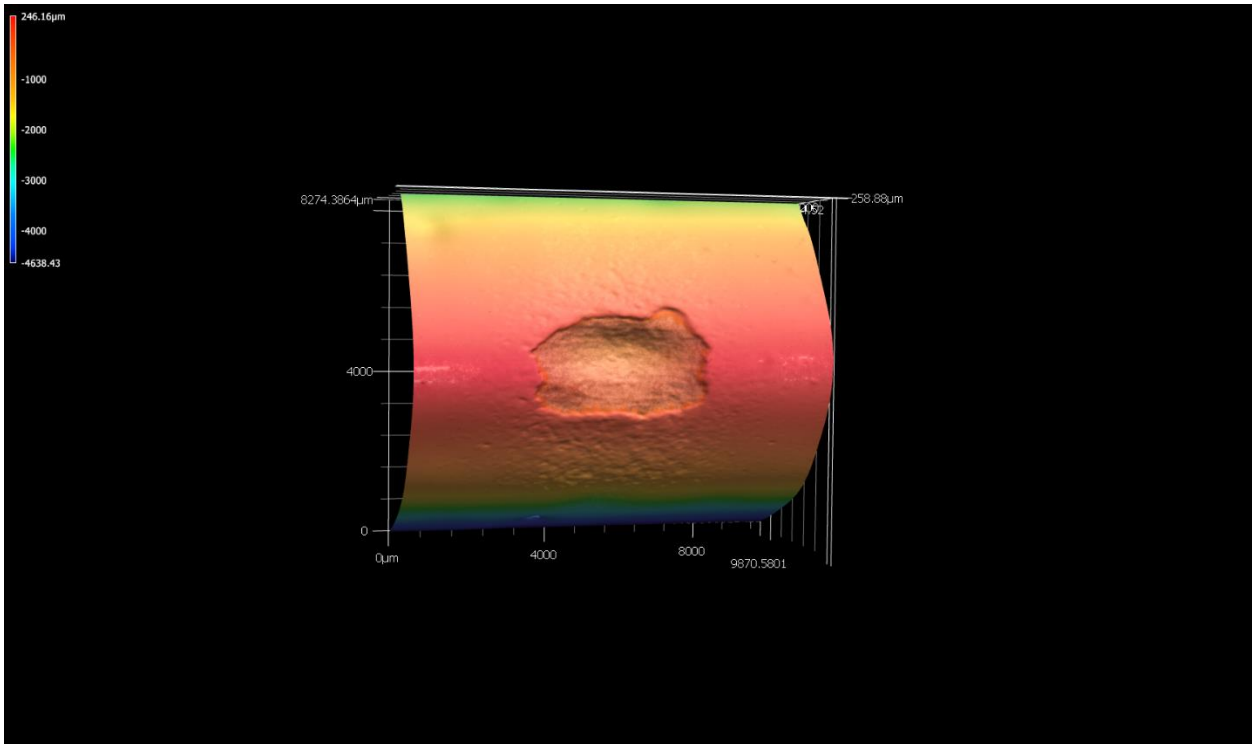


Fig. AVI-220: Erosion scar at 0° angle of impingement on the Polyurethane/IA-700 coated blade EXP6

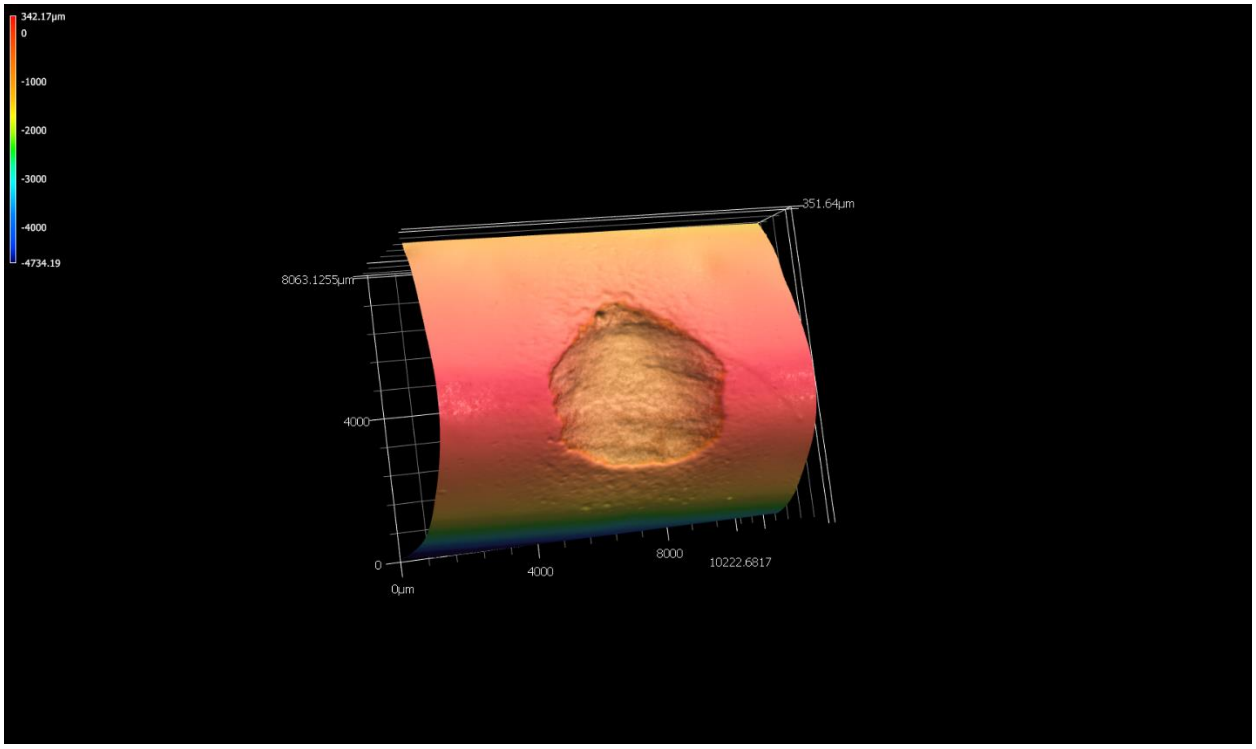


Fig. AVI-221: Erosion scar at 0° angle of impingement on the Polyurethane/IA-700 coated blade EXP7

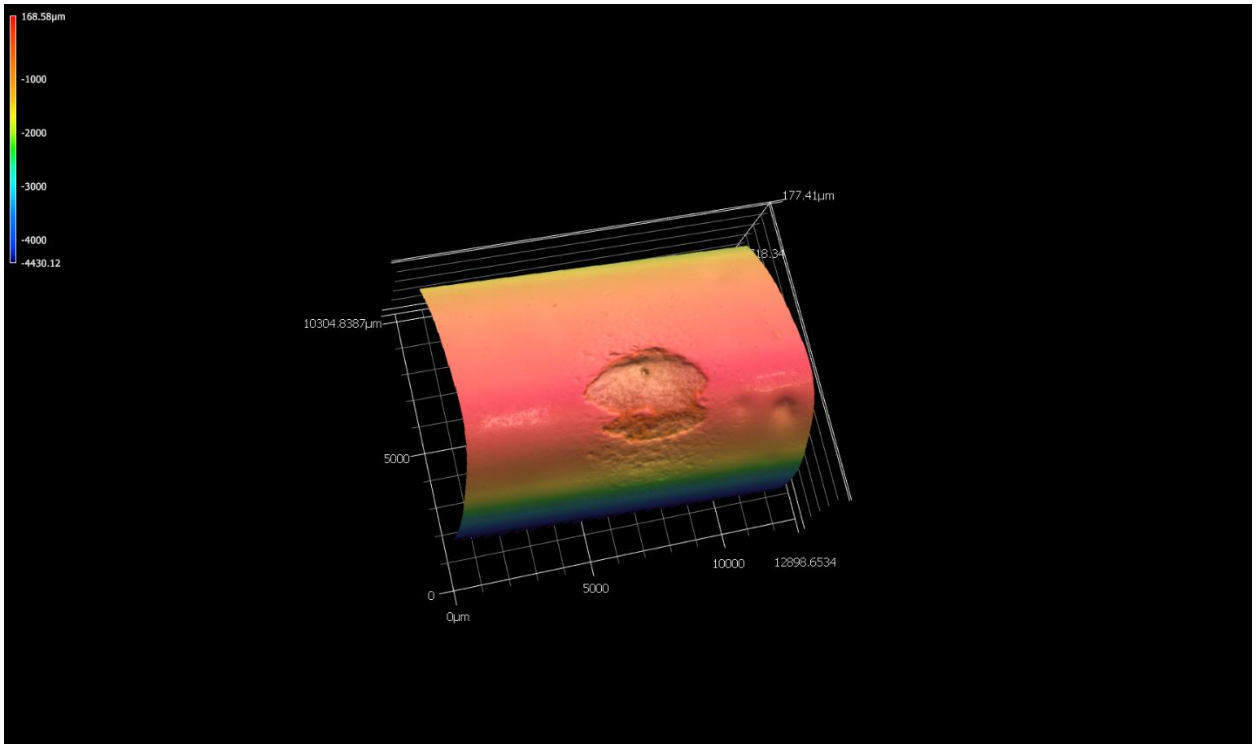


Fig. AVI-222: Erosion scar at 0° angle of impingement on the Polyurethane/IA-700 coated blade EXP8

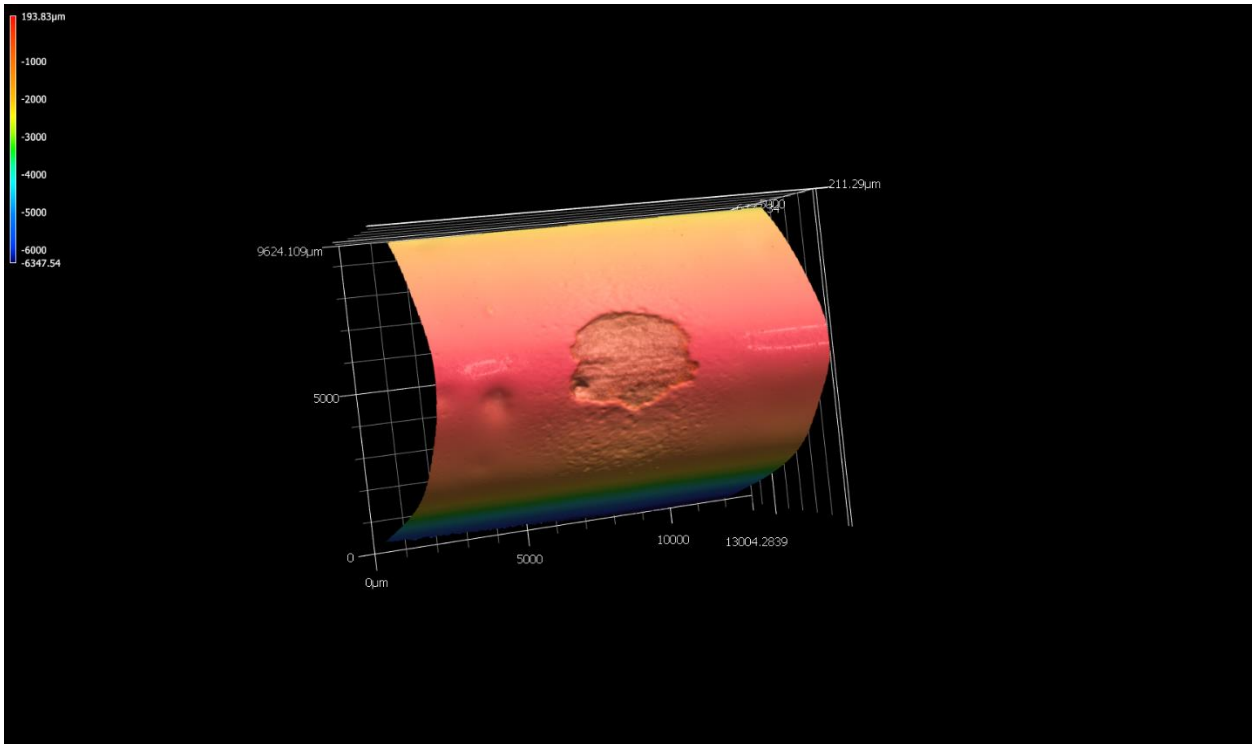


Fig. AVI-223: Erosion scar at 0° angle of impingement on the Polyurethane/IA-700 coated blade EXP9

- **5 degrees**
- **Uncoated**

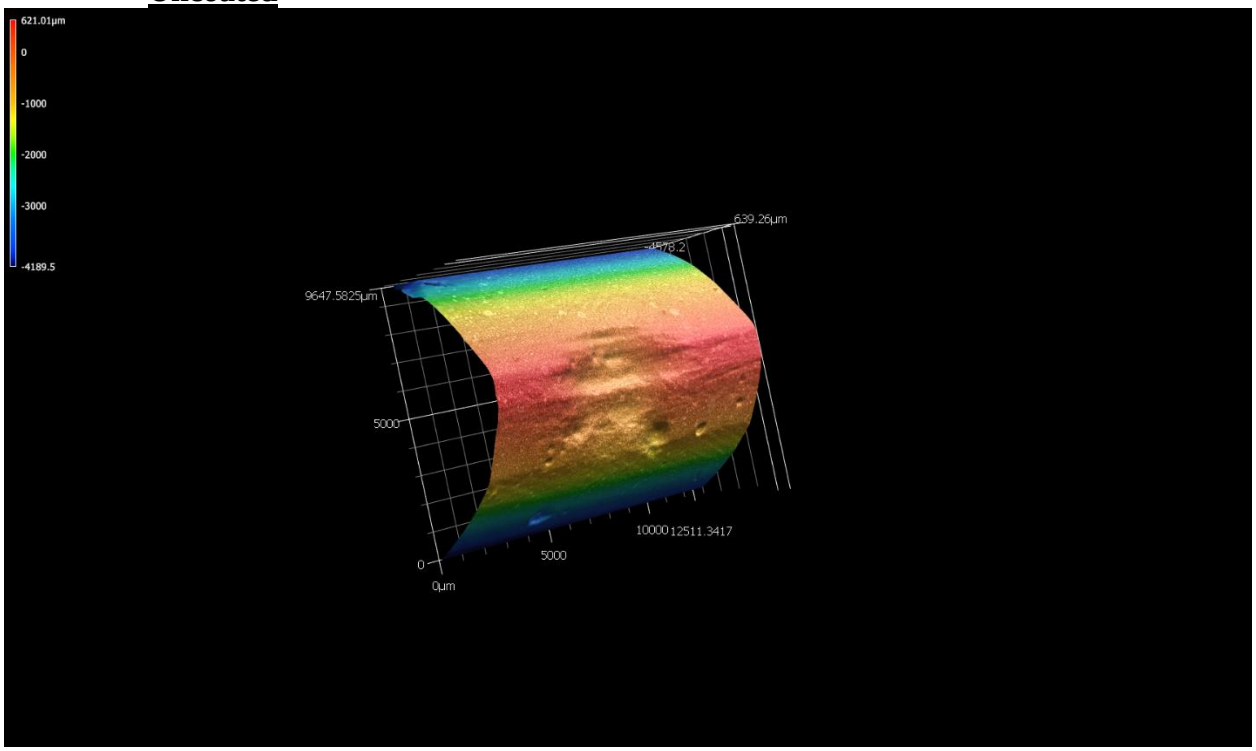


Fig. AVI-224: Erosion scar at 5° angle of impingement on the uncoated blade EXP1

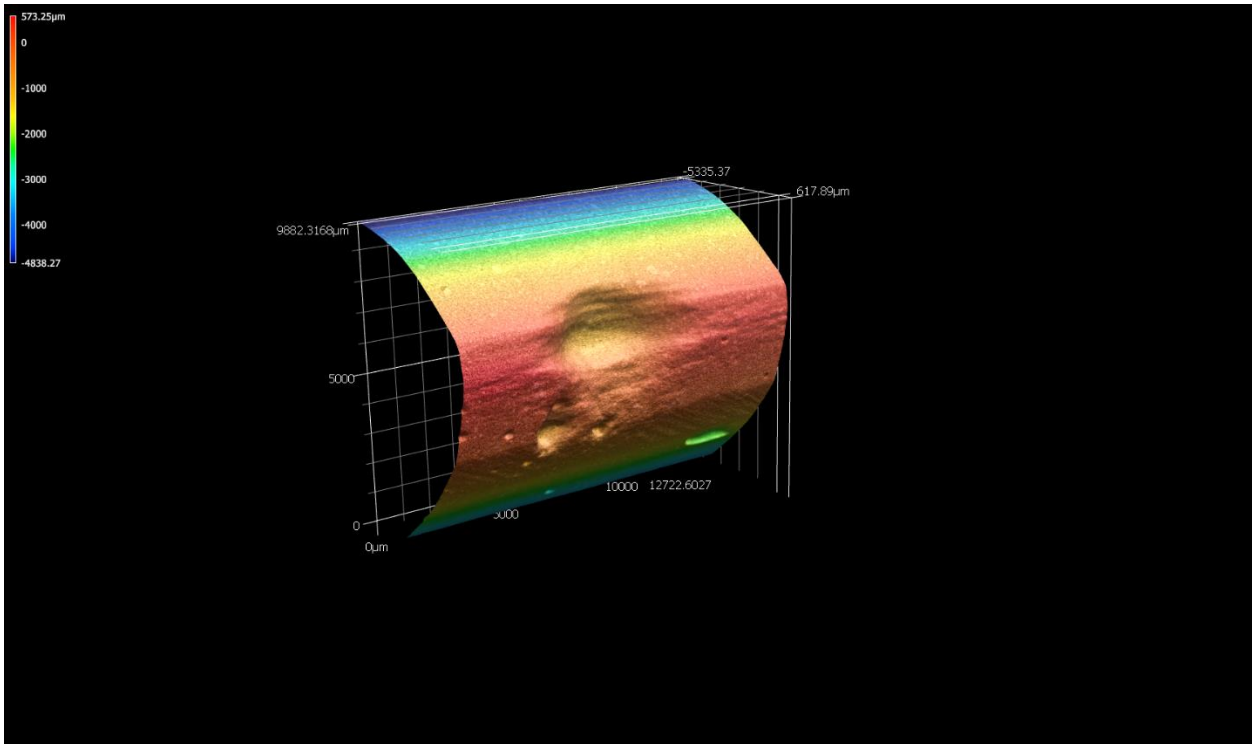


Fig. AVI-225: Erosion scar at 5° angle of impingement on the uncoated blade EXP2

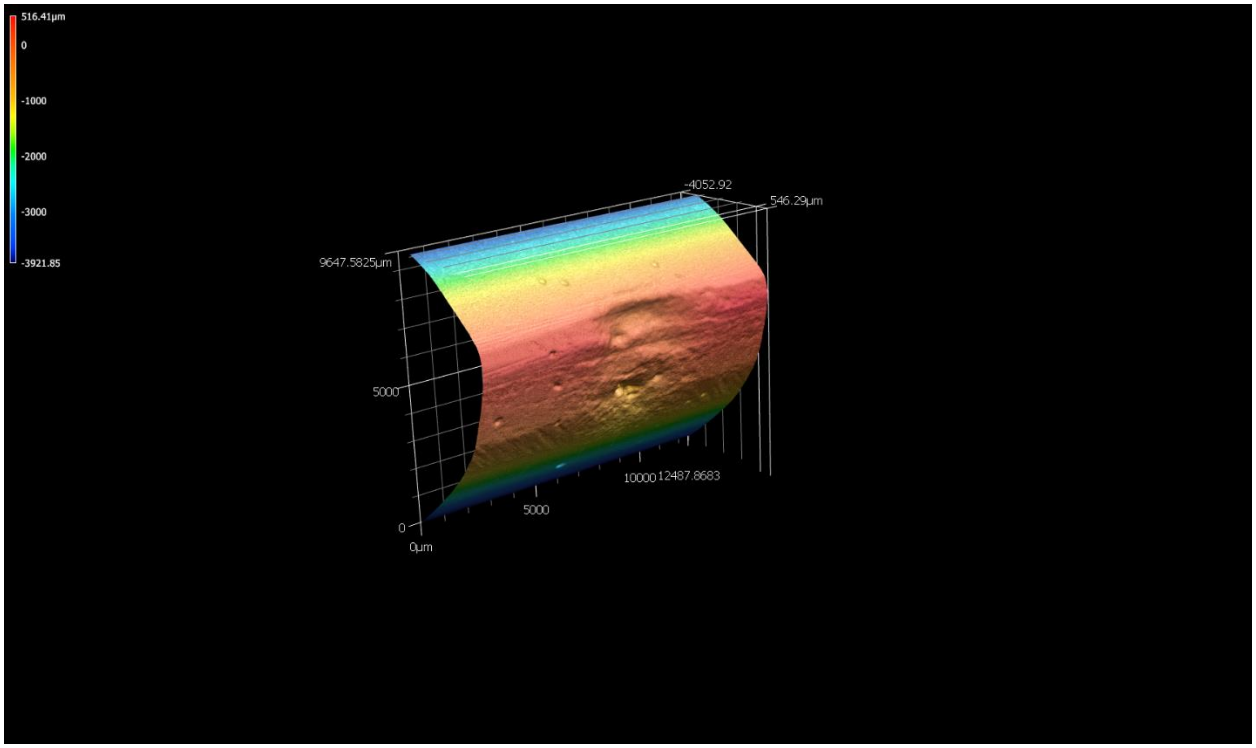


Fig. AVI-226: Erosion scar at 5° angle of impingement on the uncoated blade EXP3

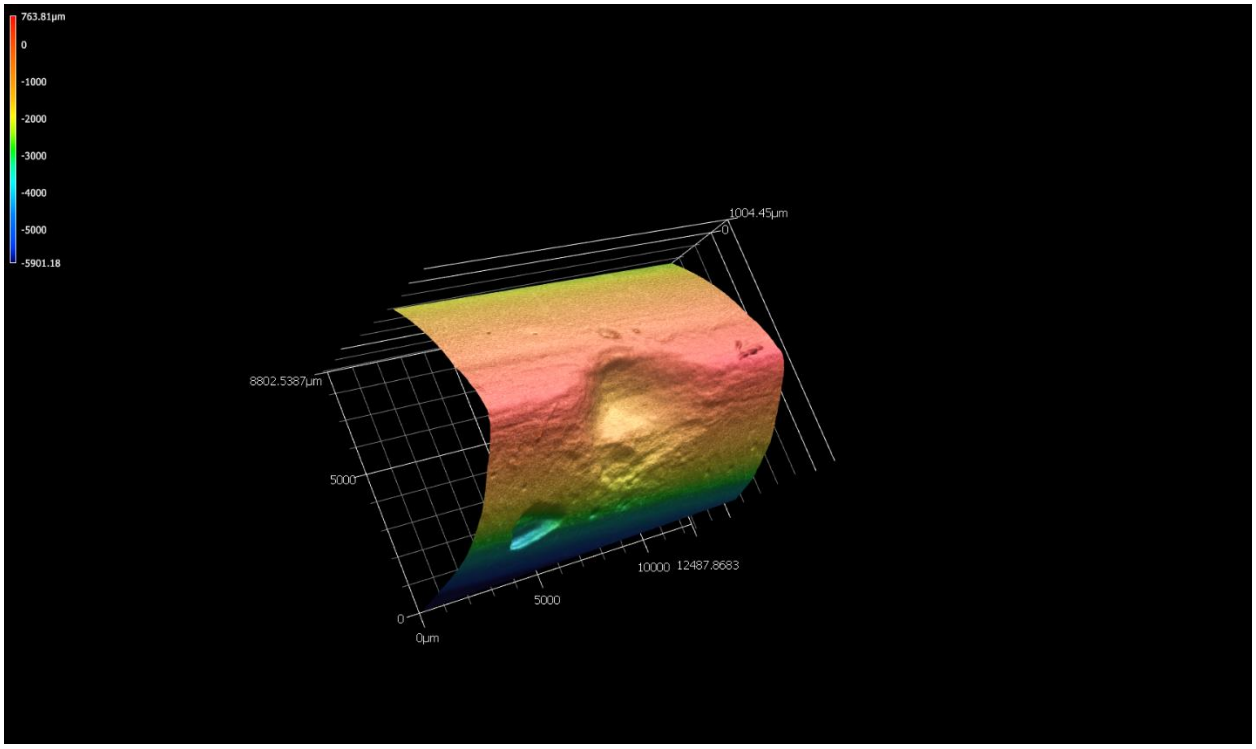


Fig. AVI-227: Erosion scar at 5° angle of impingement on the uncoated blade EXP4

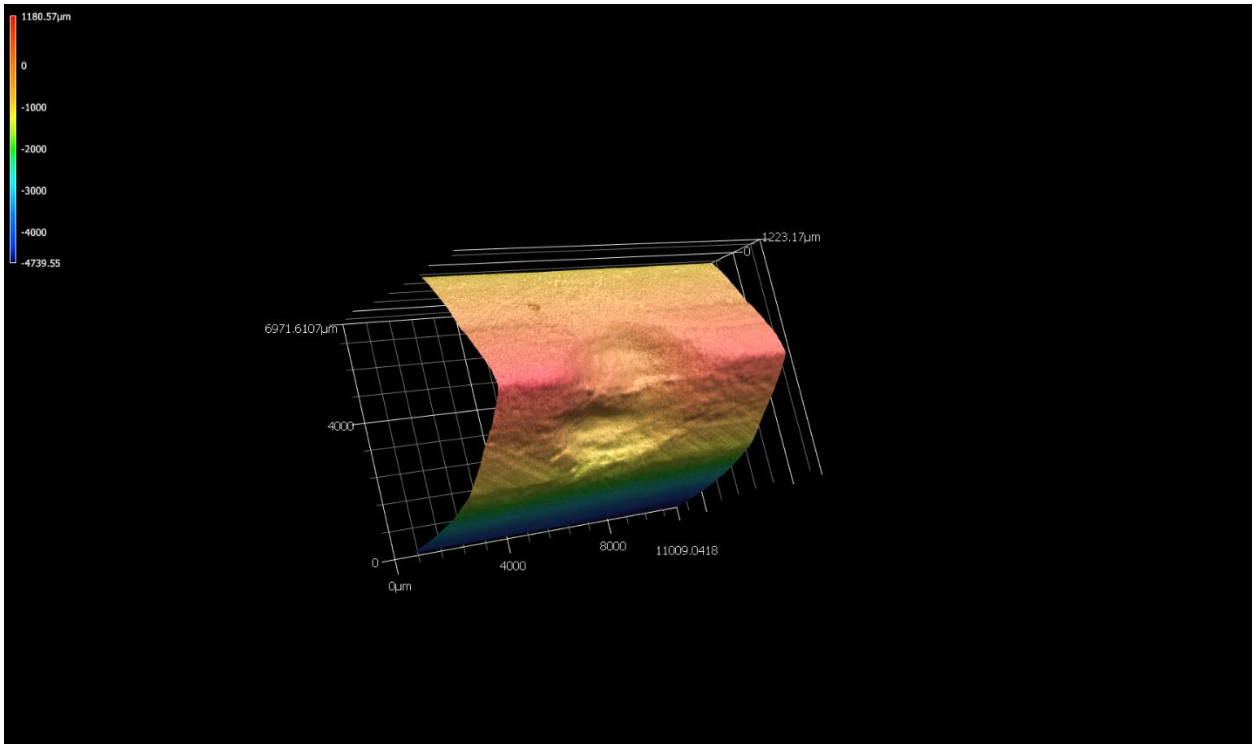


Fig. AVI-228: Erosion scar at 5° angle of impingement on the uncoated blade EXP5

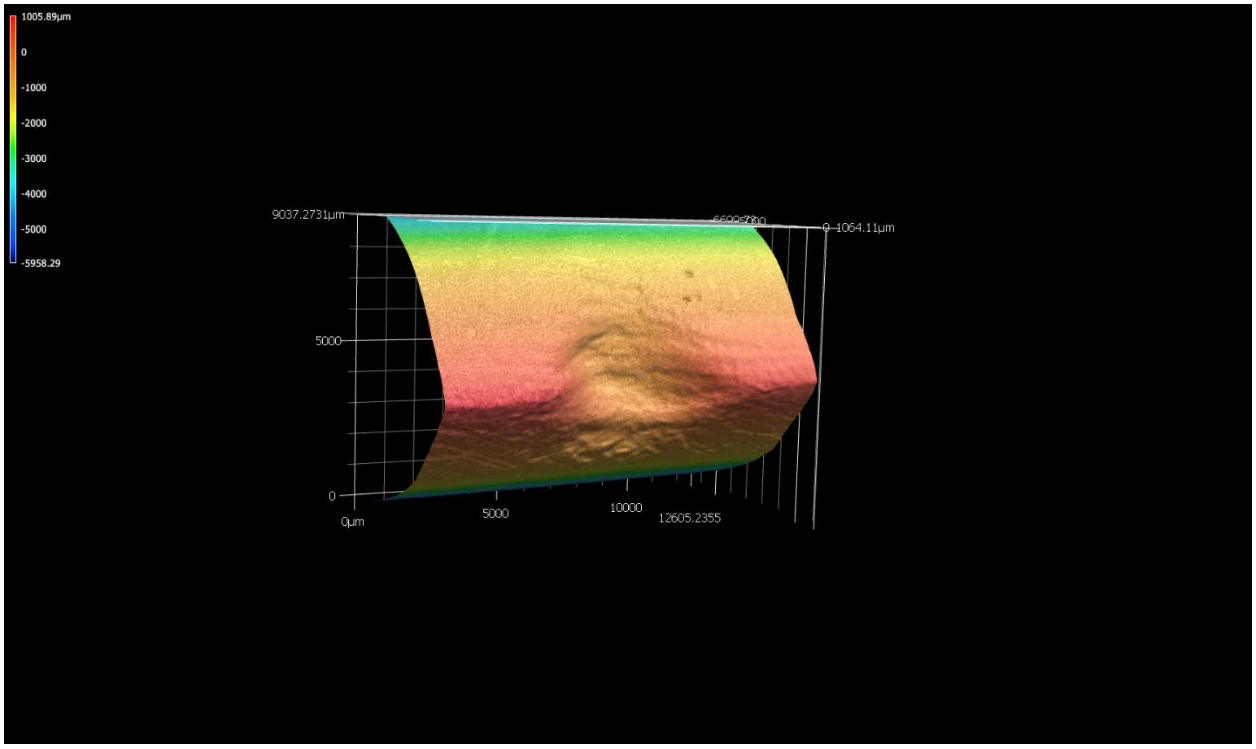


Fig. AVI-229: Erosion scar at 5° angle of impingement on the uncoated blade EXP6

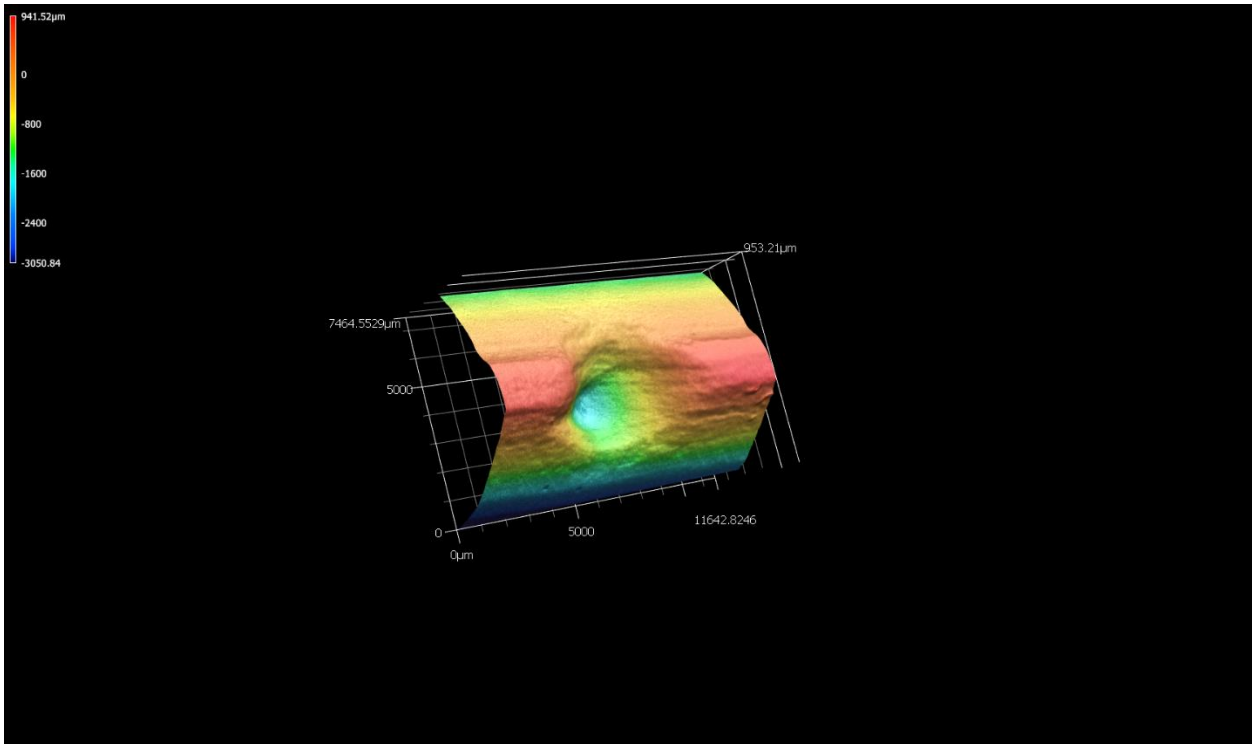


Fig. AVI-230: Erosion scar at 5° angle of impingement on the uncoated blade EXP7

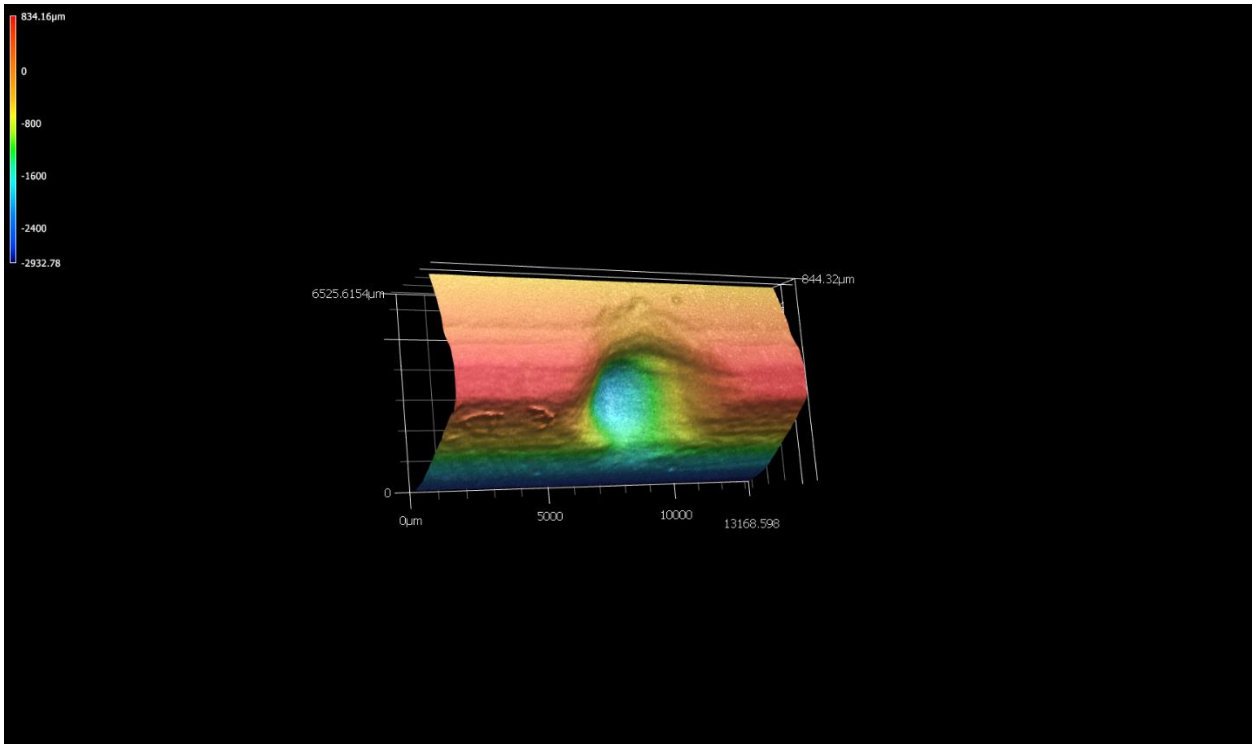


Fig. AVI-231: Erosion scar at 5° angle of impingement on the uncoated blade EXP8

- **H-146**

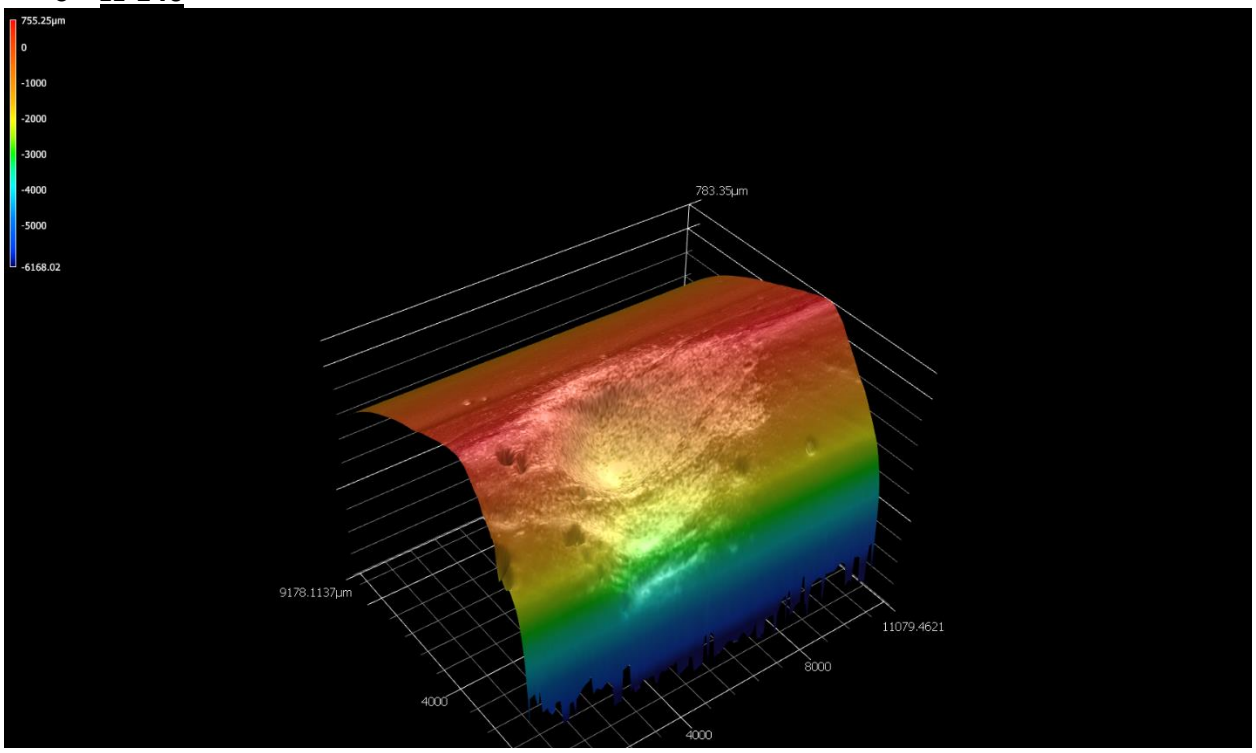


Fig. AVI-232: Erosion scar at 5° angle of impingement on the H-146 coated blade EXP1

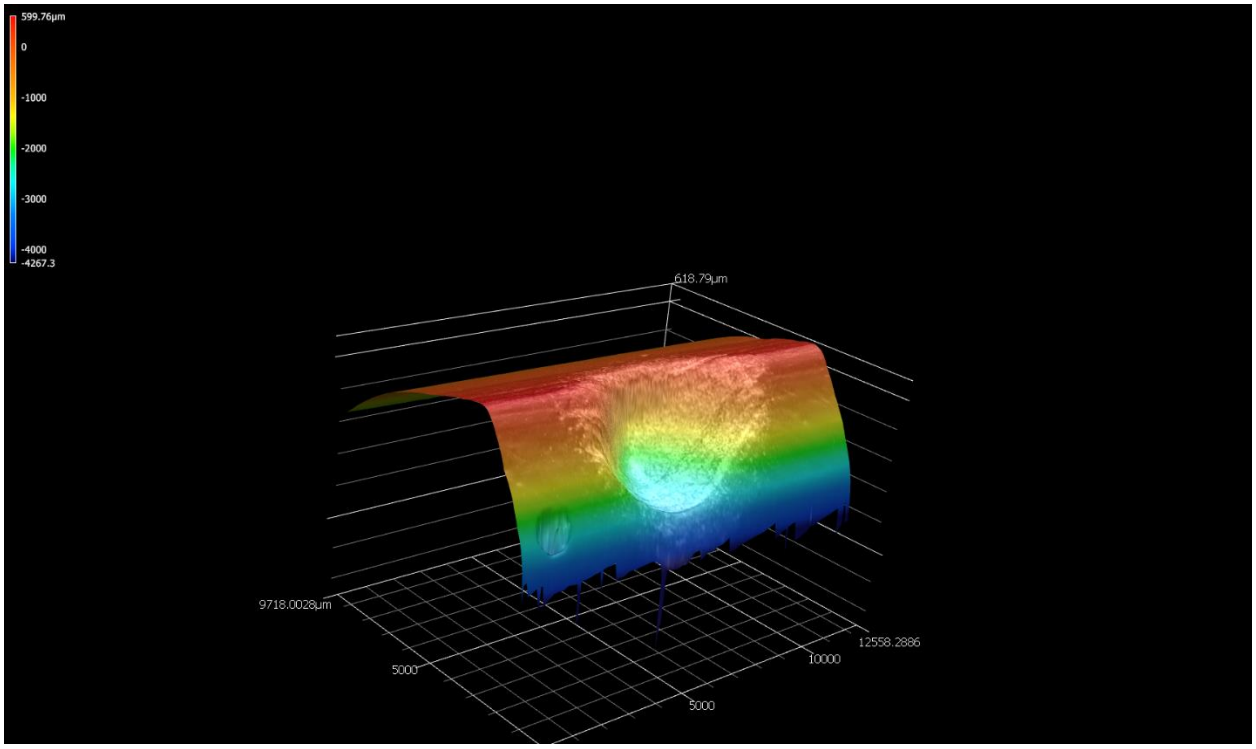


Fig. AVI-233: Erosion scar at 5° angle of impingement on the H-146 coated blade EXP2

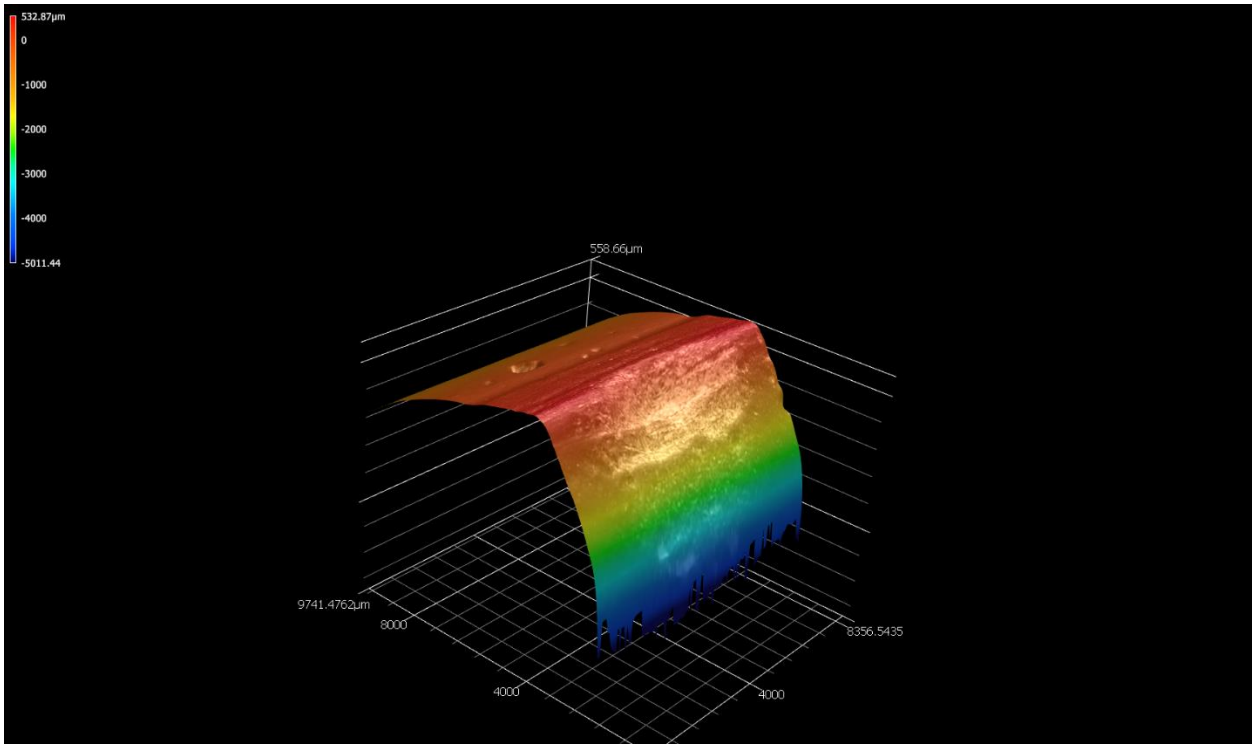


Fig. AVI-234: Erosion scar at 5° angle of impingement on the H-146 coated blade EXP3

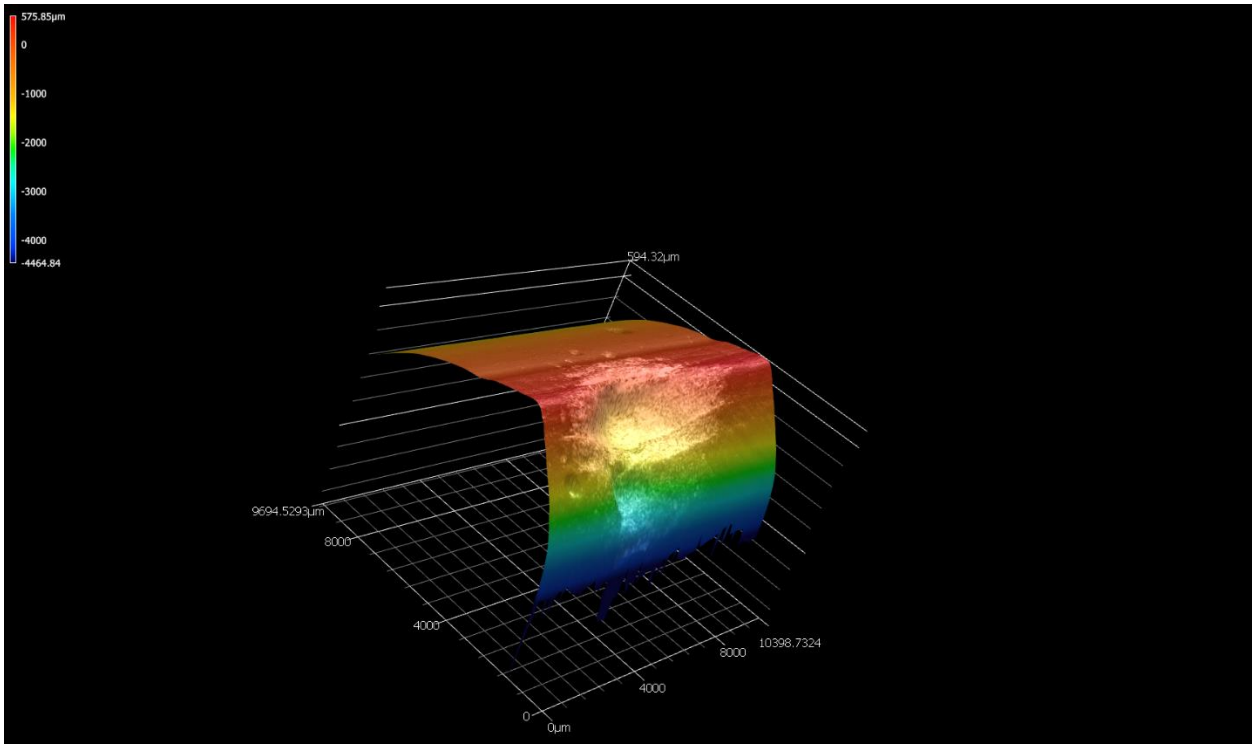


Fig. AVI-235: Erosion scar at 5° angle of impingement on the H-146 coated blade EXP4

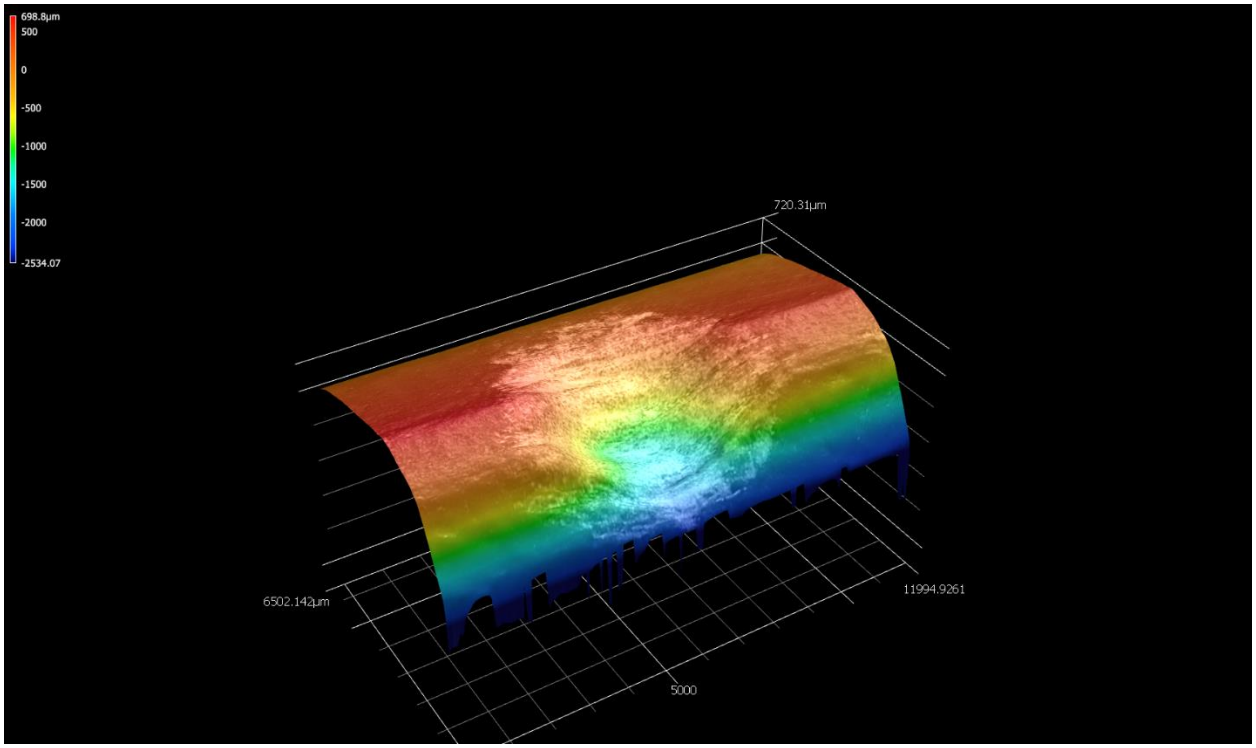


Fig. AVI-236: Erosion scar at 5° angle of impingement on the H-146 coated blade EXP5

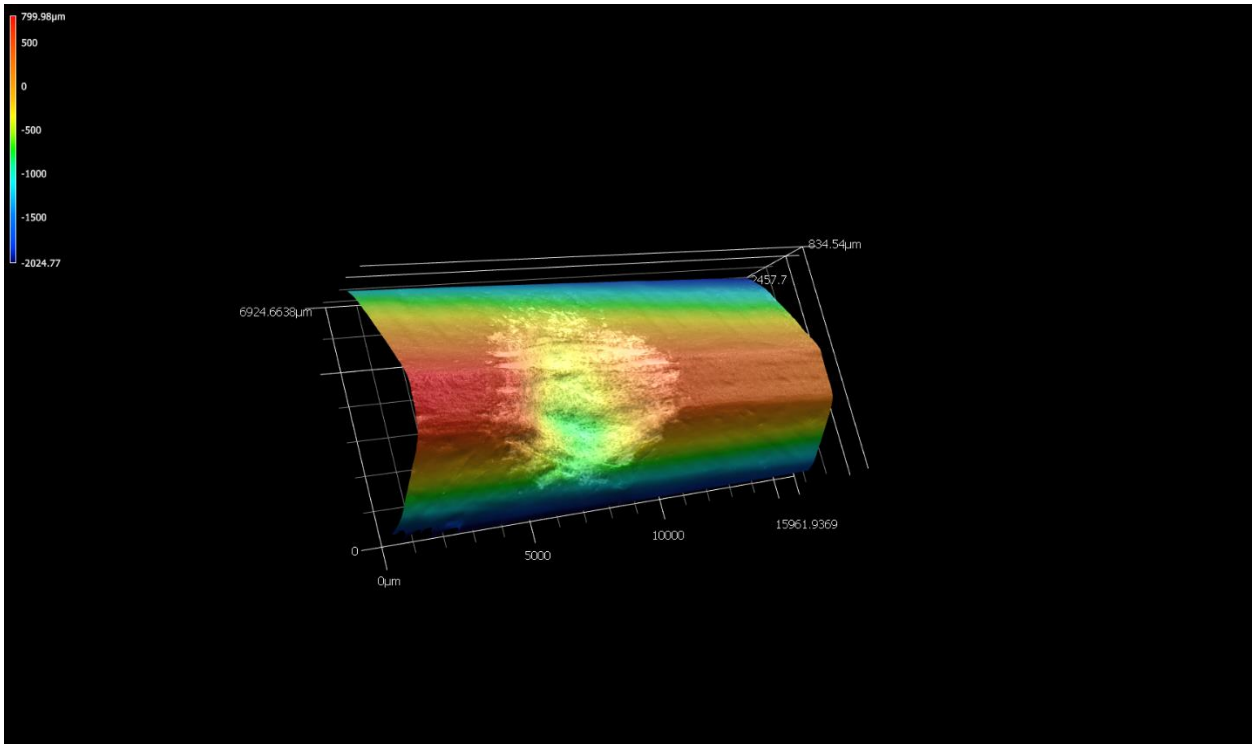


Fig. AVI-237: Erosion scar at 5° angle of impingement on the H-146 coated blade EXP6

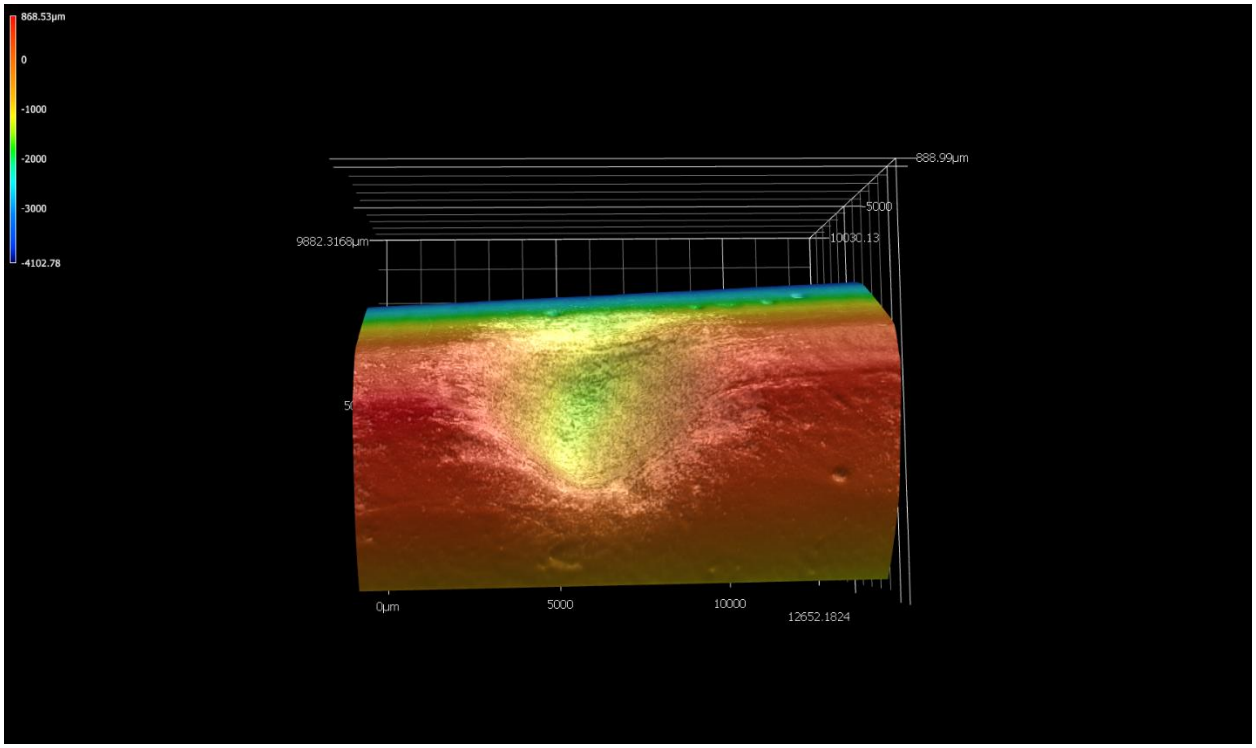


Fig. AVI-238: Erosion scar at 5° angle of impingement on the H-146 coated blade EXP7

- **Polyurethane/IA-700**

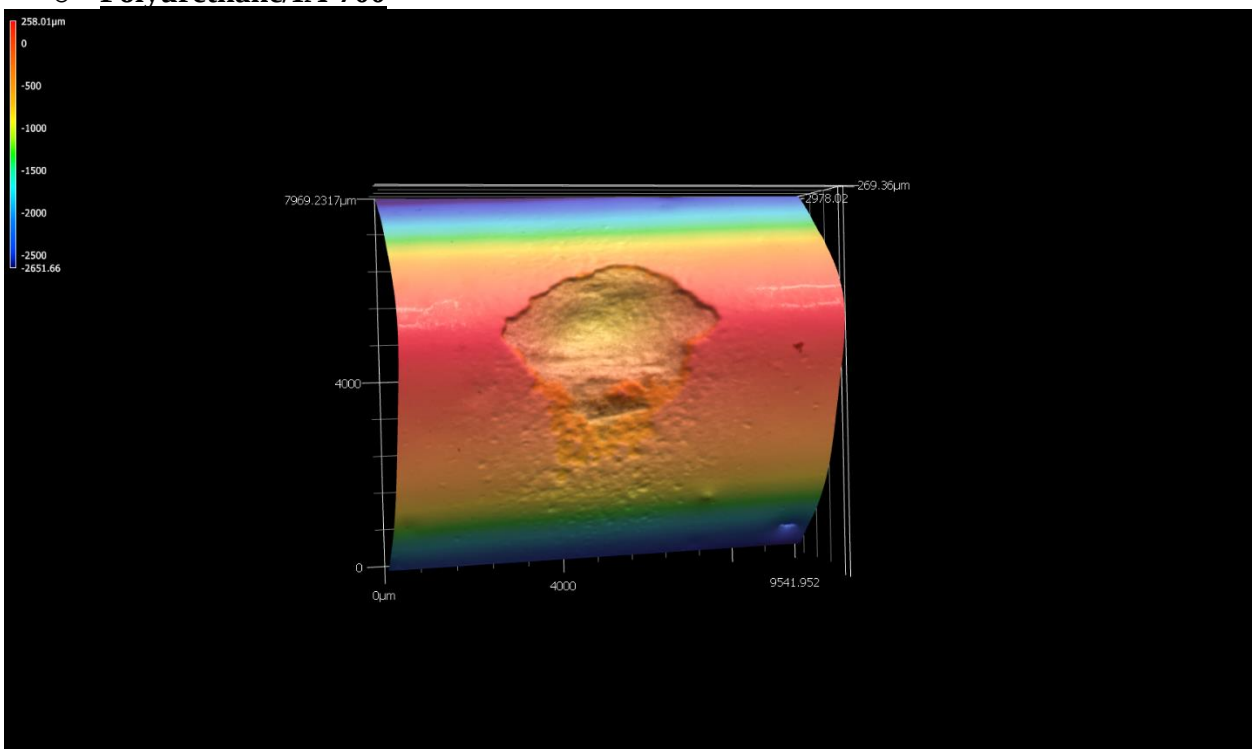


Fig. AVI-239: Erosion scar at 5° angle of impingement on the Polyurethane/IA-700 coated blade EXP1

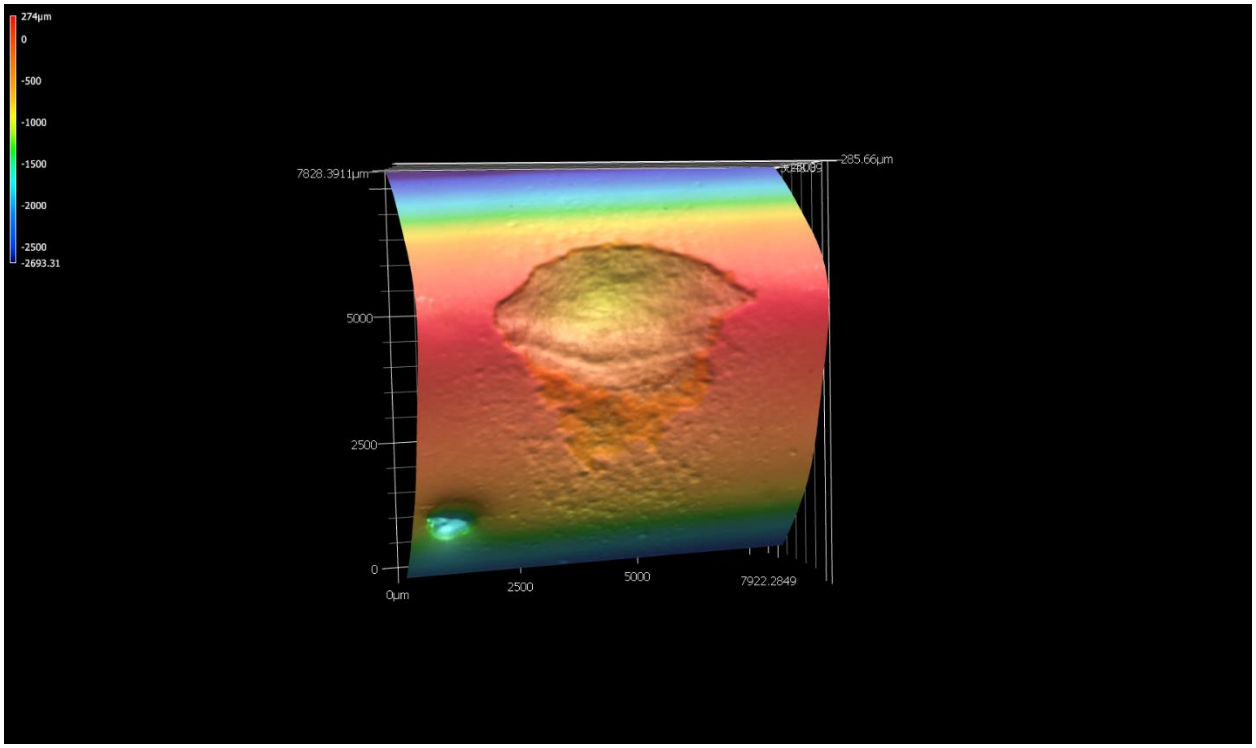


Fig. AVI-240: Erosion scar at 5° angle of impingement on the Polyurethane/IA-700 coated blade EXP2

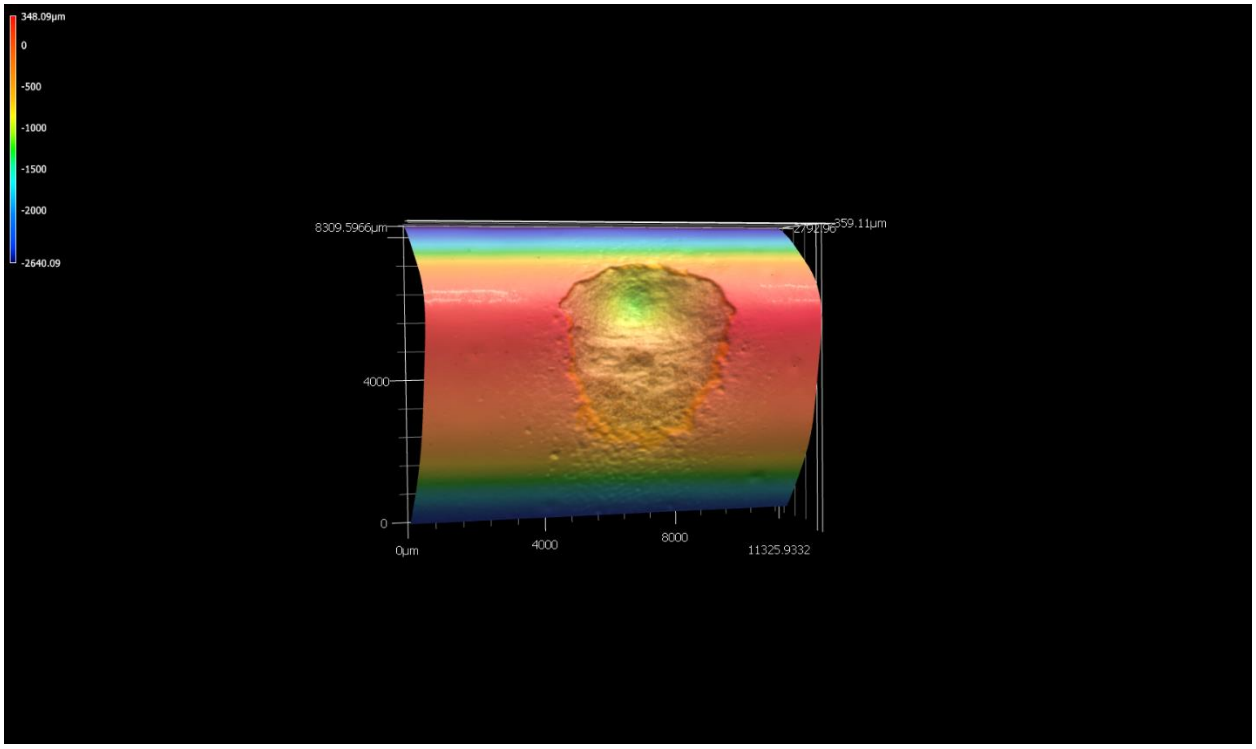


Fig. AVI-241: Erosion scar at 5° angle of impingement on the Polyurethane/IA-700 coated blade EXP3

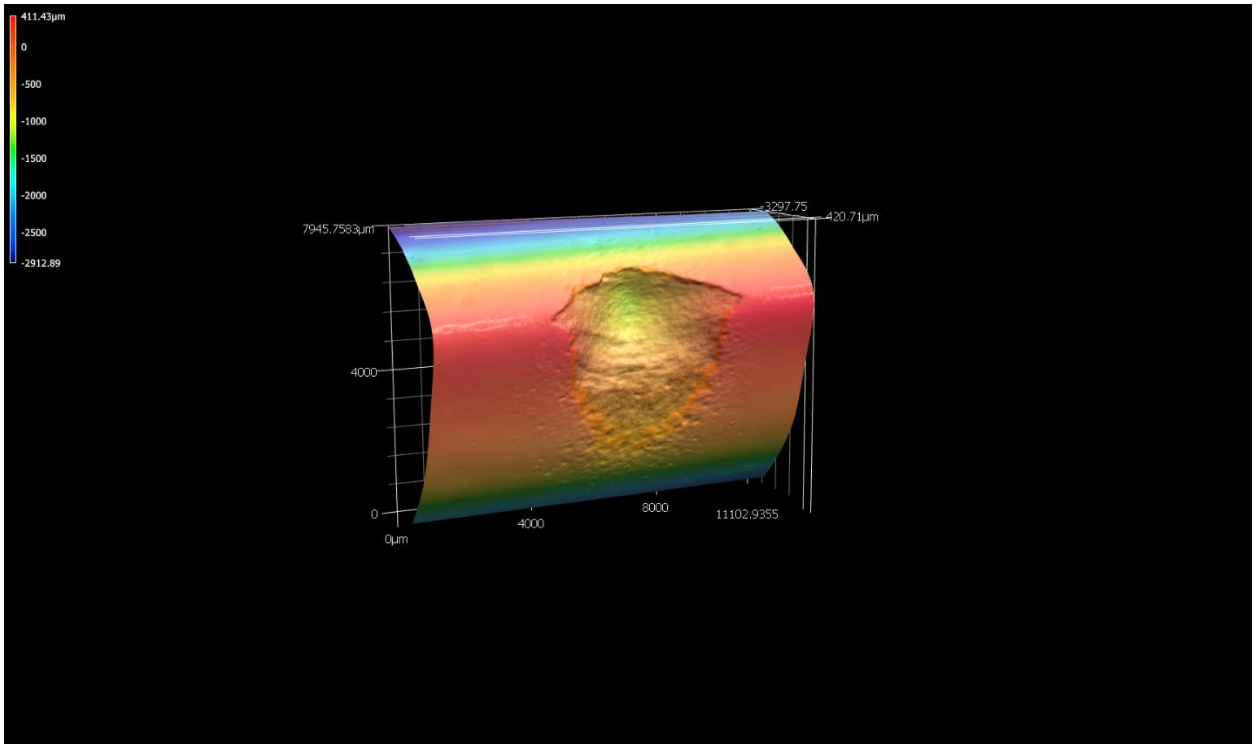


Fig. AVI-242: Erosion scar at 5° angle of impingement on the Polyurethane/IA-700 coated blade EXP4

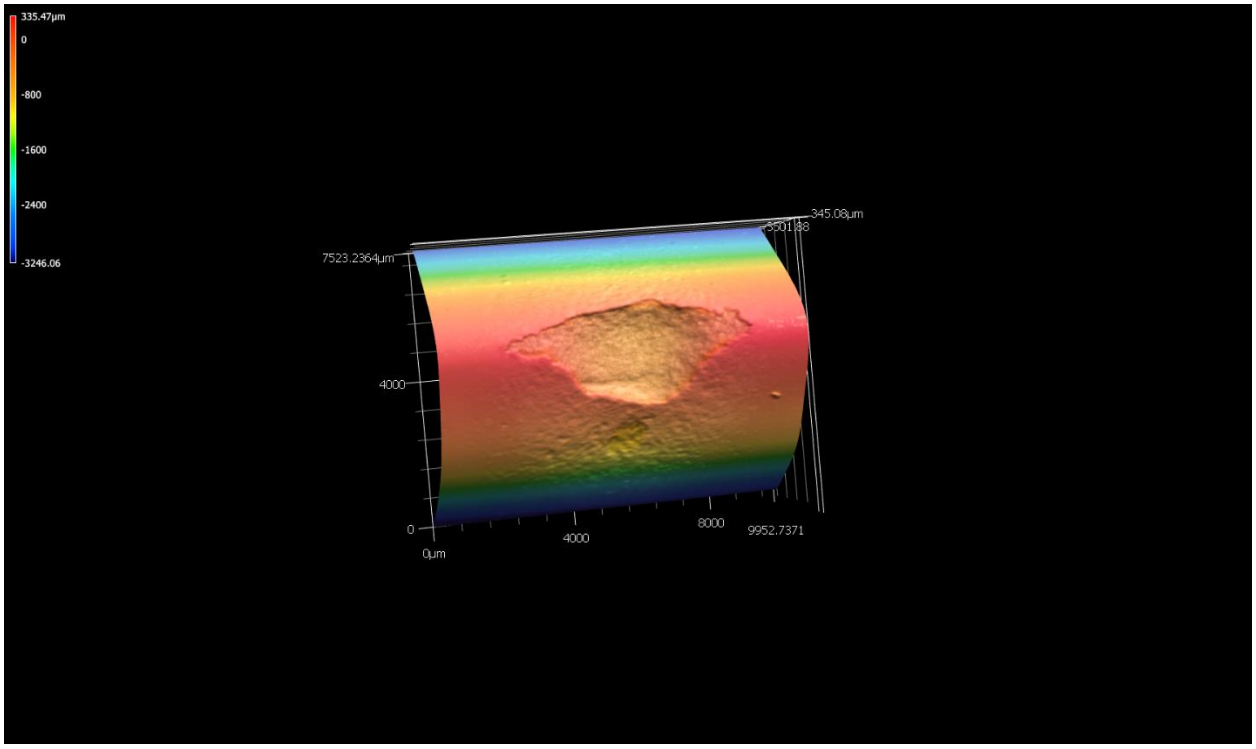


Fig. AVI-243: Erosion scar at 5° angle of impingement on the Polyurethane/IA-700 coated blade EXP5

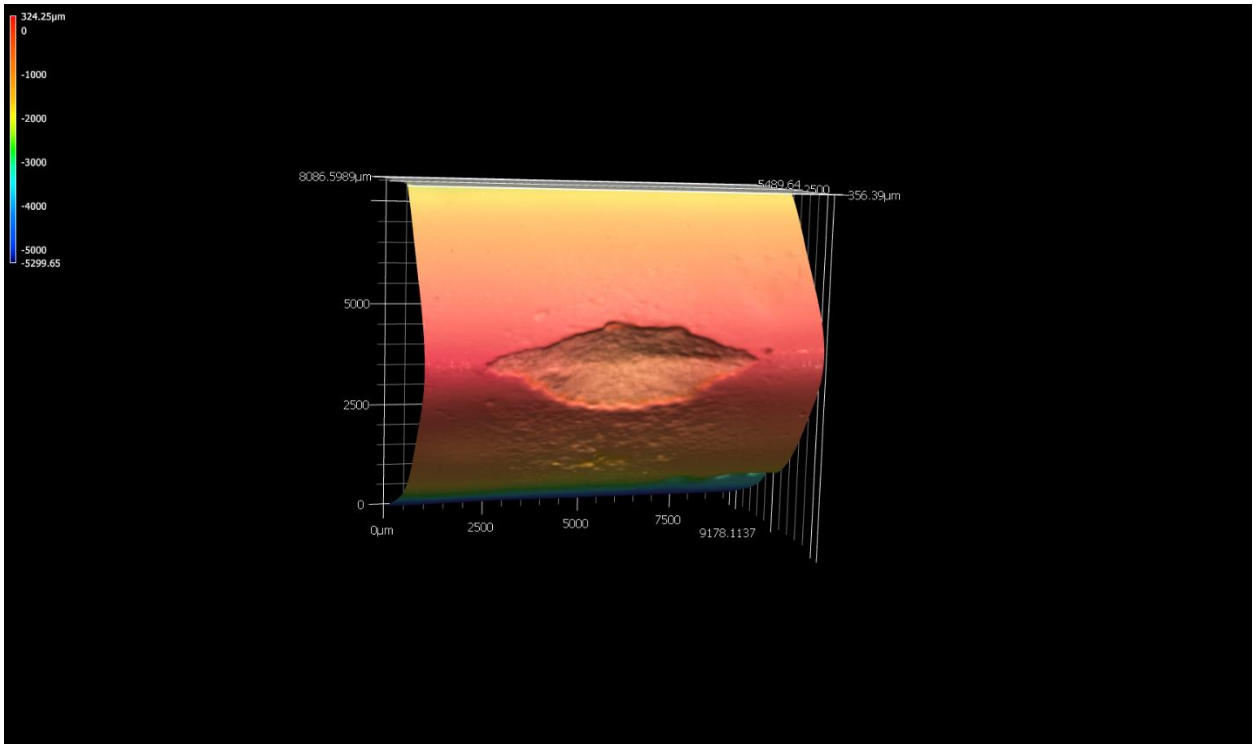


Fig. AVI-244: Erosion scar at 5° angle of impingement on the Polyurethane/IA-700 coated blade EXP6

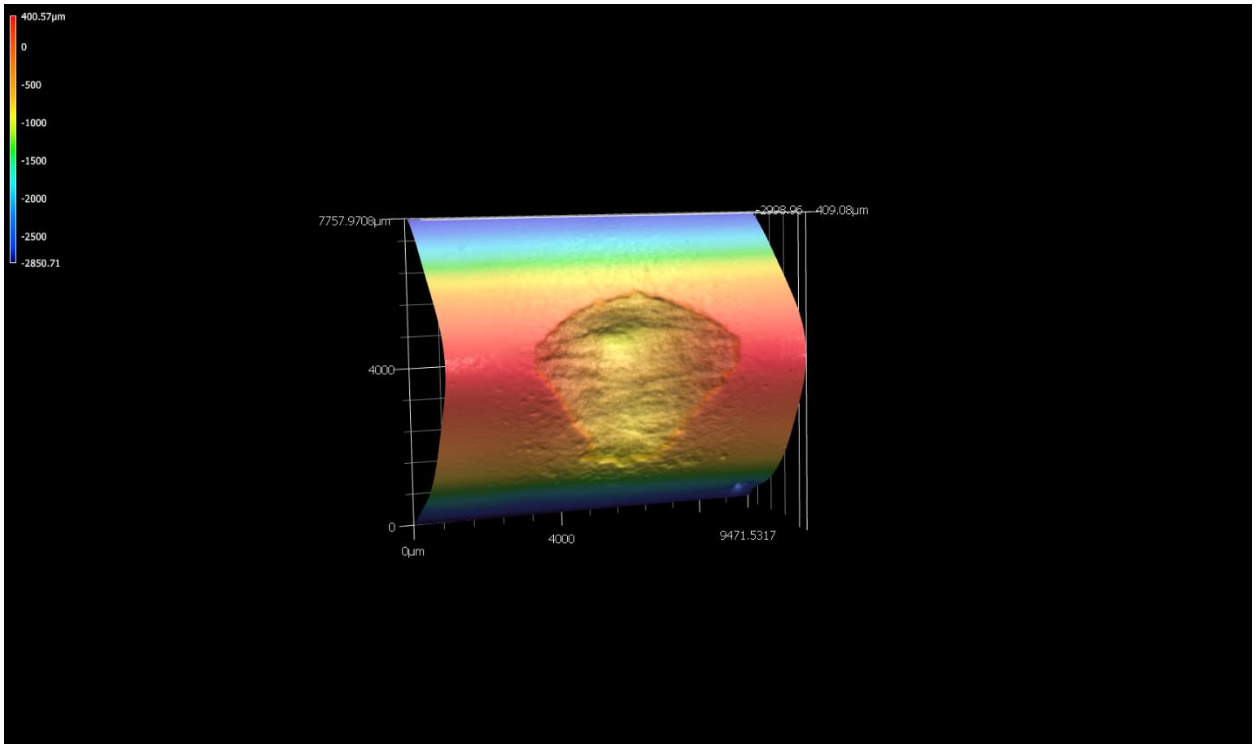


Fig. AVI-245: Erosion scar at 5° angle of impingement on the Polyurethane/IA-700 coated blade EXP7

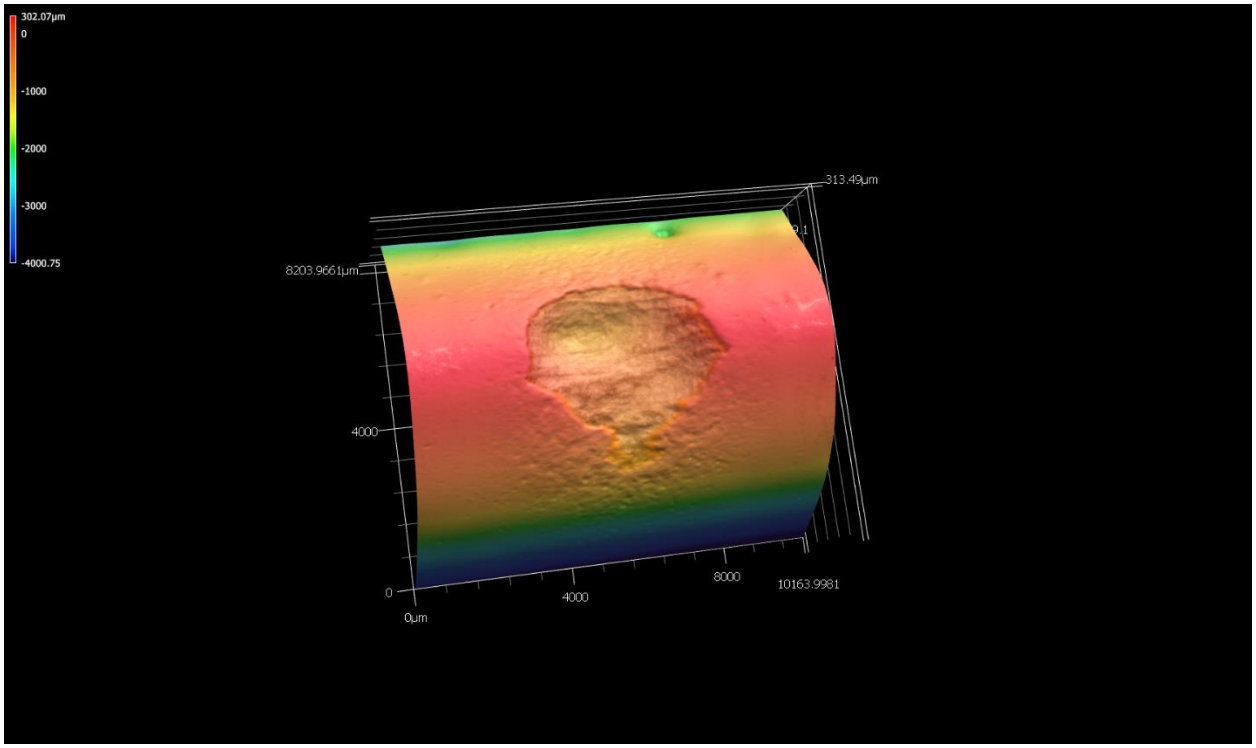


Fig. AVI-246: Erosion scar at 5° angle of impingement on the Polyurethane/IA-700 coated blade EXP8

- **10 degrees**
  - **Uncoated**

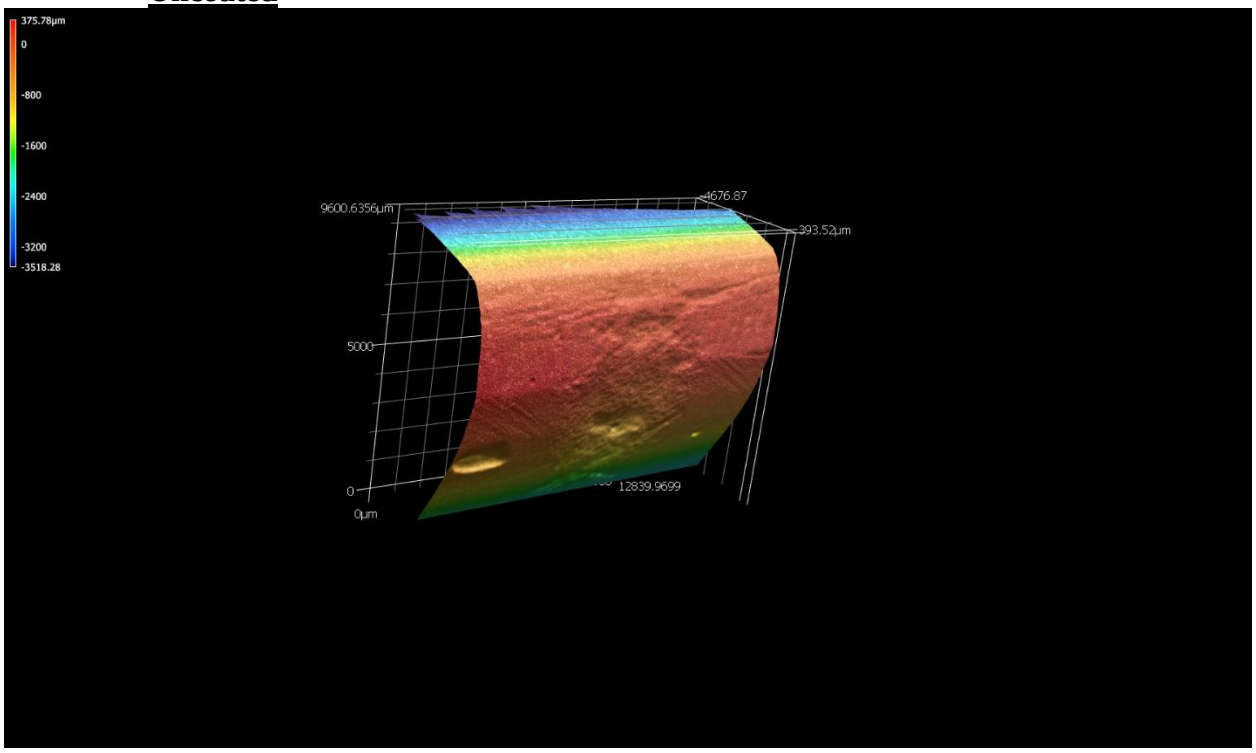


Fig. AVI-247: Erosion scar at 10° angle of impingement on the uncoated blade EXP1

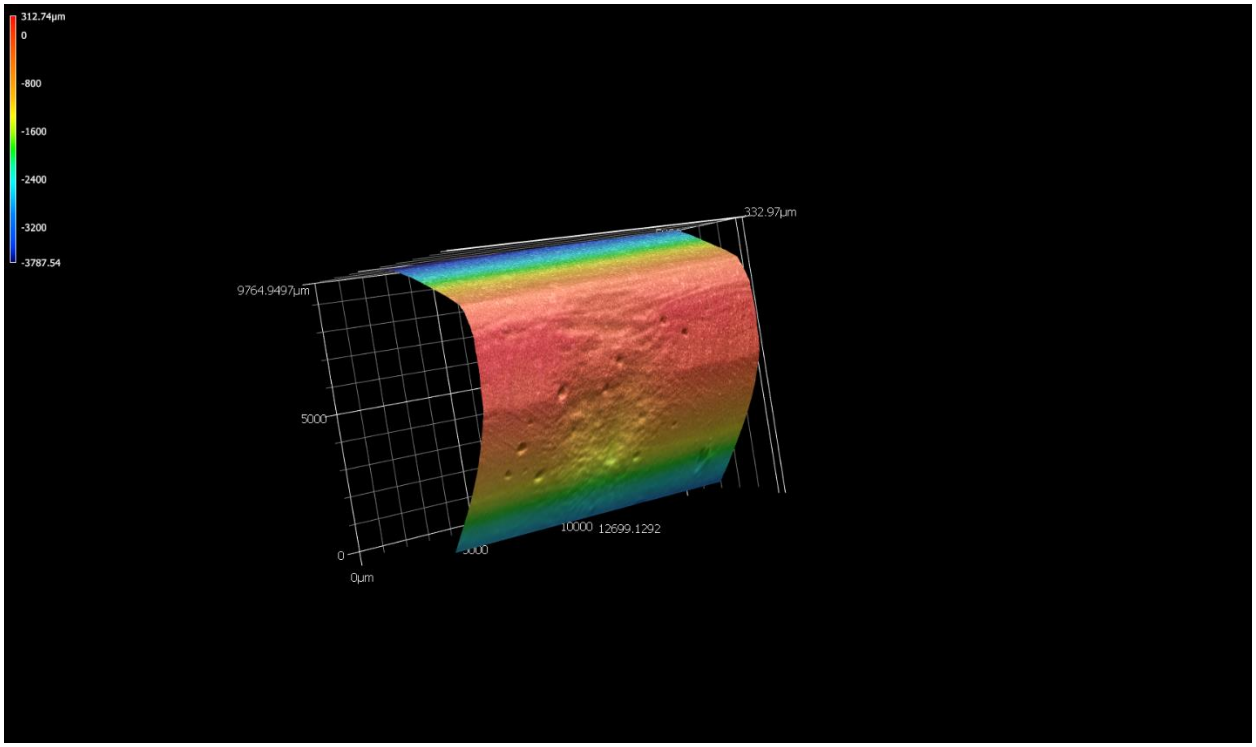


Fig. AVI-248: Erosion scar at 10° angle of impingement on the uncoated blade EXP2

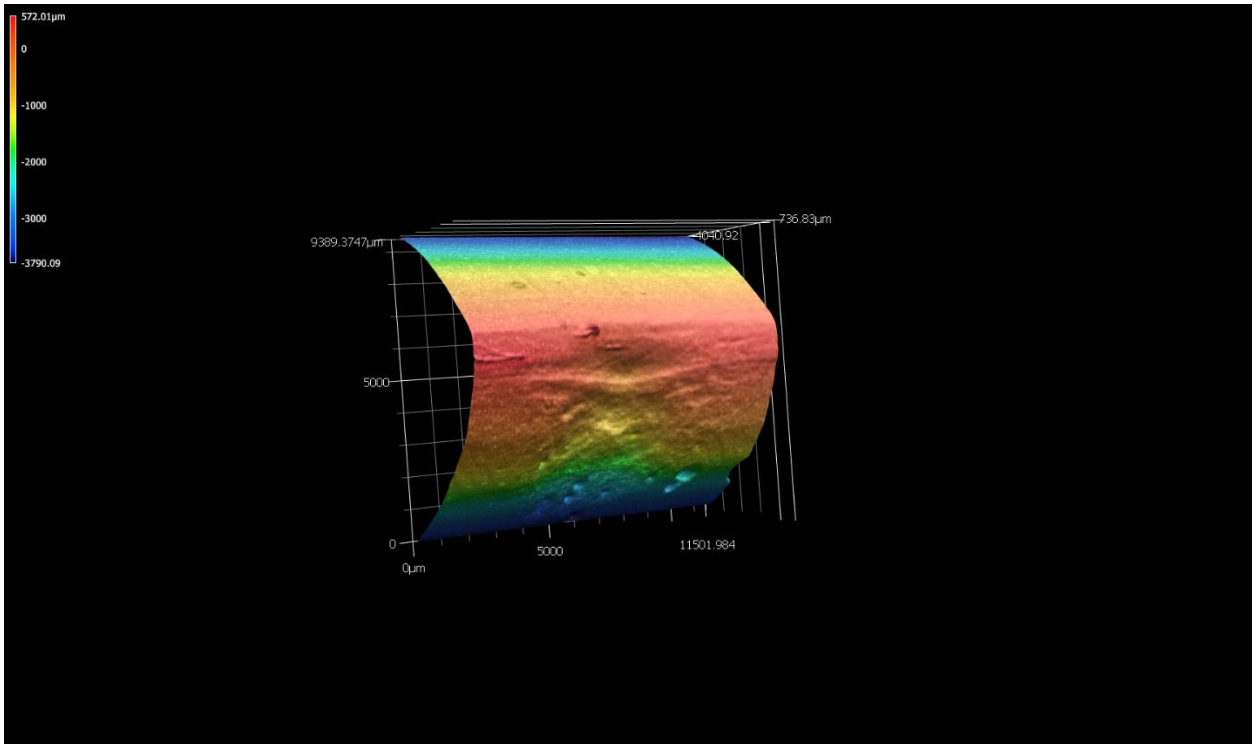


Fig. AVI-249: Erosion scar at 10° angle of impingement on the uncoated blade EXP3

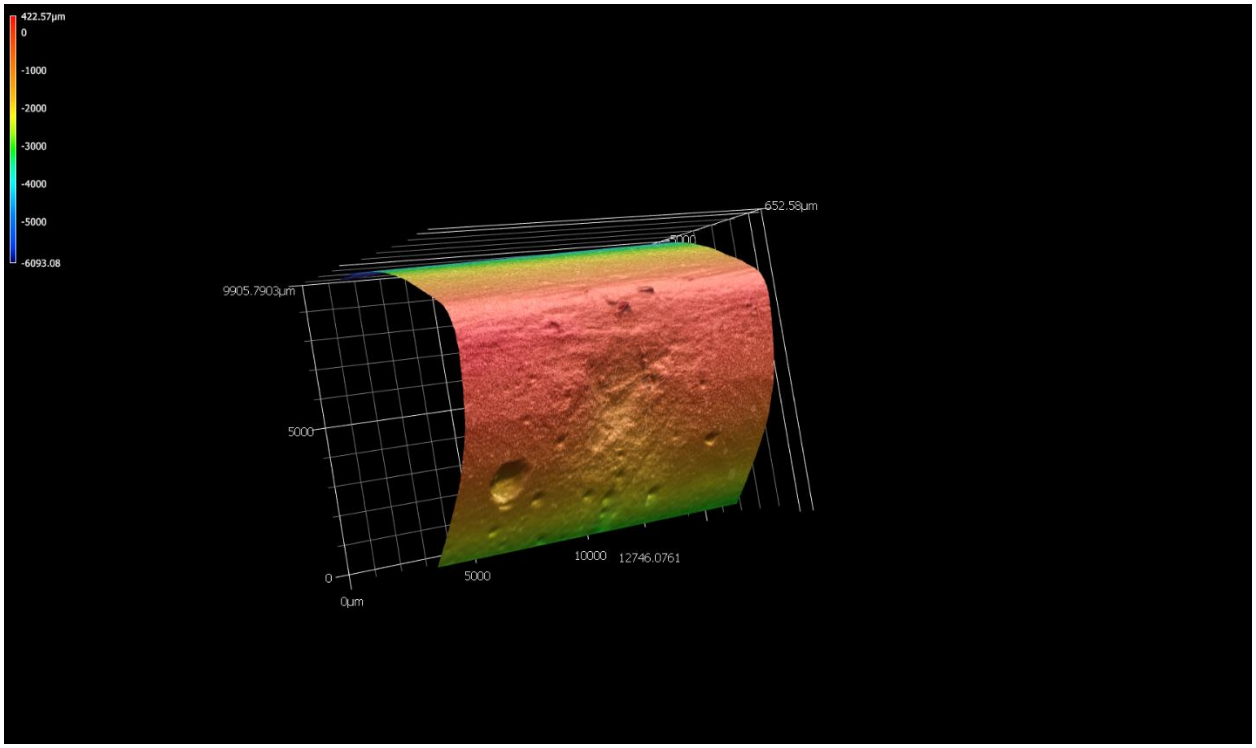


Fig. AVI-250: Erosion scar at 10° angle of impingement on the uncoated blade EXP4

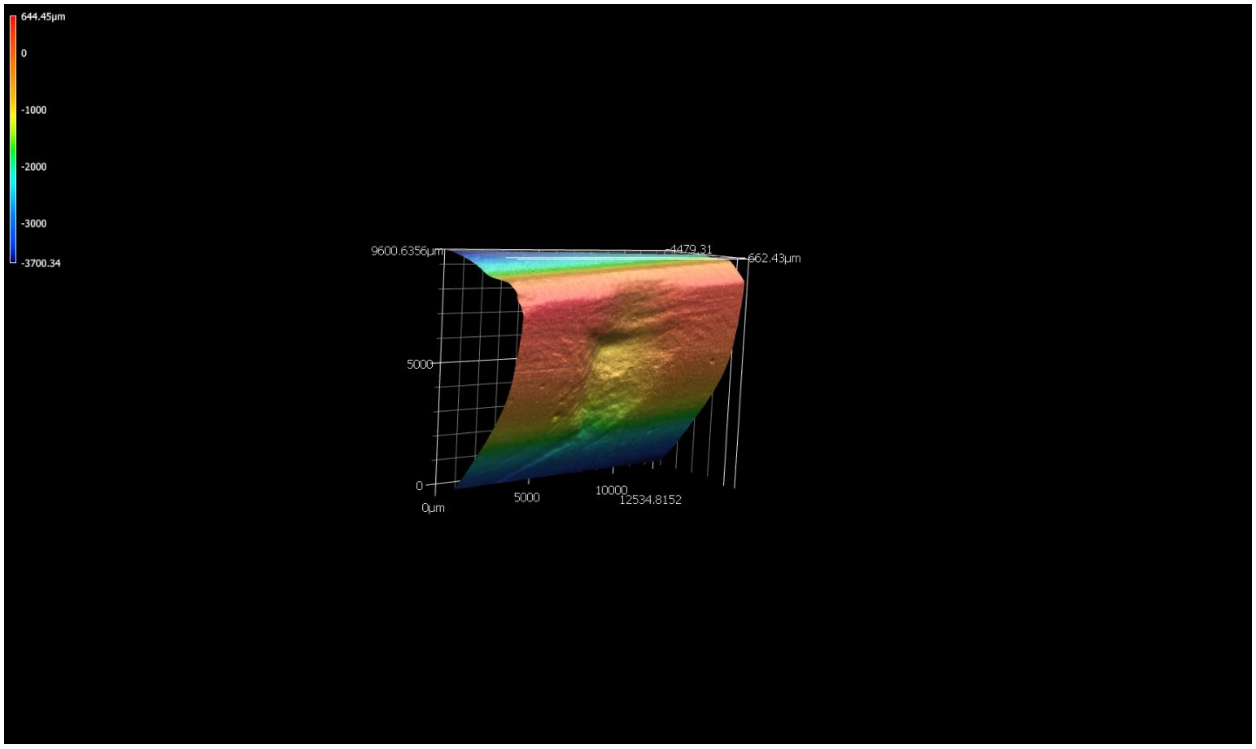


Fig. AVI-251: Erosion scar at 10° angle of impingement on the uncoated blade EXP5

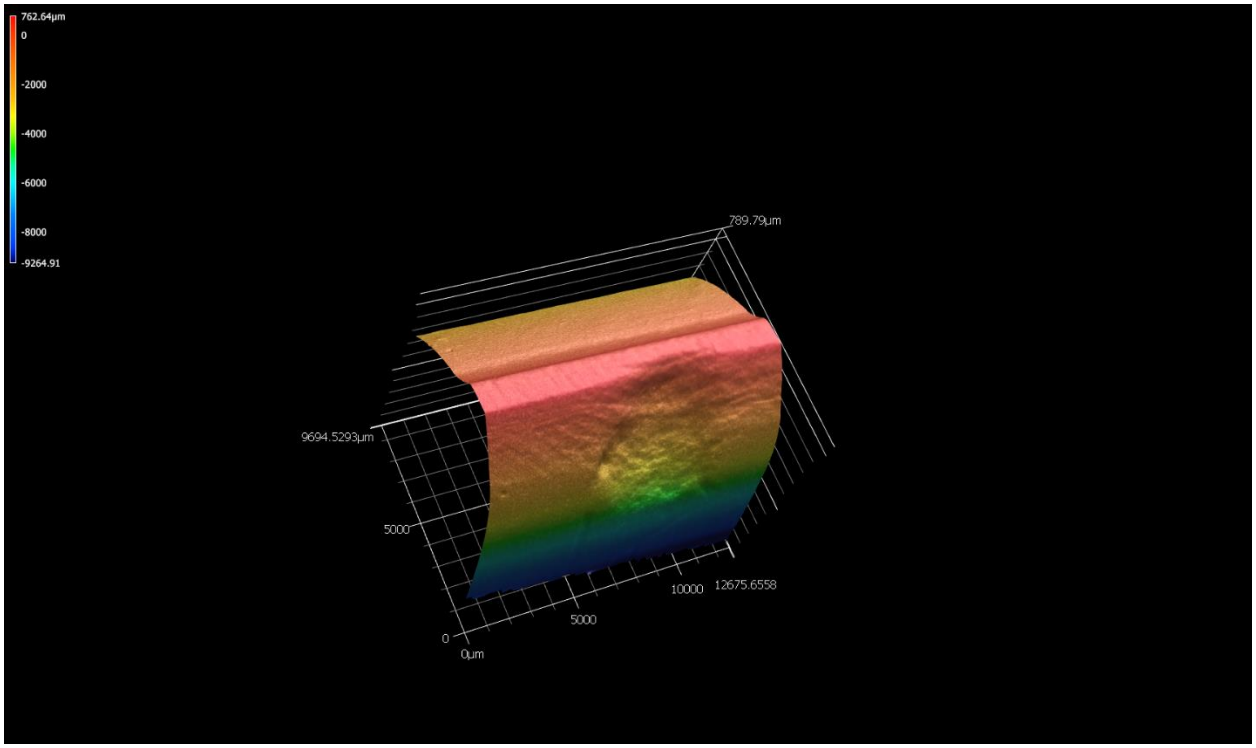


Fig. AVI-252: Erosion scar at 10° angle of impingement on the uncoated blade EXP6

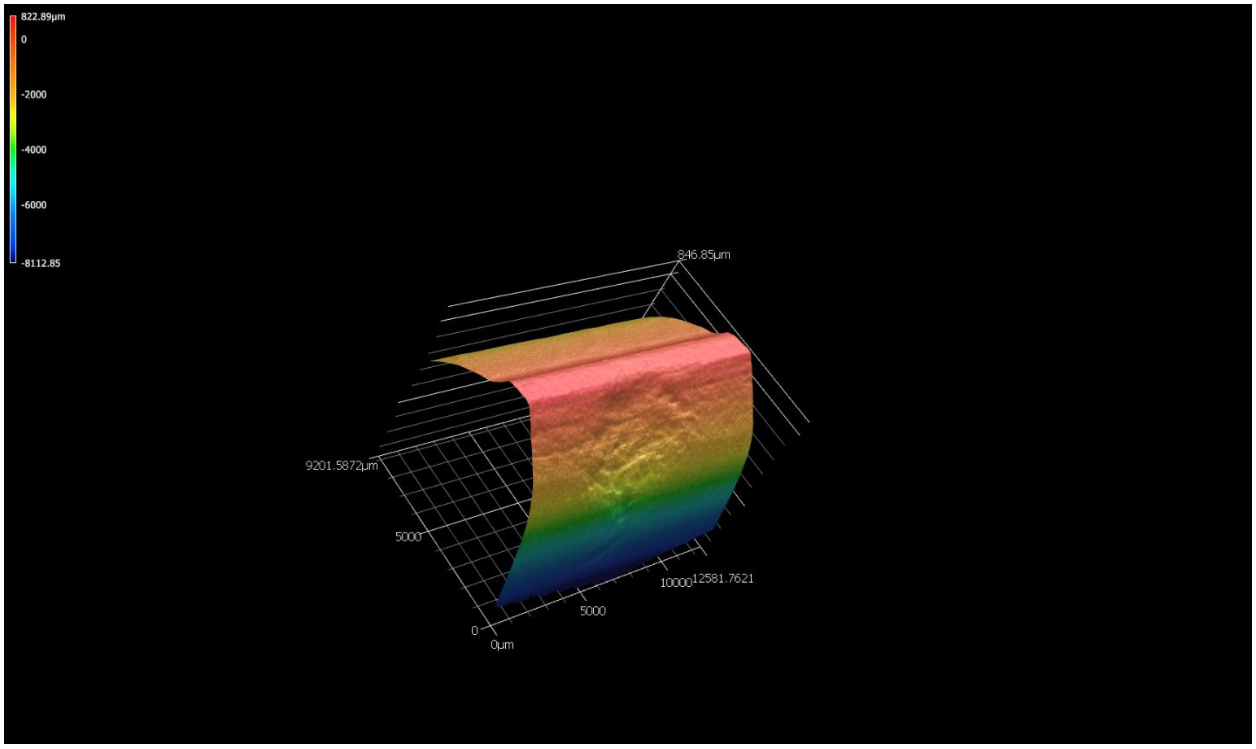


Fig. AVI-253: Erosion scar at 10° angle of impingement on the uncoated blade EXP7

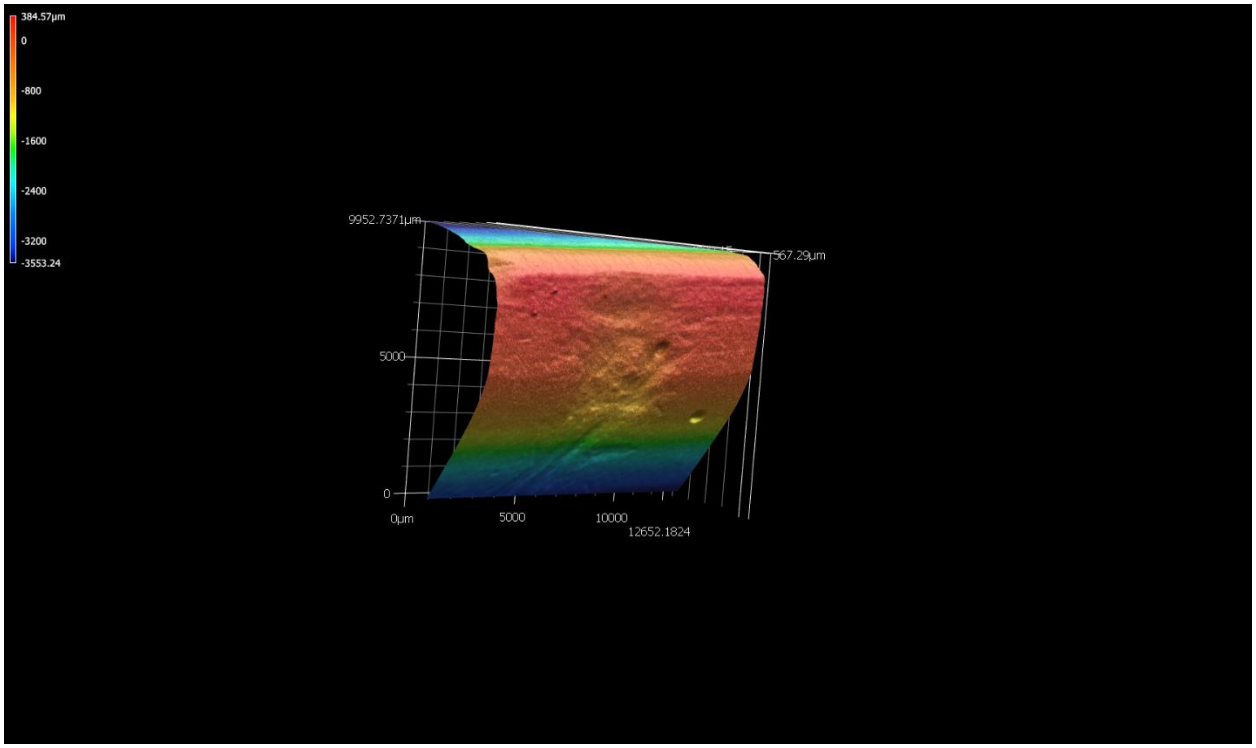


Fig. AVI-254: Erosion scar at 10° angle of impingement on the uncoated blade EXP8

- **H-146**

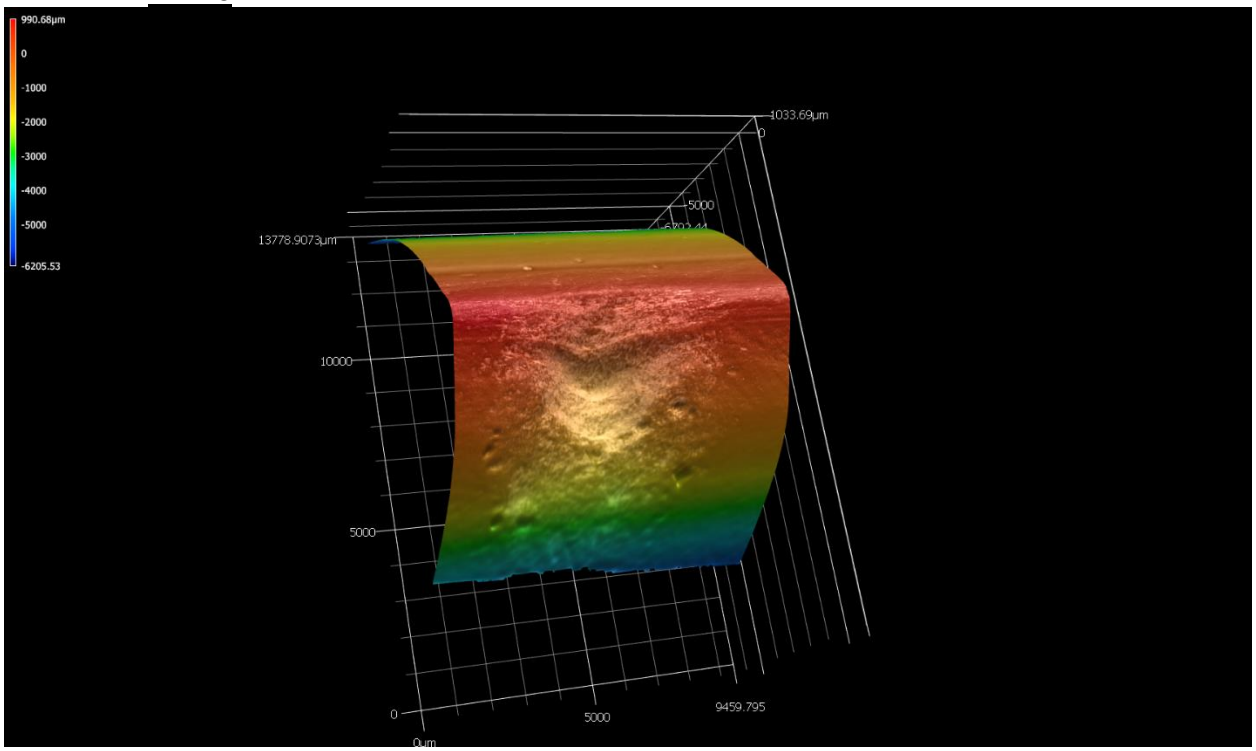


Fig. AVI-255: Erosion scar at 10° angle of impingement on the H-146 coated blade EXP1

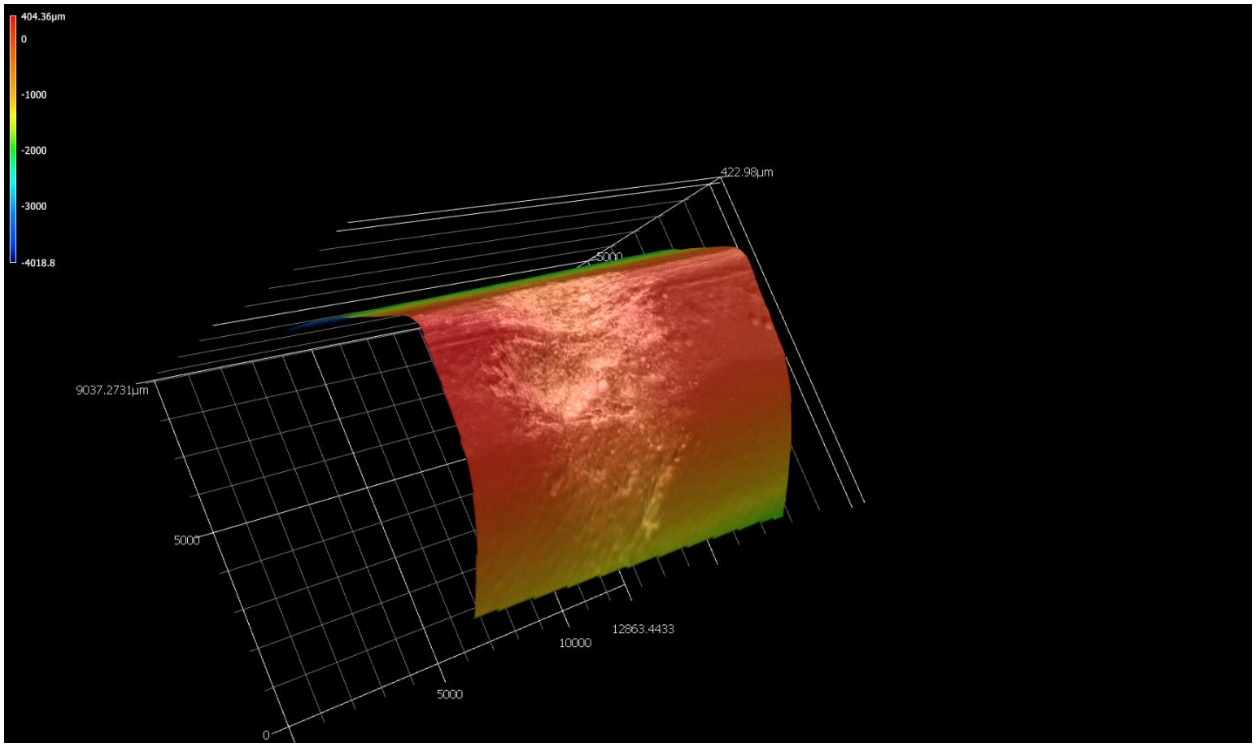


Fig. AVI-256: Erosion scar at 10° angle of impingement on the H-146 coated blade EXP2

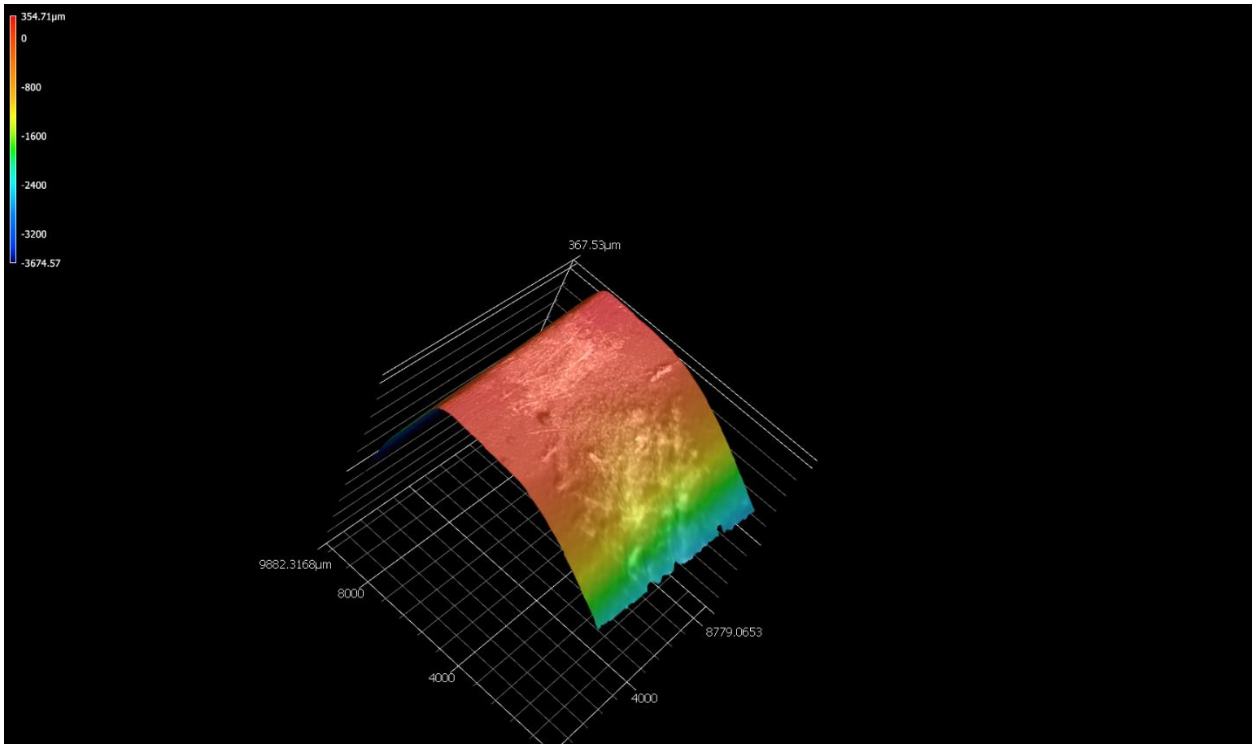


Fig. AVI-257: Erosion scar at 10° angle of impingement on the H-146 coated blade EXP3

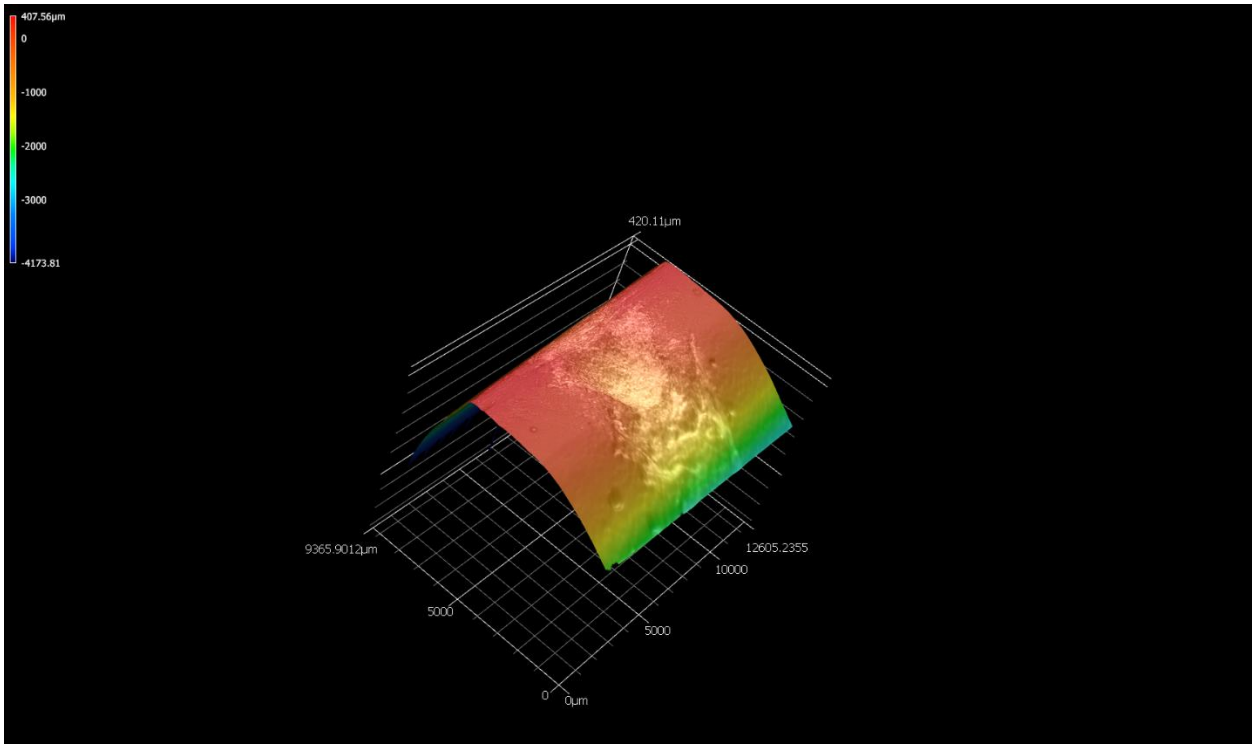


Fig. AVI-258: Erosion scar at 10° angle of impingement on the H-146 coated blade EXP4

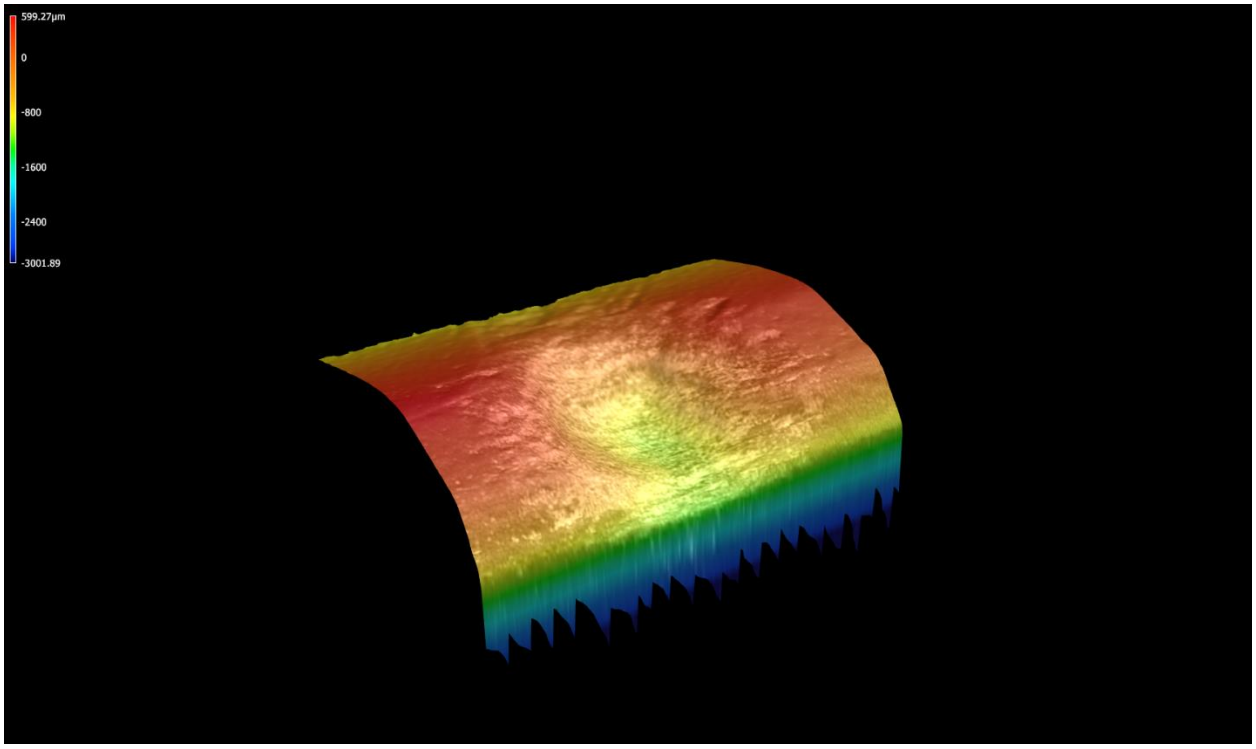


Fig. AVI-259: Erosion scar at 10° angle of impingement on the H-146 coated blade EXP5

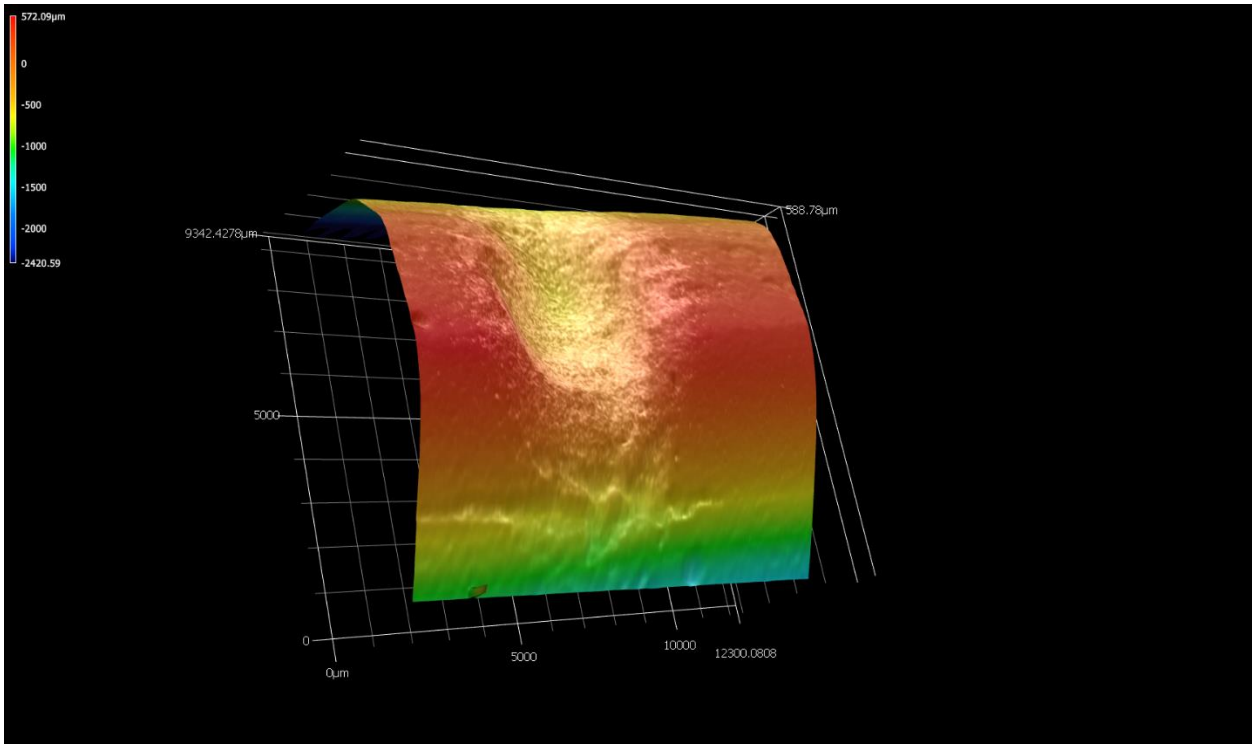


Fig. AVI-260: Erosion scar at 10° angle of impingement on the H-146 coated blade EXP6

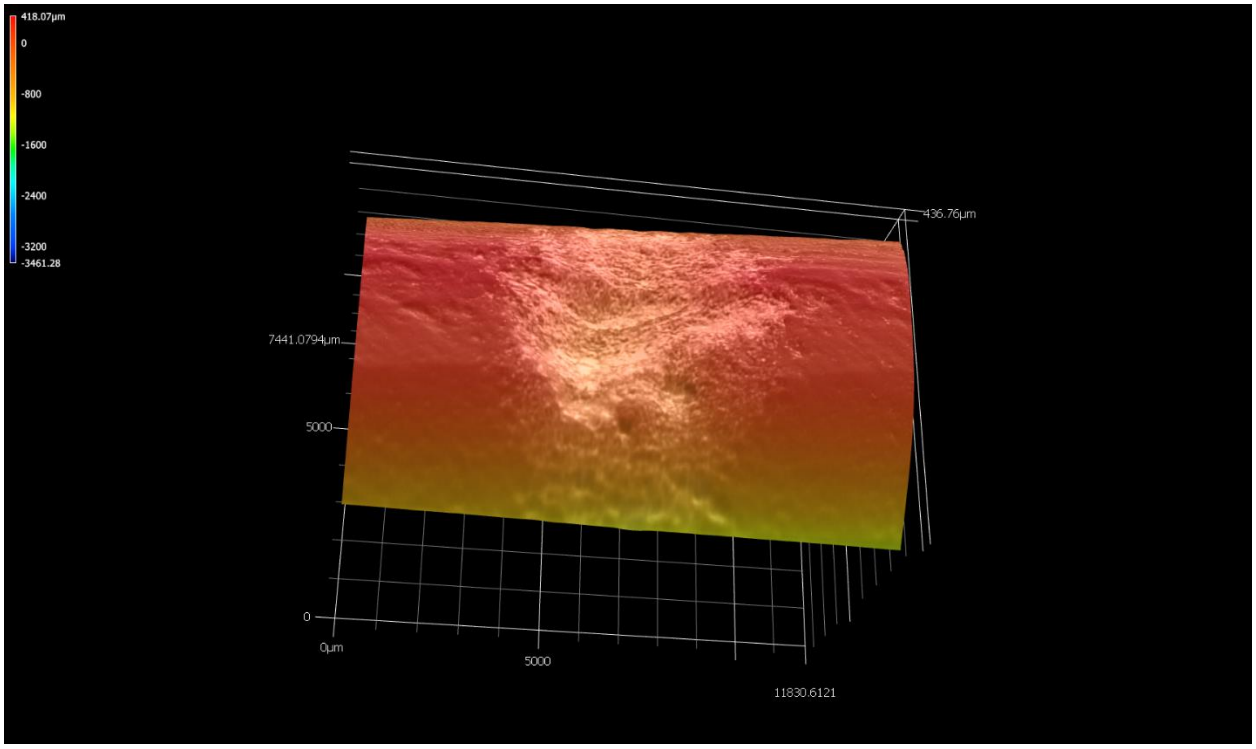


Fig. AVI-261: Erosion scar at 10° angle of impingement on the H-146 coated blade EXP7

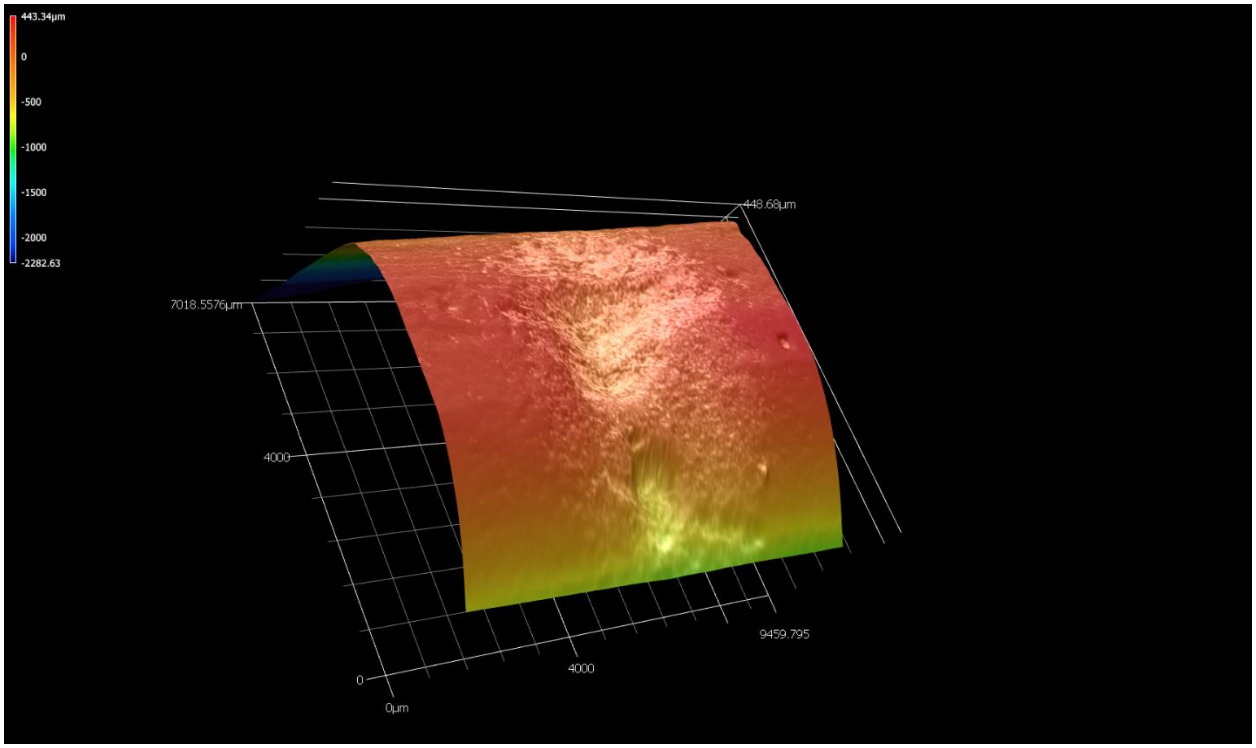


Fig. AVI-262: Erosion scar at 10° angle of impingement on the H-146 coated blade EXP8

- **Polyurethane/IA-700**

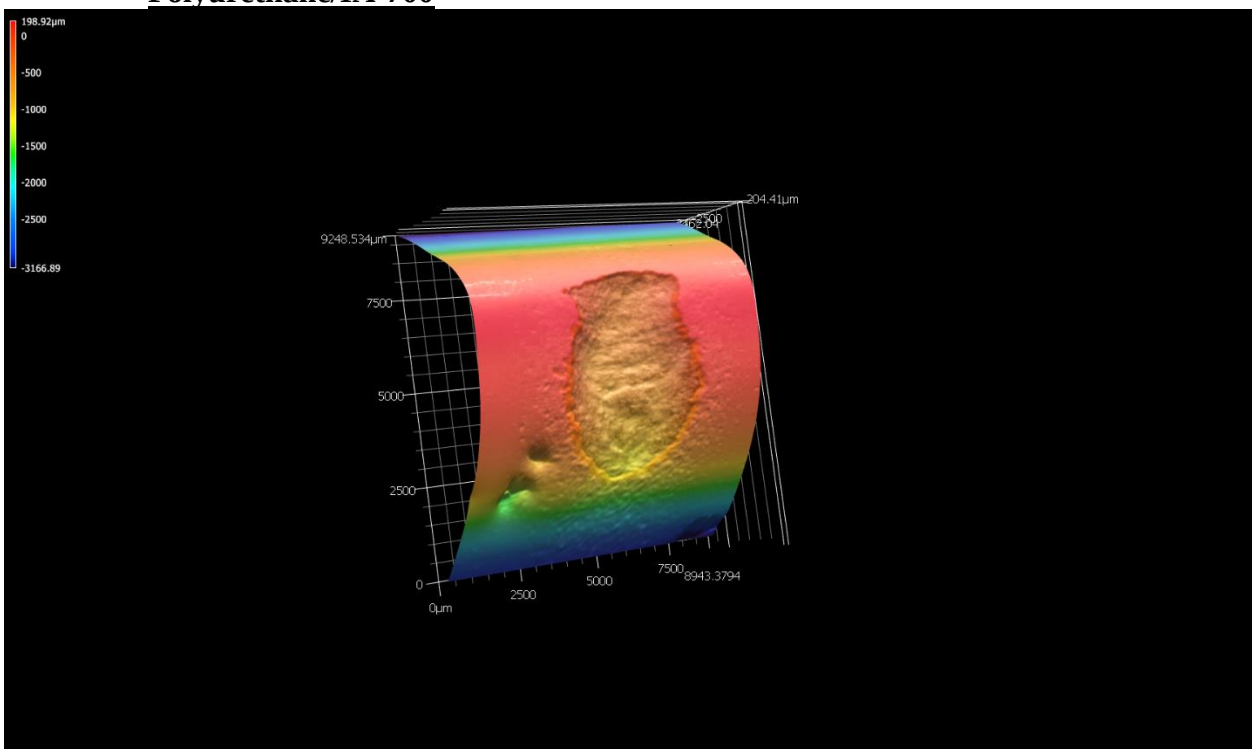


Fig. AVI-263: Erosion scar at 10° angle of impingement on the Polyurethane/IA-700 coated blade EXP1

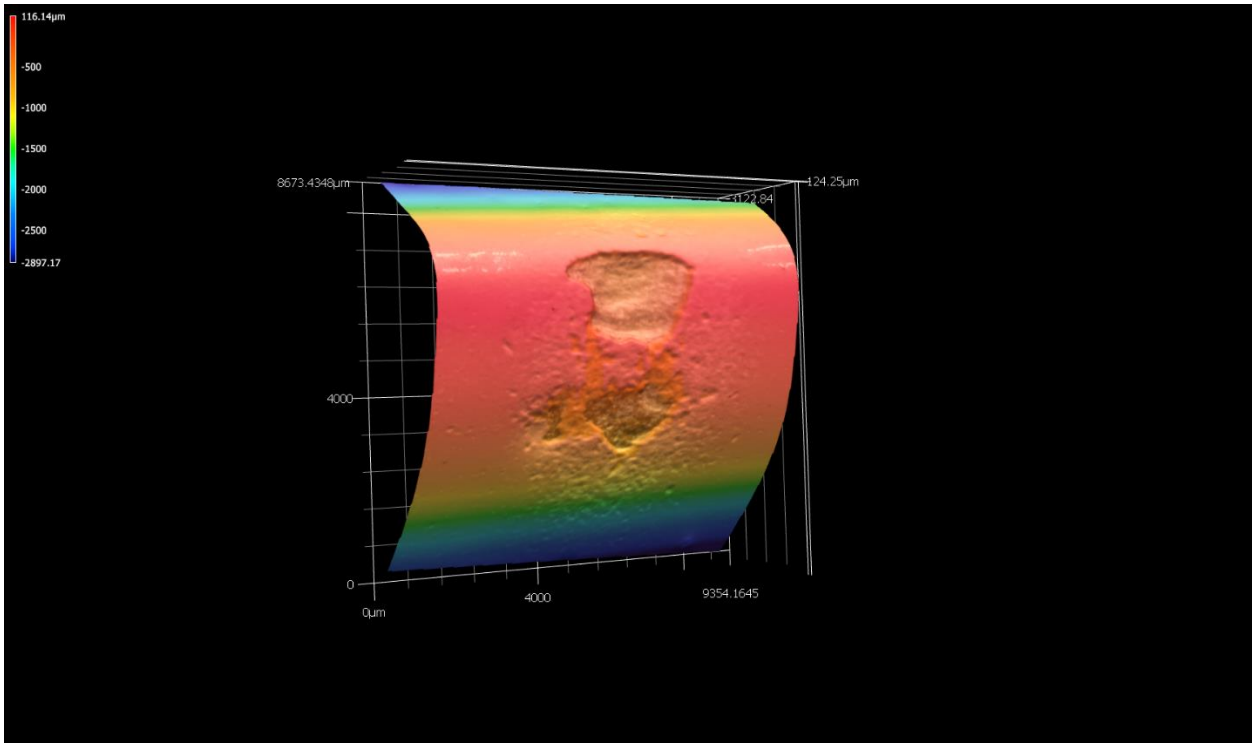


Fig. AVI-264: Erosion scar at 10° angle of impingement on the Polyurethane/IA-700 coated blade EXP2

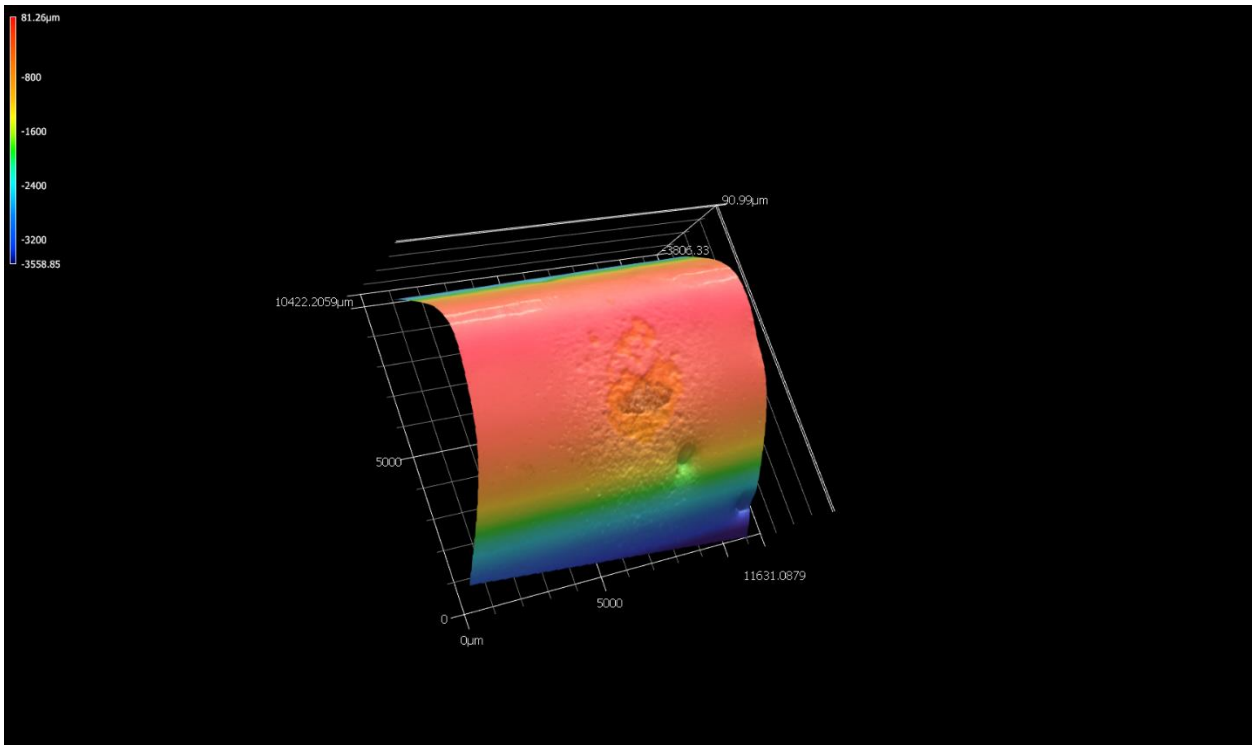


Fig. AVI-265: Erosion scar at 10° angle of impingement on the Polyurethane/IA-700 coated blade EXP3

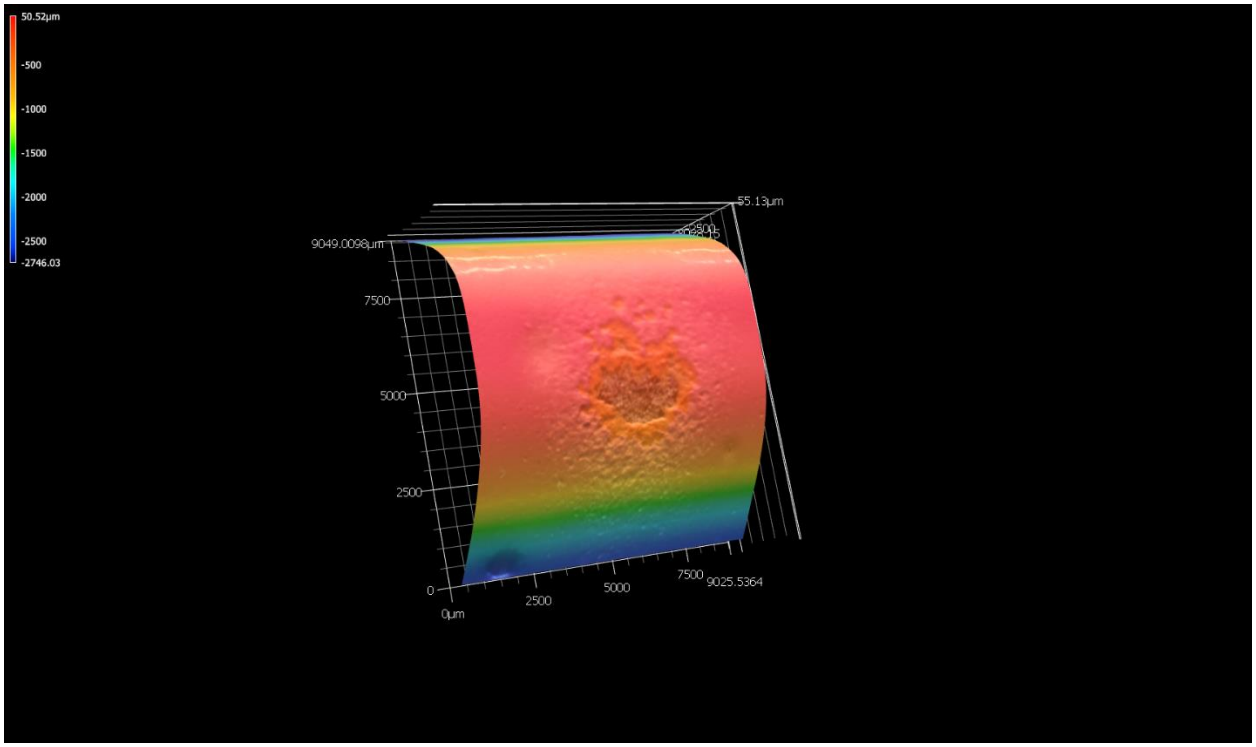


Fig. AVI-266: Erosion scar at 10° angle of impingement on the Polyurethane/IA-700 coated blade EXP4

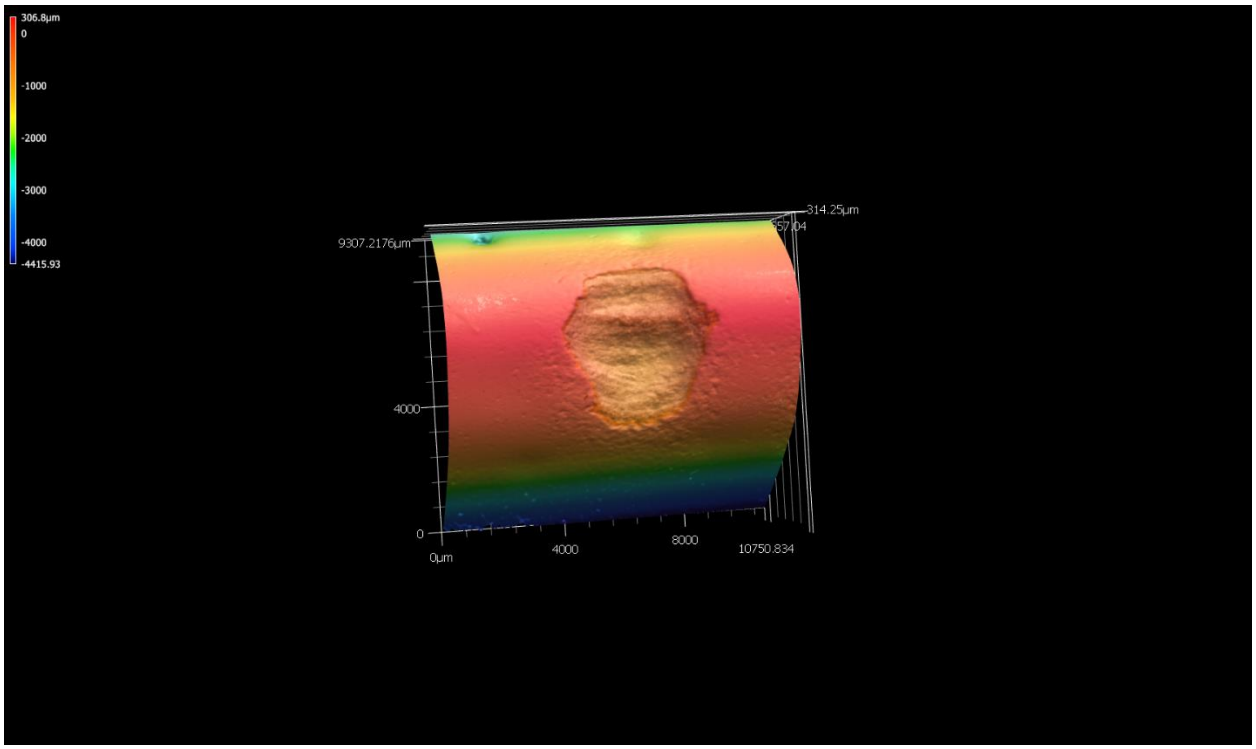


Fig. AVI-267: Erosion scar at 10° angle of impingement on the Polyurethane/IA-700 coated blade EXP5

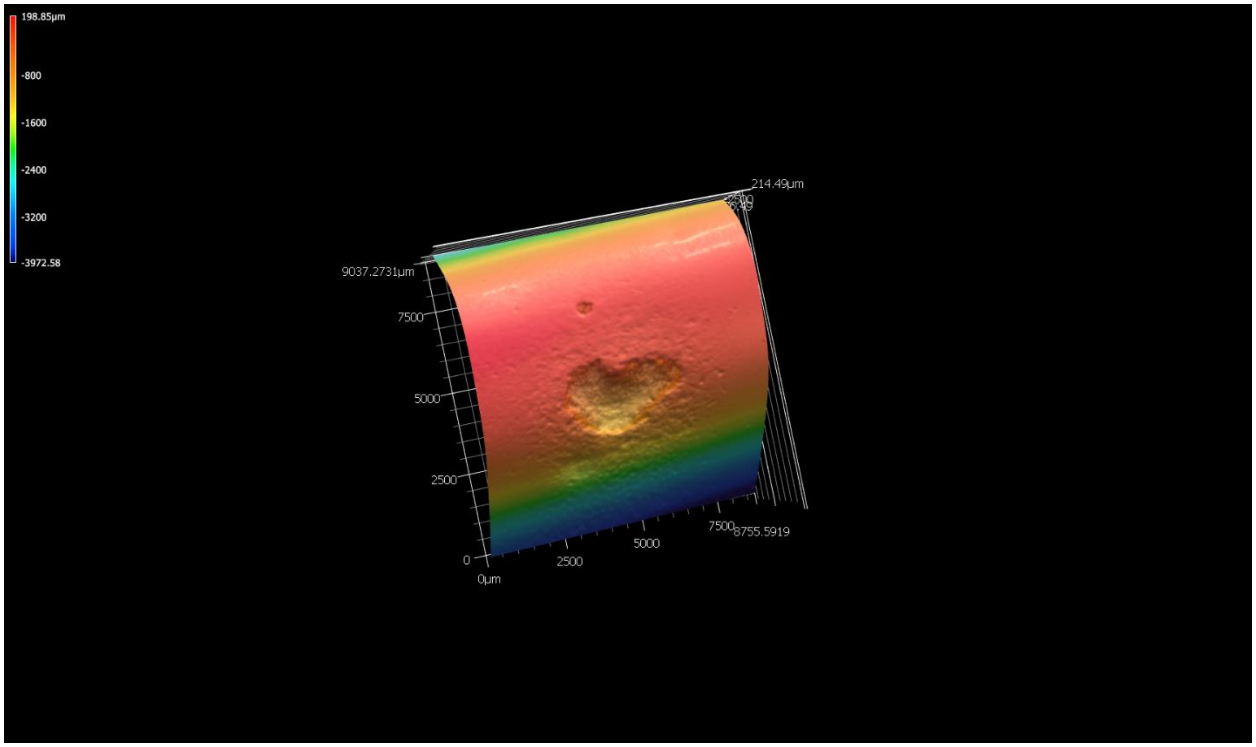


Fig. AVI-268: Erosion scar at 10° angle of impingement on the Polyurethane/IA-700 coated blade EXP8

Appendix VII: Xfoil documentation

XFOIL 6.9 User Primer THE last update 30 Nov 2001

Mark Drela, MIT Aero & Astro
Harold Youngren, Aerocraft, Inc.

General Description
==========
XFOIL is an interactive program for the design and analysis of subsonic isolated airfoils. It consists of a collection of menu-driven routines which perform various useful functions such as:

- Viscous (or inviscid) analysis of an existing airfoil, allowing
    * forced or free transition
        * transitional separation bubble(s)
    * limited trailing edge separation
    * lift and drag predictions just beyond CLmax
    * Karman-Tsien compressibility correction

- Airfoil design and redesign by interactive specification of a surface speed distribution via screen cursor or mouse. Two such facilities are implemented.
    * Full-Inverse, based on a complex-mapping formulation
    * Mixed-Inverse, an extension of XFOIL's basic panel method

  Full-inverse allows multi-point design, while Mixed-inverse allows relatively strict geometry control over parts of the airfoil.

- Airfoil redesign by interactive specification of new geometric parameters such as
    * new max thickness and/or camber
    * new LE radius
    * new TE thickness
    * new camber line via geometry specification
    * new camber line via loading change specification
    * flap deflection
    * explicit contour geometry (via screen cursor)

- Blending of airfoils

- Drag polar calculation with fixed or varying Reynolds and/or Mach numbers.

- Writing and reading of airfoil geometry and polar save files

- Plotting of geometry, pressure distributions, and polars
  (Versaplot-derivative plot package used)

XFOIL is best suited for use on a good workstation. A high-end PC is also effective, but must run Unix to support the X-Windows graphics. The source code of XFOIL is Fortran 77. The plot library also

uses a few C routines for the X-Windows interface.

History

XFOIL 1.0 was written by Mark Drela in 1986. The main goal was to combine the speed and accuracy of high-order panel methods with the new fully-coupled viscous/inviscid interaction method used in the ISES code developed by Drela and Giles. A fully interactive interface was employed from the beginning to make it much easier to use than the traditional batch-type CFD codes. Several inverse modes and a geometry manipulator were also incorporated early in XFOIL's development, making it a fairly general airfoil development system.

Since version 1.0, XFOIL has undergone numerous revisions, upgrades, hacks, and enhancements. These changes mainly originated from perceived shortcomings during actual design use, so XFOIL is now strongly geared to practical airfoil development. Harold Youngren provided the Xplot11 plot package which is a vast improvement over the grim Versaplot-type package used initially. Enhancements and suggestions from Youngren and other people were also incorporated into XFOIL itself along the way.

Over the past few years, bug reports and enhancement suggestions have slowed to practically nil, and so after a final few enhancements from version 6.8, XFOIL 6.9 is officially "frozen" and being made public. Although any bugs will likely be fixed, no further development is planned at this point. Method extensions are being planned, but these will be incorporated in a completely new next-generation code.

Note to code developers and code enhancers...
XFOIL does not exactly have the cleanest implementation, but it isn't too bad considering its vast modification history. Feel free to muck with the code as you like, provided everything is done under the GPL agreement. Drela and Youngren will not be inclined to assist with any code modifications at this point, however, since we each have a dozen other projects waiting. So proceed at your own risk.

Theory References

The general XFOIL methodology is described in

Drela, M.,
XFOIL: An Analysis and Design System for Low Reynolds Number Airfoils,
Conference on Low Reynolds Number Airfoil Aerodynamics,
University of Notre Dame, June 1989.

which also appears as a chapter in:

Low Reynolds Number Aerodynamics. T.J. Mueller (Editor).

Lecture Notes in Engineering #54. Springer Verlag. 1989.
ISBN 3-540-51884-3
ISBN 0-387-51884-3

The boundary layer formulation used by XFOIL is described in:
Drela, M. and Giles, M.B.
Viscous-Inviscid Analysis of Transonic and Low Reynolds Number Airfoils
AIAA Journal, 25(10), pp.1347-1355, October 1987.

The blunt trailing edge treatment is described in:
Drela, M.,
Integral Boundary Layer Formulation for Blunt Trailing Edges,
Paper AIAA-89-2166, August 1989.

Other related literature:
Drela, M.,
Elements of Airfoil Design Methodology,
Applied Computational Aerodynamics, (P. Henne, editor),
AIAA Progress in Aeronautics and Astronautics, Volume 125, 1990.

Drela, M.,
Low-Reynolds Number Airfoil Design for the MIT Daedalus Prototype: A Case Study,
Journal of Aircraft, 25(8), pp.724-732, August 1988.

Drela, M.,
Pros and Cons of Airfoil Optimization,
Chapter in "Frontiers of Computational Fluid Dynamics, 1998",
D.A. Caughey, M.M. Hafez, Eds.
World Scientific, ISBN 981-02-3707-3

Inviscid Formulation

The inviscid formulation of XFOIL is a simple linear-vorticity stream function panel method. A finite trailing edge base thickness is modeled
with a source panel. The equations are closed with an explicit Kutta condition. A high-resolution inviscid calculation with the default 160 panels requires seconds to execute on a RISC workstation. Subsequent
operating points for the same airfoil but different angles of attack are obtained nearly instantly.

A Karman-Tsien compressibility correction is incorporated, allowing good compressible predictions all the way to sonic conditions. The theoretical foundation of the Karman-Tsien correction breaks down in supersonic flow, and as a result accuracy rapidly degrades as the transonic regime is entered. Of course, shocked flows cannot be predicted with any certainty.

Inverse Formulation

There are two types of inverse methods incorporated in XFOIL: Full-Inverse and Mixed-Inverse. The Full-Inverse formulation

is essentially Lighthill's and van Ingen's complex mapping method, which is also used in the Eppler code and Selig's PROFOIL code. It calculates the entire airfoil geometry from the entire surface speed distribution. The Mixed-Inverse formulation is simply the inviscid panel formulation (the discrete governing equations are identical) except that instead of the panel vortex strengths being the unknowns, the panel node coordinates are treated as unknowns wherever the surface speed is prescribed. Only a part of the airfoil is altered at any one time, as will be described later. Allowing the panel geometry to be a variable results in a non-linear problem, but this is solved in a straightforward manner with a full-Newton method.

Viscous Formulation

The boundary layers and wake are described with a two-equation lagged dissipation integral BL formulation and an envelope e^n transition criterion, both taken from the transonic analysis/design ISES code. The entire viscous solution (boundary layers and wake) is strongly interacted with the incompressible potential flow via the surface transpiration model (the alternative displacement body model is used in ISES). This permits proper calculation of limited separation regions.
The drag is determined from the wake momentum thickness far downstream. A special treatment is used for a blunt trailing edge which fairly accurately accounts for base drag.

The total velocity at each point on the airfoil surface and wake, with contributions from the freestream, the airfoil surface vorticity, and the equivalent viscous source distribution, is obtained from the panel solution with the Karman-Tsien correction added. This is incorporated into the viscous equations, yielding a nonlinear elliptic system which is readily solved by a full-Newton method as in the ISES code. Execution times are quite rapid, requiring about 10 seconds on a RISC workstation for a high-resolution calculation with 160 panels. For a sequence of closely spaced angles of attack (as in a polar), the calculation time per point can be substantially smaller.

If lift is specified, then the wake trajectory for a viscous calculation
is taken from an inviscid solution at the specified lift. If alpha is specified, then the wake trajectory is taken from an inviscid solution at that alpha. This is not strictly correct, since viscous effects will
in general decrease lift and change the trajectory. This secondary correction is not performed, since a new source influence matrix would have to be calculated each time the wake trajectory is changed. This would result in unreasonably long calculation times. The effect of this
approximation on the overall accuracy is small, and will be felt mainly near or past stall, where accuracy tends to degrade anyway. In attached
cases, the effect of the incorrect wake trajectory is imperceptible.

Data Structure

==========
XFOIL stores all its data in RAM during execution. Saving of the data to files is NOT normally performed automatically, so the user must be careful to save work results before exiting XFOIL. The exception to this is optional automatic saving to disk of polar data as it's being computed in OPER (described later).

Stored airfoils and polars

XFOIL 6.9 stores multiple polars and associated airfoils and parameters during one interactive session. Each such data set is designated by its
"stored polar" index:

```
polar 1:  x,y, CL(a), CD(a)...  Re, Ma, Ncrit...
polar 2:  x,y, CL(a), CD(a)...  Re, Ma, Ncrit...
 .
 .
```

Not all of the data need to be present for each stored polar.
For example, x,y would be absent if the CL,CD polar was read in from an external file rather than computed online.

Earlier XFOIL versions in effect only allowed one stored airfoil and stored polar at a time. The new multiple storage feature makes iterative redesign considerably more convenient, since the cases can contain multiple design versions which can be easily overlaid on plots.

Current and buffer airfoils

XFOIL 6.9 retains the concept of a "current airfoil" and "buffer airfoil" used in previous versions.
These are the airfoils on which the various calculations are performed, and they are distinct from the "polar" x,y coordinates described above. The polar x,y are simply archived data, and do not directly participate in computations. The polar x,y must first be transferred into the current airfoil if they are to be used for computation.

Program Execution
=================

XFOIL is executed with

```
 % xfoil
```

When the program starts, the following top level menu and prompt appear:

```
   QUIT   Exit program

  .OPER   Direct operating point(s)
  .MDES   Complex mapping design routine
  .QDES   Surface speed design routine
  .GDES   Geometry design routine
```

```
   SAVE f Write airfoil to labeled coordinate file
   PSAV f Write airfoil to plain coordinate file
   ISAV f Write airfoil to ISES coordinate file
   MSAV f Write airfoil to MSES coordinate file
   REVE   Reverse written-airfoil node ordering

   LOAD f Read buffer airfoil from coordinate file
   NACA i Set NACA 4,5-digit airfoil and buffer airfoil
   INTE   Set buffer airfoil by interpolating two airfoils
   NORM   Buffer airfoil normalization toggle

   BEND   Display structural properties of current airfoil

   PCOP   Set current-airfoil panel nodes directly from buffer airfoil
points
   PANE   Set current-airfoil panel nodes ( 140 ) based on curvature
  .PPAR   Show/change paneling

  .PLOP   Plotting options

   WDEF f Write  current-settings file
   RDEF f Reread current-settings file
   NAME s Specify new airfoil name
   NINC   Increment name version number

   Z       Zoom    | (available in all menus)
   U       Unzoom  |

 XFOIL   c>
```

The commands preceded by a period place the user in another lower-level menu. The other commands are executed immediately and the user is prompted for another top level command. The lowercase letters i,r,f,s following some commands indicate the type of argument(s) expected by the command:

- i integer
- r real
- f filename
- s character string

Commands will be shown here in uppercase, although they are not case sensitive.

Typically, either the LOAD or the NACA command is issued first to create an airfoil for analysis or redesign. The NACA command expects an integer argument designating the airfoil:

```
 XFOIL  c>  NACA 4415
```

As with all commands, omitting the argument will produce a prompt:

```
 XFOIL  c>  NACA

 Enter NACA 4 or 5-digit airfoil designation   i>  4415
```

The LOAD command reads and processes a formatted airfoil coordinate file defining an arbitrary airfoil. It expects a filename argument:

```
 XFOIL  c>  LOAD e387.dat
```

The NACA or LOAD commands can be skipped if XFOIL is executed with a filename as an argument, as for example

```
 % xfoil e387.dat
```

which then executes the LOAD procedure before the first menu prompt is given.

Airfoil file formats

LOAD recognizes four airfoil file formats: Plain, Labeled, ISES, MSES.
All data lines are significant with the exception of lines beginning with "#", which are ignored.

Plain coordinate file

This contains only the X,Y coordinates, which run from the trailing edge, round the leading edge, back to the trailing edge in either direction:

```
X(1)  Y(1)
X(2)  Y(2)
 .     .
 .     .
X(N)  Y(N)
```

Labeled coordinate file

This is the same as the plain file, except that it also has an airfoil name string on the first line:

```
NACA 0012
X(1)  Y(1)
X(2)  Y(2)
 .     .
```

This is deemed the most convenient format to use.
The presence of the name string is automatically recognized if it does not begin with a Fortran-readable pair of numbers. Hence, "00 12 NACA Airfoil" cannot be used as a name, since the "00 12" will be interpreted as the first pair of coordinates. "0012 NACA" is OK, however.

Some Fortran implementations will also choke on airfoil names
that begin with T or F. These will be interpreted as logical
variables, defeating the name-detection logic. Beginning the
name with _T or _F is a workable solution to this "feature".

ISES coordinate file
....

This has four or five ISES grid domain parameters in addition to the
name:

```
NACA 0012
-2.0 3.0 -2.5 3.0
X(1)  Y(1)
X(2)  Y(2)
 .     .
```

If the second line has four or more numbers, then these are interpreted
as the grid domain parameters.

MSES coordinate file
....

This is the same as the ISES coordinate file, except that it can
contain multiple elements, each one separated by the line

```
999.0 999.0
```

The user is asked which of these elements is to be read in.

Buffer airfoil normalization

XFOIL will normally perform all operations on an airfoil with the
same shape and location in cartesian space as the input airfoil.
However, if the normalization flag is set (toggled with the NORM
command), the airfoil coordinates will be immediately normalized
to unit chord and the leading edge will be placed at the origin.
A message is printed to remind the user.

Buffer airfoil generation via interpolation

The INTE command is new in XFOIL 6.9, and allows interpolating
or "blending" of airfoils in various proportions. The interpolation
is performed as follows:

- -
Airfoils 0 and 1 are defined by their cubic splines,

```
  x0(s0), y0(s0)       x1(s1), y1(s1)
```

with the discrete secant arc length parameters s computed from

the coordinates x(i),y(i):

```
  s(i) = s(i-1) + sqrt[ (x(i)-x(i-1))^2 + (y(i)-y(i-1))^2 ]
```

To perform the interpolation, the discrete s0(i) points are first used to define discrete fractional parameter values s'(i) = 0...1, from the Leading Edge to the Trailing Edge:

```
 s'(i)  =   [s0(i) - s0_LE]/[s0_TE - s0_LE]
```

The s' values are computed separately on the top and bottom airfoil sides.

These fractional parameter values s' are then used to compute new spline-parameter values s0,s1 for each airfoil, separately on the top and bottom sides:

```
 s0(i)  =  s0_LE  +  s'(i) * [s0_TE - s0_LE]    ;  same as original
s0(i)
 s1(i)  =  s1_LE  +  s'(i) * [s1_TE - s1_LE]    ;  same as original
s0(i)
```

The interpolated-airfoil points are then computed by computing x,y from the splines and interpolating them:

```
 x_new(i)  =  (1-f) x0(s0(i))  +  f x1(s1(i))
 y_new(i)  =  (1-f) y0(s0(i))  +  f y1(s1(i))
```

Treating the top and bottom surface separately ensures that the leading edge point of the new airfoil is the interpolated result of the exact 0 and 1 leading edges.

- -

The polar shape of an interpolated airfoil will often be quite close to the interpolated polars of its two parent airfoils. Extrapolation can also be done by specifying a blending fraction outside the 0..1 range, although the resulting airfoil may be quite weird if the extrapolation is excessive.

A good way to use INTE is to "augment" or "tone down" the modifications to an airfoil performed in MDES or GDES. For example, say airfoil B is obtained by modifying airfoil A:

```
 A -> MDES -> B
```

Suppose the modification changed A's polar in the right direction, but not quite far enough. The additional needed change can be done by extrapolating past airfoil B in INTE:

```
Airfoil "0": A
Airfoil "1": B
Interpolating fraction 0..1 :  1.4
Output airfoil: C
```

Plotted along the "modification axis", the airfoils are:

```
A         B     C
0.0       1.0   1.4  ...
```

So airfoil C has 40% more of the change received by B in the redesign.
Aifoil C's polar will also be changed about 40% more as intended.

Airfoil node distribution matching

The INTE command can be used to impose one airfoil's node distribution
onto another airfoil shape. This is done as follows:

Airfoil 0: airfoil providing the node distribution (s'(i) values)
Airfoil 1: airfoil providing the shape (x, y values)
Interpolating fraction: 1.0

The resulting airfoil will have the shape of airfoil 1, but the
node distribution of airfoil 0.

Further buffer airfoil manipulation

The GDES facility allows very extensive manipulation of the buffer air-
foil.
This will be described in much more detail in a later section. If only
analysis is performed, the GDES facility would not normally be used.

Generation of current airfoil

When the buffer airfoil coordinates are read from a file during
startup,
or read in via the LOAD command, they are by default
also copied directly into the ``current'', or working airfoil.
Hence, no special action is needed to start analysis operations. How-
ever,
if the input airfoil has a poor point distribution (too many, too few,
poorly spaced, etc), one can use PANE to create a better panel node
distribution for the current airfoil on the splined buffer airfoil
shape.
The paneling routine increases the point density in areas of
high curvature (i.e. the leading edge) and at the trailing edge
to a degree specified by the user. The user can also increase
panel density over one additional interval on each airfoil side,
perhaps near transition. The current-airfoil paneling can be
displayed and/or modified with PPAR.

In some cases it is desirable to explicitly re-copy the buffer
airfoil into the current airfoil via PCOP. In previous XFOIL
versions this had to be done with the equivalent command sequence

```
 LOAD
 GDES
 EXEC
```

With XFOIL 6.9, the GDES,EXEC commands after LOAD are now superfluous.

The NACA command automatically invokes the paneling routine to create
a current airfoil with a suitable paneling.

Saving current airfoil coordinates

A coordinate file in any one of these four formats can be written
with the PSAV, SAVE, ISAV, or MSAV command, respectively.
When issuing the MSAV command, the user is also asked which element
in the file is to be overwritten. XFOIL can thus be used to easily
"edit" individual elements in MSES multielement configurations.
Of course, normalization should not be performed on an element if
it is to be written back to the same multielement file.
Only the current-airfoil coordinates can be saved to a file.
If the buffer or polar x,y coordinates need to be saved, they
must first be copied into the current airfoil.

Units
=====

Most XFOIL operations are performed on the airfoil's cartesian
coordinates x,y , which do not necessarily have a unit chord c.
Since the chord is ambiguous for odd shapes, the XFOIL
force coefficients CL, CD, CM are obtained by normalizing the
forces and moment with only the freestream dynamic pressure
(the reference chord is assumed to be unity). Likewise, the
XFOIL Reynolds number RE is defined with the freestream velocity
and viscosity, and an implied unit chord:

```
 CL = L / q           |     V = freestream speed
 CD = D / q           |     v = freestream kinematic viscosity
 CM = M / q           |     r = freestream density
 RE = V / v           |     q = 0.5 r V^2
```

The conventional definitions are

```
 Cl = L / q c
 Cd = D / q c
 Cm = M / q c^2
 Rc = V c / v
```

so that the conventional and XFOIL definitions differ only by
the chord factor c or c^2.

For example, a NACA 4412 airfoil is operated in the OPER menu at

```
 RE   = 500000
 ALFA = 3
```

first with chord=1.0, and then with chord=0.5 (changed with SCAL
command in the GDES menu, say). The results produced by XFOIL are:

```
 c = 1.0 :    CL = 0.80    CD = 0.0082    (RE = 500000, Rc = 500000)
 c = 0.5 :    CL = 0.40    CD = 0.0053    (RE = 500000, Rc = 250000)
```

Since CL is not normalized with the chord, it is nearly proportional to the airfoil size. It is not exactly proportional, since the true chord Reynolds number Rc is different, and there is always a weak Reynolds number effect on lift. In contrast, the CD for the smaller airfoil is significantly greater than 1/2 times the larger-airfoil CD, since chord Reynolds number has a significant impact on profile drag. Repeating the c = 0.5 case at RE = 1000000, produces the expected result that CL and CD are exactly 1/2 times their c = 1.0 values.

```
 c = 0.5 :    CL = 0.40    CD = 0.0041    (RE = 1000000, Rc = 500000)
```

Although XFOIL performs its operations with no regard to the size of the airfoil, some quantities are nevertheless defined in terms of the chord length. Examples are the camber line shape and BL trip locations, which are specified in terms of the relative x/c,y/c along and normal to the airfoil chord line. This is done only for the user's convenience. In the input and output labeling, "x,y" always refer to the cartesian coordinates, while "x/c,y/c" refer to the chord-based coordinates which are shifted, rotated, and scaled so that the airfoil's leading edge is at (x/c,y/c) = (0,0), and the airfoil's trailing edge is at (x/c,y/c) = (1,0). The two systems cooincide only if the airfoil is normalized.

Analysis

Most of the commands in the top level XFOIL menu merely put the user into some lower command level with its own menu and prompt. Issuing The OPER command, for instance, will produce the prompt

```
 .OPERi  c>
```

Typing a " ? " will result in the OPER analysis menu being displayed:

```
   <cr>     Return to Top Level
   !        Redo last ALFA,CLI,CL,ASEQ,CSEQ,VELS

   Visc r   Toggle Inviscid/Viscous mode
  .VPAR     Change BL parameter(s)
   Re   r   Change Reynolds number
   Mach r   Change Mach number
   Type i   Change type of Mach,Re variation with CL
   ITER     Change viscous-solution iteration limit
   INIT     Toggle BL initialization flag

   Alfa r   Prescribe alpha
   CLI  r   Prescribe inviscid CL
   Cl   r   Prescribe CL
   ASeq rrr Prescribe a sequence of alphas
   CSeq rrr Prescribe a sequence of CLs

   SEQP     Toggle polar/Cp(x) sequence plot display
   CINC     Toggle  minimum Cp  inclusion in polar
   HINC     Toggle hinge moment inclusion in polar
   Pacc i   Toggle auto point accumulation to active polar
```

```
   PGET f   Read new polar from save file
   PWRT i   Write polar to save file
   PSUM     Show summary of stored polars
   PLIS i   List stored polar(s)
   PDEL i   Delete stored polar
   PSOR i   Sort stored polar
   PPlo ii. Plot stored polar(s)
   APlo ii. Plot stored airfoil(s) for each polar
   ASET i   Copy stored airfoil into current airfoil
   PREM ir. Remove point(s) from stored polar
   PNAM i   Change airfoil name of stored polar
   PPAX     Change polar plot axis limits

   RGET f   Read new reference polar from file
   RDEL i   Delete stored reference polar

   GRID     Toggle Cp vs x grid overlay
   CREF     Toggle reference Cp data overlay
   FREF     Toggle reference CL,CD.. data display

   CPx      Plot Cp vs x
   CPV      Plot airfoil with pressure vectors (gee wiz)
  .VPlo     BL variable plots
  .ANNO     Annotate current plot
   HARD     Hardcopy current plot
   SIZE r   Change plot-object size
   CPMI r   Change minimum Cp axis annotation

   BL   i   Plot boundary layer velocity profiles
   BLC      Plot boundary layer velocity profiles at cursor
   BLWT r   Change velocity profile scale weight

   FMOM     Calculate flap hinge moment and forces
   FNEW rr  Set new flap hinge point
   VELS rr  Calculate velocity components at a point
   DUMP f   Output Ue,Dstar,Theta,Cf vs s,x,y to file
   CPWR f   Output x vs Cp to file
   CPMN     Report minimum surface Cp
   NAME s   Specify new airfoil name
   NINC     Increment name version number
```

The commands are not case sensitive. Some commands expect multiple arguments, but if the arguments are not typed, prompts will be issued.

The most commonly-used commands have alternative short forms, indicated by the uppercase part of the command in the menu list. For example, the menu shows...

```
   Alfa r   Prescribe alpha
   CLI  r   Prescribe inviscid CL
   Cl   r   Prescribe CL
   ASeq rrr Prescribe a sequence of alphas
   CSeq rrr Prescribe a sequence of CLs
```

The "A" command is the short alternative form of "ALFA", and "C" is the short alternative of "CL". Likewise, "AS" and "CS" are the short forms of "ASEQ" and "CSEQ". The CLI command

has no short form (as indicated by all capitals in the menu),
and must be fully typed.

Hopefully, most of the commands are self-explanatory. For inviscid cases, the CLI and CL commands are identical. For viscous cases, CLI is equivalent to specifying alpha, this being determined a priori from the specified lift coefficient via an inviscid solution. CL will return a viscous solution with the specified true viscous lift coefficient at an alpha which is determined as part of the solution (prescribing a CL above CLmax will cause serious problems, however!). The user is always prompted for any required input. When in doubt, typing a " ? " will always produce a menu.

After an ALFA, CL, or CLI command is executed, the Cp vs x distribution is displayed, and can be displayed again at any time with CPX. If the viscous mode is active, the true viscous Cp is shown as a solid line, and the inviscid Cp at that same alpha is shown as a dashed line. Each dash covers one panel, so the local dashed line density is also a useful visual indicator of panel resolution quality. If the inviscid mode is active, only the inviscid Cp is shown as a solid line.

The difference between the true viscous Cp distribution (solid line) and the inviscid Cp distribution (dashed line) is due to the modification of the effective airfoil shape by the boundary layers. This effective airfoil shape is shown superimposed on the actual current airfoil shape under the Cp vs x plot. The gap between these effective and actual shapes is equal to the local displacement thickness delta*, which can also be plotted in the VPAR menu. This is only about 1/3 to 1/2 as large as the overall boundary layer thickness, which can be visualized via the BL or BLC commands which diplay velocity profiles through the boundary layer. BL displays a number of profiles equally spaced around the airfoil's perimeter, while BLC displays profiles at cursor-selected locations. The zooming commands Z, U, may be necessary to better see these small profiles in most cases.

If the Cp reference data overlay option is enabled with CREF, initiating a Cp vs x plot will first result in the user being prompted for a formatted data file with the following format:

```
x(1)  Cp(1)
x(2)  Cp(2)
 .      .
 .      .
```

The Cp vs x plot is then displayed as usual but with the data overlaid. If FREF has been issued previously, then numerical reference values for CL, CD, etc. will be requested and added to the plot next to the computed values.

Boundary-layer quantities are plotted from the VPLO menu:

```
   H      Plot kinematic shape parameter
   DT     Plot top    side Dstar and Theta
   DB     Plot bottom side Dstar and Theta
   UE     Plot edge velocity
```

```
   CF     Plot skin friction coefficient
   CD     Plot dissipation coefficient
   N      Plot amplification ratio
   CT     Plot max shear coefficient
   RT     Plot Re_theta
   RTL    Plot log(Re_theta)

   X  rrr Change x-axis limits
   Y  rrr Change y-axis limits on current plot

   Blow   Cursor blowup of current plot
   Rese   Reset to default x,y-axis limits
   SIZE r Change absolute plot-object size
  .ANNO   Annotate plot
   HARD   Hardcopy current plot

   GRID   Toggle grid plotting
   SYMB   Toggle node-symbol plotting
   LABE   Toggle label plotting
   CLIP   Toggle line-plot clipping
```

This menu is largely self-explanatory. The skin friction coefficient plotted with the CF command is defined as

$$Cf = \tau / 0.5 \rho Q_{inf}^2$$

This differs from the standard boundary layer theory definition which uses the local Ue rather than Qinf for the normalization. Using the constant freestream reference makes Cf(x) have the same shape as the physical shear stress tau(x).

The dissipation coefficient CD' (this is NOT the drag coefficient!!!) is plotted with the CD command. CD'(x) is proportional to the local energy dissipation rate due to viscous shear and turbulent mixing. Hence, it indicates where on the airfoil drag is being created. It is in fact a much better indicator of drag production than Cf(x), since Cf does not account for pressure drag. CD', on the other hand, accounts for everything. Its relationship to the total profile drag coefficient is simply

$$CD = \int 2\, CD'\, ds$$

with the integration performed over both boundary layers and also the wake. It will be seen that if the flow is separated at the trailing edge, much of the drag contribution (energy dissipation) of CD' occurs in the wake.

As mentioned earlier, all forces are normalized with freestream dynamic pressure only. CL, CD, CM are the usual chord-based definitions only if the airfoil has a unit chord -- in general, they will scale with the airfoil's chord. Also, CM is defined about the cartesian point (xref,yref) = (0.25,0.0), which is not

necessarily the airfoil's 1/4 chord point.

-- Force calculation --

The lift and moment coefficients CL, CM, are calculated by direct surface pressure integration:

$$CL = L/q = \int Cp \, d\bar{x} \qquad CM = M/q = \int -Cp \, [(x-xref)\, dx + (y-yref)\, dy]$$

where $\bar{x} = x \cos(a) + y \sin(a)$; a = angle of attack

$\bar{y} = y \cos(a) - x \sin(a)$

The integrals performed in the counterclockwise direction around the airfoil contour. The pressure coefficient Cp is calculated using the Karman-Tsien compressibility correction.

The drag coefficient CD is obtained by applying the Squire-Young formula at the last point in the wake --- NOT at the trailing edge.

$$CD = D/q = 2\,Theta_i = 2\,Theta\,(u/V)^{(H+5)/2}$$

where Theta = momentum thickness, u = edge velocity, H = shape parameter (at end of wake)

V = freestream velocity

Theta_i = momentum thickness at "downstream infinity"

The Squire-Young formula in effect extrapolates the momentum thickness to downstream infinity. It assumes that the wake behaves in a asymptotic manner downstream of the point of application. This assumption is strongly violated in the near-wake behind an airfoil with trailing edge separation, but is always reasonable some distance behind the airfoil. Hence, the usual application of Squire-Young at the trailing edge is questionable with separation present, but its application at the last wake point (typically 1 chord downstream) is always reasonable. Also, application at the last wake point also results in the formula having a smaller effect in any case, since there u ~ V, and hence Theta_i ~ Theta.

In most 2-D airfoil experiments, drag is measured indirectly by measuring 2 Theta/c in the wake, often within one chord of the airfoil's trailing edge. For consistency, this should be compared to the Theta value predicted by XFOIL at the same wake location, rather than the "true" Cd = 2 Theta_i/c value which is effectively at downstream infinity. In general, Theta_i will be smaller than Theta. In most airfoil drag measurement experiments, this difference may amount to the drag measurement being several percent too large, unless some correction is performed.

In addition to calculating the total viscous CD from the wake momentum thickness, XFOIL also determines the friction and pressure drag components CDf,CDp of this total CD. These are calculated by

$$CDf = \int Cf \, d\bar{x} \qquad CDp = CD - CDf$$

Here, Cf is the skin friction coefficient defined with the freestream dynamic pressure, not the BL edge dynamic pressure commonly used in BL theory. Note that CDp is deduced from CD and CDf instead of being calculated via surface pressure integration. This conventional definition

$$CDp = \int Cp \, d\bar{y}$$

is NOT used, since it is typically swamped by numerical noise.

-- Transition criterion --

Transition in an XFOIL solution is triggered by one of two ways:

free transition: e^n criterion is met
forced transition: a trip or the trailing edge is encountered

The e^n method is always active, and free transition can occur upstream of the trip. The e^n method has the user-specified parameter "Ncrit", which is the log of the amplification factor of the most-amplified frequency which triggers transition. A suitable value of this parameter depends on the ambient disturbance level in which the airfoil operates, and mimics the effect of such disturbances on transition. Below are typical values of Ncrit for various situations.

situation	Ncrit	
sailplane	12-14	
motorglider	11-13	
clean wind tunnel	10-12	
average wind tunnel	9	<= standard "e^9 method"
dirty wind tunnel	4-8	

Note: The e^n method in XFOIL is actually the simplified envelope version, which is the same as the full e^n method only for flows with constant H(x). If H is not constant, the two methods differ somewhat, but this difference is typically within the uncertainty in choosing Ncrit.

The e^n method is only appropriate for predicting transition in situations where the growth of 2-D Tollmien-Schlichting waves via linear instability is the dominant transition-initiating mechanism. Fortunately, this happens to be the case in a vast majority of airfoil applications. Other possible mechanisms are:

* Crossflow instabilities. These occur on swept wings with significant favorable chordwise pressure gradients.

* Attachment-line transition. This requires large sweep, large LE radius, and a large Reynolds number. Occurs primarily on big jets.

* Bypass transition. This occurs in cases with sufficient wall roughness and/or large freestream turbulence or vibration levels. The linear-instability phase predicted by the e^n method is "bypassed", giving relatively early transition. Usually occurs in favorable pressure gradients, while the linear-instability mechanism usually dominates in adverse pressure gradients.

If any of these alternative transition mechanisms are present, the trips must be set to mimick their effect. The bypass transition mechanism can be mimicked to some extent by the e^n method by setting Ncrit to a small value --- Ncrit=1 or less. This will cause transition just after linear instability begins. For very large freestream turbulence or roughness in favorable pressure gradients, bypass transition can occur before the linear instability threshold, and in this case trips will have to be set as well.

Numerical accuracy

-- Panel density requirements --

If strong separation bubbles are present in a viscous solution, then it is very important to have good panel resolution in the region of the bubble(s). The large gradients at a bubble tend to cause significant numerical errors even if a large number of panels is used. If a separation bubble appears to be poorly resolved, it is a good idea to re-panel the airfoil with more points, and/or with points bunched around the bubble region. The paneling is controlled from the PPAR menu. A good rule of thumb is that the shape parameter Hk just after transition in the bubble should not decrease by more than 1.0 per point. Likewise, the surface velocity Ue/Vinf should not change by more than 0.05 per point past transition, otherwise there may be significant numerical errors in the drag. The point values can be observed by issuing SYMB from the VPLO menu.

Moderate chord Reynolds numbers (1-3 million, say) usually require the finest paneling, since the bubbles are still important, but very small. On many airfoils, especially those with small leading edge radii, the development of the small bubble which forms just behind the leading edge can have a significant effect on CLmax. For such cases, the default paneling density at the bubble may not be adequate. In all cases, inadequate bubble resolution results in a "ragged" or "scalloped" CL vs CD drag polar curve, so fortunately this is easy to spot.

-- Differencing order of accuracy --

The BL equations are normally discretized with two-point central differencing (i.e. the Trapezoidal Scheme), which is second-order

accurate, but only marginally stable. In particular, it has problems with the relatively stiff shape parameter and lag equations at transition, where at high Reynolds number the shape parameter must change very rapidly. Oscillations and overshoots in the shape parameter
will occur with the Trapezoidal Scheme if the grid cannot resolve this rapid change. To avoid this nasty behavior, upwinding must be introduced,
resulting in the Backward Euler Scheme, which is very stable, but has only first-order accuracy. Previous versions of XFOIL allowed a specific
constant amount of upwinding to be user-specified. Currently, XFOIL automatically introduces upwinding into the equations only in regions of rapid change (typically transition). This ensures that the overall scheme is stable and as accurate as possible.

Since only a minimal amount of upwinding is introduced in the interest of numerical accuracy, small oscillations in the shape parameter H will sometimes appear near the stagnation point if relatively coarse paneling is used there. These oscillations are primarily a cosmetic defect, and do not significantly affect the downstream development of the boundary layer. Eliminating them by increasing upwiding would in fact produce much greater errors in the overall viscous solution.

Viscous solution acceleration

The execution of a viscous case requires the solution of a large linear system every Newton iteration. The coefficient matrix of this system is 1/3 full, although most of its entries are very small. Substantial savings in CPU time (factor of 4 or more) result when these small entries are neglected. SUBROUTINE BLSOLV which solves the large Newton system ignores any off-diagonal element whose magnitude is smaller than the variable VACCEL, which is initialized in SUBROUTINE INIT, and which can be changed at runtime from the VPAR menu with the VACC command.

A nonzero VACCEL parameter should in principle degrade the convergence rate
of the viscous solution and thus result in more Newton iterations, although
the effect is usually too small to notice. For very low Reynolds number
cases (less than 100000), it MAY adversely affect the convergence rate or stability, and one should try reducing VACCEL or even setting it to zero if all other efforts at convergence are unsuccessful. The value of VACCEL has absolutely no effect on the final converged viscous solution (if attained).

Polar calculations and plotting

The polar calculation facility driven from the OPER menu deserves a detailed description. It has been considerably upgraded from previous XFOIL versions.

The simplest way to create a polar is to issue the PACC command which sets the auto polar accumulation toggle and asks for the optional save and dump filenames. If either filename is given, each computed operating point will be stored internally and also written to the specified file. If no filename is given, the automatic writing is not performed.

The polar's operating points can be computed individually with ALFA, or more conveniently en masse with ASEQ. One can also use CL or CSEQ, although these will not work close to CLmax.

The polar can be plotted anytime with PPLO. If previous polars have been
computed or read in with PGET, they can be plotted as well. If a polar is deemed incomplete, additional points can be computed as needed.

If automatic writing of a polar was not chosen (no filename was given for PACC), the polar can be written later all at once with the PWRT command. The only drawback to this approach is that if the program crashes during a polar calculation sweep for whatever reason, the computed polar and all other stored information will be lost.

If existing filenames are given to PACC, the subsequent computed points will be appended to these files, but only if the airfoil name and flow parameters in the file match the current parameters. This is to prevent clobbering of the polar file with "wrong" additional points. Messages are always produced informing the user of what's going on.

Off-line polar plotting

Polar save file(s) can also be plotted off-line with the separate program PPLOT. This is entirely menu driven, and is simply executed:

```
 % pplot
```

The file pplot.def contains plotting parameters, and is read automatically if available. If it's not available, then internal defaults are used.

Like the RGET,FREF commands in OPER, PPLOT permits reference data to be overlaid. A reference polar data file has the following form:

```
CD(1)  CL(1)
CD(2)  CL(2)
 .      .
 .      .
999.0  999.0
alpha(1)  CL(1)
alpha(2)  CL(2)
  .       .
  .       .
999.0   999.0
alpha(1)  Cm(1)
alpha(2)  Cm(2)
  .       .
  .       .
```

```
999.0   999.0
Xtr/c(1)  CL(1)
Xtr/c(2)  CL(2)
  .        .
  .        .
999.0   999.0
```

The number of points in each set (CD-CL, alpha-CL, etc.) is arbitrary, and can be zero.

The contents of a polar dump file can be selectively plotted with the separate menu-driven program PXPLOT. It is executed with:

```
 % pxplot <dump filename>
```

This allows surface plots of Cp vs x, H vs x, etc. for any or all of the saved operating points. Of course, these plots can be generated in XFOIL for any individual operating point, so PXPLOT and the dump file itself are somewhat redundant in this respect.

Re, Mach dependence

A few comments are in order on the TYPE command, which allows the user to set the dependence of the Mach and Reynolds numbers on CL. Any CL-CD polar can be of the following three types:

Type	parameters held constant		varying	fixed
1	M	, Re	lift	chord, vel.
2	M sqrt(CL)	, Re sqrt(CL)	vel.	chord, lift
3	M	, Re CL	chord	lift , vel.

* Type 1 corresponds to a given wing at a fixed velocity going over an angle of attack range, as in a wind tunnel test alpha sweep or a sudden aircraft pullup. This is also the common form for an airfoil polar.

* Type 2 corresponds to an aircraft in level flight at a given altitude undergoing trim speed changes. This is the most useful airfoil polar form for determining a drag polar for an aircraft at 1-g. For this case,
The "Mach number" input with the MACH command is actually interpreted as the product M sqrt(CL), and the "Reynolds number" input with the VISC or RE commands is actually interpreted as RE sqrt(CL). For a wing
in level flight, these products can be computed from the following exact
relations, with Re based on the mean chord:

$$M\sqrt{CL} = \left| \frac{2}{1.4} \frac{W/S}{p} \right|^{1/2} \qquad RE\sqrt{CL} = \left| \frac{1}{mu} \frac{2\,\rho\, W}{AR} \right|^{1/2}$$

W = weight p = ambient pressure

```
 S  = wing area      mu  = dynamic viscosity
 AR = aspect ratio   rho = ambient air density
```

* Type 3 corresponds to a wing of "rubber chord" with a given lift at a given speed. This is best used for selecting an optimum CL for an airfoil while taking Reynolds number changes into account. The product RE CL can be computed from the following:

$$RE\ CL = \frac{2\ W}{mu\ V\ b} \qquad b = span = \sqrt{S*AR}$$

Caution must be used with Types 2 and 3 so as to not allow the CL to go negative. In addition, with non-zero Mach and Type 2, the CL must not fall below that value which makes Mach exceed unity. Warning messages are printed when these problems occur.

Output

All output goes directly to the terminal screen. H. Youngren's plot package Xplot11 (libPlt.a) used by XFOIL drives monochrome and color X-Windows graphics, and generates B&W or color PostScript files for hardcopy. The default setup assumes color X-Windows graphics (if available), and B&W PostScript. These defaults are controlled by the IDEV and IDEVRP flags in SUBROUTINE INIT (in xfoil.f).

The Xplot11 library should work on all Unix systems. The Makefile in the ./plotlib/ directory requires some modifications for some machines.

The default X-graphics window is in Landscape mode, with a black (reverse-video) background. Normal-video can be selected by setting the Unix shell variable

```
 % setenv XPLOT11_BACKGROUND white
```

before Xfoil is started. The nicer reverse-video is restored with:

```
 % unsetenv XPLOT11_BACKGROUND
```

See the plotlib/Doc file for more info on the plot library.

Xplot11 provides a built-in Zoom/Unzoom capability which can be applied to whatever is on the screen. Zooming/Unzooming can be perfomed with the "Z" and "U" commands from nearly all the menus --- these commands are not listed to reduce clutter.

Some of the menus also have their own Blowup/Reset commands. The distinction is that XFOIL's plots don't try to adjust themselves to Zoom parameters, so a highly-"Zoomed" plot may show nothing at all. In contrast, Blowup/Reset instructs XFOIL to change its own plot scales, so a highly-"Blown-up" plot will at least show the axes.

Plot Hardcopy

For hardcopy, the current screen plot can be echoed to a PostScript file
plot.ps with the HARD command. The size of the plot objects on the screen and on hardcopy can be changed with the SIZE command from most menus. The number requested is the width of the plot in inches.

*** NOTE ***
If the plot.ps file is to be previewed with some X-Windows PostScript viewer, or imported into word-processing systems, XFOIL must be exited with QUIT in order for the plot.ps file to be properly terminated. For just printing, this may or may not be necessary.

*** NOTE ***
For the geometry plot in GDES, and the Qspec(s) plots in QDES and MDES (described below), the hardcopy plot size will also be affected if the graphics window is resized with the cursor at the window manager level. This is because the plot is always scaled so that it fills up as much of the window as possible. If the window size is left at its start-up size, the hardcopy plot widths will come out with the specified size in inches. If any window dimension is increased from its default value, then a subsequent hardcopy plot will probably not fit on a standard 8.5" x 11.0" sheet.

Full-Inverse Design Routine (MDES)

XFOIL's Full-Inverse complex-mapping facility (MDES) takes as input a speed distribution "Qspec" specified over the entire airfoil surface, modifies it somewhat to satisfy the Lighthill constraints, and generates
a new overall geometry. First a bit of the underlying theory...

The geometry and the surface velocities can both be computed from a set of complex mapping coefficients "Cn" in the form

$$x + iy = z(w;Cn)$$
$$u - iv = f(w;Cn,alpha)$$

where w= 0..2*pi is the independent parameter going around the airfoil. The z and f functions are rather complicated but this is not important here. The key to the full-inverse method is that the mapping coefficients
Cn can be computed from a known contour angle theta(w) = arctan(dy/dz) OR from a surface speed q(w) = |u-iv|. The other quantity then follows.
In summary, the operations and their commands are...

a) Direct problem: theta -> Cn -> u-iv, q (QSET)
b) Inverse problem: Qspec -> Cn -> x+iy, theta (EXEC)

Creation of seed surface speed distribution

MDES performs QSET and sets Qspec = q automatically upon entry if Qspec does not exist. This Qspec is then the starting point for subsequent design operations.

This default initialization in effect makes MDES a redesign method in which the surface speed distribution of an existing airfoil is used as a starting point to generate a new speed distribution. A ``pure'' design code which requests the entire surface speed distribution every time is often less natural to use, since airfoil design is invariably an iterative process involving repeated analyze/fix cycles. The MDES menu is shown below.

```
   <cr>   Return to Top Level
   !      Redo previous command

   INIT   Re-initialize mapping
   QSET   Reset Qspec <== Q
   AQ r.. Show/select alpha(s) for Qspec
   CQ r.. Show/select  CL(s)   for Qspec

   Symm   Toggle symmetry flag
   TGAP r Set new TE gap
   TANG r Set new TE angle

   Modi   Modify Qspec
   MARK   Mark off target segment for smoothing
   SMOO   Smooth Qspec inside target segment
   FILT   Apply Hanning filter to entire Qspec
   SLOP   Toggle modified-Qspec slope matching flag

   eXec   Execute  full-inverse calculation

   Plot   Replot Qspec (line) and Q (symbols)
   VISC   Qvis overlay toggle
   REFL   Reflected Qspec overlay toggle
   SPEC   Plot mapping coefficient spectrum

   Blow   Blowup plot region
   Rese   Reset plot scale and origin
   Wind   Plot window adjust via cursor and keys

   SIZE r Change absolute plot-object size
  .ANNO   Annotate plot
   HARD   Hardcopy current plot

   PERT   Perturb one Cn and generate geometry
```

As described above, the initial Qspec distribution is taken from "Q", the speed distribution corresponding to the current geometry at the last angle of attack employed in OPER. Qspec can be set back to this Q with QSET anytime.

Modification of surface speed distributions

-- Cursor input of modifications --
Qspec can be modified to whatever is desired with the MODI command by specifying points with the screen cursor which are then splined. The points can be entered in any order. The last point can be erased by clicking on the "Erase" button or simply typing "e" in the graphics window. The input sequence is terminated by clicking on the "Done" button or by typing "d" in the graphics window. The "Abort" button or typing "a" aborts the MODI command and returns to the MDES menu. The BLOW command can be used to enlarge regions of interest at any time by specifying opposite corners of the blowup region.

-- Modification endpoint blending --
Normally, the modified piece of Qspec(s) is blended into the current Qspec(s) with matching values and slopes at the piece endpoints. The slope matching can be turned on/off with the SLOP toggle command. If slope matching is turned off, the modified piece will match only the existing value, but a slope discontinuity will be allowed.

-- Smoothing --
Qspec can be smoothed with the SMOO command, which normally operates on the entire distribution, but can be confined to a target segment whose endpoints are selected with the MARK command. The smoothing acts to alleviate second derivatives in Qspec(s), so that with many consecutive SMOO commands Qspec(s) will approach a straight line over the target segment. If the slope-matching flag is set, the endpoint slopes are preserved.

The FILT command is an alternative smoothing procedure which acts on the Fourier coefficients of Qspec directly, and is global in its effect.
It is useful for "cleaning up" the entire Qspec(s) distribution if noise is present from some geometric glitch on the airfoil surface. Also, unintended noise might be introduced into Qspec from a poor modification via the cursor.

FILT acts by multiplying the Fourier coefficients by a Hanning window filter function raised to the power of a filter parameter "F". This tapers off the high frequencies of Qspec to varying degrees. A value of F = 0.0 gives no filtering, F = 1.0 gives the standard Hanning filter,
F = 2.0 applies the Hanning filter twice, etc. The standard Hanning filter appears to be a bit too drastic, so a filter parameter of F = 0.2 is currently used. Hence, issuing FILT five times corresponds to the standard Hanning filter. The SPEC command displays the mapping coefficient spectrum at any time.

-- Symmetry forcing --
The symmetry-forcing option (SYMM toggle) is useful when a symmetric airfoil is being designed. If active, this option zeroes out all antisymmetric (camber) Qspec changes, and doubles all symmetric (thickness) changes. This unfortunately has the annoying side effect of also doubling the numerical roundoff noise in Qspec every time a MODI operation is performed. This noise sooner or later becomes visible as high-frequency wiggles which double with each MODI command. Issuing FILT occasionally keeps this parasitic

noise growth under control.

-- Adjustment for Lighthill constraints --
The MODI, BLOW, MARK, SMOO, SLOP, FILT commands can be issued repeatedly
in any order until Qspec is modified to have the desired distribution.
In general, the surface speed distributions actually plotted will not
exactly match what was input with the cursor, since corrections are
automatically added to maintain the specified trailing edge gap and
to enforce consistency with the freestream speed. These are known
as the Lighthill constraints on the surface speed.

The trailing edge gap is initialized from the initial airfoil and can
be changed with TGAP. To reduce the "corrupting" effect of the
constraint-driven corrections, a good rule of thumb is that the
Qspec distribution should be modified so as to preserve the total CL.
The CL is simply twice the area under the Qspec(s) curve (= 2 x circulation),
so that this area should be preserved.

-- Multipoint surface speed display --
A very useful feature of the MDES facility is the ability to display
and modify a number of Qspec distributions corresponding to different
alpha or inviscid CL values. These values are displayed and/or selected
via the AQ or CQ commands. When any one Qspec distribution is modified,
the result of modification is also displayed on all the other distributions.
This allows rapid design at multiple operating points. When the Qspec
curves correspond to specified CL values, the alpha for each curve will be
adjusted after each Qspec modification so as to preserve that curve's CL.
The resulting Qspec will therefore not match the input cursor points
exactly because of this alpha correction.

Generation of new geometry

The EXEC command generates a new buffer airfoil corresponding
to the current Qspec distribution. If subsequent operations on
this airfoil are to be performed (SAVE, OPER, etc.), it is
necessary to first generate a current airfoil from this buffer
airfoil using PANE at the top level menu. This seemingly
complicated sequence is necessary because the airfoil points
generated by EXEC are uniformly spaced in the circle plane,
which gives a rather poor point (panel node) spacing distribution
on the physical airfoil. This sequence also prevents the current
airfoil from being overwritten immediately when EXEC is issued.
Once the new current airfoil is generated with PANE, it can
then be analyzed in OPER, modified in GDES, or whatever.

The PERT command allows manual input of the complex mapping
coefficients Cn which determine the geometry. These coefficients
are normally determined from Qspec(s) (this is the essence of
the inverse method). The PERT command is provided simply
as a means of allowing generation of geometric perturbation

modes, possibly for external optimization or whatever.

The manually-changed Cn values result in changes in geometry
as well as the current Qspec(s) distributions. The QSET command
will restore everything to its unperturbed state.

The Full-Inverse facility is very fast, after an initialization
calculation of several seconds (on a RISC workstation), it requires
only a fraction of a second to generate the new buffer airfoil.

Mixed-Inverse Design Routine (QDES)

XFOIL's Mixed-Inverse facility (QDES) is useful in certain redesign
problems where parts of the airfoil cannot be altered under any
circumstances. The Mixed-Inverse menu is shown below.

```
   <cr>   Return to Top Level

   QSET   Reset Qspec <== Q

   Modi   Modify Qspec
   MARK   Mark off target segment
   SMOO   Smooth Qspec inside target segment
   SLOP   Toggle modified-Qspec slope matching flag

   eXec i Execute mixed-inverse calculation
   REST   Restore geometry from buffer airfoil
   CPXX   CPxx endpoint constraint toggle

   Plot   Plot Qspec (line) and Q (symbols)
   VISC   Qvis overlay toggle
   REFL   Reflected Qspec overlay toggle

   Blow   Blowup plot region
   Rese   Reset plot scale and origin
   Wind   Plot window adjust via cursor and keys

   SIZE r Change absolute plot-object size
  .ANNO   Annotate plot
   HARD   Hardcopy current plot
```

The QDES menu above is intentionally geared for the redesign of a segment
of an existing airfoil (with its surface speed distribution calculated
previously in OPER) rather than the generation of a totally new airfoil.

Creation of seed surface speed distribution

When QDES is entered, the specified speed distribution Qspec is
initialized to the current speed distribution Q last set in OPER.
If a direct solution for the current airfoil hasn't been calculated
yet,
QDES goes ahead and calculates it, using the last-set angle of attack.

If this isn't the desired angle, it can be set in OPER using ALFA. QSET can then be used to set Qspec from the current Q distribution. The QSET command can be used anytime later to "reset" Qspec if the modification has been botched.

Modification of surface speed distribution

Qspec can be repeatedly modified with the screen cursor and the MODI command, exactly as in MDES. It is also necessary to mark off the target segment where the geometry is to be modified with the MARK command.

Generation of new airfoil geometry

EXEC modifies the airfoil over the target segment to match Qspec there as closely as possible. The remainder of the airfoil geometry is left unaltered. EXEC requests the number of Newton iterations to be performed in the inverse calculation. Although as many as six iterations may be required for convergence to machine zero, it is _not_ necessary to fully converge a Mixed-Inverse case. Two iterations are usually sufficient to get very close to the new geometry. In any case, the new surface speed distribution Q which actually results from the inverse calculation will typically differ somewhat from the specified distribution Qspec by function modes which are added to Qspec. At least two modes are added, with their magnitudes determined by geometric closure requirements at the inverse segment endpoints. As with the MDES complex-mapping routine, the necessary modifications to Qspec will be smallest if Qspec is modified so that CL (the area under the Qspec(s) curve) is roughly preserved.

Issuing PLOT after the EXEC command finishes will compare the specified (Qspec) and resulting (Q) speed distributions. If extra smoothness in the surface speed is required, the CPXX command just before EXEC will enable the addition of two additional modes which allow the second derivative in the pressure at the endpoints to be unchanged from the starting airfoil. The disadvantage of this option is that the resulting surface speed Q will now deviate more from the specified speed Qspec. It is allowable to repeatedly modify Qspec, set or reset the CPXX option, and issue the EXEC command in any order.

The Mixed-Inverse modification is performed on the current airfoil directly, in contrast to Full-Inverse which generates the buffer airfoil as its output. In fact, it is important _not_ to issue the PANE or PCOP commands at top level after doing work in the QDES menu, as the new current airfoil will be overwritten with the old buffer airfoil.

Geometry Design Routine

Executing the GDES command from the top level menu will put the user into the GDES routine. It has a rather extensive menu:

<cr>	Return to Top Level
!	Redo previous command

```
 GSET     Set buffer  airfoil <== current airfoil
 eXec     Set current airfoil <== buffer  airfoil
 SYMM     Toggle y-symmetry flag

 ADEG r   Rotate about origin (degrees)
 ARAD r   Rotate about origin (radians)
 Tran rr  Translate
 Scal r   Scale about origin
 LINS rr. Linearly-varying y scale
 DERO     Derotate (set chord line level)

 TGAP rr  Change trailing edge gap
 LERA rr  Change leading edge radius

 TCPL     Toggle thickness and camber plotting
 TFAC rr  Scale existing thickness and camber
 TSET rr  Set new thickness and camber
 HIGH rr  Move camber and thickness highpoints
.CAMB     Modify camber shape directly or via loading

 BEND     Display structural properties of buffer airfoil

 Flap rrr Deflect trailing edge flap

 Modi     Modify contour via cursor
 SLOP     Toggle modified-contour slope matching flag

 CORN     Double point with cursor (set sharp corner)
 ADDP     Add    point with cursor
 DELP     Delete point with cursor
 MOVP     Move   point with cursor

 UNIT     Normalize buffer airfoil to unit chord
 Dist     Determine distance between 2 cursor points
 CLIS     List curvatures
 CPLO     Plot curvatures
 CANG     List panel corner angles
 CADD ri. Add points at corners exceeding angle threshold

 Plot     Replot buffer airfoil
 INPL     Replot buffer airfoil without scaling (in inches)
 Blow     Blowup plot region
 Rese     Reset plot scale and origin
 Wind     Plot window adjust via cursor and keys

 TSIZ     Change tick-mark size
 TICK r   Toggle node tick-mark plotting
 GRID     Toggle grid plotting
 GPAR     Toggle geometric parameter plotting
 Over f   Overlay disk file airfoil

 SIZE r   Change absolute plot-object size
.ANNO     Annotate plot
 HARD     Hardcopy current plot

 NAME s   Specify new airfoil name
 NINC     Increment name version number
```

Creating seed buffer airfoil

The first command typically executed is GSET, which sets the temporary buffer airfoil from the current airfoil. Sometimes it might be desired to operate directly on the coordinates of an already existing buffer airfoil. It typically contains coordinates read in from a disk file by LOAD at Top Level, or coordinates generated by EXEC from the MDES menu, depending on what was done last. In either of these cases, GSET is skipped.

Point addition (typ. to Eppler and Selig airfoils)

If the buffer airfoil has an excessively coarse point spacing, additional points can be added with the CADD command. Using the PANE command at top level also does this, but CADD allows the point addition to be restricted to locations with excessive corner angles (displayed with CANG), and also to locations which fall within a specified x-range. Different spline parameters can also be used to determine the inserted spline points. For example, the command

```
 .GDES  c>  CADD 10.0  2  -0.1 0.2
```

will add spline points adjacent to each existing point whose panel angle exceeds +/-10 degrees, and only if the added point will fall within the interval -0.1 < x < 0.2. The "2" indicates that an arclength spline parameter is to be used. The PANE command will always use the arclength spline.

Some archived airfoils, notably the Eppler airfoils and some of the Selig airfoils have an excessively coarse point spacing around the leading edge. The spacing has apparently been tailored for a uniform-parameter spline, and often produces a badly shaped leading edge with the arclength-parameter spline used in Xfoil. The following command will insert additional points giving a much smoother shape for subsequent analysis.

```
 .GDES  c>  CADD 10.0  1  -0.1 1.1
```

The 10.0 degree angle tolerance can be varied as needed (1/2 of the max angle is the default). The "1" argument (also a default) specifies a uniform-parameter spline for the interpolation since this works best for Eppler airfoils), and the default x range indicates that the entire airfoil is to be treated. The CADD command can be repeated to keep reducing the max panel angle, but this may or may not improve the smoothness of the resulting splined airfoil.

Modifying buffer airfoil

Once the buffer airfoil is suitably initialized, most of the GDES commands can then be used to modify it. The resulting new shape will usually be replotted immediately in a highlighted color. The plot can be refreshed anytime with the PLOT command.

Sometimes a sequence of commands is necessary to achieve the desired effect. For instance, suppose an airfoil with the current thickness envelope is to be given an entirely new camber line. Issuing TSET and hitting a <cr> (keep same thickness) and a new camber of 0 will result in the current thickness envelope unchanged and the current camber eliminated, so that a symmetrical airfoil remains. The new camber line can then be added in the CAMB sub-menu:

```
   <cr>    Return to GDES
   TFAC rr Scale existing thickness and camber
   TSET rr Set new thickness and camber
   HIGH rr Move camber and thickness highpoints
   WRTC    Write airfoil camber x/c,y/c to file

   RDAC    Read   added camber  x/c,y/c from file
   SETC    Set    added camber  x/c,y/c from camberline
   INPC    Input  added camber  x/c,y/c from keyboard
   MODC    Modify added camber  x/c,y/c with cursor
   INPP    Input  added loading x/c,DCp from keyboard
   MODP    Modify added loading x/c,DCp with cursor
   SLOP    Toggle modified-camber,dCp slope matching flag
   SCAL r  Scale the added camber
   CLR     Clear the added camber
   ADD     Add added camber to the existing camberline

   DCPL    Toggle DCp plot
   CPLI rr Change DCp axis plot limits

   Blow    Blowup plot region
   Rese    Reset plot scale and origin

   SIZE r   Change absolute plot-object size
  .ANNO     Annotate plot
   HARD     Hardcopy current plot

..CAMB   c>
```

INPC takes the new camber line as a sequence of x/c,y/c coordinate pairs which are splined. INPP takes a sequence of x/c,delta(Cp) pairs instead. This delta(Cp) (i.e. loading) distribution, defined as

delta(Cp) = (Cp)lower - (Cp)upper

is then used in Glauert's thin-airfoil relations to define the x/c,y/c camber line.

With INPC and INPP, a slope discontinuity in y(x) or Cp(x) can be specified with two identical consecutive x/c values, which prevents splining across this point. INPP can thus easily generate a camber line with a piecewise-linear delta(Cp) loading distribution, as for example an a=0.8 NACA 6-digit airfoil:

```
 x/c delta(Cp)
 0.0   0.5
 0.8   0.5
 0.8   0.5
 1.0   0.0
```

This results in a constant delta(Cp) = 0.5 for 0.0 < x/c < 0.8 ,
then decreasing linearly to delta(Cp) = 0.0 for 0.8 < x/c < 1.0

Once a suitable added camber is input, it is added to the
existing buffer airfoil camber via the ADD command.

The various GDES commands for modifying camber-line, thickness, leading edge radius, etc. should suffice for most geometry modification tasks. If truly frustrated, the user can "draw" the new contour with the MODI command, which accepts cursor inputs in the same manner as the MDES and QDES procedures. Slope matching at the modified-piece endpoints can likewise be enabled/disabled with the SLOP toggle command. The only important difference is that here the points must be entered in consecutive order along the new contour, although one can "erase" a previously-entered point by clicking on "Erase" or type "e" in the graphics window.

A point can be doubled with the CORN command. A doubled point is useful wherever a sharp corner is required, such as at a flap break. Normally, the spline routine enforces slope continuity at all points, effectively preventing sharp corners. A doubled point, marked by a small diamond symbol on the plot, causes separate splines to be generated on each side of the corner, thus allowing the slope break. The doubled point is eliminated by clicking on it after issuing the DELP command. Using DELP on a normal single point will delete that point entirely.

The TGAP command sets the thickness (or gap) of the blunt trailing edge.
The gap "ds" is defined as the distance between the upper and lower coordinate endpoints: ds^2 = dx^2 + dy^2. If the gap is already non-zero,
then the new TE base vector (dx,dy) will have the same orientation as the old one, i.e.

$$\left.\begin{matrix} dy \\ -- \\ dx \end{matrix}\right|_{new} = \left.\begin{matrix} dy \\ -- \\ dx \end{matrix}\right|_{old}$$

If the gap is zero to begin with, then the new base vector will be perpendicular to the trailing edge bisector. If the base orientation comes out in an unexpected way, it probably means that the gap was not *exactly* zero. The fix is to first set the gap to zero, and then set it again to the desired value.

After a new gap size is input, a "blending distance/c" will also be requested. This controls how rapidly the new TE blends into the original airfoil, and is essentially the length scale for the blending function, which is exponential in x/c. The limiting values are:

distance/c = 0: Only the upper- and lower-surface TE points are changed
= 1: A linear "wedge" is added or subtracted from the air-foil

Saving buffer airfoil into current airfoil

Once the desired buffer airfoil is created, a new current airfoil is set
directly from the buffer airfoil with the EXEC command (equivalent to PCOP at top level). Alternatively, the new current airfoil can be re-paneled from the buffer airfoil with the PANE command at top level. The new current airfoil can then be analyzed in OPER. If the buffer airfoil has any doubled corner points, the doubled points will be eliminated, but a current-airfoil node will fall exactly on each buffer-airfoil corner.

Start-up Defaults
==========

XFOIL has hardwired parameters (in subr. INIT) controlling the paneling, plotting, and viscous execution. Most of these can be changed at runtime in the various menus. To avoid the need to change the parameters everytime XFOIL is executed, they can be saved to the default file xfoil.def with the WDEF command at TOP LEVEL. This file has the format:

```
   140       1.0000   0.1500   0.2000 | Npan    PPanel  TErat  REFrat
    1.0000   1.0000   1.0000   1.0000 | XrefS1  XrefS2  XrefP1 XrefP2
   10.0000   0.5500   0.0150   0.8500 | Size    plotAR  CHsize ScrnFr
   11.0000   8.5000   0.0000   0.0000 | Xpage   Ypage   Xmargn Ymargn
  F        T                          | Lcolor  Lcursor
    1.0000  -2.0000  -0.5000          | CPmax   CPmin   CPdel
    0.0900   0.7000                   | XoffAir ScalAir BLUwt
    0.0000   1.5000   0.5000          | CLmin   CLmax   CLdel
    0.0000   0.0200   0.0100          | CDmin   CDmax   CDdel
   -4.0000  10.0000   2.0000          | ALmin   ALmax   ALdel
    0.0000   0.3000   0.1000          | CMmin   CMmax   CMdel
   1         0.0000   0.0100          | MAtype  Mach    Vaccel
   1         0.0000   9.0000          | REtype  Re/10^6 Ncrit
    1.0000   1.0000                   | XtripT  XtripB
```

Line 1: Paneling parameters from the PPAR menu
Line 2: Paneling refinement locations
Line 3: Specifies the absolute plot size, the plot aspect ratio, and scales the character, number, and symbol heights
Line 4: Defines page size and page margins, in inches
Line 5: Flags for color PostScript output, cursor screen input
Line 6: Defines the Cp axis annotations
Line 7: x-offset and scale for airfoil on Cp vs x plot, BL u profile scale
Line 8: CL axis annotations on polar plot
Line 9: CD axis annotations on polar plot
Line 10: alpha axis annotations on polar plot
Line 11: CM axis annotations on polar plot
Line 12: Mach-CL dependence type, Mach number, solution acceleration parameter
Line 13: Re-CL dependence type, Reynolds number, transition parameter
Line 14: Forced transition x/c locations on top,bottom sides

This file will be read at any time with the RDEF command, thus
avoiding the manual entry of all the information.

Caveats
=======
The XFOIL code is not foolproof, and requires some level of aerodynamic
expertise and common sense on the part of the user. Although the
inviscid analysis (OPERi), geometry design (GDES), and Full-Inverse
(MDES) routines are nearly invulnerable to failure, the Mixed-Inverse
(QDES) design routines and especially the viscous analysis (OPERv)
routines will fail if a "reasonable" problem is not specified.
Typical failure scenarios are:

 - Viscous Analysis (OPERv)
     * Massive separation from excessive airfoil thickness,
         flap deflection, or angle of attack
     * Inherently unsteady flow (von Karman vortex street, etc.)
     * Poor resolution of leading edge pressure spike
     * Poor resolution of small viscous features
         (e.g. separation bubbles)
     * Reynolds number too low

 - Mixed-Inverse Surface Speed Design (QDES)
     * Re-entrant airfoil shape (negative thickness)

A possible consequence of these occurences is an arithmetic fault
causing program failure. This is unlikely, but it does happen
occasionally. It is therefore a good idea to save any previous work
before an ambitious calculation is attempted.

The following situations may give problems strictly due to numerical
roundoff:

 - Excessively small panel(s) somewhere on the airfoil

 - Airfoil located too far from origin

 - Airfoil too thin

These situations will rarely result in an arithmatic failure,
but will typically result in a "ragged" Cp distribution.
Examine the paneling in the GDES menu, making the GSET command
if neceesary to set the current paneling. Eliminate excessively
small panels my deleting one or more panel nodes with the
DELP command.

When performing viscous analysis calculations, it is always a good idea
to sequence runs so that alpha does not change too drastically from one
case to another. The Newton solution method always uses the last
available solution as a starting guess for a new solution, and works
best if the change from the old to the new solutions is reasonably
small. For this reason, it is best to perform difficult calculations

(such as past CLmax) by gradually increasing alpha. The ASEQ command in
OPER is convenient for this. If the user insists on a large change from
one point to another, it is best to force a re-initialization of the boundary layers with the INIT command from the VPAR menu in OPER before the radical calculation is performed. INIT should always be executed whenever the viscous solution blows up but the program doesn't crash.

The viscous analysis will execute no more Newton iterations than set by the current iteration limit each time an ALFA, CL, etc. command is issued. If convergence is not achieved within this limit, ALFA or CL
can be issued as often as needed (most easily with "!"), with another set of Newton iterations being performed each time. This iteration limit can be changed from its default value of 10 with the ITER command in OPER.

One should always be wary of trusting solutions which show regions of supersonic flow. Such flows can be reliably predicted only with a truly nonlinear field method (such as the MSES code). As a rule of thumb, if the maximum Mach number doesn't exceed 1.05 anywhere, shock losses will be very small, the Cp distributions will be reasonably accurate, and the drag predicted by XFOIL is likely to be accurate.

Appendix VIII: Aerodynamic performance before and after erosion

In this appendix the aerodynamic performance of the airfoils before and after erosion are presented. The aerodynamic performance results were obtained using Xfoil. The aerodynamic data presented in this appendix are for the uncoated blade, H-146 coated blade, and Polyurethane/IA-700 blades. Airfoil 1 and Airfoil 2 represent the Root section, Airfoil 3 and Airfoil 4 represent the Midspan, and Airfoil 5 and 6 represent the Tip section. For all the data represented here the following conditions are use:

XFOIL Version 6.99

Calculated polar for:

Reynolds number fixed Mach number fixed

xtrf = 1 (top) 1 (bottom)
Mach = 0 Re = 0.05 e 6 Ncrit = 9

- **Before Erosion**
    - Uncoated
        - -5°
            - Airfoil 1

Table AVIII-1: Aerodynamic performance of Airfoil 1 of the uncoated blade at -5°

alpha	CL	CD	CDp	CM	Top_Xtr	Bot_Xtr	CL/CD
------	--------	---------	---------	--------	--------	--------	--------
-5	-0.4209	0.04039	0.03229	-0.0381	1	0.1283	-10.4209
-4.5	-0.3834	0.03578	0.02654	-0.0358	1	0.1158	-10.7155
-4	-0.3446	0.03151	0.0217	-0.0334	1	0.1112	-10.9362
-3.5	-0.3028	0.02843	0.01812	-0.0307	1	0.1096	-10.6507
-3	-0.2615	0.0263	0.01574	-0.0275	1	0.1124	-9.94297
-2.5	-0.2229	0.02478	0.01404	-0.0241	1	0.1202	-8.99516
-2	-0.1836	0.02294	0.01228	-0.0223	1	0.1598	-8.00349
-1.5	-0.1997	0.02058	0.01332	-0.0035	1	0.8425	-9.7036
-1	-0.1179	0.02057	0.01274	-0.0083	1	1	-5.73165

-0.5	-0.0857	0.02095	0.01261	-0.0088	1	1	-4.09069
0	-0.0454	0.02177	0.01293	-0.0101	1	1	-2.08544
0.5	0.001	0.02296	0.01373	-0.0123	0.9974	1	0.043554
1	0.0802	0.02508	0.01553	-0.0201	0.9785	1	3.197767
1.5	0.1627	0.02728	0.01753	-0.0281	0.9559	1	5.964076
2	0.2401	0.02937	0.01954	-0.0348	0.9328	1	8.175009
2.5	0.3089	0.03134	0.02154	-0.0397	0.9097	1	9.856414
3.5	0.6254	0.02101	0.01203	-0.0465	0.6631	1	29.76678
4	0.6322	0.02271	0.01093	-0.0326	0.2467	1	27.83796
4.5	0.6736	0.02566	0.01335	-0.0303	0.2077	1	26.25097
5	0.7315	0.02824	0.01567	-0.0301	0.1846	1	25.90297
5.5	0.7885	0.03067	0.01811	-0.0299	0.1666	1	25.70916
6	0.8494	0.03452	0.02218	-0.0304	0.1598	1	24.60603
6.5	0.8997	0.03839	0.02663	-0.0294	0.156	1	23.43579
7	0.9426	0.04319	0.03209	-0.028	0.1551	1	21.8245
7.5	0.9762	0.04904	0.03862	-0.0262	0.157	1	19.9062
8	1.0024	0.05628	0.04641	-0.0246	0.1604	1	17.81095
8.5	0.9907	0.06406	0.05536	-0.0213	0.1695	1	15.46519
9	0.9541	0.07564	0.06746	-0.0202	0.181	1	12.6137
11	0.7216	0.14369	0.13552	-0.0637	0.3322	1	5.021922
11.5	0.7301	0.15075	0.14258	-0.0654	0.3181	1	4.843118
12	0.7687	0.15974	0.15166	-0.0658	0.3041	1	4.812195
12.5	0.7552	0.16392	0.15578	-0.0687	0.2882	1	4.607125
13	0.8177	0.17833	0.1704	-0.0682	0.2791	1	4.585319
13.5	0.7821	0.17748	0.16942	-0.0728	0.2638	1	4.406694
14	0.8436	0.19362	0.1859	-0.0722	0.2555	1	4.356988
14.5	0.8072	0.19093	0.18306	-0.0779	0.2434	1	4.227727
15	0.8429	0.20165	0.19396	-0.0784	0.2339	1	4.180015

- Airfoil 2

Table AVIII-2: Aerodynamic performance of Airfoil 2 of the uncoated blade at -5°

alpha	CL	CD	CDp	CM	Top_Xtr	Bot_Xtr	CL/CD
------	--------	----------	----------	--------	--------	--------	--------
-5	-0.3895	0.02587	0.01559	-0.0353	1	0.1704	-15.056
-3	-0.3274	0.02123	0.01363	0.0036	1	0.816	-15.4216
-2	-0.0845	0.0218	0.01295	-0.0174	1	1	-3.87615
-1.5	-0.114	0.02102	0.01214	-0.0095	1	1	-5.42341
-1	-0.1124	0.02057	0.01146	-0.0062	1	1	-5.46427
-0.5	-0.0753	0.02104	0.01159	-0.0079	1	1	-3.5789
0	-0.0231	0.02212	0.01237	-0.0117	0.9956	1	-1.0443
0.5	0.0592	0.02411	0.01408	-0.0205	0.9774	1	2.455413
1	0.1376	0.02604	0.01587	-0.0281	0.9563	1	5.284178

1.5	0.2115	0.02798	0.01778	-0.0345	0.9347	1	7.558971
2	0.2813	0.0299	0.01974	-0.0398	0.912	1	9.408027
2.5	0.345	0.03181	0.02175	-0.0438	0.8876	1	10.84565
3	0.4041	0.03373	0.02391	-0.0467	0.8603	1	11.98043
3.5	0.4627	0.03582	0.02627	-0.0493	0.8326	1	12.91736
4	0.6659	0.02894	0.02048	-0.0553	0.7221	1	23.00968
4.5	0.7352	0.02177	0.01357	-0.0412	0.5747	1	33.77124
5	0.7317	0.0257	0.01445	-0.0292	0.185	1	28.47082
6	0.8473	0.03253	0.02135	-0.0271	0.1461	1	26.04673
6.5	0.9098	0.03703	0.02631	-0.027	0.1429	1	24.56927
7	0.9579	0.04218	0.03188	-0.0261	0.1359	1	22.70982
8	1.017	0.05674	0.04803	-0.0223	0.1315	1	17.92386
8.5	1.0194	0.064	0.05641	-0.0191	0.137	1	15.92813
9	0.9688	0.07498	0.06819	-0.0171	0.146	1	12.92078
9.5	0.9636	0.08653	0.07992	-0.0177	0.1567	1	11.13602
10	0.8067	0.11446	0.10751	-0.0405	0.1957	1	7.047877
11	0.7866	0.15143	0.14446	-0.0627	0.3116	1	5.194479
11.5	0.7652	0.15503	0.14794	-0.0654	0.2916	1	4.935819
12	0.7612	0.16141	0.15429	-0.0682	0.2745	1	4.715941
12.5	0.7762	0.17013	0.16303	-0.0701	0.2615	1	4.562393
13	0.8259	0.18389	0.17708	-0.0694	0.244	1	4.491272
13.5	0.7963	0.18424	0.17718	-0.075	0.2293	1	4.32208
14	0.8126	0.19332	0.18639	-0.0773	0.2182	1	4.203393
14.5	0.8398	0.2043	0.19746	-0.0781	0.199	1	4.110622
15	0.8371	0.20697	0.2001	-0.0826	0.1832	1	4.044548

- Airfoil 3

Table AVIII-3: Aerodynamic performance of Airfoil 3 of the uncoated blade at -5°

alpha	CL	CD	CDp	CM	Top_Xtr	Bot_Xtr	CL/CD
------	--------	---------	---------	--------	--------	--------	--------
-4.5	-0.3688	0.02744	0.01694	-0.0354	1	0.0507	-13.4402
-4	-0.3359	0.02513	0.0143	-0.0311	1	0.0536	-13.3665
-3.5	-0.2988	0.02318	0.01191	-0.0287	1	0.0639	-12.8904
-2.5	-0.2544	0.02088	0.01241	-0.016	1	0.7089	-12.1839
-2	-0.23	0.02118	0.01218	-0.01	1	0.7666	-10.8593
-1.5	-0.2369	0.02079	0.01215	0.0059	1	0.8993	-11.3949
-1	-0.1158	0.02161	0.01252	-0.008	1	1	-5.35863
-0.5	-0.1078	0.02139	0.01203	-0.0062	1	1	-5.03974
0	-0.0349	0.02268	0.01293	-0.0148	0.986	1	-1.5388
0.5	0.0473	0.02436	0.01433	-0.0242	0.9663	1	1.941708
1	0.1216	0.02602	0.0158	-0.0317	0.9461	1	4.673328
1.5	0.1888	0.02774	0.01743	-0.0375	0.9274	1	6.806056

2	0.2521	0.02955	0.01921	-0.0422	0.9083	1	8.531303
2.5	0.3147	0.03143	0.02107	-0.0465	0.888	1	10.01273
3	0.3757	0.03335	0.02305	-0.0501	0.8664	1	11.26537
3.5	0.4337	0.03536	0.02522	-0.0531	0.8434	1	12.26527
4	0.4914	0.03739	0.02749	-0.0555	0.8171	1	13.14255
4.5	0.5572	0.03938	0.03045	-0.0584	0.789	1	14.14931
5	0.7434	0.03109	0.02363	-0.0601	0.6926	1	23.91123
5.5	0.8175	0.02678	0.02041	-0.0528	0.6228	1	30.52651
6	0.8213	0.02491	0.01653	-0.0348	0.2402	1	32.97069
6.5	0.8229	0.03244	0.02261	-0.0276	0.0972	1	25.36683
7.5	0.9185	0.04359	0.03417	-0.0237	0.0389	1	21.07135
8	0.9525	0.05127	0.04273	-0.021	0.037	1	18.57812
8.5	0.9609	0.05954	0.05185	-0.0174	0.0374	1	16.13873
9	0.9483	0.06767	0.06063	-0.014	0.0383	1	14.0136
9.5	0.9176	0.07539	0.06875	-0.0116	0.0391	1	12.17138
10	0.8811	0.08486	0.07851	-0.0139	0.04	1	10.38298
10.5	0.8447	0.09705	0.09087	-0.0208	0.0412	1	8.703761
11	0.8173	0.11126	0.10511	-0.0296	0.0427	1	7.345857
11.5	0.8034	0.1255	0.11929	-0.0372	0.0445	1	6.401594
12	0.8003	0.13818	0.13189	-0.0418	0.0464	1	5.791721
12.5	0.7911	0.15982	0.15352	-0.0556	0.0955	1	4.949944
14	0.8005	0.19172	0.18522	-0.0726	0.1257	1	4.17536
15	0.8391	0.21334	0.20677	-0.0763	0.111	1	3.933158

- Airfoil 4

Table AVIII-4: Aerodynamic performance of Airfoil 4 of the uncoated blade at -5°

alpha	CL	CD	CDp	CM	Top_Xtr	Bot_Xtr	CL/CD
------	--------	---------	---------	--------	--------	--------	--------
-5	-0.3664	0.02458	0.01341	-0.0292	1	0.0607	-14.9064
-4.5	-0.3299	0.02127	0.01081	-0.0285	1	0.1978	-15.5101
-4	-0.3167	0.02096	0.01244	-0.0197	1	0.6273	-15.1097
-3.5	-0.3151	0.02225	0.01392	-0.0062	1	0.7432	-14.1618
-1.5	-0.1261	0.02271	0.01339	-0.0051	1	1	-5.55262
-1	-0.0909	0.0231	0.01349	-0.0076	0.9944	1	-3.93506
-0.5	-0.0102	0.02472	0.01472	-0.0173	0.9749	1	-0.41262
0	0.0615	0.0263	0.01608	-0.0247	0.9569	1	2.338403
0.5	0.1314	0.02799	0.01762	-0.0311	0.9384	1	4.694534
1	0.2014	0.02984	0.01945	-0.0372	0.9208	1	6.74933
1.5	0.2617	0.03158	0.02112	-0.0413	0.9042	1	8.28689
2	0.3117	0.03335	0.02288	-0.0435	0.8867	1	9.346327
2.5	0.364	0.03536	0.02497	-0.046	0.8694	1	10.29412
3.5	0.693	0.02505	0.01669	-0.0576	0.6905	1	27.66467

4	0.7498	0.02303	0.01521	-0.0517	0.6191	1	32.55753
4.5	0.7434	0.02427	0.01382	-0.0372	0.164	1	30.63041
5	0.7538	0.02892	0.01811	-0.0315	0.0895	1	26.06501
5.5	0.7802	0.03239	0.02179	-0.0271	0.08	1	24.08768
6	0.8786	0.03861	0.02827	-0.0293	0.0773	1	22.75576
6.5	0.9416	0.04503	0.03573	-0.0277	0.0814	1	20.9105
7	0.9691	0.05407	0.04614	-0.0231	0.0896	1	17.92306
7.5	0.9721	0.06248	0.05537	-0.0185	0.0894	1	15.55858
8	0.9819	0.07231	0.06521	-0.0167	0.0786	1	13.57903
9.5	0.8492	0.10395	0.09814	-0.0189	0.1193	1	8.169312
11.5	0.7489	0.16278	0.15655	-0.0628	0.2412	1	4.600688
12	0.7651	0.17313	0.16686	-0.0645	0.2284	1	4.419223
12.5	0.7701	0.1802	0.17384	-0.0666	0.2041	1	4.273585
13	0.7777	0.18716	0.18072	-0.0687	0.1779	1	4.155268
13.5	0.8166	0.20263	0.19621	-0.0678	0.1643	1	4.030005
14	0.7989	0.20321	0.19665	-0.0746	0.1528	1	3.931401
14.5	0.8333	0.2186	0.21205	-0.0743	0.142	1	3.811985
15	0.8228	0.21883	0.21216	-0.0812	0.1317	1	3.759996

- Airfoil 5

Table AVIII-5: Aerodynamic performance of Airfoil 5 of the uncoated blade at -5°

alpha	CL	CD	CDp	CM	Top_Xtr	Bot_Xtr	CL/CD
------	--------	---------	---------	--------	--------	--------	--------
-5	-0.3338	0.02206	0.01233	-0.0388	1	0.2829	-15.1315
-4.5	-0.3057	0.02042	0.01234	-0.033	1	0.4923	-14.9706
-4	-0.2986	0.02203	0.01415	-0.0205	1	0.6565	-13.5542
-3.5	-0.2851	0.0224	0.01439	-0.0115	1	0.7315	-12.7277
-3	-0.272	0.022	0.01389	-0.0032	1	0.8037	-12.3636
-2.5	-0.2548	0.02121	0.01326	0.0058	1	0.9043	-12.0132
-2	-0.1229	0.02199	0.01353	-0.0118	1	1	-5.5889
-1.5	-0.1062	0.02187	0.01312	-0.0124	0.9968	1	-4.85597
-1	-0.0147	0.02339	0.01415	-0.0245	0.9746	1	-0.62847
-0.5	0.0708	0.02505	0.01546	-0.0345	0.9558	1	2.826347
0	0.1421	0.02655	0.01671	-0.0412	0.9351	1	5.352166
0.5	0.2118	0.02827	0.01824	-0.0471	0.9176	1	7.492041
1	0.2812	0.03005	0.01993	-0.0524	0.8989	1	9.357737
1.5	0.3274	0.03179	0.02167	-0.0538	0.8804	1	10.29884
2	0.3802	0.03376	0.02366	-0.056	0.8617	1	11.26185
2.5	0.4383	0.03585	0.02586	-0.0588	0.842	1	12.22594
3	0.4952	0.03786	0.02812	-0.0609	0.8181	1	13.07977
3.5	0.5569	0.03947	0.03002	-0.0626	0.7851	1	14.10945
4	0.6625	0.03863	0.02975	-0.0658	0.7333	1	17.14988

4.5	0.8061	0.03279	0.02491	-0.0661	0.6729	1	24.58371
5	0.8827	0.02756	0.02016	-0.0574	0.5832	1	32.0283
5.5	0.9144	0.02486	0.0167	-0.0448	0.3788	1	36.78198
6	0.9442	0.02896	0.01944	-0.0397	0.2567	1	32.60359
7.5	1.0467	0.04512	0.03555	-0.0301	0.0922	1	23.19814
9	1.0661	0.06776	0.06036	-0.0185	0.0726	1	15.73347
9.5	1.0176	0.07608	0.06929	-0.0144	0.0746	1	13.37539
10	0.9558	0.08756	0.08113	-0.0173	0.0781	1	10.91594
10.5	0.9044	0.10324	0.09682	-0.0261	0.0834	1	8.76017
11	0.8784	0.11876	0.11231	-0.0337	0.0865	1	7.39643
13	0.8094	0.18422	0.17745	-0.0749	0.1914	1	4.39366
13.5	0.8287	0.19465	0.18788	-0.0763	0.1794	1	4.257385
14	0.8331	0.20031	0.19351	-0.0798	0.1645	1	4.159053
14.5	0.8716	0.21761	0.21087	-0.0791	0.1578	1	4.005331
15	0.8505	0.21601	0.20913	-0.0873	0.1497	1	3.937318

- Airfoil 6

Table AVIII-6: Aerodynamic performance of Airfoil 6 of the uncoated blade at -5°

alpha	CL	CD	CDp	CM	Top_Xtr	Bot_Xtr	CL/CD
------	--------	---------	---------	--------	--------	--------	--------
-4.5	-0.2744	0.02596	0.01468	-0.0252	1	0.0542	-10.5701
-4	-0.2384	0.02507	0.01335	-0.023	1	0.0579	-9.50937
-3.5	-0.1987	0.02435	0.0126	-0.022	1	0.0926	-8.16016
-2.5	-0.1401	0.02366	0.01421	-0.0149	1	0.7149	-5.92139
-2	-0.0626	0.0239	0.01487	-0.02	0.9885	1	-2.61925
-1.5	0.0163	0.02584	0.01618	-0.0278	0.9697	1	0.630805
-1	0.0901	0.02775	0.01766	-0.0343	0.9503	1	3.246847
-0.5	0.1535	0.02951	0.01915	-0.0387	0.9307	1	5.201627
0	0.2165	0.03129	0.02071	-0.0427	0.909	1	6.919143
0.5	0.2794	0.03302	0.02235	-0.0463	0.8846	1	8.461538
1	0.3418	0.0347	0.02402	-0.0495	0.859	1	9.850144
1.5	0.4029	0.03638	0.02579	-0.0521	0.8339	1	11.07477
2	0.4734	0.03786	0.02736	-0.0556	0.8066	1	12.50396
2.5	0.5336	0.03911	0.02874	-0.0567	0.7741	1	13.64357
3	0.6405	0.03771	0.02773	-0.0606	0.7324	1	16.98488
4.5	0.8813	0.02364	0.01398	-0.044	0.4374	1	37.28003
5	0.9143	0.02469	0.01524	-0.0397	0.3522	1	37.03119
5.5	0.9379	0.02671	0.01702	-0.0347	0.2649	1	35.11419
6	0.9494	0.02973	0.01961	-0.0293	0.1678	1	31.93407
6.5	0.9511	0.03359	0.02287	-0.0235	0.07	1	28.31497
7	0.9581	0.03748	0.02673	-0.0188	0.0498	1	25.56297
7.5	0.9658	0.04156	0.0312	-0.0149	0.0432	1	23.23869

8	0.9714	0.04627	0.03632	-0.0115	0.0401	1	20.99416
8.5	0.9886	0.05105	0.04171	-0.0079	0.0399	1	19.36533
9	1.0349	0.05712	0.04858	-0.0043	0.0403	1	18.118
9.5	1.0379	0.06568	0.05796	-0.0021	0.0412	1	15.80238
10	1.0107	0.07545	0.06835	-0.0023	0.0418	1	13.39563
10.5	0.9716	0.08728	0.08065	-0.0066	0.0431	1	11.13199
11	0.9256	0.10217	0.09586	-0.0152	0.0443	1	9.059411
11.5	0.878	0.12161	0.11543	-0.0277	0.0463	1	7.219801
12	0.8496	0.14045	0.13417	-0.0378	0.0495	1	6.049128
12.5	0.842	0.15404	0.14766	-0.0435	0.0526	1	5.466113
13	0.8423	0.16617	0.1597	-0.0477	0.0544	1	5.068905
13.5	0.8308	0.18467	0.17805	-0.0579	0.0712	1	4.498836
15	0.8453	0.22299	0.21623	-0.076	0.1378	1	3.790753

- 0°:
- Airfoil 1

Table AVIII-7: Aerodynamic performance of Airfoil 1 of the uncoated blade at 0°

alpha	CL	CD	CDp	CM	Top_Xtr	Bot_Xtr	CL/CD
------	--------	---------	---------	--------	--------	--------	--------
-4	-0.3333	0.02282	0.01224	-0.0268	1	0.2074	-14.6056
-3	-0.3253	0.02077	0.01315	-0.0003	1	0.7894	-15.662
-2	-0.0815	0.02156	0.0128	-0.0189	1	1	-3.78015
-1.5	-0.1128	0.02082	0.01204	-0.0106	1	1	-5.41787
-1	-0.1138	0.02041	0.01141	-0.0066	1	1	-5.5757
-0.5	-0.0799	0.02087	0.01149	-0.0073	1	1	-3.82846
0	-0.0401	0.02172	0.01205	-0.0085	1	1	-1.84622
0.5	0.0184	0.02325	0.01333	-0.0129	0.9925	1	0.791398
1	0.0981	0.02523	0.01514	-0.021	0.9702	1	3.888228
1.5	0.1712	0.02721	0.01705	-0.0274	0.9483	1	6.291804
2	0.2407	0.02921	0.01908	-0.0328	0.9256	1	8.240329
2.5	0.3095	0.03125	0.02122	-0.0378	0.9008	1	9.904
3	0.3826	0.03332	0.02355	-0.0429	0.8733	1	11.48259
3.5	0.5767	0.02927	0.02028	-0.0538	0.7705	1	19.70277
4	0.6755	0.02279	0.01431	-0.0453	0.6651	1	29.64019
4.5	0.6835	0.02273	0.01185	-0.0295	0.2614	1	30.07039
5	0.7189	0.02615	0.01457	-0.0263	0.2039	1	27.4914
5.5	0.7798	0.02894	0.01733	-0.0258	0.1848	1	26.9454
6	0.8373	0.03204	0.02057	-0.0257	0.1646	1	26.13296
6.5	0.8954	0.03601	0.02471	-0.0257	0.1562	1	24.86532
7	0.9455	0.04178	0.03091	-0.0251	0.1523	1	22.63045
7.5	0.9835	0.04769	0.0376	-0.0233	0.152	1	20.62277
8	1.0133	0.05388	0.04466	-0.0211	0.1545	1	18.80661

8.5	0.9969	0.06268	0.05483	-0.0173	0.1636	1	15.90459
9	0.9835	0.07338	0.066	-0.0163	0.1724	1	13.40283
12	0.7409	0.15793	0.15048	-0.0646	0.3022	1	4.691319
13	0.7925	0.17738	0.17012	-0.0663	0.2663	1	4.467809
14	0.7975	0.18815	0.18091	-0.0711	0.2263	1	4.238639
15	0.8177	0.2038	0.19656	-0.0764	0.1942	1	4.012267

- Airfoil 2

Table AVIII-8: Aerodynamic performance of Airfoil 2 of the uncoated blade at 0°

alpha	CL	CD	CDp	CM	Top_Xtr	Bot_Xtr	CL/CD
------	--------	---------	---------	--------	--------	--------	--------
-5	-0.4178	0.02576	0.01583	-0.0369	1	0.1792	-16.2189
-4.5	-0.3786	0.02296	0.01296	-0.033	1	0.2105	-16.4895
-3.5	-0.3598	0.02158	0.01411	-0.0089	1	0.7156	-16.6728
-3	-0.3634	0.02216	0.01467	0.0071	1	0.8104	-16.3989
-2.5	-0.3236	0.02198	0.01423	0.0162	1	0.92	-14.7225
-2	-0.1208	0.02216	0.01326	-0.0121	1	0.9822	-5.45126
-1.5	-0.0836	0.02162	0.01249	-0.0156	1	1	-3.86679
-1	-0.1142	0.02079	0.01163	-0.0078	1	1	-5.49303
-0.5	-0.1013	0.02061	0.01121	-0.0064	1	1	-4.91509
0	-0.0611	0.02123	0.01145	-0.0086	1	1	-2.878
0.5	-0.0073	0.02243	0.01238	-0.0128	0.9953	1	-0.32546
1	0.0746	0.02441	0.01417	-0.0217	0.9756	1	3.056125
1.5	0.1491	0.02629	0.01596	-0.0287	0.9543	1	5.671358
2	0.2234	0.02822	0.01787	-0.0352	0.9304	1	7.916371
2.5	0.2916	0.03016	0.01988	-0.0403	0.9075	1	9.668435
3	0.3583	0.03214	0.02211	-0.0449	0.883	1	11.1481
3.5	0.4265	0.0342	0.02443	-0.0492	0.857	1	12.47076
4	0.4995	0.03636	0.02697	-0.0538	0.8304	1	13.73762
4.5	0.5527	0.03809	0.02921	-0.0544	0.7918	1	14.51037
5	0.7516	0.02576	0.01813	-0.0504	0.6546	1	29.17702
5.5	0.7739	0.02279	0.01367	-0.0337	0.3122	1	33.95788
6	0.8012	0.02773	0.01744	-0.0291	0.1991	1	28.8929
6.5	0.8669	0.03165	0.02136	-0.029	0.1715	1	27.39021
7	0.9248	0.03644	0.02658	-0.0285	0.152	1	25.3787
7.5	0.9726	0.04421	0.03501	-0.0271	0.1405	1	21.99955
8	0.9902	0.05047	0.04212	-0.023	0.1105	1	19.61958
8.5	0.997	0.05778	0.04999	-0.0194	0.0893	1	17.25511
9	0.9919	0.06576	0.05864	-0.016	0.083	1	15.08364
9.5	0.9588	0.07486	0.06832	-0.0133	0.0854	1	12.80791
10	0.9138	0.08477	0.07849	-0.0138	0.0901	1	10.77976
10.5	0.8794	0.0973	0.09108	-0.0189	0.0942	1	9.038027

11	0.873	0.11081	0.10464	-0.0228	0.098	1	7.87835
12	0.7634	0.15838	0.1519	-0.0666	0.2749	1	4.820053
13	0.7984	0.1768	0.17029	-0.0668	0.209	1	4.515837
14	0.8099	0.19045	0.18385	-0.0719	0.1689	1	4.25256
15	0.8265	0.20598	0.1993	-0.0789	0.1472	1	4.012525

- Airfoil 3

Table AVIII-9: Aerodynamic performance of Airfoil 3 of the uncoated blade at 0°

alpha	CL	CD	CDp	CM	Top_Xtr	Bot_Xtr	CL/CD
------	--------	---------	---------	--------	--------	--------	--------
-6.5	-0.529	0.03841	0.02985	-0.0396	1	0.1364	-13.7725
-6	-0.4956	0.03225	0.02267	-0.0364	1	0.1446	-15.3674
-5.5	-0.4566	0.02825	0.01822	-0.0332	1	0.1572	-16.1628
-5	-0.4184	0.02553	0.01529	-0.0301	1	0.1828	-16.3886
-4.5	-0.3796	0.02305	0.01266	-0.0263	1	0.2117	-16.4685
-3.5	-0.3657	0.02124	0.01359	-0.0013	1	0.7508	-17.2175
-3	-0.3683	0.02141	0.0138	0.015	1	0.8612	-17.2022
-2.5	-0.0821	0.02262	0.01347	-0.0212	1	0.9928	-3.62953
-2	-0.0802	0.02215	0.0129	-0.0184	1	1	-3.62077
-1.5	-0.1121	0.02144	0.01217	-0.01	1	1	-5.22854
-1	-0.1214	0.02088	0.01143	-0.0049	1	1	-5.81418
-0.5	-0.0908	0.02129	0.01152	-0.0053	1	1	-4.26491
0	-0.0523	0.02214	0.01201	-0.0064	1	1	-2.36224
0.5	0.0198	0.02387	0.01349	-0.0135	0.9847	1	0.829493
1	0.0924	0.02574	0.01521	-0.0203	0.9661	1	3.589744
1.5	0.1587	0.02764	0.01706	-0.0256	0.9485	1	5.741679
2	0.2249	0.02965	0.01907	-0.0307	0.9293	1	7.58516
2.5	0.2905	0.03166	0.02117	-0.0353	0.9068	1	9.175616
3	0.352	0.03371	0.02349	-0.0389	0.8833	1	10.44201
3.5	0.4085	0.03583	0.02585	-0.0416	0.859	1	11.40106
4	0.4686	0.03801	0.02837	-0.0444	0.8305	1	12.32833
4.5	0.6302	0.03558	0.02712	-0.0528	0.7519	1	17.7122
5.5	0.7572	0.02623	0.01564	-0.0257	0.2253	1	29.45233
6.5	0.8855	0.03594	0.02524	-0.0252	0.1426	1	24.63829
7	0.938	0.04159	0.03181	-0.0238	0.1403	1	22.5535
7.5	0.9711	0.04813	0.03946	-0.0207	0.1363	1	20.17661
8	0.9927	0.05643	0.04813	-0.0181	0.1201	1	17.59171
8.5	0.9823	0.06326	0.05604	-0.013	0.1128	1	15.52798
9	0.9612	0.07288	0.06622	-0.0099	0.1152	1	13.1888
9.5	0.9357	0.08322	0.0768	-0.0082	0.119	1	11.24369
11.5	0.746	0.15312	0.14645	-0.0571	0.3003	1	4.871996
12	0.7475	0.16029	0.1536	-0.0586	0.2759	1	4.663423

13	0.7606	0.17425	0.16751	-0.0612	0.2176	1	4.364993
13.5	0.7673	0.18237	0.17558	-0.0639	0.2015	1	4.207381
14	0.7897	0.19349	0.1867	-0.0649	0.1857	1	4.081348
14.5	0.8082	0.2035	0.19669	-0.0661	0.1643	1	3.971499

- Airfoil 4

Table AVIII-10: Aerodynamic performance of Airfoil 4 of the uncoated blade at 0°

alpha	CL	CD	CDp	CM	Top_Xtr	Bot_Xtr	CL/CD
------	--------	---------	---------	--------	--------	--------	--------
-4.5	-0.3607	0.02311	0.01589	-0.007	1	0.747	-15.608
-4	-0.3501	0.02288	0.01537	0.0031	1	0.8077	-15.3016
-3.5	-0.3395	0.02225	0.01455	0.0129	1	0.8777	-15.2584
-3	-0.1558	0.0236	0.01485	-0.0079	1	0.9775	-6.60169
-2.5	-0.1013	0.02337	0.01429	-0.0143	1	1	-4.33462
-2	-0.1265	0.02246	0.01334	-0.0075	1	1	-5.63224
-1.5	-0.1064	0.02238	0.01297	-0.0076	1	1	-4.75424
-1	-0.0426	0.02362	0.01377	-0.0145	0.9919	1	-1.80356
-0.5	0.0355	0.02537	0.01523	-0.0233	0.9747	1	1.399291
0	0.1076	0.02717	0.01685	-0.0304	0.9579	1	3.96025
0.5	0.1803	0.02912	0.01865	-0.0371	0.9404	1	6.191621
1	0.2537	0.03105	0.02053	-0.0434	0.9203	1	8.170692
1.5	0.3057	0.03271	0.02222	-0.0459	0.9025	1	9.345766
2	0.366	0.03456	0.02422	-0.0495	0.8818	1	10.59028
2.5	0.424	0.03659	0.02643	-0.0525	0.861	1	11.58787
3	0.4745	0.03883	0.02891	-0.0545	0.8408	1	12.21993
3.5	0.5426	0.04088	0.03137	-0.0579	0.8118	1	13.27299
4	0.802	0.02569	0.01822	-0.0599	0.6477	1	31.21837
4.5	0.8038	0.02418	0.01458	-0.0421	0.2238	1	33.24235
5	0.8023	0.03002	0.01923	-0.0347	0.1099	1	26.72552
5.5	0.8565	0.03415	0.02352	-0.0326	0.0925	1	25.08053
6	0.9432	0.04016	0.03003	-0.0343	0.0877	1	23.48606
6.5	0.9923	0.04778	0.03898	-0.0321	0.09	1	20.7681
7	1.0144	0.05658	0.04877	-0.0283	0.0945	1	17.9286
7.5	1.0234	0.06773	0.06052	-0.0252	0.0993	1	15.11
8	1.0073	0.07587	0.06931	-0.021	0.0988	1	13.27666
8.5	0.9808	0.08462	0.07842	-0.0181	0.0992	1	11.59064
9	0.9598	0.09489	0.0889	-0.0171	0.1008	1	10.11487
11	0.8062	0.16568	0.15942	-0.0655	0.2558	1	4.866007
11.5	0.795	0.17052	0.1642	-0.0688	0.2364	1	4.66221
12	0.7857	0.17674	0.17031	-0.0728	0.2211	1	4.445513
12.5	0.7971	0.18542	0.17895	-0.0751	0.2046	1	4.298889
13	0.807	0.19256	0.18625	-0.0772	0.1782	1	4.190902

13.5	0.8382	0.20621	0.19991	-0.0774	0.1655	1	4.064788
14	0.8305	0.20863	0.20224	-0.0831	0.1528	1	3.980731
14.5	0.8647	0.22473	0.21838	-0.083	0.1437	1	3.847728
15	0.8539	0.2243	0.21782	-0.0904	0.1345	1	3.806955

- Airfoil 5

Table AVIII-11: Aerodynamic performance of Airfoil 5 of the uncoated blade at 0°

alpha	CL	CD	CDp	CM	Top_Xtr	Bot_Xtr	CL/CD
------	--------	---------	---------	--------	--------	--------	--------
-5	-0.376	0.02187	0.01241	-0.0357	1	0.2817	-17.1925
-4.5	-0.3544	0.02032	0.01275	-0.028	1	0.5483	-17.4409
-4	-0.3503	0.02217	0.01458	-0.0135	1	0.6932	-15.8006
-3.5	-0.3361	0.02238	0.01452	-0.004	1	0.7598	-15.0179
-3	-0.323	0.02191	0.01387	0.0049	1	0.8233	-14.7421
-2	-0.0905	0.02267	0.0136	-0.0165	1	1	-3.99206
-1.5	-0.121	0.02189	0.01281	-0.009	1	1	-5.52764
-1	-0.109	0.02172	0.01232	-0.0078	1	1	-5.01842
-0.5	-0.0415	0.02294	0.01319	-0.0155	0.9884	1	-1.80907
0	0.0437	0.02476	0.01474	-0.0255	0.9698	1	1.764943
0.5	0.1148	0.02634	0.01613	-0.0324	0.9503	1	4.35839
1	0.1822	0.02806	0.01772	-0.0382	0.9319	1	6.493229
1.5	0.2468	0.02992	0.01955	-0.0431	0.9148	1	8.248663
2	0.3159	0.03199	0.02177	-0.0485	0.8979	1	9.874961
2.5	0.3609	0.03383	0.0237	-0.0498	0.8794	1	10.66805
3	0.4177	0.03585	0.02593	-0.0526	0.8574	1	11.65132
3.5	0.4645	0.03817	0.0285	-0.0541	0.8381	1	12.16924
4	0.5226	0.04043	0.03117	-0.0565	0.8123	1	12.92605
4.5	0.6321	0.04007	0.03187	-0.0606	0.7521	1	15.77489
5.5	0.7833	0.02991	0.01935	-0.0318	0.1094	1	26.18857
6.5	0.91	0.0423	0.03212	-0.0285	0.0654	1	21.513
7	0.9487	0.04957	0.04059	-0.0256	0.0638	1	19.13859
7.5	0.9675	0.05661	0.04841	-0.0218	0.0609	1	17.09062
8	0.9722	0.06392	0.05635	-0.0181	0.0588	1	15.20964
8.5	0.9496	0.07264	0.06578	-0.0143	0.0632	1	13.07269
9	0.9161	0.0809	0.07436	-0.0118	0.0659	1	11.32386
9.5	0.8791	0.09082	0.08446	-0.0138	0.0678	1	9.679586
10	0.8764	0.10248	0.09619	-0.0159	0.0724	1	8.551913
11.5	0.3637	0.04034	0.03609	-0.0173	0.1378	1	9.015865
12.5	0.3614	0.05721	0.05284	-0.0339	0.2237	1	6.317077
13	0.3831	0.06559	0.0611	-0.0373	0.2009	1	5.840829
13.5	0.4081	0.0741	0.06957	-0.0402	0.1868	1	5.507422
14	0.4247	0.08329	0.07865	-0.0446	0.1791	1	5.099052

14.5	0.4455	0.09201	0.08733	-0.0479	0.1656	1	4.841865
15	0.4732	0.10402	0.09926	-0.0505	0.1592	1	4.549125

- Airfoil 6

Table AVIII-12: Aerodynamic performance of Airfoil 6 of the uncoated blade at 0°

alpha	CL	CD	CDp	CM	Top_Xtr	Bot_Xtr	CL/CD
------	--------	---------	---------	--------	--------	--------	--------
-5	-0.2431	0.02257	0.0141	-0.0343	1	0.425	-10.7709
-4.5	-0.228	0.02362	0.0158	-0.0248	1	0.6147	-9.65284
-4	-0.2043	0.02294	0.01505	-0.0173	1	0.7455	-8.90584
-3.5	-0.1701	0.02218	0.01445	-0.0124	1	0.8578	-7.66907
-3	-0.0956	0.02231	0.01414	-0.0202	1	1	-4.28507
-2.5	-0.0505	0.02322	0.01422	-0.0225	1	1	-2.17485
-2	-0.009	0.02443	0.01499	-0.0238	1	1	-0.3684
-1.5	0.0297	0.02585	0.01607	-0.0245	1	1	1.148936
-1	0.0854	0.02799	0.01794	-0.0285	0.9918	1	3.05109
-0.5	0.1668	0.03082	0.02058	-0.0369	0.9675	1	5.41207
0	0.2461	0.03327	0.02287	-0.0442	0.9362	1	7.397054
0.5	0.3249	0.03545	0.025	-0.0505	0.9013	1	9.165021
1	0.4466	0.03563	0.0253	-0.0593	0.8366	1	12.53438
1.5	0.6369	0.02757	0.01761	-0.0675	0.7496	1	23.1012
2	0.7103	0.02483	0.01514	-0.0647	0.6945	1	28.60652
2.5	0.7618	0.02231	0.0114	-0.0544	0.4138	1	34.14612
3	0.7851	0.02612	0.01385	-0.0489	0.2746	1	30.05743
3.5	0.8509	0.02853	0.01622	-0.0501	0.2474	1	29.82475
4	0.8869	0.03045	0.0179	-0.0478	0.2108	1	29.12644
4.5	0.9239	0.03218	0.01972	-0.0455	0.1848	1	28.71038
5	0.9822	0.0341	0.02216	-0.0456	0.1791	1	28.80352
6	0.9901	0.03583	0.02431	-0.0331	0.1287	1	27.63327
7	1.0383	0.03887	0.02819	-0.0259	0.1014	1	26.71212
7.5	1.0676	0.04064	0.03043	-0.0232	0.0712	1	26.26969
8	1.0907	0.04366	0.03372	-0.02	0.0483	1	24.98168
8.5	1.1	0.04797	0.03817	-0.017	0.0438	1	22.931
9	1.1032	0.05318	0.0438	-0.0144	0.0418	1	20.74464
9.5	1.102	0.05927	0.05039	-0.0127	0.0408	1	18.59288
10	1.0979	0.06628	0.05794	-0.012	0.0405	1	16.56457
10.5	1.0884	0.0747	0.06694	-0.0126	0.0404	1	14.57028
11	1.0677	0.08547	0.07831	-0.0158	0.0407	1	12.4921
11.5	1.0309	0.10052	0.09396	-0.0233	0.0417	1	10.25567
12	0.9325	0.13491	0.12872	-0.044	0.0458	1	6.912015
12.5	0.8969	0.15565	0.14924	-0.0544	0.0485	1	5.762287
13	0.8868	0.16979	0.16326	-0.0609	0.0502	1	5.222922

13.5	0.8866	0.18176	0.17515	-0.066	0.0518	1	4.877861
14	0.8926	0.19243	0.18578	-0.0701	0.0534	1	4.63857
14.5	0.9046	0.20239	0.19574	-0.0727	0.0551	1	4.469588
15	0.8895	0.21889	0.21207	-0.0843	0.0659	1	4.063685

- 5°:
- Airfoil 1:

Table AVIII-13: Aerodynamic performance of Airfoil 1 of the uncoated blade at 5°

alpha	CL	CD	CDp	CM	Top_Xtr	Bot_Xtr	CL/CD
------	--------	---------	---------	--------	--------	--------	--------
-5	-0.4111	0.03518	0.02579	-0.0382	1	0.1135	-11.6856
-4.5	-0.3739	0.0311	0.02106	-0.0355	1	0.1117	-12.0225
-4	-0.3345	0.02844	0.01784	-0.0327	1	0.1193	-11.7616
-3.5	-0.2952	0.02551	0.01493	-0.0298	1	0.136	-11.5719
-3	-0.2557	0.02331	0.01271	-0.0265	1	0.1679	-10.9695
-2	-0.0762	0.02145	0.01336	-0.0213	1	1	-3.55245
-1.5	-0.109	0.02079	0.01267	-0.013	1	1	-5.24291
-1	-0.1152	0.02028	0.01193	-0.0084	1	1	-5.68047
-0.5	-0.0812	0.02067	0.01192	-0.0094	1	1	-3.9284
0	-0.0399	0.0215	0.01234	-0.0109	1	1	-1.85581
0.5	0.0161	0.02289	0.01342	-0.0149	0.9938	1	0.703364
1	0.0959	0.02488	0.01516	-0.0229	0.9732	1	3.854502
1.5	0.1696	0.02683	0.01698	-0.0294	0.9517	1	6.321282
2	0.2388	0.02881	0.01893	-0.0348	0.9297	1	8.288789
2.5	0.3112	0.03082	0.02099	-0.0402	0.9031	1	10.09734
3	0.3763	0.03287	0.02318	-0.0442	0.8777	1	11.44813
4	0.6768	0.02257	0.01407	-0.0475	0.6692	1	29.98671
4.5	0.6816	0.02291	0.01178	-0.0315	0.2593	1	29.7512
5	0.7215	0.02625	0.01449	-0.0288	0.2048	1	27.48571
5.5	0.7837	0.02924	0.01747	-0.0286	0.1859	1	26.80233
6	0.8451	0.03253	0.0208	-0.0288	0.1749	1	25.9791
6.5	0.8973	0.03656	0.02511	-0.0283	0.1654	1	24.54322
7	0.9436	0.04094	0.03012	-0.0272	0.163	1	23.04836
7.5	0.9813	0.04641	0.03639	-0.0257	0.1638	1	21.14415
8	1.009	0.05299	0.04366	-0.024	0.166	1	19.04133
8.5	1.0259	0.06058	0.05186	-0.0223	0.1677	1	16.93463
9	1.0374	0.06991	0.0616	-0.0213	0.1697	1	14.83908
10	0.7078	0.12855	0.12071	-0.0628	0.3745	1	5.506029
13	0.7759	0.1704	0.16275	-0.072	0.2819	1	4.553404
14	0.8528	0.1939	0.18657	-0.0718	0.2439	1	4.398143
15	0.8482	0.20385	0.19654	-0.0785	0.2179	1	4.160903

- Airfoil 2

Table AVIII-14: Aerodynamic performance of Airfoil 2 of the uncoated blade at 5°

alpha	CL	CD	CDp	CM	Top_Xtr	Bot_Xtr	CL/CD
------	--------	---------	---------	--------	--------	--------	--------
-5	-0.3878	0.0259	0.01573	-0.0357	1	0.1563	-14.973
-4.5	-0.3516	0.02378	0.01351	-0.0322	1	0.1884	-14.7855
-4	-0.3154	0.02087	0.01124	-0.0294	1	0.2621	-15.1126
-3.5	-0.3218	0.02081	0.01324	-0.0125	1	0.7134	-15.4637
-3	-0.3234	0.02136	0.01375	0.0021	1	0.8088	-15.1404
-2	-0.0857	0.02203	0.01319	-0.0171	1	1	-3.89015
-1.5	-0.1128	0.02129	0.01241	-0.0095	1	1	-5.29826
-1	-0.1138	0.02079	0.0117	-0.0057	1	1	-5.47379
-0.5	-0.078	0.02122	0.01182	-0.0072	1	1	-3.67578
0	-0.0308	0.02217	0.01247	-0.0101	0.9979	1	-1.38926
0.5	0.0499	0.02409	0.0141	-0.0188	0.9793	1	2.071399
1	0.1247	0.02601	0.01586	-0.0259	0.9604	1	4.79431
1.5	0.1932	0.0279	0.01771	-0.0316	0.9406	1	6.924731
2	0.2612	0.02988	0.0197	-0.0368	0.9187	1	8.741633
2.5	0.3247	0.03192	0.02183	-0.041	0.8964	1	10.17231
3	0.3888	0.03404	0.0242	-0.045	0.872	1	11.42186
3.5	0.468	0.03621	0.02667	-0.0504	0.8425	1	12.92461
4	0.5422	0.03761	0.0285	-0.0534	0.8008	1	14.41638
4.5	0.7454	0.02433	0.01641	-0.0481	0.6438	1	30.63707
5	0.7468	0.02461	0.01396	-0.0311	0.2362	1	30.34539
5.5	0.7931	0.02864	0.01749	-0.0287	0.1824	1	27.69204
6	0.8506	0.03206	0.02098	-0.0283	0.1511	1	26.5315
6.5	0.911	0.0369	0.0261	-0.0283	0.138	1	24.68835
7	0.9589	0.04233	0.03228	-0.0269	0.1328	1	22.65296
7.5	0.993	0.04903	0.03989	-0.0248	0.1334	1	20.25291
8	1.0115	0.05713	0.04887	-0.0225	0.1377	1	17.70523
8.5	1.0277	0.06751	0.0597	-0.0215	0.1432	1	15.22293

- Airfoil 3

Table AVIII-15: Aerodynamic performance of Airfoil 3 of the uncoated blade at 5°

alpha	CL	CD	CDp	CM	Top_Xtr	Bot_Xtr	CL/CD
------	--------	---------	---------	--------	--------	--------	--------
-5	-0.4253	0.02668	0.01678	-0.0343	1	0.163	-15.9408
-4.5	-0.387	0.02338	0.01357	-0.0303	1	0.2063	-16.5526
-4	-0.3715	0.01971	0.01258	-0.0214	1	0.5815	-18.8483
-3.5	-0.3665	0.0213	0.01404	-0.0068	1	0.7208	-17.2066
-3	-0.3637	0.0217	0.01416	0.0071	1	0.8099	-16.7604
-2.5	-0.1834	0.02287	0.0143	-0.0056	1	0.9611	-8.01924

-2	-0.0585	0.02217	0.01281	-0.0231	1	1	-2.6387
-1.5	-0.0881	0.02178	0.01241	-0.015	1	1	-4.045
-1	-0.1179	0.02099	0.0116	-0.0071	1	1	-5.61696
-0.5	-0.1052	0.0209	0.01124	-0.0054	1	1	-5.03349
0	-0.0674	0.02155	0.01159	-0.0071	1	1	-3.12761
0.5	-0.0025	0.02302	0.0128	-0.0133	0.9893	1	-0.1086
1	0.0751	0.02489	0.01445	-0.0213	0.9703	1	3.017276
1.5	0.1482	0.02676	0.01621	-0.028	0.9504	1	5.538117
2	0.214	0.0286	0.01802	-0.0332	0.9303	1	7.482517
2.5	0.2783	0.03052	0.02003	-0.0377	0.9091	1	9.118611
3	0.3401	0.0325	0.02213	-0.0416	0.8867	1	10.46462
3.5	0.3997	0.03457	0.02443	-0.0448	0.8635	1	11.56205
4	0.4669	0.03669	0.02689	-0.0487	0.8368	1	12.72554
4.5	0.5283	0.03883	0.02967	-0.0512	0.8069	1	13.60546
5	0.6987	0.03312	0.02526	-0.0552	0.7138	1	21.09601
5.5	0.8024	0.02465	0.0181	-0.0446	0.602	1	32.55172
6	0.7827	0.02672	0.01676	-0.0281	0.1577	1	29.29266
6.5	0.7952	0.03341	0.02256	-0.0221	0.0668	1	23.80126
7	0.8649	0.03866	0.02828	-0.0212	0.0523	1	22.37196
7.5	0.9162	0.04583	0.03604	-0.0199	0.0493	1	19.99127
8	0.9458	0.05339	0.04451	-0.0169	0.05	1	17.71493
8.5	0.9501	0.06164	0.0538	-0.0128	0.0525	1	15.41369
9	0.9303	0.07016	0.06306	-0.0092	0.0554	1	13.25969
9.5	0.8938	0.07828	0.07154	-0.0069	0.0572	1	11.41799
10	0.8528	0.08842	0.0819	-0.0102	0.0591	1	9.644877
10.5	0.817	0.1015	0.09506	-0.0178	0.0613	1	8.049261
11	0.8012	0.11482	0.10835	-0.0244	0.0648	1	6.977878
11.5	0.774	0.13377	0.12721	-0.0382	0.0778	1	5.786051
12.5	0.7601	0.16465	0.158	-0.0569	0.1686	1	4.616459
13	0.7724	0.17332	0.16666	-0.0594	0.1608	1	4.456497
13.5	0.8059	0.18726	0.18062	-0.0588	0.1547	1	4.303642
14	0.783	0.18935	0.18256	-0.0668	0.1441	1	4.135199
14.5	0.8138	0.20074	0.19402	-0.0668	0.1351	1	4.054
15	0.8187	0.20951	0.20271	-0.0712	0.1314	1	3.907689

- Airfoil 4

Table AVIII-16: Aerodynamic performance of Airfoil 4 of the uncoated blade at 5°

alpha	CL	CD	CDp	CM	Top_Xtr	Bot_Xtr	CL/CD
------	--------	---------	---------	--------	--------	--------	--------
-4.5	-0.327	0.0235	0.01224	-0.0327	1	0.0659	-13.9149
-4	-0.2947	0.01988	0.01119	-0.0308	1	0.5085	-14.8239
-3.5	-0.2747	0.02083	0.01224	-0.0227	1	0.6522	-13.1877

-3	-0.2773	0.02197	0.0136	-0.0082	1	0.7685	-12.6218
-2.5	-0.2988	0.02149	0.0135	0.0122	1	0.9051	-13.9041
-1	-0.1081	0.022	0.01263	-0.0068	1	1	-4.91364
-0.5	-0.0493	0.02314	0.01345	-0.013	0.9926	1	-2.13051
0	0.034	0.02491	0.0149	-0.0228	0.9719	1	1.364914
0.5	0.109	0.02667	0.01647	-0.0305	0.9523	1	4.086989
1	0.1781	0.02844	0.01814	-0.0366	0.933	1	6.262307
1.5	0.2428	0.03029	0.01998	-0.0418	0.9143	1	8.015847
2	0.3061	0.03221	0.02189	-0.0463	0.8949	1	9.50326
2.5	0.3685	0.0341	0.02385	-0.0502	0.8729	1	10.80645
3	0.4272	0.03612	0.02603	-0.0534	0.8508	1	11.82724
3.5	0.4823	0.03825	0.0284	-0.0558	0.8268	1	12.60915
4	0.5502	0.0401	0.03108	-0.059	0.797	1	13.7207
4.5	0.6222	0.04123	0.0328	-0.061	0.7558	1	15.09095
5	0.8147	0.03163	0.02478	-0.063	0.6669	1	25.75719
5.5	0.8727	0.02342	0.0167	-0.0464	0.4358	1	37.26302
6	0.8591	0.02901	0.01971	-0.0359	0.1737	1	29.61393
7.5	1.002	0.055	0.04652	-0.0291	0.0674	1	18.21818
10	0.8568	0.10199	0.09622	-0.0252	0.0813	1	8.400824
13	0.8216	0.18974	0.18356	-0.0698	0.174	1	4.330136
14	0.8284	0.20472	0.19837	-0.0775	0.1512	1	4.046503
15	0.847	0.22022	0.21373	-0.0845	0.129	1	3.846154

- Airfoil 5

Table AVIII-17: Aerodynamic performance of Airfoil 5 of the uncoated blade at 5°

alpha	CL	CD	CDp	CM	Top_Xtr	Bot_Xtr	CL/CD
------	--------	---------	---------	--------	--------	--------	--------
-5	-0.3467	0.02274	0.01307	-0.0437	1	0.2824	-15.2463
-4.5	-0.3097	0.0207	0.01214	-0.04	1	0.418	-14.9614
-4	-0.2963	0.02221	0.01423	-0.0286	1	0.6034	-13.3408
-3.5	-0.282	0.02304	0.01501	-0.0194	1	0.6859	-12.2396
-3	-0.2654	0.02297	0.01483	-0.0118	1	0.7453	-11.5542
-2.5	-0.2559	0.02238	0.01423	-0.0028	1	0.8204	-11.4343
-2	-0.2366	0.02174	0.01364	0.0046	1	0.9093	-10.8832
-1.5	-0.126	0.02221	0.01377	-0.0103	1	1	-5.67312
-1	-0.0685	0.02283	0.01395	-0.0181	0.9873	1	-3.00044
-0.5	0.0258	0.02445	0.01518	-0.0308	0.9647	1	1.055215
0	0.1064	0.02601	0.01645	-0.04	0.9434	1	4.090734
0.5	0.1852	0.02771	0.01789	-0.0478	0.9221	1	6.683508
1	0.2514	0.02942	0.01943	-0.053	0.9025	1	8.545207
1.5	0.3123	0.0312	0.02112	-0.0569	0.8821	1	10.00962
2	0.3682	0.03311	0.02305	-0.0597	0.8628	1	11.12051

2.5	0.4252	0.0351	0.02508	-0.0624	0.8423	1	12.11396
3	0.4818	0.03706	0.02715	-0.0646	0.8192	1	13.00054
3.5	0.5411	0.03887	0.02916	-0.0666	0.7918	1	13.92076
4	0.6353	0.03942	0.03026	-0.0708	0.7573	1	16.11618
4.5	0.7365	0.0376	0.02899	-0.0721	0.7084	1	19.58777
5	0.8635	0.0309	0.02298	-0.0688	0.6438	1	27.94498
5.5	0.925	0.02625	0.01885	-0.0594	0.5455	1	35.2381
6	0.9446	0.02507	0.01701	-0.0486	0.3657	1	37.6785
6.5	0.9636	0.02877	0.01949	-0.0428	0.2445	1	33.49322
7	0.9804	0.03239	0.02288	-0.0383	0.1704	1	30.2686
8	1.03	0.04464	0.03494	-0.03	0.0545	1	23.07348
8.5	1.0664	0.05219	0.04286	-0.0282	0.0476	1	20.43303
9.5	1.0608	0.06996	0.06196	-0.0211	0.0463	1	15.16295
10	1.0339	0.07716	0.06973	-0.0179	0.0467	1	13.39943
10.5	0.999	0.08521	0.07822	-0.0185	0.0475	1	11.72398
11	0.9394	0.09916	0.09266	-0.027	0.0502	1	9.473578
11.5	0.8691	0.12467	0.11829	-0.045	0.0568	1	6.971204
12	0.8528	0.14074	0.13426	-0.0532	0.0601	1	6.0594
12.5	0.8496	0.15351	0.14694	-0.0587	0.0629	1	5.534493
14	0.8459	0.19746	0.19082	-0.0818	0.1376	1	4.283906
14.5	0.8824	0.21225	0.20568	-0.081	0.1334	1	4.157362
15	0.8842	0.2212	0.21452	-0.0864	0.1317	1	3.997288

- Airfoil 6

Table AVIII-18: Aerodynamic performance of Airfoil 6 of the uncoated blade at 5°

alpha	CL	CD	CDp	CM	Top_Xtr	Bot_Xtr	CL/CD
------	--------	---------	---------	--------	--------	--------	--------
-5	-0.312	0.02446	0.0136	-0.0554	0.9494	0.0973	-12.7555
-4	-0.164	0.02337	0.0131	-0.0646	0.869	0.5485	-7.01754
-3.5	-0.1627	0.02514	0.01467	-0.056	0.8866	0.615	-6.47176
-3	-0.1669	0.02633	0.0157	-0.0454	0.9036	0.6719	-6.33878
-2.5	-0.1724	0.02687	0.01601	-0.0343	0.9228	0.7298	-6.41608
-2	-0.1785	0.02657	0.01543	-0.0236	0.9432	0.7807	-6.7181
-1.5	-0.1792	0.0255	0.01413	-0.0139	0.9713	0.823	-7.02745
-1	-0.1686	0.02396	0.01239	-0.0061	0.9983	0.8679	-7.03673
-0.5	-0.0799	0.02347	0.01157	-0.0147	1	1	-3.40435
0	-0.0175	0.02379	0.01122	-0.019	1	1	-0.7356
0.5	0.0394	0.02432	0.01131	-0.0213	1	1	1.620066
1	0.0896	0.02496	0.01169	-0.0219	1	1	3.589744
1.5	0.1373	0.02567	0.01224	-0.0219	1	1	5.348656
2	0.1824	0.0265	0.01307	-0.0217	1	1	6.883019
2.5	0.2269	0.02738	0.01398	-0.0213	1	1	8.287071

3	0.2686	0.02846	0.01527	-0.0209	1	1	9.437807
3.5	0.3093	0.02967	0.01676	-0.0205	1	1	10.42467
4	0.3467	0.0312	0.01889	-0.0202	1	1	11.11218
4.5	0.5373	0.03761	0.02728	-0.0495	0.8681	1	14.28609
5.5	0.8659	0.02361	0.01589	-0.0514	0.5602	1	36.67514
6	0.8683	0.02547	0.01632	-0.0397	0.244	1	34.09109
7	0.8857	0.03683	0.02616	-0.0263	0.0609	1	24.04833
7.5	0.9376	0.04097	0.0307	-0.0246	0.0434	1	22.88504
8.5	1.0089	0.0552	0.04651	-0.0193	0.0372	1	18.27717
9	1.0053	0.06298	0.05502	-0.0147	0.0379	1	15.96221
9.5	0.9825	0.07016	0.06271	-0.01	0.0386	1	14.00371
10	0.9491	0.07824	0.07118	-0.0082	0.0392	1	12.13062
10.5	0.9128	0.08793	0.08116	-0.0103	0.0399	1	10.38098
11	0.8772	0.09981	0.09323	-0.0157	0.0406	1	8.788699
11.5	0.8511	0.11289	0.10648	-0.0224	0.0417	1	7.539197
12	0.8078	0.13768	0.13126	-0.0397	0.0555	1	5.867228
12.5	0.8075	0.14914	0.14265	-0.0437	0.0587	1	5.414376
14.5	0.8067	0.19897	0.19229	-0.0704	0.1405	1	4.05438

- 10˚
- Airfoil 1:

Table AVIII-19: Aerodynamic performance of Airfoil 1 of the uncoated blade at 10°

alpha	CL	CD	CDp	CM	Top_Xtr	Bot_Xtr	CL/CD
------	--------	---------	---------	--------	--------	--------	--------
-4.5	-0.3934	0.02924	0.01861	-0.0308	1	0.1361	-13.4542
-4	-0.3532	0.02634	0.0156	-0.0279	1	0.1469	-13.4093
-3.5	-0.3136	0.02398	0.01324	-0.0244	1	0.1711	-13.0776
-3	-0.2816	0.01966	0.01125	-0.0208	1	0.4676	-14.3235
-2	-0.0751	0.02188	0.01334	-0.0213	1	1	-3.43236
-1.5	-0.1064	0.02122	0.01266	-0.0129	1	1	-5.01414
-1	-0.1209	0.02056	0.01182	-0.0068	1	1	-5.88035
-0.5	-0.0931	0.02084	0.01175	-0.0066	1	1	-4.46737
0	-0.0549	0.0216	0.01215	-0.0074	1	1	-2.54167
0.5	-0.0157	0.02262	0.01288	-0.0082	1	1	-0.69408
1	0.0612	0.02465	0.0147	-0.0158	0.9818	1	2.482759
1.5	0.1418	0.02683	0.01676	-0.0236	0.96	1	5.285129
2	0.2172	0.02893	0.01883	-0.0301	0.9379	1	7.507777
2.5	0.2874	0.03097	0.02095	-0.0354	0.9144	1	9.279948
3	0.3582	0.03306	0.02319	-0.0403	0.8887	1	10.83485
3.5	0.4133	0.03478	0.02512	-0.0421	0.8558	1	11.88327
4.5	0.6969	0.02064	0.01183	-0.0348	0.4936	1	33.76453
5	0.7085	0.0251	0.01365	-0.0267	0.2327	1	28.22709

5.5	0.7601	0.02798	0.01628	-0.0256	0.1944	1	27.16583
6	0.8256	0.03138	0.01963	-0.0262	0.1781	1	26.30975
6.5	0.8833	0.03496	0.02366	-0.0259	0.1711	1	25.26602
7	0.9329	0.03937	0.02865	-0.0249	0.1682	1	23.69571
7.5	0.9715	0.04479	0.03484	-0.0232	0.1689	1	21.69011
8	0.9963	0.05151	0.04249	-0.0209	0.1726	1	19.34188
8.5	1.0083	0.0594	0.05108	-0.0186	0.1762	1	16.97475
9	1.0036	0.068	0.06023	-0.0165	0.1776	1	14.75882
9.5	1.0072	0.07894	0.07142	-0.0163	0.1808	1	12.75906
10	0.8981	0.09567	0.08837	-0.0199	0.2048	1	9.387478
11	0.7238	0.1411	0.13342	-0.0592	0.3547	1	5.129695
11.5	0.7348	0.14768	0.14001	-0.0599	0.3309	1	4.975623
12	0.7341	0.15383	0.14616	-0.0617	0.3121	1	4.772151
12.5	0.758	0.16328	0.15567	-0.0629	0.2992	1	4.642332
13	0.7877	0.17233	0.16485	-0.0634	0.2797	1	4.570881
13.5	0.7691	0.17547	0.16793	-0.0671	0.2641	1	4.383085
14	0.7868	0.18435	0.17686	-0.0688	0.2496	1	4.267969
14.5	0.8219	0.19747	0.1902	-0.069	0.2286	1	4.162151

- Airfoil 2

Table AVIII-20: Aerodynamic performance of Airfoil 2 of the uncoated blade at 10°

alpha	CL	CD	CDp	CM	Top_Xtr	Bot_Xtr	CL/CD
------	--------	---------	---------	--------	--------	--------	--------
-4.5	-0.3437	0.02418	0.014	-0.0387	1	0.1767	-14.2142
-4	-0.3076	0.02185	0.01182	-0.0354	1	0.221	-14.0778
-3.5	-0.2951	0.0199	0.01232	-0.0247	1	0.6441	-14.8291
-3	-0.2924	0.02118	0.01346	-0.0109	1	0.7547	-13.8055
-2.5	-0.3015	0.02115	0.0135	0.0052	1	0.8509	-14.2553
-1.5	-0.0982	0.02111	0.01238	-0.0133	1	1	-4.65182
-1	-0.1135	0.0204	0.01155	-0.0078	1	1	-5.56373
-0.5	-0.0805	0.02063	0.01147	-0.0094	1	1	-3.90208
0	-0.0355	0.02142	0.01191	-0.0123	1	1	-1.65733
0.5	0.0459	0.02319	0.01342	-0.0214	0.9823	1	1.979301
1	0.128	0.02511	0.01517	-0.03	0.9615	1	5.097571
1.5	0.2017	0.02697	0.01693	-0.0367	0.9404	1	7.47868
2	0.2769	0.02893	0.0189	-0.0431	0.917	1	9.571379
2.5	0.3468	0.03089	0.02099	-0.0483	0.8934	1	11.22693
3	0.4187	0.03293	0.02321	-0.0533	0.8685	1	12.71485
3.5	0.4772	0.03496	0.02546	-0.0559	0.8408	1	13.64989
4	0.5384	0.03679	0.02773	-0.058	0.8057	1	14.63441
5	0.7873	0.02199	0.01428	-0.045	0.5426	1	35.80264
5.5	0.7845	0.02687	0.01592	-0.0338	0.1922	1	29.19613

6	0.8424	0.03068	0.01965	-0.0326	0.1562	1	27.45763
6.5	0.91	0.03569	0.02472	-0.033	0.1442	1	25.49734
7	0.9593	0.04033	0.03017	-0.0317	0.1349	1	23.78626
7.5	1.0019	0.04608	0.03636	-0.0305	0.1274	1	21.74262
8	1.0302	0.05318	0.04446	-0.0281	0.129	1	19.37194
8.5	1.0273	0.06237	0.05483	-0.0252	0.1351	1	16.47106
9	1.0146	0.07273	0.06577	-0.0237	0.142	1	13.95023
9.5	0.9755	0.08306	0.07651	-0.0232	0.1504	1	11.74452
10	0.8699	0.10354	0.09694	-0.0362	0.1661	1	8.401584
11	0.781	0.14708	0.14013	-0.07	0.3115	1	5.310035
11.5	0.7709	0.15331	0.14629	-0.0727	0.2934	1	5.028374
12	0.7808	0.16162	0.15461	-0.0749	0.2795	1	4.831085
12.5	0.8396	0.17648	0.16978	-0.0737	0.2627	1	4.75748
13.5	0.8162	0.18513	0.17827	-0.0817	0.2341	1	4.408794
14	0.854	0.19839	0.19165	-0.0816	0.2152	1	4.304652
14.5	0.8468	0.20021	0.19343	-0.0858	0.1972	1	4.229559
15	0.8533	0.20784	0.20104	-0.0898	0.1881	1	4.105562

- Airfoil 3

Table AVIII-21: Aerodynamic performance of Airfoil 3 of the uncoated blade at 10°

alpha	CL	CD	CDp	CM	Top_Xtr	Bot_Xtr	CL/CD
------	--------	---------	---------	--------	--------	--------	--------
-5	-0.4159	0.02516	0.01517	-0.0327	1	0.1846	-16.5302
-4	-0.3851	0.02127	0.01386	-0.0123	1	0.6606	-18.1053
-3.5	-0.3786	0.0223	0.01475	0.0009	1	0.75	-16.9776
-3	-0.3809	0.02224	0.01467	0.0161	1	0.8439	-17.1268
-2.5	-0.2174	0.02301	0.01436	0.0017	1	0.9512	-9.44807
-2	-0.0698	0.02275	0.01347	-0.0196	1	0.9979	-3.06813
-1.5	-0.093	0.02228	0.01298	-0.013	1	1	-4.17415
-1	-0.1209	0.02147	0.01212	-0.0057	1	1	-5.63111
-0.5	-0.1031	0.02157	0.01196	-0.0049	1	1	-4.77979
0	-0.0379	0.0229	0.01296	-0.0116	0.9879	1	-1.65502
0.5	0.0426	0.02467	0.01449	-0.0204	0.9667	1	1.726794
1	0.1133	0.02638	0.01605	-0.0269	0.9474	1	4.29492
1.5	0.1766	0.02814	0.01774	-0.0317	0.9296	1	6.275764
2	0.2425	0.02998	0.01957	-0.0366	0.9087	1	8.088726
2.5	0.3046	0.03185	0.02151	-0.0405	0.8872	1	9.563579
3	0.3633	0.03384	0.02363	-0.0436	0.866	1	10.73582
3.5	0.4199	0.03588	0.02603	-0.0462	0.843	1	11.7029
4	0.4804	0.03777	0.02823	-0.0486	0.8155	1	12.71909
4.5	0.5426	0.03976	0.03063	-0.0509	0.7893	1	13.64688
5	0.76	0.02177	0.01365	-0.039	0.5106	1	34.91043

5.5	0.7479	0.02675	0.01557	-0.029	0.0992	1	27.95888
6.5	0.8096	0.03553	0.02446	-0.0208	0.0523	1	22.78638
7	0.8821	0.04134	0.0308	-0.0208	0.0495	1	21.33769
7.5	0.9254	0.04834	0.0386	-0.0187	0.0498	1	19.14357
8	0.9468	0.05601	0.04705	-0.0156	0.051	1	16.90412
8.5	0.9518	0.06442	0.05609	-0.0124	0.0525	1	14.77491
9	0.9496	0.07422	0.06637	-0.0102	0.0544	1	12.7944
9.5	0.9264	0.07851	0.07123	-0.0058	0.0568	1	11.79977
10	0.8703	0.08747	0.08059	-0.0071	0.0585	1	9.949697
10.5	0.8112	0.10278	0.09608	-0.0177	0.0612	1	7.892586
11	0.7808	0.12047	0.11371	-0.0292	0.0668	1	6.481282
11.5	0.7848	0.13188	0.12507	-0.032	0.0734	1	5.950864
13	0.795	0.17837	0.17156	-0.0545	0.1632	1	4.457028
13.5	0.7696	0.18261	0.17562	-0.0623	0.1543	1	4.214446
14	0.7871	0.19096	0.18398	-0.0642	0.1448	1	4.121806
15	0.8003	0.20569	0.1986	-0.0724	0.131	1	3.890807

- Airfoil 4

Table AVIII-22: Aerodynamic performance of Airfoil 4 of the uncoated blade at 10°

alpha	CL	CD	CDp	CM	Top_Xtr	Bot_Xtr	CL/CD
------	--------	---------	---------	--------	--------	--------	--------
-4	-0.3644	0.02359	0.01623	-0.0064	1	0.7361	-15.4472
-3.5	-0.3537	0.02332	0.01569	0.0035	1	0.8015	-15.1672
-3	-0.3431	0.0225	0.01465	0.0129	1	0.8686	-15.2489
-2.5	-0.2064	0.02282	0.01419	0.0006	1	0.9608	-9.0447
-2	-0.0861	0.02282	0.01366	-0.0167	1	1	-3.77301
-1.5	-0.1154	0.02209	0.01293	-0.0093	1	1	-5.22408
-1	-0.1081	0.02179	0.01234	-0.0075	1	1	-4.96099
-0.5	-0.0619	0.02251	0.01277	-0.0116	0.998	1	-2.74989
0	0.026	0.0244	0.01438	-0.0224	0.9783	1	1.065574
0.5	0.1046	0.02618	0.01599	-0.0308	0.9583	1	3.995416
1	0.1766	0.02795	0.01765	-0.0376	0.9384	1	6.318426
1.5	0.2437	0.02976	0.01944	-0.043	0.9186	1	8.188844
2	0.3095	0.03163	0.02139	-0.0479	0.8977	1	9.785014
2.5	0.3717	0.03361	0.02359	-0.0519	0.8769	1	11.05921
3	0.4329	0.03565	0.02587	-0.0554	0.8534	1	12.14306
3.5	0.492	0.03774	0.02828	-0.0582	0.8269	1	13.03657
4	0.5598	0.03977	0.03092	-0.0615	0.7975	1	14.07594
5	0.8208	0.02246	0.01518	-0.047	0.4554	1	36.54497
5.5	0.7985	0.02958	0.0191	-0.0358	0.1156	1	26.99459
6.5	0.9169	0.04009	0.02983	-0.0332	0.0686	1	22.87104
7	0.9675	0.04715	0.0377	-0.0316	0.0681	1	20.51962

7.5	0.9957	0.05532	0.04669	-0.0287	0.0698	1	17.99892
8	1.0104	0.06625	0.05819	-0.0264	0.0725	1	15.25132
8.5	0.9992	0.07096	0.06404	-0.0209	0.0779	1	14.08117
9	0.9521	0.07939	0.07303	-0.0176	0.0818	1	11.99269
9.5	0.9016	0.08994	0.08381	-0.0202	0.0844	1	10.02446
10	0.8583	0.10422	0.09815	-0.0286	0.0885	1	8.235463
13	0.8382	0.19196	0.18563	-0.0722	0.1857	1	4.366535
14	0.8602	0.21057	0.20418	-0.0776	0.1626	1	4.085102
15	0.8626	0.22003	0.21354	-0.0866	0.1424	1	3.920374

- Airfoil 5

Table AVIII-23: Aerodynamic performance of Airfoil 5 of the uncoated blade at 10°

alpha	CL	CD	CDp	CM	Top_Xtr	Bot_Xtr	CL/CD
------	--------	---------	---------	--------	--------	--------	--------
-5	-0.3341	0.02164	0.01216	-0.0402	1	0.2891	-15.439
-4.5	-0.3074	0.0201	0.0123	-0.0336	1	0.5123	-15.2935
-4	-0.3036	0.022	0.01434	-0.0196	1	0.6698	-13.8
-3.5	-0.2915	0.02224	0.01436	-0.01	1	0.7409	-13.107
-3	-0.2779	0.02173	0.01369	-0.0018	1	0.8062	-12.7888
-2.5	-0.2581	0.0209	0.013	0.0075	1	0.9164	-12.3493
-2	-0.1113	0.02175	0.01319	-0.0129	1	1	-5.11724
-1.5	-0.1165	0.02123	0.01248	-0.0099	1	1	-5.48752
-1	-0.0353	0.02252	0.0133	-0.0205	0.9821	1	-1.5675
-0.5	0.0526	0.0242	0.0146	-0.0312	0.9622	1	2.173554
0	0.1276	0.02571	0.01586	-0.0388	0.941	1	4.963049
0.5	0.1993	0.02734	0.01733	-0.0451	0.9202	1	7.289685
1	0.2684	0.02912	0.019	-0.0506	0.9019	1	9.217033
1.5	0.3234	0.03095	0.0208	-0.0536	0.8856	1	10.44911
2	0.371	0.03288	0.02276	-0.0552	0.8677	1	11.28345
2.5	0.43	0.03494	0.02501	-0.0581	0.8476	1	12.30681
3	0.4958	0.0372	0.02749	-0.062	0.8302	1	13.32796
3.5	0.5518	0.03923	0.02979	-0.0637	0.8051	1	14.06577
4	0.654	0.0384	0.02969	-0.0664	0.7476	1	17.03125
4.5	0.7725	0.03435	0.02661	-0.0659	0.6842	1	22.48908
5	0.8806	0.02667	0.01975	-0.0574	0.5909	1	33.01837
5.5	0.8947	0.02498	0.0167	-0.0423	0.3213	1	35.81665
6	0.9114	0.03142	0.02159	-0.0362	0.171	1	29.007
7	0.9913	0.04357	0.03365	-0.031	0.0716	1	22.75189
7.5	1.0292	0.05079	0.04153	-0.0287	0.0676	1	20.26383
8	1.047	0.05891	0.05052	-0.0253	0.0677	1	17.77287
8.5	1.0305	0.06762	0.06027	-0.0206	0.0704	1	15.23957
9	0.992	0.07615	0.06936	-0.017	0.0731	1	13.02692

9.5	0.9443	0.08587	0.07937	-0.0177	0.0754	1	10.99686
10	0.9001	0.09872	0.09234	-0.0241	0.0782	1	9.117707
10.5	0.8837	0.11232	0.10593	-0.0293	0.0819	1	7.867699
12	0.8286	0.1743	0.16773	-0.0668	0.2025	1	4.753873
12.5	0.8043	0.17741	0.17071	-0.0732	0.1877	1	4.533566
13	0.8661	0.1968	0.19025	-0.0694	0.1776	1	4.400915
13.5	0.8241	0.19446	0.1877	-0.0792	0.171	1	4.23789
14	0.836	0.20177	0.19501	-0.082	0.1595	1	4.143332
14.5	0.8879	0.22337	0.21678	-0.0795	0.1518	1	3.975019
15	0.8601	0.21883	0.21206	-0.0886	0.1474	1	3.930448

- Airfoil 6

Table AVIII-24: Aerodynamic performance of Airfoil 6 of the uncoated blade at 10°

alpha	CL	CD	CDp	CM	Top_Xtr	Bot_Xtr	CL/CD
------	--------	---------	---------	--------	--------	--------	--------
-5	-0.2848	0.02255	0.01451	-0.0249	1	0.646	-12.6297
-4.5	-0.2778	0.02294	0.01499	-0.0141	1	0.7382	-12.1099
-4	-0.2684	0.02238	0.01444	-0.0048	1	0.8173	-11.9929
-3.5	-0.2379	0.022	0.01409	0.0003	1	0.9149	-10.8136
-3	-0.1426	0.0224	0.01395	-0.0129	1	1	-6.36607
-2.5	-0.0788	0.02331	0.01435	-0.0215	0.9878	1	-3.38052
-2	0.015	0.02513	0.0156	-0.0338	0.9653	1	0.596896
-1.5	0.0923	0.02673	0.01682	-0.0419	0.9425	1	3.453049
-1	0.166	0.0284	0.01823	-0.0486	0.9199	1	5.84507
-0.5	0.2336	0.03011	0.01976	-0.0538	0.8985	1	7.75822
0	0.2958	0.03179	0.02133	-0.0575	0.8774	1	9.304813
0.5	0.3546	0.03352	0.02302	-0.0605	0.8565	1	10.57876
1	0.4126	0.03524	0.02479	-0.063	0.8342	1	11.70829
1.5	0.4689	0.03712	0.02693	-0.065	0.8127	1	12.632
2	0.5237	0.03922	0.02925	-0.0669	0.793	1	13.35288
2.5	0.5736	0.04132	0.03163	-0.0677	0.7689	1	13.8819
4.5	0.875	0.0282	0.01743	-0.0428	0.1149	1	31.02837
5	0.8863	0.0322	0.02116	-0.0372	0.0745	1	27.52484
5.5	0.8987	0.03566	0.02483	-0.0315	0.0667	1	25.20191
6	0.9372	0.03988	0.02955	-0.0278	0.0622	1	23.5005
6.5	1.0431	0.0477	0.03789	-0.031	0.0618	1	21.86792
7	1.081	0.05401	0.04508	-0.028	0.0642	1	20.01481
7.5	1.0854	0.06209	0.05425	-0.023	0.0681	1	17.48108
8	1.0581	0.07014	0.06304	-0.0176	0.0711	1	15.08554
8.5	1.017	0.07827	0.07162	-0.0145	0.073	1	12.99348
9	0.9683	0.08859	0.08225	-0.0167	0.0743	1	10.93013

9.5	0.9172	0.10259	0.09641	-0.0247	0.0757	1	8.940443
10	0.8826	0.11855	0.11238	-0.0339	0.0785	1	7.44496
10.5	0.8541	0.13748	0.13126	-0.0458	0.0857	1	6.21254
11	0.8385	0.15428	0.14791	-0.0546	0.0993	1	5.434924
12	0.8158	0.18552	0.17902	-0.0751	0.1863	1	4.39737
12.5	0.8244	0.1936	0.18707	-0.0784	0.18	1	4.258264
13	0.8479	0.20401	0.1975	-0.0797	0.1741	1	4.156169
13.5	0.8738	0.2189	0.21238	-0.0814	0.1705	1	3.991777
14	0.8558	0.2179	0.21125	-0.0887	0.1607	1	3.92749
14.5	0.8758	0.22706	0.22043	-0.0906	0.1526	1	3.85713
15	0.9139	0.24792	0.24134	-0.0903	0.148	1	3.68627

- **H-146**
    - -5°
    - Airfoil 1

Table AVIII-25: Aerodynamic performance of Airfoil 1 of the H-146 coated blade at -5°

alpha	CL	CD	CDp	CM	Top_Xtr	Bot_Xtr	CL/CD
------	--------	---------	---------	--------	--------	--------	--------
-5	-0.4497	0.02878	0.0191	-0.0366	1	0.1738	-15.6254
-4.5	-0.4101	0.026	0.01597	-0.0334	1	0.179	-15.7731
-4	-0.3712	0.024	0.01343	-0.0298	1	0.1921	-15.4667
-3.5	-0.3356	0.02168	0.01147	-0.0267	1	0.2398	-15.4797
-3	-0.3351	0.02076	0.01304	-0.0124	1	0.6848	-16.1416
-2.5	-0.3338	0.0216	0.0138	0.0018	1	0.7885	-15.4537
-2	-0.3301	0.02109	0.01333	0.0165	1	0.8993	-15.652
-1.5	-0.071	0.02234	0.01321	-0.0188	1	1	-3.17816
-1	-0.0944	0.02178	0.01262	-0.0114	1	1	-4.33425
-0.5	-0.1122	0.02104	0.01177	-0.0049	1	1	-5.3327
0	-0.0902	0.02112	0.01159	-0.0042	1	1	-4.27083
0.5	-0.0514	0.02182	0.01202	-0.0058	1	1	-2.35564
1	0.0176	0.02343	0.01341	-0.0127	0.9872	1	0.751174
1.5	0.0972	0.02542	0.01525	-0.021	0.9663	1	3.823761
2	0.1731	0.02743	0.0172	-0.0282	0.9446	1	6.310609
2.5	0.2456	0.02943	0.01926	-0.0343	0.9219	1	8.345226
3	0.3137	0.03146	0.02136	-0.0394	0.8991	1	9.971392
3.5	0.3827	0.03362	0.0237	-0.0443	0.8753	1	11.38311
4	0.5575	0.03077	0.02172	-0.0546	0.7813	1	18.1183
4.5	0.6707	0.02262	0.01398	-0.0451	0.6576	1	29.65075
5	0.6734	0.02342	0.01194	-0.03	0.2109	1	28.7532
5.5	0.705	0.02682	0.01484	-0.0268	0.1651	1	26.28635
6	0.759	0.02914	0.01761	-0.0256	0.1512	1	26.04667

6.5	0.8277	0.03228	0.02081	-0.0264	0.1448	1	25.64126
7	0.8895	0.03588	0.02487	-0.0267	0.1426	1	24.79097
7.5	0.9227	0.0376	0.02695	-0.025	0.1156	1	24.53989
8	0.9714	0.04218	0.03244	-0.0239	0.1125	1	23.02987
8.5	1.007	0.04883	0.04011	-0.0215	0.107	1	20.62257
10.5	0.9306	0.08229	0.07588	-0.0107	0.085	1	11.30879
11	0.907	0.09208	0.08572	-0.0134	0.0817	1	9.85013

- Airfoil 2

Table AVIII-26: Aerodynamic performance of Airfoil 2 of the H-146 coated blade at -5°

alpha	CL	CD	CDp	CM	Top_Xtr	Bot_Xtr	CL/CD
------	--------	---------	---------	--------	--------	--------	--------
-5	-0.3531	0.02006	0.01249	-0.0213	1	0.5724	-17.6022
-4.5	-0.3553	0.02191	0.01435	-0.0046	1	0.7451	-16.2163
-4	-0.3613	0.02208	0.01452	0.0121	1	0.8463	-16.3632
-3	-0.0932	0.02293	0.01384	-0.0163	1	1	-4.06454
-2.5	-0.1161	0.0221	0.01295	-0.009	1	1	-5.25339
-2	-0.1202	0.02147	0.01213	-0.0045	1	1	-5.59851
-1.5	-0.0874	0.0218	0.01207	-0.0053	1	1	-4.00917
-1	-0.0461	0.02261	0.0126	-0.0071	1	1	-2.03892
-0.5	0.0188	0.02422	0.01399	-0.013	0.9896	1	0.776218
0	0.0917	0.02617	0.01579	-0.02	0.9722	1	3.504012
0.5	0.1612	0.02817	0.01772	-0.0261	0.9532	1	5.7224
1	0.2263	0.03022	0.01979	-0.0311	0.9333	1	7.488418
1.5	0.2895	0.03239	0.02208	-0.0356	0.9126	1	8.937944
2	0.351	0.03464	0.02449	-0.0396	0.8897	1	10.13279
2.5	0.4096	0.03694	0.02703	-0.0428	0.8647	1	11.08825
3	0.4717	0.03934	0.02991	-0.0461	0.836	1	11.99034
4.5	0.7651	0.02913	0.01801	-0.0252	0.1595	1	26.26502
5	0.8439	0.03324	0.02221	-0.0263	0.1448	1	25.38809
5.5	0.9066	0.03806	0.02775	-0.026	0.1408	1	23.82028
6.5	0.9867	0.0512	0.04198	-0.0233	0.1281	1	19.27148
7	1.0124	0.05746	0.04925	-0.0202	0.1317	1	17.61921
7.5	0.9915	0.0665	0.05953	-0.0163	0.1416	1	14.90977
8	1.0003	0.07782	0.07121	-0.0158	0.1532	1	12.85402
8.5	0.8781	0.08912	0.08279	-0.0181	0.16	1	9.853007
10.5	0.7413	0.15298	0.14603	-0.0626	0.2989	1	4.845731
11	0.7498	0.1607	0.15376	-0.0645	0.2818	1	4.665837
11.5	0.7872	0.17278	0.16609	-0.0648	0.2661	1	4.556083
12	0.7978	0.17946	0.17283	-0.0663	0.2459	1	4.445559
12.5	0.7836	0.18335	0.17664	-0.0706	0.2306	1	4.273793

13	0.8008	0.19287	0.1862	-0.0725	0.217	1	4.152019
13.5	0.8103	0.19986	0.19319	-0.0748	0.1928	1	4.054338
14	0.834	0.21181	0.20518	-0.0757	0.173	1	3.937491
15	0.8434	0.22226	0.21552	-0.0838	0.1377	1	3.794655

- Airfoil 3

Table AVIII-27: Aerodynamic performance of Airfoil 3 of the H-146 coated blade at -5°

alpha	CL	CD	CDp	CM	Top_Xtr	Bot_Xtr	CL/CD
------	--------	---------	---------	--------	--------	--------	--------
-4.5	-0.3724	0.02316	0.01299	-0.0271	1	0.1911	-16.0794
-4	-0.3552	0.01991	0.01217	-0.0193	1	0.5918	-17.8403
-3.5	-0.3616	0.02172	0.01413	-0.0013	1	0.7545	-16.6483
-3	-0.3603	0.02164	0.01396	0.0129	1	0.8495	-16.6497
-2	-0.0867	0.02239	0.01312	-0.0171	1	1	-3.87226
-1.5	-0.1148	0.02161	0.01232	-0.0092	1	1	-5.31236
-1	-0.1172	0.02115	0.01164	-0.0051	1	1	-5.54137
-0.5	-0.0845	0.0216	0.01178	-0.0059	1	1	-3.91204
0	-0.0445	0.02247	0.01236	-0.0074	1	1	-1.98042
0.5	0.032	0.02434	0.01395	-0.0155	0.9836	1	1.314708
1	0.1082	0.02636	0.01581	-0.0229	0.9654	1	4.104704
1.5	0.1725	0.02818	0.01758	-0.028	0.9476	1	6.121363
2	0.2309	0.03008	0.0195	-0.0319	0.9303	1	7.676197
2.5	0.293	0.03215	0.02165	-0.0361	0.91	1	9.11353
3	0.3521	0.03433	0.02399	-0.0396	0.8894	1	10.25634
3.5	0.4101	0.03657	0.02665	-0.0427	0.8654	1	11.21411
4	0.4713	0.03886	0.02932	-0.0459	0.8373	1	12.12815
4.5	0.5741	0.03947	0.03065	-0.0508	0.7788	1	14.54522
5	0.7414	0.02332	0.01349	-0.0311	0.2661	1	31.79245
5.5	0.7632	0.02788	0.01704	-0.0262	0.1802	1	27.37446
6	0.8331	0.03158	0.02074	-0.0264	0.1567	1	26.38062
7	0.9517	0.04243	0.03346	-0.025	0.1418	1	22.42988
8	0.9788	0.05801	0.05043	-0.0166	0.0977	1	16.87295
8.5	0.9688	0.06701	0.06019	-0.0127	0.0979	1	14.45754
9	0.9396	0.07621	0.06986	-0.0099	0.1013	1	12.32909
9.5	0.9029	0.08579	0.07962	-0.0093	0.1054	1	10.52454
10	0.8867	0.09742	0.09136	-0.0117	0.1112	1	9.101827
10.5	0.7835	0.12276	0.11635	-0.0377	0.1669	1	6.382372
12	0.772	0.16388	0.15728	-0.0578	0.242	1	4.710764
12.5	0.7861	0.17364	0.16702	-0.0587	0.2201	1	4.527183
13.5	0.7779	0.18499	0.17821	-0.0657	0.1851	1	4.205092
14	0.7871	0.19278	0.18611	-0.0683	0.1666	1	4.082892

14.5	0.8065	0.2027	0.19601	-0.0696	0.1509	1	3.978786
15	0.8139	0.20853	0.2018	-0.0732	0.137	1	3.903036

- Airfoil 4

Table AVIII-28: Aerodynamic performance of Airfoil 3 of the H-146 coated blade at -5°

alpha	CL	CD	CDp	CM	Top_Xtr	Bot_Xtr	CL/CD
------	--------	---------	---------	--------	--------	--------	--------
-5	-0.3378	0.02285	0.01284	-0.0389	1	0.1305	-14.7834
-4.5	-0.3186	0.02074	0.01307	-0.0325	1	0.5812	-15.3616
-4	-0.3238	0.02318	0.01572	-0.0159	1	0.7107	-13.9689
-3.5	-0.3283	0.02334	0.01592	-0.0012	1	0.7902	-14.066
-3	-0.3125	0.02262	0.01492	0.006	1	0.8439	-13.8152
-2.5	-0.2892	0.02181	0.01392	0.0122	1	0.9058	-13.26
-2	-0.1391	0.02283	0.01387	-0.0066	1	0.9828	-6.09286
-1.5	-0.1155	0.02252	0.01336	-0.0081	1	1	-5.12877
-1	-0.0767	0.02286	0.01343	-0.0118	0.9908	1	-3.35521
-0.5	0.0098	0.02436	0.01461	-0.0231	0.9705	1	0.402299
0	0.0833	0.02577	0.01579	-0.0312	0.9518	1	3.232441
0.5	0.1561	0.02735	0.01722	-0.0387	0.9336	1	5.707495
1	0.2215	0.02906	0.01884	-0.0445	0.9175	1	7.622161
1.5	0.2861	0.03088	0.02066	-0.0497	0.9013	1	9.264896
2	0.3524	0.03304	0.02303	-0.055	0.8865	1	10.66586
2.5	0.3942	0.03499	0.02508	-0.0562	0.8707	1	11.26608
3	0.4473	0.03705	0.02732	-0.0588	0.8536	1	12.07287
4	0.7533	0.02139	0.01364	-0.053	0.5367	1	35.21739
4.5	0.7453	0.02666	0.01583	-0.043	0.1105	1	27.95574
5	0.7696	0.03049	0.01971	-0.0385	0.0914	1	25.24106
5.5	0.8368	0.03429	0.02388	-0.037	0.085	1	24.40362
6	0.9181	0.04113	0.03157	-0.0373	0.0846	1	22.32191
7.5	0.9929	0.0635	0.05595	-0.0288	0.0674	1	15.63622
8	1.0039	0.07209	0.06515	-0.0259	0.0721	1	13.92565
8.5	0.9584	0.07909	0.07297	-0.0217	0.077	1	12.11784
9	0.9095	0.08846	0.08262	-0.0226	0.0796	1	10.28148
9.5	0.8637	0.10146	0.09571	-0.0303	0.0829	1	8.512714
11	0.7756	0.15818	0.15196	-0.0737	0.2605	1	4.903275
12	0.7989	0.17344	0.16733	-0.0751	0.1953	1	4.606204
12.5	0.8265	0.18482	0.17871	-0.0752	0.1802	1	4.471919
13	0.8221	0.18981	0.18363	-0.0797	0.1651	1	4.331173
13.5	0.8457	0.20228	0.19608	-0.081	0.1578	1	4.180838
14	0.8387	0.20546	0.19917	-0.0868	0.1454	1	4.08206
14.5	0.886	0.2253	0.2191	-0.0842	0.1366	1	3.932534

15	0.8635	0.22215	0.21578	-0.0937	0.1314	1	3.887013

- Airfoil 5

Table AVIII-29: Aerodynamic performance of Airfoil 5 of the H-146 coated blade at -5°

alpha	CL	CD	CDp	CM	Top_Xtr	Bot_Xtr	CL/CD
------	--------	---------	---------	--------	--------	--------	--------
-5	-0.3682	0.02674	0.01581	-0.0325	1	0.074	-13.7696
-4.5	-0.3375	0.0246	0.01352	-0.0285	1	0.0837	-13.7195
-4	-0.3016	0.0209	0.01051	-0.0275	1	0.2283	-14.4306
-3.5	-0.2945	0.02124	0.01239	-0.0176	1	0.6383	-13.8653
-3	-0.2773	0.02176	0.01246	-0.0095	1	0.7172	-12.7436
-2.5	-0.2495	0.02188	0.01224	-0.0053	1	0.7662	-11.4031
-2	-0.2181	0.02187	0.01202	-0.0024	1	0.8142	-9.97257
-1.5	-0.1343	0.02192	0.0127	-0.0081	1	1	-6.12682
-1	-0.0735	0.02301	0.01356	-0.0147	0.9872	1	-3.19426
-0.5	0.0102	0.02468	0.01475	-0.0246	0.9671	1	0.41329
0	0.0793	0.0262	0.01603	-0.0311	0.9481	1	3.026718
0.5	0.146	0.02782	0.01747	-0.0367	0.9295	1	5.248023
1	0.2084	0.02959	0.0191	-0.0412	0.9138	1	7.04292
1.5	0.2774	0.03149	0.02094	-0.0464	0.8972	1	8.809146
2	0.3158	0.03317	0.02264	-0.0466	0.8821	1	9.520651
3	0.6484	0.02159	0.01199	-0.057	0.674	1	30.03242
3.5	0.6995	0.02213	0.013	-0.0554	0.6491	1	31.60868
4	0.732	0.02132	0.01208	-0.0474	0.5428	1	34.33396
5	0.756	0.02778	0.01553	-0.0337	0.0629	1	27.21382
5.5	0.7821	0.03053	0.01862	-0.0295	0.0561	1	25.61743
6	0.8066	0.03358	0.02201	-0.0249	0.0534	1	24.02025
6.5	0.8586	0.03712	0.02592	-0.0225	0.0526	1	23.13039
7	0.9378	0.04316	0.03323	-0.0232	0.0546	1	21.72845
7.5	0.9783	0.05022	0.04112	-0.021	0.0573	1	19.48029
8	0.9943	0.05799	0.04966	-0.0174	0.0599	1	17.14606
8.5	0.9941	0.06617	0.05844	-0.0138	0.0621	1	15.02342
9.5	0.957	0.08083	0.07401	-0.0068	0.0668	1	11.83966
10	0.9035	0.09018	0.08371	-0.0087	0.0682	1	10.01885
10.5	0.8393	0.1061	0.09977	-0.0197	0.0697	1	7.910462
11	0.7976	0.12642	0.11996	-0.0334	0.0755	1	6.309128
11.5	0.7994	0.13833	0.13181	-0.0368	0.0838	1	5.778934
12.5	0.7893	0.17326	0.1667	-0.0566	0.1778	1	4.555581
13	0.8181	0.18712	0.18059	-0.0572	0.1753	1	4.372061
13.5	0.7831	0.18768	0.18095	-0.0656	0.1642	1	4.172528
14	0.8018	0.1964	0.18971	-0.0672	0.1572	1	4.082485

14.5	0.8409	0.21331	0.20669	-0.0666	0.1527	1	3.94215
15	0.8149	0.21105	0.20426	-0.0751	0.1457	1	3.86117

- Airfoil 6

Table AVIII-30: Aerodynamic performance of Airfoil 6 of the H-146 coated blade at -5°

alpha	CL	CD	CDp	CM	Top_Xtr	Bot_Xtr	CL/CD
------	--------	---------	---------	--------	--------	--------	--------
-5	-0.4438	0.037	0.02856	-0.0525	1	0.0865	-11.9946
-4.5	-0.4064	0.03324	0.02406	-0.0504	1	0.1048	-12.2262
-4	-0.3644	0.02744	0.01791	-0.0478	1	0.1272	-13.2799
-2	-0.2676	0.02291	0.01542	-0.0189	1	0.6967	-11.6805
-1.5	-0.2447	0.02258	0.01475	-0.0133	1	0.7531	-10.837
-1	-0.2281	0.02195	0.01387	-0.0064	1	0.8145	-10.3918
-0.5	-0.2116	0.02131	0.01334	0.0015	1	0.9061	-9.92961
0	-0.1177	0.02168	0.01339	-0.0104	1	1	-5.42897
0.5	-0.0299	0.0229	0.01404	-0.0232	0.9781	1	-1.30568
1	0.0629	0.02442	0.01512	-0.0354	0.954	1	2.575758
1.5	0.1534	0.02606	0.01645	-0.046	0.9313	1	5.886416
2	0.228	0.02768	0.01786	-0.0532	0.9103	1	8.236994
2.5	0.2977	0.0294	0.01943	-0.059	0.8901	1	10.12585
3	0.3694	0.03117	0.02115	-0.0644	0.869	1	11.85114
3.5	0.4258	0.03293	0.02293	-0.067	0.8467	1	12.93046
4	0.4787	0.03484	0.02505	-0.0688	0.8243	1	13.73995
4.5	0.5381	0.03667	0.02706	-0.0711	0.8001	1	14.67412
5	0.6127	0.03803	0.02876	-0.0742	0.7724	1	16.11097
5.5	0.6548	0.03963	0.03067	-0.0727	0.7364	1	16.52284
6	0.8339	0.02584	0.01763	-0.065	0.6172	1	32.27167
6.5	0.8831	0.02439	0.01635	-0.0593	0.5494	1	36.20746
7	0.9194	0.02409	0.01628	-0.0536	0.4618	1	38.16521
7.5	0.9343	0.02591	0.01719	-0.0462	0.2458	1	36.05944
8	0.9298	0.03184	0.02179	-0.0401	0.1011	1	29.20226
8.5	0.946	0.03659	0.02647	-0.0349	0.0739	1	25.85406
9	1.0063	0.04128	0.03155	-0.033	0.0633	1	24.37742
9.5	1.0638	0.0483	0.03909	-0.032	0.0598	1	22.02484
10	1.0897	0.05636	0.04801	-0.0292	0.0599	1	19.33463
10.5	1.0861	0.06502	0.05756	-0.0252	0.0615	1	16.70409
11	1.0494	0.07326	0.06646	-0.0212	0.0634	1	14.32432
11.5	0.9992	0.08318	0.0768	-0.0219	0.065	1	12.0125
12	0.9427	0.09728	0.09115	-0.0298	0.067	1	9.690584
12.5	0.8958	0.11542	0.10933	-0.0416	0.0702	1	7.76122
13	0.8763	0.13177	0.12559	-0.0498	0.0739	1	6.650224

13.5	0.86	0.14863	0.14238	-0.0594	0.0826	1	5.78618
14	0.8424	0.16692	0.16053	-0.0702	0.1105	1	5.046729
15	0.8872	0.20184	0.19553	-0.078	0.1699	1	4.395561

- 0°:
    - Airfoil 1:

Table AVIII-31: Aerodynamic performance of Airfoil 1 of the H-146 coated blade at 0°

alpha	CL	CD	CDp	CM	Top_Xtr	Bot_Xtr	CL/CD
------	--------	---------	---------	--------	--------	--------	--------
-5	-0.4125	0.02605	0.01547	-0.0263	1	0.1645	-15.8349
-4.5	-0.3733	0.02382	0.01324	-0.0227	1	0.1865	-15.6717
-4	-0.3558	0.01997	0.01231	-0.0149	1	0.6006	-17.8167
-3.5	-0.361	0.02149	0.01392	0.0026	1	0.7771	-16.7985
-2.5	-0.079	0.02296	0.01393	-0.0204	1	1	-3.44077
-2	-0.1005	0.02235	0.01326	-0.0131	1	1	-4.49664
-1.5	-0.1212	0.0215	0.01231	-0.0058	1	1	-5.63721
-1	-0.1094	0.02132	0.01181	-0.0031	1	1	-5.13133
-0.5	-0.0749	0.02187	0.01206	-0.0036	1	1	-3.42478
0	-0.036	0.02278	0.01272	-0.0046	1	1	-1.58033
0.5	0.0347	0.02468	0.01442	-0.0113	0.9846	1	1.405997
1	0.1122	0.0269	0.01653	-0.0189	0.9634	1	4.171004
1.5	0.1846	0.02898	0.01859	-0.0252	0.9418	1	6.36991
2	0.2529	0.03106	0.02074	-0.0305	0.9195	1	8.142305
2.5	0.3195	0.03323	0.02303	-0.0352	0.8961	1	9.614806
3	0.3842	0.03543	0.02543	-0.0392	0.87	1	10.84392
3.5	0.4366	0.03741	0.02782	-0.0408	0.8385	1	11.67068
4	0.6856	0.02607	0.01776	-0.0458	0.6914	1	26.29843
4.5	0.7046	0.02246	0.01252	-0.0267	0.2908	1	31.37133
5	0.7281	0.02676	0.01564	-0.0219	0.2005	1	27.20852
5.5	0.7783	0.02974	0.01842	-0.0208	0.1605	1	26.17014
6	0.8475	0.03371	0.02248	-0.0214	0.1423	1	25.14091
6.5	0.9054	0.0386	0.02769	-0.0211	0.133	1	23.45596
7	0.952	0.04454	0.0343	-0.0198	0.1319	1	21.37405
7.5	0.9783	0.05098	0.04195	-0.0167	0.1364	1	19.18988
8	0.9849	0.0594	0.05136	-0.0137	0.144	1	16.58081
8.5	1.0046	0.06963	0.06198	-0.0129	0.1525	1	14.42769
9.5	0.7922	0.10333	0.09629	-0.0269	0.1867	1	7.666699
11.5	0.7235	0.15432	0.14704	-0.0585	0.2972	1	4.68831
12	0.7661	0.16661	0.15948	-0.0589	0.2855	1	4.598163
12.5	0.7628	0.17078	0.16367	-0.061	0.2667	1	4.466565
13	0.7574	0.17623	0.16908	-0.0644	0.252	1	4.297793

13.5	0.7877	0.18783	0.18081	-0.0652	0.2397	1	4.193686
14	0.7909	0.19294	0.18592	-0.0675	0.2157	1	4.099202
14.5	0.8202	0.20564	0.19898	-0.0679	0.1954	1	3.988524
15	0.8107	0.2067	0.19998	-0.0728	0.1794	1	3.922109

- Airfoil 2

Table AVIII-32: Aerodynamic performance of Airfoil 2 of the H-146 coated blade at 0°

alpha	CL	CD	CDp	CM	Top_Xtr	Bot_Xtr	CL/CD
------	--------	---------	---------	--------	--------	--------	--------
-5	-0.3681	0.02418	0.01416	-0.0393	1	0.1857	-15.2233
-4.5	-0.332	0.02215	0.0121	-0.0359	1	0.2114	-14.9887
-4	-0.3143	0.02017	0.0126	-0.0274	1	0.6125	-15.5825
-3.5	-0.3082	0.02185	0.01395	-0.014	1	0.7179	-14.1053
-3	-0.3032	0.02216	0.01414	-0.0018	1	0.7971	-13.6823
-2.5	-0.3039	0.02135	0.0133	0.0116	1	0.8842	-14.2342
-2	-0.1115	0.02208	0.01324	-0.0117	1	0.9895	-5.04982
-1.5	-0.1052	0.02148	0.01233	-0.01	1	1	-4.89758
-1	-0.1074	0.0209	0.01159	-0.0066	1	1	-5.13876
-0.5	-0.0677	0.02132	0.01172	-0.0095	1	1	-3.17542
0	0.0054	0.02274	0.01289	-0.0178	0.988	1	0.237467
0.5	0.0916	0.02468	0.01465	-0.0278	0.9693	1	3.711507
1	0.166	0.02648	0.01634	-0.0352	0.9503	1	6.268882
1.5	0.2363	0.02839	0.01821	-0.0414	0.931	1	8.323353
2	0.3064	0.03042	0.02027	-0.0471	0.9105	1	10.07232
2.5	0.3741	0.03247	0.02249	-0.052	0.8889	1	11.5214
3	0.4361	0.03454	0.02476	-0.0557	0.8659	1	12.62594
3.5	0.4895	0.03668	0.02716	-0.0578	0.8405	1	13.34515
4	0.5418	0.03893	0.0299	-0.0594	0.8119	1	13.91729
5	0.7672	0.02446	0.01423	-0.0371	0.2155	1	31.36549
5.25	0.7786	0.02675	0.0161	-0.035	0.1806	1	29.10654
5.5	0.7967	0.02854	0.01777	-0.0336	0.1586	1	27.91521
5.75	0.8185	0.0303	0.01944	-0.0328	0.1384	1	27.0132
6	0.8412	0.03175	0.02102	-0.0321	0.12	1	26.49449
6.75	0.915	0.03941	0.02926	-0.0299	0.0623	1	23.21746
7	0.9384	0.0433	0.03331	-0.0291	0.0541	1	21.67206
7.25	0.956	0.04941	0.03973	-0.0283	0.0507	1	19.34831
7.5	0.968	0.05299	0.04387	-0.0266	0.0494	1	18.2676
7.75	0.9755	0.05704	0.04843	-0.025	0.0488	1	17.10203
8	0.9786	0.06128	0.05309	-0.0234	0.0486	1	15.96932
8.25	0.9776	0.06559	0.05776	-0.022	0.0486	1	14.90471
8.5	0.9724	0.06994	0.06242	-0.0207	0.0488	1	13.90335

8.75	0.9635	0.07433	0.06706	-0.0197	0.0492	1	12.96246
9	0.9504	0.0786	0.07151	-0.0186	0.0495	1	12.0916
9.25	0.9362	0.08317	0.07621	-0.0182	0.05	1	11.25646
9.5	0.9211	0.08834	0.08148	-0.0188	0.0505	1	10.42676
10.5	0.8288	0.11709	0.11076	-0.04	0.0601	1	7.078316
10.75	0.8194	0.12537	0.11899	-0.0449	0.063	1	6.535854
11	0.8152	0.13222	0.12579	-0.0483	0.0656	1	6.165482
11.25	0.8148	0.13835	0.13188	-0.0507	0.068	1	5.889411
11.5	0.8222	0.14389	0.13742	-0.0507	0.071	1	5.714087
12.25	0.802	0.17077	0.16425	-0.0707	0.1539	1	4.696375
12.5	0.8047	0.17493	0.16839	-0.0726	0.1497	1	4.600126
12.75	0.8134	0.17947	0.17293	-0.0735	0.1452	1	4.532234
13	0.8447	0.18799	0.18154	-0.0704	0.1402	1	4.493324
13.5	0.826	0.19329	0.18665	-0.0788	0.1352	1	4.273372
13.75	0.8254	0.19613	0.18947	-0.0816	0.1292	1	4.208433
14	0.8332	0.20026	0.1936	-0.0828	0.1239	1	4.160591
14.25	0.8536	0.20712	0.2005	-0.0818	0.1192	1	4.121282
14.5	0.8754	0.21828	0.21168	-0.0805	0.1166	1	4.010445
14.75	0.8675	0.21884	0.21217	-0.0851	0.1158	1	3.964083
15	0.8584	0.21817	0.21142	-0.0898	0.1132	1	3.934546

- Airfoil 3

Table AVIII-33: Aerodynamic performance of Airfoil 3 of the H-146 coated blade at 0°

alpha	CL	CD	CDp	CM	Top_Xtr	Bot_Xtr	CL/CD
------	--------	---------	---------	--------	--------	--------	--------
-3.5	-0.3886	0.02275	0.01537	0.0105	1	0.8094	-17.0813
-3	-0.2977	0.02316	0.01519	0.0119	1	0.9339	-12.8541
-2.5	-0.1393	0.0233	0.01444	-0.0099	1	0.9768	-5.97854
-2	-0.0803	0.023	0.01367	-0.0168	1	1	-3.4913
-1	-0.1174	0.0218	0.01228	-0.0047	1	1	-5.38532
0	-0.003	0.0242	0.0141	-0.0153	0.9822	1	-0.12397
0.5	0.0708	0.02603	0.01572	-0.0227	0.9653	1	2.719939
1	0.1417	0.02786	0.01741	-0.0291	0.9462	1	5.086145
1.5	0.2107	0.02974	0.01923	-0.0348	0.927	1	7.084734
2	0.2661	0.03144	0.02099	-0.038	0.908	1	8.46374
2.5	0.3166	0.03335	0.02294	-0.0403	0.8905	1	9.493253
3	0.3777	0.03537	0.02509	-0.0438	0.8673	1	10.67854
3.5	0.441	0.03743	0.02739	-0.0472	0.842	1	11.78199
4	0.5048	0.03963	0.0302	-0.0504	0.8164	1	12.73782
4.5	0.6424	0.03697	0.02843	-0.0554	0.7409	1	17.37625
5.5	0.8091	0.02448	0.01533	-0.0328	0.2939	1	33.05147

6	0.8457	0.02858	0.01874	-0.0295	0.2175	1	29.59062
6.5	0.9167	0.03342	0.02356	-0.0302	0.1792	1	27.42968
7.5	0.9629	0.04553	0.03593	-0.0226	0.0672	1	21.14869
8	0.985	0.0532	0.04466	-0.0184	0.061	1	18.51504
8.5	0.9865	0.06123	0.05353	-0.0139	0.0598	1	16.11138
9	0.9674	0.06927	0.0622	-0.0095	0.0602	1	13.96564
9.5	0.9303	0.07709	0.07041	-0.0062	0.0616	1	12.06771
10	0.8878	0.08695	0.08052	-0.0081	0.0634	1	10.21047
10.5	0.8481	0.09956	0.09325	-0.0146	0.0656	1	8.518481
11	0.8236	0.11356	0.10722	-0.0218	0.0683	1	7.252554
12.5	0.7624	0.16867	0.1621	-0.0586	0.1962	1	4.520069
13	0.7726	0.17679	0.17017	-0.0603	0.1752	1	4.370157
13.5	0.8068	0.18965	0.18307	-0.0591	0.158	1	4.254152
14	0.7871	0.19214	0.18541	-0.0662	0.1464	1	4.096492
14.5	0.8345	0.20973	0.2031	-0.0634	0.1364	1	3.978925
15	0.8091	0.20862	0.20181	-0.0725	0.1307	1	3.878343

- Airfoil 4

Table AVIII-34: Aerodynamic performance of Airfoil 4 of the H-146 coated blade at 0°

alpha	CL	CD	CDp	CM	Top_Xtr	Bot_Xtr	CL/CD
------	--------	---------	---------	--------	--------	--------	--------
-4.5	-0.3369	0.02025	0.01238	-0.0317	1	0.5407	-16.637
-4	-0.3274	0.02236	0.01453	-0.0198	1	0.6567	-14.6422
-3.5	-0.3282	0.02335	0.01555	-0.0055	1	0.7455	-14.0557
-3	-0.339	0.02266	0.01491	0.0105	1	0.8379	-14.9603
-2.5	-0.3112	0.02177	0.0138	0.0172	1	0.9162	-14.2949
-2	-0.1887	0.02237	0.01347	0.0021	1	0.9642	-8.4354
-1.5	-0.1029	0.02268	0.01344	-0.0096	1	1	-4.53704
-1	-0.1037	0.02223	0.01287	-0.0068	0.9977	1	-4.66487
-0.5	-0.0236	0.02353	0.01388	-0.0172	0.9779	1	-1.00297
0	0.0519	0.02493	0.01502	-0.0259	0.9589	1	2.081829
0.5	0.1252	0.02646	0.0164	-0.0336	0.9403	1	4.73167
1	0.1933	0.0281	0.01797	-0.0398	0.9227	1	6.879004
1.5	0.2615	0.02997	0.01992	-0.0457	0.9059	1	8.725392
2	0.3342	0.0319	0.02189	-0.0518	0.8887	1	10.47649
2.5	0.384	0.0337	0.02378	-0.054	0.8703	1	11.39466
3.5	0.6419	0.03	0.02185	-0.0663	0.7468	1	21.39667
4.5	0.7539	0.02236	0.0135	-0.0434	0.2644	1	33.71646
5	0.7532	0.02882	0.01849	-0.0367	0.1003	1	26.13463
6	0.8648	0.0376	0.02761	-0.0326	0.064	1	23
6.5	0.9256	0.04439	0.03503	-0.0315	0.0629	1	20.85154

7	0.9596	0.0523	0.04404	-0.0282	0.0673	1	18.34799
7.5	0.9742	0.06102	0.05358	-0.0248	0.0724	1	15.96526
8	0.9887	0.0731	0.066	-0.0234	0.0785	1	13.52531
8.5	0.948	0.07782	0.07171	-0.0185	0.0846	1	12.18196
9	0.8974	0.08685	0.081	-0.0187	0.0876	1	10.33276
9.5	0.8486	0.09968	0.09391	-0.0263	0.0902	1	8.513242
10	0.8272	0.11536	0.10958	-0.0356	0.1041	1	7.170596
11.5	0.7915	0.1632	0.15714	-0.0658	0.2138	1	4.849877
12	0.7806	0.17005	0.16386	-0.0703	0.1995	1	4.590415
12.5	0.835	0.18643	0.18033	-0.0675	0.1885	1	4.478893
13	0.7988	0.18625	0.17996	-0.0758	0.1757	1	4.288859
13.5	0.8421	0.20232	0.19608	-0.0743	0.1657	1	4.162218
14	0.8191	0.20205	0.19566	-0.082	0.155	1	4.053947
14.5	0.8739	0.22329	0.21701	-0.0785	0.1439	1	3.913744
15	0.8461	0.21902	0.21255	-0.088	0.1395	1	3.863118

- Airfoil 5

Table AVIII-35: Aerodynamic performance of Airfoil 5 of the H-146 coated blade at 0°

alpha	CL	CD	CDp	CM	Top_Xtr	Bot_Xtr	CL/CD
------	--------	---------	---------	--------	--------	--------	--------
-5	-0.4048	0.0235	0.01381	-0.0281	1	0.2438	-17.2255
-4.5	-0.3678	0.02134	0.01184	-0.0252	1	0.2965	-17.2352
-4	-0.3638	0.02123	0.01349	-0.0123	1	0.6496	-17.1361
-3.5	-0.3623	0.02222	0.01437	0.0018	1	0.7602	-16.3051
-3	-0.3545	0.02178	0.01383	0.0133	1	0.8413	-16.2764
-2.5	-0.1099	0.02363	0.01443	-0.0147	1	0.9867	-4.65087
-2	-0.087	0.0234	0.01402	-0.0156	1	1	-3.71795
-1.5	-0.1164	0.02269	0.01329	-0.0077	1	1	-5.13001
-1	-0.1191	0.02226	0.01266	-0.0038	1	1	-5.3504
-0.5	-0.0674	0.02322	0.01329	-0.0084	0.9925	1	-2.90267
0	0.0092	0.02482	0.01461	-0.0168	0.9741	1	0.370669
0.5	0.0757	0.02643	0.01601	-0.0228	0.9587	1	2.86417
1	0.1392	0.02812	0.01757	-0.0279	0.9421	1	4.950213
1.5	0.1983	0.02993	0.01934	-0.032	0.9276	1	6.625459
2	0.2677	0.03209	0.02157	-0.0376	0.9123	1	8.342163
2.5	0.307	0.03384	0.02359	-0.0381	0.8967	1	9.072104
3	0.3576	0.03599	0.02593	-0.0403	0.8801	1	9.936093
3.5	0.4131	0.03829	0.02853	-0.0431	0.861	1	10.78872
4	0.4679	0.04045	0.03124	-0.0452	0.8346	1	11.56737
5	0.7105	0.02897	0.01775	-0.0257	0.0824	1	24.52537
5.5	0.7499	0.03321	0.02221	-0.0216	0.066	1	22.58055

6.5	0.8742	0.0459	0.03558	-0.021	0.0466	1	19.04575
7	0.9115	0.05137	0.04192	-0.0177	0.0487	1	17.74382
7.5	0.9245	0.0588	0.05053	-0.0126	0.0537	1	15.72279
8	0.9156	0.06714	0.05962	-0.0082	0.0579	1	13.63718
8.5	0.8937	0.0751	0.068	-0.0047	0.061	1	11.90013
9	0.8611	0.08349	0.07661	-0.0032	0.0632	1	10.31381
9.5	0.8372	0.09392	0.08713	-0.0052	0.0658	1	8.913969
10.5	0.7586	0.12372	0.11707	-0.0274	0.0768	1	6.131587
11.5	0.7526	0.15734	0.15065	-0.046	0.182	1	4.783272
12	0.7707	0.16955	0.16282	-0.0475	0.1784	1	4.545562
12.5	0.7486	0.17322	0.16635	-0.0539	0.1638	1	4.321672
13	0.7891	0.18704	0.18024	-0.0523	0.1571	1	4.218884
13.5	0.7653	0.19	0.18301	-0.0599	0.1508	1	4.027895
14	0.7749	0.19708	0.19006	-0.063	0.1406	1	3.931906
14.5	0.824	0.21708	0.21014	-0.0603	0.1335	1	3.795836
15	0.7989	0.21398	0.20687	-0.0692	0.1297	1	3.733526

- Airfoil 6

Table AVIII-36: Aerodynamic performance of Airfoil 6 of the H-146 coated blade at 0°

alpha	CL	CD	CDp	CM	Top_Xtr	Bot_Xtr	CL/CD
------	--------	---------	---------	--------	--------	--------	--------
-4.5	-0.4371	0.02988	0.01956	-0.0399	1	0.1266	-14.6285
-4	-0.3994	0.02777	0.01743	-0.0377	1	0.1798	-14.3824
-3.5	-0.3618	0.02643	0.01631	-0.0355	1	0.2226	-13.689
-3	-0.3207	0.02542	0.01518	-0.0336	1	0.2525	-12.6161
-2.5	-0.2808	0.02468	0.01455	-0.0318	1	0.2921	-11.3776
-2	-0.2397	0.02383	0.01378	-0.0299	1	0.3414	-10.0587
-1.5	-0.1993	0.02322	0.01387	-0.0274	1	0.4361	-8.58312
-1	-0.1769	0.0231	0.01456	-0.0195	1	0.6525	-7.65801
0	-0.0857	0.02211	0.01413	-0.0165	1	1	-3.87607
0.5	-0.0414	0.02301	0.01455	-0.0184	1	1	-1.79922
1	0.0003	0.02417	0.01533	-0.0194	1	1	0.012412
1.5	0.0398	0.02551	0.01636	-0.0198	1	1	1.560172
2	0.0938	0.0275	0.01813	-0.0231	0.9927	1	3.410909
2.5	0.1892	0.03065	0.02114	-0.0335	0.9612	1	6.17292
3	0.2653	0.03311	0.02359	-0.0399	0.9282	1	8.012685
3.5	0.3589	0.0354	0.02597	-0.0475	0.8813	1	10.13842
4	0.5134	0.03353	0.02446	-0.0568	0.7942	1	15.31166
4.5	0.6833	0.02367	0.01518	-0.0569	0.684	1	28.86777
5	0.7111	0.02362	0.01261	-0.0435	0.3175	1	30.10584
5.5	0.763	0.02706	0.01534	-0.0422	0.2439	1	28.1966

6	0.833	0.03021	0.01833	-0.0434	0.2212	1	27.57365
6.5	0.8904	0.03324	0.02147	-0.0432	0.2073	1	26.787
7	0.9436	0.03781	0.02617	-0.043	0.1981	1	24.95636
7.5	0.9853	0.04194	0.03094	-0.0412	0.1952	1	23.49309
8	1.0171	0.04694	0.03661	-0.0386	0.1933	1	21.66809
8.5	1.0367	0.05289	0.04328	-0.0355	0.1926	1	19.60106
9	1.0426	0.06014	0.05115	-0.0322	0.1937	1	17.33622
9.5	1.0311	0.06857	0.06007	-0.0288	0.1952	1	15.03719
10	1.0031	0.07832	0.07013	-0.0262	0.1969	1	12.80771
12	0.7212	0.14921	0.14105	-0.0675	0.3387	1	4.833456
13	0.75	0.16215	0.15402	-0.0694	0.299	1	4.625347
13.5	0.8275	0.17913	0.17124	-0.068	0.2886	1	4.61955
14	0.7724	0.17562	0.16751	-0.0731	0.2729	1	4.398132
14.5	0.8098	0.18525	0.17729	-0.0733	0.2618	1	4.37139
15	0.8209	0.19443	0.18647	-0.076	0.2559	1	4.222085

- 5°:
    - Airfoil 1:

Table AVIII-37: Aerodynamic performance of Airfoil 1 of the H-146 coated blade at 5°

alpha	CL	CD	CDp	CM	Top_Xtr	Bot_Xtr	CL/CD
------	--------	---------	---------	--------	--------	--------	--------
-5	-0.4024	0.0259	0.01498	-0.0205	1	0.1531	-15.5367
-4.5	-0.3641	0.0241	0.01304	-0.0171	1	0.1672	-15.1079
-4	-0.3321	0.02037	0.01076	-0.0144	1	0.3661	-16.3034
-3.5	-0.0928	0.02388	0.01492	-0.0232	1	0.9908	-3.8861
-3	-0.0736	0.02332	0.01417	-0.0227	1	1	-3.15609
-2.5	-0.0933	0.02283	0.01362	-0.0154	1	1	-4.08673
-2	-0.116	0.02208	0.0128	-0.0076	1	1	-5.25362
-1.5	-0.1219	0.02154	0.01207	-0.0021	1	1	-5.65924
-1	-0.0962	0.02187	0.01212	-0.001	1	1	-4.39872
-0.5	-0.0613	0.02264	0.01253	-0.0011	1	1	-2.7076
0	-0.0144	0.02389	0.01356	-0.0033	0.9955	1	-0.60276
0.5	0.0657	0.0262	0.01572	-0.0115	0.9762	1	2.507634
1	0.1389	0.02833	0.0178	-0.0182	0.9557	1	4.90293
1.5	0.2101	0.03047	0.01995	-0.0241	0.9334	1	6.895307
2	0.2736	0.03254	0.02212	-0.0284	0.9115	1	8.408113
2.5	0.336	0.03469	0.02456	-0.0322	0.8867	1	9.685788
3	0.3877	0.03671	0.02679	-0.0341	0.8582	1	10.56115
3.5	0.4725	0.03816	0.02869	-0.0385	0.8098	1	12.38208
4	0.7068	0.02216	0.01408	-0.0339	0.5988	1	31.89531
4.5	0.7051	0.02494	0.014	-0.0207	0.2344	1	28.27185

5	0.7528	0.02803	0.01673	-0.0188	0.1993	1	26.85694
5.5	0.8258	0.03116	0.02009	-0.0198	0.1859	1	26.50193
6	0.8821	0.03486	0.02397	-0.0197	0.1689	1	25.30407
6.5	0.9327	0.03929	0.02904	-0.0187	0.1623	1	23.73886
7	0.9738	0.04497	0.03546	-0.0169	0.1588	1	21.65444
7.5	0.9928	0.0524	0.0444	-0.0134	0.1605	1	18.94656
8	0.986	0.06146	0.05443	-0.0097	0.1646	1	16.04295
9	0.9099	0.08103	0.07472	-0.0054	0.171	1	11.22917
9.5	0.8887	0.09385	0.08763	-0.0078	0.1758	1	9.469366
10.5	0.7304	0.14544	0.13825	-0.0506	0.3533	1	5.022002
11.5	0.7327	0.15833	0.15119	-0.0526	0.3071	1	4.627676
12	0.7267	0.16341	0.15624	-0.0542	0.2802	1	4.447096
12.5	0.7447	0.17224	0.1651	-0.0539	0.238	1	4.323618
13.5	0.7901	0.19262	0.18548	-0.0535	0.1743	1	4.101859
14	0.77	0.19384	0.18659	-0.0599	0.1617	1	3.972348
14.5	0.798	0.20693	0.19999	-0.0605	0.1515	1	3.856377
15	0.7918	0.20936	0.20233	-0.0662	0.1396	1	3.782002

- Airfoil 2

Table AVIII-38: Aerodynamic performance of Airfoil 2 of the H-146 coated blade at 5°

alpha	CL	CD	CDp	CM	Top_Xtr	Bot_Xtr	CL/CD
------	--------	---------	---------	--------	--------	--------	--------
-4.5	-0.3548	0.02467	0.01412	-0.0367	1	0.1701	-14.3818
-3.5	-0.2925	0.01951	0.01164	-0.0278	1	0.5823	-14.9923
-3	-0.2985	0.02125	0.01346	-0.0105	1	0.7554	-14.0471
-2.5	-0.3066	0.02114	0.01339	0.0056	1	0.858	-14.5033
-2	-0.0832	0.02188	0.0131	-0.0201	1	1	-3.80256
-1.5	-0.1105	0.02117	0.01236	-0.0126	1	1	-5.21965
-1	-0.1174	0.02055	0.01157	-0.0081	1	1	-5.7129
-0.5	-0.0818	0.02088	0.01157	-0.0098	1	1	-3.91762
0	-0.0374	0.02169	0.01208	-0.0124	1	1	-1.7243
0.5	0.0467	0.02359	0.01368	-0.0219	0.982	1	1.979652
1	0.1251	0.02547	0.0154	-0.0298	0.9621	1	4.911661
1.5	0.197	0.02731	0.01718	-0.0361	0.9405	1	7.213475
2	0.2668	0.02926	0.01914	-0.0417	0.9182	1	9.11825
2.5	0.3335	0.03129	0.02127	-0.0464	0.8956	1	10.65836
3	0.3961	0.0334	0.02359	-0.0503	0.8718	1	11.85928
3.5	0.4544	0.03559	0.02602	-0.0532	0.8463	1	12.76763
4	0.5137	0.03783	0.02859	-0.0557	0.8172	1	13.57917
4.5	0.7291	0.02647	0.01864	-0.0545	0.673	1	27.54439
5.5	0.777	0.02782	0.01681	-0.0316	0.1804	1	27.92955

6	0.8369	0.03135	0.02032	-0.0308	0.1486	1	26.69537
6.5	0.9037	0.03609	0.02529	-0.031	0.1368	1	25.04018
7	0.9573	0.04325	0.03294	-0.0305	0.1329	1	22.1341
7.5	0.9899	0.04824	0.039	-0.0277	0.1265	1	20.52032
8	1.0133	0.05623	0.04785	-0.0254	0.1285	1	18.02063
8.5	1.0327	0.06742	0.05954	-0.0244	0.1334	1	15.31741
9	0.9762	0.07551	0.06885	-0.0214	0.1448	1	12.92809
10	0.8134	0.11419	0.1075	-0.0457	0.1943	1	7.123216
10.5	0.74	0.13821	0.13124	-0.0685	0.3361	1	5.354171
11	0.7519	0.14605	0.13908	-0.0696	0.3137	1	5.148237
11.5	0.8071	0.16029	0.15353	-0.0692	0.2989	1	5.035249
12	0.7945	0.16404	0.15723	-0.0717	0.2778	1	4.843331
12.5	0.7854	0.16953	0.16264	-0.0749	0.2595	1	4.632808
13	0.7964	0.1778	0.17091	-0.0772	0.2448	1	4.47919
13.5	0.8263	0.18907	0.18225	-0.0776	0.2259	1	4.370339
14	0.8636	0.20238	0.19567	-0.077	0.2036	1	4.26722
14.5	0.8308	0.19965	0.19278	-0.0846	0.1913	1	4.161282
15	0.8735	0.21652	0.20978	-0.0838	0.1793	1	4.034269

- Airfoil 3

Table AVIII-39: Aerodynamic performance of Airfoil 3 of the H-146 coated blade at 5°

alpha	CL	CD	CDp	CM	Top_Xtr	Bot_Xtr	CL/CD
------	--------	---------	---------	--------	--------	--------	--------
-5	-0.4268	0.02707	0.01659	-0.0322	1	0.1613	-15.7665
-4.5	-0.387	0.0252	0.01422	-0.0288	1	0.1636	-15.3571
-4	-0.3521	0.02348	0.01252	-0.0253	1	0.1726	-14.9957
-3.5	-0.3157	0.02196	0.011	-0.0229	1	0.2006	-14.3761
-3	-0.3023	0.0203	0.01174	-0.0138	1	0.6569	-14.8916
-2.5	-0.305	0.02131	0.01291	0.0015	1	0.7872	-14.3125
-2	-0.2953	0.02085	0.01241	0.0126	1	0.8836	-14.1631
-1.5	-0.0924	0.02232	0.01303	-0.0133	1	1	-4.13978
-1	-0.1183	0.0215	0.01215	-0.0059	1	1	-5.50233
-0.5	-0.1039	0.02147	0.01185	-0.0043	1	1	-4.83931
0	-0.0674	0.02215	0.01225	-0.0057	1	1	-3.04289
0.5	0.0167	0.0241	0.01391	-0.0153	0.9808	1	0.692946
1	0.0934	0.02603	0.01565	-0.0231	0.9627	1	3.588167
1.5	0.1598	0.02778	0.01732	-0.0286	0.944	1	5.75234
2	0.2219	0.02959	0.01911	-0.033	0.9247	1	7.499155
2.5	0.2827	0.0315	0.02107	-0.0369	0.9042	1	8.974603
3	0.3437	0.03351	0.02321	-0.0406	0.8821	1	10.25664
3.5	0.4007	0.03565	0.02556	-0.0435	0.8598	1	11.23983

4	0.4557	0.03795	0.02839	-0.046	0.8367	1	12.00791
6	0.7941	0.02918	0.01876	-0.025	0.1717	1	27.21385
6.5	0.8739	0.03434	0.02431	-0.0256	0.1486	1	25.44846
8	0.9512	0.05476	0.04622	-0.0158	0.0629	1	17.37034
8.5	0.9535	0.06296	0.05521	-0.012	0.0639	1	15.14454
9	0.9384	0.07137	0.06418	-0.0087	0.0654	1	13.14838
9.5	0.9099	0.07954	0.07266	-0.0061	0.0672	1	11.43953
10	0.8782	0.0892	0.0825	-0.0069	0.069	1	9.845291
11.5	0.7469	0.15134	0.14475	-0.0533	0.2441	1	4.935245
12	0.7508	0.15896	0.1523	-0.0549	0.2207	1	4.723201
12.5	0.7544	0.16612	0.15939	-0.0569	0.1959	1	4.541295
13	0.7689	0.17501	0.16825	-0.0581	0.1767	1	4.393463
13.5	0.7818	0.18277	0.176	-0.0601	0.1617	1	4.277507
14	0.7843	0.19094	0.18408	-0.064	0.1544	1	4.107573
14.5	0.7946	0.1979	0.19102	-0.0669	0.1411	1	4.015159
15	0.8191	0.21092	0.20403	-0.0681	0.135	1	3.883463

- Airfoil 4

Table AVIII-40: Aerodynamic performance of Airfoil 4 of the H-146 coated blade at 5°

alpha	CL	CD	CDp	CM	Top_Xtr	Bot_Xtr	CL/CD
------	--------	---------	---------	--------	--------	--------	--------
-5	-0.3709	0.02276	0.01283	-0.0397	1	0.2296	-16.2961
-4	-0.3517	0.02372	0.01614	-0.015	1	0.6756	-14.8272
-3.5	-0.3407	0.02418	0.01637	-0.0046	1	0.7399	-14.0902
-3	-0.3376	0.02378	0.01587	0.0071	1	0.8093	-14.1968
-2.5	-0.3363	0.02248	0.01456	0.0197	1	0.8927	-14.96
-2	-0.2429	0.02255	0.01392	0.0112	1	0.947	-10.7716
-1.5	-0.1318	0.023	0.01396	-0.0042	1	0.9816	-5.73043
-1	-0.1092	0.02266	0.01348	-0.0056	1	1	-4.81906
-0.5	-0.0658	0.02315	0.01374	-0.0102	0.9904	1	-2.84233
0	0.0197	0.02472	0.01504	-0.0212	0.969	1	0.796926
0.5	0.101	0.02646	0.0166	-0.0306	0.9505	1	3.817082
1	0.1747	0.02815	0.01819	-0.038	0.9311	1	6.206039
1.5	0.2417	0.0299	0.01995	-0.0438	0.9131	1	8.083612
2	0.301	0.03167	0.02173	-0.0479	0.8936	1	9.504263
2.5	0.3563	0.0336	0.02375	-0.0512	0.8748	1	10.60417
3	0.4122	0.0357	0.02618	-0.0543	0.8551	1	11.54622
3.5	0.4722	0.03777	0.02851	-0.0574	0.8318	1	12.50199
4	0.5325	0.03985	0.03097	-0.06	0.8072	1	13.36261
6	0.8362	0.03664	0.026	-0.0322	0.0491	1	22.82205
6.5	0.9046	0.04287	0.03277	-0.0319	0.0491	1	21.101

7	0.945	0.05006	0.04084	-0.0294	0.0516	1	18.87735
7.5	0.9652	0.05793	0.04952	-0.0262	0.0545	1	16.66149
8	0.9694	0.06637	0.05858	-0.0231	0.0574	1	14.606
8.5	0.9642	0.07656	0.06914	-0.021	0.0602	1	12.59404
10	0.8321	0.10663	0.10029	-0.0306	0.069	1	7.80362
10.5	0.8081	0.12329	0.11689	-0.041	0.0763	1	6.554465
12.5	0.8307	0.18203	0.17559	-0.0664	0.1717	1	4.563533
13	0.7981	0.18454	0.1779	-0.0752	0.1602	1	4.324808
13.5	0.8333	0.19624	0.18965	-0.0746	0.1505	1	4.246331
14	0.8238	0.20172	0.19499	-0.0809	0.1449	1	4.083879
14.5	0.8324	0.20815	0.20138	-0.0847	0.1338	1	3.999039
15	0.8783	0.2274	0.2207	-0.0824	0.1265	1	3.862357

- Airfoil 5

Table AVIII-41: Aerodynamic performance of Airfoil 5 of the H-146 coated blade at 5°

alpha	CL	CD	CDp	CM	Top_Xtr	Bot_Xtr	CL/CD
------	--------	---------	---------	--------	--------	--------	--------
-4	-0.3194	0.02189	0.01432	-0.0183	1	0.6237	-14.5911
-3.5	-0.3069	0.02247	0.01473	-0.0081	1	0.7187	-13.6582
-3	-0.2862	0.02214	0.01413	-0.0015	1	0.7849	-12.9268
-2.5	-0.2635	0.0214	0.01346	0.0058	1	0.8786	-12.3131
-2	-0.1292	0.02233	0.01385	-0.0113	1	1	-5.78594
-1.5	-0.1214	0.02211	0.01329	-0.0099	1	1	-5.49073
-1	-0.0448	0.02358	0.01414	-0.0193	0.9843	1	-1.89992
-0.5	0.0401	0.02532	0.01547	-0.0291	0.9613	1	1.583728
0	0.1132	0.02703	0.01689	-0.036	0.9411	1	4.187939
0.5	0.1767	0.02875	0.01845	-0.0409	0.9225	1	6.146087
1	0.2422	0.03055	0.0201	-0.0455	0.9012	1	7.927987
1.5	0.3012	0.03241	0.02192	-0.0489	0.882	1	9.293428
2	0.3596	0.03442	0.02396	-0.052	0.8636	1	10.44741
2.5	0.42	0.03648	0.02627	-0.0551	0.8437	1	11.51316
3	0.4701	0.03831	0.02827	-0.0561	0.8165	1	12.27095
3.5	0.5276	0.04008	0.0303	-0.0577	0.7867	1	13.16367
4	0.605	0.04106	0.03171	-0.0601	0.7492	1	14.73453
4.5	0.6989	0.04007	0.03167	-0.0615	0.7009	1	17.44198
5	0.8438	0.03198	0.02468	-0.0591	0.6294	1	26.38524
5.5	0.9097	0.02509	0.01801	-0.0471	0.4993	1	36.25747
6	0.8873	0.02784	0.01848	-0.0335	0.1846	1	31.87141
6.5	0.8728	0.03436	0.02382	-0.0249	0.0813	1	25.40163
7	0.9053	0.03875	0.02834	-0.0208	0.0548	1	23.36258
7.5	0.9647	0.04507	0.03479	-0.0203	0.042	1	21.40448

8	1.0065	0.05285	0.04364	-0.0183	0.0414	1	19.04447
8.5	1.0158	0.06119	0.05272	-0.0146	0.0417	1	16.60075
9	1.0063	0.06936	0.06153	-0.0106	0.0424	1	14.50836
9.5	0.9841	0.07512	0.06776	-0.0066	0.0433	1	13.10037
10	0.9473	0.08298	0.0761	-0.0065	0.0444	1	11.416
10.5	0.8976	0.0951	0.0886	-0.0126	0.0459	1	9.438486
11	0.8379	0.11491	0.10857	-0.0267	0.0489	1	7.291794
11.5	0.8117	0.13355	0.12687	-0.0373	0.0543	1	6.077873
12	0.8056	0.14643	0.13965	-0.0429	0.0578	1	5.501605
12.5	0.8093	0.15757	0.15074	-0.0463	0.0609	1	5.13613
14	0.4515	0.09201	0.08722	-0.0424	0.173	1	4.907075
14.5	0.4561	0.09835	0.09349	-0.0476	0.163	1	4.637519
15	0.4993	0.11328	0.10841	-0.047	0.1517	1	4.407662

- Airfoil 6

Table AVIII-42: Aerodynamic performance of Airfoil 6 of the H-146 coated blade at 5°

alpha	CL	CD	CDp	CM	Top_Xtr	Bot_Xtr	CL/CD
------	--------	---------	---------	--------	--------	--------	--------
-5	-0.3852	0.03171	0.0225	-0.0475	1	0.084	-12.1476
-4.5	-0.3417	0.02724	0.01751	-0.044	1	0.0944	-12.5441
-2.5	-0.2682	0.02261	0.01533	-0.0103	1	0.7649	-11.862
-2	-0.2484	0.02216	0.0146	-0.0042	1	0.8177	-11.2094
-1.5	-0.2334	0.02177	0.01418	0.0038	1	0.8996	-10.7212
-1	-0.1213	0.02236	0.01423	-0.0101	1	1	-5.42487
-0.5	-0.0539	0.02313	0.01442	-0.0197	0.982	1	-2.33031
0	0.0341	0.02451	0.01535	-0.0314	0.9601	1	1.391269
0.5	0.1174	0.02604	0.0165	-0.0411	0.9379	1	4.508449
1	0.194	0.02759	0.01777	-0.0487	0.9142	1	7.031533
1.5	0.2653	0.02924	0.01924	-0.0546	0.8921	1	9.073187
2	0.3307	0.0311	0.02101	-0.0593	0.8741	1	10.63344
2.5	0.3953	0.03299	0.0229	-0.0634	0.8549	1	11.98242
3	0.4592	0.03483	0.0248	-0.0669	0.8332	1	13.18404
3.5	0.5145	0.03676	0.02686	-0.0688	0.8105	1	13.99619
4	0.5603	0.0387	0.02915	-0.0689	0.7821	1	14.47804
4.5	0.6305	0.03971	0.03054	-0.0706	0.7462	1	15.87761
5	0.724	0.03873	0.03016	-0.0719	0.701	1	18.69352
5.5	0.8566	0.03051	0.02286	-0.067	0.6285	1	28.07604
6	0.9197	0.02781	0.02065	-0.0611	0.5632	1	33.07084
6.5	0.9524	0.02486	0.01744	-0.0515	0.4355	1	38.31054
7	0.959	0.02704	0.01794	-0.0439	0.2361	1	35.46598
7.5	0.9717	0.03091	0.02128	-0.0394	0.1526	1	31.43643

8	0.9832	0.03527	0.02563	-0.0345	0.1065	1	27.87638
8.5	1.0063	0.04048	0.03111	-0.03	0.0693	1	24.85919
9	1.0693	0.04795	0.03884	-0.0294	0.0561	1	22.30031
9.5	1.096	0.05592	0.04772	-0.0266	0.0539	1	19.59943
10	1.091	0.06404	0.0566	-0.0228	0.0538	1	17.03623
10.5	1.0636	0.07194	0.06504	-0.0193	0.0541	1	14.78454
11	1.0255	0.08133	0.07485	-0.0195	0.0548	1	12.60912
11.5	0.9832	0.09313	0.08695	-0.0243	0.0557	1	10.55729
12	0.9427	0.10771	0.10168	-0.0322	0.0569	1	8.752205
12.5	0.9117	0.12365	0.11775	-0.0418	0.0587	1	7.373231
13.5	0.8578	0.16392	0.15772	-0.0663	0.073	1	5.233041
15	0.8896	0.21219	0.20598	-0.083	0.1466	1	4.192469

- 10˚
    - Airfoil 1

Table AVIII-43: Aerodynamic performance of Airfoil 1 of the H-146 coated blade at 10°

alpha	CL	CD	CDp	CM	Top_Xtr	Bot_Xtr	CL/CD
------	--------	----------	----------	--------	--------	--------	--------
-5	-0.4226	0.02694	0.01628	-0.0297	1	0.1576	-15.6867
-4.5	-0.3832	0.0244	0.0138	-0.0262	1	0.1757	-15.7049
-4	-0.3461	0.02173	0.01156	-0.0235	1	0.2401	-15.9273
-3.5	-0.3571	0.02131	0.01379	-0.0052	1	0.7355	-16.7574
-3	-0.354	0.02157	0.0139	0.0091	1	0.8315	-16.4117
-2.5	-0.0606	0.02281	0.01368	-0.0251	1	1	-2.65673
-2	-0.0817	0.02243	0.01326	-0.0177	1	1	-3.64244
-1.5	-0.1045	0.02179	0.01257	-0.0102	1	1	-4.79578
-1	-0.116	0.02115	0.0118	-0.0042	1	1	-5.48463
-0.5	-0.0893	0.02138	0.01175	-0.004	1	1	-4.1768
0	-0.0504	0.02213	0.01221	-0.0053	1	1	-2.27745
0.5	0.0044	0.02353	0.01338	-0.0093	0.9943	1	0.186995
1	0.0824	0.02556	0.01526	-0.0173	0.9736	1	3.223787
1.5	0.157	0.02762	0.01726	-0.0243	0.9518	1	5.684287
2	0.2248	0.02959	0.01923	-0.0298	0.9303	1	7.597161
2.5	0.29	0.03166	0.02138	-0.0345	0.9083	1	9.159823
3	0.352	0.03379	0.02373	-0.0384	0.8847	1	10.41728
3.5	0.4161	0.03599	0.02618	-0.0422	0.8575	1	11.56154
4	0.492	0.03804	0.0287	-0.0467	0.8238	1	12.93375
5	0.7261	0.02315	0.01296	-0.0276	0.2703	1	31.36501
5.5	0.7509	0.0276	0.01627	-0.0233	0.187	1	27.20652
6.5	0.8853	0.03462	0.02375	-0.024	0.1595	1	25.57192
7	0.9409	0.03938	0.02926	-0.0234	0.1595	1	23.89284

7.5	0.9807	0.0442	0.03517	-0.0215	0.1519	1	22.18778
8.5	1.0126	0.05389	0.04563	-0.015	0.0897	1	18.79013
9	1.0165	0.06206	0.05433	-0.0114	0.0786	1	16.37931
9.5	1.0045	0.07202	0.06475	-0.0086	0.0761	1	13.94751
10	0.9706	0.08049	0.07366	-0.0055	0.0762	1	12.05864
10.5	0.8745	0.09348	0.08717	-0.0126	0.0882	1	9.354942
11	0.8404	0.10908	0.10275	-0.0214	0.0932	1	7.704437
11.5	0.8258	0.12433	0.11793	-0.0281	0.0957	1	6.642001
13.5	0.7778	0.18081	0.17392	-0.0634	0.1741	1	4.301753
14	0.8077	0.19394	0.18724	-0.0635	0.1633	1	4.16469
14.5	0.7964	0.19705	0.19025	-0.0694	0.1508	1	4.041614
15	0.839	0.2145	0.20778	-0.0677	0.1415	1	3.911422

- Airfoil 2

Table AVIII-44: Aerodynamic performance of Airfoil 2 of the H-146 coated blade at 10°

alpha	CL	CD	CDp	CM	Top_Xtr	Bot_Xtr	CL/CD
------	--------	---------	---------	--------	--------	--------	--------
-5	-0.4266	0.02904	0.01881	-0.0319	1	0.1278	-14.6901
-4.5	-0.3853	0.02617	0.01568	-0.0283	1	0.1417	-14.723
-4	-0.3483	0.02363	0.01326	-0.0249	1	0.1778	-14.7397
-3.5	-0.3307	0.02023	0.01266	-0.0165	1	0.6261	-16.347
-3	-0.3436	0.02168	0.01424	0.0033	1	0.7966	-15.8487
-1.5	-0.1114	0.02206	0.01303	-0.0102	1	1	-5.04986
-1	-0.1219	0.02136	0.01216	-0.0045	1	1	-5.70693
-0.5	-0.0939	0.02159	0.01207	-0.0044	1	1	-4.34924
0	-0.0546	0.02234	0.01248	-0.0058	1	1	-2.44405
0.5	0.0075	0.02388	0.01376	-0.0111	0.9908	1	0.31407
1	0.0816	0.02581	0.01551	-0.0183	0.9725	1	3.161565
1.5	0.151	0.02777	0.01738	-0.0243	0.9532	1	5.437523
2	0.2189	0.02987	0.01946	-0.0298	0.933	1	7.328423
2.5	0.2846	0.03201	0.02172	-0.0347	0.9114	1	8.890972
3	0.3454	0.03415	0.024	-0.0384	0.8878	1	10.1142
3.5	0.4034	0.03637	0.02645	-0.0414	0.8624	1	11.09156
4	0.4634	0.03868	0.02907	-0.0444	0.8334	1	11.98035
4.5	0.5431	0.04072	0.03174	-0.0486	0.7953	1	13.33743
5.5	0.7514	0.0286	0.0172	-0.024	0.1662	1	26.27273
6	0.8248	0.03226	0.02088	-0.0246	0.1464	1	25.56727
6.5	0.8848	0.03657	0.02567	-0.0245	0.133	1	24.1947
7	0.9358	0.04188	0.03168	-0.0233	0.1308	1	22.34479
7.5	0.9716	0.04834	0.03905	-0.0211	0.133	1	20.0993
8	0.9933	0.05618	0.04771	-0.0187	0.138	1	17.68067

8.5	1.0073	0.06569	0.05774	-0.0169	0.1421	1	15.33415
9	0.9539	0.07432	0.06741	-0.0135	0.154	1	12.83504
9.5	0.9182	0.08597	0.0792	-0.0138	0.1641	1	10.68047
10.5	0.7189	0.13632	0.12909	-0.0573	0.341	1	5.273621
11	0.7183	0.14367	0.1364	-0.0592	0.3251	1	4.999652
11.5	0.7773	0.15776	0.15072	-0.059	0.3112	1	4.927104
13	0.7648	0.17311	0.16596	-0.0655	0.2488	1	4.418
13.5	0.7931	0.18427	0.1772	-0.0665	0.2368	1	4.30401
14	0.7977	0.18912	0.18208	-0.0691	0.2192	1	4.217957
14.5	0.802	0.19622	0.18915	-0.0727	0.2091	1	4.087249
15	0.8285	0.2059	0.19902	-0.0735	0.1935	1	4.023798

- Airfoil 3

Table AVIII-45: Aerodynamic performance of Airfoil 3 of the H-146 coated blade at 10°

alpha	CL	CD	CDp	CM	Top_Xtr	Bot_Xtr	CL/CD
------	--------	---------	---------	--------	--------	--------	--------
-4	-0.3445	0.02498	0.01402	-0.0242	1	0.0605	-13.791
-3.5	-0.3093	0.02106	0.01084	-0.0227	1	0.1939	-14.6866
-3	-0.3166	0.02122	0.01319	-0.0072	1	0.7129	-14.9199
-2.5	-0.2923	0.02131	0.01281	-0.0005	1	0.7704	-13.7166
-2	-0.2767	0.02057	0.01224	0.0117	1	0.9082	-13.4516
-1.5	-0.0997	0.022	0.01275	-0.0118	1	1	-4.53182
-1	-0.1194	0.02134	0.01196	-0.0054	1	1	-5.59513
-0.5	-0.0962	0.02162	0.01193	-0.005	1	1	-4.44958
0	-0.0347	0.0229	0.01293	-0.0108	0.9899	1	-1.51528
0.5	0.0501	0.02484	0.01461	-0.0203	0.97	1	2.016908
1	0.1176	0.0265	0.01611	-0.0264	0.9511	1	4.437736
1.5	0.1842	0.02829	0.01783	-0.0318	0.9315	1	6.511135
2	0.2502	0.03022	0.0197	-0.0369	0.9121	1	8.279285
2.5	0.3162	0.03223	0.02176	-0.0416	0.8919	1	9.810735
3	0.381	0.0343	0.02398	-0.0459	0.8711	1	11.10787
3.5	0.4375	0.03636	0.02627	-0.0485	0.8478	1	12.03245
4	0.4851	0.03856	0.02919	-0.0495	0.8223	1	12.58039
5	0.7693	0.02586	0.01902	-0.0479	0.639	1	29.74865
5.5	0.7914	0.02278	0.01481	-0.0325	0.3362	1	34.741
6	0.7945	0.02752	0.01767	-0.0267	0.1682	1	28.86991
7.5	0.9287	0.04919	0.03981	-0.0185	0.0542	1	18.87985
8	0.9452	0.05486	0.04651	-0.0141	0.0483	1	17.22931
8.5	0.9455	0.06204	0.05443	-0.0101	0.0453	1	15.24017
9	0.9272	0.06957	0.06251	-0.0064	0.0451	1	13.32758
9.5	0.8916	0.07739	0.07069	-0.0043	0.0455	1	11.52087

10	0.8546	0.088	0.08152	-0.0073	0.0497	1	9.711364
10.5	0.8279	0.10033	0.09389	-0.0123	0.0532	1	8.251769
11	0.8118	0.11382	0.10735	-0.0174	0.055	1	7.132314
12.5	0.292	0.03849	0.03434	-0.0236	0.309	1	7.586386
13	0.3246	0.0471	0.04297	-0.026	0.2529	1	6.89172
13.5	0.3526	0.05596	0.0517	-0.0285	0.2083	1	6.300929
14	0.3789	0.06531	0.06094	-0.0314	0.1868	1	5.801562
14.5	0.4126	0.07615	0.07174	-0.0327	0.1657	1	5.418253
15	0.4125	0.08205	0.07748	-0.0398	0.1595	1	5.027422

- Airfoil 4

Table AVIII-46: Aerodynamic performance of Airfoil 4 of the H-146 coated blade at 10°

alpha	CL	CD	CDp	CM	Top_Xtr	Bot_Xtr	CL/CD
------	--------	---------	---------	--------	--------	--------	--------
-5	-0.3363	0.02071	0.01166	-0.04	1	0.314	-16.2385
-4.5	-0.3305	0.02191	0.01436	-0.026	1	0.6338	-15.0844
-4	-0.3198	0.023	0.01516	-0.0149	1	0.7146	-13.9043
-3.5	-0.307	0.02295	0.01488	-0.0057	1	0.7739	-13.3769
-3	-0.3074	0.02219	0.0141	0.0067	1	0.8528	-13.8531
-2.5	-0.1981	0.0227	0.014	0.0003	1	0.9656	-8.72687
-2	-0.1012	0.02293	0.01379	-0.0132	1	1	-4.41343
-1.5	-0.1193	0.02218	0.01298	-0.0073	1	1	-5.37872
-1	-0.0821	0.02254	0.01308	-0.0104	0.9958	1	-3.64241
-0.5	0.0037	0.02417	0.01441	-0.0213	0.9762	1	0.153082
0	0.0808	0.0258	0.0158	-0.03	0.9585	1	3.131783
0.5	0.1537	0.0275	0.01736	-0.0374	0.9403	1	5.589091
1	0.2175	0.02926	0.01907	-0.0428	0.9241	1	7.433356
1.5	0.2842	0.03126	0.0212	-0.0483	0.9079	1	9.091491
2	0.3469	0.03328	0.02337	-0.0528	0.891	1	10.42368
2.5	0.3929	0.03529	0.02557	-0.0545	0.874	1	11.13347
3	0.4458	0.03754	0.02818	-0.0571	0.8552	1	11.87533
5	0.7766	0.03361	0.02255	-0.0349	0.0596	1	23.10622
5.5	0.8499	0.03808	0.02741	-0.0347	0.0515	1	22.3188
6	0.9096	0.04525	0.03542	-0.0335	0.0552	1	20.10166
6.5	0.9447	0.05418	0.04506	-0.0311	0.0594	1	17.43632
7	0.9672	0.06051	0.05255	-0.0268	0.0674	1	15.98413
7.5	0.9622	0.06987	0.06272	-0.0234	0.0758	1	13.77129
8	0.9575	0.07887	0.07222	-0.0211	0.0866	1	12.14023
8.5	0.9049	0.08682	0.08054	-0.02	0.089	1	10.42271
9	0.8552	0.09862	0.09246	-0.0265	0.0905	1	8.671669
9.5	0.8185	0.11489	0.10868	-0.0379	0.0973	1	7.124206

11	0.7804	0.1599	0.15341	-0.0681	0.2072	1	4.88055
12	0.7939	0.17667	0.17014	-0.0739	0.1849	1	4.493689
12.5	0.8523	0.19488	0.18846	-0.0703	0.1749	1	4.373461
13	0.8121	0.19289	0.18626	-0.0801	0.1647	1	4.210172
13.5	0.839	0.20344	0.19686	-0.0807	0.1543	1	4.124066
14	0.8483	0.21305	0.2064	-0.0845	0.1494	1	3.981694
14.5	0.8471	0.21641	0.20969	-0.0902	0.1387	1	3.914329
15	0.8761	0.22853	0.22187	-0.0904	0.1303	1	3.833632

- Airfoil 5

Table AVIII-47: Aerodynamic performance of Airfoil 5 of the H-146 coated blade at 10°

alpha	CL	CD	CDp	CM	Top_Xtr	Bot_Xtr	CL/CD
------	--------	---------	---------	--------	--------	--------	--------
-4.5	-0.3256	0.02144	0.01173	-0.0322	1	0.2109	-15.1866
-4	-0.3181	0.02113	0.01361	-0.0219	1	0.625	-15.0544
-3.5	-0.3176	0.02211	0.01473	-0.0077	1	0.7415	-14.3645
-3	-0.3031	0.02175	0.01412	0.0009	1	0.8122	-13.9356
-2.5	-0.2765	0.02125	0.01349	0.0087	1	0.9097	-13.0118
-2	-0.1049	0.0226	0.01398	-0.0145	1	1	-4.64159
-1.5	-0.1273	0.02189	0.01318	-0.0085	1	1	-5.81544
-1	-0.0664	0.02278	0.01355	-0.0156	0.9877	1	-2.91484
-0.5	0.0165	0.02429	0.01464	-0.0256	0.9673	1	0.679292
0	0.0977	0.02598	0.01602	-0.0344	0.9481	1	3.760585
0.5	0.1639	0.02755	0.01739	-0.04	0.9298	1	5.949183
1	0.2195	0.02919	0.01887	-0.0435	0.9129	1	7.519699
1.5	0.2808	0.03108	0.02068	-0.0475	0.8963	1	9.034749
2	0.3498	0.03311	0.02274	-0.0525	0.8797	1	10.56478
2.5	0.3882	0.03499	0.02473	-0.0527	0.8621	1	11.0946
3	0.4366	0.03711	0.02696	-0.0542	0.8425	1	11.76502
3.5	0.4889	0.03938	0.02943	-0.0561	0.8217	1	12.41493
4	0.5904	0.04018	0.03088	-0.0617	0.7808	1	14.69388
4.5	0.6827	0.03913	0.0305	-0.0628	0.7272	1	17.44697
5	0.8179	0.03253	0.02506	-0.0608	0.6594	1	25.14294
5.5	0.8931	0.02706	0.02027	-0.0517	0.5621	1	33.00443
6	0.916	0.02566	0.01776	-0.039	0.343	1	35.69758
6.5	0.9115	0.03	0.02065	-0.0315	0.1964	1	30.38333
7.5	0.9976	0.04326	0.03355	-0.0258	0.0764	1	23.06056
8	1.0355	0.05278	0.04376	-0.0239	0.0727	1	19.61917
9	1.0456	0.06997	0.06254	-0.0165	0.0736	1	14.94355
10	0.9533	0.08505	0.07878	-0.0112	0.0786	1	11.2087
11	0.8427	0.11941	0.11322	-0.0328	0.0888	1	7.057198

13	0.8177	0.18222	0.17579	-0.0646	0.1899	1	4.487433
14	0.8119	0.19559	0.18901	-0.0732	0.1713	1	4.15103
15	0.831	0.21186	0.20521	-0.0798	0.1551	1	3.922402

- Airfoil 6

Table AVIII-48: Aerodynamic performance of Airfoil 6 of the H-146 coated blade at 10°

alpha	CL	CD	CDp	CM	Top_Xtr	Bot_Xtr	CL/CD
------	--------	---------	---------	--------	--------	--------	--------
-5	-0.445	0.03888	0.03019	-0.0491	1	0.1024	-11.4455
-4.5	-0.4104	0.03338	0.0241	-0.0471	1	0.1055	-12.2948
-4	-0.3714	0.02951	0.01965	-0.0447	1	0.1212	-12.5856
-3.5	-0.3331	0.02521	0.01537	-0.0419	1	0.1678	-13.213
-3	-0.2973	0.02208	0.01274	-0.0397	1	0.2723	-13.4647
-2.5	-0.2696	0.0211	0.01333	-0.0335	1	0.5132	-12.7773
-2	-0.2646	0.0226	0.01498	-0.0206	1	0.6642	-11.708
-1.5	-0.2477	0.0225	0.01469	-0.0129	1	0.7344	-11.0089
-1	-0.2262	0.02213	0.01412	-0.0074	1	0.7953	-10.2214
-0.5	-0.2101	0.02157	0.01372	0.0008	1	0.8926	-9.74038
0	-0.0872	0.02255	0.01435	-0.0161	0.9889	1	-3.86696
0.5	0.0043	0.0239	0.01521	-0.0288	0.9629	1	0.179916
1	0.09	0.02532	0.01619	-0.039	0.9371	1	3.554502
1.5	0.1726	0.02693	0.01748	-0.0477	0.9146	1	6.409209
2	0.2483	0.02854	0.01886	-0.0543	0.8919	1	8.70007
2.5	0.3078	0.03021	0.02038	-0.0579	0.8701	1	10.18868
3	0.3613	0.03203	0.02211	-0.0603	0.8486	1	11.28005
3.5	0.4162	0.03397	0.02405	-0.0625	0.8269	1	12.25199
4	0.4736	0.03593	0.02606	-0.0647	0.8048	1	13.18119
4.5	0.5297	0.03787	0.02812	-0.0663	0.781	1	13.98733
5	0.5836	0.0397	0.03017	-0.067	0.7529	1	14.70025
5.5	0.7021	0.03771	0.02875	-0.0704	0.7067	1	18.6184
6	0.8148	0.03155	0.02306	-0.066	0.6421	1	25.82567
6.5	0.8863	0.02739	0.01919	-0.059	0.5691	1	32.35853
7	0.9212	0.02466	0.01611	-0.0486	0.4199	1	37.35604
7.5	0.9361	0.02753	0.01743	-0.0415	0.2614	1	34.00291
8	0.9727	0.03059	0.02017	-0.0389	0.2128	1	31.79797
8.5	1.0084	0.03312	0.02272	-0.0367	0.1802	1	30.44686
9.5	1.0634	0.03809	0.02813	-0.0311	0.1266	1	27.91809
10.5	1.1168	0.04878	0.03931	-0.0251	0.0721	1	22.89463
11	1.1308	0.0561	0.04756	-0.0216	0.065	1	20.15686
11.5	1.1189	0.06347	0.05555	-0.0174	0.0624	1	17.6288
12	1.0857	0.072	0.06463	-0.0153	0.0622	1	15.07917

12.5	1.0338	0.08356	0.07666	-0.0181	0.0637	1	12.37195
13	0.9698	0.10049	0.09383	-0.0278	0.0667	1	9.650712
13.5	0.9171	0.12104	0.11442	-0.0401	0.07	1	7.576834
14	0.8929	0.13874	0.13204	-0.049	0.072	1	6.435779
14.5	0.8856	0.15313	0.14637	-0.0547	0.0734	1	5.783321
15	0.8564	0.17389	0.16697	-0.0686	0.0865	1	4.924953

- **<u>Polyurethane/IA-700</u>**
  - -5°
  - Airfoil 1

Table AVIII-49: Aerodynamic performance of Airfoil 1 of the Polyurethane/IA-700 coated blade at -5°

alpha	CL	CD	CDp	CM	Top_Xtr	Bot_Xtr	CL/CD
------	--------	---------	---------	--------	--------	--------	--------
-5	-0.3888	0.03187	0.02173	-0.0307	1	0.0997	-12.1996
-4.5	-0.3516	0.02898	0.01838	-0.0277	1	0.1001	-12.1325
-4	-0.314	0.027	0.01611	-0.0247	1	0.1101	-11.6296
-3.5	-0.2768	0.02492	0.01404	-0.0214	1	0.1246	-11.1075
-3	-0.2396	0.02312	0.01223	-0.0186	1	0.1586	-10.3633
-2.5	-0.2545	0.02034	0.01283	-0.0001	1	0.8113	-12.5123
-2	-0.1211	0.02092	0.0128	-0.0115	1	1	-5.78872
-1.5	-0.1218	0.02056	0.01212	-0.0075	1	1	-5.92412
-1	-0.09	0.02107	0.01218	-0.0077	1	1	-4.27148
-0.5	-0.0527	0.02194	0.01263	-0.0082	1	1	-2.40201
0	0.0239	0.02378	0.01412	-0.0157	0.982	1	1.005046
0.5	0.0965	0.02566	0.01575	-0.0221	0.9628	1	3.760717
1	0.1645	0.02752	0.01746	-0.0274	0.9428	1	5.977471
1.5	0.2326	0.02942	0.01931	-0.0322	0.9202	1	7.906186
2	0.2969	0.03133	0.02128	-0.0362	0.8974	1	9.47654
2.5	0.4357	0.0315	0.02179	-0.0471	0.83	1	13.83175
3	0.6101	0.02557	0.0165	-0.0519	0.7352	1	23.85999
3.5	0.6725	0.02179	0.01288	-0.043	0.6452	1	30.86278
4	0.6804	0.02225	0.01116	-0.0291	0.2808	1	30.57978
4.5	0.7146	0.02532	0.01355	-0.0258	0.2235	1	28.22275
5	0.7699	0.02776	0.01593	-0.0249	0.2065	1	27.73415
5.5	0.8335	0.0303	0.01866	-0.0251	0.1983	1	27.50825
6	0.8923	0.03345	0.02195	-0.0251	0.1911	1	26.67564
6.5	0.941	0.03717	0.02619	-0.0243	0.1825	1	25.31612
7	0.9831	0.04122	0.03095	-0.0227	0.1768	1	23.85007
8	1.041	0.05141	0.04234	-0.0182	0.1576	1	20.24898
8.5	1.0459	0.05901	0.05081	-0.015	0.1569	1	17.72411
9	1.0273	0.06797	0.06045	-0.0119	0.1575	1	15.11402

9.5	0.9918	0.07812	0.07094	-0.0099	0.1602	1	12.69585
10	0.9563	0.0899	0.08285	-0.0106	0.1625	1	10.63737
11.5	0.7423	0.1517	0.14404	-0.0583	0.3137	1	4.89321
12	0.7628	0.16013	0.15267	-0.0587	0.2872	1	4.76363
12.5	0.7965	0.17309	0.16574	-0.0582	0.2587	1	4.601652
13	0.7986	0.17969	0.17231	-0.0599	0.2342	1	4.444321
13.5	0.7992	0.18449	0.1771	-0.0622	0.214	1	4.331942
14	0.7902	0.18992	0.18245	-0.0669	0.2025	1	4.160699
14.5	0.8447	0.2086	0.20135	-0.0649	0.1869	1	4.049377
15	0.8124	0.20492	0.19746	-0.0726	0.1776	1	3.964474

- Airfoil 2

Table AVIII-50: Aerodynamic performance of Airfoil 2 of the Polyurethane/IA-700 coated blade at -5°

alpha	CL	CD	CDp	CM	Top_Xtr	Bot_Xtr	CL/CD
------	--------	---------	---------	--------	--------	--------	--------
-4.5	-0.3416	0.02367	0.01365	-0.04	1	0.1704	-14.4318
-4	-0.3069	0.01963	0.01092	-0.0375	1	0.3228	-15.6342
-3.5	-0.3173	0.0214	0.01421	-0.0181	1	0.6851	-14.8271
-3	-0.3166	0.02201	0.01471	-0.0039	1	0.7748	-14.3844
-2.5	-0.3189	0.02123	0.01386	0.01	1	0.8643	-15.0212
-2	-0.2023	0.02116	0.01307	0.0011	1	0.9589	-9.56049
-1.5	-0.0893	0.02103	0.01238	-0.0149	1	1	-4.24631
-1	-0.1124	0.02025	0.01153	-0.0087	1	1	-5.55062
-0.5	-0.081	0.02044	0.01136	-0.0107	1	1	-3.96282
0	-0.0088	0.02172	0.01228	-0.0191	0.9882	1	-0.40516
0.5	0.0835	0.02358	0.01383	-0.0301	0.9666	1	3.541137
1	0.1622	0.02528	0.01535	-0.038	0.9448	1	6.416139
1.5	0.2358	0.02709	0.01708	-0.0446	0.9246	1	8.704319
2	0.3085	0.02893	0.01895	-0.0504	0.9022	1	10.66367
2.5	0.3779	0.03083	0.02094	-0.0554	0.8807	1	12.25754
3	0.4397	0.03276	0.02303	-0.0587	0.8577	1	13.42186
3.5	0.4925	0.03483	0.02543	-0.0606	0.8336	1	14.14011
4	0.5443	0.03714	0.02804	-0.0621	0.8089	1	14.65536
5.5	0.7779	0.02741	0.01639	-0.0342	0.1714	1	28.38015
6	0.8397	0.0311	0.02007	-0.0331	0.1517	1	27
6.5	0.8959	0.03527	0.02444	-0.0326	0.1298	1	25.40119
7	0.9497	0.04032	0.03003	-0.0317	0.1229	1	23.55407
7.5	0.9919	0.04663	0.0372	-0.03	0.1223	1	21.27171
8	1.0157	0.05444	0.0461	-0.0276	0.1267	1	18.65724
8.5	1.0266	0.06378	0.05619	-0.0259	0.1331	1	16.09595
9	1.009	0.07328	0.06651	-0.0244	0.1427	1	13.7691

9.5	0.9251	0.08606	0.07961	-0.0269	0.1508	1	10.74948
11	0.7617	0.14576	0.13878	-0.0733	0.3111	1	5.225714
12	0.7975	0.16273	0.15593	-0.0759	0.2793	1	4.900756
12.5	0.7933	0.16901	0.16216	-0.079	0.2628	1	4.693805
13	0.8216	0.1801	0.17334	-0.08	0.2507	1	4.56191
13.5	0.8355	0.18703	0.18033	-0.0817	0.2322	1	4.467198
14	0.8277	0.19196	0.18519	-0.0864	0.2194	1	4.311836
14.5	0.8554	0.20351	0.19682	-0.0871	0.2045	1	4.203233
15	0.8921	0.21821	0.21166	-0.0867	0.183	1	4.088264

- Airfoil 3

Table AVIII-51: Aerodynamic performance of Airfoil 3 of the Polyurethane/IA-700 coated blade at -5°

alpha	CL	CD	CDp	CM	Top_Xtr	Bot_Xtr	CL/CD
------	--------	---------	---------	--------	--------	--------	--------
-3	-0.3803	0.02237	0.01515	0.0113	1	0.8143	-17.0004
-2.5	-0.3488	0.02161	0.01409	0.0189	1	0.9011	-16.1407
-2	-0.1545	0.02236	0.01365	-0.0065	1	0.9725	-6.90966
-1.5	-0.0824	0.02203	0.01295	-0.0159	1	1	-3.74035
-1	-0.1161	0.02124	0.01215	-0.0079	1	1	-5.4661
-0.5	-0.1072	0.02108	0.01174	-0.0061	1	1	-5.08539
0	-0.0433	0.02225	0.01248	-0.0129	0.989	1	-1.94607
0.5	0.0403	0.02396	0.01389	-0.0225	0.9683	1	1.68197
1	0.1182	0.02567	0.01541	-0.0303	0.9464	1	4.604597
1.5	0.1891	0.02739	0.01703	-0.0363	0.9254	1	6.90398
2	0.2516	0.02913	0.01874	-0.0406	0.9045	1	8.637144
2.5	0.3114	0.03099	0.02064	-0.0442	0.8835	1	10.0484
3	0.3687	0.03297	0.02281	-0.0472	0.8624	1	11.18289
3.5	0.4249	0.0351	0.02513	-0.0498	0.8411	1	12.10541
4	0.4783	0.03735	0.02764	-0.0518	0.8181	1	12.80589
4.5	0.5342	0.0395	0.03016	-0.0534	0.7892	1	13.52405
5	0.7305	0.02965	0.02169	-0.0534	0.6742	1	24.63744
5.5	0.7999	0.02441	0.01727	-0.044	0.5843	1	32.76936
6	0.8101	0.02487	0.01563	-0.0302	0.2832	1	32.57338
7.75	0.9559	0.04534	0.03596	-0.0211	0.0874	1	21.08293
8	0.9715	0.04852	0.03943	-0.0197	0.0809	1	20.02267
8.25	0.9844	0.05258	0.04359	-0.0188	0.0757	1	18.72195
8.5	0.9885	0.05884	0.05013	-0.0177	0.0735	1	16.7998
8.75	0.9902	0.062	0.05377	-0.0155	0.0727	1	15.97097
9	0.99	0.06651	0.05864	-0.014	0.0728	1	14.88498
9.5	0.9872	0.07462	0.06738	-0.011	0.0747	1	13.2297
9.75	0.9724	0.07739	0.0705	-0.0091	0.0762	1	12.56493

10	0.9378	0.08068	0.07408	-0.0075	0.0781	1	11.6237
10.25	0.8975	0.08619	0.0798	-0.0096	0.0807	1	10.41304
10.5	0.8603	0.09443	0.08812	-0.0149	0.0855	1	9.110452
10.75	0.8418	0.10222	0.09591	-0.0193	0.09	1	8.235179
11	0.8327	0.1093	0.10296	-0.0226	0.0925	1	7.618481
11.25	0.8323	0.11564	0.10929	-0.0241	0.0944	1	7.197337
12	0.7484	0.15469	0.14809	-0.0591	0.2461	1	4.838063
12.25	0.7999	0.16554	0.15906	-0.0554	0.2348	1	4.832065
12.5	0.767	0.16506	0.15845	-0.0601	0.2318	1	4.646795
12.75	0.7604	0.16707	0.16042	-0.0619	0.2206	1	4.551386
13	0.7884	0.17509	0.16848	-0.0603	0.2099	1	4.502827
13.25	0.7689	0.17525	0.16855	-0.064	0.203	1	4.387447
13.75	0.7875	0.18469	0.17798	-0.0649	0.1845	1	4.263902
14	0.7834	0.18649	0.17974	-0.0672	0.1744	1	4.200761
14.5	0.8195	0.20102	0.19433	-0.0666	0.1634	1	4.076709
14.75	0.8004	0.19909	0.1923	-0.0713	0.1586	1	4.020292
15	0.8037	0.20213	0.19532	-0.0731	0.1513	1	3.976154

- Airfoil 4

Table AVIII-52: Aerodynamic performance of Airfoil 4 of the Polyurethane/IA-700 coated blade at -5°

alpha	CL	CD	CDp	CM	Top_Xtr	Bot_Xtr	CL/CD
------	--------	---------	---------	--------	--------	--------	--------
-5	-0.3896	0.02464	0.01475	-0.0336	1	0.1282	-15.8117
-4	-0.3862	0.02345	0.01656	-0.0055	1	0.7219	-16.4691
-3.5	-0.3782	0.02343	0.01625	0.0063	1	0.7929	-16.1417
-3	-0.3678	0.0226	0.01517	0.0167	1	0.8654	-16.2743
-2.5	-0.237	0.02312	0.01487	0.0053	1	0.952	-10.2509
-2	-0.0825	0.02335	0.01425	-0.0172	1	0.9999	-3.53319
-1.5	-0.1105	0.02254	0.01343	-0.0099	1	1	-4.9024
-1	-0.1207	0.02179	0.01255	-0.0055	1	1	-5.53924
-0.5	-0.0776	0.02244	0.01288	-0.0092	0.996	1	-3.45811
0	0.0138	0.02467	0.0147	-0.0206	0.974	1	0.559384
0.5	0.0925	0.02654	0.01635	-0.0289	0.9521	1	3.485305
1	0.1552	0.02809	0.01778	-0.0339	0.9319	1	5.525098
1.5	0.2223	0.02982	0.01948	-0.0393	0.9122	1	7.454728
2	0.2823	0.03157	0.02125	-0.0432	0.8923	1	8.942034
2.5	0.3395	0.0335	0.02327	-0.0464	0.8724	1	10.13433
3	0.3962	0.03558	0.02552	-0.0493	0.8514	1	11.13547
3.5	0.4503	0.03781	0.02821	-0.0517	0.8292	1	11.90955
4	0.5039	0.04013	0.03086	-0.0537	0.8044	1	12.55669
4.5	0.5744	0.04223	0.03349	-0.0569	0.7741	1	13.6017

5	0.7972	0.02868	0.02197	-0.0557	0.6427	1	27.79637
5.5	0.817	0.02469	0.01614	-0.0359	0.2763	1	33.09032
6	0.8379	0.03049	0.02066	-0.0307	0.1584	1	27.48114
6.5	0.9171	0.03923	0.02907	-0.0319	0.1053	1	23.37752
7	0.9581	0.04526	0.03605	-0.0286	0.0907	1	21.1688
7.5	0.9849	0.0535	0.04521	-0.0248	0.0891	1	18.40935
8	0.9983	0.06351	0.05565	-0.0222	0.0845	1	15.71878
9.5	0.8957	0.08863	0.08253	-0.0148	0.1013	1	10.10606
10	0.8897	0.10204	0.09593	-0.0174	0.1053	1	8.71913
11	0.7465	0.14711	0.14082	-0.0627	0.2733	1	5.074434
11.5	0.7552	0.1565	0.15016	-0.0647	0.259	1	4.825559
12	0.7841	0.16818	0.16186	-0.0649	0.2405	1	4.662267
12.5	0.7993	0.17745	0.17111	-0.0658	0.218	1	4.504367
13	0.8069	0.18514	0.17874	-0.0676	0.195	1	4.358323
14	0.8016	0.19559	0.18903	-0.0759	0.1629	1	4.098369
14.5	0.8451	0.21276	0.20627	-0.0743	0.1502	1	3.972081
15	0.8249	0.2114	0.20476	-0.0824	0.1415	1	3.902081

- Airfoil 5

Table AVIII-53: Aerodynamic performance of Airfoil 5 of the Polyurethane/IA-700 coated blade at -5°

alpha	CL	CD	CDp	CM	Top_Xtr	Bot_Xtr	CL/CD
------	--------	---------	---------	--------	--------	--------	--------
-5	-0.3376	0.02156	0.01221	-0.0409	1	0.3139	-15.6586
-4.5	-0.3091	0.02063	0.01262	-0.034	1	0.5208	-14.983
-4	-0.2942	0.02186	0.01391	-0.0235	1	0.6423	-13.4584
-3.5	-0.2752	0.02205	0.01395	-0.0161	1	0.7069	-12.4807
-3	-0.2603	0.02178	0.01361	-0.0084	1	0.7758	-11.9513
-2.5	-0.2568	0.02131	0.0132	0.0024	1	0.8576	-12.0507
-2	-0.1755	0.02159	0.01333	-0.003	1	0.9624	-8.12876
-1.5	-0.0958	0.02195	0.01332	-0.0152	0.9904	1	-4.36446
-1	-0.006	0.02311	0.01397	-0.0281	0.9657	1	-0.25963
-0.5	0.0858	0.02453	0.01501	-0.0396	0.9426	1	3.497758
0	0.1615	0.02599	0.01621	-0.0471	0.9225	1	6.213928
0.5	0.2327	0.02759	0.01762	-0.0532	0.9043	1	8.434215
1	0.303	0.02913	0.01908	-0.0583	0.8834	1	10.40165
1.5	0.3532	0.03077	0.02068	-0.06	0.8632	1	11.47871
2	0.4124	0.03237	0.02241	-0.0624	0.8403	1	12.74019
2.5	0.4637	0.0342	0.02434	-0.0638	0.8193	1	13.55848
3	0.5151	0.03615	0.02648	-0.0649	0.7981	1	14.24896
3.5	0.5644	0.03834	0.02905	-0.0659	0.7772	1	14.72092
4	0.6304	0.03978	0.03093	-0.0675	0.746	1	15.84716

4.5	0.7772	0.03508	0.0272	-0.0697	0.6887	1	22.15507
5	0.8664	0.0296	0.02244	-0.0622	0.6136	1	29.27027
6	0.9105	0.02698	0.01809	-0.0398	0.2302	1	33.74722
6.5	0.9151	0.03366	0.0236	-0.0329	0.1141	1	27.18657
7.5	1.033	0.04849	0.03913	-0.0307	0.08	1	21.30336
8	1.0513	0.05446	0.0461	-0.0267	0.0743	1	19.30408
8.5	1.0534	0.06199	0.05443	-0.0229	0.0722	1	16.99306
9	1.0345	0.07044	0.06352	-0.0193	0.0737	1	14.68626
9.5	0.9961	0.07878	0.07224	-0.0167	0.0753	1	12.64407
10	0.9519	0.08937	0.08308	-0.0195	0.077	1	10.65123
10.5	0.9149	0.10286	0.09667	-0.0259	0.0794	1	8.894614
12	0.4048	0.06462	0.06011	-0.0397	0.2391	1	6.264314
12.5	0.4155	0.07173	0.06717	-0.0442	0.2242	1	5.792555
13	0.4401	0.0814	0.07681	-0.0471	0.2174	1	5.406634
13.5	0.4523	0.08856	0.08391	-0.0515	0.204	1	5.107272
14	0.4796	0.09966	0.09499	-0.0539	0.1964	1	4.812362
14.5	0.489	0.10678	0.10206	-0.0587	0.1827	1	4.579509
15	0.5176	0.11904	0.11427	-0.0609	0.1725	1	4.348118

- Airfoil 6

Table AVIII-54: Aerodynamic performance of Airfoil 6 of the Polyurethane/IA-700 coated blade at -5°

alpha	CL	CD	CDp	CM	Top_Xtr	Bot_Xtr	CL/CD
------	--------	---------	---------	--------	--------	--------	--------
-4	-0.3125	0.02298	0.01354	-0.0354	1	0.2427	-13.5988
-3.5	-0.2737	0.02183	0.01325	-0.0334	1	0.3966	-12.5378
-3	-0.2499	0.02254	0.01447	-0.0265	1	0.5801	-11.087
-2.5	-0.2258	0.02295	0.01476	-0.0199	1	0.6756	-9.83878
-2	-0.2011	0.02279	0.01454	-0.014	1	0.7578	-8.82405
-1.5	-0.1742	0.02221	0.01442	-0.007	1	0.891	-7.84331
-1	-0.1025	0.02258	0.01431	-0.0156	1	1	-4.53942
-0.5	-0.058	0.02355	0.01475	-0.0187	1	1	-2.46285
0	0.0177	0.02556	0.01622	-0.027	0.9855	1	0.692488
0.5	0.107	0.02793	0.01817	-0.0368	0.9596	1	3.831006
1	0.1829	0.03001	0.01999	-0.0436	0.933	1	6.094635
1.5	0.254	0.03203	0.02182	-0.049	0.9055	1	7.930066
2	0.3314	0.03403	0.02375	-0.0548	0.8762	1	9.738466
2.5	0.4029	0.03584	0.02558	-0.059	0.8462	1	11.24163
3	0.4637	0.03713	0.02697	-0.0607	0.8094	1	12.48855
3.5	0.5564	0.03673	0.02677	-0.0639	0.7615	1	15.14838
4	0.669	0.03412	0.02458	-0.067	0.7157	1	19.60727
4.5	0.7864	0.02925	0.0202	-0.0674	0.6712	1	26.88547

5	0.8561	0.02647	0.0176	-0.0627	0.5993	1	32.34227
5.5	0.907	0.02553	0.01628	-0.0563	0.4824	1	35.52683
6	0.9502	0.02713	0.01716	-0.0522	0.3875	1	35.02396
6.5	0.998	0.02984	0.01977	-0.0505	0.3398	1	33.44504
7	1.048	0.03275	0.02279	-0.0494	0.3107	1	32
7.5	1.0892	0.03634	0.02702	-0.0478	0.294	1	29.97248
8	1.1306	0.03773	0.02815	-0.0454	0.2581	1	29.96554
8.5	1.157	0.03931	0.03019	-0.0416	0.2294	1	29.43271
9	1.1689	0.03964	0.03067	-0.0359	0.1883	1	29.48789
9.5	1.1556	0.04145	0.03282	-0.0279	0.1477	1	27.87937
10.5	1.1368	0.05058	0.04203	-0.0159	0.0843	1	22.47529
11	1.1431	0.05656	0.04841	-0.0128	0.0728	1	20.2104
11.5	1.1467	0.06389	0.05594	-0.0107	0.0677	1	17.94804
12	1.1209	0.07337	0.06606	-0.0102	0.0668	1	15.27736
12.5	1.0794	0.08529	0.07846	-0.0132	0.0671	1	12.65565
13	1.0295	0.10041	0.09389	-0.0203	0.0679	1	10.25296
13.5	0.898	0.14258	0.13606	-0.048	0.0835	1	6.298219
14	0.8831	0.15807	0.15142	-0.0552	0.0843	1	5.586765
14.5	0.877	0.17175	0.16502	-0.0612	0.085	1	5.106259
15	0.8833	0.18356	0.17681	-0.0649	0.0868	1	4.812051

- 0˚
    - Airfoil 1

Table AVIII-55: Aerodynamic performance of Airfoil 1 of the Polyurethane/IA-700 coated blade at 0°

alpha	CL	CD	CDp	CM	Top_Xtr	Bot_Xtr	CL/CD
------	--------	---------	---------	--------	--------	--------	--------
-4.5	-0.3698	0.02926	0.01851	-0.0365	1	0.1365	-12.6384
-4	-0.3306	0.02689	0.01564	-0.0337	1	0.1361	-12.2945
-3.5	-0.2918	0.02516	0.01376	-0.0306	1	0.1384	-11.5978
-3	-0.2548	0.02358	0.01223	-0.0277	1	0.1482	-10.8058
-2.5	-0.2143	0.022	0.01076	-0.0262	1	0.1865	-9.74091
-2	-0.2153	0.02059	0.01211	-0.0121	1	0.7564	-10.4565
-1	-0.1178	0.02043	0.01174	-0.0087	1	1	-5.76603
-0.5	-0.0848	0.02077	0.01172	-0.0098	1	1	-4.08281
0	-0.043	0.0216	0.01222	-0.0117	1	1	-1.99074
0.5	0.0293	0.02334	0.01367	-0.019	0.9855	1	1.255356
1	0.1146	0.02544	0.01557	-0.028	0.9618	1	4.504717
1.5	0.1878	0.02739	0.01741	-0.0344	0.9402	1	6.856517
2	0.257	0.0293	0.01931	-0.0398	0.9183	1	8.771331
2.5	0.3271	0.03126	0.02134	-0.0448	0.8953	1	10.46385
3	0.4325	0.03189	0.02226	-0.0519	0.8394	1	13.56225

4	0.6326	0.02257	0.01065	-0.035	0.2047	1	28.02836
4.5	0.6641	0.02594	0.01347	-0.0318	0.1541	1	25.60139
5	0.7124	0.02886	0.01637	-0.03	0.1373	1	24.68468
5.5	0.7792	0.03158	0.01929	-0.03	0.1321	1	24.67384
6	0.8428	0.03523	0.02325	-0.0302	0.1313	1	23.92279
6.5	0.897	0.03972	0.02825	-0.0297	0.1333	1	22.58308
7	0.9439	0.04555	0.03457	-0.0289	0.1365	1	20.72228
7.5	0.9776	0.05018	0.04036	-0.0263	0.1433	1	19.48187
8	0.9925	0.0582	0.04937	-0.024	0.1534	1	17.05326
8.5	0.9844	0.06713	0.05921	-0.022	0.1658	1	14.66408
9	0.9658	0.07902	0.07156	-0.0224	0.1835	1	12.22222
10.5	0.7158	0.13867	0.13097	-0.0658	0.3443	1	5.161895
11	0.725	0.14575	0.13805	-0.0673	0.3289	1	4.974271
11.5	0.7722	0.15615	0.1486	-0.0675	0.316	1	4.945245
12	0.758	0.15993	0.15232	-0.0699	0.2977	1	4.739574
12.5	0.7629	0.16657	0.15897	-0.0723	0.2844	1	4.580056
13	0.8023	0.17673	0.1693	-0.0726	0.2719	1	4.539693
13.5	0.7889	0.18017	0.17269	-0.0765	0.2586	1	4.378642
14	0.8381	0.1939	0.18667	-0.0763	0.2489	1	4.322331
14.5	0.8151	0.19409	0.18677	-0.0816	0.2372	1	4.199598
15	0.8669	0.21164	0.20485	-0.0809	0.2255	1	4.096107

- Airfoil 2

Table AVIII-56: Aerodynamic performance of Airfoil 2 of the Polyurethane/IA-700 coated blade at 0°

alpha	CL	CD	CDp	CM	Top_Xtr	Bot_Xtr	CL/CD
------	--------	---------	---------	--------	--------	--------	--------
-4.5	-0.3549	0.02971	0.01982	-0.0393	1	0.0819	-11.9455
-4	-0.3152	0.02647	0.01608	-0.0354	1	0.0917	-11.9078
-1.5	-0.1053	0.02108	0.01279	-0.0128	1	1	-4.99526
-1	-0.1135	0.02049	0.01201	-0.0084	1	1	-5.53929
-0.5	-0.0779	0.02086	0.01199	-0.0103	1	1	-3.73442
0	-0.009	0.02219	0.01282	-0.0176	0.989	1	-0.40559
0.5	0.0715	0.02394	0.01424	-0.0262	0.9695	1	2.986633
1	0.1476	0.0258	0.01583	-0.0337	0.9493	1	5.72093
1.5	0.2182	0.02763	0.01754	-0.0396	0.9288	1	7.897213
2	0.2847	0.02947	0.01935	-0.0446	0.9075	1	9.660672
2.5	0.3502	0.03138	0.02135	-0.0489	0.8847	1	11.15997
3	0.4144	0.03341	0.0235	-0.0528	0.8608	1	12.40347
3.5	0.4885	0.03545	0.02579	-0.0574	0.8339	1	13.77997
4	0.6094	0.03441	0.0255	-0.0624	0.7694	1	17.70997
4.5	0.7344	0.02218	0.01361	-0.0466	0.6009	1	33.11091

5.5	0.7701	0.02825	0.01667	-0.0309	0.1502	1	27.26018
6	0.8304	0.03139	0.01972	-0.0301	0.1383	1	26.45428
6.5	0.8992	0.03551	0.02405	-0.0305	0.1352	1	25.32244
7	0.9558	0.04068	0.02975	-0.0301	0.1358	1	23.49558
7.5	1.0021	0.04598	0.03586	-0.0287	0.1388	1	21.79426
8	1.029	0.0524	0.04345	-0.0262	0.1427	1	19.6374
8.5	1.047	0.0597	0.05117	-0.0246	0.1343	1	17.53769
9	1.0399	0.06716	0.05944	-0.022	0.1314	1	15.48392
9.5	1.0318	0.07731	0.06999	-0.021	0.1349	1	13.34627
11.5	0.7665	0.15284	0.14564	-0.0718	0.3086	1	5.015048
12.5	0.7925	0.1671	0.15993	-0.0736	0.2547	1	4.742669
13	0.8019	0.1752	0.16802	-0.076	0.2411	1	4.577055
14	0.8232	0.18977	0.18264	-0.0811	0.2121	1	4.337883
14.5	0.8745	0.20693	0.2	-0.0799	0.2026	1	4.226067
15	0.8469	0.20464	0.19759	-0.087	0.1904	1	4.138487

- Airfoil 3

Table AVIII-57: Aerodynamic performance of Airfoil 3 of the Polyurethane/IA-700 coated blade at 0°

alpha	CL	CD	CDp	CM	Top_Xtr	Bot_Xtr	CL/CD
------	--------	---------	---------	--------	--------	--------	--------
-5	-0.3917	0.02434	0.01354	-0.0308	1	0.0994	-16.0929
-4.5	-0.3754	0.01971	0.01157	-0.0258	1	0.503	-19.0462
-4	-0.3575	0.02076	0.01251	-0.0167	1	0.6399	-17.2206
-3.5	-0.3458	0.02167	0.01335	-0.006	1	0.7273	-15.9575
-3	-0.3537	0.02175	0.01363	0.0105	1	0.8289	-16.2621
-2.5	-0.2187	0.0227	0.01402	0.0024	1	0.9542	-9.63436
-2	-0.0906	0.02281	0.01365	-0.0156	1	0.996	-3.97194
-1.5	-0.1095	0.02218	0.013	-0.0101	1	1	-4.93688
-1	-0.122	0.02152	0.0122	-0.0053	1	1	-5.66914
-0.5	-0.0669	0.02248	0.01277	-0.0109	0.9912	1	-2.97598
0	0.0152	0.02409	0.01412	-0.0204	0.9693	1	0.630967
0.5	0.0888	0.02576	0.01558	-0.0277	0.9495	1	3.447205
1	0.1583	0.02746	0.0172	-0.0337	0.9291	1	5.764749
1.5	0.2216	0.0292	0.01888	-0.0382	0.9096	1	7.589041
2	0.2831	0.03101	0.02072	-0.0422	0.8892	1	9.129313
2.5	0.3416	0.03297	0.0228	-0.0455	0.87	1	10.36093
3	0.3992	0.0351	0.02525	-0.0485	0.8503	1	11.37322
3.5	0.4533	0.03731	0.02769	-0.0507	0.8285	1	12.14956
4	0.5047	0.03941	0.03008	-0.0519	0.8002	1	12.80639
4.5	0.6968	0.03294	0.02478	-0.0578	0.7061	1	21.15361
5	0.7972	0.02686	0.02009	-0.0513	0.6328	1	29.67982

5.5	0.807	0.02422	0.0157	-0.0329	0.2866	1	33.31957
7	0.9184	0.04442	0.03415	-0.0242	0.0621	1	20.67537
7.5	0.9523	0.05331	0.04378	-0.0219	0.061	1	17.86344
8	0.9724	0.06041	0.05172	-0.0186	0.0617	1	16.09667
8.5	0.9773	0.06615	0.05837	-0.0142	0.0644	1	14.774
9	0.9395	0.07399	0.06703	-0.0096	0.0684	1	12.69766
9.5	0.8921	0.0827	0.07607	-0.0088	0.0711	1	10.78718
10	0.8449	0.09476	0.08828	-0.0147	0.074	1	8.916209
10.5	0.8143	0.1091	0.10262	-0.0228	0.0783	1	7.463795
12	0.4373	0.09145	0.08662	-0.0416	0.2433	1	4.781848
12.5	0.4605	0.10063	0.09577	-0.0439	0.2319	1	4.57617
13	0.4875	0.11012	0.10523	-0.0456	0.2113	1	4.426989
13.5	0.5058	0.11824	0.1133	-0.048	0.1892	1	4.27774
14.5	0.5194	0.13072	0.12566	-0.0561	0.1589	1	3.973378
15	0.5652	0.14615	0.14113	-0.0555	0.1467	1	3.86726

- Airfoil 4

Table AVIII-58: Aerodynamic performance of Airfoil 4 of the Polyurethane/IA-700 coated blade at 0°

alpha	CL	CD	CDp	CM	Top_Xtr	Bot_Xtr	CL/CD
------	--------	---------	---------	--------	--------	--------	--------
-4	-0.3487	0.02321	0.01595	-0.007	1	0.7352	-15.0237
-3.5	-0.3472	0.02302	0.01561	0.006	1	0.8153	-15.0825
-3	-0.3328	0.02191	0.01433	0.0155	1	0.8916	-15.1894
-2.5	-0.1918	0.0223	0.01377	-0.0005	1	0.9654	-8.6009
-2	-0.0955	0.02225	0.01326	-0.0139	1	1	-4.29213
-1.5	-0.118	0.02142	0.01237	-0.0077	1	1	-5.50887
-1	-0.0901	0.02159	0.01225	-0.0091	1	1	-4.17323
-0.5	-0.0143	0.02308	0.01341	-0.0183	0.9854	1	-0.61958
0	0.0721	0.02497	0.01499	-0.0284	0.9631	1	2.887465
0.5	0.152	0.02686	0.01672	-0.0368	0.942	1	5.658972
1	0.2276	0.02871	0.0185	-0.0437	0.9211	1	7.927551
1.5	0.294	0.03046	0.02026	-0.0488	0.9005	1	9.652003
2	0.3552	0.03225	0.02211	-0.0526	0.8798	1	11.01395
2.5	0.4117	0.03422	0.02422	-0.0556	0.8591	1	12.03098
3	0.4702	0.03631	0.02671	-0.0585	0.8368	1	12.9496
3.5	0.5291	0.03853	0.02923	-0.0611	0.8133	1	13.73216
4	0.6755	0.03552	0.02713	-0.0666	0.7423	1	19.01745
4.5	0.7964	0.02821	0.02102	-0.0612	0.6591	1	28.23112
5	0.8419	0.02267	0.01544	-0.0462	0.45	1	37.13719
5.5	0.854	0.02697	0.01755	-0.0384	0.2376	1	31.66481
6	0.9137	0.03199	0.02223	-0.0374	0.1804	1	28.56205

7	1.0013	0.04821	0.03879	-0.0336	0.0956	1	20.76955
7.5	1.0222	0.05631	0.04801	-0.0293	0.0937	1	18.15308
8	1.0261	0.06526	0.05784	-0.0254	0.0933	1	15.72326
8.5	1.0082	0.07316	0.06645	-0.0216	0.0917	1	13.78075
9	0.9793	0.08187	0.07553	-0.0191	0.0926	1	11.96165
9.5	0.9521	0.09251	0.08631	-0.0192	0.0945	1	10.29186
11.5	0.8252	0.16831	0.16215	-0.0685	0.2503	1	4.902858
12	0.8052	0.17183	0.16556	-0.0727	0.2311	1	4.686027
12.5	0.7993	0.17838	0.17202	-0.0765	0.2144	1	4.480884
13	0.8084	0.18653	0.18011	-0.079	0.1961	1	4.333887
13.5	0.82	0.19408	0.18762	-0.0812	0.1726	1	4.225062
14	0.8362	0.20327	0.19677	-0.0832	0.1573	1	4.11374
14.5	0.8572	0.2124	0.20593	-0.0846	0.1419	1	4.035782
15	0.8623	0.22038	0.21381	-0.0893	0.1364	1	3.912787

- Airfoil 5

Table AVIII-59: Aerodynamic performance of Airfoil 5 of the Polyurethane/IA-700 coated blade at 0°

alpha	CL	CD	CDp	CM	Top_Xtr	Bot_Xtr	CL/CD
------	--------	---------	---------	--------	--------	--------	--------
-5	-0.3628	0.02277	0.01288	-0.0375	1	0.2495	-15.9332
-4.5	-0.3254	0.02042	0.01115	-0.0349	1	0.3263	-15.9354
-4	-0.3166	0.02076	0.01304	-0.0227	1	0.6094	-15.2505
-3.5	-0.3058	0.02157	0.01372	-0.0121	1	0.7023	-14.1771
-3	-0.2914	0.02141	0.01339	-0.0038	1	0.7729	-13.6105
-2.5	-0.2768	0.0206	0.01258	0.0043	1	0.85	-13.4369
-2	-0.1255	0.02146	0.01299	-0.0118	1	0.9868	-5.84809
-1.5	-0.1276	0.02098	0.01235	-0.0099	1	1	-6.08198
-1	-0.0414	0.02216	0.01301	-0.0218	0.9766	1	-1.86823
-0.5	0.0482	0.02359	0.01406	-0.0328	0.9532	1	2.043239
0	0.1199	0.02494	0.01515	-0.0398	0.9316	1	4.807538
0.5	0.19	0.02642	0.0164	-0.0458	0.9106	1	7.191522
1	0.2529	0.02806	0.01791	-0.0502	0.8931	1	9.01283
1.5	0.3226	0.0298	0.0196	-0.0552	0.8756	1	10.8255
2	0.3687	0.0316	0.02146	-0.0564	0.8579	1	11.66772
2.5	0.4122	0.03362	0.02352	-0.0571	0.8409	1	12.26056
3	0.4644	0.03586	0.0259	-0.0591	0.8258	1	12.95036
3.5	0.5282	0.03799	0.02829	-0.0623	0.8076	1	13.90366
4	0.5769	0.04004	0.03086	-0.0627	0.7821	1	14.40809
4.5	0.637	0.04119	0.03245	-0.0627	0.7434	1	15.46492
5	0.8221	0.02975	0.02224	-0.0582	0.6332	1	27.63361
5.5	0.8597	0.02329	0.01545	-0.0407	0.3822	1	36.91284

6	0.8679	0.02863	0.01889	-0.033	0.2037	1	30.31436
6.5	0.8975	0.03357	0.02361	-0.0292	0.1251	1	26.73518
7	0.9321	0.0403	0.03017	-0.026	0.0623	1	23.12903
7.5	0.975	0.04792	0.03822	-0.0241	0.0513	1	20.34641
8	0.9959	0.05756	0.04867	-0.0212	0.0499	1	17.30195
8.5	0.9995	0.06577	0.05763	-0.0176	0.05	1	15.1969
9	0.9907	0.0724	0.06491	-0.0138	0.0511	1	13.6837
9.5	0.9549	0.07916	0.07221	-0.0104	0.0529	1	12.06291
10	0.8955	0.09002	0.08347	-0.0146	0.0555	1	9.947789
10.5	0.8425	0.10656	0.10015	-0.0261	0.0598	1	7.906344
11	0.8188	0.12286	0.11638	-0.0356	0.0644	1	6.664496
11.5	0.8157	0.13536	0.12881	-0.0401	0.0684	1	6.026152
12	0.8019	0.15224	0.1456	-0.05	0.0873	1	5.267341
13	0.419	0.0779	0.07314	-0.0432	0.2338	1	5.378691
13.5	0.4376	0.08723	0.0824	-0.0462	0.2113	1	5.016623
14	0.4601	0.09687	0.09198	-0.0489	0.1992	1	4.749664
14.5	0.4779	0.10555	0.10057	-0.0518	0.1753	1	4.527712
15	0.5046	0.11695	0.11208	-0.0536	0.1562	1	4.314664

- Airfoil 6

Table AVIII-60: Aerodynamic performance of Airfoil 6 of the Polyurethane/IA-700 coated blade at 0°

alpha	CL	CD	CDp	CM	Top_Xtr	Bot_Xtr	CL/CD
------	--------	---------	---------	--------	--------	--------	--------
-5	-0.4137	0.02983	0.01977	-0.0395	1	0.0518	-13.8686
-4.5	-0.3736	0.02728	0.01677	-0.0364	1	0.0576	-13.695
-4	-0.3298	0.02485	0.01444	-0.0348	1	0.1071	-13.2716
-3.5	-0.2882	0.02277	0.0138	-0.0344	1	0.3567	-12.657
-3	-0.2663	0.02351	0.01542	-0.0271	1	0.5789	-11.3271
-2.5	-0.2505	0.02379	0.01571	-0.0172	1	0.709	-10.5296
-2	-0.2302	0.02329	0.0152	-0.0092	1	0.8025	-9.88407
-1.5	-0.1852	0.02313	0.01505	-0.0071	1	0.9113	-8.00692
-1	-0.1152	0.02337	0.01478	-0.0153	1	1	-4.9294
-0.5	-0.0696	0.02421	0.01503	-0.0184	1	1	-2.87485
0	-0.026	0.02538	0.01579	-0.0204	1	1	-1.02443
0.5	0.015	0.02676	0.01683	-0.0216	1	1	0.560538
1	0.0822	0.02914	0.01896	-0.0277	0.986	1	2.820865
1.5	0.1781	0.03223	0.02181	-0.0383	0.9498	1	5.525908
2	0.2621	0.03473	0.02423	-0.0459	0.9138	1	7.54679
2.5	0.3473	0.03662	0.02616	-0.0525	0.8744	1	9.483889
3	0.4152	0.03788	0.0275	-0.0558	0.8371	1	10.96093
3.5	0.4969	0.03861	0.02839	-0.06	0.7965	1	12.86972

4	0.6003	0.03699	0.02726	-0.0636	0.7448	1	16.22871
4.5	0.7312	0.03202	0.02293	-0.067	0.6955	1	22.83573
5	0.8457	0.02713	0.01845	-0.0674	0.6281	1	31.17213
5.5	0.9173	0.02575	0.0168	-0.064	0.5191	1	35.6233
6	0.9578	0.02707	0.01756	-0.0592	0.4181	1	35.38234
6.5	1.0111	0.02958	0.0199	-0.058	0.3611	1	34.18188
8	1.1075	0.03451	0.02552	-0.0468	0.249	1	32.09215
9.5	1.0517	0.04308	0.03362	-0.0219	0.0686	1	24.41272
10	1.0527	0.04858	0.03907	-0.0182	0.0523	1	21.66941
10.5	1.0487	0.05491	0.04553	-0.0157	0.0438	1	19.09852
11	1.0535	0.06133	0.05243	-0.0137	0.0389	1	17.17756
11.5	1.0515	0.06871	0.06034	-0.013	0.0358	1	15.30345
12	1.037	0.07791	0.07004	-0.0144	0.0336	1	13.31023
12.5	1.0164	0.08905	0.08174	-0.0178	0.0344	1	11.41381
13	0.9839	0.10363	0.09683	-0.0248	0.0366	1	9.494355
13.5	0.9444	0.12201	0.11553	-0.0349	0.0411	1	7.740349
14	0.8807	0.15484	0.14843	-0.0526	0.0586	1	5.687807
14.5	0.8767	0.16791	0.1614	-0.058	0.0604	1	5.221249
15	0.8797	0.17989	0.17332	-0.0623	0.0616	1	4.890211

- 5˚
    - Airfoil 1

Table AVIII-61: Aerodynamic performance of Airfoil 1 of the Polyurethane/IA-700 coated blade at 5°

alpha	CL	CD	CDp	CM	Top_Xtr	Bot_Xtr	CL/CD
------	--------	---------	---------	--------	--------	--------	--------
-5	-0.4167	0.02793	0.01768	-0.0332	1	0.164	-14.9194
-4.5	-0.378	0.02517	0.01481	-0.0299	1	0.1729	-15.0179
-4	-0.3406	0.02308	0.01267	-0.0263	1	0.1935	-14.7574
-3.5	-0.3134	0.01925	0.01119	-0.0216	1	0.5094	-16.2805
-2.5	-0.3206	0.02041	0.01277	0.011	1	0.8697	-15.708
-2	-0.075	0.02166	0.01292	-0.0198	1	1	-3.4626
-1.5	-0.1066	0.021	0.0122	-0.0116	1	1	-5.07619
-1	-0.1189	0.0204	0.01142	-0.0062	1	1	-5.82843
-0.5	-0.0885	0.02077	0.01144	-0.0067	1	1	-4.26095
0	-0.0384	0.0218	0.01215	-0.0101	0.9953	1	-1.76147
0.5	0.0455	0.02369	0.01373	-0.0192	0.9747	1	1.920642
1	0.1188	0.02545	0.01532	-0.0259	0.9539	1	4.667976
1.5	0.1869	0.02727	0.01706	-0.0314	0.9336	1	6.853685
2	0.2545	0.02915	0.01895	-0.0363	0.911	1	8.730703
2.5	0.3163	0.03114	0.021	-0.0402	0.89	1	10.15735
3	0.3779	0.03315	0.02315	-0.0436	0.8647	1	11.3997

3.5	0.4425	0.0352	0.02555	-0.0469	0.8366	1	12.57102
4	0.5159	0.03705	0.0278	-0.0504	0.8021	1	13.92443
4.5	0.7095	0.02595	0.01784	-0.0468	0.6637	1	27.34104
5.5	0.753	0.0275	0.01617	-0.0239	0.1846	1	27.38182
6	0.8191	0.03122	0.0199	-0.0237	0.1631	1	26.23639
6.5	0.8748	0.03526	0.02398	-0.0234	0.1424	1	24.80998
7.5	0.9634	0.04539	0.03569	-0.0201	0.1325	1	21.22494
8	0.9892	0.05252	0.04371	-0.0177	0.1342	1	18.83473
8.5	1.0025	0.06105	0.05296	-0.0156	0.1384	1	16.42097
9	0.9955	0.06975	0.06244	-0.0134	0.1456	1	14.2724
9.5	0.9005	0.08213	0.07526	-0.0137	0.154	1	10.96432
11	0.7197	0.14221	0.13491	-0.0589	0.3141	1	5.060826
12	0.7477	0.1578	0.15056	-0.0618	0.2848	1	4.738276
12.5	0.7506	0.16489	0.15765	-0.0643	0.2709	1	4.552126
13	0.8008	0.17801	0.17099	-0.0639	0.2573	1	4.498624
13.5	0.7745	0.17937	0.17222	-0.0686	0.2425	1	4.31789
14	0.8129	0.19311	0.18612	-0.069	0.2325	1	4.209518
14.5	0.8012	0.19442	0.18739	-0.0733	0.2171	1	4.120975
15	0.8145	0.20309	0.19611	-0.0759	0.2061	1	4.010537

- Airfoil 2

Table AVIII-62: Aerodynamic performance of Airfoil 2 of the Polyurethane/IA-700 coated blade at 5°

alpha	CL	CD	CDp	CM	Top_Xtr	Bot_Xtr	CL/CD
------	--------	---------	---------	--------	--------	--------	--------
-4.5	-0.3028	0.02658	0.01612	-0.0414	1	0.0602	-11.392
-4	-0.2693	0.02425	0.01363	-0.0375	1	0.0668	-11.1052
-3.5	-0.2284	0.02189	0.01101	-0.036	1	0.0916	-10.434
-2.5	-0.2418	0.02075	0.01315	-0.0046	1	0.832	-11.653
-1.5	-0.1105	0.01992	0.01147	-0.0105	1	1	-5.54719
-1	-0.083	0.01998	0.01118	-0.0121	1	1	-4.15415
-0.5	-0.0153	0.02105	0.01177	-0.0198	0.9914	1	-0.72684
0	0.0754	0.02275	0.01313	-0.0308	0.9714	1	3.314286
0.5	0.1581	0.02441	0.01461	-0.0396	0.9498	1	6.476854
1	0.2376	0.02619	0.01626	-0.0473	0.9291	1	9.072165
1.5	0.3062	0.02796	0.01799	-0.0527	0.908	1	10.95136
2	0.3666	0.02981	0.01989	-0.0564	0.8866	1	12.29789
2.5	0.4284	0.03178	0.02202	-0.06	0.8638	1	13.48018
3	0.4924	0.03378	0.02423	-0.0634	0.8388	1	14.57667
3.5	0.5654	0.03575	0.02655	-0.0675	0.8124	1	15.81538
5	0.7802	0.02539	0.01471	-0.038	0.2097	1	30.72863
5.5	0.8272	0.02876	0.01796	-0.0357	0.1746	1	28.76217

6	0.8933	0.03284	0.02203	-0.0354	0.1618	1	27.20158
6.5	0.9466	0.03671	0.02653	-0.0346	0.1479	1	25.78589
7	0.9969	0.04284	0.0331	-0.034	0.1421	1	23.27031
7.5	1.036	0.04952	0.0407	-0.0324	0.1424	1	20.92084
8	1.0503	0.05733	0.04991	-0.0298	0.1483	1	18.32025
8.5	1.0394	0.06815	0.06164	-0.0287	0.1569	1	15.25165
9	1.021	0.0795	0.07346	-0.0291	0.1671	1	12.84277
9.5	0.8915	0.10059	0.09443	-0.0431	0.1817	1	8.86271
11	0.7846	0.15119	0.14445	-0.0801	0.3213	1	5.189497
11.5	0.8413	0.16537	0.15899	-0.0798	0.3064	1	5.08738
12.5	0.8189	0.17427	0.16778	-0.0852	0.2663	1	4.69903
13	0.8295	0.18175	0.1753	-0.0871	0.2449	1	4.563961
13.5	0.848	0.19157	0.18519	-0.0888	0.2311	1	4.42658
14	0.8945	0.20887	0.2027	-0.0875	0.2107	1	4.282568
14.5	0.8637	0.20545	0.19911	-0.0949	0.1983	1	4.203943
15	0.8759	0.21344	0.20712	-0.0975	0.1785	1	4.103729

- Airfoil 3

Table AVIII-63: Aerodynamic performance of Airfoil 3 of the Polyurethane/IA-700 coated blade at 5°

alpha	CL	CD	CDp	CM	Top_Xtr	Bot_Xtr	CL/CD
------	--------	---------	---------	--------	--------	--------	--------
-4.5	-0.3303	0.01924	0.01171	-0.0368	1	0.4198	-17.1674
-3.5	-0.3403	0.02264	0.01543	-0.0025	1	0.7719	-15.0309
-3	-0.3404	0.02175	0.01438	0.0109	1	0.8563	-15.6506
-2.5	-0.2801	0.02105	0.01319	0.011	1	0.932	-13.3064
-2	-0.1116	0.0215	0.01259	-0.0127	1	0.9878	-5.1907
-1.5	-0.1081	0.02095	0.01192	-0.011	1	1	-5.1599
-1	-0.1031	0.02065	0.01141	-0.0091	1	1	-4.99274
-0.5	-0.0504	0.0215	0.01191	-0.0145	0.9953	1	-2.34419
0	0.041	0.02328	0.01338	-0.026	0.9727	1	1.761168
0.5	0.1245	0.02504	0.01491	-0.0353	0.9511	1	4.972045
1	0.1985	0.02675	0.0165	-0.0423	0.9301	1	7.420561
1.5	0.268	0.02848	0.01821	-0.048	0.9088	1	9.410112
2	0.3309	0.03026	0.0201	-0.0523	0.8879	1	10.93523
2.5	0.3885	0.03219	0.02215	-0.0555	0.8679	1	12.06897
3	0.4446	0.03429	0.02446	-0.0584	0.8472	1	12.96588
3.5	0.4988	0.03654	0.027	-0.0607	0.8253	1	13.65079
4	0.5538	0.03884	0.02994	-0.0627	0.8003	1	14.2585
4.5	0.632	0.03999	0.03177	-0.065	0.7574	1	15.80395
5.5	0.7936	0.0285	0.01805	-0.0365	0.1265	1	27.84561
6	0.8438	0.0347	0.02419	-0.0331	0.0824	1	24.317

6.5	0.9125	0.04093	0.03114	-0.0319	0.0744	1	22.29416
7	0.9556	0.0487	0.03986	-0.0293	0.0745	1	19.62218
7.5	0.9769	0.05682	0.0489	-0.026	0.0747	1	17.19289
8	0.9798	0.06482	0.05769	-0.0227	0.0736	1	15.11571
8.5	0.9661	0.07347	0.0669	-0.0202	0.0754	1	13.14958
9	0.9401	0.08236	0.07608	-0.0186	0.0784	1	11.41452
9.5	0.9121	0.09272	0.08656	-0.0199	0.0808	1	9.837144
10	0.7939	0.1313	0.12534	-0.0581	0.2436	1	6.046458
11	0.7796	0.1513	0.14516	-0.0676	0.2463	1	5.152677
12	0.8201	0.17344	0.16725	-0.0694	0.2169	1	4.728436
13	0.8057	0.18435	0.17798	-0.0777	0.1841	1	4.370491
14	0.8502	0.20565	0.19926	-0.0793	0.1484	1	4.134209
15	0.8897	0.22881	0.22243	-0.0827	0.127	1	3.888379

- Airfoil 4

Table AVIII-64: Aerodynamic performance of Airfoil 4 of the Polyurethane/IA-700 coated blade at 5°

alpha	CL	CD	CDp	CM	Top_Xtr	Bot_Xtr	CL/CD
------	--------	---------	---------	--------	--------	--------	--------
-5	-0.4148	0.02916	0.01914	-0.0429	1	0.0547	-14.225
-4.5	-0.378	0.02612	0.01571	-0.0383	1	0.0609	-14.4717
-4	-0.3455	0.0228	0.01236	-0.0349	1	0.0917	-15.1535
-3.5	-0.3234	0.01977	0.01189	-0.0301	1	0.5596	-16.3581
-3	-0.3155	0.02137	0.0136	-0.0173	1	0.6876	-14.7637
-2.5	-0.3359	0.02215	0.01468	0.0034	1	0.8108	-15.1648
-2	-0.3218	0.02126	0.01368	0.0149	1	0.9046	-15.1364
-1	-0.0965	0.02182	0.01278	-0.0134	1	1	-4.42255
-0.5	-0.1168	0.02114	0.01203	-0.0076	1	1	-5.52507
0	-0.0796	0.02161	0.01221	-0.0107	0.9973	1	-3.68348
0.5	0.0131	0.02339	0.01359	-0.0226	0.9742	1	0.560068
1	0.0987	0.02518	0.01513	-0.0325	0.9527	1	3.919778
1.5	0.1794	0.02696	0.01679	-0.0407	0.9315	1	6.654303
2	0.2465	0.0286	0.01837	-0.0462	0.9107	1	8.618881
2.5	0.3062	0.03028	0.02003	-0.0501	0.8904	1	10.11229
3	0.3632	0.0321	0.02193	-0.0533	0.8703	1	11.31464
3.5	0.4156	0.03412	0.02409	-0.0556	0.8506	1	12.18054
4	0.4735	0.03618	0.02642	-0.0584	0.8278	1	13.08734
4.5	0.5341	0.03833	0.02943	-0.061	0.8028	1	13.93426
5	0.6058	0.04018	0.03191	-0.0641	0.7741	1	15.07715
6	0.7802	0.02716	0.01708	-0.0372	0.1124	1	28.72607
6.5	0.7977	0.03218	0.02193	-0.0317	0.0745	1	24.78869
7	0.864	0.03704	0.02698	-0.0303	0.0621	1	23.32613

7.5	0.9292	0.04475	0.03517	-0.03	0.0594	1	20.76425
8	0.9672	0.05173	0.04309	-0.027	0.0611	1	18.69708
8.5	0.9786	0.05983	0.05235	-0.0227	0.0655	1	16.35634
9	0.9682	0.06876	0.06207	-0.0191	0.0699	1	14.08086
9.5	0.9441	0.07741	0.07114	-0.0165	0.0732	1	12.1961
10	0.9123	0.08663	0.08056	-0.0162	0.0759	1	10.53099
10.5	0.8924	0.09702	0.09114	-0.0191	0.0817	1	9.198103
11	0.8229	0.11485	0.109	-0.035	0.0858	1	7.164998
11.5	0.8002	0.13298	0.12699	-0.0465	0.1083	1	6.017446
12.5	0.775	0.16362	0.15746	-0.067	0.2015	1	4.736585
13.5	0.7903	0.18028	0.17399	-0.0726	0.1786	1	4.383736
14	0.8337	0.19572	0.18948	-0.0709	0.167	1	4.259657
14.5	0.8101	0.19638	0.18999	-0.0786	0.1552	1	4.125165
15	0.8536	0.21392	0.20757	-0.0767	0.1448	1	3.990277

- Airfoil 5

Table AVIII-65: Aerodynamic performance of Airfoil 5 of the Polyurethane/IA-700 coated blade at 5°

alpha	CL	CD	CDp	CM	Top_Xtr	Bot_Xtr	CL/CD
------	--------	---------	---------	--------	--------	--------	--------
-5	-0.3516	0.02264	0.01316	-0.0435	1	0.2711	-15.53
-4.5	-0.3123	0.0202	0.0117	-0.0409	1	0.385	-15.4604
-4	-0.3105	0.02207	0.01445	-0.0256	1	0.6538	-14.0689
-3.5	-0.303	0.02289	0.0151	-0.0141	1	0.7376	-13.2372
-3	-0.2886	0.02267	0.01464	-0.0058	1	0.7937	-12.7305
-2.5	-0.2811	0.02192	0.01381	0.0039	1	0.8671	-12.8239
-2	-0.1293	0.02275	0.01396	-0.012	1	0.9874	-5.68352
-1.5	-0.125	0.02223	0.01331	-0.0105	1	1	-5.62303
-1	-0.1068	0.02216	0.01299	-0.0107	1	1	-4.81949
-0.5	-0.013	0.02399	0.01443	-0.0233	0.9797	1	-0.54189
0	0.067	0.02562	0.01577	-0.0326	0.9601	1	2.615144
0.5	0.1474	0.02745	0.01739	-0.0413	0.941	1	5.369763
1	0.2175	0.02919	0.019	-0.0476	0.9233	1	7.451182
1.5	0.2781	0.03087	0.02068	-0.0519	0.9054	1	9.008746
2	0.3275	0.0326	0.02241	-0.0542	0.8888	1	10.04601
2.5	0.3804	0.03455	0.02442	-0.0569	0.8721	1	11.01013
3	0.4378	0.03668	0.02672	-0.06	0.8548	1	11.93566
3.5	0.4988	0.0389	0.02935	-0.0633	0.8353	1	12.82262
4	0.5535	0.04113	0.03193	-0.0654	0.8122	1	13.45733
4.5	0.6044	0.04322	0.03446	-0.0661	0.7811	1	13.98427
5.5	0.8112	0.03025	0.01946	-0.0411	0.0941	1	26.81653
6.5	0.9236	0.04093	0.03047	-0.0374	0.0507	1	22.56536

7	0.975	0.04811	0.03838	-0.0357	0.0498	1	20.26606
7.5	0.9997	0.05589	0.04718	-0.0319	0.052	1	17.88692
8	1.0014	0.06421	0.0564	-0.0275	0.0551	1	15.5957
8.5	0.9862	0.0725	0.0653	-0.0236	0.058	1	13.60276
9	0.9557	0.08043	0.07358	-0.0205	0.06	1	11.88238
9.5	0.9199	0.08985	0.08324	-0.0214	0.0618	1	10.23817
10	0.8907	0.10155	0.09505	-0.0258	0.064	1	8.771049
10.5	0.854	0.11589	0.10958	-0.0364	0.0697	1	7.369057
11	0.8231	0.13555	0.12912	-0.0499	0.0817	1	6.072298
12.5	0.4323	0.08061	0.07611	-0.0473	0.2099	1	5.362858
13	0.4557	0.08975	0.08518	-0.0503	0.1952	1	5.077437
13.5	0.4911	0.10084	0.09626	-0.0513	0.1761	1	4.870091
14	0.4909	0.10659	0.10191	-0.0574	0.1629	1	4.605498
14.5	0.5228	0.1188	0.11408	-0.0591	0.1531	1	4.400673
15	0.5269	0.12511	0.12032	-0.0647	0.1413	1	4.211494

- Airfoil 6

Table AVIII-66: Aerodynamic performance of Airfoil 6 of the Polyurethane/IA-700 coated blade at 5°

alpha	CL	CD	CDp	CM	Top_Xtr	Bot_Xtr	CL/CD
------	--------	---------	---------	--------	--------	--------	--------
-5	-0.4164	0.02799	0.0187	-0.037	1	0.2464	-14.8767
-4.5	-0.3739	0.02555	0.01593	-0.0351	1	0.2688	-14.6341
-4	-0.3311	0.02378	0.01416	-0.0333	1	0.3029	-13.9235
-3.5	-0.2904	0.02237	0.01311	-0.031	1	0.3751	-12.9817
-3	-0.2701	0.02239	0.01424	-0.0223	1	0.6017	-12.0634
-2.5	-0.2532	0.02262	0.01445	-0.0135	1	0.7114	-11.1936
-2	-0.2335	0.02222	0.01406	-0.0063	1	0.7979	-10.5086
-1.5	-0.1883	0.02196	0.01404	-0.0037	1	0.9174	-8.57468
-1	-0.1174	0.02227	0.01385	-0.0127	1	1	-5.27167
-0.5	-0.075	0.02308	0.01419	-0.0158	1	1	-3.24957
0	0.0173	0.02529	0.01592	-0.0271	0.9777	1	0.684065
0.5	0.1056	0.02752	0.01775	-0.0367	0.9539	1	3.837209
1	0.1751	0.02932	0.01933	-0.0423	0.9282	1	5.972033
1.5	0.2537	0.03132	0.02119	-0.0488	0.9013	1	8.100255
2	0.3337	0.03327	0.02308	-0.0548	0.8738	1	10.03006
2.5	0.3874	0.03495	0.02478	-0.0564	0.845	1	11.08441
3	0.4461	0.03653	0.0265	-0.0583	0.8127	1	12.21188
3.5	0.5505	0.03683	0.02707	-0.0643	0.7762	1	14.94705
4	0.6529	0.03486	0.02557	-0.0664	0.7284	1	18.7292
4.5	0.7613	0.03018	0.0213	-0.065	0.6771	1	25.22531
5	0.8271	0.02784	0.01925	-0.0602	0.6151	1	29.70905

5.5	0.8857	0.02575	0.01723	-0.054	0.5185	1	34.39612
6	0.9203	0.02622	0.01679	-0.0468	0.3848	1	35.09916
6.5	0.9647	0.02896	0.01914	-0.0441	0.3186	1	33.31146
7	1.0101	0.03149	0.02147	-0.0423	0.2787	1	32.07685
7.5	1.0352	0.03288	0.02299	-0.0383	0.2363	1	31.48418
8.5	1.0749	0.03619	0.02672	-0.0299	0.1724	1	29.70158
9	1.0818	0.03837	0.0292	-0.0245	0.1415	1	28.1939
9.5	1.0743	0.04201	0.03294	-0.0186	0.1048	1	25.57248
10	1.0825	0.04738	0.03845	-0.0145	0.0746	1	22.84719
10.5	1.1014	0.05317	0.04438	-0.0117	0.064	1	20.71469
11	1.1083	0.0607	0.05265	-0.0093	0.0603	1	18.25865
11.5	1.088	0.06967	0.06222	-0.0083	0.0592	1	15.61648
12	1.0465	0.08124	0.07431	-0.0109	0.0597	1	12.88159
12.5	0.9918	0.09675	0.09018	-0.0188	0.0615	1	10.25116
13	0.9369	0.11643	0.10999	-0.0305	0.064	1	8.046895
13.5	0.901	0.13583	0.12933	-0.0407	0.0655	1	6.633292
14	0.8526	0.1633	0.15659	-0.057	0.0739	1	5.221066
14.5	0.8473	0.17682	0.17002	-0.0634	0.0778	1	4.791879
15	0.8524	0.1883	0.18145	-0.0679	0.0826	1	4.526819

- 10˚
    - Airfoil 1

Table AVIII-67: Aerodynamic performance of Airfoil 1 of the Polyurethane/IA-700 coated blade at 10°

alpha	CL	CD	CDp	CM	Top_Xtr	Bot_Xtr	CL/CD
------	--------	---------	---------	--------	--------	--------	--------
-5	-0.4088	0.03223	0.02225	-0.0415	1	0.1355	-12.6838
-4.5	-0.3712	0.02885	0.01844	-0.0388	1	0.1366	-12.8666
-4	-0.3332	0.02624	0.01562	-0.0358	1	0.1427	-12.6982
-3.5	-0.2958	0.02429	0.01356	-0.0325	1	0.1604	-12.1779
-2	-0.2637	0.02063	0.01303	0.0001	1	0.8377	-12.7824
-1.5	-0.0955	0.02121	0.01297	-0.0162	1	1	-4.50259
-1	-0.1187	0.02041	0.01207	-0.0095	1	1	-5.81578
-0.5	-0.0925	0.02052	0.01184	-0.0098	1	1	-4.5078
0	-0.0508	0.02125	0.01216	-0.012	1	1	-2.39059
0.5	0.0115	0.02272	0.01332	-0.0175	0.992	1	0.506162
1	0.0933	0.02464	0.015	-0.026	0.9701	1	3.786526
1.5	0.1715	0.02655	0.01678	-0.0334	0.946	1	6.45951
2	0.2402	0.02846	0.01865	-0.0387	0.925	1	8.439916
2.5	0.3069	0.03041	0.02065	-0.0434	0.9027	1	10.09207
3.5	0.6189	0.02318	0.01447	-0.0552	0.7178	1	26.69974
4	0.6463	0.01994	0.01024	-0.0387	0.3846	1	32.41224

4.5	0.6649	0.02447	0.01269	-0.0336	0.2018	1	27.17205
5	0.7078	0.02702	0.01504	-0.0317	0.1673	1	26.19541
5.5	0.7682	0.0299	0.01778	-0.0313	0.1534	1	25.69231
6	0.8316	0.03302	0.0212	-0.0314	0.1466	1	25.18474
6.5	0.8884	0.03691	0.0255	-0.031	0.1441	1	24.06936
7	0.9364	0.04162	0.03087	-0.0299	0.1453	1	22.4988
7.5	0.9742	0.04735	0.03736	-0.0283	0.149	1	20.57445
8	1.004	0.05437	0.0451	-0.0268	0.1538	1	18.46607
8.5	1.0143	0.06138	0.05309	-0.0244	0.1619	1	16.52493
9	0.9795	0.07275	0.06525	-0.0229	0.1744	1	13.46392
10.5	0.3701	0.06655	0.06093	-0.037	0.3262	1	5.561232
11	0.3928	0.07355	0.0679	-0.0398	0.32	1	5.340585
11.5	0.4067	0.07873	0.07306	-0.0427	0.3037	1	5.165756
12	0.4331	0.08646	0.08078	-0.045	0.2966	1	5.009253
12.5	0.4445	0.09141	0.08577	-0.0482	0.2805	1	4.862706
13	0.474	0.10027	0.09466	-0.0502	0.2735	1	4.727236
13.5	0.48	0.10461	0.09899	-0.054	0.259	1	4.588471
14	0.5233	0.11647	0.11096	-0.0546	0.2511	1	4.493002
14.5	0.5145	0.11859	0.11303	-0.0601	0.2402	1	4.338477
15	0.5442	0.1276	0.12215	-0.0617	0.2298	1	4.26489

- Airfoil 2

Table AVIII-68: Aerodynamic performance of Airfoil 2 of the Polyurethane/IA-700 coated blade at 10°

alpha	CL	CD	CDp	CM	Top_Xtr	Bot_Xtr	CL/CD
------	--------	---------	---------	--------	--------	--------	--------
-4.5	-0.3561	0.02833	0.018	-0.0407	1	0.1054	-12.5697
-4	-0.3211	0.02524	0.0148	-0.0363	1	0.1199	-12.7219
-3.5	-0.2895	0.02206	0.01217	-0.0326	1	0.1847	-13.1233
-2.5	-0.3123	0.02142	0.01441	0.0024	1	0.8105	-14.5798
-1.5	-0.0888	0.02149	0.01315	-0.0161	1	1	-4.13215
-1	-0.1174	0.02061	0.01222	-0.0088	1	1	-5.69626
-0.5	-0.0997	0.02049	0.01177	-0.0083	1	1	-4.86579
0	-0.0324	0.02169	0.01246	-0.0156	0.9895	1	-1.49378
0.5	0.0538	0.02341	0.01385	-0.0255	0.969	1	2.298163
1	0.1346	0.02516	0.01538	-0.0337	0.9482	1	5.349762
1.5	0.2076	0.02684	0.01696	-0.0401	0.9269	1	7.734724
2	0.2725	0.02851	0.01862	-0.0446	0.9042	1	9.55805
2.5	0.3327	0.03035	0.02047	-0.0482	0.8819	1	10.96211
3	0.3966	0.03225	0.02248	-0.0519	0.8568	1	12.29767
3.5	0.4534	0.03435	0.02475	-0.0544	0.8321	1	13.19942
4	0.5132	0.03648	0.02726	-0.0568	0.8042	1	14.06798

4.5	0.5918	0.03823	0.02948	-0.0605	0.7706	1	15.47999
5	0.7684	0.0225	0.0147	-0.0462	0.572	1	34.15111
5.5	0.7663	0.02585	0.01497	-0.0335	0.1939	1	29.6441
6	0.8108	0.02948	0.01827	-0.0311	0.1557	1	27.50339
6.5	0.8744	0.03321	0.02207	-0.0308	0.1374	1	26.32942
7	0.9364	0.03872	0.02776	-0.0309	0.1316	1	24.18388
7.5	0.9808	0.04389	0.03379	-0.0293	0.1285	1	22.34678
8	1.0134	0.04998	0.04078	-0.0272	0.1259	1	20.27611
8.5	1.0358	0.05806	0.04961	-0.0252	0.1296	1	17.84017
9	1.033	0.06651	0.05903	-0.0227	0.1365	1	15.5315
9.5	0.977	0.07783	0.071	-0.0212	0.1455	1	12.553
10	0.9282	0.08979	0.08311	-0.0238	0.1552	1	10.33745
11	0.7419	0.14123	0.134	-0.0676	0.3195	1	5.253133
11.5	0.8	0.15491	0.1479	-0.0675	0.3088	1	5.164289
12	0.764	0.15675	0.14958	-0.0713	0.2891	1	4.874003
12.5	0.8282	0.17415	0.16717	-0.0708	0.2784	1	4.75567
13	0.7889	0.17201	0.16487	-0.0755	0.2594	1	4.586361
13.5	0.8286	0.18629	0.17926	-0.0762	0.2492	1	4.447904
14	0.814	0.187	0.17991	-0.0803	0.2317	1	4.352941
14.5	0.8398	0.19867	0.19168	-0.0818	0.2212	1	4.22711
15	0.8476	0.20283	0.19588	-0.0846	0.2024	1	4.178869

- Airfoil 3

Table AVIII-69: Aerodynamic performance of Airfoil 1 of the Polyurethane/IA-700 coated blade at 10°

alpha	CL	CD	CDp	CM	Top_Xtr	Bot_Xtr	CL/CD
------	--------	---------	---------	--------	--------	--------	--------
-5	-0.4164	0.02479	0.01456	-0.0304	1	0.1867	-16.7971
-4.5	-0.3817	0.02154	0.0116	-0.0266	1	0.2547	-17.7205
-4	-0.3828	0.02062	0.01296	-0.0123	1	0.6566	-18.5645
-3.5	-0.381	0.02171	0.01411	0.0027	1	0.762	-17.5495
-3	-0.3793	0.02148	0.01389	0.0179	1	0.8676	-17.6583
-2.5	-0.1579	0.02261	0.0139	-0.0085	1	0.9699	-6.98364
-2	-0.0754	0.02212	0.0129	-0.0193	1	1	-3.40868
-1.5	-0.1094	0.02139	0.01217	-0.011	1	1	-5.11454
-1	-0.1234	0.02073	0.01135	-0.0056	1	1	-5.95273
-0.5	-0.0936	0.02114	0.01144	-0.0061	1	1	-4.42763
0	-0.0293	0.02252	0.01251	-0.0123	0.9889	1	-1.30107
0.5	0.0473	0.02427	0.014	-0.0201	0.9694	1	1.948908
1	0.1196	0.02608	0.01566	-0.0266	0.9497	1	4.58589
1.5	0.188	0.02798	0.01754	-0.0321	0.9319	1	6.719085
2	0.2563	0.02994	0.01951	-0.0373	0.9131	1	8.560454

2.5	0.3137	0.03179	0.02145	-0.0405	0.8932	1	9.867883
3	0.3686	0.03379	0.02361	-0.043	0.872	1	10.90855
3.5	0.4277	0.03594	0.02617	-0.0459	0.849	1	11.90039
4	0.4882	0.03825	0.02882	-0.0487	0.8244	1	12.7634
4.5	0.5322	0.0403	0.03126	-0.0485	0.7903	1	13.20596
5	0.7595	0.02656	0.0194	-0.0461	0.6406	1	28.59563
5.5	0.7659	0.02489	0.01518	-0.027	0.2472	1	30.77139
6	0.8113	0.02987	0.01952	-0.0239	0.1751	1	27.16103
6.5	0.8702	0.03559	0.02523	-0.0229	0.1272	1	24.45069
7	0.9127	0.04128	0.03123	-0.021	0.0986	1	22.10998
8.5	0.9712	0.06526	0.05773	-0.0115	0.0963	1	14.88201
9	0.931	0.07455	0.06782	-0.0083	0.1034	1	12.48826
9.5	0.8888	0.0839	0.07738	-0.0077	0.1081	1	10.59356
10	0.8555	0.09587	0.08948	-0.0123	0.117	1	8.923542
10.5	0.7748	0.1195	0.11291	-0.0328	0.146	1	6.483682
11.5	0.4175	0.0804	0.07547	-0.0333	0.2911	1	5.192786
12	0.4207	0.08548	0.08049	-0.0368	0.273	1	4.921619
12.5	0.4313	0.09247	0.08743	-0.0401	0.2564	1	4.664215
13.5	0.4732	0.10811	0.10304	-0.0444	0.2065	1	4.377023
14	0.4847	0.11585	0.11072	-0.0481	0.1959	1	4.183858
14.5	0.5284	0.13007	0.125	-0.048	0.1801	1	4.062428
15	0.5158	0.13186	0.12669	-0.0545	0.1716	1	3.911725

- Airfoil 4

Table AVIII-70: Aerodynamic performance of Airfoil 4 of the Polyurethane/IA-700 coated blade at 10°

alpha	CL	CD	CDp	CM	Top_Xtr	Bot_Xtr	CL/CD
------	--------	---------	---------	--------	--------	--------	--------
-4	-0.3576	0.02323	0.01586	-0.0008	1	0.7633	-15.3939
-3.5	-0.3502	0.02266	0.01508	0.0101	1	0.8346	-15.4545
-3	-0.3067	0.02203	0.01417	0.0151	1	0.9242	-13.9219
-2.5	-0.1222	0.02272	0.01382	-0.0108	1	0.9843	-5.37852
-2	-0.1028	0.02226	0.01321	-0.0116	1	1	-4.61815
-1.5	-0.1169	0.02157	0.01241	-0.0067	1	1	-5.41956
-1	-0.0826	0.02201	0.01254	-0.0089	0.9995	1	-3.75284
-0.5	0.0099	0.02398	0.01412	-0.0208	0.9785	1	0.412844
0	0.0879	0.02563	0.01555	-0.0292	0.9563	1	3.429575
0.5	0.1586	0.02736	0.01713	-0.0357	0.9366	1	5.796784
1	0.2264	0.02914	0.01888	-0.0413	0.9164	1	7.769389
1.5	0.2912	0.03098	0.02071	-0.046	0.8966	1	9.399613
2	0.3545	0.03289	0.0227	-0.0502	0.8762	1	10.77835
2.5	0.4157	0.03492	0.02489	-0.0537	0.8554	1	11.90435

3	0.4734	0.03708	0.02747	-0.0564	0.8337	1	12.76699
3.5	0.5239	0.03938	0.03008	-0.058	0.8098	1	13.30371
4	0.7084	0.03302	0.02485	-0.0634	0.7142	1	21.45366
4.5	0.8132	0.02701	0.01998	-0.0582	0.6395	1	30.10737
5	0.8321	0.02372	0.01517	-0.0407	0.3195	1	35.0801
5.5	0.8608	0.02834	0.01866	-0.0362	0.2174	1	30.37403
6	0.9189	0.03365	0.02371	-0.0353	0.1572	1	27.30758
7.5	1.0254	0.05853	0.05026	-0.0277	0.0974	1	17.51922
8	1.0343	0.06792	0.06049	-0.0239	0.0994	1	15.22821
8.5	0.9878	0.07477	0.06843	-0.0185	0.1066	1	13.21118
9	0.9368	0.0839	0.07784	-0.0172	0.1115	1	11.16567
11	0.7847	0.15718	0.15085	-0.0661	0.2743	1	4.992365
11.5	0.8125	0.16886	0.16258	-0.066	0.2531	1	4.811678
12.5	0.7912	0.179	0.17256	-0.0732	0.2159	1	4.420112
13	0.7986	0.18714	0.18064	-0.076	0.1994	1	4.267393
13.5	0.8166	0.19716	0.19064	-0.0776	0.1831	1	4.141814
14	0.8269	0.20456	0.19798	-0.08	0.1607	1	4.042335
14.5	0.8506	0.21621	0.20961	-0.0807	0.1409	1	3.934138
15	0.8453	0.21846	0.21176	-0.0871	0.1295	1	3.869358

- Airfoil 5

Table AVIII-71: Aerodynamic performance of Airfoil 5 of the Polyurethane/IA-700 coated blade at 10°

alpha	CL	CD	CDp	CM	Top_Xtr	Bot_Xtr	CL/CD
------	--------	---------	---------	--------	--------	--------	--------
-5	-0.3097	0.02152	0.01184	-0.0439	1	0.2811	-14.3913
-4	-0.2678	0.02171	0.01372	-0.0259	1	0.6371	-12.3353
-3.5	-0.254	0.02207	0.014	-0.0169	1	0.7112	-11.5088
-3	-0.2377	0.02169	0.01349	-0.0099	1	0.7769	-10.959
-2.5	-0.2251	0.02099	0.01282	-0.0023	1	0.8478	-10.7242
-2	-0.1688	0.02082	0.0126	-0.0035	1	0.9429	-8.10759
-1.5	-0.0619	0.02172	0.01307	-0.0199	0.984	1	-2.84991
-1	0.0358	0.02305	0.01393	-0.0336	0.9581	1	1.553145
-0.5	0.1231	0.02434	0.01489	-0.0439	0.9318	1	5.057518
0	0.2147	0.02572	0.01604	-0.0536	0.9076	1	8.347589
0.5	0.2834	0.02719	0.01738	-0.0591	0.8872	1	10.42295
1	0.3372	0.02885	0.01894	-0.0618	0.8679	1	11.68804
1.5	0.3887	0.03072	0.02077	-0.0639	0.8501	1	12.65299
2	0.4545	0.0327	0.0229	-0.0679	0.8351	1	13.89908
2.5	0.5016	0.03472	0.02505	-0.0689	0.8156	1	14.447
3	0.5444	0.03694	0.02743	-0.0691	0.7944	1	14.73741
3.5	0.5999	0.03893	0.02972	-0.0704	0.7696	1	15.40971

4	0.6749	0.03962	0.031	-0.0716	0.7303	1	17.03433
4.5	0.8205	0.03224	0.02454	-0.0686	0.654	1	25.44975
5	0.8952	0.02753	0.02043	-0.0601	0.5738	1	32.51725
6	0.945	0.02967	0.02038	-0.0407	0.2199	1	31.85035
8	1.0577	0.05892	0.05103	-0.027	0.0767	1	17.95146
9	1.047	0.07411	0.0671	-0.0209	0.0697	1	14.12765
10.5	0.8563	0.12362	0.11726	-0.0464	0.1036	1	6.926873
11.5	0.8546	0.17054	0.16414	-0.0689	0.2302	1	5.011141
12	0.8097	0.17151	0.16492	-0.0764	0.2147	1	4.721008
12.5	0.8467	0.18579	0.17924	-0.076	0.2051	1	4.557296
13	0.828	0.18817	0.18151	-0.0816	0.1899	1	4.400276
13.5	0.8432	0.19793	0.19124	-0.0836	0.1786	1	4.260092
14.5	0.8591	0.21182	0.20505	-0.0905	0.1512	1	4.055802
15	0.8781	0.22024	0.2136	-0.0923	0.1397	1	3.987014

- Airfoil 6

Table AVIII-72: Aerodynamic performance of Airfoil 6 of the Polyurethane/IA-700 coated blade at 10°

alpha	CL	CD	CDp	CM	Top_Xtr	Bot_Xtr	Cl/CD
------	--------	---------	---------	--------	--------	--------	--------
-5	-0.3978	0.02808	0.01807	-0.0411	1	0.2145	-14.1667
-4.5	-0.3577	0.02615	0.01583	-0.0392	1	0.2339	-13.6788
-4	-0.3146	0.02459	0.01391	-0.0374	1	0.2491	-12.7938
-3.5	-0.2741	0.0231	0.01261	-0.0353	1	0.2775	-11.8658
-3	-0.2379	0.02163	0.01255	-0.0323	1	0.4472	-10.9986
-2.5	-0.2288	0.02282	0.01417	-0.0216	1	0.6538	-10.0263
-2	-0.2122	0.02302	0.01441	-0.0139	1	0.737	-9.21807
-1.5	-0.1946	0.02261	0.0142	-0.0068	1	0.8262	-8.60681
-1	-0.1222	0.02262	0.01441	-0.0123	1	1	-5.4023
-0.5	-0.0257	0.02452	0.01571	-0.0258	0.9776	1	-1.04812
0	0.06	0.02626	0.01702	-0.0358	0.9515	1	2.284844
0.5	0.1407	0.02808	0.01851	-0.0438	0.9262	1	5.010684
1	0.2147	0.02987	0.02007	-0.05	0.9021	1	7.187814
1.5	0.2847	0.03163	0.02166	-0.0549	0.8784	1	9.000948
2	0.3502	0.03334	0.02328	-0.0587	0.8548	1	10.5039
2.5	0.4114	0.03505	0.02501	-0.0614	0.8316	1	11.73752
3	0.4705	0.03681	0.02681	-0.0636	0.8081	1	12.78185
3.5	0.5315	0.03833	0.02844	-0.0652	0.7802	1	13.86642
4	0.5805	0.03982	0.03011	-0.0648	0.747	1	14.5781
4.5	0.7015	0.03787	0.02854	-0.0693	0.7102	1	18.5239
5	0.8164	0.03324	0.02445	-0.0689	0.6645	1	24.56077
5.5	0.8882	0.03011	0.02156	-0.064	0.6063	1	29.49851

6	0.9514	0.0265	0.01784	-0.0573	0.5244	1	35.90189
6.5	0.9719	0.02565	0.01669	-0.0483	0.4036	1	37.89084
7	0.9838	0.02781	0.01779	-0.0411	0.2792	1	35.37576
7.5	1.0064	0.03075	0.02022	-0.0369	0.2203	1	32.72846
8	1.0468	0.03362	0.02298	-0.0349	0.1915	1	31.13623
8.5	1.089	0.03636	0.02592	-0.0332	0.1695	1	29.9505
9	1.1177	0.03904	0.02887	-0.0303	0.1475	1	28.62961
9.5	1.1431	0.04223	0.0325	-0.0271	0.1272	1	27.06843
11	1.1564	0.06119	0.05272	-0.0147	0.0728	1	18.89851
12	1.0802	0.08062	0.07334	-0.013	0.0715	1	13.39866
13	0.9683	0.11315	0.10638	-0.0296	0.0746	1	8.557667
14	0.8614	0.16452	0.15754	-0.0607	0.0872	1	5.235838

- **After Erosion**
    - Uncoated
        - -5°
            - Airfoil 1

Table AVIII-73: Aerodynamic performance of Airfoil 1 of the uncoated blade at -5°

alpha	CL	CD	CDp	CM	Top_Xtr	Bot_Xtr	CL/CD
------	--------	---------	---------	--------	--------	--------	--------
-4	-0.3549	0.03481	0.0255	-0.035	1	0.1023	-10.1953
-3.5	-0.314	0.03073	0.02089	-0.0328	1	0.098	-10.218
-3	-0.2709	0.02788	0.01759	-0.0302	1	0.0968	-9.71664
-2.5	-0.2294	0.0259	0.01538	-0.0269	1	0.1002	-8.85714
-2	-0.1902	0.02421	0.01353	-0.0241	1	0.111	-7.85626
-1.5	-0.161	0.02043	0.01292	-0.0191	1	0.6849	-7.88057
-1	-0.1191	0.02043	0.01294	-0.0094	1	1	-5.82966
-0.5	-0.0922	0.02061	0.01256	-0.0094	1	1	-4.47356
0	-0.0511	0.02133	0.01277	-0.011	1	1	-2.39569
0.5	-0.0088	0.02235	0.01332	-0.0125	1	1	-0.39374
1	0.0643	0.02421	0.01483	-0.0194	0.9852	1	2.655927
1.5	0.1463	0.0264	0.01677	-0.0275	0.965	1	5.541667
2	0.2267	0.02853	0.01879	-0.0349	0.9417	1	7.946022
2.5	0.2984	0.03048	0.02075	-0.0403	0.9177	1	9.790026
3	0.362	0.03222	0.02262	-0.0439	0.8882	1	11.23526
3.5	0.6082	0.02177	0.01284	-0.0493	0.6975	1	27.93753
4	0.6194	0.02171	0.01029	-0.0337	0.2606	1	28.53063
4.5	0.6537	0.02497	0.01276	-0.0307	0.2006	1	26.17942
5	0.7077	0.02749	0.01504	-0.0299	0.183	1	25.74391
5.5	0.7727	0.03002	0.0178	-0.0303	0.1758	1	25.73951
6	0.834	0.03316	0.02118	-0.0305	0.1725	1	25.15078
6.5	0.8879	0.03699	0.02548	-0.0302	0.1719	1	24.00378
7	0.9336	0.04076	0.0294	-0.0295	0.162	1	22.90481
8	0.9969	0.04727	0.03676	-0.026	0.1265	1	21.08949
8.5	1.0233	0.05225	0.04239	-0.0239	0.123	1	19.58469
9	1.0366	0.0586	0.04945	-0.0215	0.1225	1	17.68942
9.5	1.0287	0.06631	0.05783	-0.0188	0.1235	1	15.5135
10	0.9911	0.07553	0.06754	-0.0164	0.1263	1	13.12194
10.5	0.9367	0.08752	0.07974	-0.0183	0.1303	1	10.7027
11	0.9179	0.1	0.09229	-0.0224	0.1339	1	9.179
12.5	0.7587	0.16234	0.15439	-0.0703	0.2883	1	4.673525
13	0.7732	0.16908	0.16115	-0.0716	0.2685	1	4.572983
13.5	0.789	0.17543	0.16774	-0.0728	0.2456	1	4.49752
14	0.829	0.18606	0.1785	-0.0724	0.2284	1	4.455552

14.5	0.8165	0.18816	0.18058	-0.0768	0.2142	1	4.339392
15	0.8642	0.20255	0.19517	-0.076	0.2053	1	4.266601

- Airfoil 2

Table AVIII-74: Aerodynamic performance of Airfoil 2 of the uncoated blade at -5°

alpha	CL	CD	CDp	CM	Top_Xtr	Bot_Xtr	CL/CD
------	--------	---------	---------	--------	--------	--------	--------
-5	-0.3493	0.02566	0.01511	-0.0422	1	0.1587	-13.6126
-4.5	-0.314	0.02276	0.01246	-0.0383	1	0.1932	-13.7961
-3.5	-0.2918	0.02105	0.01341	-0.0161	1	0.7225	-13.8622
-3	-0.2863	0.02135	0.01354	-0.0042	1	0.8026	-13.4098
-2.5	-0.2846	0.0206	0.01277	0.0085	1	0.8941	-13.8155
-2	-0.087	0.02124	0.01256	-0.0165	1	1	-4.09605
-1.5	-0.1136	0.02046	0.01173	-0.0094	1	1	-5.5523
-1	-0.0931	0.02035	0.01135	-0.0094	1	1	-4.57494
-0.5	-0.0481	0.02099	0.01165	-0.0127	1	1	-2.29157
0	0.0308	0.02259	0.01297	-0.0215	0.9847	1	1.363435
0.5	0.1187	0.02455	0.01473	-0.0312	0.9641	1	4.835031
1	0.1973	0.02644	0.01652	-0.0388	0.9437	1	7.462179
1.5	0.271	0.02832	0.01845	-0.0451	0.9215	1	9.569209
2	0.3413	0.03024	0.02044	-0.0503	0.8981	1	11.28638
2.5	0.4043	0.03213	0.02248	-0.054	0.8723	1	12.58326
3	0.4638	0.03404	0.02463	-0.0566	0.8429	1	13.62515
3.5	0.5243	0.03622	0.02718	-0.0593	0.8151	1	14.47543
4.5	0.7656	0.02137	0.01357	-0.0433	0.5071	1	35.82592
5	0.7669	0.02692	0.01586	-0.0341	0.1749	1	28.48811
5.5	0.824	0.03071	0.01948	-0.0326	0.1451	1	26.83165
6	0.8893	0.03497	0.0239	-0.0324	0.1327	1	25.43037
6.5	0.9401	0.04034	0.02991	-0.0315	0.1223	1	23.30441
7	0.9815	0.04641	0.03684	-0.0298	0.1204	1	21.14846
7.5	1.0103	0.05406	0.04532	-0.0278	0.1227	1	18.68849
8	1.0311	0.06422	0.05602	-0.0267	0.1268	1	16.05575
8.5	0.9931	0.07275	0.06587	-0.0241	0.1376	1	13.65086
9.5	0.848	0.10656	0.09989	-0.0417	0.1667	1	7.957958
11.5	0.7792	0.16055	0.15347	-0.0765	0.2739	1	4.853317
12	0.8279	0.1745	0.16769	-0.076	0.2602	1	4.744413
12.5	0.8145	0.17724	0.17037	-0.0796	0.2416	1	4.595464
13	0.8137	0.18375	0.17683	-0.0834	0.2277	1	4.428299
13.5	0.8379	0.19394	0.18707	-0.0846	0.2131	1	4.320408
14	0.8751	0.20732	0.20055	-0.0844	0.1942	1	4.221011
14.5	0.8517	0.2061	0.1992	-0.0916	0.1826	1	4.13246
15	0.8954	0.22356	0.21679	-0.0907	0.1724	1	4.005189

- Airfoil 3

Table AVIII-75: Aerodynamic performance of Airfoil 3 of the uncoated blade at -5°

alpha	CL	CD	CDp	CM	Top_Xtr	Bot_Xtr	CL/CD
------	--------	---------	---------	--------	--------	--------	--------
-5	-0.3857	0.02305	0.01334	-0.0303	1	0.1909	-16.7332
-4	-0.3857	0.02287	0.01589	-0.0011	1	0.7393	-16.8649
-3.5	-0.3785	0.0227	0.01544	0.0108	1	0.8161	-16.674
-3	-0.3527	0.02197	0.01442	0.0183	1	0.8934	-16.0537
-2.5	-0.1328	0.02314	0.01438	-0.0104	1	0.9805	-5.73898
-2	-0.0898	0.02276	0.0137	-0.015	1	1	-3.94552
-1.5	-0.1207	0.02193	0.01285	-0.0073	1	1	-5.50388
-1	-0.111	0.02175	0.01242	-0.0055	1	1	-5.10345
-0.5	-0.0504	0.02291	0.01322	-0.0117	0.9905	1	-2.19991
0	0.0321	0.02469	0.01471	-0.0209	0.9701	1	1.300122
0.5	0.1073	0.02647	0.01625	-0.0283	0.9508	1	4.053646
1	0.1719	0.02815	0.01782	-0.0333	0.9316	1	6.106572
1.5	0.234	0.02993	0.01955	-0.0376	0.9117	1	7.818243
2	0.2943	0.03183	0.02151	-0.0413	0.8918	1	9.245994
2.5	0.3581	0.03393	0.02371	-0.0453	0.8718	1	10.55408
3	0.4248	0.03603	0.02602	-0.0494	0.8485	1	11.79017
3.5	0.4845	0.03809	0.02843	-0.0519	0.8221	1	12.71987
4	0.5322	0.04004	0.03069	-0.0522	0.7893	1	13.29171
5	0.8138	0.02533	0.01797	-0.047	0.5962	1	32.12791
5.5	0.821	0.02519	0.01561	-0.0318	0.2806	1	32.5923
6	0.8677	0.02931	0.01915	-0.0296	0.2171	1	29.60423
6.5	0.9291	0.03344	0.02351	-0.0294	0.1857	1	27.78409
7	0.9814	0.03891	0.02944	-0.0282	0.1618	1	25.22231
7.5	1.0147	0.04659	0.0372	-0.0259	0.1256	1	21.77935
9	1.012	0.0707	0.06362	-0.0131	0.0977	1	14.314
10	0.9459	0.0899	0.08339	-0.0099	0.1002	1	10.52169
12	0.3421	0.05415	0.04934	-0.0308	0.3071	1	6.317636
13	0.3846	0.06936	0.0646	-0.0375	0.2668	1	5.544983
14	0.433	0.08766	0.08289	-0.0431	0.2206	1	4.939539
15	0.4674	0.10435	0.09949	-0.0504	0.1822	1	4.479157

- Airfoil 4

Table AVIII-76: Aerodynamic performance of Airfoil 4 of the uncoated blade at -5°

alpha	CL	CD	CDp	CM	Top_Xtr	Bot_Xtr	CL/CD
------	--------	---------	---------	--------	--------	--------	--------
-5	-0.3587	0.02784	0.0177	-0.0339	1	0.0637	-12.8843
-4.5	-0.3258	0.02589	0.01552	-0.03	1	0.0699	-12.584
-4	-0.2904	0.02396	0.0131	-0.0276	1	0.0864	-12.1202

-3.5	-0.266	0.02101	0.01242	-0.0231	1	0.6035	-12.6606
-3	-0.2709	0.02234	0.01407	-0.0082	1	0.7591	-12.1262
-2.5	-0.2595	0.02222	0.01378	0.0011	1	0.8318	-11.6787
-2	-0.1079	0.02342	0.01457	-0.0123	1	1	-4.60717
-1.5	-0.1288	0.0226	0.01368	-0.0062	1	1	-5.69912
-1	-0.0789	0.02335	0.01413	-0.0113	0.9902	1	-3.37901
-0.5	0.0008	0.02495	0.01537	-0.0207	0.9708	1	0.032064
0	0.0786	0.02668	0.01682	-0.0289	0.9517	1	2.946027
0.5	0.1423	0.02829	0.0182	-0.0342	0.9346	1	5.030046
1	0.2033	0.03002	0.01973	-0.0387	0.9167	1	6.772152
1.5	0.2637	0.03187	0.02144	-0.0427	0.8995	1	8.274239
2	0.4874	0.02766	0.0174	-0.0606	0.7986	1	17.62111
2.5	0.568	0.02721	0.01708	-0.063	0.7724	1	20.87468
3	0.6433	0.02479	0.01457	-0.0602	0.716	1	25.94998
3.5	0.6974	0.02524	0.01517	-0.0595	0.6935	1	27.63074
4	0.754	0.02517	0.0153	-0.0581	0.6658	1	29.9563
4.5	0.8055	0.02353	0.01405	-0.0529	0.6031	1	34.23289
5	0.8417	0.02265	0.01306	-0.0465	0.5068	1	37.16115
5.5	0.8744	0.02327	0.01358	-0.0416	0.3684	1	37.57628
6	0.8803	0.0271	0.01592	-0.0352	0.1763	1	32.48339
6.5	0.8961	0.0306	0.01925	-0.0306	0.1375	1	29.28431
7	0.9189	0.03352	0.02238	-0.0269	0.1137	1	27.41348
7.5	0.9543	0.03695	0.02616	-0.0241	0.0947	1	25.82679
8	1.0304	0.04353	0.03337	-0.0252	0.0723	1	23.67103
8.5	1.0651	0.05056	0.04172	-0.0227	0.063	1	21.06606
9	1.0753	0.05817	0.05009	-0.0191	0.06	1	18.48547
9.5	1.061	0.06576	0.05836	-0.0146	0.0594	1	16.13443
10	1.0223	0.07385	0.06697	-0.0111	0.0599	1	13.84292
10.5	0.9699	0.08459	0.07812	-0.0131	0.0611	1	11.46589
11	0.9078	0.10052	0.09427	-0.0224	0.0632	1	9.031039
11.5	0.8602	0.1204	0.11386	-0.0351	0.0661	1	7.144518
12	0.8412	0.13672	0.13009	-0.0436	0.0685	1	6.152721
12.5	0.8354	0.1498	0.1431	-0.0493	0.0708	1	5.576769
14.5	0.8633	0.20922	0.20254	-0.0722	0.1401	1	4.126279
15	0.8406	0.21005	0.20322	-0.0812	0.1343	1	4.001904

- Airfoil 5

Table AVIII-77: Aerodynamic performance of Airfoil 5 of the uncoated blade at -5°

alpha	CL	CD	CDp	CM	Top_Xtr	Bot_Xtr	CL/CD
------	--------	---------	---------	--------	--------	--------	--------
-5	-0.3609	0.0244	0.01471	-0.0372	1	0.172	-14.791
-4.5	-0.3254	0.02204	0.01255	-0.0347	1	0.2443	-14.7641

-4	-0.3094	0.02091	0.01344	-0.0263	1	0.5671	-14.7967
-3.5	-0.3075	0.02234	0.01487	-0.0128	1	0.6957	-13.7645
-3	-0.2935	0.02229	0.01459	-0.0042	1	0.7682	-13.1673
-2.5	-0.2816	0.02141	0.01369	0.005	1	0.8546	-13.1527
-2	-0.1252	0.02236	0.0142	-0.0126	1	0.9913	-5.59928
-1.5	-0.1299	0.0218	0.01338	-0.0099	1	1	-5.95872
-1	-0.0662	0.02282	0.01392	-0.0175	0.9871	1	-2.90096
-0.5	0.0208	0.02455	0.01522	-0.028	0.9666	1	0.847251
0	0.0975	0.02618	0.01645	-0.0357	0.9458	1	3.724217
0.5	0.1685	0.02791	0.01794	-0.0419	0.927	1	6.037263
1	0.2406	0.02973	0.01962	-0.0478	0.9076	1	8.092836
1.5	0.2927	0.03138	0.02119	-0.0501	0.8877	1	9.327597
2	0.3426	0.03326	0.02303	-0.0519	0.8691	1	10.30066
2.5	0.3983	0.03522	0.02504	-0.0543	0.8483	1	11.30892
3	0.4549	0.03719	0.02716	-0.0565	0.8249	1	12.23178
3.5	0.5212	0.03887	0.02905	-0.0592	0.7954	1	13.4088
4	0.672	0.03611	0.02699	-0.0665	0.7393	1	18.6098
4.5	0.7981	0.02961	0.02111	-0.0637	0.669	1	26.95373
5	0.859	0.02554	0.01728	-0.0548	0.5762	1	33.63352
5.5	0.8663	0.02506	0.01498	-0.0404	0.3089	1	34.56903
6	0.8978	0.02928	0.01828	-0.0366	0.2194	1	30.66257
7	1.0116	0.037	0.02625	-0.0359	0.1738	1	27.34054
7.5	1.0639	0.04246	0.03203	-0.0356	0.1651	1	25.05652
8	1.0981	0.04833	0.03874	-0.0333	0.1627	1	22.72088
8.5	1.1201	0.05516	0.04641	-0.0305	0.1629	1	20.30638
9	1.1332	0.0631	0.05513	-0.0278	0.1648	1	17.9588
9.5	1.0729	0.07161	0.06464	-0.0219	0.1706	1	14.98254
10	0.9374	0.08954	0.08262	-0.0256	0.1787	1	10.46906
10.5	0.9462	0.10195	0.0952	-0.0281	0.1887	1	9.28102
12	0.7677	0.16013	0.15268	-0.0711	0.3163	1	4.79423
12.5	0.8273	0.17473	0.16762	-0.0713	0.3078	1	4.734734
13	0.7925	0.1745	0.16726	-0.0747	0.2911	1	4.541547
13.5	0.8287	0.18742	0.18046	-0.0756	0.2825	1	4.42162
14	0.8461	0.19582	0.18901	-0.0765	0.2588	1	4.320805
14.5	0.8516	0.20222	0.19547	-0.0781	0.2344	1	4.211255
15	0.8541	0.20798	0.20123	-0.0805	0.2097	1	4.106645

- Airfoil 6

Table AVIII-78: Aerodynamic performance of Airfoil 6 of the uncoated blade at -5°

alpha	CL	CD	CDp	CM	Top_Xtr	Bot_Xtr	CL/CD
------	--------	---------	---------	--------	--------	--------	--------
-4.5	-0.3796	0.03978	0.03174	-0.042	1	0.1116	-9.54248

-4	-0.3349	0.03465	0.02541	-0.0406	1	0.1052	-9.66522
-3.5	-0.2912	0.03095	0.02115	-0.0384	1	0.1064	-9.40872
-3	-0.2505	0.02841	0.01841	-0.0356	1	0.1138	-8.81732
-2.5	-0.2122	0.02659	0.01642	-0.0324	1	0.1303	-7.98044
-2	-0.1839	0.02318	0.01572	-0.0266	1	0.6187	-7.93356
-1.5	-0.1862	0.02348	0.0164	-0.0129	1	0.7947	-7.93015
-1	-0.1254	0.02318	0.01609	-0.0141	1	1	-5.40984
-0.5	-0.0787	0.02406	0.0163	-0.018	0.9979	1	-3.27099
0	0.0133	0.02633	0.01785	-0.0287	0.9758	1	0.505127
0.5	0.091	0.02832	0.01936	-0.036	0.9529	1	3.213277
1	0.1632	0.03031	0.02096	-0.0418	0.9303	1	5.384362
1.5	0.2373	0.03228	0.02269	-0.0473	0.9054	1	7.351301
2	0.3177	0.03411	0.02435	-0.053	0.879	1	9.313984
2.5	0.3731	0.03561	0.0258	-0.0546	0.8511	1	10.47739
3	0.4371	0.0371	0.02734	-0.0569	0.8207	1	11.78167
3.5	0.5342	0.03768	0.02808	-0.062	0.7865	1	14.17728
4	0.6436	0.03574	0.02645	-0.065	0.7391	1	18.00783
4.5	0.7651	0.03104	0.02216	-0.0655	0.6847	1	24.64884
5	0.8595	0.02668	0.01784	-0.0616	0.6092	1	32.21514
5.5	0.9032	0.02488	0.01582	-0.0533	0.4973	1	36.30225
6	0.9131	0.0265	0.01593	-0.0431	0.3236	1	34.4566
6.5	0.9416	0.02977	0.0183	-0.0389	0.24	1	31.62916
7	0.9795	0.03247	0.02068	-0.0363	0.1989	1	30.16631
7.5	1.0206	0.035	0.02307	-0.0343	0.1728	1	29.16
8	1.0584	0.03752	0.02574	-0.0321	0.1525	1	28.20896
8.5	1.1105	0.04096	0.02902	-0.0319	0.1398	1	27.11182
9	1.1447	0.0444	0.03304	-0.0292	0.1313	1	25.78153
9.5	1.1739	0.04745	0.03631	-0.0263	0.121	1	24.73973
10	1.1989	0.05195	0.04107	-0.0237	0.1134	1	23.07796
10.5	1.2029	0.0566	0.04641	-0.019	0.1086	1	21.25265
11	1.1921	0.0621	0.05247	-0.0138	0.1057	1	19.19646
11.5	1.1575	0.06966	0.06061	-0.0095	0.1055	1	16.61642
12	1.0858	0.08241	0.07394	-0.0102	0.1088	1	13.17559
12.5	1.0139	0.10081	0.09264	-0.0182	0.1143	1	10.05753
13	0.7934	0.17032	0.16219	-0.069	0.2775	1	4.65829
14	0.8108	0.18291	0.17485	-0.0733	0.2506	1	4.432781
15	0.8779	0.20232	0.19463	-0.0722	0.2094	1	4.339166

- 0°
- Airfoil 1

Table AVIII-79: Aerodynamic performance of Airfoil 1 of the uncoated blade at 0°

alpha	CL	CD	CDp	CM	Top_Xtr	Bot_Xtr	CL/CD
------	--------	---------	---------	--------	--------	--------	--------
-5	-0.4294	0.03165	0.02182	-0.0349	1	0.1244	-13.5671
-4.5	-0.3964	0.02898	0.01901	-0.0322	1	0.1503	-13.6784
-4	-0.3546	0.02631	0.01592	-0.0291	1	0.1578	-13.4778
-3.5	-0.3149	0.02404	0.01344	-0.0255	1	0.1714	-13.099
-3	-0.2762	0.02165	0.01139	-0.0229	1	0.2323	-12.7575
-1.5	-0.1004	0.02142	0.01305	-0.0137	1	1	-4.68721
-1	-0.1209	0.02064	0.01214	-0.0069	1	1	-5.85756
-0.5	-0.0968	0.0208	0.01196	-0.0062	1	1	-4.65385
0	-0.0589	0.02153	0.01227	-0.0072	1	1	-2.73572
0.5	-0.0131	0.02266	0.01307	-0.0092	0.9971	1	-0.57811
1	0.0745	0.02497	0.01512	-0.0186	0.9757	1	2.98358
1.5	0.15	0.02699	0.01699	-0.0254	0.954	1	5.557614
2	0.2207	0.02895	0.01898	-0.031	0.9311	1	7.623489
2.5	0.2866	0.03089	0.02102	-0.0353	0.9053	1	9.278084
3	0.3494	0.03293	0.02321	-0.0389	0.8792	1	10.61039
3.5	0.471	0.03338	0.02418	-0.047	0.8182	1	14.11025
4	0.655	0.02538	0.01696	-0.0487	0.7113	1	25.80772
5	0.697	0.02595	0.01439	-0.0241	0.1859	1	26.85934
5.5	0.7517	0.0295	0.01771	-0.0225	0.1506	1	25.48136
6	0.8228	0.03411	0.02211	-0.0232	0.1386	1	24.12196
6.5	0.8787	0.03904	0.02754	-0.0224	0.1367	1	22.50768
7	0.9211	0.04429	0.03356	-0.0203	0.1348	1	20.79702
7.5	0.9467	0.0474	0.03689	-0.0178	0.108	1	19.97257
8	0.9709	0.05284	0.0424	-0.0159	0.0921	1	18.37434
8.5	0.9773	0.05874	0.04919	-0.012	0.0857	1	16.63773
9	0.9721	0.06563	0.05666	-0.0088	0.0817	1	14.81182
9.5	0.9584	0.0725	0.06385	-0.0062	0.0784	1	13.21931
11	0.7397	0.1448	0.13708	-0.0516	0.269	1	5.108425
11.5	0.7679	0.15472	0.14701	-0.0512	0.2482	1	4.963159
12	0.7558	0.15957	0.15179	-0.0545	0.2288	1	4.736479
12.5	0.7449	0.16571	0.15784	-0.0585	0.213	1	4.495202
13	0.7702	0.17606	0.16817	-0.0594	0.2022	1	4.374645
13.5	0.7753	0.18163	0.17372	-0.0622	0.1861	1	4.268568
14	0.78	0.18915	0.18119	-0.0658	0.1777	1	4.123711
14.5	0.7954	0.19604	0.18808	-0.068	0.1645	1	4.057335
15	0.8097	0.20502	0.19703	-0.0708	0.1576	1	3.949371

- Airfoil 2

Table AVIII-80: Aerodynamic performance of Airfoil 2 of the uncoated blade at 0°

alpha	CL	CD	CDp	CM	Top_Xtr	Bot_Xtr	CL/CD
------	--------	---------	---------	--------	--------	--------	--------
-4	-0.3804	0.02097	0.01373	-0.0142	1	0.674	-18.1402
-3.5	-0.3742	0.022	0.01464	-0.0006	1	0.7628	-17.0091
-3	-0.3756	0.02204	0.01449	0.0148	1	0.8556	-17.0417
-2.5	-0.1938	0.02283	0.01426	-0.0031	1	0.9601	-8.48883
-2	-0.0674	0.02225	0.01293	-0.021	1	1	-3.02921
-1.5	-0.0985	0.02164	0.01232	-0.0128	1	1	-4.55176
-1	-0.1212	0.02083	0.01142	-0.006	1	1	-5.81853
-0.5	-0.0949	0.02099	0.0113	-0.0063	1	1	-4.5212
0	-0.0543	0.02175	0.01178	-0.0082	1	1	-2.49655
0.5	0.0032	0.02317	0.01297	-0.0129	0.9933	1	0.13811
1	0.0824	0.02517	0.01482	-0.0211	0.9733	1	3.273739
1.5	0.1571	0.02717	0.01674	-0.0281	0.9528	1	5.782113
2	0.2268	0.02909	0.01868	-0.0338	0.9316	1	7.796494
2.5	0.2945	0.03107	0.02076	-0.0389	0.9096	1	9.478597
3	0.3578	0.03313	0.02298	-0.043	0.8876	1	10.79988
3.5	0.4149	0.03517	0.02525	-0.0458	0.8619	1	11.79699
4	0.4765	0.03723	0.02786	-0.0487	0.8312	1	12.79882
4.5	0.5495	0.039	0.03018	-0.0519	0.7933	1	14.08974
5	0.7539	0.02141	0.01363	-0.038	0.4761	1	35.21252
5.5	0.7534	0.02668	0.01599	-0.0289	0.1891	1	28.23838
6	0.8089	0.03017	0.01944	-0.0276	0.1567	1	26.8114
6.5	0.8833	0.03482	0.02432	-0.0287	0.1447	1	25.3676
7	0.9398	0.04027	0.03068	-0.0278	0.1424	1	23.33747
7	0.9398	0.04027	0.03068	-0.0278	0.1424	1	23.33747
7.25	0.962	0.04384	0.03483	-0.0267	0.143	1	21.94343
8	0.989	0.05309	0.0444	-0.0216	0.0848	1	18.62874
8.5	0.9836	0.0613	0.05386	-0.0167	0.0775	1	16.04568
8.75	0.9755	0.06499	0.05796	-0.0144	0.0737	1	15.01
9	0.9653	0.06926	0.06254	-0.0127	0.074	1	13.93734
9.5	0.9306	0.07753	0.07119	-0.0098	0.075	1	12.0031
10	0.8941	0.08766	0.08131	-0.0112	0.0787	1	10.19963
10.5	0.8672	0.09992	0.09362	-0.0155	0.0814	1	8.678943
12	0.7481	0.15888	0.15241	-0.0646	0.2727	1	4.708585
13	0.8038	0.18086	0.17437	-0.0617	0.1927	1	4.444322
13.5	0.7801	0.18328	0.17667	-0.0685	0.1819	1	4.256329
14	0.7904	0.19118	0.18451	-0.0709	0.1619	1	4.134324
14.5	0.8116	0.20159	0.19491	-0.0721	0.1462	1	4.025993

15	0.817	0.20707	0.20035	-0.0761	0.1321	1	3.945526

- Airfoil 3

Table AVIII-81: Aerodynamic performance of Airfoil 3 of the uncoated blade at 0°

alpha	CL	CD	CDp	CM	Top_Xtr	Bot_Xtr	CL/CD
------	--------	---------	---------	--------	--------	--------	--------
-3.5	-0.3657	0.0214	0.01398	-0.0001	1	0.7527	-17.0888
-3	-0.3636	0.02144	0.01397	0.0144	1	0.8522	-16.959
-2	-0.0846	0.02241	0.01343	-0.0168	1	1	-3.7751
-1.5	-0.1171	0.02158	0.01257	-0.0085	1	1	-5.42632
-1	-0.12	0.02113	0.01189	-0.0043	1	1	-5.67913
-0.5	-0.088	0.02163	0.01206	-0.0048	1	1	-4.06842
0	-0.0385	0.02276	0.01284	-0.0079	0.9951	1	-1.69156
0.5	0.0396	0.02474	0.01457	-0.0158	0.9773	1	1.600647
1	0.1126	0.02665	0.01632	-0.0224	0.9578	1	4.225141
1.5	0.1758	0.02845	0.01805	-0.027	0.9385	1	6.179262
2	0.2349	0.03036	0.02	-0.0307	0.9197	1	7.737154
2.5	0.2952	0.03243	0.02215	-0.0343	0.8993	1	9.102683
3	0.3561	0.03453	0.02441	-0.0378	0.8751	1	10.31277
3.5	0.414	0.0367	0.02687	-0.0405	0.8497	1	11.28065
4	0.4967	0.0387	0.02929	-0.0456	0.816	1	12.83463
5	0.726	0.02465	0.01382	-0.0261	0.2058	1	28.86771
5.5	0.7626	0.02871	0.01736	-0.0227	0.1689	1	26.56217
6	0.8369	0.03294	0.02148	-0.0236	0.1492	1	25.4068
6.5	0.8972	0.03747	0.02663	-0.0232	0.1437	1	23.94449
7	0.9424	0.04227	0.03195	-0.0218	0.133	1	22.29477
7.5	0.9786	0.05016	0.04033	-0.0204	0.1284	1	19.50957
8	1.0024	0.05608	0.04722	-0.017	0.1306	1	17.87447
8.5	0.9823	0.06461	0.05703	-0.0124	0.1386	1	15.20353
9	0.9574	0.07476	0.06765	-0.0104	0.1463	1	12.80631
11	0.751	0.14788	0.14067	-0.0538	0.3163	1	5.078442
11.5	0.7362	0.15241	0.14512	-0.0559	0.2956	1	4.830392
12	0.733	0.1588	0.15146	-0.0582	0.2772	1	4.615869
12.5	0.7465	0.16725	0.15993	-0.0599	0.2626	1	4.463378
13	0.7999	0.18253	0.17545	-0.0589	0.2441	1	4.382293
13.5	0.7675	0.18155	0.17433	-0.0641	0.2281	1	4.227486
14	0.7765	0.1887	0.18146	-0.0666	0.2091	1	4.114997
14.5	0.8022	0.19973	0.19255	-0.0675	0.195	1	4.016422
15	0.807	0.20428	0.19709	-0.0709	0.1792	1	3.95046

- Airfoil 4

Table AVIII-82: Aerodynamic performance of Airfoil 4 of the uncoated blade at 0°

alpha	CL	CD	CDp	CM	Top_Xtr	Bot_Xtr	CL/CD
------	--------	---------	---------	--------	--------	--------	--------
-4.5	-0.3499	0.03469	0.02384	-0.0312	1	0.1162	-10.0865
-4	-0.3119	0.03244	0.02117	-0.0293	1	0.1177	-9.61467
-3.5	-0.2708	0.03021	0.01863	-0.0273	1	0.1179	-8.96392
-3	-0.2289	0.02798	0.01629	-0.0243	1	0.1154	-8.18084
-2.5	-0.1907	0.02669	0.01493	-0.0212	1	0.1169	-7.145
-2	-0.1486	0.02546	0.01347	-0.0196	1	0.1277	-5.83661
-1.5	-0.1177	0.02351	0.0142	-0.0151	1	0.6848	-5.00638
-1	-0.0512	0.02356	0.01477	-0.0143	0.9849	1	-2.17317
-0.5	0.0328	0.02522	0.01583	-0.0234	0.9653	1	1.300555
0	0.1017	0.02684	0.01709	-0.0292	0.947	1	3.789121
0.5	0.1685	0.02857	0.0187	-0.0344	0.9283	1	5.897795
1	0.2365	0.03054	0.0207	-0.0396	0.9112	1	7.743942
1.5	0.2944	0.03236	0.02258	-0.0427	0.8919	1	9.097651
2	0.3435	0.03428	0.02461	-0.0444	0.8727	1	10.02042
2.5	0.3938	0.03642	0.02694	-0.0461	0.8527	1	10.81274
3	0.4458	0.03871	0.02951	-0.048	0.8307	1	11.5164
3.5	0.5142	0.04082	0.03238	-0.0511	0.8023	1	12.59677
4	0.6784	0.02755	0.01598	-0.0288	0.0867	1	24.62432
4.5	0.706	0.03079	0.01927	-0.0246	0.0727	1	22.92952
5	0.7686	0.03432	0.02295	-0.0234	0.0676	1	22.3951
5.5	0.8393	0.03905	0.02799	-0.0237	0.066	1	21.49296
6	0.8897	0.04483	0.03434	-0.0223	0.0668	1	19.84609
6.5	0.9243	0.05175	0.04189	-0.0199	0.0686	1	17.86087
7	0.9506	0.05984	0.05053	-0.0177	0.0713	1	15.8857
7.5	0.9482	0.0649	0.0568	-0.0122	0.078	1	14.61017
8	0.923	0.07367	0.0662	-0.0087	0.0841	1	12.52884
8.5	0.8938	0.08237	0.07513	-0.0068	0.0884	1	10.85104
9	0.8649	0.09225	0.08526	-0.0088	0.0961	1	9.37561
9.5	0.7756	0.11416	0.10724	-0.0267	0.1081	1	6.793973
10.5	0.7253	0.15112	0.14413	-0.0537	0.2353	1	4.799497
11	0.7601	0.16285	0.15586	-0.0536	0.2277	1	4.667485
11.5	0.7506	0.16742	0.16035	-0.0571	0.2095	1	4.483335
12	0.7469	0.17427	0.1671	-0.0609	0.198	1	4.285878
12.5	0.7808	0.18438	0.17724	-0.0606	0.185	1	4.234733
13	0.7677	0.18908	0.18181	-0.0661	0.1756	1	4.060186
13.5	0.79	0.1974	0.19015	-0.0673	0.1639	1	4.002026
14	0.8014	0.20635	0.19903	-0.0704	0.158	1	3.883693

14.5	0.8032	0.21026	0.2029	-0.0751	0.1466	1	3.820032
15	0.8596	0.23209	0.22482	-0.0714	0.1377	1	3.703736

- Airfoil 5

Table AVIII-83: Aerodynamic performance of Airfoil 5 of the uncoated blade at 0°

alpha	CL	CD	CDp	CM	Top_Xtr	Bot_Xtr	CL/CD
------	--------	---------	---------	--------	--------	--------	--------
-3.5	-0.2674	0.02999	0.0194	-0.0348	1	0.0771	-8.91631
-3	-0.2311	0.02844	0.01766	-0.0323	1	0.0772	-8.12588
-2.5	-0.1973	0.02724	0.01647	-0.0298	1	0.0832	-7.24302
-2	-0.1631	0.02661	0.01576	-0.0275	1	0.0918	-6.12927
-1.5	-0.127	0.02605	0.01505	-0.026	1	0.1006	-4.87524
-1	-0.0757	0.02575	0.01458	-0.0275	0.9957	0.1212	-2.93981
-0.5	-0.0247	0.02489	0.01652	-0.0246	0.9784	0.7566	-0.99237
0	0.0581	0.02499	0.01686	-0.0288	0.9582	1	2.32493
0.5	0.1385	0.02673	0.01829	-0.0369	0.9382	1	5.181444
1	0.2011	0.02827	0.01965	-0.0414	0.9189	1	7.113548
1.5	0.261	0.03005	0.02138	-0.0452	0.8998	1	8.685524
2	0.3193	0.03202	0.02337	-0.0485	0.882	1	9.971893
2.5	0.3852	0.03425	0.02585	-0.0526	0.8644	1	11.24672
3	0.4413	0.03645	0.02848	-0.0548	0.8441	1	12.107
4	0.656	0.03126	0.02024	-0.0305	0.0634	1	20.98528
4.5	0.7282	0.0358	0.02498	-0.0301	0.0631	1	20.34078
5	0.7847	0.04149	0.03116	-0.0286	0.0658	1	18.91299
5.5	0.8276	0.04928	0.03945	-0.0268	0.0697	1	16.79383
6	0.8631	0.05367	0.04505	-0.0226	0.08	1	16.08161
7.5	0.8461	0.08287	0.0765	-0.018	0.1484	1	10.20997
8	0.767	0.09642	0.09006	-0.027	0.1536	1	7.954781
10	0.7101	0.14691	0.14016	-0.0594	0.2492	1	4.833572
10.5	0.7146	0.15439	0.14754	-0.0613	0.2295	1	4.628538
11	0.7506	0.16567	0.15881	-0.0604	0.2159	1	4.530694
11.5	0.7521	0.17084	0.16391	-0.0629	0.1961	1	4.402365
12	0.7454	0.17698	0.16993	-0.0672	0.1832	1	4.211775
12.5	0.8082	0.19459	0.18762	-0.0627	0.1678	1	4.153348
13	0.7683	0.19183	0.18468	-0.0723	0.1595	1	4.005109
13.5	0.7924	0.20045	0.1933	-0.073	0.1471	1	3.953106
14	0.8119	0.21194	0.20472	-0.0751	0.1416	1	3.830801
14.5	0.8053	0.21299	0.20568	-0.0813	0.1317	1	3.780929
15	0.8298	0.22211	0.21481	-0.0821	0.1223	1	3.735987

- Airfoil 6

Table AVIII-84: Aerodynamic performance of Airfoil 6 of the uncoated blade at 0°

alpha	CL	CD	CDp	CM	Top_Xtr	Bot_Xtr	CL/CD
------	--------	---------	---------	--------	--------	--------	--------
-5	-0.2999	0.03458	0.02492	-0.0341	1	0.1377	-8.67264
-4.5	-0.2596	0.03148	0.02156	-0.0323	1	0.1566	-8.24651
-4	-0.2165	0.0295	0.01912	-0.03	1	0.1668	-7.33898
-3.5	-0.1755	0.02793	0.01758	-0.0278	1	0.1845	-6.28357
-3	-0.1336	0.0271	0.01677	-0.026	1	0.2168	-4.92989
-2.5	-0.0891	0.02545	0.01698	-0.0245	1	0.4942	-3.50098
-2	-0.0556	0.02435	0.01736	-0.018	1	1	-2.28337
-1.5	-0.0136	0.02555	0.01798	-0.0187	1	1	-0.53229
-1	0.0257	0.02697	0.01899	-0.0189	1	1	0.952911
-0.5	0.0789	0.02906	0.02079	-0.0216	0.9926	1	2.715072
0	0.167	0.03227	0.0238	-0.0301	0.9617	1	5.175085
0.5	0.2693	0.03579	0.02729	-0.0396	0.9234	1	7.524448
1.5	0.606	0.02452	0.0133	-0.0393	0.2469	1	24.71452
2	0.6648	0.0272	0.01562	-0.0382	0.2065	1	24.44118
2.5	0.7475	0.03045	0.01855	-0.0403	0.1883	1	24.54844
3	0.8108	0.03355	0.02188	-0.0398	0.1795	1	24.16692
3.5	0.8624	0.03704	0.02538	-0.0383	0.1669	1	23.28294
4.5	0.9374	0.0461	0.03548	-0.0322	0.1521	1	20.33406
5	0.9587	0.05209	0.04214	-0.028	0.1511	1	18.40468
5.5	0.9639	0.05937	0.05008	-0.0234	0.153	1	16.23547
6	0.9556	0.06781	0.05901	-0.0193	0.1572	1	14.09232
6.5	0.9646	0.07793	0.06937	-0.0177	0.1641	1	12.37777
8.5	0.6696	0.14425	0.13622	-0.0573	0.3127	1	4.641941
9	0.6804	0.15179	0.14369	-0.0583	0.2962	1	4.482509
9.5	0.7218	0.16082	0.15274	-0.0572	0.2781	1	4.488248
10	0.7003	0.16479	0.15659	-0.0609	0.2618	1	4.249651
10.5	0.7619	0.17951	0.17132	-0.0583	0.246	1	4.244332
11	0.7301	0.17817	0.16988	-0.0633	0.2278	1	4.097772
11.5	0.7833	0.19385	0.1856	-0.0614	0.2175	1	4.040753
12	0.753	0.19141	0.18303	-0.0676	0.2035	1	3.933964
12.5	0.7947	0.2029	0.19458	-0.0663	0.193	1	3.916708
13	0.7987	0.21041	0.20201	-0.07	0.1884	1	3.795922
13.5	0.7934	0.21113	0.20267	-0.075	0.1767	1	3.757874
14	0.8178	0.21913	0.21068	-0.0758	0.1679	1	3.732031
14.5	0.8709	0.24319	0.23483	-0.0738	0.1625	1	3.581151
15	0.8427	0.23339	0.22491	-0.0821	0.1587	1	3.610695

- 5°
- Airfoil 1:

Table AVIII-85: Aerodynamic performance of Airfoil 1 of the uncoated blade at 5°

alpha	CL	CD	CDp	CM	Top_Xtr	Bot_Xtr	CL/CD
------	--------	---------	---------	--------	--------	--------	--------
-5	-0.4322	0.03972	0.03086	-0.0376	1	0.1012	-10.8812
-4.5	-0.4001	0.03485	0.02537	-0.0349	1	0.0968	-11.4806
-4	-0.3626	0.03107	0.02096	-0.0321	1	0.0957	-11.6704
-3.5	-0.3231	0.02851	0.01771	-0.0292	1	0.1028	-11.3329
-3	-0.2855	0.02645	0.01557	-0.0265	1	0.1275	-10.794
-2.5	-0.2467	0.02418	0.01338	-0.023	1	0.1489	-10.2026
-0.5	-0.1045	0.02077	0.01235	-0.007	1	1	-5.0313
0	-0.0673	0.0214	0.0125	-0.0079	1	1	-3.14486
0.5	-0.0274	0.02236	0.0131	-0.0089	1	1	-1.2254
1	0.0451	0.02422	0.01465	-0.0157	0.984	1	1.862097
1.5	0.1207	0.02625	0.01649	-0.0226	0.9631	1	4.598095
2	0.1919	0.02826	0.0184	-0.0284	0.9414	1	6.790517
2.5	0.2607	0.0303	0.02044	-0.0335	0.9182	1	8.60396
3	0.3349	0.03234	0.02257	-0.0389	0.891	1	10.3556
3.5	0.5365	0.02934	0.02022	-0.0533	0.7924	1	18.28562
4.5	0.6463	0.02407	0.01191	-0.029	0.2019	1	26.85085
5	0.688	0.02695	0.0145	-0.0266	0.1719	1	25.52876
5.5	0.7509	0.02942	0.017	-0.0265	0.1603	1	25.52345
6	0.8156	0.03241	0.02005	-0.027	0.1553	1	25.16507
6.5	0.8737	0.03603	0.02397	-0.0269	0.1544	1	24.24924
7	0.9231	0.04034	0.02888	-0.026	0.1564	1	22.88299
7.5	0.9614	0.04571	0.03529	-0.0244	0.161	1	21.0326
8	0.9916	0.05222	0.04243	-0.0228	0.1664	1	18.98889
8.5	1.0086	0.05908	0.05011	-0.0206	0.1741	1	17.07177
9	0.9767	0.07045	0.06235	-0.0187	0.1885	1	13.86373
11	0.7058	0.13987	0.13168	-0.0611	0.3561	1	5.046114
11.5	0.7153	0.14677	0.13857	-0.0626	0.3405	1	4.873612
12	0.7451	0.15562	0.14747	-0.0634	0.3243	1	4.787945
12.5	0.7468	0.16033	0.15217	-0.0647	0.2978	1	4.657893
13	0.7707	0.16871	0.16079	-0.0655	0.2793	1	4.568194
13.5	0.8113	0.17955	0.17178	-0.0655	0.2605	1	4.518519
14	0.7859	0.1808	0.17292	-0.07	0.2449	1	4.346792
14.5	0.8074	0.19039	0.18256	-0.0718	0.2348	1	4.240769
15	0.8178	0.19583	0.18805	-0.0743	0.2193	1	4.176071

- Airfoil 2

Table AVIII-86: Aerodynamic performance of Airfoil 2 of the uncoated blade at 5°

alpha	CL	CD	CDp	CM	Top_Xtr	Bot_Xtr	CL/CD
------	--------	---------	---------	--------	--------	--------	--------
-4.5	-0.3781	0.02481	0.01458	-0.0356	1	0.1447	-15.2398
-4	-0.3441	0.02265	0.01236	-0.0319	1	0.1714	-15.1921
-3.5	-0.3131	0.01912	0.01085	-0.0293	1	0.4524	-16.3755
-3	-0.3071	0.02045	0.01267	-0.016	1	0.6974	-15.0171
-2.5	-0.3116	0.02123	0.01352	-0.0005	1	0.8047	-14.6773
-2	-0.2944	0.02095	0.01314	0.0123	1	0.9244	-14.0525
-1.5	-0.0826	0.02176	0.01294	-0.0172	1	1	-3.79596
-1	-0.11	0.02105	0.0122	-0.0095	1	1	-5.22565
-0.5	-0.1095	0.02061	0.01156	-0.0061	1	1	-5.31295
0	-0.0722	0.02107	0.01165	-0.008	1	1	-3.42667
0.5	-0.0227	0.02206	0.01236	-0.0114	0.9974	1	-1.02901
1	0.0627	0.02411	0.01417	-0.021	0.9782	1	2.600581
1.5	0.1415	0.0261	0.016	-0.0289	0.9587	1	5.421456
2	0.2147	0.02801	0.01786	-0.0353	0.9373	1	7.66512
3	0.3488	0.03197	0.02202	-0.0451	0.8934	1	10.91023
3.5	0.4168	0.03413	0.02439	-0.0496	0.8694	1	12.21213
4	0.4684	0.03599	0.02648	-0.0509	0.8368	1	13.01473
4.5	0.5506	0.03748	0.02855	-0.055	0.795	1	14.6905
5.5	0.746	0.02535	0.01463	-0.0312	0.2151	1	29.42801
6	0.7973	0.02932	0.01821	-0.0293	0.1693	1	27.19304
6.5	0.8552	0.03335	0.02205	-0.0292	0.1384	1	25.64318
7	0.9124	0.03786	0.02725	-0.0286	0.128	1	24.09931
7.5	0.9602	0.04361	0.03361	-0.0274	0.1236	1	22.01789
8	0.992	0.0505	0.04154	-0.0252	0.1256	1	19.64356
8.5	1.0025	0.05913	0.05123	-0.0226	0.1316	1	16.95417
9	1.0082	0.06914	0.06179	-0.0213	0.1384	1	14.58201
9.5	0.9479	0.07917	0.07256	-0.0198	0.1483	1	11.97297
10	0.8756	0.09458	0.088	-0.0266	0.1592	1	9.257771
11	0.7392	0.14092	0.13383	-0.0659	0.3148	1	5.245529
11.5	0.7753	0.15095	0.14399	-0.0664	0.3012	1	5.136138
12.5	0.7683	0.16387	0.15693	-0.0718	0.2676	1	4.688473
13	0.8301	0.17968	0.17296	-0.0705	0.2541	1	4.61988
13.5	0.7953	0.17917	0.17231	-0.076	0.2378	1	4.438801
14	0.8115	0.18851	0.1817	-0.0783	0.228	1	4.304811
14.5	0.8272	0.1957	0.18896	-0.0804	0.2122	1	4.226878
15	0.8285	0.20195	0.19518	-0.0847	0.2014	1	4.102501

- Airfoil 3

Table AVIII-87: Aerodynamic performance of Airfoil 3 of the uncoated blade at 5°

alpha	CL	CD	CDp	CM	Top_Xtr	Bot_Xtr	CL/CD
------	--------	---------	---------	--------	--------	--------	--------
-5	-0.3862	0.02524	0.01459	-0.034	1	0.163	-15.3011
-4.5	-0.3481	0.02279	0.01214	-0.0304	1	0.1962	-15.2742
-4	-0.3427	0.02042	0.0127	-0.018	1	0.6544	-16.7826
-3.5	-0.3403	0.02163	0.01384	-0.0031	1	0.7615	-15.7328
-3	-0.3489	0.02148	0.01374	0.0144	1	0.8744	-16.243
-2	-0.08	0.0218	0.0127	-0.017	1	1	-3.66972
-1.5	-0.1115	0.02107	0.01197	-0.009	1	1	-5.29188
-1	-0.1056	0.02081	0.0115	-0.0066	1	1	-5.07448
-0.5	-0.0672	0.02141	0.0118	-0.0086	1	1	-3.13872
0	-0.004	0.02277	0.01287	-0.0146	0.9911	1	-0.17567
0.5	0.0809	0.02478	0.01467	-0.0239	0.9722	1	3.26473
1	0.1518	0.02657	0.01636	-0.0303	0.9532	1	5.71321
1.5	0.2266	0.0286	0.01836	-0.0369	0.9333	1	7.923077
2	0.2915	0.03046	0.02029	-0.0415	0.9118	1	9.569928
2.5	0.3479	0.03237	0.02237	-0.0444	0.8898	1	10.74761
3	0.4065	0.03445	0.02466	-0.0475	0.8661	1	11.79971
3.5	0.4681	0.03662	0.02713	-0.0506	0.8399	1	12.78263
4	0.5455	0.03865	0.0297	-0.0549	0.8082	1	14.11384
5	0.7561	0.02386	0.01404	-0.0314	0.2627	1	31.68902
5.5	0.7881	0.0285	0.01781	-0.0274	0.1773	1	27.65263
6.5	0.9128	0.03856	0.02832	-0.0263	0.1294	1	23.6722
7	0.9542	0.04579	0.03601	-0.0248	0.1179	1	20.83861
7.5	0.9824	0.05374	0.0449	-0.0219	0.1178	1	18.28061
8	0.9988	0.06412	0.05596	-0.0196	0.1196	1	15.57704
8.5	1.0013	0.07335	0.0659	-0.0172	0.1201	1	13.65099
9	0.9236	0.08163	0.07512	-0.0147	0.1368	1	11.31447
10.5	0.7601	0.14367	0.13689	-0.0609	0.3151	1	5.290597
11	0.7481	0.14963	0.14275	-0.0631	0.2944	1	4.999666
11.5	0.7481	0.15705	0.15013	-0.0652	0.2757	1	4.763451
12	0.7601	0.16544	0.15858	-0.0667	0.2564	1	4.594415
12.5	0.77	0.17284	0.16596	-0.0681	0.2314	1	4.454987
13	0.8026	0.18534	0.17852	-0.0681	0.2139	1	4.33042
13.5	0.8002	0.18935	0.18249	-0.0713	0.1956	1	4.226036
14	0.8027	0.19675	0.18982	-0.0752	0.1848	1	4.079797
14.5	0.8431	0.21297	0.20611	-0.0739	0.1663	1	3.958774
15	0.824	0.21134	0.20436	-0.0813	0.1551	1	3.898931

- Airfoil 4

Table AVIII-88: Aerodynamic performance of Airfoil 4 of the uncoated blade at 5°

alpha	CL	CD	CDp	CM	Top_Xtr	Bot_Xtr	CL/CD
------	--------	---------	---------	--------	--------	--------	--------
-4.5	-0.3473	0.02011	0.01201	-0.0262	1	0.5949	-17.27
-4	-0.3461	0.02201	0.01421	-0.0111	1	0.7118	-15.7247
-3.5	-0.3603	0.02254	0.01498	0.0075	1	0.8154	-15.9849
-3	-0.3434	0.02164	0.0139	0.0155	1	0.8783	-15.8688
-2.5	-0.2289	0.02201	0.01339	0.0057	1	0.9529	-10.3998
-2	-0.0883	0.02232	0.01317	-0.0147	1	0.998	-3.95609
-1.5	-0.1141	0.0216	0.01243	-0.0082	1	1	-5.28241
-1	-0.103	0.02143	0.01206	-0.0073	1	1	-4.80635
-0.5	-0.0289	0.02278	0.01308	-0.0163	0.9858	1	-1.26866
0	0.0542	0.02448	0.01452	-0.0261	0.9655	1	2.214052
0.5	0.1332	0.02622	0.0161	-0.0344	0.9445	1	5.080092
1	0.2079	0.02803	0.0178	-0.0413	0.9242	1	7.417053
1.5	0.2756	0.02979	0.01957	-0.0466	0.9034	1	9.251427
2	0.3307	0.03162	0.02145	-0.0497	0.8838	1	10.45857
2.5	0.391	0.03356	0.02354	-0.0532	0.8617	1	11.65077
3	0.4533	0.03558	0.02581	-0.0566	0.8379	1	12.7403
3.5	0.5182	0.03772	0.02882	-0.0599	0.8131	1	13.73807
4	0.5647	0.04	0.03153	-0.0604	0.7842	1	14.1175
4.5	0.7439	0.03278	0.02583	-0.0629	0.6968	1	22.69372
5	0.7979	0.02285	0.01491	-0.0396	0.3077	1	34.91904
5.5	0.7825	0.03074	0.02056	-0.0314	0.0889	1	25.45543
6.5	0.9072	0.04233	0.0329	-0.0282	0.0613	1	21.43161
7	0.9462	0.04989	0.04136	-0.0256	0.0621	1	18.96572
7.5	0.9647	0.05817	0.05047	-0.0223	0.0646	1	16.58415
8	0.9679	0.0673	0.06021	-0.0195	0.0674	1	14.38187
8.5	0.9712	0.07674	0.0701	-0.0174	0.0713	1	12.65572
9	0.3468	0.0037	-0.00006	0.0253	0.1147	1	93.72973
13	0.7915	0.1858	0.17952	-0.0732	0.1664	1	4.259957
14	0.8101	0.20167	0.19528	-0.0799	0.1475	1	4.016958
15	0.8393	0.21944	0.21298	-0.0856	0.1329	1	3.824736

- Airfoil 5

Table AVIII-89: Aerodynamic performance of Airfoil 5 of the uncoated blade at 5°

alpha	CL	CD	CDp	CM	Top_Xtr	Bot_Xtr	CL/CD
------	--------	---------	---------	--------	--------	--------	--------
-5	-0.3565	0.03524	0.02499	-0.0455	1	0.106	-10.1163
-4.5	-0.3177	0.03175	0.02108	-0.0439	1	0.104	-10.0063
-4	-0.2788	0.02927	0.01825	-0.042	1	0.1032	-9.52511

-3.5	-0.2413	0.02756	0.01634	-0.0396	1	0.1041	-8.75544
-3	-0.206	0.02645	0.01504	-0.0369	1	0.1069	-7.78828
-2.5	-0.1714	0.02542	0.01397	-0.0348	1	0.113	-6.74272
-2	-0.1325	0.02479	0.01325	-0.0339	1	0.1306	-5.3449
-1.5	-0.1014	0.02316	0.01416	-0.0301	1	0.6385	-4.37824
-1	-0.0937	0.02362	0.01519	-0.0184	0.9933	0.8138	-3.96698
0	0.091	0.02564	0.01696	-0.0378	0.9467	1	3.549142
0.5	0.1682	0.02728	0.01838	-0.0455	0.925	1	6.165689
1	0.2372	0.02903	0.01999	-0.0512	0.9048	1	8.170858
1.5	0.3014	0.03086	0.02179	-0.0555	0.8841	1	9.766688
2	0.3632	0.0328	0.02375	-0.059	0.8634	1	11.07317
2.5	0.4249	0.03482	0.02588	-0.0623	0.8428	1	12.20276
3	0.4829	0.03681	0.02812	-0.0644	0.819	1	13.11872
3.5	0.544	0.03843	0.03005	-0.0659	0.7866	1	14.15561
4	0.6348	0.03845	0.03068	-0.0682	0.7406	1	16.50975
4.5	0.8175	0.02655	0.01991	-0.0625	0.624	1	30.79096
6	0.8994	0.03983	0.02965	-0.0356	0.0784	1	22.58097
6.5	0.9412	0.04587	0.03611	-0.0332	0.0662	1	20.51886
8	0.9653	0.06807	0.06048	-0.0222	0.0567	1	14.18099
8.5	0.9419	0.07616	0.06899	-0.019	0.0582	1	12.36738
9	0.9075	0.08499	0.07807	-0.0183	0.0595	1	10.67773
9.5	0.8885	0.09772	0.09085	-0.0208	0.0622	1	9.092305
10	0.7461	0.141	0.13458	-0.0643	0.237	1	5.291489
11	0.7568	0.15915	0.15257	-0.0695	0.218	1	4.755262
12	0.7709	0.17525	0.16852	-0.0745	0.1909	1	4.398859
13	0.7917	0.19091	0.18406	-0.0797	0.1651	1	4.14698
14	0.8147	0.20604	0.19908	-0.0857	0.142	1	3.954087
15	0.8404	0.22114	0.21407	-0.092	0.1222	1	3.800307

- Airfoil 6

Table AVIII-90: Aerodynamic performance of Airfoil 6 of the uncoated blade at 5°

alpha	CL	CD	CDp	CM	Top_Xtr	Bot_Xtr	CL/CD
------	--------	---------	---------	--------	--------	--------	--------
-5	-0.345	0.03952	0.0303	-0.0342	1	0.0955	-8.72976
-4	-0.2731	0.03289	0.02269	-0.0298	1	0.0838	-8.30344
-3.5	-0.2343	0.03064	0.02	-0.0275	1	0.0812	-7.64687
-3	-0.1971	0.02911	0.01828	-0.0249	1	0.0815	-6.77087
-2.5	-0.1507	0.02818	0.01719	-0.0241	0.9959	0.0855	-5.34776
-2	-0.0627	0.02754	0.01629	-0.0308	0.9749	0.1095	-2.27669
-0.5	0.1637	0.02782	0.01945	-0.0427	0.9087	1	5.884256
0	0.2267	0.02954	0.02093	-0.0465	0.8884	1	7.67434
0.5	0.2856	0.03133	0.02264	-0.0492	0.8667	1	9.115863

1	0.3417	0.03327	0.0246	-0.0512	0.8457	1	10.27051
1.5	0.3974	0.0353	0.02674	-0.0529	0.8234	1	11.25779
2	0.4504	0.0374	0.02909	-0.0539	0.7996	1	12.04278
2.5	0.5116	0.03909	0.03109	-0.0549	0.7675	1	13.08775
3	0.6976	0.02167	0.01335	-0.0351	0.3538	1	32.19197
3.5	0.6943	0.0286	0.01772	-0.0264	0.133	1	24.27622
4.5	0.8137	0.03832	0.02738	-0.0234	0.0843	1	21.23434
5	0.8619	0.04383	0.03353	-0.0209	0.0821	1	19.66461
5.5	0.896	0.05063	0.041	-0.0178	0.083	1	17.69702
6	0.9168	0.05912	0.05007	-0.0148	0.0852	1	15.50744
6.5	0.9322	0.06731	0.05877	-0.0121	0.0871	1	13.84935
7	0.9297	0.0734	0.06544	-0.0085	0.0883	1	12.66621
8	0.759	0.10181	0.09493	-0.0208	0.1214	1	7.455063
9	0.3459	0.06988	0.06486	-0.0313	0.2592	1	4.949914
9.5	0.3701	0.07725	0.07217	-0.0332	0.2542	1	4.790939
10	0.377	0.08382	0.07862	-0.0368	0.2459	1	4.497733
10.5	0.3999	0.09069	0.08542	-0.0384	0.2311	1	4.409527
11	0.4089	0.09739	0.09202	-0.0419	0.2198	1	4.198583
11.5	0.4572	0.11	0.10471	-0.041	0.2041	1	4.156364
12	0.4419	0.11165	0.10613	-0.047	0.1941	1	3.957904
12.5	0.489	0.12494	0.11948	-0.0459	0.1805	1	3.913879
13	0.476	0.12666	0.12107	-0.0523	0.1728	1	3.758093
13.5	0.5049	0.13607	0.13045	-0.0531	0.1587	1	3.71059
14	0.5099	0.1423	0.13658	-0.0576	0.151	1	3.583275
14.5	0.5269	0.14943	0.14367	-0.0602	0.1393	1	3.526066
15	0.5501	0.1602	0.15436	-0.0621	0.1311	1	3.433833

- 10˚
- Airfoil 1:

Table AVIII-91: Aerodynamic performance of Airfoil 1 of the uncoated blade at 10°

alpha	CL	CD	CDp	CM	Top_Xtr	Bot_Xtr	CL/CD
------	--------	---------	---------	--------	--------	--------	--------
-4.5	-0.3676	0.02651	0.01565	-0.028	1	0.1552	-13.8665
-4	-0.3296	0.02396	0.01331	-0.0247	1	0.1858	-13.7563
-3.5	-0.2933	0.02023	0.01098	-0.022	1	0.3459	-14.4983
-3	-0.3128	0.02058	0.01307	-0.0007	1	0.7848	-15.1992
-2	-0.098	0.0216	0.013	-0.0155	1	1	-4.53704
-1.5	-0.1244	0.02074	0.01205	-0.0078	1	1	-5.99807
-1	-0.1072	0.02072	0.01167	-0.0061	1	1	-5.17375
-0.5	-0.0711	0.02135	0.01195	-0.0067	1	1	-3.33021
0	-0.0322	0.02229	0.01259	-0.0074	1	1	-1.44459
0.5	0.031	0.02401	0.01405	-0.0125	0.9893	1	1.291129

1	0.1072	0.02606	0.01596	-0.0197	0.9682	1	4.113584
1.5	0.1783	0.02808	0.01793	-0.0256	0.9463	1	6.349715
2	0.2454	0.0301	0.01996	-0.0306	0.9238	1	8.152824
2.5	0.3113	0.03217	0.02213	-0.035	0.8988	1	9.676717
3	0.3823	0.03422	0.02443	-0.0396	0.8692	1	11.17183
3.5	0.63	0.02556	0.01677	-0.05	0.7256	1	24.64789
4	0.6884	0.02114	0.01254	-0.039	0.5992	1	32.56386
4.5	0.6905	0.02433	0.01287	-0.0269	0.2325	1	28.3806
5	0.7388	0.02741	0.0156	-0.0252	0.1979	1	26.95367
5.5	0.8053	0.0302	0.01855	-0.0256	0.185	1	26.66556
6	0.8677	0.03369	0.02226	-0.0259	0.1794	1	25.75542
6.5	0.9217	0.0384	0.02719	-0.0258	0.1741	1	24.0026
7	0.9603	0.04246	0.03216	-0.0237	0.1679	1	22.61658
7.5	0.9931	0.0482	0.03869	-0.0217	0.1679	1	20.60373
8	1.0144	0.05529	0.04652	-0.0195	0.1698	1	18.3469
8.5	1.0313	0.06453	0.05626	-0.0181	0.1731	1	15.98171
9	0.9415	0.07508	0.06785	-0.0143	0.1847	1	12.53996
11	0.7372	0.14575	0.13811	-0.0586	0.3413	1	5.057976
11.5	0.7292	0.15107	0.1434	-0.0605	0.3227	1	4.826901
12	0.7399	0.15864	0.15101	-0.0623	0.3083	1	4.664019
13.5	0.782	0.18047	0.17315	-0.0668	0.2496	1	4.33313
14	0.7866	0.18751	0.18021	-0.0698	0.2322	1	4.194976
14.5	0.8366	0.20404	0.19689	-0.0673	0.1963	1	4.100176
15	0.8121	0.20238	0.1951	-0.0738	0.1829	1	4.012748

- Airfoil 2

Table AVIII-92: Aerodynamic performance of Airfoil 2 of the uncoated blade at 10°

alpha	CL	CD	CDp	CM	Top_Xtr	Bot_Xtr	CL/CD
------	--------	---------	---------	--------	--------	--------	--------
-4	-0.353	0.02148	0.0148	-0.0121	1	0.7122	-16.4339
-3.5	-0.3632	0.02229	0.01533	0.006	1	0.8189	-16.2943
-2.5	-0.0703	0.02244	0.01349	-0.0224	1	1	-3.1328
-2	-0.098	0.02189	0.01291	-0.0146	1	1	-4.47693
-1.5	-0.1216	0.02104	0.012	-0.0074	1	1	-5.77947
-1	-0.101	0.021	0.01167	-0.0068	1	1	-4.80952
-0.5	-0.0602	0.02166	0.012	-0.0088	1	1	-2.77932
0	-0.0171	0.02265	0.01268	-0.0108	0.9999	1	-0.75497
0.5	0.0672	0.02481	0.01463	-0.0201	0.9794	1	2.708585
1	0.1453	0.02686	0.01657	-0.0277	0.9588	1	5.409531
1.5	0.2184	0.02882	0.0185	-0.0342	0.9376	1	7.578071
2	0.2913	0.03082	0.02056	-0.0401	0.9144	1	9.451655
2.5	0.3644	0.03288	0.0228	-0.0456	0.8896	1	11.08273

3	0.4235	0.03487	0.02498	-0.0486	0.864	1	12.14511
3.5	0.4762	0.03688	0.02724	-0.0503	0.8333	1	12.91215
4	0.5671	0.03813	0.02914	-0.0552	0.7904	1	14.8728
4.5	0.777	0.02502	0.01737	-0.0528	0.6509	1	31.05516
5	0.7732	0.02466	0.01433	-0.0342	0.2437	1	31.35442
5.5	0.8138	0.02944	0.01832	-0.0313	0.171	1	27.64266
6	0.8877	0.03404	0.02294	-0.0325	0.1494	1	26.07814
7	0.9861	0.04377	0.03383	-0.0304	0.1285	1	22.52913
7.5	1.0207	0.05042	0.04133	-0.0281	0.1288	1	20.24395
8	1.027	0.05833	0.05047	-0.0242	0.1337	1	17.60672
8.5	1.0142	0.06785	0.06077	-0.0212	0.1404	1	14.94768
9	1.0279	0.07991	0.07309	-0.0213	0.1488	1	12.86322
10	0.7326	0.13242	0.1254	-0.0622	0.3272	1	5.532397
10.5	0.7506	0.14138	0.13442	-0.064	0.3191	1	5.309096
11	0.7468	0.1487	0.14169	-0.0665	0.3037	1	5.022192
11.5	0.8039	0.16224	0.15545	-0.0661	0.2912	1	4.955005
12	0.7755	0.16453	0.15761	-0.0699	0.2724	1	4.713426
12.5	0.7798	0.17199	0.1651	-0.0727	0.259	1	4.533985
13	0.8402	0.18813	0.18152	-0.0714	0.2433	1	4.466061
13.5	0.8029	0.18671	0.1799	-0.0777	0.2294	1	4.300252
14	0.8378	0.20016	0.19349	-0.0783	0.218	1	4.185651

- Airfoil 3

Table AVIII-93: Aerodynamic performance of Airfoil 3 of the uncoated blade at 10°

alpha	CL	CD	CDp	CM	Top_Xtr	Bot_Xtr	CL/CD
------	--------	---------	---------	--------	--------	--------	--------
-5	-0.4009	0.02311	0.01206	-0.0287	1	0.0932	-17.3475
-4.5	-0.3757	0.01938	0.01039	-0.0261	1	0.4231	-19.386
-4	-0.3483	0.0196	0.01078	-0.0203	1	0.5823	-17.7704
-3.5	-0.3351	0.02077	0.01214	-0.0101	1	0.6994	-16.1338
-3	-0.313	0.02108	0.01223	-0.0032	1	0.758	-14.8482
-2.5	-0.2907	0.02101	0.01168	0.003	1	0.8116	-13.8363
-1.5	-0.1049	0.02182	0.0123	-0.0105	1	1	-4.80752
-1	-0.1205	0.0212	0.01159	-0.005	1	1	-5.68396
-0.5	-0.0914	0.02161	0.01178	-0.0058	1	1	-4.22952
0	-0.0177	0.02318	0.01313	-0.0139	0.9848	1	-0.76359
0.5	0.0652	0.02508	0.01486	-0.0231	0.9645	1	2.599681
1	0.1354	0.02679	0.01646	-0.0293	0.9443	1	5.054125
1.5	0.205	0.02862	0.01829	-0.0351	0.9246	1	7.162823
2	0.274	0.03053	0.02021	-0.0404	0.9044	1	8.974779
2.5	0.3395	0.03237	0.02217	-0.0446	0.8828	1	10.48811

3	0.4007	0.03415	0.02431	-0.0476	0.8602	1	11.73353
4	0.6807	0.02142	0.01286	-0.0437	0.6095	1	31.77871
4.5	0.6722	0.02468	0.01262	-0.0314	0.0886	1	27.23663
5	0.697	0.02842	0.01633	-0.0272	0.0528	1	24.52498
5.5	0.7272	0.03157	0.01981	-0.0233	0.0465	1	23.03453
6	0.78	0.03531	0.02427	-0.0211	0.043	1	22.09006
6.5	0.8487	0.04082	0.03027	-0.0208	0.0429	1	20.79128
7	0.8954	0.04756	0.03784	-0.0187	0.0449	1	18.82675
7.5	0.9171	0.05512	0.04638	-0.0152	0.0478	1	16.63824
8	0.92	0.06307	0.05509	-0.0117	0.0506	1	14.58697
8.5	0.9068	0.07103	0.06358	-0.0086	0.0529	1	12.76644
9	0.8781	0.07864	0.0715	-0.0062	0.0543	1	11.16607
9.5	0.8436	0.08801	0.08107	-0.0081	0.0557	1	9.585274
10	0.815	0.09961	0.09275	-0.0131	0.0575	1	8.181909
10.5	0.7972	0.11173	0.10502	-0.0205	0.062	1	7.135058
11	0.7581	0.13206	0.12524	-0.0363	0.0712	1	5.740572
12.5	0.7536	0.17103	0.16413	-0.0579	0.1556	1	4.406245
13	0.7845	0.18176	0.17491	-0.0576	0.1485	1	4.316131
13.5	0.7743	0.18818	0.18119	-0.0638	0.1424	1	4.114677
14	0.7812	0.19483	0.18781	-0.0675	0.1325	1	4.009649
14.5	0.8346	0.21411	0.2072	-0.0638	0.1249	1	3.897996
15	0.8109	0.21291	0.20584	-0.073	0.1223	1	3.808652

- Airfoil 4

Table AVIII-94: Aerodynamic performance of Airfoil 4 of the uncoated blade at 10°

alpha	CL	CD	CDp	CM	Top_Xtr	Bot_Xtr	CL/VD
------	--------	---------	---------	--------	--------	--------	--------
-5	-0.3713	0.01956	0.0118	-0.0351	1	0.3828	-18.9826
-4.5	-0.3526	0.0205	0.01313	-0.0258	1	0.5979	-17.2
-4	-0.3288	0.02123	0.01348	-0.0185	1	0.6671	-15.4875
-3.5	-0.3098	0.0217	0.0137	-0.0103	1	0.7305	-14.2765
-3	-0.3058	0.02172	0.01368	0.0016	1	0.8107	-14.0792
-2	-0.1044	0.02215	0.01315	-0.0122	1	0.9912	-4.71332
-1.5	-0.1106	0.02158	0.01251	-0.009	1	1	-5.12512
-1	-0.1061	0.02128	0.01201	-0.0071	1	1	-4.9859
-0.5	-0.0376	0.02246	0.01288	-0.0153	0.9877	1	-1.67409
0	0.0497	0.0242	0.01426	-0.0259	0.9669	1	2.053719
0.5	0.1258	0.02584	0.01571	-0.0338	0.9459	1	4.868421
1	0.196	0.02757	0.01734	-0.0401	0.9264	1	7.109177
1.5	0.2608	0.02933	0.0191	-0.0451	0.9067	1	8.89192
2	0.3223	0.03119	0.021	-0.0492	0.8863	1	10.33344
2.5	0.3812	0.03316	0.02309	-0.0526	0.8659	1	11.49578

3	0.4399	0.03519	0.02534	-0.0556	0.8428	1	12.50071
3.5	0.4987	0.03731	0.02813	-0.0581	0.8174	1	13.36639
4.5	0.6254	0.04078	0.03273	-0.0617	0.7529	1	15.33595
5	0.7554	0.02675	0.0158	-0.0365	0.0966	1	28.23925
5.5	0.7751	0.03119	0.02022	-0.0316	0.0657	1	24.85091
6	0.8261	0.03522	0.0249	-0.0287	0.0558	1	23.45542
6.5	0.8974	0.0413	0.03143	-0.0284	0.0534	1	21.72881
7	0.9433	0.04864	0.03968	-0.0262	0.0554	1	19.3935
7.5	0.9627	0.05685	0.04892	-0.0227	0.0589	1	16.93404
8	0.9634	0.06541	0.05823	-0.0195	0.0624	1	14.72863
8.5	0.9501	0.07413	0.06743	-0.017	0.0653	1	12.81667
9	0.9262	0.08327	0.07682	-0.0153	0.0677	1	11.12285
13	0.8031	0.18578	0.17943	-0.0723	0.1622	1	4.322855
14	0.8146	0.20078	0.19431	-0.0801	0.1443	1	4.057177
15	0.84	0.21754	0.21101	-0.0868	0.131	1	3.861359

- Airfoil 5

Table AVIII-95: Aerodynamic performance of Airfoil 5 of the uncoated blade at 10°

alpha	CL	CD	CDp	CM	Top_Xtr	Bot_Xtr	CL/CD
------	--------	---------	---------	--------	--------	--------	--------
-5	-0.3566	0.02029	0.01158	-0.0376	1	0.3589	-17.5752
-4.5	-0.3391	0.02124	0.01361	-0.028	1	0.5627	-15.9652
-4	-0.3247	0.02245	0.01473	-0.0173	1	0.6691	-14.4633
-3.5	-0.3083	0.02256	0.01452	-0.0088	1	0.7305	-13.6658
-3	-0.2895	0.0222	0.01392	-0.0021	1	0.788	-13.0405
-2.5	-0.2726	0.02138	0.01299	0.0048	1	0.8528	-12.7502
-2	-0.1369	0.02189	0.0132	-0.0084	1	0.9807	-6.254
-1.5	-0.122	0.0215	0.01261	-0.0089	1	1	-5.67442
-1	-0.0859	0.02192	0.01271	-0.012	0.9966	1	-3.9188
-0.5	0.0036	0.02366	0.01408	-0.0235	0.9756	1	0.152156
0	0.0836	0.02531	0.01543	-0.0323	0.954	1	3.303042
0.5	0.1541	0.027	0.01693	-0.0389	0.9352	1	5.707407
1	0.2241	0.02881	0.01864	-0.0448	0.9161	1	7.778549
1.5	0.2939	0.03076	0.02063	-0.0504	0.8994	1	9.554616
2	0.3461	0.03255	0.02245	-0.0528	0.8812	1	10.63287
2.5	0.3927	0.03453	0.02452	-0.0542	0.8636	1	11.37272
3	0.4425	0.03671	0.02697	-0.0561	0.8459	1	12.05394
3.5	0.4964	0.03899	0.02953	-0.0583	0.8253	1	12.73147
4	0.5867	0.03982	0.0309	-0.0624	0.7811	1	14.7338
4.5	0.7447	0.03519	0.02764	-0.0669	0.7123	1	21.16226
5.5	0.8325	0.02803	0.01831	-0.0372	0.1839	1	29.70032
6.5	0.9384	0.04106	0.03099	-0.0325	0.078	1	22.85436

7	0.9823	0.04833	0.03902	-0.0301	0.0753	1	20.32485
7.5	1	0.05651	0.04826	-0.026	0.0774	1	17.69598
8	0.996	0.06542	0.05804	-0.0217	0.0813	1	15.2247
8.5	0.9783	0.07447	0.0676	-0.0185	0.0851	1	13.13683
9	0.9553	0.08421	0.07756	-0.0165	0.0887	1	11.34426
10	0.8288	0.1122	0.10589	-0.0342	0.101	1	7.386809
12	0.4527	0.08812	0.08335	-0.0447	0.2242	1	5.137313
12.5	0.4645	0.09478	0.08997	-0.0481	0.2078	1	4.900823
13	0.4781	0.10313	0.09825	-0.0518	0.2004	1	4.635896
13.5	0.4988	0.11152	0.10667	-0.0542	0.185	1	4.47274
14	0.5103	0.12008	0.11517	-0.0582	0.1774	1	4.249667
14.5	0.5269	0.12805	0.12312	-0.0612	0.1645	1	4.114799
15	0.5524	0.14035	0.13537	-0.0633	0.1575	1	3.935875

- Airfoil 6

Table AVIII-96 Aerodynamic performance of Airfoil 6 of the uncoated blade at 10°

alpha	CL	CD	CDp	CM	Top_Xtr	Bot_Xtr	CL/CD
------	--------	---------	---------	--------	--------	--------	--------
-5	-0.2425	0.01989	0.01133	-0.0382	1	0.3853	-12.1921
-4.5	-0.212	0.02054	0.012	-0.0338	1	0.5339	-10.3213
-4	-0.1829	0.02136	0.01237	-0.0303	1	0.5981	-8.56273
-3.5	-0.1642	0.02217	0.01332	-0.024	1	0.6875	-7.40641
-3	-0.1526	0.02204	0.01346	-0.0153	1	0.7973	-6.92377
-2.5	-0.0495	0.0225	0.0141	-0.0245	0.9764	1	-2.2
-2	0.042	0.02382	0.01462	-0.0367	0.9523	1	1.763224
-1.5	0.1287	0.02532	0.01562	-0.0466	0.9304	1	5.082938
-1	0.1984	0.02676	0.01675	-0.0527	0.9077	1	7.414051
-0.5	0.2652	0.02834	0.01813	-0.0577	0.8868	1	9.357798
0	0.3277	0.02997	0.01969	-0.0615	0.8656	1	10.93427
0.5	0.3841	0.03173	0.02142	-0.064	0.8449	1	12.10526
1	0.4381	0.03361	0.0234	-0.066	0.824	1	13.03481
1.5	0.4919	0.03557	0.02558	-0.0676	0.8026	1	13.82907
2	0.5456	0.03754	0.02791	-0.0689	0.7803	1	14.53383
4	0.8377	0.03148	0.02049	-0.0362	0.0596	1	26.61055
5	0.8604	0.03491	0.02428	-0.0316	0.0581	1	24.64623
5.5	0.9222	0.03896	0.02916	-0.0289	0.0599	1	23.67043
6	0.9982	0.04627	0.0373	-0.0283	0.065	1	21.57337
6.5	1.0289	0.05494	0.0469	-0.0252	0.0703	1	18.7277
7	1.0393	0.06542	0.05799	-0.0224	0.0747	1	15.88658
8	0.9801	0.07955	0.07352	-0.0152	0.0822	1	12.32055
8.5	0.9289	0.08989	0.08409	-0.0188	0.0828	1	10.33374
9	0.8787	0.10449	0.09876	-0.0288	0.0833	1	8.409417

9.5	0.841	0.123	0.11715	-0.0412	0.0876	1	6.837398
10	0.8379	0.13719	0.13129	-0.047	0.1015	1	6.107588
12	0.8464	0.19589	0.18977	-0.074	0.1921	1	4.320792
13	0.8361	0.20582	0.1995	-0.0836	0.1736	1	4.062287
14	0.8567	0.22224	0.21581	-0.0908	0.1612	1	3.854842
15	0.9223	0.25756	0.25123	-0.0912	0.144	1	3.580913

- **H-146**
  - -5˚
  - Airfoil 1

Table AVIII-97: Aerodynamic performance of Airfoil 1 of the H-146 coated blade at -5°

alpha	CL	CD	CDp	CM	Top_Xtr	Bot_Xtr	CL/CD
------	--------	---------	---------	--------	--------	--------	--------
-5	-0.4473	0.03077	0.02096	-0.0332	1	0.1227	-14.5369
-4.5	-0.4123	0.02694	0.01711	-0.03	1	0.1725	-15.3044
-4	-0.3707	0.02422	0.01421	-0.0261	1	0.1964	-15.3055
-3.5	-0.3336	0.02123	0.01194	-0.0232	1	0.2941	-15.7136
-3	-0.3466	0.02162	0.01446	-0.004	1	0.7418	-16.0315
-2.5	-0.3472	0.02181	0.01436	0.0112	1	0.8419	-15.9193
-2	-0.0679	0.02333	0.01453	-0.022	1	1	-2.91042
-1.5	-0.0883	0.02286	0.014	-0.0148	1	1	-3.86264
-1	-0.1103	0.02211	0.01319	-0.0073	1	1	-4.98869
-0.5	-0.1114	0.02163	0.01251	-0.0029	1	1	-5.15025
0	-0.0805	0.02204	0.01251	-0.0031	1	1	-3.65245
0.5	-0.0416	0.02289	0.01309	-0.0043	1	1	-1.81739
1	0.0223	0.02461	0.0146	-0.0099	0.9893	1	0.906136
1.5	0.0997	0.02674	0.01657	-0.0177	0.9684	1	3.728497
2	0.1717	0.02877	0.01853	-0.0241	0.947	1	5.968022
2.5	0.24	0.03077	0.02054	-0.0296	0.924	1	7.799805
3	0.3052	0.03286	0.02275	-0.0342	0.9003	1	9.287888
3.5	0.3687	0.03503	0.02509	-0.0383	0.8747	1	10.52526
4	0.4542	0.03722	0.02762	-0.0446	0.8427	1	12.20312
5.5	0.7247	0.02797	0.01621	-0.0249	0.1624	1	25.9099
6.5	0.8618	0.03632	0.02461	-0.0265	0.1301	1	23.72797
7	0.9141	0.04124	0.03016	-0.0258	0.1296	1	22.16537
7.5	0.9564	0.04738	0.03692	-0.0245	0.1316	1	20.18573
8	0.9882	0.05264	0.04312	-0.0218	0.1365	1	18.7728
8.5	0.9842	0.06098	0.05267	-0.0178	0.1464	1	16.13972
9	1.0081	0.07076	0.06276	-0.0174	0.1558	1	14.24675
12	0.726	0.155	0.14747	-0.0607	0.2954	1	4.683871
13	0.7702	0.17156	0.16416	-0.0633	0.2678	1	4.489391

14	0.8164	0.19089	0.18371	-0.0662	0.2439	1	4.276809
15	0.8418	0.20692	0.1999	-0.0709	0.2217	1	4.068239

- Airfoil 2

Table AVIII-98: Aerodynamic performance of Airfoil 2 of the H-146 coated blade at -5°

alpha	CL	CD	CDp	CM	Top_Xtr	Bot_Xtr	CL/CD
------	--------	---------	---------	--------	--------	--------	--------
-5	-0.3658	0.03223	0.02137	-0.0375	1	0.0592	-11.3497
-4.5	-0.3279	0.02946	0.01831	-0.0349	1	0.0592	-11.1303
-4	-0.2905	0.02731	0.01599	-0.0317	1	0.0605	-10.6371
-3.5	-0.2546	0.02537	0.0139	-0.0289	1	0.0648	-10.0355
-3	-0.2143	0.02414	0.01245	-0.0278	1	0.0763	-8.87738
-2.5	-0.1772	0.02086	0.01205	-0.0258	1	0.6202	-8.49473
-2	-0.2106	0.02161	0.01349	-0.0021	1	0.8519	-9.74549
-1	-0.0993	0.02146	0.01261	-0.0065	1	1	-4.62721
-0.5	-0.0562	0.02206	0.01288	-0.0092	1	1	-2.5476
0	0.0115	0.02356	0.01405	-0.0159	0.9907	1	0.488115
0.5	0.0892	0.02548	0.01574	-0.024	0.9728	1	3.500785
1	0.1629	0.02746	0.01763	-0.0309	0.9534	1	5.932265
1.5	0.2344	0.02955	0.01975	-0.0371	0.9332	1	7.932318
2	0.301	0.03159	0.02189	-0.0421	0.911	1	9.528332
2.5	0.3664	0.0338	0.02428	-0.0466	0.888	1	10.84024
3	0.4285	0.03609	0.02686	-0.0503	0.8633	1	11.8731
3.5	0.4845	0.03846	0.02961	-0.0528	0.8363	1	12.5975
4.5	0.7168	0.02701	0.01608	-0.0314	0.159	1	26.53832
6	0.9026	0.04111	0.03094	-0.0292	0.111	1	21.95573
6.5	0.9437	0.04796	0.03881	-0.0268	0.1136	1	19.67681
7	0.9647	0.05656	0.04849	-0.024	0.1211	1	17.05622
7.5	0.9708	0.06541	0.05804	-0.0216	0.1234	1	14.84177
8	0.9673	0.07551	0.06856	-0.0203	0.1268	1	12.81022

- Airfoil 3

Table AVIII-99: Aerodynamic performance of Airfoil 3 of the H-146 coated blade at -5°

alpha	CL	CD	CDp	CM	Top_Xtr	Bot_Xtr	CL/CD
------	--------	---------	---------	--------	--------	--------	--------
-4.5	-0.3655	0.03113	0.02032	-0.0291	1	0.0702	-11.7411
-4	-0.3274	0.02905	0.01797	-0.0262	1	0.0718	-11.2702
-3.5	-0.2908	0.02646	0.01529	-0.0227	1	0.0757	-10.9902
-3	-0.2558	0.025	0.0137	-0.0197	1	0.082	-10.232
-2.5	-0.2182	0.02399	0.01235	-0.0177	1	0.0938	-9.09546

-2	-0.1908	0.02117	0.01241	-0.0131	1	0.6538	-9.01275
-1	-0.1104	0.02141	0.01273	-0.0049	1	1	-5.15647
-0.5	-0.0753	0.022	0.01288	-0.0056	1	1	-3.42273
0	-0.0175	0.02337	0.01387	-0.0102	0.9924	1	-0.74882
0.5	0.0638	0.02549	0.01572	-0.0185	0.974	1	2.502942
1	0.1301	0.02729	0.01734	-0.0238	0.9566	1	4.767314
1.5	0.191	0.02913	0.01919	-0.028	0.9381	1	6.556814
2	0.2522	0.03117	0.0213	-0.0319	0.9187	1	8.091113
2.5	0.3122	0.03333	0.02361	-0.0355	0.8977	1	9.366937
3	0.3705	0.0356	0.02616	-0.0385	0.8748	1	10.4073
3.5	0.4305	0.03795	0.02894	-0.0414	0.8479	1	11.34387
5.5	0.7932	0.03782	0.02651	-0.0208	0.065	1	20.97303
6	0.8425	0.04335	0.0327	-0.0191	0.0639	1	19.43483
6.5	0.8778	0.04988	0.04017	-0.0164	0.0652	1	17.59824
7	0.9002	0.05735	0.0483	-0.0137	0.0676	1	15.6966
7.5	0.9188	0.06707	0.05845	-0.0119	0.0713	1	13.69912
8	0.894	0.07221	0.06474	-0.0068	0.0792	1	12.38056
8.5	0.8549	0.08083	0.0737	-0.0049	0.0843	1	10.57652
10.5	0.7551	0.14849	0.1414	-0.0448	0.2322	1	5.085191
11	0.7299	0.15299	0.14574	-0.0496	0.213	1	4.7709
11.5	0.728	0.16049	0.15315	-0.0529	0.1988	1	4.536108
12.5	0.7459	0.17535	0.16807	-0.0578	0.1728	1	4.253778
13	0.8001	0.19082	0.18363	-0.0546	0.1618	1	4.192957
13.5	0.7667	0.19015	0.18278	-0.0635	0.1518	1	4.03208
14	0.801	0.20104	0.19374	-0.0629	0.141	1	3.984282
14.5	0.8031	0.2082	0.20081	-0.0675	0.1368	1	3.857349
15	0.8029	0.21152	0.20407	-0.0729	0.1271	1	3.795859

- Airfoil 4

Table AVIII-100: Aerodynamic performance of Airfoil 4 of the H-146 coated blade at -5°

alpha	CL	CD	CDp	CM	Top_Xtr	Bot_Xtr	CL/CD
------	--------	---------	---------	--------	--------	--------	--------
-4.5	-0.3707	0.02908	0.01884	-0.0344	1	0.1036	-12.7476
-4	-0.3332	0.02654	0.01629	-0.0312	1	0.1283	-12.5546
-3.5	-0.2962	0.02365	0.01358	-0.0275	1	0.1771	-12.5243
-2.5	-0.318	0.02278	0.01565	0.0077	1	0.8332	-13.9596
-2	-0.1056	0.02443	0.01614	-0.0134	1	0.9915	-4.32255
-1.5	-0.0994	0.02401	0.01554	-0.0115	1	1	-4.13994
-1	-0.1203	0.02315	0.01461	-0.0051	1	1	-5.19654
-0.5	-0.0864	0.02349	0.0146	-0.0072	0.9943	1	-3.67816
0	-0.0072	0.02511	0.01587	-0.0163	0.9754	1	-0.28674

0.5	0.0632	0.02679	0.01724	-0.0232	0.959	1	2.359089
1	0.1354	0.02873	0.01902	-0.0299	0.9424	1	4.712844
1.5	0.193	0.03042	0.02061	-0.0337	0.926	1	6.34451
2	0.2454	0.03232	0.02248	-0.0365	0.9121	1	7.592822
2.5	0.308	0.03452	0.02474	-0.0407	0.8962	1	8.922364
3	0.3686	0.03671	0.02713	-0.0443	0.8781	1	10.04086
3.5	0.4107	0.03883	0.02941	-0.0451	0.8594	1	10.57687
4	0.4873	0.04098	0.03193	-0.0495	0.8279	1	11.89117
5	0.7294	0.02724	0.01586	-0.0295	0.1593	1	26.7768
5.5	0.7676	0.03054	0.01886	-0.0268	0.1279	1	25.13425
6	0.8367	0.03427	0.02261	-0.0275	0.1058	1	24.41494
6.5	0.8903	0.03779	0.02631	-0.0269	0.087	1	23.55914
7	0.925	0.04098	0.02968	-0.025	0.0658	1	22.57199
8	0.9928	0.05373	0.04378	-0.0205	0.0582	1	18.47757
8.5	1.0042	0.06045	0.05121	-0.017	0.0579	1	16.61208
9	1.0003	0.06765	0.05902	-0.0134	0.0584	1	14.7864
9.5	0.9797	0.07515	0.06695	-0.0098	0.0592	1	13.03659
10	0.9473	0.08343	0.07554	-0.0081	0.0601	1	11.35443
10.5	0.9174	0.09446	0.08675	-0.0101	0.0616	1	9.712047
11	0.8219	0.11628	0.10905	-0.0284	0.0705	1	7.068283
11.5	0.8041	0.13243	0.12513	-0.0373	0.0785	1	6.071887
12.5	0.7916	0.16779	0.16057	-0.0578	0.1789	1	4.717802
13	0.7883	0.17575	0.16844	-0.0623	0.1701	1	4.485349
13.5	0.7985	0.18254	0.17523	-0.065	0.1587	1	4.374384
14	0.8451	0.19658	0.18935	-0.0626	0.1525	1	4.299013
14.5	0.8138	0.19718	0.18981	-0.0722	0.1436	1	4.127193
15	0.8302	0.20442	0.19708	-0.0746	0.1357	1	4.061246

- Airfoil 5

Table AVIII-101: Aerodynamic performance of Airfoil 1 of the H-146 coated blade at -5°

alpha	CL	CD	CDp	CM	Top_Xtr	Bot_Xtr	CL/CD
------	--------	---------	---------	--------	--------	--------	--------
-4	-0.3118	0.03701	0.02803	-0.0323	1	0.073	-8.42475
-3.5	-0.2704	0.03463	0.02473	-0.0293	1	0.0647	-7.80826
-3	-0.2323	0.03289	0.02259	-0.0266	1	0.0629	-7.06294
-2.5	-0.1951	0.02971	0.01938	-0.0238	1	0.0687	-6.56681
-2	-0.1556	0.0286	0.01823	-0.0221	0.9983	0.0918	-5.44056
-1	-0.0117	0.02543	0.01811	-0.0224	0.9657	1	-0.46009
-0.5	0.0608	0.02698	0.01897	-0.0289	0.9464	1	2.253521
0	0.1335	0.02887	0.02046	-0.0351	0.9298	1	4.624177
0.5	0.1901	0.03048	0.02189	-0.0382	0.912	1	6.236877

1	0.241	0.03229	0.02326	-0.04	0.8965	1	7.463611
1.5	0.3062	0.03445	0.02541	-0.044	0.8803	1	8.888244
2	0.3488	0.0364	0.02742	-0.0444	0.8637	1	9.582418
2.5	0.3994	0.03852	0.02973	-0.0457	0.8424	1	10.36864
4	0.7222	0.03176	0.02008	-0.0276	0.1062	1	22.73929
4.5	0.7858	0.03469	0.02325	-0.0271	0.0972	1	22.65206
5	0.8387	0.03974	0.02815	-0.027	0.0827	1	21.10468
5.5	0.8743	0.04125	0.03033	-0.0239	0.0712	1	21.19515
6	0.9116	0.04504	0.03409	-0.0223	0.0624	1	20.23979
6.5	0.9442	0.05193	0.04141	-0.0203	0.0603	1	18.18217
7	0.9654	0.0574	0.04737	-0.017	0.0597	1	16.81882
7.5	0.9758	0.06307	0.0536	-0.0133	0.0593	1	15.4717
8	0.9692	0.06752	0.05865	-0.0086	0.0573	1	14.35427
8.5	0.9436	0.07322	0.06479	-0.004	0.0559	1	12.88719
9	0.9094	0.08144	0.07331	-0.0027	0.0571	1	11.1665
9.5	0.8804	0.09237	0.0844	-0.005	0.0593	1	9.531233

- Airfoil 6

Table AVIII-102: Aerodynamic performance of Airfoil 1 of the H-146 coated blade at -5°

alpha	CL	CD	CDp	CM	Top_Xtr	Bot_Xtr	CL/CD
------	--------	---------	---------	--------	--------	--------	--------
-4	-0.431	0.04368	0.03653	-0.0361	1	0.1047	-9.86722
-2.5	-0.32	0.03214	0.02265	-0.0281	1	0.1043	-9.95644
-2	-0.2808	0.03024	0.02034	-0.0249	1	0.1028	-9.28571
-1.5	-0.2442	0.02893	0.01887	-0.0216	1	0.1064	-8.44106
-1	-0.2083	0.02814	0.01784	-0.0188	1	0.1168	-7.40227
-0.5	-0.1659	0.02692	0.01676	-0.0177	1	0.1707	-6.1627
0.5	-0.0493	0.02692	0.01913	-0.0171	0.9788	1	-1.83135
1	0.0251	0.02907	0.02072	-0.0238	0.9596	1	0.863433
1.5	0.0923	0.03103	0.02203	-0.0286	0.94	1	2.974541
2	0.1516	0.03279	0.02362	-0.0317	0.9197	1	4.623361
2.5	0.2073	0.03463	0.0254	-0.0342	0.9014	1	5.986139
3	0.2641	0.03657	0.02738	-0.0366	0.8808	1	7.221766
3.5	0.3287	0.03852	0.02949	-0.0396	0.8545	1	8.533229
4	0.4242	0.03931	0.03058	-0.0443	0.8057	1	10.79115
5	0.69	0.02481	0.01338	-0.0329	0.1776	1	27.81137
5.5	0.7113	0.02755	0.01553	-0.0281	0.1266	1	25.81851
6	0.7381	0.02961	0.01738	-0.0241	0.1048	1	24.92739
6.5	0.7647	0.03171	0.01939	-0.02	0.0925	1	24.11542
7	0.8044	0.03403	0.0218	-0.0171	0.0865	1	23.63797
7.5	0.871	0.03668	0.02476	-0.0173	0.0797	1	23.74591

8.5	0.9709	0.04393	0.03222	-0.0156	0.0609	1	22.10107
9	1.0099	0.04863	0.03738	-0.0135	0.0589	1	20.76702
9.5	1.0341	0.05301	0.04241	-0.0103	0.0582	1	19.50764
10	1.0456	0.05761	0.04751	-0.0063	0.0578	1	18.14963
10.5	1.0393	0.06261	0.053	-0.0013	0.0578	1	16.59958
11	1.0176	0.06872	0.05959	0.003	0.0578	1	14.80792
11.5	0.9779	0.07702	0.06834	0.0044	0.0581	1	12.6967
12	0.9065	0.09141	0.08316	-0.0013	0.0582	1	9.916858
12.5	0.8174	0.11675	0.10855	-0.0179	0.0586	1	7.001285
13	0.7929	0.13385	0.12564	-0.0276	0.0592	1	5.923795
13.5	0.7864	0.14574	0.1375	-0.0339	0.0585	1	5.395911
14	0.787	0.15588	0.14762	-0.0389	0.059	1	5.048755
14.5	0.7907	0.16523	0.15697	-0.0435	0.0588	1	4.785451
15	0.7988	0.17365	0.16555	-0.0475	0.0596	1	4.600058

- 0°
- Airfoil 1:

Table AVIII-103: Aerodynamic performance of Airfoil 1 of the H-146 coated blade at 0°

alpha	CL	CD	CDp	CM	Top_Xtr	Bot_Xtr	CL/CD
------	--------	---------	---------	--------	--------	--------	--------
-4	-0.3424	0.0402	0.02992	-0.0311	1	0.1596	-8.51741
-3.5	-0.3104	0.03847	0.02809	-0.0291	1	0.1666	-8.06862
-2.5	-0.2554	0.03541	0.02551	-0.0247	1	0.239	-7.21265
-2	-0.2187	0.03276	0.0231	-0.023	1	0.2495	-6.67582
-1.5	-0.1751	0.031	0.02108	-0.0222	1	0.2589	-5.64839
-1	-0.1293	0.02856	0.01864	-0.0211	1	0.2681	-4.52731
-0.5	-0.0811	0.02678	0.01675	-0.0199	1	0.2736	-3.02838
0	-0.0298	0.02519	0.01481	-0.0178	1	0.2547	-1.18301
0.5	0.0184	0.02455	0.01398	-0.0157	1	0.2294	0.749491
2	0.16	0.02267	0.01234	-0.0077	1	1	7.057786
2.5	0.2514	0.02524	0.0153	-0.0178	0.9709	1	9.96038
3	0.3408	0.02768	0.01826	-0.027	0.9383	1	12.31214
4	0.6038	0.02371	0.01292	-0.0221	0.1914	1	25.46605
4.5	0.6618	0.02753	0.01683	-0.0206	0.1511	1	24.03923
6	0.8028	0.04887	0.04002	-0.0147	0.0972	1	16.42726
6.5	0.8269	0.0567	0.04932	-0.0113	0.1118	1	14.58377
7	0.8377	0.06819	0.06178	-0.0109	0.1467	1	12.28479
9	0.6945	0.12061	0.11428	-0.0489	0.3111	1	5.758229
9.5	0.7064	0.12837	0.12199	-0.0488	0.2805	1	5.502843
10	0.7461	0.14032	0.13397	-0.0465	0.2515	1	5.317132
10.5	0.7411	0.1471	0.14063	-0.0485	0.2287	1	5.038069

11	0.7509	0.15567	0.14914	-0.0495	0.2069	1	4.823665
11.5	0.7703	0.16587	0.1593	-0.0497	0.1856	1	4.643998
12	0.7433	0.16779	0.16106	-0.0566	0.1727	1	4.429942
12.5	0.755	0.17648	0.16968	-0.0587	0.1593	1	4.278105
13	0.7764	0.18675	0.17991	-0.0593	0.1404	1	4.15743
13.5	0.7768	0.19102	0.18411	-0.0635	0.1252	1	4.06659
14	0.7875	0.19963	0.19263	-0.0666	0.1169	1	3.944798
14.5	0.7951	0.20526	0.19821	-0.0707	0.1058	1	3.873624
15	0.8378	0.22534	0.21834	-0.0683	0.0982	1	3.717937

- Airfoil 2

Table AVIII-104: Aerodynamic performance of Airfoil 2 of the H-146 coated blade at 0°

alpha	CL	CD	CDp	CM	Top_Xtr	Bot_Xtr	CL/CD
------	--------	---------	---------	--------	--------	--------	--------
-3	-0.3648	0.02254	0.01519	0.0129	1	0.8431	-16.1846
-1.5	-0.1065	0.02255	0.0138	-0.01	1	1	-4.72284
-1	-0.1203	0.02169	0.01281	-0.0043	1	1	-5.54633
-0.5	-0.0916	0.02187	0.01271	-0.0049	1	1	-4.18839
0	-0.0455	0.02275	0.01332	-0.0079	0.9979	1	-2
0.5	0.0337	0.02464	0.01495	-0.0164	0.9798	1	1.367695
1	0.1068	0.02654	0.01665	-0.0234	0.9613	1	4.024115
1.5	0.1751	0.02849	0.01853	-0.0291	0.9423	1	6.146016
2	0.2412	0.03056	0.02049	-0.0342	0.9228	1	7.89267
2.5	0.3048	0.03268	0.02273	-0.0386	0.9019	1	9.326805
3	0.3653	0.03486	0.02515	-0.0422	0.879	1	10.47906
3.5	0.4239	0.0371	0.02773	-0.0452	0.8528	1	11.42588
4	0.4915	0.03948	0.03053	-0.0489	0.8228	1	12.44934
4.5	0.6822	0.02576	0.01447	-0.0299	0.1641	1	26.48292
5	0.7168	0.02923	0.01759	-0.0268	0.1205	1	24.52275
6	0.8551	0.0389	0.02742	-0.0278	0.0945	1	21.98201
6.5	0.8991	0.04269	0.03201	-0.0258	0.0878	1	21.06114
7	0.9363	0.04783	0.03781	-0.0238	0.083	1	19.57558
7.5	0.9619	0.05426	0.04505	-0.0211	0.0833	1	17.72761
8	0.9719	0.06195	0.05354	-0.0181	0.087	1	15.68846
8.5	0.9708	0.07051	0.06263	-0.0157	0.091	1	13.76826
9.5	0.8621	0.09087	0.08392	-0.0165	0.106	1	9.487179
10	0.8647	0.10313	0.09627	-0.0197	0.1191	1	8.384563
11.5	0.7469	0.15914	0.15207	-0.0638	0.2707	1	4.693352
12	0.7676	0.16782	0.16076	-0.0647	0.2498	1	4.573948
12.5	0.7871	0.17635	0.16931	-0.0656	0.228	1	4.463283
13	0.8073	0.18518	0.17816	-0.0664	0.206	1	4.359542

13.5	0.7915	0.18732	0.18022	-0.0717	0.1909	1	4.22539
14	0.8017	0.19517	0.18803	-0.0748	0.1784	1	4.107701
14.5	0.8291	0.20627	0.19914	-0.0753	0.1603	1	4.019489
15	0.8426	0.21353	0.20636	-0.0775	0.138	1	3.94605

- Airfoil 3

Table AVIII-105: Aerodynamic performance of Airfoil 3 of the H-146 coated blade at 0°

alpha	CL	CD	CDp	CM	Top_Xtr	Bot_Xtr	CL/CD
------	--------	---------	---------	--------	--------	--------	--------
-5	-0.414	0.03886	0.0302	-0.0338	1	0.0852	-10.6536
-4.5	-0.378	0.03692	0.02731	-0.0305	1	0.0783	-10.2384
-4	-0.3421	0.03347	0.02342	-0.0281	1	0.0788	-10.2211
-3.5	-0.3027	0.03083	0.02044	-0.0258	1	0.0791	-9.81836
-3	-0.2633	0.02833	0.0179	-0.0231	1	0.0825	-9.29403
-2.5	-0.2266	0.02692	0.01643	-0.0199	1	0.0857	-8.41753
-2	-0.19	0.0259	0.01519	-0.0173	1	0.0916	-7.33591
-1.5	-0.1502	0.02529	0.01431	-0.0159	1	0.1035	-5.93911
-1	-0.123	0.02316	0.01512	-0.0104	1	0.7166	-5.31088
-0.5	-0.0718	0.02284	0.01525	-0.0076	0.9965	1	-3.14361
0	0.0134	0.02474	0.01659	-0.0168	0.976	1	0.541633
0.5	0.0855	0.02649	0.01784	-0.0232	0.9569	1	3.227633
1.5	0.2275	0.03045	0.0208	-0.0344	0.9201	1	7.471264
2	0.2825	0.03225	0.0227	-0.0371	0.9007	1	8.75969
2.5	0.3339	0.03424	0.02488	-0.0392	0.8807	1	9.751752
3	0.3906	0.03644	0.02744	-0.0419	0.8578	1	10.71899
3.5	0.4561	0.03873	0.03018	-0.0452	0.8307	1	11.7764
5.5	0.7925	0.04152	0.03027	-0.0209	0.0485	1	19.08719
6	0.8229	0.04227	0.03147	-0.0179	0.0337	1	19.46771
7	0.8757	0.05261	0.04283	-0.013	0.0254	1	16.64512
7.5	0.8897	0.05785	0.04868	-0.0096	0.0241	1	15.37943
8	0.8891	0.06388	0.05523	-0.0061	0.0237	1	13.91828
8.5	0.8699	0.07023	0.062	-0.0024	0.0237	1	12.38644
9	0.84	0.07811	0.0702	-0.0018	0.0243	1	10.75406
9.5	0.8048	0.08847	0.08081	-0.0056	0.0251	1	9.096869
10	0.7724	0.10142	0.09389	-0.013	0.0259	1	7.615855
10.5	0.7545	0.1147	0.10717	-0.0193	0.0275	1	6.57803
11.5	0.736	0.14582	0.13836	-0.0383	0.0387	1	5.047319
12	0.74	0.1556	0.14808	-0.0427	0.041	1	4.755784
12.5	0.746	0.16489	0.15731	-0.0469	0.0419	1	4.524228
13	0.7568	0.17356	0.16595	-0.05	0.0447	1	4.360452
13.5	0.7714	0.18218	0.17455	-0.052	0.0469	1	4.234274

15	0.7969	0.20918	0.20156	-0.0681	0.0787	1	3.809638

- Airfoil 4

Table AVIII-106: Aerodynamic performance of Airfoil 4 of the H-146 coated blade at 0°

alpha	CL	CD	CDp	CM	Top_Xtr	Bot_Xtr	CL/CD
------	--------	---------	---------	--------	--------	--------	--------
-5	-0.3558	0.03251	0.02243	-0.0434	1	0.0784	-10.9443
-4.5	-0.3199	0.02966	0.01937	-0.0412	1	0.0819	-10.7856
-4	-0.2854	0.02766	0.01745	-0.0389	1	0.0913	-10.3181
-3.5	-0.2496	0.02655	0.01612	-0.0362	1	0.0992	-9.40113
-3	-0.2142	0.02527	0.01476	-0.0335	1	0.1066	-8.47645
-2.5	-0.1738	0.02408	0.01352	-0.0327	1	0.1294	-7.21761
-2	-0.1725	0.02313	0.01562	-0.0191	1	0.7295	-7.45785
-1.5	-0.1977	0.02264	0.01547	0.0009	1	0.8703	-8.73233
-1	-0.1093	0.02276	0.01518	-0.0058	1	1	-4.80228
-0.5	-0.0382	0.0238	0.01573	-0.0148	0.9826	1	-1.60504
0	0.0394	0.0252	0.01674	-0.024	0.9641	1	1.563492
0.5	0.1146	0.02678	0.01809	-0.0321	0.9455	1	4.279313
1	0.1901	0.02863	0.01978	-0.0396	0.9284	1	6.639888
1.5	0.2561	0.03044	0.02175	-0.0451	0.9105	1	8.413272
2	0.3075	0.03233	0.0232	-0.0479	0.8953	1	9.51129
2.5	0.3689	0.03458	0.02566	-0.0521	0.8786	1	10.66802
3	0.4313	0.03681	0.02826	-0.0558	0.8575	1	11.71692
3.5	0.493	0.03921	0.03125	-0.0591	0.8356	1	12.57332
4.5	0.7212	0.03174	0.02114	-0.0342	0.0838	1	22.72212
5	0.7981	0.03722	0.02674	-0.0346	0.0778	1	21.44277
5.5	0.8532	0.04441	0.03436	-0.0337	0.0754	1	19.21189
6	0.8883	0.05186	0.04252	-0.0312	0.0732	1	17.12881
6.5	0.9133	0.05808	0.04953	-0.0279	0.0718	1	15.72486
7	0.9273	0.06586	0.05793	-0.0252	0.0721	1	14.07987
9	0.7135	0.13064	0.12443	-0.066	0.3189	1	5.461574
9.5	0.7205	0.13895	0.13272	-0.0674	0.3004	1	5.185318
10	0.7319	0.14718	0.14086	-0.0684	0.2782	1	4.972822
10.5	0.7464	0.15559	0.14919	-0.0694	0.2567	1	4.797223
11	0.7645	0.16455	0.15809	-0.07	0.2353	1	4.646004
11.5	0.7806	0.17293	0.1664	-0.0708	0.2124	1	4.513965
12	0.7927	0.18074	0.17413	-0.0721	0.1888	1	4.385858
12.5	0.8081	0.18895	0.18228	-0.073	0.1657	1	4.276793
13.5	0.8082	0.19949	0.19263	-0.0818	0.1348	1	4.051331
14	0.8304	0.20906	0.20226	-0.0825	0.1176	1	3.972065
14.5	0.8362	0.21356	0.20671	-0.087	0.1032	1	3.915527

15	0.8586	0.2251	0.2182	-0.0881	0.095	1	3.814305

- Airfoil 5

Table AVIII-107: Aerodynamic performance of Airfoil 5 of the H-146 coated blade at 0°

alpha	CL	CD	CDp	CM	Top_Xtr	Bot_Xtr	CL/CD
------	--------	---------	---------	--------	--------	--------	--------
-5	-0.3693	0.0286	0.01743	-0.0361	1	0.1429	-12.9126
-4.5	-0.3319	0.0266	0.01529	-0.0332	1	0.1448	-12.4774
-4	-0.2964	0.0252	0.01386	-0.03	1	0.1509	-11.7619
-3.5	-0.2614	0.02407	0.01266	-0.0271	1	0.1631	-10.86
-3	-0.2229	0.02232	0.01121	-0.0261	1	0.2165	-9.98656
-2.5	-0.2356	0.0222	0.01369	-0.0088	1	0.7473	-10.6126
-2	-0.2384	0.02162	0.01331	0.0055	1	0.8683	-11.0268
-1.5	-0.1171	0.02248	0.01394	-0.0073	1	1	-5.20907
-1	-0.0973	0.02244	0.01361	-0.0073	0.9965	1	-4.33601
-0.5	-0.0138	0.02403	0.0148	-0.0175	0.9779	1	-0.57428
0	0.0599	0.02553	0.01604	-0.0251	0.9595	1	2.346259
0.5	0.1323	0.0273	0.01769	-0.0319	0.9442	1	4.846154
1	0.1884	0.02885	0.01919	-0.0355	0.9285	1	6.530329
1.5	0.2459	0.03063	0.02096	-0.0391	0.9114	1	8.028077
2	0.3062	0.03266	0.02306	-0.0429	0.8952	1	9.375383
2.5	0.3741	0.03491	0.02553	-0.0475	0.8782	1	10.71613
3	0.4146	0.03689	0.0277	-0.048	0.8598	1	11.23882
3.5	0.4738	0.03911	0.03026	-0.0507	0.8361	1	12.11455
4	0.5482	0.04057	0.03241	-0.0533	0.7933	1	13.51245
4.5	0.7088	0.02982	0.019	-0.0281	0.1104	1	23.76928
5	0.7777	0.03471	0.02386	-0.0273	0.079	1	22.40565
5.5	0.8295	0.04021	0.02965	-0.0261	0.0624	1	20.6292
6	0.8678	0.04527	0.03514	-0.0242	0.0507	1	19.16943
7.5	0.9161	0.0667	0.05884	-0.014	0.0525	1	13.73463
8	0.8855	0.07497	0.06776	-0.0104	0.0564	1	11.81139
8.5	0.8456	0.08357	0.07665	-0.01	0.0589	1	10.11846
9	0.8077	0.09493	0.08814	-0.0154	0.062	1	8.508375
9.5	0.7877	0.10763	0.10083	-0.0216	0.0659	1	7.318591
10	0.7913	0.12445	0.1177	-0.0271	0.0909	1	6.358377
11	0.755	0.16093	0.15403	-0.0557	0.2039	1	4.691481
11.5	0.7688	0.16931	0.16245	-0.0564	0.1815	1	4.540783
12	0.7983	0.18016	0.17327	-0.055	0.1595	1	4.431061
12.5	0.7648	0.18205	0.17499	-0.0644	0.1536	1	4.201044
13.5	0.7883	0.19802	0.19085	-0.0698	0.1328	1	3.980911
14	0.7951	0.20404	0.19682	-0.0738	0.1231	1	3.896785

14.5	0.8433	0.22184	0.21472	-0.0706	0.1146	1	3.801388

- Airfoil 6

Table AVIII-108: Aerodynamic performance of Airfoil 6 of the H-146 coated blade at 0°

alpha	CL	CD	CDp	CM	Top_Xtr	Bot_Xtr	CL/CD
------	--------	---------	---------	--------	--------	--------	--------
-5	-0.3676	0.05621	0.05064	-0.026	1	0.2122	-6.53976
-4.5	-0.3147	0.04198	0.03497	-0.0354	1	0.1453	-7.49643
-4	-0.271	0.03562	0.02768	-0.0355	1	0.1427	-7.60809
-3.5	-0.2296	0.03175	0.02326	-0.0341	1	0.1646	-7.2315
-3	-0.1885	0.02924	0.02037	-0.0322	1	0.189	-6.44665
-2.5	-0.145	0.02754	0.01835	-0.0303	1	0.1973	-5.26507
-2	-0.1028	0.02658	0.01715	-0.0283	1	0.2115	-3.86757
-1.5	-0.0571	0.02598	0.01675	-0.0273	1	0.2477	-2.19784
-1	-0.024	0.02519	0.018	-0.0227	1	0.6431	-0.95276
-0.5	0.0485	0.02524	0.01869	-0.0263	0.9893	1	1.921553
0	0.1299	0.02755	0.0206	-0.0336	0.9661	1	4.715064
1	0.4708	0.02438	0.01386	-0.0399	0.1448	1	19.31091
1.5	0.5207	0.02654	0.01582	-0.0374	0.1251	1	19.61944
2	0.5862	0.02945	0.01853	-0.0364	0.1146	1	19.90492
2.5	0.65	0.03277	0.02192	-0.0352	0.1125	1	19.83522
3	0.7056	0.0368	0.02623	-0.0334	0.1133	1	19.17391
3.5	0.7536	0.04172	0.03154	-0.0312	0.1159	1	18.06328
4	0.7926	0.04682	0.03714	-0.0285	0.1163	1	16.92866
4.25	0.8089	0.04928	0.03988	-0.0269	0.1154	1	16.41437
4.5	0.8229	0.05181	0.0427	-0.0253	0.1144	1	15.88303
4.75	0.8346	0.05467	0.04584	-0.0237	0.1139	1	15.26614
5	0.8441	0.05787	0.04929	-0.0222	0.1142	1	14.58614
5.25	0.8519	0.06152	0.05314	-0.0209	0.1156	1	13.84753
5.5	0.8608	0.06622	0.058	-0.0201	0.118	1	12.99909
6	0.7901	0.07969	0.07275	-0.0202	0.1651	1	9.914669
6.25	0.8208	0.08548	0.07842	-0.0203	0.1711	1	9.602246
7	0.626	0.12262	0.11576	-0.0591	0.3612	1	5.105203
7.25	0.6133	0.12492	0.11797	-0.0595	0.3462	1	4.909542
7.5	0.6358	0.12888	0.1219	-0.0587	0.3355	1	4.933271
7.75	0.633	0.13225	0.12518	-0.0592	0.3245	1	4.786389
8	0.642	0.13508	0.12797	-0.0589	0.3109	1	4.752739
8.5	0.6474	0.14158	0.13437	-0.0597	0.2894	1	4.57268
9	0.6637	0.14885	0.14155	-0.0599	0.269	1	4.458851
9.5	0.6878	0.1567	0.14933	-0.0593	0.2464	1	4.389279
10	0.729	0.16689	0.15954	-0.057	0.2235	1	4.368147

10.5	0.7032	0.16813	0.16066	-0.0621	0.2072	1	4.182478
11	0.732	0.17836	0.17083	-0.062	0.1969	1	4.104059
11.5	0.7287	0.18154	0.17394	-0.0653	0.1803	1	4.013991
12	0.7538	0.19163	0.18397	-0.0657	0.1701	1	3.933622
12.5	0.7527	0.19434	0.18661	-0.0696	0.155	1	3.873109
13	0.7924	0.20817	0.20042	-0.0679	0.1445	1	3.806504
13.5	0.7781	0.20724	0.1994	-0.0747	0.1357	1	3.754584
14	0.8003	0.2142	0.20635	-0.0754	0.1248	1	3.736228
14.5	0.8422	0.23241	0.22469	-0.0735	0.1192	1	3.623768
15	0.8263	0.22826	0.22042	-0.0815	0.1157	1	3.619995

- 5°
- Airfoil 1

Table AVIII-109: Aerodynamic performance of Airfoil 1 of the H-146 coated blade at 5°

alpha	CL	CD	CDp	CM	Top_Xtr	Bot_Xtr	CL/CD
------	--------	----------	----------	--------	--------	--------	--------
-5	-0.4223	0.02789	0.01669	-0.0279	1	0.1316	-15.1416
-4.5	-0.3833	0.02565	0.01438	-0.0246	1	0.1345	-14.9435
-4	-0.3479	0.02412	0.01268	-0.0213	1	0.1437	-14.4237
-3.5	-0.3109	0.02256	0.01112	-0.019	1	0.1717	-13.781
-2.5	-0.3142	0.0208	0.0125	0.0103	1	0.8563	-15.1058
-2	-0.0886	0.02242	0.01335	-0.0165	1	1	-3.95183
-1.5	-0.1115	0.02172	0.01259	-0.0088	1	1	-5.13352
-1	-0.1173	0.02118	0.01189	-0.0036	1	1	-5.53824
-0.5	-0.0895	0.02151	0.01182	-0.0031	1	1	-4.16086
0	-0.0524	0.02229	0.01235	-0.0039	1	1	-2.35083
0.5	0.0064	0.02384	0.01369	-0.0085	0.992	1	0.268456
1	0.0817	0.02581	0.01556	-0.0159	0.9722	1	3.16544
1.5	0.153	0.02784	0.01753	-0.0222	0.9514	1	5.49569
2	0.2218	0.02992	0.01963	-0.0278	0.9295	1	7.413102
2.5	0.2874	0.03204	0.02185	-0.0325	0.9068	1	8.970037
3	0.3486	0.03419	0.02422	-0.0362	0.8829	1	10.19596
3.5	0.41	0.03632	0.0266	-0.0395	0.8535	1	11.28855
4	0.4961	0.03844	0.02931	-0.0452	0.8186	1	12.90583
5.5	0.7613	0.02834	0.01749	-0.0218	0.185	1	26.86309
6	0.8296	0.03215	0.02131	-0.0222	0.1604	1	25.80404
6.5	0.8921	0.03703	0.02644	-0.0223	0.1503	1	24.09128
7	0.9357	0.04259	0.03273	-0.0207	0.1427	1	21.96995
7.5	0.9687	0.04932	0.04051	-0.0182	0.1426	1	19.64112
8	0.9893	0.05765	0.04959	-0.0158	0.1452	1	17.16045
8.5	0.9972	0.06693	0.05947	-0.0135	0.1466	1	14.89915

9	0.9237	0.07622	0.06973	-0.0102	0.16	1	12.11887
9.5	0.8612	0.08985	0.08329	-0.0145	0.1747	1	9.584864
10.5	0.6973	0.13632	0.1292	-0.0548	0.3421	1	5.11517
11	0.7294	0.14728	0.14024	-0.0558	0.3301	1	4.952471
11.5	0.7498	0.1562	0.1492	-0.0563	0.3075	1	4.800256
12	0.7647	0.16444	0.15747	-0.057	0.2845	1	4.650328
12.5	0.7693	0.17033	0.16338	-0.0585	0.2639	1	4.516527
13	0.7535	0.17422	0.16717	-0.0622	0.247	1	4.324991
13.5	0.7635	0.18221	0.17516	-0.0645	0.2325	1	4.19022
14	0.7823	0.1912	0.18433	-0.0658	0.2129	1	4.091527
14.5	0.8215	0.20654	0.1998	-0.0654	0.1927	1	3.977438
15	0.7979	0.20448	0.19761	-0.0719	0.1799	1	3.902093

- Airfoil 2

Table AVIII-110: Aerodynamic performance of Airfoil 2 of the H-146 coated blade at 5°

alpha	CL	CD	CDp	CM	Top_Xtr	Bot_Xtr	CL/CD
------	--------	---------	---------	--------	--------	--------	--------
-4.5	-0.3636	0.02579	0.01504	-0.0339	1	0.1365	-14.0985
-4	-0.3256	0.02417	0.01328	-0.0307	1	0.1529	-13.4712
-3.5	-0.2862	0.02165	0.01115	-0.0292	1	0.2178	-13.2194
-2.5	-0.2982	0.02121	0.01343	0.0036	1	0.8486	-14.0594
-2	-0.0848	0.02221	0.01358	-0.0195	1	1	-3.8181
-1.5	-0.1109	0.02149	0.01282	-0.0119	1	1	-5.16054
-1	-0.1178	0.02086	0.01198	-0.0072	1	1	-5.64717
-0.5	-0.0833	0.02117	0.01196	-0.0086	1	1	-3.93481
0	-0.0395	0.02198	0.01246	-0.011	1	1	-1.79709
0.5	0.0266	0.02355	0.01377	-0.0171	0.9897	1	1.129512
1	0.1065	0.02557	0.01563	-0.0254	0.969	1	4.165037
1.5	0.1807	0.02755	0.01753	-0.0322	0.9477	1	6.558984
2	0.2523	0.02953	0.01953	-0.0382	0.9256	1	8.543854
2.5	0.3198	0.03156	0.02166	-0.0431	0.9023	1	10.13308
3	0.3818	0.0337	0.02415	-0.0469	0.8789	1	11.32938
3.5	0.4485	0.03594	0.02672	-0.051	0.8526	1	12.47913
4	0.5168	0.03824	0.02954	-0.0546	0.8231	1	13.51464
4.5	0.7029	0.02165	0.01246	-0.0348	0.3035	1	32.46651
5	0.7213	0.02657	0.01593	-0.0296	0.1814	1	27.14716
5.5	0.7753	0.03041	0.0194	-0.0284	0.1425	1	25.4949
6	0.8464	0.03461	0.02411	-0.0284	0.1302	1	24.45536
6.5	0.9049	0.04031	0.03043	-0.0276	0.127	1	22.44852
7	0.9446	0.04739	0.03867	-0.025	0.1311	1	19.93248
7.5	0.9659	0.0552	0.04742	-0.022	0.1304	1	17.49819

8	0.9713	0.06371	0.05664	-0.0191	0.1273	1	15.24564
8.5	0.948	0.07476	0.06834	-0.0176	0.138	1	12.68058
12	0.7608	0.16598	0.1594	-0.0689	0.254	1	4.583685
13	0.7806	0.18189	0.17523	-0.0723	0.2061	1	4.291605
14	0.8159	0.20037	0.19364	-0.0748	0.1644	1	4.071967
15	0.8377	0.21642	0.20959	-0.081	0.1414	1	3.870714

- Airfoil 3

Table AVIII-111: Aerodynamic performance of Airfoil 3 of the H-146 coated blade at 5°

alpha	CL	CD	CDp	CM	Top_Xtr	Bot_Xtr	CL/CD
------	--------	---------	---------	--------	--------	--------	--------
-3.5	-0.3086	0.0245	0.01326	-0.0213	1	0.1396	-12.5959
-3	-0.2733	0.02318	0.01209	-0.0194	1	0.1678	-11.7903
-2.5	-0.2559	0.02075	0.01246	-0.0116	1	0.6717	-12.3325
-2	-0.2727	0.02127	0.0133	0.0082	1	0.8517	-12.8209
-1.5	-0.0984	0.02253	0.01384	-0.0109	1	1	-4.36751
-1	-0.1184	0.02176	0.01295	-0.0043	1	1	-5.44118
-0.5	-0.0962	0.02195	0.01281	-0.0037	1	1	-4.38269
0	-0.0558	0.02278	0.01332	-0.0055	0.9986	1	-2.44952
0.5	0.0281	0.02484	0.01509	-0.0149	0.979	1	1.13124
1	0.0973	0.02661	0.01669	-0.0211	0.961	1	3.65652
1.5	0.1634	0.02844	0.01844	-0.0264	0.942	1	5.745429
2	0.2262	0.03036	0.02052	-0.0308	0.9227	1	7.450593
2.5	0.288	0.03241	0.02273	-0.0349	0.9026	1	8.886146
3	0.3483	0.03458	0.02516	-0.0384	0.8811	1	10.0723
3.5	0.4055	0.03683	0.02777	-0.0413	0.8572	1	11.01005
4	0.4619	0.03915	0.03061	-0.0436	0.8298	1	11.79821
5	0.6995	0.03007	0.01946	-0.0222	0.1108	1	23.26239
6	0.8415	0.04352	0.03388	-0.0213	0.0996	1	19.33594
6.5	0.8731	0.0506	0.04192	-0.0174	0.0974	1	17.25494
7	0.8875	0.05763	0.0498	-0.0132	0.0932	1	15.39997
7.25	0.8924	0.0624	0.05487	-0.0117	0.0973	1	14.30128
7.5	0.9091	0.06811	0.0608	-0.011	0.1047	1	13.34753
7.75	0.8793	0.07113	0.06449	-0.0082	0.1126	1	12.36187
8	0.8687	0.07651	0.07004	-0.0075	0.1197	1	11.35407
8.5	0.8154	0.08569	0.07953	-0.0081	0.1332	1	9.515696
8.75	0.7833	0.09235	0.08619	-0.0126	0.1371	1	8.481862
10	0.6783	0.13651	0.13002	-0.0519	0.3174	1	4.968867
11	0.7018	0.15226	0.14562	-0.0523	0.2553	1	4.609221
11.5	0.7126	0.15949	0.15279	-0.0529	0.2251	1	4.467992
12	0.7195	0.16732	0.16053	-0.0548	0.2053	1	4.300143

12.5	0.7342	0.17611	0.16926	-0.0562	0.1888	1	4.168985
13	0.7735	0.19008	0.18332	-0.0546	0.1702	1	4.069339
13.5	0.7497	0.19037	0.18339	-0.0617	0.1583	1	3.938121
14	0.7828	0.20437	0.19746	-0.0614	0.1468	1	3.830308
14.5	0.7723	0.20547	0.19845	-0.0676	0.1361	1	3.7587
15	0.8161	0.22447	0.21749	-0.0655	0.1248	1	3.635675

- Airfoil 4

Table AVIII-112: Aerodynamic performance of Airfoil 4 of the H-146 coated blade at 5°

alpha	CL	CD	CDp	CM	Top_Xtr	Bot_Xtr	CL/CD
------	--------	---------	---------	--------	--------	--------	--------
-5	-0.4024	0.02577	0.01387	-0.0312	1	0.0647	-15.6151
-4	-0.3343	0.02403	0.01156	-0.0268	1	0.072	-13.9118
-2	-0.309	0.02232	0.01392	0.0172	1	0.8937	-13.8441
0	-0.0586	0.02379	0.01434	-0.0075	0.9931	1	-2.46322
1	0.0968	0.02733	0.01747	-0.0251	0.9531	1	3.541895
2	0.2298	0.03105	0.02115	-0.0366	0.9163	1	7.400966
6	0.8247	0.04936	0.04006	-0.0244	0.0506	1	16.70786
7	0.8686	0.06293	0.0555	-0.0165	0.063	1	13.80264
8	0.8467	0.07966	0.07331	-0.0109	0.0828	1	10.62892
12	0.7727	0.17694	0.17046	-0.0543	0.1652	1	4.367017
13	0.7792	0.19229	0.18563	-0.0613	0.1419	1	4.052213
14	0.8101	0.21202	0.20525	-0.0654	0.12	1	3.820866
15	0.8	0.21719	0.21022	-0.0785	0.1061	1	3.683411

- Airfoil 5

- Table AVIII-113: Aerodynamic performance of Airfoil 5 of the H-146 coated blade at 5°

alpha	CL	CD	CDp	CM	Top_Xtr	Bot_Xtr	CL/CD
------	--------	---------	---------	--------	--------	--------	--------
-5	-0.4008	0.02536	0.01403	-0.0323	1	0.15	-15.8044
-4.5	-0.3668	0.0245	0.0132	-0.0303	1	0.1805	-14.9714
-4	-0.3293	0.02348	0.01216	-0.0281	1	0.1987	-14.0247
-3.5	-0.2936	0.02248	0.0113	-0.0261	1	0.229	-13.0605
-3	-0.2659	0.02094	0.01172	-0.0224	1	0.5169	-12.6982
-2.5	-0.2619	0.02213	0.01325	-0.0108	1	0.7003	-11.8346
-2	-0.2513	0.02216	0.01345	-0.0012	1	0.7957	-11.3403
-1.5	-0.2081	0.02189	0.01353	0.0023	1	0.9144	-9.50662
-1	-0.1287	0.02242	0.01377	-0.0077	1	1	-5.74041
-0.5	-0.066	0.02358	0.01448	-0.0147	0.9882	1	-2.79898
0	0.018	0.02541	0.01593	-0.0244	0.9672	1	0.708383

0.5	0.0977	0.02729	0.01755	-0.0324	0.9464	1	3.580066
1	0.1597	0.02893	0.01903	-0.0369	0.9271	1	5.520221
1.5	0.215	0.03072	0.02073	-0.04	0.9101	1	6.998698
2	0.2753	0.03258	0.02262	-0.0434	0.8896	1	8.449969
2.5	0.3335	0.03459	0.02468	-0.0465	0.8711	1	9.641515
3	0.392	0.03655	0.02678	-0.0491	0.849	1	10.72503
4	0.5019	0.04048	0.03137	-0.0523	0.7957	1	12.39872
4.25	0.545	0.04107	0.03221	-0.0542	0.777	1	13.27003
4.5	0.5898	0.04108	0.03259	-0.0553	0.7518	1	14.35735
4.75	0.706	0.03595	0.02828	-0.0585	0.7036	1	19.63839
5	0.8072	0.0235	0.01598	-0.0467	0.5518	1	34.34894
5.25	0.8005	0.02318	0.01454	-0.0378	0.3314	1	34.53408
5.5	0.7826	0.02701	0.01648	-0.0322	0.1352	1	28.97445
5.75	0.7799	0.02997	0.01891	-0.0284	0.0895	1	26.02269
6	0.788	0.0319	0.02075	-0.0257	0.0698	1	24.70219
6.25	0.7988	0.03386	0.02267	-0.0234	0.061	1	23.59126
6.5	0.8184	0.03529	0.02428	-0.0219	0.0527	1	23.19071
6.75	0.8417	0.03694	0.02602	-0.0208	0.048	1	22.7856
7	0.8736	0.03922	0.02839	-0.0206	0.0448	1	22.27435
7.25	0.9101	0.04261	0.03202	-0.0212	0.043	1	21.35884
7.5	0.9375	0.04676	0.0365	-0.021	0.0421	1	20.04919
7.75	0.9551	0.05057	0.04067	-0.0199	0.0419	1	18.88669
8	0.9677	0.05397	0.04441	-0.0184	0.042	1	17.93033
8.25	0.9766	0.05715	0.04792	-0.0166	0.0423	1	17.08836
8.5	0.9811	0.06043	0.05155	-0.0147	0.0424	1	16.23531
8.75	0.9826	0.06348	0.05491	-0.0126	0.0427	1	15.47889
9	0.9797	0.0666	0.05833	-0.0105	0.043	1	14.71021
9.25	0.9708	0.06982	0.0618	-0.0081	0.0431	1	13.90433
9.5	0.9585	0.07287	0.06508	-0.0059	0.0433	1	13.15356
9.75	0.9365	0.07626	0.06884	-0.0042	0.0454	1	12.28036
10	0.913	0.0809	0.07371	-0.0044	0.0463	1	11.28554
10.25	0.8755	0.08785	0.08091	-0.0075	0.048	1	9.965851
10.5	0.8438	0.09577	0.08897	-0.0125	0.0492	1	8.810692
10.75	0.8155	0.10518	0.09842	-0.0189	0.0509	1	7.753375
11	0.7965	0.11452	0.10776	-0.0248	0.053	1	6.955117
11.25	0.7859	0.12301	0.11621	-0.0295	0.0551	1	6.388911
11.5	0.781	0.12977	0.12293	-0.0327	0.0569	1	6.01834
11.75	0.7793	0.13578	0.1289	-0.0351	0.0588	1	5.739431
12	0.7808	0.14117	0.13427	-0.0365	0.0607	1	5.53092

- Airfoil 6

Table AVIII-114: Aerodynamic performance of Airfoil 6 of the H-146 coated blade at 5°

alpha	CL	CD	CDp	CM	Top_Xtr	Bot_Xtr	CL/CD
------	--------	---------	---------	--------	--------	--------	--------
-4	-0.3535	0.04037	0.03273	-0.0293	1	0.1483	-8.7565
-3.5	-0.3136	0.03587	0.02745	-0.0281	1	0.1325	-8.74268
-2.5	-0.232	0.03135	0.02185	-0.024	1	0.1186	-7.40032
-2	-0.1922	0.02978	0.02002	-0.0216	1	0.116	-6.454
-1.5	-0.1261	0.02897	0.01894	-0.0235	0.9888	0.119	-4.35278
-1	-0.0463	0.02845	0.01825	-0.0285	0.9705	0.1405	-1.62742
0	0.1152	0.02767	0.01997	-0.0358	0.9305	1	4.163354
0.5	0.1837	0.02929	0.02117	-0.0405	0.9099	1	6.271765
1	0.2324	0.03094	0.02258	-0.042	0.8915	1	7.511312
1.5	0.2848	0.03281	0.02423	-0.0438	0.8723	1	8.68028
2	0.3438	0.03479	0.02625	-0.0461	0.8496	1	9.88215
2.5	0.398	0.03691	0.02853	-0.0477	0.8272	1	10.78299
3	0.4753	0.03847	0.03048	-0.0508	0.7924	1	12.35508
3.5	0.6287	0.02625	0.01552	-0.0281	0.1234	1	23.95048
4	0.6623	0.03035	0.01951	-0.0233	0.0947	1	21.82208
4.5	0.7261	0.0338	0.02316	-0.022	0.0789	1	21.48225
5.5	0.8117	0.04246	0.03205	-0.0188	0.0457	1	19.11682
6	0.8458	0.04627	0.03648	-0.0156	0.038	1	18.27966
6.5	0.8702	0.05009	0.04061	-0.0127	0.0312	1	17.37273
7.5	0.8773	0.06111	0.05243	-0.0057	0.0236	1	14.35608
8	0.861	0.06677	0.05854	-0.0016	0.0225	1	12.89501
8.5	0.8314	0.07439	0.06654	-0.0005	0.0225	1	11.17623
9	0.7949	0.08473	0.07717	-0.004	0.0233	1	9.381565
9.5	0.7603	0.09761	0.09021	-0.0109	0.0245	1	7.789161
10	0.712	0.12416	0.11703	-0.0277	0.038	1	5.734536
11	0.7078	0.14676	0.13943	-0.038	0.0416	1	4.82284
12	0.7191	0.16579	0.15832	-0.046	0.0433	1	4.337415
13	0.7366	0.18341	0.17582	-0.0538	0.0435	1	4.016139
14	0.757	0.19941	0.19182	-0.0618	0.0427	1	3.796199
15	0.7861	0.21546	0.20781	-0.0679	0.0451	1	3.648473

- 10˚
- Airfoil 1

Table AVIII-115: Aerodynamic performance of Airfoil 1 of the H-146 coated blade at 10°

alpha	CL	CD	CDp	CM	Top_Xtr	Bot_Xtr	CL/CD
------	--------	---------	---------	--------	--------	--------	--------
-5	-0.4461	0.02692	0.01702	-0.029	1	0.1736	-16.5713
-4	-0.3714	0.02137	0.01192	-0.0222	1	0.2931	-17.3795
-3	-0.3705	0.02165	0.01419	0.0082	1	0.8062	-17.1132
-2	-0.0747	0.02268	0.01353	-0.0203	1	1	-3.29365
-1.5	-0.0973	0.02212	0.01292	-0.0127	1	1	-4.39873
-1	-0.1173	0.02138	0.01208	-0.0054	1	1	-5.48644
-0.5	-0.1039	0.02132	0.01175	-0.0029	1	1	-4.87336
0	-0.0699	0.02192	0.01206	-0.0033	1	1	-3.18887
0.5	-0.0314	0.02285	0.01268	-0.0043	1	1	-1.37418
1	0.0446	0.02483	0.01447	-0.0121	0.983	1	1.796214
1.5	0.1222	0.02695	0.01649	-0.0198	0.9626	1	4.534323
2	0.1945	0.02898	0.01852	-0.0261	0.9412	1	6.711525
2.5	0.2616	0.03102	0.02061	-0.0313	0.9195	1	8.433269
3	0.326	0.03311	0.02283	-0.0357	0.8966	1	9.845968
3.5	0.3973	0.0354	0.02546	-0.0407	0.8714	1	11.22316
4	0.4439	0.03734	0.02765	-0.0416	0.8405	1	11.88806
5	0.7369	0.02214	0.01425	-0.0361	0.566	1	33.28365
5.5	0.7373	0.02581	0.01492	-0.0241	0.2234	1	28.56645
6	0.7939	0.02916	0.01801	-0.0232	0.1902	1	27.22565
6.5	0.8631	0.03258	0.02167	-0.024	0.1773	1	26.49171
7	0.9149	0.03643	0.02614	-0.0234	0.1606	1	25.11392
7.5	0.9642	0.04162	0.03178	-0.0226	0.1515	1	23.16675
8	0.9986	0.04893	0.03999	-0.0204	0.1483	1	20.40875
8.5	1.0088	0.05535	0.04758	-0.0162	0.1419	1	18.22584
9	1.0218	0.06264	0.05516	-0.0137	0.1251	1	16.31226
9.5	1.002	0.07161	0.06488	-0.01	0.1244	1	13.99246
10	0.9646	0.08046	0.07411	-0.0073	0.1245	1	11.98857
10.5	0.9245	0.09098	0.08476	-0.0079	0.1257	1	10.16157
11.5	0.7553	0.15048	0.14354	-0.0563	0.3295	1	5.019272
12.5	0.7431	0.16126	0.15432	-0.0599	0.2904	1	4.608086
13	0.7472	0.16879	0.16207	-0.062	0.2724	1	4.426803
13.5	0.7897	0.18136	0.17477	-0.0586	0.2156	1	4.354323
14	0.806	0.19186	0.18526	-0.0595	0.1935	1	4.20098
14.5	0.7822	0.1924	0.18566	-0.0658	0.1802	1	4.065489
15	0.7981	0.20253	0.19576	-0.0678	0.1685	1	3.940651

- Airfoil 2

Table AVIII-116: Aerodynamic performance of Airfoil 2 of the H-146 coated blade at 10°

alpha	CL	CD	CDp	CM	Top_Xtr	Bot_Xtr	CL/CD
------	--------	---------	---------	--------	--------	--------	--------
-5	-0.3595	0.02791	0.01735	-0.0357	1	0.0954	-12.8807
-4.5	-0.3225	0.02496	0.01446	-0.0317	1	0.1173	-12.9207
-3.5	-0.3249	0.02211	0.015	-0.0011	1	0.7948	-14.6947
-2.5	-0.0867	0.02249	0.01375	-0.0184	1	1	-3.85505
-2	-0.1097	0.02176	0.01296	-0.0112	1	1	-5.04136
-1.5	-0.1171	0.02107	0.01211	-0.0064	1	1	-5.55766
-1	-0.0829	0.02133	0.01203	-0.0078	1	1	-3.88654
-0.5	-0.0382	0.02212	0.01245	-0.0105	1	1	-1.72694
0	0.0319	0.02374	0.01379	-0.0175	0.9881	1	1.343724
0.5	0.1084	0.0257	0.01552	-0.0253	0.9703	1	4.217899
1	0.181	0.02768	0.01741	-0.032	0.9506	1	6.539017
1.5	0.2487	0.02969	0.01941	-0.0375	0.9299	1	8.376558
2	0.3136	0.03177	0.02161	-0.0422	0.908	1	9.870947
2.5	0.3755	0.03396	0.02394	-0.0462	0.8851	1	11.05713
3	0.4379	0.03622	0.02644	-0.0499	0.8594	1	12.09001
3.5	0.5114	0.03851	0.02923	-0.0545	0.8296	1	13.27967
4.5	0.7349	0.02543	0.01449	-0.0329	0.1987	1	28.89894
5.5	0.8431	0.03276	0.02143	-0.0306	0.1357	1	25.73565
6	0.9071	0.03714	0.02633	-0.0305	0.1304	1	24.4238
6.5	0.9581	0.04261	0.03257	-0.0295	0.1306	1	22.48533
7	0.9964	0.04941	0.04019	-0.0279	0.1341	1	20.16596
7.5	1.0277	0.05864	0.05011	-0.0267	0.1389	1	17.52558
8	1.0104	0.06616	0.0591	-0.0229	0.1514	1	15.27207
8.5	1.0054	0.07696	0.07037	-0.0224	0.1646	1	13.06393
9	0.877	0.09274	0.08621	-0.0292	0.1736	1	9.456545
10	0.7393	0.13849	0.13143	-0.0678	0.3399	1	5.338292
10.5	0.7792	0.14928	0.14242	-0.0686	0.3285	1	5.219721
11.5	0.7701	0.16158	0.15465	-0.0731	0.2912	1	4.76606
12	0.7885	0.17046	0.16358	-0.0746	0.2749	1	4.625719
12.5	0.8026	0.17805	0.17121	-0.076	0.252	1	4.507723
13	0.8523	0.1933	0.18665	-0.0748	0.2318	1	4.409208
13.5	0.8206	0.19163	0.18484	-0.0811	0.217	1	4.282211
14	0.8438	0.20285	0.1962	-0.0826	0.2065	1	4.159724
14.5	0.8497	0.2077	0.20107	-0.0861	0.1902	1	4.090997
15	0.8617	0.21675	0.21014	-0.0894	0.1816	1	3.975548

- Airfoil 3

Table AVIII-117: Aerodynamic performance of Airfoil 3 of the H-146 coated blade at 10°

alpha	CL	CD	CDp	CM	Top_Xtr	Bot_Xtr	CL/CD
------	--------	---------	---------	--------	--------	--------	--------
-5	-0.4063	0.02262	0.01301	-0.0291	1	0.2538	-17.962
-4.5	-0.397	0.02082	0.0137	-0.0178	1	0.6006	-19.0682
-4	-0.3911	0.02258	0.01528	-0.0034	1	0.7175	-17.3206
-3.5	-0.3821	0.02276	0.01521	0.0081	1	0.7937	-16.7882
-3	-0.3677	0.02211	0.01434	0.0206	1	0.8942	-16.6305
-2.5	-0.1323	0.02339	0.01441	-0.0106	1	0.9793	-5.65626
-2	-0.0774	0.02302	0.01364	-0.0168	1	1	-3.36229
-1.5	-0.1064	0.02231	0.01294	-0.009	1	1	-4.76916
-1	-0.1158	0.02174	0.01221	-0.0041	1	1	-5.32659
-0.5	-0.0863	0.02217	0.01235	-0.0047	1	1	-3.89265
0	-0.0236	0.02362	0.01354	-0.0107	0.9899	1	-0.99915
0.5	0.0539	0.02554	0.01525	-0.0189	0.9698	1	2.110415
1	0.1263	0.02749	0.01706	-0.0258	0.9507	1	4.594398
1.5	0.1942	0.02939	0.01892	-0.0314	0.932	1	6.60769
2	0.2616	0.03135	0.02095	-0.0366	0.9128	1	8.344498
2.5	0.3246	0.0333	0.02303	-0.0408	0.8925	1	9.747748
3	0.3832	0.0353	0.02523	-0.044	0.8706	1	10.85552
3.5	0.4445	0.03741	0.02777	-0.0471	0.8456	1	11.88185
4	0.4909	0.03953	0.03022	-0.0479	0.8173	1	12.41842
5	0.7783	0.02209	0.01444	-0.0364	0.4241	1	35.23314
5.5	0.7912	0.02669	0.01693	-0.0289	0.2306	1	29.64406
7	0.9288	0.04588	0.03634	-0.022	0.0707	1	20.24412
8.5	0.9447	0.06866	0.06123	-0.0104	0.0595	1	13.7591
9	0.9211	0.07651	0.06947	-0.007	0.0606	1	12.03895
9.5	0.8916	0.08554	0.07871	-0.006	0.0622	1	10.42319
10	0.8171	0.10023	0.09386	-0.016	0.0769	1	8.15225
10.5	0.8028	0.11484	0.10849	-0.0233	0.0889	1	6.990596
12.5	0.772	0.17467	0.16801	-0.0574	0.1939	1	4.419763
13	0.7883	0.18385	0.17716	-0.0582	0.1724	1	4.287735
13.5	0.7731	0.18717	0.18036	-0.0644	0.1611	1	4.13047
14	0.7865	0.19572	0.18887	-0.0665	0.1465	1	4.018496
15	0.8082	0.21107	0.20413	-0.0728	0.1245	1	3.829061

- Airfoil 4

Table AVIII-118: Aerodynamic performance of Airfoil 4 of the H-146 coated blade at 10°

alpha	CL	CD	CDp	CM	Top_Xtr	Bot_Xtr	CL/CD
------	--------	---------	---------	--------	--------	--------	--------
-4.5	-0.387	0.02021	0.01157	-0.0303	1	0.3768	-19.1489
-4	-0.3901	0.02244	0.01489	-0.013	1	0.672	-17.3841
-3.5	-0.3807	0.02318	0.01536	-0.0012	1	0.7453	-16.4236
-3	-0.3704	0.02288	0.01473	0.009	1	0.8105	-16.1888
-2	-0.1455	0.02361	0.01415	-0.0081	1	0.9779	-6.16264
-1.5	-0.0889	0.02351	0.01388	-0.0146	1	1	-3.78137
-1	-0.1129	0.02277	0.01313	-0.0073	1	1	-4.95828
-0.5	-0.1113	0.02235	0.01258	-0.004	1	1	-4.97987
0	-0.0769	0.02287	0.01292	-0.0055	1	1	-3.36248
0.5	0.0001	0.02464	0.01446	-0.0144	0.9841	1	0.004058
1	0.081	0.0267	0.0164	-0.0233	0.9664	1	3.033708
1.5	0.1498	0.02856	0.01821	-0.0296	0.9497	1	5.245098
3.5	0.563	0.02406	0.01159	-0.0363	0.0562	1	23.39983
4	0.6007	0.02641	0.01428	-0.0334	0.0504	1	22.74517
4.5	0.6336	0.0292	0.01742	-0.0295	0.0494	1	21.69863
5	0.6918	0.03262	0.02112	-0.0276	0.0509	1	21.20785
5.5	0.7765	0.03843	0.0273	-0.0285	0.0561	1	20.20557
6	0.8304	0.04599	0.03539	-0.0273	0.0614	1	18.0561
6.5	0.8703	0.05143	0.04197	-0.0233	0.0709	1	16.92203
7	0.8929	0.06071	0.05229	-0.0203	0.0818	1	14.70763
7.5	0.8962	0.0684	0.06105	-0.0161	0.0997	1	13.10234
8	0.8745	0.07723	0.07058	-0.0137	0.1182	1	11.32332
8.5	0.851	0.08961	0.08321	-0.0148	0.1483	1	9.496708
9	0.7918	0.10016	0.09348	-0.021	0.1466	1	7.905351
11	0.7273	0.1505	0.14352	-0.0547	0.2244	1	4.832558
13	0.7856	0.18776	0.18085	-0.0609	0.1719	1	4.184065
14	0.8128	0.20641	0.19942	-0.0655	0.1502	1	3.937794
15	0.8112	0.21419	0.20707	-0.0751	0.1322	1	3.787292

- Airfoil 5

Table AVIII-119: Aerodynamic performance of Airfoil 5 of the H-146 coated blade at 10°

alpha	CL	CD	CDp	CM	Top_Xtr	Bot_Xtr	CL/CD
------	--------	---------	---------	--------	--------	--------	--------
-4	-0.2973	0.02258	0.01176	-0.0247	1	0.1172	-13.1665
-2	-0.191	0.02218	0.01156	-0.0049	1	0.7982	-8.61136
-1	-0.0705	0.02336	0.01278	-0.0122	0.9902	0.933	-3.01798

0	0.0876	0.02709	0.01629	-0.0296	0.9515	1	3.233666
1	0.2024	0.03047	0.01986	-0.0374	0.9168	1	6.642599
2	0.3199	0.03439	0.02383	-0.0448	0.8863	1	9.302123
3	0.4164	0.03827	0.02797	-0.0479	0.8491	1	10.88059
6	0.8754	0.04538	0.03517	-0.022	0.0509	1	19.29044
7	0.9307	0.06016	0.05145	-0.0149	0.0592	1	15.47041
8	0.8867	0.07601	0.06875	-0.0059	0.0683	1	11.66557
9	0.8108	0.09508	0.08821	-0.0101	0.0709	1	8.527556
13	0.7633	0.19012	0.18293	-0.0624	0.1516	1	4.014833
15	0.8228	0.2253	0.21796	-0.0726	0.1235	1	3.65202

- Airfoil 6

Table AVIII-120: Aerodynamic performance of Airfoil 6 of the H-146 coated blade at 10°

alpha	CL	CD	CDp	CM	Top_Xtr	Bot_Xtr	CL/CD
------	--------	---------	---------	--------	--------	--------	--------
-5	-0.3187	0.02193	0.01205	-0.0359	1	0.1989	-14.5326
-4.5	-0.2773	0.02087	0.01124	-0.0347	1	0.3121	-13.287
-4	-0.2479	0.02119	0.01214	-0.0304	1	0.5374	-11.6989
-3.5	-0.2187	0.02202	0.01291	-0.0265	1	0.6116	-9.93188
-3	-0.1928	0.02275	0.01363	-0.022	1	0.6705	-8.47473
-2.5	-0.1724	0.02327	0.01427	-0.0162	1	0.7451	-7.40868
-2	-0.1425	0.02359	0.01428	-0.0132	1	0.7957	-6.0407
-1.5	-0.0715	0.02385	0.01511	-0.017	0.9901	1	-2.9979
-1	0.0224	0.02601	0.01677	-0.0282	0.9666	1	0.861207
-0.5	0.095	0.02771	0.01812	-0.0349	0.9439	1	3.428365
0	0.1665	0.02948	0.01951	-0.0406	0.9215	1	5.647897
0.5	0.2321	0.0313	0.02111	-0.0447	0.9006	1	7.415335
1	0.2921	0.03315	0.02284	-0.0476	0.8809	1	8.811463
1.5	0.35	0.03503	0.02469	-0.0498	0.8613	1	9.991436
2	0.4075	0.0371	0.02695	-0.0517	0.8427	1	10.98383
2.5	0.465	0.03908	0.02911	-0.053	0.8199	1	11.89867
3	0.6894	0.02898	0.01995	-0.0558	0.7162	1	23.78882
3.5	0.7725	0.02218	0.01273	-0.043	0.5809	1	34.82867
4	0.8098	0.02245	0.01374	-0.036	0.4942	1	36.07127
4.5	0.8256	0.02439	0.01463	-0.0274	0.2454	1	33.84994
5	0.8266	0.02953	0.01828	-0.0208	0.0656	1	27.99187
6	0.8593	0.03674	0.02599	-0.0085	0.0454	1	23.38868
6.5	0.9272	0.04151	0.03131	-0.0056	0.0434	1	22.33679
7	0.9921	0.0492	0.03977	-0.0035	0.0441	1	20.16463
7.5	1.0124	0.05715	0.04869	0.0006	0.0454	1	17.71479
8	1.0086	0.06516	0.05736	0.005	0.0466	1	15.47882

8.5	0.9861	0.07297	0.06562	0.009	0.0475	1	13.51377
9	0.9556	0.08166	0.07466	0.0102	0.0483	1	11.70218
10	0.8874	0.1012	0.09486	0.0012	0.0502	1	8.768775
10.5	0.8413	0.1177	0.11135	-0.0131	0.0518	1	7.147833
11	0.8049	0.13931	0.13283	-0.0299	0.0567	1	5.777762
11.5	0.7974	0.15281	0.14623	-0.0375	0.062	1	5.218245
13.5	0.8483	0.21037	0.20379	-0.0558	0.1369	1	4.032419
14	0.8211	0.20968	0.20292	-0.0668	0.1322	1	3.915967
14.5	0.8295	0.21648	0.20969	-0.0711	0.1248	1	3.831763
15	0.8473	0.22515	0.2185	-0.073	0.1192	1	3.763269

- Polyurethane/IA-700
  - -5˚
  - Airfoil 1

Table AVIII-121: Aerodynamic performance of Airfoil 1 of the Polyurethane/IA-700 coated blade at -5°

alpha	CL	CD	CDp	CM	Top_Xtr	Bot_Xtr	CL/CD
------	--------	---------	---------	--------	--------	--------	--------
-5	-0.3912	0.03237	0.02243	-0.0362	1	0.1143	-12.0853
-4.5	-0.3531	0.02916	0.01872	-0.0333	1	0.1137	-12.1091
-4	-0.3145	0.02674	0.01611	-0.0305	1	0.1203	-11.7614
-3.5	-0.2756	0.02513	0.01429	-0.0274	1	0.1341	-10.967
-3	-0.2374	0.02313	0.01232	-0.0246	1	0.1619	-10.2637
0.5	0.0794	0.02467	0.01492	-0.0237	0.9725	1	3.218484
1	0.1498	0.02651	0.01658	-0.0295	0.9531	1	5.650698
1.5	0.2188	0.02838	0.01838	-0.0348	0.9316	1	7.709655
2	0.2848	0.03031	0.02031	-0.0393	0.9101	1	9.396239
2.5	0.3499	0.03223	0.02237	-0.0432	0.8854	1	10.85635
3	0.5447	0.02946	0.02026	-0.0567	0.7909	1	18.48948
3.5	0.6553	0.02408	0.01526	-0.0519	0.6999	1	27.21346
4	0.696	0.02057	0.01174	-0.0394	0.5394	1	33.83568
4.5	0.7084	0.02404	0.01271	-0.0307	0.2468	1	29.46755
5	0.7537	0.02668	0.01499	-0.0288	0.214	1	28.24963
5.5	0.8115	0.02908	0.01743	-0.0284	0.1962	1	27.90578
6	0.8738	0.03202	0.02047	-0.0287	0.1884	1	27.28919
6.5	0.9325	0.03618	0.02488	-0.029	0.1848	1	25.77391
7	0.9792	0.04013	0.02949	-0.0278	0.1828	1	24.4007
7.5	1.0144	0.04384	0.03407	-0.0255	0.1737	1	23.13869
8	1.0518	0.04837	0.03886	-0.0241	0.1623	1	21.74488
8.5	1.0684	0.05516	0.04646	-0.0213	0.157	1	19.36911
9	1.0633	0.06128	0.05345	-0.0173	0.1462	1	17.3515
9.5	1.0686	0.0705	0.06287	-0.0152	0.1335	1	15.15745

10	1.0268	0.08034	0.0732	-0.0124	0.1333	1	12.78068
12	0.7663	0.15664	0.14926	-0.0644	0.2938	1	4.892109
12.5	0.7991	0.16877	0.16147	-0.0635	0.2592	1	4.734846
13	0.8306	0.18152	0.17435	-0.0629	0.2352	1	4.575804
13.5	0.7929	0.18085	0.17352	-0.0693	0.2208	1	4.384296
14	0.82	0.19314	0.18586	-0.07	0.2078	1	4.245625
14.5	0.8585	0.20745	0.20026	-0.0687	0.1843	1	4.138347
15	0.8253	0.20412	0.19677	-0.077	0.1757	1	4.04321

- Airfoil 2

Table AVIII-122: Aerodynamic performance of Airfoil 2 of the Polyurethane/IA-700 coated blade at -5°

alpha	CL	CD	CDp	CM	Top_Xtr	Bot_Xtr	CL/CD
------	--------	---------	---------	--------	--------	--------	--------
-5	-0.4626	0.03169	0.02137	-0.032	1	0.0968	-14.5977
-4.5	-0.4225	0.02869	0.01778	-0.0287	1	0.1037	-14.7264
-3.5	-0.3511	0.02205	0.01213	-0.0225	1	0.2345	-15.9229
-2.5	-0.3775	0.02232	0.01495	0.0157	1	0.8544	-16.9131
-1.5	-0.0942	0.02386	0.01491	-0.0161	1	1	-3.94803
-1	-0.1231	0.02284	0.01386	-0.0085	1	1	-5.38967
-0.5	-0.1328	0.02199	0.01282	-0.0035	1	1	-6.03911
0	-0.1021	0.02236	0.01285	-0.004	1	1	-4.56619
0.5	-0.0457	0.02378	0.01396	-0.0085	0.9921	1	-1.92178
1	0.0336	0.02604	0.01594	-0.0165	0.9721	1	1.290323
1.5	0.1014	0.02788	0.01762	-0.0222	0.953	1	3.637016
2	0.1677	0.02971	0.01939	-0.0272	0.934	1	5.644564
2.5	0.2258	0.03149	0.02117	-0.0306	0.9148	1	7.17053
3	0.2817	0.03343	0.02319	-0.0336	0.8949	1	8.426563
3.5	0.3374	0.03555	0.02549	-0.0364	0.8737	1	9.490858
4	0.3974	0.03779	0.02796	-0.0395	0.8492	1	10.51601
4.5	0.4728	0.04021	0.03075	-0.0441	0.8212	1	11.75827
5	0.6334	0.03533	0.02696	-0.048	0.7199	1	17.92811
6	0.7564	0.02812	0.01703	-0.0228	0.1766	1	26.899
7	0.9029	0.03788	0.02729	-0.0249	0.1301	1	23.8358
7.5	0.9506	0.0439	0.03407	-0.0232	0.1288	1	21.65376
8	0.9807	0.05188	0.04242	-0.0213	0.1215	1	18.90324
8.5	0.9863	0.05683	0.04839	-0.0161	0.1161	1	17.35527
9	0.9868	0.06529	0.05747	-0.0125	0.1188	1	15.11411
9.5	0.9809	0.07366	0.06639	-0.0095	0.1243	1	13.31659
10	0.881	0.08268	0.07591	-0.0072	0.1317	1	10.65554
10.5	0.8441	0.09682	0.09009	-0.0127	0.1419	1	8.71824
11.5	0.399	0.08231	0.07676	-0.0321	0.3071	1	4.847528

12	0.4144	0.0893	0.08373	-0.0349	0.2979	1	4.640538
12.5	0.4408	0.09679	0.09126	-0.0366	0.2809	1	4.554189
13	0.4426	0.10174	0.09616	-0.0401	0.265	1	4.350305
13.5	0.4657	0.10892	0.10334	-0.0417	0.2383	1	4.275615
14	0.4758	0.11529	0.10969	-0.0449	0.2222	1	4.126984
14.5	0.5087	0.12628	0.12088	-0.046	0.2106	1	4.02835
15	0.5082	0.12973	0.12431	-0.0503	0.1958	1	3.917367

- Airfoil 3

Table AVIII-123: Aerodynamic performance of Airfoil 3 of the Polyurethane/IA-700 coated blade at -5°

alpha	CL	CD	CDp	CM	Top_Xtr	Bot_Xtr	CL/CD
------	--------	---------	---------	--------	--------	--------	--------
-4.5	-0.3708	0.02744	0.01674	-0.0317	1	0.0769	-13.5131
-4	-0.3387	0.02468	0.01398	-0.0274	1	0.092	-13.7237
-3.5	-0.3208	0.02014	0.01244	-0.0206	1	0.5912	-15.9285
-3	-0.3554	0.02214	0.01514	0.0058	1	0.8007	-16.0524
-2.5	-0.2949	0.02214	0.01469	0.0124	1	0.9317	-13.3198
-2	-0.0966	0.02266	0.01405	-0.0158	1	0.9917	-4.26302
-1.5	-0.0988	0.02213	0.01344	-0.0129	1	1	-4.46453
-1	-0.1219	0.02133	0.01254	-0.0064	1	1	-5.71496
-0.5	-0.0958	0.02159	0.01242	-0.0069	1	1	-4.43724
0	-0.0113	0.02329	0.01361	-0.017	0.9816	1	-0.48519
0.5	0.0678	0.025	0.015	-0.0252	0.9599	1	2.712
1	0.141	0.02678	0.01661	-0.0319	0.9391	1	5.265123
1.5	0.2125	0.02863	0.01845	-0.0378	0.9186	1	7.422284
2	0.2792	0.03042	0.02022	-0.0424	0.8972	1	9.178172
2.5	0.347	0.03232	0.02221	-0.0469	0.876	1	10.73639
3	0.4034	0.03425	0.02428	-0.0494	0.8541	1	11.7781
4	0.5212	0.03845	0.02902	-0.0542	0.806	1	13.55527
4.25	0.5248	0.03972	0.03035	-0.0521	0.7922	1	13.21249
4.75	0.7409	0.02836	0.01993	-0.0528	0.6717	1	26.12482
5	0.7727	0.02623	0.01801	-0.0486	0.6338	1	29.45864
5.25	0.7974	0.02279	0.01498	-0.0406	0.5462	1	34.98903
5.5	0.7917	0.02327	0.01381	-0.0319	0.301	1	34.02235
5.75	0.7969	0.0257	0.01533	-0.0288	0.2326	1	31.00778
6	0.8098	0.02761	0.01681	-0.027	0.1999	1	29.32995
6.25	0.8272	0.02923	0.01826	-0.0257	0.1746	1	28.29969
6.5	0.8523	0.03091	0.01983	-0.0251	0.1577	1	27.5736
6.75	0.8831	0.03268	0.02175	-0.0248	0.1441	1	27.02264
7	0.921	0.03568	0.02452	-0.0257	0.1327	1	25.81278
7.25	0.9436	0.03749	0.02675	-0.0246	0.1221	1	25.16938

7.5	0.9648	0.04032	0.02951	-0.0243	0.1086	1	23.92857
7.75	0.9838	0.04276	0.03241	-0.0229	0.1008	1	23.00748
8	1.0029	0.04599	0.03551	-0.0227	0.0908	1	21.80691
8.25	1.0126	0.04853	0.03858	-0.0207	0.0852	1	20.86544
8.5	1.0223	0.05119	0.04169	-0.019	0.0805	1	19.9707
8.75	1.0302	0.05456	0.04546	-0.0173	0.0783	1	18.88196
9	1.0339	0.05817	0.04946	-0.0155	0.0774	1	17.77377
9.25	1.0327	0.06197	0.05363	-0.0137	0.0771	1	16.66452
9.5	1.0255	0.06595	0.05796	-0.0119	0.0774	1	15.54966
9.75	1.012	0.07003	0.06234	-0.0101	0.0778	1	14.45095
10	0.9919	0.07398	0.06652	-0.0083	0.0788	1	13.40768
10.25	0.9674	0.07854	0.07127	-0.0077	0.0799	1	12.31729
10.5	0.9414	0.08388	0.07675	-0.0089	0.0811	1	11.22318
10.75	0.9153	0.09024	0.08321	-0.0117	0.0826	1	10.14295
11	0.8898	0.09766	0.0907	-0.0158	0.0841	1	9.111202
11.25	0.8733	0.10505	0.0981	-0.0197	0.086	1	8.313184
11.5	0.8609	0.1126	0.10564	-0.0234	0.0874	1	7.645648
11.75	0.8636	0.11859	0.11163	-0.0244	0.0891	1	7.282233
12.75	0.7735	0.16712	0.16001	-0.0618	0.2188	1	4.628411
13	0.7758	0.17038	0.16328	-0.0631	0.2107	1	4.553351
13.25	0.8173	0.17929	0.1723	-0.06	0.2012	1	4.558536
13.5	0.7878	0.1786	0.17148	-0.0651	0.1961	1	4.410974
13.75	0.7901	0.18163	0.1745	-0.0667	0.1881	1	4.350052
14	0.8345	0.19104	0.18409	-0.0629	0.1795	1	4.368195
14.25	0.825	0.19408	0.18704	-0.0664	0.1776	1	4.250824
14.5	0.8058	0.19324	0.18611	-0.0709	0.1716	1	4.169944
14.75	0.8114	0.19648	0.18936	-0.0723	0.1644	1	4.129682
15	0.8297	0.20196	0.1949	-0.0717	0.1589	1	4.108239

- Airfoil 4

Table AVIII-124: Aerodynamic performance of Airfoil 4 of the Polyurethane/IA-700 coated blade at -5°

alpha	CL	CD	CDp	CM	Top_Xtr	Bot_Xtr	CL/CD
------	--------	---------	---------	--------	--------	--------	--------
-5	-0.3372	0.02621	0.01646	-0.0467	1	0.1632	-12.8653
-4.5	-0.2979	0.02299	0.01332	-0.0434	1	0.2161	-12.9578
-4	-0.2677	0.02021	0.0128	-0.0382	1	0.5333	-13.2459
-3.5	-0.27	0.02227	0.01498	-0.0224	1	0.6955	-12.1239
-3	-0.265	0.02263	0.01521	-0.0108	1	0.7761	-11.7101
-2.5	-0.2601	0.02205	0.01454	-0.0003	1	0.8513	-11.7959
-1.5	-0.1217	0.02201	0.01384	-0.0099	1	1	-5.5293
-1	-0.0669	0.02258	0.01403	-0.0167	0.9869	1	-2.9628

-0.5	0.0183	0.02404	0.01506	-0.0277	0.9663	1	0.761231
0	0.1027	0.0257	0.01641	-0.0374	0.9451	1	3.996109
0.5	0.1767	0.02742	0.01789	-0.0447	0.9268	1	6.444201
1	0.2456	0.02915	0.01951	-0.0505	0.9074	1	8.425386
1.5	0.3056	0.03093	0.02124	-0.0544	0.8889	1	9.880375
2	0.3644	0.03288	0.02321	-0.0579	0.8711	1	11.08273
2.5	0.4225	0.03487	0.0253	-0.0609	0.8509	1	12.11643
3	0.4801	0.03706	0.02771	-0.0636	0.831	1	12.95467
3.5	0.5365	0.03924	0.03017	-0.0657	0.8067	1	13.67227
4	0.7734	0.02456	0.01668	-0.0625	0.6454	1	31.49023
4.5	0.7686	0.02454	0.01389	-0.0447	0.2078	1	31.32029
5	0.7982	0.02866	0.0175	-0.0408	0.1561	1	27.85066
5.5	0.8635	0.03266	0.02157	-0.04	0.1335	1	26.43907
6	0.9241	0.03753	0.02657	-0.0398	0.1133	1	24.62297
6.5	0.9729	0.04419	0.03338	-0.0393	0.1012	1	22.01629
7	1.0077	0.04899	0.03907	-0.0367	0.0964	1	20.5695
7.5	1.0342	0.05624	0.04707	-0.0342	0.0981	1	18.38905
8	1.0515	0.06553	0.0569	-0.0324	0.1012	1	16.04609
8.5	1.0342	0.07189	0.0644	-0.0282	0.1085	1	14.38587
9	0.9752	0.08215	0.07518	-0.0264	0.1151	1	11.87097
10	0.7812	0.14339	0.13652	-0.0739	0.3117	1	5.448079
11	0.7983	0.15772	0.1508	-0.0766	0.2695	1	5.061501
12	0.8493	0.17889	0.17201	-0.0784	0.2421	1	4.74761
13	0.8306	0.18805	0.18103	-0.0868	0.214	1	4.41691
14	0.8609	0.20403	0.19703	-0.0918	0.1923	1	4.219478
15	0.9202	0.22837	0.22164	-0.0937	0.1715	1	4.029426

- Airfoil 5

Table AVIII-125: Aerodynamic performance of Airfoil 5 of the Polyurethane/IA-700 coated blade at -5°

alpha	CL	CD	CDp	CM	Top_Xtr	Bot_Xtr	CL/CD
------	--------	---------	---------	--------	--------	--------	--------
-5	-0.2705	0.02604	0.01621	-0.0468	1	0.1206	-10.3879
-4.5	-0.2272	0.02203	0.01296	-0.0453	1	0.2456	-10.3132
-3.5	-0.2102	0.02301	0.01583	-0.0217	1	0.7246	-9.13516
-3	-0.2003	0.02255	0.0153	-0.0126	1	0.804	-8.88248
-2.5	-0.1869	0.02182	0.01468	-0.004	1	0.904	-8.56554
-2	-0.0504	0.02292	0.01517	-0.0234	0.9788	1	-2.19895
-1.5	0.0449	0.0242	0.01586	-0.0362	0.9514	1	1.855372
-1	0.1356	0.02573	0.01692	-0.0467	0.9295	1	5.270113
-0.5	0.2103	0.02717	0.01808	-0.0534	0.9065	1	7.740155
0	0.2825	0.0287	0.01938	-0.0589	0.8862	1	9.843206

0.5	0.3495	0.03036	0.02091	-0.0631	0.8682	1	11.51186
1	0.4077	0.03204	0.02255	-0.0655	0.8493	1	12.72472
1.5	0.4493	0.03404	0.02455	-0.0657	0.8321	1	13.19918
2	0.5048	0.03582	0.02645	-0.0671	0.8102	1	14.09269
2.5	0.5557	0.03786	0.02866	-0.0679	0.7889	1	14.67776
3	0.7146	0.03222	0.02358	-0.0706	0.7195	1	22.17877
3.5	0.8224	0.02383	0.01504	-0.06	0.6057	1	34.51112
4	0.8569	0.02295	0.01401	-0.0524	0.5075	1	37.33769
4.5	0.8613	0.02561	0.01466	-0.0432	0.2201	1	33.63139
5	0.8822	0.02935	0.01743	-0.0394	0.154	1	30.05792
5.5	0.9168	0.03204	0.02029	-0.0364	0.1323	1	28.61423
6	0.9654	0.03462	0.02305	-0.0345	0.1202	1	27.88562
6.5	1.0135	0.03779	0.02613	-0.0332	0.1042	1	26.81926
7	1.0497	0.04083	0.02925	-0.031	0.086	1	25.70904
8	1.1265	0.05093	0.04042	-0.027	0.0699	1	22.11859
8.5	1.1468	0.05648	0.0465	-0.0242	0.0675	1	20.30453
9	1.1516	0.06269	0.05327	-0.0209	0.0664	1	18.36976
9.5	1.1337	0.06957	0.06071	-0.017	0.0664	1	16.29582
10	1.0929	0.07838	0.07007	-0.0156	0.0672	1	13.94361
10.5	1.0018	0.09611	0.0884	-0.0247	0.07	1	10.42347
11	0.9128	0.12495	0.11745	-0.0445	0.0759	1	7.305322
11.5	0.8971	0.14041	0.13289	-0.0524	0.0789	1	6.389146
12	0.8973	0.15186	0.14433	-0.0571	0.0812	1	5.908732
13	0.8615	0.18956	0.18215	-0.0821	0.165	1	4.544735
14	0.9031	0.20623	0.19896	-0.0853	0.1569	1	4.379091
15	0.9192	0.22211	0.21488	-0.0935	0.1517	1	4.13849

- Airfoil 6

Table AVIII-126: Aerodynamic performance of Airfoil 6 of the Polyurethane/IA-700 coated blade at -5°

alpha	CL	CD	CDp	CM	Top_Xtr	Bot_Xtr	CL/CD
------	--------	---------	---------	--------	--------	--------	--------
-4.5	-0.3233	0.03904	0.03076	-0.0372	1	0.095	-8.28125
-4	-0.2781	0.03489	0.02571	-0.0356	1	0.0899	-7.97077
-3.5	-0.235	0.03205	0.02239	-0.0334	1	0.0905	-7.33229
-3	-0.1941	0.03007	0.02019	-0.0308	1	0.0957	-6.45494
-2.5	-0.1542	0.0289	0.01883	-0.0281	1	0.1058	-5.33564
-2	-0.108	0.02718	0.01718	-0.0269	1	0.1591	-3.97351
-1.5	-0.084	0.0242	0.0178	-0.0167	1	1	-3.47107
-1	-0.0016	0.02625	0.01886	-0.0252	0.984	1	-0.06095
-0.5	0.0908	0.02865	0.02054	-0.0347	0.9575	1	3.169284
0	0.167	0.03073	0.0222	-0.0407	0.93	1	5.434429

0.5	0.2445	0.03288	0.02404	-0.0463	0.9022	1	7.436131
1	0.3171	0.03499	0.02599	-0.0506	0.8749	1	9.062589
1.5	0.3875	0.03687	0.02784	-0.0538	0.8432	1	10.5099
2	0.495	0.03663	0.02759	-0.0583	0.7933	1	13.51351
2.5	0.6109	0.03362	0.02485	-0.0599	0.7372	1	18.17073
3	0.736	0.02613	0.0176	-0.0555	0.6633	1	28.16686
3.5	0.7924	0.02309	0.01414	-0.047	0.5526	1	34.31789
4	0.81	0.0239	0.01389	-0.0377	0.3681	1	33.89121
4.5	0.8295	0.0271	0.01573	-0.0319	0.2503	1	30.60886
5	0.8685	0.02989	0.0181	-0.0291	0.2035	1	29.05654
5.5	0.919	0.03244	0.02046	-0.0277	0.1767	1	28.32922
6	0.9754	0.03519	0.02341	-0.0268	0.1627	1	27.7181
6.5	1.0284	0.03825	0.02643	-0.026	0.1516	1	26.88627
7.5	1.0984	0.04371	0.03258	-0.0207	0.1264	1	25.12926
8	1.1203	0.04668	0.0359	-0.0171	0.1141	1	23.99957
8.5	1.1392	0.04911	0.03861	-0.0132	0.1038	1	23.1969
9	1.1563	0.05218	0.04167	-0.0099	0.0944	1	22.15983
9.5	1.15	0.05565	0.04574	-0.0045	0.0879	1	20.66487
10	1.1413	0.06021	0.05075	-0.0007	0.0824	1	18.95532
10.5	1.1417	0.06301	0.05355	0.0018	0.0758	1	18.11935
11.5	1.0961	0.07961	0.07084	0.0009	0.071	1	13.76837
12.5	0.8263	0.16081	0.15289	-0.049	0.0885	1	5.138362
13	0.8233	0.17159	0.16364	-0.0547	0.0828	1	4.798065
13.5	0.8251	0.182	0.17404	-0.0597	0.0828	1	4.533516
14	0.829	0.19227	0.18428	-0.0647	0.0861	1	4.311645
14.5	0.8389	0.20145	0.19347	-0.0685	0.0897	1	4.164309
15	0.8599	0.21095	0.20302	-0.0699	0.0938	1	4.076321

- 0˚
- Airfoil 1

Table AVIII-127: Aerodynamic performance of Airfoil 1 of the Polyurethane/IA-700 coated blade at 0°

alpha	CL	CD	CDp	CM	Top_Xtr	Bot_Xtr	CL/CD
------	--------	---------	---------	--------	--------	--------	--------
-5	-0.4	0.02995	0.01948	-0.0367	1	0.1381	-13.3556
-4.5	-0.3638	0.02689	0.01635	-0.0338	1	0.1495	-13.5292
-4	-0.3261	0.02457	0.01395	-0.0306	1	0.1696	-13.2723
-3.5	-0.2875	0.02241	0.01184	-0.0275	1	0.2103	-12.8291
-3	-0.2856	0.02036	0.01268	-0.014	1	0.7007	-14.0275
-2.5	-0.2873	0.02071	0.01305	0.001	1	0.8185	-13.8725
-2	-0.0816	0.02158	0.01318	-0.0194	1	1	-3.78128
-1.5	-0.1132	0.02076	0.01234	-0.0113	1	1	-5.45279

-1	-0.1108	0.02037	0.0117	-0.0081	1	1	-5.43937
-0.5	-0.0748	0.02087	0.01185	-0.0094	1	1	-3.58409
0	-0.0316	0.02181	0.01245	-0.0114	0.999	1	-1.44888
0.5	0.0567	0.02393	0.0143	-0.0213	0.9781	1	2.369411
1	0.1336	0.0258	0.01601	-0.0286	0.9556	1	5.178295
1.5	0.2051	0.02769	0.01783	-0.0345	0.9328	1	7.407006
2	0.2736	0.0296	0.01978	-0.0395	0.9096	1	9.243243
2.5	0.3385	0.03159	0.02187	-0.0436	0.8865	1	10.71542
3	0.4006	0.0337	0.02416	-0.047	0.863	1	11.88724
4.5	0.6807	0.02481	0.01324	-0.0296	0.2003	1	27.43652
5	0.7284	0.0278	0.01595	-0.0276	0.1736	1	26.20144
5.5	0.7933	0.03057	0.01897	-0.0274	0.1623	1	25.95028
6	0.854	0.03432	0.02271	-0.0275	0.1529	1	24.88345
6.5	0.9048	0.03877	0.02758	-0.0267	0.1468	1	23.33763
7	0.9493	0.04391	0.03337	-0.0254	0.147	1	21.61922
7.5	0.985	0.05045	0.04062	-0.0238	0.1487	1	19.52428
8	1.0122	0.05616	0.0472	-0.0215	0.1532	1	18.0235
8.5	0.9866	0.06588	0.05813	-0.0184	0.1637	1	14.97571
9	0.9927	0.07728	0.06976	-0.0186	0.1735	1	12.8455
9.5	0.8408	0.09757	0.09022	-0.0289	0.1954	1	8.617403
11	0.732	0.14555	0.13793	-0.0639	0.3298	1	5.0292
11.5	0.7361	0.15247	0.14483	-0.0657	0.3141	1	4.827835
12	0.7895	0.16468	0.15722	-0.0655	0.2999	1	4.794146
12.5	0.7637	0.16668	0.15912	-0.0688	0.2819	1	4.581833
13	0.7878	0.17683	0.16939	-0.0702	0.2713	1	4.455126
13.5	0.8384	0.19133	0.18409	-0.0692	0.249	1	4.381958
14	0.7996	0.18799	0.1806	-0.075	0.2338	1	4.253418
14.5	0.828	0.20023	0.19294	-0.076	0.2223	1	4.135244
15	0.8628	0.21464	0.20747	-0.0758	0.1989	1	4.019754

- Airfoil 2

Table AVIII-128: Aerodynamic performance of Airfoil 2 of the Polyurethane/IA-700 coated blade at 0°

alpha	CL	CD	CDp	CM	Top_Xtr	Bot_Xtr	CL/CD
------	--------	---------	---------	--------	--------	--------	--------
-5	-0.3958	0.02962	0.01914	-0.038	1	0.1319	-13.3626
-4.5	-0.358	0.02575	0.0153	-0.0348	1	0.1454	-13.9029
-4	-0.3207	0.02319	0.01273	-0.031	1	0.1727	-13.8292
-3	-0.3173	0.02131	0.01385	-0.0028	1	0.7779	-14.8897
-2.5	-0.3156	0.02064	0.01307	0.0113	1	0.8852	-15.2907
-2	-0.0759	0.02152	0.01279	-0.02	1	1	-3.52695
-1.5	-0.1067	0.02088	0.01212	-0.012	1	1	-5.11015

-1	-0.112	0.0204	0.01146	-0.0079	1	1	-5.4902
-0.5	-0.0768	0.02083	0.01155	-0.0095	1	1	-3.68699
0	-0.0113	0.02212	0.01252	-0.016	0.99	1	-0.51085
0.5	0.0767	0.02404	0.01415	-0.0259	0.9693	1	3.190516
1	0.1549	0.0259	0.01585	-0.0336	0.95	1	5.980695
1.5	0.2297	0.02772	0.01762	-0.0401	0.9278	1	8.286436
2	0.2939	0.02949	0.0194	-0.0445	0.9067	1	9.96609
2.5	0.357	0.03138	0.02143	-0.0483	0.8841	1	11.37667
3	0.4263	0.03336	0.0236	-0.0526	0.8583	1	12.77878
3.5	0.4874	0.03535	0.02585	-0.0552	0.8299	1	13.78784
4	0.5362	0.03753	0.0284	-0.0559	0.7999	1	14.28724
4.5	0.7224	0.02739	0.01935	-0.0526	0.6722	1	26.37459
5	0.7521	0.02216	0.01266	-0.0334	0.3072	1	33.93953
5.5	0.7699	0.02723	0.01617	-0.0283	0.1795	1	28.27396
6	0.8275	0.03068	0.01963	-0.0268	0.1553	1	26.97197
6.5	0.8893	0.03498	0.024	-0.0266	0.139	1	25.4231
7	0.9422	0.03981	0.02942	-0.0256	0.1323	1	23.66742
7.5	0.9833	0.04606	0.03657	-0.0238	0.1317	1	21.34824
8	1.0064	0.05387	0.04538	-0.0213	0.1353	1	18.68201
8.5	1.0141	0.06303	0.05529	-0.0192	0.14	1	16.08916
9	1.0073	0.07282	0.06559	-0.0178	0.1422	1	13.83274
9.5	1.0011	0.0832	0.07632	-0.0174	0.146	1	12.03245
10.5	0.7358	0.13731	0.13013	-0.0643	0.332	1	5.358677
11	0.7584	0.14623	0.13912	-0.0654	0.319	1	5.18635
11.5	0.7512	0.1528	0.14562	-0.0678	0.3021	1	4.91623
12	0.7706	0.16201	0.15487	-0.0689	0.2857	1	4.756497
12.5	0.794	0.17138	0.16429	-0.0693	0.2631	1	4.632979
13	0.8105	0.17895	0.17196	-0.0704	0.2433	1	4.529198
13.5	0.7954	0.18308	0.17599	-0.0749	0.2295	1	4.344549
14	0.8379	0.19828	0.1913	-0.0745	0.2165	1	4.225842
14.5	0.8212	0.19838	0.19133	-0.0795	0.2005	1	4.13953
15	0.8334	0.20665	0.19959	-0.0822	0.1872	1	4.032906

- Airfoil 3

Table AVIII-129: Aerodynamic performance of Airfoil 3 of the Polyurethane/IA-700 coated blade at 0°

alpha	CL	CD	CDp	CM	Top_Xtr	Bot_Xtr	CL/CD
------	--------	---------	---------	--------	--------	--------	--------
-4.5	-0.3486	0.02253	0.01456	-0.0092	1	0.7207	-15.4727
-4	-0.3488	0.02267	0.01473	0.0049	1	0.8022	-15.386
-3.5	-0.34	0.02169	0.0137	0.016	1	0.8891	-15.6754
-3	-0.1791	0.02245	0.01369	-0.0029	1	0.9678	-7.97773

-2.5	-0.0959	0.02239	0.01334	-0.0141	1	1	-4.28316
-2	-0.121	0.02156	0.01246	-0.0076	1	1	-5.61224
-1.5	-0.0964	0.02174	0.0124	-0.0083	1	1	-4.43422
-1	-0.0095	0.02347	0.01381	-0.0193	0.9814	1	-0.40477
-0.5	0.0679	0.02508	0.01524	-0.0276	0.9609	1	2.707337
0	0.1412	0.02679	0.01691	-0.0346	0.94	1	5.270623
0.5	0.2121	0.02863	0.01874	-0.0406	0.9204	1	7.408313
1	0.2846	0.03057	0.0208	-0.0464	0.9007	1	9.309781
1.5	0.3407	0.03242	0.02283	-0.0494	0.8815	1	10.50895
2	0.3897	0.03446	0.02511	-0.0511	0.8619	1	11.30876
2.5	0.4381	0.03679	0.02777	-0.0528	0.8431	1	11.90813
3	0.4984	0.03898	0.0305	-0.0552	0.8163	1	12.78604
5	0.8325	0.04268	0.03227	-0.0279	0.055	1	19.50562
5.5	0.872	0.04912	0.03947	-0.0253	0.0547	1	17.75244
6	0.8989	0.05939	0.05044	-0.0231	0.0578	1	15.13554
6.5	0.9137	0.06297	0.05522	-0.0178	0.0653	1	14.51008
7	0.9042	0.07189	0.06481	-0.0147	0.0727	1	12.57755
8	0.8793	0.09468	0.08815	-0.0139	0.1022	1	9.287072
8.5	0.8179	0.10348	0.0971	-0.0195	0.1009	1	7.903943
9.5	0.7226	0.14428	0.1377	-0.0582	0.2501	1	5.008317
10	0.7335	0.15189	0.14525	-0.059	0.2245	1	4.829153
10.5	0.7411	0.15961	0.1529	-0.0607	0.2029	1	4.643193
11	0.7593	0.16891	0.16215	-0.0615	0.1876	1	4.495293
11.5	0.7846	0.17803	0.17136	-0.0614	0.1697	1	4.407122
12	0.769	0.18311	0.17629	-0.0677	0.1588	1	4.199661
12.5	0.8189	0.19901	0.19225	-0.0645	0.1469	1	4.114869
13	0.7895	0.19851	0.19157	-0.0738	0.1396	1	3.97713
13.5	0.8137	0.20791	0.20099	-0.0746	0.1283	1	3.913713
14	0.8278	0.2182	0.21122	-0.0776	0.1241	1	3.793767
14.5	0.8254	0.22073	0.21367	-0.0841	0.1156	1	3.73941
15	0.8438	0.22892	0.22185	-0.0863	0.1078	1	3.686004

- Airfoil 4

Table AVIII-130: Aerodynamic performance of Airfoil 4 of the Polyurethane/IA-700 coated blade at 0°

alpha	CL	CD	CDp	CM	Top_Xtr	Bot_Xtr	CL/CD
------	--------	---------	---------	--------	--------	--------	--------
-5	-0.3494	0.02844	0.0171	-0.04	1	0.0791	-12.2855
-4.5	-0.3154	0.02638	0.01488	-0.0363	1	0.0931	-11.956
-4	-0.2859	0.02437	0.01341	-0.0345	1	0.1525	-11.7316
-2	-0.1193	0.02269	0.01439	-0.0117	1	0.9903	-5.25782
-1.5	-0.125	0.02204	0.01364	-0.0088	1	1	-5.67151

-1	-0.051	0.023	0.01418	-0.0186	0.9804	1	-2.21739
-0.5	0.0284	0.02427	0.01516	-0.028	0.9584	1	1.170169
0	0.1058	0.02576	0.01645	-0.036	0.9379	1	4.107143
0.5	0.1756	0.02734	0.01789	-0.0421	0.9189	1	6.422824
1	0.2364	0.02904	0.01955	-0.0463	0.9017	1	8.140496
1.5	0.2967	0.03094	0.02145	-0.0501	0.8853	1	9.589528
2	0.3631	0.03304	0.02366	-0.0546	0.8696	1	10.98971
2.5	0.4037	0.03508	0.02582	-0.055	0.8514	1	11.50798
3	0.4516	0.03734	0.0283	-0.0563	0.8317	1	12.09427
3.5	0.5062	0.03966	0.03097	-0.0582	0.8081	1	12.76349
4	0.577	0.04135	0.03343	-0.0602	0.7704	1	13.95405
5	0.7791	0.03456	0.02309	-0.0314	0.0779	1	22.5434
5.5	0.846	0.04011	0.02894	-0.0311	0.0763	1	21.092
6	0.8961	0.04716	0.03653	-0.0298	0.0776	1	19.00127
6.5	0.934	0.0511	0.0415	-0.026	0.083	1	18.27789
7	0.9501	0.05913	0.05056	-0.0224	0.0918	1	16.06799
7.5	0.9724	0.068	0.05988	-0.0205	0.102	1	14.3
8	0.9246	0.07701	0.0699	-0.0172	0.1138	1	12.00623
9	0.8319	0.10283	0.09608	-0.0263	0.1417	1	8.090052
10.5	0.7383	0.15119	0.14423	-0.064	0.2634	1	4.883259
11	0.7422	0.15867	0.15162	-0.0661	0.2464	1	4.677633
11.5	0.7752	0.16975	0.16268	-0.0661	0.2329	1	4.566716
12	0.7892	0.17684	0.16974	-0.0673	0.2136	1	4.462791
12.5	0.7739	0.18117	0.17394	-0.0722	0.1993	1	4.271679
13	0.808	0.1935	0.18626	-0.0722	0.1878	1	4.175711
13.5	0.8011	0.19615	0.18884	-0.0767	0.1728	1	4.084119
14	0.8258	0.20772	0.20038	-0.078	0.165	1	3.975544
14.5	0.8228	0.21035	0.20294	-0.0831	0.1524	1	3.911576
15	0.8677	0.22859	0.22166	-0.0814	0.1437	1	3.795879

- Airfoil 5

Table AVIII-131: Aerodynamic performance of Airfoil 5 of the Polyurethane/IA-700 coated blade at 0°

alpha	CL	CD	CDp	CM	Top_Xtr	Bot_Xtr	CL/CD
------	--------	---------	---------	--------	--------	--------	--------
-4.5	-0.3097	0.0247	0.01307	-0.0293	1	0.135	-12.5385
-2.5	-0.2484	0.02072	0.01265	0.0035	1	0.8643	-11.9884
-2	-0.1236	0.02155	0.01321	-0.0107	1	1	-5.7355
-1.5	-0.0894	0.02186	0.01319	-0.014	0.9907	1	-4.08966
-1	-0.0006	0.02333	0.01425	-0.0251	0.9669	1	-0.02572
-0.5	0.0746	0.02479	0.0154	-0.0328	0.9455	1	3.009278
0	0.1476	0.02638	0.01677	-0.0393	0.9246	1	5.595148

0.5	0.2128	0.02806	0.01836	-0.044	0.9068	1	7.583749
1	0.2741	0.02976	0.02001	-0.0476	0.8885	1	9.210349
1.5	0.3363	0.0316	0.02193	-0.0511	0.8717	1	10.64241
2	0.3756	0.03351	0.02401	-0.0511	0.8551	1	11.20859
3	0.5956	0.02428	0.01229	-0.0341	0.0782	1	24.53048
3.5	0.6273	0.02735	0.01556	-0.0303	0.0619	1	22.93601
4	0.6611	0.03018	0.01867	-0.0263	0.0568	1	21.90524
4.5	0.7177	0.03346	0.0222	-0.0241	0.0549	1	21.44949
5	0.7887	0.03828	0.02735	-0.0234	0.0565	1	20.60345
5.5	0.8403	0.04421	0.03401	-0.0214	0.0604	1	19.00701
6	0.8766	0.05129	0.04175	-0.0188	0.0648	1	17.09105
6.5	0.9095	0.05817	0.04933	-0.0161	0.0711	1	15.63521
7	0.9049	0.06624	0.05861	-0.0117	0.0825	1	13.66093
7.5	0.8966	0.07478	0.06779	-0.0093	0.0958	1	11.98984
7.75	0.8672	0.07939	0.07266	-0.0085	0.0999	1	10.92329
8	0.843	0.08392	0.07721	-0.0089	0.1017	1	10.04528
8.25	0.8204	0.08976	0.08311	-0.0113	0.105	1	9.139929
9.5	0.7106	0.13892	0.13216	-0.052	0.2601	1	5.115174
10	0.7348	0.14964	0.14284	-0.0525	0.2515	1	4.910452
11	0.7295	0.16208	0.15512	-0.0573	0.2127	1	4.500864
11.5	0.7678	0.17481	0.16788	-0.0563	0.2025	1	4.392197
12	0.7539	0.17771	0.17067	-0.0607	0.1854	1	4.242305
12.5	0.7626	0.18597	0.17894	-0.0633	0.1758	1	4.100661
13	0.779	0.19333	0.18629	-0.0648	0.1613	1	4.02938
13.5	0.7879	0.20184	0.19475	-0.068	0.1551	1	3.903587
14	0.7911	0.20647	0.19932	-0.0722	0.143	1	3.831549
14.5	0.8399	0.22641	0.21935	-0.0692	0.1344	1	3.709642
15	0.8175	0.22203	0.21483	-0.0782	0.1296	1	3.681935

- Airfoil 6

Table AVIII-132: Aerodynamic performance of Airfoil 6 of the Polyurethane/IA-700 coated blade at 0°

alpha	CL	CD	CDp	CM	Top_Xtr	Bot_Xtr	CL/CD
------	--------	---------	---------	--------	--------	--------	--------
-4.5	-0.3338	0.0367	0.02656	-0.0278	1	0.0952	-9.09537
-4	-0.2952	0.03268	0.02208	-0.0258	1	0.0979	-9.03305
-3.5	-0.2589	0.03056	0.01994	-0.0237	1	0.1132	-8.47186
-3	-0.2202	0.02857	0.01792	-0.0213	1	0.1399	-7.70739
-1	-0.0543	0.02505	0.0171	-0.013	1	1	-2.16766
-0.5	0.0229	0.02727	0.01883	-0.0205	0.9823	1	0.839751
0	0.1129	0.03002	0.0212	-0.0296	0.9576	1	3.760826
0.5	0.1966	0.03208	0.02304	-0.0366	0.9221	1	6.128429

1	0.276	0.0342	0.02505	-0.0422	0.8897	1	8.070175
1.5	0.3473	0.03582	0.02666	-0.0457	0.8509	1	9.695701
2	0.4529	0.03716	0.02816	-0.0527	0.8123	1	12.18784
2.5	0.5502	0.03579	0.02703	-0.0544	0.7529	1	15.37301
3	0.672	0.03158	0.02324	-0.0554	0.6936	1	21.27929
3.5	0.7855	0.0258	0.01774	-0.0523	0.6154	1	30.44574
4	0.8303	0.02445	0.01563	-0.043	0.4558	1	33.9591
4.5	0.8638	0.02707	0.01698	-0.037	0.3265	1	31.90986
5	0.9076	0.03034	0.01967	-0.0342	0.2595	1	29.9143
6	0.9908	0.03779	0.02719	-0.0287	0.1848	1	26.21858
6.5	1.0242	0.04212	0.03169	-0.0254	0.1591	1	24.31624
7	1.0542	0.04847	0.03823	-0.0225	0.1437	1	21.74954
7.5	1.0555	0.05506	0.04573	-0.0168	0.1377	1	19.17
8	1.0378	0.06278	0.05414	-0.0112	0.1354	1	16.53074
8.5	0.9903	0.07124	0.06308	-0.0055	0.1363	1	13.9009
9	0.9223	0.08272	0.07484	-0.0051	0.14	1	11.14966
9.5	0.8717	0.0981	0.09029	-0.0106	0.1441	1	8.885831
10	0.8012	0.12636	0.11858	-0.0276	0.1716	1	6.340614
11	0.7039	0.1601	0.15216	-0.055	0.268	1	4.396627
11.5	0.7633	0.17499	0.16716	-0.0532	0.2538	1	4.361964
12	0.7268	0.17438	0.16643	-0.0581	0.2374	1	4.167909
12.5	0.784	0.19098	0.18309	-0.0563	0.2261	1	4.105142
13	0.748	0.18852	0.18051	-0.0624	0.2131	1	3.967749
13.5	0.7881	0.20016	0.19221	-0.0615	0.2016	1	3.93735
14	0.7864	0.20664	0.19861	-0.0656	0.1965	1	3.805652
14.5	0.7862	0.20934	0.20128	-0.0697	0.1832	1	3.755613
15	0.8528	0.23495	0.2271	-0.066	0.1723	1	3.629708

- 5°
- Airfoil 1

Table AVIII-133: Aerodynamic performance of Airfoil 1 of the Polyurethane/IA-700 coated blade at 5°

alpha	CL	CD	CDp	CM	Top_Xtr	Bot_Xtr	CL/CD
------	--------	---------	---------	--------	--------	--------	--------
-5	-0.4105	0.02913	0.01872	-0.0374	1	0.136	-14.092
-4.5	-0.3742	0.02633	0.01578	-0.0342	1	0.1458	-14.2119
-4	-0.3389	0.02421	0.01365	-0.0309	1	0.1722	-13.9983
-3.5	-0.3019	0.02177	0.01136	-0.0278	1	0.2231	-13.8677
-2.5	-0.307	0.02079	0.01305	0.0025	1	0.8174	-14.7667
-1.5	-0.1016	0.0211	0.0124	-0.0141	1	1	-4.81517
-1	-0.12	0.02038	0.01155	-0.008	1	1	-5.88813
-0.5	-0.0923	0.02062	0.01146	-0.0083	1	1	-4.47624

0	-0.0522	0.02139	0.01186	-0.01	1	1	-2.44039
0.5	0.0356	0.02333	0.0135	-0.02	0.9795	1	1.525932
1	0.1143	0.02517	0.01514	-0.0278	0.9593	1	4.54112
1.5	0.1872	0.02702	0.01689	-0.0342	0.9392	1	6.928201
2	0.2614	0.02897	0.01883	-0.0403	0.9176	1	9.023127
2.5	0.3236	0.03082	0.02078	-0.0441	0.896	1	10.49968
3	0.3867	0.03281	0.02291	-0.0478	0.873	1	11.78604
3.5	0.4461	0.03481	0.02513	-0.0504	0.8456	1	12.81528
4	0.5001	0.03677	0.02745	-0.0517	0.813	1	13.60076
4.5	0.703	0.02772	0.01956	-0.0531	0.6893	1	25.36075
5	0.7449	0.0213	0.01256	-0.0348	0.3998	1	34.97183
5.5	0.7571	0.02647	0.01543	-0.028	0.2015	1	28.60219
6	0.8077	0.03001	0.01853	-0.0266	0.1622	1	26.91436
6.5	0.8718	0.03352	0.02249	-0.0263	0.149	1	26.00835
7	0.9296	0.03833	0.0276	-0.026	0.143	1	24.25254
7.5	0.9763	0.04412	0.03407	-0.0247	0.1423	1	22.12829
8	1.0044	0.05078	0.04189	-0.022	0.1463	1	19.77944
8.5	1.0097	0.05924	0.05137	-0.0193	0.1509	1	17.04423
9	0.9959	0.06834	0.06112	-0.0171	0.1531	1	14.57272
9.5	0.9629	0.07866	0.07178	-0.0162	0.1577	1	12.24129
10	0.8656	0.09877	0.09198	-0.0269	0.1882	1	8.763795
11	0.7264	0.14111	0.13377	-0.0631	0.3368	1	5.147757
11.5	0.743	0.14991	0.1426	-0.0646	0.3232	1	4.956307
12	0.7547	0.15706	0.14986	-0.0655	0.2994	1	4.80517
12.5	0.7993	0.16968	0.16261	-0.0652	0.2797	1	4.710632
13	0.7841	0.17218	0.16506	-0.0681	0.2604	1	4.553955
13.5	0.7818	0.17845	0.17129	-0.0714	0.2461	1	4.381059
14	0.8216	0.19247	0.18544	-0.0714	0.2318	1	4.268717
15	0.8185	0.20073	0.19363	-0.0784	0.1957	1	4.077617

- Airfoil 2

Table AVIII-134: Aerodynamic performance of Airfoil 2 of the Polyurethane/IA-700 coated blade at 5°

alpha	CL	CD	CDp	CM	Top_Xtr	Bot_Xtr	CL/CD
------	--------	---------	---------	--------	--------	--------	--------
-5	-0.4179	0.02764	0.01693	-0.0324	1	0.1345	-15.1194
-4.5	-0.3793	0.02508	0.01424	-0.0288	1	0.1454	-15.1236
-4	-0.344	0.02305	0.01234	-0.0257	1	0.1874	-14.9241
-3.5	-0.338	0.02028	0.01253	-0.0138	1	0.6623	-16.6667
-3	-0.3424	0.02128	0.01358	0.0027	1	0.7918	-16.0902
-2	-0.078	0.0222	0.01325	-0.0196	1	1	-3.51351
-1.5	-0.1109	0.02147	0.01252	-0.0114	1	1	-5.16535

-1	-0.1234	0.02082	0.0117	-0.0061	1	1	-5.92699
-0.5	-0.0923	0.02121	0.0117	-0.0068	1	1	-4.35172
0	-0.0484	0.02213	0.01231	-0.009	0.9981	1	-2.18708
0.5	0.0355	0.02416	0.01406	-0.0182	0.9794	1	1.469371
1	0.1077	0.02595	0.01567	-0.0247	0.9602	1	4.150289
1.5	0.1803	0.02793	0.01756	-0.0309	0.9417	1	6.455424
2	0.2428	0.02973	0.01939	-0.0352	0.9224	1	8.166835
2.5	0.2999	0.03159	0.0213	-0.0383	0.902	1	9.493511
3	0.3569	0.03362	0.02348	-0.0412	0.8805	1	10.6157
3.5	0.4219	0.03577	0.02595	-0.0449	0.855	1	11.7948
4	0.4924	0.03802	0.02856	-0.0488	0.8273	1	12.95108
5.5	0.7517	0.02707	0.01592	-0.0249	0.1883	1	27.76875
6	0.8112	0.03052	0.01921	-0.0239	0.161	1	26.57929
6.5	0.8824	0.0351	0.02417	-0.0246	0.152	1	25.1396
7	0.9358	0.04039	0.03024	-0.0235	0.1502	1	23.1691
7.5	0.9753	0.04564	0.0359	-0.0217	0.1363	1	21.36941
8	1.0027	0.05452	0.04551	-0.0195	0.1336	1	18.39142
8.5	1.005	0.06163	0.05385	-0.0151	0.1376	1	16.30699
9	0.9655	0.07207	0.06517	-0.0122	0.1469	1	13.3967
9.5	0.954	0.08391	0.07726	-0.0121	0.1578	1	11.36932
10	0.8274	0.10218	0.09546	-0.0252	0.1742	1	8.097475
11	0.7215	0.14181	0.13472	-0.0581	0.3251	1	5.087794
11.5	0.7278	0.14966	0.14257	-0.0596	0.3062	1	4.863023
12	0.7396	0.15795	0.15088	-0.061	0.2872	1	4.682494
12.5	0.7586	0.1674	0.16035	-0.062	0.2679	1	4.531661
13	0.7615	0.17345	0.16637	-0.0638	0.2417	1	4.390314
13.5	0.7717	0.18068	0.17359	-0.0655	0.217	1	4.271087
14	0.8057	0.19378	0.18676	-0.0654	0.2007	1	4.157808
14.5	0.7997	0.19656	0.18949	-0.0695	0.1839	1	4.068478
15	0.8081	0.2047	0.19758	-0.0728	0.1744	1	3.947728

- Airfoil 3

Table AVIII-135: Aerodynamic performance of Airfoil 3 of the Polyurethane/IA-700 coated blade at 5°

alpha	CL	CD	CDp	CM	Top_Xtr	Bot_Xtr	CL/CD
------	--------	---------	---------	--------	--------	--------	--------
-5	-0.3929	0.02153	0.01193	-0.032	1	0.278	-18.249
-4.5	-0.3902	0.02099	0.01348	-0.0177	1	0.6238	-18.5898
-4	-0.3836	0.02229	0.01472	-0.004	1	0.7218	-17.2095
-3.5	-0.3775	0.02225	0.01453	0.0082	1	0.8034	-16.9663
-3	-0.3579	0.02132	0.01342	0.0173	1	0.8812	-16.7871
-2.5	-0.1706	0.02208	0.01308	-0.0052	1	0.9676	-7.72645

-2	-0.0806	0.02177	0.01242	-0.0175	1	1	-3.70234
-1.5	-0.1155	0.021	0.01167	-0.0093	1	1	-5.5
-1	-0.1107	0.02076	0.0112	-0.007	1	1	-5.33237
-0.5	-0.0551	0.02177	0.01191	-0.0124	0.9928	1	-2.53101
0	0.0299	0.02347	0.01335	-0.0223	0.9717	1	1.273967
0.5	0.1116	0.02526	0.01499	-0.0309	0.9509	1	4.418052
1	0.1832	0.02699	0.01674	-0.0371	0.9308	1	6.787699
1.5	0.2514	0.02876	0.01853	-0.0424	0.9107	1	8.741307
2	0.3077	0.0305	0.02035	-0.0453	0.8905	1	10.08852
2.5	0.361	0.03242	0.02243	-0.0477	0.8703	1	11.1351
3	0.4119	0.03453	0.02493	-0.0495	0.8503	1	11.92876
3.5	0.464	0.03681	0.02756	-0.0514	0.8285	1	12.60527
4.5	0.6752	0.02642	0.01524	-0.0294	0.0953	1	25.5564
5.5	0.7558	0.0338	0.02282	-0.0229	0.0566	1	22.36095
6	0.8269	0.03925	0.0287	-0.0223	0.0558	1	21.06752
6.5	0.8754	0.04599	0.03624	-0.0203	0.0584	1	19.03457
7	0.906	0.05378	0.04479	-0.0176	0.0621	1	16.84641
7.5	0.9311	0.06306	0.05458	-0.0156	0.0669	1	14.7653
8	0.9153	0.06961	0.0624	-0.011	0.0759	1	13.14897
8.5	0.9282	0.08083	0.07384	-0.0104	0.0887	1	11.48336
9	0.8668	0.08761	0.08106	-0.0096	0.0909	1	9.893848
9.5	0.8077	0.1007	0.09426	-0.0189	0.0932	1	8.020854
10.5	0.7332	0.14248	0.13585	-0.0529	0.23	1	5.145985
11	0.7562	0.15252	0.1459	-0.0538	0.2238	1	4.958038
11.5	0.7447	0.15924	0.1525	-0.0578	0.2071	1	4.676589
12	0.779	0.17162	0.16489	-0.0573	0.1974	1	4.539098
12.5	0.7692	0.17589	0.16908	-0.0616	0.1803	1	4.373188
13	0.7731	0.18392	0.17702	-0.0651	0.1711	1	4.203458
13.5	0.7899	0.19188	0.18498	-0.0668	0.1572	1	4.116635
14	0.7986	0.20066	0.1937	-0.0702	0.1505	1	3.979866
14.5	0.8033	0.20592	0.1991	-0.0743	0.1384	1	3.90103
15	0.8478	0.22505	0.21831	-0.0724	0.1307	1	3.767163

- Airfoil 4

Table AVIII-136: Aerodynamic performance of Airfoil 4 of the Polyurethane/IA-700 coated blade at 5°

alpha	CL	CD	CDp	CM	Top_Xtr	Bot_Xtr	CL/CD
------	--------	---------	---------	--------	--------	--------	--------
-4.5	-0.3502	0.03336	0.02144	-0.0396	1	0.083	-10.4976
-4	-0.3131	0.0299	0.01778	-0.0372	1	0.0811	-10.4716
-3.5	-0.2754	0.02762	0.01541	-0.0343	1	0.0797	-9.97104
-3	-0.2391	0.02608	0.0138	-0.0311	1	0.0796	-9.16794

-2.5	-0.2029	0.02499	0.01247	-0.0287	1	0.0819	-8.11925
-2	-0.1638	0.02407	0.01141	-0.0279	1	0.09	-6.80515
-1.5	-0.1203	0.02334	0.0108	-0.0281	1	0.126	-5.15424
-1	-0.0997	0.02243	0.01257	-0.0219	1	0.7026	-4.44494
-0.5	-0.0793	0.02297	0.01344	-0.0146	0.9947	0.8293	-3.45233
0	0.0179	0.0237	0.0146	-0.0242	0.9711	0.9686	0.755274
0.5	0.0987	0.02528	0.01597	-0.0329	0.9495	1	3.904272
1	0.1718	0.02689	0.0175	-0.0396	0.9279	1	6.388992
1.5	0.2398	0.02873	0.01942	-0.0448	0.9075	1	8.346676
2	0.3045	0.03062	0.02139	-0.0492	0.8889	1	9.944481
2.5	0.3714	0.03248	0.02343	-0.0535	0.8693	1	11.43473
3	0.4389	0.03441	0.02571	-0.0574	0.849	1	12.75501
4	0.6308	0.02653	0.01531	-0.0352	0.0821	1	23.77686
4.5	0.6679	0.02979	0.0188	-0.0315	0.0732	1	22.42028
5	0.7372	0.03367	0.02305	-0.0304	0.0699	1	21.89486
5.5	0.8046	0.03902	0.0288	-0.0299	0.071	1	20.62019
6	0.8542	0.04562	0.03603	-0.028	0.075	1	18.72424
6.5	0.8946	0.05381	0.04473	-0.0262	0.0802	1	16.62516
7	0.9111	0.05991	0.05222	-0.0217	0.0932	1	15.20781
7.5	0.914	0.06869	0.06188	-0.019	0.1095	1	13.30616
8.5	0.8455	0.09093	0.08486	-0.0206	0.143	1	9.298361

- Airfoil 5

Table AVIII-137: Aerodynamic performance of Airfoil 5 of the Polyurethane/IA-700 coated blade at 5°

alpha	CL	CD	CDp	CM	Top_Xtr	Bot_Xtr	CL/CD
------	--------	---------	---------	--------	--------	--------	--------
-5	-0.3208	0.02424	0.01341	-0.0402	1	0.2	-13.2343
-4.5	-0.2835	0.02258	0.01154	-0.0374	1	0.2177	-12.5554
-4	-0.2441	0.02037	0.01013	-0.0361	1	0.3063	-11.9833
-3.5	-0.2442	0.0215	0.0128	-0.0221	1	0.6758	-11.3581
-3	-0.2331	0.02202	0.01329	-0.0126	1	0.7583	-10.5858
-2.5	-0.2299	0.02141	0.01287	-0.0014	1	0.8516	-10.738
-2	-0.1188	0.02185	0.01333	-0.0111	1	1	-5.43707
-1.5	-0.0847	0.02206	0.01328	-0.0145	0.991	1	-3.83953
-1	0.0013	0.02345	0.01432	-0.0255	0.9695	1	0.055437
-0.5	0.0863	0.02506	0.01567	-0.0354	0.9494	1	3.443735
0	0.1585	0.0266	0.01702	-0.0423	0.9301	1	5.958647
0.5	0.2231	0.02825	0.01856	-0.0474	0.9112	1	7.897345
1	0.2811	0.03003	0.02032	-0.051	0.8939	1	9.360639
1.5	0.3371	0.03194	0.02249	-0.054	0.8768	1	10.55416
2	0.398	0.03408	0.02487	-0.0576	0.8609	1	11.6784

2.5	0.4518	0.03626	0.02741	-0.0599	0.8431	1	12.46001
3	0.4972	0.03857	0.03007	-0.0608	0.8227	1	12.89085
3.5	0.5701	0.04071	0.03287	-0.0642	0.7951	1	14.00393
4.5	0.766	0.03265	0.02207	-0.0333	0.0908	1	23.46095
5.5	0.8801	0.0448	0.03479	-0.0313	0.0667	1	19.64509
6	0.9183	0.05089	0.04196	-0.0277	0.0709	1	18.0448
6.5	0.9364	0.05908	0.05118	-0.0241	0.0786	1	15.8497
7	0.9596	0.07049	0.06287	-0.0228	0.0876	1	13.61328
7.5	0.9191	0.07674	0.07028	-0.0189	0.0991	1	11.9768
8	0.8944	0.08653	0.08035	-0.0186	0.1133	1	10.3363
8.5	0.826	0.0996	0.09351	-0.0276	0.1164	1	8.293173
10.5	0.7538	0.1574	0.15094	-0.067	0.2319	1	4.789072
11	0.7657	0.16607	0.15954	-0.0687	0.2171	1	4.610706
11.5	0.8061	0.17875	0.17224	-0.067	0.1991	1	4.50965
12	0.7871	0.18116	0.17453	-0.0726	0.1826	1	4.344778
12.5	0.7944	0.18922	0.18251	-0.0757	0.1712	1	4.198288
13.5	0.8158	0.20414	0.19733	-0.0816	0.1479	1	3.996277
14	0.8347	0.2122	0.20539	-0.0834	0.1356	1	3.933553
14.5	0.8558	0.22456	0.21788	-0.0852	0.1301	1	3.811008
15	0.8522	0.22594	0.21916	-0.0919	0.1211	1	3.771798

- Airfoil 6

Table AVIII-138: Aerodynamic performance of Airfoil 6 of the Polyurethane/IA-700 coated blade at 5°

alpha	CL	CD	CDp	CM	Top_Xtr	Bot_Xtr	CL/CD
------	--------	---------	---------	--------	--------	--------	--------
-5	-0.3547	0.0332	0.02175	-0.0327	1	0.1489	-10.6837
-4.5	-0.3136	0.03086	0.01916	-0.0311	1	0.1509	-10.162
-4	-0.2742	0.02931	0.01764	-0.029	1	0.1567	-9.35517
-3.5	-0.2351	0.02839	0.01666	-0.027	1	0.1672	-8.28108
-3	-0.1965	0.02746	0.01575	-0.0251	1	0.19	-7.15586
-1.5	-0.1017	0.02543	0.01709	-0.0114	1	1	-3.99921
-1	-0.0597	0.02651	0.01774	-0.0136	1	1	-2.25198
-0.5	-0.0122	0.02811	0.01899	-0.0165	0.9967	1	-0.43401
0	0.0831	0.03157	0.02211	-0.0274	0.9656	1	2.632246
0.5	0.1623	0.03425	0.02457	-0.0346	0.9354	1	4.738686
1	0.2297	0.03629	0.02653	-0.0393	0.9062	1	6.329567
1.5	0.3003	0.03814	0.02837	-0.0441	0.8793	1	7.873623
2	0.3645	0.03964	0.03006	-0.0473	0.8475	1	9.195257
2.5	0.4545	0.04071	0.03129	-0.0527	0.8106	1	11.16433
3	0.557	0.03993	0.03079	-0.057	0.7653	1	13.94941
3.5	0.6893	0.03416	0.02551	-0.0585	0.7031	1	20.17857

5	0.8738	0.02706	0.01699	-0.0398	0.3044	1	32.2912
6	0.9784	0.03304	0.02244	-0.0382	0.2103	1	29.61259
6.5	1.0513	0.03666	0.02627	-0.0403	0.1922	1	28.67703
7.5	1.0611	0.04005	0.03023	-0.0268	0.1313	1	26.49438
9.5	1.0493	0.06259	0.05417	-0.0059	0.0462	1	16.76466
10	1.0239	0.07133	0.06349	-0.0042	0.0454	1	14.35441
10.5	0.978	0.08314	0.07583	-0.0066	0.046	1	11.76329
11	0.9113	0.10113	0.09423	-0.0164	0.0489	1	9.011174
11.5	0.8575	0.12245	0.11567	-0.0294	0.0532	1	7.002858
12	0.8289	0.14146	0.1346	-0.0393	0.0548	1	5.859607
12.5	0.8189	0.15586	0.14891	-0.046	0.0557	1	5.254074
13	0.8166	0.16864	0.1616	-0.0515	0.0562	1	4.842268
13.5	0.8228	0.18006	0.17297	-0.0551	0.0573	1	4.569588
14	0.8082	0.1967	0.18952	-0.0669	0.0725	1	4.108795
15	0.8216	0.21894	0.21173	-0.0784	0.1106	1	3.752626

- 10˚
- Airfoil 1

Table AVIII-139: Aerodynamic performance of Airfoil 1 of the Polyurethane/IA-700 coated blade at 10°

alpha	CL	CD	CDp	CM	Top_Xtr	Bot_Xtr	CL/CD
------	--------	---------	---------	--------	--------	--------	--------
-4.5	-0.3493	0.02717	0.01663	-0.0347	1	0.1427	-12.8561
-4	-0.3104	0.02511	0.01432	-0.0315	1	0.1483	-12.3616
-3.5	-0.2728	0.02325	0.01239	-0.0283	1	0.1629	-11.7333
-3	-0.2344	0.01961	0.01059	-0.0267	1	0.3962	-11.9531
-2	-0.0888	0.02109	0.01281	-0.0177	1	1	-4.21053
-1.5	-0.1188	0.02025	0.01191	-0.01	1	1	-5.86667
-1	-0.1004	0.02021	0.01153	-0.0092	1	1	-4.96784
-0.5	-0.0607	0.02086	0.01181	-0.011	1	1	-2.90988
0	0.0018	0.02228	0.0129	-0.0166	0.9915	1	0.08079
0.5	0.0844	0.02415	0.01448	-0.0252	0.9692	1	3.494824
1	0.1607	0.02603	0.01621	-0.0322	0.9472	1	6.173646
1.5	0.2292	0.0279	0.01804	-0.0375	0.9258	1	8.215054
2	0.2934	0.02985	0.02	-0.0418	0.9044	1	9.829146
2.5	0.3571	0.03183	0.02211	-0.0457	0.8809	1	11.21898
3	0.5902	0.02508	0.01623	-0.0562	0.748	1	23.5327
3.5	0.6371	0.02006	0.01125	-0.0407	0.5813	1	31.75972
4	0.6485	0.02349	0.01186	-0.0314	0.2125	1	27.60749
4.5	0.6913	0.02614	0.01428	-0.029	0.1866	1	26.44606
5	0.7504	0.02887	0.01686	-0.0284	0.173	1	25.99238
5.5	0.8077	0.03186	0.01982	-0.0283	0.1553	1	25.35154

6	0.8646	0.0354	0.02375	-0.0279	0.1502	1	24.42373
6.5	0.9146	0.03963	0.0286	-0.0268	0.1481	1	23.07848
7	0.9567	0.04486	0.03454	-0.0254	0.1484	1	21.32635
7.5	0.9898	0.05125	0.04163	-0.0238	0.1508	1	19.31317
8	1.0194	0.05913	0.05004	-0.0228	0.1545	1	17.23998
8.5	0.9835	0.06829	0.06059	-0.0198	0.1664	1	14.40182
9	0.9895	0.07893	0.07152	-0.0202	0.1779	1	12.53642
11	0.7378	0.14734	0.1397	-0.0662	0.3219	1	5.007466
11.5	0.7467	0.15459	0.14696	-0.068	0.3083	1	4.830196
12	0.7842	0.16397	0.15649	-0.0683	0.2941	1	4.782582
12.5	0.7704	0.16804	0.1605	-0.0715	0.2785	1	4.584623
13	0.8341	0.18385	0.17661	-0.0707	0.2691	1	4.536851
13.5	0.7971	0.18206	0.17467	-0.0757	0.254	1	4.378227
14	0.8495	0.19851	0.19154	-0.0754	0.2455	1	4.279381
14.5	0.8218	0.19618	0.18911	-0.0808	0.2319	1	4.18901
15	0.8703	0.21361	0.20681	-0.0786	0.1988	1	4.074247

- Airfoil 2

Table AVIII-140: Aerodynamic performance of Airfoil 2 of the Polyurethane/IA-700 coated blade at 10°

alpha	CL	CD	CDp	CM	Top_Xtr	Bot_Xtr	CL/CD
------	--------	---------	---------	--------	--------	--------	--------
-5	-0.2952	0.02078	0.0116	-0.0358	1	0.2494	-14.206
-4	-0.3083	0.02152	0.01444	-0.0025	1	0.7955	-14.3262
-3.5	-0.3036	0.0206	0.01344	0.0105	1	0.8961	-14.7379
-3	-0.0843	0.02129	0.01284	-0.0188	1	1	-3.95961
-2.5	-0.1152	0.02049	0.01202	-0.0113	1	1	-5.62225
-2	-0.1046	0.02018	0.01142	-0.0099	1	1	-5.18335
-1.5	-0.0615	0.02074	0.01159	-0.013	1	1	-2.96528
-1	0.0246	0.02243	0.01283	-0.0232	0.9816	1	1.096745
-0.5	0.1101	0.02429	0.01441	-0.0326	0.9621	1	4.53273
0	0.1841	0.02598	0.01596	-0.0393	0.9406	1	7.08622
0.5	0.2565	0.02781	0.01774	-0.0454	0.9194	1	9.223301
1	0.3258	0.02968	0.01962	-0.0505	0.8971	1	10.97709
1.5	0.3879	0.03154	0.02158	-0.054	0.873	1	12.29867
2	0.4462	0.03355	0.02382	-0.0568	0.8487	1	13.29955
2.5	0.501	0.03571	0.0262	-0.0588	0.8226	1	14.02968
3	0.5739	0.0376	0.0285	-0.0622	0.7908	1	15.2633
3.5	0.7537	0.02627	0.01828	-0.0555	0.6561	1	28.69052
4	0.77	0.02316	0.01314	-0.0369	0.2636	1	33.24698
4.5	0.7931	0.02788	0.01663	-0.0329	0.1696	1	28.44692
5	0.8516	0.03149	0.02019	-0.0316	0.1444	1	27.04351

5.5	0.9154	0.03562	0.02483	-0.0313	0.1345	1	25.69905
6	0.9699	0.04081	0.03059	-0.0305	0.1326	1	23.76623
6.5	1.0098	0.04711	0.03791	-0.0287	0.1356	1	21.43494
7	1.0329	0.05505	0.04684	-0.0266	0.1415	1	18.76294
8.5	0.9697	0.08772	0.08135	-0.0256	0.1732	1	11.05449
10	0.7619	0.14753	0.14041	-0.0732	0.3232	1	5.164373
10.5	0.8003	0.15809	0.15127	-0.0737	0.3093	1	5.062306
11.5	0.7938	0.17004	0.16316	-0.0788	0.2737	1	4.668313
12	0.8085	0.17718	0.17036	-0.0802	0.2486	1	4.563156
12.5	0.824	0.18584	0.17907	-0.0822	0.2345	1	4.433922
13	0.8812	0.20372	0.19722	-0.0803	0.2165	1	4.325545
13.5	0.844	0.19997	0.19328	-0.088	0.2047	1	4.220633
14	0.8783	0.21463	0.20809	-0.0881	0.1929	1	4.092159
14.5	0.8718	0.21601	0.20944	-0.0935	0.1779	1	4.035924
15	0.885	0.22406	0.21749	-0.0961	0.1549	1	3.949835

- Airfoil 3

Table AVIII-141: Aerodynamic performance of Airfoil 3 of the Polyurethane/IA-700 coated blade at 10°

alpha	CL	CD	CDp	CM	Top_Xtr	Bot_Xtr	CL/CD
------	--------	---------	---------	--------	--------	--------	--------
-5	-0.3968	0.02443	0.01404	-0.0336	1	0.1774	-16.2423
-4.5	-0.362	0.02179	0.01152	-0.0299	1	0.2197	-16.6131
-3.5	-0.3479	0.02121	0.01325	-0.0058	1	0.7294	-16.4026
-3	-0.3561	0.02124	0.01343	0.011	1	0.8371	-16.7655
-2.5	-0.199	0.02194	0.01328	-0.0015	1	0.9582	-9.07019
-2	-0.0756	0.02168	0.01251	-0.019	1	1	-3.48708
-1.5	-0.1103	0.02094	0.01179	-0.0107	1	1	-5.26743
-1	-0.1162	0.02043	0.01109	-0.0068	1	1	-5.68771
-0.5	-0.0818	0.02093	0.01129	-0.0083	1	1	-3.90827
0	0.0005	0.02259	0.01259	-0.0178	0.9817	1	0.022134
0.5	0.0826	0.0244	0.01419	-0.0265	0.9615	1	3.385246
1	0.1526	0.02608	0.01577	-0.0326	0.9416	1	5.851227
1.5	0.2208	0.02793	0.01758	-0.038	0.9233	1	7.905478
2	0.2894	0.02987	0.01958	-0.0431	0.904	1	9.688651
2.5	0.3424	0.03171	0.02154	-0.0455	0.8839	1	10.79786
3	0.3967	0.03376	0.02391	-0.0479	0.8628	1	11.75059
3.5	0.4545	0.03594	0.02635	-0.0505	0.8398	1	12.64608
4	0.522	0.03824	0.02906	-0.054	0.8145	1	13.65063
4.5	0.5927	0.03925	0.03063	-0.055	0.7662	1	15.10064
5.5	0.7748	0.02641	0.01653	-0.0273	0.2157	1	29.33737
6.5	0.8684	0.03976	0.02908	-0.0229	0.0785	1	21.84105

7	0.9064	0.04438	0.03435	-0.0204	0.0631	1	20.42361
7.5	0.9393	0.05183	0.0426	-0.0179	0.0623	1	18.12271
8	0.9489	0.05996	0.0518	-0.0142	0.065	1	15.82555
8.5	0.9361	0.06878	0.06141	-0.0111	0.069	1	13.61006
9	0.9069	0.07729	0.07034	-0.0089	0.0719	1	11.73373
9.5	0.8712	0.08661	0.07985	-0.0102	0.0746	1	10.05888
10.5	0.786	0.11857	0.1119	-0.0321	0.0911	1	6.628996
11.5	0.4097	0.07747	0.07264	-0.0363	0.2616	1	5.288499
12	0.4225	0.08508	0.08017	-0.0396	0.2433	1	4.965914
12.5	0.4411	0.0934	0.08843	-0.0425	0.2294	1	4.722698
13	0.4779	0.10466	0.09969	-0.0433	0.2118	1	4.566214
13.5	0.4772	0.10893	0.1039	-0.0481	0.1951	1	4.380795
14	0.4931	0.11692	0.1118	-0.0511	0.1742	1	4.217414
14.5	0.5082	0.12513	0.11997	-0.0545	0.1597	1	4.061376
15	0.5544	0.14056	0.13544	-0.0537	0.1456	1	3.944223

- Airfoil 4

Table AVIII-142: Aerodynamic performance of Airfoil 4 of the Polyurethane/IA-700 coated blade at 10°

alpha	CL	CD	CDp	CM	Top_Xtr	Bot_Xtr	CL/CD
------	--------	---------	---------	--------	--------	--------	--------
-4.5	-0.3426	0.02172	0.01398	-0.0222	1	0.653	-15.7735
-4	-0.3279	0.02243	0.01448	-0.0129	1	0.7186	-14.6188
-3.5	-0.3176	0.02248	0.01439	-0.0032	1	0.7842	-14.1281
-3	-0.3141	0.02177	0.01369	0.008	1	0.8643	-14.4281
-2.5	-0.195	0.02251	0.01372	-0.0017	1	0.9663	-8.66282
-2	-0.1155	0.02268	0.01357	-0.0127	1	1	-5.09259
-1.5	-0.1236	0.02207	0.01284	-0.009	0.9988	1	-5.60036
-1	-0.038	0.02348	0.01393	-0.0205	0.9767	1	-1.6184
-0.5	0.0374	0.02491	0.01512	-0.0293	0.9579	1	1.501405
0	0.112	0.02651	0.01647	-0.037	0.9383	1	4.224821
0.5	0.1818	0.02822	0.01805	-0.0434	0.9202	1	6.44224
1	0.2459	0.02992	0.01969	-0.0483	0.9023	1	8.218583
3	0.4579	0.03788	0.0282	-0.0585	0.8357	1	12.08817
3.5	0.5134	0.04022	0.03112	-0.0608	0.816	1	12.76479
5.5	0.8352	0.03937	0.02851	-0.0323	0.0459	1	21.21412
6	0.891	0.04725	0.03699	-0.0312	0.0473	1	18.85714
6.5	0.9317	0.05239	0.04297	-0.0281	0.0506	1	17.78393
7	0.947	0.05985	0.05166	-0.0235	0.0575	1	15.82289
7.5	0.9473	0.0686	0.06108	-0.0202	0.0632	1	13.80904
8.5	0.9005	0.08462	0.07804	-0.0156	0.0749	1	10.64169
9	0.8524	0.09529	0.08892	-0.0207	0.0763	1	8.945325

9.5	0.81	0.11074	0.10439	-0.0319	0.0801	1	7.31443
10	0.7661	0.14041	0.13405	-0.0569	0.2106	1	5.456164
12	0.8087	0.18001	0.17345	-0.0662	0.1799	1	4.492528
13	0.8129	0.19435	0.18765	-0.0737	0.1559	1	4.18266
14	0.8522	0.21595	0.20923	-0.0769	0.1352	1	3.946284
15	0.8523	0.22338	0.21654	-0.0876	0.118	1	3.815471

- Airfoil 5

Table AVIII-143: Aerodynamic performance of Airfoil 5 of the Polyurethane/IA-700 coated blade at 10°

alpha	CL	CD	CDp	CM	Top_Xtr	Bot_Xtr	CL/CD
------	--------	---------	---------	--------	--------	--------	--------
-4.5	-0.225	0.02013	0.01107	-0.0356	1	0.5662	-11.1773
-4	-0.2136	0.02149	0.01268	-0.0259	1	0.6652	-9.93951
-3.5	-0.2044	0.02179	0.01306	-0.0163	1	0.7473	-9.38045
-3	-0.1891	0.0212	0.01246	-0.0094	1	0.8179	-8.91981
-2.5	-0.1605	0.02082	0.0119	-0.006	1	0.8841	-7.70893
-2	-0.0507	0.02172	0.01273	-0.0209	0.9841	1	-2.33425
-1.5	0.0502	0.0233	0.01399	-0.0349	0.9573	1	2.154506
-1	0.1372	0.02476	0.01526	-0.045	0.9306	1	5.541195
-0.5	0.2204	0.02626	0.01658	-0.0535	0.9063	1	8.392993
0	0.2851	0.02788	0.01805	-0.0586	0.8861	1	10.22597
0.5	0.3439	0.02962	0.01973	-0.0622	0.8675	1	11.6104
1.5	0.4695	0.03344	0.0239	-0.0695	0.8352	1	14.04007
2	0.5779	0.03161	0.02261	-0.0727	0.7758	1	18.28219
2.5	0.7102	0.02161	0.01288	-0.061	0.6298	1	32.86441
3	0.7361	0.02098	0.01189	-0.0512	0.45	1	35.0858
3.5	0.7402	0.02686	0.01485	-0.0449	0.0538	1	27.55771
4	0.7709	0.03016	0.01859	-0.041	0.0446	1	25.56034
4.5	0.8034	0.03365	0.02248	-0.0368	0.0414	1	23.87519
5	0.8675	0.03839	0.02785	-0.0347	0.0409	1	22.59703
5.5	0.9262	0.0453	0.03546	-0.0329	0.0429	1	20.44592
6	0.9584	0.05295	0.04397	-0.0299	0.0456	1	18.10009
6.5	0.9715	0.06127	0.05303	-0.0266	0.0482	1	15.85605
7	0.9692	0.0702	0.06251	-0.0238	0.0504	1	13.80627
7.5	0.969	0.07933	0.07203	-0.0219	0.0538	1	12.2148
8	0.9341	0.08508	0.07827	-0.0195	0.0559	1	10.97908
8.5	0.8872	0.09519	0.08865	-0.0241	0.0565	1	9.320307
9	0.842	0.11028	0.10384	-0.0355	0.0578	1	7.635111
9.5	0.8149	0.1282	0.12168	-0.0477	0.0629	1	6.356474
10	0.8151	0.14051	0.13393	-0.0522	0.0711	1	5.801011
11	0.8018	0.17186	0.16522	-0.0723	0.1576	1	4.665425

11.5	0.8088	0.18012	0.17344	-0.0757	0.1512	1	4.49034
12	0.8328	0.19051	0.18384	-0.0765	0.1453	1	4.371424
12.5	0.8475	0.20207	0.19535	-0.079	0.1412	1	4.194091
13	0.836	0.20458	0.19775	-0.086	0.1306	1	4.086421
13.5	0.8571	0.21398	0.20715	-0.0874	0.1233	1	4.005515
14	0.8901	0.23159	0.22478	-0.0872	0.1191	1	3.84343
14.5	0.8746	0.22907	0.22212	-0.0962	0.1141	1	3.818047
15	0.8867	0.23581	0.22884	-0.1002	0.1063	1	3.760231

- Airfoil 6

Table AVIII-144: Aerodynamic performance of Airfoil 6 of the Polyurethane/IA-700 coated blade at 10°

alpha	CL	CD	CDp	CM	Top_Xtr	Bot_Xtr	CL/CD
------	--------	---------	---------	--------	--------	--------	--------
-5	-0.2795	0.02826	0.01728	-0.0401	1	0.1535	-9.8903
-4.5	-0.2421	0.02652	0.01554	-0.0387	1	0.1614	-9.12896
-4	-0.2042	0.02568	0.01456	-0.0369	1	0.164	-7.95171
-3.5	-0.169	0.0252	0.01398	-0.035	1	0.1691	-6.70635
-3	-0.1318	0.02506	0.0136	-0.0338	1	0.179	-5.25938
-2.5	-0.0908	0.02462	0.01337	-0.0339	1	0.2121	-3.68806
-2	-0.0408	0.02462	0.0157	-0.031	0.9817	0.7307	-1.65719
-1.5	0.0406	0.02452	0.01622	-0.0352	0.9582	1	1.655791
-1	0.1267	0.0261	0.01731	-0.0449	0.9327	1	4.854406
-0.5	0.2122	0.02781	0.01869	-0.0534	0.9095	1	7.630349
0	0.2815	0.0295	0.02016	-0.0585	0.8865	1	9.542373
0.5	0.3442	0.03123	0.02176	-0.062	0.8631	1	11.02145
1	0.4101	0.03305	0.02355	-0.0656	0.8407	1	12.40847
1.5	0.4735	0.03489	0.02549	-0.0684	0.8179	1	13.57122
2	0.5274	0.03674	0.02744	-0.0694	0.7923	1	14.35493
2.5	0.5885	0.0382	0.02916	-0.0703	0.7611	1	15.40576
3	0.6666	0.03799	0.02931	-0.0707	0.7175	1	17.54672
3.5	0.7687	0.03451	0.02639	-0.0687	0.6661	1	22.2747
4	0.868	0.02888	0.02111	-0.0629	0.6035	1	30.0554
4.5	0.9166	0.02578	0.01802	-0.0536	0.4951	1	35.55469
5	0.9367	0.02678	0.01769	-0.0441	0.3161	1	34.9776
5.5	0.9803	0.03072	0.0211	-0.0412	0.2448	1	31.91081
7	1.0979	0.04428	0.03529	-0.0341	0.1466	1	24.79449
8	1.1312	0.06067	0.05238	-0.0277	0.1089	1	18.64513
8.5	1.1123	0.0685	0.06107	-0.0228	0.1073	1	16.23796
9	1.0762	0.07726	0.07033	-0.019	0.1074	1	13.92959
9.5	1.0326	0.08782	0.08116	-0.0185	0.1085	1	11.75814
10.5	0.8409	0.13773	0.13108	-0.0546	0.1514	1	6.105424

11.5	0.7953	0.17065	0.16383	-0.0764	0.247	1	4.660416
12	0.8104	0.18022	0.17344	-0.0779	0.2315	1	4.496726
12.5	0.8284	0.18844	0.1817	-0.0792	0.2144	1	4.396094
13	0.8322	0.19698	0.19019	-0.0828	0.2065	1	4.224794
13.5	0.8416	0.20321	0.19643	-0.0855	0.1908	1	4.141528
14	0.8709	0.21811	0.21138	-0.0863	0.1835	1	3.992939
14.5	0.8592	0.21811	0.21129	-0.0927	0.1714	1	3.939297
15	0.9048	0.23865	0.23196	-0.0905	0.1584	1	3.791326

VITA

Abdullah F. Alajmi

Education

Ph.D. in Mechanical Engineering: Department of Mechanical Engineering, University of Washington, Seattle. Dissertation: *Characterization and Modeling of the Leading Edge Erosion of Wind Turbine Blades due to Sand Particles Impingement.*
Chair: M. Ramulu. August, 2021.

Master of Science in Mechanical Engineering: Department of Mechanical Engineering, University of Washington, Seattle. Thesis: *Conceptual Design of a Circulating Fluidized Bed Reactor as a Thermochemical Thermal Energy Storage System for Applications in Concentrated Solar Thermal Power Plants.*
Chair: John Kramlich. August, 2016.

Bachelor of Science, Department of Mechanical Engineering, University of Portland, 2013

Publications

[1] A. F. Alajmi, "Conceptual Design of a Circulating Fluidized Bed Reactor as a Thermochemical Thermal Energy Storage System for Applications in Concentrated Solar Thermal Power Plants," University of Wshington, 2016.

[2] A. F. Alajmi, B. P. Hu, and M. Ramulu, "Experimental solid particle erosion of silicon nitride: Optical investigation," *Ceram. Int.*, vol. 47, no. 2, pp. 2743–2750, 2021.

[3] A. F. Alajmi and M. Ramulu, "Solid Particle Erosion of Graphene-based Coatings," *Wear*, p. 203686, 2021.

[4] Alajmi, A. F., and Ramulu, M. (2021). "Characterization of the leading-edge erosion of wind turbine blades by sand particles impingement". In *Energy.* (In press).

[5] Bin Abdullah, M. S., Alajmi, A. F., and Ramulu, M. (2021). "Solid Particle Erosion Behavior of Electron Beam Melted (EBM) Ti6Al4V at Different Built Orientation". In *Advanced Manufacturing.* (In press).

Presentations at Professional Meetings

A. F. Alajmi and M. Ramulu, "Solid Particle Erosion of Graphene-based Coatings," Presented at *the 23rd International Confrence on Wear of Materials.* April, 2021.

Honors and Awards

Tau Beta Pi Engineering Honor Society, Member Oct. 2011 –present

Scholarship from Ministry of Higher Education in Kuwait – Bachelor
Sept.2009 – May 2013

Dean's list Fall 2009 – Spring 2013

Scholarship from Ministry of Higher Education in Kuwait – Master's
Aug. 2013 – Aug. 2015

Scholarship from Kuwait University – Master's and PhD Sept. 2015 – Aug. 2021